

**FLORIDA SOLAR**



**ENERGY CENTER®**

## CONTRACT REPORT

### **Understanding the Dehumidification Performance of Air-Conditioning Equipment at Part-Load Conditions**

#### **Final Report FSEC-CR-1537-05**

Don B. Shirey, III  
Hugh I. Henderson, Jr.  
Richard A. Raustad

January 2006

DOE/NETL Project No. DE-FC26-01NT41253

University of Central Florida / Florida Solar Energy Center  
1679 Clearlake Road  
Cocoa, FL 32922  
(321) 638-1000

CDH Energy Corp.  
P.O. Box 641  
132 Albany St.  
Cazenovia, NY 13035-0641  
(315) 655-1063

1679 Clearlake Road, Cocoa, FL 32922-5703 ♦ Phone: 321-638-1000 ♦ Fax: 321-638-1010  
[www.fsec.ucf.edu](http://www.fsec.ucf.edu)



A Research Institute of the University of Central Florida

## **DISCLAIMER**

This report was prepared as an account of work sponsored by an agency of the United States Government. Neither the United States Government nor any agency thereof, nor any of their employees, makes any warranty, express or implied, or assumes any legal liability or responsibility for the accuracy, completeness, or usefulness of any information, apparatus, product, or process disclosed, or represents that its use would not infringe privately owned rights. Reference herein to any specific commercial product, process, or service by trade name, trademark, manufacturer, or otherwise does not necessarily constitute or imply its endorsement, recommendation, or favoring by the United States Government or any agency thereof. The views and opinions of authors expressed herein do not necessarily state or reflect those of the United States Government or any agency thereof.

## Abstract

Air conditioner cooling coils typically provide both sensible cooling and moisture removal. Data from a limited number of field studies (Khattar et al. 1985; Henderson and Rengarajan 1996; Henderson 1998) have demonstrated that the moisture removal capacity of a cooling coil degrades at part-load conditions – especially when the supply fan operates continuously while the cooling coil cycles on and off. Degradation occurs because moisture that condenses on the coil surfaces during the cooling cycle evaporates back into air stream when the coil is off. This degradation affects the ability of cooling equipment to maintain proper indoor humidity levels and may negatively impact indoor air quality.

This report summarizes the results of a comprehensive project to better understand and quantify the moisture removal (dehumidification) performance of cooling coils at part-load conditions. A review of the open literature was initially conducted to learn from previous research on this topic. Detailed performance measurements were then collected for eight cooling coils in a controlled laboratory setting to understand the impact of coil geometry and operating conditions on transient moisture condensation and evaporation by the coils. Measurements of cooling coil dehumidification performance and space humidity levels were also collected at seven field test sites. Finally, an existing engineering model to predict dehumidification performance degradation for single-stage cooling equipment at part-load conditions (Henderson and Rengarajan 1996) was enhanced to include a broader range of fan control strategies and an improved theoretical basis for modeling off-cycle moisture evaporation from cooling coils. The improved model was validated with the laboratory measurements, and this report provides guidance for users regarding proper model inputs. The model is suitable for use in computerized calculation procedures such as hourly or sub-hourly building energy simulation programs (e.g., DOE’s EnergyPlus building energy simulation program, <http://www.energyplus.gov> ).

## Table of Contents

1	Introduction.....	1-1
2	Literature Review.....	2-1
2.1	Summary of Technical Documents.....	2-1
2.1.1	Transient Moisture Removal by Cooling Coils at Startup.....	2-2
2.1.2	Modeling and Experimental Studies of Moisture Retention on Cooling Coils ...	2-4
2.1.3	Field Measurements of Latent Capacity Degradation at Part-Load Conditions ..	2-7
2.1.4	Transient Moisture Evaporation from a Wetted Surface .....	2-10
2.2	Analysis of Existing Data Sets of Field Measurements.....	2-11
2.3	Impacts of Fan Overrun on Seasonal Energy Efficiency Ratio .....	2-12
2.4	Review of Manufacturer’s Product Information.....	2-13
3	Laboratory Testing.....	3-1
3.1	Testing Facility and Experimental Setup.....	3-1
3.2	Instrumentation and Monitored Variables .....	3-4
3.3	Description of Tests .....	3-7
3.4	Test Results.....	3-10
3.4.1	Steady-State Tests.....	3-10
3.4.2	Cyclic Tests.....	3-32
3.5	Cyclic Tests with Fan Delay .....	3-35
3.5.1	Fan Overrun Delay.....	3-35
3.5.2	“Drain-Down” Fan Delay .....	3-37
3.6	Impact of Oil on New Coils.....	3-40
3.6.1	Experiences with Coil 2.....	3-40
3.6.2	Tracking Performance for Other “New” Coils .....	3-43
4	Field Testing .....	4-1
4.1	Description of Field Test Sites.....	4-1
4.2	Instrumentation .....	4-3
4.3	One-Time and Auxiliary Measurements.....	4-6
4.4	Documentation of Coil and System Information .....	4-7
4.5	Analysis of Collected Data .....	4-8
4.5.1	Verification of Latent Capacity Measurements .....	4-8
4.5.2	Analysis of Field Measurements.....	4-9
4.5.3	Part-Load Sensible Heat Ratio.....	4-18
4.5.4	Impact of Supply Air Fan Control on Indoor Humidity Levels.....	4-21
5	Model Development and Validation.....	5-1
5.1	Original LHR Model from Henderson and Rengarajan.....	5-1
5.1.1	Summary of Original LHR Calculation Procedure.....	5-3
5.2	Better Predictions of Off-Cycle Moisture Evaporation .....	5-5
5.2.1	Deriving a Model for Transient Moisture Evaporation .....	5-5
5.2.2	Validation of the Transient Moisture Evaporation Model.....	5-9
5.3	An Improved Latent Degradation Model.....	5-22
5.4	Modeling Latent Capacity Degradation for Off-Cycle Fan Control Strategies.....	5-25
5.4.1	A Simple Model to Consider Supply Air Fan Delays.....	5-26
5.4.2	A General Model to Consider Two Types of Off-Cycle Fan Operation .....	5-26



5.4.3	Demonstrating the Utility of the New LHR Models.....	5-28
5.5	Validation of LHR Degradation Models.....	5-32
5.5.1	Validating Constant Fan Operation .....	5-32
5.5.2	Validating the AUTO Fan Mode .....	5-41
5.5.3	Validating the LHR Degradation Model for Fan Drain-Down Delays.....	5-44
5.6	Recommended Model Parameters for Various Cooling Systems.....	5-45
5.7	Part-Load Latent Performance for Modulating and Staged DX Systems.....	5-47
5.7.1	Part-Load Latent Performance for Modulating DX Coils .....	5-47
5.7.2	Considering the Impact of Cooling Coil Circuiting and Staging.....	5-49
5.7.3	Approaches for Modeling Multi-Stage, Cycling DX Systems .....	5-52
5.8	Latent Degradation with Modulating Chilled Water Coils.....	5-54
6	Summary of Findings.....	6-1
6.1	Summary of Laboratory and Field Test Findings.....	6-1
6.2	Best Practices to Mitigate Latent Capacity Degradation .....	6-3
6.2.1	The Importance of Proper Equipment Sizing .....	6-3
6.2.2	The Importance of Capacity Staging and Coil Circuiting .....	6-4
6.2.3	The Importance of Coil Temperature Control .....	6-4
6.2.4	The Impact of Off-Cycle Moisture Evaporation from the Cooling Coil .....	6-5
7	Conclusions and Recommendations .....	7-1
7.1	Conclusions.....	7-1
7.2	Recommendations for Further Work .....	7-3
8	References.....	8-1

Appendix A:	Literature Review Bibliography
Appendix B:	Summary of Katipamula and O’Neal (1991)
Appendix C:	Summary of Cooling Coil Moisture Retention Studies (Jacobi et al.)
Appendix D:	Summary of Khattar Field Study (Khattar et al. 1987)
Appendix E:	Analysis of Existing Data Sets of Field Measurements
Appendix F:	Impacts of Fan Overrun on Seasonal Energy Efficiency Ratio (SEER)
Appendix G:	Analysis of Manufacturer’s Evaporator Specifications
Appendix H:	Laboratory Test Summaries
Appendix I:	Field Test Site Summaries

## List of Figures

Figure 1-1. On-Cycle Condensation and Off-Cycle Evaporation of Moisture from a Cooling Coil (Henderson 1990).....	1-1
Figure 2-1. Effective Sensible Heat Ratio Versus Compressor Percent On-time.....	2-4
Figure 2-2. Real-time Moisture Retention for Plain Fin-and-tube Heat Exchangers (Yin and Jacobi 2000).....	2-5
Figure 2-3. Moisture Retention Impacts of Hydrophilic Coatings (Kim and Jacobi 2000) .....	2-6
Figure 2-4. Air-conditioner Transient Performance During Start-up .....	2-7
Figure 2-5. Moisture Removal Versus Air-conditioner Compressor Run-time Fraction .....	2-8
Figure 2-6. Moisture Removal and Addition Under Fan ON Operating Mode.....	2-9
Figure 2-7. Comparison of Measured SHR with First-generation Latent Degradation Model .....	2-10
Figure 2-8. Frequency Distribution for Number of Coil Rows .....	2-14
Figure 2-9. Frequency Distribution for Coil Fin Spacing.....	2-15
Figure 3-1. Control Room.....	3-1
Figure 3-2. Outdoor Test Chamber.....	3-1
Figure 3-3. Indoor Test Chamber.....	3-2
Figure 3-4. Schematic of Vertical Flow Test Configuration .....	3-3
Figure 3-5. Schematic of Horizontal Flow Test Configuration .....	3-3
Figure 3-6. Schematic of Psychrometric Chambers/Coil Testing Apparatus at FSEC.....	3-4
Figure 3-7. Tipping Bucket Calibration Multiplier.....	3-7
Figure 3-8. Cyclic Tests Shown on NEMA Thermostat Curve ( $N_{max}=3$ ).....	3-9
Figure 3-9. Comparing Steady-State Latent Capacity Calculated From Psychrometric State Points and Condensate Removal Rates, Coil 1 .....	3-11
Figure 3-10. Comparing Steady-State Latent Capacity Calculated From Psychrometric State Points and Condensate Removal Rates, All Coils .....	3-11
Figure 3-11. Variation of Steady State SHR with Entering Humidity and Nominal Air Flow, Coil 1.....	3-12
Figure 3-12. Laboratory Test Data for a Typical Test Run .....	3-13
Figure 3-13. Comparing Stored Moisture Mass Calculated by Integrating Sensible and Latent Off-Cycle Capacity (Integrated with a 1-minute Delay), Coil 1 .....	3-15
Figure 3-14. Comparing “twet” (Calculated with Off-Cycle Sensible and Steady State Latent) to the Condensate Delay Time, Coil 1 .....	3-16
Figure 3-15. Comparing “twet” (Calculated with Off-Cycle Sensible and Steady State Latent) to the Condensate Delay Time, All Coils .....	3-17
Figure 3-16. Impact of Dew Point and Coil Wettedness on Condensate Delay Time, Coil 1..	3-18
Figure 3-17. Measured Variation of Initial Evaporation Rate with Wet-Bulb Depression, Coil 1 .....	3-19
Figure 3-18. Evaporative Effectiveness Versus Airflow for Coil 1.....	3-20
Figure 3-19. Comparing Measured and Predicted Initial Moisture Evaporation Rates.....	3-21
Figure 3-20. Variation of Retained Moisture (Based on Off-Cycle Sensible) with Flow and Dew Point, Coil 1 .....	3-22
Figure 3-21. Variation of Retained Moisture with Dew Point at 400 cfm/ton, All Coils.....	3-22
Figure 3-22. Variation of Retained Moisture with Dew Point at 300 cfm/ton, All Coils.....	3-23

Figure 3-23. Variation of Retained Moisture with Air Flow at Nominal Entering Air Conditions of 80°F dry bulb, 60.4°F dew point, Coil 1 .....	3-24
Figure 3-24. Variation of Retained Moisture with Air Flow at Nominal Entering Air Conditions of 80°F dry bulb, 60.4°F dew point, All Coils.....	3-24
Figure 3-25. Variation of Wet-Dry Pressure Drop with Entering Conditions and Air Flow Rate for Coil 1 .....	3-25
Figure 3-26. Trend of Wet-Dry Pressure Drop with Flow at Nominal Entering Conditions of 80°F, 60.4°F dew point for Coil 1 .....	3-26
Figure 3-27. Trend of Various Parameters with Saturated Suction Temperature for Coil 1 ....	3-27
Figure 3-28. Trend of Steady-State Sensible Heat Ratio with Coil Temperature for All Coils	3-28
Figure 3-29. Trend of Steady-State Latent Capacity with Coil Temperature for All Coils.....	3-28
Figure 3-30. Variation in Moisture Retention with Coil Temperature, All Coils.....	3-29
Figure 3-31. Variation of Wet-Dry Pressure Drop with Moisture Retention, All Coils.....	3-29
Figure 3-32. Normalized Wet-Dry Pressure Drop with Normalized Moisture Mass, All Coils .....	3-30
Figure 3-33. Off-Cycle Sensible Capacity for Runs 16 and 25: Coils 1-4 .....	3-31
Figure 3-34. Off-Cycle Sensible Capacity for Runs 16 and 25: Coils 5-8 .....	3-32
Figure 3-35. Comparing Measured Latent Degradation to the LHR Models for Coil 1 .....	3-34
Figure 3-36. Measured AUTO Fan Latent Degradation for Coil 1 .....	3-34
Figure 3-37. Test Results for Coil 2 with NO Fan Overrun Delay (AUTO Fan).....	3-36
Figure 3-38. Test Results for Coil 2 with 1.5-minute Fan Overrun Delay .....	3-36
Figure 3-39. Test Results for Coil 8 with Drain-Down Cycle (5 minutes).....	3-37
Figure 3-40. Measured Latent Degradation for Coil 8 “Drain-Down Cycle” Tests.....	3-38
Figure 3-41. Comparing Condensate Removal Rates with Various Drain-Down Delay Times (0.5 Coil Runtime Fraction).....	3-39
Figure 3-42. Comparing Condensate Removal Rates with Various Drain-Down Delay Times (0.688 Coil Runtime Fraction).....	3-40
Figure 3-43. Change in Steady-State Coil Performance for Initial Tests with Coil 2 .....	3-41
Figure 3-44. Change in Moisture Retention for Initial Tests with Coil 2.....	3-42
Figure 3-45. Change in Moisture Retention for Initial Tests with Coil 4.....	3-43
Figure 3-46. Change in Moisture Retention for Initial Tests with Coil 5.....	3-44
Figure 3-47. Change in Moisture Retention for Initial Tests with Coil 8.....	3-44
Figure 4-1. Residential Air Handler (Site 1, 2 <sup>nd</sup> Floor Unit) .....	4-3
Figure 4-2. Commercial Air Handler (Site 7).....	4-3
Figure 4-3. Schematic of Sensor Locations for DX Systems .....	4-5
Figure 4-4. Schematic of Sensor Locations for Chilled Water Systems.....	4-5
Figure 4-5. Comparison of Latent Capacity Calculated From Psychrometric State Points and Condensate Removal Rates, Site 1 .....	4-9
Figure 4-6. Monitoring Condensate Delay Time at Site 1 .....	4-10
Figure 4-7. Impact of Dew Point on Condensate Delay Time for Site 2 at First Stage.....	4-11
Figure 4-8. Impact of Dew Point Temperature on Condensate Delay Time for Site 4 .....	4-11
Figure 4-9. Trend of Sensible Capacity for Several “Wetted” Off Cycles, Site 1.....	4-13
Figure 4-10. Variation of Peak Off-Cycle Evaporation Rate with Wet-Bulb Depression, Site 1 .....	4-13
Figure 4-11. Trend of Sensible Capacity for Several “Wetted” Off Cycles, Site 2.....	4-14
Figure 4-12. Thermostat Cycling Curve for 2nd Floor AC Unit at Site 1 .....	4-17

Figure 4-13. Thermostat Cycling Curve for 1st Floor AC Unit at Site 1 .....	4-17
Figure 4-14. Thermostat Cycling for 2 <sup>nd</sup> Stage Compressor Operation at Site 4 .....	4-18
Figure 4-15. Measured Latent Degradation for 1 <sup>st</sup> Floor AC Unit at Site 1 .....	4-19
Figure 4-16. Measured Latent Degradation for Site 4 (DB: 70-75°F, RH: 45-55%) .....	4-20
Figure 4-17. Measured Latent Degradation for Site 2 (RH: 50-55%) .....	4-21
Figure 4-18. Daily Humidity Ratios for AUTO vs Constant Fan Modes at Site 1 .....	4-22
Figure 4-19. Daily Humidity Ratios for AUTO vs Constant Fan Modes at Site 2 .....	4-23
Figure 4-20. Daily Humidity Ratios for AUTO vs Constant Fan Modes at Site 3 .....	4-23
Figure 4-21. Enhanced Fan Mode for Stage 1 Cooling at Site 2 .....	4-25
Figure 4-22. Enhanced Fan Mode for Stage 2 Cooling at Site 2 .....	4-25
Figure 4-23. Impact of Control Modes on Indoor Humidity at Site 2: Enhanced vs. AUTO... 4-26	4-26
Figure 4-24. Impacts of Control Modes on Indoor Humidity: Single Stage vs. Two Stage.... 4-26	4-26
Figure 4-25. Details of a 2 <sup>nd</sup> Stage Cycle for Site 2 (Enhanced Mode)..... 4-27	4-27
Figure 5-1. Graphical Representation of LHR Model Parameters .....	5-2
Figure 5-2. Three Possible Modes of Off-Cycle Moisture Evaporation..... 5-3	5-3
Figure 5-3. Off-Cycle Moisture Evaporation Rate for Various Conditions .....	5-8
Figure 5-4. Moisture Mass Remaining on the Coil for Various Conditions..... 5-8	5-8
Figure 5-5. Comparing Measured and Modeled Evaporation Rates: Coil 1, 400 cfm/ton .....	5-10
Figure 5-6. Comparing Measured and Modeled Evaporation Rates: Coil 1, 300 cfm/ton .....	5-10
Figure 5-7. Comparing Measured and Modeled Evaporation Rates: Coil 1, 200 cfm/ton .....	5-11
Figure 5-8. Comparing Measured and Modeled Evaporation Rates: Coil 2, 400 cfm/ton .....	5-11
Figure 5-9. Comparing Measured and Modeled Evaporation Rates: Coil 2, 300 cfm/ton .....	5-12
Figure 5-10. Comparing Measured and Modeled Evaporation Rates: Coil 2, 200 cfm/ton .....	5-12
Figure 5-11. Comparing Measured and Modeled Evaporation Rates: Coil 3, 400 cfm/ton .....	5-13
Figure 5-12. Comparing Measured and Modeled Evaporation Rates: Coil 3, 300 cfm/ton .....	5-13
Figure 5-13. Comparing Measured and Modeled Evaporation Rates: Coil 3, 200 cfm/ton .....	5-14
Figure 5-14. Comparing Measured and Modeled Evaporation Rates: Coil 4, 400 cfm/ton .....	5-14
Figure 5-15. Comparing Measured and Modeled Evaporation Rates: Coil 4, 300 cfm/ton .....	5-15
Figure 5-16. Comparing Measured and Modeled Evaporation Rates: Coil 4, 200 cfm/ton .....	5-15
Figure 5-17. Comparing Measured and Modeled Evaporation Rates: Coil 5, 400 cfm/ton .....	5-16
Figure 5-18. Comparing Measured and Modeled Evaporation Rates: Coil 5, 300 cfm/ton .....	5-16
Figure 5-19. Comparing Measured and Modeled Evaporation Rates: Coil 5, 200 cfm/ton .....	5-17
Figure 5-20. Comparing Measured and Modeled Evaporation Rates: Coil 6, 400 cfm/ton .....	5-17
Figure 5-21. Comparing Measured and Modeled Evaporation Rates: Coil 6, 300 cfm/ton .....	5-18
Figure 5-22. Comparing Measured and Modeled Evaporation Rates: Coil 6, 200 cfm/ton .....	5-18
Figure 5-23. Comparing Measured and Modeled Evaporation Rates: Coil 7, 400 cfm/ton .....	5-19
Figure 5-24. Comparing Measured and Modeled Evaporation Rates: Coil 7, 300 cfm/ton .....	5-19
Figure 5-25. Comparing Measured and Modeled Evaporation Rates: Coil 7, 200 cfm/ton .....	5-20
Figure 5-26. Comparing Measured and Modeled Evaporation Rates: Coil 8, 400 cfm/ton .....	5-20
Figure 5-27. Comparing Measured and Modeled Evaporation Rates: Coil 8, 300 cfm/ton .....	5-21
Figure 5-28. Comparing Measured and Modeled Evaporation Rates: Coil 8, 200 cfm/ton .....	5-21
Figure 5-29. Example of a Quasi-Steady ON/OFF Cycle .....	5-22
Figure 5-30. Comparing the New and Original LHR Models .....	5-24
Figure 5-31. Moisture Balance Concept with Two Off-Cycle Intervals .....	5-27
Figure 5-32. Impact of a Brief Fan Shutdown: 2, 4, 6, 8 and 10 minutes..... 5-28	5-28
Figure 5-33. Predicting Latent Degradation for Lower Off-Cycle Airflow Rates .....	5-29

Figure 5-34. Predicting Latent Degradation for a Brief Period of Low Off-Cycle Airflow.....	5-30
Figure 5-35. Predicting Latent Degradation with Fan Overrun Delay .....	5-31
Figure 5-36. Predicting Latent Degradation with a Fan Overrun Delay and Reduced Off-Cycle Airflow.....	5-32
Figure 5-37. Comparing LHR Model to Lab Data: Coils 1-4, 80°F db, 60°F dp.....	5-34
Figure 5-38. Comparing LHR Model to Lab Data: Coils 5-8, 80°F db, 60°F dp.....	5-35
Figure 5-39. Comparing LHR Model to Lab Data: Coils 2-4, 75°F db, 64°F dp.....	5-36
Figure 5-40. Comparing LHR Model to Lab Data: Coils 5-8, 75°F db, 64°F dp.....	5-37
Figure 5-41. Comparing LHR Model to Lab Data: Coils 2-4, 75°F db, 56°F dp.....	5-38
Figure 5-42. Comparing LHR Model to Lab Data: Coils 5-8, 75°F db, 56°F dp.....	5-39
Figure 5-43. Comparing LHR Model to Lab Data: Coils 2-4, 300 cfm/ton .....	5-40
Figure 5-44. Comparing LHR Model to Lab Data: Coils 5-8, 300 cfm/ton .....	5-41
Figure 5-45. Measured LHR Degradation: Coils 1-4, AUTO Fan at Nominal Conditions.....	5-42
Figure 5-46. Measured LHR Degradation: Coils 5-8, AUTO Fan at Nominal Conditions.....	5-43
Figure 5-47. Comparing LHR Model to Lab Data: Coil 8, AUTO Fan .....	5-44
Figure 5-48. Comparing LHR Model to Lab Data: Coil 8, “Drain-Down Delays”.....	5-45
Figure 5-49. Variation of Coil Retained Moisture Mass with Airflow.....	5-46
Figure 5-50. Impact of Compressor Loading on Cooling Coil Process Line .....	5-48
Figure 5-51. Variation of SHR with Compressor Loading for a Modulated Coil .....	5-49
Figure 5-52. Cooling Coil Circuiting Options .....	5-50
Figure 5-53. Trends of Measured SHR with Chilled Water Flow, Coil 8.....	5-55
Figure 5-54. Trends of SHR with Chilled Water Flow from CCDET.....	5-55
Figure 5-55. Trends of Measured Capacity with Chilled Water Flow, Coil 8.....	5-56
Figure 5-56. Trends of Capacity with Chilled Water Flow from CCDET .....	5-56
Figure 5-57. Trends of Measured SHR with Cooling Capacity, Coil 8.....	5-57
Figure 5-58. Trends of SHR with Cooling Capacity from CCDET .....	5-57
Figure 6-1. Comparing Measured Coil Moisture Retention from Field and Laboratory Measurements .....	6-2
Figure 6-2. Comparing NTU K-Factor from Field and Laboratory Measurements .....	6-2

## List of Tables

Table 2-1. Impact of Fan Overrun on Actual Operating Efficiency .....	2-13
Table 2-2. Variations in Coil Geometry by Equipment Type.....	2-14
Table 2-3. Enhanced Fan Control Schemes for Improved Dehumidification .....	2-16
Table 3-1. Description of Lab-Tested Cooling Coils.....	3-2
Table 3-2. Data Points for Monitoring DX Cooling Coils.....	3-5
Table 3-3. Data Points for Monitoring the Chilled Water Cooling Coil .....	3-6
Table 3-4. Tipping Bucket Calibration Data.....	3-6
Table 3-5. Summary of Steady-State Test Conditions Corresponding to Each Run or Test.....	3-8
Table 3-6. Cyclic Test Conditions .....	3-9
Table 3-7. Comparing Measured Performance Parameters for the Lab-Tested Cooling Coils	3-14
Table 3-8. Change in Performance for Coil 2.....	3-41
Table 3-9. Change in Moisture Retention for All Coils.....	3-43
Table 4-1. Field Test Sites .....	4-2
Table 4-2. Field Site Coil Descriptions.....	4-2
Table 4-3. Data Points for Field Monitoring .....	4-4
Table 4-4. One-Time Measurements .....	4-6
Table 4-5. Indoor Coil Geometry for Unit 1 (Upstairs) at Field Site 1 .....	4-7
Table 4-6. Nameplate Data for Cooling System at Field Site 1.....	4-8
Table 4-7. Comparing Measured Performance Parameters for the Field-Tested Cooling Coils .....	4-15
Table 5-1. Normalized Model Inputs for 1996 LHR Model.....	5-1
Table 5-2. Average Parameters Used for Moisture Evaporation Model Inputs .....	5-9
Table 5-3. Model Parameters Used to Compare Original and New LHR Models .....	5-24
Table 5-4. Guidelines to Determine Parameters for the LHR Degradation Models.....	5-46
Table 5-5. Part-Load Performance for a “Face Split” Coil.....	5-51
Table 5-6. Part-Load Performance for a “Row Split” Coil.....	5-51
Table 5-7. Part-Load Performance for an “Intertwined” Coil .....	5-52
Table 5-8. Comparison of Dehumidification Performance for Different Coil Arrangements..	5-52

# 1 Introduction

Data from a limited number of field studies (Khattar et al. 1985; Henderson and Rengarajan 1996; Henderson 1998) have demonstrated that the moisture removal capacity of a cooling coil degrades at part-load conditions – especially when the supply fan operates continuously. Degradation occurs because moisture that condenses on the coil surfaces during the cooling cycle evaporates back into air stream when the coil is off (see Figure 1-1). As a result, a cooling coil that cycles on and off in response to a thermostat signal will have less net moisture removal as the system spends more time with the coil deactivated.

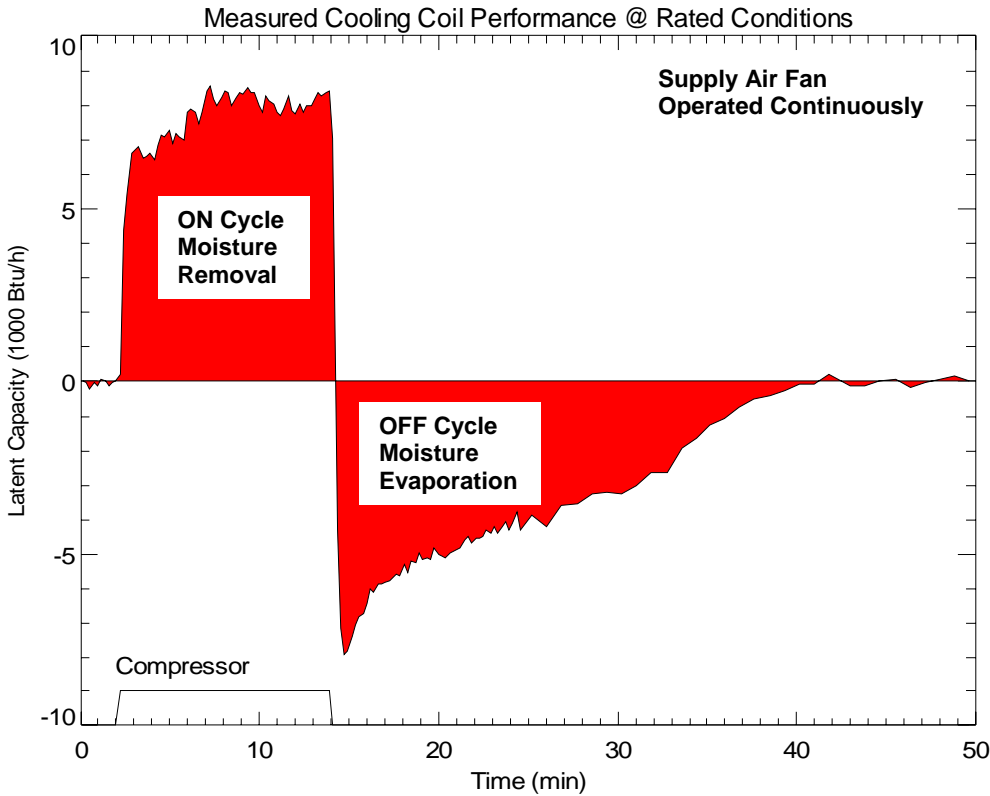


**Figure 1-1. On-Cycle Condensation and Off-Cycle Evaporation of Moisture from a Cooling Coil (Henderson 1990)**

Understanding the moisture-removal performance of cooling equipment over the range of expected operating conditions is critical to predicting the indoor humidity levels that result when meeting cooling and dehumidification loads in real building applications. While most systems can maintain adequate humidity levels at full load or design conditions if sized properly, indoor humidity can often drift above the generally accepted limit of 60% RH at part load. Most current analysis tools and building simulation models do not account for these part-load effects. Therefore, equipment manufacturers and HVAC system designers do not have the tools they need to evaluate the impacts of their design choices.

The objective of this project was to better understand and quantify the moisture removal (dehumidification) performance of cooling coils at part-load conditions. The project addressed the following specific issues:

- Moisture retention characteristics of modern cooling coils
- Moisture evaporation rate from deactivated cooling coils
  - constant and variable air volume applications
  - single-speed and multiple-speed compressors
- Impacts of coil geometry and operating conditions on moisture retention and evaporation
- The role that building and air conditioner controls play in latent cooling capacity degradation
- Resulting moisture removal capacity of systems at part-load conditions and the impact this part-load performance has on space humidity levels

This project included four major tasks: 1) Literature review, 2) Detailed cooling coil measurements in the laboratory, 3) Field measurements of coil dehumidification performance and resulting indoor humidity levels, and 4) Development and validation of methods to predict latent part-load degradation. The end product is an improved mathematical model to account for latent part-load degradation which can help design professionals more confidently predict the energy consumption, indoor humidity impacts, and life-cycle costs of their design choices.

A comprehensive review of the open literature was completed at the beginning of the project. This included locating and analyzing existing data sets to quantify the amount of moisture removal degradation at part-load conditions. Information was also sought regarding measurements of cooling coil transient moisture removal at startup, models for transient mass and heat transfer by cooling coils, and modeling or experimental studies of moisture retention on cooling coils. Furthermore, information was sought regarding transient evaporation studies or models that considered a declining amount of moisture on a surface. Major findings from the literature review are summarized in Section 2 of this report.

Detailed measurements of coil performance were also collected in a controlled laboratory setting to understand the impact of coil geometry and operating conditions on transient moisture condensation and evaporation by the coil. A total of eight coils were tested: seven direct expansion coils and one chilled water coil. More than forty (40) steady-state and cycling tests were performed on each coil. A description of the coils, test facility and experimental setup, tests performed on each coil, and the test results are summarized in Section 3.

Another task involved collecting field measurements of cooling coil dehumidification performance and space humidity conditions. Seven field test sites were recruited to participate in this project and a total of eight cooling coils were monitored. Cooling coil types included residential and commercial direct expansion (DX) systems, and commercial chilled water coils. The residential systems included single-stage constant air volume systems, as well as single-stage and two-stage systems with a variable-speed supply air fan. The commercial DX system was a typical two-stage rooftop packaged unit, and the chilled water coils included one constant-air-volume system and one variable-air-volume system. Section 4 of this report describes the test sites, instrumentation, and analysis and discussion of the measured data.



The field and laboratory data were used to refine and validate a mathematical model that can be used to predict the degradation in cooling coil dehumidification performance for a wide range of operating conditions. The model is suitable for use in computerized calculation procedures such as hourly building energy simulation models (e.g., DOE's EnergyPlus building energy simulation program, <http://www.energyplus.gov>). Model development and validation with laboratory test data collected as part of this project are presented in Section 5. Section 6 summarizes and compares the field and laboratory test findings, and provides guidance on best practices for equipment manufacturers and design professionals. Section 7 provides conclusions and recommendations for further work.

## 2 Literature Review

A comprehensive review of the open literature was completed at the beginning of this project. The primary focus was to collect information on the following relevant topics:

- Measurements of cooling coil transient moisture removal at startup
- Models for transient mass and heat transfer by cooling coils
- Modeling and experimental studies of moisture retention on cooling coils
- Transient evaporation studies or models that consider a declining amount of moisture on a surface

More than forty technical papers, research reports, journal articles, and standards were collected as part of this effort. Pertinent information obtained from these documents is summarized below in Section 2.1.

In addition to the review of existing technical literature, existing sets of field measurements were located and analyzed in hopes of quantifying the amount of moisture removal degradation at part-load conditions for these sites. The data were also analyzed to determine if the amount of moisture retention on the cooling coils could be estimated. A summary of the analysis results is provided in Section 2.2.

Another aspect of this task was to investigate the impacts of fan overrun on the test and rating procedure for determining seasonal energy efficiency ratio (SEER) (Federal Register 2005, ARI 2005). The appropriate ARI test standard procedures were analyzed along with reports from previous studies. Laboratory tests on a single coil were performed as part of this project to provide additional information, and the results of this investigation are summarized in Section 2.3.

Finally, manufacturer's product information was reviewed to support the laboratory and field testing tasks associated with this project. Specifically, manufacturer's product data were collected and analyzed to provide guidance for selecting the direct expansion cooling coils to be tested in the laboratory as part of this project. Manufacturer's data were also collected to understand the operation of currently-available residential products with variable-speed air handlers for improved dehumidification performance, and to assist with selecting equipment to be monitored at two of the field test sites. The results of the manufacturer's data review are provided in Section 2.4 below.

### **2.1 Summary of Technical Documents**

A comprehensive review of the open literature was completed at the beginning of the project. Information was sought regarding moisture removal during cooling coil startup, models for transient mass and heat transfer by cooling coils, and modeling or experimental studies of moisture retention on cooling coils. Furthermore, information was sought regarding transient evaporation studies or models that considered a declining amount of moisture on a surface.

A total of 46 technical papers, research reports, journal articles, and standards were collected as part of this effort. A complete listing of the collected documents is provided in Appendix A. While these documents pertained to the topics of interest in a general sense, only a few provided information that was directly applicable to this project. The following sections describe the applicable information and its implications for the project.

### **2.1.1 Transient Moisture Removal by Cooling Coils at Startup**

Katipamula and O'Neal (1991) performed a literature review and laboratory tests related to the transient dehumidification performance of residential direct-expansion heat pumps when operating in cooling mode. A summary of their work is provided in Appendix B. The project focused on quantifying part-load performance losses for the case when the cooling coil and supply air fan cycle on and off in tandem (AUTO fan mode). For buildings located in hot and humid climates, the authors note that the dehumidification capabilities of a heat pump are important in achieving and maintaining comfort in the conditioned space. They also note that since heat pumps operate at a part-load condition for many hours of the year, understanding their dehumidification response is essential to quantifying both comfort and efficiency.

The authors drew a number of conclusions from the literature that they reviewed:

1. The performance losses due to transient effects can be as much as 20 percent.
2. It takes 6-15 minutes to achieve steady state performance after compressor start-up.
3. The transient response is affected by the number of on-off cycles and percent compressor on-time during each on-off cycle.
4. The mass of the heat exchangers (indoor and outdoor coils) affects transient losses.
5. The off-cycle migration of refrigerant from the condenser to the evaporator causes significant losses in capacity.
6. The relationship between cooling load factor (CLF) and part-load factor (PLF) is nonlinear.
7. Compressor power is relatively unaffected due to part-load operation.
8. The transient performance is independent of outdoor temperature.

The authors noted that much of the research on heat pump transient losses had been confined to the heating mode of operation. For the cooling mode, the research had focused on quantifying the effects of heat exchanger mass, the impact of off-cycle refrigerant migration on transient sensible capacity, and the effects of cycling (percent on-time and cycling rate) on cooling performance. The authors indicated that transient dehumidification performance had not been addressed thus far. Therefore, they completed a series of laboratory tests to characterize the transient dehumidification response of a nominal 3-ton (10.5 kW) air-to-air heat pump by varying percent on-time, thermostat cycling rate, indoor dry-bulb temperature and indoor humidity while keeping outdoor dry-bulb temperature and air flow rates constant. As mentioned previously, all tests were performed with the compressor and supply air fan cycling on and off in tandem (AUTO fan mode).

The test results highlighted several trends, including:

1. For nearly all tests, moisture was added to the supply air stream immediately after compressor start-up, and dehumidification of the air began after 60 to 150 seconds of compressor operation depending on the entering air conditions.
2. The heat pump's latent cooling (dehumidification) capacity took 3 to 15 minutes to reach steady state after compressor startup. The time required for latent capacity to reach steady state increased as the number of on/off cycles per hour increased, and the time to reach steady state also increased as inlet air humidity levels decreased (at a constant inlet air temperature).
3. The loss in latent capacity was greater than the loss in sensible capacity as the compressor runtime was decreased and as the number of on/off cycles per hour increased. So oversized equipment, which is commonly installed, will cycle on/off more often which will negatively impact dehumidification performance.

Finally, the authors developed a relationship for normalized sensible and latent cooling capacity as a function of percent compressor on-time and inlet air relative humidity. While the form of the correlation was consistent with previous models, the authors note that the model coefficients will vary from system to system. The resulting "effective" sensible heat ratio (sensible capacity divided by sensible plus latent capacity) based on their correlation evaluated at 50% RH inlet air conditions is shown in Figure 2-1 below. The difference between the SHR calculated by the normalized capacity correlations and the measured steady-state SHR is due to the correlation coefficients being the best fit of the measured data (i.e., the normalized correlations do not evaluate to exactly 1.0 for 50% RH with percent on-time of 1.0).

The results in Figure 2-1 are similar to those found by Khattar et al. (1987) through field measurements. Khattar also showed a modest amount of degradation in dehumidification performance (i.e., increase in sensible heat ratio) with lower compressor runtime fractions when the supply air fan cycles on/off with the compressor. Khattar went on to show that the amount of latent degradation is substantially greater when the supply air fan operates continuously while the compressor cycles on/off to meet the thermostat set point temperature. See Section 2.1.3 for further discussion of the Khattar study.

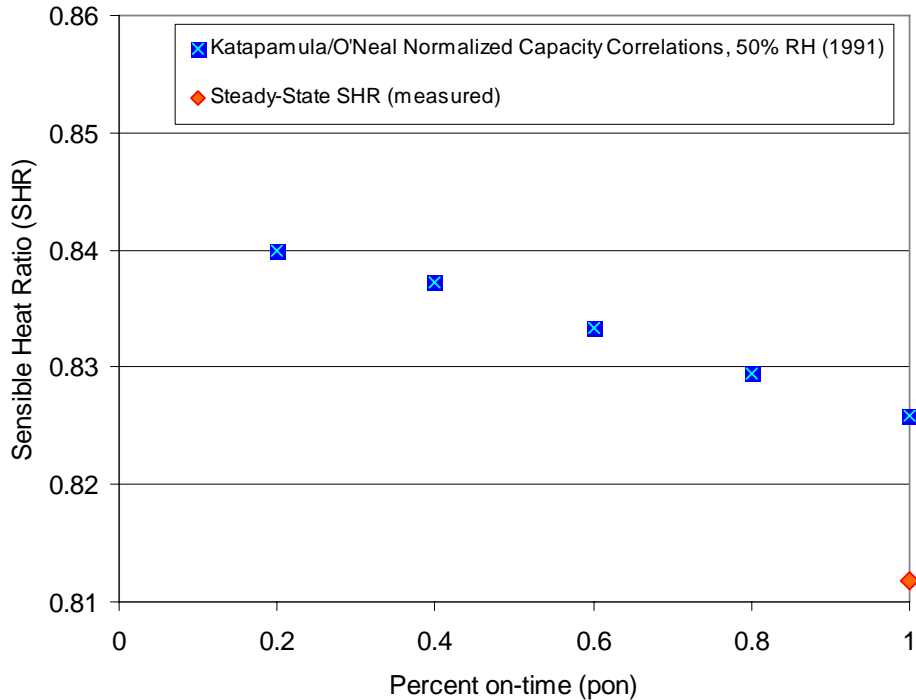


**Figure 2-1. Effective Sensible Heat Ratio Versus Compressor Percent On-time**

### 2.1.2 Modeling and Experimental Studies of Moisture Retention on Cooling Coils

Jacobi et al. completed a series of laboratory studies measuring moisture retention on cooling coils (Korte and Jacobi 1997, Yin and Jacobi 2000, Kim and Jacobi 2000). A summary of their results is presented here, with additional details provided in Appendix C.

The researchers developed experimental techniques to dynamically measure condensate accumulation on cooling coil surfaces. Initial experiments used a load cell for these measurements. However, later experiments used a calibrated balance to directly weigh the coil during each test.

A wide range of heat exchanger geometries was evaluated, including variations in fin spacing, fin type (plain, wavy, slit), and number of coil tube rows in the direction of air flow. The impacts of coil coatings (corrosion resistant and hydrophilic) were also investigated. The tests were performed at relatively hot and humid enter air conditions of 95°F (35°C) dry-bulb temperature and 75°F (23.9°C) dew point temperature. A glycol-water mixture was circulated through the coil tubes, with the coil inlet fluid temperature maintained between 32-38°F (0-3.3°C) which assured the air-side coil surfaces were fully wetted. These studies did not look at other entering air/fluid conditions since they were primarily focused on coil geometry and surface issues.

Figure 2-2 shows moisture retention on the cooling coil as a function of time for three plain fin-and-tube heat exchangers with different fin spacing. In all cases moisture retention on the air-side coil surfaces grows steadily after cold fluid begins flowing through the heat exchanger tubes, with the maximum amount of moisture retention increasing with greater fin densities. For

the case of 12 fins per inch (2.12 mm fin spacing), the measurements detected an “overshoot” of moisture retention. This implies that a certain amount of moisture builds up before it begins shedding off the coil. Moisture retention on the coil eventually settles out to a slightly lower steady-state value. This moisture “overshoot” was not observed for the closer fin densities that were tested (i.e., 16 fpi and 20 fpi). Coils with wavy and louvered fins were tested over the same range of fin spacing but did not exhibit this “overshoot” effect.

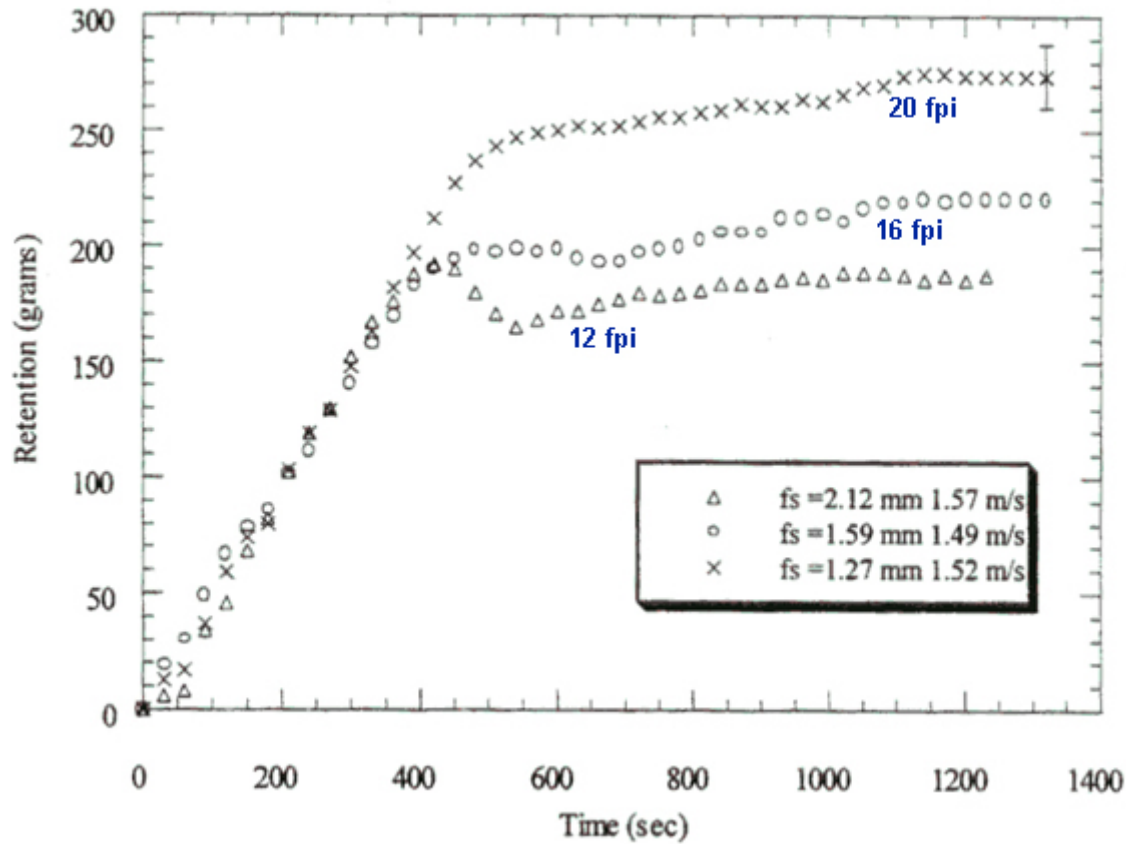


**Figure 2-2. Real-time Moisture Retention for Plain Fin-and-tube Heat Exchangers (Yin and Jacobi 2000)**

The studies also showed that hydrophilic coil coatings significantly reduce moisture retention (Figure 2-3). These coatings increase surface wettability and reduce the thickness of condensed moisture droplets. Not only can the coatings decrease moisture retention but they can also significantly reduce the air-side pressure drop leading to reduced fan power requirements. The wettability of hydrophilic coatings tends to degrade over time, however, and research on improving their long-term performance continues (Hong and Webb 2001, Yamazaki et al. 2000).

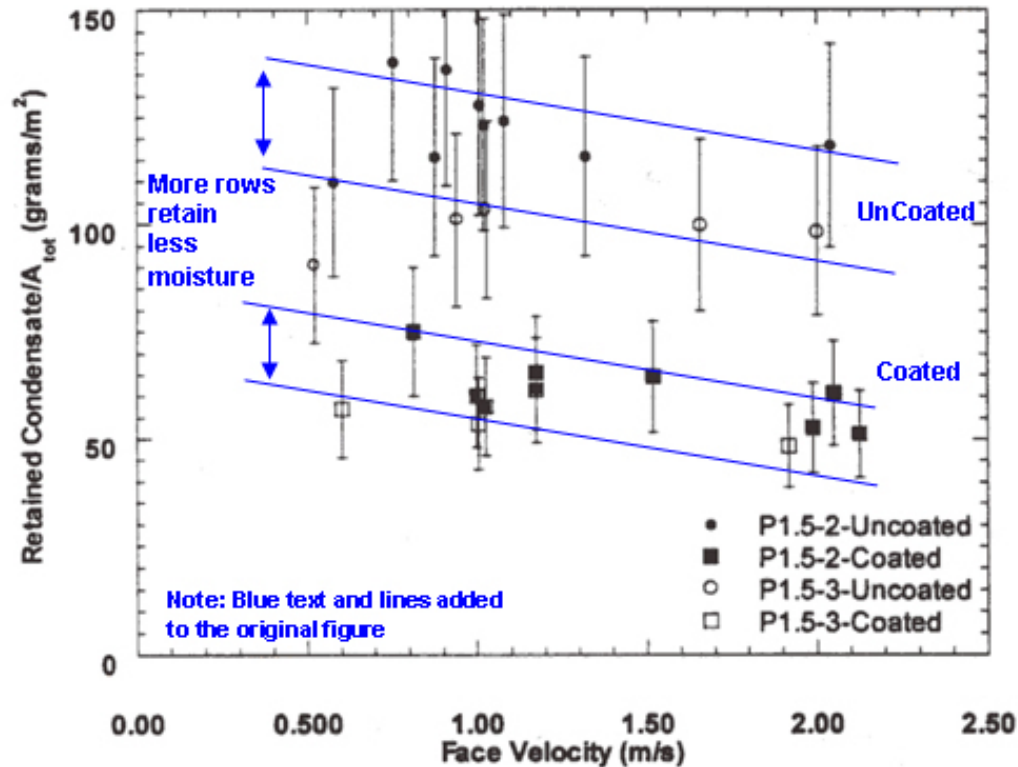


**Figure 2-3. Moisture Retention Impacts of Hydrophilic Coatings (Kim and Jacobi 2000)**

The authors presented most of their results in terms of mass of retained moisture (maximum at steady-state conditions) per unit area of air-side coil surface (i.e., grams/m<sup>2</sup>, or lb/ft<sup>2</sup>). The test results indicate the following:

1. With a coil face velocity of 2 m/sec (394 ft/min), which is typical for commercial and residential air conditioners, moisture retention varied from approximately 70-120 grams/m<sup>2</sup> (0.014-0.025 lb/ft<sup>2</sup>) depending on number of coil rows, fin type, fin spacing and coil coating (if any).
2. Fin enhancements (i.e., wavy or slit versus plain) increase moisture retention, on the order of 10-20 grams/m<sup>2</sup> (0.002-0.004 lb/ft<sup>2</sup>) for the coils that were tested.
3. Moisture retention increases as fin density increases (i.e., fin spacing decreases).
4. While total moisture retention increases with the number of coil tube rows, moisture retention per unit of surface area decreases slightly. This is due to air velocity-driven sweeping of the moisture. Deeper coils with more tube rows have longer fin lengths, allowing more time for moisture droplets to reach their maximum size which causes them to be shed from the coil.
5. Surface coatings decrease moisture retention.
6. Moisture retention tends to decrease slightly or remain constant with increasing air flow.

### 2.1.3 Field Measurements of Latent Capacity Degradation at Part-Load Conditions

Of the literature review documents located as part of this project, field testing performed by Khattar et al. in 1983 was the earliest effort to begin quantifying the latent capacity degradation of direct expansion (DX) cooling equipment under part-load conditions (Khattar et al. 1985, Khattar et al. 1987). Like Katipamula and O'Neal, Khattar observed that latent capacity took longer to reach steady state after compressor startup than sensible capacity (Figure 2-4). In addition, a series of tests were performed on a small packaged air conditioner (29,600 Btu/h, 8.67 kW) to determine the impact of supply air fan operation mode on dehumidification performance. The fan was operated in the AUTO mode (fan cycles on/off with compressor) and ON mode (fan runs continuously while compressor cycles on/off to meet thermostat set point temperature). The test results, shown in Figure 2-5, were expressed in terms of moisture removal per unit of electricity consumed. These results show a modest degradation in moisture removal capacity with fan AUTO mode (similar to Katipamula and O'Neal), with a much greater degradation for fan ON mode. One item to note, however, is that the test points shown in Figure 2-5 were collect at different entering air relative humidity conditions. Adjusting for differences in inlet air humidity would change the results somewhat, but not the overall trend (see Appendix D).

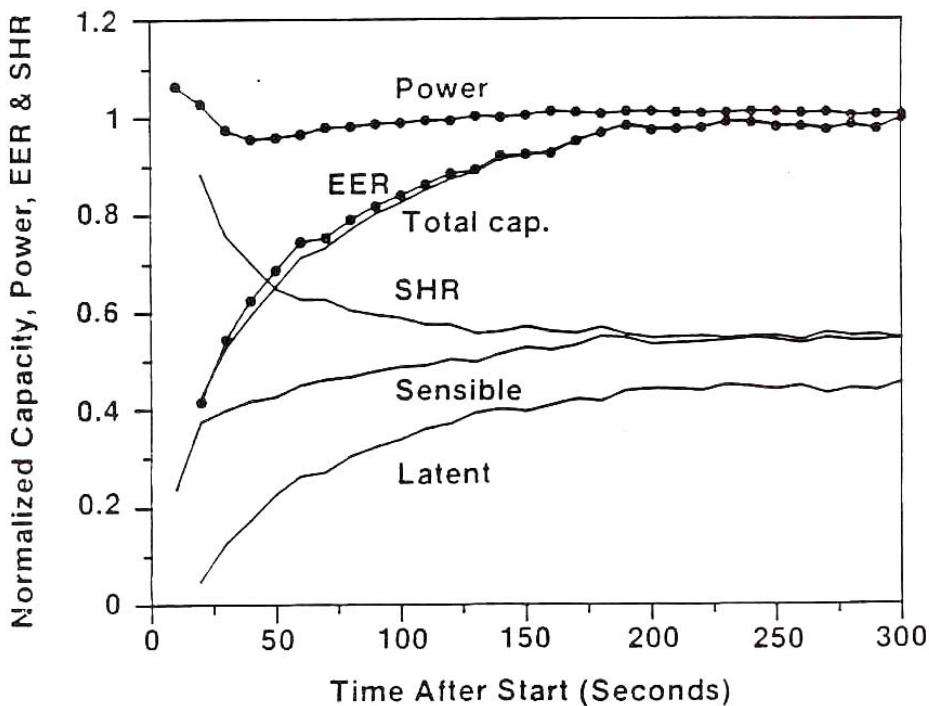
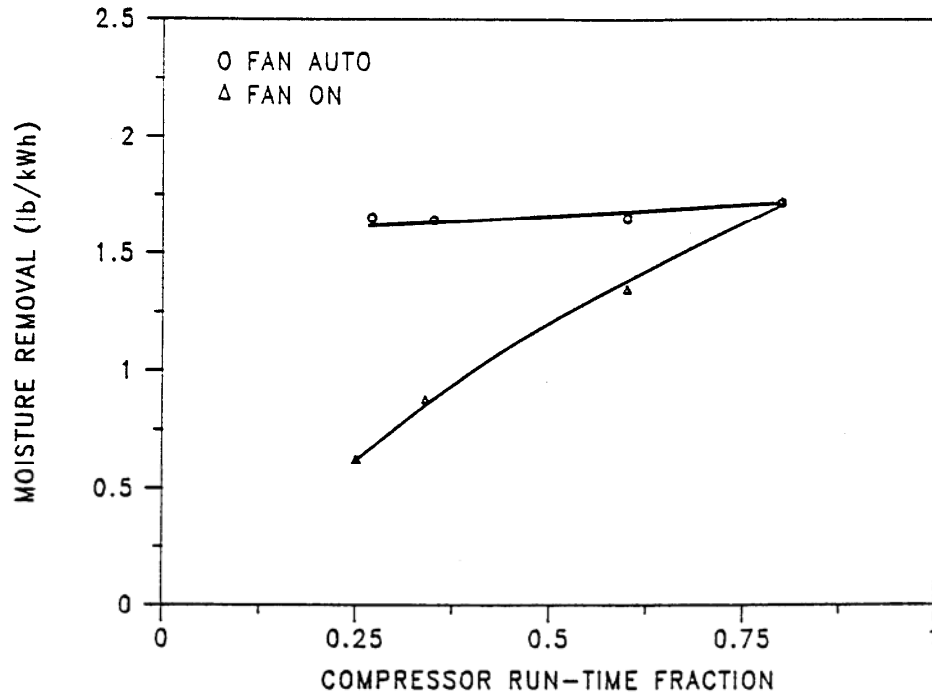


Figure 2-4. Air-conditioner Transient Performance During Start-up





**Figure 2-5. Moisture Removal Versus Air-conditioner Compressor Run-time Fraction**

One of the major objectives of the literature review was to collect information that would be useful for developing and validating models and approaches to quantify latent capacity degradation at part-load conditions. A first-generation model was previously developed by Henderson and Rengarajan (1996) to predict latent capacity degradation with continuous supply air fan operation. Model inputs include the amount of moisture retained by the coil under normal operation (i.e., fully wetted) and the initial rate of moisture evaporation from the cooling coil when the compressor turns off. Appendix D summarizes the efforts to extract these model inputs from the Khattar field study, primarily using Figure 2-6. For the cooling coil that was tested, the amount of moisture retained on the coil was estimated at 0.63 lb (0.29 kg), or about 0.26 lb per ton of total cooling capacity (0.033 kg/kW).

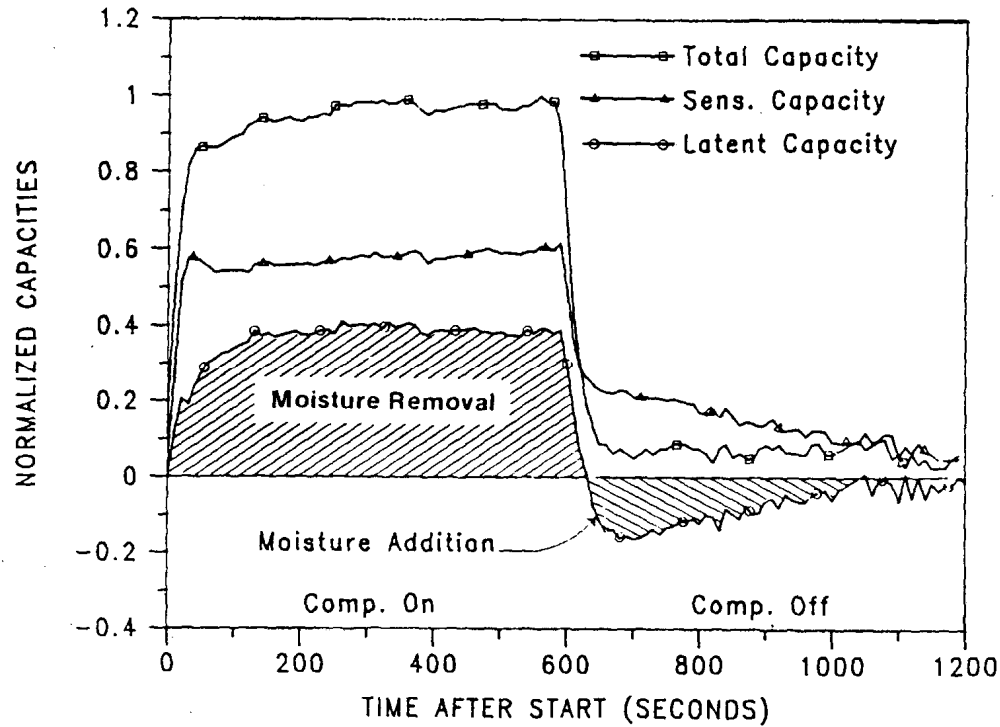


**Figure 2-6. Moisture Removal and Addition Under Fan ON Operating Mode**

Henderson (1998) also collected field test data on the part-load dehumidification performance of a 3-ton (10.5 kW) water-to-air heat pump with fan ON mode. The collected information was used to validate the Henderson and Rengarajan first-generation mathematical model for latent degradation. Figure 2-7 compares the measured trend in sensible heat ratio with the results of the latent degradation model. Based on field measurements, the amount of moisture retained on the cooling coil was estimated at 2.1 lb (0.95 kg), or about 0.7 lb per ton of total cooling capacity (0.09 kg/kW). This amount of retained moisture was noticeably higher than the retained moisture for the Khattar field test unit.

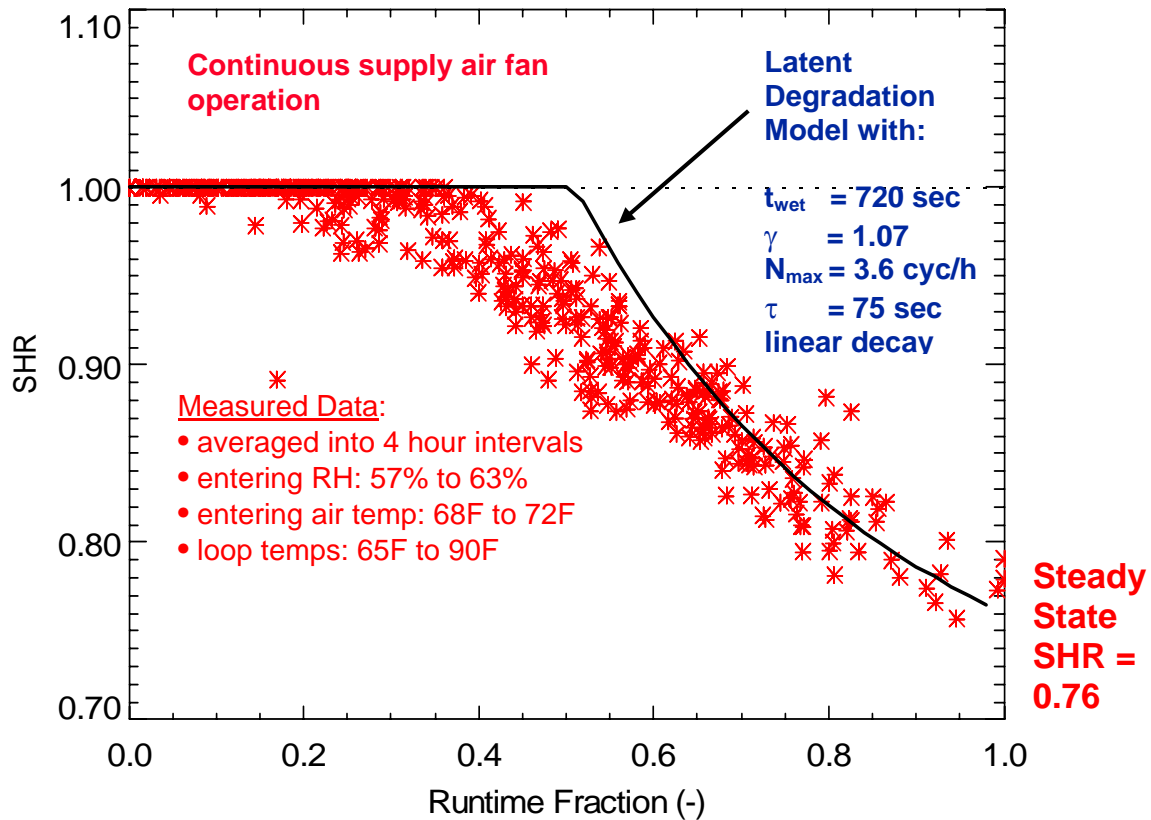


**Figure 2-7. Comparison of Measured SHR with First-generation Latent Degradation Model**

#### 2.1.4 Transient Moisture Evaporation from a Wetted Surface

When a wet cooling coil is deactivated while the supply air fan continues to operate, the retained moisture on the coil begins to evaporate into the air stream. One aspect of the literature review was to try to locate information related to transient evaporation studies or models that considered a declining amount of moisture on a surface. Unfortunately, information on this specific subject was not found. However, studies on evaporative cooling were located and they proved to be useful for this project.

The original latent degradation model developed by Henderson and Rengarajan (1996) considered linear decay, exponential decay, and constant moisture evaporation rates. Laboratory measurements (Henderson 1990) had indicated that a linear or exponential decay of moisture evaporation rate over time was more appropriate. However, the choice of moisture evaporation profile was not based on engineering equations for the process of interest.

In many ways, the process of moisture evaporation from a wet cooling coil after the coil is turned off is analogous to a direct evaporative cooler. The exception is the amount of moisture on the

wet cooling coil decreases over time as air flow continues over the coil, as opposed to a direct evaporative cooler where the moisture on the media is replenished to maintain the desired cooling effect.

Stabat et al. (2001) reviewed both principal and simulation models for indirect and direct evaporative cooling systems. Their goal was to identify a simplified pre-design tool to evaluate the feasibility of evaporative cooling systems, and a more detailed design tool to estimate annual water and energy consumption. As part of their review of existing models, the authors derived an equation for the “saturation effectiveness” of a direct evaporative cooler:

$$\eta \cong 1 - e^{-NTU}$$

where:

$$\eta = \text{saturation effectiveness} = \frac{T_{o,db} - T_{i,db}}{T_{i,wb} - T_{i,db}} = \frac{\omega_{o,db} - \omega_{i,db}}{\omega_{i,wb} - \omega_{i,db}}$$

$$NTU = \frac{\beta'}{\dot{m}_a} = \text{Number of transfer units}$$

$T_{o,db}$  = Outlet air dry-bulb temperature

$T_{i,db}$  = Inlet air dry-bulb temperature

$T_{i,wb}$  = Inlet air wet-bulb temperature

$\omega_{o,db}$  = Outlet air humidity ratio

$\omega_{i,db}$  = Inlet air humidity ratio

$\omega_{i,wb}$  = Inlet air humidity ratio at saturated conditions based on  $T_{i,wb}$

$\dot{m}_a$  = air mass flow rate

$\beta'$  = constant

This equation, along with other assumptions, was used to develop a model for transient moisture evaporation from a cooling coil. The improved moisture evaporation model was subsequently integrated into the original latent capacity degradation model from Henderson and Rengarajan. See Section 5 of this report for more details regarding this model development effort.

## 2.2 Analysis of Existing Data Sets of Field Measurements

In addition to reviewing and summarizing technical documents, the literature review effort also involved locating and analyzing existing data sets of field measurements that may be relevant to this study. Specifically, the authors of this report had collected data at field test sites for other purposes, but it was anticipated that the type and quality of data collected would provide pertinent information. The existing data sets that were analyzed are summarized below:

1. Constant-air-volume chilled water cooling coil in a Florida commercial building
2. Residential water-to-air, direct expansion heat pumps at 12 North Carolina sites
3. Two commercial direct expansion packaged units in Texas

Details regarding the analysis of these data sets are provided in Appendix E. The goal was to quantify the amount of moisture removal degradation at part-load conditions for these sites. In addition, efforts were made to estimate moisture retention on the direct expansion cooling coils by measuring the delay time between compressor startup and the first measurement of condensate removal (“condensate delay time”) starting from a dry coil.

The analysis of residential heat pump data provided the most useful information. In fact, one of these twelve sites was used by Henderson (1998) to validate the original latent degradation model (Figure 2-7), so analysis primarily focused on the other 11 homes. Condensate delay times were computed for several of the test sites, and the trends in delay time with varying inlet air conditions were similar to those seen from the laboratory and field tests completed as part of this project. Graphs of “effective” sensible heat ratio as a function of runtime fraction were generated for two of the sites, and the degradation in dehumidification performance at reduced runtime fractions was similar to that shown in Figure 2-7.

### **2.3 Impacts of Fan Overrun on Seasonal Energy Efficiency Ratio**

One well-known aspect of the SEER test procedure is the potential to improve the SEER of the unit using fan overrun strategies. Because of the test procedure details, keeping the fan on for a short period after the compressor cycles off can increase the cyclic EER determined at dry coil conditions (Test D) and decrease the degradation coefficient ( $C_D$ ), thereby increasing the calculated SEER. The literature cited in this section universally implies that this type of fan delay would hurt the latent performance of the unit at part-load conditions.

To evaluate the impact of fan overrun, a direct expansion cooling coil (coil 2, see Section 3) was tested in accordance with the DOE test procedures that are given in Appendix C of ARI 210/240-2005 (ARI 2005). The focus was on Tests C and D, which operate the coil at “dry coil” conditions to determine the efficiency degradation at cyclic conditions<sup>1</sup>. Historically these tests have been completed at dry coil conditions to make the test more manageable and repeatable. Work at the National Institute of Standards and Technology (NIST) had shown that transient measurements of humidity (or wet bulb) were difficult and that a cyclic test at dry-coil conditions yielded the same result as at wet-coil conditions (Kelly and Parken 1978). The laboratory instrumentation available in this study made it possible to accurately measure transient performance at wet-coil conditions.

The details of the laboratory testing related to Test D of the SEER Test Procedure are given in Appendix F. As expected, adding a 90-second fan delay resulted in a slightly lower calculated value of  $C_D$  at dry-coil conditions (80°F [26.7°C] inlet air dry-bulb temperature, 58°F [14.4°C] inlet air wet-bulb temperature). The cyclic EER increases because the integration time for delivered capacity is also increased by 90 seconds. The additional 90 seconds of off-cycle sensible capacity appear to be provided by coil thermal mass as well as by evaporating the modest amounts of moisture that collected on the coil (some moisture likely formed even at these dry entering air conditions).

---

<sup>1</sup> The procedures for Tests C and D call for entering air with low enough moisture content so no condensate forms on the indoor coil (57°F [13.9°C] or lower wet-bulb temperature is recommended). The FSEC test facility was able to achieve 58°F [14.4°C] entering air wet-bulb temperature.

Analogous cyclic testing at wet-coil conditions demonstrated that there is no real gain in cyclic efficiency at actual operating conditions due to a 90-second fan overrun. A cyclic test similar to Test D, but at wet-coil conditions (80°F [26.7°C] inlet air dry-bulb, 60.4°F [15.8°C] inlet air dew point), indicated that the Gross EER of the system (not accounting for supply fan power and heat) changed by less than 1% with the fan delay. When the impact of the supply fan power and heat is accounted for, the fan delay actually decreased the Net EER by 4%. Table 2-1 summarizes the impact of a 90-second fan delay on gross and net efficiency for this test coil.

**Table 2-1. Impact of Fan Overrun on Actual Operating Efficiency**

	<b>Gross EER (Btu/Wh)</b>	<b>Net EER (Btu/Wh)</b>
Cycling (AUTO) Fan	11.15	9.47
90 sec Fan Overrun	11.09 (-1%)	9.10 (-4%)
Notes:	$\text{Gross EER} = \frac{(Q_{\text{sensible}} + Q_{\text{condensate}})}{\text{Unit Power}}$ $\text{Net EER} = \frac{(Q_{\text{sensible}} + Q_{\text{condensate}} - Q_{\text{fanheat}})}{(\text{Unit Power} + \text{Fan Power})}$	

Not only does the fan delay not result in an actual efficiency benefit, it also severely degrades the latent capacity of the unit (see Appendix F). At wet-coil conditions with 6 minutes of compressor on-time and 24 minutes off-time (i.e., 20% compressor runtime), the cyclic latent capacity provided by the unit (measured as condensate removal after 3 repetitions of the test) decreased by 44% with a 90-second fan delay after the compressor cycled off. So the fan delay, often added by manufacturers to slightly improve the calculated SEER, actually resulted in a small efficiency loss for the coil tested here (-4%) and significantly degraded the latent capacity of the unit (-44%) at 20% compressor runtime. In general, we speculate that the impacts of fan delay on efficiency for other coils will be small ( $\pm 5\%$ ) but the degradation in latent capacity will be significant (20% to 50%).

## **2.4 Review of Manufacturer’s Product Information**

Manufacturer’s product information was reviewed to understand the geometric details of cooling coils used in currently-available equipment. Characteristics for direct-expansion cooling coils were compiled for more than 500 residential and commercial air-conditioning products from four major U.S. equipment manufacturers. This information was analyzed to guide the selection of coils to be tested in the laboratory (see Section 3). The goal was to determine the range of common coil geometries and variations by equipment type.

The cooling coil information was analyzed in a number of different ways, with details provided in Appendix G. One portion of the analysis focused on cooling coils in both residential and commercial packaged equipment (as of 2002). Another part of the analysis considered information for all coils for which data were collected (packaged units, air handlers, and evaporator coils). Considering the information for all cooling coils, the typical evaporator coil is 3-rows deep and has just over 14 fins per inch. The evaporator face area for all coils averaged 1.23 ft<sup>2</sup> per nominal rated ton (0.033 m<sup>2</sup>/kW) and the total amount of evaporator surface area

averaged 103.6 ft<sup>2</sup>/ton (2.74 m<sup>2</sup>/kW). Coil geometry variations by equipment type are shown in Table 2-2.

**Table 2-2. Variations in Coil Geometry by Equipment Type**

	Evaporator Face Area (ft <sup>2</sup> /ton)	Evaporator Fin Surface Area (ft <sup>2</sup> /ton)	Evaporator Rows (-)	Evaporator Fin Spacing (fpi)
Residential Packaged	1.41	113.5	2.8	14.9
Commercial Packaged	1.15	101.3	3.1	14.6
All coils	1.23	103.6	3.0	14.3

Note: Fin surface area is gross fin area: coil face area (ft<sup>2</sup>) x coil depth (in) x fin spacing (fpi) x 2

Figure 2-8 shows the frequency distribution for number of coil rows by equipment type. The frequency distribution for fin spacing by system type is shown in Figure 2-9, indicating most direct expansion cooling coils have 12 – 16 fins per inch (4.7 – 6.3 fins/cm). These figures show that there are some coil geometry differences based on equipment type, and the analysis also showed that there are some variations based on coil size as well.

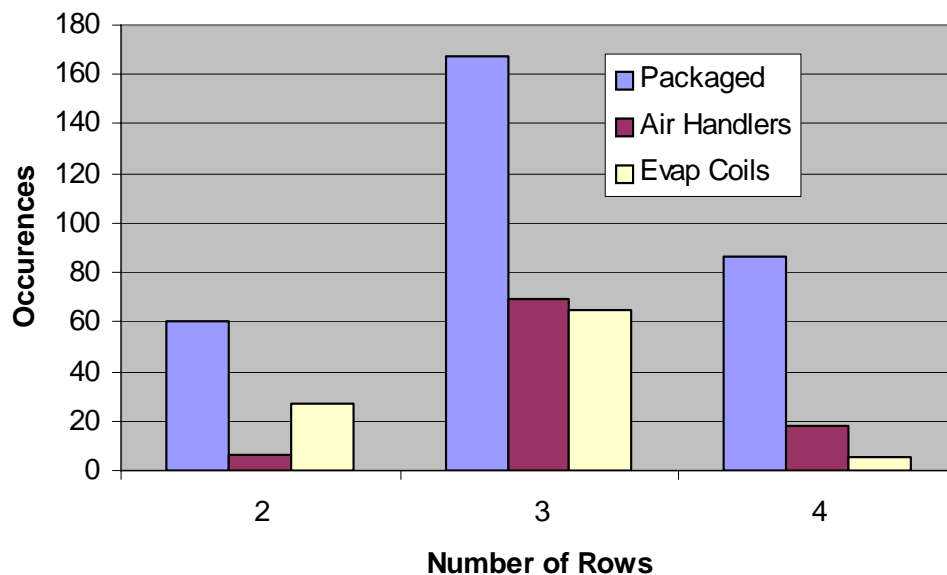


**Figure 2-8. Frequency Distribution for Number of Coil Rows**

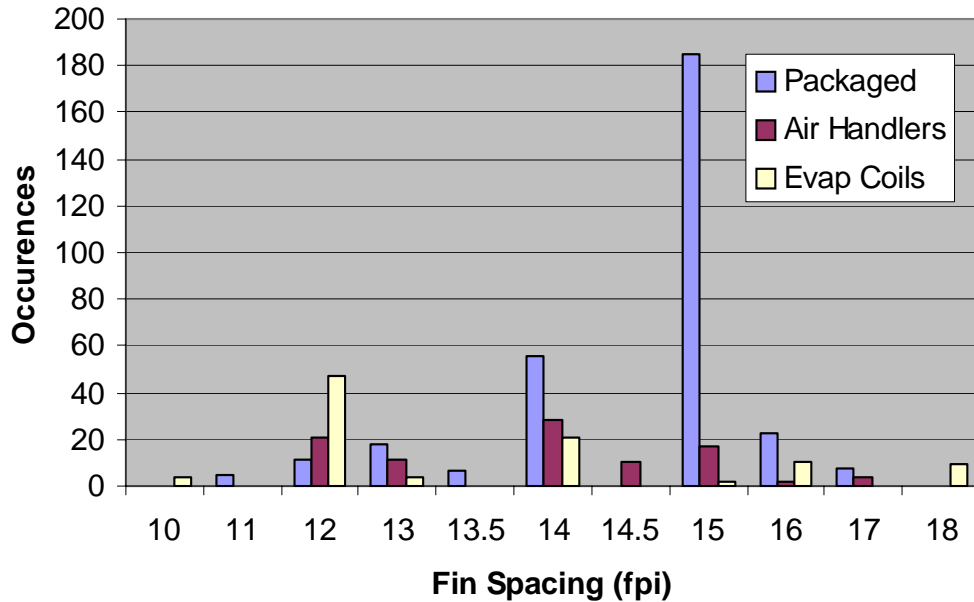


**Figure 2-9. Frequency Distribution for Coil Fin Spacing**

In addition to collecting information on cooling coil characteristics, another area of interest was new variable-speed residential equipment with improved dehumidification performance which is being heavily marketed in humid climates like the southeastern U.S. Several equipment manufacturers have implemented supply fan control schemes intended to limit latent capacity degradation or enhance steady-state latent capacity. Fan delays as well as brief operating periods at lower fan speeds are often used to enhance latent capacity. Manufacturer’s data were collected to understand the operation of these new residential products, and a summary of the enhanced fan control schemes being used is listed in Table 2-3. The collected information was also used to assist with selecting equipment to be monitored at two field test sites (see Section 4).



**Table 2-3. Enhanced Fan Control Schemes for Improved Dehumidification**

<b>Manufacturer</b>	<b>Soft Start Time &amp; Flow</b>	<b>Dehumidify Time &amp; Flow</b>	<b>Off-Cycle Delay Time &amp; Flow</b>	<b>Humidistat Option</b>	<b>Comments</b>
Trane	1 minute at 50% full air flow	Up to 7.5 minutes at 80% full air flow	3 minutes at 50% full air flow	80% of full flow when humidistat enabled	Without humidistat (Comfort-R™ enhanced mode), air handler ramps up to 100% full flow after 8.5 minutes. Cooling is terminated when thermostat set point is reached, at which time the compressor is turned off and the fan operates at 50% flow for 3 minutes.
Goodman	Time not given, ramp	NA	Time not given, stepped to 50% full air flow	Reduced air flow when humidistat enabled (exact percentage not given)	Standard fan operation, with ramp up and ramp down, is primarily targeted toward avoiding warm or cold air “blasts” at start-up and modest efficiency gains at shut down. An optional humidistat can be installed to reduce air flow and improve dehumidification.
Carrier Standard (ENH mode)	30 seconds with no airflow	150 seconds at 70% full flow	None (for “added comfort”)	Standard humidistat reduces flow to 80%	Thermostat controls compressor operation. Humidistat simply limits the maximum air flow to 80%.
Carrier Thermidistat™ (Cool to Dehumidify, or Superdehumidify)		Max run time in this mode is 10 minutes ON, 10 minutes OFF.	Depends on settings, “None” suggested for maximum dehumidification	Thermidistat™ allows overcooling based on dehumidify signal by up to 1.7°C (3°F). RH set point is reset 2% up for every 0.6°C (1°F) of overcooling.	Superdehumidify limits maximum air flow to 80% to limit overcooling. The manufacturer suggests removing the 90 second off-cycle fan delay for maximum dehumidification performance. If fan is set to continuous, the fan signal is removed for 5 minutes after the compressor turns off.
Lennox	30 seconds at 50% full flow	Up to 7.5 minutes at 80% full flow	30 seconds at 50% flow	EfficiencyPlus™ control indicates degree of deviation from RH set point with lights. Varies indoor blower speed and compressor speed (if applicable), but control details not given	Compressor operation controlled by thermostat unless EfficiencyPlus™ humidistat is installed.
Nordyne	None in De-Hum mode	10 minutes at 75% flow	Not given	Standard humidistat reduces airflow by unspecified amount	Air handler settings provide two soft start and off-cycle delay options for “energy efficiency and comfort”. De-Hum setting provides reduced flow for up to 10 minutes to improve dehumidification.

Source: Manufacturer’s published technical literature (circa 2001, 2002)

# 3 Laboratory Testing

Detailed measurements of cooling coil performance were collected in a controlled laboratory setting to understand the impact of coil geometry and operating conditions on transient moisture condensation and evaporation by the coils. A total of eight coils were tested: seven direct-expansion coils and one chilled-water coil. More than forty (40) steady state and cycling tests were performed on each coil. This section describes the test facility and experimental setup, detailed measurements that were made, tests performed on each coil, and the test results.

## 3.1 Testing Facility and Experimental Setup

An existing laboratory facility was used to collect detailed measurements on the part-load dehumidification performance of selected direct-expansion (DX) and chilled water (CW) cooling coils. The facility contains two psychrometric chambers that were used to maintain various air conditions (dry-bulb temperature and humidity levels) while testing coil performance. Both chambers were utilized to test the direct expansion coils (indoor coil in one chamber and the air-cooled condensing unit in the adjacent outdoor chamber), while only one chamber was required for testing the chilled water coil. The control room set up and outdoor test chamber are shown in Figure 3-1 and Figure 3-2 below. The condenser section shown below in the outdoor test chamber utilizes a variable-speed scroll compressor that was used for testing all DX coils selected for this project.

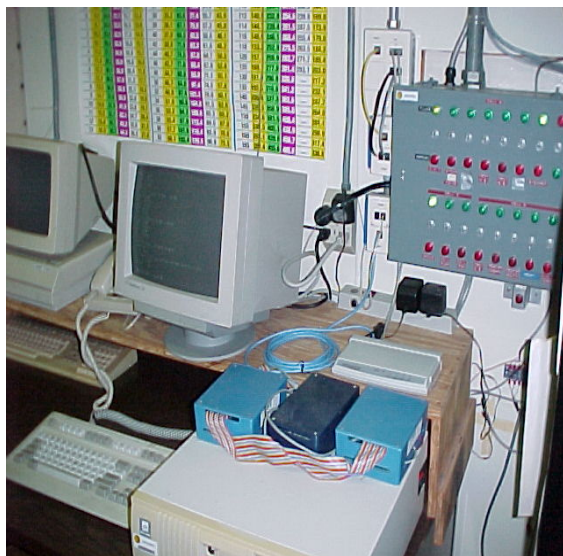


**Figure 3-1. Control Room**



**Figure 3-2. Outdoor Test Chamber**

The indoor test chamber is shown in Figure 3-3 with coil 1 installed for testing. The figure shows the air handler's vertical flow configuration in the left pane and the air flow measurement station and electric steamer in the right pane. Each air handler or coil was installed after completion of the entire series of tests for the previous coil. All coils except coils 4 and 8 were configured as shown in Figure 3-3 with the supply air fan included in the coil cabinet.



**Figure 3-3. Indoor Test Chamber**

A total of seven direct-expansion coils and one chilled-water coil were tested in the laboratory facility. The DX coils were selected to represent the range of common coil geometries based on manufacturer’s product information (see Section 2.4). The chilled water coil was selected as a common configuration yet different from the two chilled water coils being monitored as part of the field tests. Each coil was installed within the indoor chamber of the test facility. The characteristics of the tested coils are provided in Table 3-1 below.

**Table 3-1. Description of Lab-Tested Cooling Coils**

Coil	Configuration	Type	Description, expansion device	Rows	Fin Spacing (fpi)	Cooling Capacity (ton / kW)	Fin Surface Area (ft <sup>2</sup> / m <sup>2</sup> )
1	Vert. AHU, Fan On	DX	Slanted coil with plain fins, orifice	3	13	2.9 / 10.2	243.8 / 22.7
2	Vert. AHU, Fan Off	DX	A-coil with lanced sine-wave fins, TXV	3	15.5	2.4 / 8.4	237.8 / 22.1
3	Vert. AHU, Fan Off	DX	A-coil with lanced sine-wave fins, TXV (Coil 2 with low air flow)	3	15.5	1.4 / 4.9	237.8 / 22.1
4	Horiz. Casing, No Fan	DX	Vertical coil with wavy fins, orifice	2	14	1.8 / 6.3	137.4 / 12.8
5	Vert. AHU, Fan Off	DX	Slanted coil with wavy fins, orifice	4	12	2.3 / 8.1	162.7 / 15.1
6	Vert. AHU, Fan Off	DX	A-coil with wavy fins, TXV	3	13	1.6 / 6.0	231.1 / 21.5
7	Vert. AHU, Fan Off	DX	A-coil with wavy fins, TXV (Coil 6 with high air flow)	3	13	2.0 / 7.0	231.1 / 21.5
8	Horiz. Casing, No Fan	CW	Vertical coil with wavy fins, no expansion device	4	10	1.5 / 5.3	157.5 / 14.6

Notes: Additional information for each coil is provided in Appendix H.

AHU = air handling unit, TXV = thermostatic expansion valve

Fin surface area is gross fin area: coil face area (ft<sup>2</sup>) x coil depth (in) x fin spacing (fpi) x 2

Schematic representations of the vertical and horizontal airflow test configurations are shown in Figure 3-4 and Figure 3-5 below. Coils 1 through 3 and 5 through 7 were air handler assemblies that were tested in the vertical configuration shown in Figure 3-4. Each air handler included a fan (though the fan was not operated in every case). Coils 4 and 8 were stand alone cased coils tested with horizontal airflow as shown in Figure 3-5. All coils were tested using a booster fan to overcome the pressure drop of the airflow measurement station and to control the airflow rate through the unit.

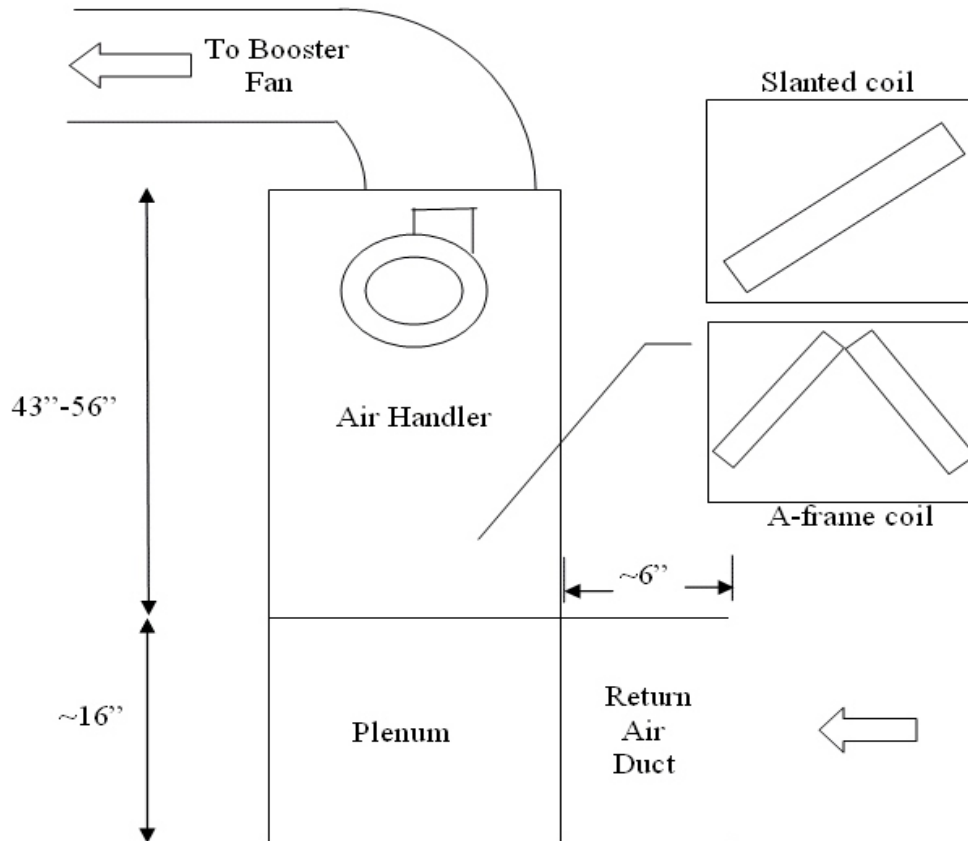


**Figure 3-4. Schematic of Vertical Flow Test Configuration**

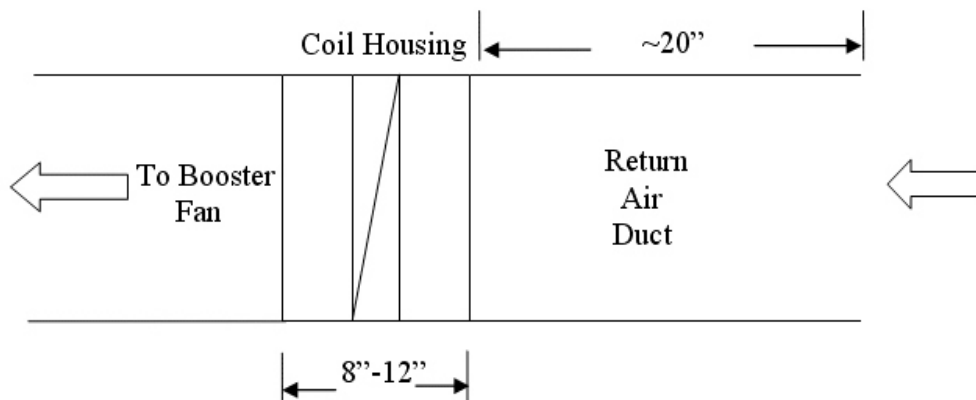


**Figure 3-5. Schematic of Horizontal Flow Test Configuration**

The test facility is capable of testing air-conditioning systems with cooling capacities up to 3 tons (10.5 kW) while maintaining constant temperature and humidity conditions as specified in ASHRAE Standard 37 (ASHRAE 1988). The instrumentation used in the lab is schematically shown in Figure 3-6. The instrumentation and room controls were configured to allow for transient testing of air conditioner performance. The controls in the indoor test chamber were programmed to maintain constant space conditions using proportional and integral control of multiple heaters and an electric steamer as the cooling coil cycled on and off. Outdoor test chamber temperature was maintained using a chilled water coil and a variable-speed fan, and a heater was used to trim the chamber temperature when the DX condenser cycled off. To minimize deviations in chamber conditions when the cooling coil cycled on or off, control signals to the heaters, steamer, and other control equipment were adjusted immediately prior to these transition periods in anticipation of the rapid change in loads.

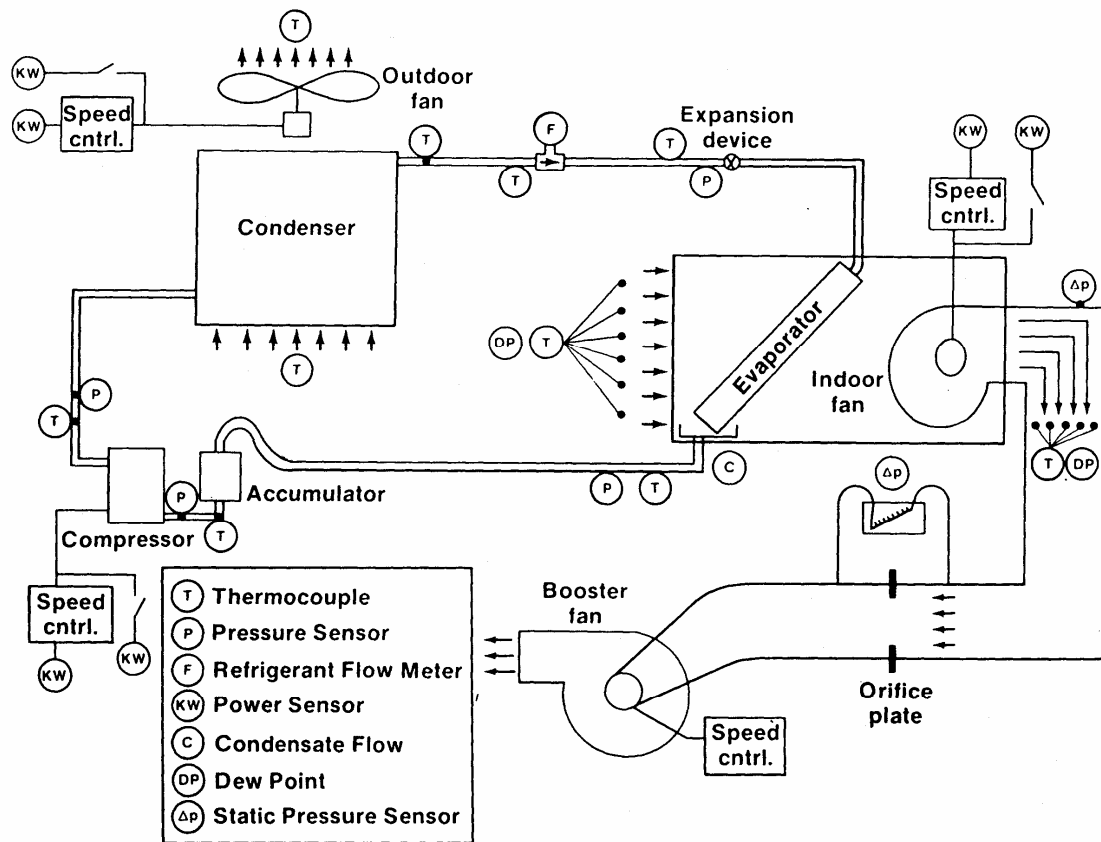


Figure 3-6. Schematic of Psychrometric Chambers/Coil Testing Apparatus at FSEC

### 3.2 Instrumentation and Monitored Variables

The test facility contains a dedicated laboratory-grade data acquisition and control system. The facility is fully instrumented to monitor and maintain the desired conditions required for each test. Additional instrumentation is used to measure the performance of the air-conditioning system being tested. For this project, the system performance measurements were collected at 15-second intervals. The measured data were continuously transferred to a mainframe computer system for processing, storage, and analysis.

Table 3-2 below describes the monitored variables and instrumentation used to evaluate the performance of the DX coils. Dry-bulb temperature measurements were made using type-T thermocouples with an accuracy of  $\pm 1^\circ\text{F}$ . Chilled mirror hygrometers with an accuracy of  $\pm 0.36^\circ\text{F}$  were used to measure the dewpoint temperature of air entering and leaving the cooling coil. Air flow measurements were made by measuring pressure drop across an ASME MFC-3M-1984 orifice plate. Air-side pressure measurements were made using differential pressure transducers with accuracies of  $\pm 1.0\%$  of full scale ( $\pm 0.025$  in WC). Refrigerant pressures were monitored using pressure transducers with  $\pm 0.13\%$  full-scale accuracy ( $\pm 0.325$  psi). Electrical energy consumption was measured using  $\pm 0.5\%$  watt-hour transducers. Condensate removal was monitored using a rain-gauge tipping bucket calibrated at 0.0087 lbs/tip.

**Table 3-2. Data Points for Monitoring DX Cooling Coils**

<b>Description</b>	<b>Instrumentation</b>
Coil entering air dew point temperature	Chilled mirror hygrometer with sampling pump
Coil entering air dry-bulb temperature	Type-T thermocouple array
Supply air dew point temperature	Chilled mirror hygrometer with sampling pump
Supply air dry-bulb temperature	Type-T thermocouple array
Supply air fan power	Watt-hour transducer
Air volume flow rate across coil	Calibrated orifice plate, pressure transducer
Refrigerant pressure at coil outlet (compressor suction)	Pressure transducer
Refrigerant temperature at coil outlet	Surface-mounted type-T thermocouple
Refrigerant pressure at expansion device inlet (condenser outlet)	Pressure transducer
Refrigerant temperature at expansion device inlet	Surface-mounted type-T thermocouple
Liquid refrigerant flow rate	Turbine flow meter
Compressor power	Watt-hour transducer
Compressor speed	Control voltage to inverter
Condensate removal rate	Calibrated rain gauge (tipping bucket)
Evaporator coil tube temperature (3 places)	Surface-mounted type-T thermocouples
Cooling coil air-side pressure drop	Pressure transducer
Condenser entering air temperature	Type-T thermocouple
Condenser leaving air temperature	Type-T thermocouple

The monitored variables and instrumentation for the chilled water coil tests are shown in Table 3-3 below. Many of the data points are identical to those monitored for the DX coils. However, measurements of chilled water flow rate and coil inlet/outlet water temperatures were added while the DX refrigerant system variables were omitted. Chilled water flow rate through the test coil was measured using a positive displacement flow meter with an accuracy of 1.5% of reading and a resolution of 1 pulse per 0.01 gallon.

**Table 3-3. Data Points for Monitoring the Chilled Water Cooling Coil**

<b>Description</b>	<b>Instrumentation</b>
Coil entering air dew point temperature	Chilled mirror hygrometer with sampling pump
Coil entering air dry-bulb temperature	Type-T thermocouple array
Supply air dew point temperature	Chilled mirror hygrometer with sampling pump
Supply air dry-bulb temperature	Type-T thermocouple array
Air volume flow rate across coil	Calibrated orifice plate, pressure transducer
Cooling coil water flow rate	Positive displacement flow meter
Cooling coil water inlet temperature	Type-T thermocouple (metal-sheathed insertion probe)
Cooling coil water outlet temperature	Type-T thermocouple (metal-sheathed insertion probe)
Condensate removal rate	Calibrated rain gauge (tipping bucket)
Cooling coil tube temperature (3 places)	Surface-mounted type-T thermocouples
Cooling coil air-side pressure drop	Pressure transducer
Chilled water pump speed	Control voltage to inverter

As previously described, condensate removal was monitored using a rain-gauge tipping bucket calibrated at approximately 0.0087 lbs/tip. However, the calibration of the tipping bucket varies with flow rate. To accurately measure condensate at varying flow rates, the tipping bucket was calibrated at 3 discrete flow rates and a calibration curve fit was used during analysis. The calibration data and calibration multiplier for the initial tipping bucket are shown in Table 3-4 and Figure 3-7, respectively. The tipping bucket was replaced twice over the testing period (before testing coil 5 and coil 7) and similar calibrations were performed and calibration curve fits used during the subsequent analyses.

**Table 3-4. Tipping Bucket Calibration Data**

<b>Sample Time (hr)</b>	<b>No of tips</b>	<b>Measured Water (lb)</b>	<b>Multiplier (lb/tip)</b>	<b>Flow Rate (lb/hr)</b>	<b>(tips/min)</b>
0.20778	120	0.9714	0.0081	4.675	9.63
0.08833	110	0.9716	0.0088	11	20.75
0.05972	103	0.9716	0.0094	16.27	28.74



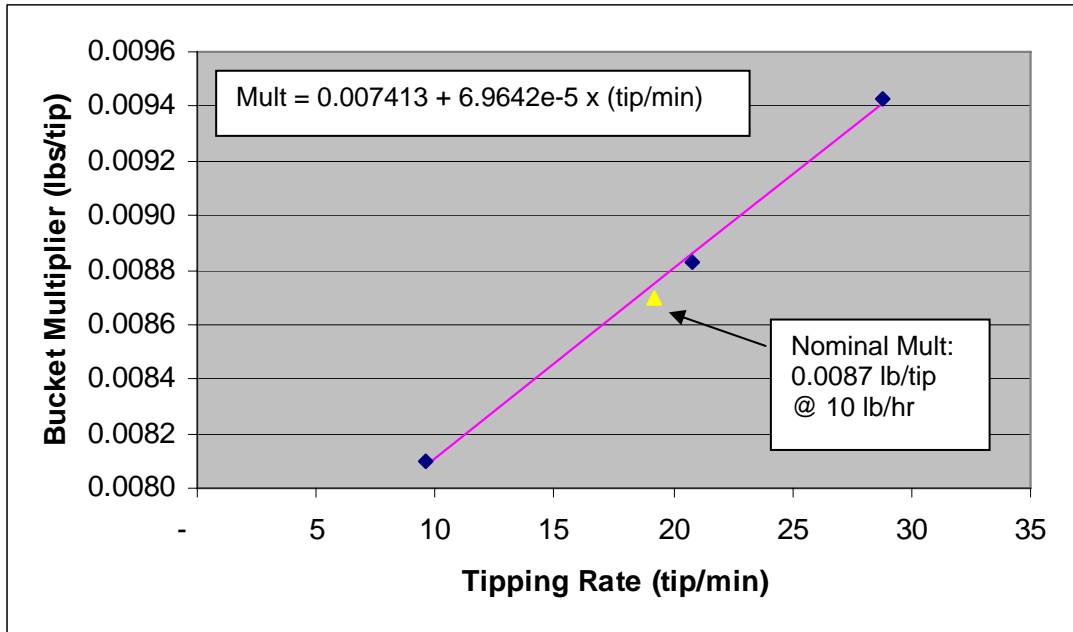


**Figure 3-7. Tipping Bucket Calibration Multiplier**

Additional measurements were collected during the tests to identify control issues associated with the test procedures for each coil. These measurements included monitoring the control voltage sent to the heater and steamer load centers, the temperature of the chilled water holding tank, and the control voltage sent to the air flow booster fan. This additional information was collected and stored at the same 15-second interval as the test coil data points denoted in Table 3-2 and Table 3-3 above.

### **3.3 Description of Tests**

A series of steady-state and cyclic tests were performed on each coil. Table 3-5 summarizes the steady-state tests that were performed. For each of these tests, the coil was turned off for a long period of time (typically 45-60 minutes, or longer in some cases) with continuous air flow across the coil at the prescribed flow rate. This was done to completely dry off the cooling coil. Then, the cooling coil was turned on for a similar length of time (> 45 minutes) to reach steady-state conditions. The coil was then turned off for a long period until measurements indicated the coil was completely dry again. For some of the low humidity tests, the compressor on time exceeded 4 hours.

These tests were performed for a combination of two entering air dry-bulb temperatures, three entering air humidity levels, and four air flow rates (tests 3 through 24 in Table 3-5). These tests were performed primarily to quantify the amount of moisture retention by each coil, and to determine the moisture evaporation rates from the coil over time once coil operation was terminated. Test 25 involved operating at an air flow rate of approximately 400 cfm/ton (0.054 m<sup>3</sup>/s•kW) when the coil was on, then decreasing the airflow rate by 50% during periods when the coil was off. This test was performed to assess the impact of this change on moisture evaporation from the coil since various manufacturers are now using this control strategy for continuous fan operation (fan ON mode).



Steady-state tests 1 and 2 operated the cooling coil at significantly different temperatures than were measured during the baseline tests (3 and 4). The different coil temperatures were achieved by adjusting the compressor speed of the variable-speed condensing unit (for coils 1 through 7) or adjusting the entering water temperature (for coil 8). These tests were performed to determine if coil temperature impacted the amount of moisture retained or the rate and profile of moisture evaporation from the coil.

**Table 3-5. Summary of Steady-State Test Conditions Corresponding to Each Run or Test**

Air Flow Rate	Test Number					
	Entering Coil Conditions (dry bulb/wet bulb, dew point temperatures)					
	80/67°F, 60°F dp	80/72°F, 68°F dp	80/62°F, 50°F dp	75/68°F, 64°F dp	75/63°F, 56°F dp	75/58°F, 45°F dp
400 cfm/ton	4 (or 3)	5	6	7	8	9
300 cfm/ton	10	11	12	13	14	15
200 cfm/ton	16	17	18	19	20	21
450 cfm/ton	22	23	24			
400-200 cfm/ton (ON & OFF)	25					
400 cfm/ton with low coil temperature	1					
400 cfm/ton with high coil temperature	2					

Note: Test 1 and 2 sought to operate the coil at a 3-5°F higher and a 3-5°F lower coil temperature compared to the baseline (tests 3 and 4). For coil 1 a lower suction was not possible, so a 2<sup>nd</sup> higher coil temperature was tested (see Figure 3-28). See Appendix H for the specific temperatures used for each coil.

In addition to steady-state tests, a series of quasi-steady cyclic tests were performed on each coil with differing lengths of coil on and off times (Table 3-6). As shown by Figure 3-8, the lengths of the on and off times were selected to correspond with the NEMA thermostat curve with a maximum cycle rate ( $N_{max}$ ) of 3 cycles/hour at 50% duty cycle (NEMA 1990). The tests were conducted with the fan continuously providing air flow over the cooling coil (CONST) and also with the fan cycling on and off in tandem with the cooling coil (AUTO). Each test was repeated multiple times to reach quasi-steady state conditions. Some additional cyclic tests were also completed for two of the coils with various fan delay control strategies (see Section 3.5).

**Table 3-6. Cyclic Test Conditions**

CONST FAN	AUTO FAN	Number of Times Test Repeated	ON Time (minutes)	OFF Time (minutes)	Runtime Fraction (-)	Cycle Rate (cycles/h)
Test Number						
31	41	2	45	45	0.500	0.667
32	42	3	30	6	0.833	1.667
33	43	3	16	7.25	0.688	2.581
34	44	3	10	10	0.500	3.000
35	45	3-5	7	17.5	0.286	2.449
	46	3-5	5.5	55	0.091	0.992

Notes: All tests performed with 80°F db/60.4°F dp inlet air and 400 cfm/ton air flow. Tests 45 and 46 were repeated up to 5 times for coils 5 – 8.

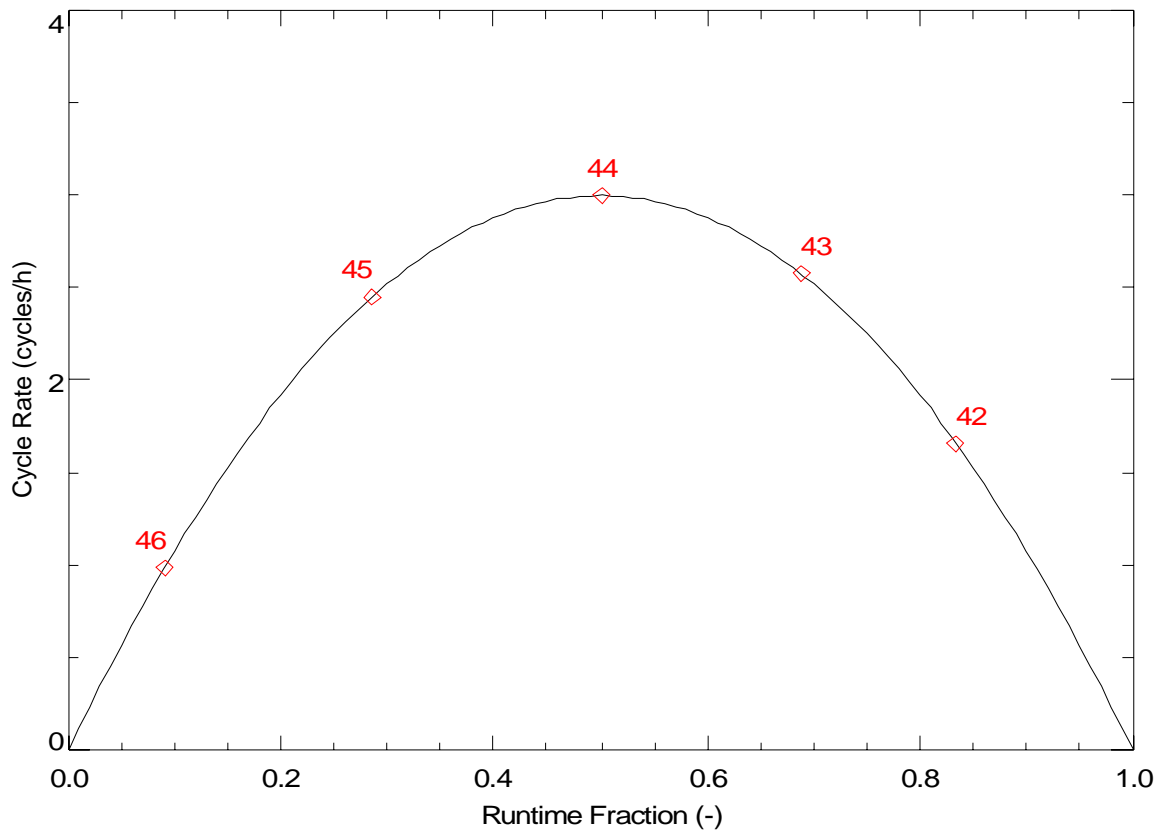


**Figure 3-8. Cyclic Tests Shown on NEMA Thermostat Curve ( $N_{max}=3$ )**

For coil 1, the cyclic tests shown in Table 3-6 were performed at a single nominal entering air condition (80°F [26.7°C] inlet air dry-bulb, 60.4°F [15.8°C] dew point) and air flow rate (400 cfm/ton [0.054 m<sup>3</sup>/s•kW]). For the seven other coils, the cyclic tests were performed at nominal conditions as well as other operating conditions in the constant fan mode:

- Tests 51-55, inlet air conditions of 75°F dry bulb/64°F dewpoint (23.9°C/17.8°C) with air flow at 400 cfm/ton (0.054 m<sup>3</sup>/s•kW),
- Tests 61-65, inlet air conditions of 75°F dry bulb/56°F dewpoint (23.9°C/13.3°C) with air flow at 400 cfm/ton (0.054 m<sup>3</sup>/s•kW),
- Tests 71-75, original inlet air conditions (80°F dry bulb/60.4°F dewpoint [26.7°C/15.8°C]) but at a reduced air flow rate of 300 cfm/ton (0.041 m<sup>3</sup>/s•kW).

The quasi-steady cyclic tests were performed to determine the overall degradation in dehumidification performance at various coil cycling rates. This information was used to validate mathematical models to predict latent capacity degradation over a wide range of operating conditions. Model development and validation are described further in Section 5.

### **3.4 Test Results**

The eight cooling coils were subjected to the battery of tests described in Section 3.3. In most cases a given test series was repeated several times until operating conditions and test stability were maintained. The test results were summarized, plotted, and analyzed in a number of different ways. The full set of standardized results for each coil is provided in Appendix H. The following sections show typical test results and the standard data analyses that were performed for each coil. The results for the first test coil (coil 1) are shown to serve as an example, with results for all test coils also shown in some cases to show variations among the coils.

#### **3.4.1 Steady-State Tests**

##### Steady-State Performance

Accurate measurement of coil dehumidification was of critical importance for the laboratory tests, and two methods were used to measure dehumidification performance. First, a calibrated rain-gauge tipping bucket was used to measure the volume of condensed water exiting the coil's drain pan. Measured condensate flow multiplied by the latent heat of condensation for water (1060 Btu/lb, 2466 kJ/kg) yielded the latent cooling rate. The second method used the measured psychrometric conditions of air entering and leaving the coil along with measured air flow rate across the coil to calculate the coil's dehumidification (latent cooling) rate. Moist air properties were computed using the psychrometric routines from the ASHRAE Secondary Toolkit (Brandemuehl 1993) and the hourly barometric pressure readings from nearby Melbourne International Airport. The results of the two methods were plotted against each other for all tests when the coil reached steady-state operating conditions. The resulting plot for coil 1, shown in Figure 3-9, indicates relatively good agreement between the two methods, although some deviation occurs at low latent removal rates. The numbers shown in Figure 3-9 represent the test run numbers as specified in Table 3-5. Figure 3-10 shows similar agreement between the two methods for all test coils. The solid lines in Figure 3-10 denote  $\pm 15\%$  difference between the two calculation methods.

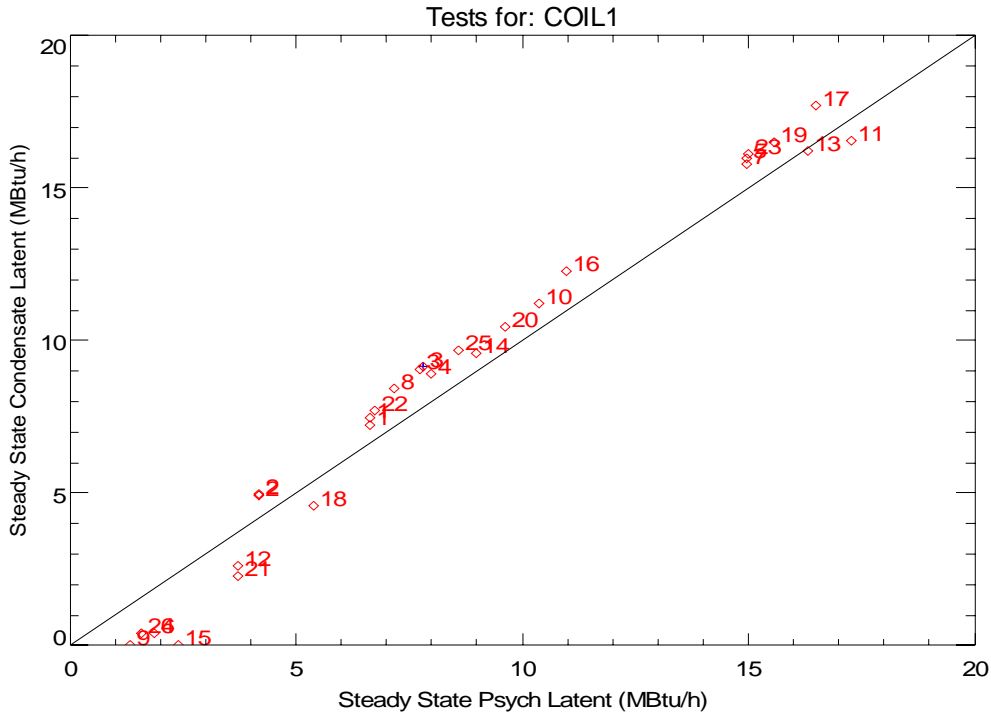


**Figure 3-9. Comparing Steady-State Latent Capacity Calculated From Psychrometric State Points and Condensate Removal Rates, Coil 1**

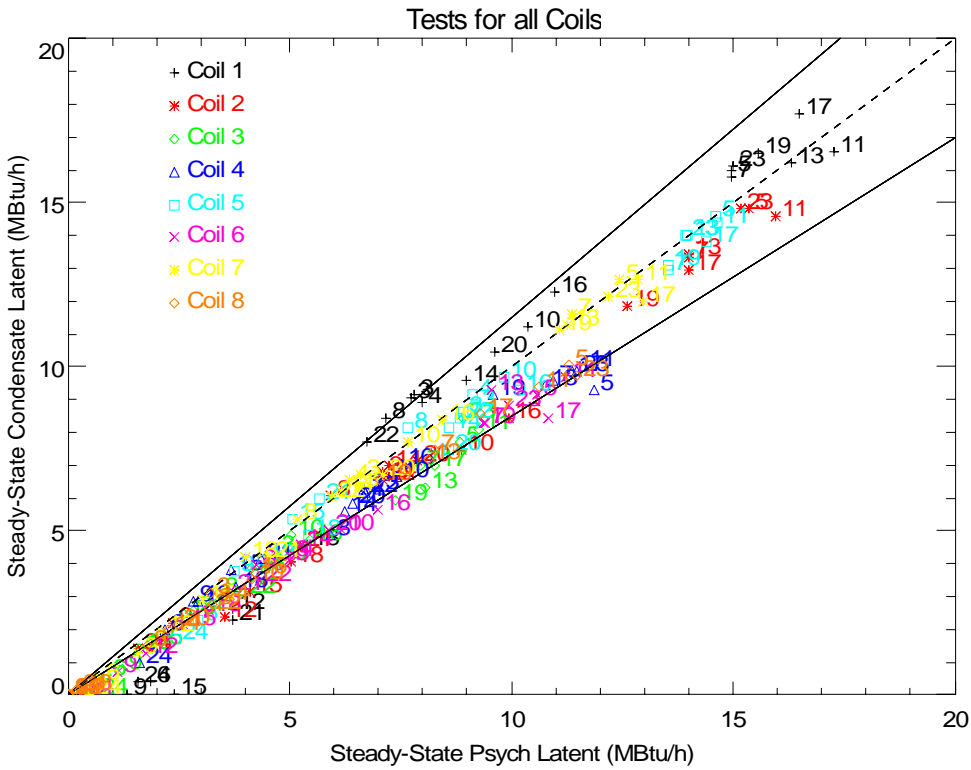


**Figure 3-10. Comparing Steady-State Latent Capacity Calculated From Psychrometric State Points and Condensate Removal Rates, All Coils**

The steady-state sensible heat ratio (SHR) was also calculated and plotted versus entering air relative humidity and air flow rate across the cooling coil. The temperature and humidity of air entering and leaving the cooling coil, along with the measured air flow, were used to calculate the sensible heat ratio. SHR is the sensible cooling capacity divided by the total (sensible plus latent) cooling capacity of the coil. Figure 3-11 for coil 1 shows that the sensible heat ratio decreases as the relative humidity entering the coil increases. The figure also shows that SHR tends to decrease as air flow across the cooling coil decreases. All tested coils exhibited these same general trends.

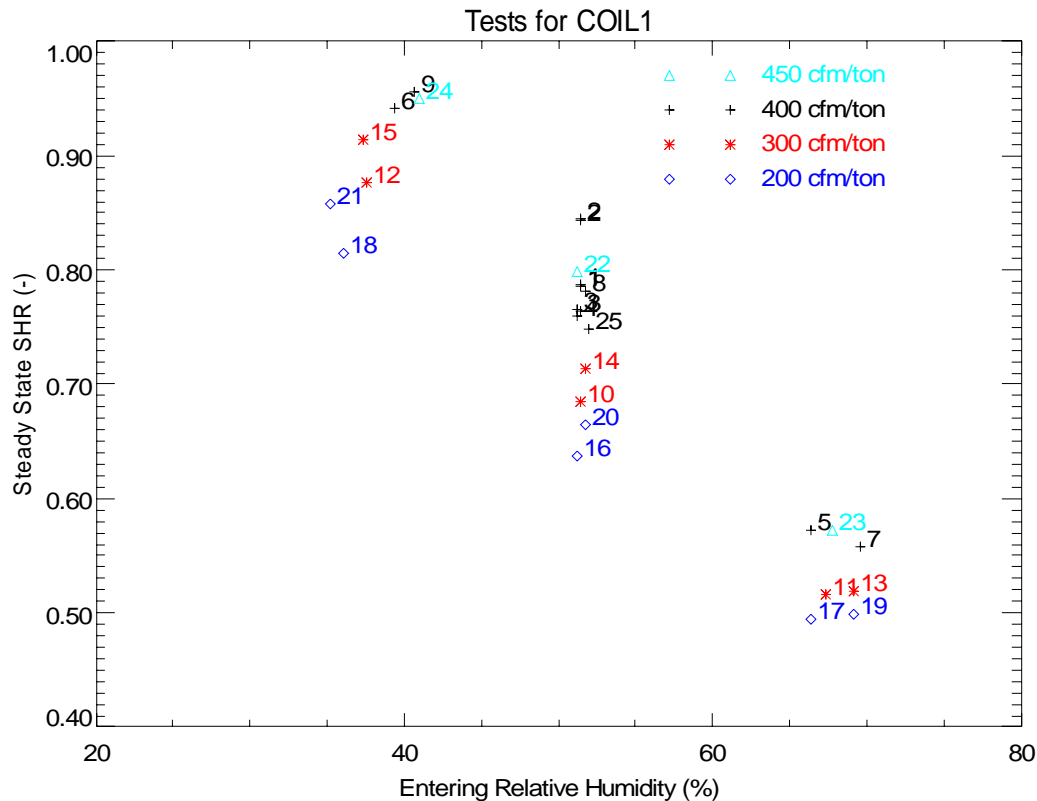


**Figure 3-11. Variation of Steady State SHR with Entering Humidity and Nominal Air Flow, Coil 1**

Typical Transient Performance

For each steady-state coil test denoted in Table 3-5, the measured cooling capacity of the coil was calculated and plotted versus time for each coil on/off cycle. The sensible (QS) and latent (QL) capacity of the coil were calculated based on the measured entering and leaving air conditions and air flow rate. Latent capacity was also calculated based on measured condensate removal (QC) and the latent heat of condensation for water. The resulting plot for coil 1, run 4 is shown in Figure 3-12.

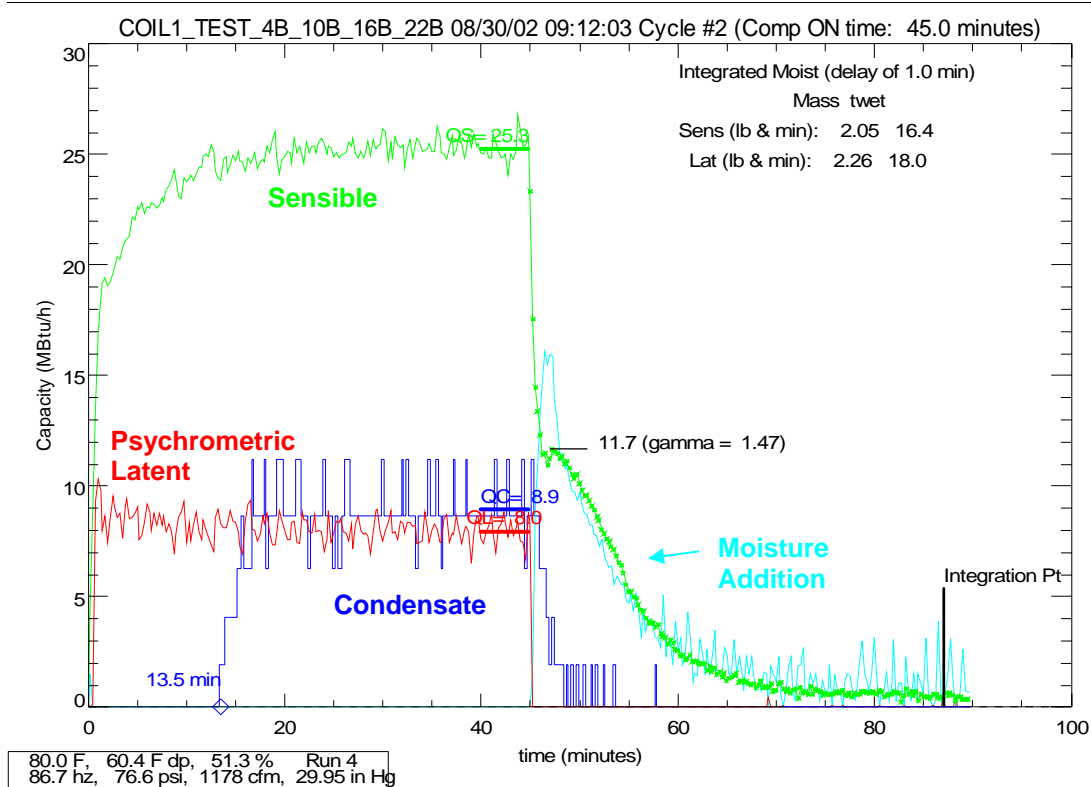


**Figure 3-12. Laboratory Test Data for a Typical Test Run**

Starting with a dry coil, Figure 3-12 shows that psychrometric sensible and latent capacity rise to their steady-state values within 15 minutes after the cooling cycle begins for this test coil at these test conditions. However, there is a lag before enough moisture builds up on the coil for condensate to begin flowing from the drain pan, a delay of 13.5 minutes for the coil 1 test shown in Figure 3-12. This condensate “delay time” is an indicator of the amount of moisture retained on the cooling coil. Condensate delay time is relatively easy to measure at field test sites, and may be used to estimate coil moisture retention if detailed psychrometric or condensate measurements are not available.

The cooling coil is operated for a long period of time to assure steady-state operation has been achieved (45 minutes in Figure 3-12). At this point the latent capacity calculated from psychrometric properties of moist air and the measured airflow (8.9 MBtu/h [2.6 kW]) is approximately equal to the latent capacity determined from the condensate flow rate (8.0 MBtu/h [2.3 kW]). The compressor is then turned off and the fan continues to operate until the coil is completely dry (time = 90 minutes in Figure 3-12).

At the beginning of the compressor off cycle (time = 45 minutes), sensible capacity continues to be delivered due to continuous fan operation but capacity quickly drops as the system makes the transition to an evaporative cooler. The transition takes about 1 to 2 minutes after the compressor stops operating while refrigerant migration inside the coil and system subsides. Starting at the transition point identified in Figure 3-12 as “gamma” (11.7 MBtu/h [3.4 kW]), the sensible cooling is approximately equal to the latent energy associated with moisture addition. Integrating the latent (or sensible) capacity over the off cycle provides an indication of the amount of moisture that is retained on the coil surfaces. In this case, starting the integration after a one-

minute delay and continuing to the designated integration point, a moisture mass of about 2 lbs [0.9 kg] is retained on the coil based on sensible capacity (slightly higher when integrating latent capacity which is harder to measure precisely). The designated integration point is selected as the point at which the supply air dew point temperature first reaches the average terminal value (defined as the average for the last 1.5 minutes of the off cycle). Dividing the moisture mass (based on the integrated off-cycle sensible capacity) by the steady-state latent capacity indicates that  $t_{wet}$  is 16.4 minutes in this case, which is fairly close to the measured condensate delay time of 13.5 minutes. The parameter  $t_{wet}$  is used in the latent degradation model developed by Henderson and Rengarajan (1996), which is described further in Section 5.

Table 3-7 summarizes the measured moisture retention, condensate delay time, and the calculated value of  $t_{wet}$  for all tested coils. Moisture retention varied from approximately 8 to 12 lbs per 1,000 ft<sup>2</sup> (39 to 59 g/m<sup>2</sup>) of fin area. The one exception was coil 4 which held nearly 14 lbs per 1,000 ft<sup>2</sup> (68 g/m<sup>2</sup>) of fin area. The condensate delay time varied from 12 minutes to 34 minutes for the lab test coils at nominal conditions. Similar variations were observed for the model parameter  $t_{wet}$ .

**Table 3-7. Comparing Measured Performance Parameters for the Lab-Tested Cooling Coils**

	Capacity (tons)	Fin Surface Area (ft <sup>2</sup> )	Retained Moisture Mass		Cond Delay Time (min)	$t_{wet}$ (min)
			(lb)	(lb/kft <sup>2</sup> )		
Coil 1 (Slanted coil, 3 row, 13 fpi, plain fins, orifice)	2.9	243.8	2.1	8.6	13.5	16.5
Coil 2 (A-coil, 3 rows, 15.5 fpi, lanced sine-wave fins, TXV)	2.4	237.8	2.0	8.4	16.3	17.0
Coil 3 (Coil 2 with low air flow) (A-coil, 3 rows, 15.5 fpi, lanced sine-wave fins, TXV)	1.4	237.8	2.0	8.4	32.5	29.0
Coil 4 (vertical coil, 2 rows, 14 fpi, wavy fins, orifice)	1.8	137.4	1.9	13.8	23.5	18.5
Coil 5 (slanted coil, 4 rows, 12 fpi, wavy fins, orifice)	2.3	162.7	1.4	8.6	11.5	9.5
Coil 6 (A-coil, 3 rows, 13 fpi, wavy fins, TXV)	1.6	231.1	2.7	11.7	34.0	33.0
Coil 7 (Coil 6 with high air flow) (A-coil, 3 rows, 13 fpi, wavy fins, TXV)	2.0	231.1	2.7	11.7	27.0	27.0
Coil 8 (vertical chilled-water coil, 4 rows, 10 fpi, wavy fins, 46°F entering water temp.)	1.5	157.5	1.4	8.9	26.5	25.0

- Notes:
- 1- Cooling capacity includes sensible and latent cooling at nominal conditions. Nominal conditions correspond to ASHRAE Test A test point.
  - 2- Fin surface area is gross fin area: coil face area (ft<sup>2</sup>) x coil depth (in) x fin spacing (fpi) x 2
  - 3- Condensate delay time and  $t_{wet}$  are average for all tests at nominal conditions (tests 3 and 4).
  - 4- Retained moisture based on off-cycle integration of sensible capacity at nominal conditions (test 4).

## Part-Load Latent Capacity Parameters

As described above, integrating the latent and sensible measurements during the compressor off cycle provides an indication of moisture retention by the cooling coil. If it is assumed that the coil acts as an evaporative cooler, the sensible and latent capacities during the compressor off cycle should be equal. To check this assumption, off-cycle integrated sensible and latent capacities were calculated for each steady state test, converted to mass using the latent heat of condensation, and plotted against each other. This was done for all eight test coils, and the resulting plot for coil 1 is shown in Figure 3-13. For coil 1, the integrated latent capacity significantly exceeded the integrated sensible capacity for several test cases. Further investigation showed these deviations occurred at high inlet air dew point temperatures. Results for the other seven coils showed good overall agreement between the two methods for all tests with no bias at high inlet humidity conditions. Since we expect that off-cycle latent and sensible capacity should sum to zero, we have selected the integrated off-cycle sensible capacity as the most reliable indication of moisture held on the cooling coil.

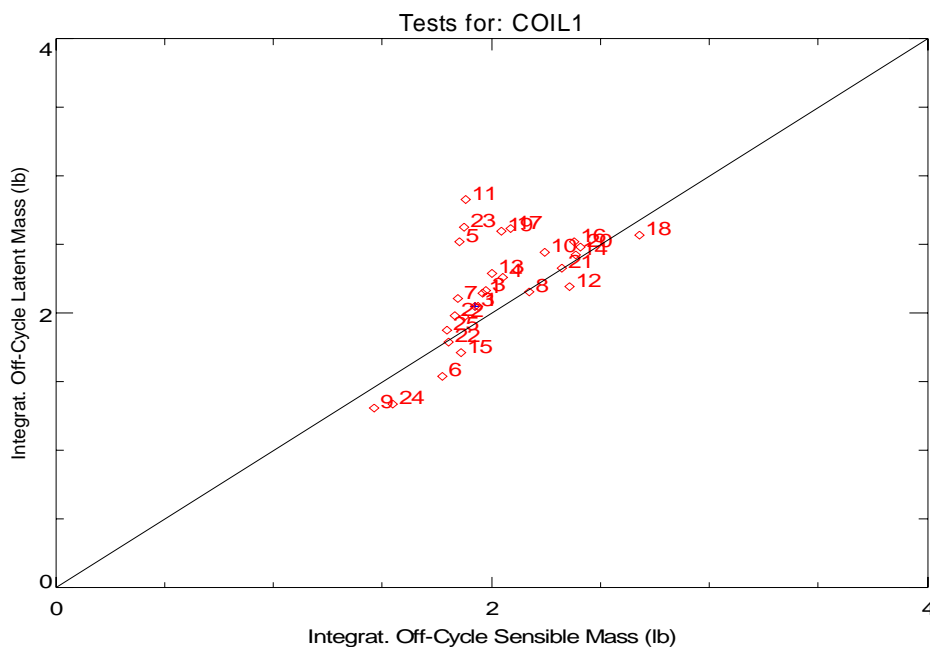
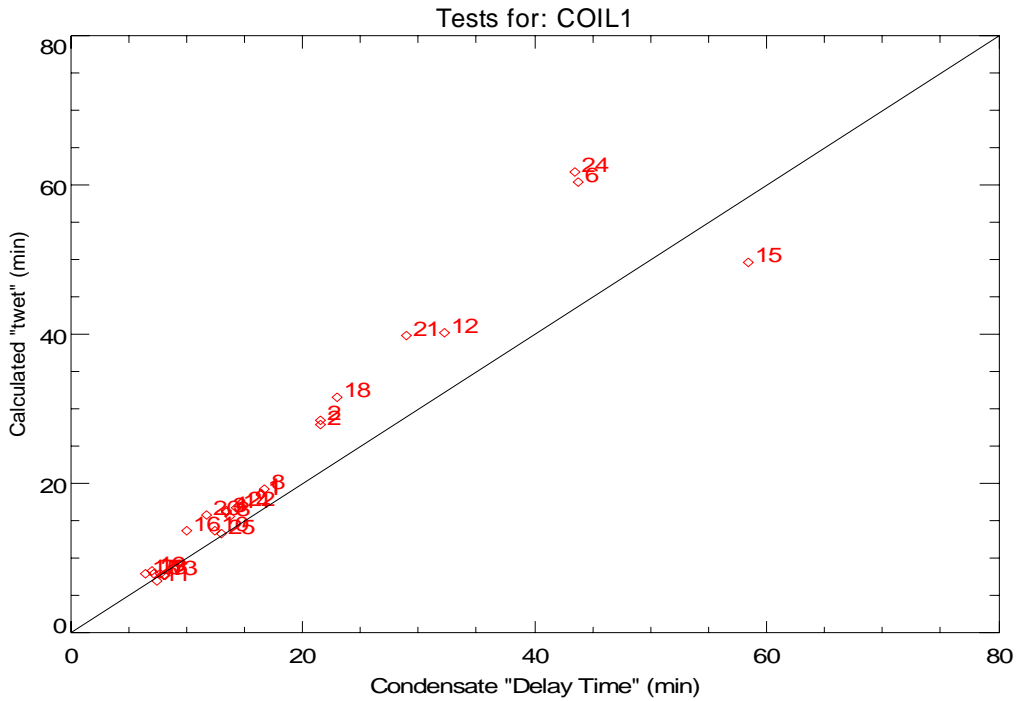


**Figure 3-13. Comparing Stored Moisture Mass Calculated by Integrating Sensible and Latent Off-Cycle Capacity (Integrated with a 1-minute Delay), Coil 1**

As mentioned previously, the model parameter  $t_{\text{wet}}$  is the moisture retained on the cooling coil times the enthalpy of condensation for water (1060 Btu/lb, 2466 kJ/kg) divided by the steady-state latent capacity of the cooling coil. The parameter should physically correspond to the time it takes for moisture to first fall from the coil (ignoring startup delays and other effects). Figure 3-14 compares the calculated  $t_{\text{wet}}$  (determined by integrating sensible capacity during the off-cycle and then dividing by the steady-state psychrometric latent capacity during the on-cycle) to the condensate delay time for all the test runs. There is relatively good agreement between these two values for coil 1 at short to moderate delay times, but the difference between them increases significantly at longer delay times (because as coil inlet air conditions get drier the integration error to find  $t_{\text{wet}}$  gets larger, or because the coil is only partially wetted at the lower inlet air dew

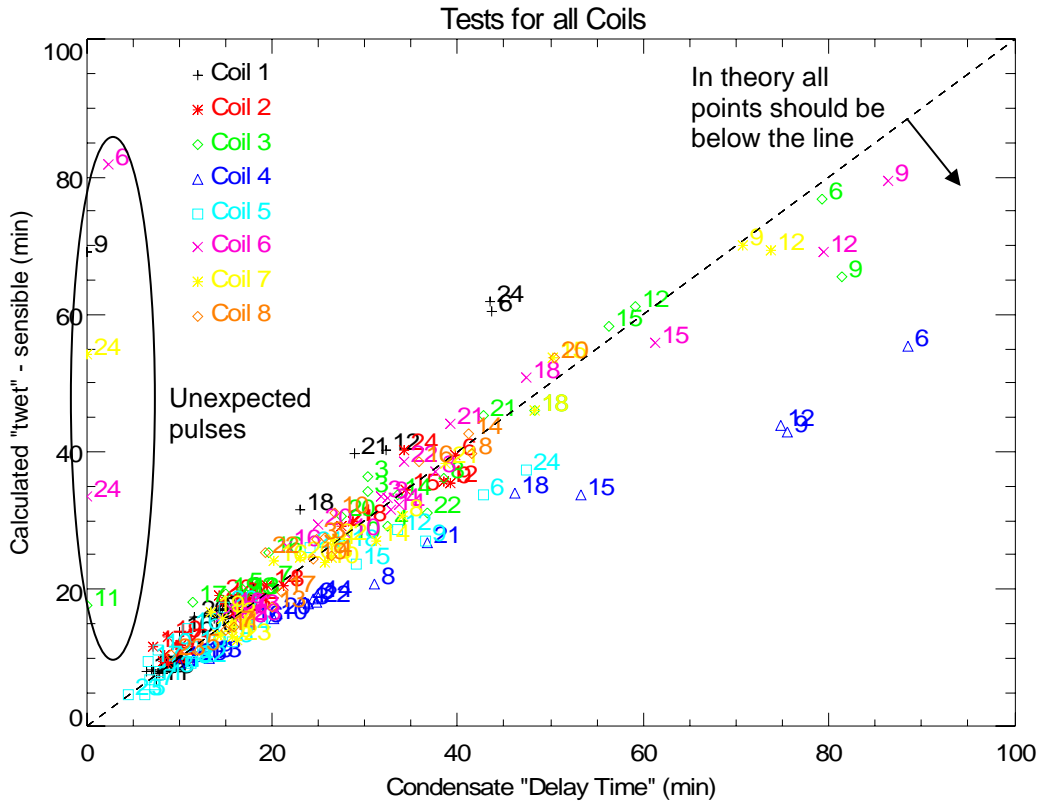


point temperatures). In theory the condensate delay time would always be greater than or equal to  $t_{wet}$  (due to startup losses), so the trend seen for coil 1 was unexpected.



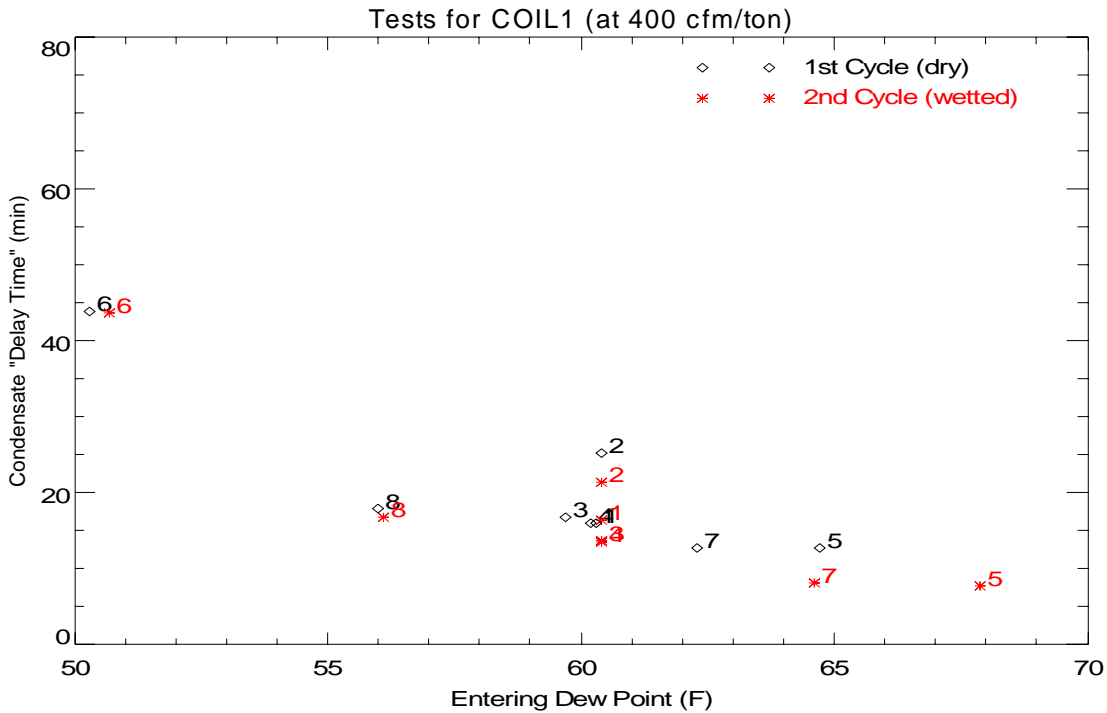
**Figure 3-14. Comparing “twet” (Calculated with Off-Cycle Sensible and Steady State Latent) to the Condensate Delay Time, Coil 1**

Figure 3-15 shows the same comparison of  $t_{wet}$  versus condensate delay time for all eight test coils. In general, all coils except coil 1 and coil 4 exhibited the expected trend of condensate delay time being greater than or equal to  $t_{wet}$ . For a few of the coils, a few unexpected or “stray” condensate pulses were recorded near the start of coil operation for a couple of the runs. These outlier points (condensate delay times < 4 minutes) are circled on the plot. The tipping bucket measurements for coil 4 started to “stick” or respond slowly (impacting delay times), and the sensor was subsequently replaced for the remaining coils.



**Figure 3-15. Comparing “twet” (Calculated with Off-Cycle Sensible and Steady State Latent) to the Condensate Delay Time, All Coils**

Figure 3-16 shows the impact of entering air dew point temperature on measured condensate delay time. As expected, the figure shows that the delay time increases as entering air humidity levels decrease (all coils showed this trend). Different symbols are shown on the plot for the 1<sup>st</sup> and 2<sup>nd</sup> cycles in each test sequence. For coil 1, the delay time was slightly higher for the first cycle when the fin surfaces were totally dry. For the 2<sup>nd</sup> cycle, the coil apparently may have had better wettability than it did for the 1<sup>st</sup> cycle. However, this trend was not consistent for all of the test coils. For certain coils, there was virtually no difference between the values calculated for the 1<sup>st</sup> and 2<sup>nd</sup> cycles.



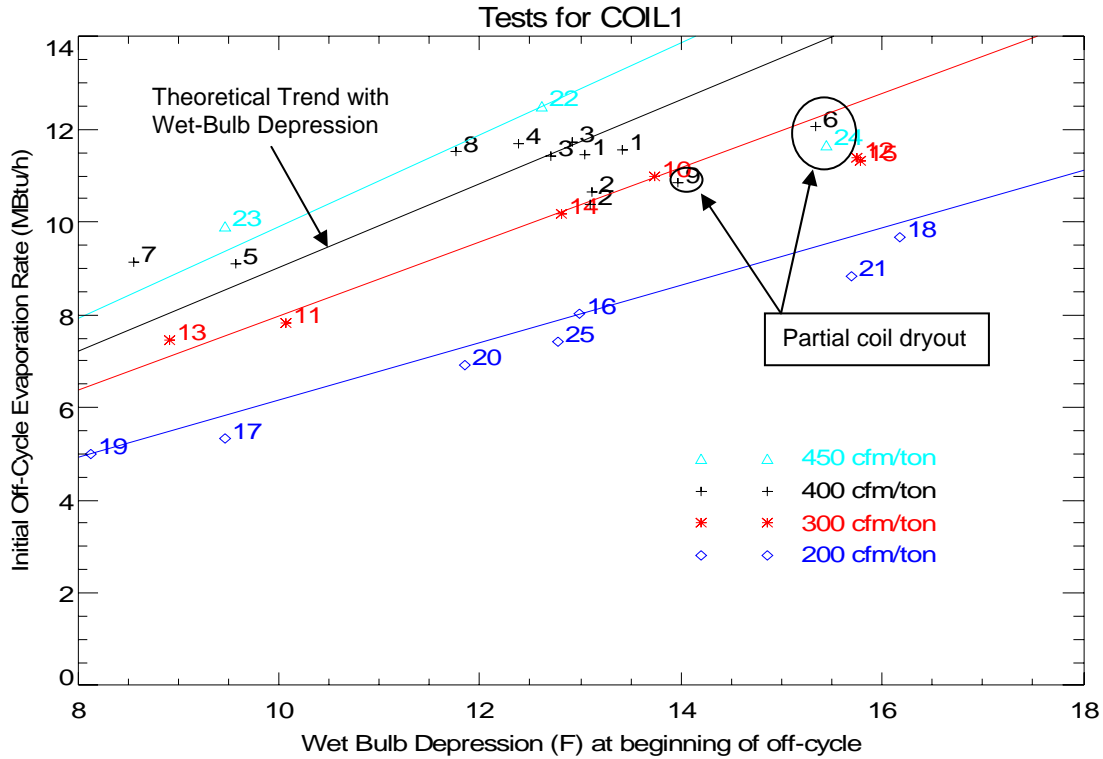
**Figure 3-16. Impact of Dew Point and Coil Wettedness on Condensate Delay Time, Coil 1**

Figure 3-17 shows that the initial off-cycle moisture evaporation rate varies with wet-bulb depression. As expected, the evaporation rate increases as the entering air wet-bulb depression increases (i.e., entering air dry-bulb temperature minus wet-bulb temperature) and as air flow rates increase.

The latent degradation model developed by Henderson and Rengarajan (1996) used the following simple evaporative cooler model to predict the moisture evaporation rate at off-design conditions:

$$q_{evap} = q_{evap_o} \frac{(DB - WB)}{(80 - 67)}$$

where  $q_{evap_o}$  is the evaporation rate at the nominal entering air conditions of 80°F dry bulb (DB) and 67°F wet bulb (WB). This simple model is shown as the lines in Figure 3-17. For each air flow rate, the line is based on the nominal test results at 80°F DB/67°F WB extended to pass through zero. The measured data show essentially the same slope as the theoretical lines. The notable exceptions are the points with higher airflow and drier entering conditions (e.g., runs 6, 9 and 24). These runs have a much lower initial moisture evaporation rate because the entering air dew point temperature was close to the cooling coil temperature, so the fin surfaces were not fully wetted. The smaller wetted surface area reduces the initial moisture evaporation rate. The results for the other six DX coils were similar to those shown here for coil 1. The results for the chilled water coil (coil 8) showed more deviation from the theoretical trends (because the entire surface was rarely fully wetted).



**Figure 3-17. Measured Variation of Initial Evaporation Rate with Wet-Bulb Depression, Coil 1**

Stabat et al. (2001) reviewed the theoretical performance of direct evaporative coolers and showed that the saturation effectiveness of an evaporative cooler is:

$$\eta_{evp} = 1 - e^{-NTU} \quad \text{where} \quad NTU = K/cfm^{0.2} \quad \text{for an air-water mixture.}$$

The line shown on Figure 3-18 is the best fit for the equation above to the measured data for coil 1. The resulting constant K was 5.76, which is equivalent to an NTU of 1.40 at 1,200 cfm. The resulting K constants and NTU values for all eight coils are used later for model validation (see Section 5.2). While there is considerable scatter due to the experimental uncertainty of predicting the initial off-cycle moisture evaporation rate, the slope of the line is still fairly representative of the overall trend (this was true for all eight test coils).

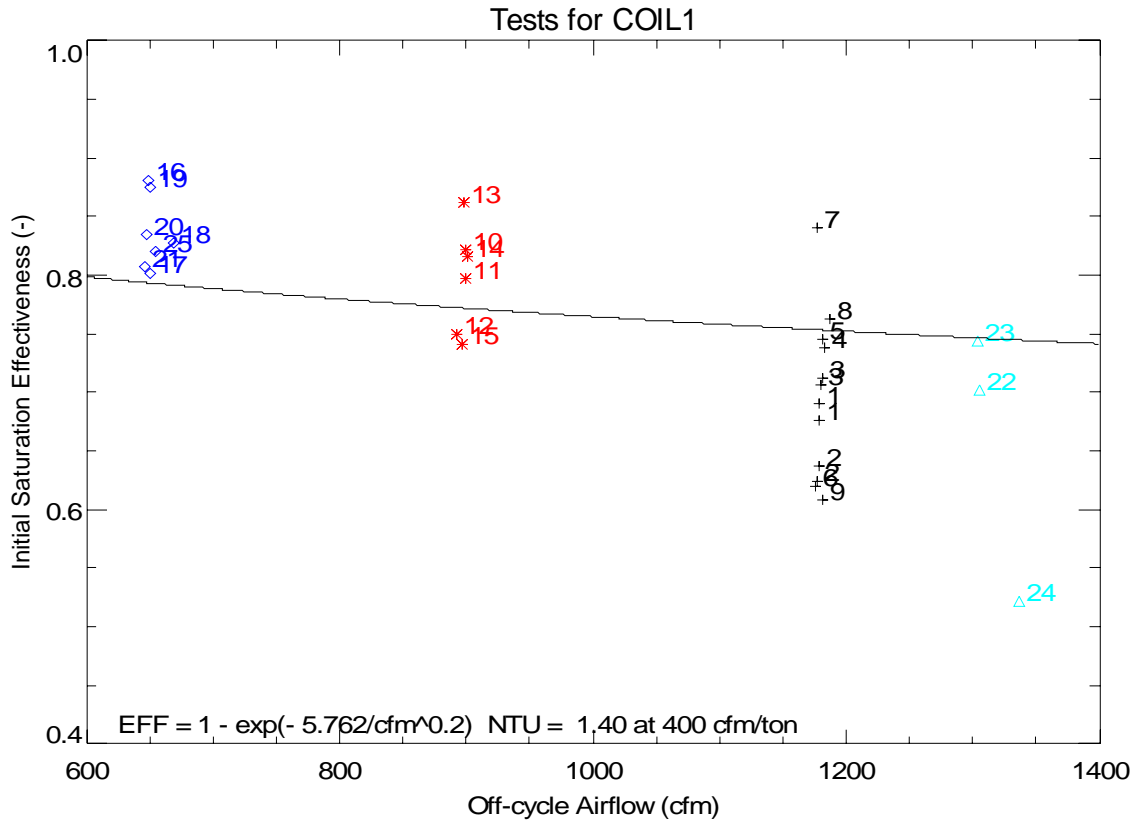


**Figure 3-18. Evaporative Effectiveness Versus Airflow for Coil 1**

Figure 3-19 compares the measured initial off-cycle moisture evaporation rate for each coil 1 test to the predicted initial evaporation rate using the effectiveness model above. The model and measured data generally agree when presented in this form (i.e., the overall agreement visually appears better than in Figure 3-18 above). Again, the variation that occurs for runs 6, 9, and 24 was due to partial coil dryout. The results for the other six DX coils were very similar to those shown here for coil 1. The results for the chilled water coil (coil 8) were similar but showed greater variations for more tests (see Appendix H).

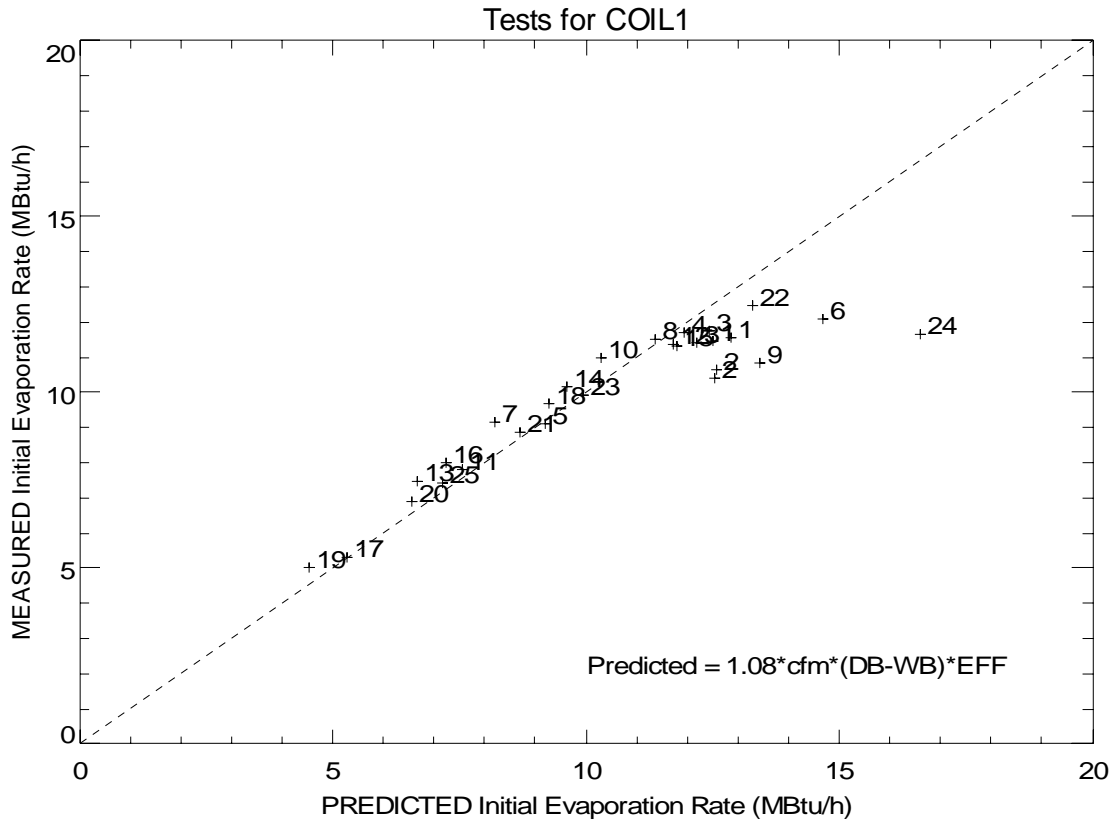


**Figure 3-19. Comparing Measured and Predicted Initial Moisture Evaporation Rates**

Figure 3-20 shows the impact of entering air humidity and air flow rate on the amount of moisture retained on cooling coil 1. At higher entering dew point temperatures, the moisture holding capacity of the coil approaches the equilibrium value (approximately 2 lbs [0.9 kg] for coil 1). The greater scatter and magnitude at lower dew points may be due to the fact that integration of the off-cycle evaporation rate includes the error associated with integrating the “tail” of the profile. Also, the lower retained moisture values for runs 6, 9 and 24 are due to partial coil dryout at the lower entering air dew point conditions.

The trends shown in Figure 3-20 for coil 1 were not consistent with the results for the other coils. Figure 3-21 and Figure 3-22 show the impact of entering air humidity on moisture retention for all test coils with airflow of 400 cfm/ton (0.054 m<sup>3</sup>/s•kW) and 300 cfm/ton (0.034 m<sup>3</sup>/s•kW), respectively. Some coils (e.g., coil 5) show a slight decrease in moisture retention with increasing inlet air dew point temperature, while others show either very little variation (coil 4) or a slight increase (e.g., coil 2 and coil 3). The chilled water coil (coil 8) showed the greatest dependence of retained moisture on entering air dew point temperature. This strong impact of dew point temperature implies that the chilled water coil is not fully wetted until very high inlet air dew points are reached, which makes sense given that the water temperature continuously increases as it travels through the coil (i.e., temperature glide). In contrast a large portion of the DX coil is at or near the saturated suction temperature.

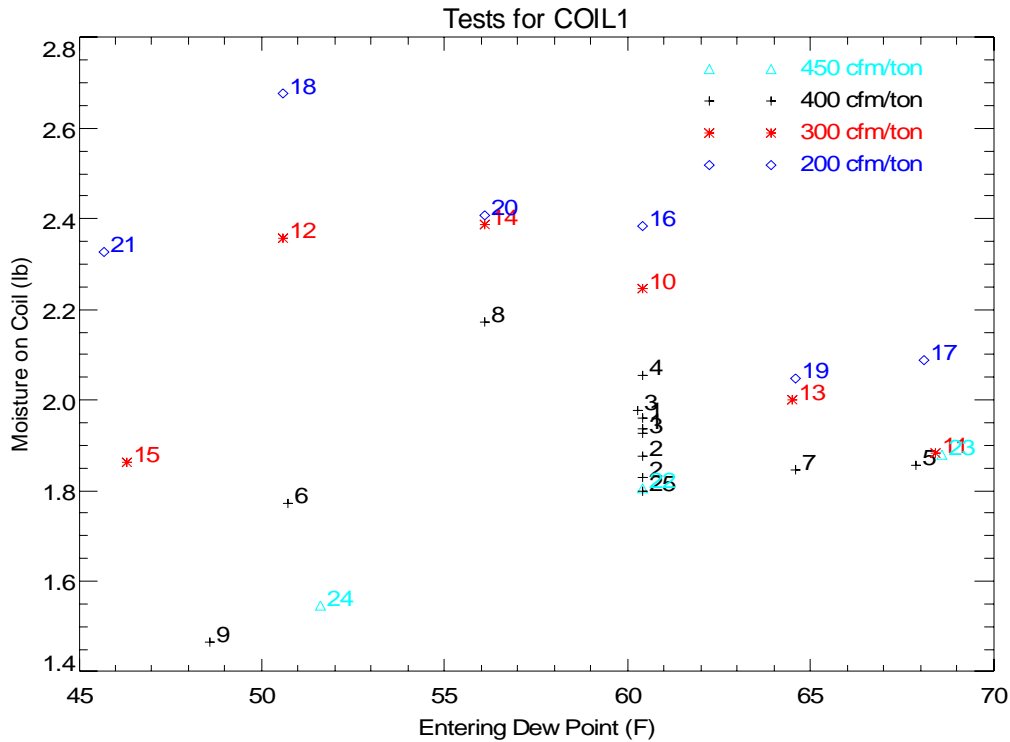


Figure 3-20. Variation of Retained Moisture (Based on Off-Cycle Sensible) with Flow and Dew Point, Coil 1

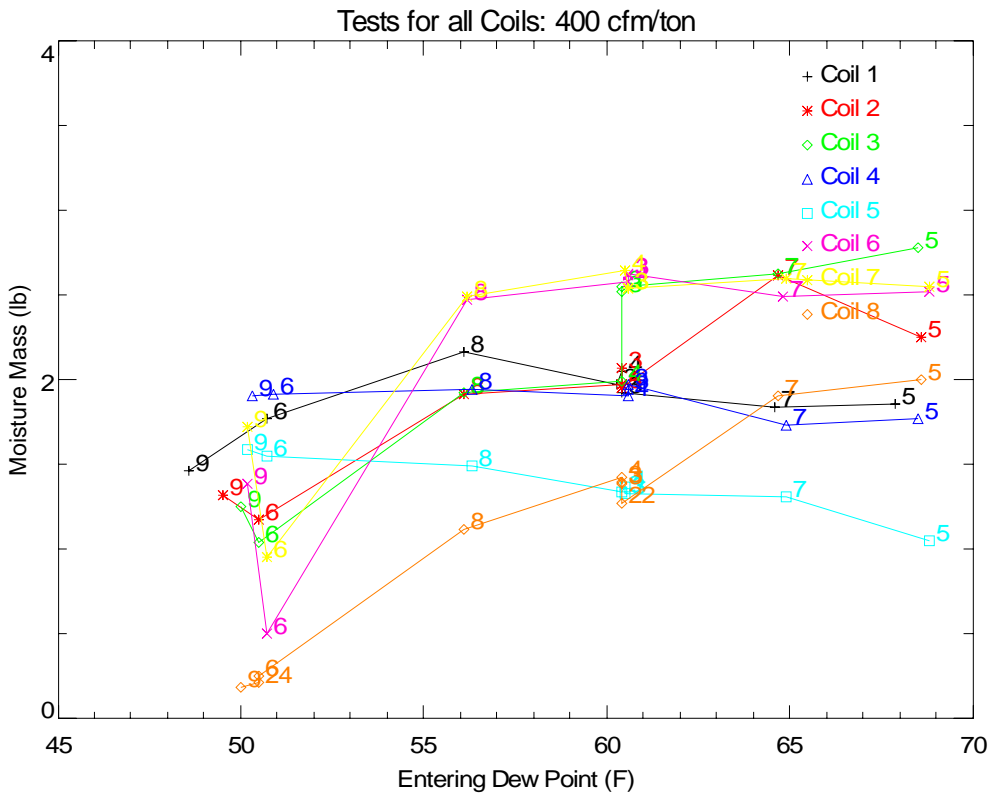
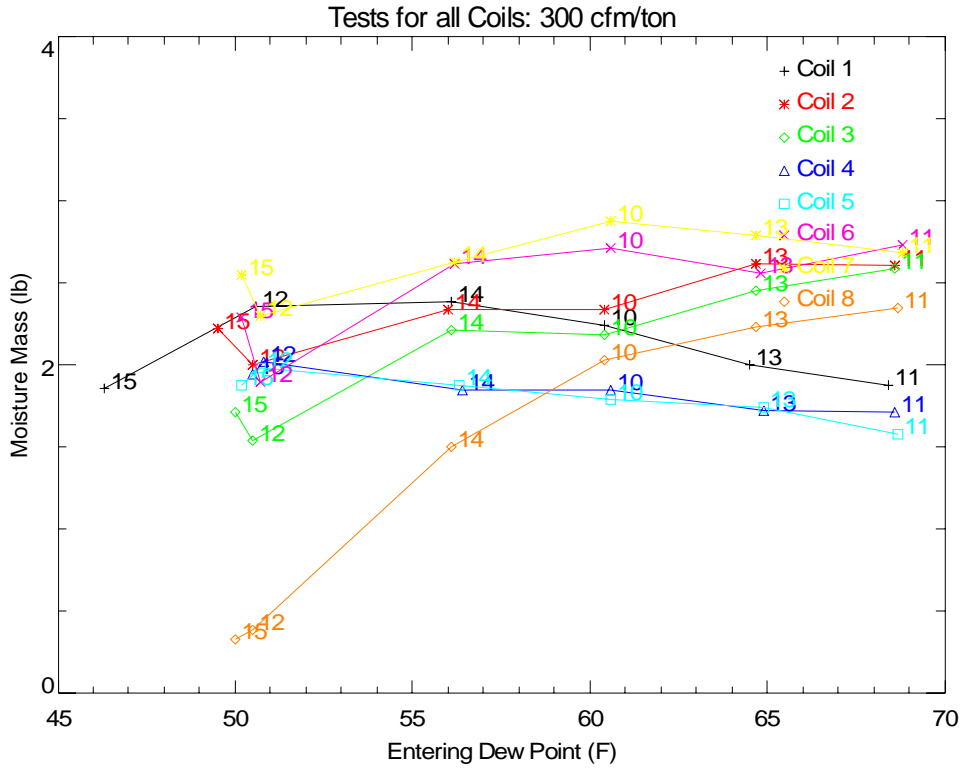


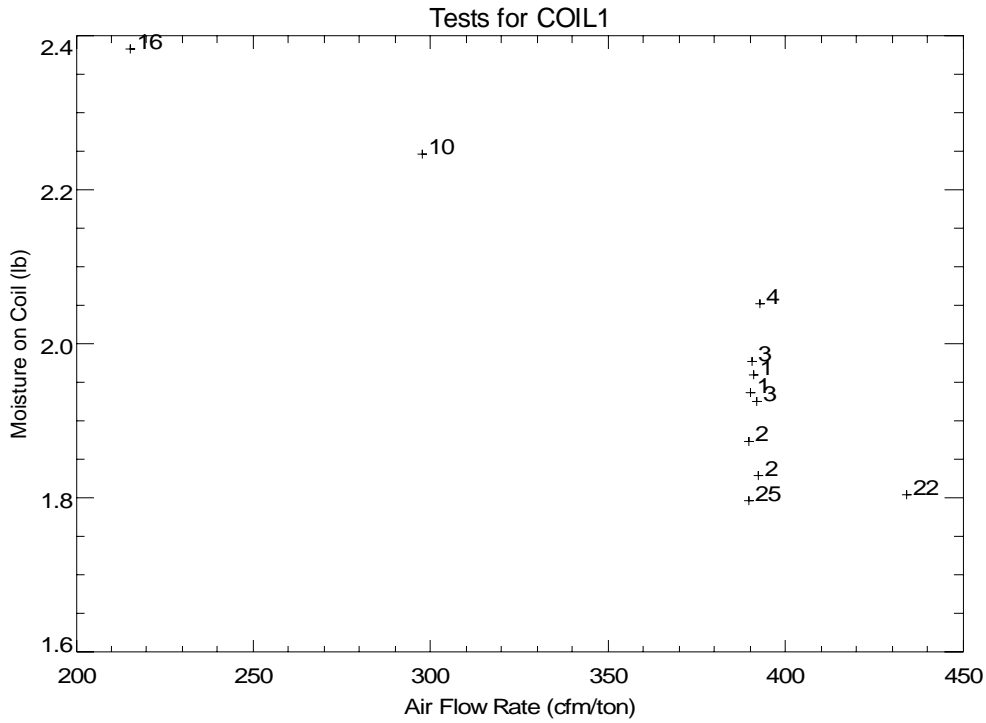
Figure 3-21. Variation of Retained Moisture with Dew Point at 400 cfm/ton, All Coils



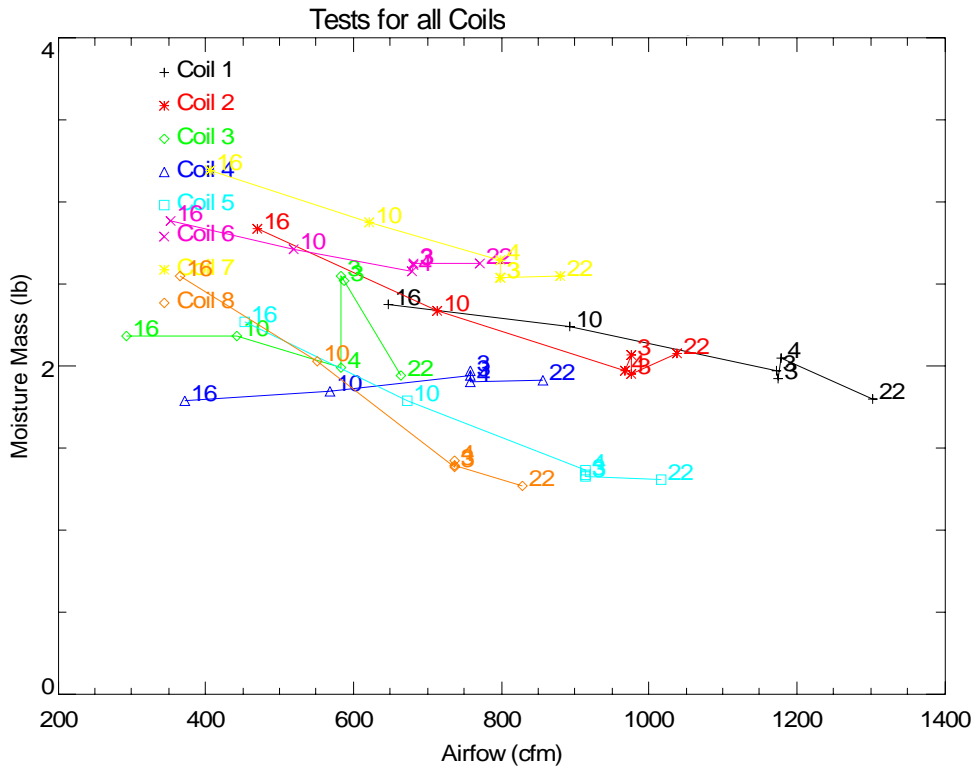
**Figure 3-22. Variation of Retained Moisture with Dew Point at 300 cfm/ton, All Coils**

Figure 3-23 shows a 10-20% decrease in the amount of retained moisture on coil 1 with higher air flow rates. The same general trend was seen for the other coils as shown in Figure 3-24, although the percentage decrease varied by coil. The one exception was coil 4 which showed a modest increase in retained moisture with higher air flow rates. Coil 4 had significant refrigerant distribution problems which may have contributed to this unexpected trend.





**Figure 3-23. Variation of Retained Moisture with Air Flow at Nominal Entering Air Conditions of 80°F dry bulb, 60.4°F dew point, Coil 1**



**Figure 3-24. Variation of Retained Moisture with Air Flow at Nominal Entering Air Conditions of 80°F dry bulb, 60.4°F dew point, All Coils**

Another way to detect the amount of retained moisture is to measure the static air-side pressure drop across the cooling coil. The difference between the pressure drop across the coil under wet and dry conditions can provide an indication of the amount of retained moisture (the wet coil pressure drop is measured at steady-state conditions while the dry coil pressure drop is taken as the average pressure drop during the last part of the off cycle). Figure 3-25 shows the variation of the wet-dry pressure difference for coil 1 with various entering air dew point temperatures at multiple air flow rates. Comparing the values for each air flow rate generally shows a trend of pressure drops reaching a plateau once the humidity of the entering air is sufficiently high to fully wet the coil.

The variation of wet-dry pressure difference with entering air dew point temperature was similar for most of the other test coils. Notable exceptions were coil 4 which showed virtually no variation, and coil 5 which showed a slight decrease in wet-dry pressure difference over the range of inlet air dew point temperatures. The results for coil 8, the chilled water coil, showed that moisture retention was a very strong function of the entering air dew point temperature, particularly at the higher air flow rates of 400 cfm/ton (0.054 m<sup>3</sup>/s•kW) and 450 cfm/ton (0.061 m<sup>3</sup>/s•kW).

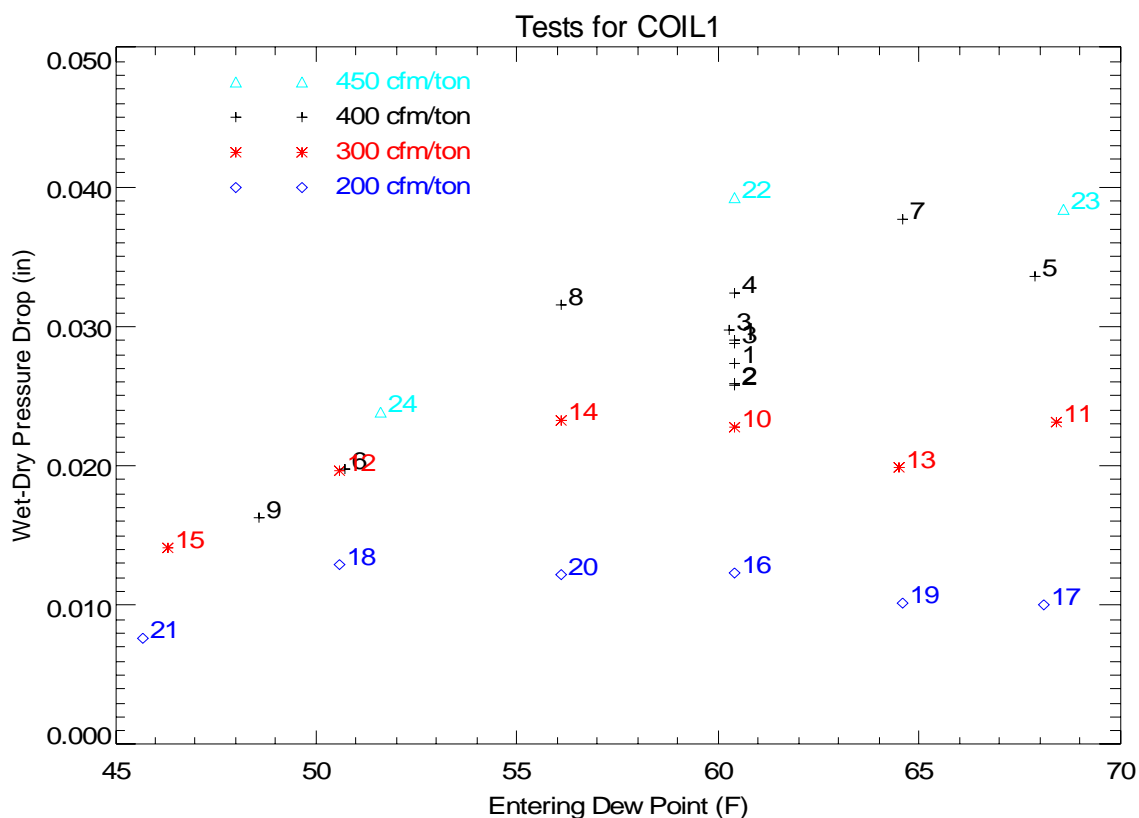


**Figure 3-25. Variation of Wet-Dry Pressure Drop with Entering Conditions and Air Flow Rate for Coil 1**

Figure 3-26 confirms that the wet-dry pressure drop is nearly a linear function of air flow rate, which implies laminar flow in the wetted cooling coil. The trend shown here for coil 1 was seen

for all test coils. The impact of air flow on wet-dry pressure drop was greatest for the 4-row chilled water coil (coil 8).

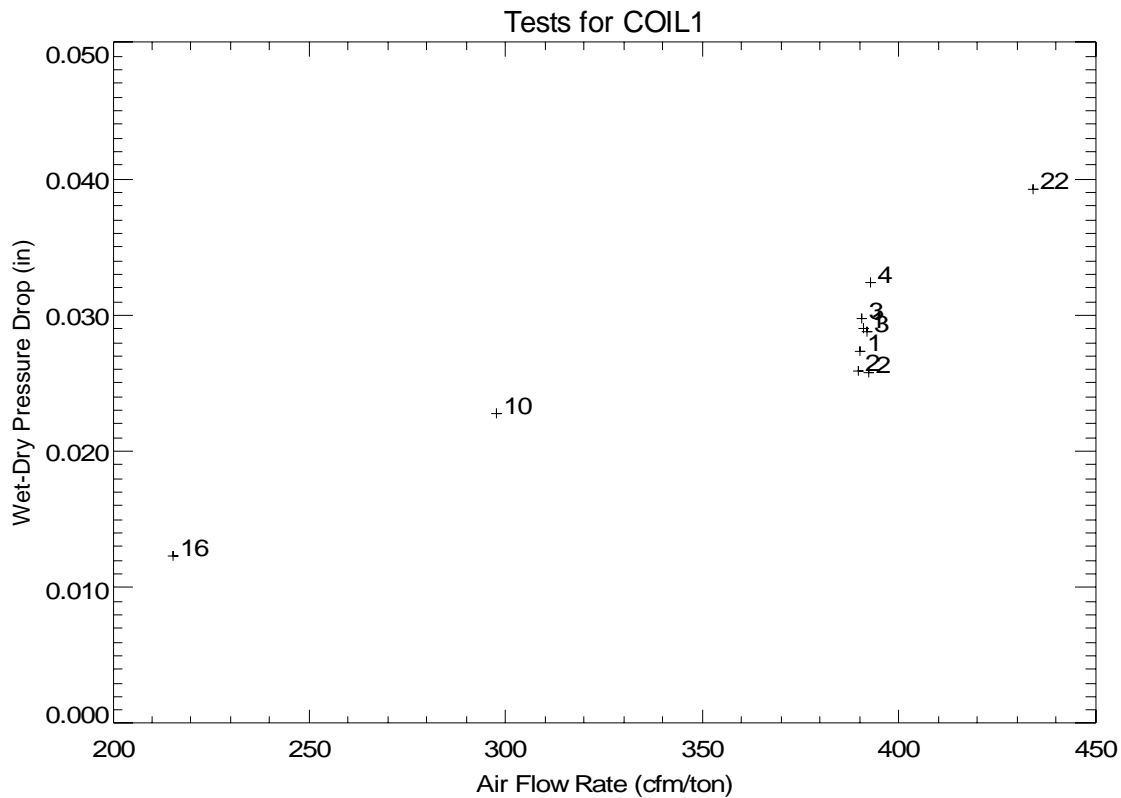


**Figure 3-26. Trend of Wet-Dry Pressure Drop with Flow at Nominal Entering Conditions of 80°F, 60.4°F dew point for Coil 1**

The series of plots in Figure 3-27 were developed using the results from runs 1-3 to determine the impact of coil temperature (saturated suction temperature for the DX coils and water inlet temperature for the chilled water coil) on latent cooling performance and moisture retention. All tests were run at the same nominal air flow (400 cfm/ton, 0.054 m<sup>3</sup>/s•kW) and entering air conditions (80°F [26.7°C] dry bulb, 60.4°F [15.8°C] dew point). The plots in Figure 3-27 for steady-state sensible heat ratio and steady-state latent capacity show the expected trend of increased dehumidification performance with a colder coil. This trend was consistent for all test coils, as shown in Figure 3-28 and Figure 3-29.

In Figure 3-27, the trends for coil 1 related to moisture retention on the coil and wet-dry pressure drop both confirm that more moisture is retained when this coil is colder (i.e., lower saturated suction temperature). However, this trend was not consistent for all test coils. Figure 3-30 shows the variation of moisture retention with coil temperature for all test coils. While coils 1, 3, 6, 7 and 8 showed the expected trend of reduced moisture retention with warmer coil temperature, coils 4 and 5 showed the opposite trend and coil 2 showed no clear trend at all. The reason for the unexpected results is not known.

Figure 3-31 shows the relationship between wet-dry pressure drop and the amount of retained moisture for the different coil temperatures. The results generally show that the increase in

moisture mass is corroborated by the increase in air-side pressure drop. Figure 3-32 attempts to normalize the trends. Generally the coils with fewer fins per inch and more rows (e.g., coil 8 and coil 5) tend to show more static pressure variation on a percentage basis.

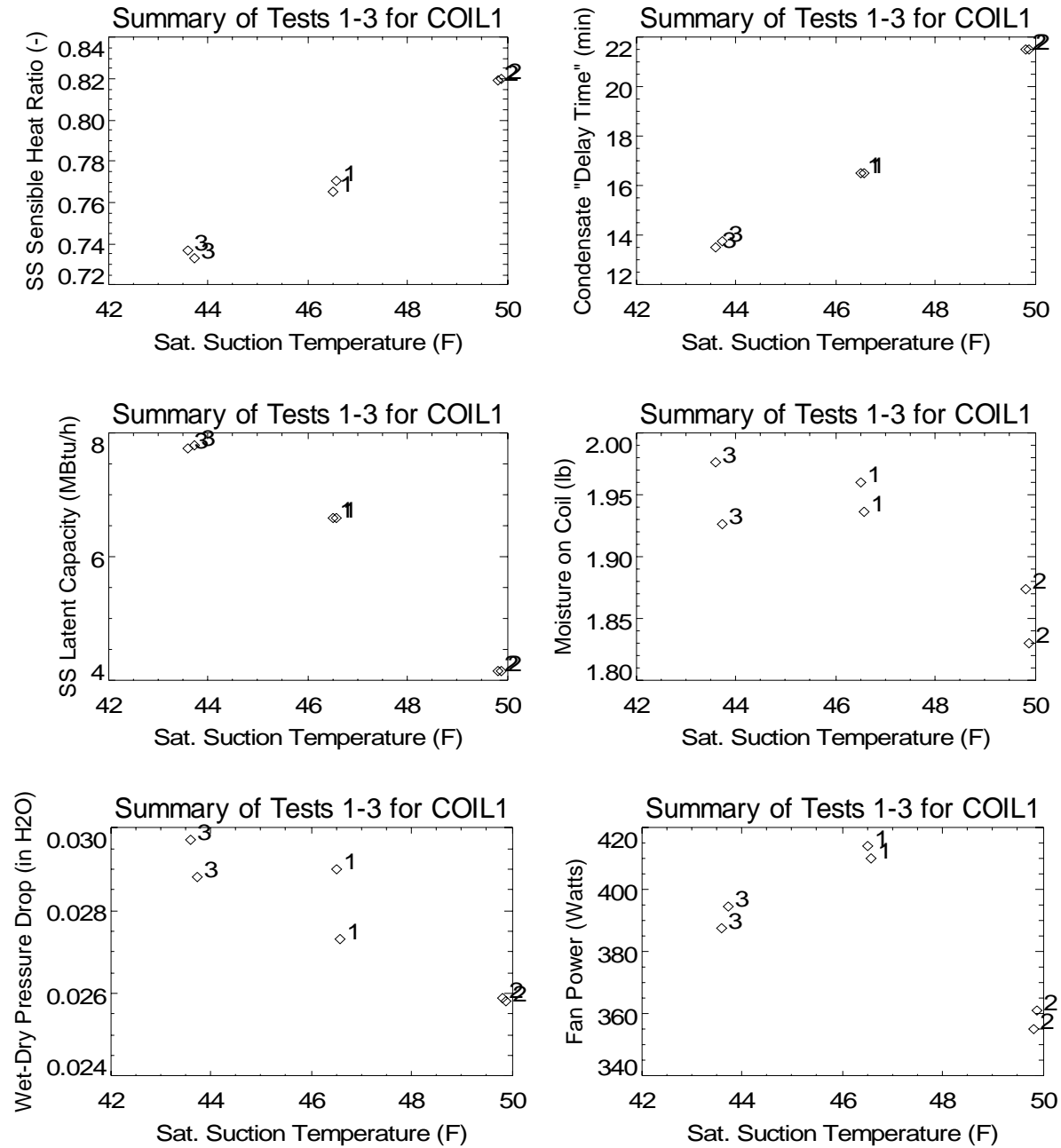


**Figure 3-27. Trend of Various Parameters with Saturated Suction Temperature for Coil 1**

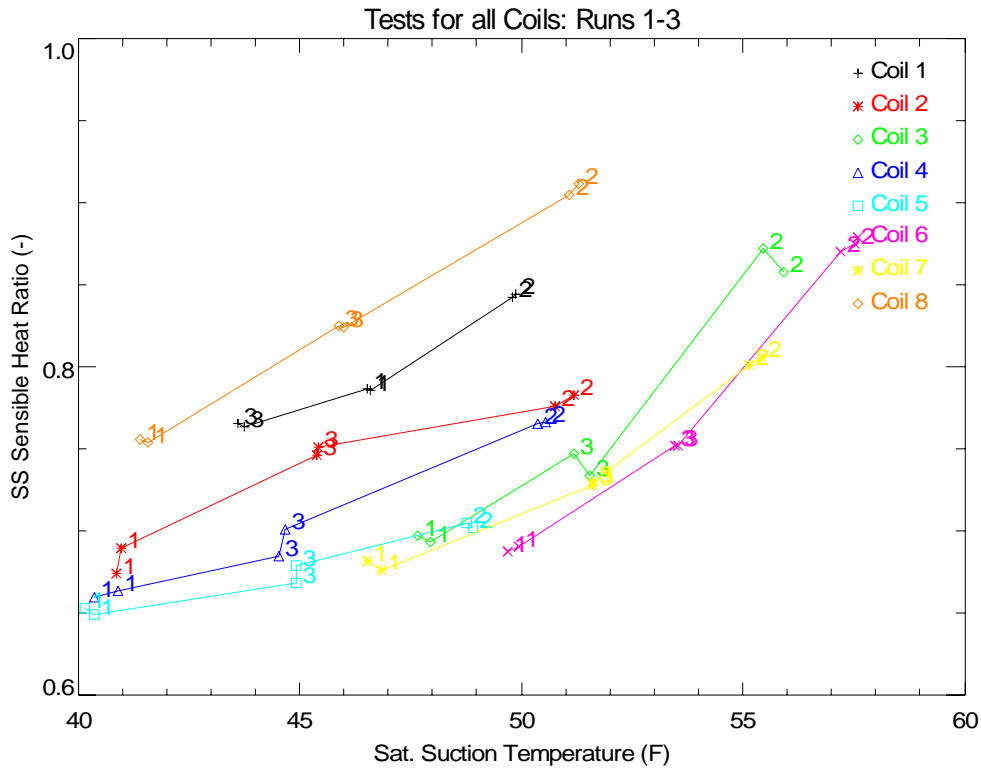


Figure 3-28. Trend of Steady-State Sensible Heat Ratio with Coil Temperature for All Coils

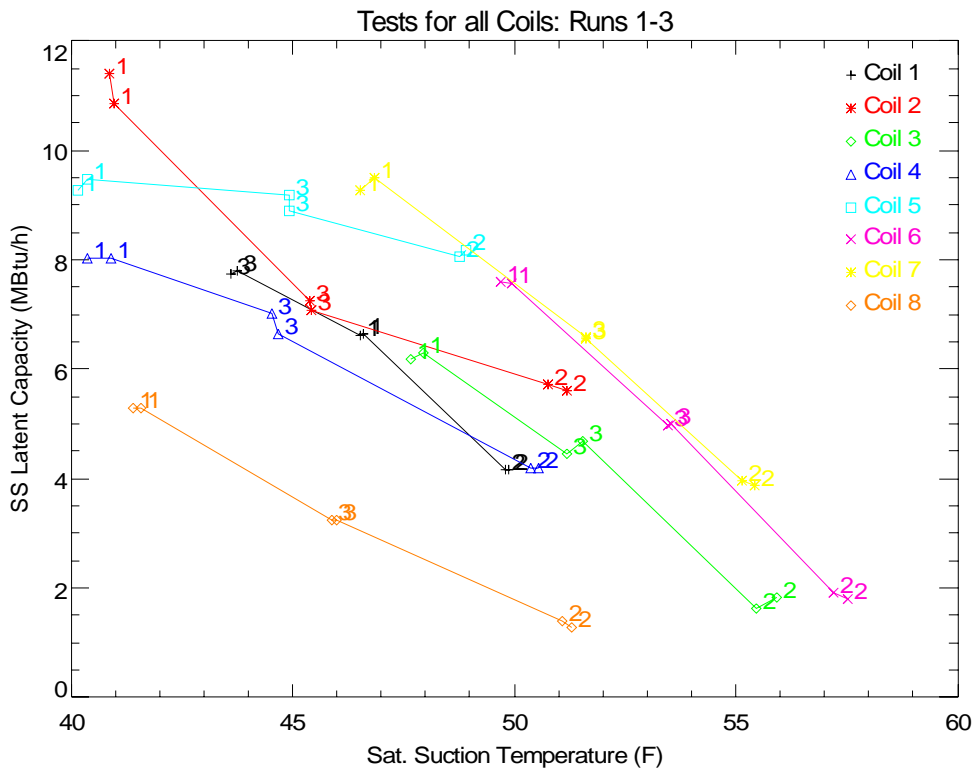


Figure 3-29. Trend of Steady-State Latent Capacity with Coil Temperature for All Coils

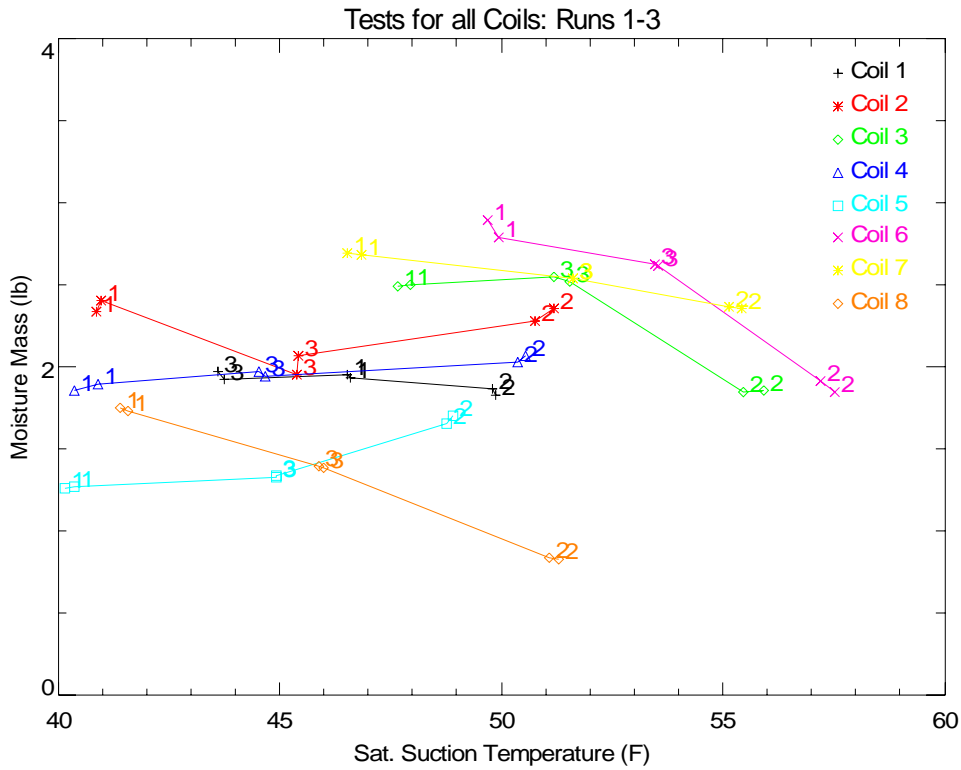


Figure 3-30. Variation in Moisture Retention with Coil Temperature, All Coils

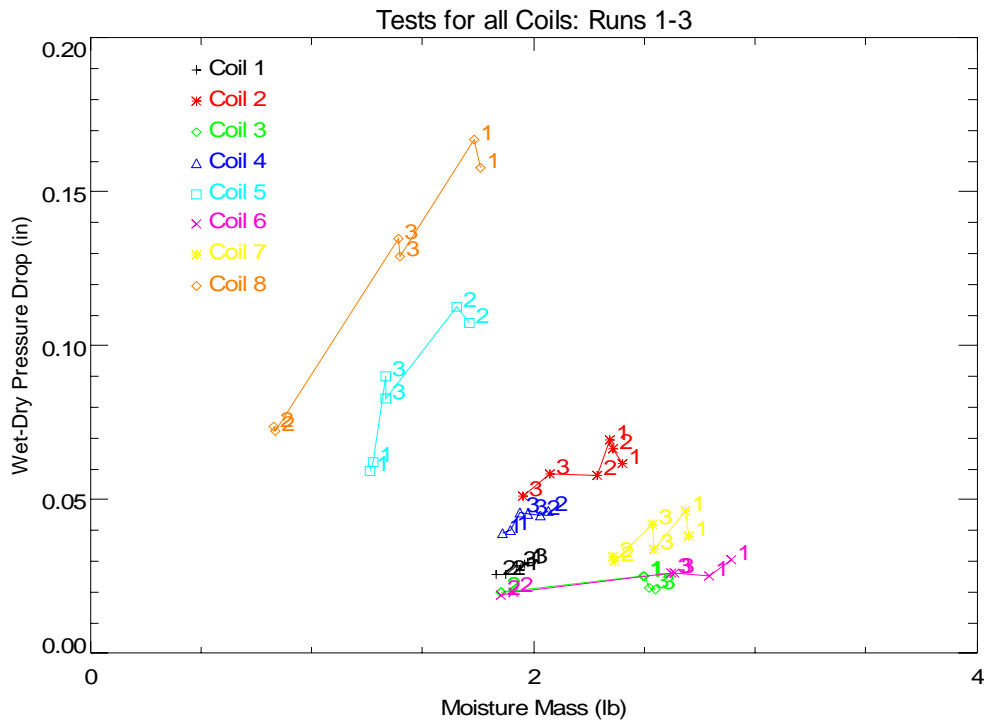
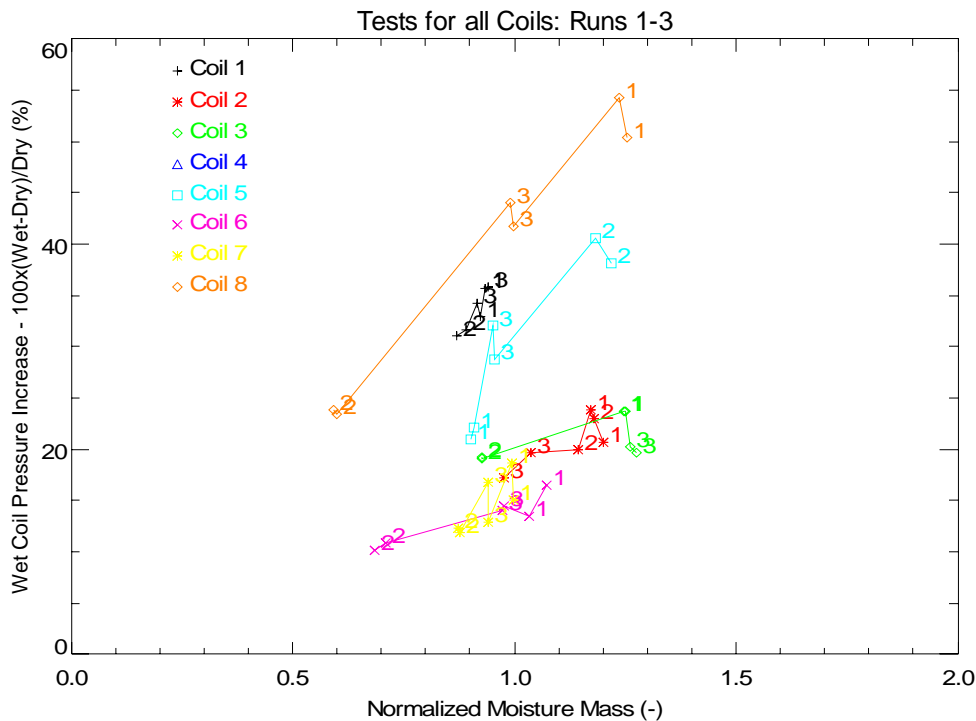


Figure 3-31. Variation of Wet-Dry Pressure Drop with Moisture Retention, All Coils



**Figure 3-32. Normalized Wet-Dry Pressure Drop with Normalized Moisture Mass, All Coils**

One of the laboratory tests (run 25) maintained the airflow at 400 cfm per ton ( $0.054 \text{ m}^3/\text{s}\cdot\text{kW}$ ) during the coil on cycle, but decreased the airflow to 200 cfm per ton ( $0.027 \text{ m}^3/\text{s}\cdot\text{kW}$ ) during the coil off cycle. This test was completed to check the assumption that the off-cycle evaporation process should be the same regardless of what happened during the previous on cycle. Figure 3-33 and Figure 3-34 compare the off-cycle sensible cooling capacity for run 25 to the off-cycle sensible capacity for run 16, which maintained 200 cfm per ton for the entire on/off cycle.

The plots show that while the initial evaporation rates (indicated by the sensible cooling provided) are similar, the shape of the curve and the total amount of moisture evaporated are different. Run 16, which ran at 200 cfm per ton during the on cycle, typically accumulated more moisture on the coil. As a result the evaporation rate for run 16 remains higher in the middle of the evaporation process than run 25. The amount of moisture on the coil for run 25 is in better agreement with the nominal  $M_o$  (which was also determined at 400 cfm per ton during the on and off cycle) than the amount of retained moisture for run 16. The one exception was coil 4 (Figure 3-33) which showed very similar results for both runs. These results are consistent with results shown in Figure 3-24 that show more moisture typically accumulates on a coil at lower airflow rates.

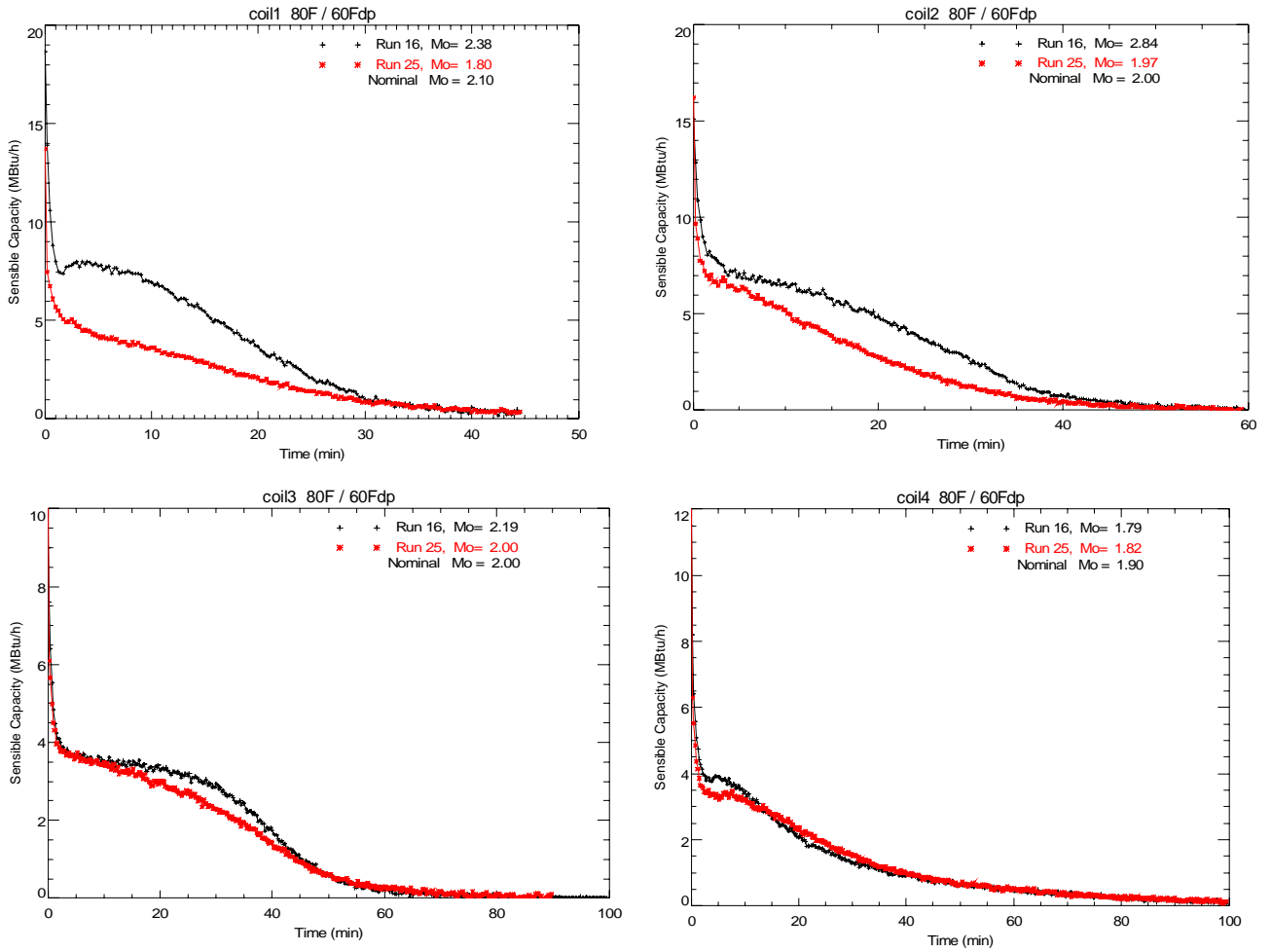


**Figure 3-33. Off-Cycle Sensible Capacity for Runs 16 and 25: Coils 1-4**



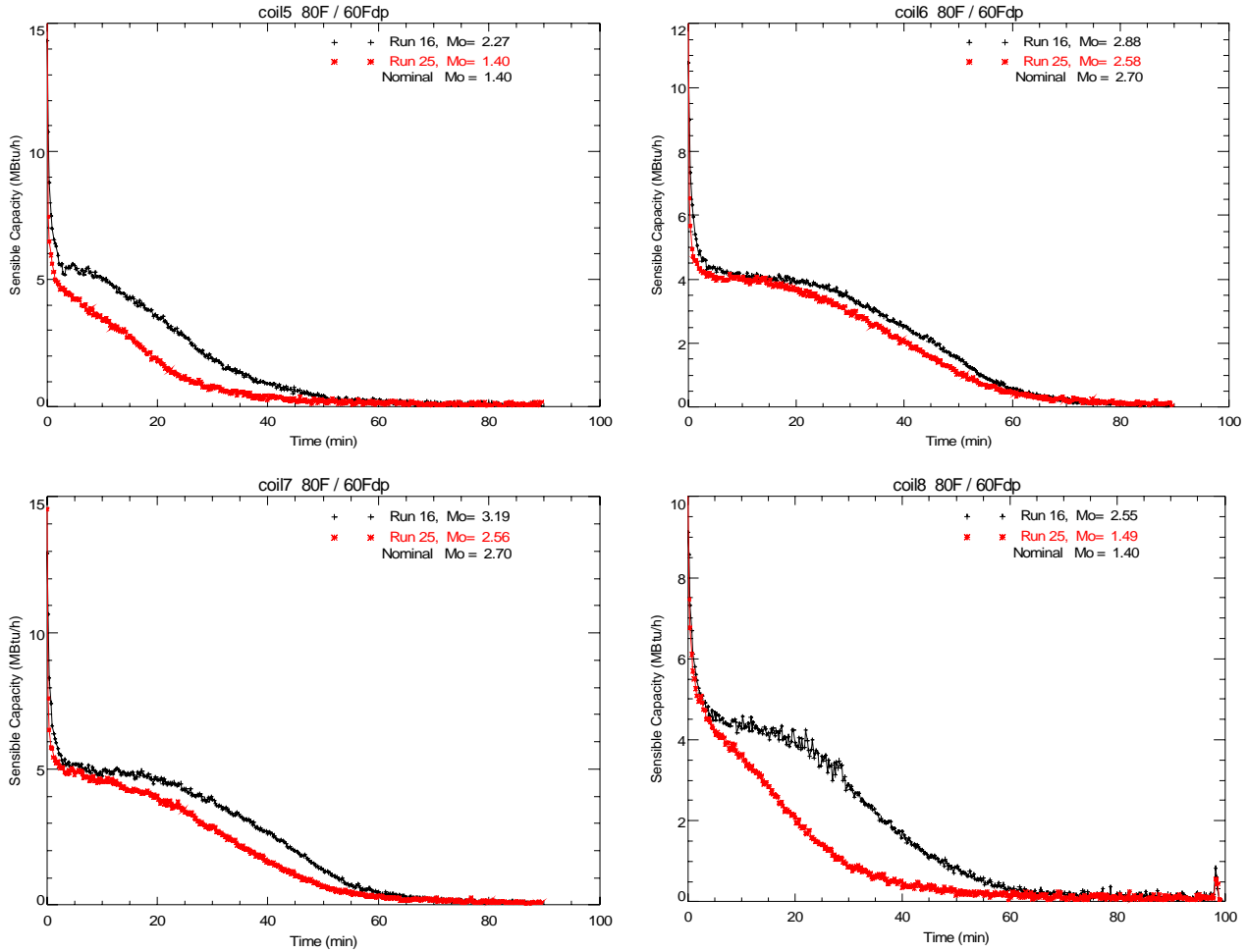


**Figure 3-34. Off-Cycle Sensible Capacity for Runs 16 and 25: Coils 5-8**

### 3.4.2 Cyclic Tests

In addition to the steady-state tests, a series of quasi-steady cyclic tests was also completed to quantify the overall part-load degradation of latent capacity. As explained previously in Section 3.3 these tests were completed for each coil with differing lengths of coil on and off times, which were selected to correspond with the NEMA thermostat curve with a maximum cycle rate of 3 cycles per hour at 50% duty cycle (NEMA 1990). The test results were used to validate latent degradation engineering models (see Section 5.5).

The series of cyclic tests was performed on coil 1 with nominal air flow (400 cfm/ton, 0.054 m<sup>3</sup>/s·kW) and nominal entering air conditions (80°F [26.7°C] dry-bulb, 60.4°F [15.8°C] dew point). The tests were conducted with the fan continuously providing air flow over the cooling coil (CONST) and also with the fan cycling on and off in tandem with the cooling coil (AUTO). Each test was repeated multiple times to reach quasi-steady state conditions (Table 3-6).

For coils 2 through 8, these same tests described above were conducted and additional tests were performed at other operating conditions with continuous fan operation:

- Tests 51-55, inlet air conditions of 75°F dry bulb/64°F dewpoint (23.9°C/17.8°C) with air flow at 400 cfm/ton (0.054 m<sup>3</sup>/s•kW),
- Tests 61-65, inlet air conditions of 75°F dry bulb/56°F dewpoint (23.9°C/13.3°C) with air flow at 400 cfm/ton (0.054 m<sup>3</sup>/s•kW),
- Tests 71-75, original inlet air conditions (80°F dry bulb/60.4°F dewpoint [26.7°C/15.8°C]) but at a reduced air flow rate of 300 cfm/ton (0.041 m<sup>3</sup>/s•kW).

The additional tests provided data that allowed the engineering models to be validated over a wider range of operating conditions.

Figure 3-35 shows the net impact of part-load operation on the dehumidification performance of coil 1 with continuous supply air fan operation. The “effective” sensible heat ratio is plotted as a function of cooling coil runtime fraction. The delivered sensible capacity is obtained using the integrated dry-bulb temperature difference across the cooling coil and air flow rate for the entire on/off cycle, while the latent capacity is obtained by measuring the moisture removed at the condensate drain (measured using the rain gauge tipping bucket). The sensible heat ratio is the delivered sensible capacity divided by the total (sensible plus latent) capacity for the on/off cycle. As mentioned previously, each test was repeated several times to reach quasi-steady state conditions, and the symbols in the figure denote the test results for each cycle (repetition) for a given coil runtime fraction. Note that the results for the 2<sup>nd</sup> and 3<sup>rd</sup> cycle for each runtime fraction show good agreement, indicating quasi-steady state had been reached.

The results for these tests were used to validate latent degradation engineering models. Figure 3-35 shows the results for various models (solid and dotted lines), which are in good agreement with the measured data (diamond, star and triangle symbols). The engineering models and the model validation efforts are thoroughly discussed in Section 5.

Figure 3-36 shows that some latent degradation can be detected in the AUTO fan mode as well (i.e., when the supply air flow across the cooling coil starts and stops with compressor operation). The sensible heat ratio is again plotted as a function of coil runtime fraction, and the sensible and latent capacity for the entire coil on/off cycle are calculated in the same way as they were for Figure 3-35. In Figure 3-36, the symbols again represent the test results for each on/off cycle for a given coil runtime fraction and the results for the 2<sup>nd</sup> and 3<sup>rd</sup> cycle show good agreement. The lines in Figure 3-36 do not represent the engineering models, but are simply lines drawn point-to-point for the 2<sup>nd</sup> and 3<sup>rd</sup> cycle to allow the trend to be more easily observed. The development and validation of a new engineering model to account for latent performance degradation with AUTO fan operation are summarized in Sections 5.4 and 5.5.2, respectively.

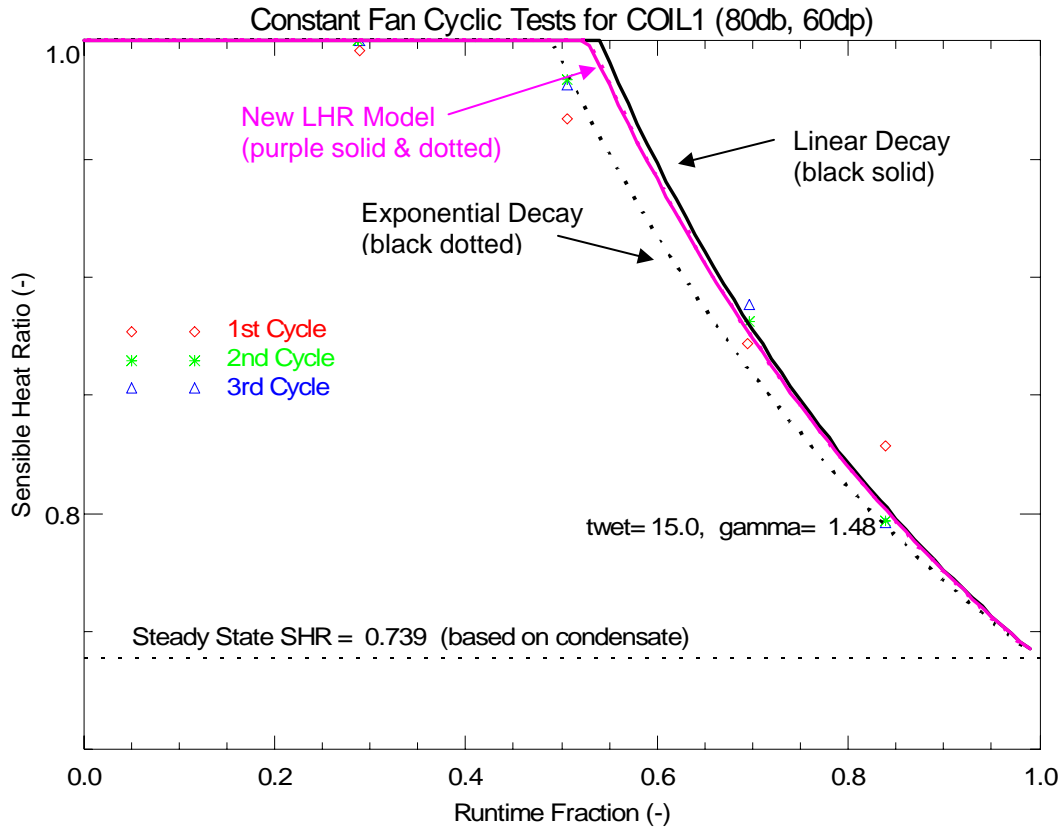


Figure 3-35. Comparing Measured Latent Degradation to the LHR Models for Coil 1

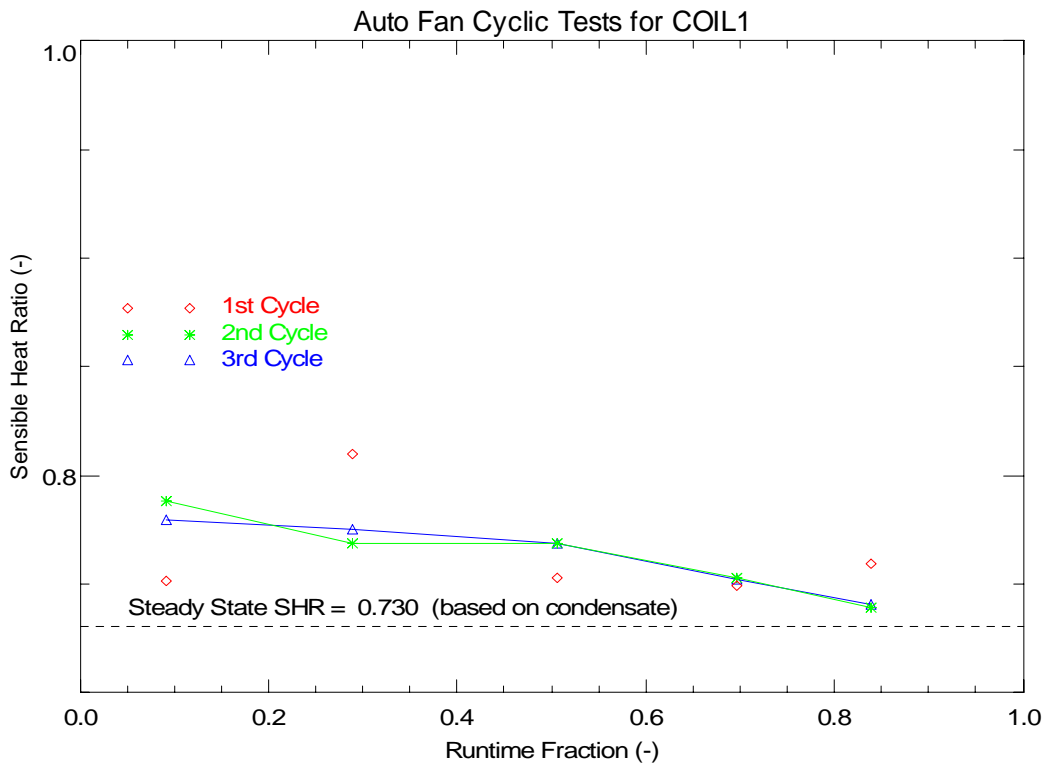


Figure 3-36. Measured AUTO Fan Latent Degradation for Coil 1

### **3.5 Cyclic Tests with Fan Delay**

In addition to the standardized tests performed on all coils as described in Section 3.4, additional tests were performed on two of the coils with alternate fan control schemes implemented. A series of cyclic tests was performed on coil 2 to help assess the impact of fan overrun (fan operation for 90 seconds after the cooling coil turns off) on latent removal. The test results are presented below. A detailed analysis of how fan overrun strategies affect the SEER calculation procedure is also given in Appendix F. A model for predicting the impact of fan overrun on part-load dehumidification performance is described later in Section 5.4.

Test data were also collected for coil 8 with a type of fan delay scheme that shuts the fan off for a fixed period immediately after a cooling cycle. This type of fan shutdown is often claimed to allow the moisture on the coil to “drain down” before fan operation resumes. Data for this series of tests are presented in Section 3.5.2, and a model for predicting the impact of this fan delay scheme is described in Section 5.4.

#### **3.5.1 Fan Overrun Delay**

Figure 3-37 shows test data for the 3<sup>rd</sup> quasi-steady cycle for coil 2 with the compressor running for 6 minutes and off for 24 minutes (20% runtime fraction). This test is similar to Test D<sup>2</sup> that is required for the SEER test procedure (ARI 2005) except coil 2 is wet (Test D specifies dry-coil conditions). In this case the fan cycles on and off with the compressor (AUTO fan). Figure 3-38 shows similar data for a cycle where the fan ran for an additional 1.5 minutes after the end of the cooling cycle. The condensate collected over an on-off cycle was 0.578 lbs with no fan overrun delay (Figure 3-37) and 0.322 lb with a 1.5-minute fan overrun delay (Figure 3-38). So the fan delay degraded the effective latent capacity of the unit by 44%. Clearly even a modest fan overrun delay degrades latent removal at these conditions.

---

<sup>2</sup> This test was slightly different from Test D in that dampers were not installed on both sides of the coil to absolutely stop air flow through the coil during the off-cycle. Instead, a sheet metal cover was placed over the return air opening during the off-cycle to minimize (or stop) air flow.

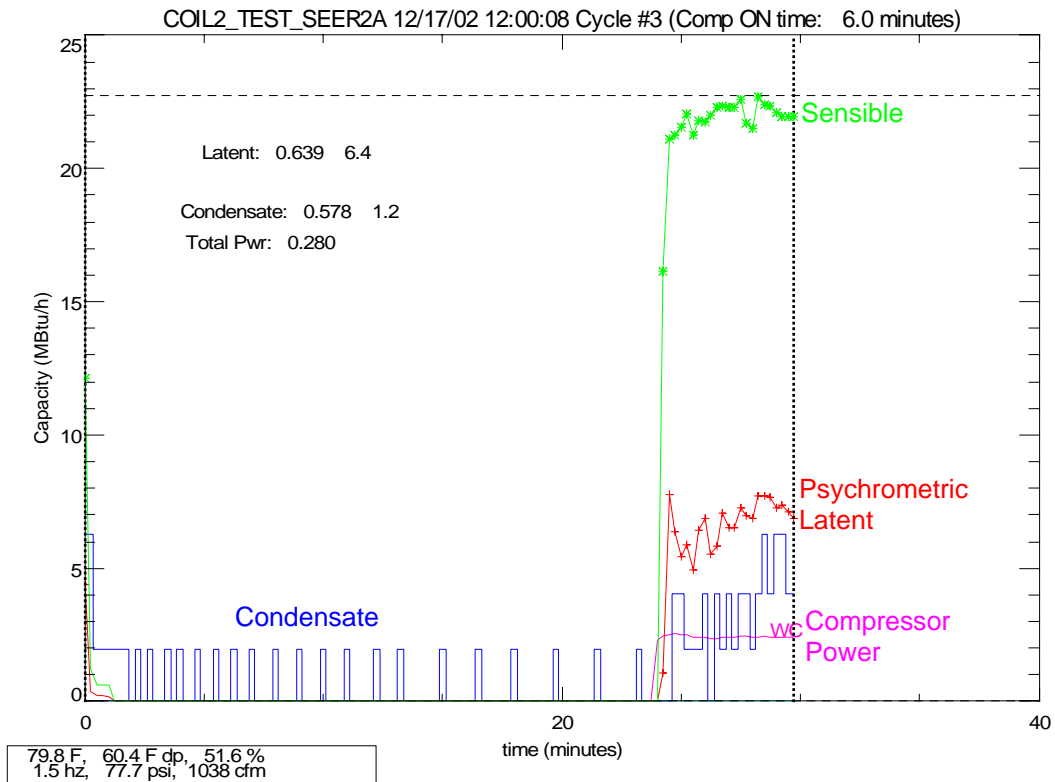


Figure 3-37. Test Results for Coil 2 with NO Fan Overrun Delay (AUTO Fan)

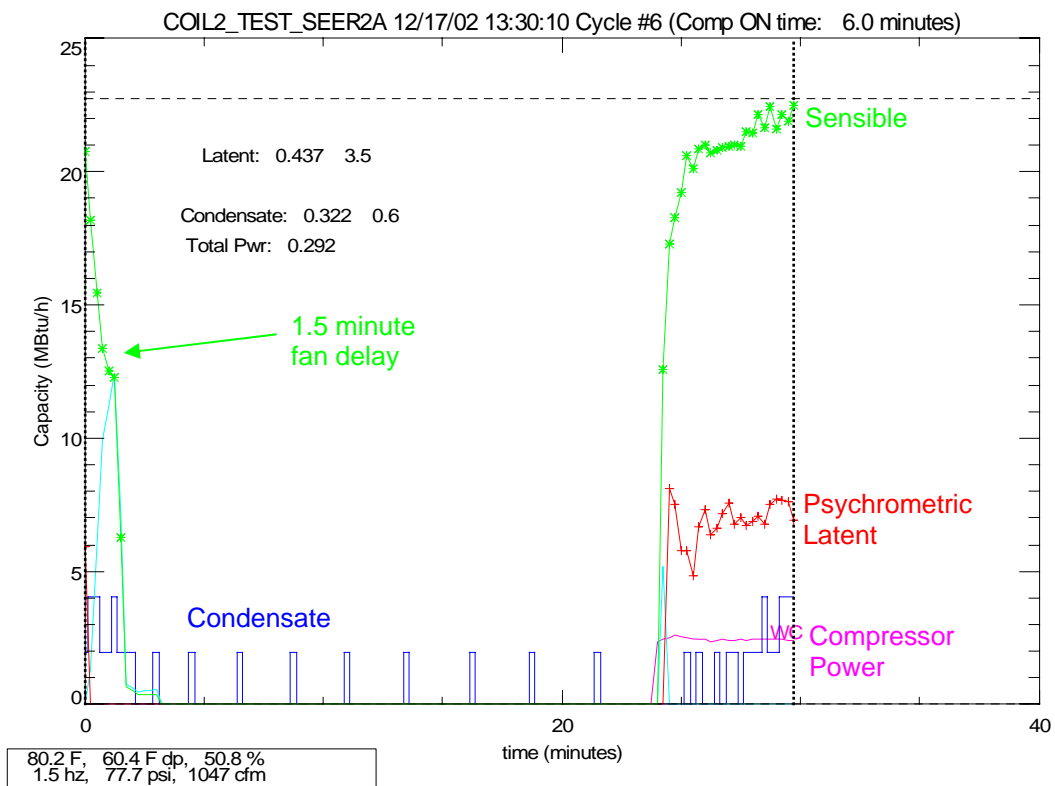
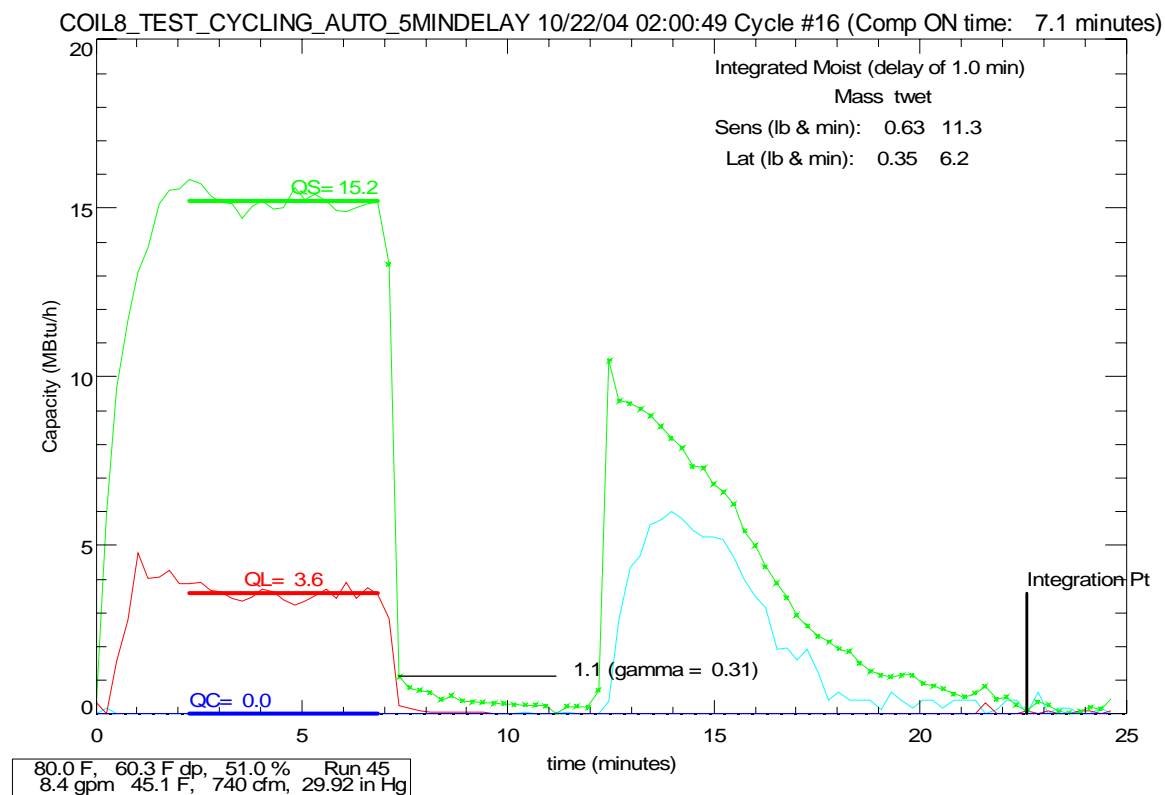


Figure 3-38. Test Results for Coil 2 with 1.5-minute Fan Overrun Delay

### 3.5.2 “Drain-Down” Fan Delay

Tests were also performed to study the impact of a fan “drain-down cycle”. This control strategy turns the fan off for a fixed interval (a few minutes) immediately after a cooling cycle to drain moisture from the coil. Fan operation is restarted after the fixed interval, presumably with little or no penalty to dehumidification performance. Many of the laboratory tests performed on coils 1-7 did not indicate a large amount of moisture draining from the cooling coil during the off cycle with AUTO fan operation, so a series of tests was performed on coil 8 to directly measure the impacts of a “drain-down cycle”.

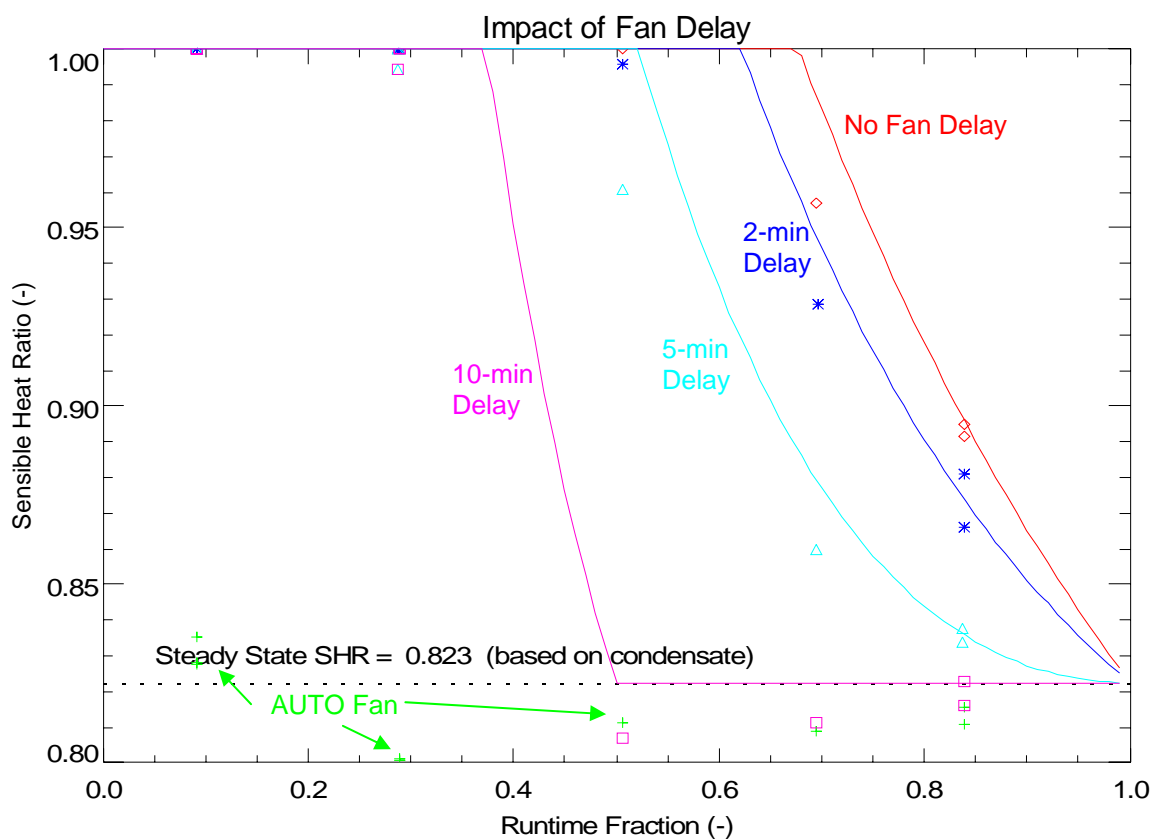
For coil 8, the quasi-steady cyclic tests with AUTO fan operation (Table 3-6, runs 41-46) were rerun with coil drain-down periods lasting 2, 5 and 10 minutes after the cooling coil was turned off. The supply air fan restarted after this drain-down period and ran until the end of the off cycle. The measured sensible and latent cooling capacity of coil 8 for a typical test with 5-minute drain-down period is shown in Figure 3-39.



**Figure 3-39. Test Results for Coil 8 with Drain-Down Cycle (5 minutes)**

Figure 3-40 shows the net impact of coil drain-down (fan delay) on part-load dehumidification performance. The “effective” sensible heat ratio is plotted as a function of coil runtime fraction, with the symbols representing the test results and the lines representing the results from the latent degradation model developed as part of this project. See Section 5.5.3 for more details regarding validation of the new model with data collected from these tests on coil 8.

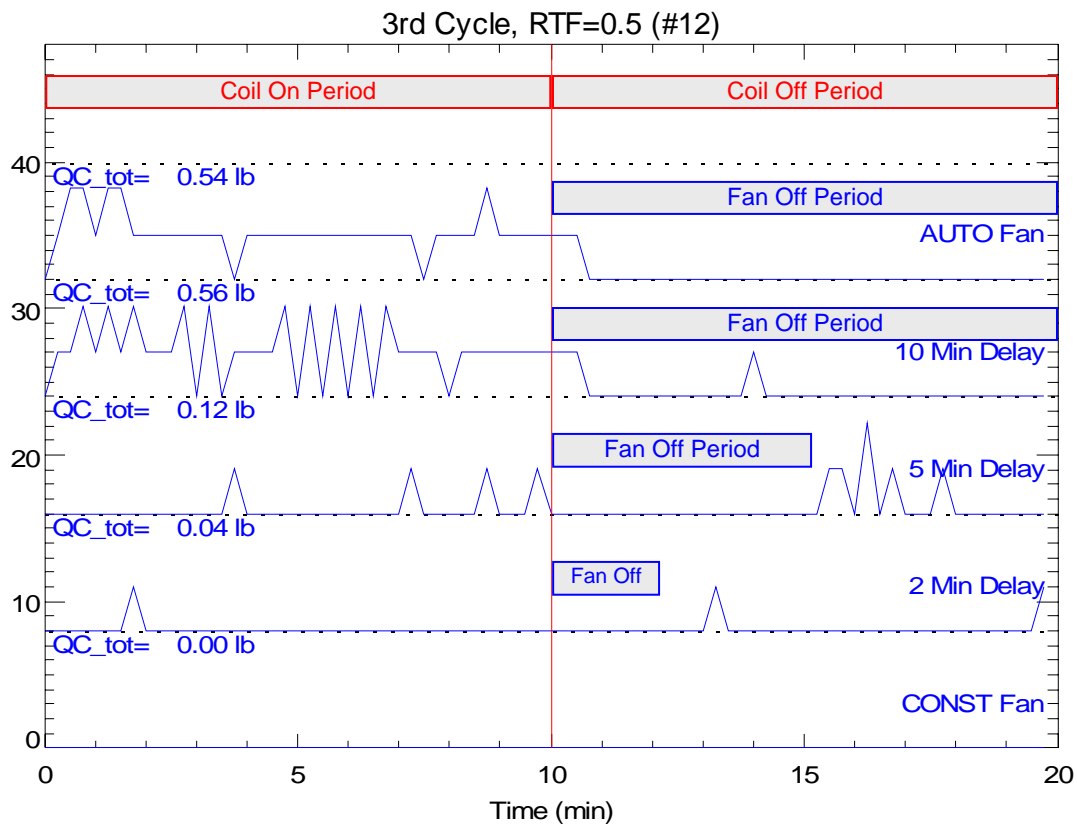
The green “+” symbols in Figure 3-40 represent the results for true AUTO fan control with no fan operation when the cooling coil is off. For this case, the SHR remains basically unchanged near 0.82 for all coil runtime fractions that were tested. The red diamond symbols represent the test results with continuous fan operation (no fan delay). The blue “\*” and aqua “Δ” symbols show the impact of 2-minute and 5-minute coil drain-down periods, which show only minor improvement in dehumidification performance over the constant fan operation case (no fan delay). For the 10-minute fan delay, the cooling coil “off” time for runtime fractions from 0.5 to 1.0 was less than or equal to 10 minutes (Table 3-6, runs 42-44). For these cases, the fan remained off for the entire period when the cooling coil was off, yielding the same results as the true AUTO fan case (green “+” symbols). With the 10-minute delay for coil runtime fractions of 0.29 and 0.09, the coil provided no net dehumidification over the complete on/off cycle (SHR ≈ 1).



**Figure 3-40. Measured Latent Degradation for Coil 8 “Drain-Down Cycle” Tests**

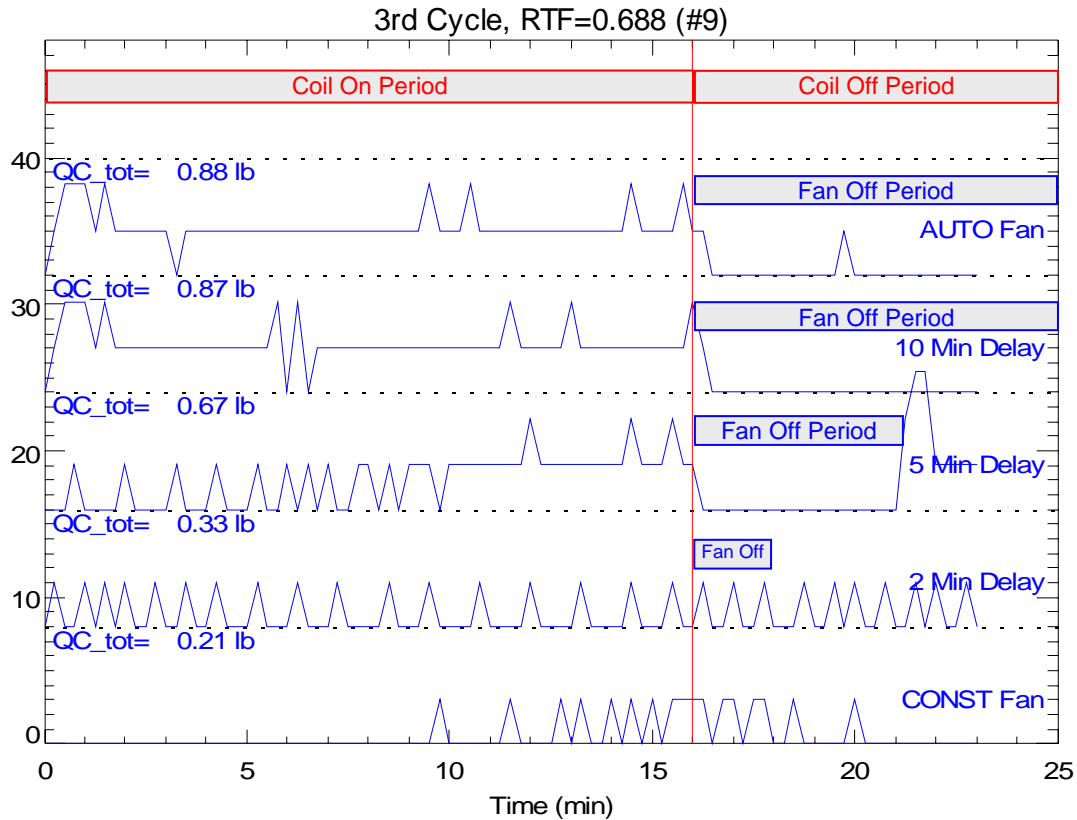
These results indicate that reasonable fan drain-down periods of 2 to 5 minutes yield only modest improvement in part-load dehumidification performance compared to continuous fan operation. However, the improvement is not caused by additional moisture draining from the coil while the fan is off, but is simply a result of the fan running for less time when the coil is off (thereby evaporating less moisture from the wet coil). Section 5.5.3 will confirm this point by comparing the test data to a theoretical model that only accounts for the reduced moisture evaporation from the wet cooling coil due to shorter fan runtimes during the coil off cycle.

Figure 3-41 and Figure 3-42 illustrate this point in a different way by comparing the net condensate removal (QC\_tot) with various drain-down delay times. The graphs are for two different coil runtime fractions (0.5 and 0.688). In some cases a “surge” of condensate is apparent when the fan restarts during the coil off cycle (e.g., the case of the 5-minute delay). However, the most prevalent reason for the loss of latent capacity is because fan operation during the coil off cycle evaporates moisture from the wet coil, and it takes more time for moisture to buildup and fall from the coil during the subsequent cooling cycle. For the AUTO fan case, there is little to no off-cycle evaporation because the fan is off. Therefore, moisture starts to fall from the coil almost immediately at the beginning of the cooling cycle. As the fan is on for longer portions of the coil off cycle, less and less condensate is removed by the system.



**Figure 3-41. Comparing Condensate Removal Rates with Various Drain-Down Delay Times (0.5 Coil Runtime Fraction)**





**Figure 3-42. Comparing Condensate Removal Rates with Various Drain-Down Delay Times (0.688 Coil Runtime Fraction)**

### 3.6 Impact of Oil on New Coils

Most of the coils tested in the laboratory were purchased new and installed in the laboratory facility for testing. Several other researchers (e.g., Korte and Jacobi 1997) have observed that the performance of a new cooling coil is affected by the light coating of machine oil that is left on the fin and tube surfaces during manufacturing. This section presents measured performance data that was collected immediately after coil installation, but prior to conducting the steady-state and cyclic tests described in Sections 3.4 and 3.5.

#### 3.6.1 Experiences with Coil 2

The first new coil tested in the lab was coil 2. A change in coil performance was observed over the course of the initial testing period, apparently related to oil remaining on the exterior surfaces of the coil due to the manufacturing process.

Table 3-8, Figure 3-43, and Figure 3-44 show that the trend of various parameters across the initial part of the test period. While the steady-state sensible and latent capacities remained roughly the same for this initial period,  $t_{wet}$ , the condensate delay time, and the amount of moisture retained on the coil all changed substantially. The most rapid change occurs during the

first few days of testing. The initial values of  $t_{wet}$  are 50-60% of the ultimate values after the surface oil had been washed off of the fins by multiple operating cycles.

**Table 3-8. Change in Performance for Coil 2**

	Run 3 10/14/02	Run 4 10/18/02	Run 4a 10/29/02	Run 3a 11/6/02
Sensible Capacity (MBtu/h)	21.3	21.8	21.6	21.8
Latent Capacity (MBtu/h)	7.8	7.2	7.6	7.8
Latent Capacity Based on Condensate (MBtu/h)	7.5	6.9	7	7.4
Moisture Retention on Coil (lb)	1.67	2.14	2.32	2.51
$t_{wet}$ (minutes)	13.7	18.8	19.4	20.6
Condensate Delay Time (minutes)	9.7	14.8	17	18
Peak Evaporation Rate (MBtu/h)	10.7	11.2	11.5	11.9
Gamma	1.37	1.54	1.51	1.52

Notes: Moisture retention on coil and  $t_{wet}$  based on integrated sensible capacity during the coil off cycle.

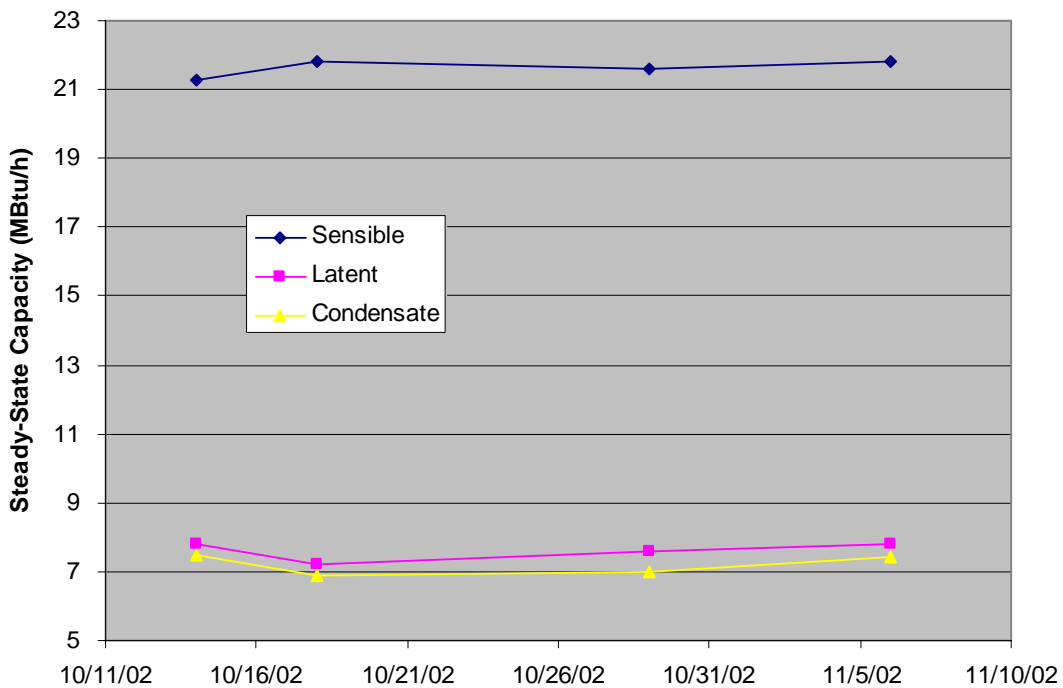


**Figure 3-43. Change in Steady-State Coil Performance for Initial Tests with Coil 2**

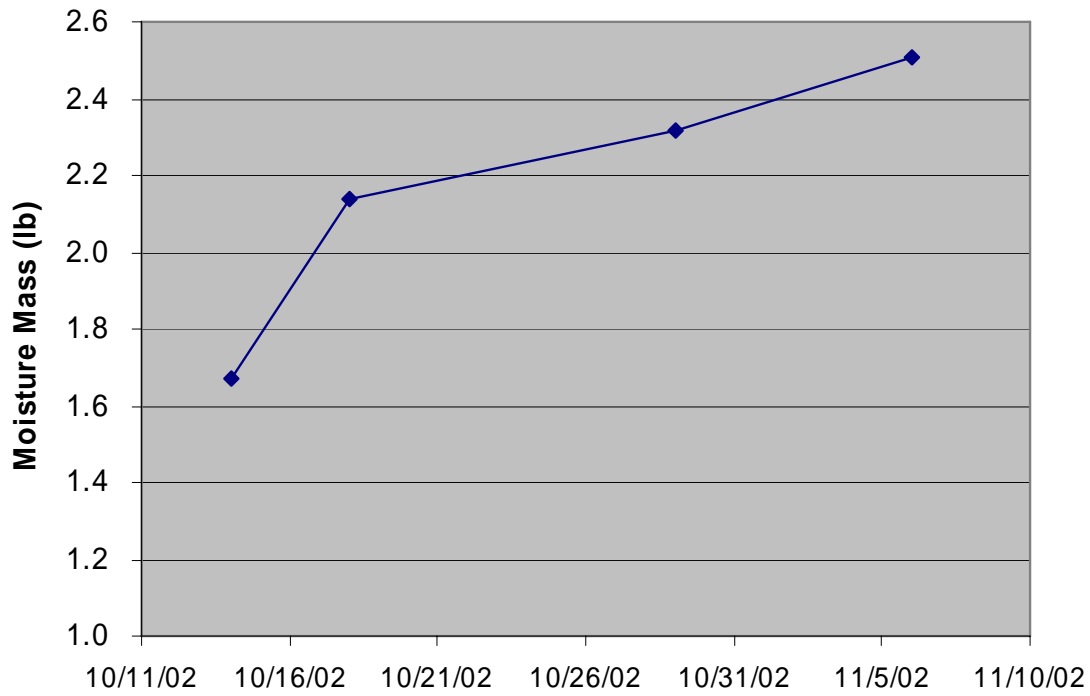
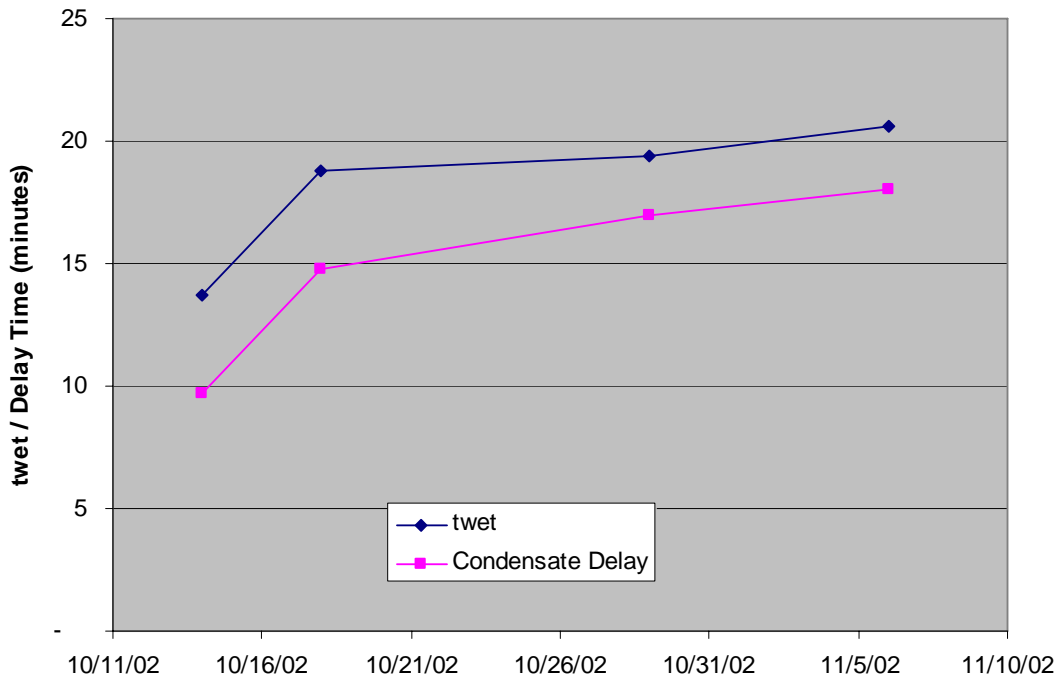


**Figure 3-44. Change in Moisture Retention for Initial Tests with Coil 2**

### 3.6.2 Tracking Performance for Other “New” Coils

In order to more carefully track the change in performance for a new coil, a procedure was established for the subsequent testing that ran a new coil through a series of on-off tests at wet coil conditions (i.e., steady state test 3, Table 3-5). The coil was repeatedly run for 20 to 30 cycles with the coil on for 120 minutes and off until the coil was dry. Figure 3-45, Figure 3-46 and Figure 3-47 show the changes in moisture retention over time for coils 4, 5 and 8, respectively. Tests were also run for coil 6, but a refrigerant leak in the middle of these tests invalidated the series. Similar to coil 2, no perceptible changes in steady-state performance could be detected for these 3 coils. However, the moisture holding capacity of the coil did noticeably change as the coil was “washed” by continued operation.

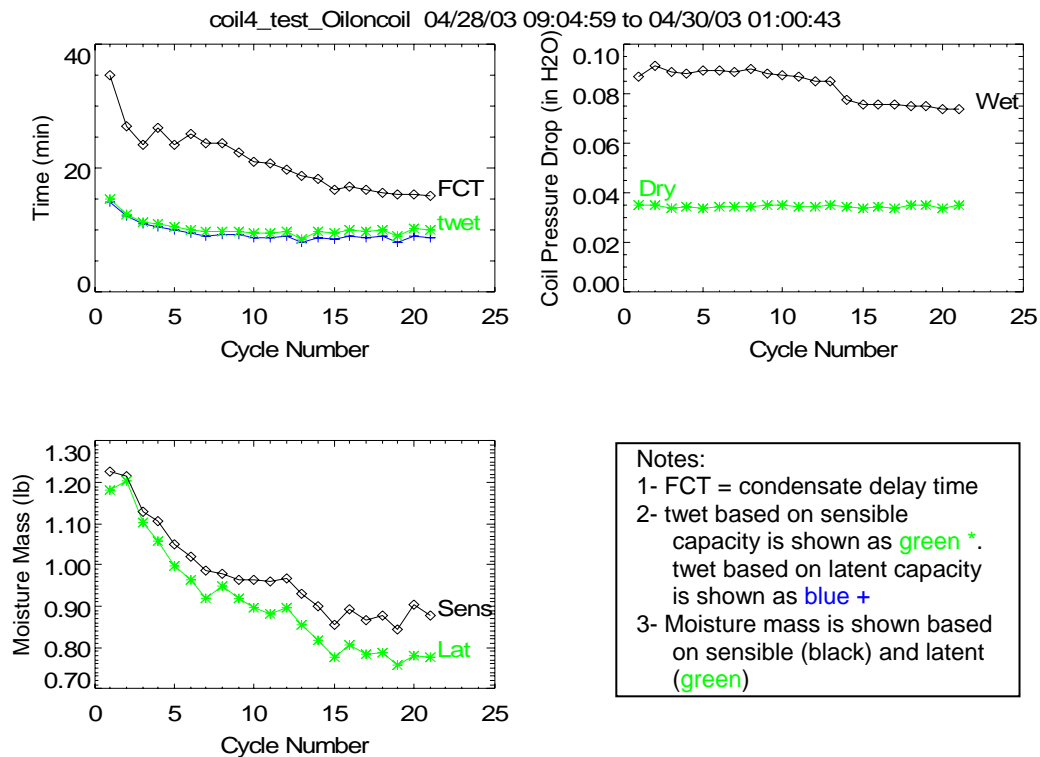


**Figure 3-45. Change in Moisture Retention for Initial Tests with Coil 4**

The results for coil 4 were somewhat surprising in that amount of moisture retained on the coil decreased as time progressed. The other coils were similar to coil 2 in that the mass of water increased with time. Less consistent trends are apparent with the wet coil pressure drop. Table 3-9 summarizes the change in moisture retention as the initial oil coating washes away.

**Table 3-9. Change in Moisture Retention for All Coils**

	Ratio of Initial Moisture Mass to Final Mass
Coil 2	0.67
Coil 4	1.50
Coil 5	0.89
Coil 6	0.66

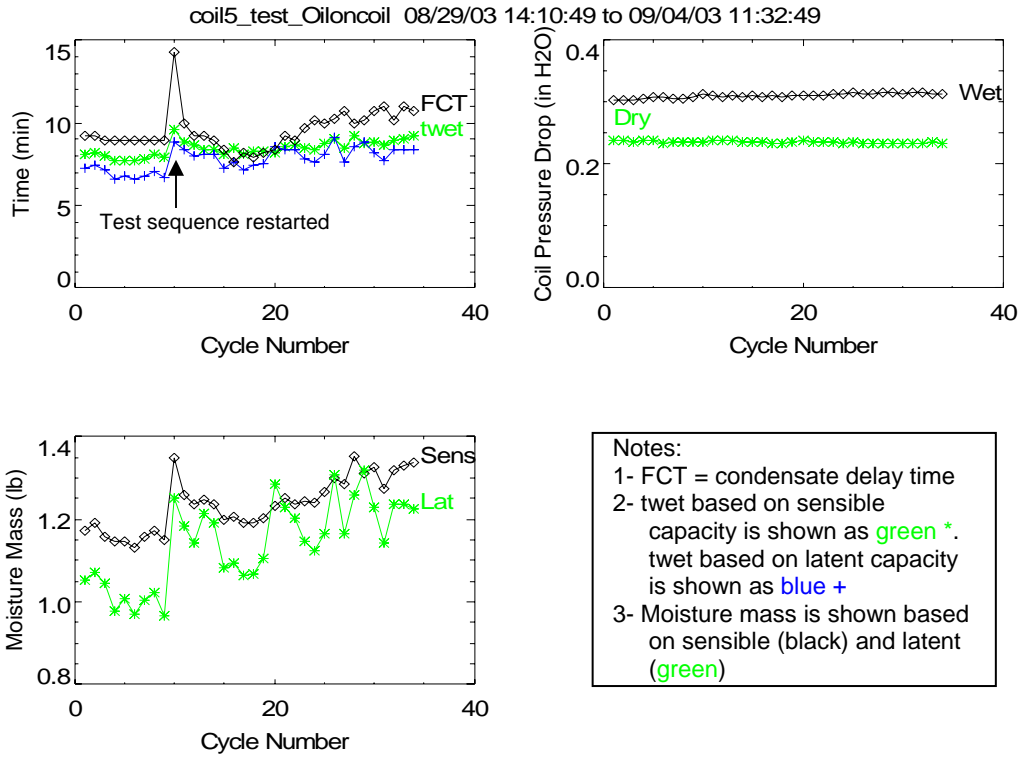


Figure 3-46. Change in Moisture Retention for Initial Tests with Coil 5

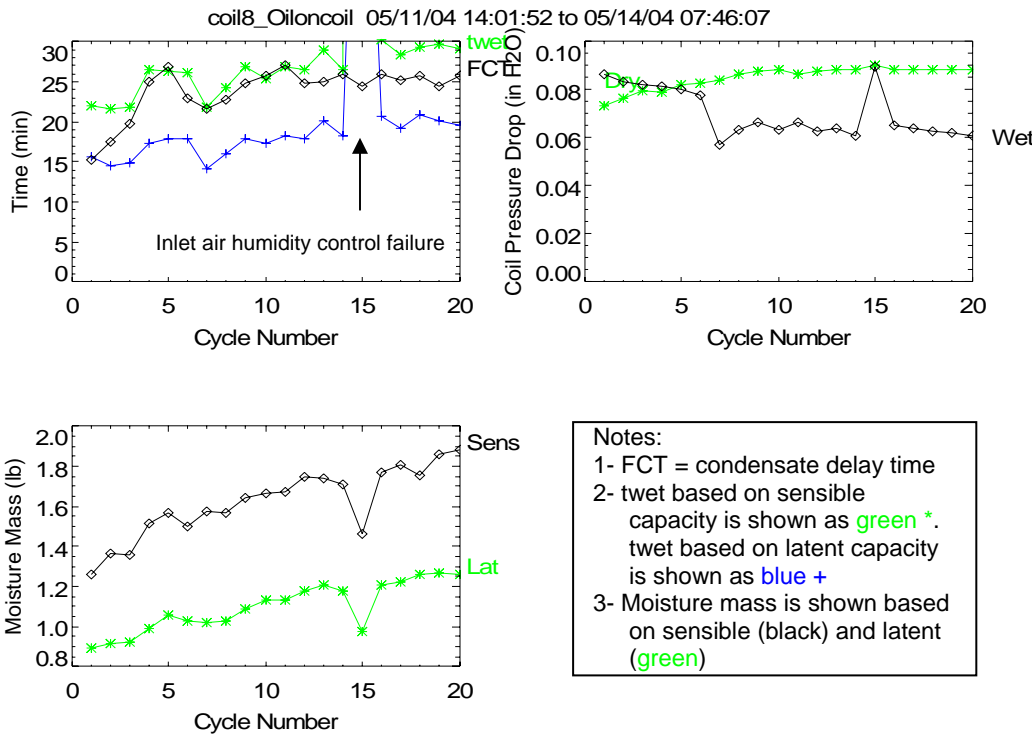


Figure 3-47. Change in Moisture Retention for Initial Tests with Coil 8

## 4 Field Testing

The field testing portion of this project involved monitoring the performance of residential and commercial cooling systems to understand the degradation of latent (dehumidification) capacity at part-load conditions. Field measurements were also collected to understand the impact of supply air fan operation on indoor humidity levels. Eight cooling systems were monitored at seven field test sites. The systems included residential split direct expansion (DX) equipment (single-stage and two-stage condensing units), a commercial rooftop unit, and chilled water coils in both constant air volume and variable air volume applications. This section summarizes the test sites and monitored data. Details regarding each site are provided in Appendix I.

The monitored data collected from the field sites generally support the laboratory test results (Section 3). Degradation of moisture removal performance occurred with continuous supply air fan operation for both DX and chilled water coils. In addition, systems operating with AUTO fan control (supply air fan cycles on and off in tandem with the cooling coil) showed some degree of moisture removal degradation, although to a lesser extent than for continuous fan operation.

A brief description of the field test locations and cooling system types are documented in Section 4.1. Instrumentation used to monitor system performance is described in Section 4.2. One-time measurements were recorded while on site to install the monitoring equipment, and the results are discussed in Section 4.3. Information about each coil and system was carefully documented, and an example of the collected information is provided in Section 4.4. Analysis and discussion of the measured data are provided in Section 4.5.

### **4.1 Description of Field Test Sites**

Table 4-1 below describes the field test sites selected for this project. The sites were chosen to cover a range of climates and applications. Four test sites involved monitoring residences with split DX systems. A commercial rooftop packaged unit (DX) serving a large retail store was monitored at another site. Two test sites were selected to monitor the performance of chilled water coils: a variable-air-volume air handler serving an office building and a constant-air-volume air handler serving a laboratory building. The sites were located in four eastern states, ranging from Florida to Connecticut.

The systems were monitored under normal operation as selected by the building owner. This included operating parameters such as unit scheduling, set points and fan control. If the supply air fan typically operated in the AUTO mode (fan cycles on/off in tandem with the cooling coil), the building operators were asked to operate the supply air fan continuously for one or two weeks to also capture data with that mode of fan operation. If a system had multiple fan control options, building operators were asked to operate the fan in each mode for several weeks to monitor the impacts of the various fan control strategies.

A basic description of each field test coil is shown in Table 4-2. Detailed information was documented for the coils at each field test site (e.g., manufacturer's name, model number, coil face area, coil depth, fin spacing, etc.), and this information is located in Appendix I. This

information was needed to assess and compare the moisture retention characteristics of the field-tested cooling coils with those tested in the laboratory (Section 3). Documentation of coil and system information is described further in Section 4.4.

The test sites and cooling systems were extensively photographed to document site conditions and installation characteristics. For example, Figure 4-1 and Figure 4-2 show the residential direct-expansion unit for site 1 (2<sup>nd</sup> floor unit) and the commercial chilled-water air handler for site 7.

**Table 4-1. Field Test Sites**

Site	Site Description	System Description
1	Residence in Herndon, Virginia	Two single-stage split DX systems (2.5-ton and 3-ton) with upflow air handling units (AHUs) and inverted A-coils.
2	Residence in Merritt Island, Florida	3-ton, two-stage split DX unit with variable-speed air handler. Air handler is an upflow A-coil design.
3	Residence in Danbury, Connecticut	4-ton, single-stage DX coil for a geothermal water-to-air heat pump. Air handler is a conventional A-coil design.
4	Retail store in Brookline, Massachusetts	10-ton, two-stage rooftop package DX coil with natural gas heater. DX coil used face-split design.
5	Residence in Cocoa, Florida	3.5-ton, single-stage DX unit with variable-speed air handler. Air handler is a conventional upflow A-coil design.
6	Laboratory building in Cocoa, Florida	AHU with 6-row chilled water coil. Constant air volume application with 2-way modulating water valve.
7	Office building in Cocoa, Florida	AHU with 6-row chilled water coil. Variable-air-volume system.

**Table 4-2. Field Site Coil Descriptions**

Site	Type	Description, expansion device	Rows	Fin Spacing (fpi)	Nominal Cooling Capacity (ton / kW)	Fin Surface Area (ft <sup>2</sup> / m <sup>2</sup> )
1	DX	1 <sup>st</sup> floor, inverted A-coil with wavy fins, fixed orifice	3	11	3.0 / 10.5	241.5 / 22.4
		2 <sup>nd</sup> floor, inverted A-coil with wavy fins, fixed orifice	3	11	2.5 / 8.8	241.5 / 22.4
2	DX	A-coil with wavy fins, TXV	4	14	3.0 / 10.5	446.3 / 41.5
3	DX	A-coil with wavy fins, fixed orifice	4	14	4.0 / 14.1	469.5 / 43.6
4	DX	2-stage vertical slab coil with straight fins, face-split coil, TXV	3	13	10.0 / 35.2	762.3 / 70.8
5	DX	A-coil with sine-wave lanced fins, hard shut-off TXV	3	15.5	3.5 / 12.3	508.1 / 47.2
6	CW	Vertical slab coil with wavy fins, no expansion device, 2-way modulating valve	6	12	2.9 / 10.1	499.6 / 46.4
7	CW	Vertical slab coil with straight fins, no expansion device, 2-way modulating valve	6	11	7.0 / 24.5	1008.7 / 93.7

Notes: Additional information for each coil is provided in Appendix I

Fin surface area is gross fin area: coil face area (ft<sup>2</sup>) x coil depth (in) x fin spacing (fpi) x 2

DX = direct expansion, CW = chilled water, TXV = thermostatic expansion valve



**Figure 4-1. Residential Air Handler (Site 1, 2<sup>nd</sup> Floor Unit)**



**Figure 4-2. Commercial Air Handler (Site 7)**

## **4.2 Instrumentation**

A data logger was installed at each site and programmed to scan each channel at 5-second or 10-second intervals (varied by site). Analog channels were averaged and other points were summed over one-minute logging intervals. Event records were also recorded each time the supply air fan or compressor turned on or off and when condensate removal first began (i.e., the tipping bucket produces its first pulse). For certain field test sites, the data were also logged at 15-minute intervals so that a continuous record of overall performance was available.

The instrumentation used at each site was selected to quantify the parameters of interest for each situation. One of the most important measurements was the amount of condensate removed by the cooling coil. The operating parameters that drive steady-state latent removal performance, such as the psychrometric conditions (temperature and humidity) of air entering the cooling coil and the coil temperature itself, were also measured. Leaving psychrometric conditions were monitored to understand the mode and rate of moisture evaporation from a deactivated cooling coil. The parameters measured are listed in Table 4-3. The general locations of the data collection points are shown in Figure 4-3 for DX systems and in Figure 4-4 for chilled water systems. For DX systems, additional monitoring points are listed in Table 4-3, such as coil suction pressure, suction temperature, and compressor power. For DX systems with variable speed fan motors, fan speed and supply air velocity were also measured. For chilled water systems, the water flow rate through the coil was determined by measuring the pressure drop across a circuit-setter and converting to flow rate using manufacturer's data for pressure drop versus water flow rate. The temperature of the entering and leaving water was also measured for chilled water coils.



**Table 4-3. Data Points for Field Monitoring**

<b>Point Type</b>	<b>Point Name</b>	<b>Description</b>	<b>Eng. Units</b>	<b>Sensor Type</b>
Analog	TAM	Temperature of mixed air entering coil	°F	Type-T thermocouple
Analog	RHM	RH of mixed air entering coil	%RH	Humidity transducer
Analog	TAS	Temperature of supply air leaving coil	°F	Type-T thermocouple
Analog	RHS	RH of supply air leaving coil	%RH	Humidity transducer
Analog	DPC	Static air-side pressure drop across the coil	in H <sub>2</sub> O	Pressure transducer
Analog	TAO	Outdoor air temperature	°F	Type-T thermocouple or RTD
Count	FC	Condensate flow rate	lb	Calibrated rain gauge (tipping bucket)
Count	WF	Supply air fan energy (except site 4)	kWh	Watt-hour transducer
Digital	SF	Supply fan status	minutes	Current switch
<b>Additional Data Points for DX Coils (sites 1 through 5)</b>				
Analog	TSUC	Evaporator/compressor suction temperature	°F	Type-T thermocouple
Analog	PSUC	Evaporator/compressor suction pressure	psi	Pressure transducer
Digital	SCx	Coil/compressor status #x (x=1, 2...)	minutes	Current status switch
Count	WU	AC condenser unit energy (except site 4 was total RTU energy)	kWh	Watt-hour transducer
Analog	IB	Fan current	amps	Current transducer
Analog	TLIQ	Liquid refrigerant temp (before exp. valve)	°F	Type-T thermocouple
Analog	TEVAP	Evaporator temp (1 <sup>st</sup> U-bend after exp. valve)	°F	Type-T thermocouple
<b>Additional Data Points for DX Coils with Variable Speed Fans (sites 2 and 5)</b>				
Analog	VF	Fan Speed (site 2 only)	rpm	Photo tachometer
Analog	FA	Supply Air Velocity	fpm	Pitot tube
Analog	RHO	RH of outdoor air	%RH	Humidity transducer
<b>Additional Data Points for Chilled Water Coils (sites 6 and 7)</b>				
Analog	TCWE	Chilled water temperature entering coil	°F	Type-T thermocouple
Analog	TCWL	Chilled water temperature leaving coil	°F	Type-T thermocouple
Analog	DPCW	Chilled water flow rate	gpm	Transducer measuring pressure drop across water flow circuit-setter
Analog	SVALV	Valve position/signal, CW valve	%	Voltage divider

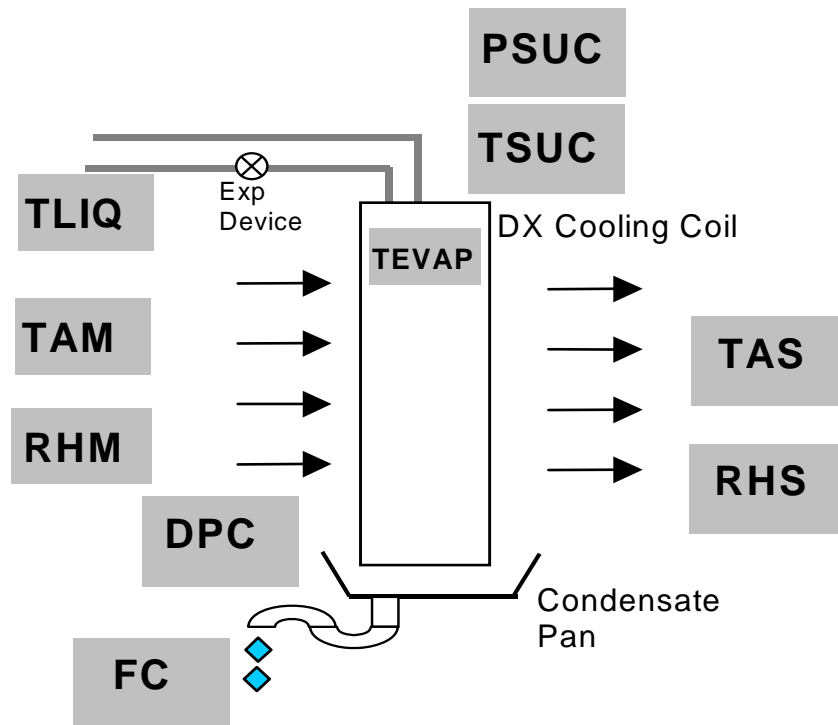


Figure 4-3. Schematic of Sensor Locations for DX Systems

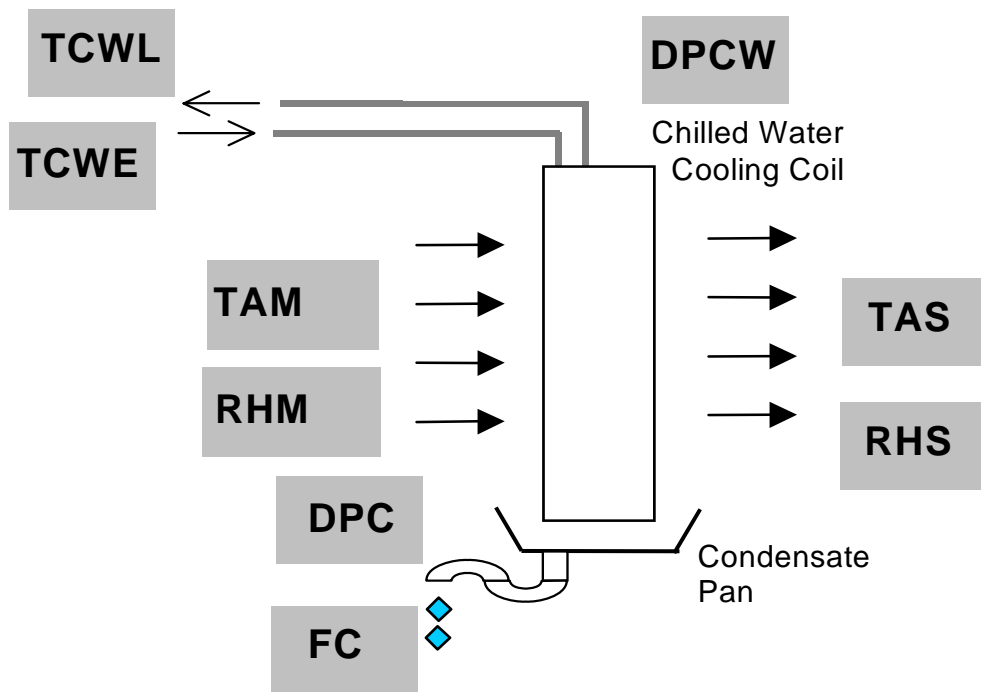


Figure 4-4. Schematic of Sensor Locations for Chilled Water Systems

### 4.3 One-Time and Auxiliary Measurements

In addition to the continuously monitored data, one-time measurements of various other parameters were collected to aid in the data analysis and potentially assist in developing and validating the engineering models being developed as part of this project (Section 5). These measurements were also used to confirm and enhance the continuously recorded data. The specific number of one-time measurements was dependent on system type and physical constraints at each field site. Table 4-4 lists the one-time measurements including air flow, measurements of supply duct stratification, and static air pressure before and after the cooling coil.

**Table 4-4. One-Time Measurements**

<b>Point Name</b>	<b>Description</b>	<b>Instrument</b>	<b>Notes</b>
FA1	Air flow by multi-point velocity traverse	Anemometer or pitot tube	Equal area method
FA2	Air flow using electric heater elements	Measure power & coil $\Delta T$	Current transducer and hand-held temperature probe
To, Rho	Supply air stratification (T & RH)	Handheld T/RH probe	Equal area method
Ti, Rhi	Mixed air stratification (T & RH)	Handheld T/RH probe	Equal area method
Dpin	Static Pressure, Entering Coil	Pressure transducer	Existing sensor or hand-held probe
Dpout	Static Pressure, Leaving Coil	Pressure transducer	Existing sensor or hand-held probe

Air flow measurements were used with continuous readings of air conditions (T & RH) entering and leaving the cooling coil to determine the total, latent and sensible capacity as well as the sensible heat ratio (SHR). Temperature and humidity stratification measurements confirmed that the cooling systems were operating as expected.

At some of the sites, battery-powered data loggers were deployed to measure air temperature and relative humidity in the conditioned zone itself. These measurements were compared to the air conditions entering the cooling coil to detect any major differences. These measurements were also used to determine the impact of part-load latent degradation on space humidity levels. The sensors were calibrated with more accurate instruments, and these portable data loggers were time synchronized to the main data logger at the site. For site 5, zone temperature and humidity levels were measured by sensors connected directly to the main data logger for this site (i.e., battery-powered loggers were not used for this site).

## 4.4 Documentation of Coil and System Information

For each test site, the following information was documented for each monitored cooling system. Digital photographs were also taken to document sensor locations as applicable.

- Air conditioner manufacturer and model number
- Nominal cooling capacity and heating type
- Other nameplate data for each system component
- Design data from mechanical drawings when available
- Cooling coil specifications (e.g. # of rows, fin spacing, coil face area, coil dimensions)
- Air handler dip switch settings that are set by the installer which impact the air handler operation and control sequences (sites 2 and 5 only, DX coils with variable-speed AHUs)
- General layout of the duct system and location of the AC components in the building

An example of the information documented at each field test site is shown in Table 4-5 and Table 4-6 for site 1. Complete descriptions for each field test site are provided in Appendix I.

**Table 4-5. Indoor Coil Geometry for Unit 1 (Upstairs) at Field Site 1**

Coil Type	“V” coil (inverted “A” coil)	
Coil Face Area	542.9 sq. in. 574.9 sq. in. w/o blockage	
Number of rows x Tubes/row	3 x 18	
Fin spacing	11 fpi	
Tubing diameter	1/4"	
Coil depth	2.75 in	
Exp device	orifice	
Notes:	Small sheet metal “L” bracket at bottom of coil partially blocks air flow around a portion of the lower right side coil. This appears to be the same coil as Unit #2, with smaller angle between the coil sides.	

**Table 4-6. Nameplate Data for Cooling System at Field Site 1**

Unit and Location	Size/Type	System	Model Number	Comments
Unit 1 – Upstairs	2.5-ton Heat Pump	Condensing Unit	York E1FD030B06A	Single-stage
		Air Handling Unit	York (unknown)	Constant air volume
Unit 2 – 1 <sup>st</sup> Floor and Basement	3.0-ton Heat Pump	Condensing Unit	York E1FD036S06B	Single-stage
		Air Handling Unit	York G/HC036SB	Constant air volume

## 4.5 Analysis of Collected Data

The field-monitored data were used to quantify the part-load latent (moisture) removal performance of these systems. The data were also used, along with the laboratory test results (Section 3), to develop and validate engineering models to predict latent degradation at part-load conditions (Section 5). The following sections describe the types of data analyses that were performed. Detailed analysis results for each field site are provided in Appendix I.

### 4.5.1 Verification of Latent Capacity Measurements

Accurate measurement of coil dehumidification was of primary importance for the field tests, and two methods were used to measure dehumidification performance. First, a calibrated rain-gauge tipping bucket was used to measure the volume of condensed water exiting the coil’s drain pan. Measured condensate flow multiplied by the latent heat of condensation for water yielded the latent cooling rate. The second method used the measured psychrometric conditions of air entering and leaving the cooling coil along with the measured air flow rate (one-time measurement for most sites, or continuous measurements for sites 2, 5 and 7) to calculate the coil’s dehumidification (latent cooling) rate. The results of these two methods were plotted against each other for all monitored coils for periods when the coil was at steady-state conditions (e.g., after 15-30 minutes of compressor runtime for DX systems).

Figure 4-5 shows the results of these calculations for the 2<sup>nd</sup> floor unit at field site 1. The data shown in the figure were collected at times when there were at least 30 minutes of continuous compressor operation. This data was limited to periods where the entering air temperature was greater than 73°F and the relative humidity was between 48% and 52%. The figure shows fairly good agreement between the latent capacity calculation methods. The trend of slightly higher psychrometric-based latent capacity compared to condensate removal is consistent with what was observed for many of the other field test sites. Comparison of the two calculation methods was made for each of the field test sites with results shown in Appendix I.

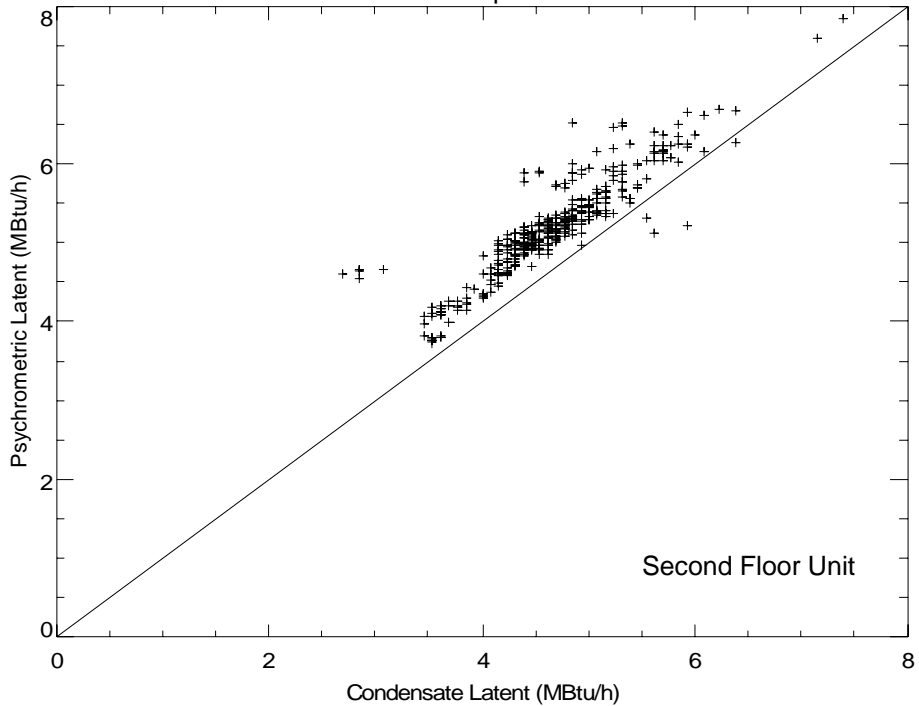


**Figure 4-5. Comparison of Latent Capacity Calculated From Psychrometric State Points and Condensate Removal Rates, Site 1**

#### 4.5.2 Analysis of Field Measurements

##### Time to First Condensate Pulse

One key indication of the coil's moisture-holding capacity is the time it takes for condensate to first fall from the coil and exit the unit through the condensate drain line (Figure 4-6). This time to first condensate pulse, along with the steady-state latent capacity of the coil, can be used to estimate the moisture-holding capacity of the cooling coil. This time delay is similar to the parameter  $t_{wet}$  from the latent degradation model developed by Henderson and Rengarajan (1996), which is described further in Section 5.

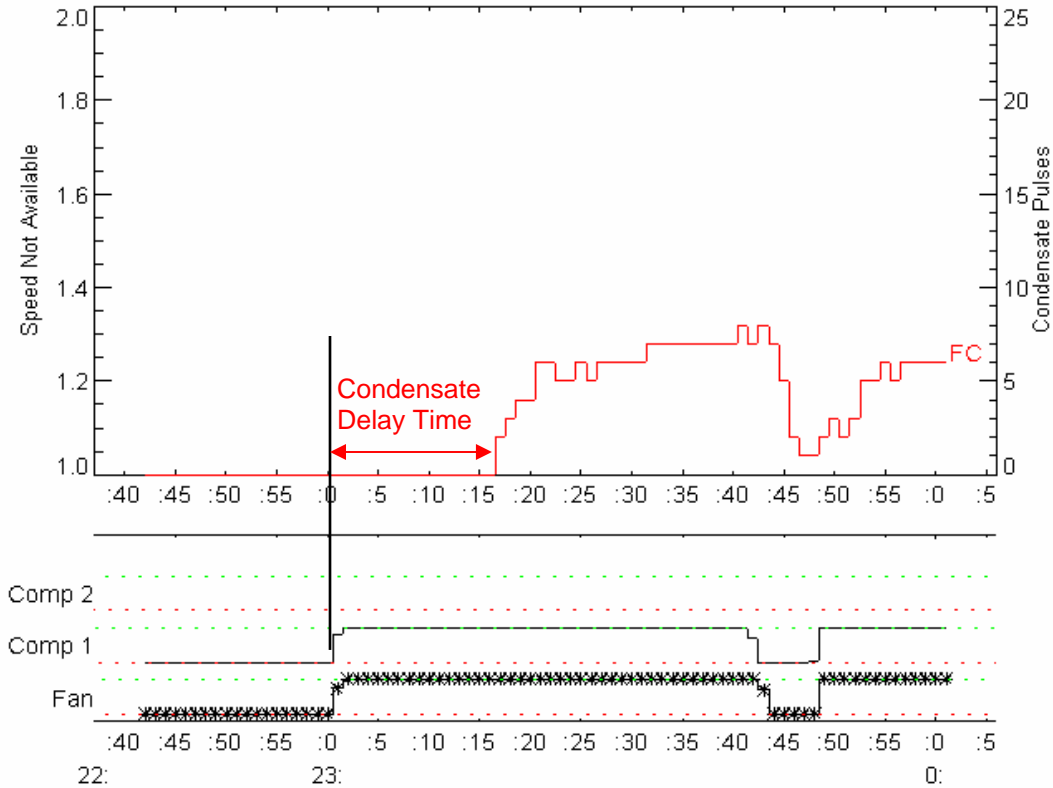


**Figure 4-6. Monitoring Condensate Delay Time at Site 1**

The time to first condensate pulse was monitored at all field test sites. However the major challenge in obtaining meaningful information was finding time periods where the coil was dry prior to the start of a cooling cycle, and having the coil remain in continuous operation until condensed moisture began to exit the drain pan. For sites 1 through 4, the following criteria were applied to filter the measured data for meaningful values of time to first condensate pulse:

- No condensate pulses in the previous 2 hours before compressor startup (dry coil at start),
- Compressor was continuously on at least until the first condensate pulse occurred,
- First measured condensate pulse was followed by at least one other condensate pulse (to confirm that the first pulse wasn't a stray measurement).

Using these criteria, only a single value (approximately 16 minutes) was located for the two DX units at site 1, and no values were obtained for site 3. For sites 2 and 4, applying these criteria to the measured data yielded a sufficient number of data points to correlate the time to first condensate pulse to the dew point temperature of air entering the coil (Figure 4-7 and Figure 4-8). For both sites, the condensate delay time decreases as the dew point temperature of the entering air increases. This trend is consistent with data collected in the laboratory (Figure 3-16). Note that the time to first condensate pulse for sites 2 and 4 were quite different. At a nominal entering air dew point temperature of 60-61°F (15.6-16.1°C), the condensate delay time was around 10 minutes for site 4 whereas it was 4-to-5 times longer (40-50 minutes) for the coil at site 2 (with this two-stage unit operating at first stage).

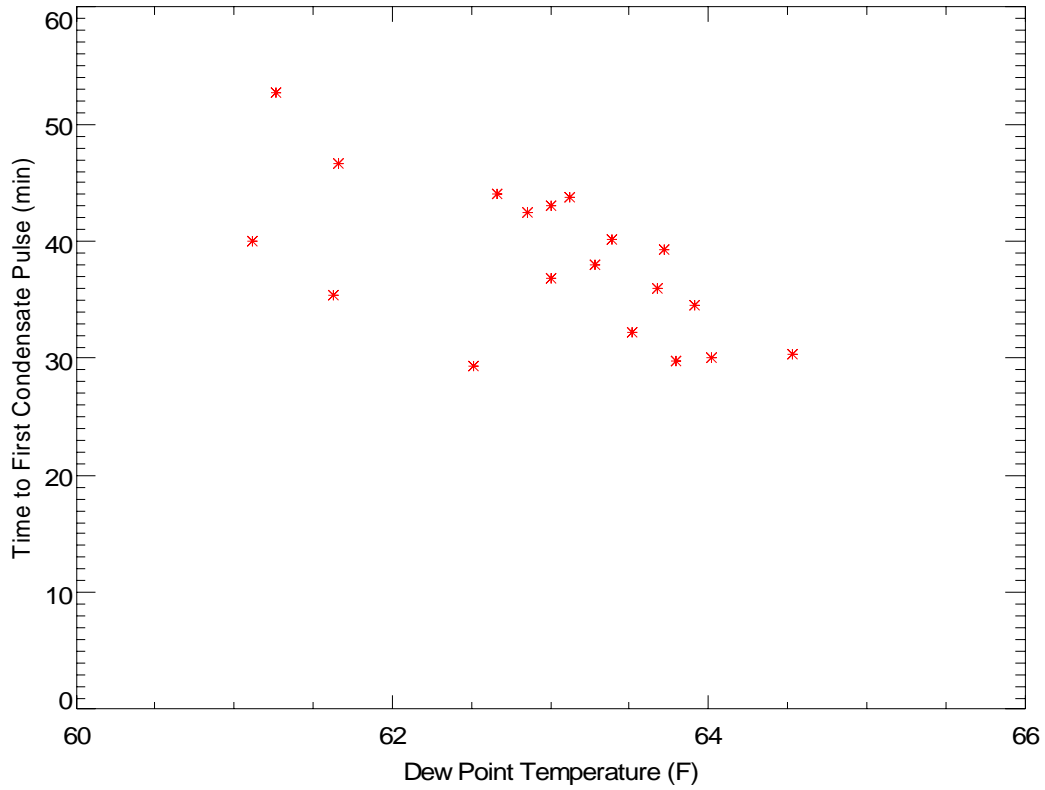


**Figure 4-7. Impact of Dew Point on Condensate Delay Time for Site 2 at First Stage**

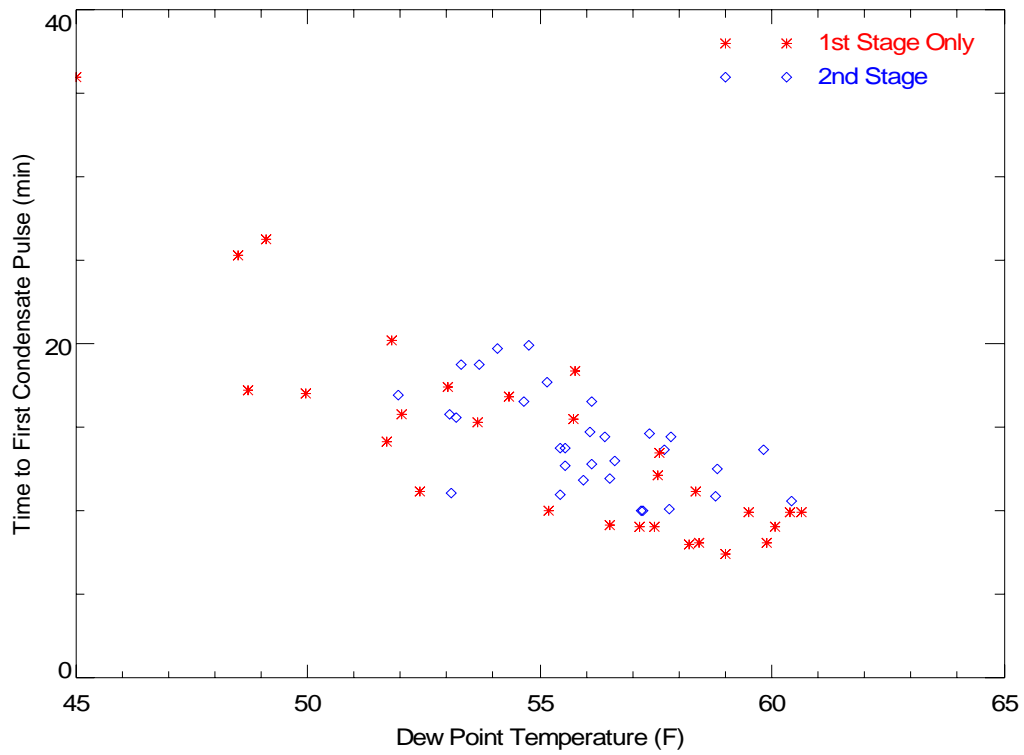


**Figure 4-8. Impact of Dew Point Temperature on Condensate Delay Time for Site 4**



For site 5, a single test was performed to measure the time to first condensate pulse. The test started with a completely dry cooling coil. Based on this one test, the condensate delay time for the coil at this site was approximately 35 minutes.

For the chilled water coils at sites 6 and 7, the chilled water control valve is not controlled in an on/off fashion like the DX coils (sites 1 through 5). Instead, chilled water flow rate through the coil is varied based on the measured space temperature in relation to the set point temperature. Therefore, specific tests were conducted to measure condensate delay time for these coils. The chilled water control valve was fully opened for a period of time to produce a fully-wetted coil. Then, water flow through the coil was stopped (using an isolation valve) for several hours while the supply air fan continued to operate. Once the moisture on the cooling coil had been fully evaporated into the supply air stream, the chilled water isolation valve was reopened to provide full flow through the cooling coil and measurements were collected until condensate removal was detected by the tipping bucket mechanism. The air flow rate across the coil for the variable-air-volume system (site 7) was fixed at its design value for this test, while the air flow across the coil for the constant-air-volume system (site 6) remained at its normal value.

This test sequence was conducted twice for each chilled water coil. For site 6, the time to first condensate pulse varied from 21 to 30 minutes. The variation was caused by a difference in inlet air humidity level and water flow rate between the two tests. For site 7, the time to first condensate pulse was 15 to 16 minutes for both tests (similar operating conditions for both tests).

#### Measurement of Off-Cycle Moisture Evaporation Rate to Estimate Coil Moisture Retention

Moisture retention on the coil was also estimated for some of the field test sites by integrating the sensible capacity delivered by the cooling coil during the coil off cycle. This method of estimating coil moisture retention was also used during lab testing (Figure 3-12) since lab measurements indicated that the coil operates as an evaporative cooler during the coil off cycle with latent capacity approximately equal to sensible capacity. When available, collected field data were screened to provide information regarding off-cycle moisture evaporation after the compressor operated for a sufficient time to yield a fully-wetted coil surface.

For example, the first floor unit for site 1 was operated in the constant fan mode for an extended period of time. Figure 4-9 shows the off-cycle sensible capacity for several “wetted” cycles during times when the compressor had just stopped operating, and one or more condensate pulses had occurred during the last 10 minutes of compressor operation. The plot includes symbols (\*) at 2 minutes after compressor shutdown, which is about the time that refrigerant dynamics have subsided and sensible capacity is then driven by the moisture evaporation process. The shape of the sensible evaporation curve is similar to the evaporation curves found for other field test sites and for coils tested in the laboratory (e.g., Figure 3-33 and Figure 3-34).

For the curves in Figure 4-9, the initial evaporation rate is approximately 10 MBtu/h two minutes after the compressor is turned off. Figure 4-10 clearly shows that the off-cycle evaporation rate is a function of the wet-bulb depression (i.e., entering air dry-bulb temperature minus the entering air wet-bulb temperature). The line in Figure 4-10 shows the theoretical trend of moisture evaporation projected to zero evaporation at no wet-bulb depression, with the measured data showing good agreement with this theoretical trend. Integration of the sensible off-cycle capacity in Figure 4-9 yields an estimate of coil moisture retention of approximately 1.9 pounds.

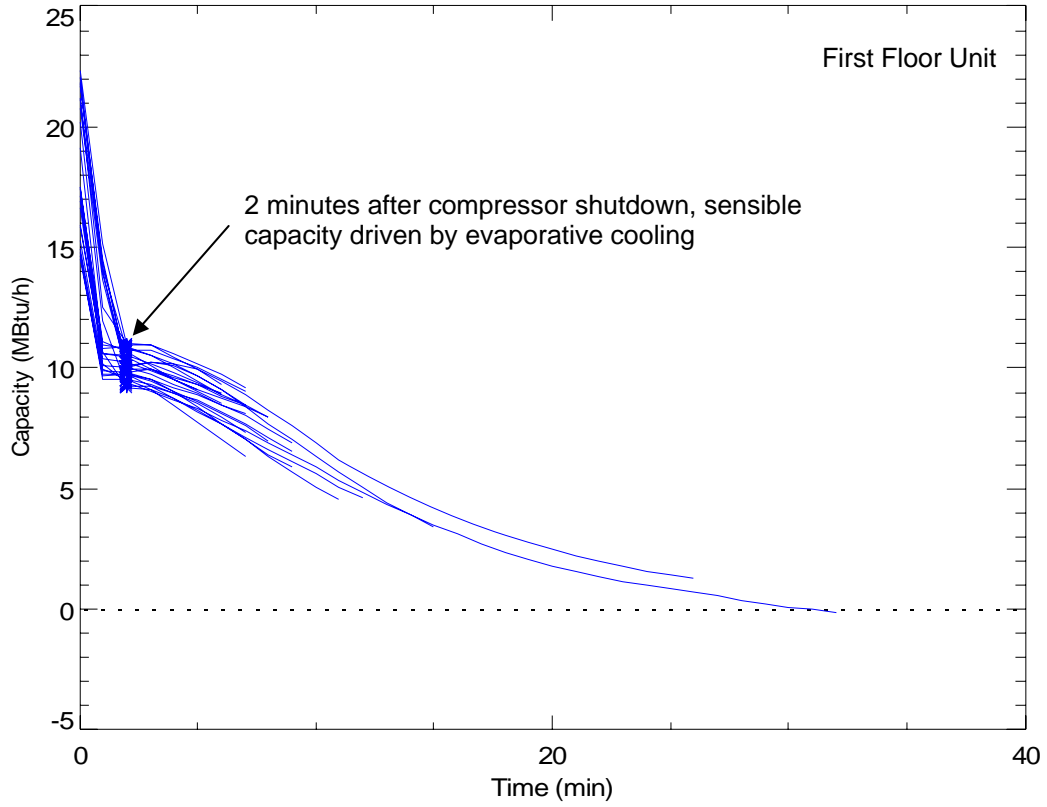


**Figure 4-9. Trend of Sensible Capacity for Several “Wetted” Off Cycles, Site 1**

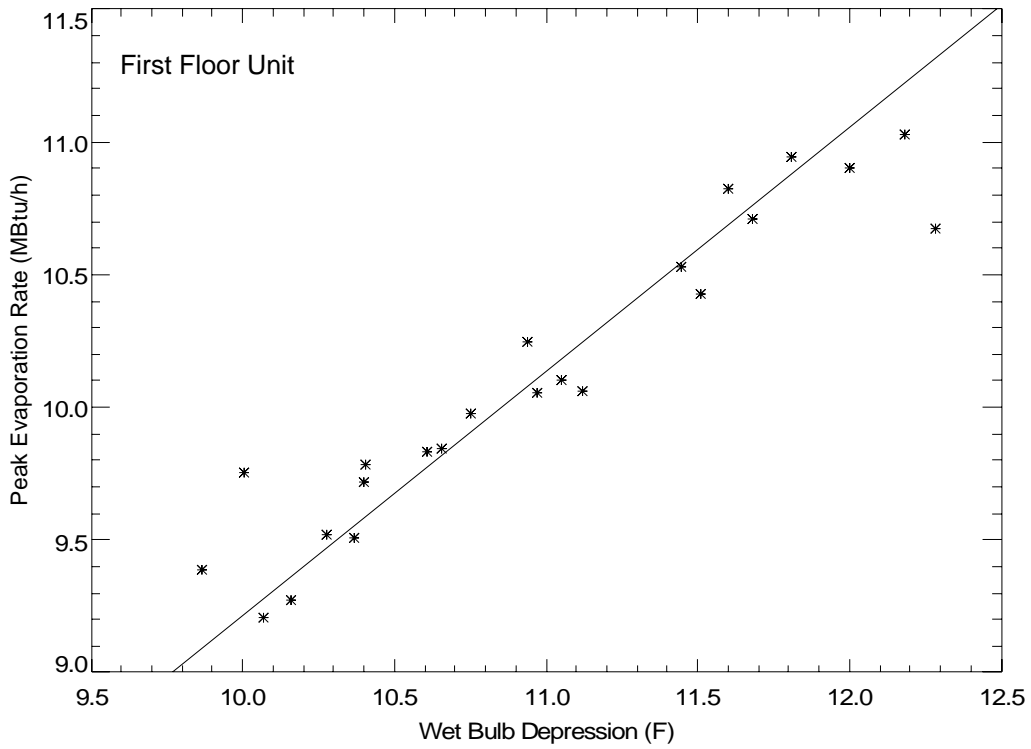


**Figure 4-10. Variation of Peak Off-Cycle Evaporation Rate with Wet-Bulb Depression, Site 1**

Similar data were collected and analyzed for several other sites. For example, the off-cycle moisture evaporation rate versus time for the cooling coil at site 2 is shown in Figure 4-11. Integrating the off-cycle evaporation rate for this coil (beginning 4 minutes after compressor shutdown) yields an estimated 5.6 pounds of moisture retained on this coil. This amount of moisture retention is significantly larger than the estimated moisture retention for the coil at site 1 (Figure 4-9). This difference is primarily due to the fact that the site 2 coil has 85% more finned surface area than the site 1 (downstairs unit) coil.

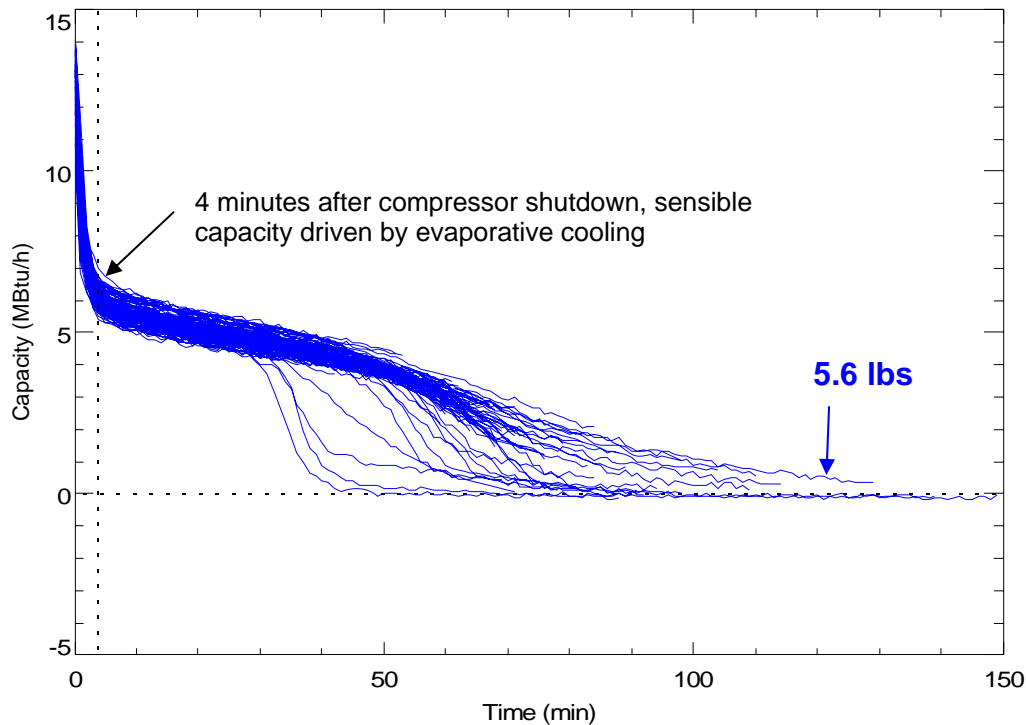


**Figure 4-11. Trend of Sensible Capacity for Several “Wetted” Off Cycles, Site 2**

As described previously, the chilled water coils at sites 6 and 7 were not controlled in an on/off fashion like the DX coils. Instead, chilled water flow through the coil was varied based on the difference between the measured space temperature and the set point temperature. Therefore, specific tests were conducted to measure off-cycle sensible capacity in order to estimate moisture retention on the cooling coil. The space set point temperature was reduced and the coil operated with full chilled water flow to yield a fully-wetted coil, then water flow was stopped while the fan continued to operate until the moisture on the coil was completely evaporated back into the supply air stream. The air flow rate across the coil for the variable-air-volume system (site 7) was fixed at its design value for this test, while the air flow across the coil for the constant-air-volume system (site 6) remained at its normal value. Integrating the off-cycle sensible capacity and dividing by the heat of vaporization for water resulted in moisture retention estimates of approximately 3.4 pounds and 7.5 pounds for the coils at sites 6 and 7, respectively.

Estimates of moisture retention parameters based on measured data for all field-tested coils are shown in Table 4-7. The moisture performance characteristics (i.e., retained moisture mass and condensate delay time) were determined from actual operating conditions as opposed to a

reference set of test conditions as was done for the coils tested in the laboratory (Table 3-7). As the laboratory tests indicated, the moisture retention characteristics of cooling coils vary with operating conditions, particularly chilled water coils. Therefore, direct comparison of these estimated values should be done with caution but can be used for general trend comparisons with the laboratory test results (see Section 6). No moisture performance characteristics could be estimated for the coil at site 3 due to insufficient data.

**Table 4-7. Comparing Measured Performance Parameters for the Field-Tested Cooling Coils**

	Capacity (tons)	Fin Surface Area (ft <sup>2</sup> )	Retained Moisture Mass		Condensate Delay Time (min)
			(lb)	(lb/kft <sup>2</sup> )	
Site 1, Second Floor (Inverted A-coil, 3 row, 13 fpi, orifice)	2.5	241.5	na	na	15.2
Site 1, First Floor (Inverted A-coil, 3 rows, 13 fpi, orifice)	3.0	241.5	1.9	8.0	16.4
Site 2, First stage (A-coil, 3 rows, 14 fpi, TXV)	1.5	446.3	5.6	12.5	40-50
Site 4 (Vertical slab coil, 3 rows, 13 fpi, TXV)	10.0	762.3	5.7	7.4	8-12
Site 5 (A-coil, 3 rows, 15.5 fpi, lanced sine-wave fins, hard shut-off TXV)	3.5	508.1	5.2	10.2	35
Site 6 (Vertical slab chilled-water coil, 6 rows, 12 fpi, wavy fins, 46°F entering water temp.)	2.9	499.6	3.4	6.8	21-30
Site 7 (Vertical slab chilled-water coil, 6 rows, 11 fpi, straight fins, 46°F entering water temp.)	7.2	1008.7	7.5	7.4	15-16

- Notes: 1- Cooling capacity is the nominal rated capacity (sites 1-5) or the design cooling capacity (sites 6-7).  
 2- Surface area is gross fin area: coil face area (ft<sup>2</sup>) x coil depth (in) x fin spacing (fpi) x 2  
 3- Retained moisture and condensate delay time are estimated from field measurements. See Appendix I for details.  
 4- na = not available from measured data.

## Thermostat Cycling Rate

One input to the latent capacity degradation model by Henderson and Rengarajan (1996, Section 5.1), and the improved degradation model developed as part of this project (Section 5.3), is the maximum thermostat cycling rate. Thermostat behavior for single-stage AC systems (on/off control) is expected to follow a parabolic trend with runtime fraction corresponding with the NEMA thermostat curve (NEMA 1990) as shown in Figure 4-12 and Figure 4-13 below. The single-parameter parabolic curve is defined as:

$$N = 4 \cdot N_{\max} \cdot X \cdot (1-X)$$

where  $N_{\max}$  is the peak cycling rate which occurs at a runtime fraction ( $X$ ) of 0.5. Most residential and small commercial systems have a value of  $N_{\max}$  around 3 cycles/hour. For the first floor and second floor AC units at field site 1 (Figure 4-12 and Figure 4-13), the values of  $N_{\max}$  calculated from the average  $N$  for  $X$  in the range of 0.48-0.52 are 2.9 and 3.5 cycles/hour, respectively. In each case the measured data were determined from 1-minute records by calculating the exact length of each total on/off cycle ( $t_{\text{cyc}}$ ) as well as the compressor runtime ( $t_{\text{on}}$ ). Then for each cycle the runtime fraction ( $X = t_{\text{on}}/t_{\text{cyc}}$ ) and the cycle rate ( $N = 1/t_{\text{cyc}}$ ) were determined. The shape of these curves is representative of the curve used for testing cooling coils in the laboratory where a peak cycling rate of 3.0 was used (see Section 3). The degree of scatter for the first floor AC unit is most likely due to user thermostat adjustment, thermostat setup and setback, and any built-in control delays in the AC unit.

The peak cycling rates,  $N_{\max}$ , for the coils at site 1 were similar to those seen for other DX coil test sites (the on/off cycling rate was not applicable to chilled water coil sites 6 and 7).  $N_{\max}$  generally ranged from 2.4 to 3.5 cycles/hour. The notable exception was the rooftop packaged unit at site 4 (Figure 4-14). For this 2-stage system, the peak cycling rate for the 2<sup>nd</sup> stage compressor was only 0.9 cycles/hour. The time clock controls for this unit were causing very long coil operating times with very little on/off cycling for the 2<sup>nd</sup> stage compressor.

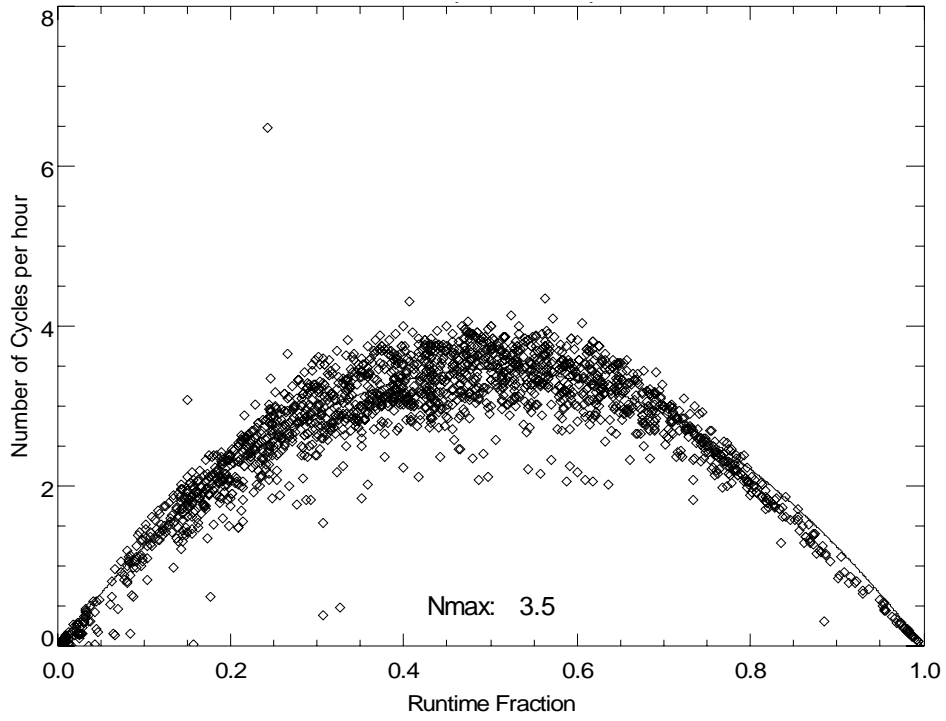


**Figure 4-12. Thermostat Cycling Curve for 2nd Floor AC Unit at Site 1**

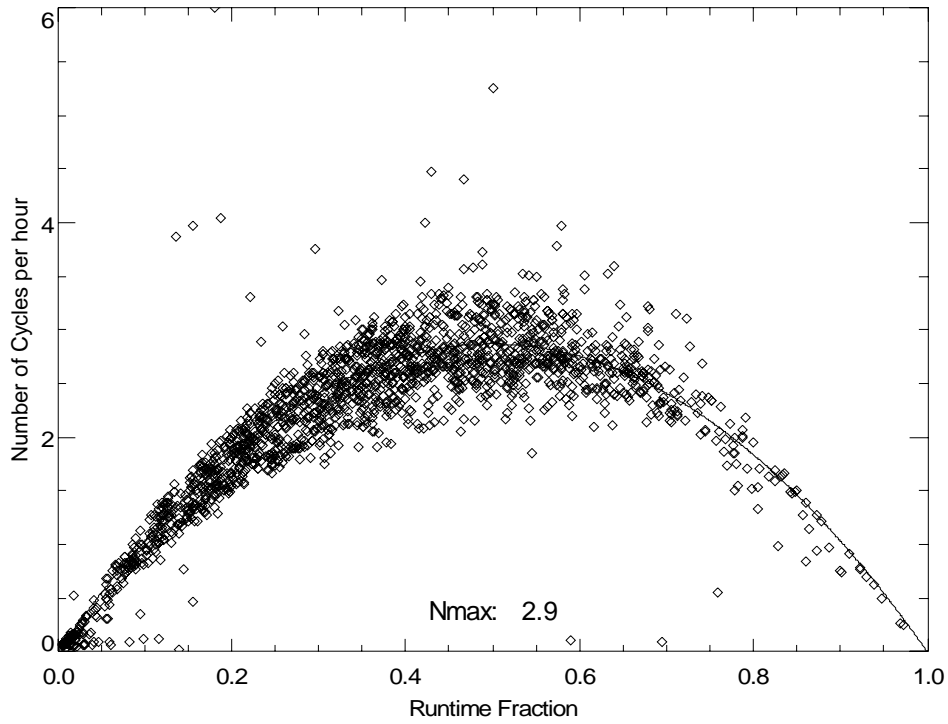


**Figure 4-13. Thermostat Cycling Curve for 1st Floor AC Unit at Site 1**

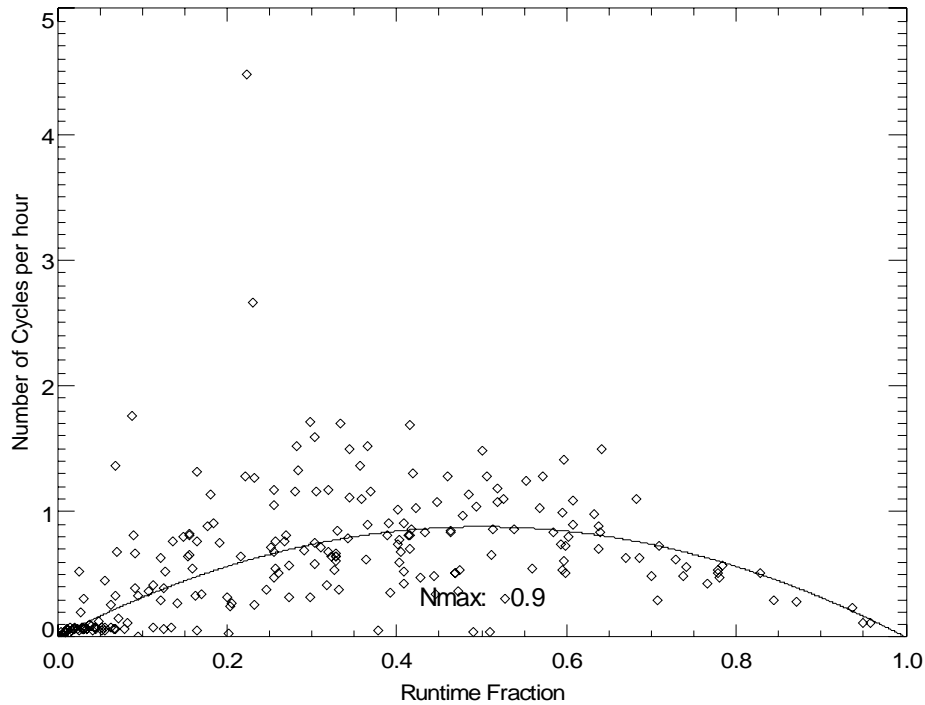


**Figure 4-14. Thermostat Cycling for 2<sup>nd</sup> Stage Compressor Operation at Site 4**

### 4.5.3 Part-Load Sensible Heat Ratio

The moisture removal capacity of a cooling coil is reduced at part-load conditions. Figure 4-15 shows the net impact of part-load operation on the dehumidification performance of the 1<sup>st</sup> floor unit at site 1. The “effective” sensible heat ratio is plotted as a function of cooling coil runtime fraction (RTF). The delivered sensible capacity is obtained using the integrated dry-bulb temperature difference across the cooling coil and air flow rate for the entire on/off cycle, while the latent capacity is obtained by measuring the moisture removed at the condensate drain (measured using the rain gauge tipping bucket). The sensible heat ratio is the delivered sensible capacity divided by the total (sensible plus latent) capacity for the on/off cycle. The data used to generate Figure 4-15 was restricted to times when the hourly average entering air conditions were 71-74°F (21.7-23.3°C) and 48-52% relative humidity.

Figure 4-15 shows resulting degradation in part-load dehumidification performance with the fan operated continuously and with the fan cycling on/off in tandem with the cooling coil (AUTO fan). Consistent with laboratory test results (Section 3.4.2), continuous supply air fan operation significantly degraded dehumidification capacity (i.e., increased sensible heat ratio) as coil runtime fraction decreased. For this coil, below approximately 60% runtime fraction the unit provided no net dehumidification to the conditioned space (SHR = 1). Similar trends were seen with for all single-stage DX coils tested with constant fan operation (both the field and laboratory tests associated with this project). The line in Figure 4-15 shows the results for the latent degradation model developed by Henderson and Rengarajan (1996), with good agreement between the model and the measured data. In this case the parameters for the model were determined using measured data from the site (see Appendix I).

Latent degradation at part-load operation is also common when the fan is configured to operate in tandem with the compressor (AUTO fan mode operation), although the degradation is less severe than when the fan operates continuously. Data collected at site 1 with AUTO fan control (Figure 4-15) shows a marked increase in sensible heat ratio as the compressor/fan runtime fraction decreases. This latent degradation at lower coil runtime fractions was also seen for other field test sites and in laboratory tests, although to a lesser extent than the degradation seen for this system.

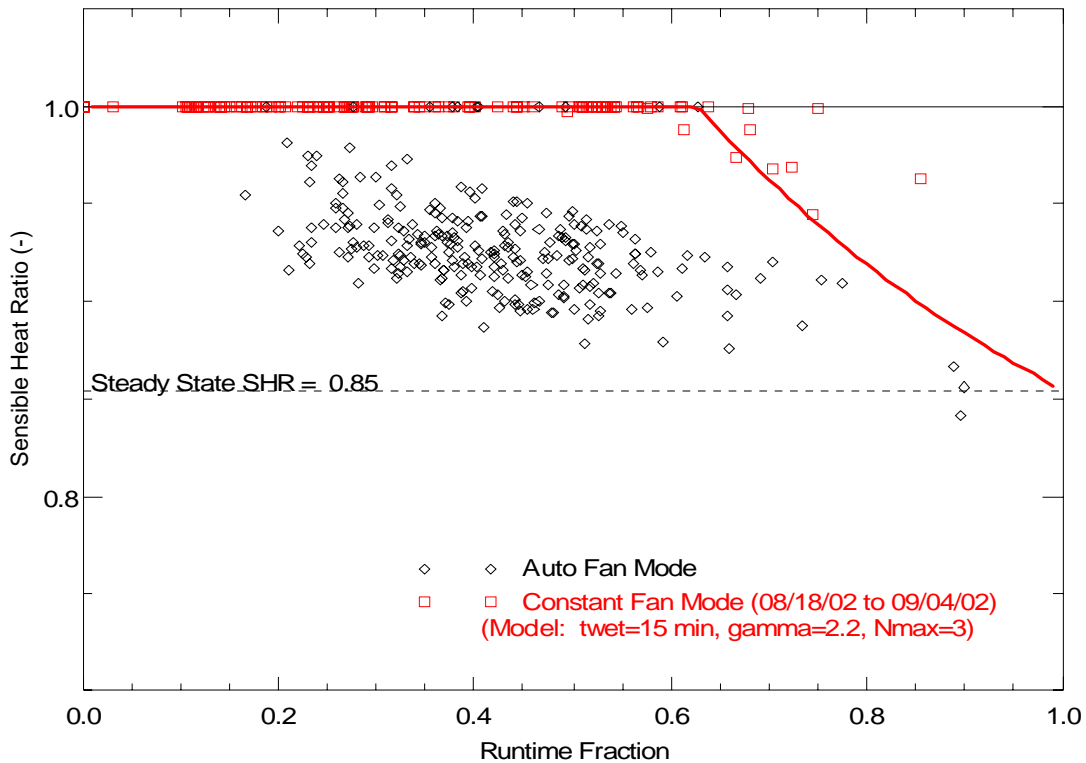


**Figure 4-15. Measured Latent Degradation for 1<sup>st</sup> Floor AC Unit at Site 1**

Figure 4-16 shows the sensible heat ratio versus compressor runtime fraction for the two-stage commercial rooftop unit at site 4. Data are only included in the plot for periods when the hourly average entering air conditions were 70-75°F (21.1-23.9°C) and 45-55% relative humidity. Both the RTF and SHR are averaged on an hourly basis. The runtime fraction in this case is summation of the runtime fraction for compressor 1 (SC1) and the runtime fraction for compressor 2 (SC2) divided by 2.

There is little to no degradation at runtime fractions above 0.5, since compressor 1 is running continuously at these conditions. The lack of degradation seen for the 2<sup>nd</sup> stage compressor is also influenced by the abnormally low cycle rate for this cooling stage (Figure 4-14). Only a mild amount of degradation is apparent as compressor 1 cycles on and off (for RTFs below 0.5), even with continuous fan operation.



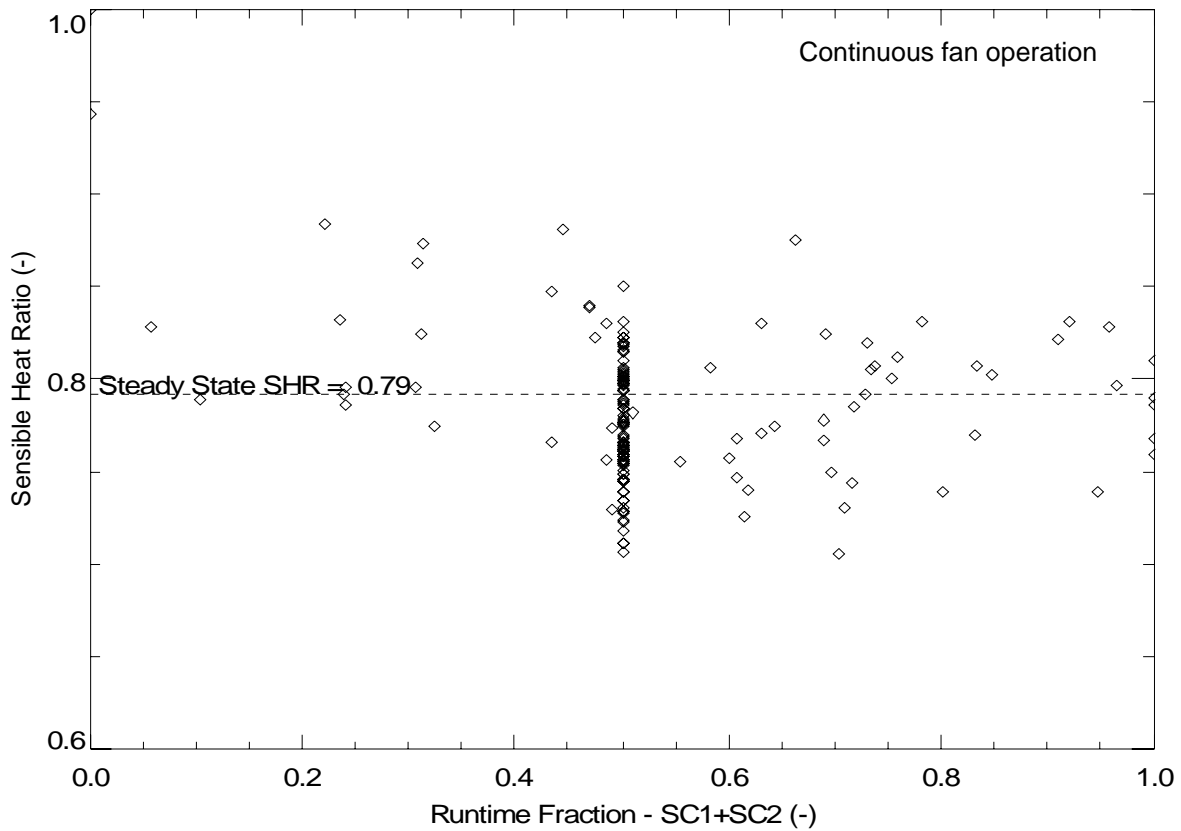


**Figure 4-16. Measured Latent Degradation for Site 4 (DB: 70-75°F, RH: 45-55%)**

Figure 4-17 shows the sensible heat ratio versus compressor runtime fraction for the two-stage residential unit with variable-speed air handler at site 2. With AUTO fan control, there was little to no latent degradation during 2<sup>nd</sup> stage operation (runtime fraction 0.5 to 1.0). However significant degradation was seen during 1<sup>st</sup> stage operation (runtime fraction 0 to 0.5) when the 1<sup>st</sup> stage compressor was cycling on and off in tandem with the fan. There was insufficient data available at these same operating conditions to generate comparable results for constant fan mode.

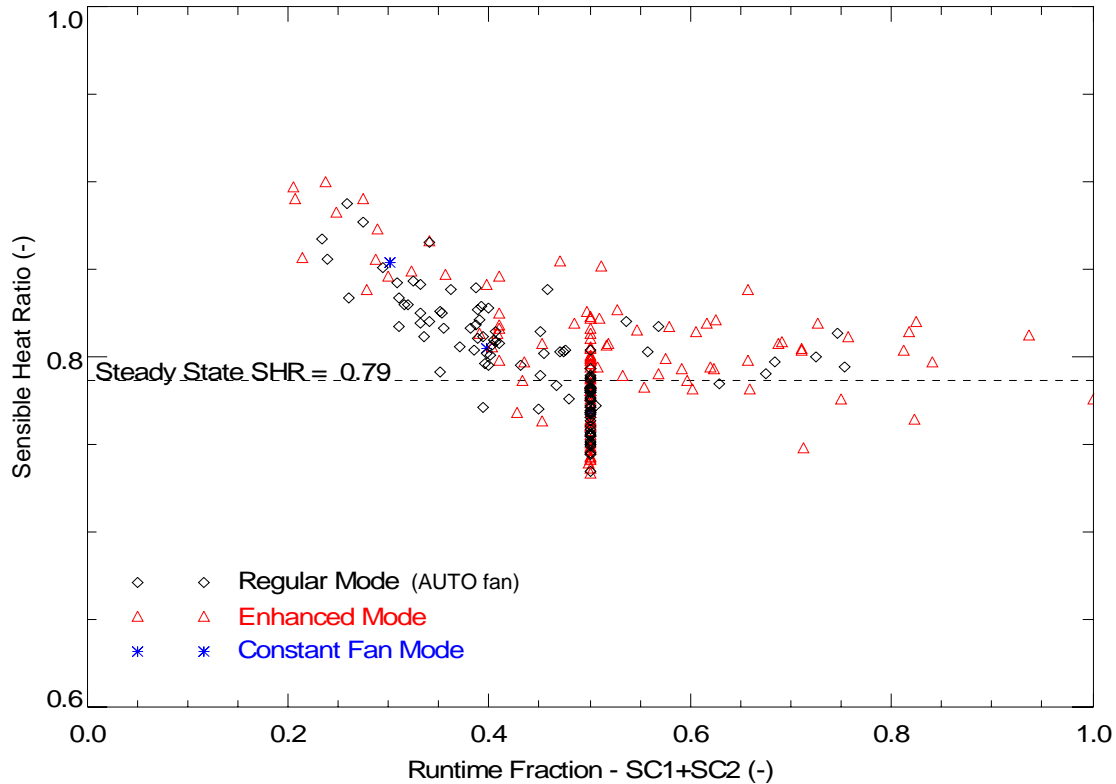


**Figure 4-17. Measured Latent Degradation for Site 2 (RH: 50-55%)**

#### 4.5.4 Impact of Supply Air Fan Control on Indoor Humidity Levels

Section 4.5.3 above discussed the impacts of two common fan control modes (constant fan mode and AUTO fan mode) on the dehumidification performance of cooling coils at part-load conditions. The measured field data indicated varying degrees of latent capacity (dehumidification) degradation at part-load conditions depending on the fan control mode. Reduced dehumidification performance can impact indoor humidity conditions, which may lead to occupant discomfort, indoor air quality problems, and increased energy use. Measurements of indoor humidity levels from the field test sites were therefore analyzed to determine the impacts due to various fan control strategies that are commonly used.

Figure 4-18 shows indoor versus outdoor humidity levels for site 1 (1<sup>st</sup> floor unit) with constant fan and AUTO fan operating modes. The plotted data points represent daily average values of absolute humidity levels for days with cooling coil activity. Results from this study and others indicate that continuous fan operation causes greater degradation in latent cooling (dehumidification) capacity at part-load conditions than AUTO fan operation, with the expectation of higher indoor humidity levels for the constant fan case. Figure 4-18, however, shows only a modest tendency toward higher indoor humidity levels with constant fan mode compared to AUTO fan mode. This can be partially explained by Figure 4-15, which shows that this cooling coil has significant latent capacity degradation with AUTO fan control mode, not too different from the degradation seen for constant fan mode. As explained previously, the latent degradation for this coil with AUTO fan operation was greater than we have seen for other coils.

In addition, this multi-story residence was conditioned by two cooling systems, so the operation of the other system (2<sup>nd</sup> floor unit) may have impacted the air conditions on the 1<sup>st</sup> floor of the residence.

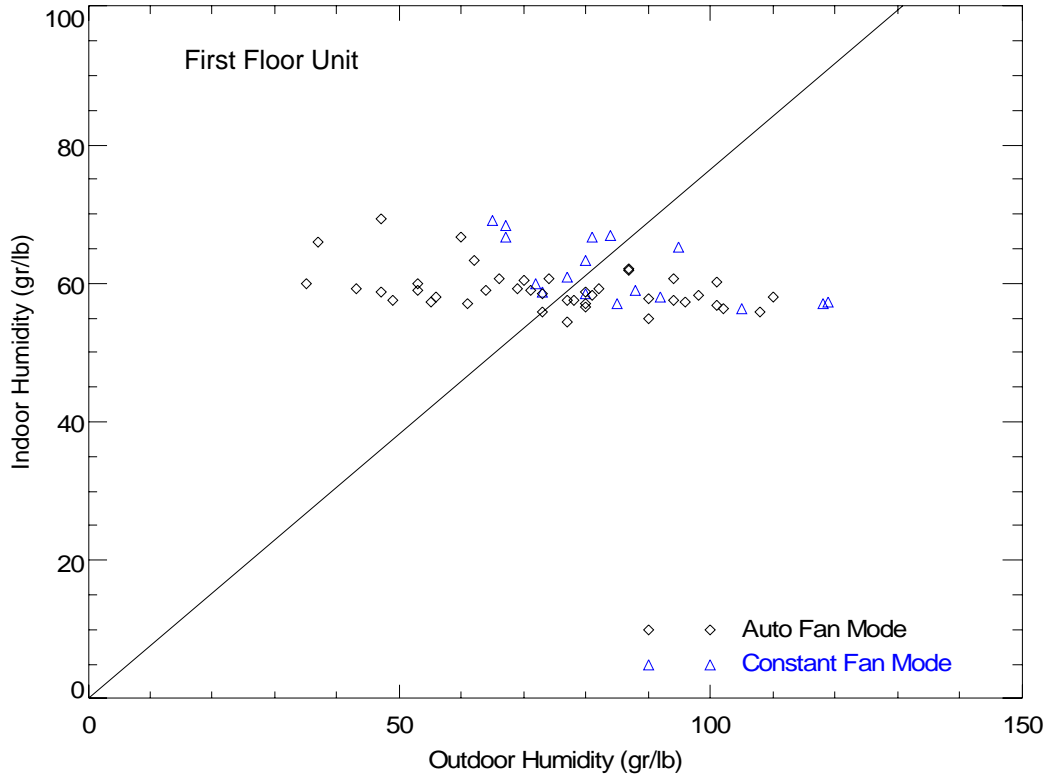


**Figure 4-18. Daily Humidity Ratios for AUTO vs Constant Fan Modes at Site 1**

Figure 4-19 and Figure 4-20 show the same plot of indoor versus outdoor humidity levels for site 2 and site 3, respectively. For these sites, constant fan mode definitely caused higher indoor humidity levels when compared to AUTO fan mode at similar outdoor humidity levels. For site 2, indoor humidity levels were consistently 10-20 grains/lb (0.0014-0.0028 kg/kg) lower with AUTO fan mode. With indoor temperatures near 78°F for this site, these absolute humidity level reductions due to AUTO fan mode are equivalent to approximately 8-15% reduction in relative humidity.

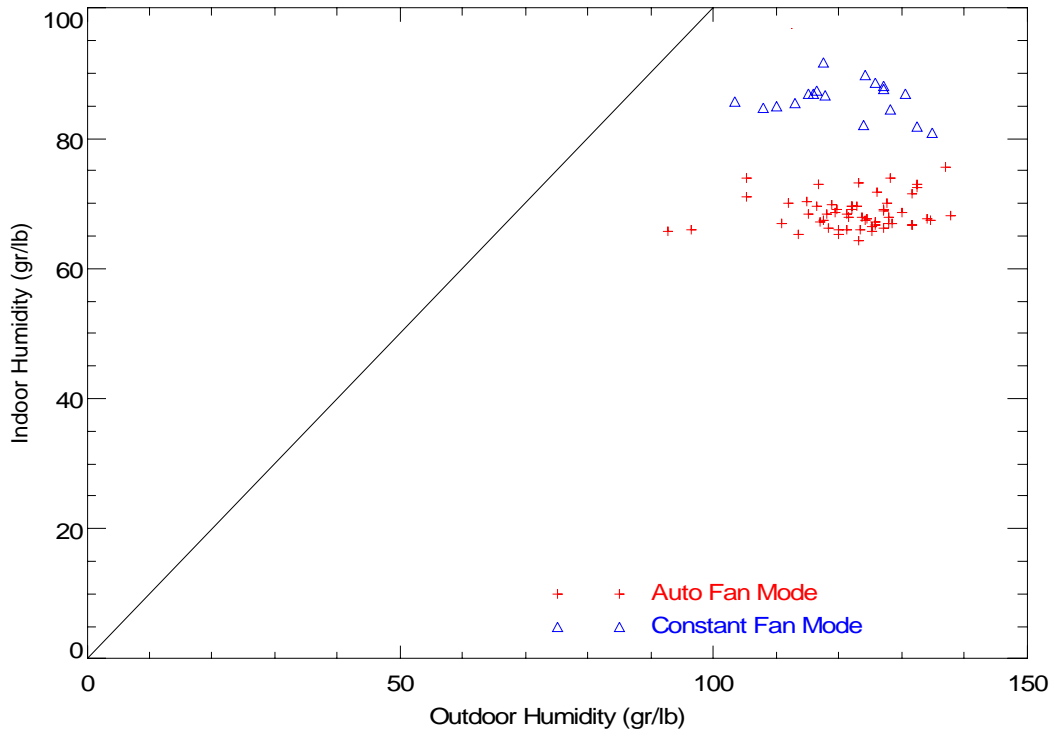


**Figure 4-19. Daily Humidity Ratios for AUTO vs Constant Fan Modes at Site 2**

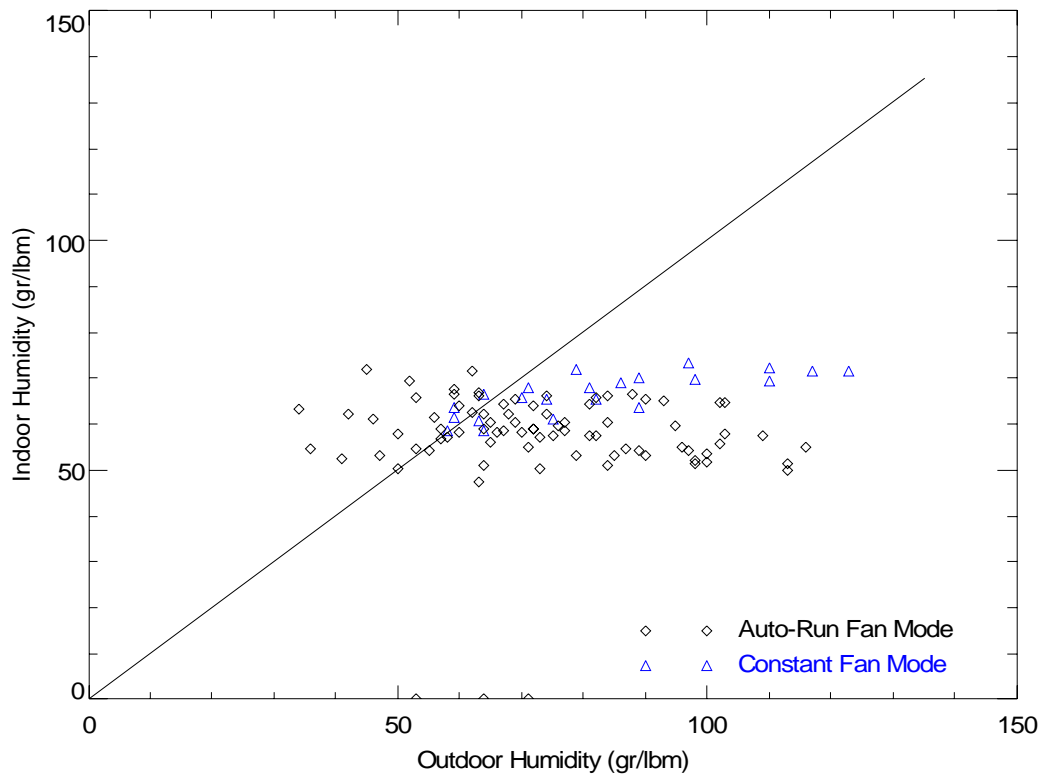


**Figure 4-20. Daily Humidity Ratios for AUTO vs Constant Fan Modes at Site 3**

As explained previously (Section 2.4), one area of interest for this project was new residential equipment with variable-speed supply air fan capabilities that can be used to improve dehumidification performance. This equipment is being heavily marketed in humid climates like the southeastern U.S. Several equipment manufacturers have implemented supply fan control schemes intended to limit latent capacity degradation or enhance steady-state latent capacity. Fan delays as well as brief operating periods at lower fan speeds are often used to enhance latent capacity. As part of the literature review portion of this project, manufacturer's data were collected to understand the operation of these new residential products, and a summary of the enhanced fan control schemes being used is listed in Table 2-3. This information was also used to select the equipment to be monitored at site 2 and site 5. Site 2 has a two-stage heat pump with variable-speed supply air fan, while site 5 has a single-stage unit with a variable-speed fan. Indoor humidity levels were monitored at these two sites to assess the benefits of the various supply fan control schemes provided by the manufacturer's of these units.

In addition to the conventional constant fan and AUTO fan control modes, the air handlers at sites 2 and 5 also had an "enhanced" dehumidification mode where fan speed was reduced at the beginning of each cooling cycle. The fan speed was eventually ramped up to the nominal value as the cooling cycle continued. Figure 4-21 shows the enhanced fan control used for stage 1 cooling at site 2. The fan initially operates at 50% flow for 1 minute after the 1<sup>st</sup> stage compressor starts. The air flow ramps up to 80% flow for the next 7.5 minutes, and up to 100% flow thereafter. When the 1<sup>st</sup> stage compressor turns off, the fan stays at 100% flow for three minutes before ramping off<sup>3</sup>. Note that 1<sup>st</sup> stage cooling represents approximately 50% of the maximum cooling capacity of this unit, so 100% flow for 1<sup>st</sup> stage cooling is about 50% of the air flow rate when 2<sup>nd</sup> stage cooling is active.

Figure 4-22 shows how the unit at site 2 switches up to (and back from) 2<sup>nd</sup> stage cooling. Both compressors are off for 1 minute before the 2<sup>nd</sup> stage compressor is enabled. During the 1-minute break, the fan ramps up (or down) to the required speed without any enhanced mode delays.

Indoor humidity levels for site 2 were monitored with this enhanced dehumidification mode and compared to humidity readings with AUTO fan control, and the results are shown in Figure 4-23. The plotted data points represent daily average values of absolute humidity levels for days with cooling coil activity. The results in Figure 4-23 indicate that the enhanced fan control provided little difference in indoor humidity levels for this site. The unit at site 5 had a slightly different enhanced fan control strategy, but it too provided only a modest difference in indoor humidity levels compared to conventional AUTO fan control (see Appendix I5).

One theory for the modest humidity impact at site 2 with enhanced fan control was that two-stage compressor operation already provides sufficient humidity control so that enhanced fan control provides little additional benefit. To test this hypothesis, the unit controls at site 2 were set to operate the system as a single-stage unit (in high stage) with enhanced fan control as well as regular (AUTO) fan control. The indoor humidity levels provided by these control modes were compared to the enhanced fan control with two-stage cooling operation. Figure 4-25 shows that the same indoor humidity was maintained for all three of these control options.

---

<sup>3</sup> It is possible that the design engineers had intended a reduction to 50% flow during this period. The manufacturer's literature indicated 50% flow during this shutdown period, and this was seen when this unit was briefly reconfigured to operate as a single-stage unit.

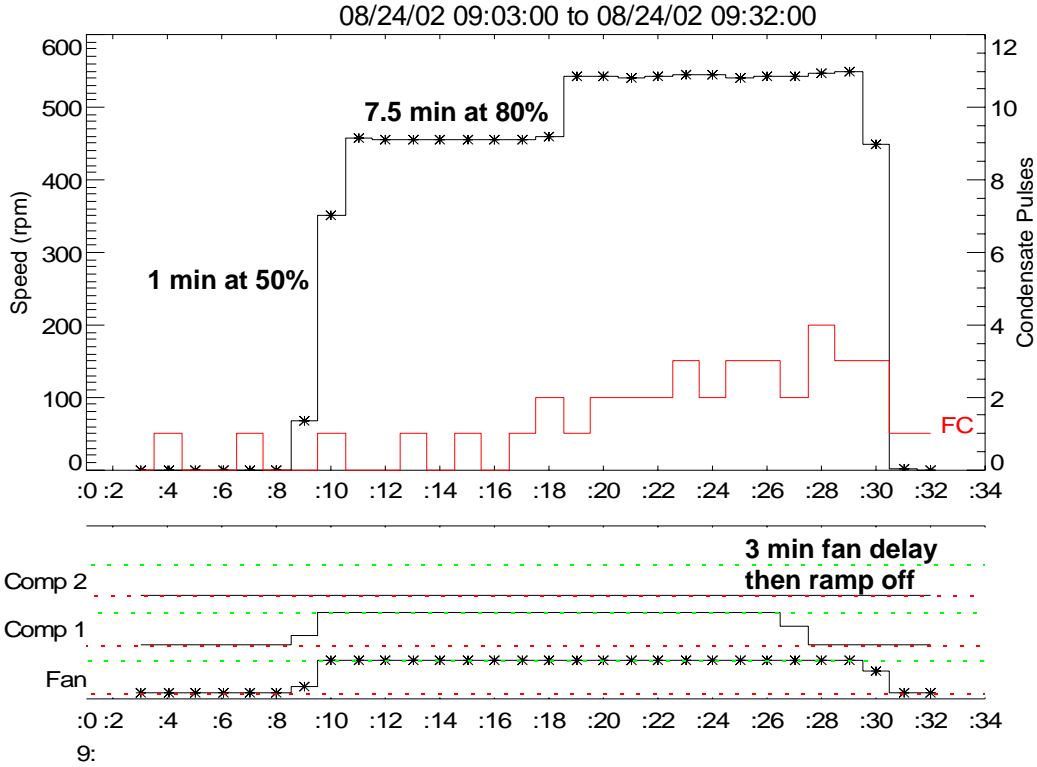


**Figure 4-21. Enhanced Fan Mode for Stage 1 Cooling at Site 2**

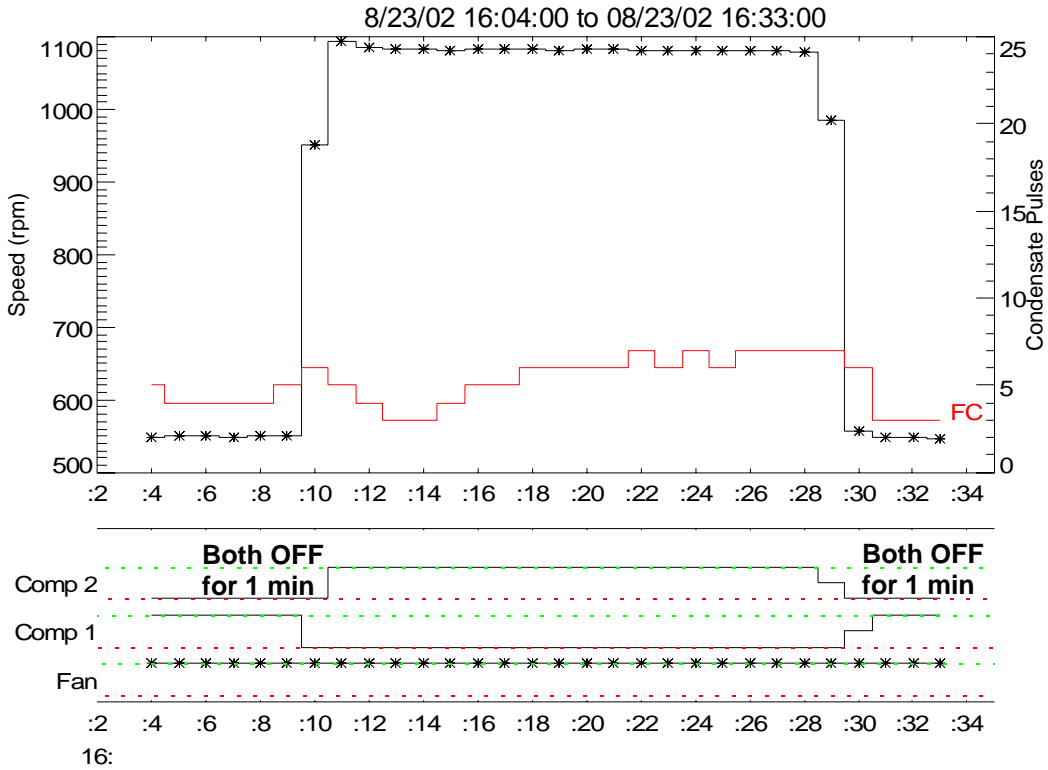


**Figure 4-22. Enhanced Fan Mode for Stage 2 Cooling at Site 2**

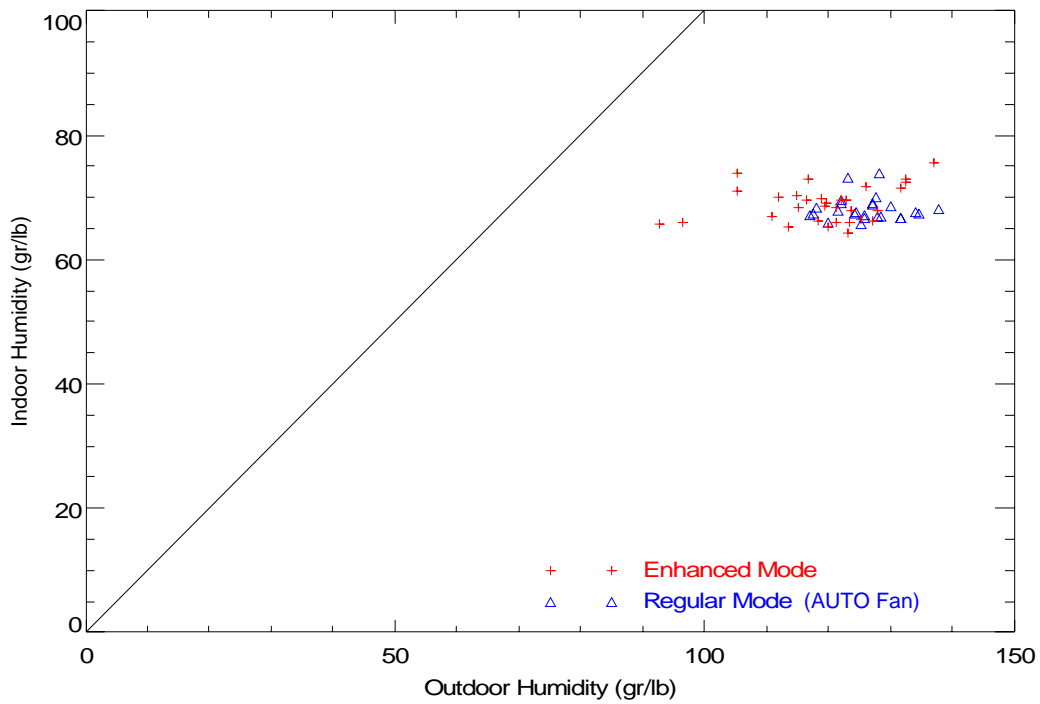


**Figure 4-23. Impact of Control Modes on Indoor Humidity at Site 2: Enhanced vs. AUTO**

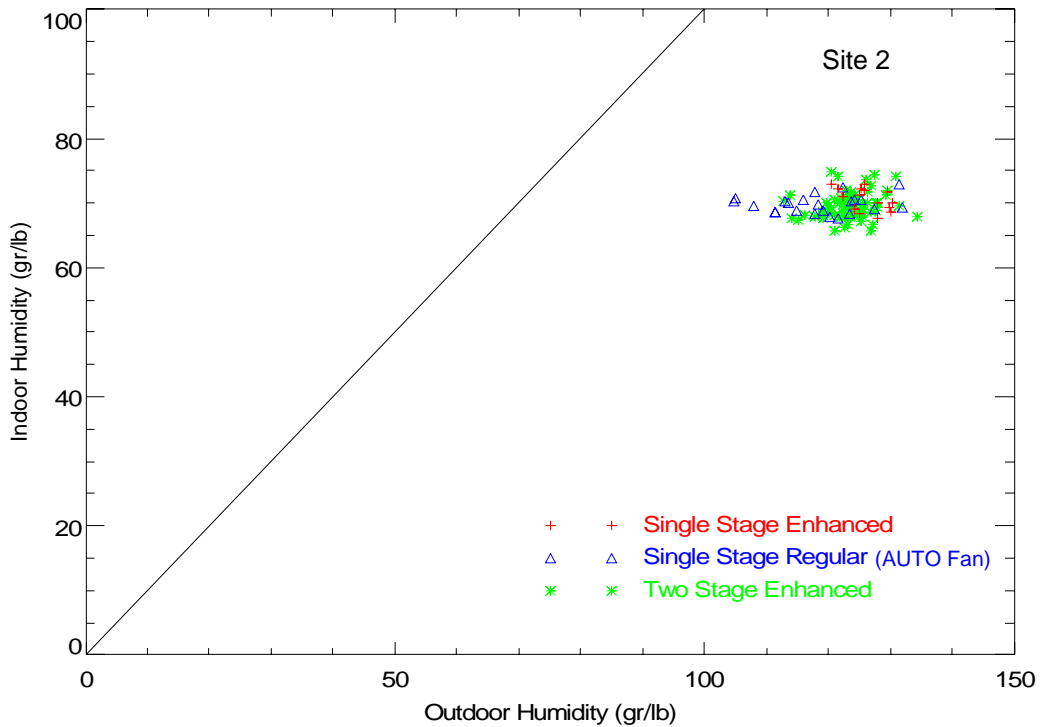


**Figure 4-24. Impacts of Control Modes on Indoor Humidity: Single Stage vs. Two Stage**

One unexpected finding at site 2 was the difference in coil operating temperatures during 1<sup>st</sup> and 2<sup>nd</sup> stage operation. As shown in Figure 4-25, the unit at site 2 has a slightly lower saturated suction temperature during 2<sup>nd</sup> stage operation than during 1<sup>st</sup> stage operation. This lower coil temperature yields slightly better dehumidification performance (lower steady-state sensible heat ratio) during 2<sup>nd</sup> stage operation. If 1<sup>st</sup> stage operation had provided better dehumidification than 2<sup>nd</sup> stage operation, we would have seen better overall dehumidification with this two-stage unit. However, the dehumidification penalty expected with shorter compressor runtimes when the system was configured as a single-stage unit was apparently negated by the improved 2<sup>nd</sup> stage dehumidification performance.

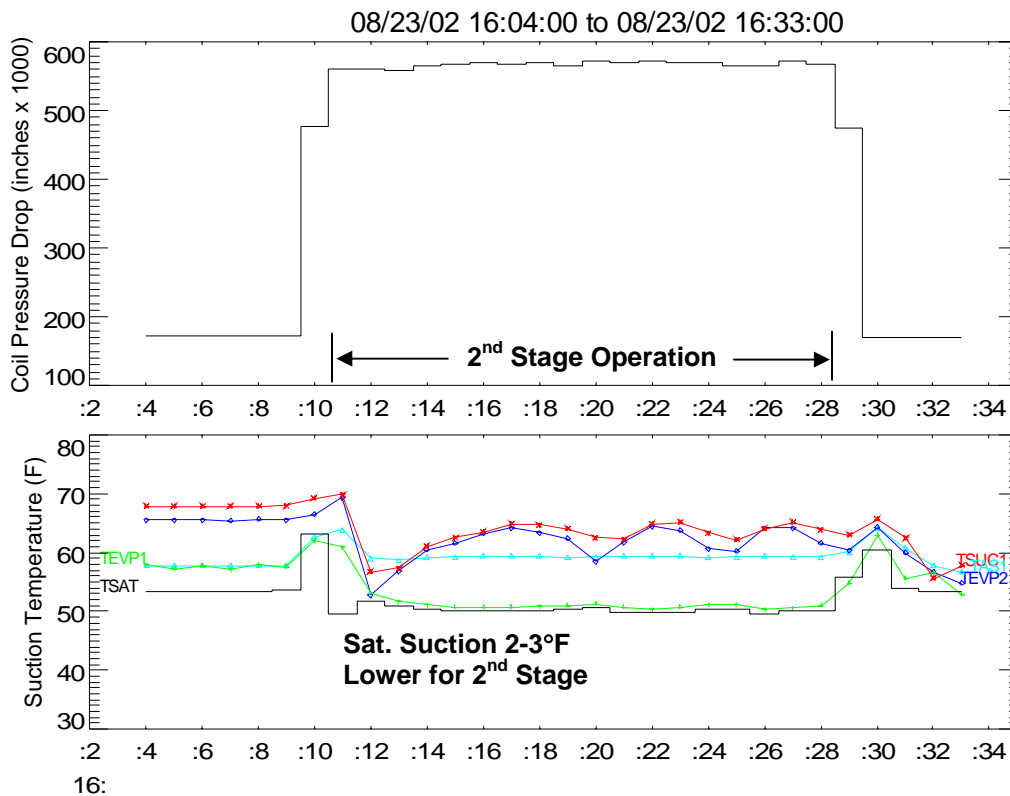


**Figure 4-25. Details of a 2<sup>nd</sup> Stage Cycle for Site 2 (Enhanced Mode)**



# 5 Model Development and Validation

This section develops and validates algorithms and engineering models to predict the part-load latent performance of cooling coils in various applications and configurations. This section also provides guidance on how to apply these latent degradation models for a wide variety of systems.

## 5.1 Original LHR Model from Henderson and Rengarajan

Henderson and Rengarajan (1996) developed a simple engineering model to predict the variation of latent capacity with cooling load fraction or runtime for a cycling air conditioner. The model was developed to predict how the latent heat ratio (LHR)<sup>4</sup> varies with runtime fraction (X) for a single-stage coil that has continuous supply air fan operation. Subsection 5.1.1 below summarizes the details of the calculation procedure from the original paper (for the case of linear decrease in moisture evaporation rate). The model requires the normalized parameters given in Table 5-1 as inputs to describe the characteristics of a cooling system. Figure 5-1 shows the graphical representation of these parameters.

**Table 5-1. Normalized Model Inputs for 1996 LHR Model**

Model Input	Description
$t_{wet}$	The nominal time after cooling startup when moisture starts to drain from the condensate pan. Defined as the maximum moisture holding capacity of the cooling coil ( $M_o$ ) divided by the steady-state latent removal capacity ( $Q_L$ ): $t_{wet} = M_o/Q_L$ .
$\gamma$	The ratio of the initial off-cycle evaporation rate ( $Q_e$ ) and the steady-state latent removal capacity ( $Q_L$ ): $\gamma = Q_e/Q_L$ .
$N_{max}$	The maximum thermostat cycling rate. Typically 3 cycles per hour for most cooling systems. $N_{max}$ mostly depends on the dynamic characteristics of the thermostat.
$\tau$	Time constant of latent capacity at startup. Typically 30 to 90 seconds.

The original LHR model was derived based on the following assumptions:

1. For a given cooling coil system all surfaces in the condensate removal path have a fixed capacity to hold water ( $M_o$ ). These surfaces include the cooling coil fins and tubes, the condensate pan, and the condensate drain. Once a fixed mass of water  $M_o$  has collected on the surfaces, additional condensate drains from the unit as cooling continues. Only condensate that drains from the unit is considered to be "removed" from the air.
2. Condensate removal always begins once the surfaces have collected a mass of water  $M_o$ , irregardless of the initial mass of water on the surfaces. Hysteresis effects that might be

<sup>4</sup> LHR is one minus the sensible heat ratio (1-SHR). SHR and LHR are sometimes used interchangeably in this section.

caused by previous wetting, surface tension, or dirty coil surfaces are assumed to be negligible.

3. The instantaneous latent capacity of a cooling system at startup is described by a first-order, exponential response with a time constant  $\tau$ . The time constant  $\tau$  is the same for total, sensible and latent capacity at startup.
4. The evaporation process is adiabatic, or sensible cooling provided during the off cycle is equal to the energy associated with moisture addition to the air stream. Thermal capacitance effects of the coil are neglected.

The sections that follow will evaluate many of these underlying assumptions.

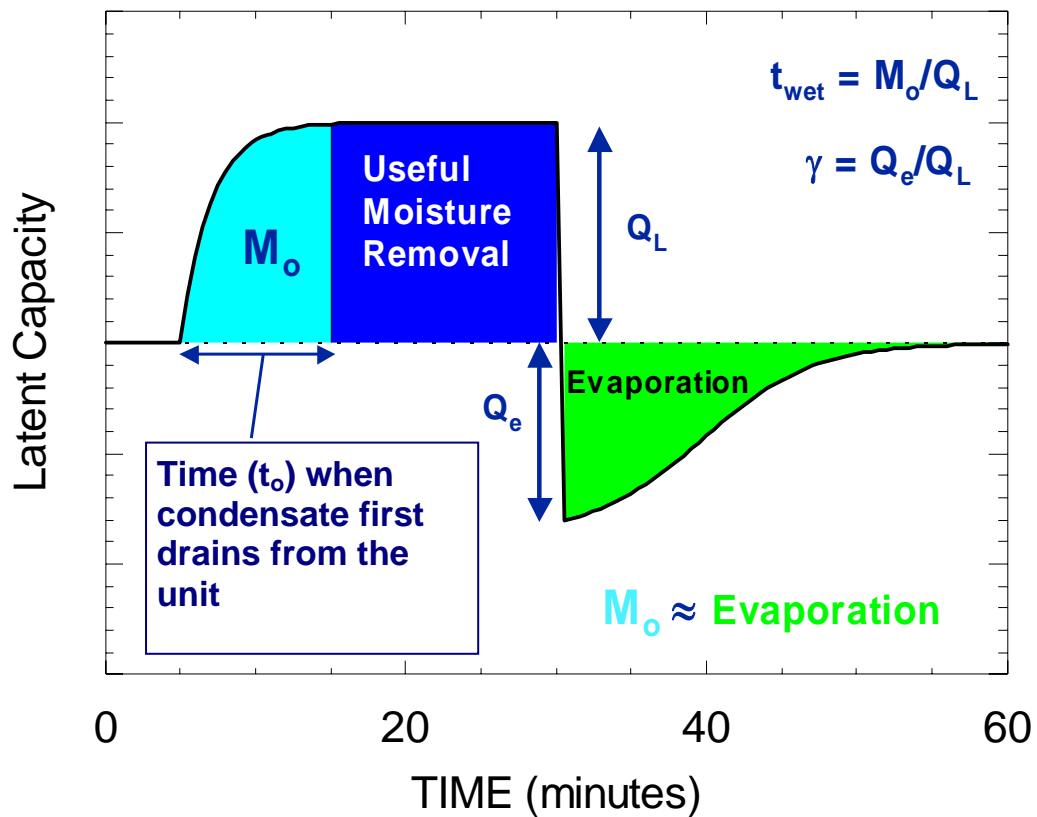


**Figure 5-1. Graphical Representation of LHR Model Parameters**

The original model assumed three possible modes of moisture evaporation from the coil during the off cycle:

1. moisture evaporation rate decreases linearly with time,
2. moisture evaporation rate is constant with time,
3. moisture evaporation rate decreases exponentially with time.

Figure 5-2 shows these three possible modes of moisture evaporation. In all cases the initial amount of moisture on the coil is assumed to be  $M_o$  (or  $M_{initial}$  if the full amount of moisture has not yet built up on the coil). These evaporation models were fairly crude approximations of observations from previous laboratory tests. Section 5.2 develops more sophisticated models to predict moisture evaporation.

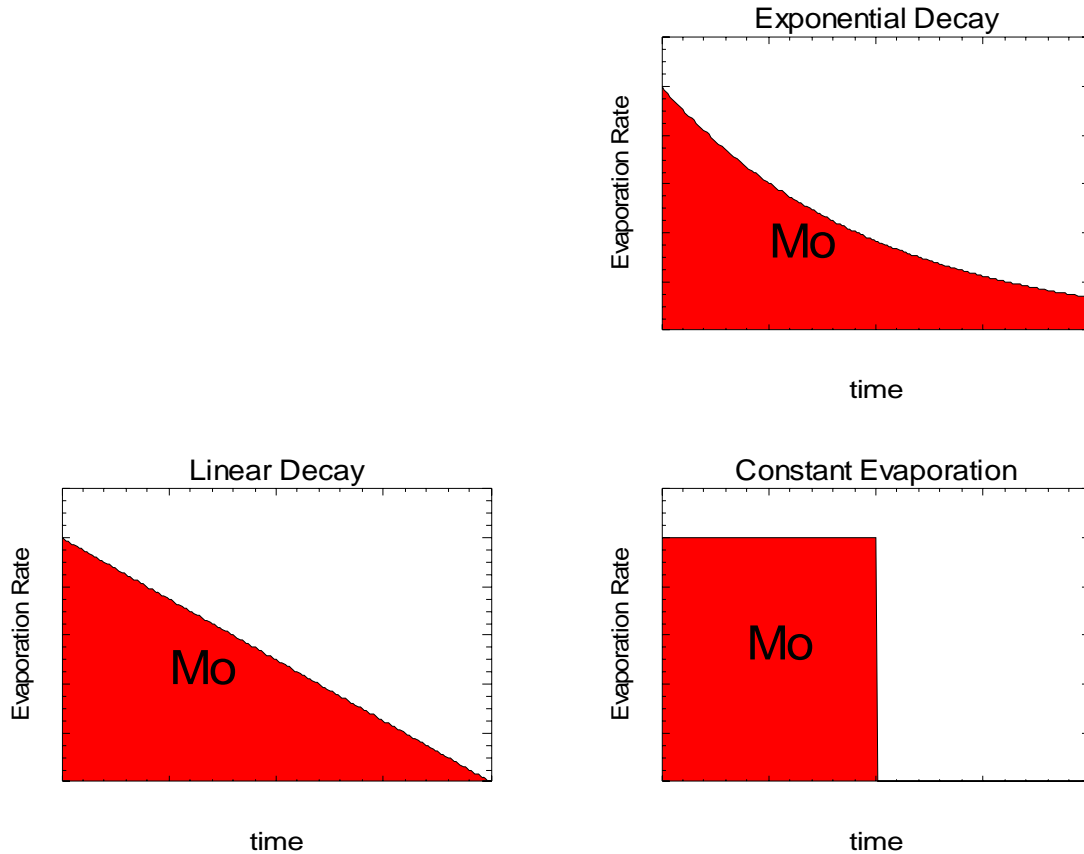


**Figure 5-2. Three Possible Modes of Off-Cycle Moisture Evaporation**

### 5.1.1 Summary of Original LHR Calculation Procedure

This subsection summarizes the calculation procedure for the latent heat ratio (LHR) part-load model described in Henderson and Rengarajan (1996). The variables are defined at the end of this subsection.

Use equations 5-1 and 5-2 to find  $X$  from CLF (if CLF is an independent variable):

$$X = \frac{CLF}{PLF(CLF)} \quad (5-1)$$

where PLF is determined by successive substitution from equation 5-2.

$$PLF_{i+1} = 1 - 4\tau N_{\max}(1 - CLF/PLF_i) \left[ 1 - e^{\frac{-1}{4\tau N_{\max}(1 - CLF/PLF_i)}} \right] \quad (5-2)$$

Use equations 5-3 and 5-4 to calculate  $t_{on}$  and  $t_{off}$  given X:

$$t_{on} = \frac{3600}{4N_{\max}(1 - X)} \quad (5-3)$$

$$t_{off} = \frac{3600}{4N_{\max}X} \quad (5-4)$$

Use a cooling coil performance map to calculate steady-state latent capacity as a function of the entering conditions  $Q_L(DB, WB)$ . Then use equations 5-5 and 5-6 to correct  $t_{wet}$  and  $\gamma$  to the actual operating conditions:

$$t_{wet} = t_{wet, rated} \frac{Q_{L, rated}}{Q_L(DB, WB)} \quad (5-5)$$

$$\gamma = \gamma_{rated} \frac{(DB - WB)}{(DB_{rated} - WB_{rated})} \frac{Q_{L, rated}}{Q_L(DB, WB)} \quad (5-6)$$

Use equation 5-7 (assuming a linear decay evaporation model) to solve for  $t_o$ , time after startup when moisture starts to drain from the unit.  $t_o$  must be determined by successive substitution.

$$t_o^{j+1} = \gamma t_{off} - \left\{ \frac{\gamma^2}{4t_{wet}} \right\} t_{off}^2 - \tau \left( e^{-\frac{t_o^j}{\tau}} - 1 \right), \quad t_{off} \leq \frac{2t_{wet}}{\gamma} \quad (5-7)$$

Use equation 5-8 and  $LHR_{ss}$  to calculate the part-load LHR:

$$\frac{LHR}{LHR_{ss}} = \frac{|t_{on} - t_o|^+}{(t_{on} + \tau(e^{-\frac{t_{on}}{\tau}} - 1))} \quad (5-8)$$

Equation 5-8 assumes that  $t_o \gg \tau$  which is nearly always true with constant fan operation. A more exact formulation of this equation that would apply when  $t_o \approx \tau$  is:

$$\frac{LHR}{LHR_{ss}} = \frac{|t_{on} - t_o + \tau(e^{-\frac{t_{on}}{\tau}} - e^{-\frac{t_o}{\tau}})|^+}{(t_{on} + \tau(e^{-\frac{t_{on}}{\tau}} - 1))} \quad (5-9)$$

Equation 5-9 was not given in Henderson and Rengaragan (1996) since it is usually not required for cases with constant supply air fan operation. However, some of the special fan control cases in the section below will require this more exact formulation.

Variables

<i>DB</i>	-	Dry-bulb temperature entering cooling coil (°F)
<i>WB</i>	-	Wet-bulb temperature entering cooling coil (°F)
<i>LHR</i>	-	Latent heat ratio at part load (-)
<i>LHR<sub>ss</sub></i>	-	Latent heat ratio at steady-state conditions ( $Q_L/(Q_S+Q_L)$ )
<i>M<sub>o</sub></i>	-	Energy of maximum condensate holding capacity of cooling coil (Btu)
<i>Q<sub>e</sub></i>	-	Initial evaporation rate (Btu/h)
<i>Q<sub>L</sub></i>	-	Steady-state latent capacity of cooling coil (Btu/h)
<i>Q<sub>S</sub></i>	-	Steady-state sensible capacity of cooling coil (Btu/h)
<i>t</i>	-	Time (s)
<i>t<sub>o</sub></i>	-	Time after coil startup when moisture begins to drain from the unit (s)
<i>t<sub>off</sub></i>	-	Duration of cooling coil off cycle (s)
<i>t<sub>on</sub></i>	-	Duration of cooling coil on cycle (s)
<i>t<sub>wet</sub></i>	-	Nominal time until moisture begins to drain from the unit, $M_o/Q_L$ (s)
$\tau$	-	Time constant of cooling coil response at startup (s)
$\gamma$	-	Ratio of initial evaporation rate and steady-state capacity $Q_e/Q_L$ (-)
<i>N<sub>max</sub></i>	-	Maximum cycling rate (cycles/h)
<i>X</i>	-	Runtime fraction (-)
<i>CLF</i>	-	Cooling load fraction: ratio of load and capacity (-)
<i>PLF</i>	-	Part load factor: ratio of part load and steady state efficiency (-)

**5.2 Better Predictions of Off-Cycle Moisture Evaporation**

A weak point in the original LHR degradation model from Henderson and Rengarajan (1996) was how moisture evaporated from the coil during the off cycle. This section derives a more sophisticated model to predict off-cycle evaporation and compares it to laboratory test data.

**5.2.1 Deriving a Model for Transient Moisture Evaporation**

Cooling Coil as an Evaporative Cooler

There is good evidence (see Figure 3-12) that a cooling coil quickly becomes an evaporative cooler during the off cycle. For an evaporative cooler the evaporation rate can be defined as:

$$q_{evp} = \frac{1.08 \cdot cfm \cdot (DB - WB) \cdot \eta_{evp}}{1060} \quad (\text{lb/h}) \quad (5-10)$$

Stabat et al. (2001) reviewed the theoretical performance of direct evaporative coolers and showed that the saturation effectiveness of an evaporative cooler is:

$$\eta_{evp} = 1 - e^{-NTU} \quad (-) \quad (5-11)$$

where NTU is the number of transfer units based on the mass transfer. They went on to show that for an air-water mixture below 50°C, the NTU can be expressed in the form:

$$NTU = \frac{K \cdot A}{cfm^{0.2}} \quad (-) \quad (5-12)$$

When the coil first turns off, its fully wetted surface ( $A_o$ ) holds a fixed amount of moisture ( $M_o$ ). However, as the water evaporates we can assume that the wetted surface area shrinks in proportion to the amount of moisture remaining on the coil, or:

$$A = \frac{M \cdot A_o}{M_o} \quad (ft^2) \quad (5-13)$$

### Mass Balance

Based on a mass balance, the rate of moisture evaporation must equal the change in moisture on the coil:

$$\frac{dM}{dt} = -q_{evp} \quad (lb/h) \quad (5-14)$$

Combining equations 5-10 through 5-14 results in a differential equation of the form:

$$\frac{dM}{dt} = \beta \cdot (1 - e^{-\alpha M}) \quad (lb/h) \quad (5-15)$$

where

$$\beta = \frac{-1.08 \cdot cfm \cdot (DB - WB)}{1060} \quad \text{and} \quad \alpha = \frac{K \cdot A_o}{M_o \cdot cfm^{0.2}} = \frac{NTU_o}{M_o}$$

Rearranging and integrating equation 5-15 results in:

$$\int_0^t dt = \frac{1}{\beta} \cdot \int_{M_s}^M \frac{dM}{1 - e^{-\alpha M}} \quad (5-16)$$

From the CRC Math handbook, this integral has the following solution:

$$t = \frac{M}{\beta} + \frac{1}{\alpha\beta} \cdot \ln(1 - e^{-\alpha M}) - \left[ \frac{M_s}{\beta} + \frac{1}{\alpha\beta} \cdot \ln(1 - e^{-\alpha M_s}) \right] \quad (5-17)$$

where the constant term in square brackets is also referred to as  $t_o$  below.  $M_s$  is the amount of moisture on the coil at the beginning of the off cycle. Rearranging equation 5-17 to express the moisture mass ( $M$ ) remaining on the coil as function of time:

$$M = \frac{1}{\alpha} \cdot \ln(e^{\alpha\beta(t+t_o)} + 1) \quad (\text{lb}) \quad (5-18a)$$

or rearranging to get rid of  $t_o$ , by using the term in brackets from equation 5-17 as an exponent of  $e$ ,

$$e^{\alpha\beta t_o} = e^{\alpha M_s} (1 - e^{-\alpha M_s}) = (e^{\alpha M_s} - 1)$$

equation 5-18a becomes:

$$M = \frac{1}{\alpha} \cdot \ln(e^{\alpha\beta t} \cdot (e^{\alpha M_s} - 1) + 1) \quad (\text{lb}) \quad (5-18b)$$

Recalling the definition of  $q_{evp}$  given by equation 5-15, the evaporation rate can be expressed as:

$$q_{evp} = -\beta \cdot (1 - e^{-\ln(e^{\alpha\beta t} \cdot (e^{\alpha M_s} - 1) + 1)}) \quad (\text{lb/h}) \quad (5-19a)$$

or rearranging yields:

$$q_{evp} = -\beta \cdot \left( \frac{e^{\alpha\beta t} \cdot (e^{\alpha M_s} - 1)}{e^{\alpha\beta t} \cdot (e^{\alpha M_s} - 1) + 1} \right) \quad (\text{lb/h}) \quad (5-19b)$$

### Resulting Moisture Evaporation Trends

Figure 5-3 and Figure 5-4 below show the resulting trends of the evaporation rate and remaining moisture mass using the parameters below for a hypothetical 3-ton coil:

Total coil fin area ( $A_o$ ) = 300 ft<sup>2</sup>

cfm = 1200 cfm

Nominal  $\eta_{evp}$  = 0.918 (NTU = 2.5) at 1200 cfm

Moisture mass ( $M_o$ ) = 3.5 lbs

The thin lines on each plot show the trend for the coil at the nominal air flow of 1200 cfm (400 cfm/ton). The thicker line shows the impact of decreasing the airflow to 900 cfm (300 cfm/ton).

These evaporation trends are more consistent with the field and laboratory observations from FSEC (Henderson 1990; Henderson 1998; Khattar et al. 1985) and by others (Shen et al. 2004). The initial evaporation rates increase at drier entering conditions and as the off-cycle airflow increases. At certain operating conditions, such as humid entering air with lower airflow, the trends become nearly linear – at least partially justifying the initial assumption of linear evaporation in the original LHR model. The next section compares the moisture evaporation model to measured laboratory data for various coils.

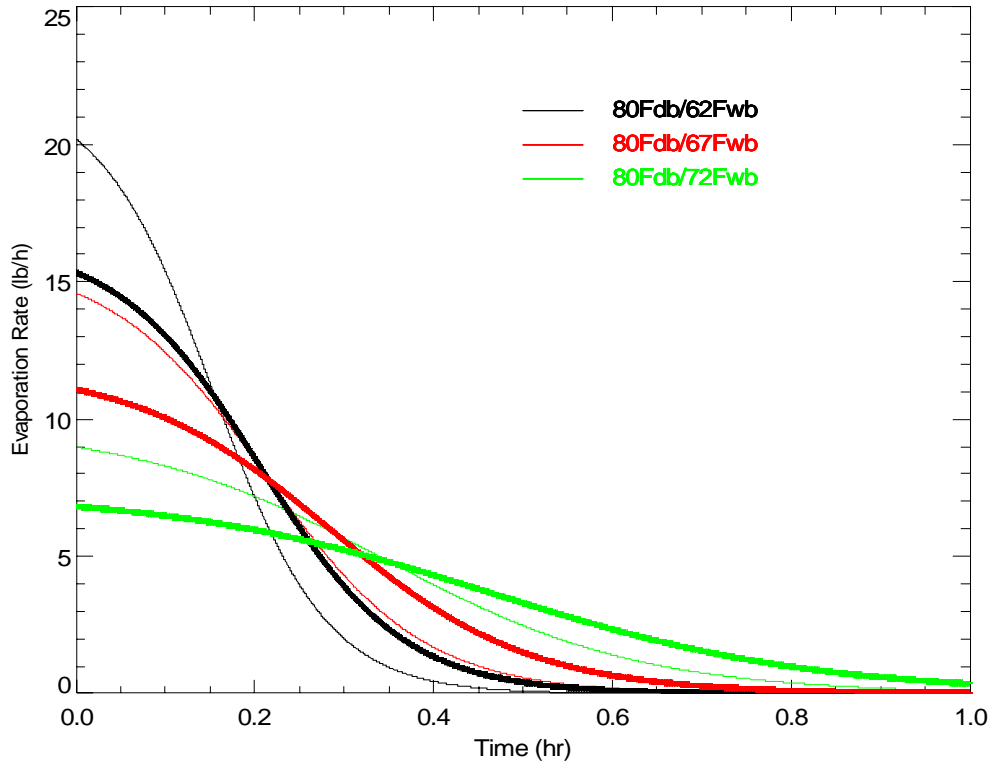


**Figure 5-3. Off-Cycle Moisture Evaporation Rate for Various Conditions**

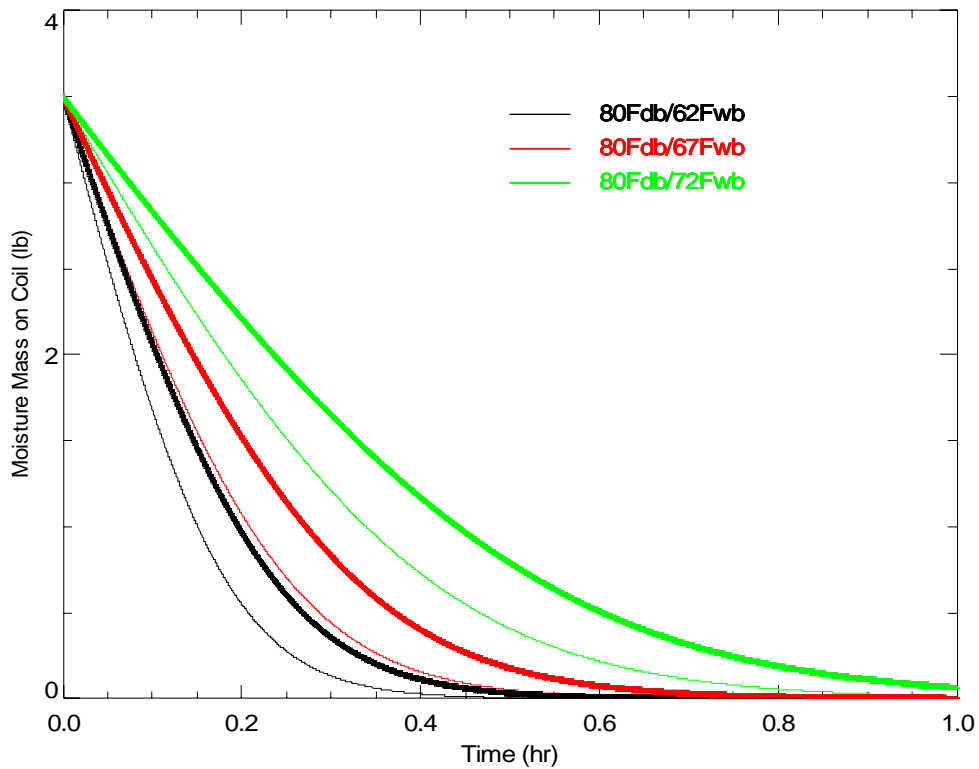


**Figure 5-4. Moisture Mass Remaining on the Coil for Various Conditions**



## 5.2.2 Validation of the Transient Moisture Evaporation Model

The moisture evaporation rate trends – as measured by the off-cycle sensible cooling – are shown for all 8 of the laboratory-tested coils in Figure 5-5 through Figure 5-28. Each figure corresponds to one air flow rate (expressed as cfm per ton) and shows the various entering air conditions. For each plot the measured data are shown with symbols. The moisture evaporation model derived above is shown on each plot as a thick line with the color corresponding to each set of measured points. Table 5-2 lists the model parameters that were used in each case. These values were determined from the laboratory tests for each coil (see the coil test summaries given in Section 3 and Appendix H). The plot also includes a “thin line” corresponding to each test run. This thin line corresponds to the evaporation model using parameters that are determined using only the test results for each specific run. Generally there are only modest differences between the thin line with test run specific parameters and the thick line, which uses average model parameters (from Table 5-2) for all the runs for a given coil.

**Table 5-2. Average Parameters Used for Moisture Evaporation Model Inputs**

	<b>Nominal Capacity (tons)</b>	<b>NTU Factor (K)</b>	<b>Factor x Area (K·A<sub>o</sub>)</b>	<b>Moisture Mass (M<sub>o</sub>)</b>
Coil 1	2.9	0.024	5.76	2.1
Coil 2	2.4	0.030	7.23	2.0
Coil 3 (Coil 2 with low flow)	1.4	0.032	7.60	2.0
Coil 4	1.8	0.029	4.00	1.9
Coil 5	2.3	0.032	5.17	1.4
Coil 6	1.6	0.043	9.99	2.7
Coil 7 (Coil 6 with high flow)	2	0.039	9.00	2.7
Coil 8	1.5	0.036	5.64	1.4

Notes: K is the constant in the NTU equation:  $NTU_o = K \cdot A_o / cfm^{0.2}$ .  
The actual cfm is the nominal capacity (tons) x the cfm/ton value.  
Then use  $\alpha = NTU_o / M_o$  and  $\beta = -1.08 \cdot cfm \cdot (DB-WB) / 1060$  with equation 5-19b converted to MBtu/h.

Generally there is good agreement between the moisture evaporation model and measured data. Agreement is better for lower air flows and more humid conditions since the evaporation process is slower and the instruments are better able to follow the dynamics of the process. Conversely, tests with lower humidity and high air flow show the most deviation from the measured trends because the thermocouples cannot respond fast enough. The match is always poor for the first 1-2 minutes of the off-cycle since refrigerant dynamics and the thermal capacitance of the coils can affect the measured sensible cooling.

The model generally explains the overall changes in moisture evaporation from the cooling coil with airflow and entering humidity. The initial moisture evaporation rate changes by nearly a factor of three as operating conditions change from 80°F dry bulb and 50°F dew point at 400 cfm/ton (Run 6) to 75°F dry bulb and 64°F dew point at 200 cfm/ton (Run 19).

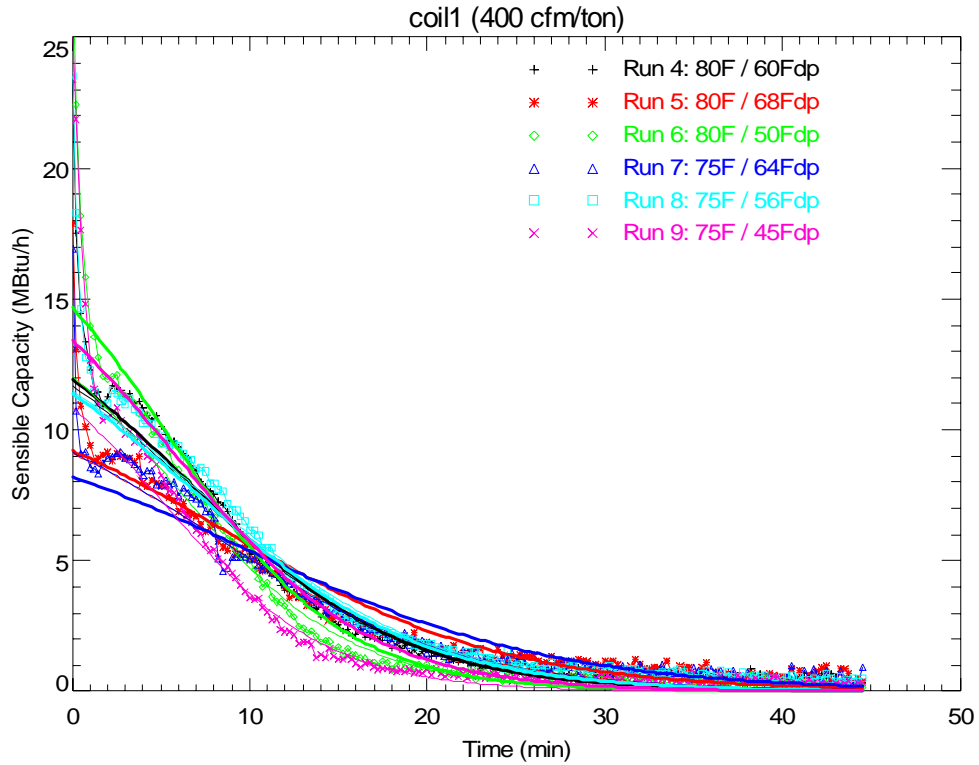


**Figure 5-5. Comparing Measured and Modeled Evaporation Rates: Coil 1, 400 cfm/ton**

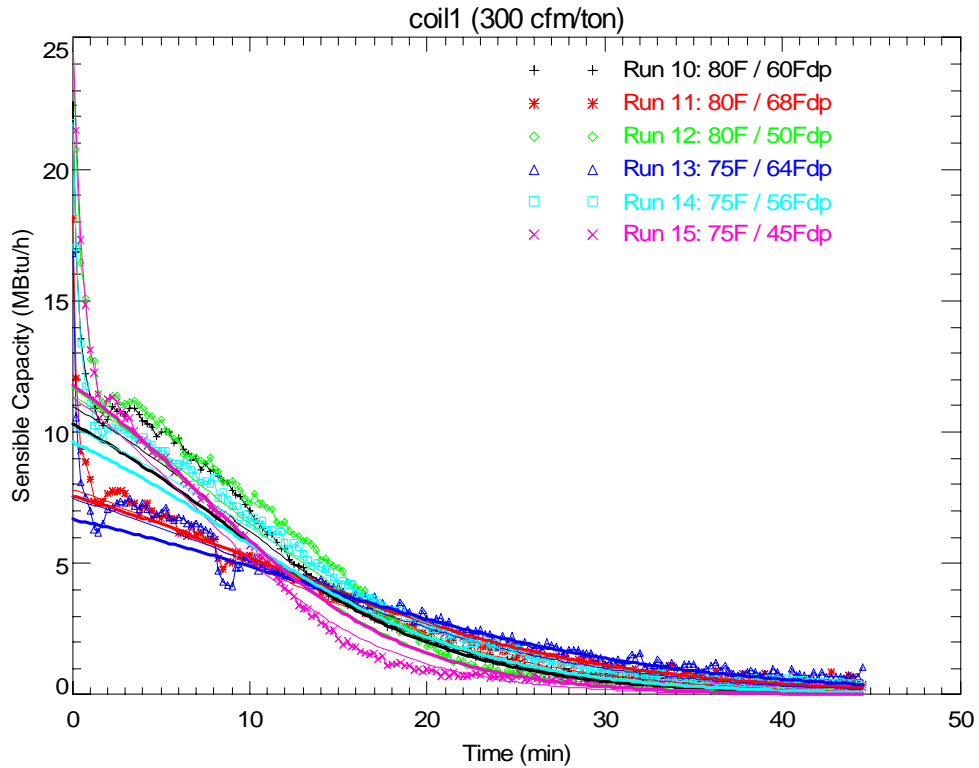


**Figure 5-6. Comparing Measured and Modeled Evaporation Rates: Coil 1, 300 cfm/ton**

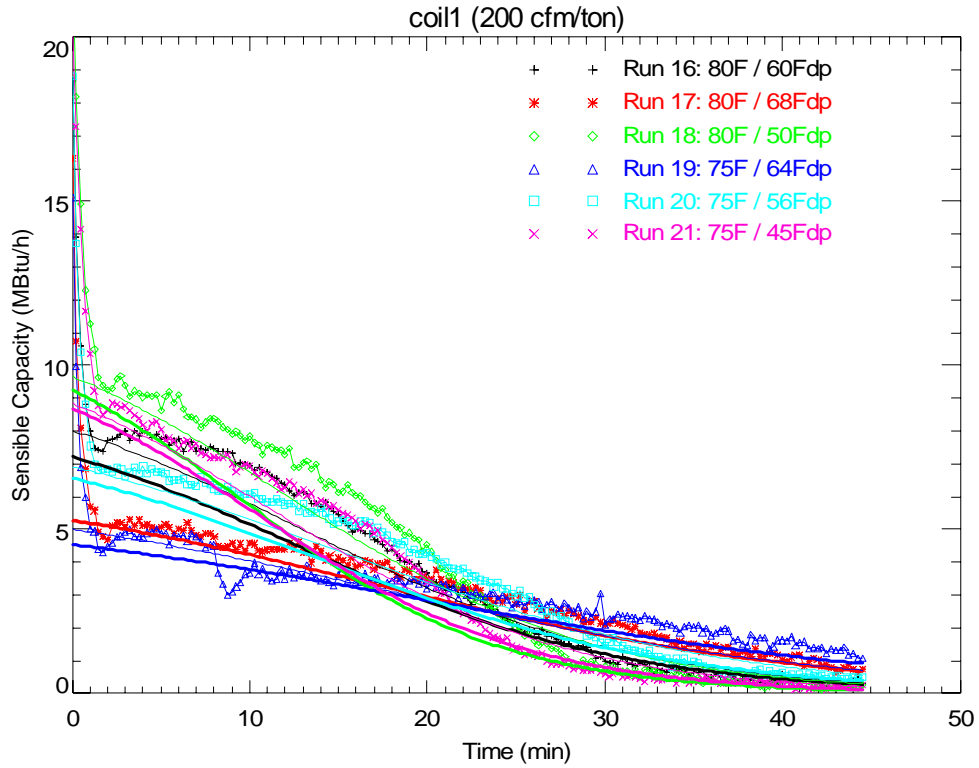


Figure 5-7. Comparing Measured and Modeled Evaporation Rates: Coil 1, 200 cfm/ton

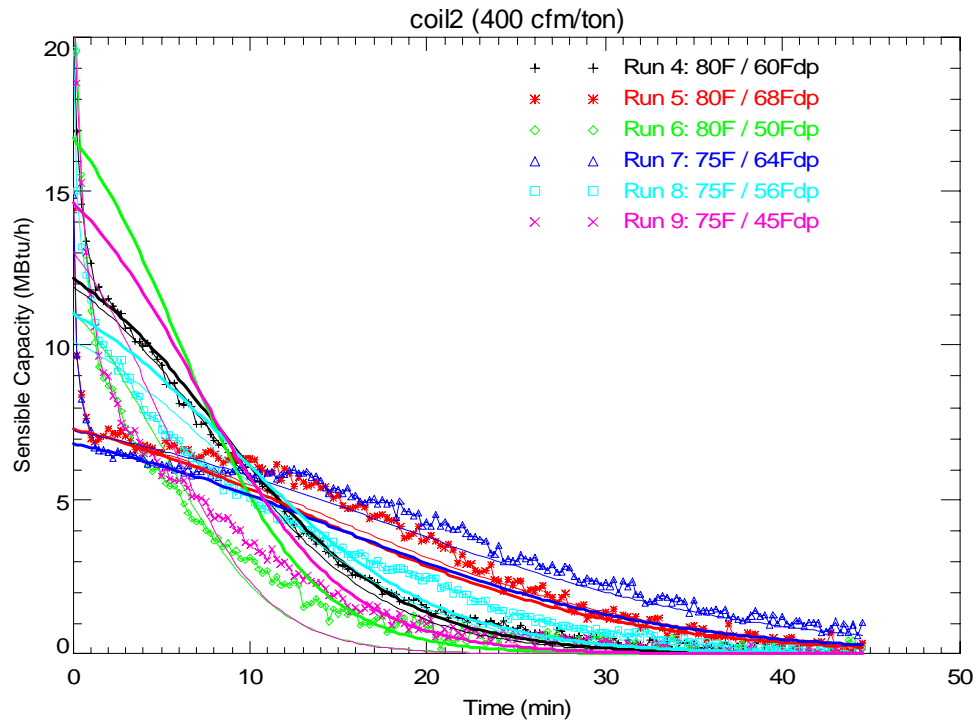


Figure 5-8. Comparing Measured and Modeled Evaporation Rates: Coil 2, 400 cfm/ton

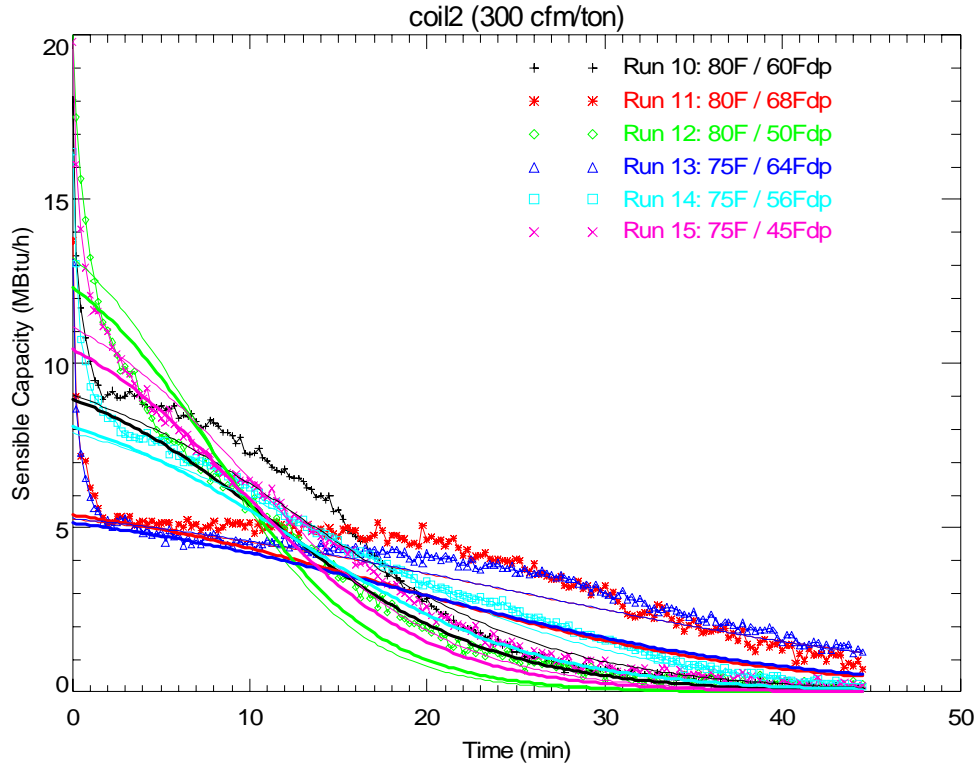


Figure 5-9. Comparing Measured and Modeled Evaporation Rates: Coil 2, 300 cfm/ton

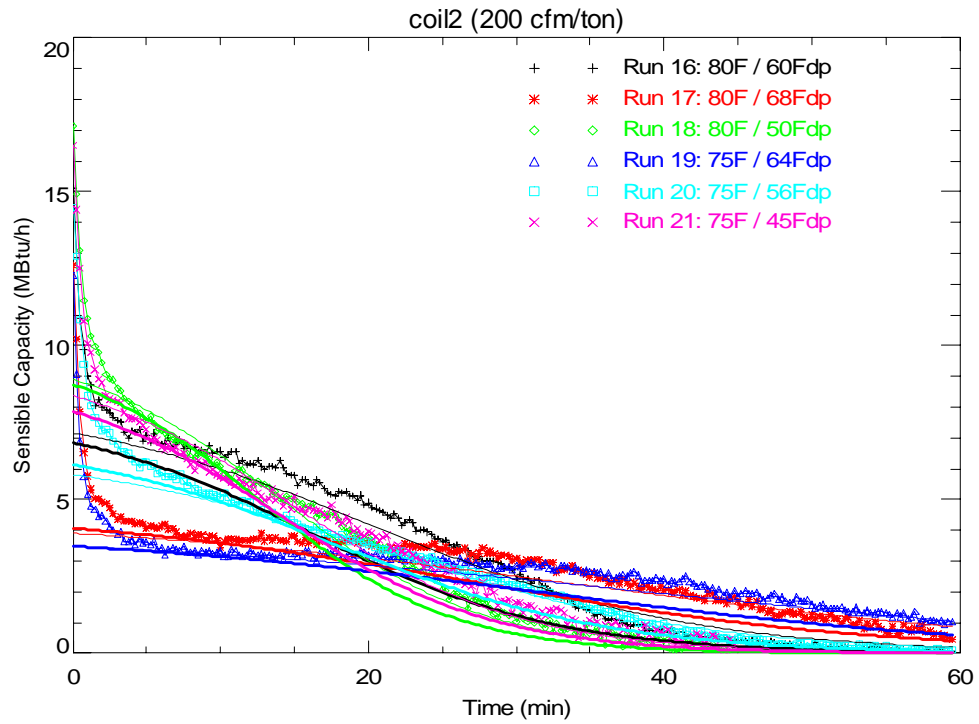


Figure 5-10. Comparing Measured and Modeled Evaporation Rates: Coil 2, 200 cfm/ton

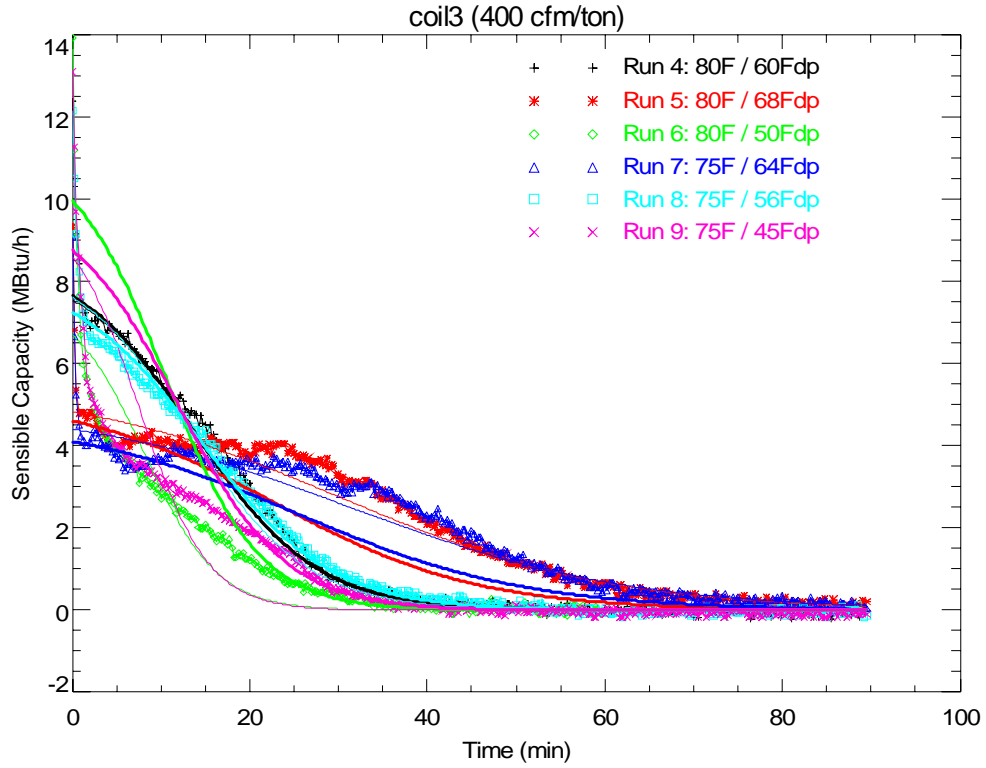


Figure 5-11. Comparing Measured and Modeled Evaporation Rates: Coil 3, 400 cfm/ton

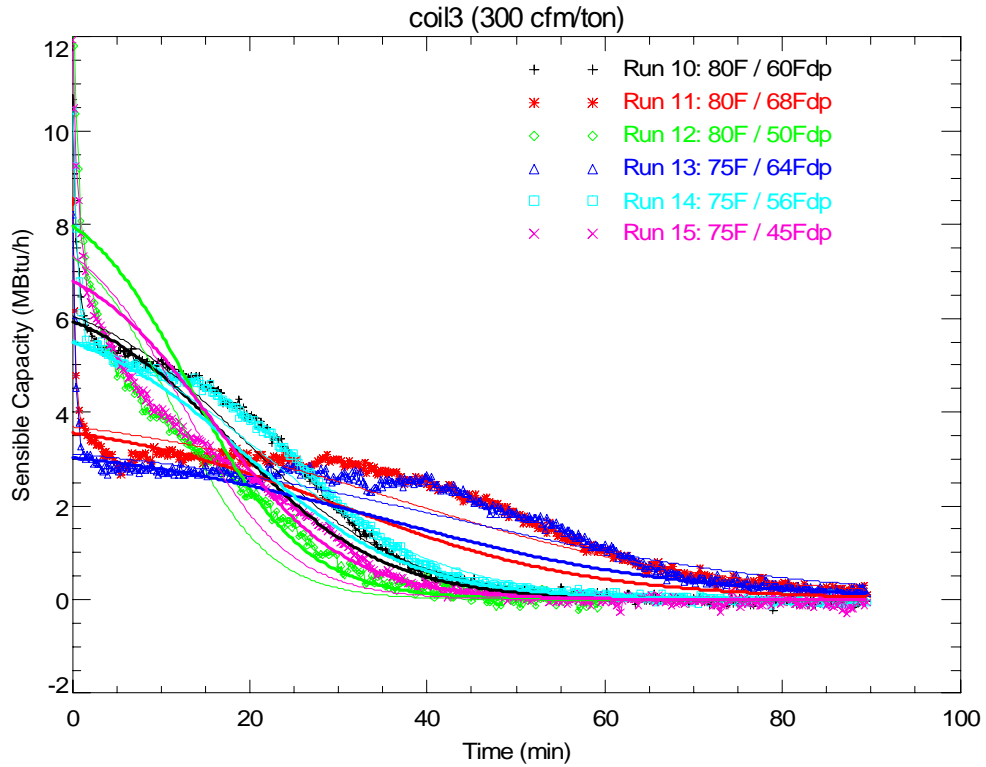
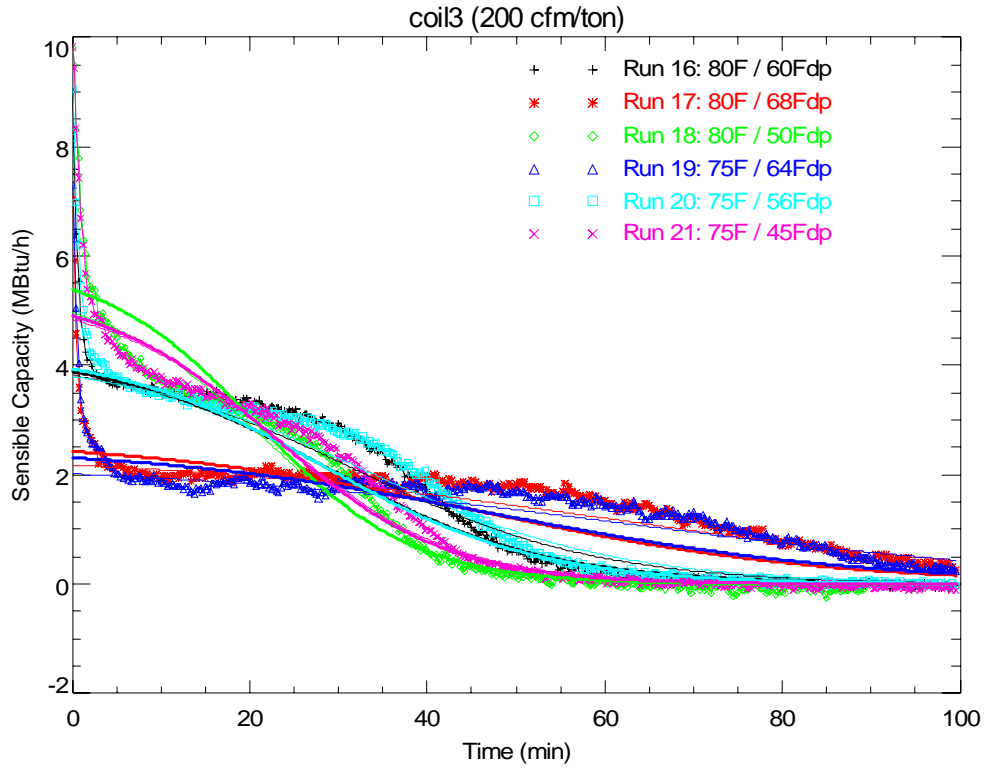
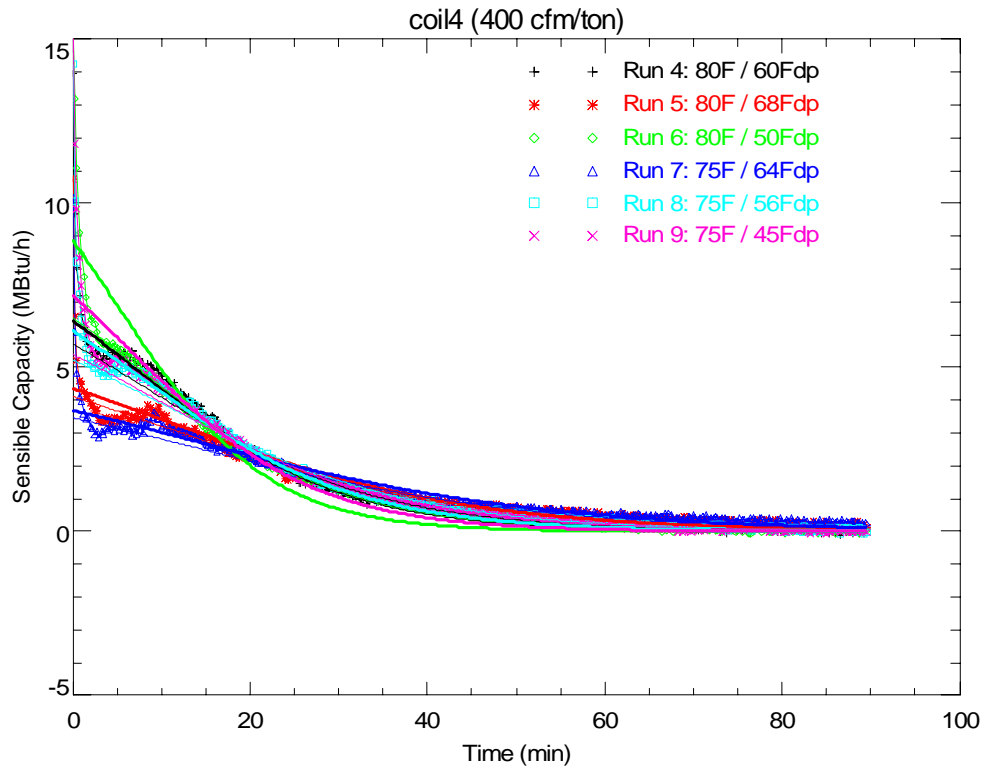


Figure 5-12. Comparing Measured and Modeled Evaporation Rates: Coil 3, 300 cfm/ton



**Figure 5-13. Comparing Measured and Modeled Evaporation Rates: Coil 3, 200 cfm/ton**



**Figure 5-14. Comparing Measured and Modeled Evaporation Rates: Coil 4, 400 cfm/ton**

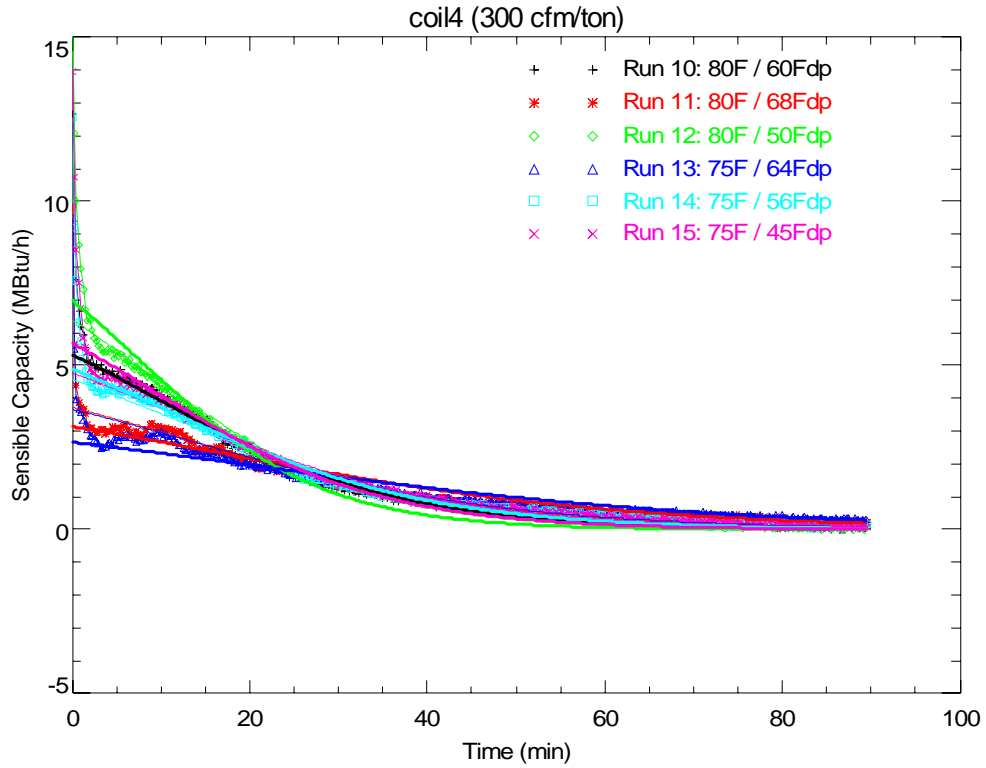


Figure 5-15. Comparing Measured and Modeled Evaporation Rates: Coil 4, 300 cfm/ton

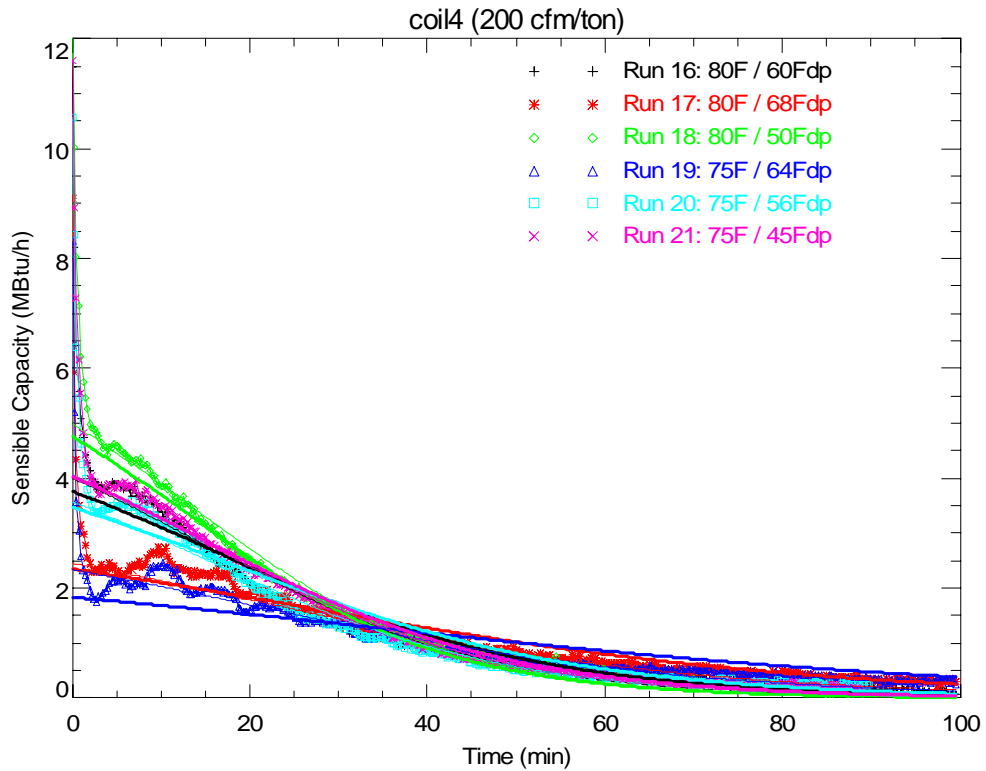


Figure 5-16. Comparing Measured and Modeled Evaporation Rates: Coil 4, 200 cfm/ton

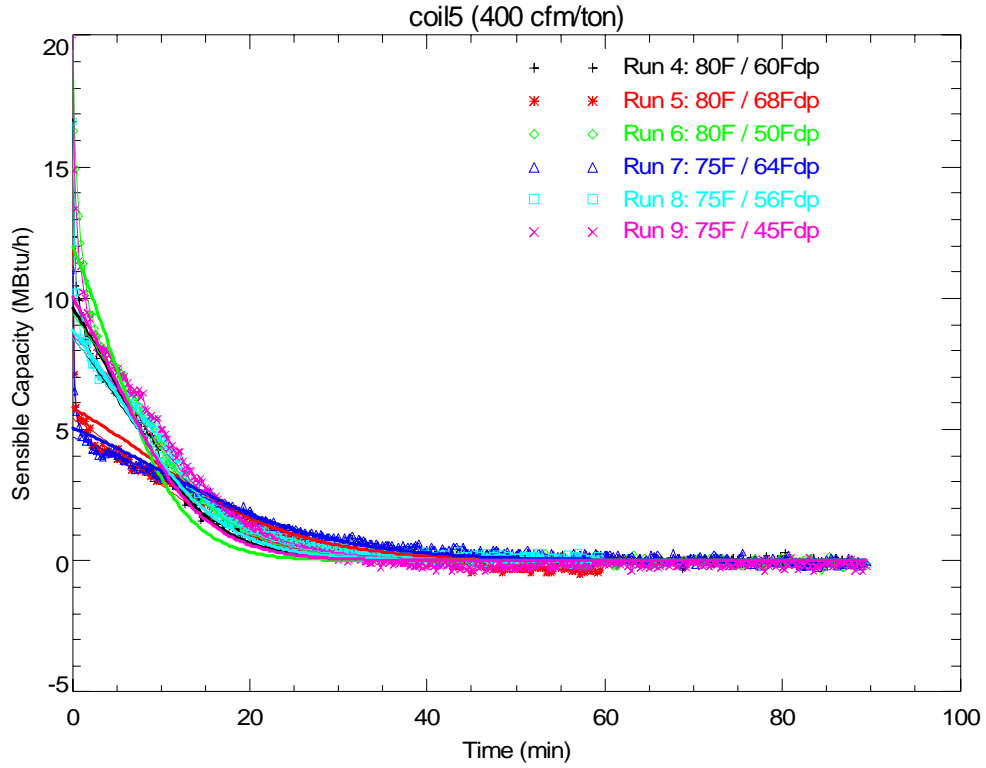


Figure 5-17. Comparing Measured and Modeled Evaporation Rates: Coil 5, 400 cfm/ton

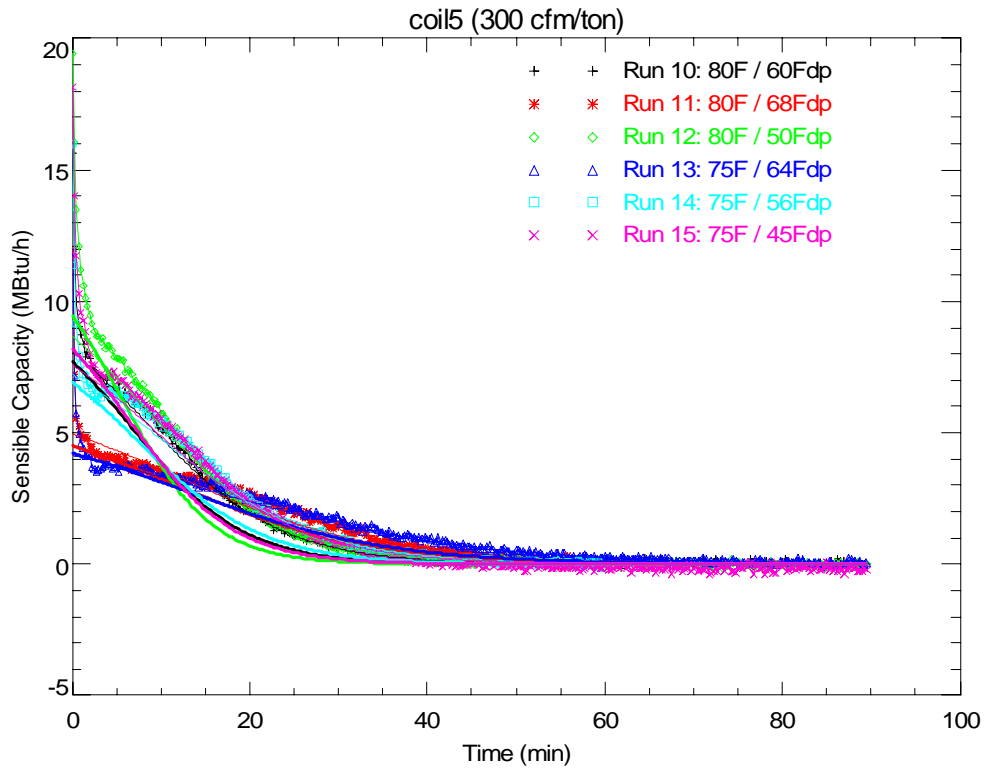
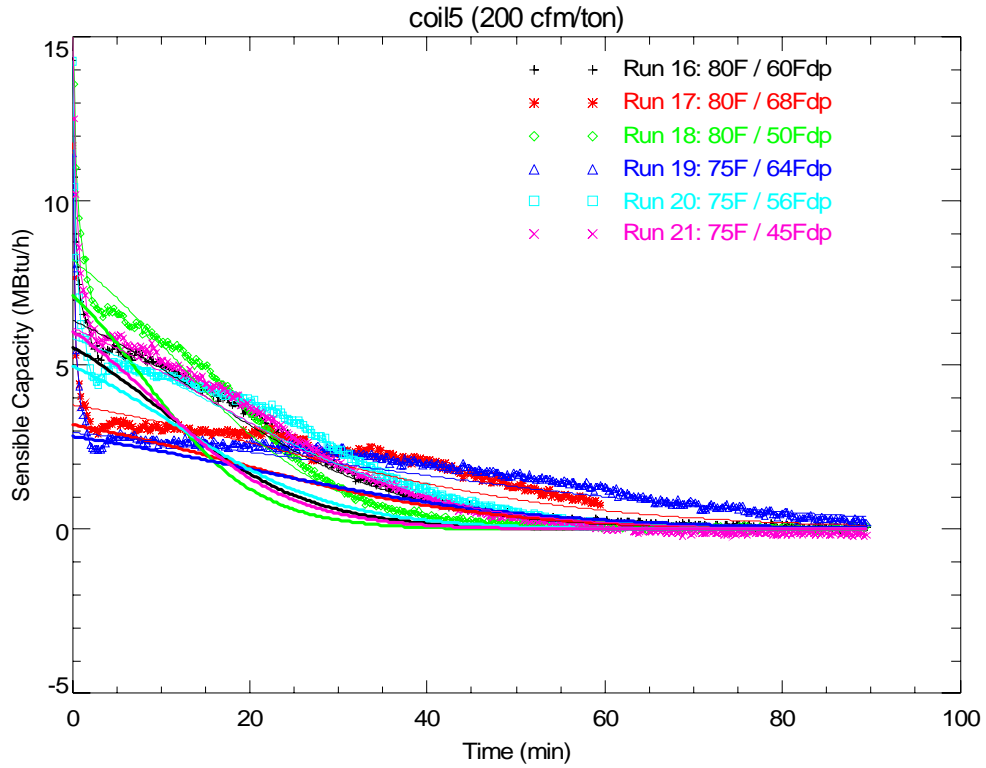
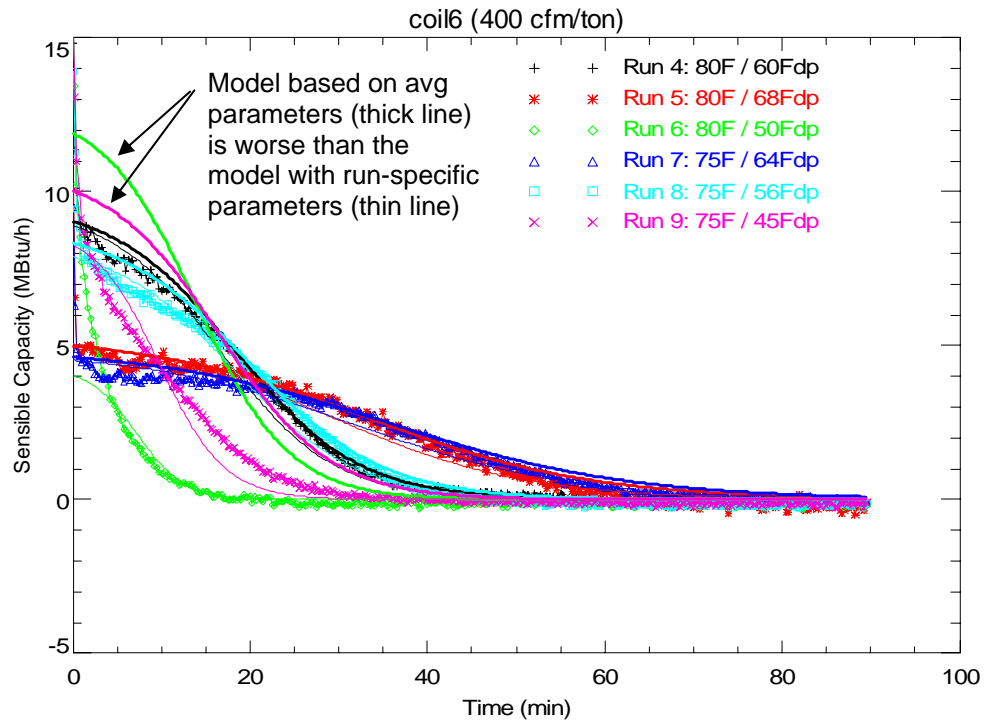


Figure 5-18. Comparing Measured and Modeled Evaporation Rates: Coil 5, 300 cfm/ton





**Figure 5-19. Comparing Measured and Modeled Evaporation Rates: Coil 5, 200 cfm/ton**



**Figure 5-20. Comparing Measured and Modeled Evaporation Rates: Coil 6, 400 cfm/ton**

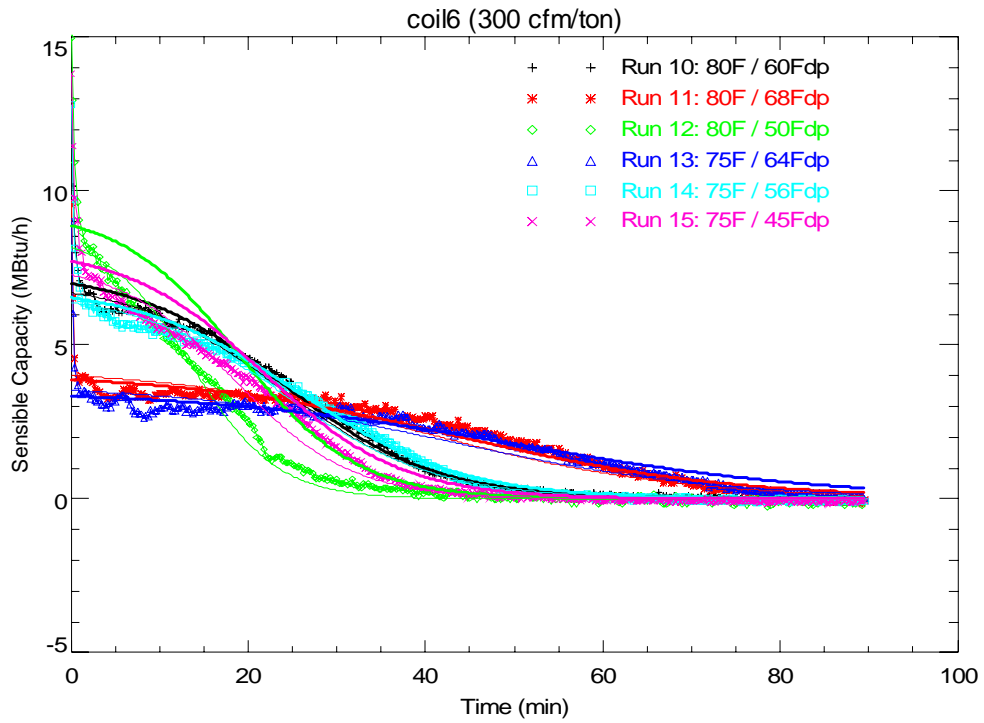


Figure 5-21. Comparing Measured and Modeled Evaporation Rates: Coil 6, 300 cfm/ton

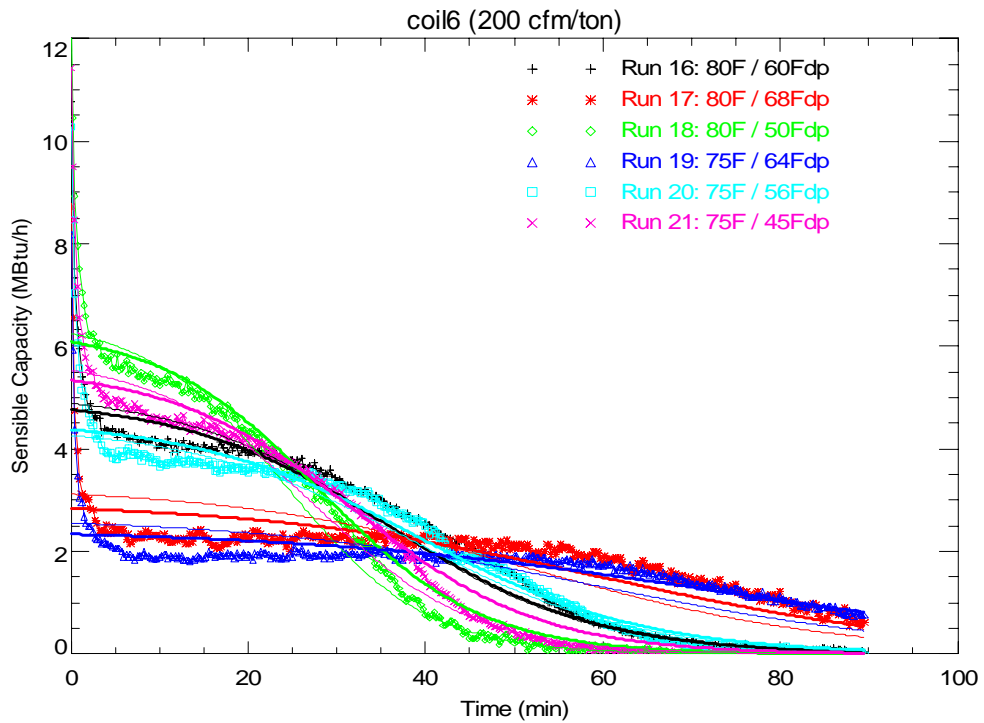
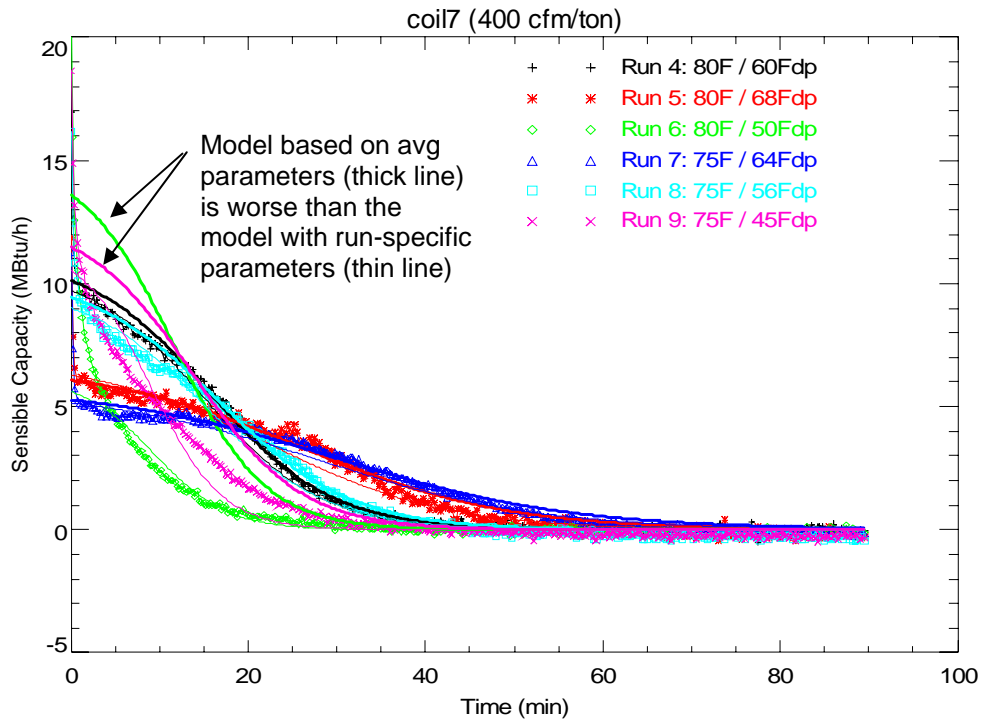
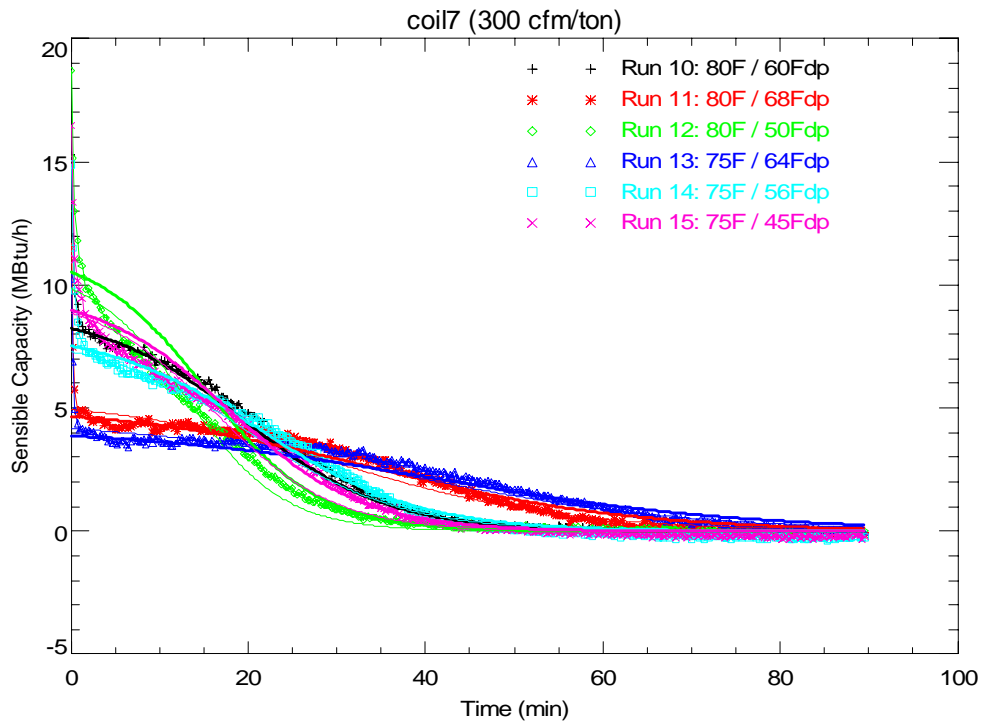


Figure 5-22. Comparing Measured and Modeled Evaporation Rates: Coil 6, 200 cfm/ton



**Figure 5-23. Comparing Measured and Modeled Evaporation Rates: Coil 7, 400 cfm/ton**



**Figure 5-24. Comparing Measured and Modeled Evaporation Rates: Coil 7, 300 cfm/ton**

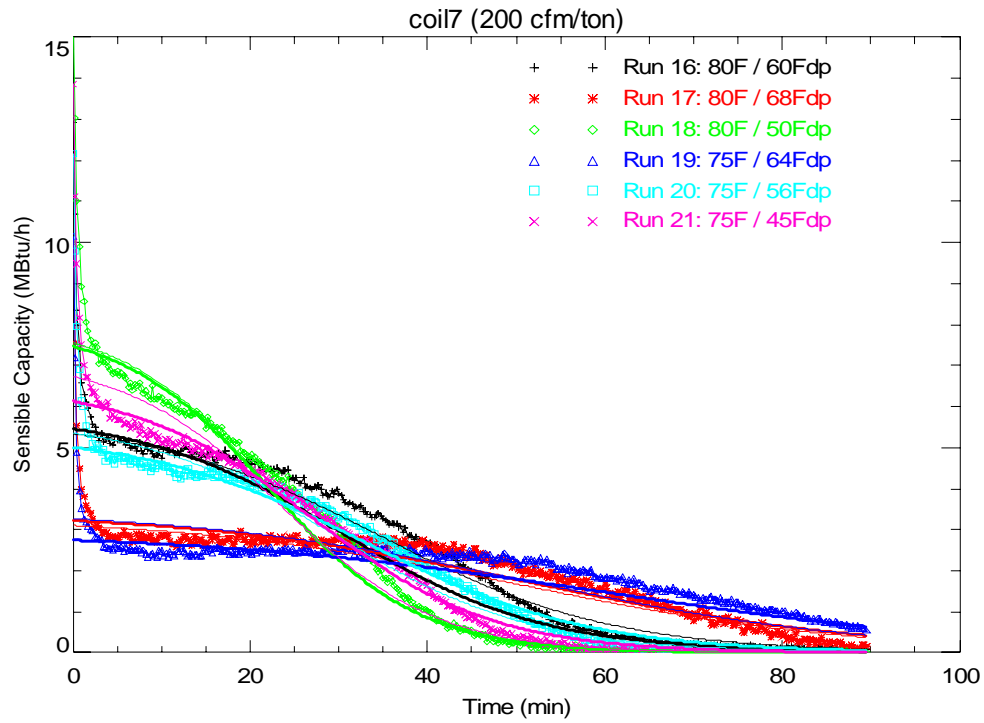


Figure 5-25. Comparing Measured and Modeled Evaporation Rates: Coil 7, 200 cfm/ton

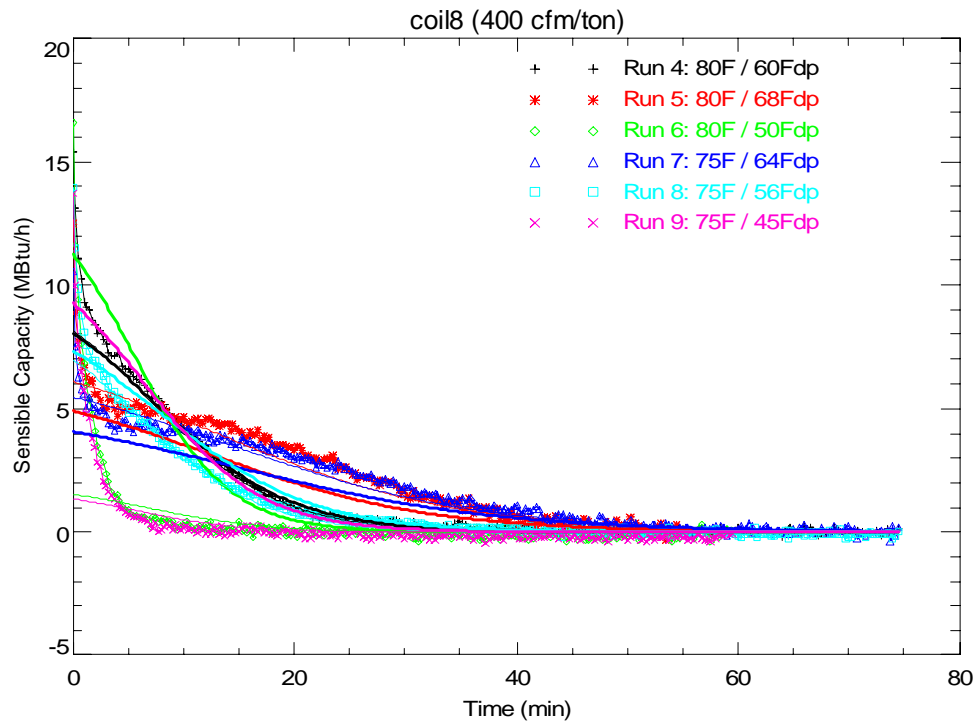


Figure 5-26. Comparing Measured and Modeled Evaporation Rates: Coil 8, 400 cfm/ton

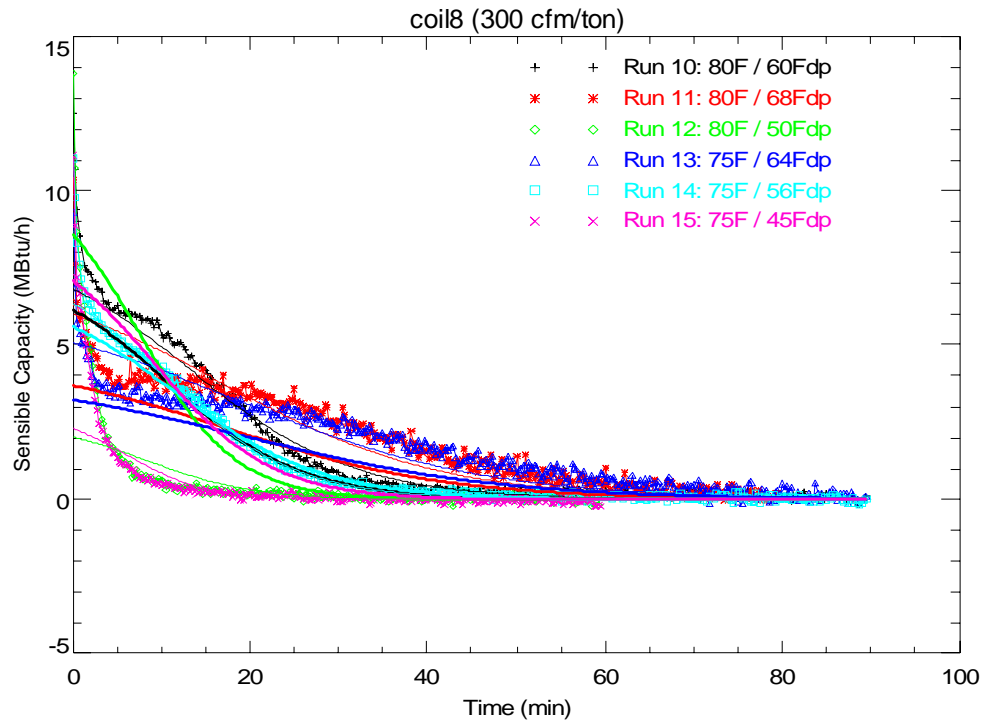


Figure 5-27. Comparing Measured and Modeled Evaporation Rates: Coil 8, 300 cfm/ton

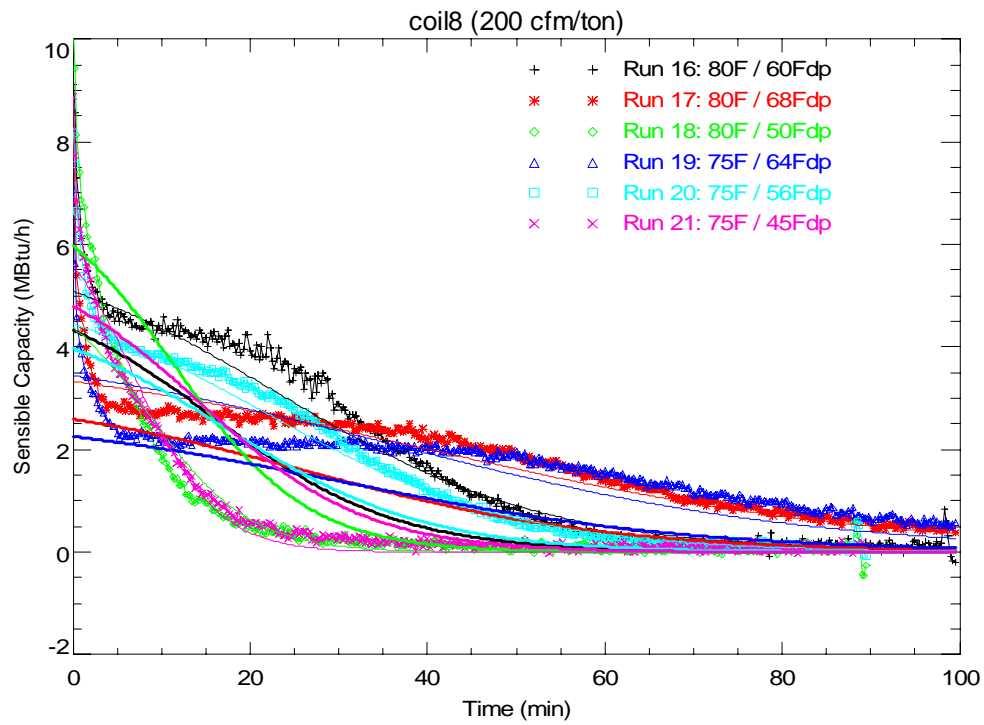
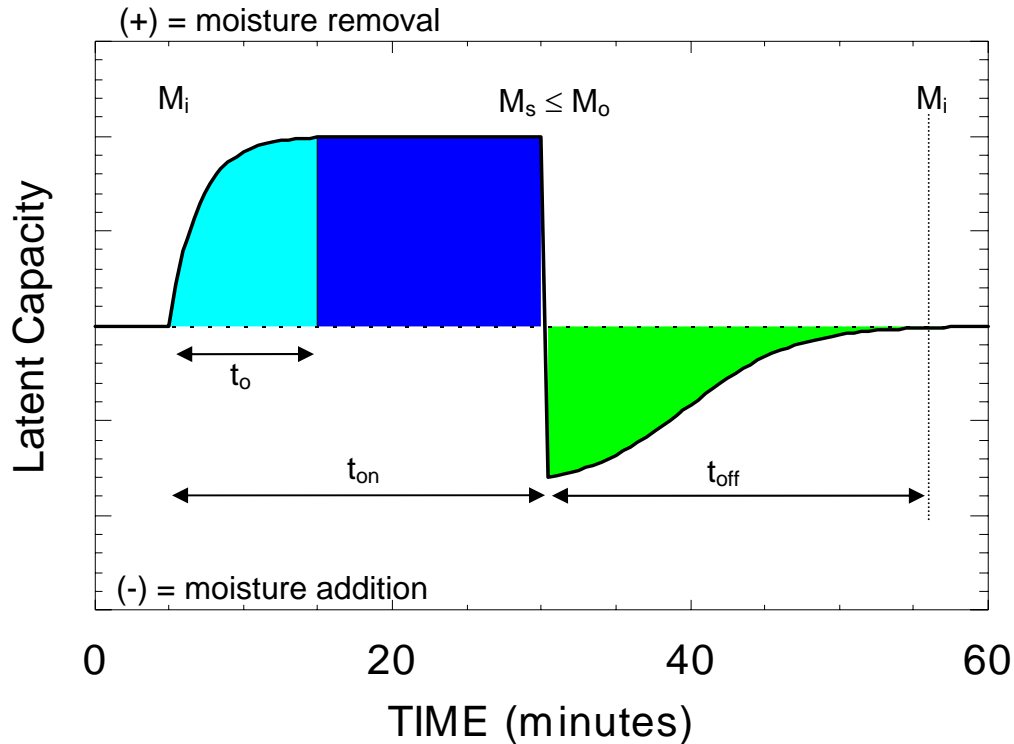


Figure 5-28. Comparing Measured and Modeled Evaporation Rates: Coil 8, 200 cfm/ton

### 5.3 An Improved Latent Degradation Model

With the more realistic moisture evaporation model given by equation 5-19b available, it is possible to develop a more refined LHR degradation function similar to that developed previously by Henderson and Rengarajan (1996). As in the original model, a quasi-steady moisture balance can be used to solve for the value of  $t_o$  - the time when the mass of moisture on the coil reaches  $M_o$  and condensate starts to drain from the unit. Figure 5-29 illustrates this concept.



**Figure 5-29. Example of a Quasi-Steady ON/OFF Cycle**

$M_i$  is the amount of moisture on the coil at compressor or cooling coil startup.  $M_s$  is the amount of moisture on the coil at the end of the on cycle or the beginning of the off cycle.  $M_s$  must be less than or equal to  $M_o$  as long as  $t_{on} < t_o$  and equal to  $M_o$  if  $t_{on} \geq t_o$ . Adopting equation 5-18b, we can express  $M_i$  as:

$$M_i = \left( \frac{1}{\alpha} \right) \ln \left( e^{\alpha \beta t_{off}} \cdot (e^{\alpha M_s} - 1) + 1 \right) \quad (5-20)$$

and for the compressor on cycle:

$$M_s = M_i + Q_L \left( t_{on} + \tau \cdot (e^{-t_{on}/\tau} - 1) \right) \quad (5-21)$$

These equations can be simplified and made dimensionless with the following terms:

$$f_i \equiv \frac{M_i}{M_o}, \quad f_s \equiv \frac{M_s}{M_o}, \quad t_{wet} = \frac{M_o}{Q_L}, \quad NTU_o = \alpha M_o$$

Also, if we define:

$$t_p \equiv \frac{1060 \cdot M_o}{1.08 \cdot cfm \cdot (DB - WB)} = \frac{Moisture\_Mass}{Evap\_Potential}$$

then

$$\alpha\beta = -\left(\frac{NTU_o}{t_p}\right) \quad \text{and} \quad t_p = -\left(\frac{M_o}{\beta}\right)$$

Equations 5-20 and 5-21 can then be rearranged to be in terms of the fractions  $f$  instead of  $M$ :

$$f_i = \left(\frac{1}{NTU_o}\right) \ln\left(e^{-NTU_o \cdot t_{off}/t_p} \cdot (e^{NTU_o \cdot f_s} - 1) + 1\right) \quad (5-22)$$

and

$$f_s = f_i + \left(\frac{1}{t_{wet}}\right) (t_{on} + \tau \cdot (e^{-t_{on}/\tau} - 1)) \quad (5-23)$$

Equation 5-22 can be substituted into equation 5-23. The result is equation 5-24 which can be solved by successive substitution to find  $f_s$ .  $f_s$  is limited to be less than or equal to 1. Then,  $f_i$  can be found with equation 5-22 and equation 5-23 can be rearranged to find  $t_o$  as shown below in equation 5-25 (replacing  $f_s$  with 1 and  $t_{on}$  with  $t_o$ ).

$$f_s = \left(\frac{1}{NTU_o}\right) \ln\left(e^{-NTU_o \cdot t_{off}/t_p} \cdot (e^{NTU_o \cdot f_s} - 1) + 1\right) + \left(\frac{1}{t_{wet}}\right) (t_{on} + \tau \cdot (e^{-t_{on}/\tau} - 1)) \quad (5-24)$$

$$t_o = (1 - f_i) \cdot t_{wet} - \tau \cdot (e^{-t_o/\tau} - 1) \quad (5-25)$$

The same procedures from Henderson and Rengarajan (1996) are then used to find the LHR ratio with  $t_o$  (i.e., using either equation 5-8 or 5-9).

Figure 5-30 shows the new LHR function as blue symbols and compares it to the original degradation function with linear evaporation. While the two functions use different parameters, the same basic coil characteristics were used in each case. Table 5-3 below lists the assumed coil parameters and calculated values for each model parameter.

**Table 5-3. Model Parameters Used to Compare Original and New LHR Models**

Steady State:	$Q_T = 36 \text{ MBtu/h}$ , $Q_L = 9 \text{ MBtu/h}$ , $\text{SHR} = 0.75$ $\text{cfm} = 1200$ , $\text{WB depression} = 13^\circ\text{F}$
Moisture Mass:	$M_o = 2.4 \text{ lbs}$ , $A_o = 300 \text{ ft}^2$
Evaporation:	$\text{NTU}_o = 2.2$ , $\text{NTU}_o = K \cdot A_o / \text{cfm}^{0.2}$ $\eta_{\text{evp}} = 1 - e^{-\text{NTU}} = 0.887$
Cycling:	$N_{\text{max}} = 3 \text{ cycles/h}$ , $\tau = 60 \text{ sec}$
Calculated Values:	$t_{\text{wet}} = 3600 \cdot M_o \cdot 1.06 / Q_L = 1018 \text{ sec}$ $t_p = 3600 \cdot M_o \cdot 1060 / (1.08 \cdot \text{cfm} \cdot \text{WB}_{\text{depress}}) = 544 \text{ sec}$ $\gamma = 1.08 \cdot \text{cfm} \cdot \text{WB}_{\text{depress}} \cdot \eta_{\text{evp}} / (Q_L \cdot 1000) = 1.66$

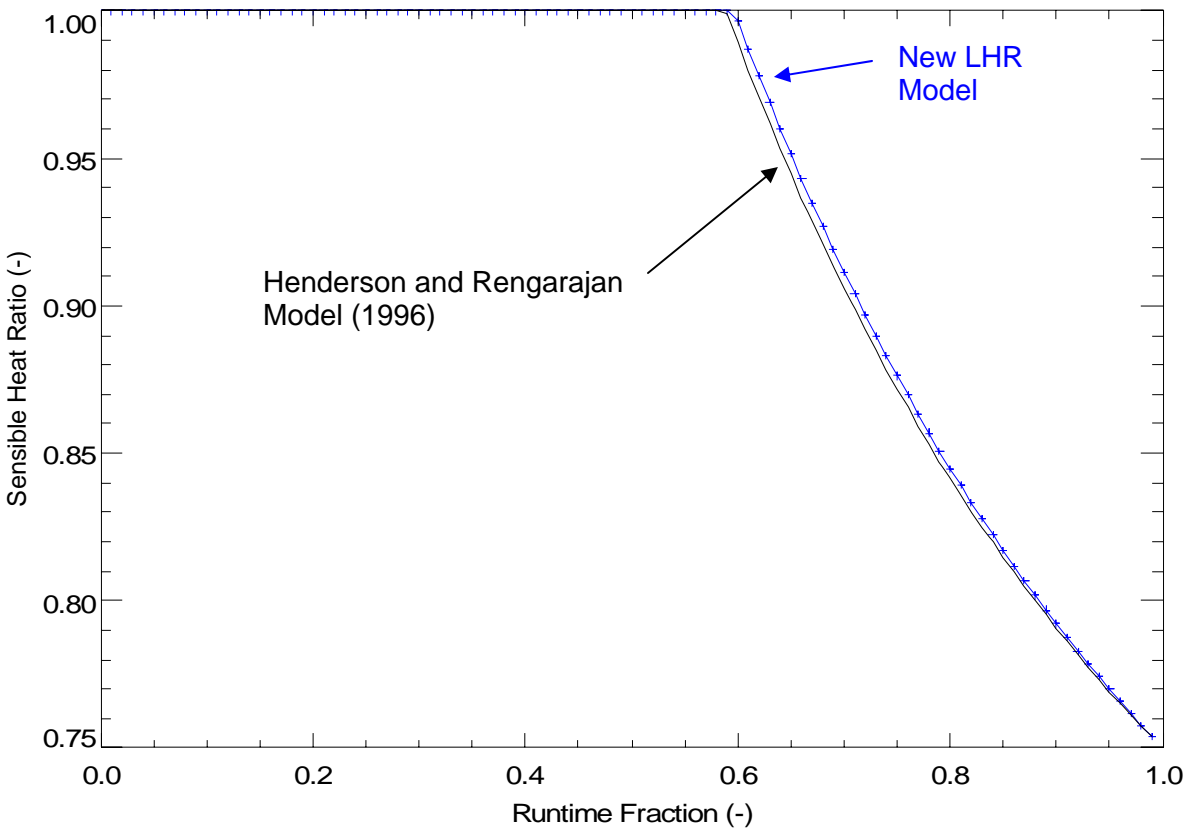


**Figure 5-30. Comparing the New and Original LHR Models**

The expression for evaporation rate in equation 5-19b can now be rearranged in terms of  $\text{NTU}_o$  and  $t_p$ :

$$q_{\text{evp}} = Q_L \frac{t_{\text{wet}}}{t_p} \cdot \left( \frac{e^{-\text{NTU}_o t / t_p} \cdot (e^{\text{NTU}_o M_s / M_o} - 1)}{e^{-\text{NTU}_o t / t_p} \cdot (e^{\text{NTU}_o M_s / M_o} - 1) + 1} \right) \quad (\text{lb/h}) \quad (5-26)$$



The conversion between the original model parameters ( $t_{wet}$  and  $\gamma$ ) and the new parameters ( $t_p$  and  $NTU_o$ ) can be completed with the equations listed below:

$$\begin{aligned}\gamma &= \frac{q_i}{Q_L} = \frac{1.08 \cdot cfm \cdot (DB - WB)}{1060 \cdot Q_L} (1 - e^{-NTU_o}) \\ &= \left( \frac{M_o}{Q_L} \right) \cdot \left( \frac{1.08 \cdot cfm \cdot (DB - WB)}{1060 \cdot M_o} \right) (1 - e^{-NTU_o})\end{aligned}\quad (5-27)$$

where  $q_i$  = initial moisture evaporation rate from a fully-wetted coil (same as  $Q_e$  in Section 5.1.1 above).

Therefore,  $t_p$  is defined as:

$$t_p = \frac{t_{wet}}{\gamma} (1 - e^{-NTU_o}) \quad (s) \quad (5-28)$$

and

$$NTU_o = -\ln(1 - \eta_{evp}) \quad (-) \quad (5-29)$$

Because of the extra degree of freedom in the new model formulation – i.e., the moisture mass on the coil at the beginning of the off cycle is now a variable instead of constant – the new model has one extra parameter. Therefore, while  $t_p$  is essentially a function of the other parameters,  $NTU_o$  must be determined from experimental data with equation 5-29 above.

Many of the plots in Section 3 and Section 5.5 compare the laboratory test data to both the original LHR degradation model as well as the new model developed in this section.

## **5.4 Modeling Latent Capacity Degradation for Off-Cycle Fan Control Strategies**

Many air-conditioning systems use supply air fan control strategies during the off cycle other than constant fan operation. Possible off-cycle fan control strategies include:

1. Turn off the fan when cooling is not provided (i.e., AUTO fan),
2. Keep the fan on for a fixed interval after cooling and then turn the fan off for the remainder of the coil off cycle (Fan Overrun Strategy),
3. Turn the fan off for a fixed interval after cooling and then activate the fan for the remainder of the coil off cycle (“Coil Drain-Down” Strategy),
4. Decrease the airflow during all or part of the coil off cycle.

### 5.4.1 A Simple Model to Consider Supply Air Fan Delays

When the supply air fan does not run for part of the coil off cycle, the simplest approach is to assume that no moisture evaporation occurs when the fan is off. So the value of  $t_{off}$ , which corresponds to the time during the coil off cycle when the fan is on, is adjusted. Equation 5-4 becomes:

$$t_{off} = \left| \frac{3600}{4N_{max} X} - t_{delay-drain} \right|^+ \quad (5-30)$$

$$t_{off} = \left| \frac{3600}{4N_{max} X} \right| \leq t_{delay-overrun} \quad (5-31)$$

Equation 5-30 applies when the fan shuts down for a fixed interval ( $t_{delay-drain}$ ) after a cooling cycle; this is commonly referred to as a drain-down cycle. Equation 5-31 applies when the fan stays on for a fixed interval ( $t_{delay-overrun}$ ) after a cooling cycle, then shuts down for the rest of the off cycle.

The fan delay concepts can be applied to either the original LHR degradation model or the new degradation model derived above.

### 5.4.2 A General Model to Consider Two Types of Off-Cycle Fan Operation

The most general way to consider the various fan control strategies can all be considered by breaking the off cycle into separate intervals and repeating the quasi-steady moisture balance above. Figure 5-31 shows this concept graphically. The figure is similar to Figure 5-29, which had assumed a single, uniform off-cycle interval.

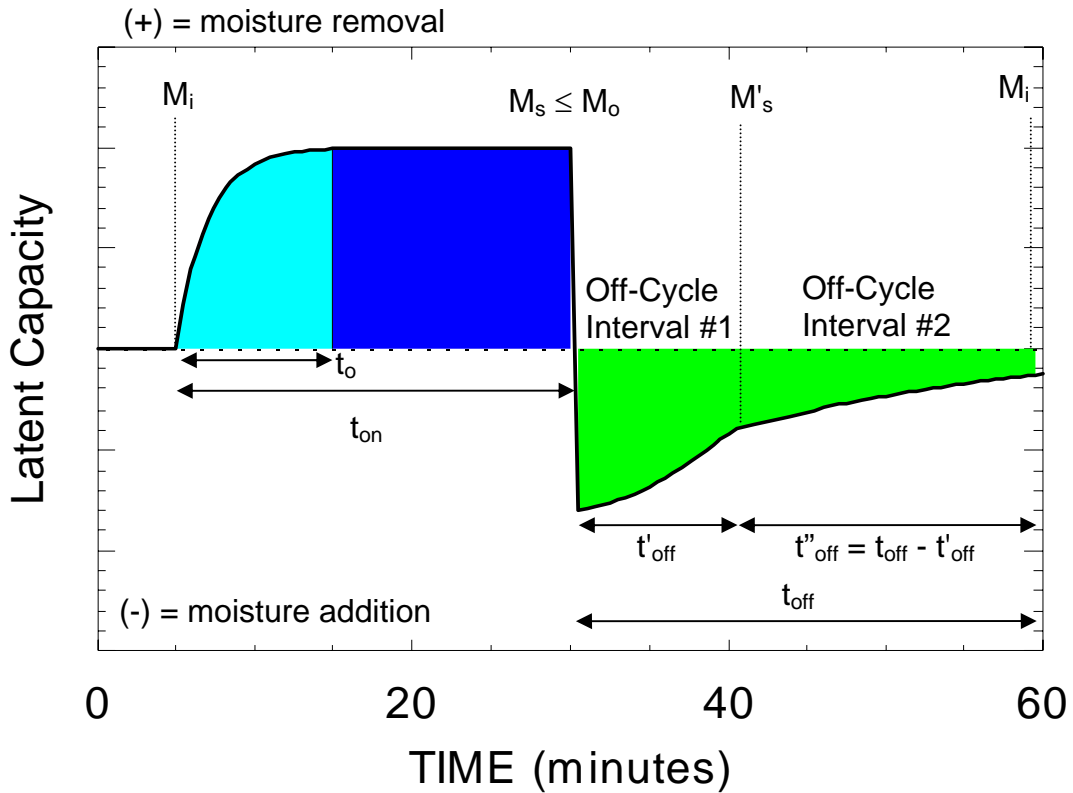


**Figure 5-31. Moisture Balance Concept with Two Off-Cycle Intervals**

The moisture balance still iterates in order to equate the moisture fraction on the coil at the beginning and end of the overall cycle, similar to equations 5-22 and 5-23 above. For simplification, equation 5-22 is expressed in functional form as:

$$f_i = F_{5-22}(t''_{off}, f'_s, t'_p, NTU'_o, \dots) \quad (5-31)$$

where  $f'_s$  is the fraction of moisture on the coil at the intermediate point between the two off-cycle intervals.  $f'_s$  is determined by:

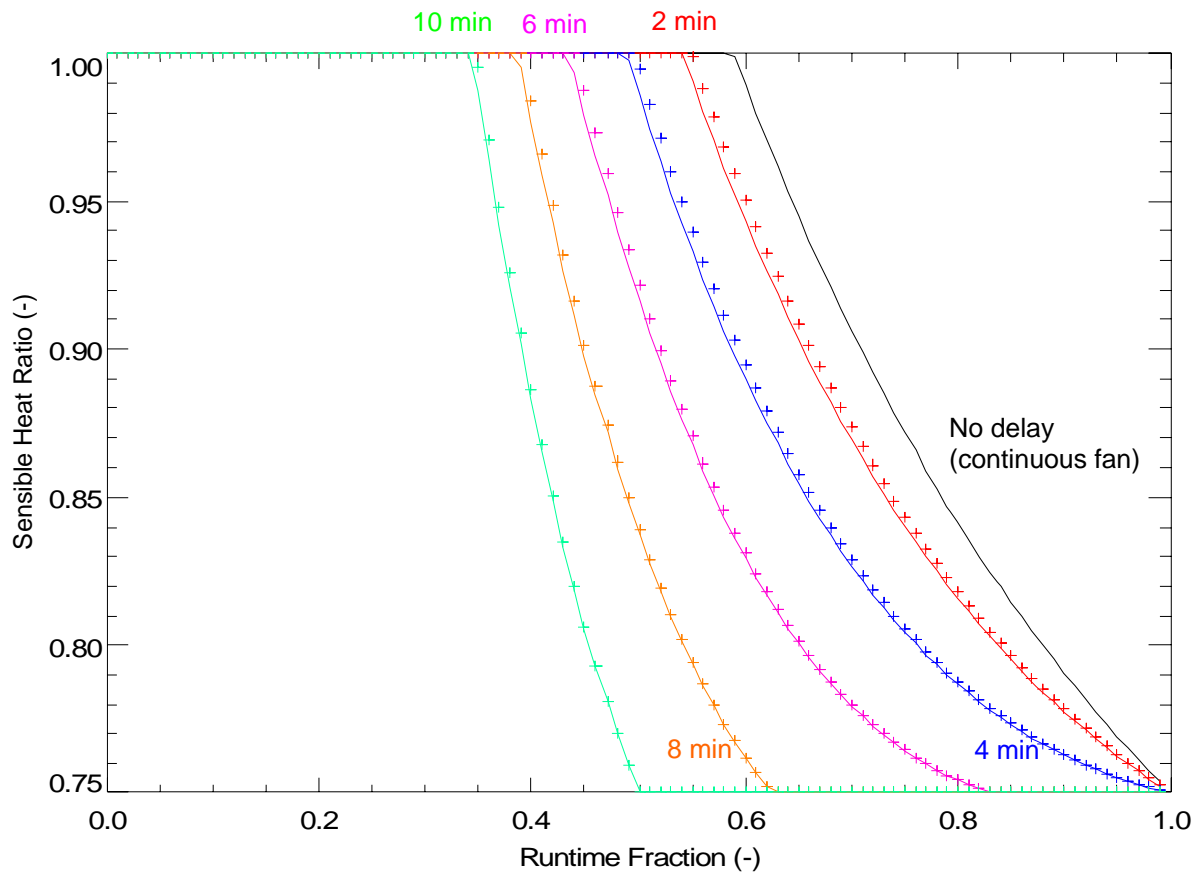
$$f'_s = F_{5-22}(t'_{off}, f_s, t'_p, NTU'_o, \dots) \quad (5-32)$$

where  $t'_{off}$ ,  $t'_p$  and  $NTU'_o$  are all evaluated at the flow rate and conditions (DB, WB) corresponding to off-cycle interval #1.  $t''_{off}$ ,  $t_p$  and  $NTU_o$  are evaluated at the flow rate and conditions associated with off-cycle interval #2. Of course the parameters  $t_{wet}$ ,  $M_o$  and  $\tau$  are also required by these equations, though these values are only a function of the on-cycle performance of the cooling coil and are not affected by changes during the off cycle.

The calculation procedure again requires iterations by successive substitution and starts with an initial guess of  $f_s$ , then equations 5-32, 5-31 and 5-23 are evaluated to provide a new estimate for  $f_s$ . Iterations continue until  $f_s$  converges.

### 5.4.3 Demonstrating the Utility of the New LHR Models

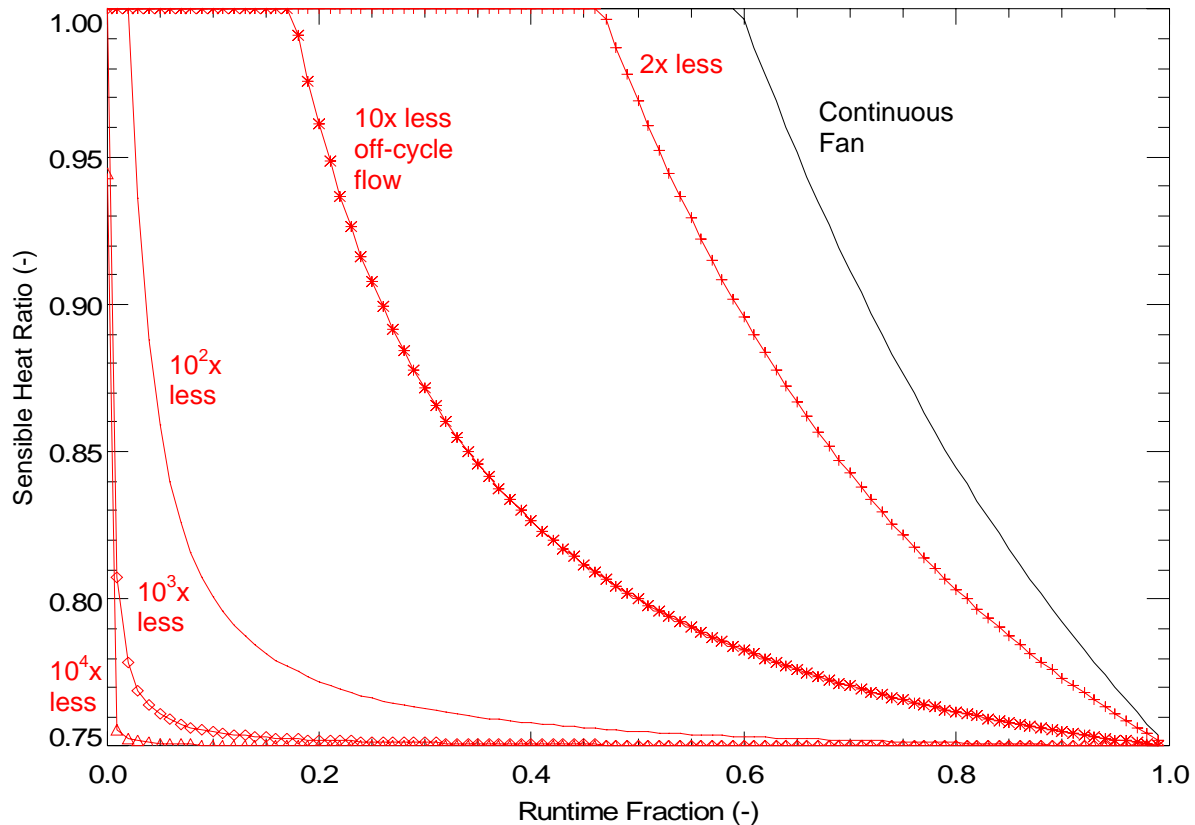
The models developed above can consider a number of fan control scenarios. Figure 5-32 shows the impact of a brief fan shutdown after a cooling cycle – often referred to as a drain-down cycle. Latent degradation trends are shown for delays ( $t_{\text{delay-drain}}$ ) of 2 to 10 minutes (using the base parameters from Table 5-3). The line and symbols represent the time delays with the different models. The line represents the original 1996 LHR degradation model with delay times added. The symbols add the delay model to the new LHR degradation model derived above (Section 5.3). The two models are in very close agreement.



**Figure 5-32. Impact of a Brief Fan Shutdown: 2, 4, 6, 8 and 10 minutes**

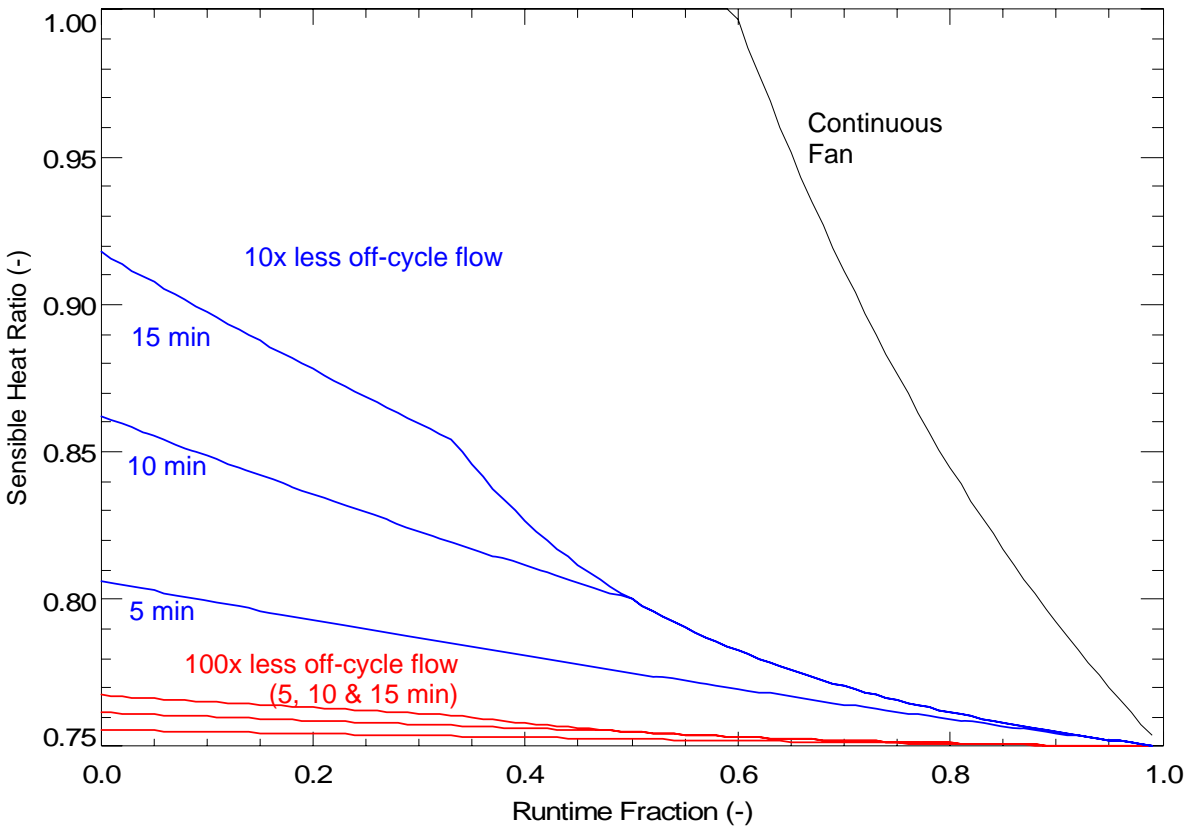
Figure 5-33 shows the impact of changing the values of  $NTU_o$  and  $t_p$  to correspond to lower air flow rates during the entire coil off cycle. The plot shows the impact of reducing the off-cycle flow to be 2, 10, 100, 1000, and 10000 times less than the on-cycle airflow. Flow reductions

greater than 100 are representative of the AUTO fan mode, where some small amount of airflow across the coil is driven by natural convection even though the fan is off. Cutting the off-cycle airflow in half has only a modest impact compared to constant fan operation. Even at the lowest off-cycle flow rates, the SHR still approaches 1 at very small coil runtime fractions. This occurs because the off-cycle length is more than 4 hrs at a runtime fraction of 0.02 – enough time for even a modest evaporation rate to remove all the moisture from the coil.



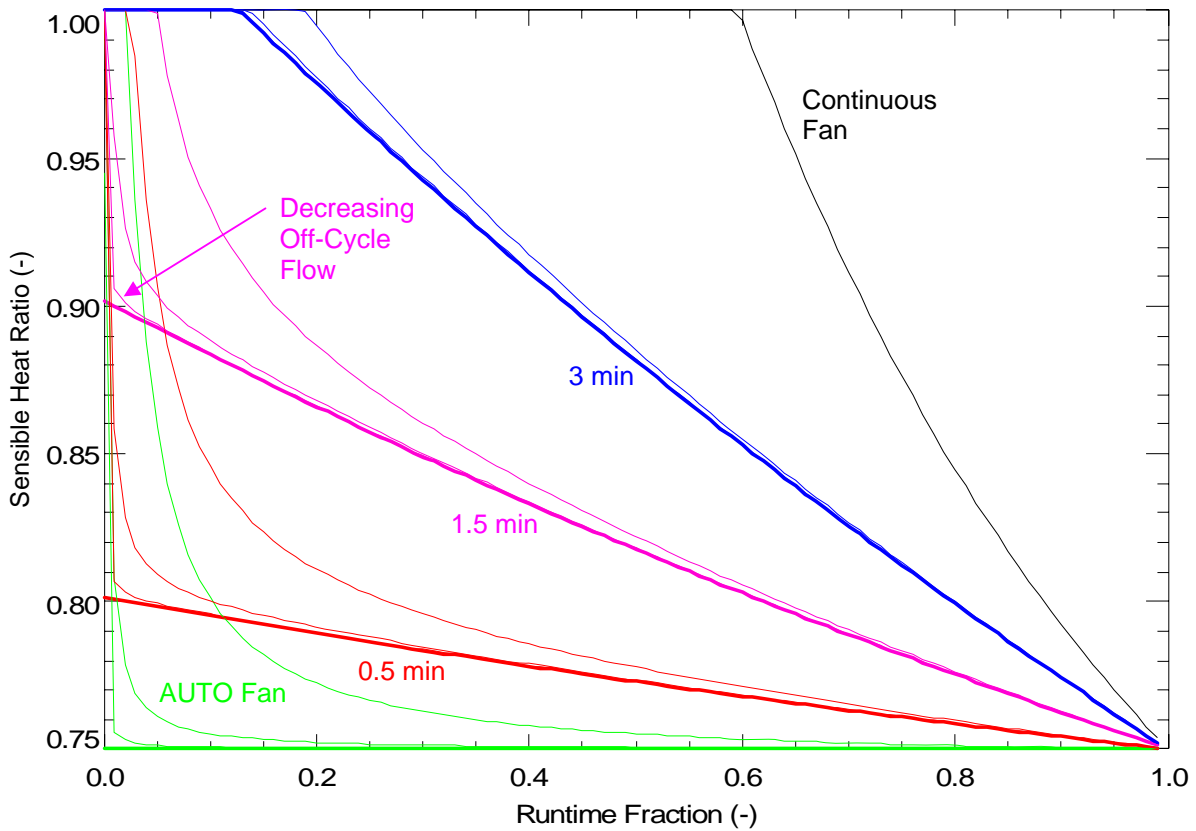
**Figure 5-33. Predicting Latent Degradation for Lower Off-Cycle Airflow Rates**

The trends shown in Figure 5-33 are not fully consistent with our measured observations of a coil in the AUTO fan mode – i.e., we have never observed SHR asymptotically approaching 1 at low coil runtime fractions (however 0.09 was the lowest runtime fraction tested). An alternate way to consider the AUTO fan mode might be to think of the off cycle as a brief period of thermosyphon-induced airflow that eventually subsides. This alternate concept is shown in Figure 5-34 using the two off-cycle interval approach described in Section 5.4.2. The lines on the plot assume off-cycle flows are 10 and 100 times lower than the on-cycle flow for brief periods of 5, 10 and 15 minutes after the cooling cycle ends. After these brief low airflow periods, the flow is assumed to fully stop for the remainder of the coil off cycle.



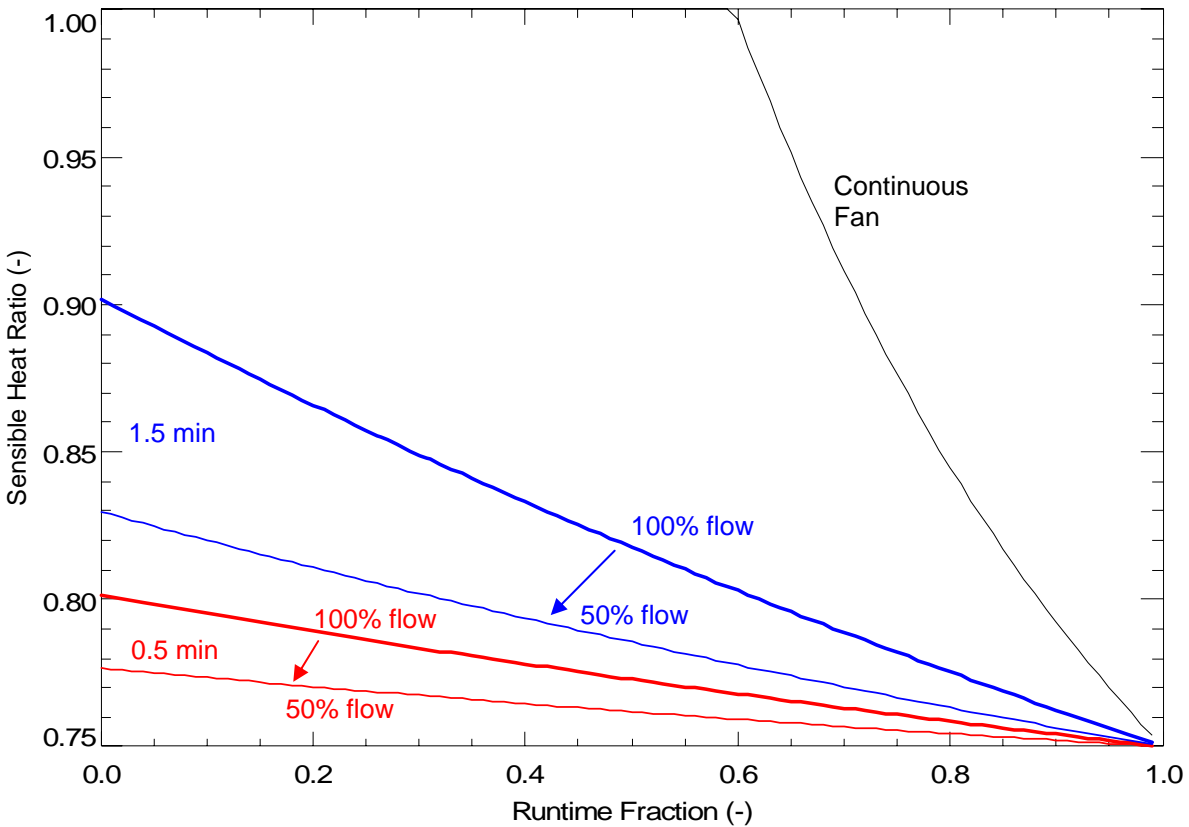
**Figure 5-34. Predicting Latent Degradation for a Brief Period of Low Off-Cycle Airflow**

Figure 5-35 shows the impact of a fan overrun strategy that keeps the fan on at the same airflow rate for a fixed length of time after the cooling on cycle. The overrun delays ( $t_{\text{delay-overrun}}$ ) shown on the plot are for 0.5, 1.5, and 3 minutes. In each case the thicker line is for the simple model that added a fan delay (and assumes no evaporation for the remainder of the off-cycle when the fan is off). The thinner lines associated with each time delay use the two off-cycle interval model and assume that the 2<sup>nd</sup> interval in the off-cycle when the fan is off has a very small airflow ( $10^2$ ,  $10^3$ , and  $10^4$  times less are shown on the plot). As expected the two models converge at very small off-cycle flow rates.



**Figure 5-35. Predicting Latent Degradation with Fan Overrun Delay**

Some manufacturers implement fan delays that maintain 50% of full flow for a brief period (see Table 2-3). Figure 5-36 shows the impact of reducing airflow during the fan delay. The reduced air flow during the fan delay does, in part, mitigate the latent degradation.



**Figure 5-36. Predicting Latent Degradation with a Fan Overrun Delay and Reduced Off-Cycle Airflow**

## 5.5 Validation of LHR Degradation Models

### 5.5.1 Validating Constant Fan Operation

The laboratory tests for each coil included a set of quasi-steady tests with continuous supply air fan operation at several cycling rates that corresponded to a maximum cycle rate ( $N_{\max}$ ) of 3 cycles/hr. The series of quasi-steady tests also included an initial run to estimate the model parameters  $t_{\text{wet}}$ ,  $\gamma$ ,  $M_0$ , etc.

Figure 5-37 through Figure 5-46 compare the measured laboratory data (symbols) to the various LHR degradation models. The original LHR model is shown as a black solid line (assuming linear decay for the off-cycle moisture evaporation rate) and a black dotted line (assuming exponential decay for the off-cycle moisture evaporation rate). The values of  $t_{\text{wet}}$  and  $\gamma$  used in each case are given in the table associated with each figure. These values were calculated using the data associated with each test run.



The new LHR degradation model (from Section 5.2) requires the parameters  $t_p$  and NTU. These parameter values were calculated based on two different assumptions.

Option 1. (Solid pink line) The values were calculated using measured data from the initial test in the series (i.e., run specific parameters). In this case the parameters were determined using:

$$t_{p1} \equiv \frac{1060 \cdot M_o}{1.08 \cdot cfm \cdot (DB - WB)} = \frac{Moisture\_Mass}{Evap\_Potential}$$

$$NTU_1 = -\ln(1 - \eta_{evp\_measured})$$

Option 2. (Dotted pink line) The values were calculated using the average properties of the coil based on many tests. In this case the NTU is based on a curve fit of the results for all the runs for that coil. The parameters were determined using:

$$NTU_2 = \frac{K_{curvefit}}{cfm^{0.2}}$$

$$t_{p2} = \frac{t_{wet}}{\gamma} (1 - e^{-NTU_2})$$

Overall the LHR degradation models are in good agreement with the measured data at the various operating conditions (when considering the measured test results for the 2<sup>nd</sup>, 3<sup>rd</sup>, and 4<sup>th</sup> cycles when quasi-steady state had been reached). While the new LHR degradation model does incorporate a more accurate prediction of off-cycle moisture evaporation, it still predicts similar LHR variation as the original LHR model. The more accurate off-cycle prediction of moisture evaporation rate does not result in a substantial improvement since the time to evaporate moisture from the coil is similar in both cases.

Coil 8, the chilled water coil, demonstrated the most deviation between the model and measured data. The larger differences in this case may be due to the confounding influence of the added coil mass of the chilled water system. The additional mass of the coil may confound our experimental procedures which use off-cycle sensible capacity to determine the mass of moisture on the coil. Similarly, the water temperature glide through the chilled water coil – which affects if the coil fins are fully wetted – may also have had an impact on the results for this coil.

Coil	Condition (°F db, °F dp)	Original Model (black lines)		New Model Run-Specific Parameters (solid pink line)		New Model Averaged Parameters (dotted pink line)	
		$t_{wet}$ (min)	$\gamma$	$t_{p1}$ (min)	$NTU_1$ (-)	$t_{p2}$ (min)	$NTU_2$ (-)
1	80/60	15.0	1.48	7.4	1.29	7.7	1.40
2	80/60	17.3	1.50	9.2	1.60	9.7	1.83
3	80/60	29.6	1.81	14.3	2.06	14.4	2.12
4	80/60	17.3	0.92	11.8	1.00	12.3	1.07

Note: Air flow rate is 400 cfm/ton

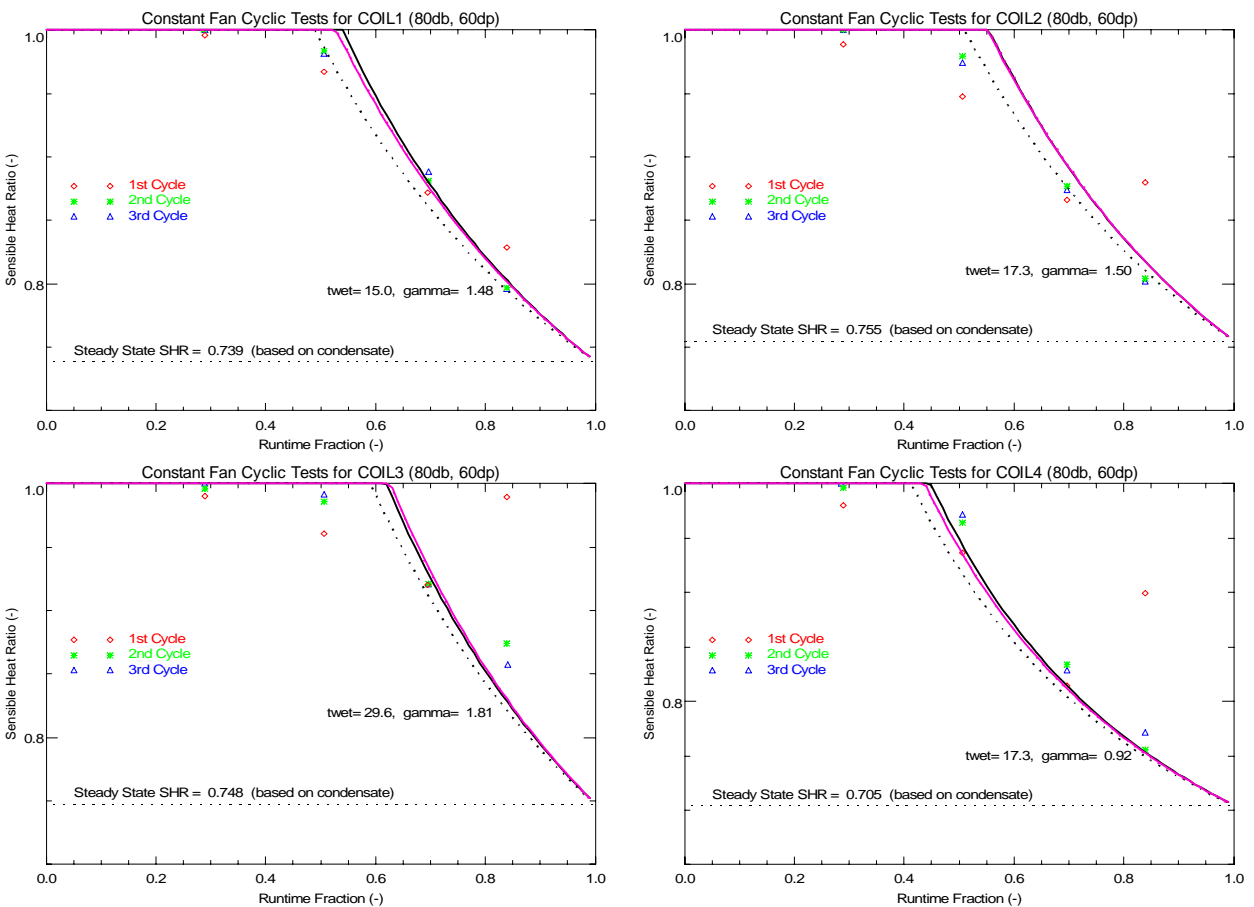


Figure 5-37. Comparing LHR Model to Lab Data: Coils 1-4, 80°F db, 60°F dp

Coil	Condition (°F db, °F dp)	Original Model (black lines)		New Model Run-Specific Parameters (solid pink line)		New Model Averaged Parameters (dotted pink line)	
		$t_{wet}$ (min)	$\gamma$	$t_{p1}$ (min)	$NTU_1$ (-)	$t_{p2}$ (min)	$NTU_2$ (-)
5	80/60	8.7	0.88	6.1	0.95	7.3	1.32
6	80/60	31.9	1.68	16.9	2.20	17.6	2.58
7	80/60	24.5	1.57	13.6	2.06	14.2	2.37
8	80/60	27.8	2.46	9.2	1.66	8.8	1.50

Note: Air flow rate is 400 cfm/ton

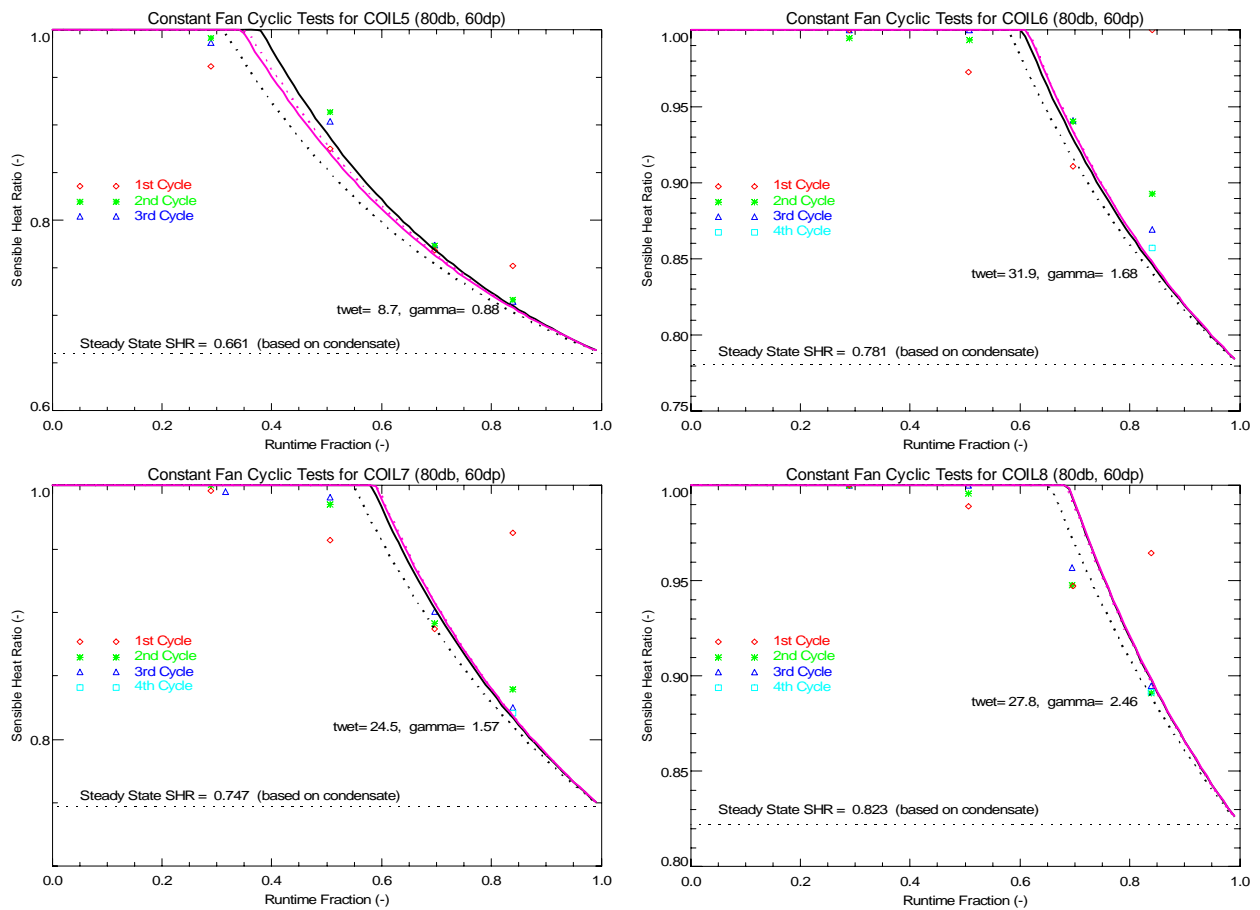


Figure 5-38. Comparing LHR Model to Lab Data: Coils 5-8, 80°F db, 60°F dp

Coil	Condition (°F db, °F dp)	Original Model (black lines)		New Model Run-Specific Parameters (solid pink line)		New Model Averaged Parameters (dotted pink line)	
		$t_{wet}$ (min)	$\gamma$	$t_{p1}$ (min)	$NTU_1$ (-)	$t_{p2}$ (min)	$NTU_2$ (-)
2	75/64	11.2	0.49	19.6	1.88	19.3	1.83
3	75/64	21.3	0.59	34.1	3.08	31.9	2.12
4	75/64	9.6	0.47	15.4	1.42	13.3	1.07

Note: Air flow rate is 400 cfm/ton

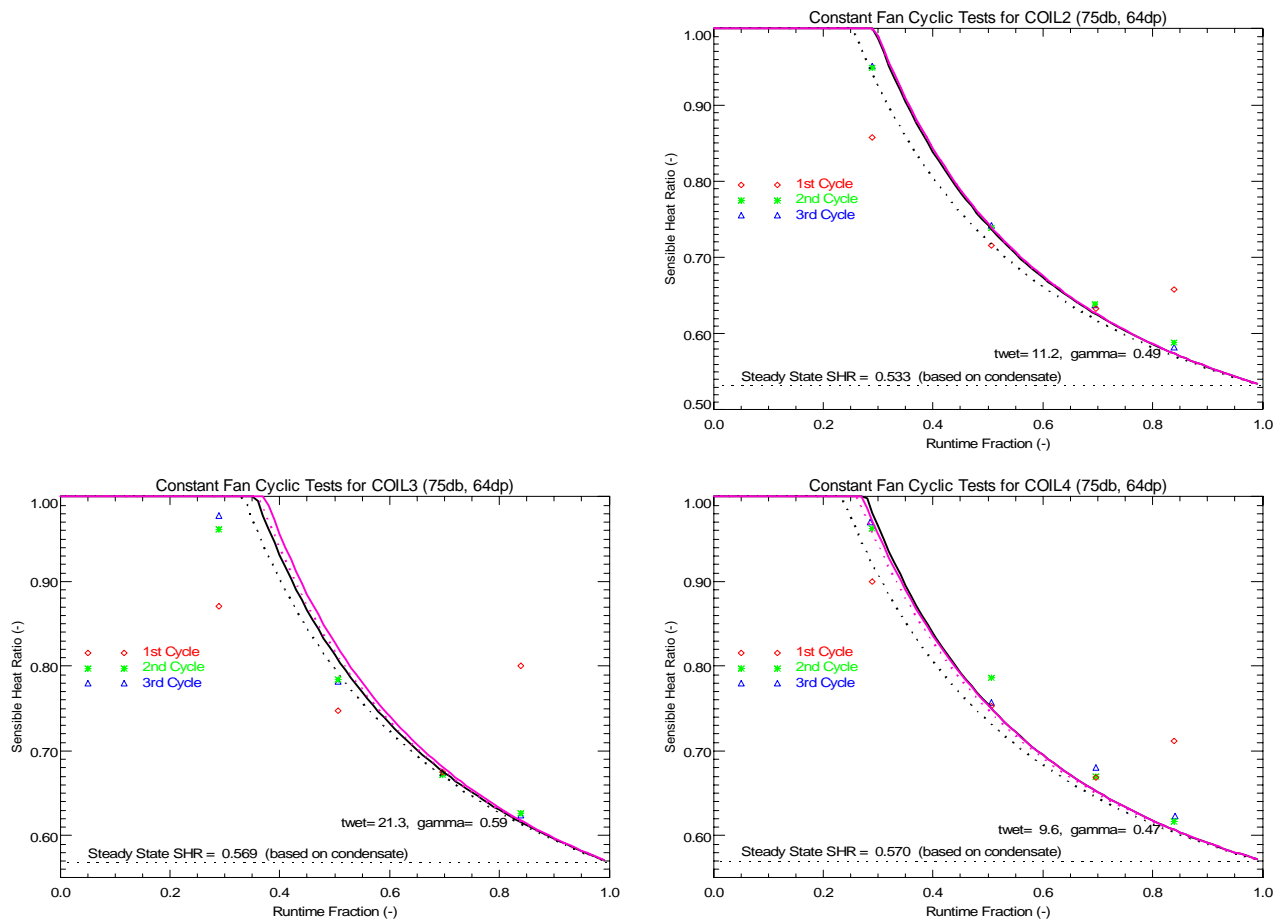


Figure 5-39. Comparing LHR Model to Lab Data: Coils 2-4, 75°F db, 64°F dp

Coil	Condition (°F db, °F dp)	Original Model (black lines)		New Model Run-Specific Parameters (solid pink line)		New Model Averaged Parameters (dotted pink line)	
		$t_{wet}$ (min)	$\gamma$	$t_{p1}$ (min)	$NTU_1$ (-)	$t_{p2}$ (min)	$NTU_2$ (-)
5	75/64	5.5	0.40	10.2	1.35	10.1	1.32
6	75/64	17.6	0.55	29.4	2.49	29.7	2.58
7	75/64	15.4	0.58	26.8	na	24.3	2.37
8	75/64	15.8	0.68	19.7	1.87	18.2	1.50

Notes: Air flow rate is 400 cfm/ton. na – indicates effectiveness greater than 1 so  $NTU_1$  was invalid.

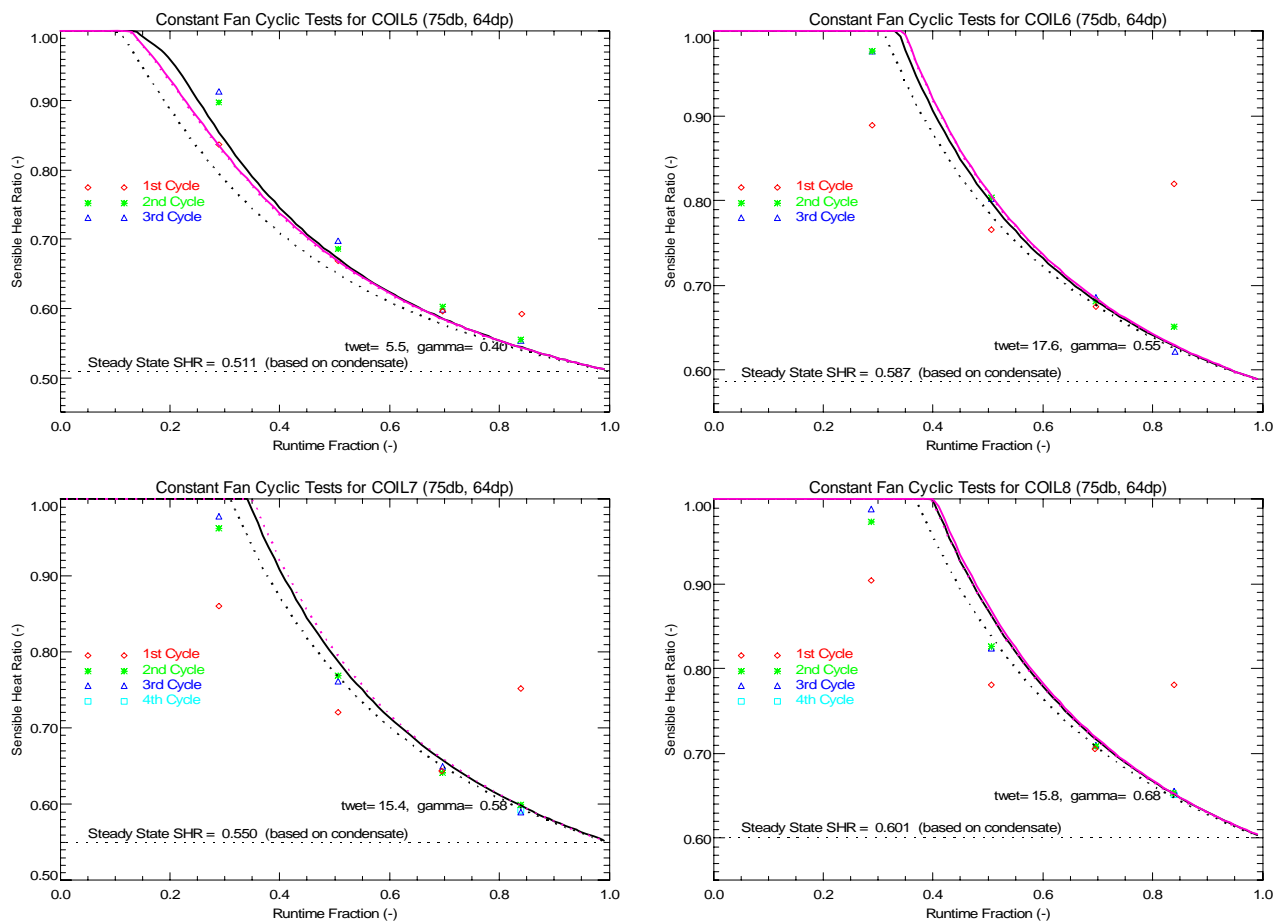


Figure 5-40. Comparing LHR Model to Lab Data: Coils 5-8, 75°F db, 64°F dp

Coil	Condition (°F db, °F dp)	Original Model (black lines)		New Model Run-Specific Parameters (solid pink line)		New Model Averaged Parameters (dotted pink line)	
		$t_{wet}$ (min)	$\gamma$	$t_{p1}$ (min)	$NTU_1$ (-)	$t_{p2}$ (min)	$NTU_2$ (-)
2	75/56	21.6	1.80	9.8	1.67	10.0	1.83
3	75/56	36.3	2.15	15.8	2.78	14.9	2.12
4	75/56	20.8	0.92	12.7	0.82	14.9	1.07

Note: Air flow rate is 400 cfm/ton

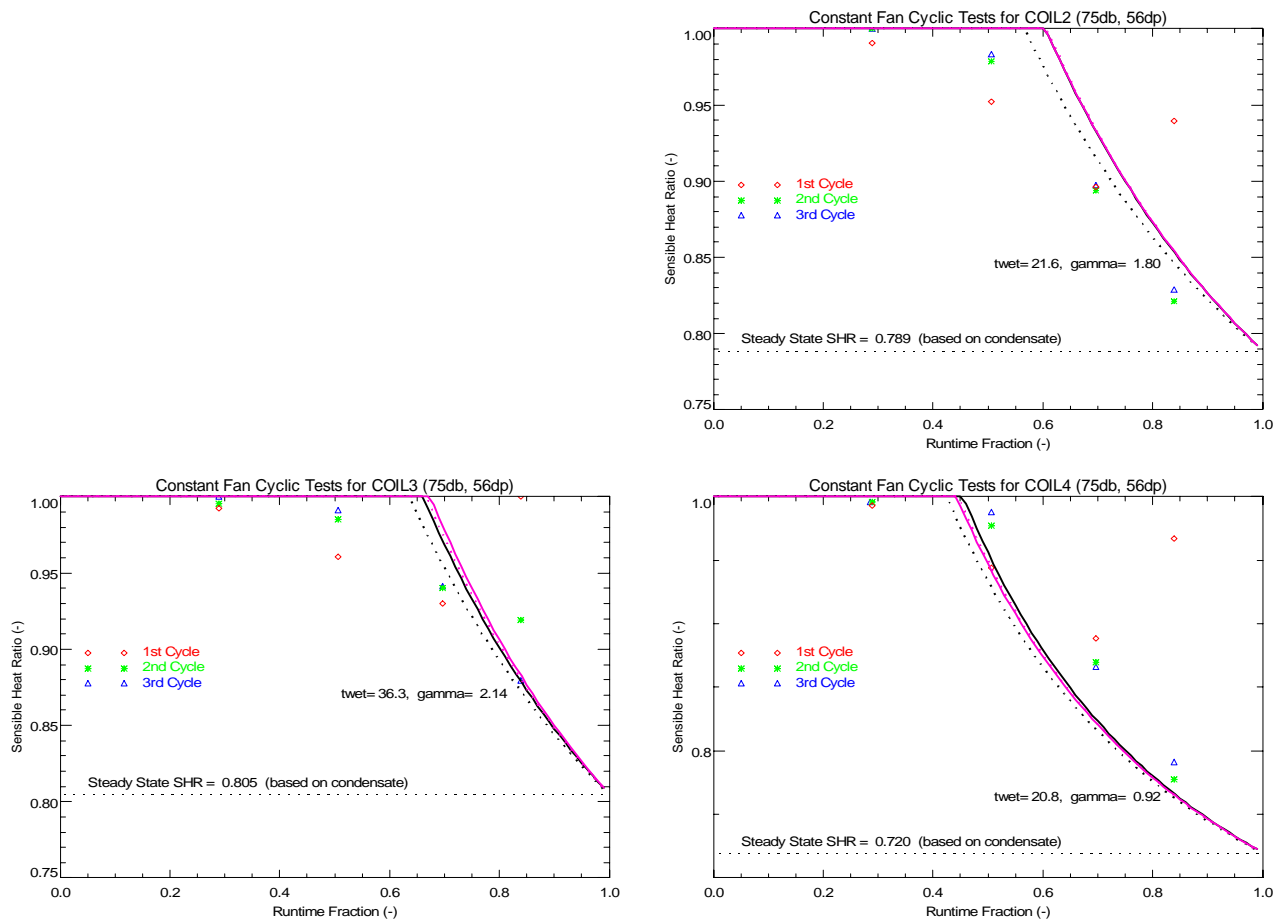


Figure 5-41. Comparing LHR Model to Lab Data: Coils 2-4, 75°F db, 56°F dp

Coil	Condition (°F db, °F dp)	Original Model (black lines)		New Model Run-Specific Parameters (solid pink line)		New Model Averaged Parameters (dotted pink line)	
		$t_{wet}$ (min)	$\gamma$	$t_{p1}$ (min)	$NTU_1$ (-)	$t_{p2}$ (min)	$NTU_2$ (-)
5	75/56	12.7	1.12	8.3	1.31	8.3	1.32
6	75/56	37.8	1.91	17.2	2.01	18.3	2.57
7	75/56	33.4	1.74	16.6	2.08	17.4	2.37
8	75/56	46.0	4.45	6.9	1.13	8.0	1.50

Note: Air flow rate is 400 cfm/ton

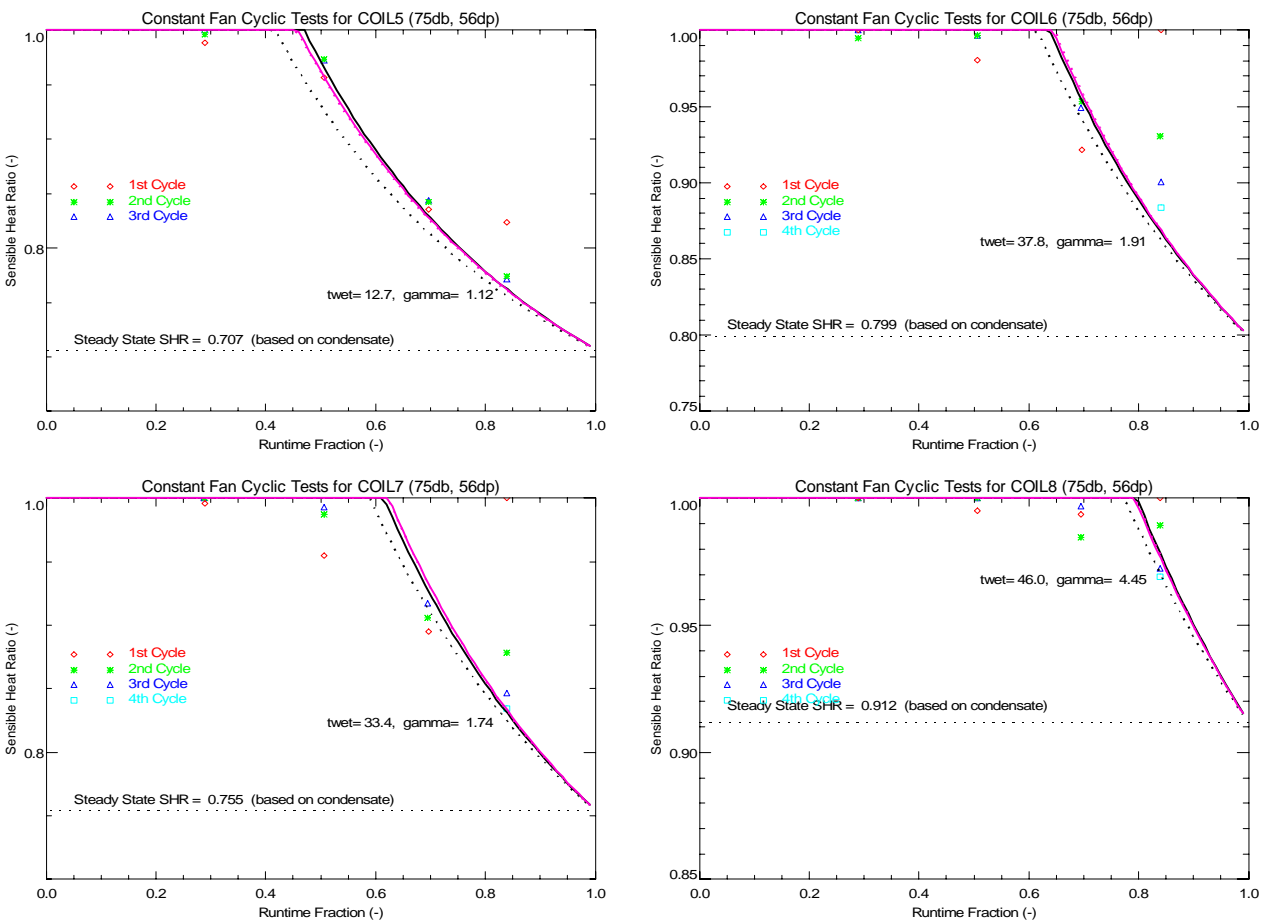


Figure 5-42. Comparing LHR Model to Lab Data: Coils 5-8, 75°F db, 56°F dp

Coil	Condition (°F db, °F dp)	Original Model (black lines)		New Model Run-Specific Parameters (solid pink line)		New Model Averaged Parameters (dotted pink line)	
		$t_{wet}$ (min)	$\gamma$	$t_{p1}$ (min)	$NTU_1$ (-)	$t_{p2}$ (min)	$NTU_2$ (-)
2	80/60	16.9	0.97	10.9	1.78	14.9	1.94
3	80/60	28.7	1.23	16.2	2.29	20.8	2.23
4	80/60	15.2	0.73	10.7	1.13	14.1	1.13

Note: Air flow rate is 300 cfm/ton

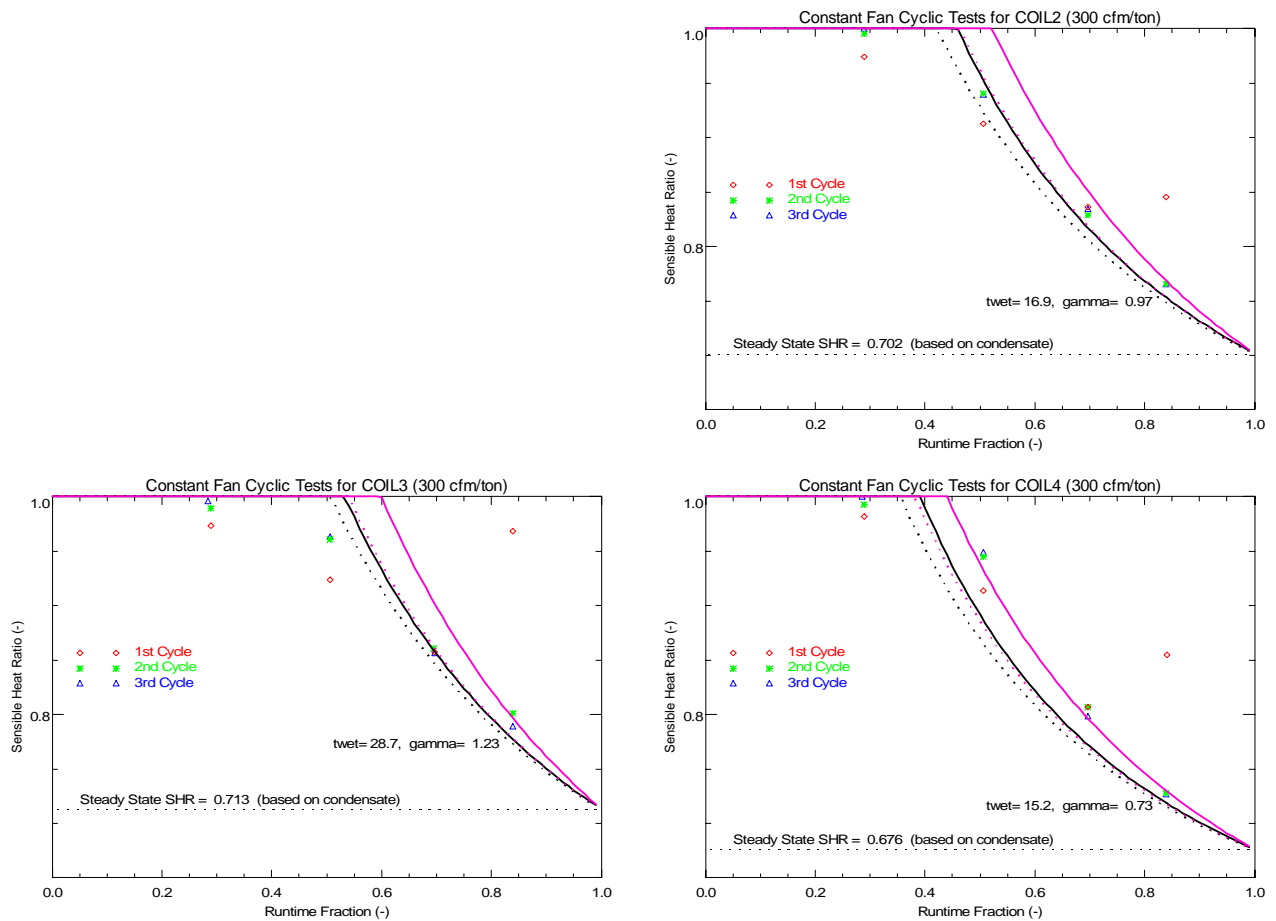


Figure 5-43. Comparing LHR Model to Lab Data: Coils 2-4, 300 cfm/ton



Coil	Condition (°F db, °F dp)	Original Model (black lines)		New Model Run-Specific Parameters (solid pink line)		New Model Averaged Parameters (dotted pink line)	
		$t_{wet}$ (min)	$\gamma$	$t_{p1}$ (min)	$NTU_1$ (-)	$t_{p2}$ (min)	$NTU_2$ (-)
5	80/60	11.9	0.77	8.6	1.42	11.6	1.40
6	80/60	27.6	1.07	17.8	2.47	24.1	2.73
7	80/60	24.2	1.08	15.6	2.37	20.6	2.50
8	80/60	29.3	1.77	11.5	2.57	13.2	1.59

Note: Air flow rate is 300 cfm/ton

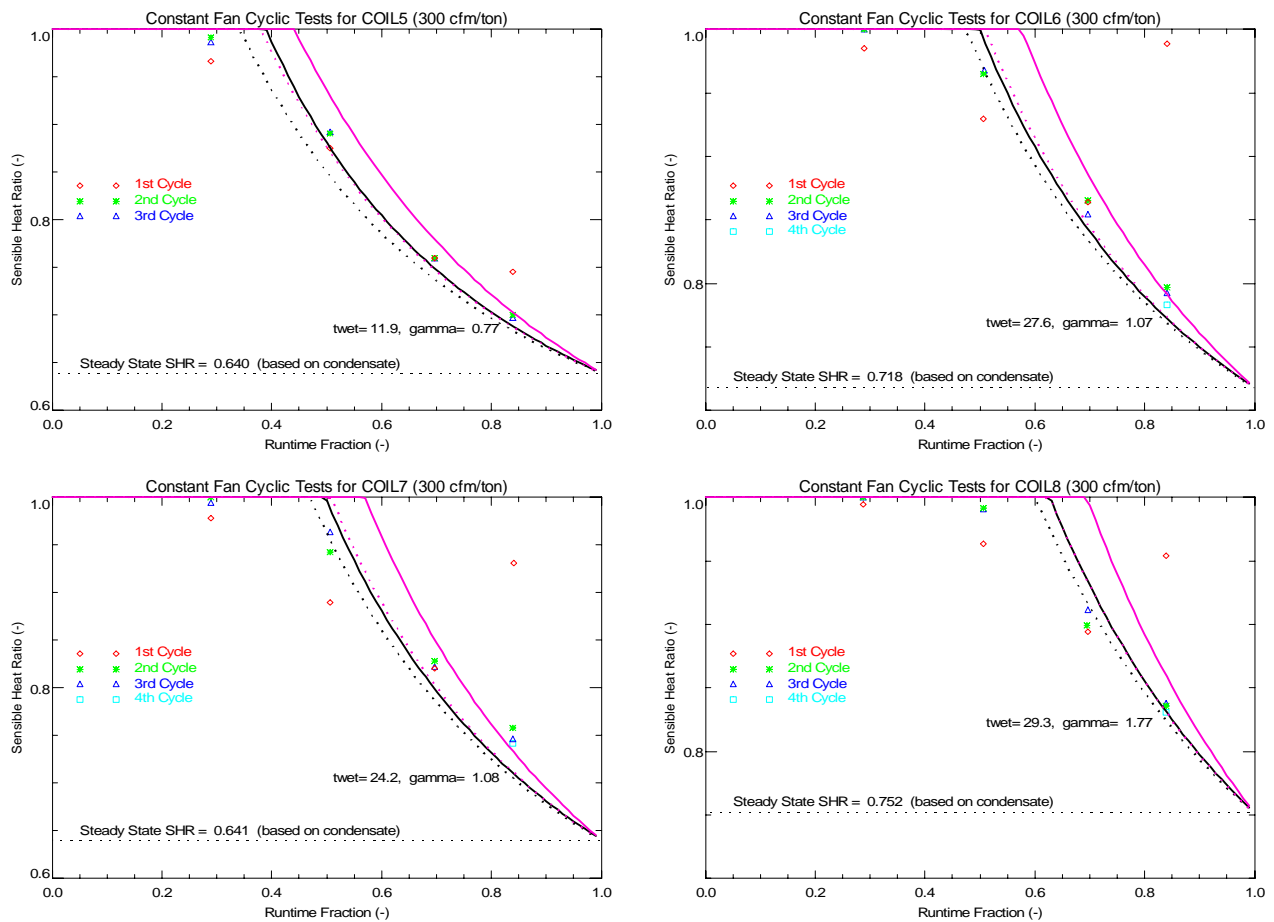


Figure 5-44. Comparing LHR Model to Lab Data: Coils 5-8, 300 cfm/ton

### 5.5.2 Validating the AUTO Fan Mode

Quasi-steady cyclic data were also collected with the fan cycling on and off with the cooling coil for all eight test coils. These results are shown in Figure 5-45 and Figure 5-46 for nominal operating conditions (80°F db, 60°F dp, 400 cfm/ton). For the test points with very low runtime

fraction we found that additional cycles were required to achieve quasi-steady conditions (i.e., cycle  $n+1$  yields the same result as cycle  $n$ ). Lines in these figures are simply drawn from point-to-point for the final cycles at each coil/fan runtime fraction to allow easier viewing of the general trends (i.e., they are not model predictions). For all coils except coil 2, some amount of SHR degradation was detected. Figure 5-33 and Figure 5-34 in Section 5.4.3 presented two possible ways to consider moisture evaporation when the fan is off during the coil off cycle:

- Scenario 1. A tiny amount of airflow through the coil when the fan is off (e.g., 100 times less flow than the on-cycle airflow) causes moisture to evaporate from the coil,
- Scenario 2. A tiny amount of airflow occurs only for a brief period at the beginning of the off cycle because the system is cold; after a brief period, the system warms and all airflow stops.

The observed trends from the lab testing seem to imply a mix of these two possible scenarios. Coils 1, 2 and 5 show a nearly linear trend that is consistent with Scenario 2 (flow for a brief period). In contrast, coils 3, 4, 6, 7 and 8 show trends (the SHR approaching 1 at very low runtime fractions) that are consistent with Scenario 1.

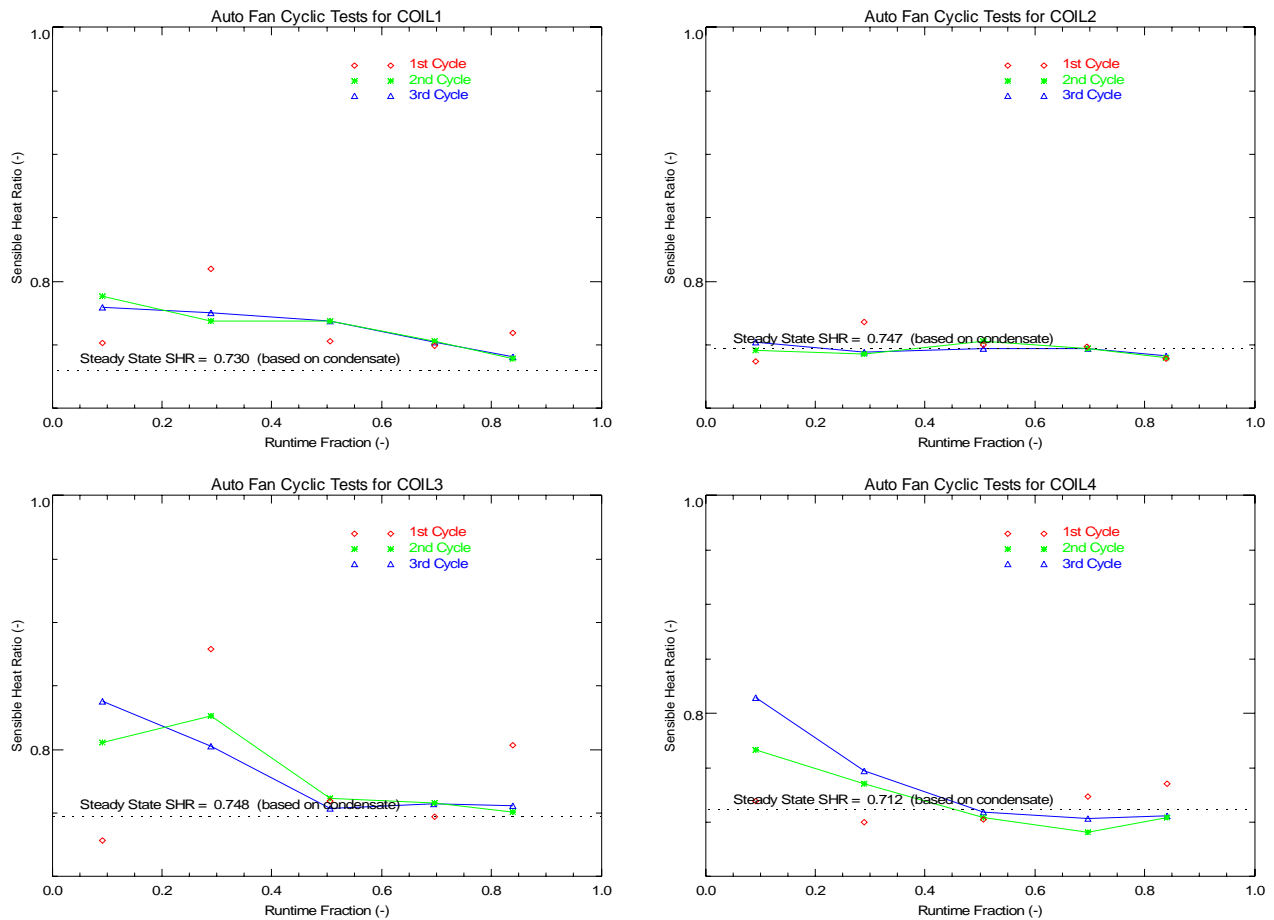


**Figure 5-45. Measured LHR Degradation: Coils 1-4, AUTO Fan at Nominal Conditions**

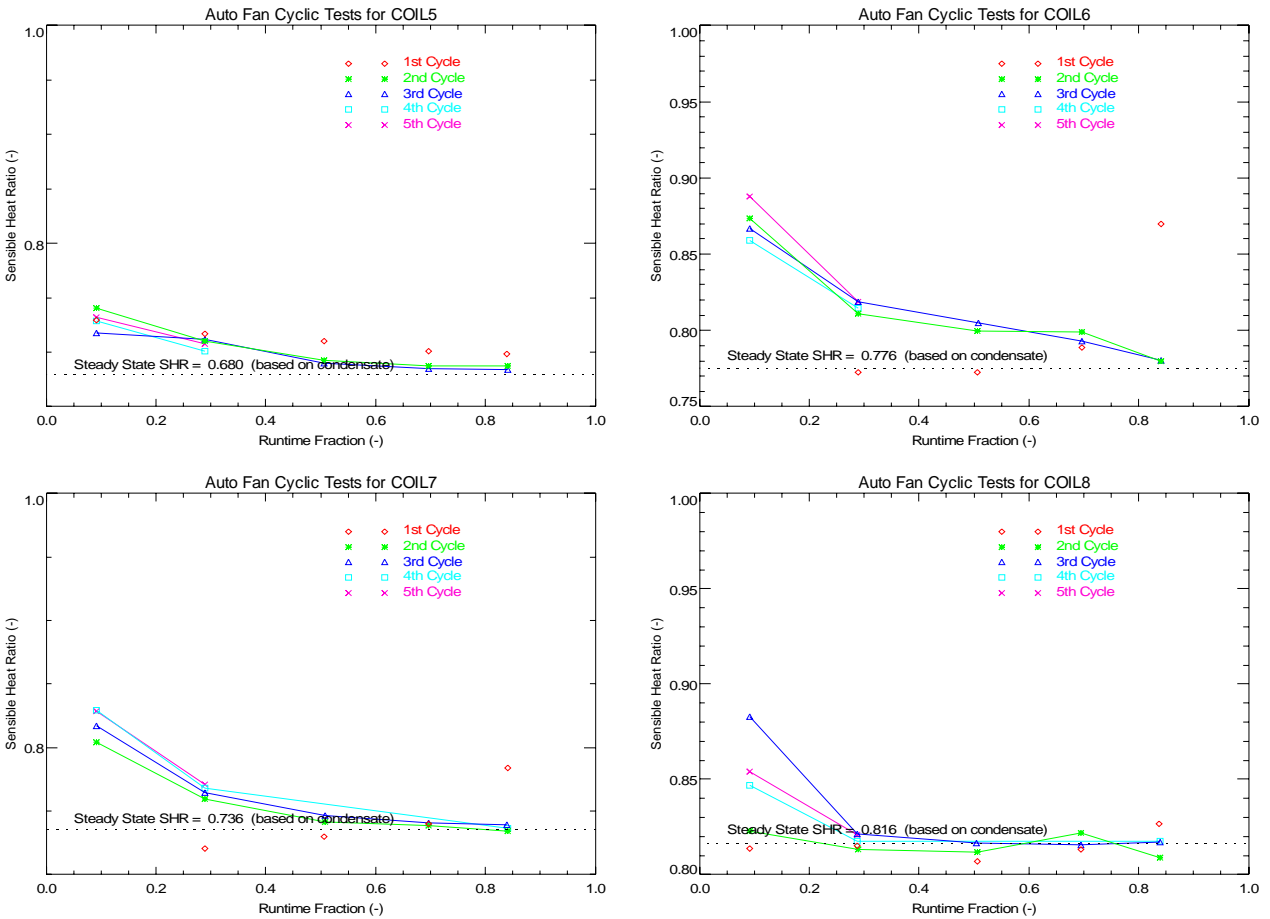


**Figure 5-46. Measured LHR Degradation: Coils 5-8, AUTO Fan at Nominal Conditions**

The laboratory setup and instrumentation were not able to measure very low airflow rates such as might be expected with the fan off. For coil 8, we did use a handheld hot-wire anemometer in an attempt to sense any airflow with the fan off. The hot wire probe was not able to consistently detect airflow, but about 1 of 20 readings did detect a flow of 20-40 fpm. If we average all the readings the implied velocity would be 1-2 fpm, or about 250-500 times less than the on-cycle airflow. This equates to 2-4 cfm. During the same period the orifice flow meter indicated a pressure drop of 0.002 inches, which implies 44 cfm. Both of these airflow readings are well below the threshold of each instrument, though probably provide an order of magnitude indication of off-cycle airflow.

Figure 5-47 compares the laboratory data for coil 8 to the new LHR model assuming that the off-cycle airflow is 250 times less than the on-cycle flow over the entire coil off cycle (Scenario 1). The model is in fairly good agreement with the 4<sup>th</sup> and 5<sup>th</sup> cycles of the measured data.

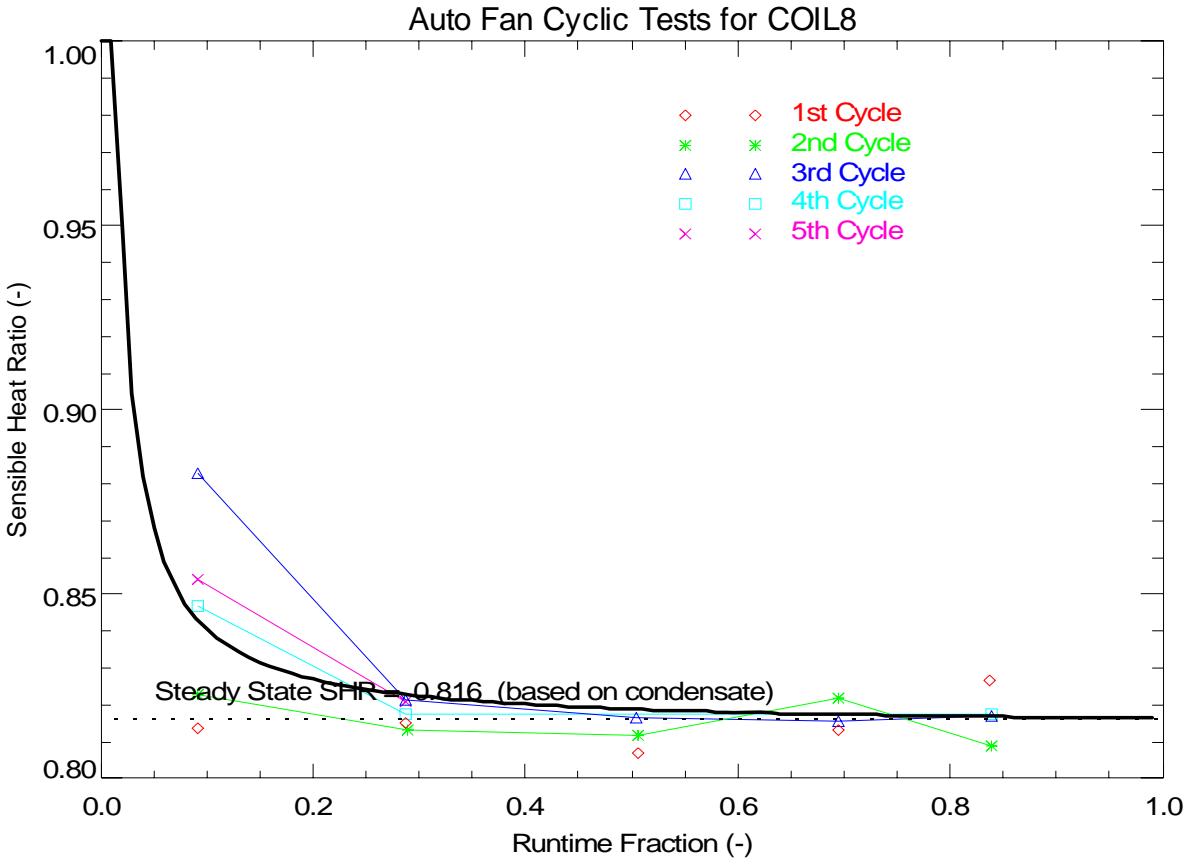


**Figure 5-47. Comparing LHR Model to Lab Data: Coil 8, AUTO Fan**

### 5.5.3 Validating the LHR Degradation Model for Fan Drain-Down Delays

A special case of fan delay is when the fan turns off for a fixed interval right after a cooling cycle ends. This type of delay is often called a “drain-down cycle” because of the misguided belief that water drains from the coil when the fan is off for a few minutes. Section 5.4.1 derived a model to handle this type of fan delay. The model inherently assumes that moisture drain down does not occur, but instead that moisture remains on the coil until the fan is activated again. This model assumption is largely supported by the lab testing results.

Figure 5-48 compares the measured LHR degradation trends (symbols) to the theoretical model developed in Section 5.4.1 (lines). The LHR degradation model is in good agreement with the data, confirming the assumption that little-to-no moisture is removed from the coil during the brief fan shutdown period.

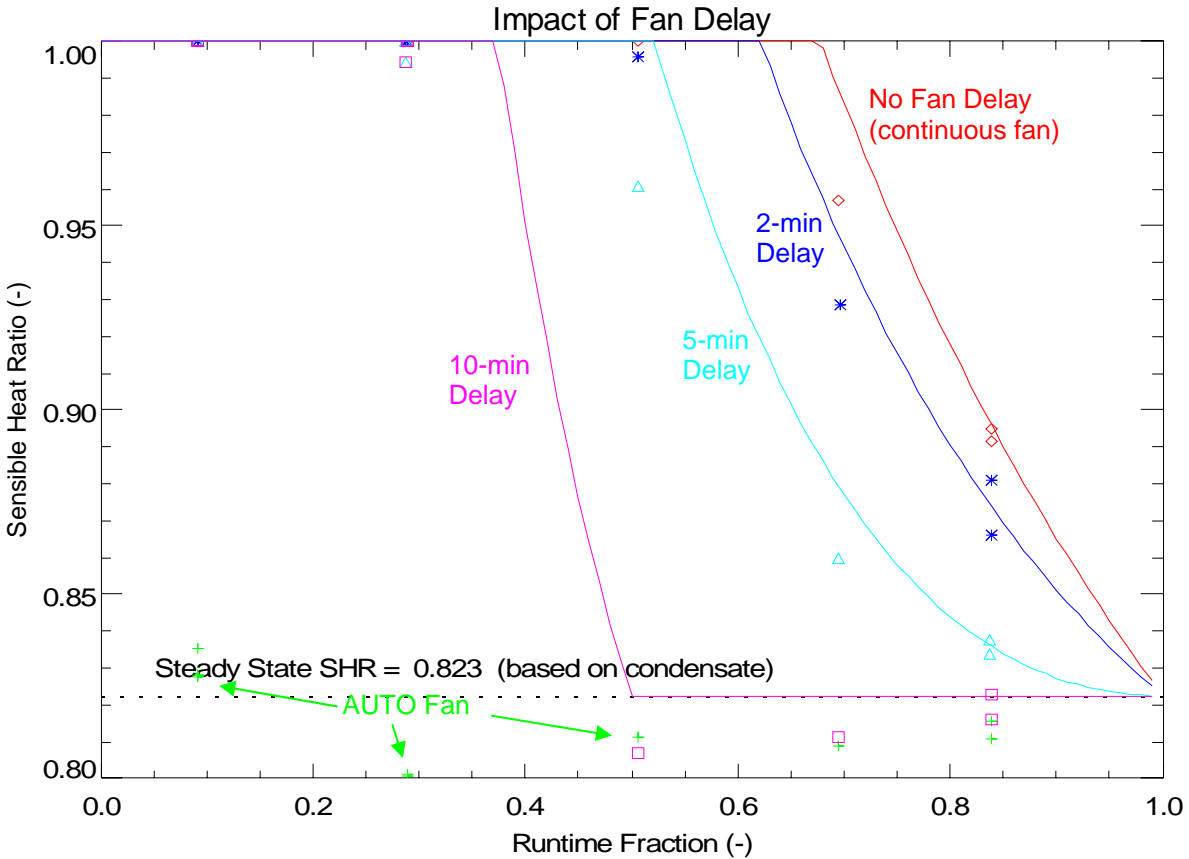


**Figure 5-48. Comparing LHR Model to Lab Data: Coil 8, “Drain-Down Delays”**

## 5.6 Recommended Model Parameters for Various Cooling Systems

The latent degradation of a cooling coil at part-load conditions depends on several aspects of cooling system performance that are generally not provided by equipment manufacturers or available in the literature. Therefore, we have developed the set of guidelines below in Table 5-4 to help users intelligently select model parameters for a given cooling system based on a minimal amount of knowledge. We assume that the following basic information is available:

- Total cooling capacity and sensible heat ratio (SHR),
- Airflow rate,
- Coil face area, fins spacing, and coil depth (to find total fin area).

It is generally better to determine the information above at the actual operating conditions of interest. Alternatively, the calculations described in the sections above – along with a steady-state cooling performance map – can also be used to correct rated model parameters to the proper values at different operating conditions. These corrections for operating conditions would apply to  $Q_L$ ,  $t_{wet}$ , and  $t_p$ .

**Table 5-4. Guidelines to Determine Parameters for the LHR Degradation Models**

Parameter	Equation Form	Suggested Value	Observed Range of Values
Latent Capacity ( $Q_L$ , Btu/h)	$Q_L = Q_T \cdot SHR$	SHR near 0.75 at nominal conditions	0.5-1.0 depending on actual operating conditions
Total Fin Area ( $A_o$ , ft <sup>2</sup> )	$A_o = 2 \cdot (\text{face area, ft}^2) \cdot (\text{fpi}) \cdot (\text{depth, in})$	Approx. 100 ft <sup>2</sup> per ton	50-150 ft <sup>2</sup> per ton
Moisture Mass ( $M_o$ , lb)	$M_o = K1 \cdot A_o / 1000$	$K1 = 8$ lb per 1000 ft <sup>2</sup> (at nominal conditions)	$K1 = 7-14$ lb per 1000 ft <sup>2</sup>
Evaporation $NTU_o$	$NTU_o = (K2 \cdot A_o) / \text{cfm}^{0.2}$	$K2 = 0.03$	$K2 = 0.024-0.043$
$t_{wet}$ (sec)	$t_{wet} = 3600 \cdot (M_o \cdot 1060) / Q_L$		
$t_p$ (sec)	$t_p = \frac{3600 \cdot (M_o \cdot 1060)}{1.08 \cdot \text{cfm} \cdot (\text{DB-WB})}$		
$\gamma$	$\gamma = \frac{(1.08 \cdot \text{cfm} \cdot (\text{DB-WB})) \cdot (1 - e^{-NTU_o})}{Q_L \cdot 1060}$		

Note: nominal conditions are 80°F dry-bulb temperature, 60°F dewpoint temperature, 400 cfm/ton.

The guidelines above assume that the moisture holding capacity of the coil does not change with operating conditions. In fact the data shown in the laboratory section did imply some variation with airflow. To account for this variation with airflow, we have developed the simple relationship shown in Figure 5-49. This linear adjustment factor approximately accounts for the variation shown from the lab-tested coils.

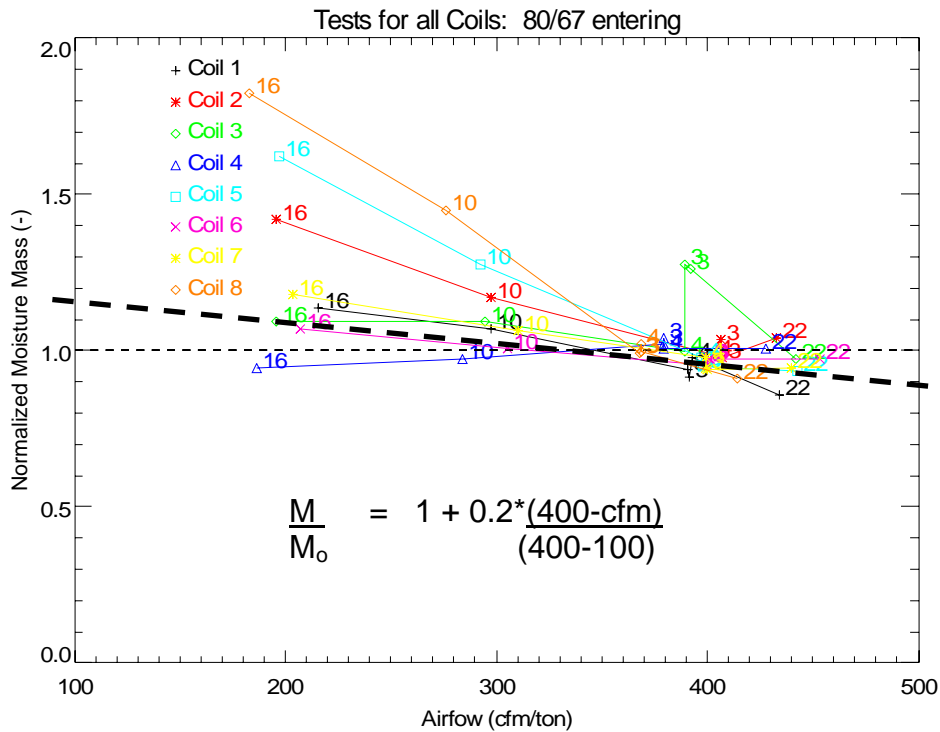


**Figure 5-49. Variation of Coil Retained Moisture Mass with Airflow**

## **5.7 Part-Load Latent Performance for Modulating and Staged DX Systems**

The improved latent degradation model described in Section 5.3 is primarily applicable to direct expansion (DX) cooling coils that cycle on and off to meet cooling requirements. However, some DX cooling systems modulate compressor capacity to meet the cooling load. Section 5.7.1 below presents a method for modeling part-load dehumidification performance for these capacity-modulated systems that relies on a steady-state DX coil performance model instead of the improved “cyclic” latent degradation model developed as part of this project.

Another method for varying DX equipment capacity is to provide multiple stages of compressor capacity and more than one refrigeration circuit. Several common coil circuiting arrangements are used, and both coil circuiting and compressor staging impact part-load dehumidification performance. Section 5.7.2 describes these issues and identifies the circuiting arrangement that provides the best dehumidification performance.

Finally, there are multi-stage cycling DX systems whose performance is best modeled using a combination of steady-state and cyclic models. Section 5.7.3 describes the mix of latent degradation modeling techniques that must be employed for these types of systems.

### **5.7.1 Part-Load Latent Performance for Modulating DX Coils**

Some direct expansion (DX) air-conditioning systems modulate compressor capacity in response to the cooling load instead of cycling a single compressor on and off. These systems can use multiple compressors, a compressor with unloaders, or a variable-speed compressor to modulate refrigerant flow to a single-circuit cooling coil (see Section 5.7.2 for coils with multiple refrigerant circuits). Since less refrigerant flow is sent to the cooling coil during part-load conditions, this method of capacity control causes the coil surface to get warmer at part load. As a result, the apparatus dew point of the coil increases.

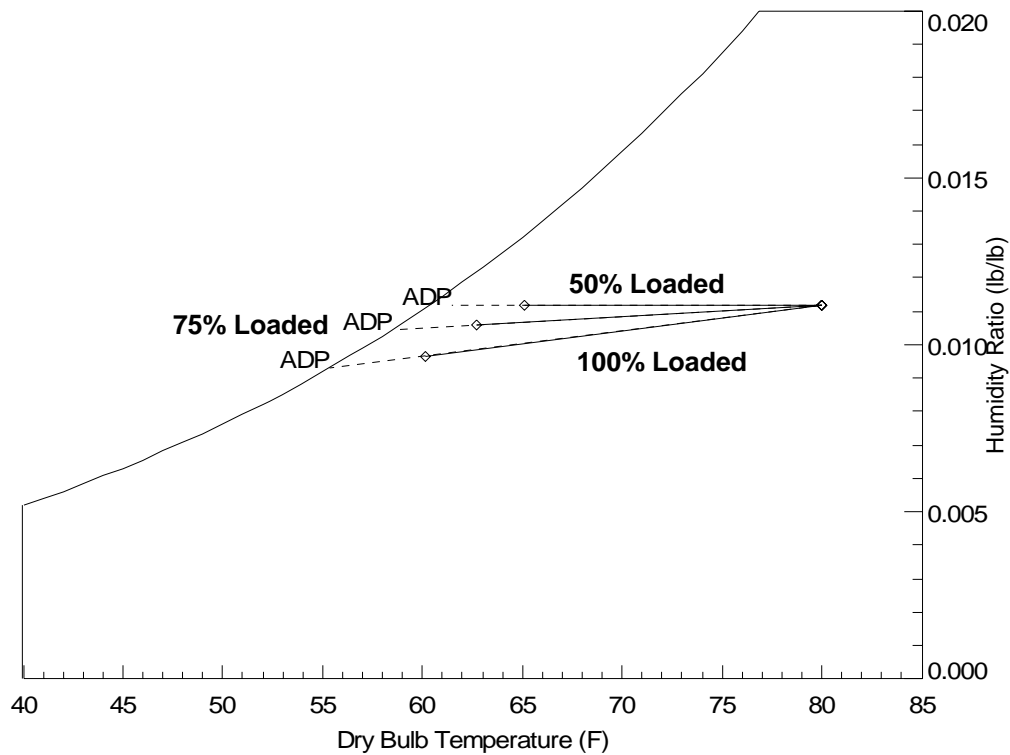
One way to emulate the part-load latent performance of these systems is to apply the apparatus dew point (ADP) / Bypass Factor (BF) approach developed by Henderson, Rengarajan and Shirey (1992) to predict the sensible and latent performance at different inlet air conditions. This steady-state AC coil model is also given in the ASHRAE Secondary Toolkit as DXDOE (Brandemuehl 1993) and in the EnergyPlus Engineering Manual (EnergyPlus Development Team 2005). The model combines empirical predictions of total capacity with the ADP/BF calculations to find the mix of sensible and latent capacity. The model first determines the BF and ADP corresponding to design or rated conditions. At other operating conditions, the BF and the enthalpy difference ( $\Delta h$ ) across the coil (which are known) are used to solve for the new operating ADP. The ADP is determined by knowing the enthalpy corresponding to the point where the process line intersects with the saturation line on the psychrometric chart. The ADP can be found using the relationship between the saturation temperature and enthalpy for moist air, or by iteration using psychrometric functions for moist air properties. Once the ADP is determined, the SHR of the coil can be calculated as well. The model depends on the definition of BF, which is only a function of air flow rate (and not entering air conditions).

For the case of a modulating coil, the total capacity and enthalpy difference ( $\Delta h$ ) decrease in proportion to compressor capacity:

$$\Delta h = LF \cdot \Delta h_o$$

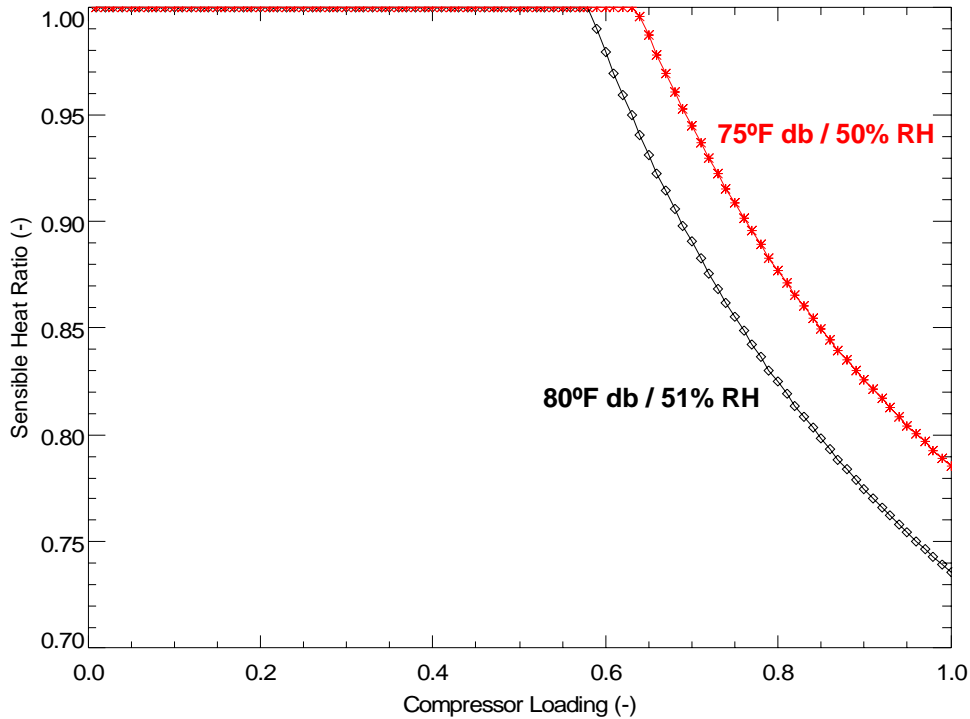
where  $\Delta h_o$  is the enthalpy difference across the coil at full load conditions and LF is the loading fraction of the compressors. The calculations use the reduced  $\Delta h$  with BF to find the new ADP at each capacity level. Figure 5-50 shows how the process line for a typical DX cooling coil changes as the compressor loading decreases. At 50% loading, the coil only provides sensible cooling. At 75% compressor loading the SHR has dropped to 0.855. At full load the SHR decreases further to 0.736. As the compressor loading decreases, the ADP of the coil warms from 55°F at full load to more than 61°F at 50% load.

Figure 5-51 shows trends of SHR with compressor loading factor for a typical DX cooling coil. With the compressors fully loaded, the SHR of the coil is 0.736 at nominal conditions of 80°F dry-bulb temperature and 51% RH (67°F wet-bulb temperature). The SHR of the coil reaches 1.0 when the compressor capacity drops below 60% in this case. Figure 5-51 also shows the SHR trend for entering air conditions of 75°F and 50% RH. The fully-loaded SHR is just under 0.79 for this operating condition. The latent capacity approaches zero when the compressor loading drops to 65%.



**Figure 5-50. Impact of Compressor Loading on Cooling Coil Process Line**





**Figure 5-51. Variation of SHR with Compressor Loading for a Modulated Coil**

### 5.7.2 Considering the Impact of Cooling Coil Circuiting and Staging

Many cooling systems have multiple stages of compressor capacity and more than one refrigeration circuit. Usually a compressor is dedicated to a specific refrigeration circuit or section in a cooling coil. The part-load latent performance of a cooling coil depends on both the compressor staging as well as how the coil is circuited. Figure 5-52 shows the three basic coil circuited arrangements (assuming 2 equal stages of capacity):

- **Face-Split Coils.** This arrangement breaks the coil into sections vertically, mimicking the performance of two single-stage cooling units operating in parallel. When circuit 1 is on (usually the bottom of the coil), approximately half of the total cooling capacity is applied to half of the air flow. This results in an SHR for stage 1 that is roughly equivalent to the SHR for full-load operation (i.e., stages 1 and 2 are operating).
- **Row-Split Coils.** This arrangement breaks the coil into sections horizontally, mimicking the performance of two single-stage cooling units operating in series. When circuit 1 is on, approximately half of the total cooling capacity is applied to the full air flow. This results in an SHR for stage 1 that is higher than the SHR for full-load operation.
- **Intertwined Coils.** This arrangement breaks the coil into small sections, mimicking the performance of a single coil with modulating refrigerant flow. When circuit 1 is on, each section of the coil can effectively use the fins of neighboring sections of the coil that are

unused. This arrangement can result in performance that approaches a single refrigerant circuit with modulating refrigerant flow (as discussed in Section 5.7.1).

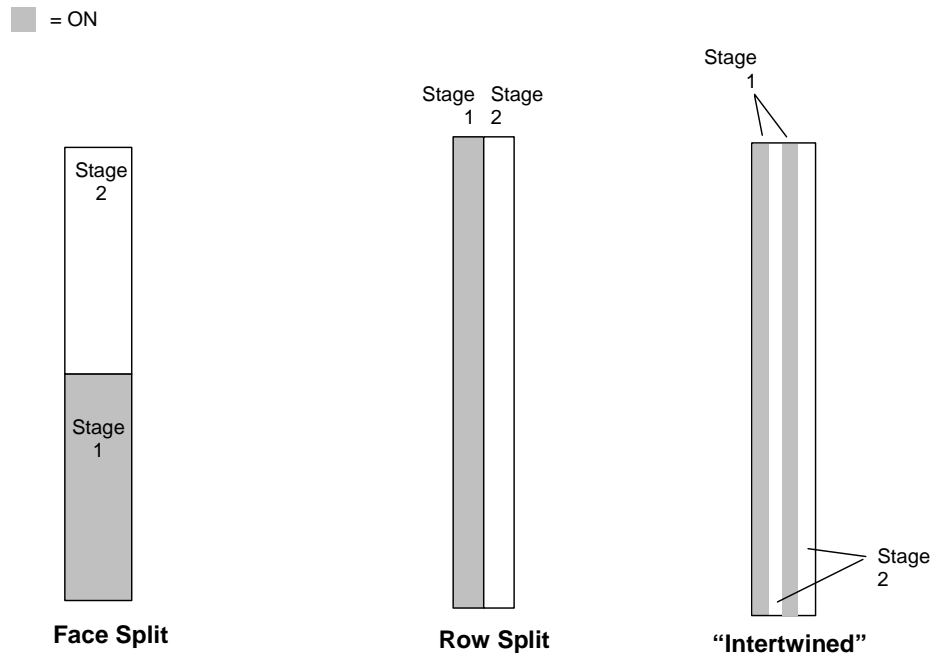


**Figure 5-52. Cooling Coil Circuiting Options**

The face split arrangement offers the best dehumidification performance at part-load conditions. The first-stage coil typically provides similar steady-state dehumidification performance (i.e., SHR) as the fully-operating coil since both air flow and refrigeration capacity decrease at roughly the same rate. In fact, part-load (first stage) dehumidification performance usually improves since the airflow through the active coil section is slightly reduced because air can more easily flow through the inactive, dry sections of the coil. Table 5-5 shows the calculated supply air dew point for a hypothetical 10-ton system that is face split using the steady-state coil model from Henderson, Rengarajan and Shirey (1992). Table 5-6 gives the operating conditions for the same system at 50% capacity but with a row-split coil.

The supply air conditions are 57.4°F dry bulb (db) and 54°F dewpoint (dp) for the 10-ton system at full load (see top section of each table). For the face split coil at 50% capacity, the air conditions leaving the cooling coil are 56.2°F db and 53.3°F dp (Table 5-5). When this air is mixed with bypassed air entering the unit the supply conditions for the entire system become 66.5°F db and 56.7°F dp. In contrast, Table 5-6 shows that the supply air conditions for the row-split case at 50% capacity are slightly cooler but more humid at 64.1°F db and 57.0°F dp (compared to the “system” supply air conditions for the face-split coil in Table 5-5). The intertwined coil – which is assumed to approach the performance of a single coil with modulated refrigerant flow – has very poor dehumidification performance (Table 5-7). Using the calculation method for a modulated coil described in Section 5.7.1 above, the supply conditions are 62.4°F db and 59°F dp when the intertwined coil is operating at 50% capacity.

**Table 5-5. Part-Load Performance for a “Face Split” Coil**

10-ton unit, 4000 cfm, 75DB/65WB entering air (~60%RH), 95°F outdoors

<p><b>100% Capacity (100% airflow)</b>            Coil Condition Wet            Total Capacity (10<sup>3</sup> Btu/h) 112.98            Sensible Capacity (10<sup>3</sup> Btu/h) 75.90            Latent Capacity (10<sup>3</sup> Btu/h) 37.08            Sensible heat Ratio (SHR) 0.672            Apparatus Dew Point (ADP) 53.3            Bypass Factor (BF) 0.195</p>	<p><b>Supply Air</b>            DB = 57.4°F            w = 0.0895 lb/lb            DP = 54.0°F</p>
<p><b>50% Capacity (45% of full airflow)</b>            Coil Condition Wet            Total Capacity (10<sup>3</sup> Btu/h) 55.26            Sensible Capacity (10<sup>3</sup> Btu/h) 36.51            Latent Capacity (10<sup>3</sup> Btu/h) 18.75            Sensible heat Ratio (SHR) <b>0.661</b>            Apparatus Dew Point (ADP) 52.7            Bypass Factor (BF) 0.163</p>	<p><b>COIL 1 Supply Air</b>            DB = 56.2°F            w = 0.0871 lb/lb            DP = 53.3°F</p>
<p><b>Mixed Conditions (full airflow)</b>            (55% entering + 45% supply conditions)            Sensible heat Ratio (SHR) <b>0.661</b></p>	<p><b>SYSTEM Supply Air</b>            DB = 66.5°F            w = 0.0991 lb/lb            DP = 56.7°F</p>

**Table 5-6. Part-Load Performance for a “Row Split” Coil**

10-ton unit, 4000 cfm, 75DB/65WB entering air (~60%RH), 95°F outdoors

<p><b>100% Capacity (100% airflow)</b>            Coil Condition Wet            Total Capacity (10<sup>3</sup> Btu/h) 112.98            Sensible Capacity (10<sup>3</sup> Btu/h) 75.90            Latent Capacity (10<sup>3</sup> Btu/h) 37.08            Sensible heat Ratio (SHR) 0.672            Apparatus Dew Point (ADP) 53.3            Bypass Factor (BF) 0.195</p>	<p><b>Supply Air</b>            DB = 57.4°F            w = 0.0895 lb/lb            DP = 54.0°F</p>
<p><b>50% Capacity with COIL 1 (100% airflow)</b>            Coil Condition Wet            Total Capacity (10<sup>3</sup> Btu/h) 64.12            Sensible Capacity (10<sup>3</sup> Btu/h) 46.96            Latent Capacity (10<sup>3</sup> Btu/h) 17.16            Sensible heat Ratio (SHR) <b>0.732</b>            Apparatus Dew Point (ADP) 55.6            Bypass Factor (BF) 0.442</p>	<p><b>Supply Air</b>            DB = 64.1°F            w = 0.0999 lb/lb            DP = 57.0°F</p>

**Table 5-7. Part-Load Performance for an “Intertwined” Coil**

10-ton unit, 4000 cfm, 75DB/65WB entering air (~60%RH), 95°F outdoors

<b>100% Capacity (100% airflow)</b>		<b>Supply Air</b> DB = 57.4°F w = 0.0895 lb/lb DP = 54.0°F
Coil Condition Wet		
Total Capacity (10 <sup>3</sup> Btu/h)	112.98	
Sensible Capacity (10 <sup>3</sup> Btu/h)	75.90	
Latent Capacity (10 <sup>3</sup> Btu/h)	37.08	
Sensible heat Ratio (SHR)	0.672	
Apparatus Dew Point (ADP)	53.3	
Bypass Factor (BF) 0.195		
<b>50% Capacity Intertwined/Modulated COIL (100% airflow)</b>		<b>Supply Air</b> DB = 62.4°F w = 0.1078 lb/lb DP = 59.0°F
Coil Condition Wet		
Total Capacity (10 <sup>3</sup> Btu/h)	56.49	
Sensible Capacity (10 <sup>3</sup> Btu/h)	54.29	
Latent Capacity (10 <sup>3</sup> Btu/h)	2.20	
Sensible heat Ratio (SHR)	<b>0.961</b>	
Apparatus Dew Point (ADP)	59.5	
Bypass Factor (BF) 0.195		
Comp Loading Factor (LF) 0.500		

Table 5-8 summarizes the performance of the face-split, row-split and intertwined coil arrangements. The best part-load dehumidification performance is provided by the face-split coil (SHR=0.66). The row-split coil has slightly less latent capacity (SHR=0.73). The intertwined coil – which is assumed to approach a single-circuit coil with modulated refrigerant flow – provides nearly no latent capacity (SHR=0.96).

**Table 5-8. Comparison of Dehumidification Performance for Different Coil Arrangements**

	Supply Temperature (°F)	Supply Dew Point (°F)	Sensible Heat Ratio
Full Load	57.4	54.0	0.67
50% Capacity – Face Split	66.5	56.7	0.66
50% Capacity – Row Split	64.1	57.0	0.73
50% Capacity – Intertwined/Modulated	62.4	59.0	0.96

### 5.7.3 Approaches for Modeling Multi-Stage, Cycling DX Systems

Many cooling systems are a relatively complex mix of both cycling and modulating systems. One example is a residential two-stage system. This system usually has a single refrigerant circuit that is served by multiple or modulating compressors. The unit effectively modulates between its capacity stages to meet the load. In the case of most residential systems, the supply fan also modulates with capacity stages to ensure that good dehumidification is provided at each stage. At very low loads, the unit cycles between the lowest cooling stage and off to meet the cooling load.

In these cases, a mix of latent degradation modeling techniques must be employed:

1. The unit effectively functions like a cycling system at low-load conditions, so the part-load latent degradation calculation methods summarized in Section 5.3 are used. The model parameters must be calculated using the steady-state performance and other physical characteristics for the low-stage cooling system.
2. Once modulation between capacity stages starts to occur, then empirical or semi-empirical methods to predict steady-state performance must be applied (such as the calculation approaches described in Sections 5.7.1 and 5.7.2). In time steps with mixed operation, some method of proportioning the amount of operation at each stage must be applied.

The mixed approach to applying part-load latent degradation is similar to what is required for part-load efficiency calculations.

For multi-stage commercial DX systems with face-split coils with dedicated compressors, the part-load latent degradation calculations summarized in Section 5.3 can be applied as if the two coil sections are separate cooling systems (e.g., installed in parallel each with their own runtime fraction).

## **5.8 Latent Degradation with Modulating Chilled Water Coils**

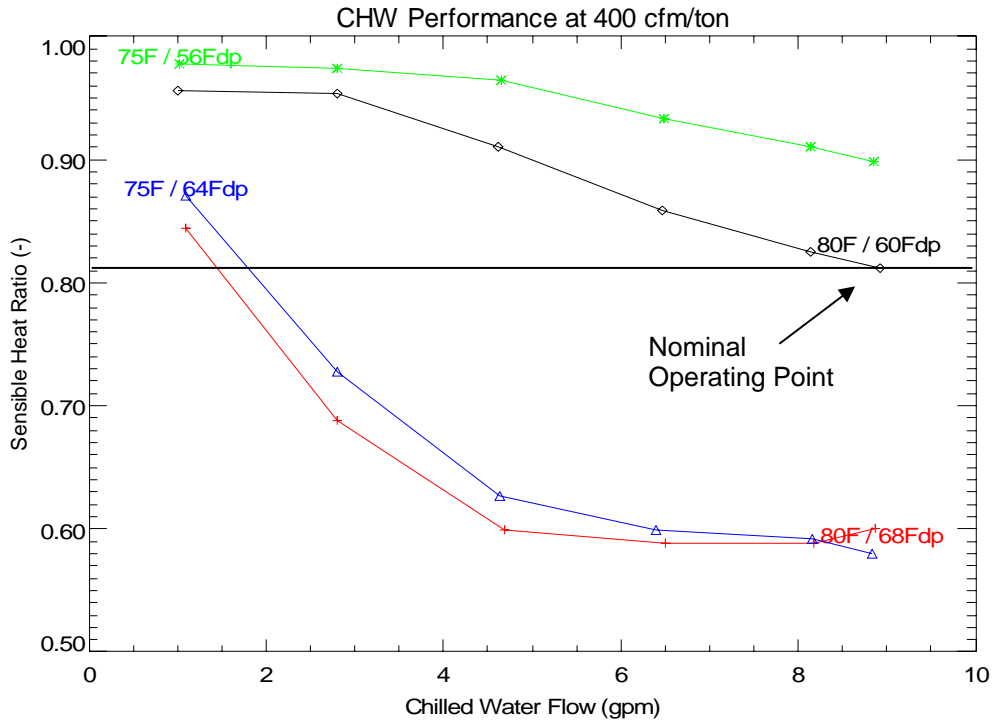
The data shown for coil 8 in Section 5.5 demonstrates that a chilled water coil that cycles on and off (using a quick-acting two-way water valve) behaves the same at part-load conditions as a cycling DX coil and compressor. However, most chilled water coils are applied with modulating valves that reduce the water flow through the coil when less cooling is required. When the chilled water flow is modulated the latent capacity of the coil decreases faster than the sensible cooling capacity. As a result, the SHR of a modulating chilled water coil changes at part-load conditions.

Figure 5-53 and Figure 5-55 show the measured trends of SHR and total cooling capacity with chilled water flow rate. The detailed chilled water coil model CCDET<sup>5</sup> from the ASHRAE Secondary Toolkit (Brandemuehl 1993) was also used to model the performance of coil 8. These performance trends are shown in Figure 5-54 and Figure 5-56. The CCDET model inputs included the geometric data for this coil given in Appendix H and the fluid properties of the chilled water loop (21% propylene glycol). While the magnitude of the SHR and capacity predicted by CCDET are in some cases quite different from the measured data, the overall performance variations with water flow are consistent with the laboratory measurements.

Figure 5-57 shows how the measured SHR changes with cooling load instead of water flow rate. Figure 5-58 shows the same data from the CCDET model. This set of plots, normalized for the capacity differences between the coils, shows similar trends for the measured data and CCDET predictions. This cursory comparison of measured performance data to one model implies that detailed chilled water coil models that endeavor to accurately predict mixed wet-dry performance at steady-state conditions can reasonably predict the loss of latent capacity at lower chilled water flow rates.

---

<sup>5</sup> Other similarly detailed chilled water coil models include the model by Elmahdy and Mitalas (1977), a slightly modified version of which is used in EnergyPlus, as well as the Type 56 chilled water model used in TRNSYS (Braun 1988).



**Figure 5-53. Trends of Measured SHR with Chilled Water Flow, Coil 8**

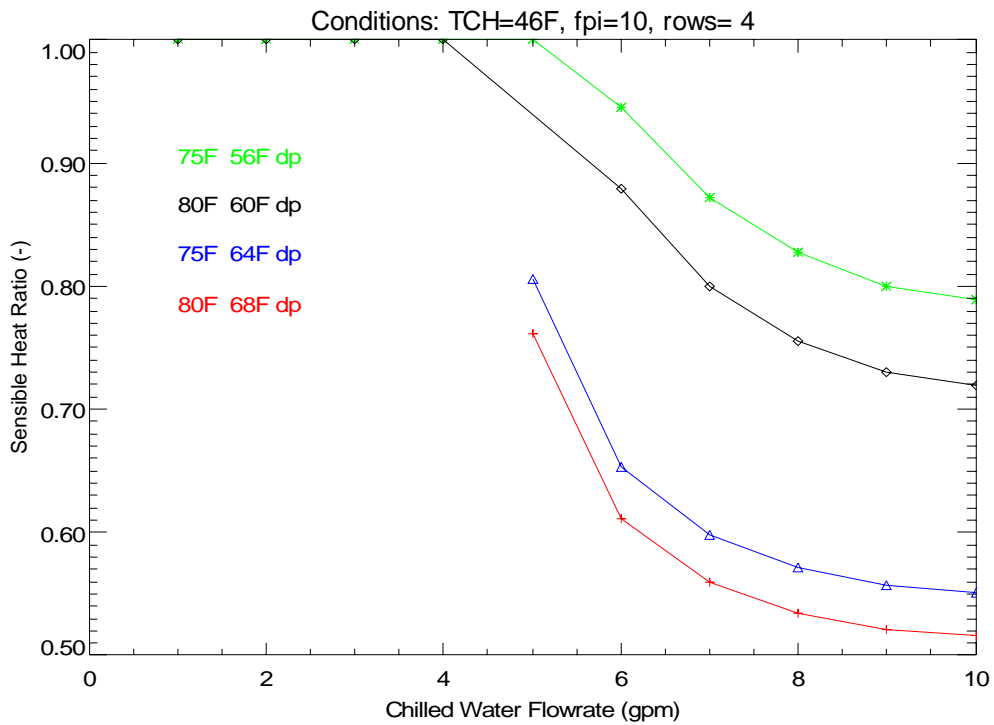


**Figure 5-54. Trends of SHR with Chilled Water Flow from CCDET**

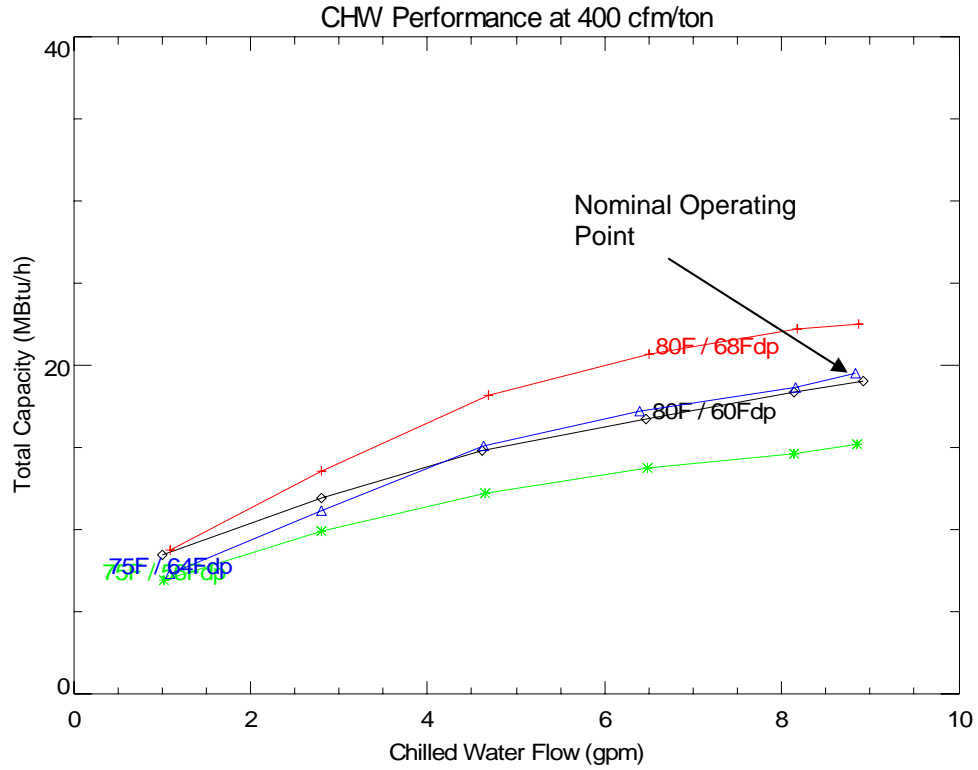


Figure 5-55. Trends of Measured Capacity with Chilled Water Flow, Coil 8

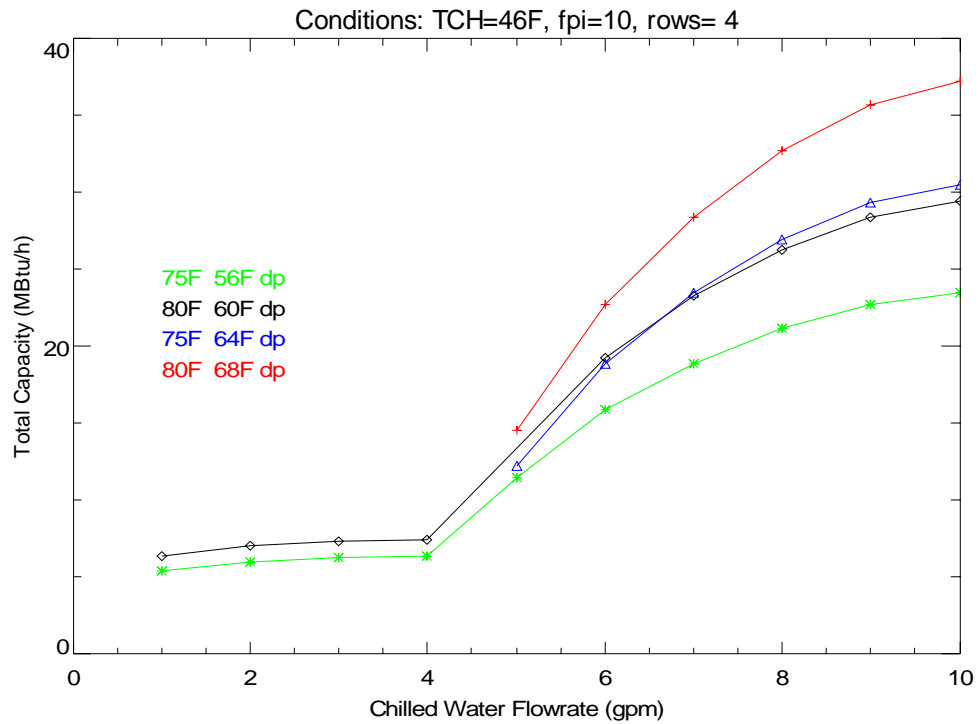


Figure 5-56. Trends of Capacity with Chilled Water Flow from CCDET



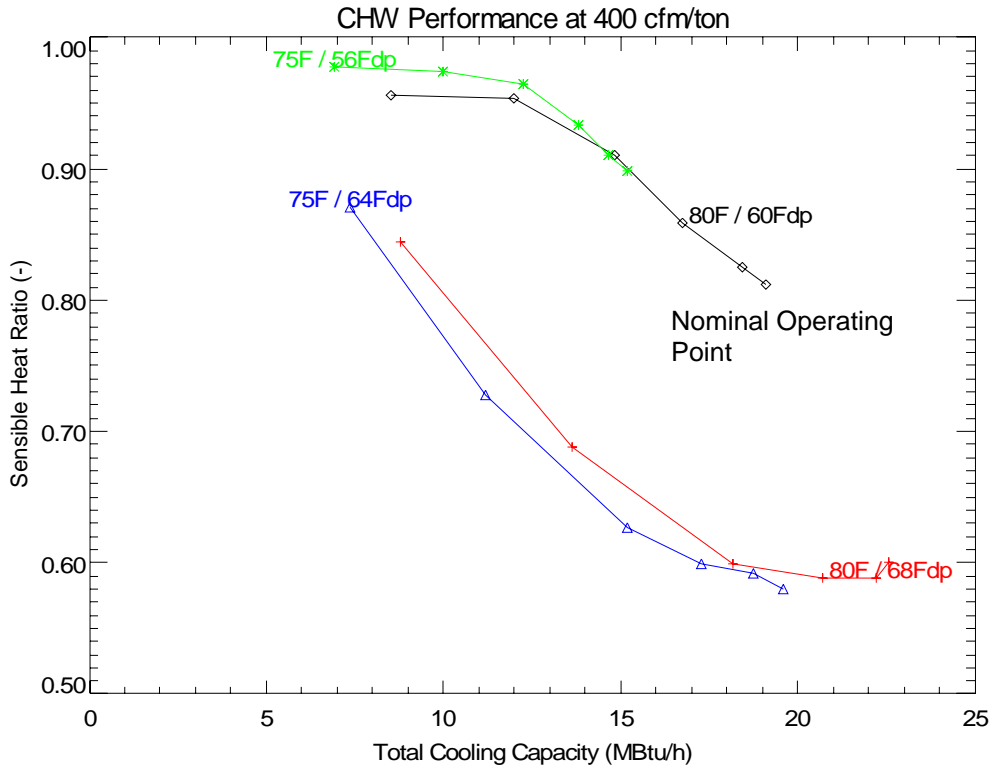


Figure 5-57. Trends of Measured SHR with Cooling Capacity, Coil 8

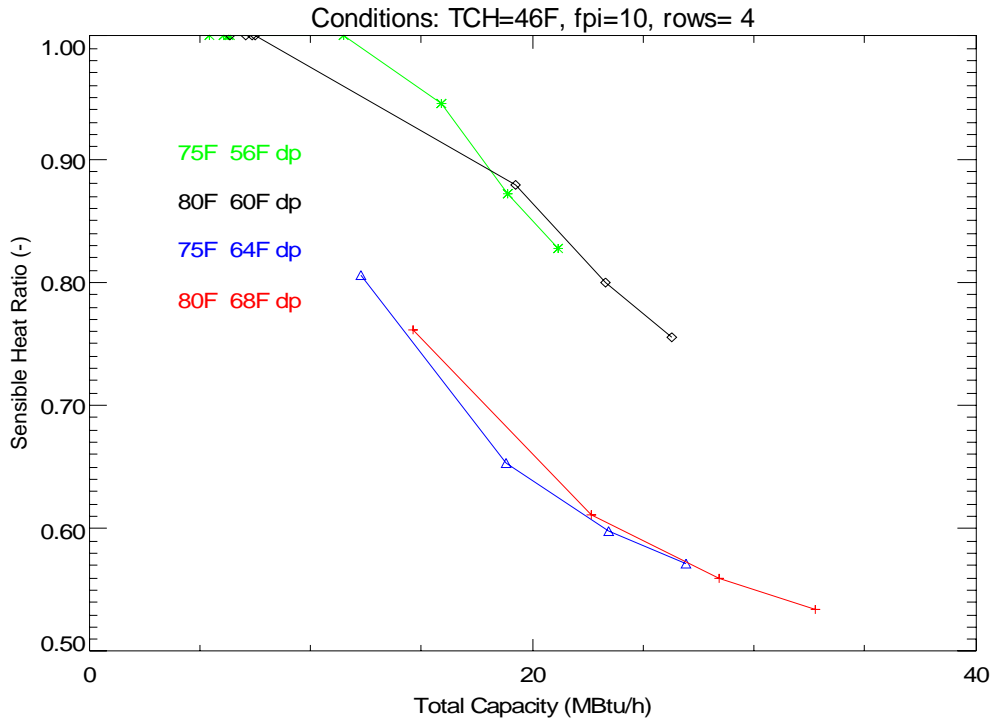


Figure 5-58. Trends of SHR with Cooling Capacity from CCDET

# 6 Summary of Findings

This section summarizes and compares the key findings from laboratory and field testing conducted as part of this project, and also discusses how the results can be applied to design, install and operate cooling systems with better part-load dehumidification performance.

## 6.1 Summary of Laboratory and Field Test Findings

The laboratory data collected as part of this study provided the most definitive and credible results related to the details of coil dehumidification performance as well as how part-load performance can be modeled. The laboratory results were more definitive because instrumentation accuracy and precision were much better and operating conditions were more carefully controlled than at the field test sites. All of the model validation efforts in Section 5 were completed using laboratory data. However, the field data were also able to corroborate many of the laboratory findings. Figure 6-1 below compares the measured moisture retention values from the laboratory and field testing. The laboratory testing found moisture retention values of 8 to 14 lb per thousand square feet of gross fin surface area<sup>6</sup>. The majority of the lab-tested coils were closer to 8 lbs per thousand square feet. The moisture-holding capacity of the coils at the field test sites are determined by various means that were often less accurate. However, the resulting moisture retention rates were still close to the laboratory-determined values.

Another fundamental measure of coil performance is the constant  $k$  that is related to the NTU associated with the performance of the coil as an evaporative cooler during the off cycle (see Sections 3.4 and 5.2). Figure 6-2 compares the  $k$  factor values determined from laboratory and field testing. The  $k$  factor should, in theory, depend on the thermo-physical properties of air and water near 40-60°F, as well as the properties related to surface tension of water on the fin material. Since the coils all use similar fin materials and operate at similar temperatures, the calculated  $k$  factors were very similar for all lab-tested coils, ranging from 0.024 to 0.043. Attempts to determine the  $k$  factor from some field test sites resulted in  $k$  factors of similar order, but with significant variations. The differences between the field and lab tests in this case primarily resulted from the inability to find periods with consistent and meaningful operating conditions in the field. For instance, the two-stage cooling unit at field site 2 typically cycled from 1<sup>st</sup> stage to off (instead of from 2nd stage to off). Therefore, the coil was not fully wetted at the beginning of the off cycle and the measured evaporation rate was lower than would have been expected at laboratory test conditions.

---

<sup>6</sup> Gross fin surface area is based on simple fin area calculations and ignores the area corrections associated with tube voids and fin collars, as described in Section 3.

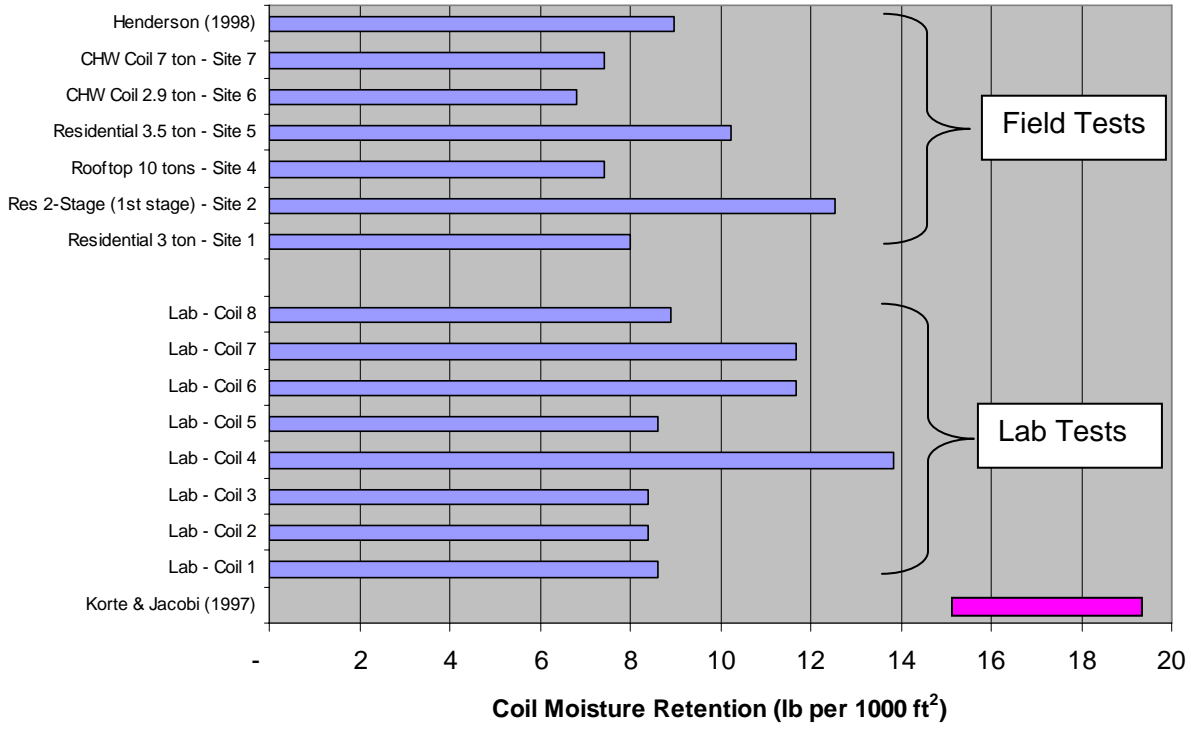


**Figure 6-1. Comparing Measured Coil Moisture Retention from Field and Laboratory Measurements**

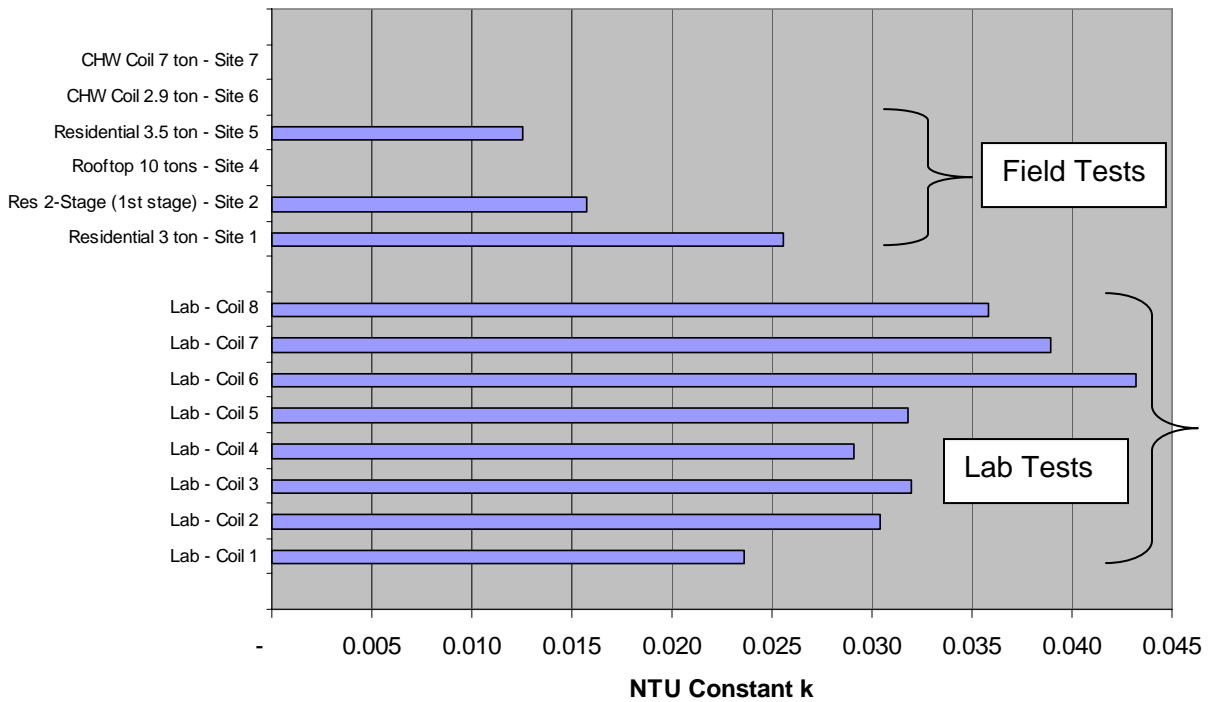


**Figure 6-2. Comparing NTU K-Factor from Field and Laboratory Measurements**

While the field data yielded less accurate measurements of coil performance details, it did provide realistic feedback on the net impacts of latent degradation in real buildings. The field testing from site 1 and other sites demonstrated that latent degradation was also a significant issue with the AUTO fan mode (supply air fan cycles on/off in tandem with the cooling coil). Since AUTO fan degradation strongly depends on the magnitude of off-cycle airflows, the coil and duct arrangements of a given system appear to have a significant impact on the rate of latent degradation.

For many of the field sites, we were able to determine the necessary model parameters to develop a part-load curve to predict latent degradation for the cooling unit (see Section 4). In all cases the latent degradation model was shown to match the measured latent degradation trend. This confirmation of the latent degradation model with field data provided further confidence that the model is valid for a wide range of operating conditions and coil configurations.

Field test data also demonstrated the impact of latent degradation on space humidity levels in a building. We were also able to evaluate the net impacts of enhanced control approaches that have been developed by several equipment manufacturers. At several sites, tests were run with the various enhanced control features both enabled and disabled. These different control periods were compared at similar outdoor humidity conditions to discern the impact of the control change on indoor humidity. Generally we found no observable impact of these enhanced control modes on space humidity levels. The only control change observed to significantly impact space humidity levels was the difference between the AUTO and continuous fan modes. The results from the laboratory testing and the model development efforts have generally corroborated the performance trends we have observed in the field.

## ***6.2 Best Practices to Mitigate Latent Capacity Degradation***

### **6.2.1 The Importance of Proper Equipment Sizing**

The field and laboratory results presented in this report clearly indicate the importance of equipment sizing. Single-stage cooling units that operate at less than 50% of full load with continuous fan operation were typically shown to provide no latent capacity. Similarly, single-circuit DX systems with modulating compressors and chilled water coils lose most of their dehumidification capacity below 50-60% loading.

Clearly, engineers and designers can mitigate the negative impact of latent degradation by ensuring equipment is not significantly oversized compared to the expected cooling loads in a building application. Oversizing AC equipment increases the amount of time spent at part load and results in higher space humidity levels. Carefully sizing equipment to match the cooling load requirements results in better humidity control and higher system efficiency since part-load losses are minimized. These impacts can be quantified by using the latent degradation models developed in this report with building simulation tools such as EnergyPlus.

## 6.2.2 The Importance of Capacity Staging and Coil Circuiting

Multiple stages of cooling capacity can greatly mitigate the impact of latent degradation at part load. Field measurements for a 10-ton [35 kW] packaged rooftop in a retail application (field test site 4) showed that having two stages of cooling capacity (with face split coil) significantly reduced the impact of latent degradation. The SHR of the cooling coil was maintained near the full-load level even at 1<sup>st</sup> stage operation because the cooling coil was face split (i.e., compressor 1 serving the bottom half of the coil). In this application, the system spent many hours with the first stage operating continuously. As a result, humidity control was reasonably maintained in this commercial application even with continuous supply fan operation. In contrast, a single-stage rooftop would have resulted in extremely poor space humidity control in this application since the compressor would have operated for all but a few hours of the year at less than a 50% runtime fraction.

A multi-stage cooling unit with a row-split coil (i.e., compressor 1 serving the entering rows of the cooling coil) or an intertwined coil (i.e., compressor 1 effectively serving the entire coil area) would have resulted in less latent capacity at part load and in poorer humidity control. While these coil circuiting arrangements can result in improved part-load efficiency, they clearly result in poorer dehumidification performance at part load.

## 6.2.3 The Importance of Coil Temperature Control

Cooling systems provide good part-load dehumidification when the coil is always maintained at cold conditions (i.e., below the dewpoint temperature of the entering air). The residential two-stage unit at field test site 2 reduced the supply airflow for first stage of cooling capacity, though the coil suction temperature actually increased slightly at this condition. Better dehumidification performance would have been realized if the airflow rate had been slightly less than 50% flow at 50% capacity. Manufacturers have considerable flexibility with variable-speed supply blowers available for residential equipment. Strategies that persistently maintain lower airflows and supply air temperatures for low stage can improve latent performance. While many manufacturers reduce airflows for a few minutes at the beginning of an operating cycle, the long operating cycles typical of low-stage operation reduce the efficacy of this approach. Equipment manufacturers may be concerned that consistently lower airflow rates will lead to coil freeze up or duct sweating. One possible answer may be to use simple refrigerant line temperature switches to sense when the risk of freezeup or sweating is high.

Modulated chilled water coils in large commercial systems also experience latent degradation at part-load conditions. Field testing of a constant-air-volume chilled water coil in a Florida commercial building (field test site 6) confirmed the expected drop in latent capacity as the water flow rate through the chilled water coil modulates to match the load requirements while the air flow rate remains at the design value. In constant-air-volume applications where improved humidity control is important, designers should consider controlling cooling capacity by bypassing air around the coil. The air bypass method clearly provides better humidity control at part load compared to systems that modulate capacity by varying the chilled water flow rate.

Chilled water coils in variable air volume (VAV) systems (field test site 7) typically provide good dehumidification at part-load conditions since they are consistently controlled to a cold discharge air temperature. Chilled water temperature reset strategies, which are often implemented in VAV systems to improve energy efficiency, eliminate or reduce this natural advantage that VAV systems provide.

#### **6.2.4 The Impact of Off-Cycle Moisture Evaporation from the Cooling Coil**

Operation in the AUTO fan mode, with the fan cycling on and off with the compressor, nearly always improves the dehumidification performance of a cooling system. However, continuous fan operation is often required to provide ventilation, filtration, uniform mixing of the space, and/or constant sound levels.

Strategies to minimize moisture evaporation from the coil during the off cycle improve dehumidification performance. Off-cycle evaporation from the coil can be reduced by:

- turning off the fan for all or part of the off cycle,
- using lower supply airflow rates during the off cycle,
- bypassing air around the coil during the off cycle.

All of these strategies can improve dehumidification performance. The models developed and presented in Section 5 can be used to quantify the impacts of these strategies.

Many equipment manufacturers use fan delay strategies ostensibly to extract additional cooling from a coil at the end of an operating cycle. These strategies are used in residential applications where AUTO fan control is the norm. While this strategy may (or may not) slightly improve the energy efficiency of a system, our findings demonstrate that it clearly degrades the latent removal capacity of a system. Measured data showed a 44% reduction in net condensate removal at a runtime fraction of 20% with only a 90-second fan delay. The measured increase in gross cooling efficiency with the fan delay was about 1%. Fan delay strategies have a significant negative impact on dehumidification capacity and should be avoided in any application where high humidity is a concern.

# 7 Conclusions and Recommendations

## 7.1 Conclusions

The latent capacity of a cooling coil degrades at part-load conditions. This degradation is most significant when the supply air fan operates continuously with a single-stage cooling coil. However, some degradation also occurs with modulated and multi-stage cooling systems as well. Continuous supply air fan operation is used in nearly all commercial buildings to provide the outdoor air ventilation requirements prescribed by ANSI/ASHRAE Standard 62.1 (ASHRAE 2004a) and to provide air circulation for occupant comfort. Continuous fan operation is also becoming more prevalent for residential applications for a variety of reasons, including central air filtration (e.g., UV<sub>C</sub> lamps or high-efficiency air filters) and new recommendations for whole-building ventilation with outdoor air (ASHRAE 2004b). The impact of latent capacity degradation must be considered in these circumstances.

The results from this research project confirm and quantify the impact equipment oversizing has on humidity control. Whether operating with continuous fan operation, as is common in commercial applications, or in the AUTO fan mode, as most residential systems do, dehumidification performance degrades at part-load conditions. Oversizing air-conditioning equipment increases the time spent at part load and results in higher space humidity levels. Carefully sizing equipment to match the cooling load requirements results in better humidity control and higher system efficiency since part-load losses are minimized.

Modulated chilled water coils also experience latent degradation at part-load conditions. Field testing of a constant air volume chilled water coil in a Florida commercial building confirmed the expected drop in latent capacity as the water flow rate through the chilled water coil modulates to match the sensible cooling load requirements. In constant air volume applications where improved humidity control is important, designers should consider controlling cooling capacity by bypassing air around the coil. The air bypass method clearly provides better humidity control at part load compared to systems that modulate capacity by varying the chilled water flow rate. Variable air volume systems also provide good dehumidification when controlled to an appropriate discharge air temperature.

AUTO fan control, where the supply air fan cycles on and off with the cooling coil, nearly always improves the dehumidification performance of a cooling system. However, continuous fan operation is often required as noted above. Strategies are available to minimize moisture evaporation during the coil off cycle and improve dehumidification performance. These strategies include turning off the fan for all or part of the coil off cycle, using lower supply airflow rates during the coil off cycle, and/or bypassing air around the coil during the off cycle. The improved latent degradation model developed as part of this project can be used to quantify the impacts of these strategies on dehumidification performance. The latent degradation model can also be incorporated into dynamic building energy simulation programs (e.g., DOE's EnergyPlus program), providing a tool for evaluating the implications of equipment design and operating strategies on indoor humidity levels during part-load operation.

Multiple stages of cooling capacity can greatly mitigate the impact of latent degradation at part load. For example, field measurements of a 10-ton (35kW) rooftop packaged unit showed that having two stages of cooling capacity significantly reduced the impact of latent degradation even with continuous supply air fan operation. This two-stage cooling system had a single cooling coil with two independent refrigerant circuits and a single compressor for each circuit. The cooling coil was configured in the face-split arrangement, with the bottom half of the coil served by compressor 1 (1<sup>st</sup> stage cooling) and the top half of the coil served by compressor 2 (2<sup>nd</sup> stage of cooling). This combination of multiple cooling stages and coil circuiting yielded good part-load dehumidification performance.

Smaller residential equipment can also benefit from multiple stages of cooling capacity. For these systems, the cooling coil is typically composed of a single refrigerant circuit. Therefore, the key to good part-load dehumidification performance for this type of system is to properly vary the supply air fan speed with cooling capacity to maintain cold coil temperatures at each stage of cooling. Air flow will likely need to be reduced in greater proportion than total cooling capacity to keep coil temperatures low at part load (e.g., 50% reduction in total cooling capacity may require a 55-60% reduction in airflow rate).

Many equipment manufacturers use fan delay strategies to extract additional cooling from a coil at the end of a cooling cycle. These strategies are used in residential applications where AUTO fan control is the norm. While this strategy may (or may not) slightly improve the energy efficiency of a system, our findings demonstrate that it clearly degrades the latent removal capacity of a system. Fan delay strategies have a significant negative impact on dehumidification capacity and should be avoided in any application where high humidity is a concern. Equipment manufacturers almost always provide a means to disable this fan delay strategy (described in the installation documents).

Residential equipment with variable-speed supply air fans are being offered by several equipment manufacturers. In addition to reduced fan energy consumption, these supply air fans give manufacturers the flexibility to vary fan speed to improve performance under various operating conditions. Several equipment manufacturers have implemented supply fan control schemes intended to limit latent capacity degradation or enhance steady-state dehumidification. These schemes include a combination of reduced air flow rate at the beginning of the cooling cycle, and sometimes also include a fan delay (i.e., continued fan operation for a brief period after the compressor turns off). Field measurements collected during this project for two such systems indicated little-to-no reduction in indoor humidity levels with these “enhanced dehumidification” control strategies compared to conventional AUTO fan control. Fan delay (overrun) is included as part of this control scheme by some manufacturers, and this aspect of the control should be eliminated since project results clearly indicate that this degrades dehumidification performance.

Some manufacturers are also providing supply air fan controls where fan operation is stopped for a fixed interval right after the cooling coils ends, with fan operation restarted after the fixed interval. This type of fan delay is often called a “drain-down cycle” because of the misguided belief that water drains from the coil when the fan is off for a few minutes. Project results



indicate that reasonable fan drain-down periods of 2 to 5 minutes yield only modest improvement in part-load dehumidification performance compared to continuous fan operation.

## **7.2 Recommendations for Further Work**

The results from this project and previous research have led to a good understanding of the dehumidification (latent cooling) performance of single-stage DX cooling coils at part-load conditions. An existing engineering model to predict latent capacity degradation at part load was enhanced as part of this project to include a broader range of fan control strategies and an improved theoretical basis for modeling off-cycle moisture evaporation from the cooling coil. The improved model was validated with laboratory measurements, and this project has yielded better guidance for users regarding proper inputs for the model.

The majority of laboratory and field tests to date regarding part-load dehumidification performance of cooling coils have focused on single-stage DX cooling equipment, which is typically used in residential and light commercial applications. As part of this project, testing was expanded to include one two-stage rooftop packaged unit (field site) and three chilled water coils (two field sites and one lab test coil). While this expansion has provided better insight into the part-load dehumidification performance of these commercial systems, further study is clearly warranted for these equipment types. Two-stage DX rooftop packaged units are used extensively in commercial and institutional applications, making this equipment a particularly high priority for future work. The improved latent degradation model developed as part of this project may be able to properly model part-load latent performance for 2-stage constant air volume DX equipment, but additional laboratory and field testing is needed to validate the model predictions and to provide users with guidance for model inputs specific to this type of equipment.

Another recommendation is to implement the improved latent degradation model in various analysis tools, including DOE's state-of-the-art EnergyPlus™ building energy simulation program. The original latent degradation model by Henderson and Rengarajan (1996) was implemented in EnergyPlus in 2003 by the Florida Solar Energy Center (FSEC). Therefore, the improved model developed as part of this project should be relatively easy to incorporate in EnergyPlus. In addition, the guidance developed during this project for selecting proper model inputs should be included as part of the EnergyPlus user documentation. FSEC is part of DOE's EnergyPlus development team, and updating EnergyPlus with this latest latent degradation model will be proposed to the DOE Analysis Tools Technology Development Manager for consideration in FY2007.

Once EnergyPlus has been updated with the improved latent degradation model, the next important step would be to use EnergyPlus to demonstrate the ramifications of fan controls on indoor humidity levels and energy consumption. A series of simulations should be completed to demonstrate both good and bad practices so building professionals and owners/operators better understand the impacts of different fan control strategies. In many cases building designers and owner/operators are unable to perform part-load analyses, or don't realize the importance of doing so. Publications containing these simulation results will raise overall awareness of this critical aspect of system performance, and provide some general guidance on "do's and don'ts"

regarding fan controls. With the benefit of this guidance, part-load analysis for a specific application can be more focused on viable solutions.

Another important follow up to this project would be to partner with HVAC equipment manufacturers to develop equipment designs and control algorithms that mitigate the impacts of part-load latent degradation, and/or improve the overall dehumidification performance of systems for applications where it is required. A critical first step would be to conduct a thorough market evaluation. For example EnergyPlus, with the updated latent degradation model, could be used as part of an extensive simulation study to determine the impact of part-load latent degradation on indoor humidity levels and energy use for a variety of commercial and residential applications across a range of geographic locations. Prototypical buildings can be modeled with conventional HVAC systems as well as systems that use enhanced control techniques and/or other system improvements to increase dehumidification performance. The results of the market evaluation would clearly identify which HVAC markets have the greatest issue with high humidity control, and the extent to which commercially-available enhanced control techniques can improve indoor humidity control and occupant comfort. HVAC equipment designers will benefit by better understanding the limitations and benefits of technologies and control strategies already available in the marketplace, and the results will identify markets for equipment manufacturers where further humidity enhancements are required.

Following the market evaluation, it is important to assist industry partners in evaluating and incorporating new enhanced dehumidification strategies in their products. This project identified several control strategies that are currently used to enhance dehumidification, and field test results showed that some strategies were more effective than others. One way to assist industry partners would be to work with them to systematically assess the efficacy of various control strategies using laboratory testing and computer simulations. Laboratory tests could be performed to determine the impact of various control scenarios on coil dehumidification performance, and the updated latent-degradation engineering model resulting from this project could be used to assess the impact of the control strategies on indoor humidity levels in various building applications. Depending on the laboratory test results, this may require further updates or enhancements to the latent-degradation engineering model. Any model improvements could be incorporated into EnergyPlus, and ultimately make their way into the wide array of mainstream energy analysis and load sizing software tools that will be used by hundreds of engineers and designers throughout the industry.

## 8 References

ARI. 2005. ARI Standard 210/240, 2005 Standard for Unitary Air-Conditioning and Air-Source Heat Pump Equipment. Arlington, VA.: Air-Conditioning and Refrigeration Institute.

<http://www.ari.org/std/standards.html>

ASHRAE. 1988. ANSI/ASHRAE Standard 37-1988, Methods of Testing for Rating Unitary Air-Conditioning and Heat Pump Equipment. Atlanta, GA: American Society of Heating, Refrigerating, and Air-Conditioning Engineers, Inc.

ASHRAE. 2004a. ANSI/ASHRAE Standard 62.1-2004, Ventilation for Acceptable Indoor Air Quality. Atlanta, GA: American Society of Heating, Refrigerating, and Air-Conditioning Engineers, Inc.

ASHRAE. 2004b. ANSI/ASHRAE Standard 62.2-2004, Ventilation and Acceptable Indoor Air Quality in Low-Rise Residential Buildings. Atlanta, GA: American Society of Heating, Refrigerating, and Air-Conditioning Engineers, Inc.

Brandemuehl, M. 1993. HVAC2 Toolkit: Algorithms and Subroutines for Secondary HVAC Systems Energy Calculations. Atlanta, GA: American Society of Heating, Refrigerating, and Air-Conditioning Engineers, Inc.

Braun, J.E., "Methodologies for the Design and Control of Chilled Water Systems," Ph. D. Thesis, University of Wisconsin - Madison, 1988.

EnergyPlus Development Team. 2005. EnergyPlus Engineering Reference, Version 1.2.3, 13 December 2005. Washington, DC: U. S. Department of Energy.

<http://www.energyplus.gov/pdfs/engineeringreference.pdf>

Federal Register 2005. 10 CFR Part 430. Energy Conservation Program for Consumer Products: Test Procedure for Residential Central Air Conditioners and Heat Pumps; Final Rule. Vol. 70, No. 195, October 11, 2005.

<http://a257.g.akamaitech.net/7/257/2422/01jan20051800/edocket.access.gpo.gov/2005/pdf/05-15601.pdf>

Henderson, H.I. 1990. An Experimental Investigation of the Effects of Wet and Dry Coil Conditions on Cyclic Performance in the SEER Procedure, Proceedings of USNC/IIR Refrigeration Conference at Purdue University, July 1990, West Lafayette, IN.

Henderson, H.I., K. Rengarajan, D.S. Shirey. 1992. The Impact of Comfort Control on Air Conditioner Energy Use in Humid Climates. ASHRAE Transactions Vol. 98 Part 2, June 1992.

Henderson, H.I., Jr., and K. Rengarajan. 1996. A Model to Predict the Latent Capacity of Air Conditioners and Heat Pumps at Part-Load Conditions with Constant Fan Operation. ASHRAE Transactions, Vol. 102, Part 1, pp. 266-274.

- Henderson, H.I., Jr. 1998. The Impact of Part-Load Air-Conditioner Operation on Dehumidification Performance: Validating a Latent Capacity Degradation Model. Proceedings of ASHRAE IAQ and Energy 98, pp. 115-122.
- Hong, K., and R. Webb. 2001. Wetting Coatings for Dehumidifying Heat Exchangers. ASHRAE Transactions, Vol. 107, Part 1.
- Katipamula, S., and D.L. O'Neal. 1991. Transient Dehumidification Characteristics of a Heat Pump in Cooling Mode. ASME Transactions, Vol. 113, November, pp. 264-271.
- Kelly, G.E. and W.H. Parken. 1978. Method of testing, rating and estimating the seasonal performance of central air conditioners and heat pumps operating in the cooling mode. NBSIR 77-1271, Report by National Bureau of Standards. April.
- Khattar, M.K., N. Ramanan, and M. Swami. 1985. Fan Cycling Effects on Air Conditioner Moisture Removal Performance in Warm, Humid Climates. FSEC-PF-75-85. Cape Canaveral: Florida Solar Energy Center.
- Khattar, M.K., M.V. Swami, and N. Ramanan. 1987. Another Aspect of Duty Cycling: Effects on Indoor Humidity. ASHRAE Transactions, Vol. 93, Part 1, pp. 1678-1687.
- Kim, G. J., and A.M. Jacobi. 2000. Condensate Accumulation Effects on the Air-Side Thermal Performance of Slit-Fin Surfaces. ACRC CR-26. Air Conditioning and Refrigeration Center, Urbana, IL.
- Korte, C.M., and A.M. Jacobi. 1997. Condensate Retention and Shedding Effects on Air-Side Heat Exchanger Performance. ACRC TR-132, Air Conditioning and Refrigeration Center, Urbana, IL.
- NEMA. 1990. Residential controls – Electric wall-mounted room thermostats. NEMA Standards Publication No. DC 3. Rosslyn, VA: National Electrical Manufacturers Association.
- Shen, B., J. Braun, and E. Groll. 2004. Steady State Cyclic Performance Testing of Packaged R-410A Units. Final Report. Baseline test report prepared by Purdue University for Southern California Edison Co. November. <http://www.hdac-des-pier.com/index.html>
- Stabat, P., D. Marchio, and M. Orphelin. 2001. Pre-Design and Design Tools for Evaporative Cooling. ASHRAE Transactions, Vol. 107, Part 1, pp. 501-510.
- Yamazaki, E., T. Uehara, and C. Yoshida. 2000. Development of Heat Exchangers with Non-Chromate High Corrosion Resistance Treatment. SAE 2000 World Congress, 2000-01-0572.
- Yin, J., and A.M. Jacobi. 2000. Condensate Retention Effects on the Air-Side Heat Transfer Performance of Plain and Wavy-Louvered Heat Exchangers. ACRC TR-158. Air Conditioning and Refrigeration Center, Urbana, IL.

## **APPENDIX A**

### **Literature Review Bibliography**

**Table A-1. Literature Search Bibliography**

Ref.	Description
1	Shirey, D.B. 1993. Demonstration of Efficient Humidity Control Techniques at an Art Museum. ASHRAE Transactions Vol. 99, Part 1, pp. 694-703.
2	Liu, M., S.Y. Liang, T.N. Wong, and G.K. Nathan. 1997. Performance Study of Finned Tube Evaporators in a Humid Environment. ASME Asia Congress and Exhibition, pp. 1-6.
3	O'Neal, D.L., N. Chan, S. Somasundaram, and S. Katkipamula. 1987. An Evaluation of Steady-State Dehumidification Characteristics of Residential Central Air Conditioners. Final Report. ESL-PA-87/06-01. Energy Systems Laboratory, Texas A&M University.
4	Katipamula, S., D. O'Neal, and S. Somasundaram. 1987. Determination of the Transient Dehumidification Characteristics of High Efficiency Central Air Conditioners. Final Report. ESL-TR-87/07-03. Energy Systems Laboratory, Texas A&M University.
5	Korte, C.M., and A.M. Jacobi. 1997. Condensate Retention and Shedding Effects on Air-Side Heat Exchanger Performance. ACRC TR-132. Air Conditioning and Refrigeration Center, Urbana, IL.
6	Yin, J., and A.M. Jacobi. 2000. Condensate Retention Effects on the Air-Side Heat Transfer Performance of Plain and Wavy-Louvered Heat Exchangers. ACRC TR-158. Air Conditioning and Refrigeration Center, Urbana, IL.
7	Kim, G. J., and A.M. Jacobi. 2000. Condensate Accumulation Effects on the Air-Side Thermal Performance of Slit-Fin Surfaces. ACRC CR-26. Air Conditioning and Refrigeration Center, Urbana, IL.
8	a ARI. 1994. ARI Standard 210/240, 1994 Standard for Unitary Air-Conditioning and Air-Source Heat Pump Equipment. Arlington, VA.: Air-Conditioning and Refrigeration Institute.
	b ARI. 2003. ARI Standard 210/240, 2003 Standard for Unitary Air-Conditioning and Air-Source Heat Pump Equipment. Arlington, VA.: Air-Conditioning and Refrigeration Institute.
9	Van Aken, G. J. 1994. Thermal Modeling of Cooling and Heating Coils. AIRAH Journal, pp. 16-20.
10	P. Oppenheim. 1991. Energy Implications of Blower Overrun Strategies for a Zoned Residential Forced-Air System. ASHRAE Transactions, Vol. 97, Part 2, pp. 354-362.
11	Hong, K., and R. Webb. 2001. Wetting Coatings for Dehumidifying Heat Exchangers. ASHRAE Transactions, Vol. 107, Part 1.
12	Chen, T.D., J.C. Conklin, and V.D. Baxter. 1999. Dehumidification: Prediction of Condensate Flow Rate for Plate-Fin Tube Heat Exchangers Using the Latent j Factor. ORNL/CP-100589. Oak Ridge, TN: Oak Ridge National Laboratory.
13	Katipamula, S., D.L. O'Neal, and S. Somasundaram. 1988. Simulation of Dehumidification Characteristics of Residential Central Air Conditioners. ASHRAE Transactions, Vol. 94, Part 2, pp. 829-849.
14	Mirth, D.R., S. Ramadhyani, and D.C. Hittle. 1993. Thermal Performance of Chilled-Water Cooling Coils Operating at Low Water Velocities. ASHRAE Transactions, Vol. 99, Part 1, pp. 43-53.

15	Mirth, D.R., and S. Ramadhyani. 1995. Performance of Chilled-Water Cooling Coils. ASHRAE HVAC&R Research Journal, Vol. 1, No. 2, pp. 160-172.
16	Bocanegra, L.M., and A.Y. Khan. 1992. Parametric Analysis of Heat and Mass Transfer Performance of a Counterflow, Cooling and Dehumidification Coil. ASME Winter Annual Meeting, Anaheim, CA, 92-WA/HT-1, pp. 1-6.
17	Khan, A. Y. 1994. Heat and Mass Transfer Performance Analysis of Cooling Coils at Part-Load Operating Conditions. ASHRAE Transactions, Vol. 100, Part 1, pp. 54-62.
18	Katipamula, S., and D.L. O'Neal. 1991. Transient Dehumidification Characteristics of a Heat Pump in Cooling Mode. ASME Transactions, Vol. 113, November, pp. 264-271.
19	Krakov, K.I., S. Lin, and Z. Zeng. 1995. Analytical Determination of PID Coefficients For Temperature and Humidity Control During Cooling and Dehumidifying by Compressor and Evaporator Fan Speed Variation. ASHRAE Transactions, Vol. 101, Part 1, pp. 343-354.
20	Krakov, K.I., S. Lin, and Z. Zeng. 1995. Temperature and Humidity Control During Cooling and Dehumidifying by Compressor and Evaporator Fan Speed Variation. ASHRAE Transactions, Vol. 101, Part 1, pp. 292-304.
21	Oskarsson, S.P., K.I. Krakow, and S. Lin. 1990. Evaporator Models for Operation with Dry, Wet, and Frosted Finned Surfaces, Part I: Heat Transfer and Fluid Flow Theory. ASHRAE Transactions, Vol. 96, Part 1, pp. 373-380.
22	Oskarsson, S.P., K.I. Krakow, and S. Lin. 1990. Evaporator Models for Operation with Dry, Wet, and Frosted Finned Surfaces, Part II: Evaporator Models and Verification. ASHRAE Transactions, Vol. 96, Part 1, pp. 381-392.
23	Henderson, H.I., Jr., and K. Rengarajan. 1996. A Model to Predict the Latent Capacity of Air Conditioners and Heat Pumps at Part-Load Conditions with Constant Fan Operation. ASHRAE Transactions, Vol. 102, Part 1, pp. 266-274.
24	Henderson, H.I., Jr. 1998. The Impact of Part-Load Air-Conditioner Operation on Dehumidification Performance: Validating a Latent Capacity Degradation Model. Proceedings of ASHRAE IAQ and Energy 98, pp. 115-122.
25	Miller, J.D. 1984. Development and Validation of a Moisture Mass Balance Model for Predicting Residential Cooling Energy Consumption. ASHRAE Transactions, Vol. 90, Part 2B, pp. 275-293.
26	Khattar, M.K., N. Ramanan, and M. Swami. 1985. Fan Cycling Effects on Air Conditioner Moisture Removal Performance in Warm, Humid Climates. FSEC-PF-75-85. Cape Canaveral: Florida Solar Energy Center.
27	O'Neal, D.L., and S. Katipamula. 1991. Performance Degradation During On-Off Cycling of Single-Speed Air Conditioners and Heat Pumps: Model Development and Analysis. ASHRAE Transactions, Vol. 97, Part 2, pp. 316-323.
28	Katipamula, S., and D.L. O'Neal. 1991. Performance Degradation During On-Off Cycling of Single-Speed Heat Pumps Operating In the Cooling Mode: Experimental Results. ASHRAE Transactions, Vol. 97, Part 2, pp.331-339.
29	Hu, X., L. Zhang, and A.M. Jacobi. 1994. Surface Irregularity Effects of Droplets and Retained Condensate on Local Heat Transfer to Finned Tubes in Cross-Flow. ASHRAE Transactions, Vol. 100, Part 1, pp.375-381.
30	Mehendale, S.S., and A.M. Jacobi. 2000. Evaporative Heat Transfer in Mesoscale Heat Exchangers. ASHRAE Transactions, Vol. 106, Part 1, pp. 446-452.

31	Mirth, D.R., and S. Ramadhyani. 1993. Comparison of Methods of Modeling the Air-Side Heat and Mass Transfer in Chilled-Water Cooling Coils. ASHRAE Transactions, Vol. 99, Part 2, pp. 285-299.
32	Khattar, M.K., M.V. Swami, and N. Ramanan. 1987. Another Aspect of Duty Cycling: Effects on Indoor Humidity. ASHRAE Transactions, Vol. 93, Part 1, pp. 1678-1687.
33	Chen, P.L., H.M. Qin, Y.J. Huang, and H.F. Wu. 1991. A Heat and Mass Transfer Model for Thermal and Hydraulic Calculations of Indirect Evaporative Cooler Performance. ASHRAE Transactions, Vol. 97, Part 2, pp. 852-865.
34	Yamazaki, E., T. Uehara, and C. Yoshida. 2000. Development of Heat Exchangers with Non-Chromate High Corrosion Resistance Treatment. SAE 2000 World Congress, 2000-01-0572.
35	McLaughlin, W., and R. Webb. 2000. Wet Air Side Performance of Louver Fin Automotive Evaporators. SAE 2000 World Congress, 2000-01-0574
36	McLaughlin, W., and R. Webb. 2000. Condensate Drainage and Retention in Louver Fin Automotive Evaporators. SAE 2000 World Congress, 2000-01-0575
37	Stabat, P., D. Marchio, and M. Orphelin. 2001. Pre-Design and Design Tools for Evaporative Cooling. ASHRAE Transactions, Vol. 107, Part 1, pp. 501-510.
38	Liesen, R.J., and C.O. Pedersen. 1991. Development and Demonstration of an Evaporative Cooler Simulation Model for the BLAST Energy Analysis Computer Program. ASHRAE Transactions, Vol. 97, Part 2, pp.866-873.
39	Doty, S. 2001. Applying DX Equipment in Humid Climates. ASHRAE Journal, Vol. 43, No. 3 (March), pp. 30-34.
40	Parker, D.S., J.R. Sherwin, R.A. Raustad, and D.B. Shirey. 1997. Impact of Evaporator Coil Airflow in Residential Air-Conditioning Systems. ASHRAE Transactions, Vol. 103, Part 2, pp.395-405.
41	Katipamula, S. 1989. A Study of the Transient Behavior During Start-up of Residential Heat Pumps. PhD Dissertation, Department of Mechanical Engineering, Office of the Graduate College of Texas A&M University.
42	Murphy, W.E., and V.W. Goldschmidt. 1984. Transient Response of Air Conditioners – A Qualitative Interpretation Through a Sample Case. ASHRAE Transactions, Vol. 90, Part 1B, pp. 997-1008.
43	Bullock, C.E. 1987. Dynamic Loss Reduction with Electric Heat Pumps. HEAT PUMPS: Prospects in Heat Pump Technology and Marketing, IEA Heat Pump Conference, Ch. 11, pp. 143-157.
44	Huang, Y.J. 2001. Algorithms for direct and indirect evaporative cooling. <i>Detailed Design Tools for Low Energy Cooling Technologies</i> , International Energy Agency Annex 28, Subtask 2.b Report.
45	Katipamula, S., D. O’Neal, and S. Somasundaram. 1989. Simulation of Dehumidification Characteristics of High Efficiency Residential Central Air-Conditioners in Hot and Humid Climates. Fifth Annual Symposium on Improving Building Energy Efficiency in Hot and Humid Climates, pp. 220-229.
46	El Sherbini, A.I. and A. M. Jacobi. 2003. Modeling Condensate Drops Retained on the Air-Side of Heat Exchangers. Report TR-209. Air Conditioning and Refrigeration Center, Department of Mechanical and Industrial Engineering, University of Illinois at Urbana-Champaign, February.



## **APPENDIX B**

### **Summary of Katipamula and O'Neal (1991)**

## Transient Dehumidification Characteristics of a Heat Pump in Cooling Mode

Srinivas Katipamula and Dennis L. O'Neal

*Journal of Solar Energy Engineering, Transactions of the ASME*

Volume 113, November 1991, pp 264 – 271

This paper summarizes a literature review and laboratory test results related to transient performance of residential heat pumps when operating in the cooling mode.

The literature review discusses research results from the late 1970s through 1991 that describe the magnitude of transient losses as well as the probable causes. Several studies note that the magnitude of the performance degradation is a function of the percent on-time (i.e., the compressor run time divided by the total cycle time) and the compressor cycling rate (cycles per hour). A field study by Parken et al.<sup>1</sup> found that

$$\frac{\dot{Q}_{ss}^l}{\dot{Q}_{ss}^s} \neq \frac{\dot{Q}_{cyc}^l}{\dot{Q}_{cyc}^s} \quad (1)$$

where the quantities  $\dot{Q}_{ss}^l$  and  $\dot{Q}_{ss}^s$  are the latent and sensible steady-state cooling capacities, and  $\dot{Q}_{cyc}^l$  and  $\dot{Q}_{cyc}^s$  are the latent and sensible cooling done over a complete on-off cycle. This relationship indicates that cycling losses do not affect the latent and sensible performance in the same proportion. However, the authors could not quantify the latent (dehumidification) performance in the field since they were only measuring the dry-bulb temperature change across the cooling coil.

The authors draw a number of conclusions from their literature review:

- 1) The losses due to transient effects can be as much as 20 percent.
- 2) It takes 6-15 minutes to achieve steady state performance after compressor start-up.
- 3) The transient response is affected by the number of on-off cycles and percent on-time during each on-off cycle.
- 4) The mass of the heat exchangers (indoor and outdoor coils) affects transient losses.
- 5) The off-cycle migration of refrigerant from the condenser to the evaporator causes significant losses in capacity.
- 6) The relationship between cooling load factor (CLF) and part-load factor (PLF) is nonlinear.
- 7) Compressor power is relatively unaffected due to part-load operation.
- 8) The transient performance is independent of outdoor temperature.

The authors note that much of the research on heat pump transient losses has been confined to the heating mode of operation. For the cooling mode, the research has focused on quantifying the effects of heat exchanger mass, off-cycle phenomena on the transient sensible capacity, and effects of cycling (percent on-time and cycling rate) on the cooling performance of the unit. The authors indicate that transient dehumidification performance has not been addressed thus far.

The paper notes that a number of variables affect the transient performance of residential heat pumps: (i) percent on-time of the compressor, (ii) thermostat cycling rate, (iii) indoor dry-bulb temperature, (iv) outdoor dry-bulb temperature, and (v) indoor relative humidity. The authors devised a series of laboratory tests to characterize the transient dehumidification response of a nominal 3-ton (10.6 kW) heat pump by varying percent on-time, thermostat cycling rate, indoor dry-bulb temperature and indoor humidity while keeping outdoor dry-bulb temperature and air flow rates constant. The physical characteristics of the heat pump are described in Table B-1.

---

<sup>1</sup> Parken, W.H., Didion, D.A., Wojuechowski, P.H., and Chein, L., 1985, "Field Performance of Three Residential Heat Pumps in the Cooling Mode," NBSIR 85-3107, NBS, Washington, D.C.

**Table B-1. Characteristics of the 3-ton (10.6 kW) Air-to-Air Heat Pump Test Unit**

Characteristic	Outdoor Coil	Indoor Coil
shape	horse shoe, vertical	vertical
number of rows	two rows, four circuits	four rows, four circuits
refrigerant tubing	3/8" (0.95 cm) diameter copper	3/8" (0.95 cm) diameter copper
fin spacing	20 fins/inch (7.9 fins/cm)	12 fins/inch (4.7 fins/cm)
fin type	Wavy	wavy
ref. tubing passes	30	17
coil face area	17.5 ft <sup>2</sup> (1.62 m <sup>2</sup> )	3.75 ft <sup>2</sup> (0.35 m <sup>2</sup> )
rated flow	1900 cfm (53.8 m <sup>3</sup> /min)	1250 cfm (35.4 m <sup>3</sup> /min)

Note: Katipamula<sup>2</sup> indicates the expansion device is a bleed-type TXV

The heat pump was instrumented to measure numerous air-side and refrigerant-side performance parameters. During the transient tests, the data were collected at a scan rate of 7 seconds at compressor start-up and the scan rate was gradually increased to 30 seconds after five minutes of compressor operation.

The heat pump was first tested under both steady-state and cycling conditions as recommended by the Department of Energy (DOE)<sup>3</sup> – tests A through D. For all tests, the air flow rate across the indoor coil remained constant at 1,200 cfm (34 m<sup>3</sup>/min). For the steady-state test, the air entered the cooling coil at a dry-bulb temperature of 80°F (26.7°C) and 50% relative humidity and the air entered the outdoor coil at 95°F (35°C). For the cycling tests, the cooling coil entering dry-bulb temperature was varied between 72°F (22.2°C) and 80°F (26.7°C) and the humidity was varied between 20 and 67% RH. The percent on-time of the compressor and supply air fan was varied at three discrete levels for the cycling tests: 20, 50 and 80 percent over a broad range of cycling rates (0.8 to 10 cycles per hour).

Figure B-1 shows the normalized capacity of the system (integrated actual cooling delivered divided by the steady-state capacity) at various cycling rates and percent on-times. At high percent on-times and relatively low cycle rates, the cycling losses were quite low resulting in normalized capacities above 0.9. The cycling losses increase as percent on-time decreases and also as the cycling rate increases. Note that the degradation in normalized latent capacity is always greater than for the normalized sensible capacity.

Figures B-2 and B-3 show the moisture removal response of the system at various inlet air humidity conditions for two different percent on-times (80% and 20%). It is noted that the moisture removal is negative for the first 60 to 90 seconds after compressor and fan operation begin. This is due to the moisture left on the coil from the previous compressor cycle. When compressor and supply air fan operation begin, the coil temperature is above the dew point temperature of the air, and moisture left on the coil from the previous compressor cycle begins to evaporate back into the supply air stream. While this trend is similar for the 80% and 20% on-time cases, the moisture removal rate becomes positive earlier with the lower percent on-time. The authors attribute this to the low on-time (7 minutes) for the 20% on-time case which did not allow the system to reach steady state operation; hence, the moisture accumulation on the coil was less for the 20% on-time case (7 minutes of compressor/fan operation) versus the 80% on-time case (27 minutes of compressor/fan operation). Although not stated in the paper, 7 minutes of compressor operation at 20% on-time and 27 minutes at 80% on-time yields a cycling rate of about 1.75 cycles per hour and a maximum cycling rate of about 2.73 cycles per hour (at 50% on-time) when the following thermostat cycling equations are used:

<sup>2</sup> Katipamula, S. 1989. A study of the transient behavior during start-up of residential heat pumps. PhD Dissertation, Department of Mechanical Engineering, Office of the Graduate College of Texas A&M University.

<sup>3</sup> ARI Standard 210/240, "Standard for Unitary Air-Conditioning and Air-Source Heat Pump Equipment", Air-Conditioning and Refrigeration Institute, Arlington, VA.

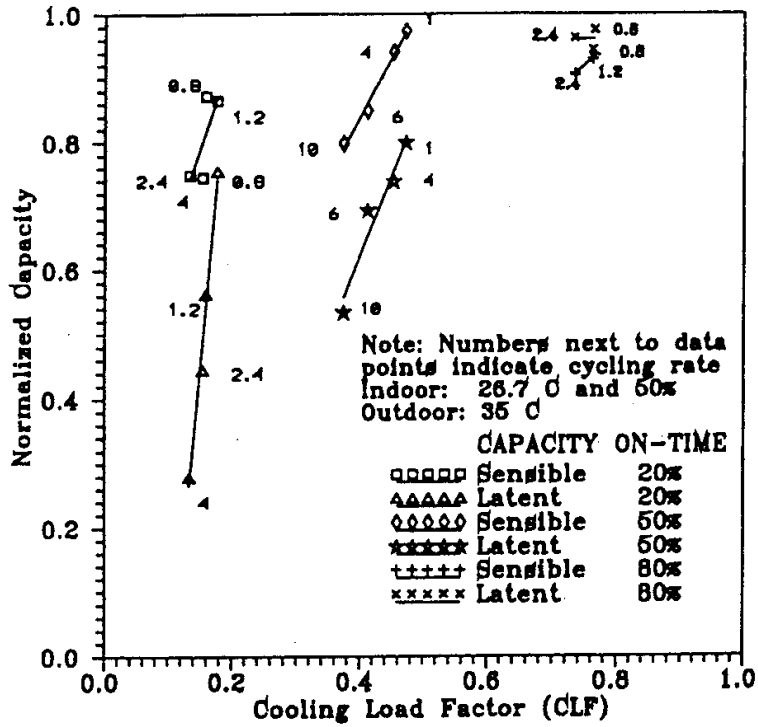


Figure B-1. Normalized sensible and latent capacities at various cycling rates and percent on-times

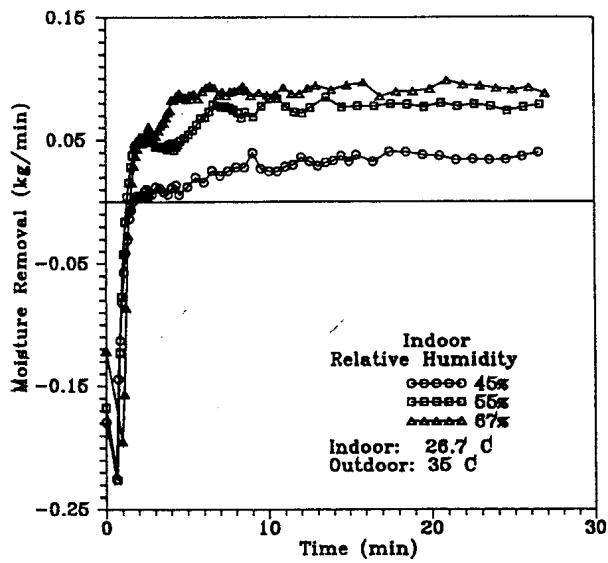


Figure B-2. Moisture removal at various inlet air relative humidities (80% on-time)

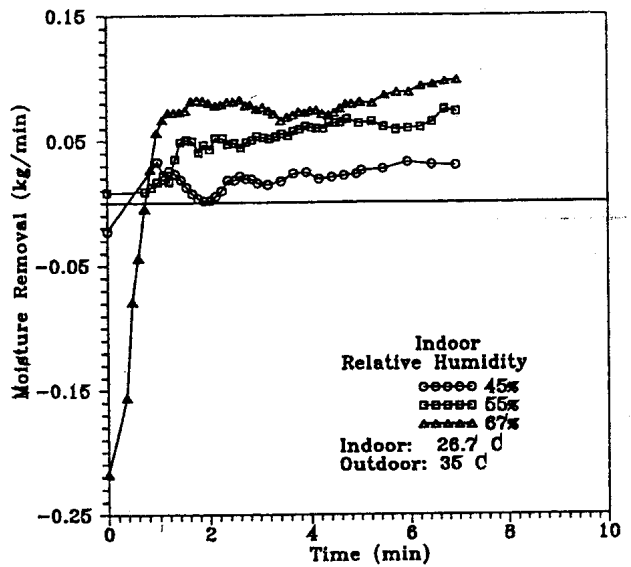


Figure B-3. Moisture removal at various inlet air relative humidities (20% on-time)

$$N_{\max} = \frac{1}{4t_{on}(1-X)} \quad (2)$$

$$N = 4N_{\max}X(1-X) \quad (3)$$

where

- $N_{\max}$  = maximum cycling rate (at on-time of 50%)
- $N$  = actual cycling rate
- $t_{on}$  = compressor on-time
- $X$  = percent on-time, ratio of the time AC is ON to the time for a complete ON & OFF cycle

Figures B-4 and B-5 show the normalized latent and sensible capacities at various inlet air relative humidity levels and system on-times. The normalized capacities increase linearly with an increase in inlet air relative humidity (at a constant inlet air dry-bulb temperature) for a given percent on-time. The solid lines shown in the figures represent the best linear curve fit through the data points. Note that the slope of the lines increases as percent on-time decreases. The trends for normalized latent (Figure B-4) and sensible (Figure B-5) capacities are similar, but the slopes of the lines for normalized sensible capacity are smaller than those for latent. Thus, system cycling degrades the net delivered latent capacity more than the net sensible capacity for any set of operating conditions, and the difference increases with lower system on-times and lower inlet air relative humidity (at a constant inlet air dry-bulb temperature). Unfortunately, the authors do not provide the actual cycling rates or the maximum cycling rate for the data shown in Figures B-4 and B-5.

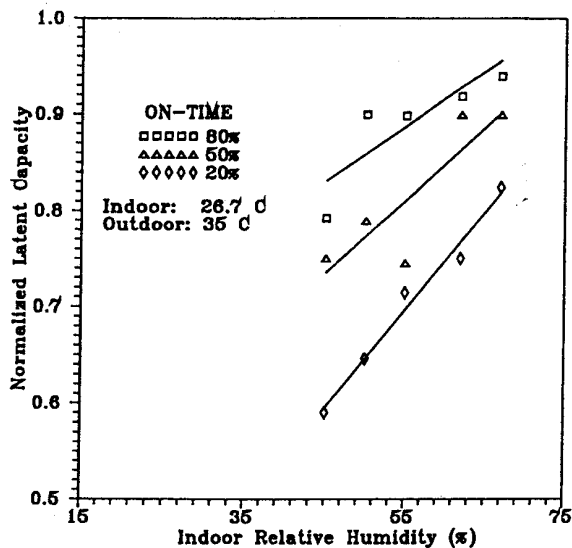


Figure B-4. Change in normalized latent capacity with indoor relative humidity

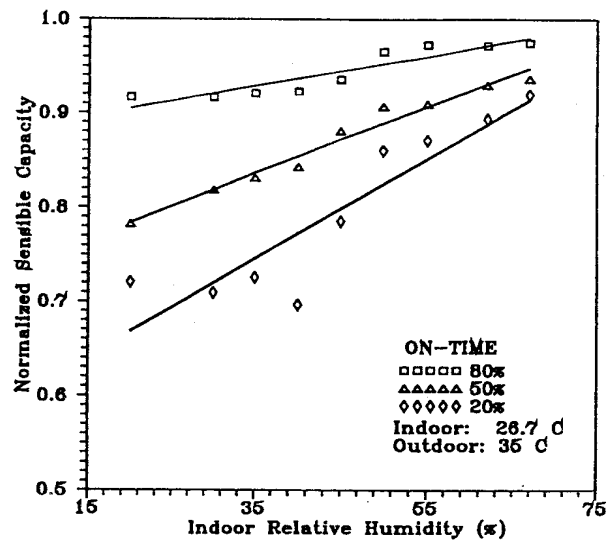


Figure B-5. Change in normalized sensible capacity with indoor relative humidity

The change in normalized sensible and latent capacities at a constant 50% inlet relative humidity for a range of inlet air dry-bulb temperatures and at two levels of percent on-time (50% and 80%) are shown in Figures B-6 and B-7. The normalized latent capacity decreased with decreasing inlet air temperature. On the other hand, there was very little change in normalized sensible capacity at various inlet air temperatures for a given percent on-time. In both cases the normalized capacity decreases with a decrease in percent on-time for the same inlet air conditions.

The change in normalized sensible and latent capacities at a constant entering air dewpoint temperature (58°F or 14.4°C) for a range of inlet air dry-bulb temperatures and at two levels of percent on-time (50% and 80%) are shown in Figures B-8 and B-9. There was a slight increase in normalized latent capacity with increase in inlet air temperature at 50% on-time and 80% on-time (Figure B-8). In contrast, the normalized sensible capacity decreased slightly at 80% on-time and increased slightly at 50% on-time with increasing inlet air temperature. Based on the test data used to develop these figures, the authors note that the time at which dehumidification began increased with an increase in inlet air temperature. At 22.2°C (72°F) inlet air temperature dehumidification began 60 seconds after system startup, whereas it took 120 seconds at 26.7°C (80°F).

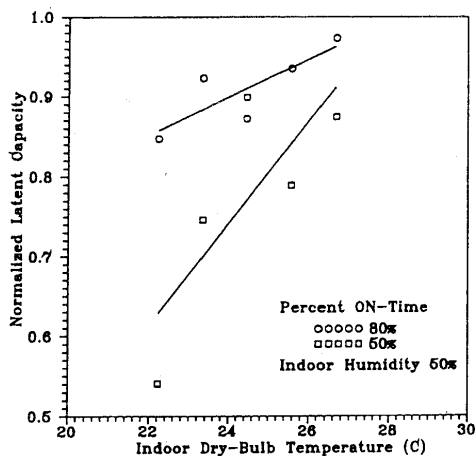


Figure B-6. Normalized latent capacity versus inlet air temperature at a constant relative humidity

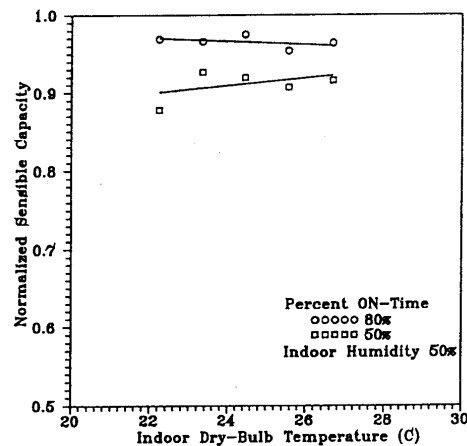


Figure B-7. Normalized sensible capacity versus inlet air temperature at a constant relative humidity

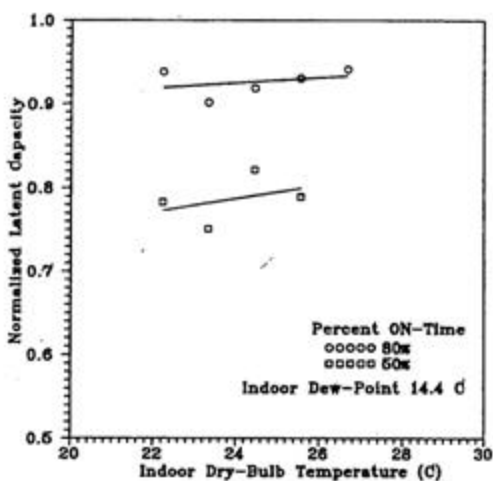


Figure B-8. Normalized latent capacity versus inlet air temperature at a constant dewpoint

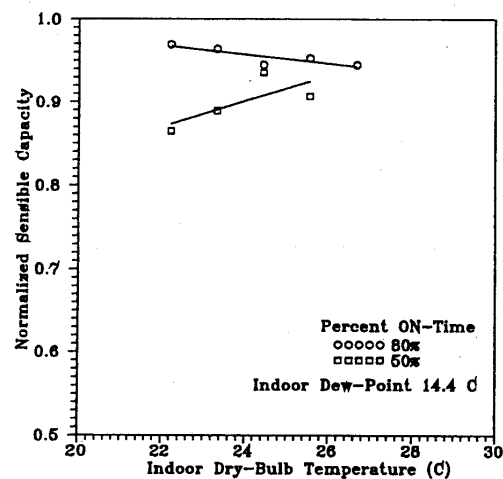


Figure B-9. Normalized sensible capacity versus inlet air temperature at a constant dewpoint

Finally, the authors developed an empirical correlation for normalized capacity as a function of percent on-time and inlet air relative humidity. The measured data suggested the capacity varies exponentially with percent on-time and linearly with inlet air relative humidity. The regression model is shown below in equation 4 and the regression constants (a and β) which provide the best fit of the measured data are provided in Table B-2.

$$Cap_{nor} = 1. - e^{(-a \times pon)} + b \times rh_i \times e^{(-a \times pon)} \quad (4)$$

where

pon = percent on-time

rh<sub>i</sub> = inlet air relative humidity

**Table B-2. Regression Constants**

Capacity	a	β
Latent	1.391	1.121
Sensible	2.779	1.343

The normalized capacity predicted by equation 4 was compared to the measured data. While curve-fit statistics were not provided, a graphical comparison indicated good agreement of predicted versus actual for normalized latent capacity, and also good agreement for normalized sensible capacity except at the lower end of the measured values (normalized sensible capacity near 0.7). The authors note that a and β are system constants and may vary from system to system.

For almost all tests, moisture was added to the supply air stream at start-up and dehumidification began 60 to 150 seconds after start-up depending on inlet air conditions. The authors conclude that, if the unit operates for less than 2 minutes, it will add moisture to the air rather than remove it. Using equation 5 below, the maximum thermostat cycling rate ( $N_{max}$ ) at 50% on-time would have to be greater than 7.5 cycles per hour to have a minimum on-time of less than 2 minutes. Henderson et al.<sup>4</sup> found maximum cycling rates ranging from 0.15 to 4.1 for a sample of 30 homes in Central Florida. With  $N_{max}$  of 4.1, the minimum on-time from equation 5 would be 3.7 minutes.

$$N_{max} = \frac{60}{(4 \times t_{on,min})} \quad (5)$$

<sup>4</sup> Henderson, Jr., H.I., Raustad, R., and Rengarajan, K. 1991. Measuring thermostat and air conditioner performance in Florida homes. FSEC-RR-24-91. Cocoa, FL: Florida Solar Energy Center.

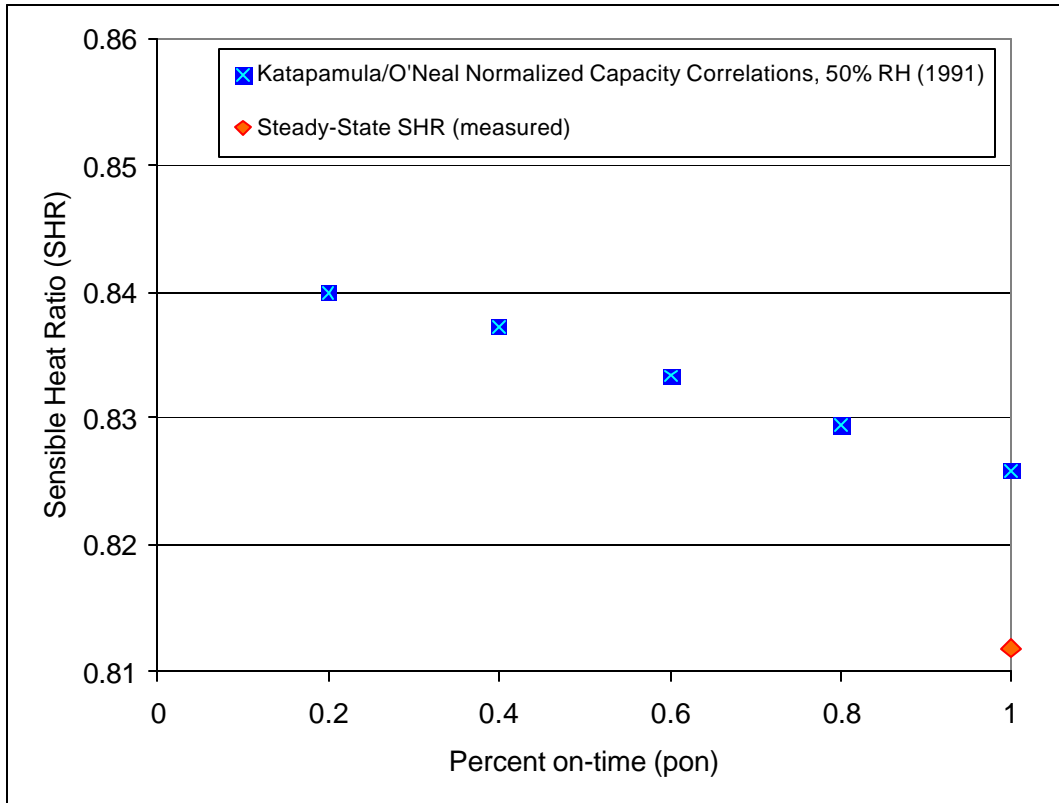


**Figure B-10. Effective Sensible Heat Ratio Versus Percent On-Time**

Figure B-10 manipulates the data provided in the Katipamula and O’Neal paper and plots it in a different format. The data points are for 80°F/50%RH inlet air and 95°F outdoor air. The steady-state sensible and latent capacities for this condition are from Katipamula (1989)<sup>5</sup>.

<sup>5</sup> Katipamula, S. 1989. A study of the transient behavior during start-up of residential heat pumps. PhD Dis sertation, Department of Mechanical Engineering, Office of the Graduate College of Texas A&M University.



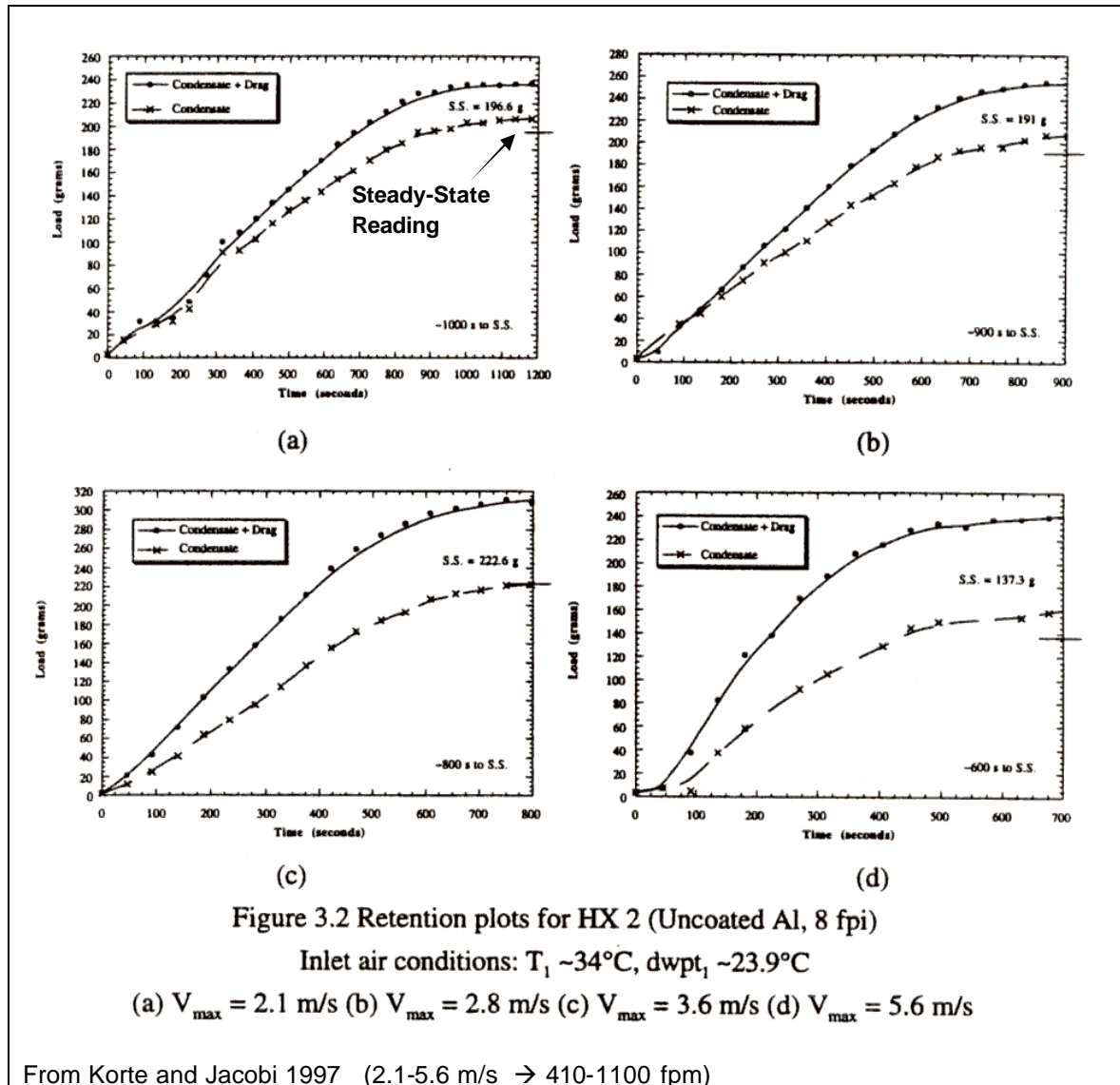
## **APPENDIX C**

### **Summary of Cooling Coil Moisture Retention Studies (Jacobi et al.)**

## Condensate Retention Testing at the University of Illinois

### 1997 Study

Section 3 of Korte and Jacobi (1997) takes measurements of the moisture retained on cooling coils. The measurements looked at both transient and steady state readings. A load cell was used to take transient readings of moisture retained on the coil. The steady state readings were made by removing and weighing the coil on a scale. The coil was arranged horizontally so that air flow was downward through the coil (in the same direction as gravity). The transient and steady state readings were found to agree very well. The original reason to take transient readings was to investigate whether any pulsating behavior could be detected. But moisture was found to asymptotically reach a constant value (in the 2000 study they changed the measurement procedure and did detect overshoot). The time to reach steady state was typically 600-800 seconds at various velocities for the 4 fpi coil. For the 8 fpi coil the time to steady state is 600-1000 seconds.

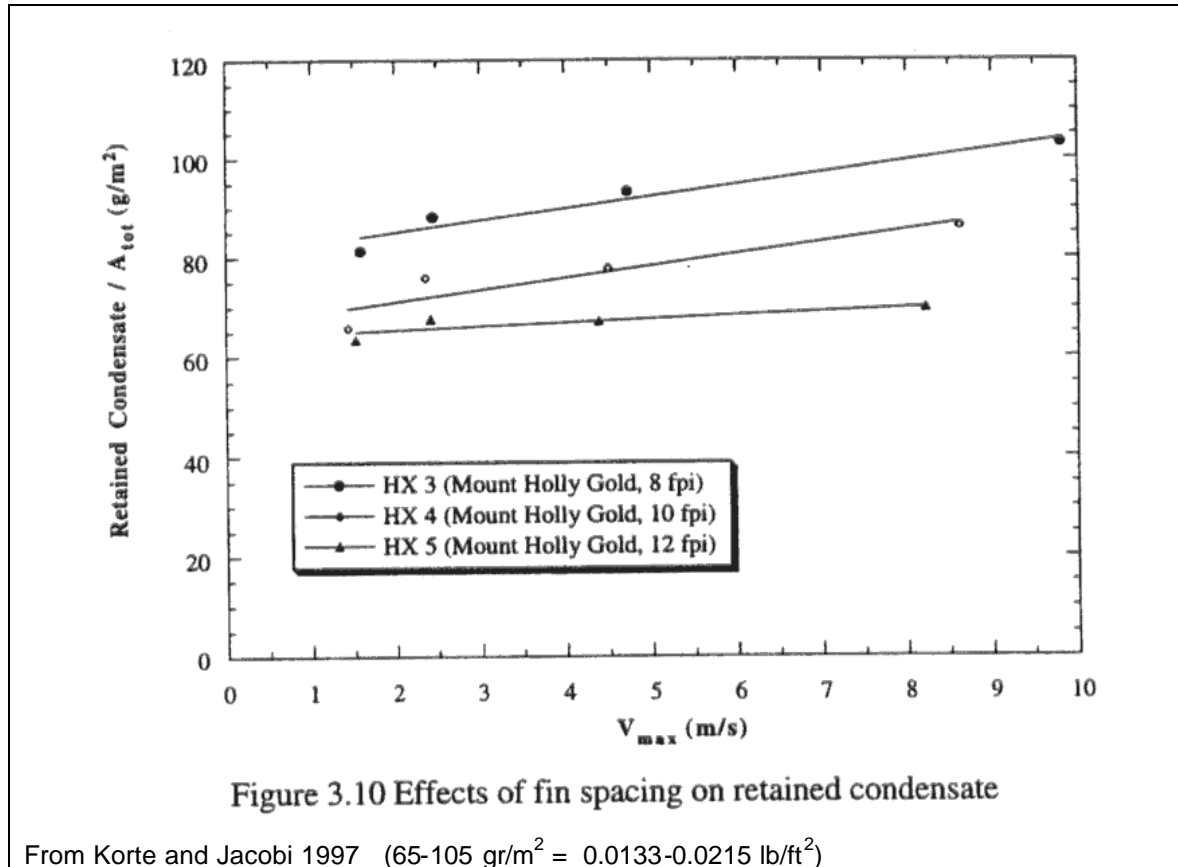


The amount of moisture that can be retained on the coil was found to change after several wet-dry cycles. The wettability of the coil changed as the factory-applied oil coating wore off. After several test cycles, the 4 and 8 fpi coils were found to have the same moisture holding capacity per total area. This was because the water droplets became flatter so that less fin-to-fin bridging occurred.

The first 4 & 8 fpi coils showed that more condensate was retained at lower velocities. The other coils showed the opposite behavior: more moisture retained at higher velocity. The range of the velocities considered ranged from 300 to 2000 fpm (1.5 to 10 m/s).

Other findings shown in the figures below:

- Less moisture retained for closer fin spacings (fig 3-10).
- Less velocity-dependence at closer fin spacings (fig 3-10)
- Hydrophilic coatings (e.g. Hycor) also reduce velocity dependence (fig 3-12)



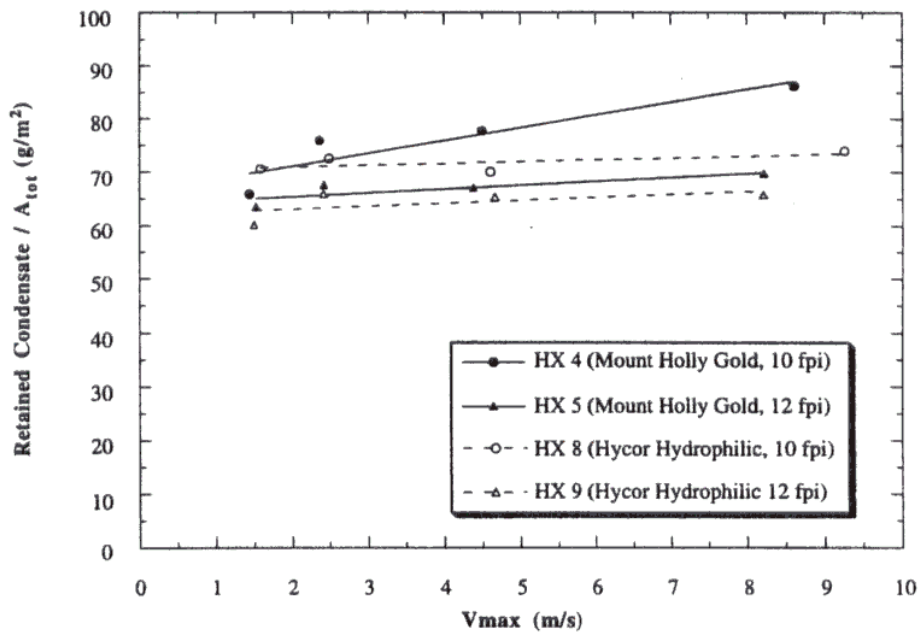
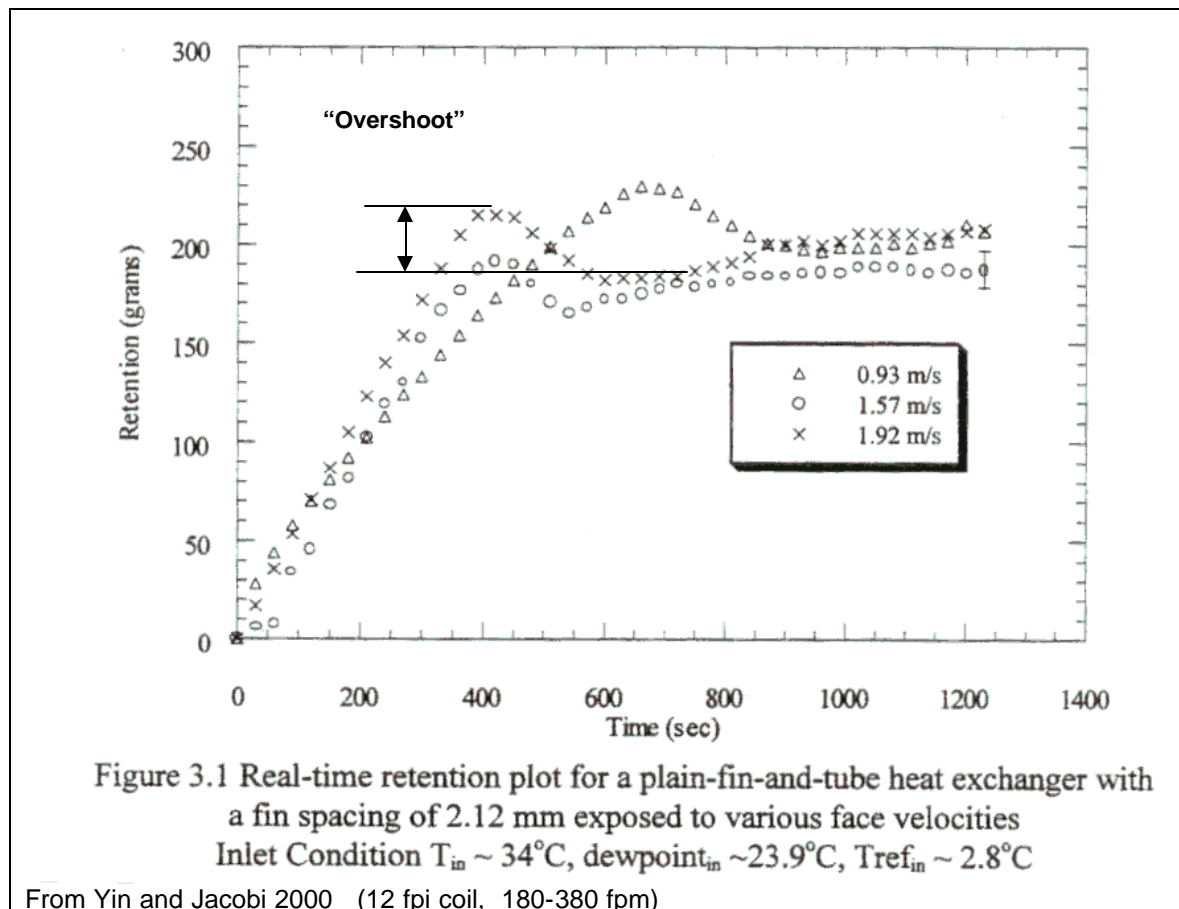


Figure 3.12 Effects of hydrophilic surface coating on retained condensate

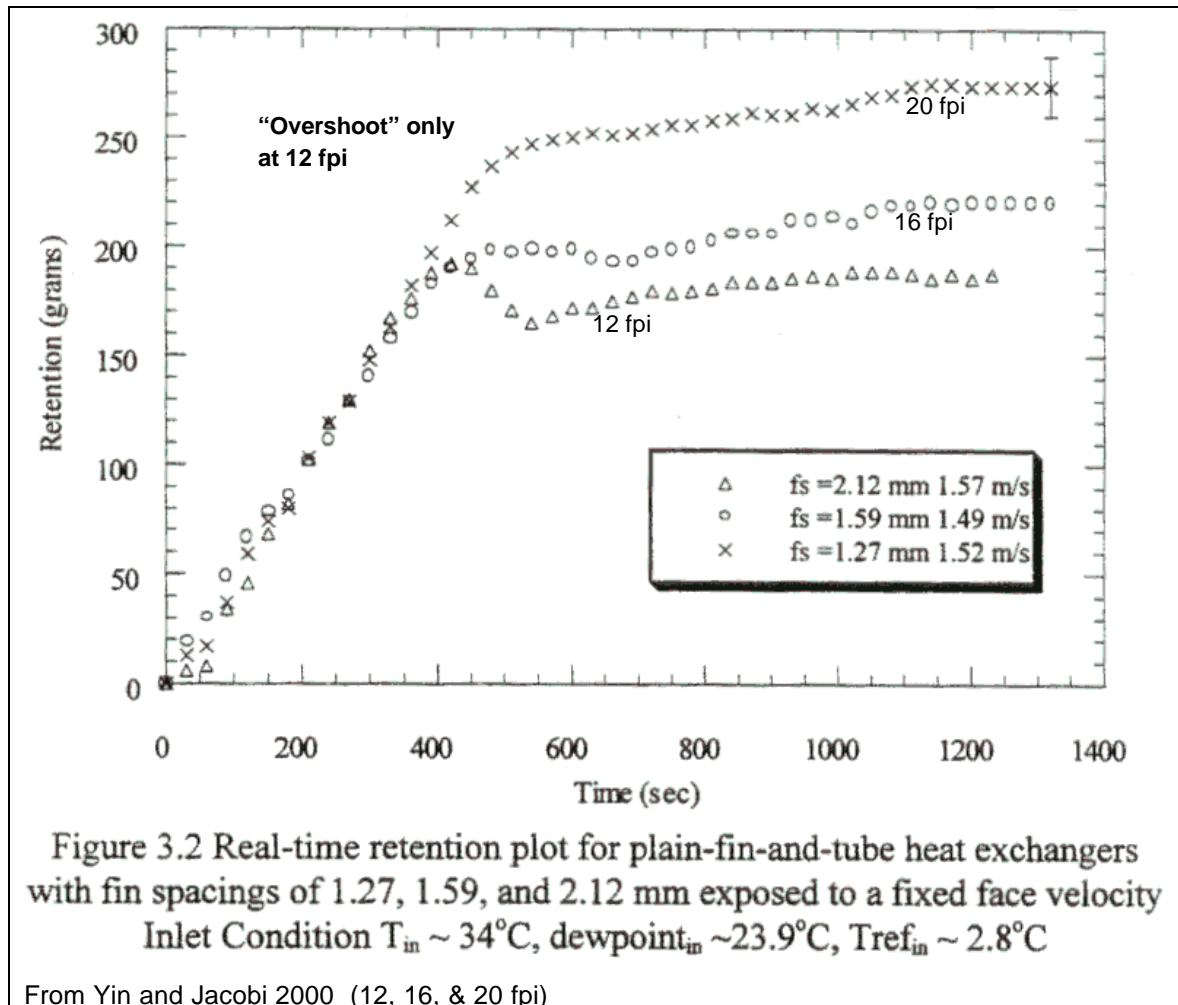
From Korte and Jacobi 1997

## 2000 Study

In 2000 the University of Illinois completed further testing on moisture retention. Kim and Jacobi (2000) looked at slit fin coils while Yin and Jacobi (2000) evaluated wavy-louvered fins. Both tests also re-examined the moisture retention characteristics of plain fin coils as well. They developed a new apparatus to measure the transient moisture collection on the coil (this apparatus did not require the drag forces to be separated from the condensate weight). In this test setup airflow through the coil was horizontal with condensate draining downward from the coil. The new apparatus was able to detect an initial “overshoot” in the mass of moisture retained on the coil. The overshoot implies that a certain quantity of moisture must first build up on a dry coil before the formed droplets start to fall from the fin surfaces. At that point, surface tension forces, gravitational forces, and velocity/shear forces are in balance and a quasi-steady state condition is eventually reached. The moisture on the coil ultimately settles out to a slightly lower steady state value. The steady-state measurements were still confirmed by removing the coil and weighing the condensate.



The “overshoot” effect was only observed for coils with 12 fpi or less; the figure below shows that no overshoot occurs for greater fin densities.



The testing of plain fins showed that the mass of moisture retention did increase for greater fin densities from 12 to 20 fpi (the opposite trend was found in 1997). The different pattern may have been due to the coil configuration. Moisture retention rates were typically 80-120  $\text{gr}/\text{m}^2$  (0.0164-0.0245  $\text{lb}/\text{ft}^2$ ) for plain fins. Wavy fins retain about 10-20% more water than plain fins. More water is retained because less sweeping takes place.

All testing was completed at 93°F & 75°F dp (56% rh & 131 gr/lb) entering air conditions with the entering fluid at 37°F (34°C, 24°C dp, 2.8°C fluid). These conditions are typical of outdoor air on a very humid day. These studies did not look at other entering conditions since they were primarily focused on coil geometry and surface issues.

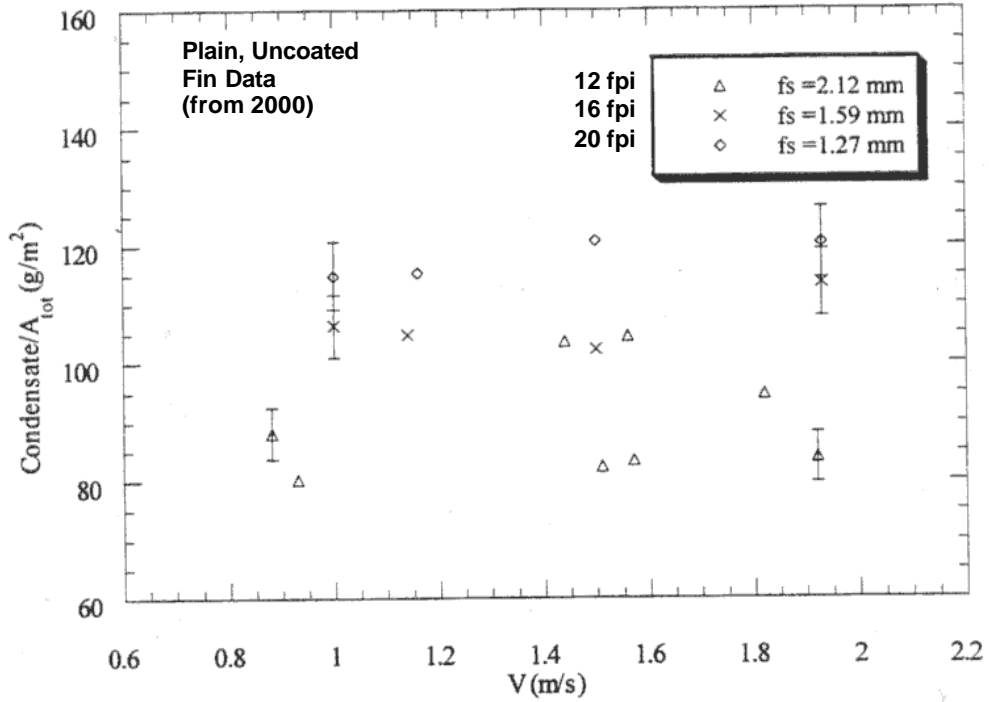
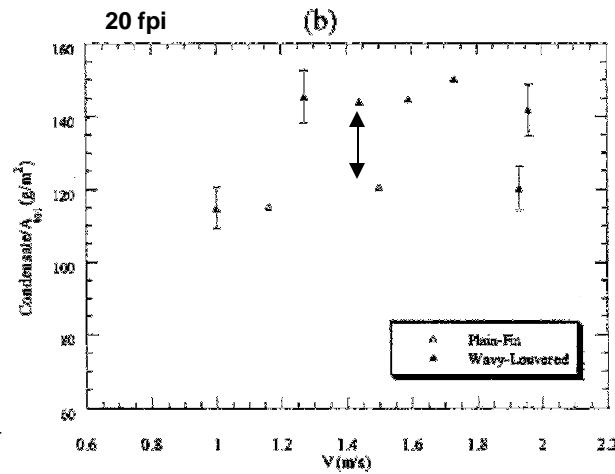
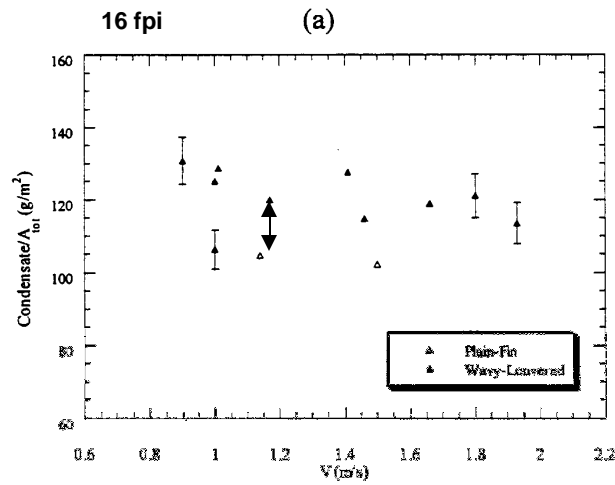
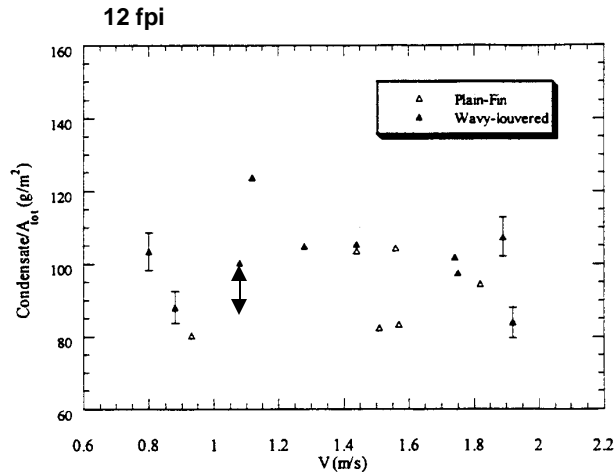


Figure 3.5 Condensate retention /  $A_{tot}$  for plain-fin-and-tube heat exchangers under steady-state conditions  
Inlet Condition  $T_{in} \sim 34^{\circ}\text{C}$ ,  $dewpoint_{in} \sim 23.9^{\circ}\text{C}$ ,  $T_{ref,in} \sim 2.8^{\circ}\text{C}$

From Yin and Jacobi 2000



Wavy Fins Hold  
10-20 gr/m<sup>2</sup>  
more moisture



(c)  
Figure 3.7 Steady-state condensate retention /  $A_{tot}$  for wavy-louvered versus plain-fin heat exchangers with varying fin spacings (a) 2.12 mm (b) 1.59 mm (c) 1.27 mm  
Inlet Condition  $T_{in} \sim 34^\circ C$ , dewpoint<sub>in</sub>  $\sim 23.9^\circ C$ ,  $T_{ref,in} \sim 2.8^\circ C$

From Yin and Jacobi 2000

Results from Kim and Jacobi (2000) also show that a coil with more rows retains less moisture (per unit surface area) since more droplets are removed by velocity-driven sweeping of condensate. Figure 3.5 below compares coated and uncoated fins with either 2 or 3 rows.

The 2000 studies both found that velocity had little or no impact on moisture retention, though the velocity range was limited to 200-400 fpm (0.9 to 2 m/s). Figure 3.5 from Kim and Jacobi (2000) did show a mild decrease in retention with higher velocities.

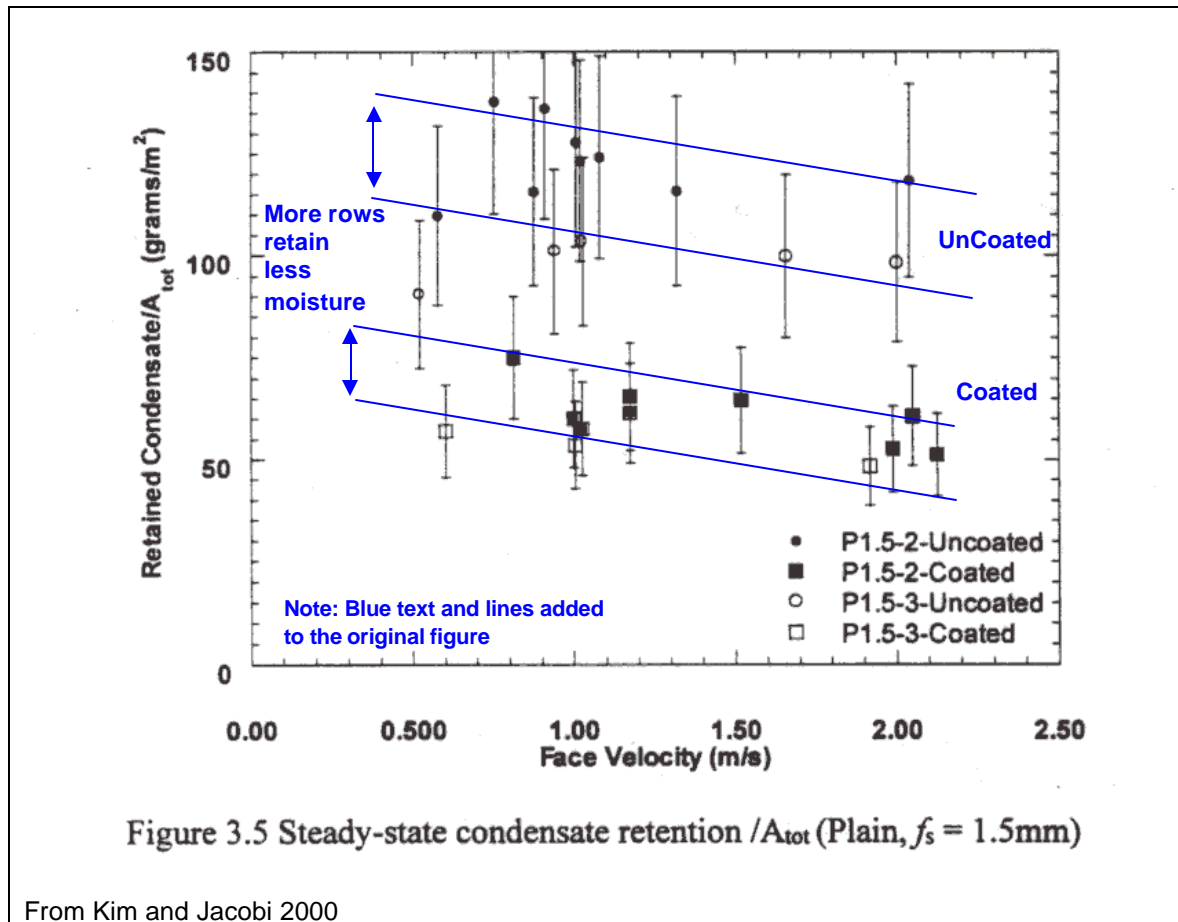


**Table C-1. Summary Table for Plain Fin Coils from All Studies**

<b>Reference</b>	<b>Coil Details</b>	<b>Moisture Retention @ 2 m/s [394 fpm]</b>
Korte & Jacobi (1997)	HX 4 (coated w/ Mount Holly Gold) 2 row coil, 10 fpi	70 g/m <sup>2</sup>
	HX 5 (coated w/ Mount Holly Gold) 2 row coil, 12 fpi	65 g/m <sup>2</sup>
Yin & Jacobi (2000)	12 fpi, 2 row	80-90 g/m <sup>2</sup>
	16 fpi, 2 row	105-120 g/m <sup>2</sup>
	20 fpi, 2 row	115-125 g/m <sup>2</sup>
Kim & Jacobi (2000)	17 fpi, 2 row, uncoated	95-140 g/m <sup>2</sup>
	17 fpi, 3 row, uncoated	80-120 g/m <sup>2</sup>

The studies also showed the following trends in coil moisture retention:

- Impact of wavy fin: 10-20 g/m<sup>2</sup> increase
- Impact of more rows (2 → 3 rows): 15-25 g/m<sup>2</sup> decrease
- Impact of hydrophilic coating: 5-40 g/m<sup>2</sup> decrease
- Impact of less airflow (394 → 98 fpm): 20 g/m<sup>2</sup> increase, though it's highly variable (some tests show little change or a slight decrease with decreasing airflow)

## 2003 Study

A more recent summary modeling study by El Sherbini and Jacobi (2003) developed more accurate models for moisture retention on a cooling coil. They also reviewed the previous work and made the following observations about previous work at their facility:

- At lower velocities and closer fin spacing there is more potential for condensate bridging – and as a result more condensate retention, (p. 1)
- They generally stated that the Yin and Jacobi testing found very little impact of velocity on condensate retention (in spite of some graphs we have pulled out above that seem to show the opposite).

The model they developed could be used to predict the fin spacing where bridging would first occur. They found that coils with fin spacing closer than 10-11 fpi are likely to have bridging (and their model would in theory under predict condensate retention at this point).

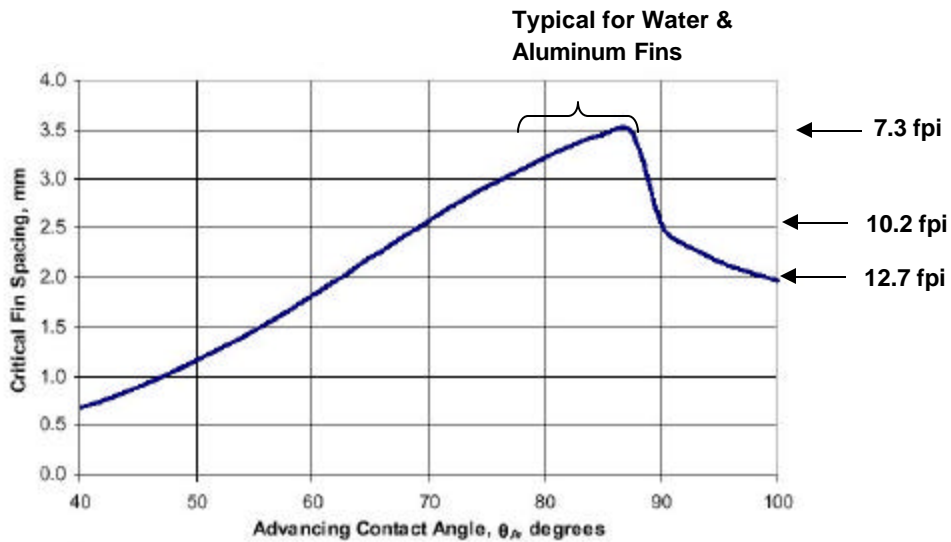


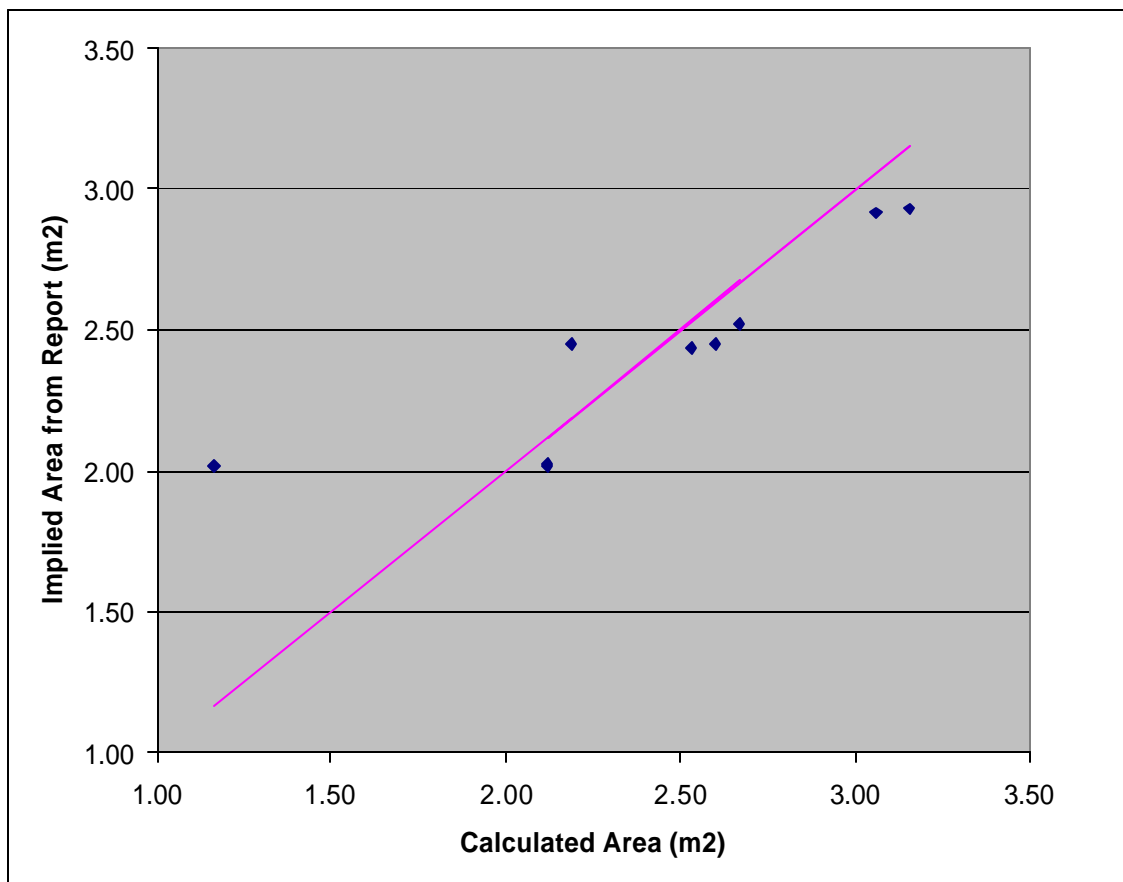
Figure 5.3 Critical fin spacing, beyond which condensate bridging cannot occur, as a function of the advancing contact angle.

### Concern about total fin area calculations

Korte & Jacobi (1997) was the only report to provide coil geometric data and also imply what the total coil area was (in table 3.3). The figure below compares our calculated area which we calculated as:

$$\text{Total area} = \text{gross fin area} - \text{tube hole area} + \text{exposed tube area}$$

Our calculations are typically 4-6% greater than the values implied by the report. If we used just the gross fin area (ignoring tube voids and exposed tube areas in the calculations) the calculated gross area is 11-15% greater than the implied area from the report.



As a result, we can not be totally certain how to calculate total areas for our coils, when we apply these retained condensate values to coil geometries. However, the good news is that the uncertainty in reported condensate values is  $\pm 10\%$  while the difference in the area calculations is smaller at approximately 5%.

## **APPENDIX D**

### **Summary of Khattar Field Study (Khattar et al. 1987)**

The plot below is Figure 4 from Khattar et al.<sup>6</sup> which shows the transient performance of the AC coil in FSEC's PV House (located at the old FSEC site in Cape Canaveral. FSEC relocated to Cocoa in 1995). The nominal performance of this unit was 29.6 MBtu/h with an SHR of 0.78. Khattar reported that the data for this graph corresponded to operating conditions of 80°F db/68.9°F wb (57.4% RH) air entering the cooling coil and an outdoor air dry-bulb temperature of 82°F. The steady state SHR at this condition was 0.63.

One problem with this plot was the obvious offset of the total and sensible data above zero. If we offset the "zero point" to +0.05, then the total capacity approaches zero and the sensible and latent sum to zero during the off cycle. This offset is shown on the plot below with a dotted line. The red and green lines over-laid on the original figure now show the adjusted latent capacity during the on cycle (red) and during the off cycle (green).

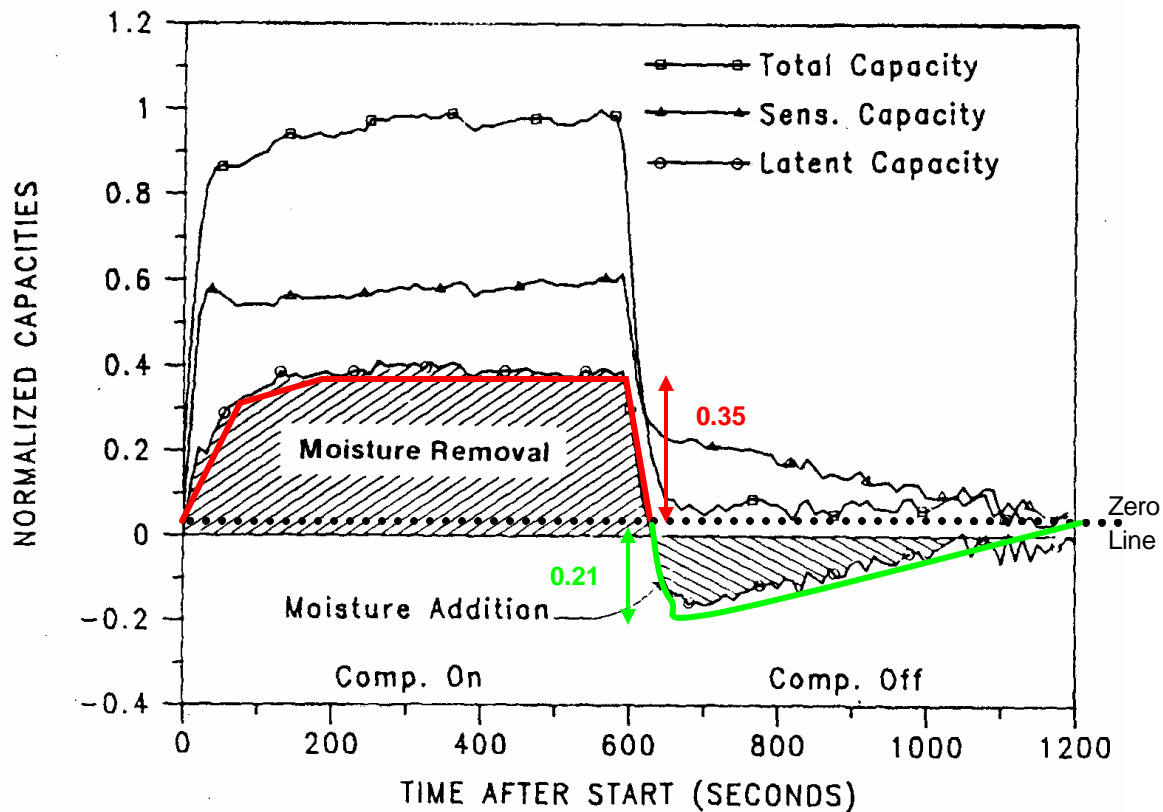


**Figure D-1. Moisture Removal and Addition Under Fan ON Operating Mode**

The relative heights of these adjusted on- and off-cycle profiles were used to find gamma, a parameter used in the first-generation latent degradation model developed by Henderson and Rengarajan<sup>7</sup>:

$$\text{gamma} = 0.21 / 0.35 = 0.6$$

<sup>6</sup> Khattar, M.K., M.V. Swami, and N. Ramanan. 1987. Another Aspect of Duty Cycling: Effects on Indoor Humidity. ASHRAE Transactions Vol. 93, Part 1, pp. 1678-1687.

<sup>7</sup> Henderson, H.I., Jr., and K. Rengarajan. 1996. A Model to Predict the Latent Capacity of Air Conditioners and Heat Pumps at Part-Load Conditions with Constant Fan Operation. ASHRAE Transactions Vol. 102, Part 1, pp. 266-274.

Similarly the area under the off-cycle latent capacity (the area under the green triangle) was estimated graphically using the height and duration times one half:

$$\text{Off-cycle Area} = 0.21 \times 600 \text{ sec} \times \frac{1}{2} = 63$$

Therefore, to graphically find  $t_{\text{wet}}$ , we divide the area by the steady-state latent capacity during the on cycle (0.35) to find the time in seconds:

$$t_{\text{wet}} \sim 63 / 0.35 = 180 \sim 200 \text{ seconds}$$

Khattar does not provide the absolute value of the latent capacity for the transient testing from Figure 4. However, if we use the DOE\_AC function with the nominal rating conditions of 30 MBtu/h and 0.78 SHR, and apply the reported operating conditions of 80°F db/68.9°F wb entering the cooling coil and 82°F outdoor dry-bulb temperature, we predict:

Total capacity:	32.6 MBtu/h
Latent capacity:	11.4 MBtu/h
SHR:	0.65

Since the predicted SHR is close the value of 0.63 reported by Khattar, we can have reasonable confidence that the latent capacity predicted by DOE\_AC is representative. Based on the latent capacity of 11.4 MBtu/h, we can calculate the following values:

$$\text{Moisture Mass: } \frac{200 \text{ seconds} \times 11.4 \text{ MBtu/h}}{3600 \text{ seconds/h} \times 1.060 \text{ MBtu/lb}} = 0.597 \text{ lbs}$$

Initial

$$\text{Evaporation Rate: } 0.6 \times 11.4 \text{ MBtu/h} = 6.8 \text{ MBtu/h}$$

The evaporator coil on the Bard unit salvaged from the PV House (which is assumed to be similar to the original unit tested by Khattar) has a face area of 1.1 ft<sup>2</sup>/ton. The coil is 2.5 inches deep with 10.5 fins per inch. So the coil surface area (144.4 ft<sup>2</sup>) is modest compared to typical AC units that we are testing in the laboratory. The modest fin area at least partially explains why the mass of moisture held on the fins is relatively low in this case. However, the normalized moisture mass is still only 4 lbs per 1,000 ft<sup>2</sup> of fin area, or about half of what we have seen for other coils in the lab.

The data from Table 2 in Khattar are summarized below. The data points were taken by recording the average values collected over one-week periods. The runtime fraction was increased by lowering the thermostat. Therefore, the operating conditions were not held constant in each case.



**Table D-1. Summary of Khattar Data**

<b>Runtime Fraction (CONST Fan)</b>	<b>Operating Conditions (CONST Fan)</b>	<b>CONST Fan Moisture Removal (lb/kWh)</b>	<b>AUTO Fan Moisture Removal (lb/kWh)</b>	<b>Latent Degradation Fraction</b>
0.25	80°F & 65%	0.62	1.65	0.376
0.34	77°F & 70%	0.87	1.64	0.530
0.60	76°F & 70%	1.34	1.65	0.812
0.80	71°F & 75%	1.72	1.72	1.000

The latent degradation fraction was determined by dividing the lb/kWh value from the constant fan tests by the values from the auto fan tests. Taking the ratio of values at least partially corrects for the different operating conditions. However, while the space temperatures were the same for each row in the table, the space humidity was typically 10% lower in auto fan mode.

Figure D-2 below compares the measured data to the model. It attempts to develop a separate LHR curve for each data point / test condition to compensate for the variations in  $t_{wet}$  and  $\gamma$ . These values were adjusted in each case using the DOE\_AC function to predict steady state latent capacity and SHR at each set of conditions. Then  $\gamma$  and  $t_{wet}$  were calculated using:

$$t_{wet} = \frac{0.597 \text{ lbs} \times 1.06 \text{ MBtu/lb}}{QL_{ss}}$$

$$\gamma = \frac{6.8 \text{ MBtu/h} \times (DB - WB)}{QL_{ss} (80-68.9)}$$

$$SHR = 1 - (1 - SHR_{ss}) \times FLHR(t_{wet}, \gamma, \dots)$$

where  $QL_{ss}$  and  $SHR_{ss}$  are determined with DOE\_AC with the conditions from each point (i.e., DB & WB).

Using these relations to correct back to nominal conditions of 80°F db, 67°F wb, and 95°F outdoors, the values of  $t_{wet}$  and  $\gamma$  at ARI conditions become:

$t_{wet}$ : 323 seconds  
 $\gamma$ : 1.13  
 Steady State: 7.0 MBtu/h latent, SHR = 0.759

Figures D-2 and D-3 plot each data point and the theoretical curve corresponding to the conditions associated with that point. DOE\_AC predicts a steady state SHR of 0.50-0.55 for the cool, humid operating conditions. The model significantly deviates from the data points for low

runtime fractions. The humid conditions significantly increase  $QL_{ss}$  and reduce the evaporation rate.

Figure D-3 arbitrarily increases the mass of moisture on the coil by 50% and shows that this change brings the theoretical curves more in line with measured data. The reasons for deviations between the model and the data could be due to the inaccuracies of the graphical integration techniques above. There is also uncertainty associated with the conversion of Khattar's data into a LHR ratio since the entering conditions in the auto and constant fan modes were not exactly equivalent – especially at lower runtime fractions when space humidity levels could be different by 10% RH.

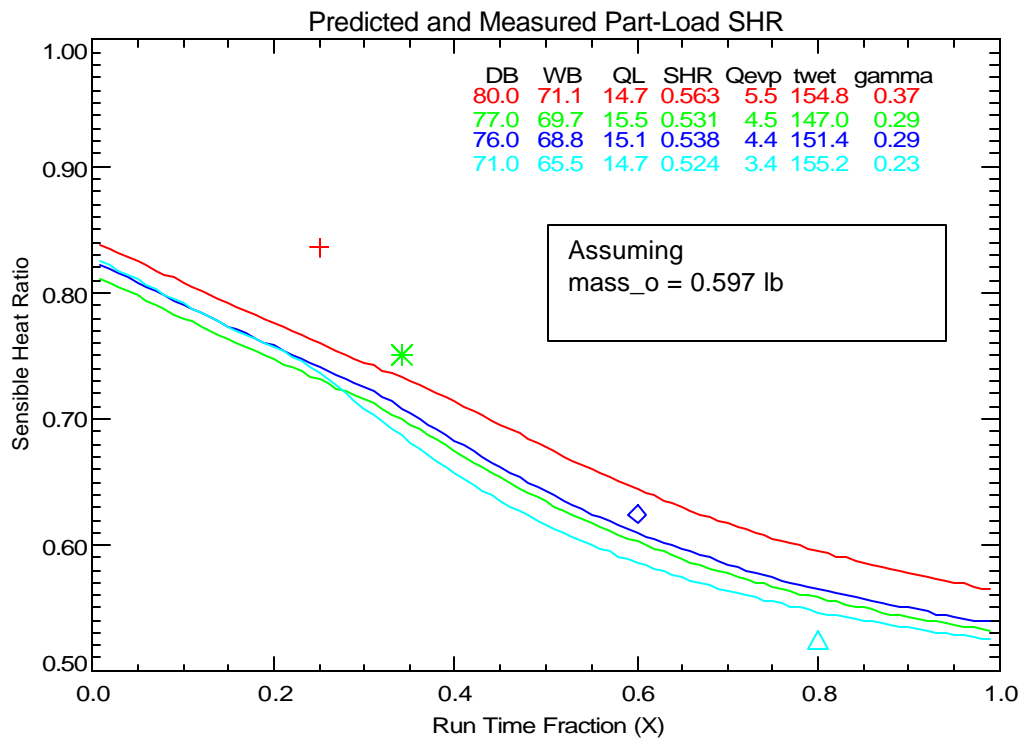


**Figure D-2. Sensible Heat Ratio Versus Run Time Fraction (Mo = 0.597 lb)**

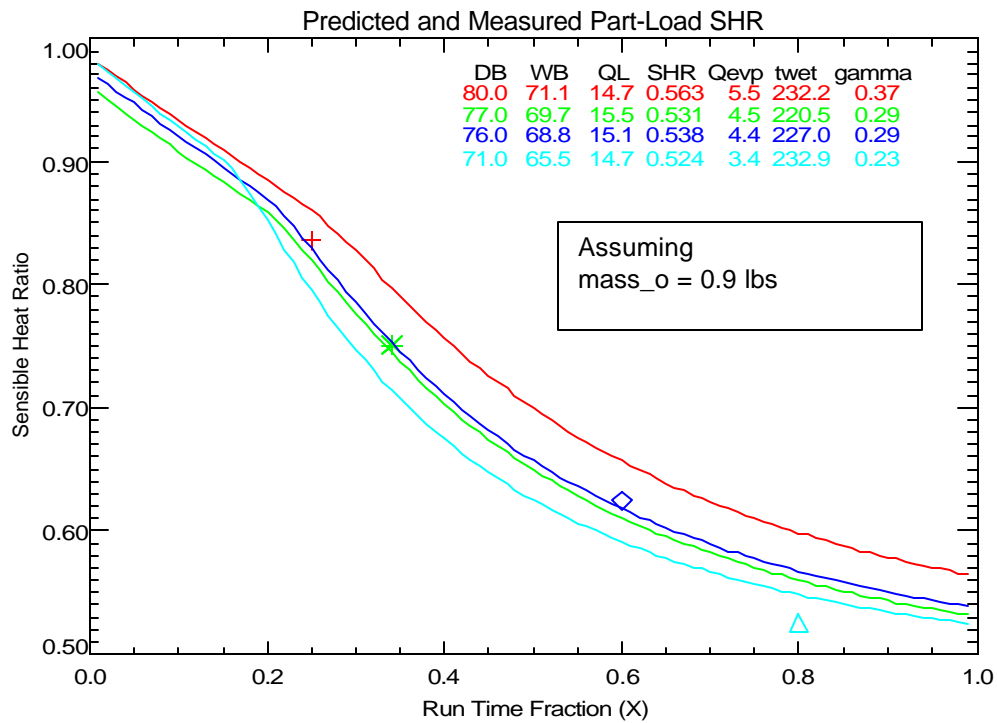


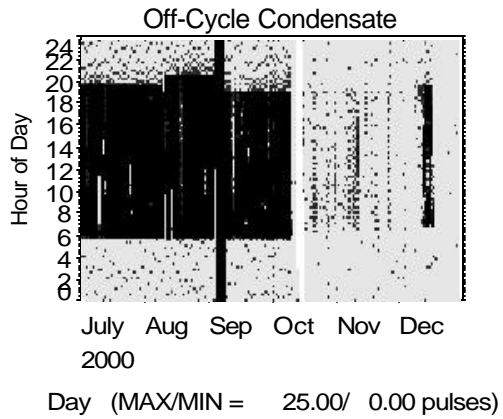
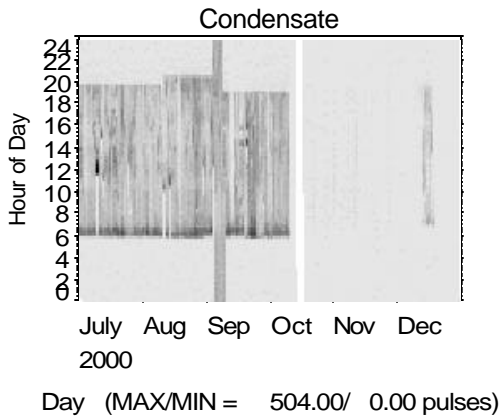
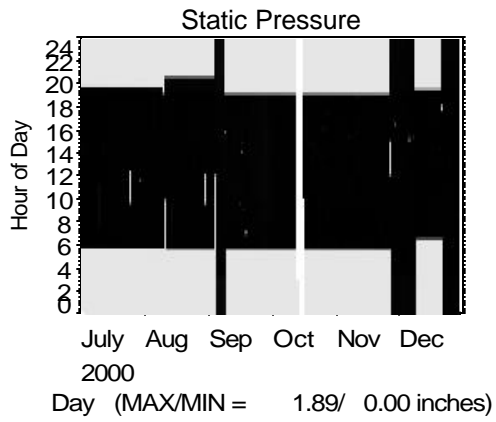
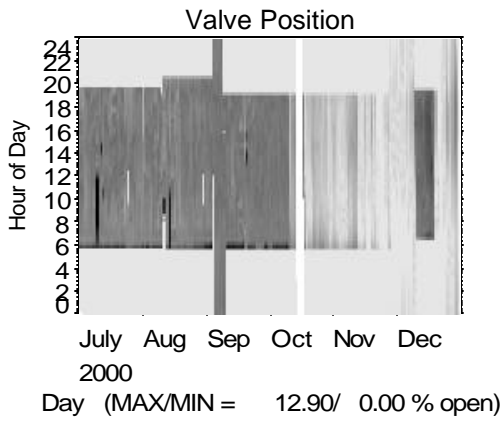
**Figure D-3. Sensible Heat Ratio Versus Run Time Fraction (Mo = 0.9 lb)**

## **APPENDIX E**

### **Analysis of Existing Data Sets of Field Measurements**

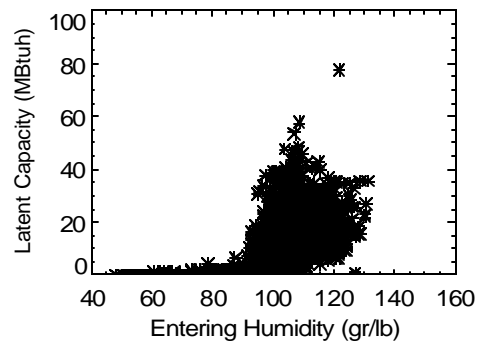
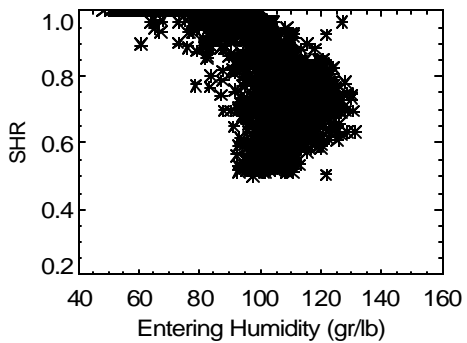
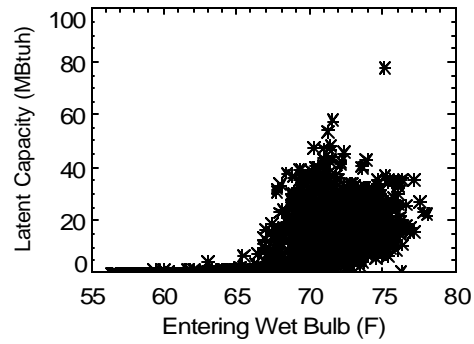
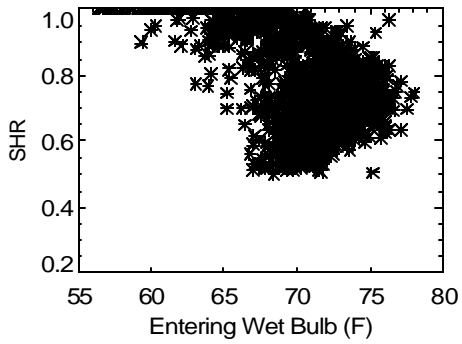
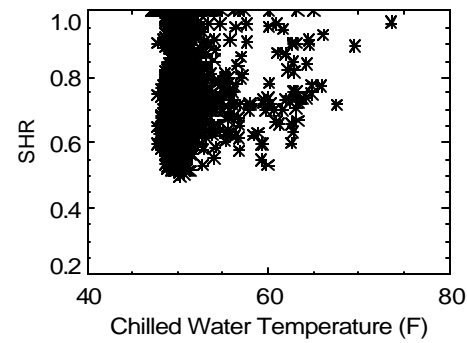
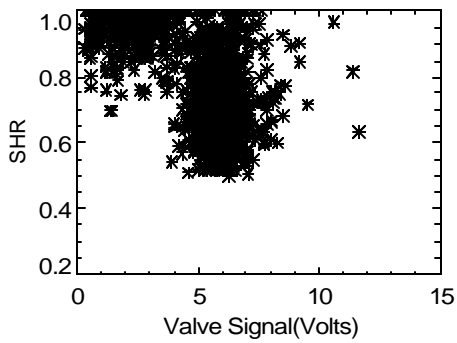
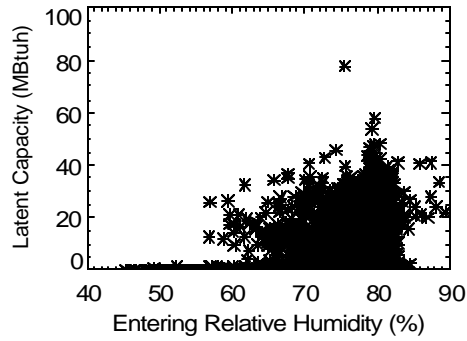
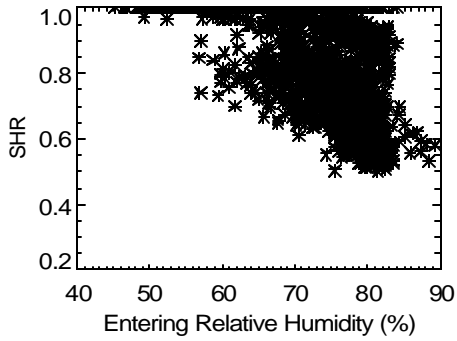
## **Constant-Air-Volume Chilled Water Coil in a Florida Commercial Building**

Cocoa Beach Country Club  
15-minute Data

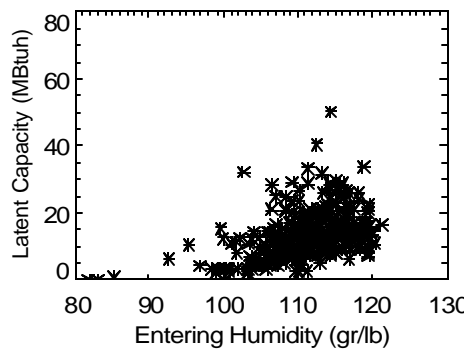
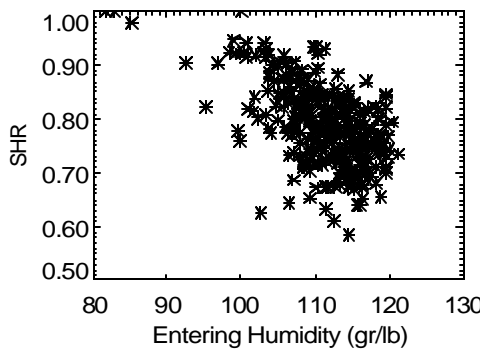
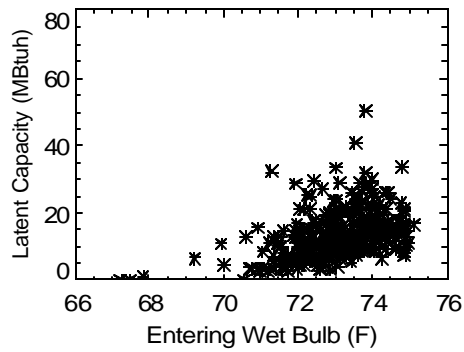
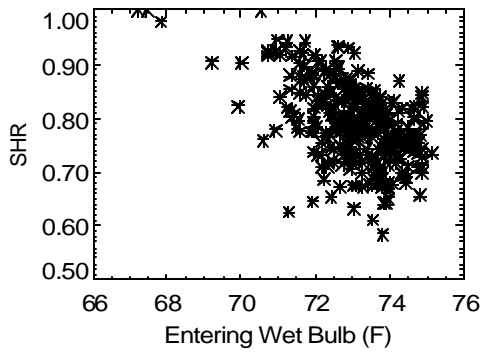
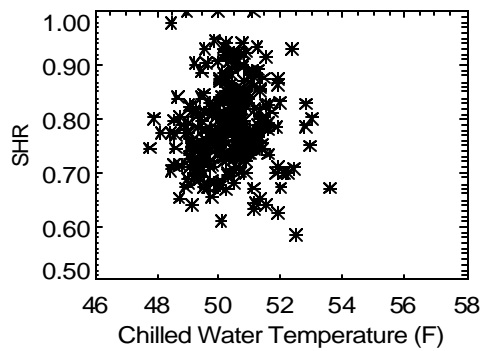
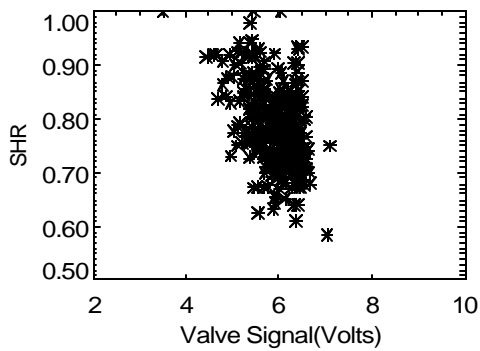
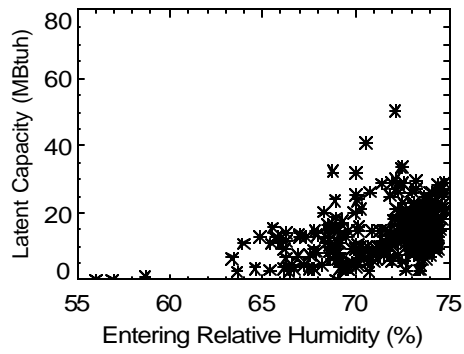
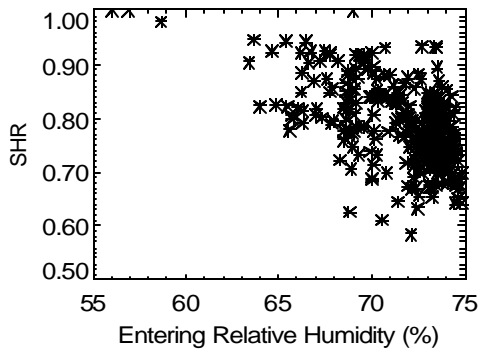


Assumed parameters: 3468 cfm & 200 pulse/gal (0.0417 lb/pulse)

All the data (with the AHU fan on):

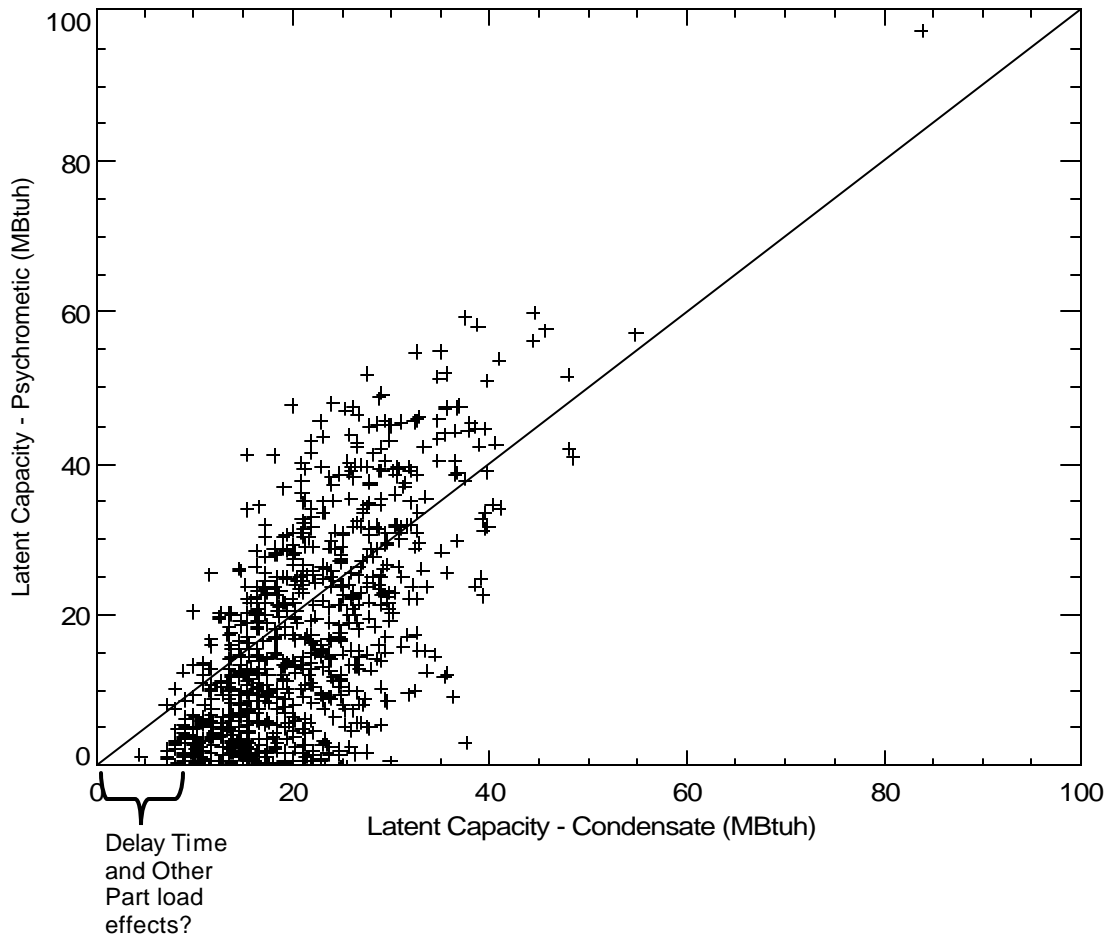


Data near design conditions (entering air temp 78-82°F, CW<60°F, entering RH 55-75%):

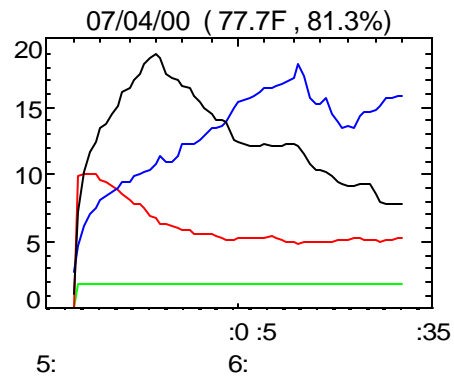
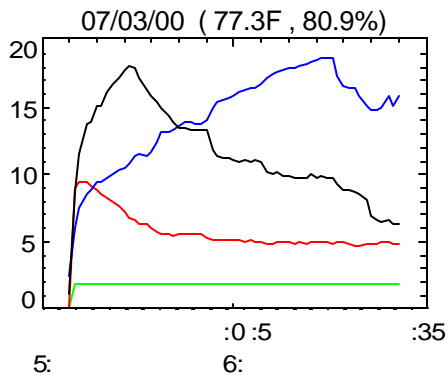
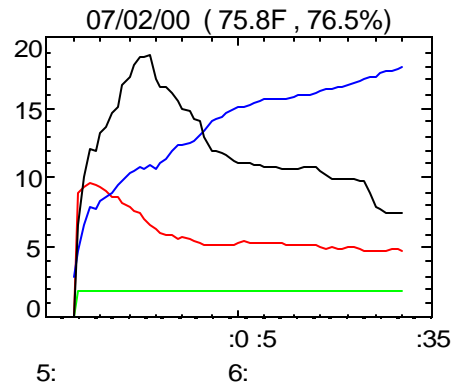
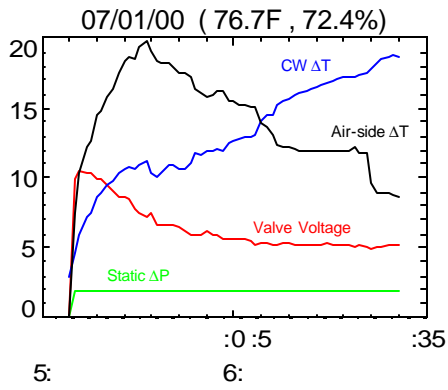


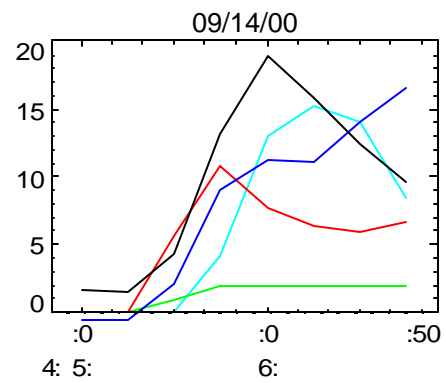
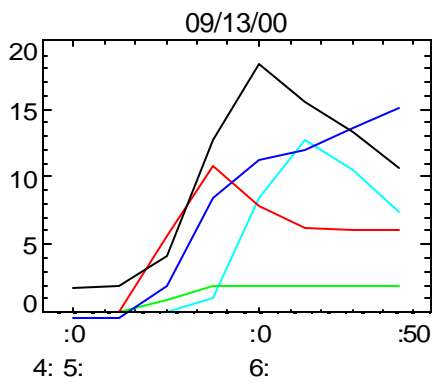
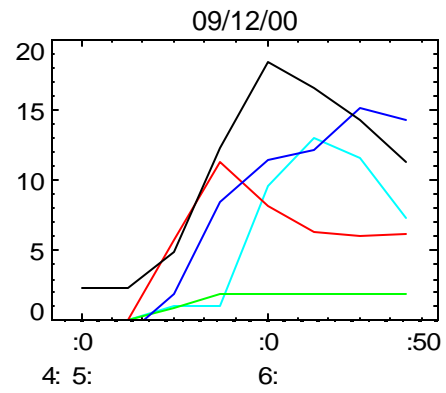
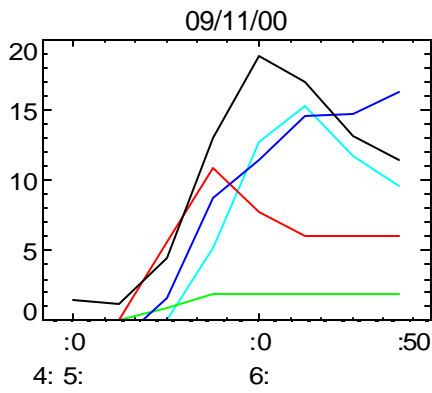
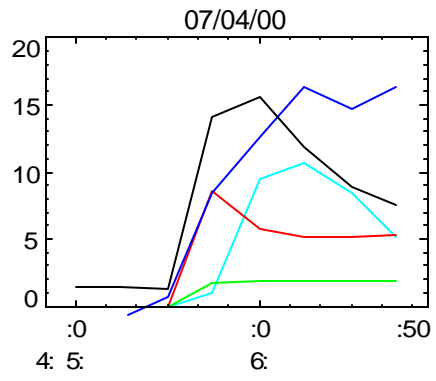
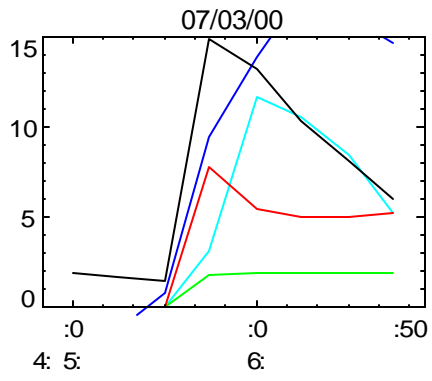
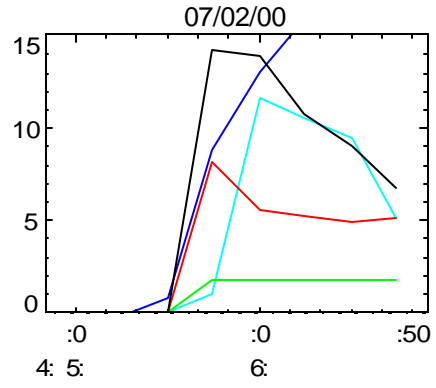
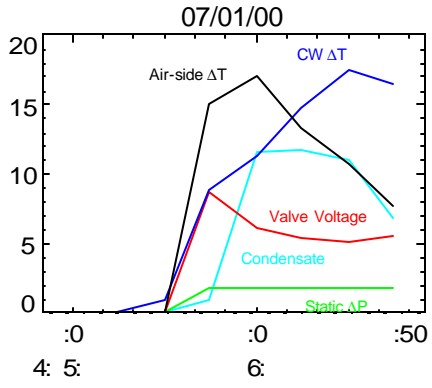


The latent capacity can be calculated by using psychrometric air-side measurements and also by measured condensate pulses. The two methods agree best at higher capacities. All the data is shown.



The 1-minute data shows no real variation in static pressure at startup, so that's not so useful.





## **Residential Water-to-Air, Direct Expansion Heat Pumps at 12 North Carolina Sites**

## Condensate Time Delay

This section calculates the time after compressor startup until the condensate pulse is detected by the condensate pump (see Figure E-1). This delay time is another indication of a coil's moisture holding capacity and the parameter  $t_{\text{wet}}$  in the latent degradation model. We have looked at the data from 12 residential water-source heat pump sites in North Carolina (site 1 was the system used in Henderson 1998). The 15-minute data includes the exact time when the compressor turns on but the precise time of the condensate pulse is not known, since it could have occurred and at any time during the 15 minute recording interval (therefore we only know the time delay within  $\pm 7.5$  minutes). Figure E-1 illustrates this concept.

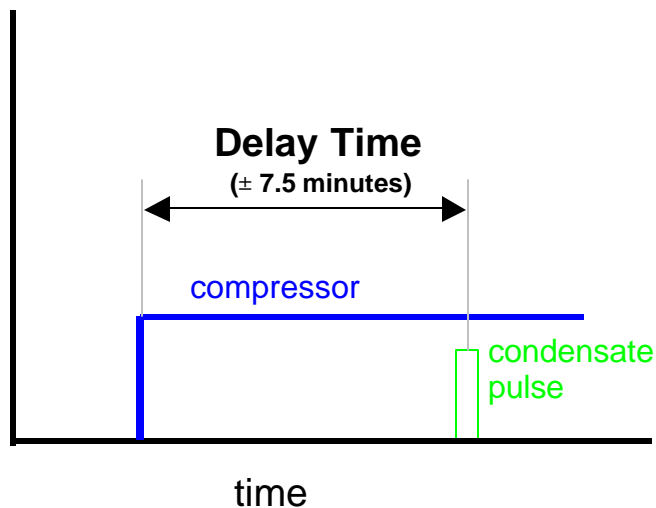


**Figure E-1. Delay Time for First Condensate Pulse from the Evaporator Coil**

We reviewed the data set for all 12 sites and found the occurrences listed in Table E-1 where the compressor had been off for an extended time (i.e., several hours) and then came on. Therefore, we have a fair confidence that the coil was starting up fully dry under these conditions<sup>8</sup>. Figure E-2 shows the data from one occurrence at Site 1 on 3/27/97.

---

<sup>8</sup> However we are less certain about the amount water initially in the condensate pump sump. Therefore, we can not precisely be sure that the first pump cycle corresponds to exactly 0.5 lb of water falling from the drain pan.

**Table E-1. Occurrences where the Evaporator Coil is Starting from Dry Conditions**

Site	Fan Control Mode	Date	Time of Compressor Startup	Delay Time (minutes)	Entering <sup>1</sup> Air Temp (F)	Entering <sup>1</sup> Air RH (%)	Change in Fan Speed
1	AUTO	12/25/97	15:33:21	49.2	70.0	45.1	off-med
1	CONST	02/19/97	22:18:06	49.4	72.0	37.8	low-med
1	CONST	02/22/97	14:09:34	12.9	73.6	48.6	low-med
1	CONST	02/27/97	20:48:46	18.7	73.3	47.1	low-med
1	CONST	03/27/97	15:36:38	45.9	71.6	42.2	low-med
2	AUTO	05/19/97	14:05:20	302.2	81.6	48.1	off-med
3	AUTO	03/29/97	14:08:40	88.8	70.5	46.9	off-med
3	AUTO	05/18/97	17:57:20	55.2	79.2	41.2	off-med
3	AUTO	05/30/97	20:03:40	63.8	74.1	53.1	off-med
3	AUTO	06/15/97	18:29:35	52.9	78.6	44.2	off-med
3	AUTO	06/20/97	15:33:35	18.9	76.8	44.9	off-med
3	AUTO	06/25/97	15:30:45	21.7	76.9	47.5	off-med
3	AUTO	07/10/97	6:08:30	14.0	76.9	56.7	off-med
3	AUTO	09/08/97	14:00:50	66.7	77.3	45.0	off-med
3	AUTO	09/16/97	5:59:45	22.8	76.3	56.7	off-med
3	AUTO	09/21/97	12:23:30	29.0	76.0	52.7	off-med
3	AUTO	10/04/97	11:47:15	50.2	71.0	51.4	off-med
6	CONST	05/19/97	16:32:40	49.8	80.4	47.8	low-med
8	AUTO	05/15/97	9:43:09	24.4	70.9	60.9	off-med
8	AUTO	03/03/97	16:26:11	26.3	72.6	61.5	off-med
9	CONST	06/23/97	16:56:50	55.7	74.3	57.6	low-med
11	AUTO	09/23/97	19:48:58	18.5	72.5	69.5	off-med

Notes: 1 – Entering air conditions measured at the time of compressor startup  
 2 – Site 2 had a very long delay time that could not be explained. So it was excluded.

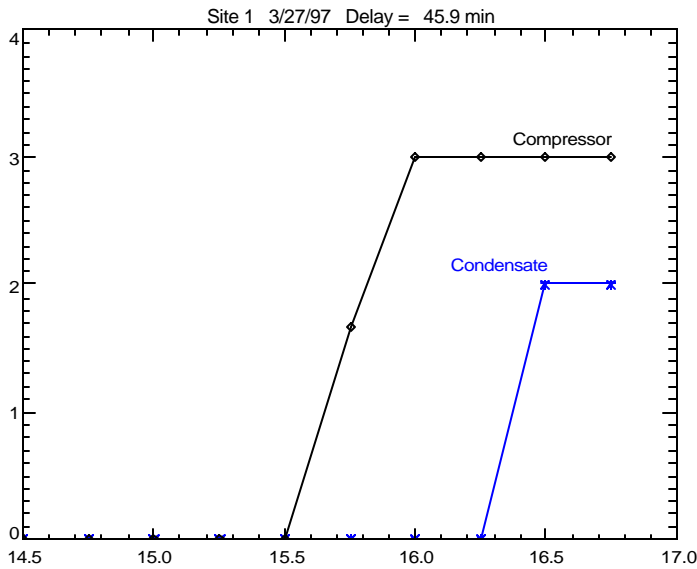


**Figure E-2. Data Demonstrating Delay Time from Site 1 on 3/27/97**

Figure E-3 shows that the delay time is dependent on the entering conditions. Data from each site is identified by its number. The variables best able to predict the variation in latent capacity appear to be the humidity ratio and wet bulb temperature. At less humid conditions, the delay time approaches 100 minutes. The delay is longer since less moisture forms on the evaporator coil and it takes longer for the coil's holding capacity ( $M_o$ ) to be reached. Near design conditions (i.e., an entering wet bulb of 67°F) the delay time approaches 20 minutes, which is close to value of 12 minutes determined for Site 1 in (Henderson 1998). Table E-2 shows that the cooling coils at the sites all have similar characteristics (in terms of number of rows, face velocity, etc.).

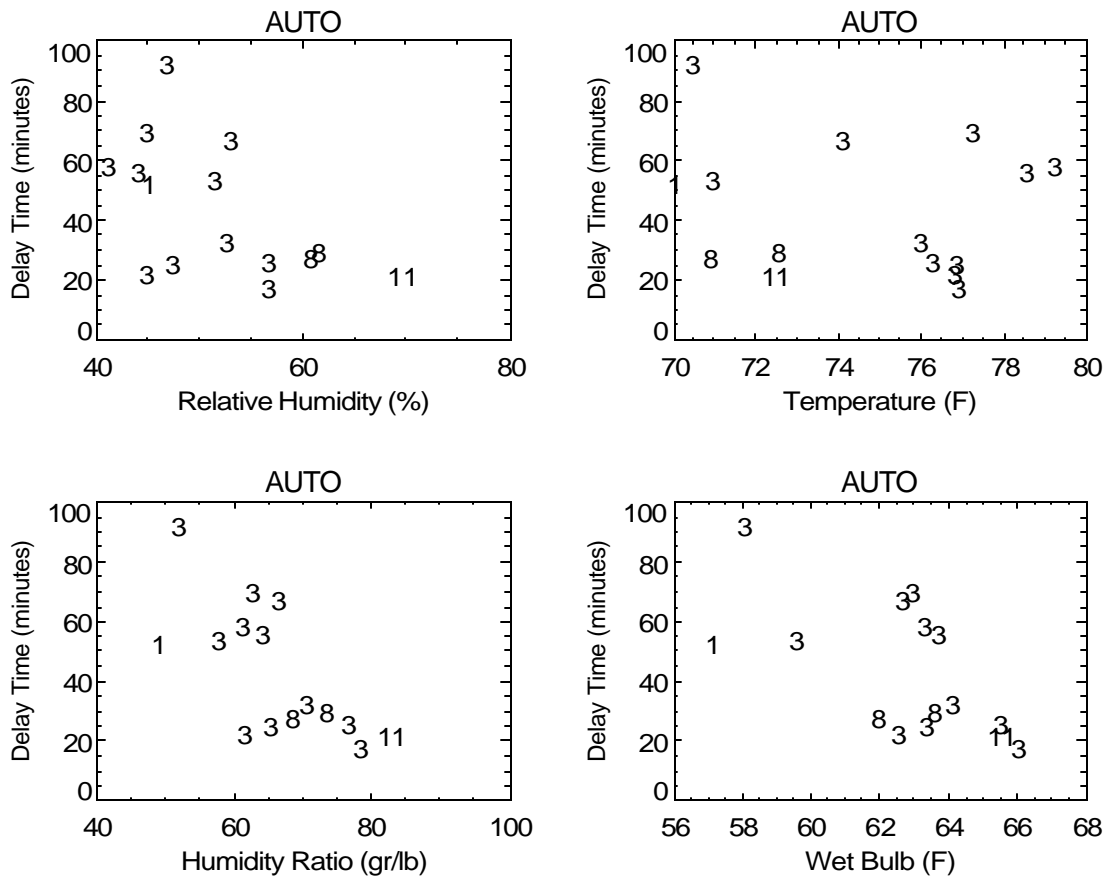


**Figure E-3. The Variation in Delay Time with Entering Conditions (Various Sites, AUTO Fan Mode)**

Figure E-4 and Figure E-5 show the same variation in time delay for Sites 1 and 3 individually. Since the plots focus on moisture buildup at startup, the differences between the AUTO and CONST fan mode should be small. The data for Site 3 shows that at design conditions, the delay time approaches 10-15 minutes. The data for Site 1 also shows a strong trend and a minimum delay near 10 minutes. Though, conditions are cooler than design conditions.

**Table E-2. Characteristics of Cooling Coils**

	Unit Model	Coil Face Area (ft <sup>2</sup> )	No of Rows	Supply Air (scfm)	Face Velocity (fpm)
Site 1	ATV034	3.8	3	1,291	344
Site 2	ATH016	2.6	3	891	339
Site 3	ATV022	3.3	3	1,257	377
Site 4					
Site 5					
Site 6	ATH034	3.8	3	1,288	343
Site 7					
Site 8	ATH034	3.8	3	1,290	344
Site 9	ATV045	4.9	3	1,148	236
Site 10	ATV057	5.6	3	1,417	255
Site 11	ATH046	4.9	3	1,456	300
Site 12	ATH057	5.6	3	1,708	307
Average:					316

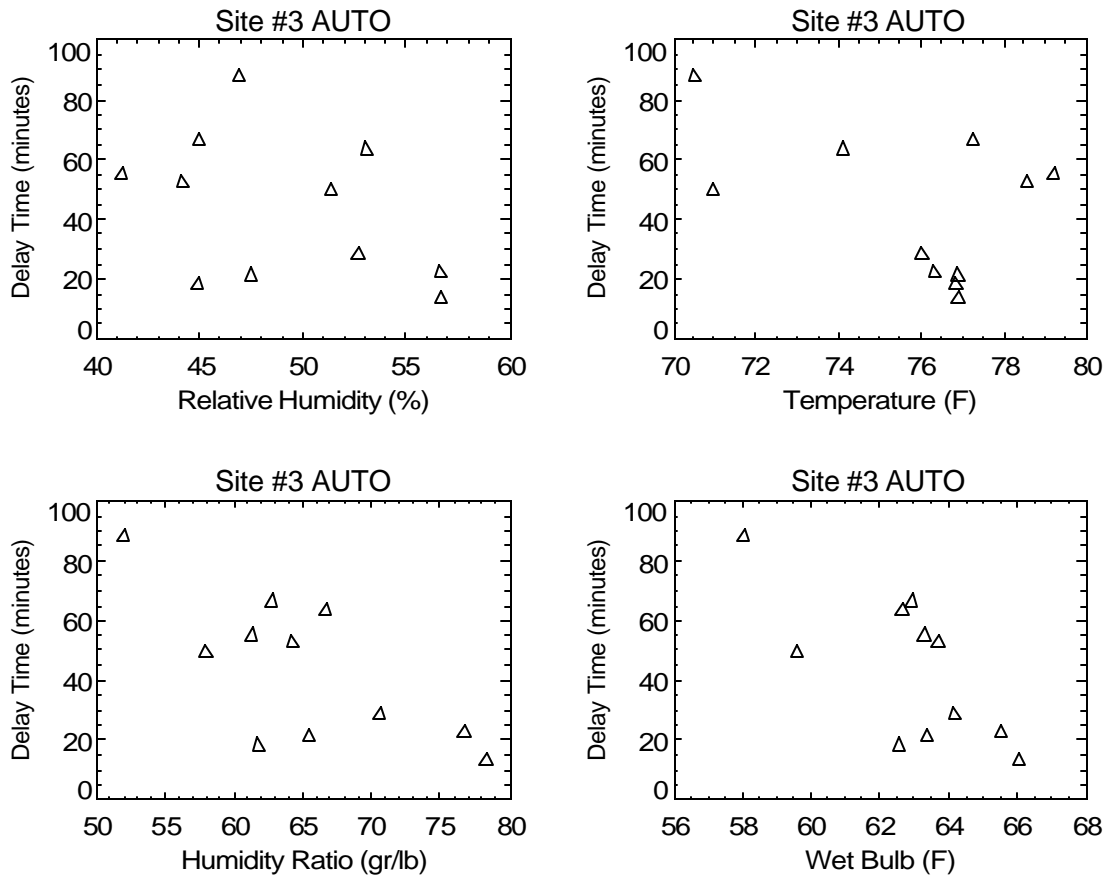


**Figure E-4. The Variation in Delay Time with Entering Conditions (Site 3, AUTO Fan Mode)**



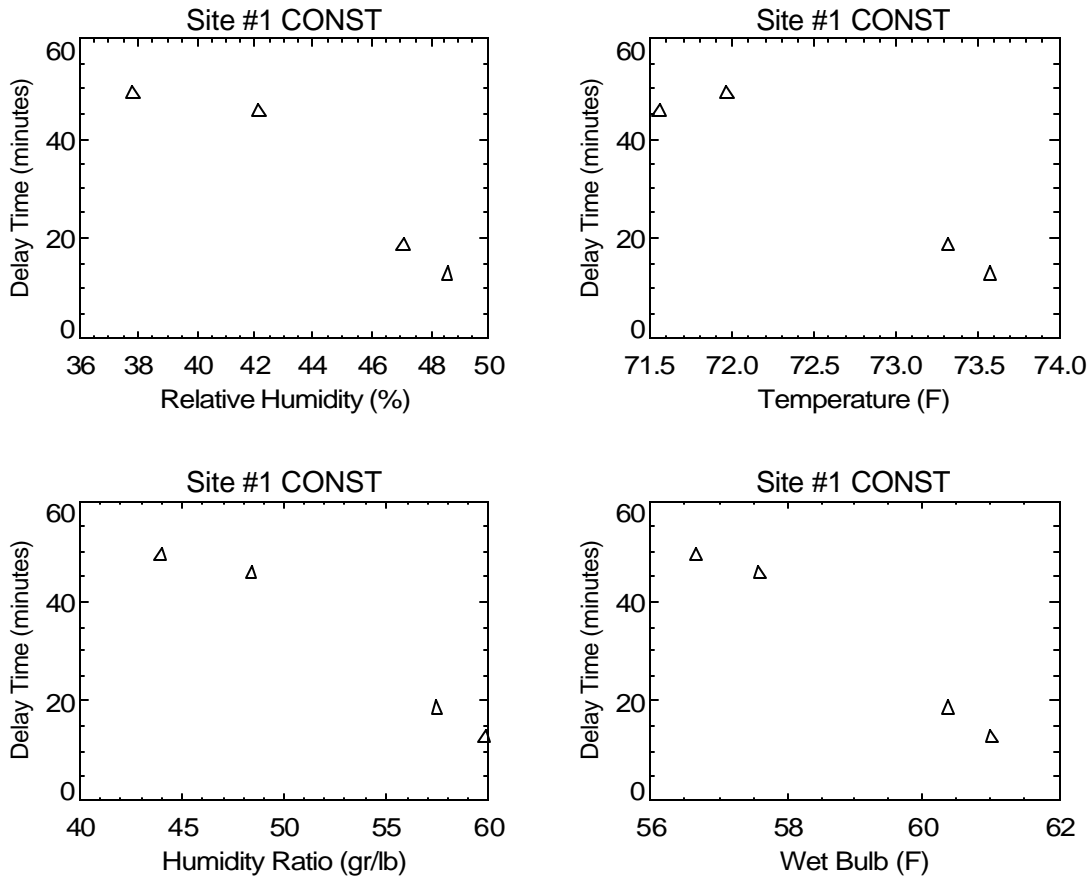


**Figure E-5. The Variation in Delay Time with Entering Conditions (Site 1, CONST Fan Mode)**

## Site 9 Latent Capacity Degradation Trends

This water-source heat pump ran in the constant fan mode from June 12, 1997 through August 24, 1997 when the cooling loads were largest. The occupants set the cooling set point very low at this site. The temperature entering the coil was around 72°F. Figure E-6 shows that the steady-state SHR of the cooling coil was dependent on the entering relative humidity. The steady-state SHR was very high at this site. High condenser loop temperatures alone do not seem to explain the high SHR. The low space temperature may have also caused the higher than expected SHR.

The heat pump is a Waterfurnace ATV045 with 28" x 25" three-row coil. The face area is 4.9 ft<sup>2</sup> for this nominally 4-ton system. The supply air flow during the cooling mode is 1,288 cfm (face velocity is 343 fpm).

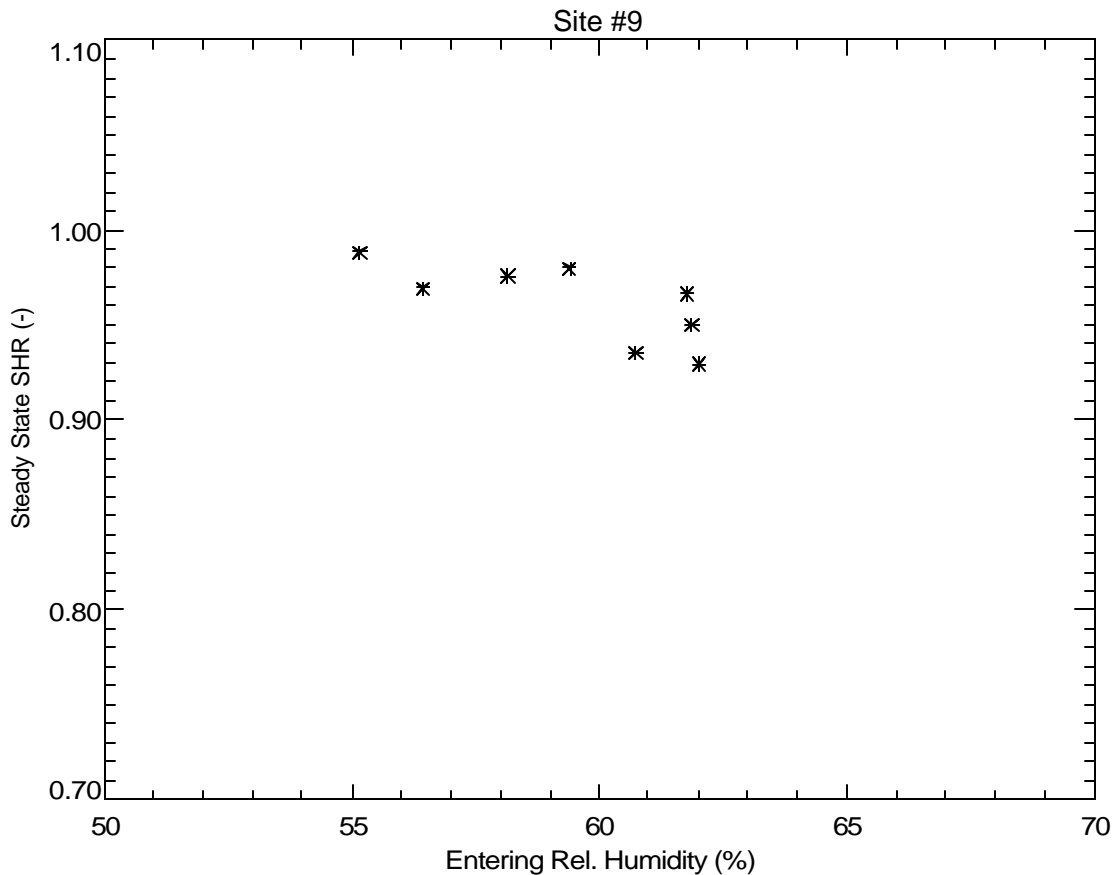


**Figure E-6. The Trend of Steady State SHR with Entering Relative Humidity**

Figure E-7 shows the trend of effective SHR with runtime fraction. Most of the data are for an SHR of 1. It is not clear what causes the lack of latent capacity.

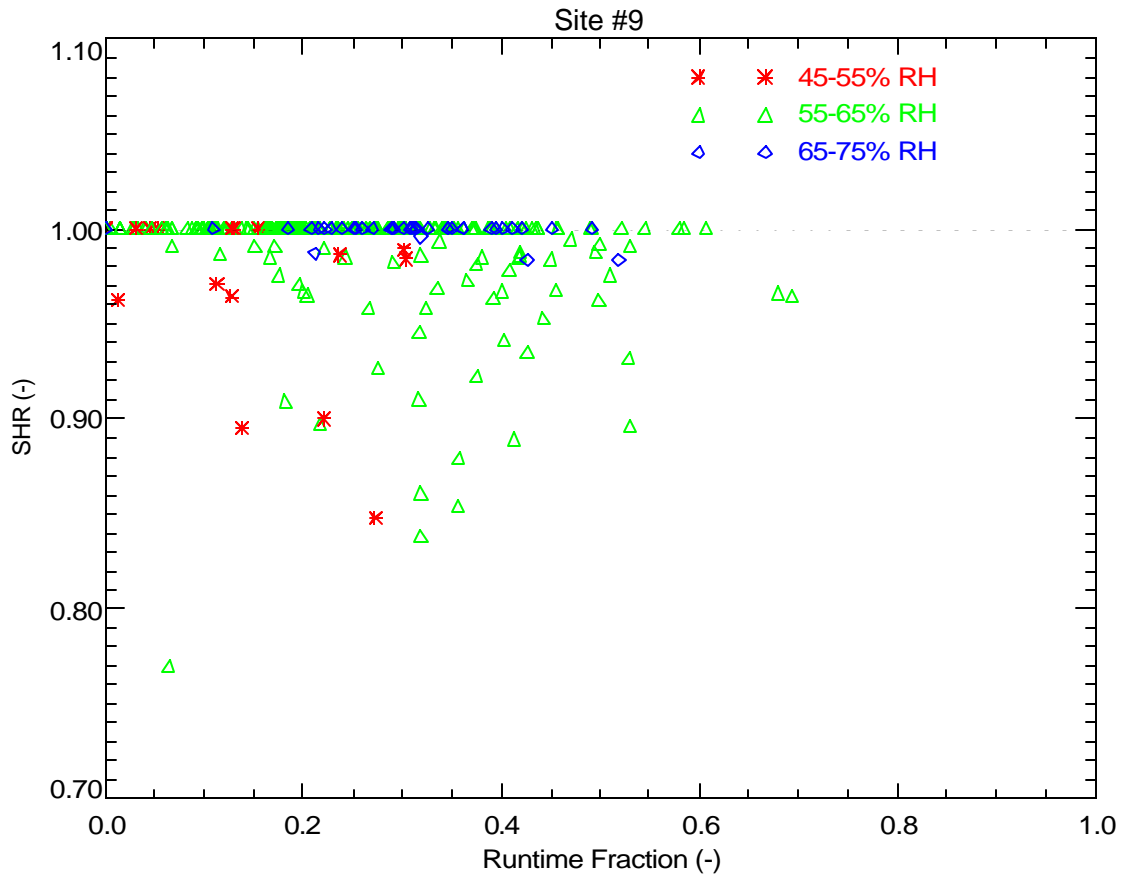
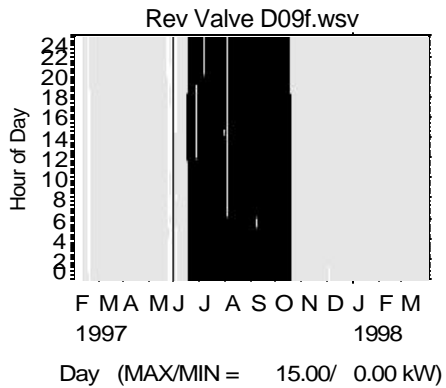
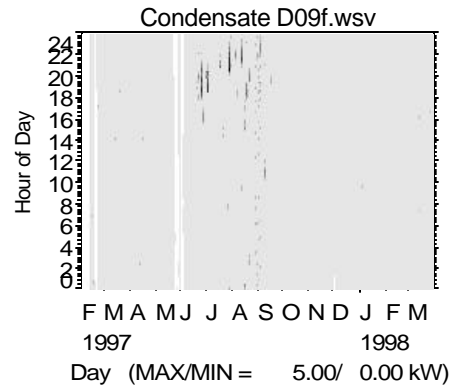
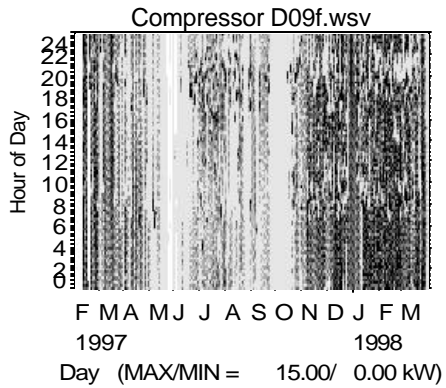
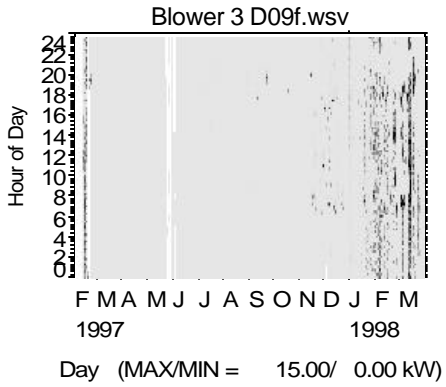
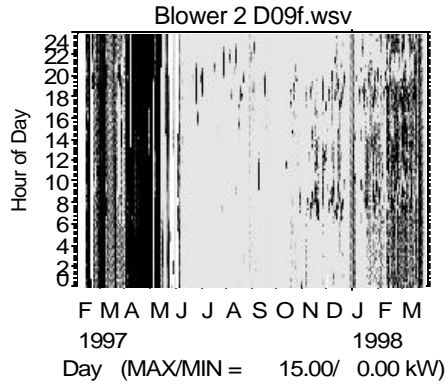
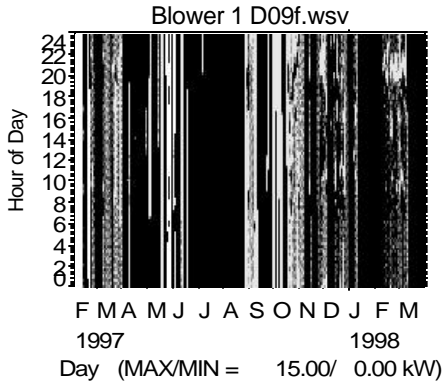


**Figure E-7. The Trend of SHR with Runtime Fraction at Various Entering Relative Humidity Levels**



**Site 12**  
**Latent Capacity Degradation Trends**

This water-source heat pump ran in the constant fan mode for more than 6 months from May through December 1997. We focused our analysis on data from June through October when the cooling loads were largest. The occupants set the cooling set point very low at this site. The temperature entering the coil was consistently 70-72°F. Figure E-8 shows that the steady-state SHR of the cooling coil was dependent on the entering relative humidity.

The heat pump is a Waterfurnace ATH057 with 20"x 40" three-row coil. This unit has a two speed compressor and ECM fan motor. The face area is 5.6 ft<sup>2</sup> for this nominally 5-ton system. The supply air flow during the cooling mode is 1,708 cfm (face velocity is 307 fpm).

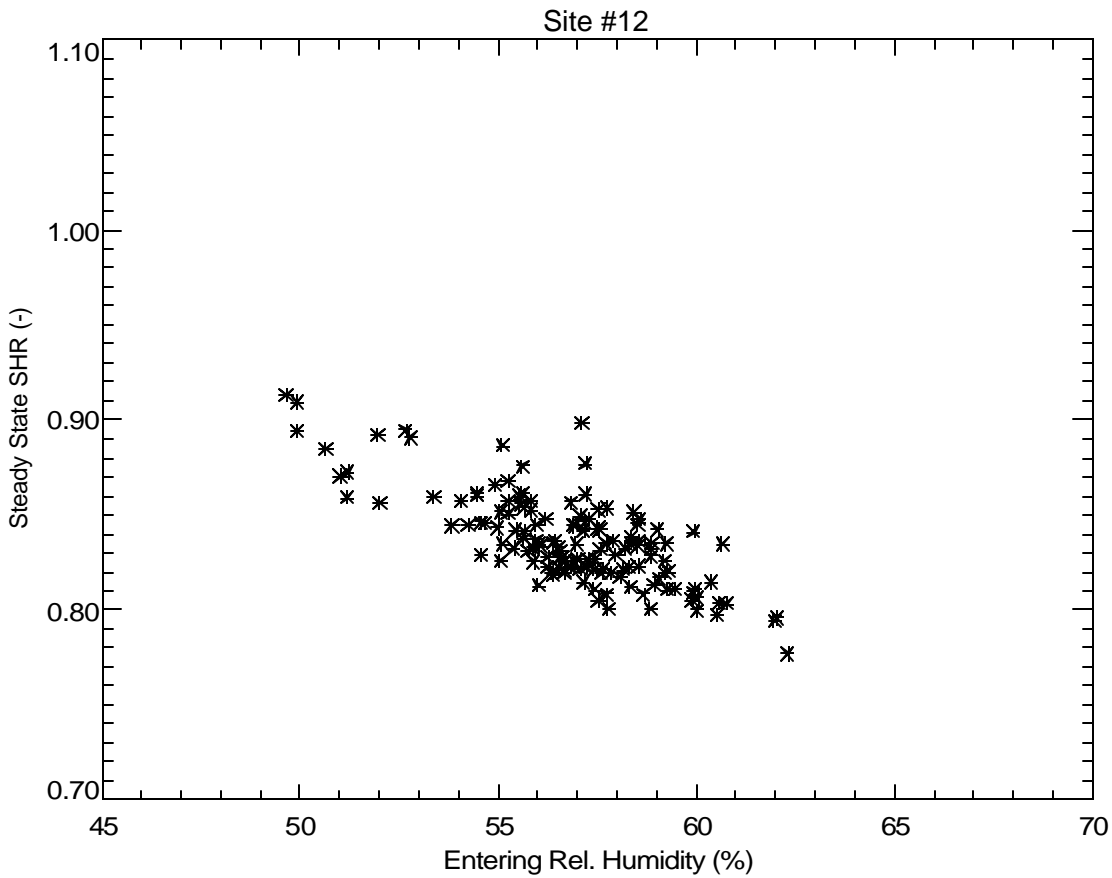


**Figure E-8. The Trend of Steady State SHR with Entering Relative Humidity**

Figure E-9 shows the trend of effective SHR with runtime fraction. The trends of SHR depend on the entering humidity for this system. While the latent degradation trends make sense at higher humidity levels (i.e., 55-65% and 65-75%), the trend is essentially flat at the lower humidity level (45-55%).

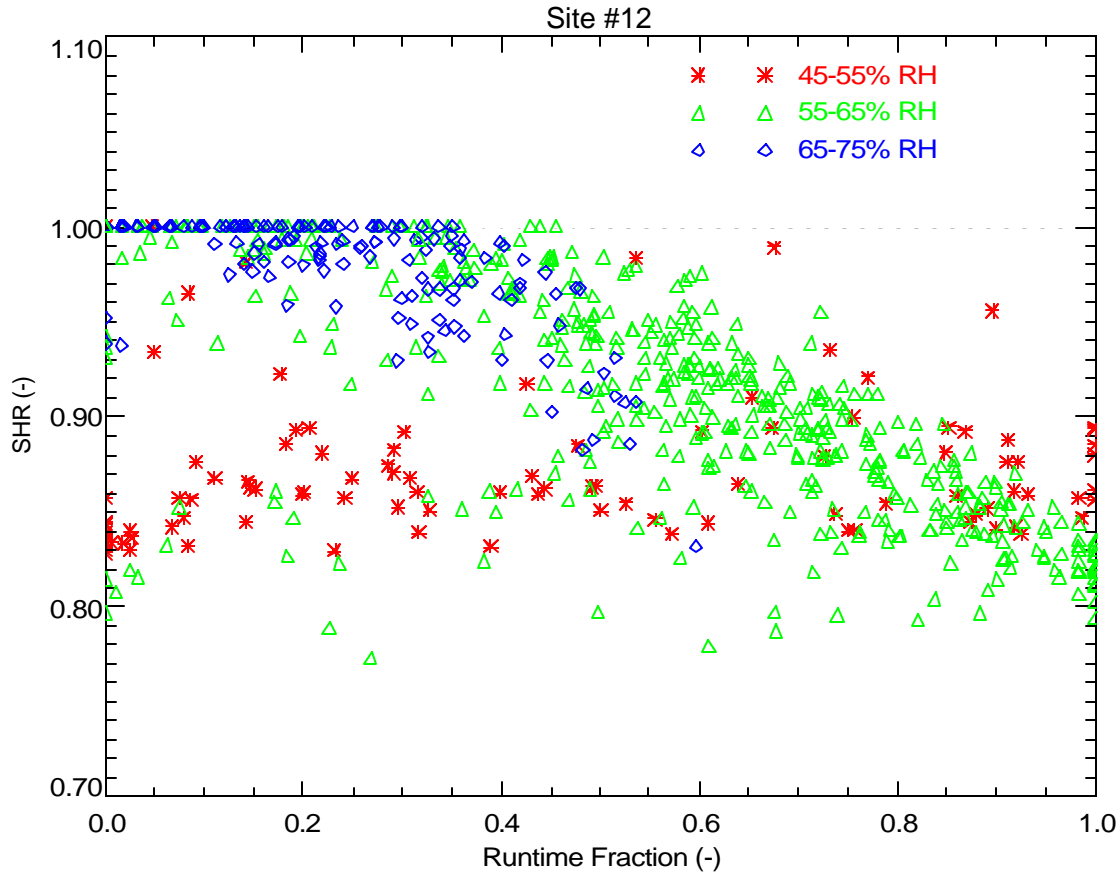
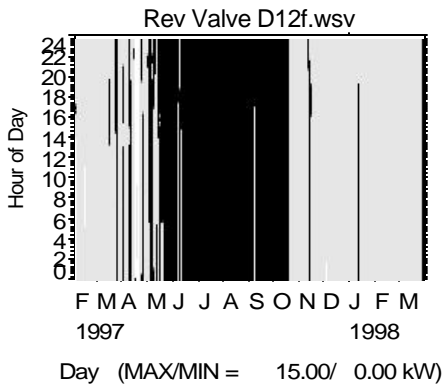
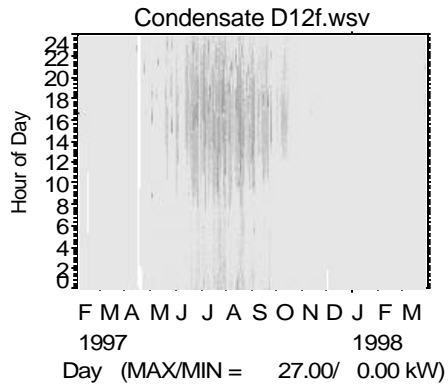
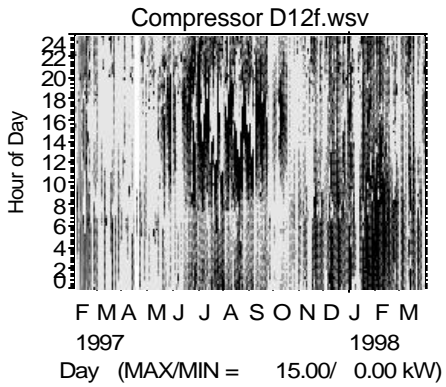
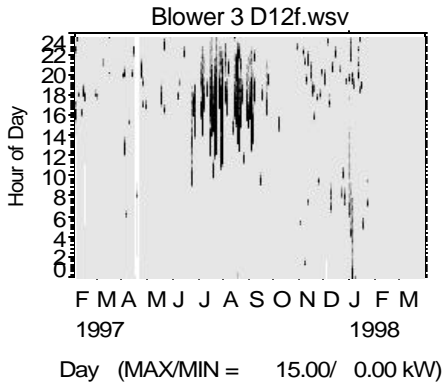
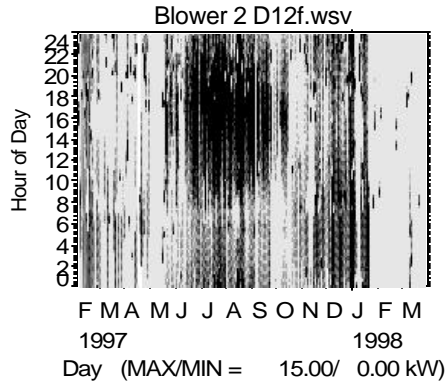
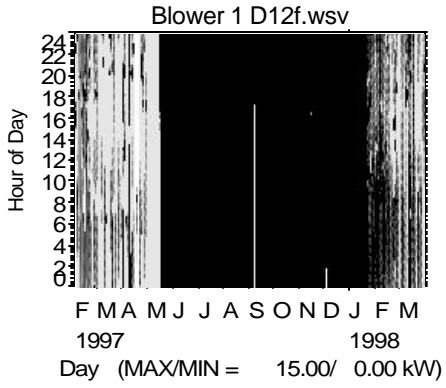


**Figure E-9. The Trend of SHR with Runtime Fraction at Various Entering Relative Humidity Levels**

The reason for the flatter trend may be due to the varying air flow with this system. The medium speed air flow of 1,708 cfm is used for the cooling during the on-cycle. However, the low speed air flow of 785 cfm, which is used during the off-cycle, would reduce the evaporation rate. This may explain why the latent capacity degradation is lower.

However, it is not fully clear why this would have more impact at drier conditions.



**Two commercial direct expansion packaged units in Texas**



## Condensate Time Delay – Unitary Rooftop Unit

This section calculates the time after compressor startup until the condensate pulse is detected by the condensate pump on a pair of Carrier unitary rooftop units in Houston, TX. The 5-minute data includes the exact time when the compressor turns on but the precise time of the condensate pulse is not known, since it could have occurred at any time during the 5-minute recording interval (therefore we only know the time delay within  $\pm 2.5$  minutes).

The airflow for the 25-ton unit was determined using the air enthalpy and condensate removal method. This method provided an airflow of 8,250 SCFM, or a normalized airflow of 330 SCFM/ton. Normalized indoor fan power for this unit was 0.67 watt/SCFM.

Airflow measurements for the 27.5-ton unit were inconclusive. Airflow for this unit was estimated using the normalized fan power for the 25-ton unit and the measured fan power. This estimate yields an airflow of 11,000 SCFM, or a normalized airflow of 400 SCFM/ton.

**Table E-3. Characteristics of Cooling Coils**

	Unit Model	Coil Face Area (ft <sup>2</sup> )	No of Rows	Fin Spacing / Tube Diameter	Supply Air (scfm)	Face Velocity (fpm)
Unit 1	50DJ-030	23.4	4	15 FPI, ½" Dia	11,000	470
Unit 2	50DJ-028	23.4	4	15 FPI, ½" Dia	8,250	352

Both units operated under a time-clock control, with separate operating patterns for weekends and weekdays. Condensate delay was calculated using data for the first two hours of startup each morning, under the assumption that the coil was sufficiently dry after being shutdown all night.

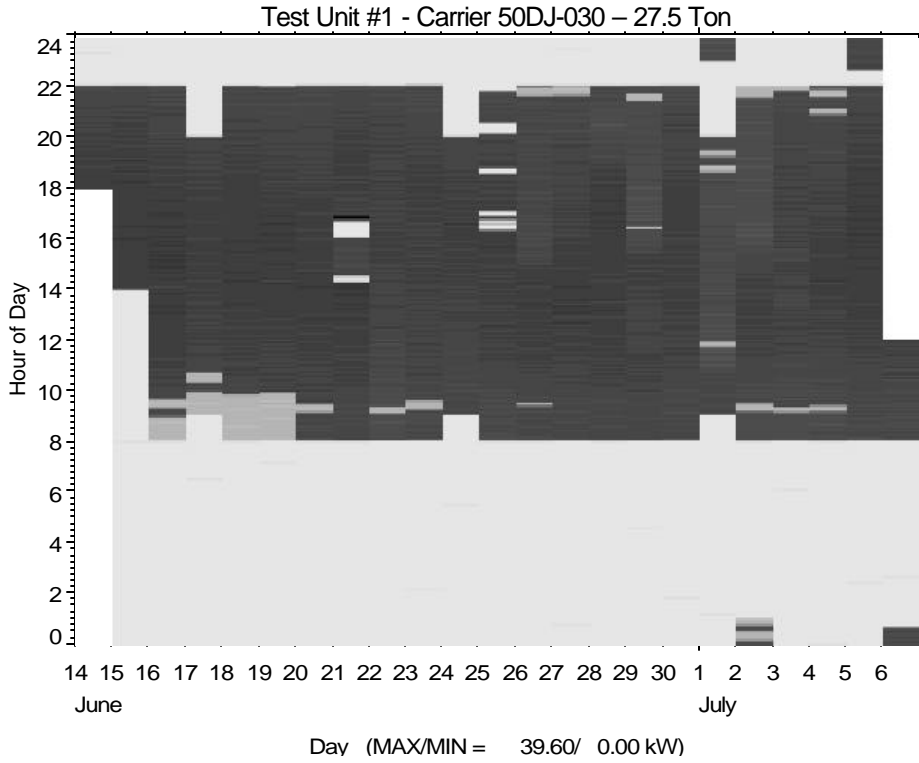


**Figure E-10. Test Unit #1 Operating Patterns**

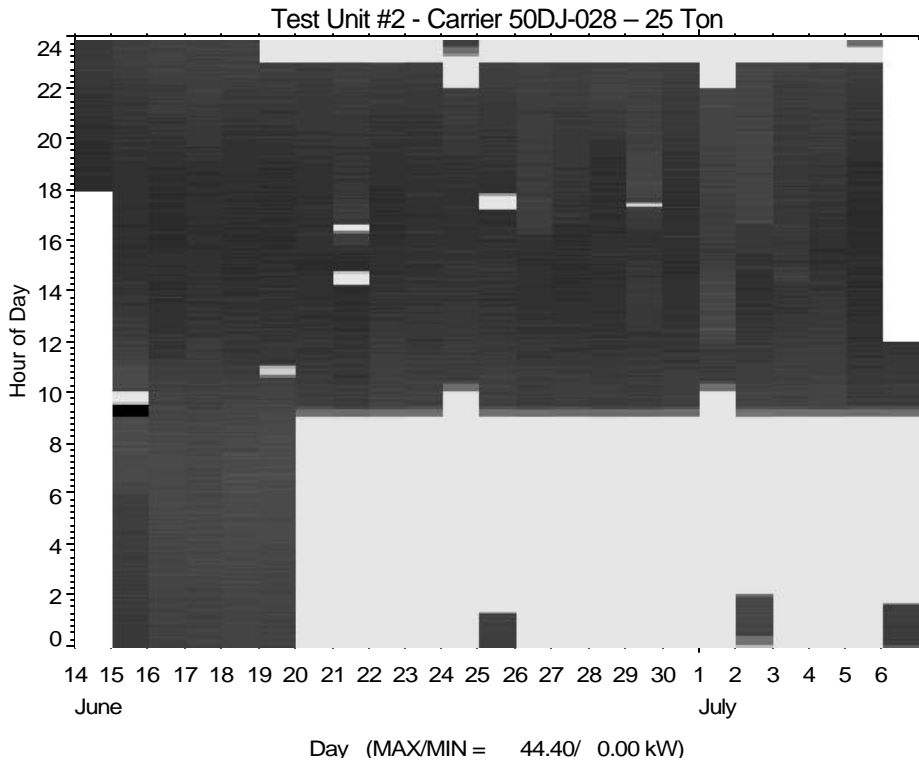


**Figure E-11. Test Unit #2 Operating Patterns**

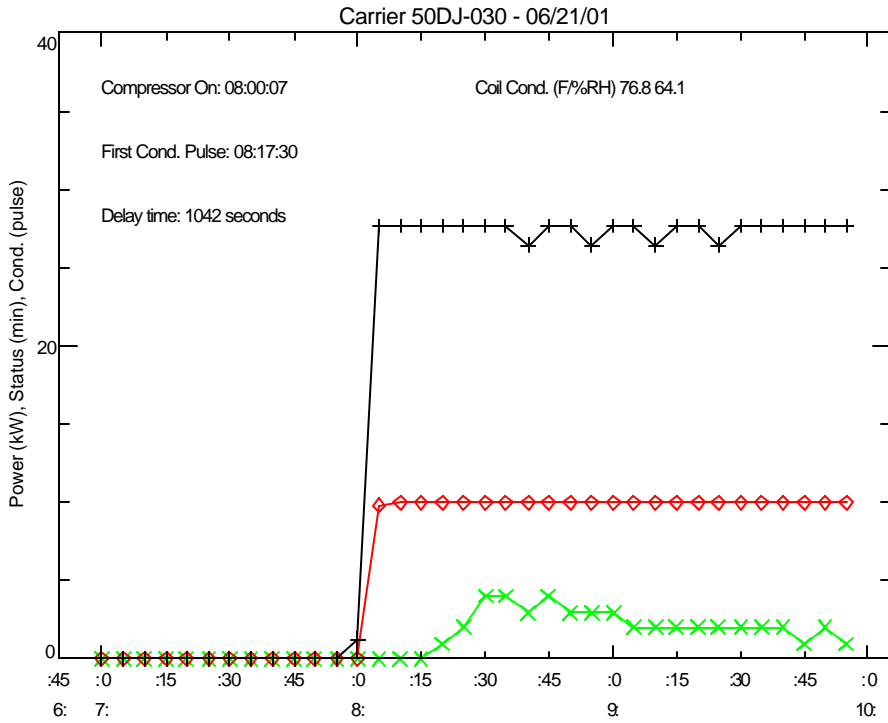


**Figure E-12. Sample Condensate Delay Data for Carrier 50DJ-030**

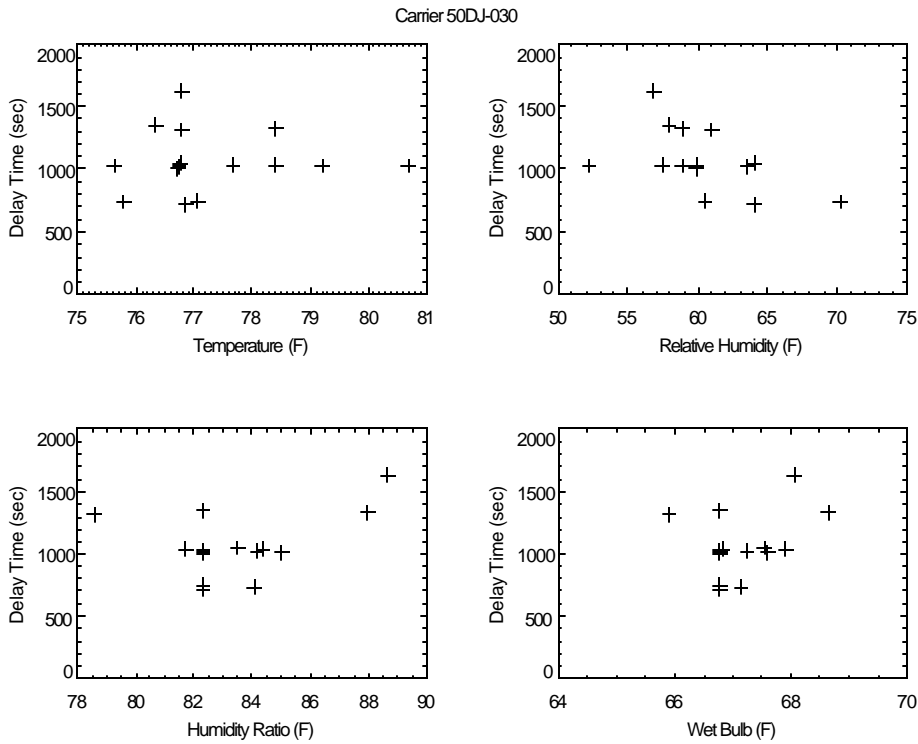


**Figure E-13. Condensate Delay Variation with Return Conditions for Carrier 50DJ-030**  
 Average Delay Time: 1,066 seconds (17.8 minutes)

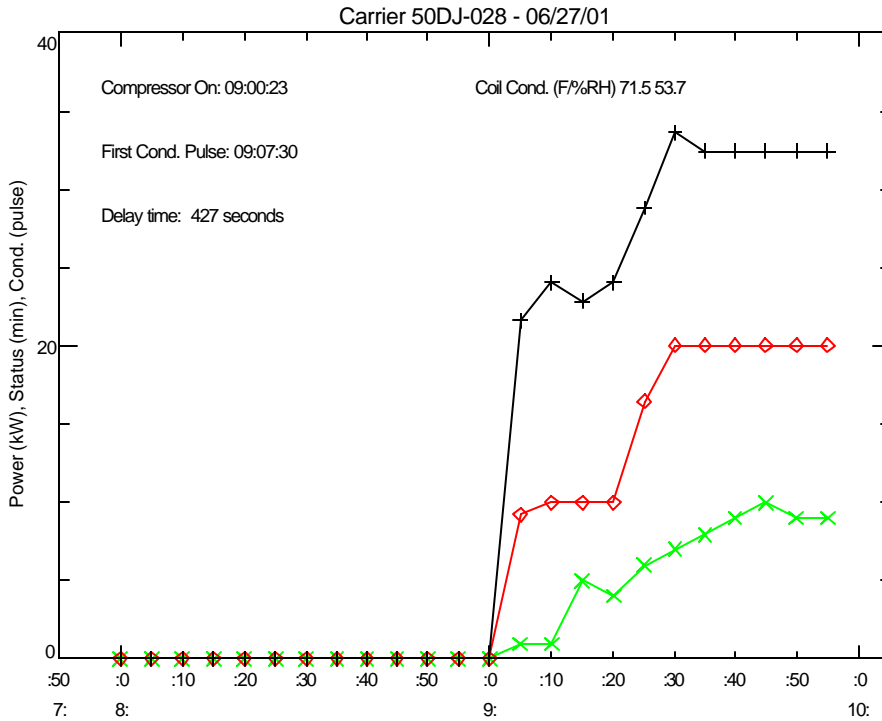


**Figure E-14. Sample Condensate Delay Data for Carrier 50DJ-028**

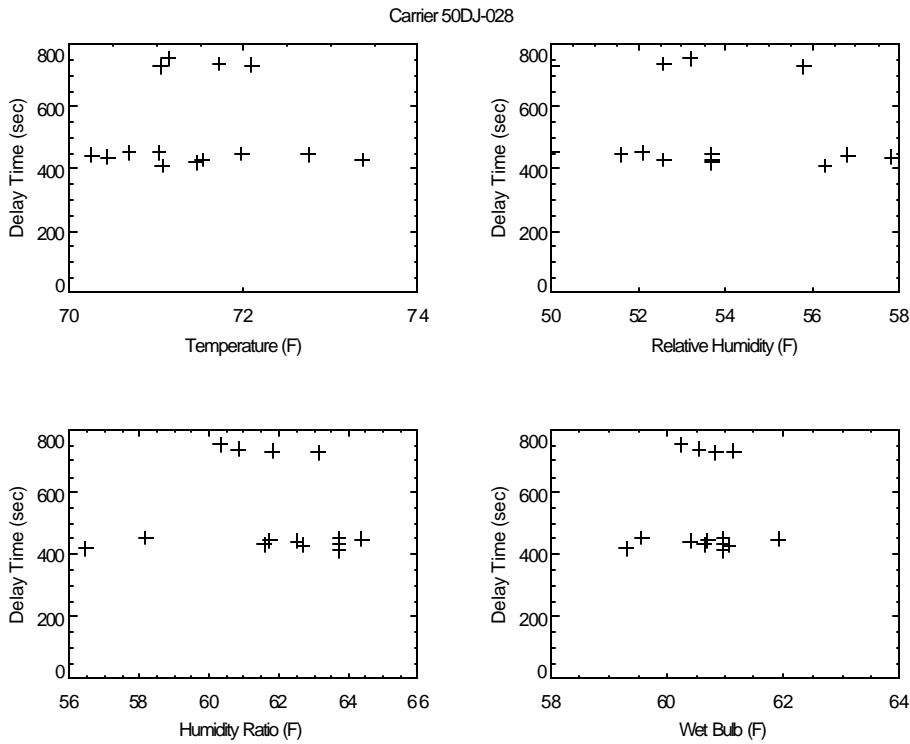


**Figure E-15. Condensate Delay Variation with Return Conditions for Carrier 50DJ-028**  
 Average Delay Time: 522 seconds (8.7 minutes)

## **APPENDIX F**

### **Impacts of Fan Overrun on Seasonal Energy Efficiency Ratio (SEER)**

Running the supply air fan for a period after the compressor turns off may decrease the degradation coefficient (Cd) and in turn increase the resulting Seasonal Energy Efficiency Ratio (SEER). To a certain extent, this small efficiency gain may be an artifact of the test procedure details for Tests C and D that are described in “Appendix M” of the Federal Rating Procedures and are included as part of ARI Standard 210/240-94. The text from Section 4.1.1.2 is quoted below:

*...During this last cycle, which is referred to as the test cycle, the indoor and outdoor test room ambient conditions shall remain within the tolerances specified in A4.1.3 during the cyclic dry-coil tests, all air moving equipment on the condenser side shall cycle “on” and “off” when the compressor cycles “on” and “off”. **The indoor air moving equipment shall also cycle “off” as governed by any automatic controls normally installed with the unit. This last requirement applies to units having an indoor fan time delay.** Units not supplied with an indoor fan time delay shall have the indoor air moving equipment cycle “on” and “off” as the compressor cycles “on” and “off”.*

While supply fan overrun strategies may produce a lower value of Cd – and as a result a higher SEER – we have evidence that this control approach negatively impacts the dehumidification performance of the unit. Furthermore we suspect that this control strategy does not actually increase seasonal energy efficiency in actual applications but is an artifact of the test procedure details.

The cyclic test procedure developed by NIST was specified to use “dry coil” conditions because of the difficulty of accurately measuring transient wet bulb temperatures. Kelly and Parken (1978) reported that the ratio of cyclic to steady state efficiency was similar at wet and dry coil conditions. Therefore, the dry test was conceived to require only thermocouple grids to measure the transient response of air conditioner cooling capacity. In order to eliminate cumulative impact of small errors in the temperature difference, the procedure only integrates the temperature difference when the fan operates. The equations to find the sensible capacity are:

$$Q_{cyc, dry} = \frac{60 \times \dot{V} \times C_{pa} \times \Gamma}{V_n' \times (1 + W_n)}$$

and

$$\Gamma = \int_{(time\ indoor\ fan\ on)}^{(time\ indoor\ fan\ off)} [T_{a1}(t) - T_{a2}(t)] dt$$

where:

$\dot{V}$  = indoor air flow rate (cfm)

$C_{pa}$  = specific heat of air (Btu/lb-F)

$V_n'$  = specific volume of air (ft<sup>3</sup>/lb)

$W_n$  = humidity ratio (lb/lb)

$Q_{cyc, dry}$  = total cooling over a cycle consisting of one compressor “off” period & one compressor “on” period (Btu)

$T_{a1}(t)$  = dry-bulb temperature of air entering the indoor coil (F) at time (t)

$T_{a2}(t)$  = dry-bulb temperature of air leaving the indoor coil (F) at time (t)

Since the sensible capacity integration is only during fan operation, extending fan operation also extends the integration period and tends to increase the cyclic sensible capacity. Fan power is

small for a short interval, so the result is often to increase the cyclic EER. The laboratory data presented in the next section illustrates this concept.

### SEER Cyclic Testing Results

Table F-1 summarizes the measurements and calculations for finding the degradation coefficient as per the federal test procedures and ARI 210/240. These tests were completed in the Laboratory at FSEC on Coil 2 in December 2002. Sheetmetal was manually placed over the return air entrance when the fan was off in an effort to mimic the damper arrangement specified in ARI 210/240. The test approach for a given set of entering conditions was to:

1. Run one cycle (Test #1) with the compressor on for 60 minutes to determine the steady state capacity and EER.
2. Run three 30-minute cycles with the compressor off for 24 minutes and on for 6 minutes. The supply fan cycles on and off with the compressor. For the third cycle (Test #3) integrate the required cyclic capacity and power readings.
3. Run three 30-minute cycles with the compressor off for 24 minutes and on for 6 minutes. The supply fan remains on for 90 seconds after compressor stops. For the third cycle (Test #6) integrate the required cyclic capacity and power readings.
4. Run three 30-minute cycles with the compressor off for 24 minutes and on for 6 minutes. The supply fan remains on continuously. For the third cycle (Test #9) integrate the required cyclic capacity and power readings.

At dry coil conditions, the steady state results from Test #1 correspond to Test C conditions. The integrated cyclic results from Tests #3 and #6 correspond to Test D. The results in Table F-1 show that the calculated Cd for this system is 0.065 with no fan delay. Figure F-1 graphically shows this data.

The gross EER for the system at Test B conditions, excluding the indoor blower effects, is 12.36 Btu/Wh (see Table F-2). If we take away the fan heat and add in the fan power assuming that the supply fan uses the default 0.365 Watts per cfm, then the net EER at Test B conditions is 10.26 Btu/Wh. Applying the Cd calculation, the SEER of the system becomes 9.92 Btu/Wh.

If the fan operates for another 90 seconds after the compressor stops, then the cyclic sensible capacity integrated over 7.5 minutes (instead of 6 minutes) increases slightly and the resulting value of Cd decreases slightly to 0.062 (see Table F-1 and Figure F-2). The SEER with fan overrun controls becomes 9.94.

**Table F-1. Summary of Conventional Test C and Test D Measurements and Calculations to Find Cd**

	Test C (dry steady state)			Test D (dry cyclic)				Part Load Fraction (PLF)	Degradation Coefficient (Cd)
	Steady-State Sensible NET Capacity (Mbtu/h)	Steady State Unit & Fan Power (kW)	Steady-State NET EER (Btu/Wh)	Cyclic Sensible NET Capacity (MBtu)	Cyclic Unit & Fan Power (kWh)	Cyclic NET EER (Btu/Wh)	Cooling Load Fraction (CLF)		
	[1]	[2] + [3]	[4] = [1]/([2]*[3])	[5]	[6] + [7]	[8] = [5] / ([6]*[7])	[9] = [5] / ([1]*[9.5])	[10] = [8] / [4]	[11] = ([1-10])/([1-9])
Dry Coil Test - No Fan Delay	24.8	2.735	9.07	2.289	0.267	8.58	0.18	0.95	0.065
Dry Coil Test - w/ 90 sec delay	24.8	2.735	9.07	2.373	0.275	8.61	0.19	0.95	0.062

Notes

1. [5] is the sensible capacity integrated only when the fan is on

2. The compressor power [6] is integrated over the entire 30 minute interval, the fan power [7] is only integrated when the fan

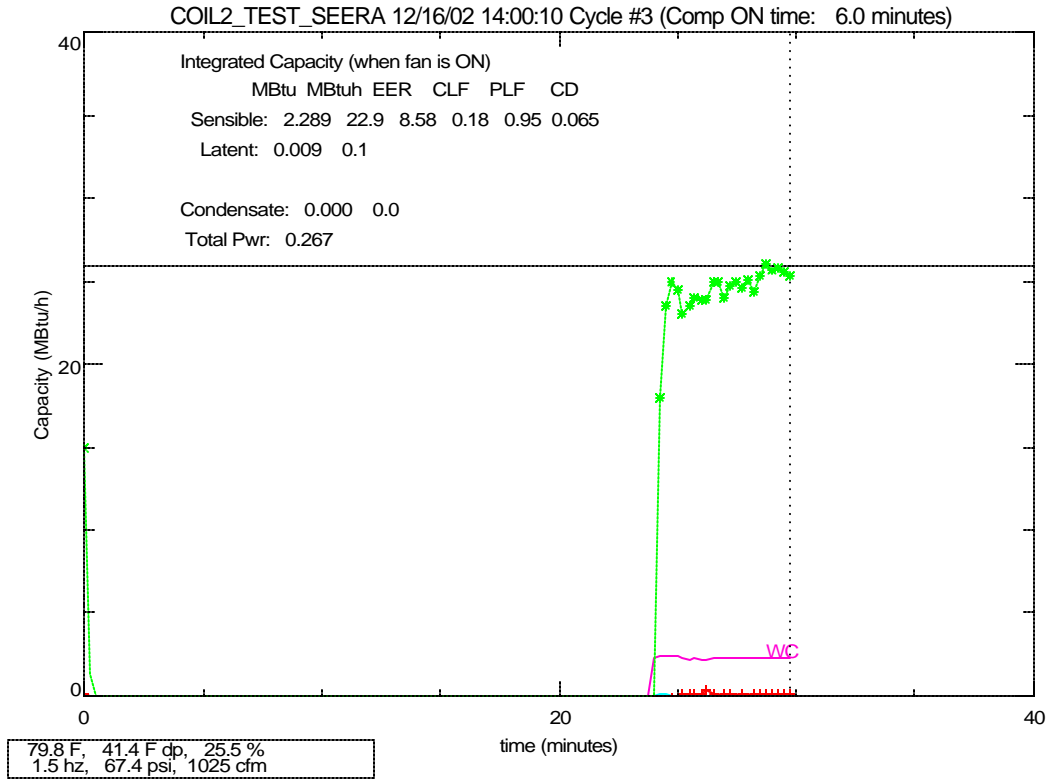


**Figure F-1. Integrated Sensible Capacity for Dry Coil Cyclic Test – No Fan Overrun**

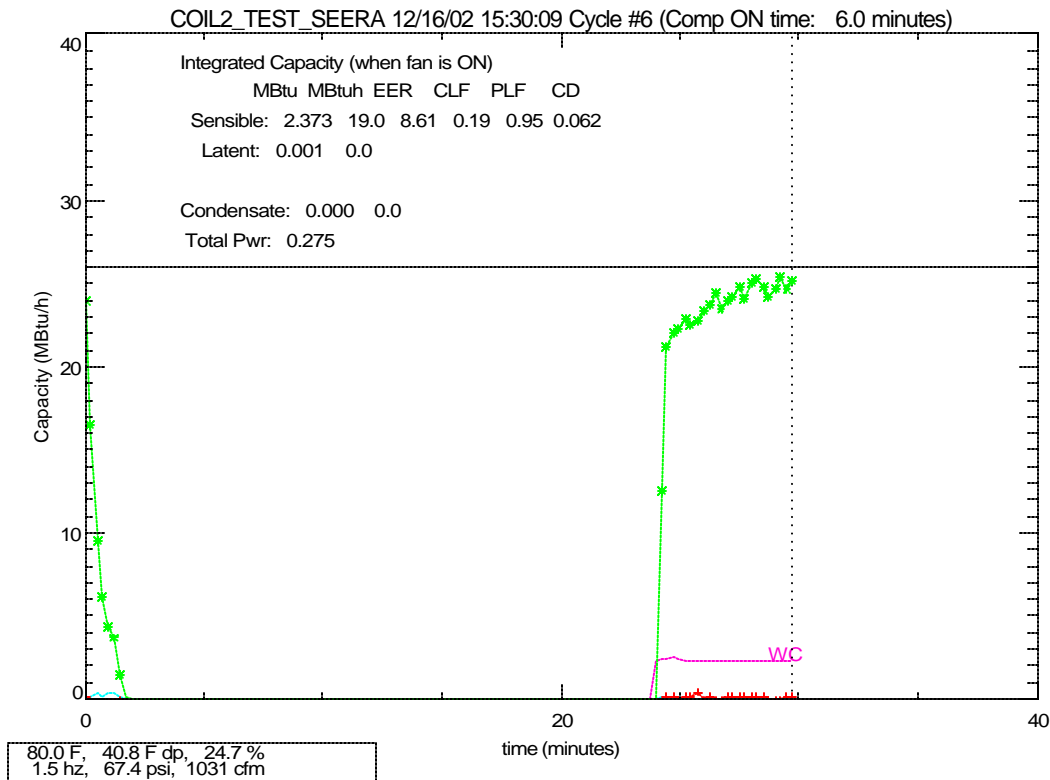


**Figure F-2. Integrated Sensible Capacity for Dry Coil Cyclic Test – with 90 sec Fan Overrun**



## Wet Coil Test Procedure to Find Cd

Several researchers have also completed cyclic tests in the lab at wet coil conditions (Henderson 1990; Shen et al. 2004). Both papers demonstrated that the Cd calculated at wet conditions was generally the same as the value calculated with the dry coil tests – as had been reported by Kelly and Parken (1978). In these cases the laboratory instrumentation was able to measure the transient latent capacity. Both datasets demonstrate that an alternate method to find Cd at wet coil conditions would be possible without the added expense of transient humidity measurements. Table F-2 shows the steady state test results at Test B conditions and completes a modified cyclic test at wet coil conditions with the fan running continuously. Basing all calculations on gross capacity and EER, a similar value of Cd is determined. In this case the sensible capacity is integrated over the entire 30-minute interval. Since the sensible capacity over the entire interval is equivalent to total capacity, the need for transient humidity measurements is eliminated. The value of 0.057 calculated for Cd with this approach is very similar to value of 0.065 calculated by the traditional dry coil method.

**Table F-2. Alternative Wet Coil Measurements and Calculations to Find Cd**

	Test B (wet steady state)			"Modified Test D" (wet cyclic)				Part Load Fraction (PLF)	Degradation Coefficient (Cd)
	Steady-State Total GROSS Capacity (MBtu/h)	Steady State Unit Power (kW)	Steady-State GROSS EER (Btu/Wh)	Cyclic Sensible NET Capacity (MBtu)	Cyclic Unit Power (kWh)	Cyclic Gross EER (Btu/Wh)	Cooling Load Fraction (CLF)		
Wet Coil Test	[1*] 30.4	[2] 2.463	[4]= [1*] / [2] 12.36	[5*] 2.875	[6] 0.244	[8] = [5*] / [6] 11.78	[9] = [5*] / ([1*] × 0.5) 0.19	[10] = [8] / [4] 0.95	[11] = (1 - [10]) / (1 - [9]) 0.057

Notes

1. The SHR of the coil (based on gross capacity) is 0.75
2. [1\*] is the steady-state total capacity (sensible and latent) of the cooling coil w/o fan heat
3. [5\*] is the integrated sensible capacity of the coil over the 30 minute interval with the fan operating continuously  
The sensible and total capacity are equivalent over the interval since there is no net condensate removal

## Is the Efficiency Benefit of Fan Overrun Real?

At actual wet coil cyclic conditions, the fan overrun strategy clearly decreases the latent capacity of the cooling coil. Figure F-3 and Figure F-4 illustrate this point. Both graphs show the sensible and latent capacity for the third cycle of cyclic operation at wet coil conditions. The condensate removed by the coil is also shown. The total condensate removed over the cycle with the fan cycling off (Figure F-3) is equivalent to 0.578 MBtu (0.545 lbs). With the fan remaining on for an additional 90 seconds (Figure F-4), the total condensate removed drops by 44% to 0.322 MBtu (0.304 lbs). The impact is especially strong because the value of  $t_{wet}$  for this coil is greater than 6 minutes.

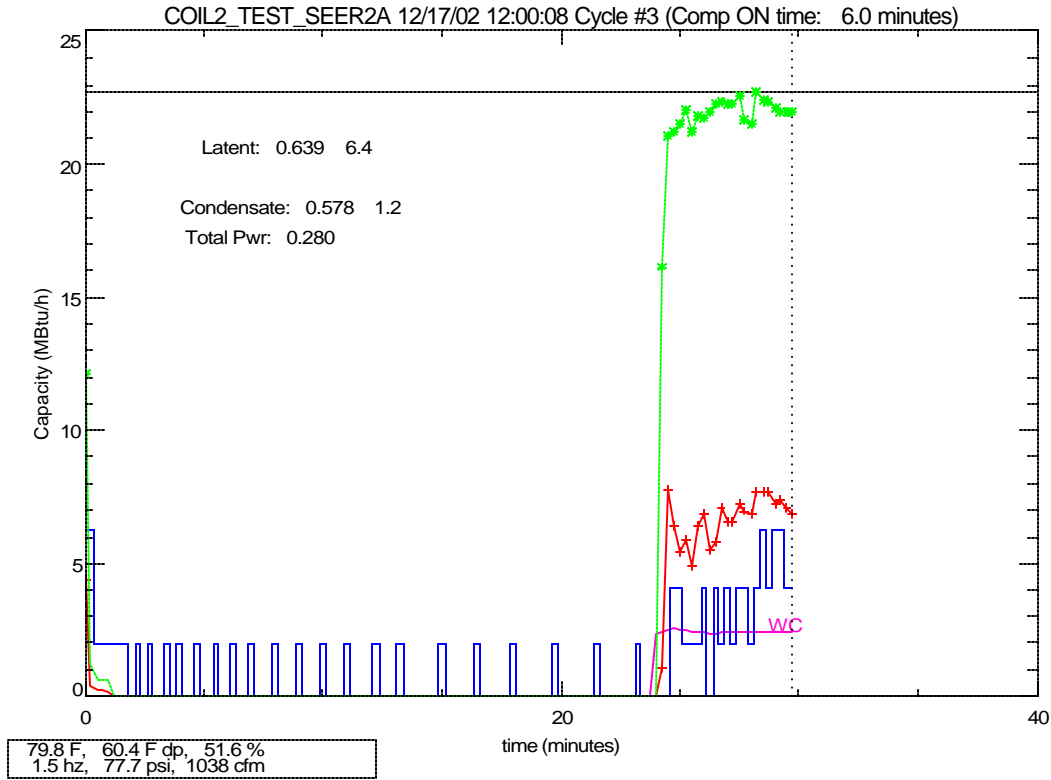


**Figure F-3. Cyclic Sensible and Latent Capacity for Cyclic Test – Fan Cycles with Compressor**

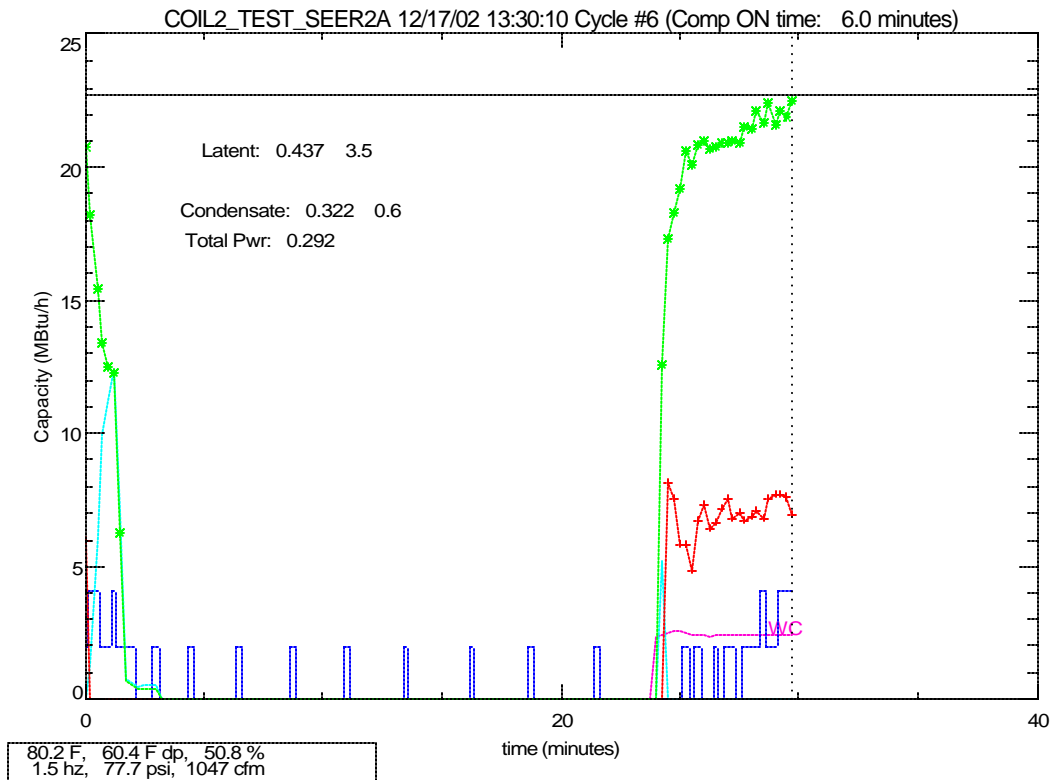


**Figure F-4. Cyclic Sensible and Latent Capacity for Cyclic Test – Fan Cycles with Compressor**

While it is clear that latent capacity degrades, perhaps there is still an efficiency benefit? To test this assumption we determined the cyclic capacity and EER by adding the integrated sensible capacity (when the fan operated) and condensate to get total capacity. We then calculated the EER on a gross and net basis. The results in Table F-3 show that the EER on a gross basis dropped slightly when the 90 second fan overrun strategy was used. This small impact makes sense because fan operation should in theory adiabatically convert latent capacity into sensible cooling. When the additional fan power and fan heat is considered, the Net EER of the system actually decreases by 4%.

**Table F-3. Impact of Fan Control on Gross and Net Efficiency**

	Gross EER (Btu/Wh)	Net EER (Btu/Wh)
Cycling Fan	11.15	9.47
90 sec Fan Overrun	11.09 (-1%)	9.10 (-4%)
Notes:	$\text{Gross EER} = \frac{(Q_{\text{sensible}} + Q_{\text{condensate}})}{\text{Unit Power}}$ $\text{Net EER} = \frac{(Q_{\text{sensible}} + Q_{\text{condensate}} - \text{Fan Heat})}{(\text{Unit Power} + \text{Fan Power})}$	

### Summary

This analysis demonstrates that the fan overrun strategy – which can result in a modest increase in the calculated SEER – actually degrades both latent capacity and part load efficiency. The SEER boost is an artifact of the calculation and test procedures to determine the cyclic sensible capacity. In reality, the gross coil efficiency is not affected by the additional fan operation: it simply changes moisture on the coil into sensible cooling. After considering the additional fan power, the Net efficiency actually decreases slightly.

### References

Henderson, H.I. 1990. An Experimental Investigation of the Effects of Wet and Dry Coil Conditions on Cyclic Performance in the SEER Procedure, Proceedings of USNC/IIR Refrigeration Conference at Purdue University, July 1990, West Lafayette, IN.

Kelly, G.E. and W.H. Parken. 1978. Method of testing, rating and estimating the seasonal performance of central air conditioners and heat pumps operating in the cooling mode. NBSIR 77-1271, Report by National Bureau of Standards. April.

Shen, B., J. Braun, and E. Groll. 2004. Steady State Cyclic Performance Testing of Packaged R-410A Units. Final Report. Baseline test report prepared by Purdue University for Southern California Edison Co. November. [www.hdac-des-pier.com/index.html](http://www.hdac-des-pier.com/index.html).

## **APPENDIX G**

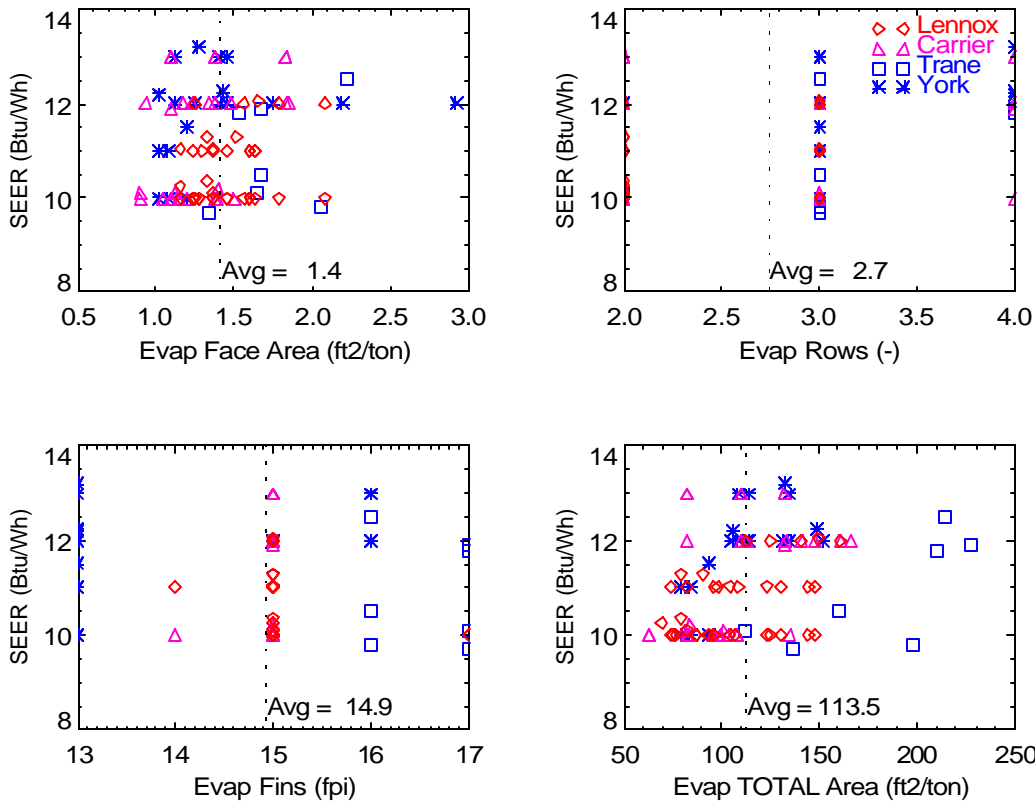
### **Analysis of Manufacturer's Evaporator Specifications**

Equipment specifications from several manufacturers were entering into a data base for analysis (more than 500 entries). Data were entered for packaged and split systems, air handlers and evaporator coils.

For most equipment, basic information about the evaporator coil was available. This information typically included coil face area, number of rows and fin spacing. For this data we could calculate the total fin area of the coil using the equation below. The equation assumes that the evaporator row spacing was 1 inch.

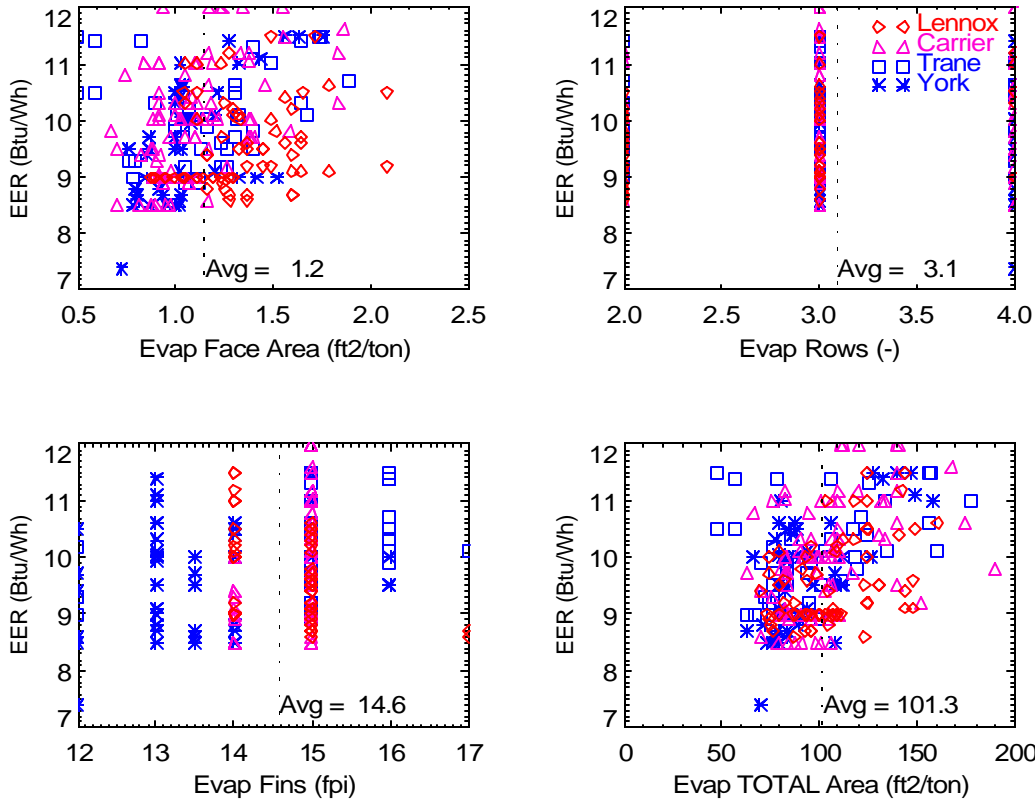
$$\text{Total Area (ft}^2\text{)} = 2 \times (\text{Face Area}) \times (\text{fpi}) \times (\text{rows})$$

Figure G-1 shows that SEER has only a weak relationship to normalized face area for residential equipment. The total evaporator fin area (which includes the impact of rows and fins) does demonstrate a slightly more noticeable trend. On average, these residential evaporators had 1.4 ft<sup>2</sup> of face area and 113.5 ft<sup>2</sup> of total fin area per nominal ton, with about 15 fpi and slightly less than 3 rows.



**Figure G-1. Variation of (residential) SEER with evaporator coil characteristics**

Figure G-2 shows the same data for commercial packaged units that are rated according to EER. A more consistent trend of EER with evaporator size is apparent for these units. Compared to residential units, the face area and total fin area of the evaporator are slightly lower (this probably reflects the greater premium placed on keeping unit size/ volume smaller for commercial rooftop units).



**Figure G-2. Variation of (commercial) EER with evaporator coil characteristics**

The normalized evaporator face area and total fin area are plotted against unit size in Figure G-3. The data are for packaged systems as well as air handlers and evaporator coils (though the larger units are mostly packaged systems). Not surprisingly, evaporator size is highly variable for smaller systems, but becomes more predictable at large sizes.

	Evaporator Face Area (ft <sup>2</sup> /ton)	Evaporator Total Area (ft <sup>2</sup> /ton)	Evaporator Rows (-)	Evaporator Fin Spacing (fpi)
Residential Packaged	1.41	113.5	2.8	14.9
Commercial Packaged	1.15	101.3	3.1	14.6
All units	1.23	103.6	3.0	14.3

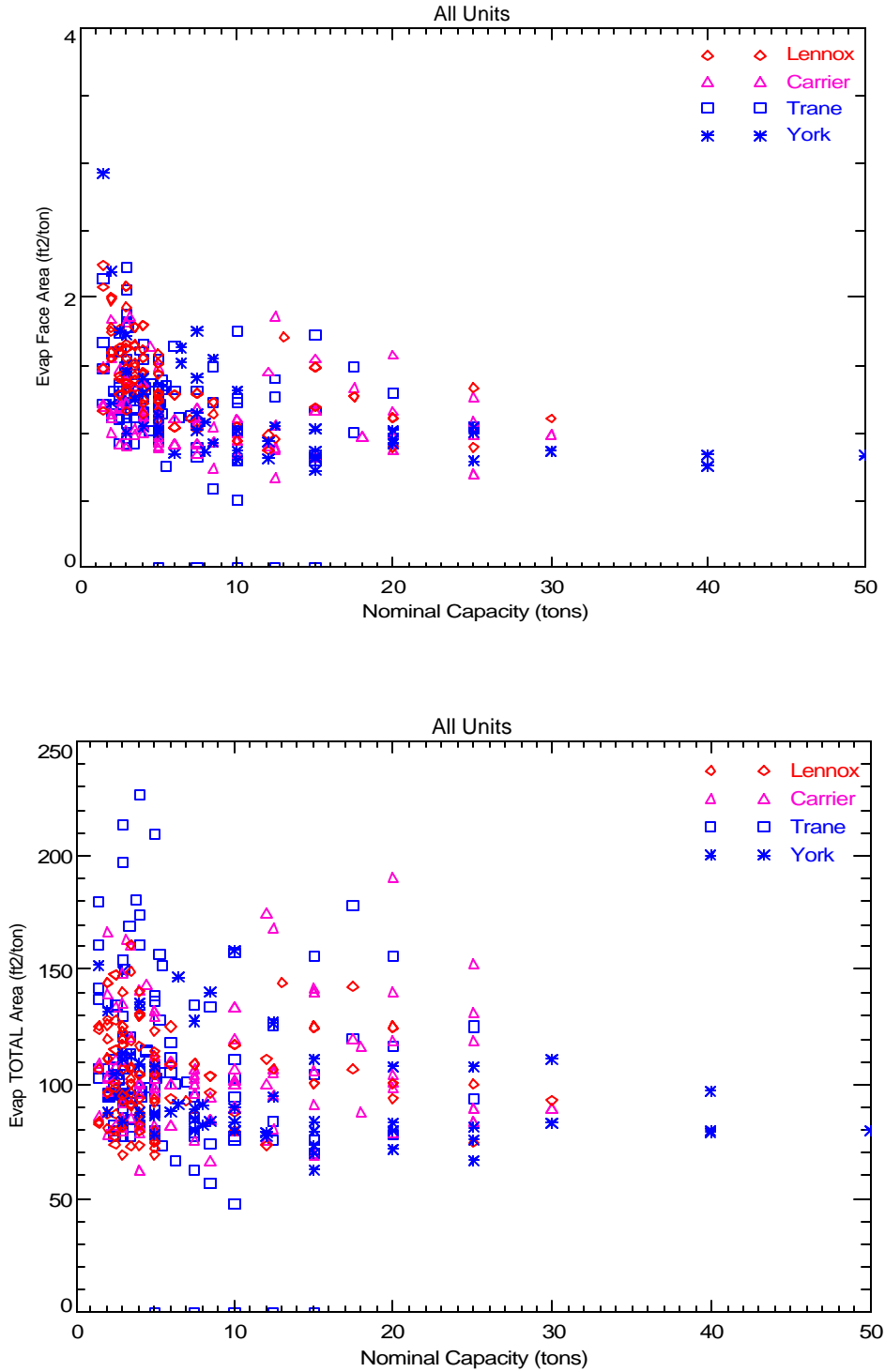


**Figure G-3. Variation of coil size with unit tons (packaged units, air handlers, evap coils)**

Jacobi and his co-workers completed a series of laboratory measurements of the amount of moisture that could be retained on a coil. They looked at several factors including fin type, velocity, etc. The typical range of moisture retention was from 50-120 gram per m<sup>2</sup> of fin face

area. While not all the details for each coil are not known in this case, the plot below assumes that all the coils can hold 74 grams/m<sup>2</sup> (or 0.015 lb/ft<sup>2</sup>). Based on this, the average evaporator holds about 1.5-2 lbs of water per nominal ton. The moisture holding capacity of the unit from Henderson (1998) is included on the plot for reference. This value (about 2.1 lbs for a 3 ton unit) is towards the low end of the range.

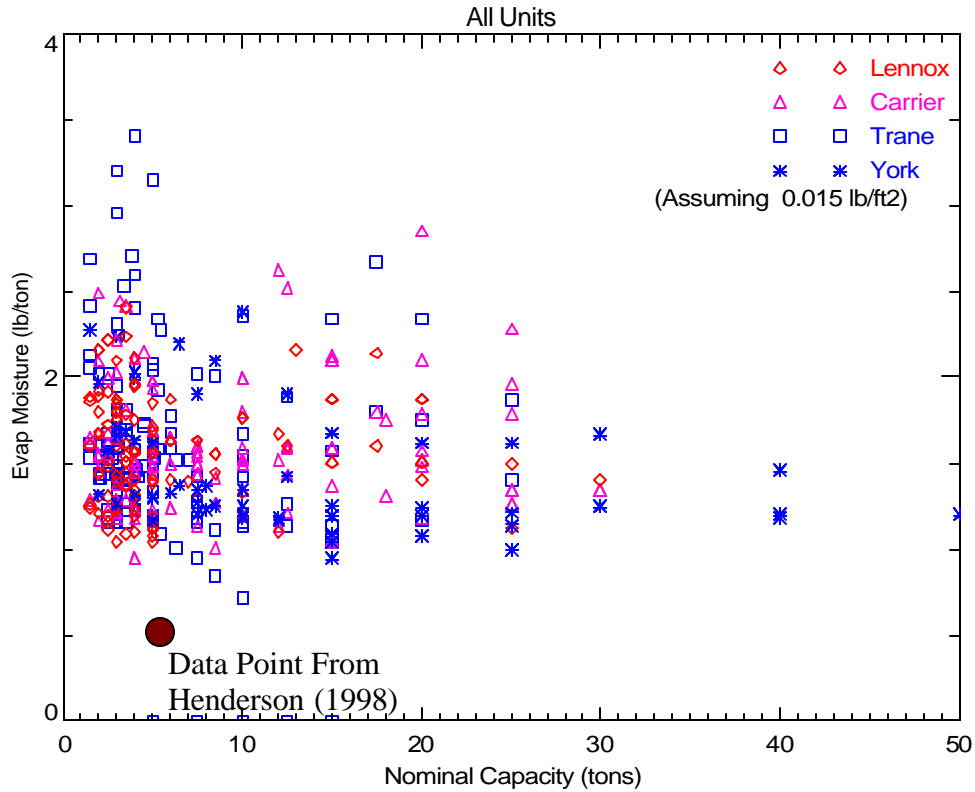
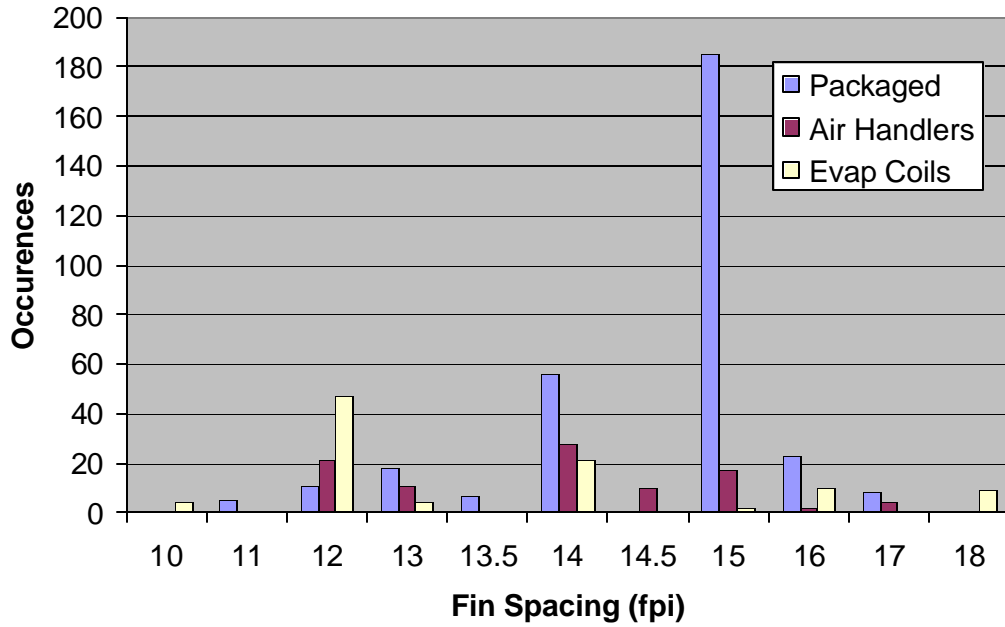
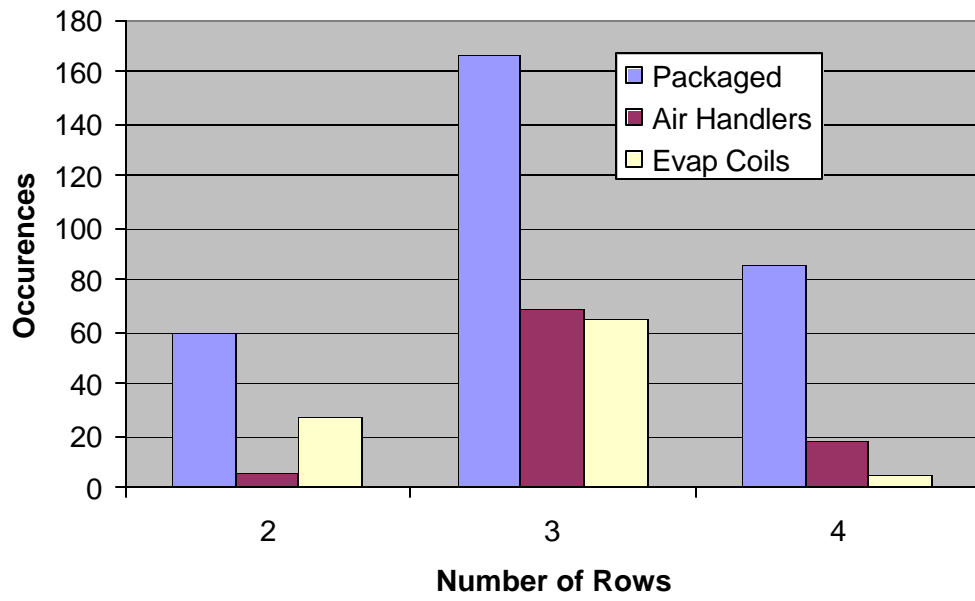


**Figure G-4. Predicted moisture retention on evaporator coils (based on Jacobi et al)**





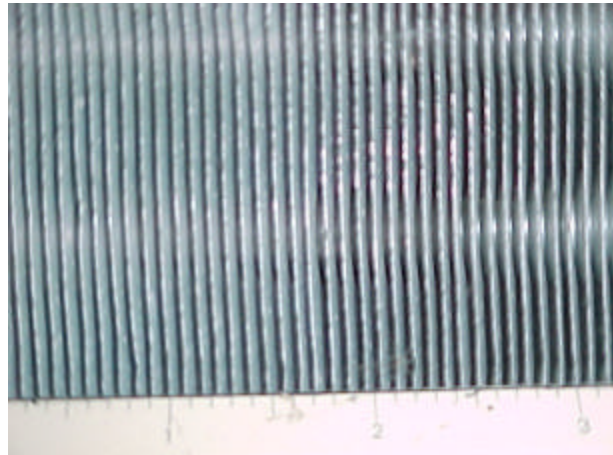
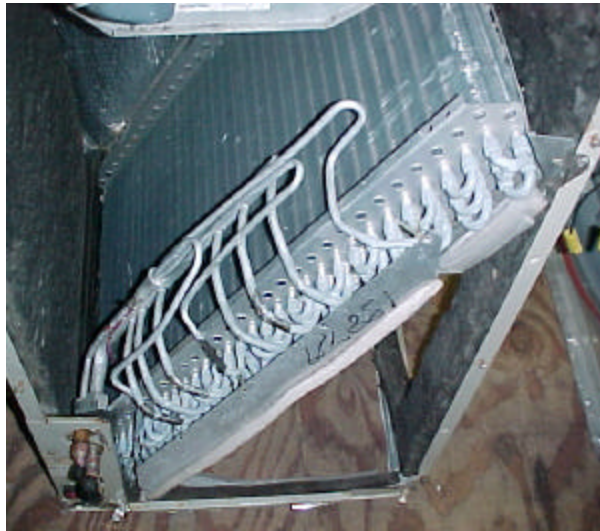
## **APPENDIX H**

### **Laboratory Test Summaries**

## **APPENDIX H1**

### **Summary of Laboratory Data for Coil 1**

**Summary of Laboratory Data for Coil 1  
November 2005**



13 fpi, conventional flat fin

Manufacturer:	Carrier (circa 1990)
Model number:	40QV036300
Nominal size:	3 tons
Baseline Size and Airflow (Test 4):	2.9 tons / 1180 cfm
Coil type:	slanted coil, 3 rows, 13 fpi
	3 circuits
Coil dimensions:	3.75 ft <sup>2</sup> face area
	18-5/8 in x 29 in
Coil thickness:	2.5 in
Tube diameter:	3/8 in OD aluminum
Tube spacing, within row (vert):	1 in
Tube spacing, row-to-row (horiz):	7/8 in
Expansion device:	fixed orifice
Unit supply fan:	on
Compressor power:	inverter

**Table 1. Summary of Steady State Test Conditions Corresponding to Each Run or Test**

	<i>Entering Coil Conditions</i>					
	<i>80/67°F 60°F dp</i>	<i>80/72°F 68°F dp</i>	<i>80/62°F 50°F dp</i>	<i>75/68°F 64°F dp</i>	<i>75/63°F 56°F dp</i>	<i>75/58°F 45°F dp</i>
400 cfm/ton	#4 (or 3)	#5	#6	#7	#8	#9
300 cfm/ton	#10	#11	#12	#13	#14	#15
200 cfm/ton	#16	#17	#18	#19	#20	#21
450 cfm/ton	#22	#23	#24			
400-200 cfm/ton (ON & OFF)	#25					
Med suction (46°F)	#1					
High suction (50°F)	#2					

Notes: Tests 4-25 all at nominal suction of 44°F (set at nominal conditions of test #3/4). This coil used a fixed orifice expansion device, with nominal superheat of 12 – 13°F set during Test 4. The orifice setting established during Test 4 was not changed for the remaining tests. The Table 1 test points denote the target testing conditions. Drier test conditions with dew points below 50°F (such as Tests #9, #15, and #21) could not be achieved. In these cases, entering conditions were typically held near 50°F dp. For each test, the compressor is ON for 45-60 minutes and then the compressor is OFF for 45-60 minutes. The supply air fan runs continuously for all tests (when the compressor is both ON and OFF).

**Steady State Performance**

The nominal performance characteristics for this coil (based on steady-state conditions from Run #4 below) are:

Total Capacity:	34.2 MBtu/h (2.9 tons)
Sensible Capacity:	25.3 MBtu/h
Latent Capacity (condensate):	8.9 MBtu/h
Sensible Heat Ratio:	0.74

Latent capacity can be calculated two ways: 1) using dew point readings and air flow, and 2) the condensate flow rate. Figure 1 compares the latent capacity calculated these two ways. The number of each data point corresponds to the run or test number listed in Table 1. In general, condensate readings resulted in a slightly higher capacity (except at very low latent capacities).

Figure 2 shows the trend of steady-state sensible heat ratio (SHR) with relative humidity and airflow rate. The sensible and latent cooling capacities used to calculate SHR in Figure 2 are based on airflow measurements and the psychrometric conditions entering and leaving the cooling coil. This performance map is typical for a cooling coil (i.e., SHR is mostly a function of the entering relative humidity, with some dependence on the air flow rate).

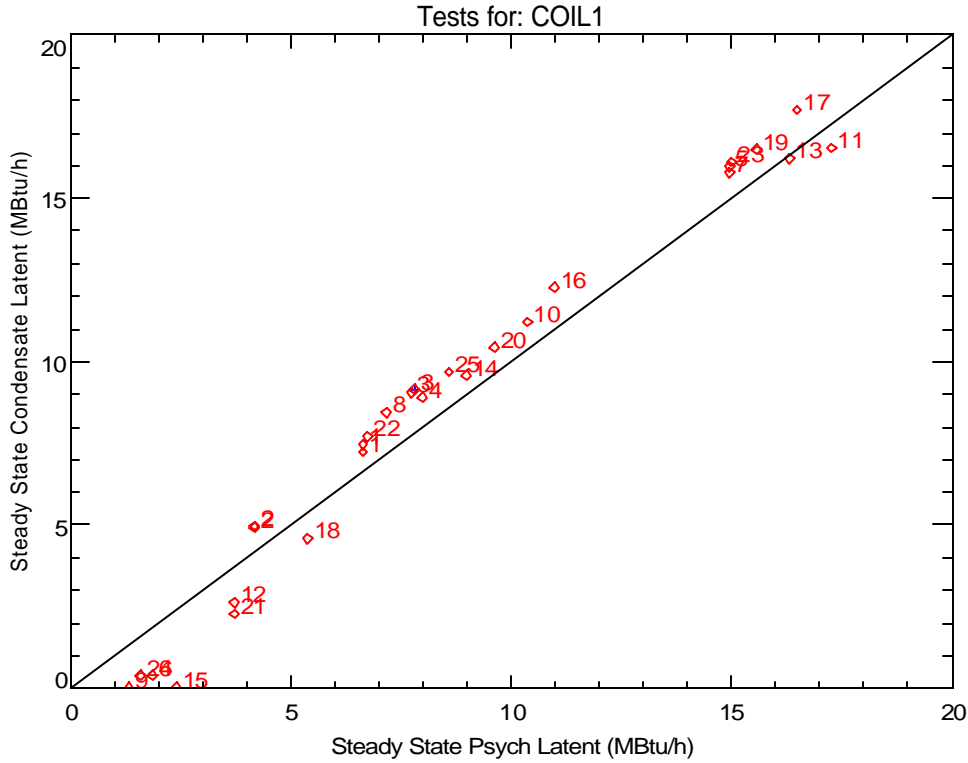


**Figure 1. Comparing Steady-State Latent Capacity Calculated From Psychrometric State Points and Condensate Removal Rates**

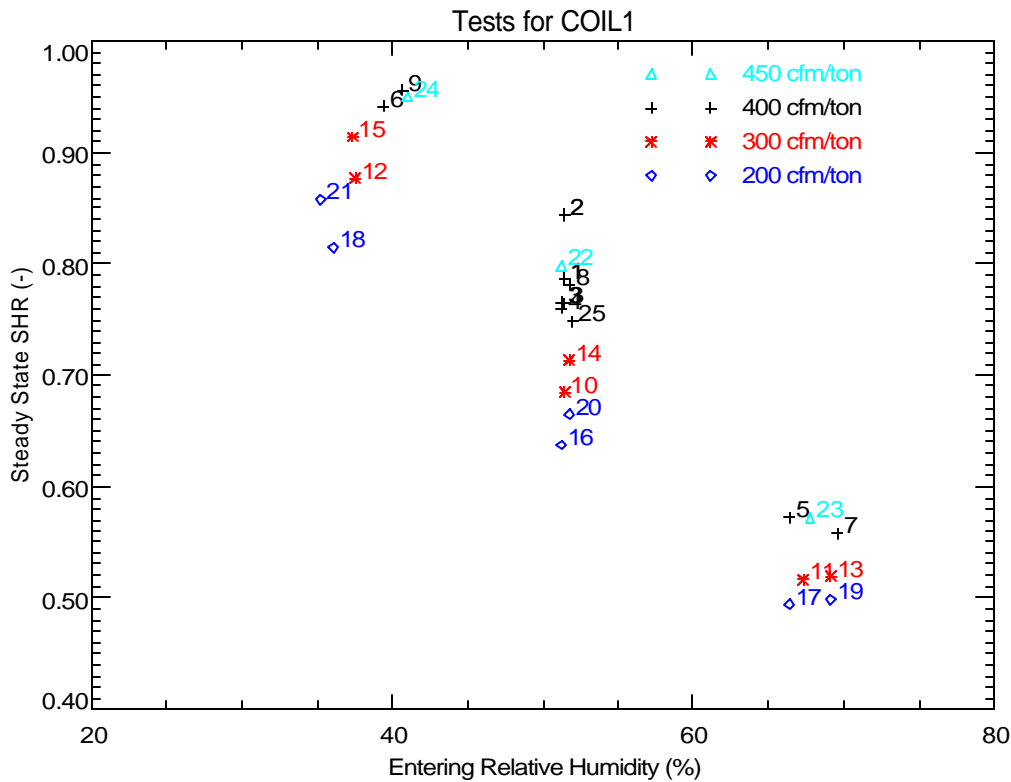


**Figure 2. Variation of Steady State SHR with Entering Humidity and Nominal Air Flow**

## **Typical Transient Performance**

Figure 3 shows the typical transient performance of the cooling coil at nominal conditions (i.e., for Cycle 2 of Run #4). The compressor runs for 45 minutes and is off for 45 minutes. The supply fan and booster fan remain on during the entire test. The booster is an external fan used to overcome air pressure drop due to instrumentation and assist with maintaining the desired air flow rate. A portion of the moisture removed by the coil during the compressor on cycle evaporates back into the air stream during the off cycle. During the off cycle the coil acts as an evaporative cooler, so the sensible capacity is nearly equal to the absolute value of the latent capacity (i.e., the sum of latent and sensible is zero).

If we integrate the off cycle sensible capacity (after allowing a 1-minute off-cycle delay to account for refrigerant movement and other transient effects), we can determine the energy associated with the moisture retained on the coil. To minimize the integration of any measurement errors, the off-cycle integration stops at the time labeled “Integration Pt.” on the plot. This point corresponds to the time when the temperature and dew point differences across the coil have first reached the terminal values (i.e., the averages from the end of the off-cycle). In this case the integration indicates that the sensible cooling is equivalent to 2.05 lbs of moisture being retained on the coil. The integrated latent capacity – which is harder to measure precisely – equals 2.26 lbs.

The value “ $t_{wet}$ ” from Henderson and Rengarajan (1996) can then be calculated by dividing the retained moisture mass (expressed as Btu, or mass x 1060 Btu/lb) and the steady state psychrometric latent capacity ( $QL = 8.0$  MBtu/h). The values of  $t_{wet}$  based on integrated sensible and latent off-cycle capacity are 16.4 and 18.0 minutes, respectively. These values of  $t_{wet}$  are similar but not identical to the measured delay of 13.5 minutes for the first condensate pulse to fall from the drain pan. The value of  $\gamma$  (1.47), which is the initial off-cycle moisture evaporation rate divided by the steady-state psychrometric latent capacity, uses the off-cycle moisture evaporation rate determined from sensible capacity (i.e., 11.7 MBtu/h) once the refrigerant flow rate has reached zero (and all coil heat and mass transfer with the air stream is assumed to be adiabatic). The off-cycle sensible capacity also shows a clear change in the decay trend at this point. For this unit it took about 2.0 minutes for refrigerant flow to settle to zero.

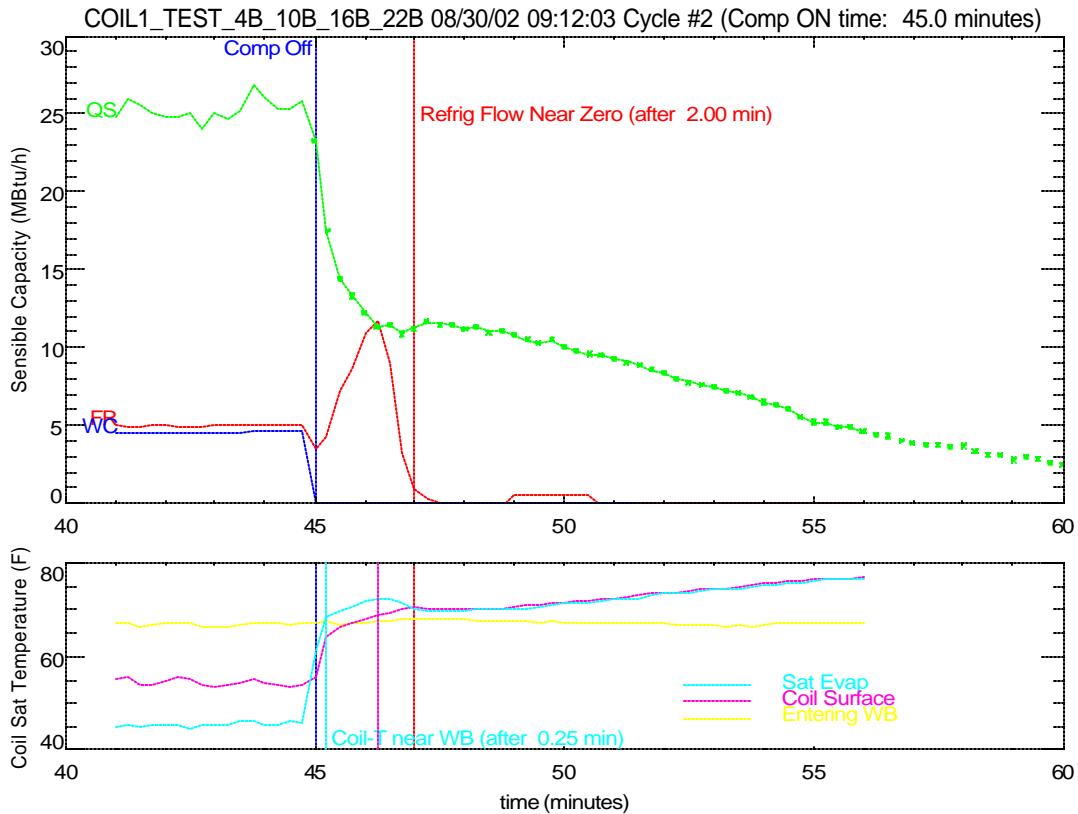
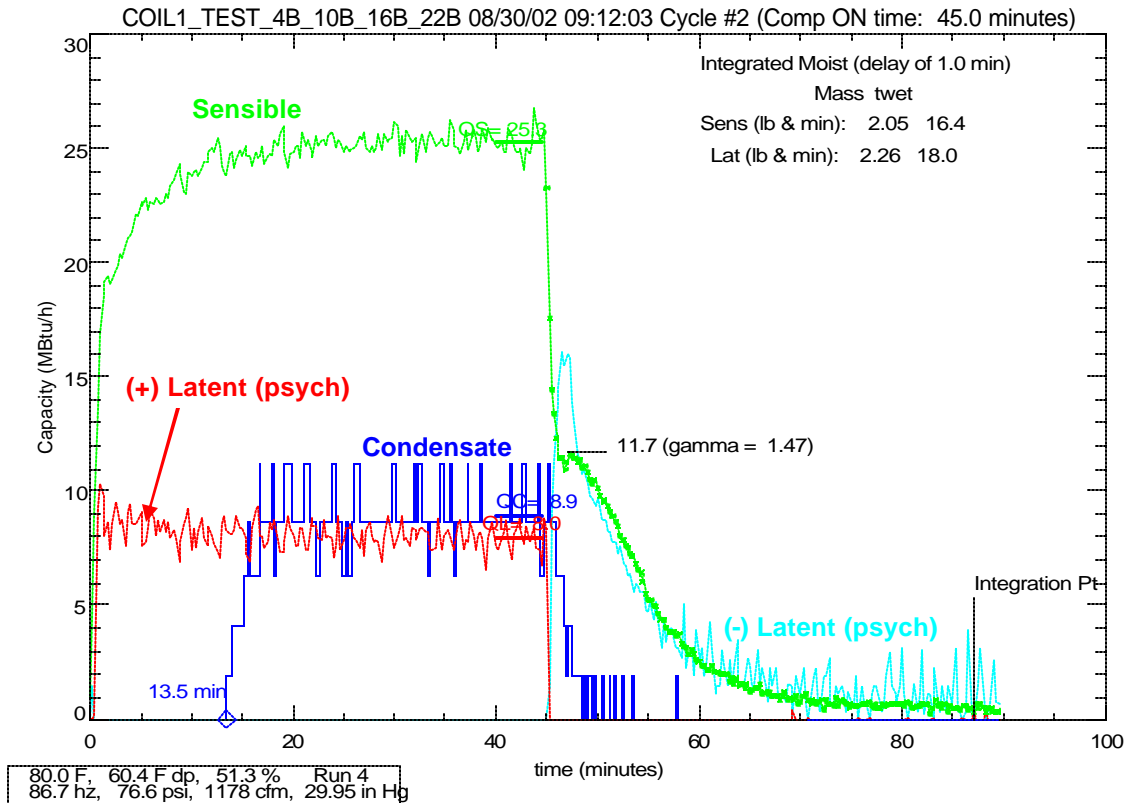


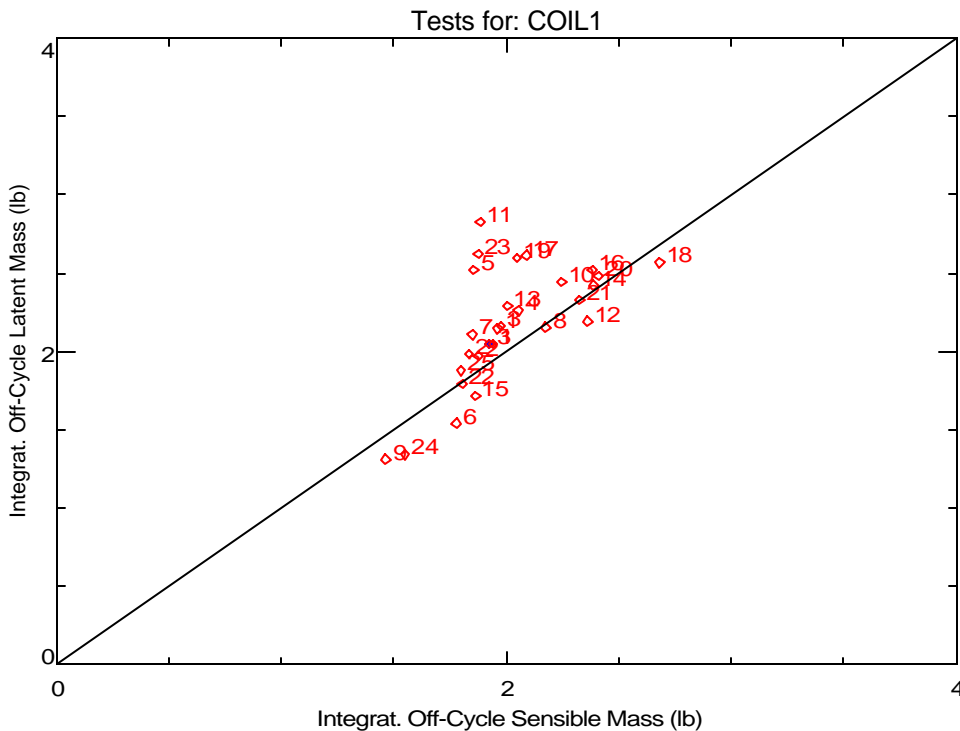
Figure 3. Example Plots of Detailed Data for Coil 1



## Part Load Latent Capacity Parameters

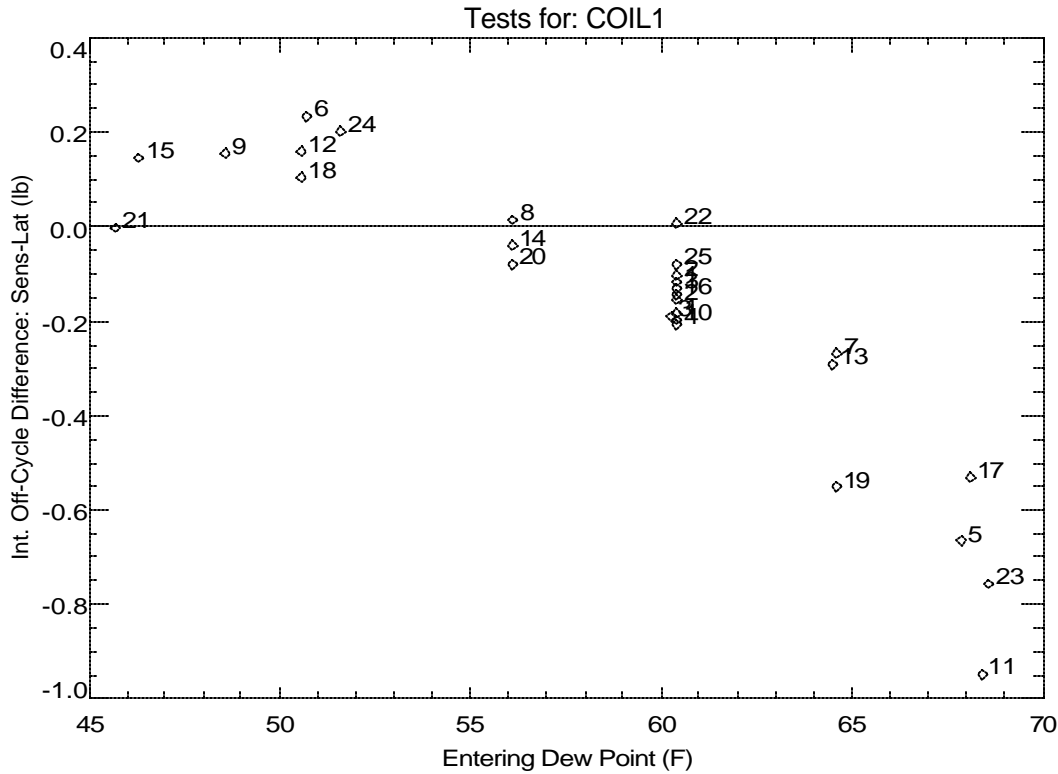
The amount of moisture held on the cooling coil (and drain pan) can be calculated by integrating the off-cycle capacity from the coil (and dividing by the heat of vaporization, 1060 Btu/lb, to get the moisture mass). The integration is delayed for the first minute of the off-cycle so that the overshoot response of the chilled dew point hygrometers does not skew the results of the integration<sup>1</sup>. The integration terminates once steady state conditions are reached for the off cycle. If we assume the coil acts as an evaporative cooler, sensible and latent capacity should be equal. Figure 4 compares the off-cycle integrated latent and sensible capacity calculated for each run. In this case, the integrated latent capacity significantly exceeds the integrated sensible capacity for several test cases. As Figure 5 shows, the two tend to match for test conditions near nominal dew point conditions (60°F). At higher dew points the integrated off-cycle latent capacity is much higher. We believe this is a systematic error with the delta dew point measurements at off-design conditions.

Since we expect that off-cycle latent and sensible capacity should sum to zero, we have selected the integrated off-cycle sensible capacity as the most consistent and believable indication of the moisture mass held on the cooling coil (and drain pan).



**Figure 4. Comparing Stored Moisture Mass Calculated by Integrating Sensible and Latent Off-Cycle Capacity (Integrated with a 1 minute delay)**

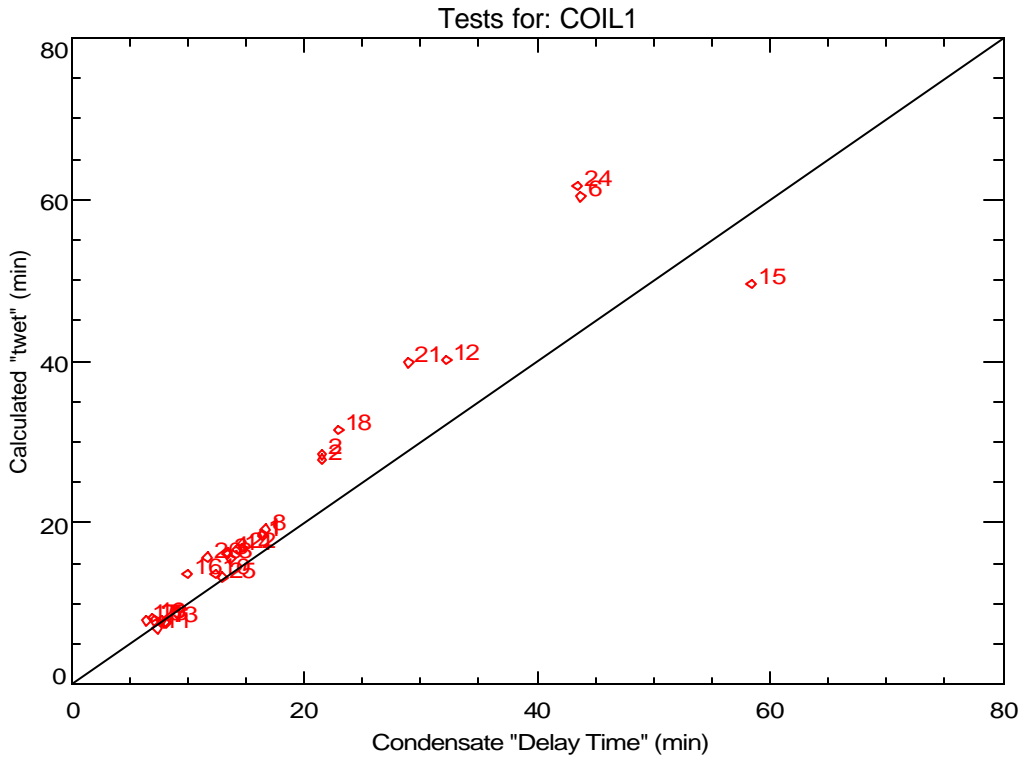
<sup>1</sup> The 1-minute delay causes the estimate of moisture mass to be low by as much as 0.18 lbs (or 9%).



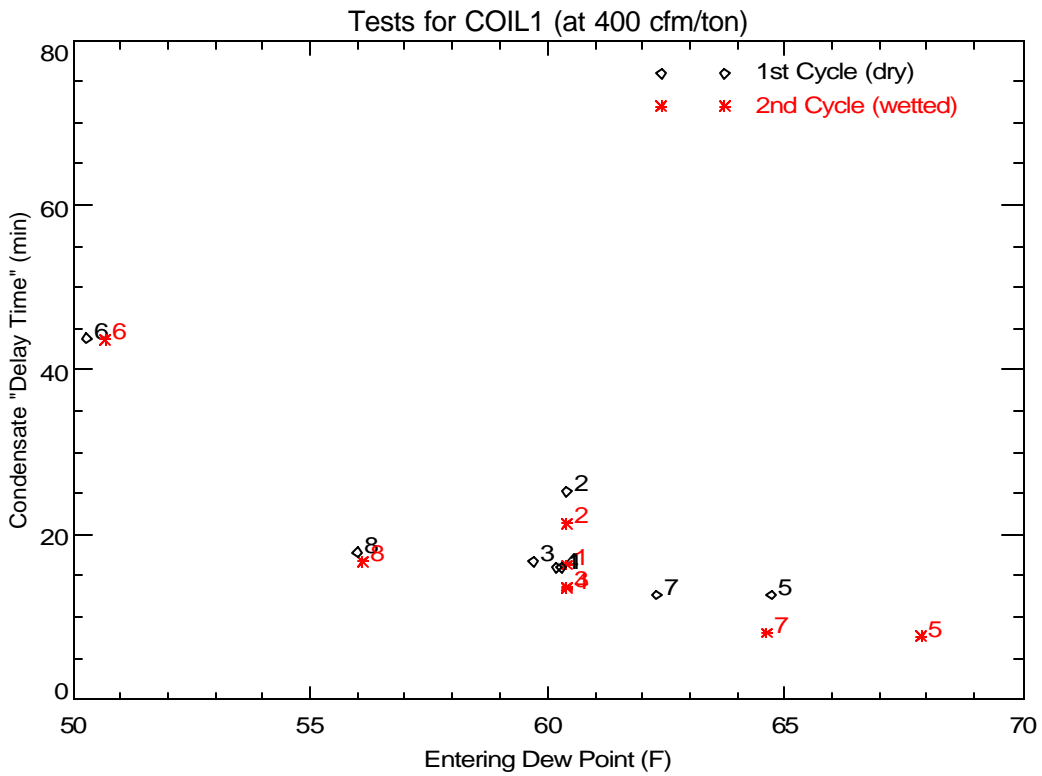
**Figure 5. Variation of Off-Cycle Sensible-Latent Difference with Entering Dew Point**

The parameter “twet” is the moisture mass held on the cooling coil times the enthalpy of vaporization (1060 Btu/lb) divided by the steady-state latent capacity of the cooling coil. The parameter should physically correspond to the time it takes for moisture to first fall from the coil (ignoring startup delays and other effects). Figure 6 compares the calculated “twet” (determined from integrating sensible capacity during the off-cycle and then dividing by the steady-state psychrometric latent capacity during the on-cycle) to the condensate delay time for all the test runs. There is relatively good agreement between these two values, but the difference between them increases at longer condensate delay times (because as coil inlet air conditions get drier the integration error to find twet is larger, or because the coil is only partially wetted at lower inlet air dew point temperatures).

Figure 7 shows the condensate delay time is a function of the entering air dew point temperature as would be expected. Different symbols are shown on the plot for the 1<sup>st</sup> and 2<sup>nd</sup> cycles in each test sequence. The delay time was slightly higher for the first cycle when the fin surfaces were totally dry. For the 2<sup>nd</sup> cycle, the coil apparently may have had better wettability than it did for the 1<sup>st</sup> cycle.



**Figure 6. Comparing “twet” (calculated with off-cycle sensible and steady state latent) to the Condensate Delay Time**



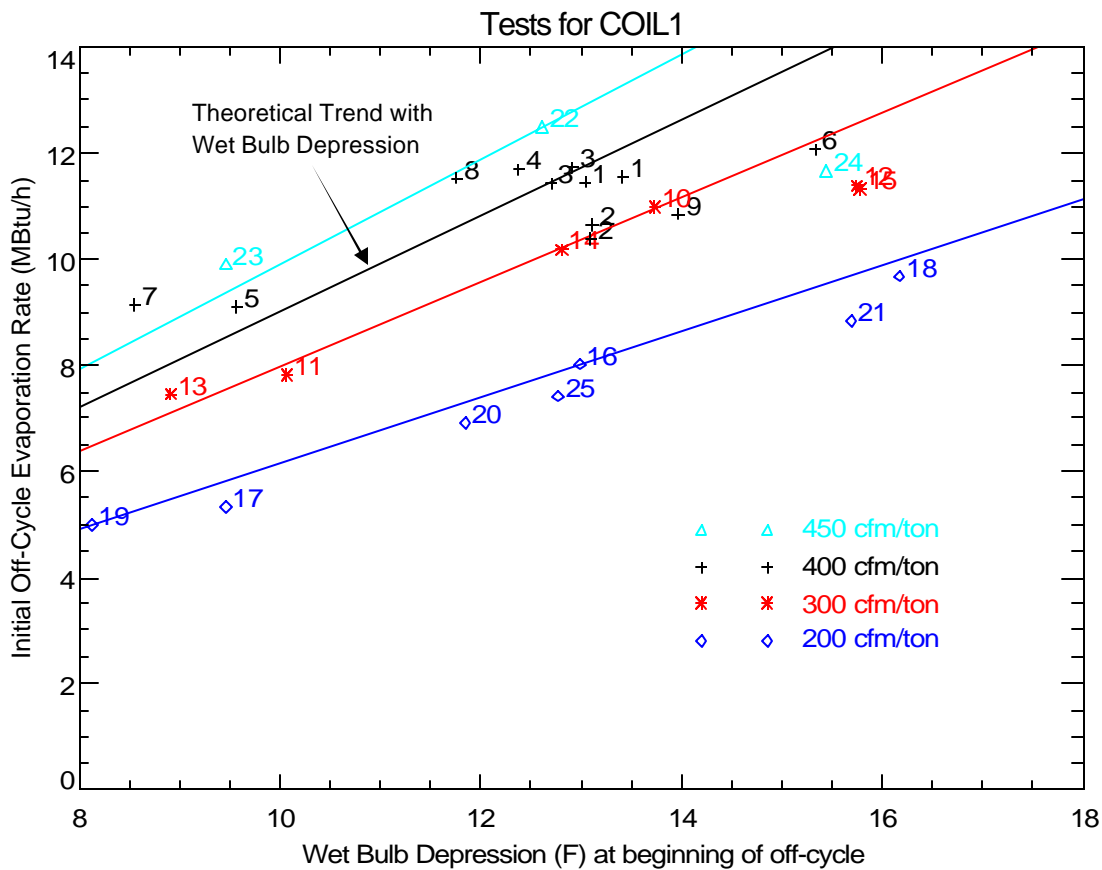
**Figure 7. Impact of Dew Point and Coil Wettedness on Condensate Delay Time**

Figure 8 shows the initial off-cycle moisture evaporation rate varies with wet bulb depression. As expected, the evaporation rate is highest when the entering air has a larger wet bulb depression (i.e., has a lower relative humidity) and higher air flow rate.

The model developed by Henderson and Rengarajan (1996) used the following simple evaporative cooler model to predict the moisture evaporation rate at off-design conditions:

$$Q_{\text{evap}} = Q_{\text{evap}_o} \times \frac{(DB - WB)}{(80 - 67)}$$

where  $Q_{\text{evap}_o}$  is the evaporation rate at the nominal entering air conditions of 80°F dry bulb (DB) and 67°F wet bulb (WB). This simple model is shown as the lines in Figure 8. For each air flow rate, the line is based on the nominal test results at 80°F DB/67°F WB extended to pass through zero. The measured data show essentially the same slope as the theoretical lines. The notable exceptions are the points with higher airflow and drier entering conditions (e.g., Runs #6, #9 and #24). These runs have a much lower initial moisture evaporation rate because the entering air dew point temperature was close to the cooling coil temperature, so the fin surfaces were not fully wetted. The smaller wetted surface area reduces the initial moisture evaporation rate.



**Figure 8. Measured Variation of Initial Evaporation Rate with Wet Bulb Depression**

Stabat et al. (2001) reviewed the theoretical performance of direct evaporative coolers and showed that the saturation effectiveness of an evaporative cooler is:

$$h_{evp} = 1 - e^{-NTU} \quad \text{where} \quad NTU = K/cfm^{0.2} \quad \text{for an air-water mixture.}$$

The line shown on Figure 9 is the best fit for the equation above to the measured data. The resulting constant K was 5.76, which is equivalent to an NTU of 1.40 at 1,200 cfm. While there is considerable scatter due to the experimental uncertainty of predicting the initial off-cycle moisture evaporation rate, the slope of the line is still fairly representative of the overall trend.

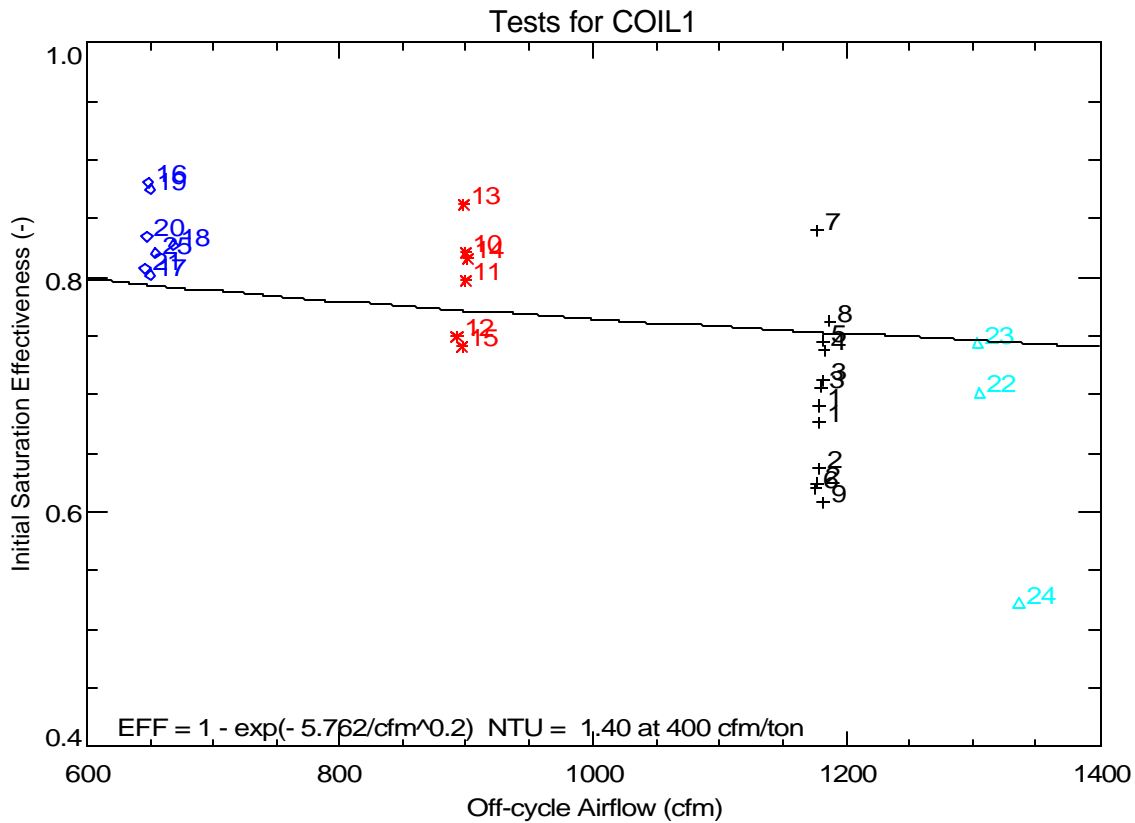


**Figure 9. Evaporative Effectiveness versus Airflow**

Figure 10 compares the measured initial off-cycle moisture evaporation rate for each test to the predicted initial evaporation rate using the effectiveness model above. The model and measured data generally agree when presented in this form (i.e., the overall agreement visually appears better than in Figure 9 above). Again, the variation that occurs for Tests #6, #9, and #24 was due to partial coil dryout, as mentioned above.

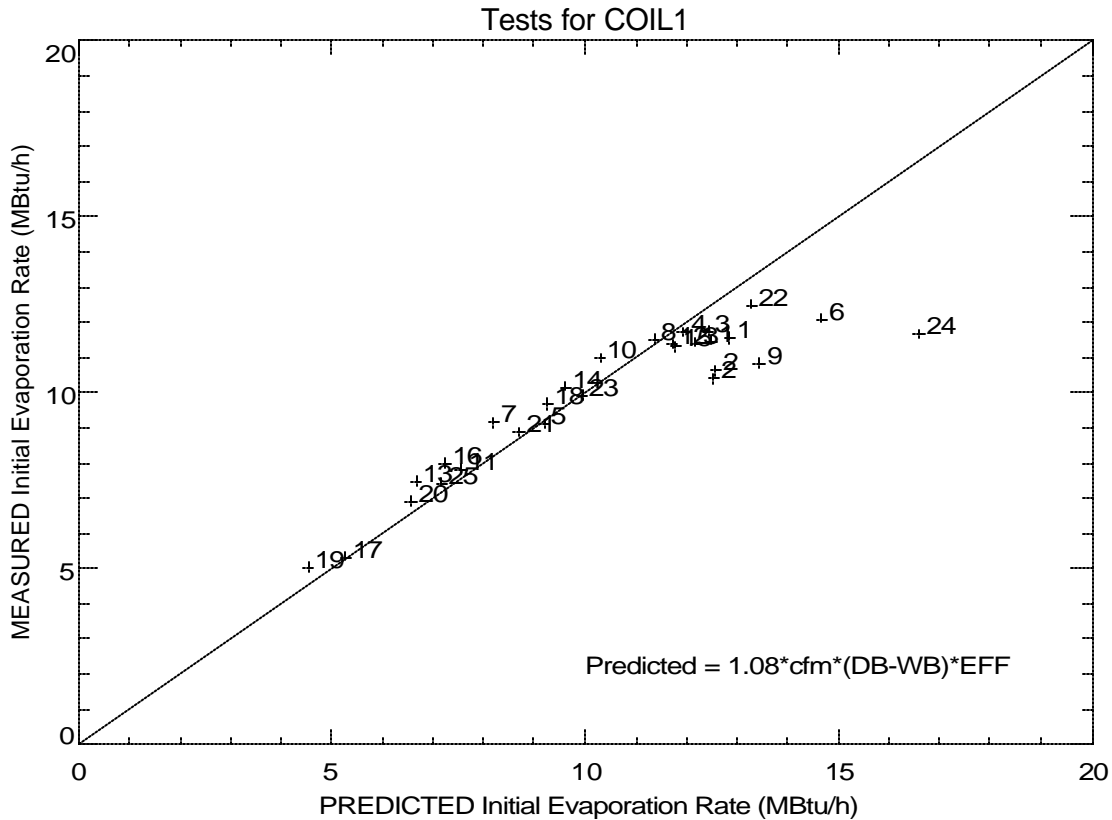


**Figure 10. Comparing Measured and Predicted Initial Moisture Evaporation Rates**

One question of interest is whether the amount of moisture retained on the cooling coil is a function of air flow or entering air conditions. Figures 11 and 12 show how the retained moisture varies with these conditions. At higher dew points (Figure 11), the high condensate flow rate has the effect of causing the amount of retained moisture to approach equilibrium. The greater scatter and magnitude at lower dew points may be due to the fact that integration of the off-cycle evaporation rate includes the error associated with integrating the “tail” of the profile. Also, the lower retained moisture values for Test #6, #9 and #24 are due to partial coil dryout at the lower entering air dewpoint conditions.

Figure 12 does show a 10-20% decrease in the amount of retained moisture on the cooling coil with higher air flow rates.

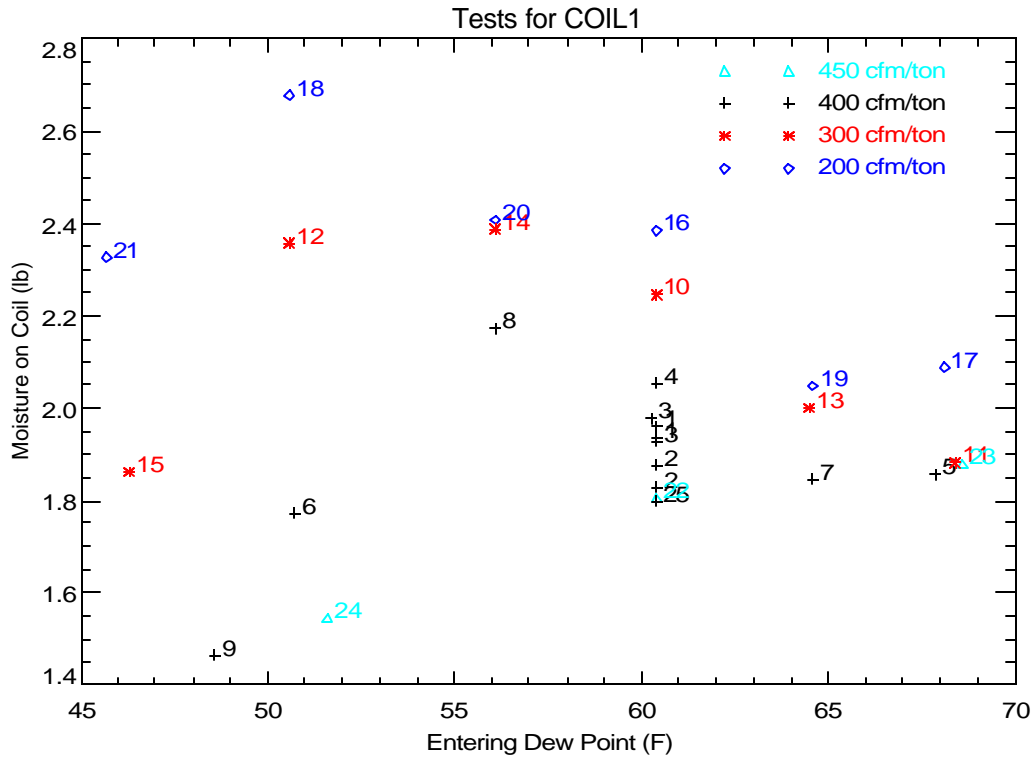


Figure 11. Variation of Retained Moisture (based on Off-Cycle Sensible) with Flow and Dew Point

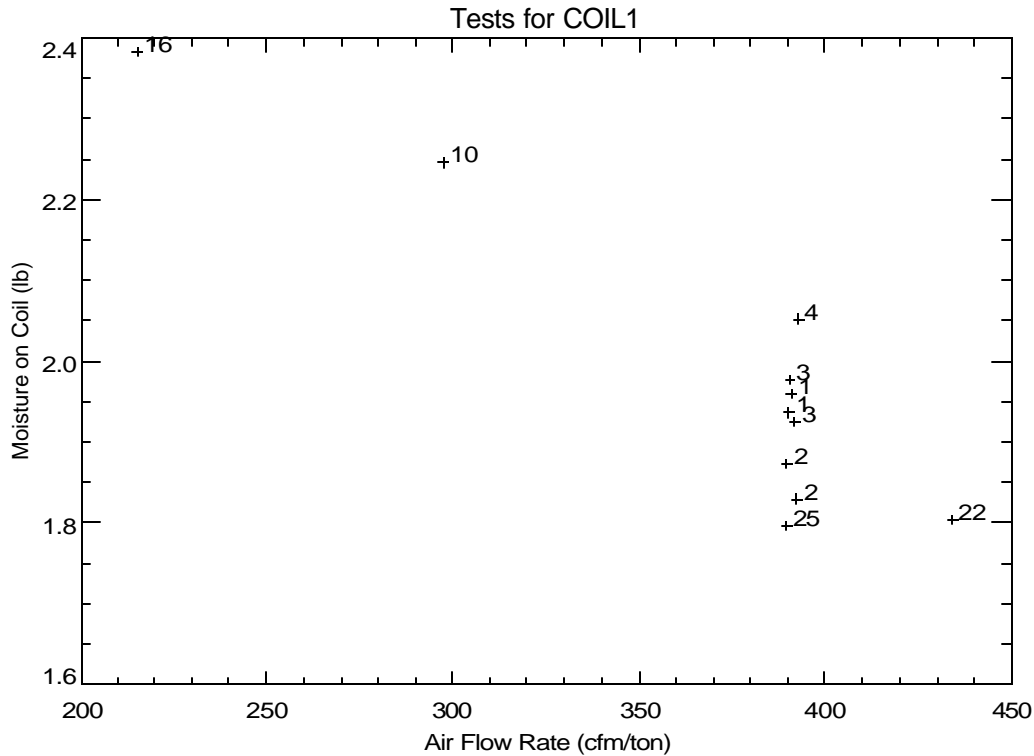
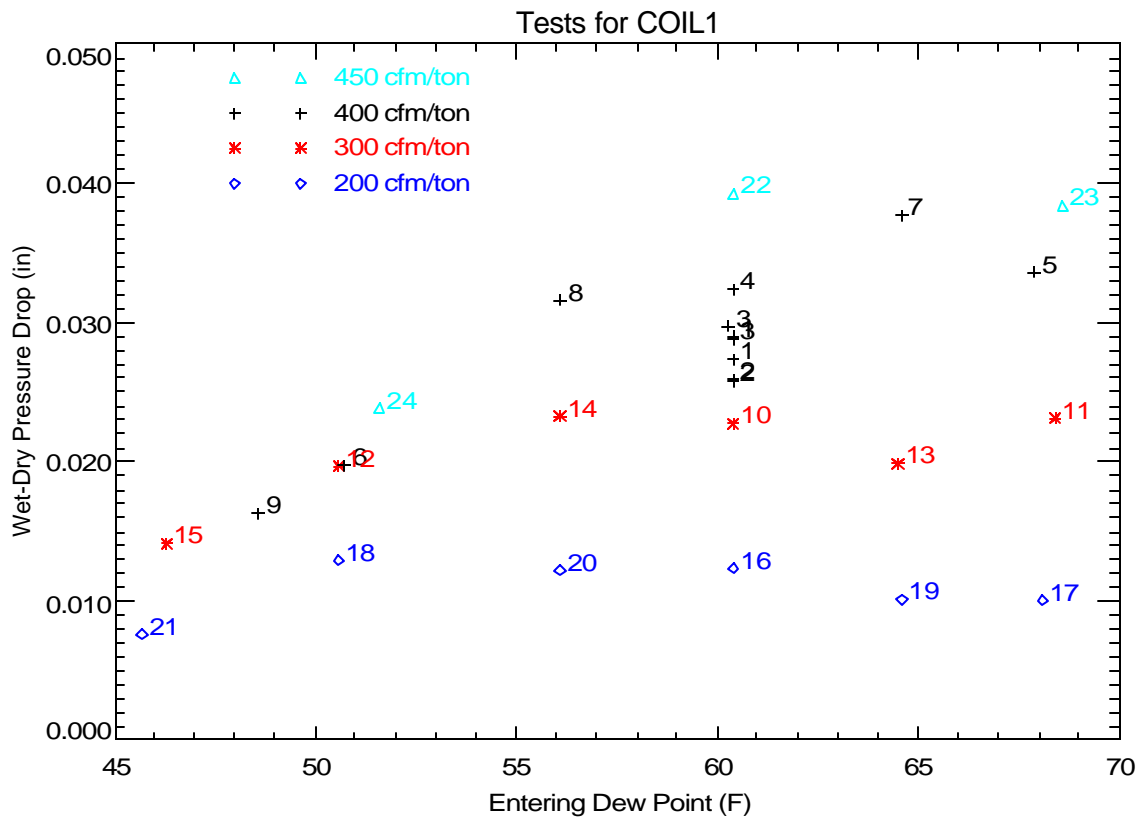


Figure 12. Variation of Retained Moisture with Air Flow at Nominal Entering Conditions of 80°F, 60.4°F dew point

Another way to detect the amount of retained moisture is to measure the static air-side pressure drop across the cooling coil. The difference between the pressure drop across the coil under wet and dry conditions should provide an indication of the amount of retained moisture (the wet coil pressure drop is measured at steady-state conditions while the dry coil pressure drop is taken as the average pressure drop during the last part of the off-cycle). Figure 13 shows the variation of the wet-dry pressure difference with various entering air dew point temperatures at multiple air flow rates. Comparing the values for each air flow rate generally shows a trend of pressure drops reaching a plateau once the humidity of the entering air is sufficiently high to fully wet the coil. At a given air flow rate, the pressure drop does not increase substantially with dew points above 60°F.



**Figure 13. Variation of Wet-Dry Pressure Drop with Entering Conditions and Air Flow Rate**

Figure 14 confirms that the wet-dry pressure drop is mostly a function of air flow rate. The linear trend also implies laminar flow in the wetted cooling coil.



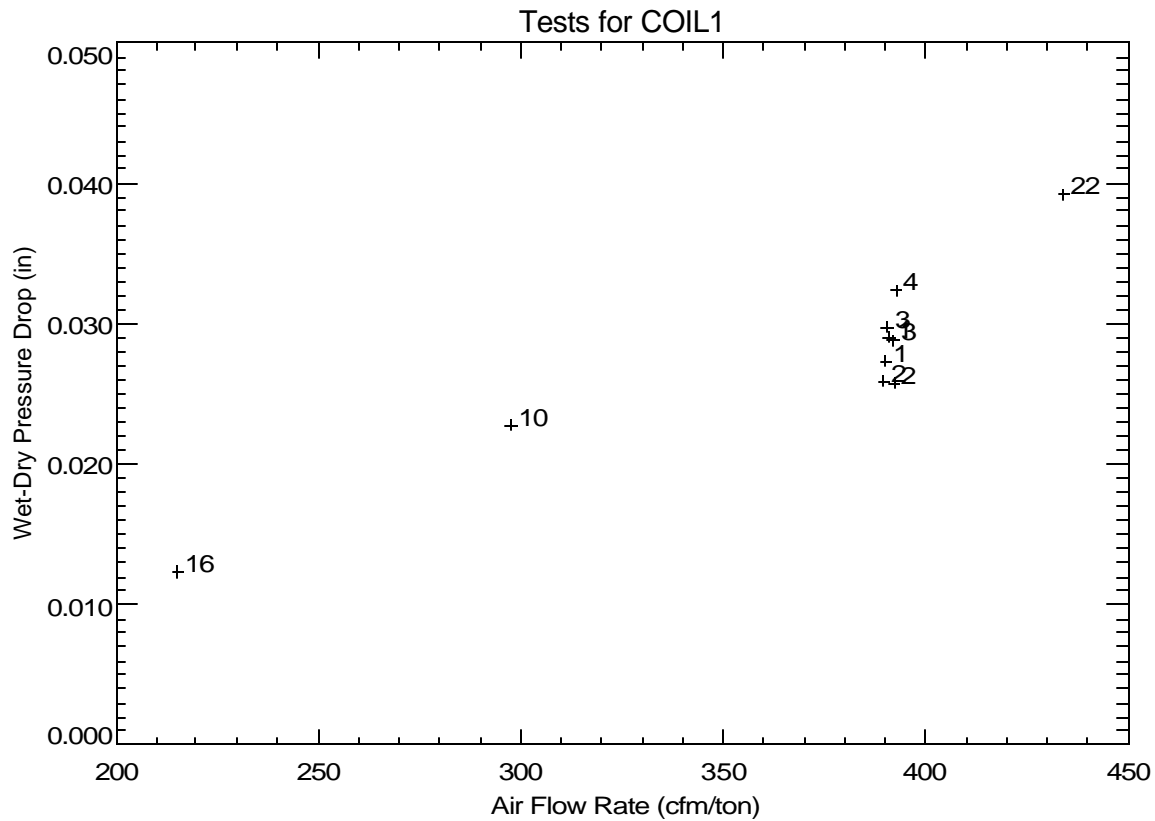


**Figure 14. Trend of Wet-Dry Pressure Drop with Flow at Nominal Entering Conditions of 80°F, 60.4°F dew point**

The series of plots in Figure 15 show the impact of coil suction temperature on performance. The plots for moisture on coil and wet-dry pressure drop both confirm that more moisture is retained when the coil is colder (i.e., lower saturated suction temperature).

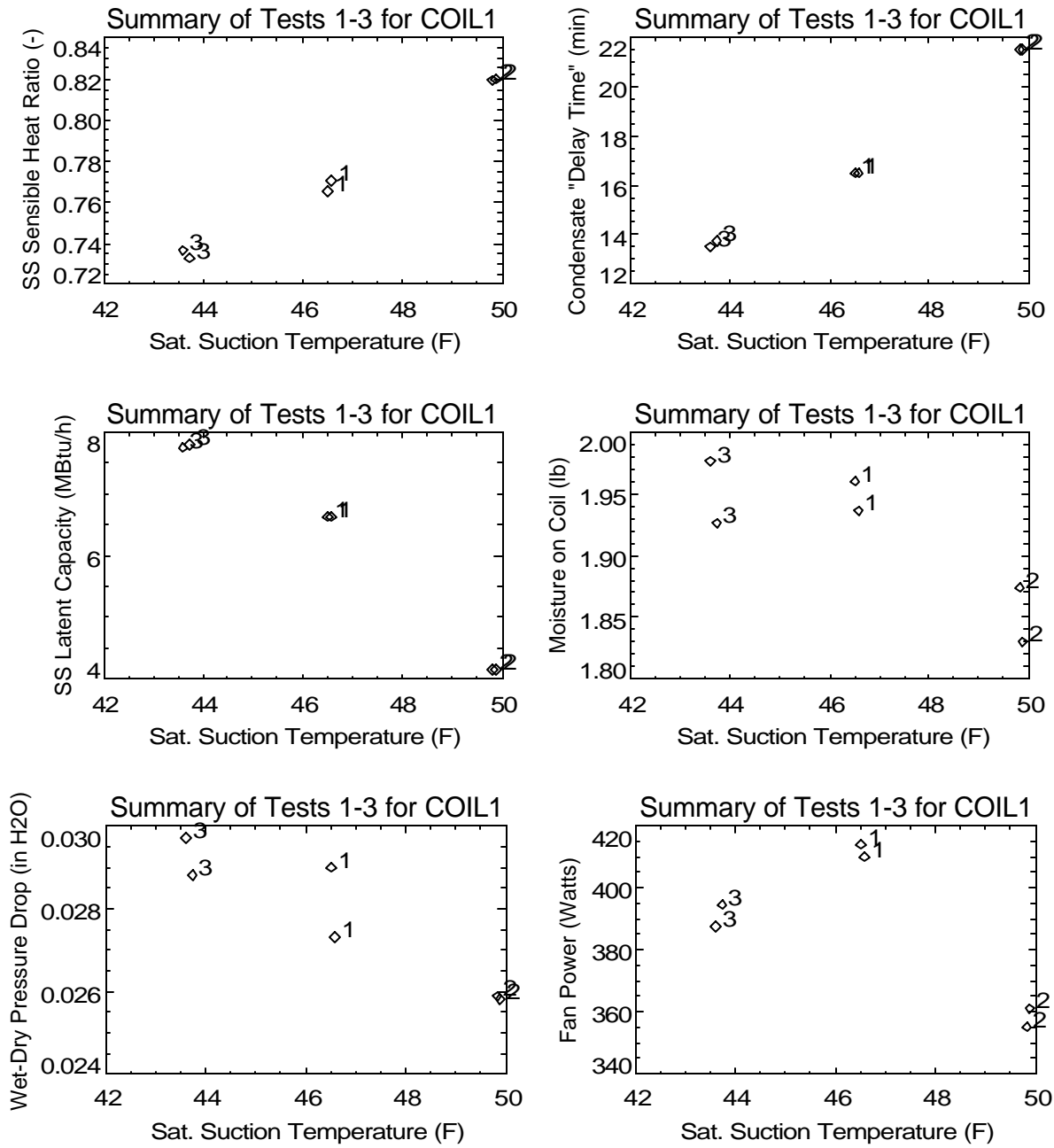


**Figure 15. Trend of Various Parameters with Saturated Suction Temperature**

## Overall Latent Degradation Trends

Several quasi-steady cyclic tests were also completed in the laboratory to quantify the overall part-load degradation of latent capacity. Table 2 lists the cycling test runs. These conditions correspond to a conventional thermostat with a maximum cycle rate of 3 cycles per hour (at 50% runtime).

**Table 2. Cyclic Test Conditions**

CONST FAN	AUTO FAN	Number of Times Test Repeated	ON Time (minutes)	OFF Time (minutes)	Runtime Fraction (-)	Cycle Rate (cycles/h)
Run						
31	41	2	45	45	0.500	0.667
32	42	3	30	6	0.833	1.667
33	43	3	16	7.25	0.688	2.581
34	44	3	10	10	0.500	3.000
35	45	3	7	17.5	0.286	2.449
	46	3	5.5	55	0.091	0.992

Note: All tests performed with 80°F db/60.4°F dp inlet air and 400 cfm/ton air flow.

Figures 16 and 17 show the net impact of part-load system operation based on cyclic tests completed in the lab.

Figure 16 is for the constant fan mode (continuous air flow over the cooling coil while the coil cycles on/off). The measured data compare well to the model from Henderson and Rengarajan (1996) with the following model parameters obtained from the test sequence ( $t_{wet} = 15.0$  minutes,  $\gamma = 1.48$ ,  $N_{max} = 3$ ,  $\tau = 20$  seconds). These parameters were taken from the 2<sup>nd</sup> occurrence of Test #31 which was completed as part of the suite of cycling tests listed in Table 2. The latent time constant ( $\tau$ ) of 20 seconds comes from qualitative observation of the coil's response time. The black solid line corresponds to the linear off-cycle evaporation model (Henderson and Rengarajan 1996). The black dotted line assumes an off-cycle evaporation trend that corresponds to an exponential decay.

The purple line is the new part load LHR model that uses the more realistic moisture evaporation model from Stabat et al. (2001) and also allows for variable amounts of moisture on the coil at the end of the on cycle. The parameters NTU and  $t_p$  were determined from the specific measured data from each test (the purple solid line) as well as the average NTU and  $t_p$  from all the data (the purple dotted line), including Figure 9 above. For this coil the two trends were the same. The parameter  $t_p$  is defined in the improved model development section of this report.

For this coil the black dotted line in Figure 16, which corresponds to the standard model with exponential decay in the off cycle, best matches the measured data. In general the data corresponding to the 2<sup>nd</sup> and 3<sup>rd</sup> repetition of each test, once quasi-steady conditions had been reached, showed the best agreement with the models.

Figure 17 shows that some latent degradation can be detected in the AUTO fan mode as well (i.e., when the supply air flow across the cooling coil starts and stops with compressor operation). The 2<sup>nd</sup> and 3<sup>rd</sup> repetition (cycle) show good agreement with each other.

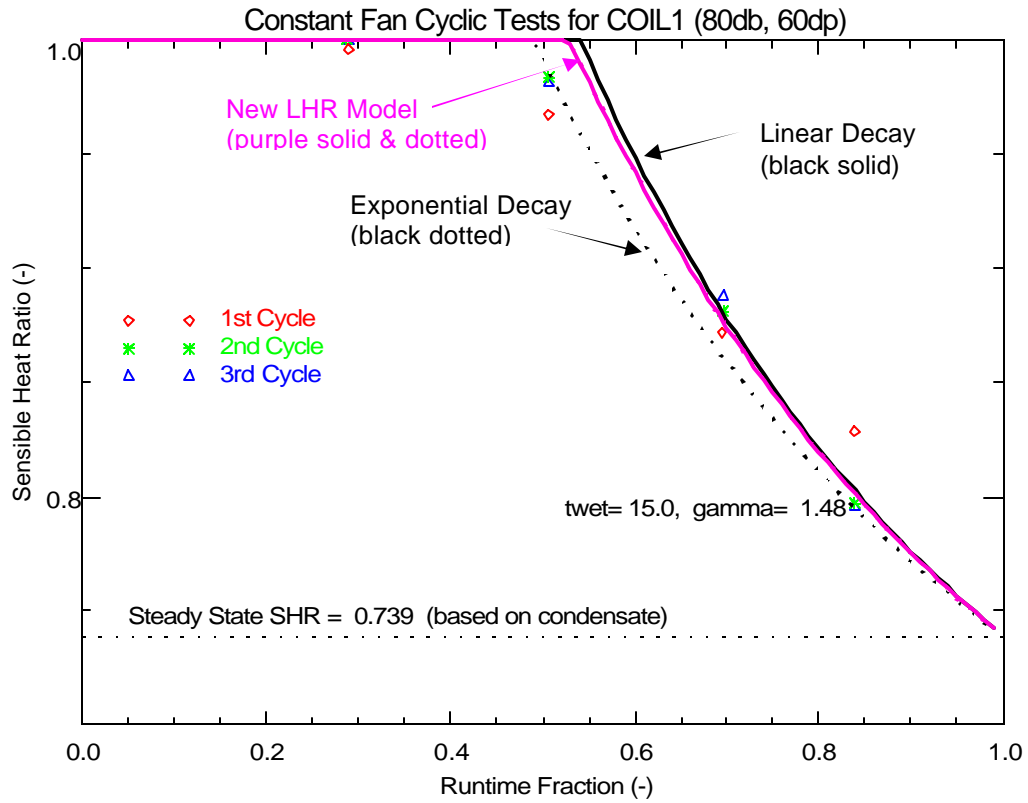


Figure 16. Comparing Measured Latent Degradation to the LHR Models

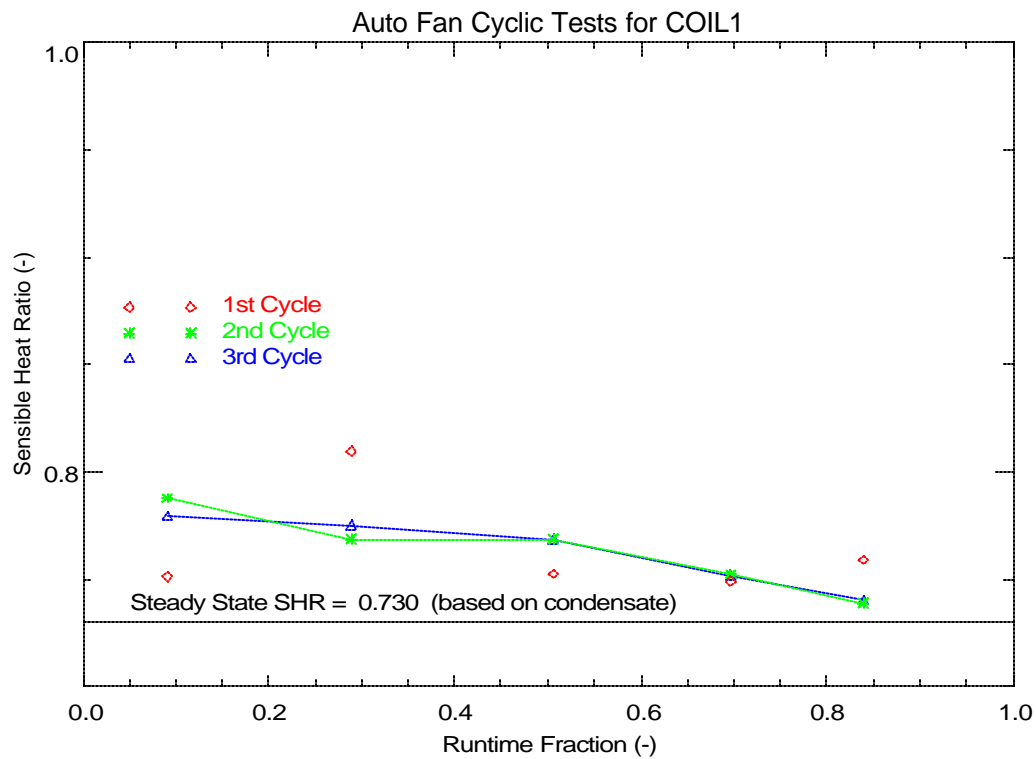
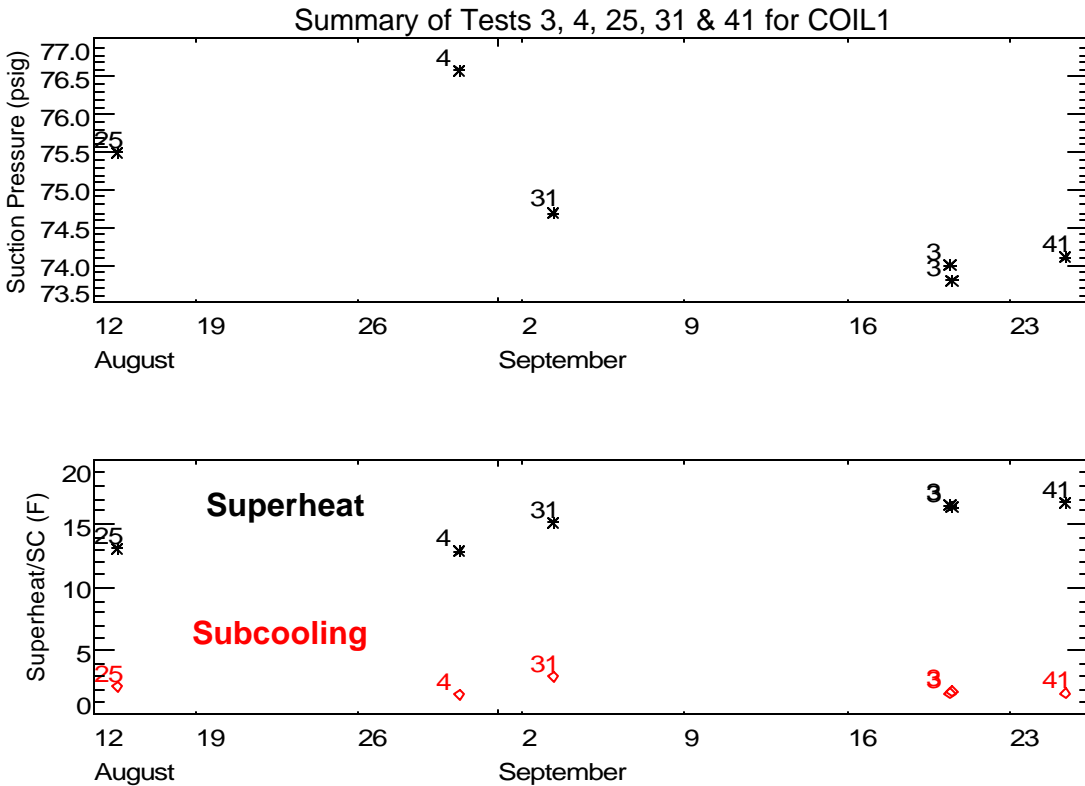


Figure 17. Measured AUTO Fan Latent Degradation

The tests were completed over a period of 6-7 weeks. Figure 18 shows some evidence of a very modest change in suction pressure and superheat that might imply some loss of charge over the period. However, the suction pressure only dropped by about 1 psig over the 6-week period.



**Figure 18. Long-term Variation in Suction Pressure, Superheat and Subcooling**

**References**

Henderson, H., and K. Rengarajan. 1996. A model to predict the latent capacity of air conditioners and heat pumps at part-load conditions with constant fan operation. *ASHRAE Transactions* 102(1): 266-274.

Stabat, P., Marchio, D. and M. Orphelin. 2001. Pre-Design and Design Tools for Evaporative Cooling. *ASHRAE Transactions* 107 (1): 501-510.

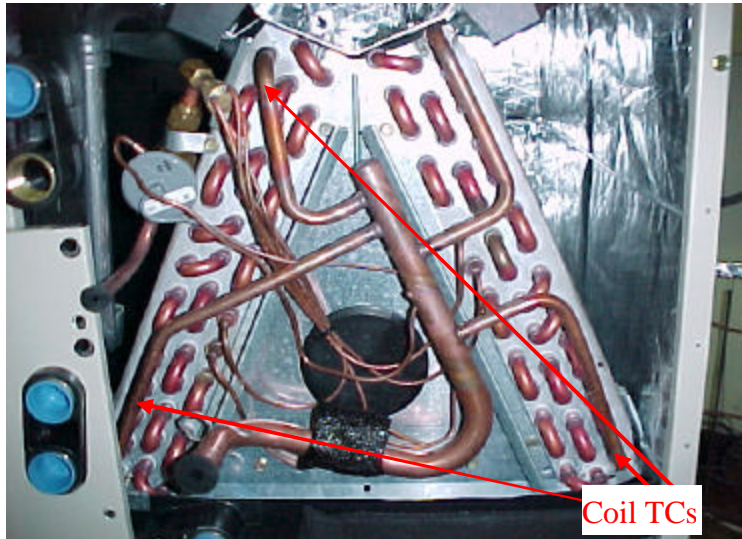
**COIL 1 Test Runs**

File Name	Date	Start Time	Sequence No.	Run/Test No.	Inlet DB (F)	Inlet DewPt (F)	Air Flow (cfm)	Test Duration (min)	Comp Runtime (min)
Coil1_Test_1.out	10/7/2002	10:31:56	1	1	79.9	60.3	1180.3	119.8	60
Coil1_Test_1.out	10/7/2002	12:31:56	2	1	79.9	60.4	1173.5	119.8	60
Coil1_Test_1.out	10/7/2002	14:31:56	3	1	79.9	60.4	1171.1	120.3	60
Coil1_Test_2.out	10/4/2002	9:33:57	1	2	79.9	60.4	1187.5	119.7	60
Coil1_Test_2.out	10/4/2002	11:33:55	2	2	79.9	60.4	1176.8	119.8	60
Coil1_Test_2.out	10/4/2002	13:33:55	3	2	79.9	60.4	1169.8	120	60
Coil1_Test_3b.out	9/20/2002	7:28:13	1	3	79.3	59.7	1186.6	119.8	60
Coil1_Test_3b.out	9/20/2002	9:28:13	2	3	79.9	60.4	1175.4	119.7	60
Coil1_Test_3b.out	9/20/2002	11:28:12	3	3	79.9	60.3	1172.5	120	60
Coil1_Test_4b_10b_16b_22b.out	8/30/2002	7:42:04	1	4	79.9	60.2	1188.2	89.7	45
Coil1_Test_4b_10b_16b_22b.out	8/30/2002	9:12:03	2	4	80	60.4	1178.6	89.7	45
Coil1_Test_4b_10b_16b_22b.out	8/30/2002	10:42:02	3	10	79.9	60.4	892.6	89.8	45
Coil1_Test_4b_10b_16b_22b.out	8/30/2002	12:12:02	4	16	80	60.4	646.6	89.8	45
Coil1_Test_4b_10b_16b_22b.out	8/30/2002	13:42:02	5	22	80	60.4	1303.1	89.8	45
Coil1_Test_4a_10a_16a_22a_25a.out	8/15/2002	15:25:22	6	25	79.6	60.4	1168.6	89.8	45
Coil1_Test_5a,11a,17a,23a.out	8/19/2002	8:42:28	1	5	79.5	64.7	1186.7	89.7	45
Coil1_Test_5a,11a,17a,23a.out	8/19/2002	10:12:27	2	5	80.1	67.9	1175.8	89.7	45
Coil1_Test_5a,11a,17a,23a.out	8/19/2002	11:42:26	3	11	80.2	68.4	893.4	89.8	45
Coil1_Test_5a,11a,17a,23a.out	8/19/2002	13:12:26	4	17	80.3	68.1	647.3	89.8	45
Coil1_Test_5a,11a,17a,23a.out	8/19/2002	14:42:26	5	23	80.2	68.6	1301.6	89.8	45
Coil1_Test_6b_12b_18b_24b.out	9/19/2002	9:30:09	1	6	77	50.3	1186.9	89.7	45
Coil1_Test_6b_12b_18b_24b.out	9/19/2002	11:00:08	2	6	77.3	50.7	1176.3	89.7	45
Coil1_Test_6b_12b_18b_24b.out	9/19/2002	12:30:07	3	12	78.6	50.6	888.1	89.7	45
Coil1_Test_6b_12b_18b_24b.out	9/19/2002	14:00:06	4	18	79.9	50.6	667.2	89.7	45
Coil1_Test_6b_12b_18b_24b.out	9/19/2002	15:30:04	5	24	77.1	51.6	1335.1	89.7	45
Coil1_Test_7a,13a,19a.out	8/20/2002	10:30:23	1	7	75.1	62.3	1180.8	89.7	45
Coil1_Test_7a,13a,19a.out	8/20/2002	12:00:22	2	7	75.2	64.6	1168.5	89.7	45
Coil1_Test_7a,13a,19a.out	8/20/2002	13:30:20	3	13	75.3	64.5	890.1	89.7	45
Coil1_Test_7a,13a,19a.out	8/20/2002	15:00:17	4	19	75.4	64.6	648.3	89.7	45
Coil1_Test_8b_14b_20b.out	9/5/2002	7:58:04	1	8	74.9	56	1185.5	89.8	45
Coil1_Test_8b_14b_20b.out	9/5/2002	9:28:04	2	8	75	56.1	1183.2	89.7	45
Coil1_Test_8b_14b_20b.out	9/5/2002	10:58:03	3	14	75	56.1	895	89.7	45
Coil1_Test_8b_14b_20b.out	9/5/2002	12:28:03	4	20	75	56.1	646.7	89.7	45
Coil1_Test_9a,15a,21a.out	8/26/2002	9:02:45	1	9	73.6	48	1185.5	89.7	45
Coil1_Test_9a,15a,21a.out	8/26/2002	10:32:44	2	9	74	48.6	1177.5	89.8	45
Coil1_Test_9a,15a,21a.out	8/26/2002	12:02:44	3	15	73.9	46.3	892.6	89.8	45
Coil1_Test_9a,15a,21a.out	8/26/2002	13:32:45	4	21	75	45.7	646.6	89.7	45
Coil1_Test_Cycling.out	9/3/2002	8:39:14	1	31	80	60.4	1185.2	89.8	45
Coil1_Test_Cycling.out	9/3/2002	10:09:14	2	31	79.9	60.4	1175.7	89.8	45
Coil1_Test_Cycling.out	9/3/2002	11:39:14	3	32	80	60.4	1170.5	35.8	30
Coil1_Test_Cycling.out	9/3/2002	12:15:14	4	32	79.9	60.4	1171.4	35.8	30
Coil1_Test_Cycling.out	9/3/2002	12:51:14	5	32	79.9	60.3	1171.2	35.8	30
Coil1_Test_Cycling.out	9/3/2002	13:27:14	6	33	79.9	60.4	1171.9	23	16
Coil1_Test_Cycling.out	9/3/2002	13:50:28	7	33	79.9	60.4	1172.6	23	16
Coil1_Test_Cycling.out	9/3/2002	14:13:43	8	33	79.9	60.4	1171.6	23	16
Coil1_Test_Cycling.out	9/3/2002	14:36:58	9	34	80	60.3	1174.3	19.7	10
Coil1_Test_Cycling.out	9/3/2002	14:56:58	10	34	80	60.4	1173.9	19.7	10
Coil1_Test_Cycling.out	9/3/2002	15:16:57	11	34	80.2	60.4	1171.4	19.8	10
Coil1_Test_Cycling.out	9/3/2002	15:36:57	12	35	80.3	60.3	1174.7	24.3	7
Coil1_Test_Cycling.out	9/3/2002	16:01:27	13	35	80.5	60.4	1178.2	24.2	7
Coil1_Test_Cycling.out	9/3/2002	16:25:56	14	35	80.5	60.4	1176.1	24.3	7
Coil1_Test_Cycling_auto a.out	9/25/2002	8:11:54	1	41	78.9	59.7	1190.1	89.8	45
Coil1_Test_Cycling_auto a.out	9/25/2002	9:41:54	2	41	79.8	60.4	1186.2	89.7	45
Coil1_Test_Cycling_auto a.out	9/25/2002	11:11:53	3	42	79.8	60.4	1183.3	35.8	30
Coil1_Test_Cycling_auto a.out	9/25/2002	11:47:53	4	42	79.7	60.4	1180.5	35.8	30
Coil1_Test_Cycling_auto a.out	9/25/2002	12:23:53	5	42	79.7	60.3	1178.8	35.8	30
Coil1_Test_Cycling_auto a.out	9/25/2002	12:59:53	6	43	79.5	60.2	1177.1	23	16
Coil1_Test_Cycling_auto a.out	9/25/2002	13:23:08	7	43	79.5	60.3	1176.3	23	16
Coil1_Test_Cycling_auto a.out	9/25/2002	13:46:23	8	43	79.6	60.4	1179	23	16
Coil1_Test_Cycling_auto a.out	9/25/2002	14:09:38	9	44	79.4	60.3	1175.1	19.8	10
Coil1_Test_Cycling_auto a.out	9/25/2002	14:29:38	10	44	79.4	60.1	1176.9	19.8	10
Coil1_Test_Cycling_auto a.out	9/25/2002	14:49:38	11	44	79.3	60.2	1176.9	19.8	10
Coil1_Test_Cycling_auto2.out	9/30/2002	12:29:52	3	45	79.3	60.5	1183.7	24.3	7
Coil1_Test_Cycling_auto2.out	9/30/2002	12:54:22	4	45	79.3	60.3	1177.7	24.3	7
Coil1_Test_Cycling_auto2.out	9/30/2002	13:18:52	5	45	79.4	60.3	1181.4	24.3	7
Coil1_Test_Cycling_auto2.out	9/30/2002	13:43:22	6	46	79.4	59.9	1179.1	60.3	5.5
Coil1_Test_Cycling_auto2.out	9/30/2002	14:43:52	7	46	79.4	60.4	1185.2	60.3	5.5
Coil1_Test_Cycling_auto2.out	9/30/2002	15:44:22	8	46	79.4	60.4	1182.1	60.3	5.5

## **APPENDIX H2**

### **Summary of Laboratory Data for Coil 2**

**Summary of Laboratory Data for Coil 2**  
**November 2005**



15.5 fpi, lanced sine wave fin

Manufacturer & Model number:	Carrier FK4CNF002000AGAA
Nominal size:	1 ½ - 3 tons
Baseline Size and Airflow (Test 4):	2.4 tons / 970 cfm
Coil type:	“A” coil, 3 rows, 15.5 fpi (aluminum fins)
Coil dimensions:	3.41 ft <sup>2</sup> total finned face area (face area = 3.46 ft <sup>2</sup> per manufacturers literature) 2 slabs @ (13 7/8 in x 17 11/16 in) 3.2 ft <sup>2</sup> finned face area exposed to air flow 2 slabs @ (13 3/8 in x 17 ¼ in)
Coil thickness:	2 ¼ in
Tube diameter:	3/8 in OD copper
Tube spacing:	1 in within row (vert); ¾ in row-to-row (horiz)
Expansion device:	TXV (6-8°F superheat)
Unit supply fan:	off
Compressor power:	60 hz, direct

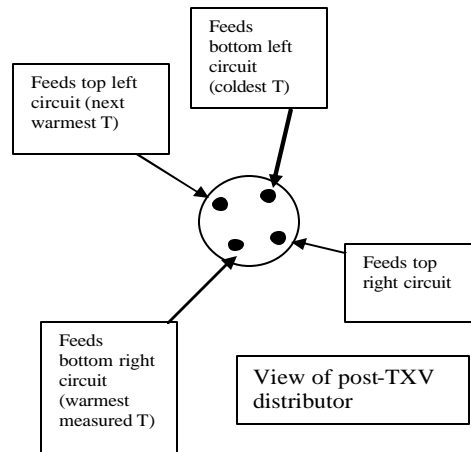
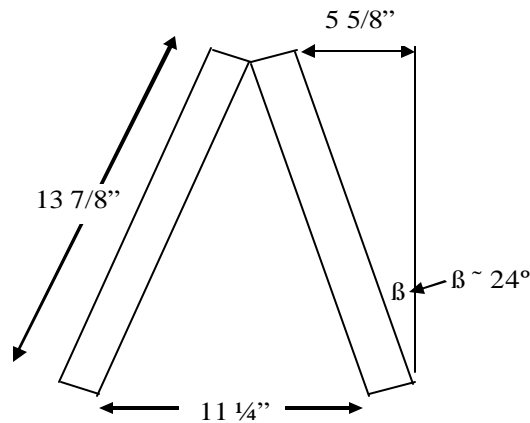




**Table 1. Summary of Steady State Test Conditions Corresponding or Each Run or Test**

	<i>Entering Coil Conditions</i>					
	<i>80/67°F 60°F dp</i>	<i>80/72°F 68°F dp</i>	<i>80/62°F 50°F dp</i>	<i>75/68°F 64°F dp</i>	<i>75/63°F 56°F dp</i>	<i>75/58°F 45°F dp</i>
400 cfm/ton	#4 (or 3)	#5	#6	#7	#8	#9
300 cfm/ton	#10	#11	#12	#13	#14	#15
200 cfm/ton	#16	#17	#18	#19	#20	#21
450 cfm/ton	#22	#23	#24			
400-200 cfm/ton (ON & OFF)	#25					
Low suction (41°F)	#1					
High suction (51°F)	#2					

Notes: Tests 4-25 all at nominal suction of 45 °F (set at nominal conditions of test #3/4). A thermal expansion device was used, with nominal superheat of 6-8°F set during Test 4. The refrigerant charge established during Test 4 was not changed for the remaining tests. The Table 1 test points denote the target testing conditions. Drier test conditions with dew points below 50°F (such as Tests #9, #15, and #21) could not be achieved. In these cases, entering conditions were typically held near 50°F dp. For each test, the compressor is ON for 45-90 minutes and then the compressor is OFF for 45-60 minutes. The booster fan runs continuously for all tests (when the compressor is both ON and OFF).

**Steady State Performance**

The nominal performance characteristics for this coil (based on steady-state conditions from Run #4 below) are:

Total Capacity:	28.5 MBtu/h (2.4 tons)
Sensible Capacity:	21.8 MBtu/h
Latent Capacity (condensate):	6.7 MBtu/h
Sensible Heat Ratio:	0.77

Latent capacity can be calculated two ways: 1) using dew point readings and air flow, and 2) the condensate flow rate. Figure 1 compares the latent capacity calculated these two ways. The number of each data point corresponds to the test number listed in Table 1. In general, the condensate readings resulted in a slightly lower capacity.

Figure 2 shows the trend of steady-state sensible heat ratio (SHR) with relative humidity and airflow rate. The cooling capacities used to calculate SHR in Figure 2 are based on airflow measurements and the psychrometric conditions entering and leaving the cooling coil. This performance map is typical of a cooling coil (i.e., SHR is mostly a function of the entering relative humidity, with some dependence on the air flow rate).

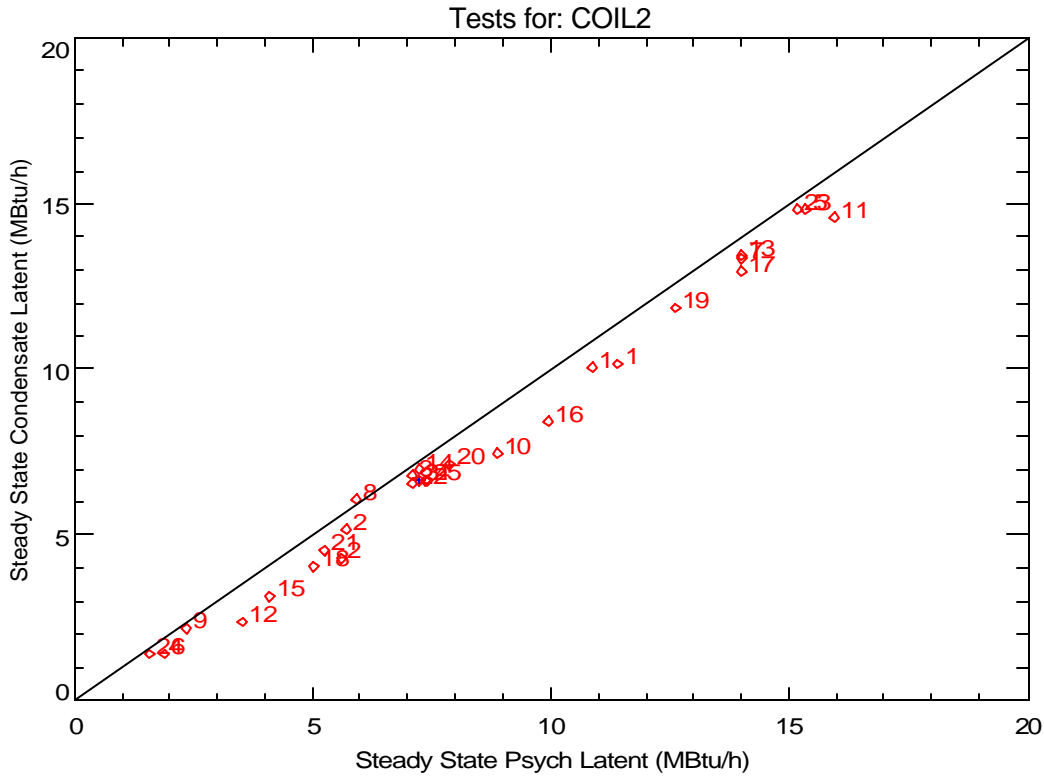


**Figure 1. Comparing Steady-State Latent Capacity Calculated From Psychrometric State Points and Condensate Removal Rates**

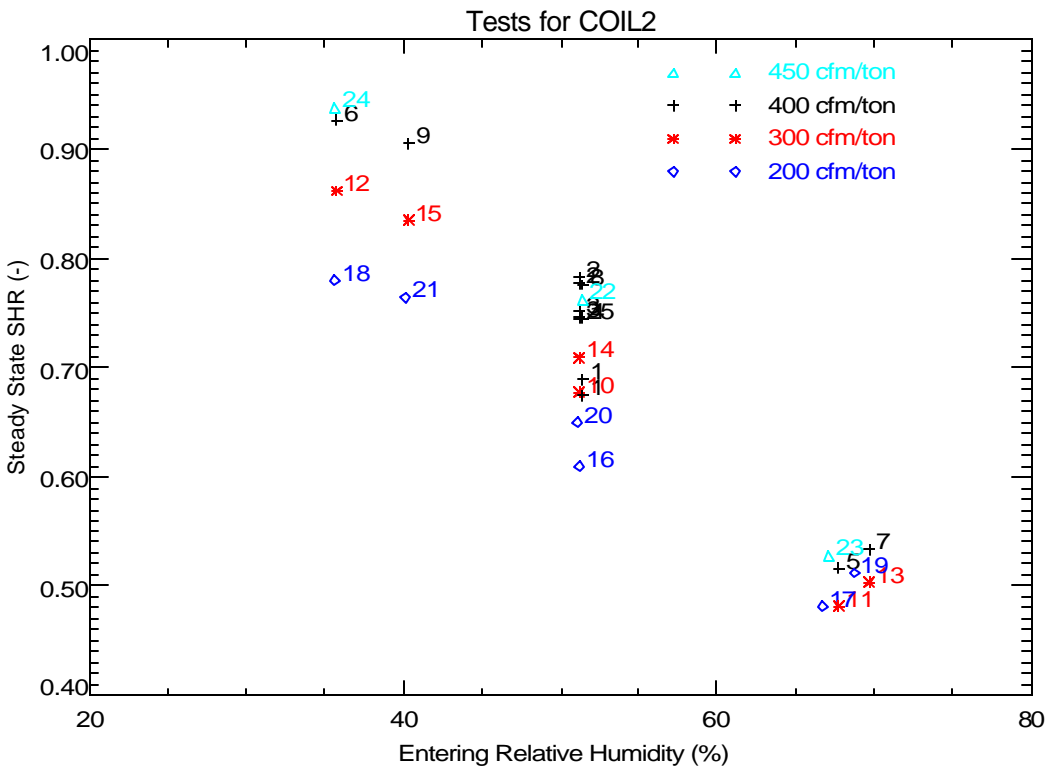


**Figure 2. Variation of Steady State SHR with Entering Humidity and Nominal Air Flow**

## **Typical Transient Performance**

Figure 3 shows the typical transient performance of the cooling coil at nominal conditions (i.e., for Cycle 2 of Run #4). The compressor runs for 45 minutes and is off for 45 minutes. The booster fan remains on during the entire test (separate external fan used to maintain the desired air flow rate across the cooling coil). A portion of the moisture removed by the coil during the compressor on cycle evaporates back into the air stream during the off cycle. During the off cycle the coil acts as an evaporative cooler, so the sensible capacity is nearly equal to the absolute value of the latent capacity (i.e., the sum of latent and sensible is zero).

If we integrate the off cycle sensible capacity (after allowing for a 1-minute off-cycle delay to account for refrigerant movement and other transient effects), we can determine the energy associated with the moisture retained on the coil. To minimize the integration of any measurement errors, the off-cycle integration stops at the time labeled “Integration Pt.” on the plot. This point corresponds to the time when the temperature and dew point differences across the coil have first reached the terminal values (i.e., the averages from the end of the off-cycle). In this case the integration indicates that the sensible cooling is equivalent to 1.98 lbs of moisture being retained on the coil. The integrated latent capacity – which is harder to measure precisely – equals 1.97 lbs.

The value “twet” from Henderson and Rengarajan (1996) can then be calculated by dividing the retained moisture mass (expressed as Btu; mass x 1060 Btu/lb) and the steady state psychrometric latent capacity ( $Q_L=7.4$  MBtu/h). The values of twet based on integrated sensible and latent off-cycle capacity are 17.0 and 16.9 minutes respectively. These values of twet are similar but not identical to the measured delay of 16.3 minutes for the first condensate pulse to fall from the drain pan. The value of gamma (1.60), which is the initial off-cycle moisture evaporation rate divided by the steady-state psychrometric latent capacity, uses the off-cycle moisture evaporation rate (11.9 MBtu/h) once the saturated coil temperature is within 1°F of the entering air wet-bulb temperature. At this point where gamma is determined, it is assumed that all coil heat and mass transfer with the air stream is adiabatic (the refrigerant flow could not be used as an indicator of this point for this coil since it used a TXV that totally shut off refrigerant flow during the off cycle). The off-cycle sensible capacity also shows a change in the decay trend at this point. In this case it took about 1.5 minutes for coil temperature to approach the wet bulb within the specified tolerance.

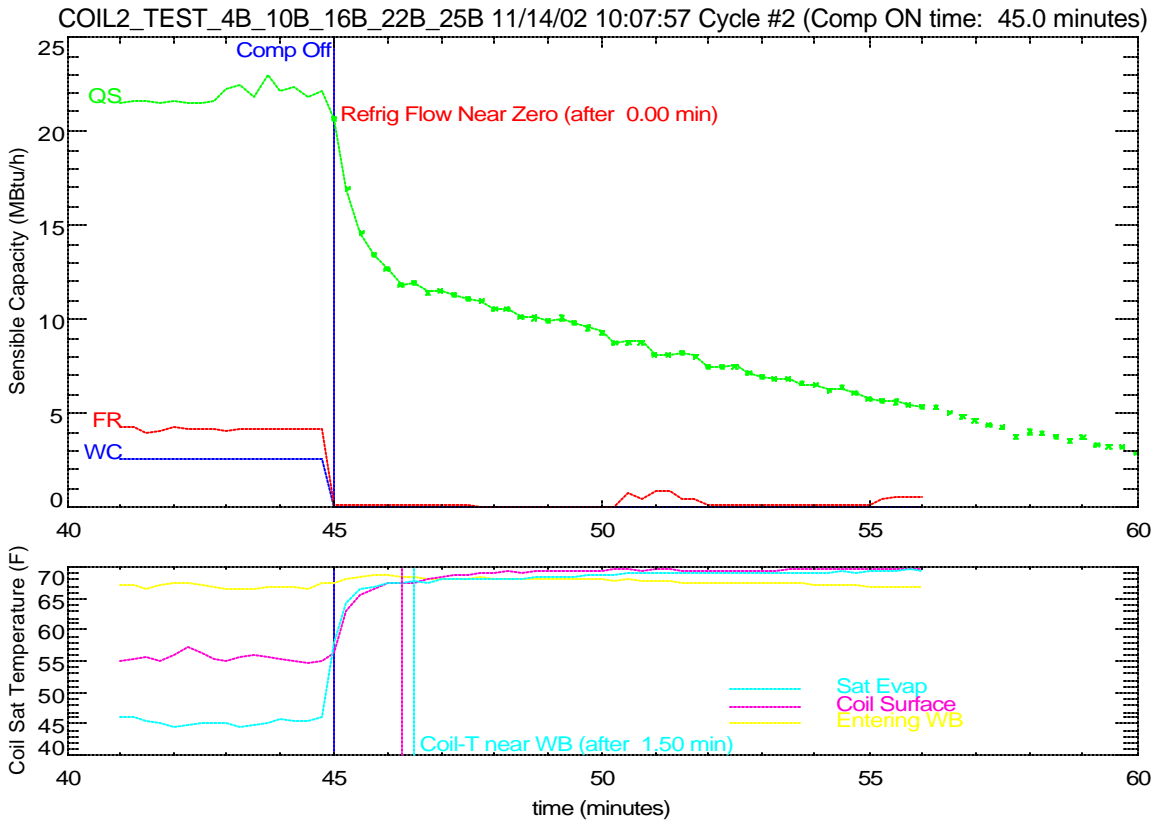
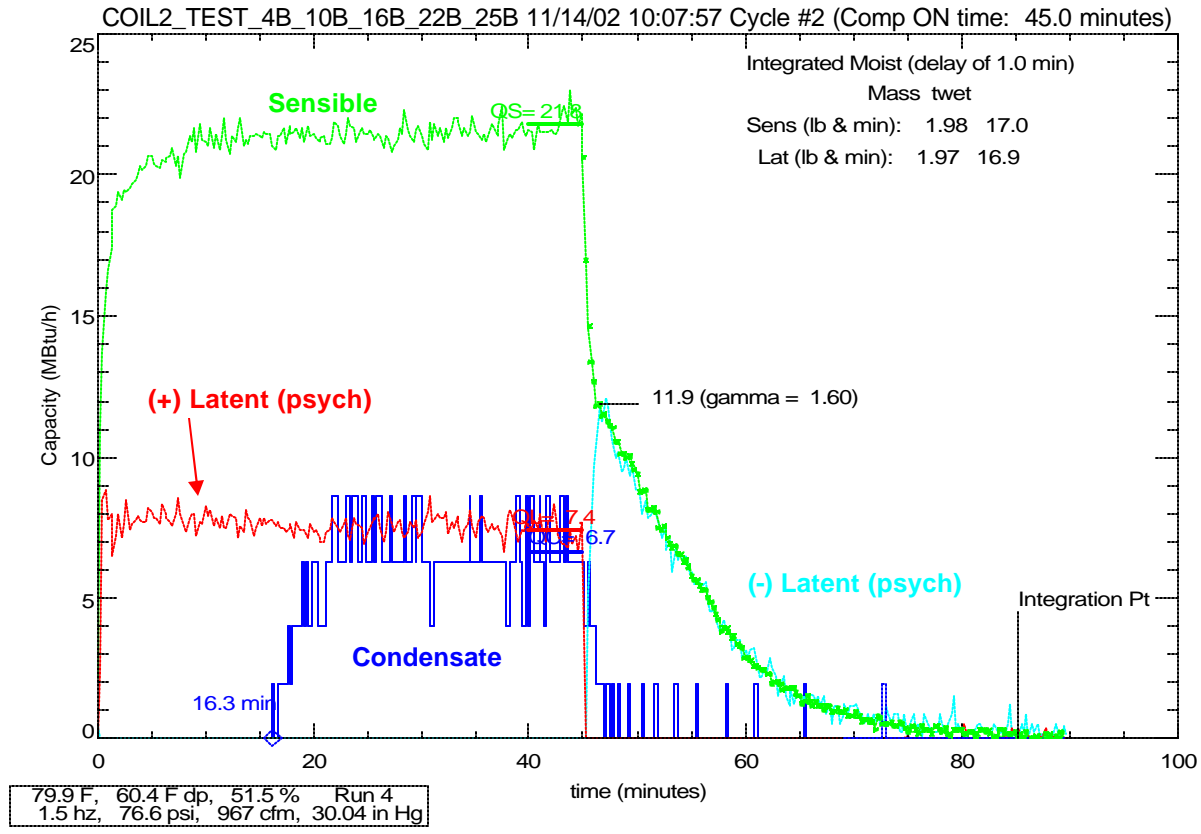
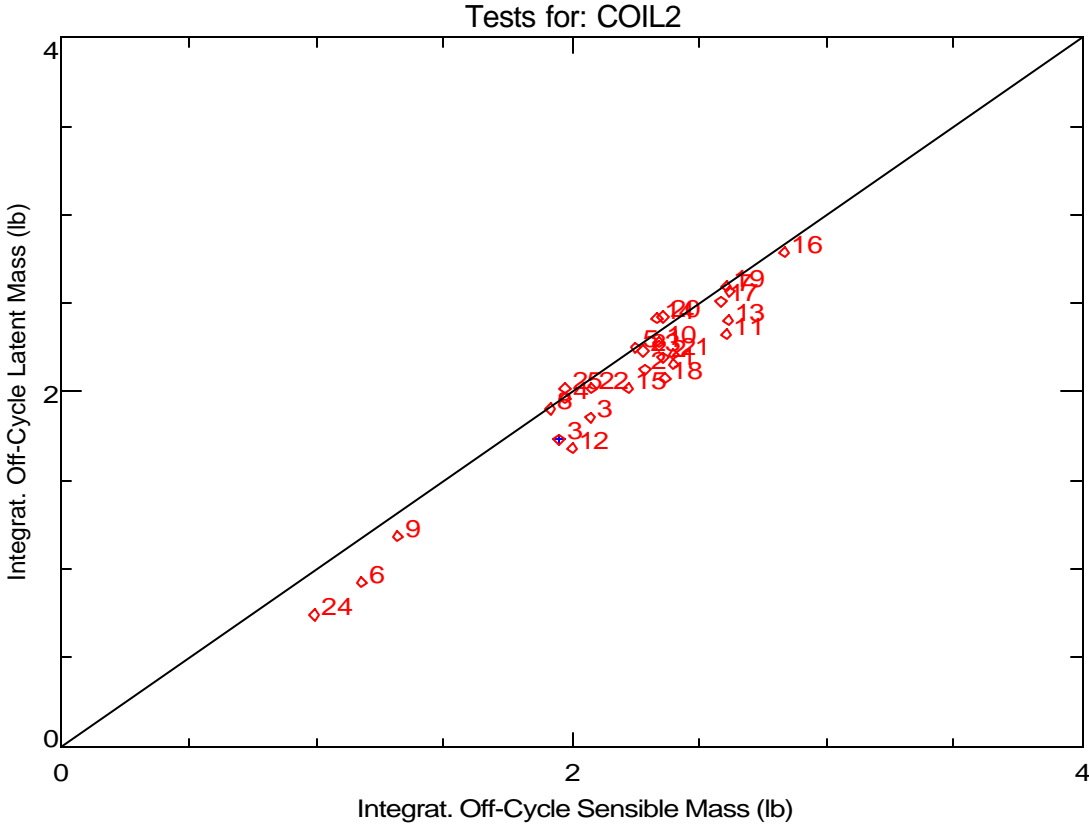


Figure 3. Example Plots of Detailed Data for Coil 2

**Part Load Latent Capacity Parameters**

The amount of moisture held on the cooling coil (and drain pan) can be calculated by integrating the off-cycle capacity from the coil (and dividing by the heat of vaporization, 1060 Btu/lb, to get the moisture mass). The integration is delayed for the first minute of the off-cycle so that the overshoot response of the chilled mirror dew point hygrometers does not skew the results of the integration<sup>1</sup>. The integration terminates once steady state conditions are reached for the off cycle. If we assume the coil acts as an evaporative cooler, sensible and latent capacity should be equal. Figure 4 compares the off-cycle integrated latent and sensible capacity calculated for each run. In this case the integrated sensible capacity is about the same as the integrated latent capacity. Figure 5 shows that the bias is not a function of dew point as was observed from tests of Coil 1.

Since we expect that off-cycle latent and sensible capacity should sum to zero, we have selected the integrated off-cycle sensible capacity as the most consistent and believable indication of the moisture mass held on the cooling coil (and drain pan).



**Figure 4. Comparing Stored Moisture Mass Calculated by Integrating Sensible and Latent Off-Cycle Capacity (Integrated with a 1 minute delay)**

<sup>1</sup> The 1-minute delay causes the estimate of moisture mass to be low by as much as 0.19 lbs (or 9%).

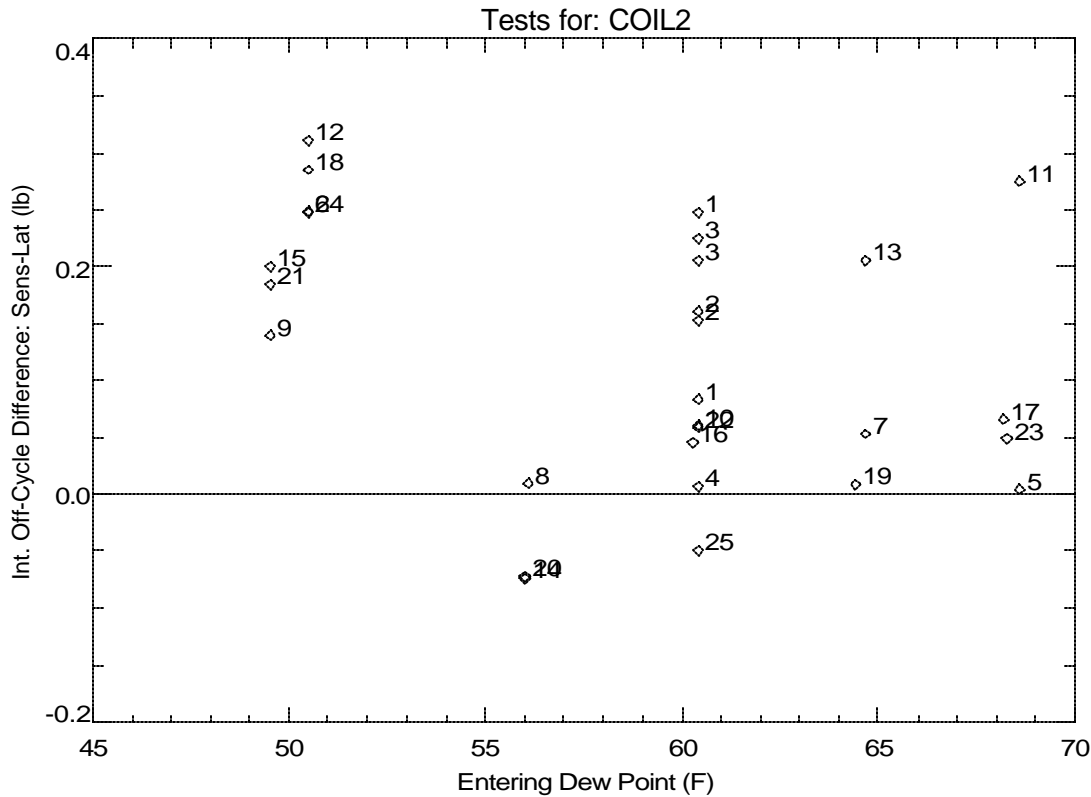


**Figure 5. Variation of Off-Cycle Sensible-Latent Difference with Entering Dew Point**

The parameter “twet” is the moisture mass held on the cooling coil times the enthalpy of vaporization (1060 Btu/lb) divided by the steady-state latent capacity of the cooling coil. The parameter should physically correspond to the time it takes for moisture to first fall from the coil (ignoring startup delays and other effects). Figure 6 compares the calculated “twet” (determined from integrating sensible capacity during the off-cycle and then dividing by the steady-state psychrometric latent capacity during the on-cycle) to the condensate delay time for all the test runs. There is relatively good agreement between these two values.

Figure 7a and 7b show that both twet and the condensate delay time are a function of the entering air dew point temperature. Figure 7b uses different symbols to show the 1<sup>st</sup> and 2<sup>nd</sup> cycles in each test sequence with flow rate of 400 cfm/ton for all tests. The delay time was sometimes higher for the first cycle when the fin surfaces were totally dry. For the 2<sup>nd</sup> cycle, the coil may have had better watability than it did for the 1<sup>st</sup> cycle in some cases.

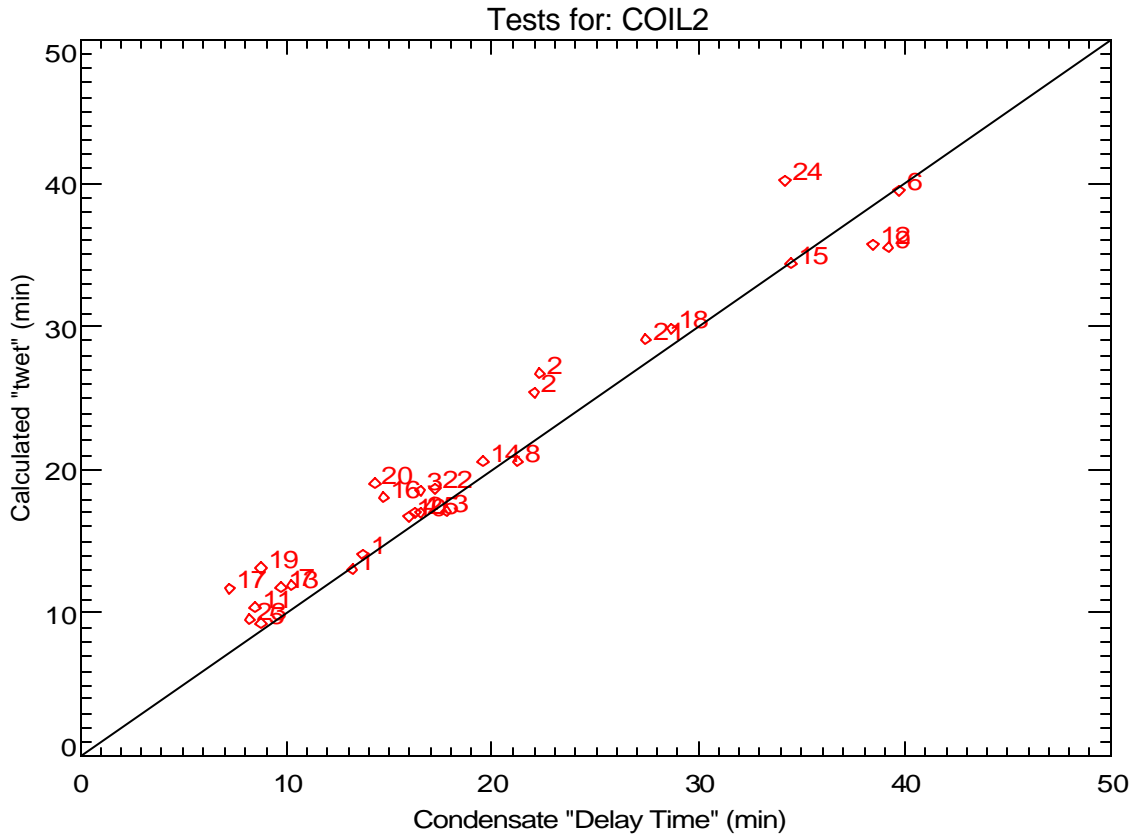


**Figure 6. Comparing “twet” (calculated with off-cycle sensible and steady state latent) to the Condensate Delay Time**

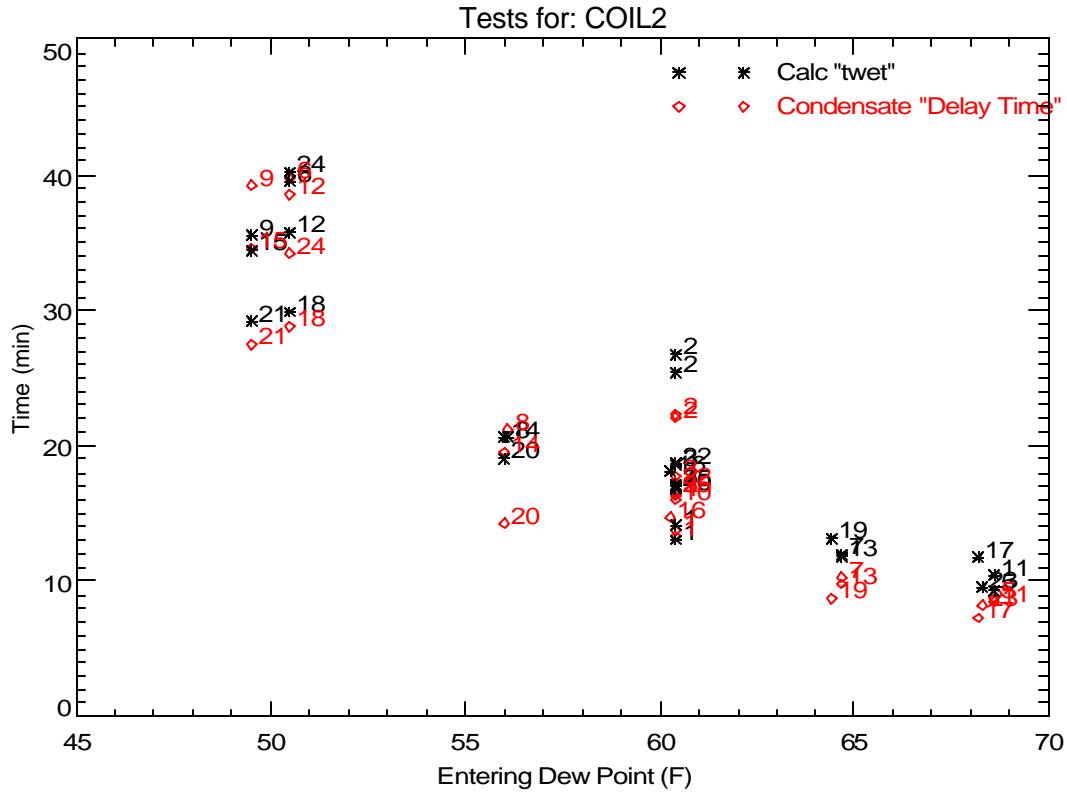


Figure 7a. Impact of Dew Point on “twet” and Condensate Delay Time

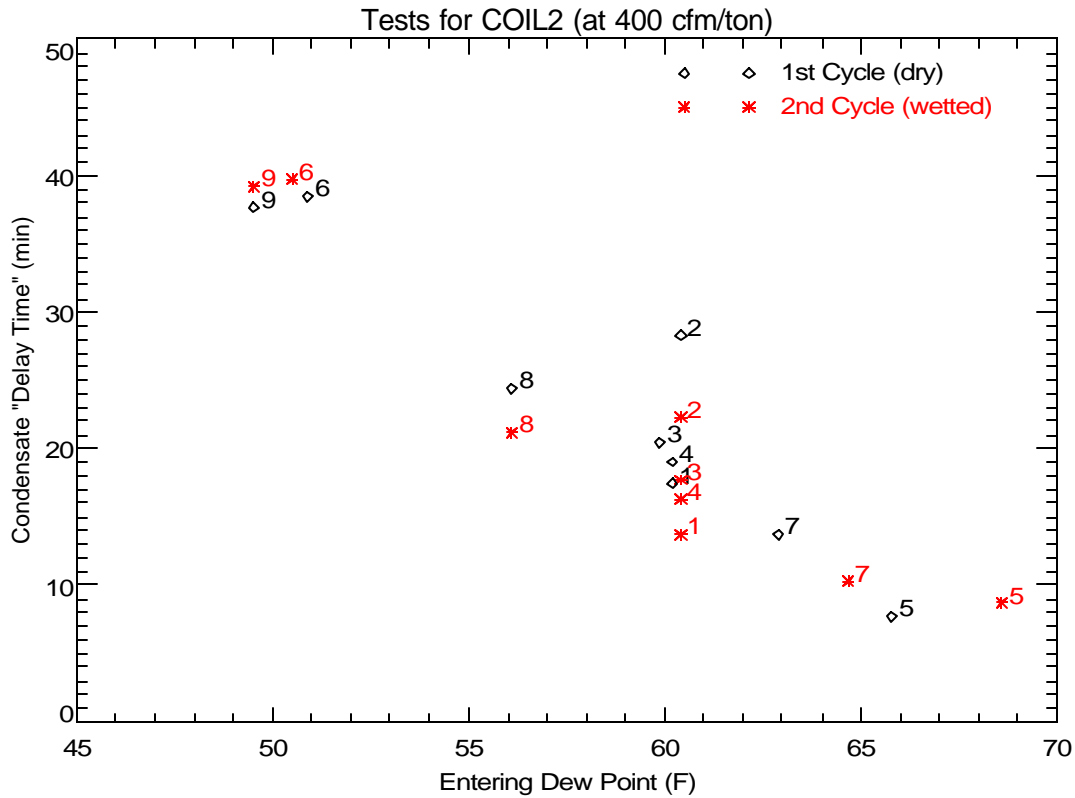


Figure 7b. Impact of Dew Point and Coil Wettedness on Condensate Delay Time

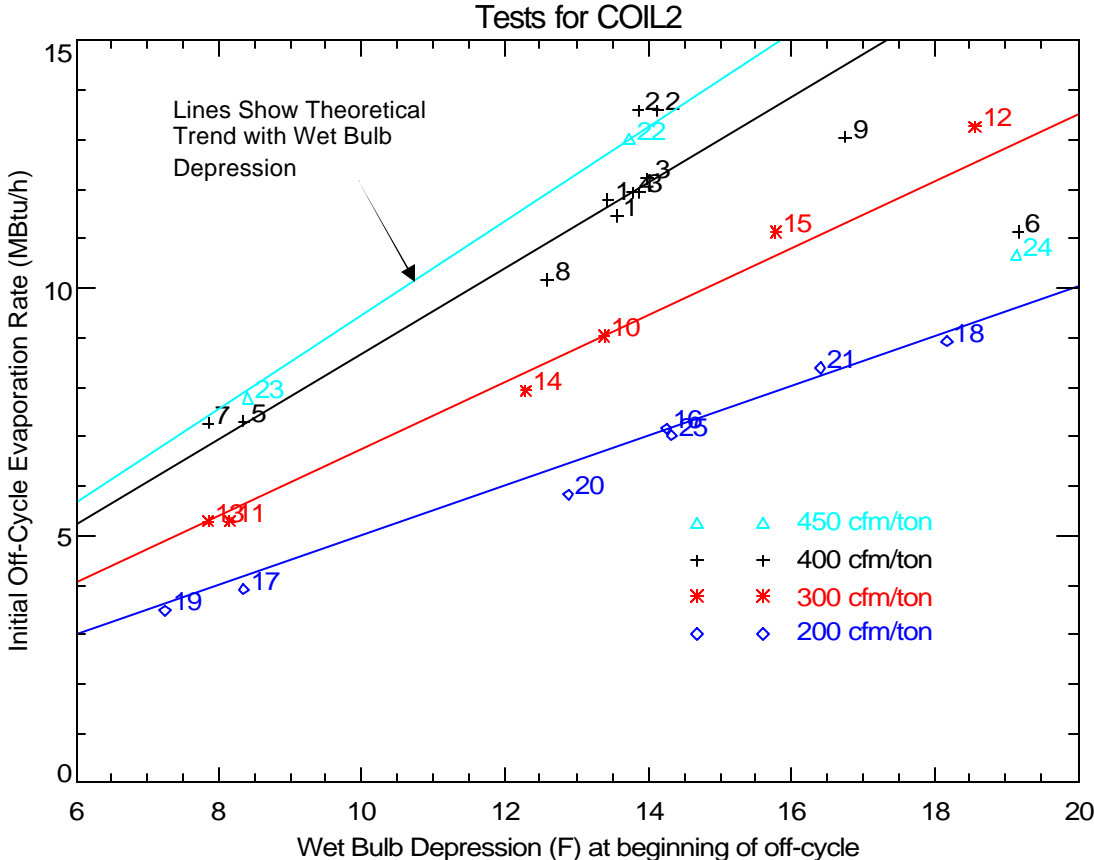


Figure 8 shows the initial off-cycle moisture evaporation rate varies with wet bulb depression. As expected, the evaporation rate is highest when the entering air has a larger wet bulb depression (i.e., has a lower relative humidity) and a higher airflow rate.

The model developed by Henderson and Rengarajan (1996) used the following simple evaporative cooler model to predict the moisture evaporation rate at off-design conditions:

$$Q_{\text{evap}} = Q_{\text{evap}_o} \times \frac{(DB - WB)}{(80 - 67)}$$

where  $Q_{\text{evap}_o}$  is the evaporation rate at the nominal entering air conditions of 80°F dry bulb (DB) and 67°F wet bulb (WB). This simple model is shown as the lines in Figure 8. For each airflow rate, the line is based on the nominal test results at 80°F DB/67°F WB extended to pass through zero. The measured data show essentially the same slope as the theoretical lines. The notable exceptions are the points with higher airflow and drier entering conditions. Specifically, Tests #6, #9, and #24 deviate significantly from the lines. These runs have a much lower initial moisture evaporation rate because the entering air dew point temperature was close to the cooling coil temperature, so the fin surfaces were not fully wetted (as shown in Figure 4 above). The smaller wetted surface area reduces the initial moisture evaporation rate.



**Figure 8. Measured Variation of Initial Evaporation Rate with Wet Bulb Depression**

Stabat et al. (2001) reviewed the theoretical performance of direct evaporative coolers and showed that the saturation effectiveness of an evaporative cooler is:

$$h_{evp} = 1 - e^{-NTU} \quad \text{where} \quad NTU = K/cfm^{0.2} \quad \text{for an air-water mixture.}$$

The line shown on Figure 9 is the best fit of the equation above to the measured data. The resulting constant K was 7.23, which is equivalent to an NTU of 1.83 at 1,000 cfm. While there is considerable scatter due to the experimental uncertainty of predicting the initial off-cycle moisture evaporation rate, the slope of the line is still representative of the overall trend.

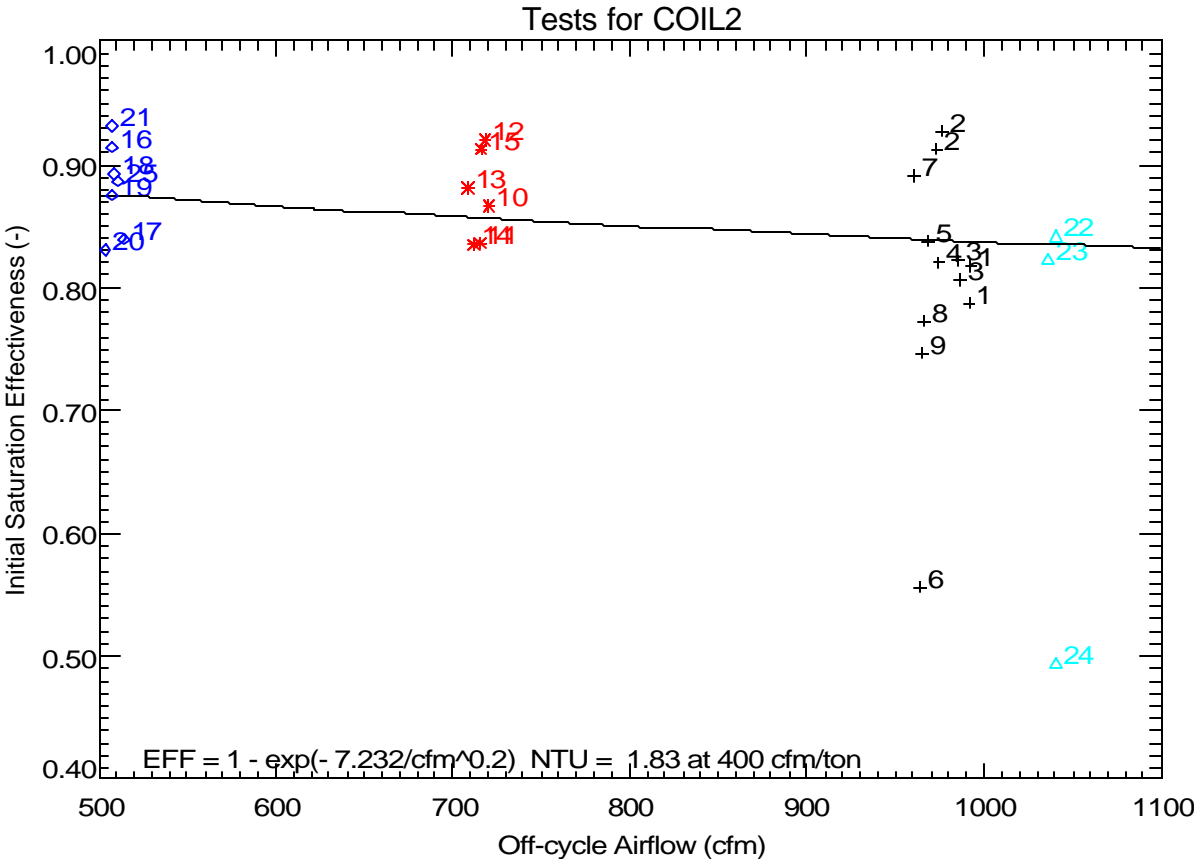


**Figure 9. Evaporative Effectiveness versus Airflow**

Figure 10 compares the measured initial off-cycle moisture evaporation rate for each test to the predicted initial evaporation rate using the effectiveness model above. The model and measured data generally agree when presented in this form (i.e., the overall agreement visually appears better than in Figure 9 above). Again, the variation that occurs for Tests #6, #9, and #24 was due to partial coil dryout, as mentioned above.

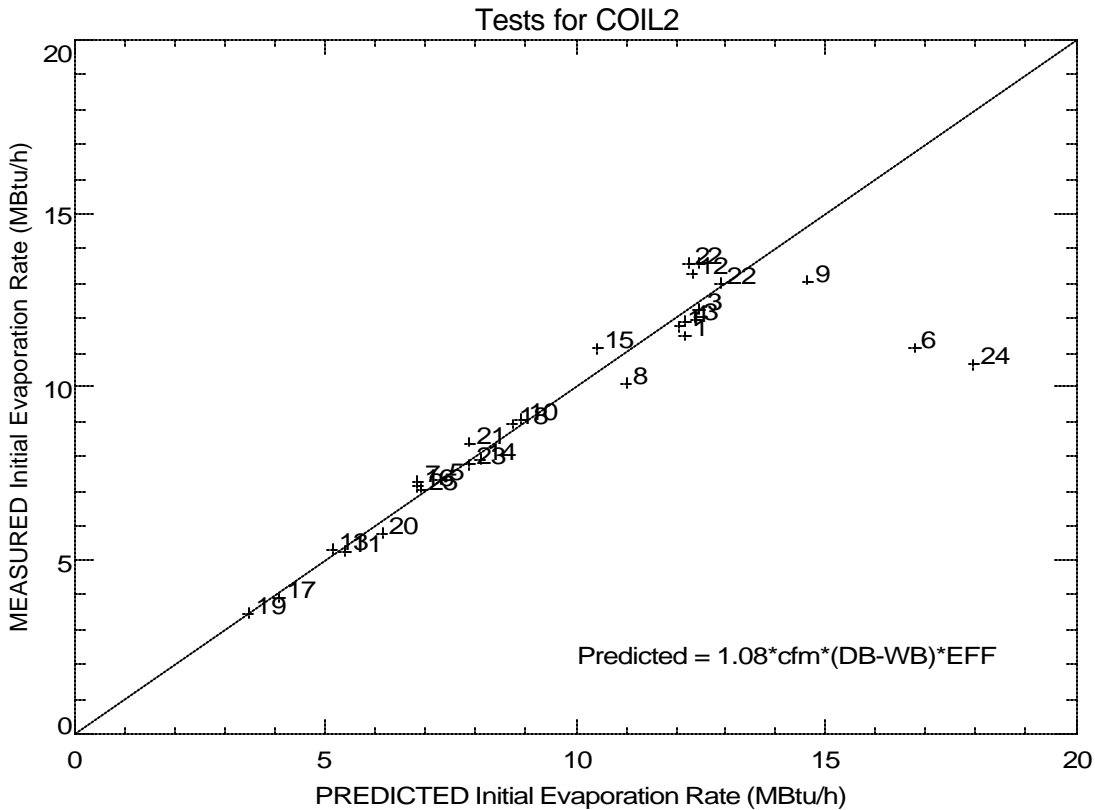


**Figure 10. Comparing Measured and Predicted Initial Moisture Evaporation Rates**

Figure 11 and Figure 12 below evaluate whether the amount of moisture retained on the cooling coil is a function of air flow or entering air conditions. At higher dew points (Figure 11) the moisture holding capacity of the coil approaches the equilibrium value. At lower dew points the moisture holding capacity is slightly less, especially for Tests #6, #9, and #24. For these tests, portions of the cooling coil were not fully wetted, since the coil surfaces were warmer than the entering air dew point temperature. For the other test conditions, where the coil surfaces were fully wetted, the amount of retained moisture on the cooling coil ranges from 2.0 to 2.7 lbs.

Figure 12 shows a 10-20% decrease in the amount of retained moisture with higher air flow rates. This variation of retained moisture with air flow rate for Coil 2 is similar to that seen for Coil 1.

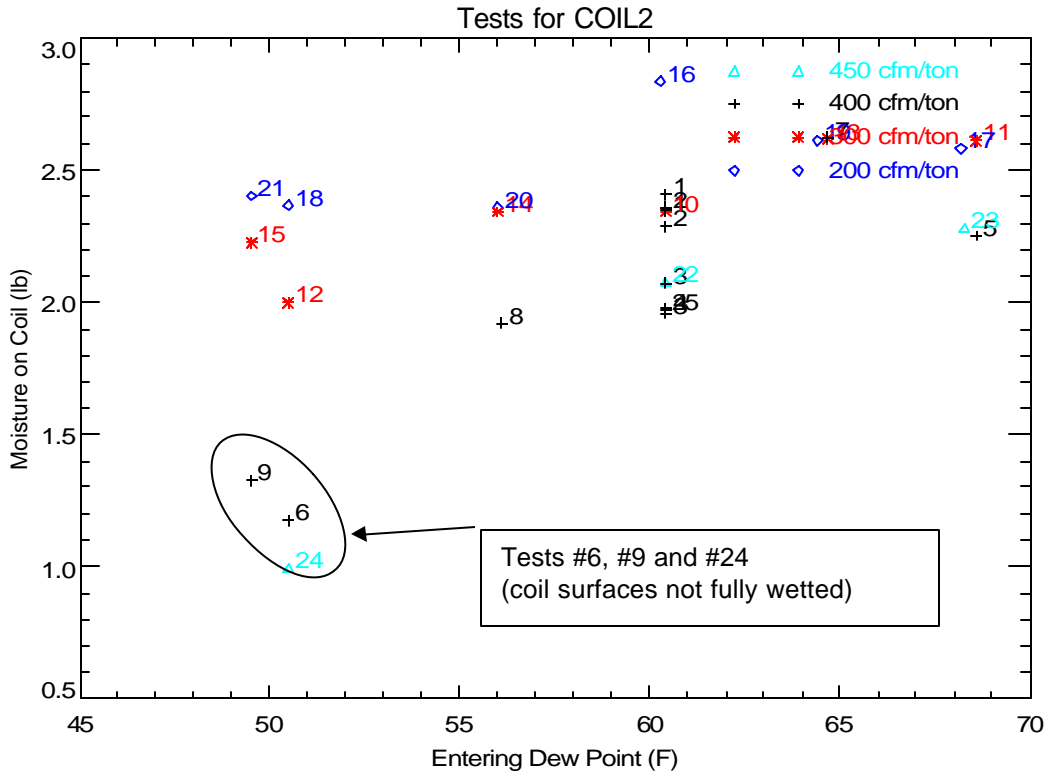


Figure 11. Variation of Retained Moisture (based on Off-Cycle Sensible) with Flow and Dew Point

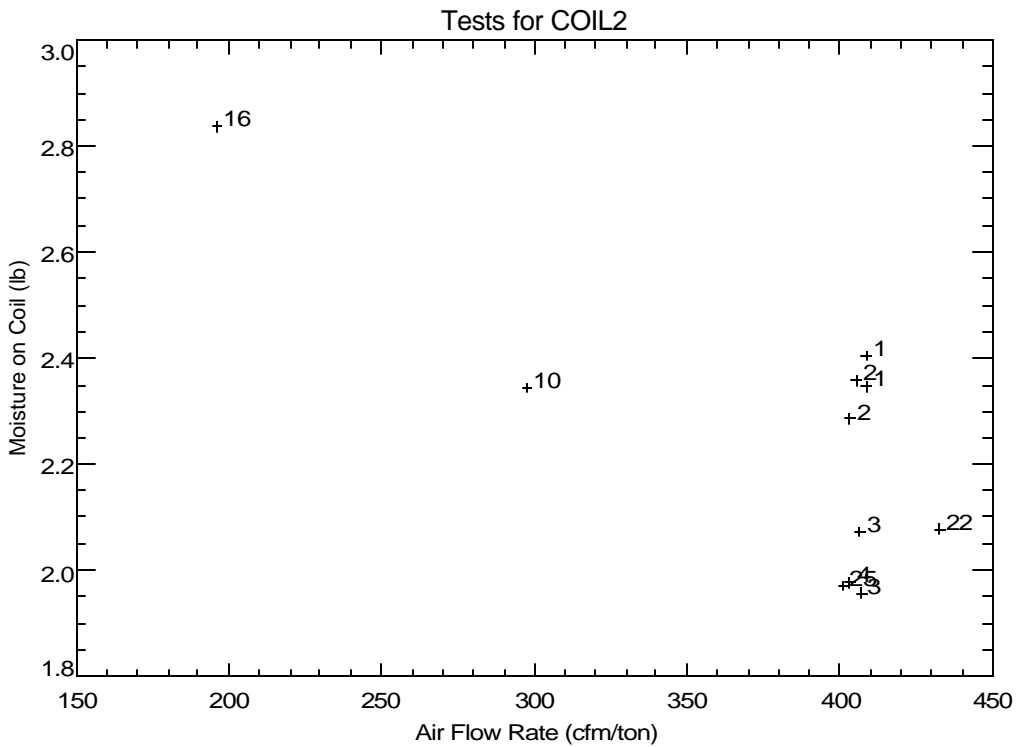
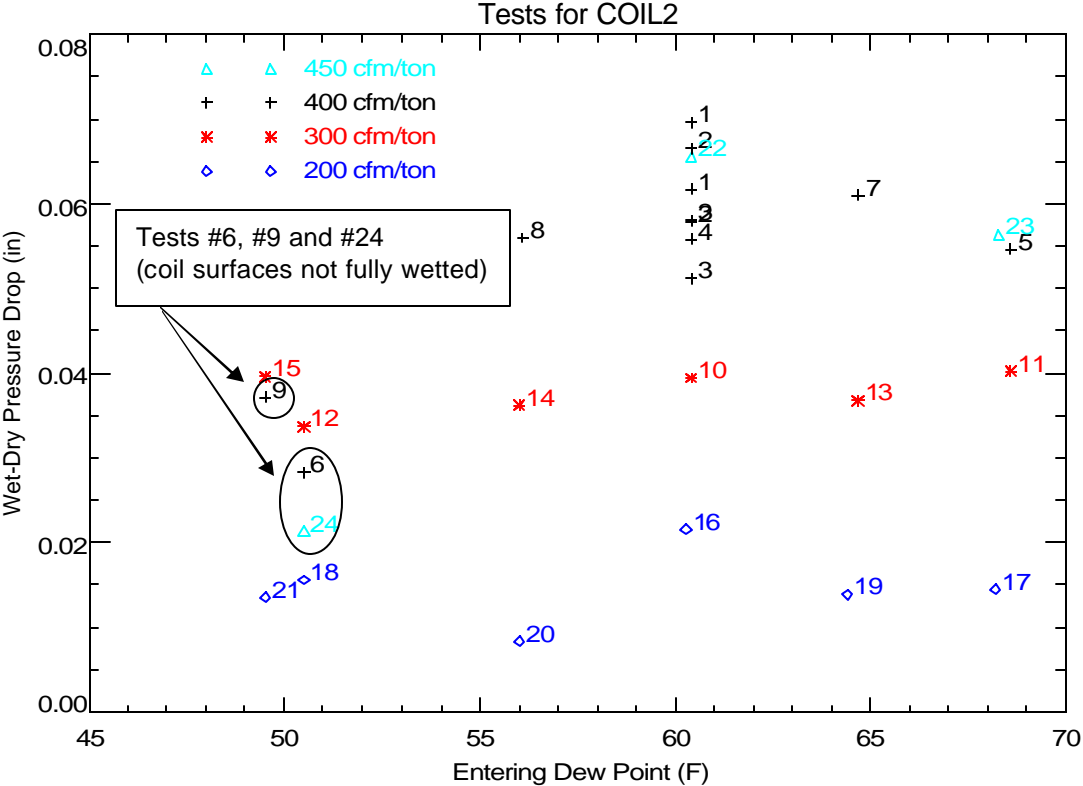


Figure 12. Variation of Retained Moisture with Air Flow at Nominal Entering Conditions of 80°F, 60.4°F dew point

Another way to detect the amount of retained moisture is to measure the static air-side pressure drop across the cooling coil. The difference between the pressure drop across the coil under wet and dry conditions should provide an indication of the amount of retained moisture (the wet coil pressure drop is measured at steady-state conditions while the dry coil pressure drop is taken as the average pressure drop during the last part of the off-cycle). Figure 13 shows the variation of the wet-dry pressure difference with various entering humidity conditions at multiple air flow rates. Comparing the values for each air flow rate generally shows a trend of pressure drops reaching a plateau once the humidity of the entering air is sufficiently high to fully wet the coil. For air flow rates of 200 cfm/ton and 300 cfm/ton, the wet-dry pressure difference remained fairly constant for the range of entering air dew point temperatures that were tested, indicating a fully wetted coil. The wet-dry pressure drops for Tests #6, #9, and #24 are all significantly lower than expected, again confirming that less moisture was retained on the cooling coil at these drier/higher air flow conditions.



**Figure 13. Variation of Wet-Dry Pressure Drop with Entering Conditions and Air Flow Rate**

Figure 14 confirms that the wet-dry pressure drop is a linear function of air flow rate, which implies laminar flow in the wetted cooling coil.

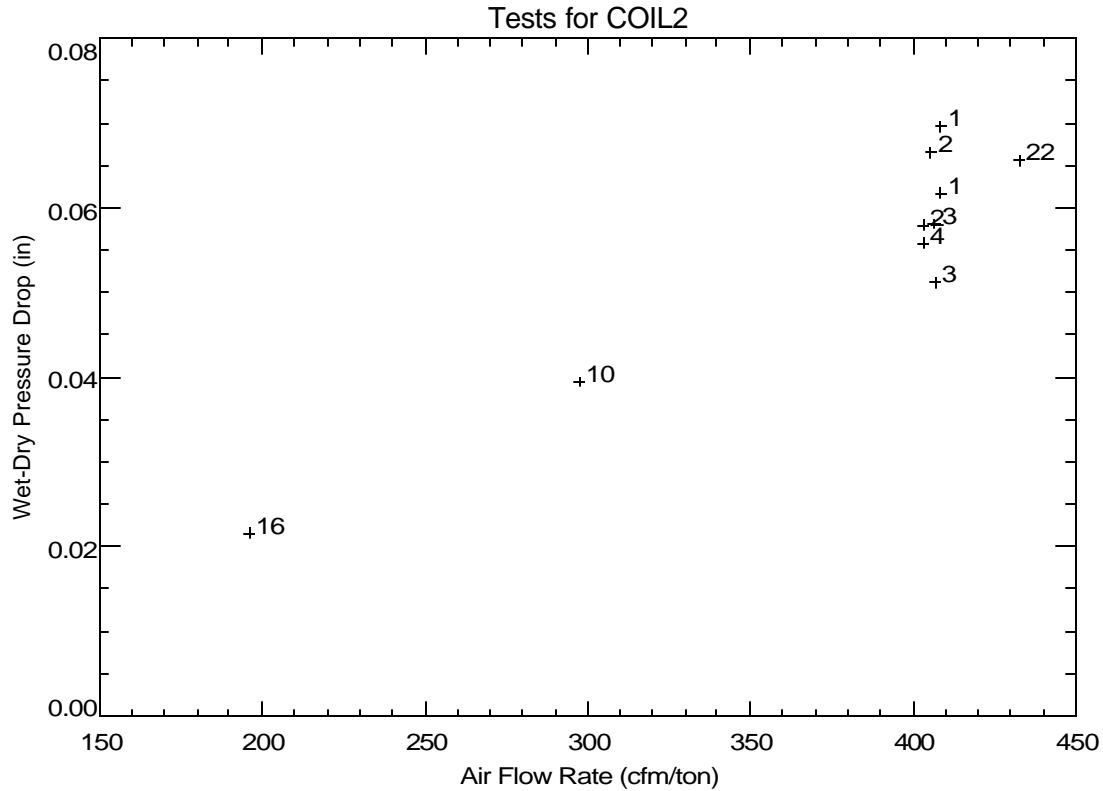


**Figure 14. Trend of Wet-Dry Pressure Drop with Flow at Nominal Entering Conditions of 80°F, 60.4°F dew point**

The series of plots in Figure 15 show the impact of coil suction temperature on performance. The steady-state performance of the system shows the expected trends of lower SHR and greater latent capacity at lower coil temperatures (i.e., lower saturated suction temperatures). However, both the mass of moisture on the coil and the wet-dry pressure drop imply that less moisture was retained on the coil for Test 3. It is not clear what caused this unexpected result.

The graph of fan power versus saturated suction temperature in Figure 15 is not relevant since the AHU fan was turned off during all tests. For this cooling coil, an external booster fan was used to obtain the desired air flow rate for each test.

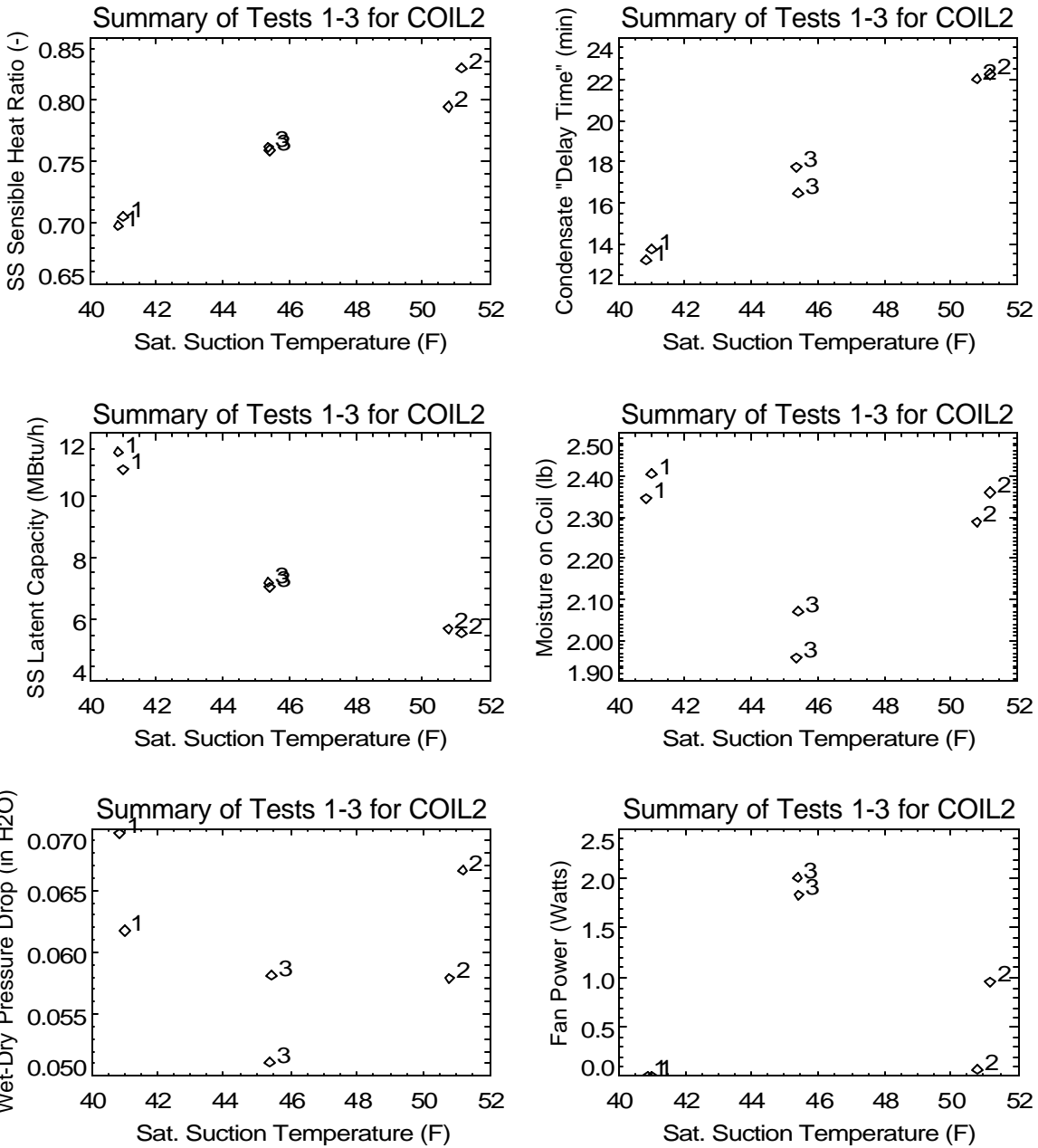


**Figure 15. Trend of Various Parameters with Saturated Suction Temperature**

## Overall Latent Degradation Trends

Several quasi-steady cyclic tests were also completed in the laboratory to quantify the overall part-load degradation of latent capacity. Table 2 lists the cycling test runs. These conditions correspond to a conventional thermostat with a maximum cycle rate of 3 cycles per hour (at 50% runtime).

**Table 2. Cyclic Test Conditions**

CONST FAN <sup>1</sup>	AUTO FAN <sup>2</sup>	Number of Times Test Repeated	ON Time (minutes)	OFF Time (minutes)	Runtime Fraction (-)	Cycle Rate (cycles/h)
Run						
31	41	2	45	45	0.500	0.667
32	42	3	30	6	0.833	1.667
33	43	3	16	7.25	0.688	2.581
34	44	3	10	10	0.500	3.000
35	45	3	7	17.5	0.286	2.449
	46	3	5.5	55	0.091	0.992

Notes: <sup>1</sup>Constant fan tests performed at 80°F db/60.4°F dp inlet air with 400 cfm/ton (runs 31-35) and 300 cfm/ton (runs 71-75) air flow. Tests also conducted at 75°F db/56°F dp (runs 61-65) and 75°F db/64°F dp (runs 51-55) inlet air with 400 cfm/ton air flow.

<sup>2</sup>Auto fan tests performed at 80°F db/60.4°F dp inlet air with 400 cfm/ton air flow.

Figure 16 through Figure 19 show the net impact of part-load system operation based on cyclic tests completed in the lab. All of these tests are in the constant fan mode (continuous air flow over the cooling coil while the coil cycles on/off), but at various entering air and flow rate conditions:

- Nominal: 80°F & 60.4°F dew pt. with 400 cfm/ton (Figure 16)
- Humid: 75°F & 64°F dew pt. with 400 cfm/ton (Figure 17)
- Dry: 75°F & 56°F dew pt. with 400 cfm/ton (Figure 18)
- Low Flow: 80°F & 60.4°F dew pt. with 300 cfm/ton (Figure 19)

The measured data generally compare well to the model from Henderson and Rengarajan (1996) using the model parameters shown on each plot. These parameters were always taken from the 2<sup>nd</sup> occurrence of the first test in each sequence (i.e., Tests #31, 51, 61 and 71), which were completed as part of the suite of cycling tests listed in Table 2 for the constant fan mode. The latent time constant ( $\tau$ ) of 20 seconds was selected based on qualitative observations of the coil's response time. The solid black line corresponds to the linear off-cycle evaporation model. The black dotted line assumes an off-cycle evaporation trend that corresponds to an exponential decay. The purple line is the new part load LHR model that uses the more realistic evaporation model from Stabat et al. (2001) and also allows for variable amounts of moisture on the coil at the end of the on cycle. The parameters NTU and  $t_p$  were determined from the specific measured data from each test sequence (the purple solid line) as well as the average NTU and  $t_p$  from all the data (the purple dotted line), including Figure 9 above. The parameter  $t_p$  is defined in the improved model development section of this report.

In general the measured data corresponding to the later repetitions of each test (i.e., 2<sup>nd</sup> and 3<sup>rd</sup> cycle) showed the best agreement with the models, since quasi-steady conditions had been achieved.



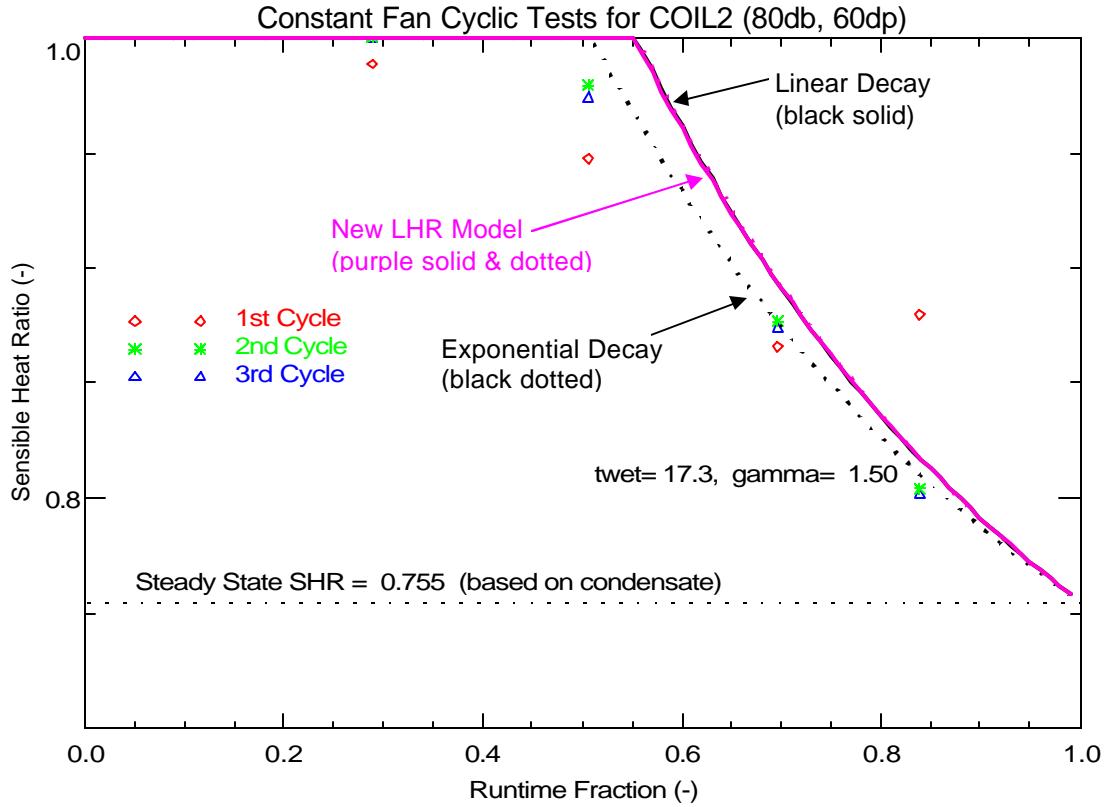


Figure 16. Comparing Measured Latent Degradation to the LHR Models: Nom. Conditions (80°F / 60.4°Fdp)

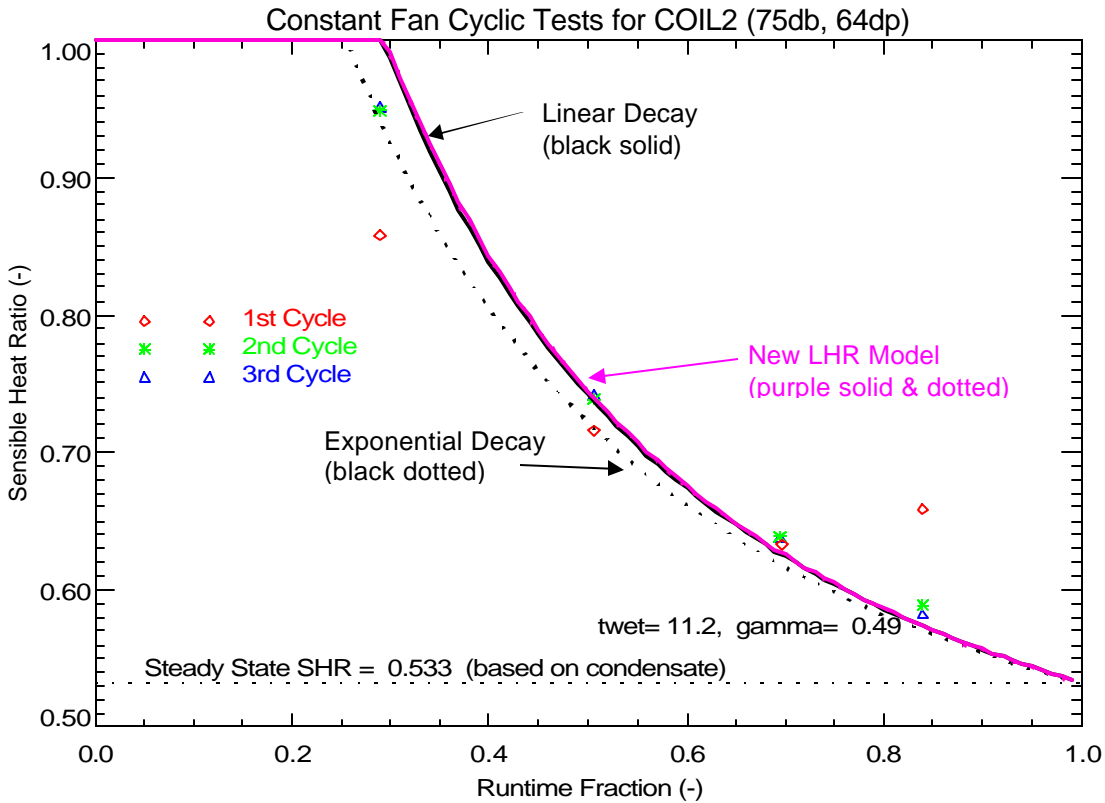


Figure 17. Comparing Measured Latent Degradation to the LHR Models: (75°F / 64°Fdp)

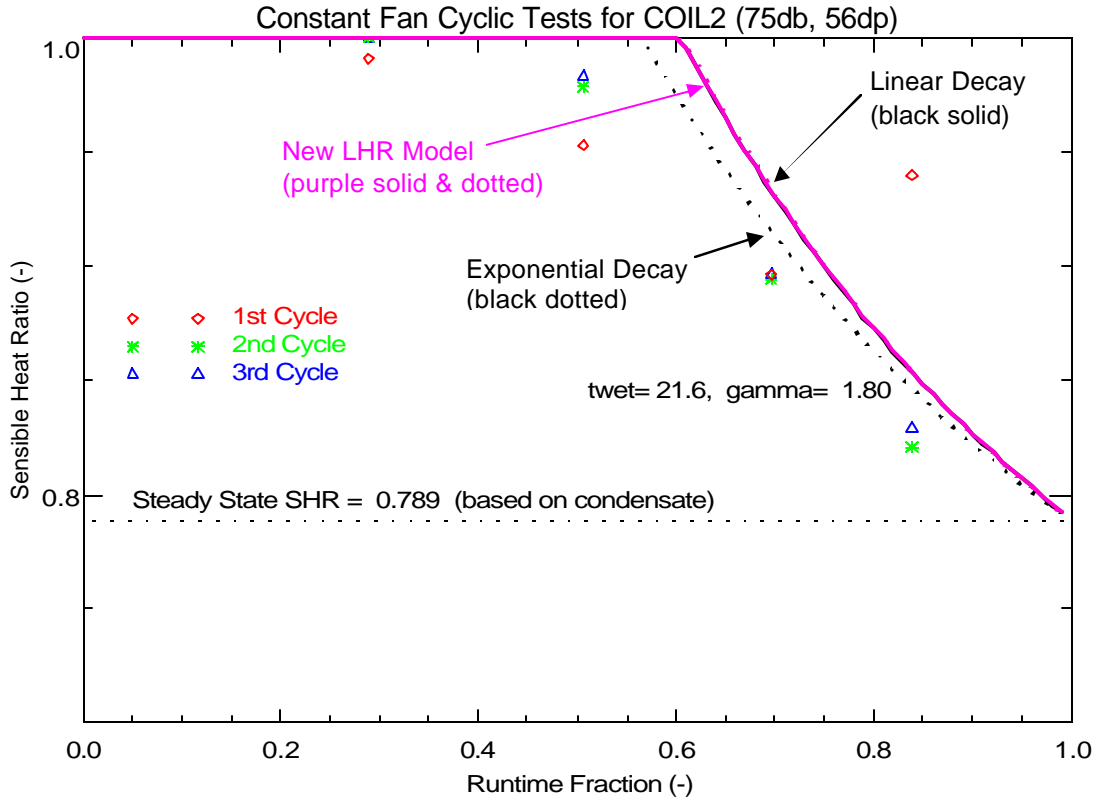


Figure 18. Comparing Measured Latent Degradation to the LHR Models: (75°F / 56°Fdp)

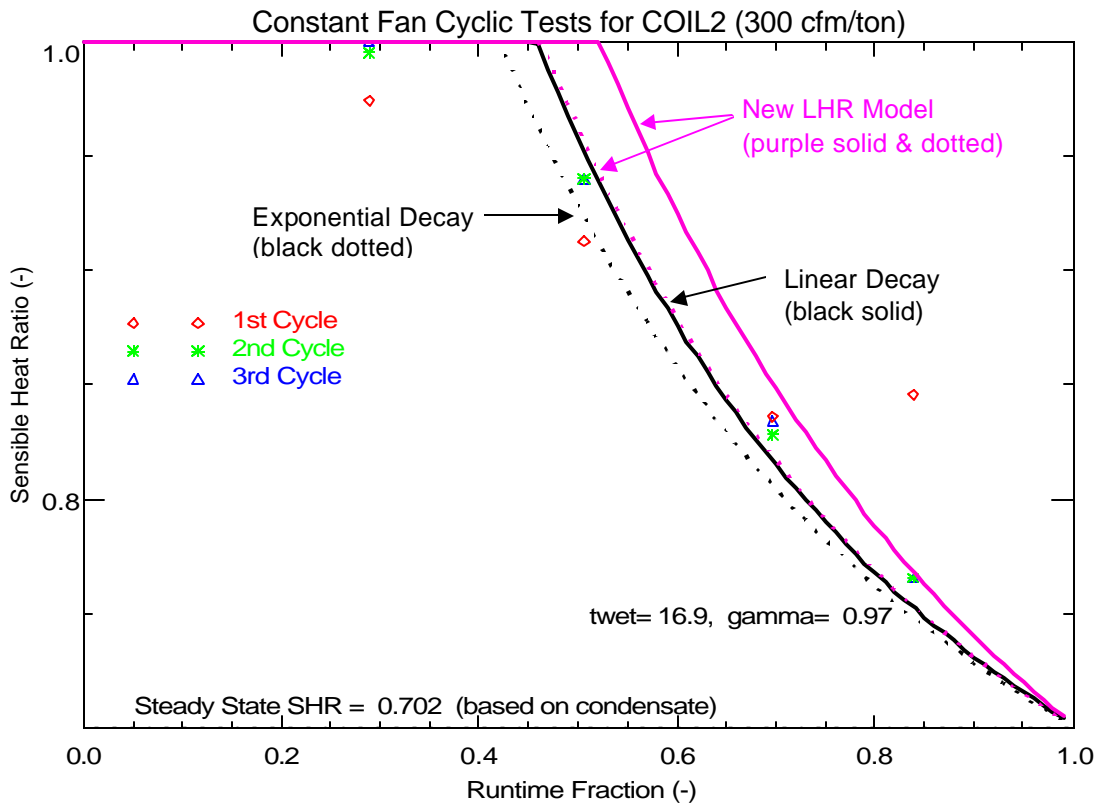
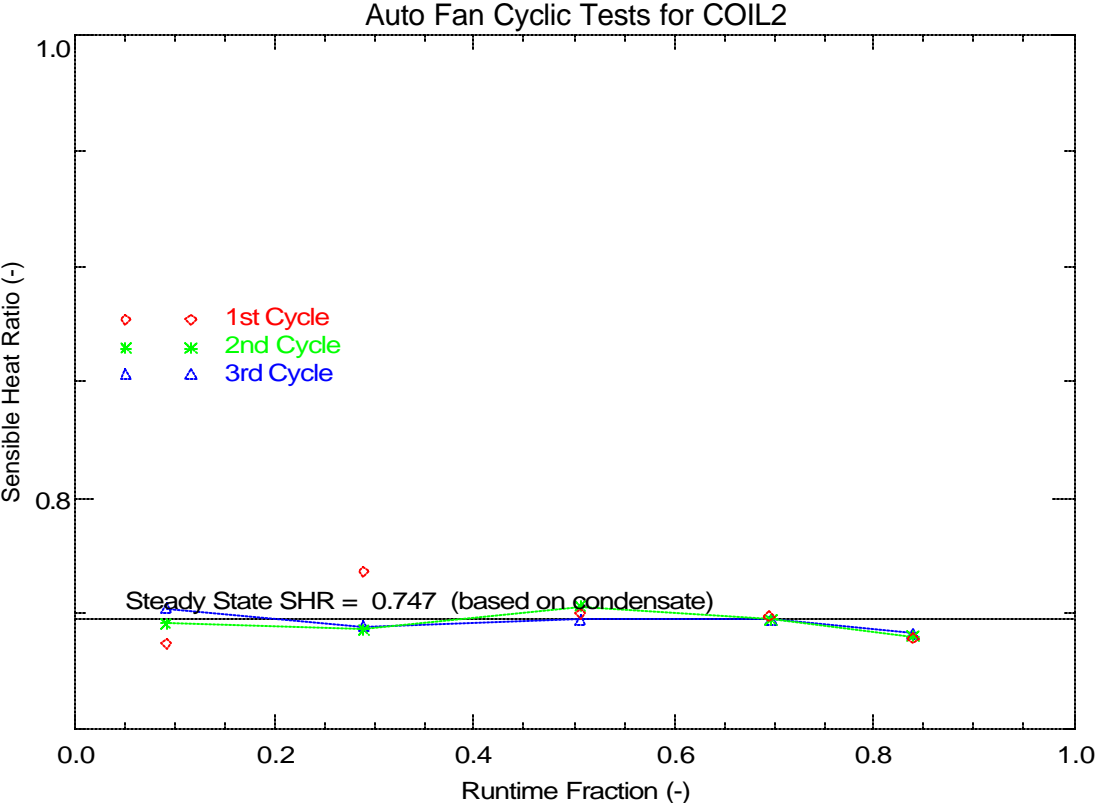


Figure 19. Comparing Measured Latent Degradation to the LHR Models: 300 cfm/ton, 80°F / 60.4°Fdp

Figure 20 shows very little latent degradation can be detected in the AUTO fan mode (i.e., the supply air flow across the cooling coil starts and stops with compressor operation) for Coil 2. The other coils have shown more variation. The 2<sup>nd</sup> and 3<sup>rd</sup> repetition (cycle) show good agreement with each other.



**Figure 20. Measured AUTO Fan Latent Degradation**

The tests were completed over a period of 6-7 weeks. Figure 21 shows little evidence of a change in suction pressure, subcooling or superheat over the test period. This implies that no significant loss of refrigerant charge occurred over the test period.

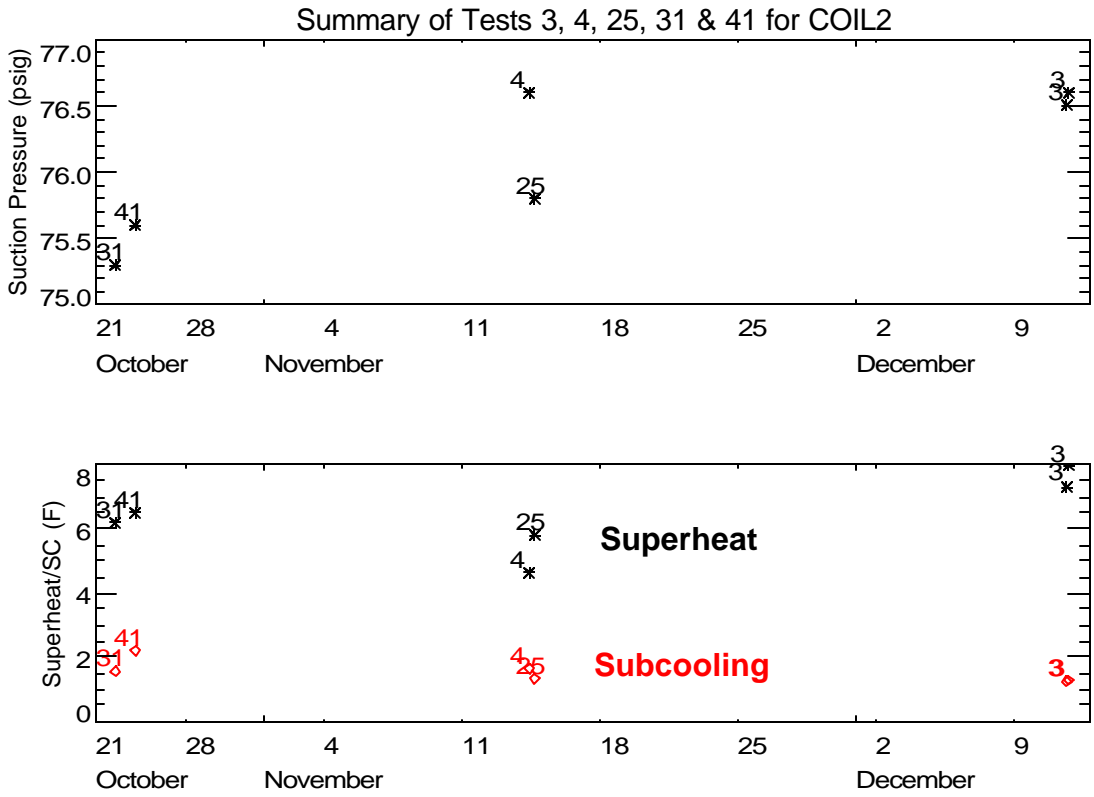


Figure 21. Long-Term Variation in Suction Pressure, Superheat and Subcooling

**References**

Henderson, H., and K. Rengarajan. 1996. A model to predict the latent capacity of air conditioners and heat pumps at part-load conditions with constant fan operation. *ASHRAE Transactions* 102(1): 266-274.

Stabat, P., Marchio, D. and M. Orphelin. 2001. Pre-Design and Design Tools for Evaporative Cooling. *ASHRAE Transactions* 107 (1): 501-510.

**COIL 2 Test Runs**

File Name	Date	Start Time	Sequence No.	Run/Test No.	Inlet DB (F)	Inlet DewPt (F)	Air Flow (cfm)	Test Duration (min)	Comp Runtime (min)
Coil2 Test 1.out	12/6/2002	9:43:49	1	1	79.9	60.2	984.1	118.5	58.5
Coil2 Test 1.out	12/6/2002	11:42:34	2	1	79.9	60.4	981.2	119.8	59.7
Coil2 Test 1.out	12/6/2002	13:42:34	3	1	79.9	60.4	981.1	149.5	89.7
Coil2 Test 2.out	12/5/2002	9:10:07	1	2	80	60.4	980.2	119	58.5
Coil2 Test 2.out	12/5/2002	11:09:21	2	2	80	60.4	973.1	119.8	59.3
Coil2 Test 2.out	12/5/2002	13:09:21	3	2	80	60.4	967.5	155	95.3
Coil2 Test 3b.out	12/11/2002	16:04:07	1	3	80.1	59.9	977.8	119.7	60
Coil2 Test 3b.out	12/11/2002	18:04:05	2	3	80	60.4	976.8	119.7	60
Coil2 Test 3b.out	12/11/2002	20:04:04	3	3	80	60.4	976.2	149.7	90
Coil2 Test 4b 10b 16b 22b 25b.out	11/14/2002	8:37:58	1	4	79.6	60.2	972.9	89.7	45
Coil2 Test 4b 10b 16b 22b 25b.out	11/14/2002	10:07:57	2	4	79.9	60.4	967.3	89.8	45
Coil2 Test 4b 10b 16b 22b 25b.out	11/14/2002	11:37:57	3	10	80	60.4	713.9	89.8	45
Coil2 Test 4b 10b 16b 22b 25b.out	11/14/2002	13:07:57	4	16	79.9	60.3	470.2	104.8	45
Coil2 Test 4b 10b 16b 22b 25b.out	11/14/2002	14:52:58	5	22	79.9	60.4	1037.8	89.8	45
Coil2 Test 4b 10b 16b 22b 25b.out	11/14/2002	16:22:59	6	25	80	60.4	962.3	104.5	45
Coil2 Test 5b 11b 17b 23b.out	11/20/2002	7:49:25	1	5	80.1	65.8	968.3	89.8	45
Coil2 Test 5b 11b 17b 23b.out	11/20/2002	9:19:26	2	5	80.2	68.6	965.3	89.8	45
Coil2 Test 5b 11b 17b 23b.out	11/20/2002	10:49:26	3	11	80.2	68.6	709.7	119.7	60
Coil2 Test 5b 11b 17b 23b.out	11/20/2002	12:49:26	4	17	80.3	68.2	482.9	134.7	60
Coil2 Test 5b 11b 17b 23b.out	11/20/2002	15:04:26	5	23	80.2	68.3	1030.1	135	60
Coil2 Test 6b 12b 18b 24b.out	12/10/2002	17:37:14	1	6	80.1	50.9	957.8	134.7	90
Coil2 Test 6b 12b 18b 24b.out	12/10/2002	19:52:14	2	6	80	50.5	960.6	134.7	90
Coil2 Test 6b 12b 18b 24b.out	12/10/2002	22:07:13	3	12	80	50.5	712.6	134.8	90
Coil2 Test 6b 12b 18b 24b.out	12/11/2002	0:22:14	4	18	80.1	50.5	469.2	134.7	90
Coil2 Test 6b 12b 18b 24b.out	12/11/2002	2:37:14	5	24	80.1	50.5	1039.8	134.7	90
Coil2 Test 7b 13b 19b.out	11/15/2002	7:20:16	1	7	75.2	62.9	965.6	119.7	60
Coil2 Test 7b 13b 19b.out	11/15/2002	9:20:16	2	7	75.3	64.7	960.1	119.7	60
Coil2 Test 7b 13b 19b.out	11/15/2002	11:20:15	3	13	75.3	64.7	705.6	119.8	60
Coil2 Test 7b 13b 19b.out	11/15/2002	13:20:16	4	19	75.4	64.4	477.7	139.7	60
Coil2 Test 8 14 20.out	10/23/2002	7:29:56	1	8	75.2	56.1	969.5	89.8	45
Coil2 Test 8 14 20.out	10/23/2002	8:59:56	2	8	75.2	56.1	961	89.8	45
Coil2 Test 8 14 20.out	10/23/2002	10:29:56	3	14	75.2	56	708.2	89.8	45
Coil2 Test 8 14 20.out	10/23/2002	11:59:56	4	20	75.3	56	459.1	104.8	45
Coil2 Test 9c 15c 21c.out	12/11/2002	4:52:14	1	9	75.4	49.5	963.7	134.7	90
Coil2 Test 9c 15c 21c.out	12/11/2002	7:07:14	2	9	75.2	49.5	962.6	134.7	90
Coil2 Test 9c 15c 21c.out	12/11/2002	9:22:13	3	15	75.2	49.5	714.1	134.8	90
Coil2 Test 9c 15c 21c.out	12/11/2002	11:37:14	4	21	75.4	49.5	471.7	135	90
Coil2 Test Cycling Constant.out	10/24/2002	7:49:55	1	31	80.1	60.1	964.5	89.7	45
Coil2 Test Cycling Constant.out	10/24/2002	9:19:54	2	31	80.1	60.4	959.6	89.8	45
Coil2 Test Cycling Constant.out	10/24/2002	10:49:54	3	32	80.1	60.4	955.6	35.8	30
Coil2 Test Cycling Constant.out	10/24/2002	11:25:54	4	32	80.3	60.4	949.4	35.8	30
Coil2 Test Cycling Constant.out	10/24/2002	12:01:54	5	32	80.2	60.4	947.1	35.8	30
Coil2 Test Cycling Constant.out	10/24/2002	12:37:54	6	33	80.5	60.3	951	23	16
Coil2 Test Cycling Constant.out	10/24/2002	13:01:09	7	33	80.5	60.4	947.7	23	16
Coil2 Test Cycling Constant.out	10/24/2002	13:24:24	8	33	80.4	60.4	947.4	23	16
Coil2 Test Cycling Constant.out	10/24/2002	13:47:39	9	34	80.6	60.4	946.3	19.8	10
Coil2 Test Cycling Constant.out	10/24/2002	14:07:39	10	34	80.6	60.4	944.3	19.8	10
Coil2 Test Cycling Constant.out	10/24/2002	14:27:39	11	34	80.5	60.3	946.2	19.8	10
Coil2 Test Cycling Constant.out	10/24/2002	14:47:39	12	35	80.7	60.4	947.3	24.3	7
Coil2 Test Cycling Constant.out	10/24/2002	15:12:09	13	35	80.4	60.3	942.6	24.3	7
Coil2 Test Cycling Constant.out	10/24/2002	15:36:39	14	35	80.5	60.2	946.8	24.3	7
Coil2 Test Cycling auto.out	10/25/2002	7:20:07	1	41	79.9	60.3	964.3	89.7	45
Coil2 Test Cycling auto.out	10/25/2002	8:50:06	2	41	79.9	60.4	959.1	89.7	45
Coil2 Test Cycling auto.out	10/25/2002	10:20:05	3	42	79.9	60.3	953.4	35.8	30
Coil2 Test Cycling auto.out	10/25/2002	10:56:05	4	42	80.1	60.4	950.1	35.8	30
Coil2 Test Cycling auto.out	10/25/2002	11:32:05	5	42	80.1	60.3	948.3	35.8	30
Coil2 Test Cycling auto.out	10/25/2002	12:08:05	6	43	80.2	60.3	946.8	23	16
Coil2 Test Cycling auto.out	10/25/2002	12:31:19	7	43	80.2	60.3	943.1	23	16
Coil2 Test Cycling auto.out	10/25/2002	12:54:33	8	43	80.1	60.2	944	23	16
Coil2 Test Cycling auto.out	10/25/2002	13:17:48	9	44	80.2	60.3	935.5	19.7	10
Coil2 Test Cycling auto.out	10/25/2002	13:37:47	10	44	80.1	60.3	936.1	19.7	10
Coil2 Test Cycling auto.out	10/25/2002	13:57:46	11	44	79.9	60.3	939.1	19.8	10
Coil2 Test Cycling auto2.out	10/28/2002	16:07:20	3	45	79.5	60.2	936.7	24.3	7
Coil2 Test Cycling auto2.out	10/28/2002	16:31:50	4	45	79.6	60.2	933.3	24.3	7
Coil2 Test Cycling auto2.out	10/28/2002	16:56:20	5	45	79.6	60.2	932.8	24.2	7
Coil2 Test Cycling auto2.out	10/28/2002	17:20:49	6	46	79.6	60.1	930.8	60.2	5.5
Coil2 Test Cycling auto2.out	10/28/2002	18:21:17	7	46	79.4	60.3	930.2	60.3	5.5
Coil2 Test Cycling auto2.out	10/28/2002	19:21:47	8	46	79.4	60.1	938.4	60.3	5.5

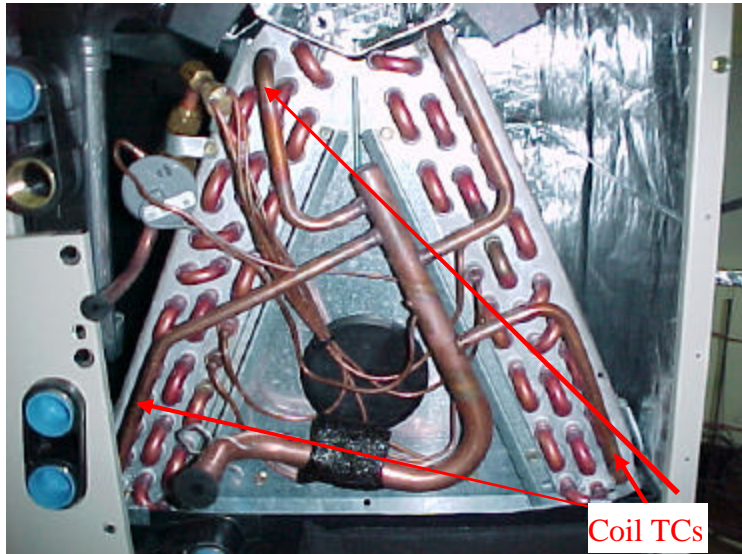
**COIL 2 Test Runs (cont)**

File Name	Date	Start Time	Sequence No.	Run/Test No.	Inlet DB (F)	Inlet DewPt (F)	Air Flow (cfm)	Test Duration (min)	Comp Runtime (min)
Coil2 Test Cycling Constant 75 64.out	11/7/2002	8:06:52	1	51	75.3	64	965.1	89.7	45
Coil2 Test Cycling Constant 75 64.out	11/7/2002	9:36:51	2	51	75.3	64.7	962.2	89.8	45
Coil2 Test Cycling Constant 75 64.out	11/7/2002	11:06:51	3	52	75.4	64.7	962.4	35.8	30
Coil2 Test Cycling Constant 75 64.out	11/7/2002	11:42:51	4	52	75.5	64.7	961.1	35.8	30
Coil2 Test Cycling Constant 75 64.out	11/7/2002	12:18:51	5	52	75.4	64.6	958.8	35.7	30
Coil2 Test Cycling Constant 75 64.out	11/7/2002	12:54:50	6	53	75.6	64.6	959.6	23	16
Coil2 Test Cycling Constant 75 64.out	11/7/2002	13:18:05	7	53	75.7	64.6	961.7	23	16
Coil2 Test Cycling Constant 75 64.out	11/7/2002	13:41:19	8	53	75.7	64.6	957.9	23	16
Coil2 Test Cycling Constant 75 64.out	11/7/2002	14:04:33	9	54	75.8	64.6	959	19.8	10
Coil2 Test Cycling Constant 75 64.out	11/7/2002	14:24:33	10	54	75.8	64.6	960.2	19.8	10
Coil2 Test Cycling Constant 75 64.out	11/7/2002	14:44:33	11	54	75.8	64.6	958.4	19.7	10
Coil2 Test Cycling Constant 75 64.out	11/7/2002	15:04:32	12	55	75.9	64.6	958.2	24.3	7
Coil2 Test Cycling Constant 75 64.out	11/7/2002	15:29:02	13	55	76	64.6	966.4	24.3	7
Coil2 Test Cycling Constant 75 64.out	11/7/2002	15:53:32	14	55	75.9	64.6	962.8	24.2	7
Coil2 Test Cycling Constant 75 56.out	11/8/2002	8:22:21	1	61	75.1	56	972.2	89.7	45
Coil2 Test Cycling Constant 75 56.out	11/8/2002	9:52:20	2	61	75.1	56.1	965.7	89.8	45
Coil2 Test Cycling Constant 75 56.out	11/8/2002	11:22:20	3	62	75.2	56.1	960.2	35.8	30
Coil2 Test Cycling Constant 75 56.out	11/8/2002	11:58:20	4	62	75.2	56.1	954.5	35.8	30
Coil2 Test Cycling Constant 75 56.out	11/8/2002	12:34:20	5	62	75.2	56.1	952.6	35.8	30
Coil2 Test Cycling Constant 75 56.out	11/8/2002	13:10:20	6	63	75.3	56.1	953.5	23	16
Coil2 Test Cycling Constant 75 56.out	11/8/2002	13:33:35	7	63	75.3	56.1	954.1	23	16
Coil2 Test Cycling Constant 75 56.out	11/8/2002	13:56:50	8	63	75.3	56.1	953.1	23	16
Coil2 Test Cycling Constant 75 56.out	11/8/2002	14:20:05	9	64	75.4	56.1	952.8	19.8	10
Coil2 Test Cycling Constant 75 56.out	11/8/2002	14:40:05	10	64	75.3	56	952.8	19.8	10
Coil2 Test Cycling Constant 75 56.out	11/8/2002	15:00:05	11	64	75.4	56	954.3	19.8	10
Coil2 Test Cycling Constant 75 56.out	11/8/2002	15:20:05	12	65	75.5	56.1	956.1	24.3	7
Coil2 Test Cycling Constant 75 56.out	11/8/2002	15:44:35	13	65	75.7	56.1	956.2	24.3	7
Coil2 Test Cycling Constant 75 56.out	11/8/2002	16:09:05	14	65	75.8	56.2	957.3	24.3	7
Coil2 Test Cycling Constant 300.out	12/10/2002	8:54:04	1	71	80.6	60.3	725.2	89.8	45
Coil2 Test Cycling Constant 300.out	12/10/2002	10:24:04	2	71	80.1	60.3	722.8	89.7	45
Coil2 Test Cycling Constant 300.out	12/10/2002	11:54:03	3	72	80.1	60.3	723	35.8	30
Coil2 Test Cycling Constant 300.out	12/10/2002	12:30:03	4	72	80.2	60.3	722	35.8	30
Coil2 Test Cycling Constant 300.out	12/10/2002	13:06:03	5	72	80.2	60.4	720.2	35.8	30
Coil2 Test Cycling Constant 300.out	12/10/2002	13:42:03	6	73	80.3	60.3	720.3	23	16
Coil2 Test Cycling Constant 300.out	12/10/2002	14:05:18	7	73	80.1	60.3	720.2	23	16
Coil2 Test Cycling Constant 300.out	12/10/2002	14:28:33	8	73	80.3	60.4	719.4	23	16
Coil2 Test Cycling Constant 300.out	12/10/2002	14:51:48	9	74	80.3	60.4	720.4	19.8	10
Coil2 Test Cycling Constant 300.out	12/10/2002	15:11:48	10	74	80.1	60.4	720.8	19.8	10
Coil2 Test Cycling Constant 300.out	12/10/2002	15:31:48	11	74	80.2	60.3	721.3	19.8	10
Coil2 Test Cycling Constant 300.out	12/10/2002	15:51:48	12	75	80.4	60.3	721.7	24.3	7
Coil2 Test Cycling Constant 300.out	12/10/2002	16:16:18	13	75	80.3	60	722.3	24.3	7
Coil2 Test Cycling Constant 300.out	12/10/2002	16:40:48	14	75	80.5	60.3	724.3	24.2	7

## **APPENDIX H3**

### **Summary of Laboratory Data for Coil 3**

**Summary of Laboratory Data for Coil 3 (same physical coil as Coil 2)  
November 2005**



15.5 fpi, lanced sine wave fin

Manufacturer & Model number:	Carrier FK4CNF002000AGAA
Nominal size:	1 ½ - 3 tons
Baseline Size and Airflow (Test 4):	1.4 tons / 585 cfm
Coil type:	“A” coil, 3 rows, 15.5 fpi (aluminum fins)
Coil dimensions:	3.41 ft <sup>2</sup> total finned face area (face area = 3.46 ft <sup>2</sup> per manufacturers literature) 2 slabs @ (13 7/8 in x 17 11/16 in) 3.2 ft <sup>2</sup> finned face area exposed to air flow 2 slabs @ (13 3/8 in x 17 ¼ in)
Coil thickness:	2 ¼ in
Tube diameter:	3/8 in OD copper
Tube spacing:	1 in within row (vert); ¾ in row-to-row (horiz)
Expansion device:	TXV (5-6°F superheat)
Unit supply fan:	off
Compressor power:	60 hz, direct

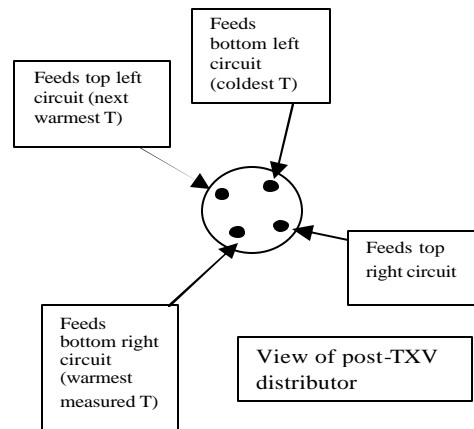
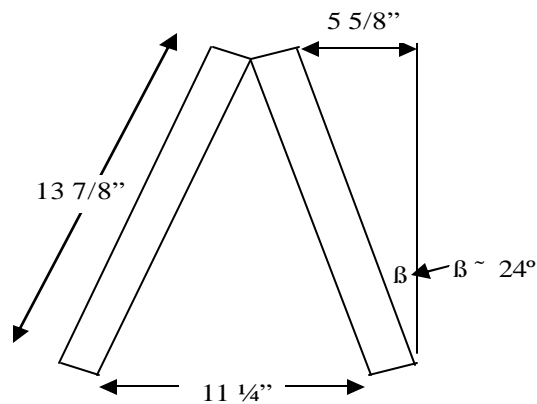




**Table 1. Summary of Steady State Test Conditions Corresponding to Each Run or Test**

	<i>Entering Coil Conditions</i>					
	<i>80/67°F 60°F dp</i>	<i>80/72°F 68°F dp</i>	<i>80/62°F 50°F dp</i>	<i>75/68°F 64°F dp</i>	<i>75/63°F 56°F dp</i>	<i>75/58°F 45°F dp</i>
400 cfm/ton	#4 (or 3)	#5	#6	#7	#8	#9
300 cfm/ton	#10	#11	#12	#13	#14	#15
200 cfm/ton	#16	#17	#18	#19	#20	#21
450 cfm/ton	#22	#23	#24			
400-200 cfm/ton (ON & OFF)	#25					
Low suction (48°F)	#1					
High suction (56°F)	#2					

Notes: Tests 4-25 all at nominal suction of 51°F (set at nominal conditions of test #3/4). A thermal expansion device was used, with nominal superheat of 5-6°F. The refrigerant charge established during Test 4 was not changed for the remaining tests. The Table 1 test points denote the target testing conditions. Drier test conditions with dew points below 50°F (such as Tests #9, #15, and #21) could not be achieved. In these cases, entering conditions were typically held near 50°F dp. For each test, the compressor is ON for 90-180 minutes and then the compressor is OFF for 60-180 minutes. The booster fan runs continuously for all tests (when the compressor is both ON and OFF).

### **Steady State Performance**

The nominal performance characteristics for this coil (based on steady-state conditions from Run #4 below) are:

Total Capacity:	16.7 MBtu/h (1.4 tons)
Sensible Capacity:	12.9 MBtu/h
Latent Capacity (condensate):	3.8 MBtu/h
Sensible Heat Ratio:	0.77

Latent capacity can be calculated two ways: 1) using dew point readings and air flow, and 2) the condensate flow rate. Figure 1 compares the latent capacity calculated these two ways. The number of each data point corresponds to the test number listed in Table 1. In general, the condensate readings resulted in a slightly lower capacity.

Figure 2 shows the trend of steady-state sensible heat ratio (SHR) with relative humidity and airflow rate. The cooling capacities used to calculate SHR in Figure 2 are based on airflow measurements and the psychrometric conditions entering and leaving the cooling coil. This performance map is typical of a cooling coil (i.e., SHR is mostly a function of the entering relative humidity, with some dependence on the air flow rate).

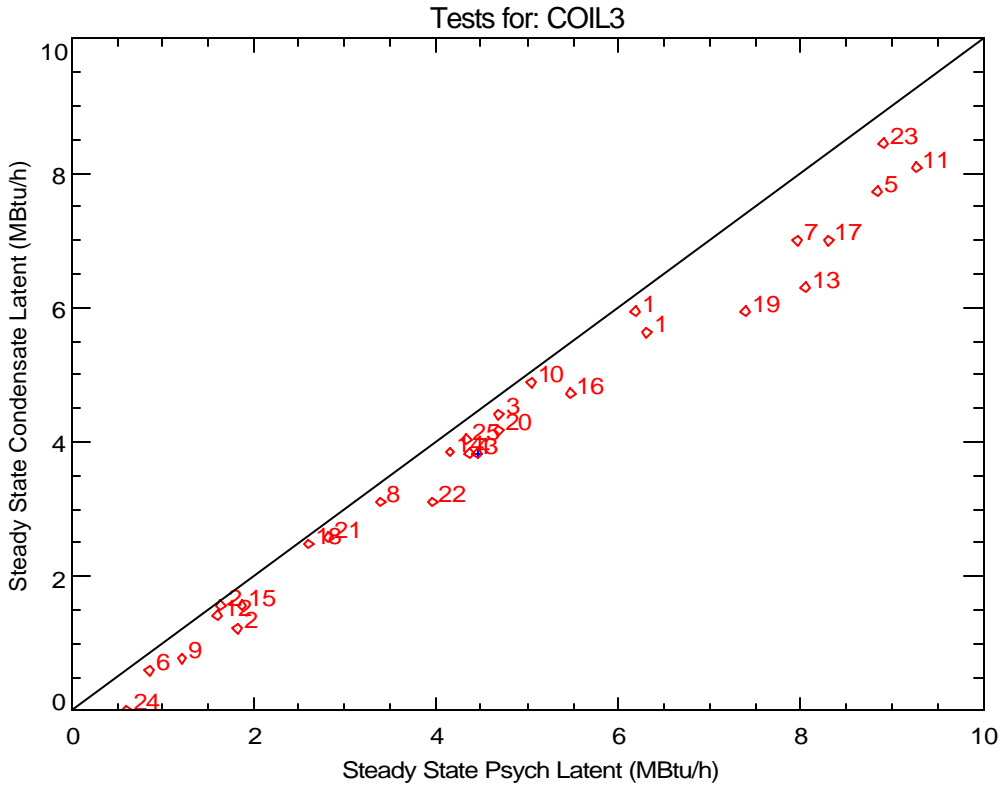


**Figure 1. Comparing Steady-State Latent Capacity Calculated From Psychrometric State Points and Condensate Removal Rates**

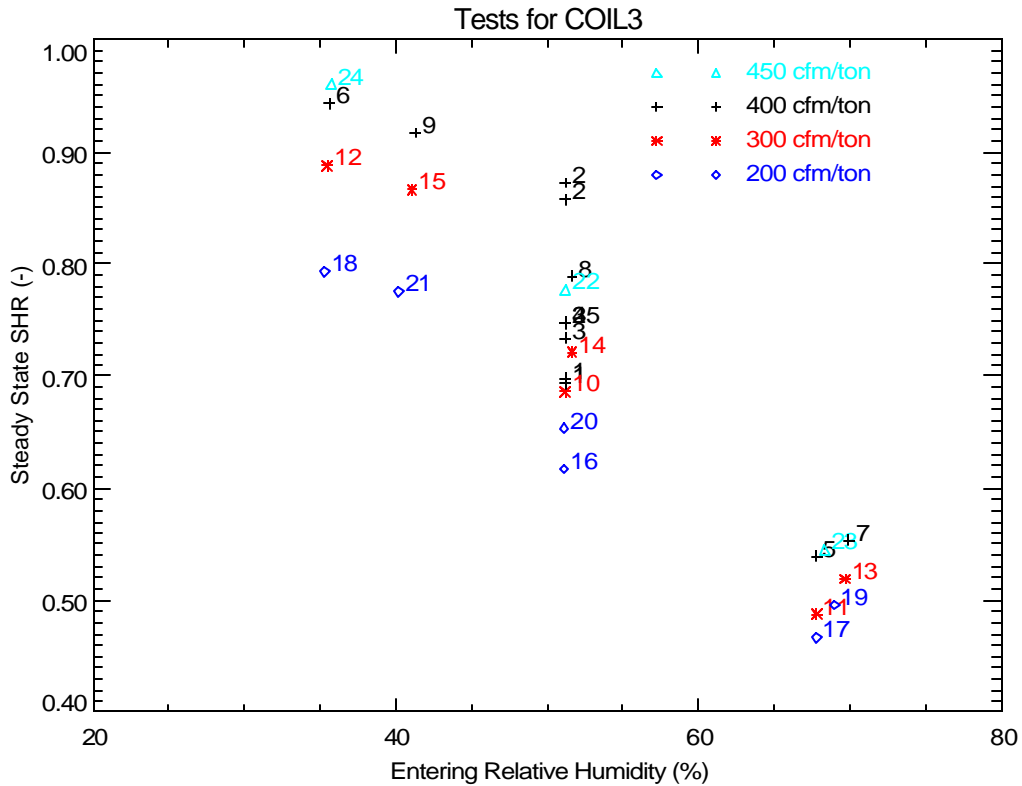


**Figure 2. Variation of Steady State SHR with Entering Humidity and Nominal Air Flow**

## **Typical Transient Performance**

Figure 3 shows the typical transient performance of the cooling coil at nominal conditions (i.e., for Cycle 2 of Run #4). The compressor runs for 90 minutes and is off for 90 minutes<sup>1</sup>. The booster fan remains on during the entire test (separate external fan used to maintain the desired air flow rate across the cooling coil). A portion of the moisture removed by the coil during the compressor on cycle evaporates back into the air stream during the off cycle. During the off cycle the coil acts as an evaporative cooler, so the sensible capacity is nearly equal to the absolute value of the latent capacity (i.e., the sum of latent and sensible is zero).

If we integrate the off cycle sensible capacity (after allowing for a 1-minute off-cycle delay to account for refrigerant movement and other transient effects), we can determine the energy associated with the moisture retained on the coil. To minimize the integration of any measurement errors, the off-cycle integration stops at the time labeled “Integration Pt.” on the plot. This point corresponds to the time when the temperature and dew point differences across the coil have first reached the terminal values (i.e., the averages from the end of the off-cycle). In this case the integration indicates that the sensible cooling is equivalent to 2.00 lbs of moisture being retained on the coil. The integrated latent capacity – which is harder to measure precisely – equals 2.02 lbs. These values are nearly the same as was recorded for coil 2 (as would be expected, since coil 3 was the same physical coil as coil 2 but operating at a lower cooling capacity).

The value “twet” from Henderson and Rengarajan (1996) can then be calculated by dividing the retained moisture mass (expressed as Btu; mass x 1060 Btu/lb) and the steady state psychrometric latent capacity ( $QL=4.4$  MBtu/h). Figure 3 shows that the values of twet based on integrated sensible and latent off-cycle capacity are 29.1 and 29.5 minutes respectively. These values of twet are similar to the measured delay of 32.5 minutes for the first condensate pulse to fall from the drain pan. The value of gamma (1.73), which is the initial off-cycle moisture evaporation rate divided by the steady-state psychrometric latent capacity, uses the off-cycle moisture evaporation rate (7.6 MBtu/h) once the saturated coil temperature is within 1°F of the entering air wet-bulb temperature. At this point where gamma is determined, it is assumed that all coil heat and mass transfer with the air stream is adiabatic (the refrigerant flow could not be used as the indicator for this point for this coil since it used a TXV that totally shut off refrigerant flow during the off cycle). The off-cycle sensible capacity also shows a change in the decay trend at this point. In this case it took about 1 minute for coil temperature to approach the wet bulb within the specified tolerance.

---

<sup>1</sup> The runtime was increased from 45 minutes for the previous coil tests to ensure steady state was achieved during the on cycle and full moisture evaporation occurred during the off cycle.

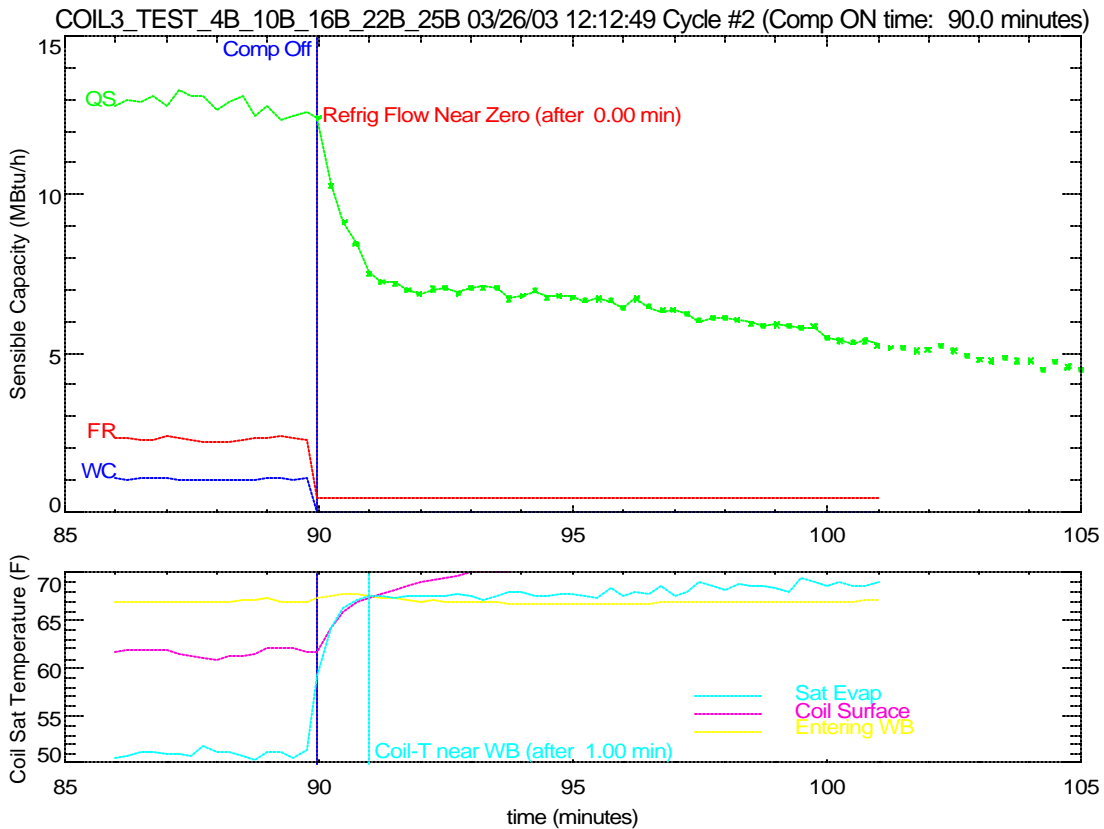
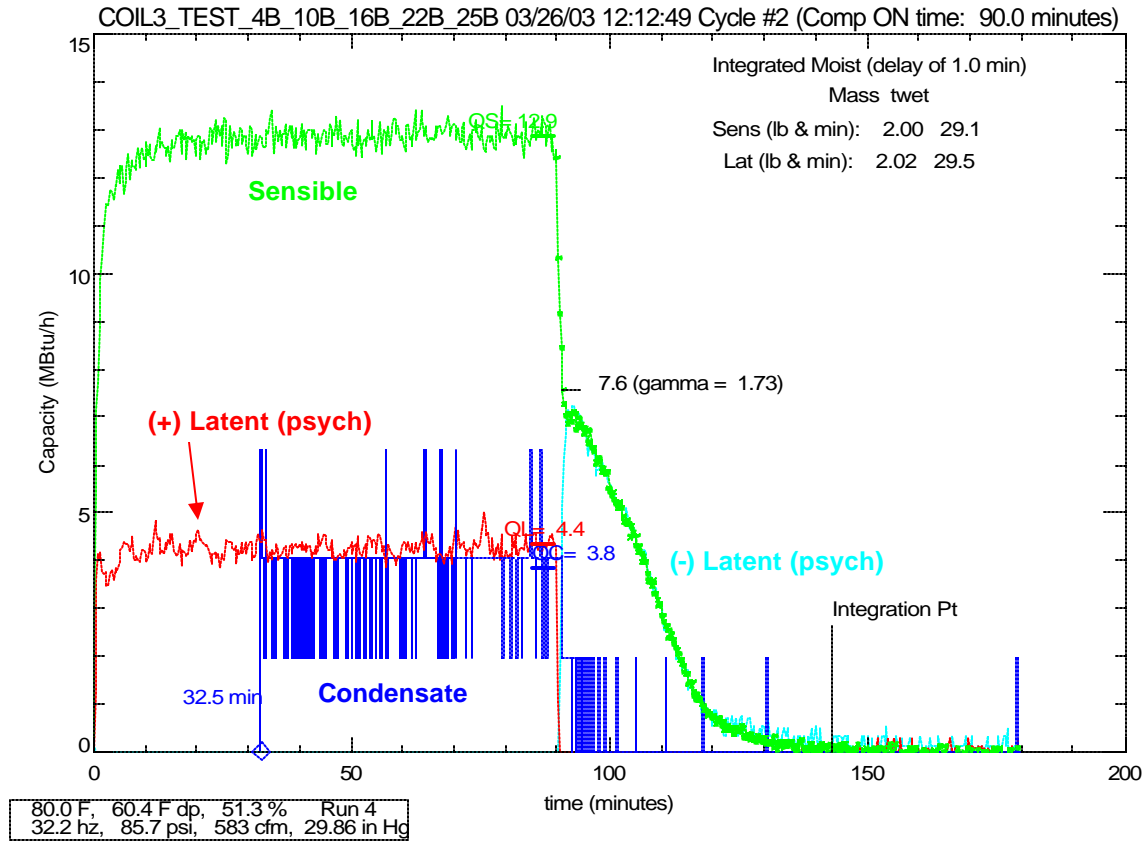
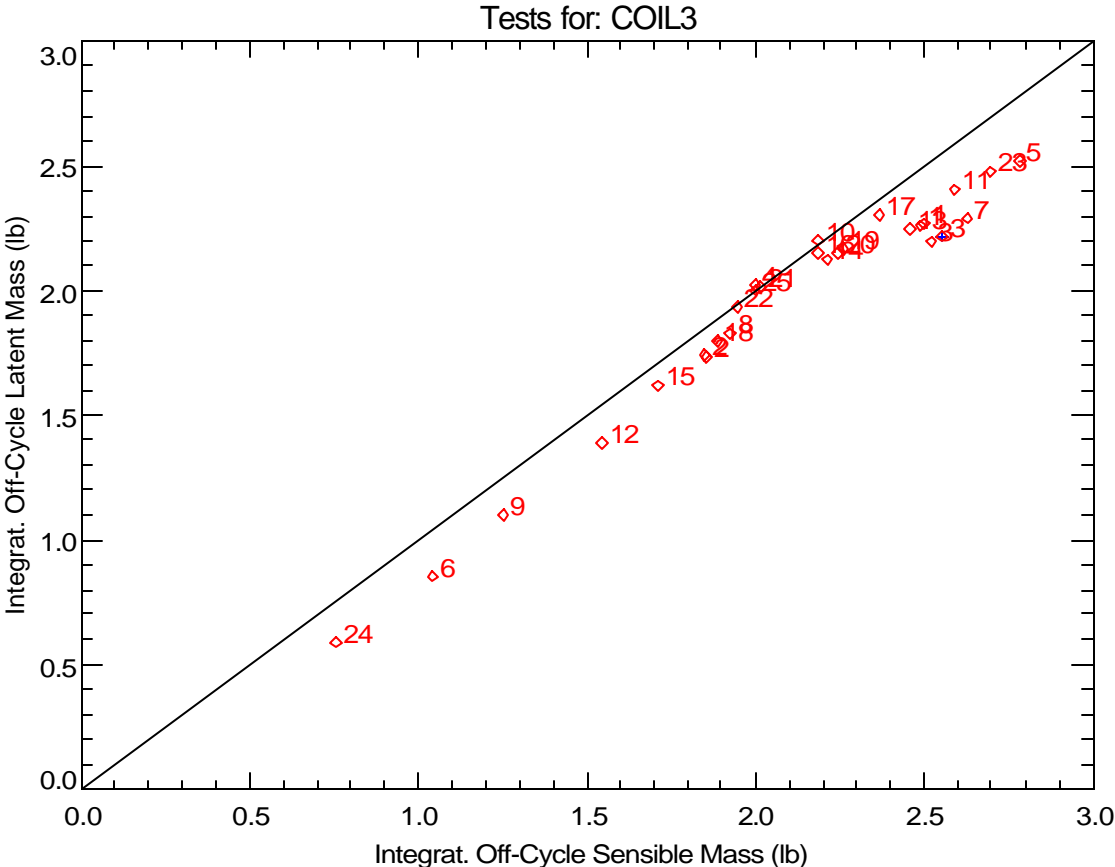


Figure 3. Example Plots of Detailed Data for Coil 3

**Part Load Latent Capacity Parameters**

The amount of moisture held on the cooling coil (and drain pan) can be calculated by integrating the off-cycle capacity from the coil (and dividing by the heat of vaporization, 1060 Btu/lb, to get the moisture mass). The integration is delayed for the first minute of the off-cycle so that the overshoot response of the chilled dew point hygrometers does not skew the results of the integration<sup>2</sup>. The integration terminates once steady state conditions are reached for the off cycle. If we assume the coil acts as an evaporative cooler, then sensible and latent capacity should be equal. Figure 4 compares the off-cycle integrated latent and sensible capacity calculated for each run. A systematic bias is evident: the integrated sensible capacity is typically greater than the latent capacity. Figure 5 shows that the bias is not a function of dew point as was observed from tests of Coil 1.

Since we expect that off-cycle latent and sensible capacity should sum to zero, we have selected the integrated off-cycle sensible capacity as the most consistent and believable indication of the moisture mass held on the cooling coil (and drain pan).



**Figure 4. Comparing Stored Moisture Mass Calculated by Integrating Sensible and Latent Off-Cycle Capacity (Integrated with a 1 minute delay)**

<sup>2</sup>The 1-minute delay causes the estimate of moisture mass to be low by as much as 0.12 lbs (or 6%).

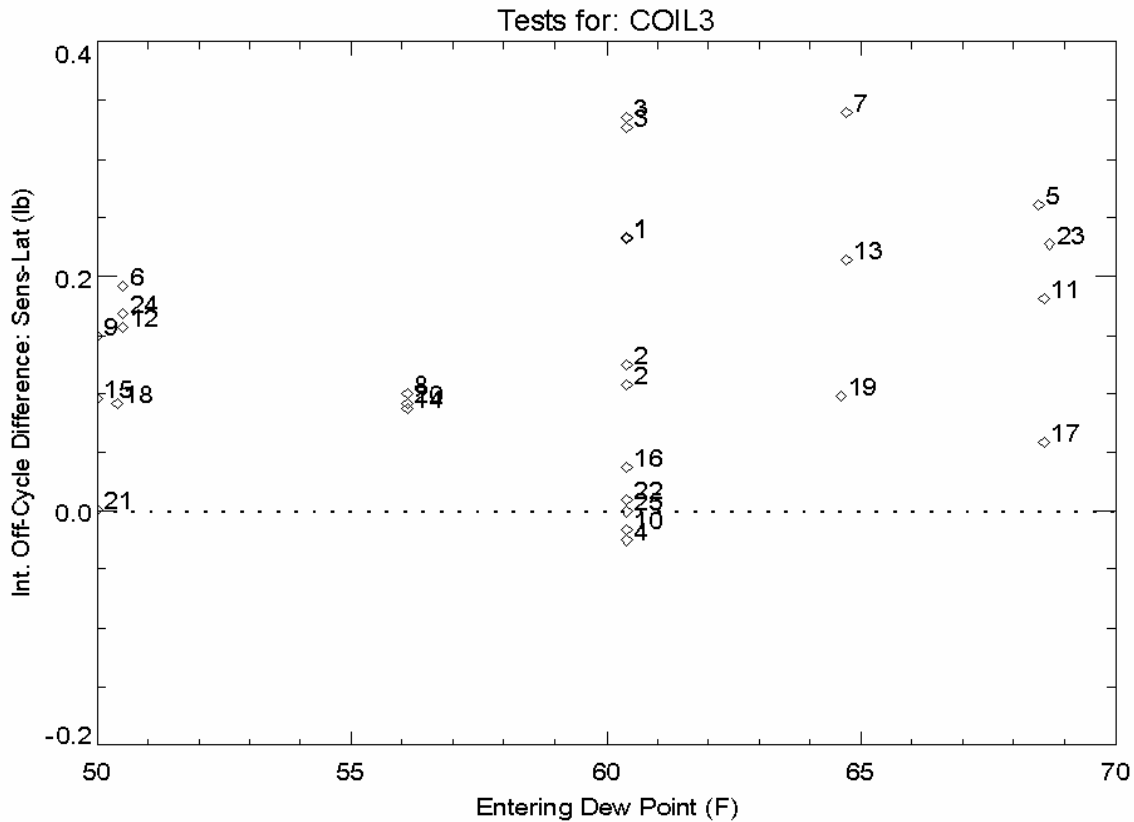


**Figure 5. Variation of Off-Cycle Sensible-Latent Difference with Entering Dew Point**

The parameter “twet” is the moisture mass held on the cooling coil times the enthalpy of vaporization (1060 Btu/lb) divided by the steady-state latent capacity of the cooling coil. The parameter should physically correspond to the time it takes for moisture to first fall from the coil (ignoring startup delays and other effects). Figure 6 compares the calculated “twet” (determined from integrating sensible capacity during the off-cycle and then dividing by the steady-state psychrometric latent capacity during the on-cycle) to the condensate delay time for all test runs. There is relatively good agreement between these two values, with the exception of Tests #2, #9 and #24, which have either drier entering conditions, warmer coil temperatures, or higher air flows.

Figure 7a and 7b show that both twet and the condensate delay time are a function of the entering air dew point temperature. Figure 7b uses different symbols to show the 1<sup>st</sup> and 2<sup>nd</sup> cycles in each test sequence with flow rate of 400 cfm/ton for all tests. The delay time was generally the same for the first and second cycles for this coil.

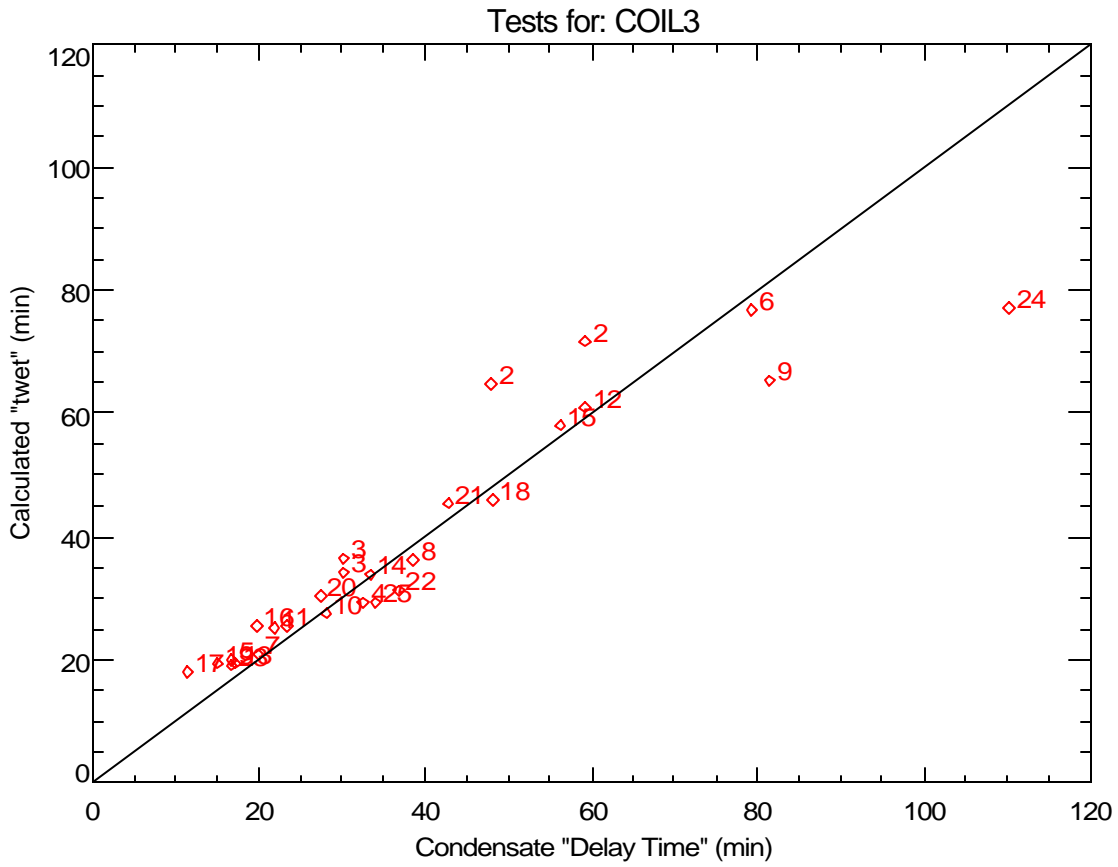


**Figure 6. Comparing “twet” (calculated with off-cycle sensible and steady state latent) to the Condensate Delay Time**

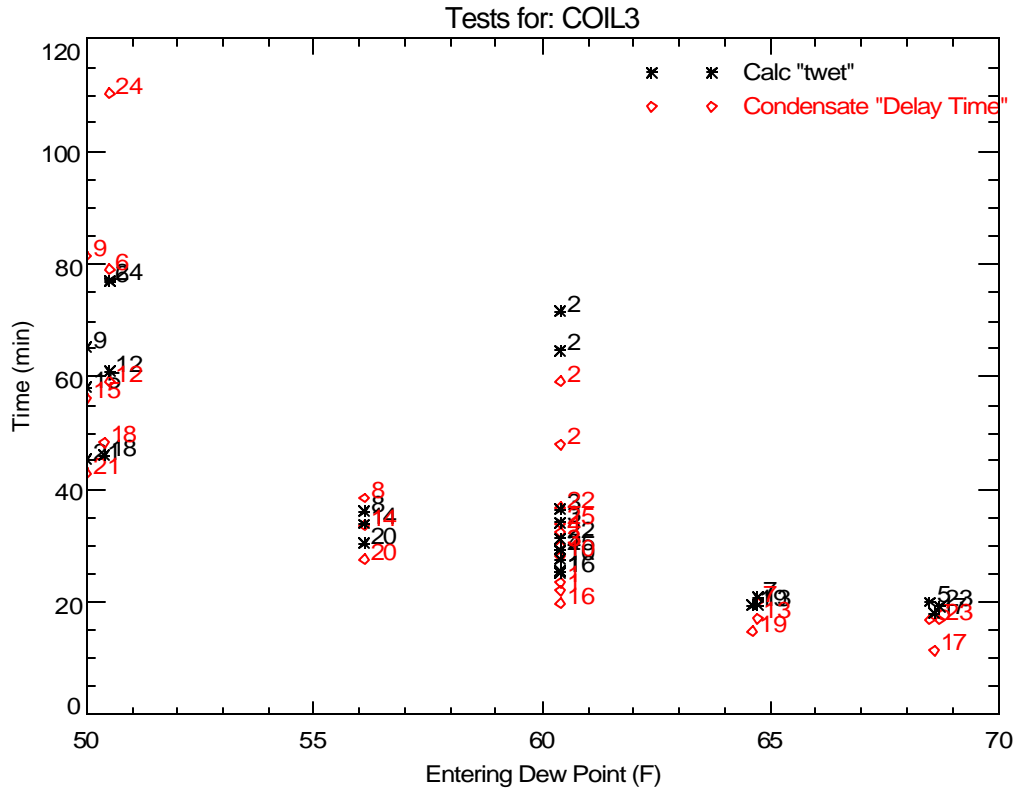


Figure 7a. Impact of Dew Point on “twet” and Condensate Delay Time

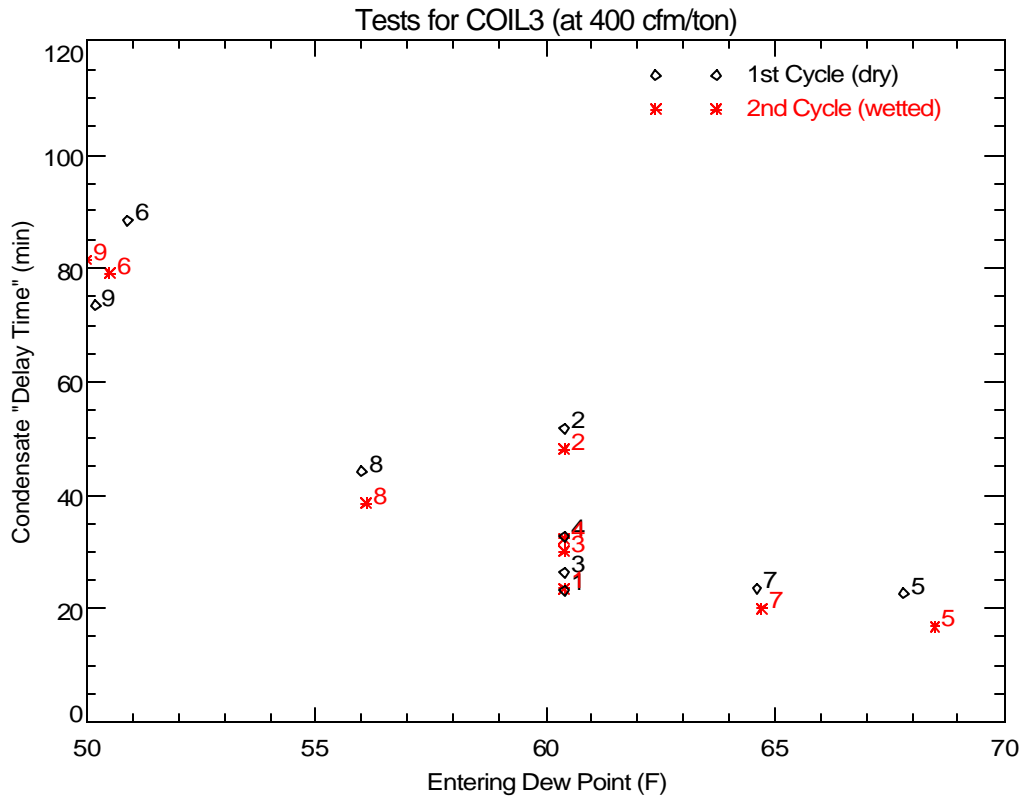


Figure 7b. Impact of Dew Point and Coil Wettedness on Condensate Delay Time

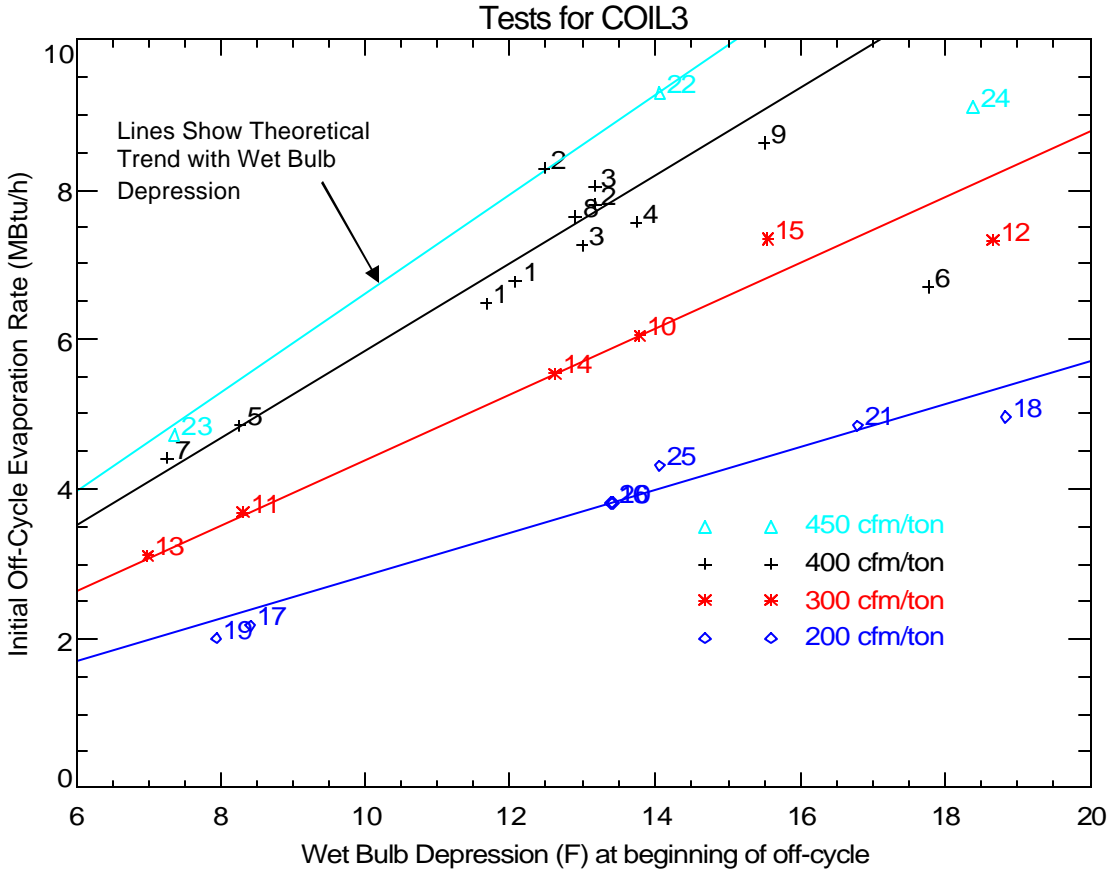


Figure 8 shows the initial off-cycle moisture evaporation rate varies with wet bulb depression. As expected, the evaporation rate is highest when the entering air has a larger wet bulb depression (i.e., has a lower relative humidity) and a higher airflow rate.

The model developed by Henderson and Rengarajan (1996) used the following simple evaporative cooler model to predict the moisture evaporation rate at off-design conditions:

$$Q_{\text{evap}} = Q_{\text{evap}_o} \times \frac{(DB - WB)}{(80 - 67)}$$

where  $Q_{\text{evap}_o}$  is the evaporation rate at the nominal entering air conditions of 80°F dry bulb (DB) and 67°F wet bulb (WB). This simple model is shown as the lines in Figure 8. For each air flow rate, the line is based on the nominal test results at 80°F DB/67°F WB extended to pass through zero. The measured data show essentially the same slope as the theoretical lines. The notable exceptions are the points with higher air flow and drier entering air conditions. Specifically, Tests #6 and #24 deviate significantly from the line. These runs have a much lower initial moisture evaporation rate because the entering air dew point temperature was close to the cooling coil temperature, so that the fin surfaces were not fully wetted. The smaller wetted surface area reduces the initial moisture evaporation rate.

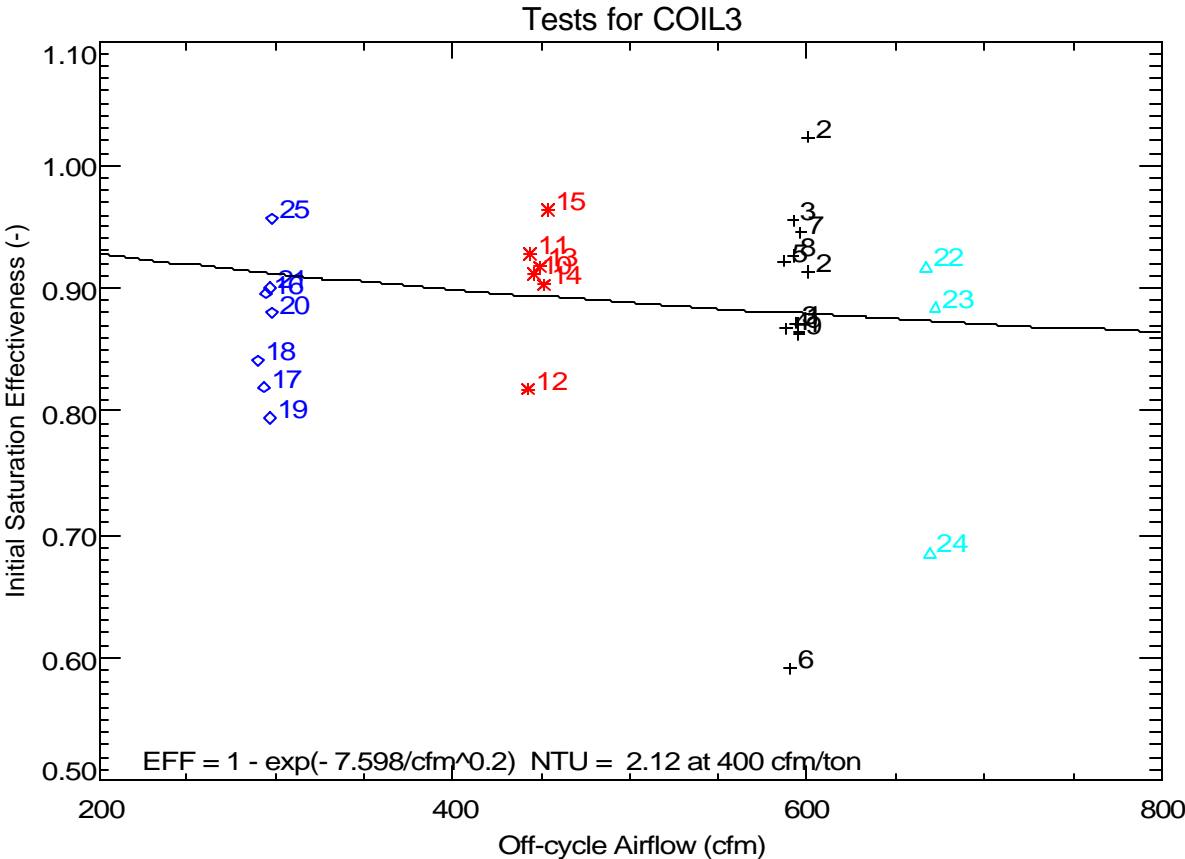


**Figure 8. Measured Variation of Initial Evaporation Rate with Wet Bulb Depression**

Stabat et al. (2001) reviewed the theoretical performance of direct evaporative coolers and showed that the saturation effectiveness of an evaporative cooler is:

$$h_{evp} = 1 - e^{-NTU} \quad \text{where} \quad NTU = K/cfm^{0.2} \quad \text{for an air-water mixture.}$$

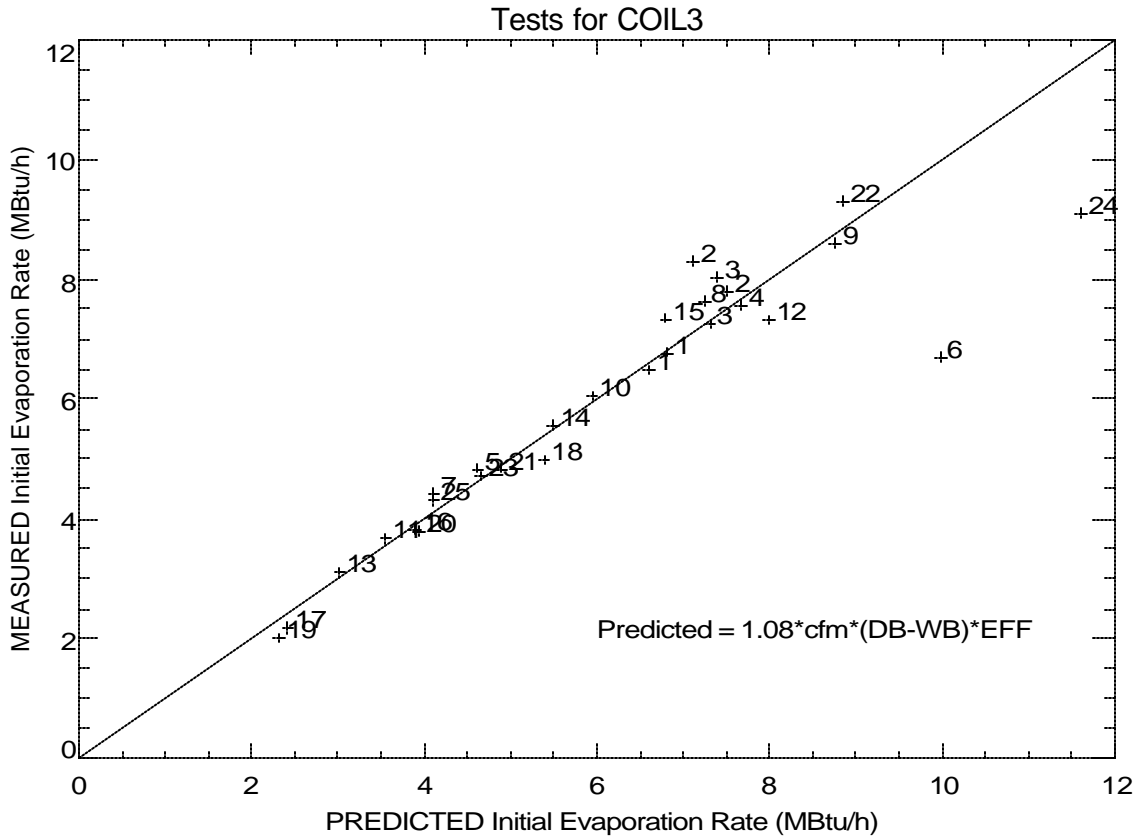
The line shown on Figure 9 is the best fit of the equation above to the measured data. The resulting constant K was 7.6<sup>3</sup>, which is equivalent to an NTU of 2.12 at 600 cfm. While there is considerable scatter due to the experimental uncertainty of predicting the initial off-cycle moisture evaporation rate, the slope of the line is still fairly representative of the overall trend.



**Figure 9. Evaporative Effectiveness versus Airflow**

Figure 10 compares the measured initial off-cycle moisture evaporation rate for each test to the predicted initial evaporation rate using the effectiveness model above. The model and measured data generally agree when presented in this form (i.e., the overall agreement visually appears better than in Figure 9 above). Again, the variation that occurs for Tests #6 and #24 was due to partial coil dryout, as mentioned above.

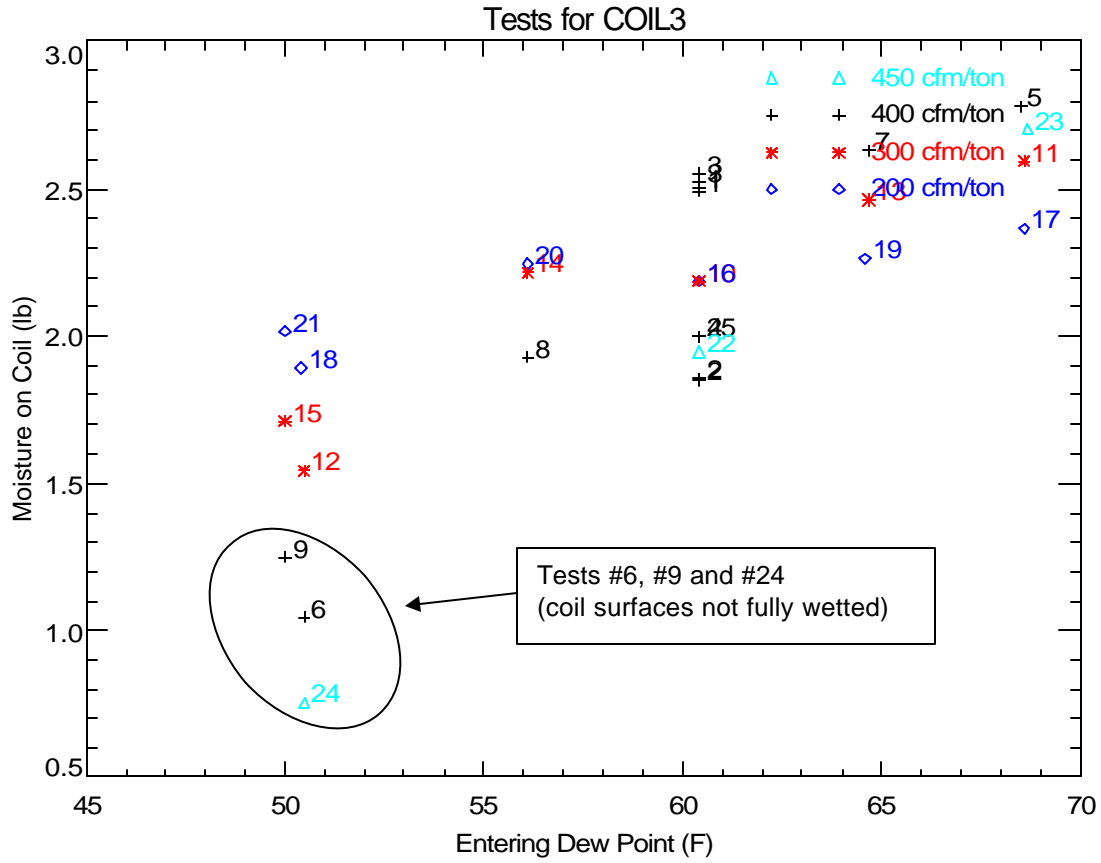
<sup>3</sup> For Coil #2, which was the same physical coil, K=7.23 which is in good agreement with the value of 7.6 calculated here.



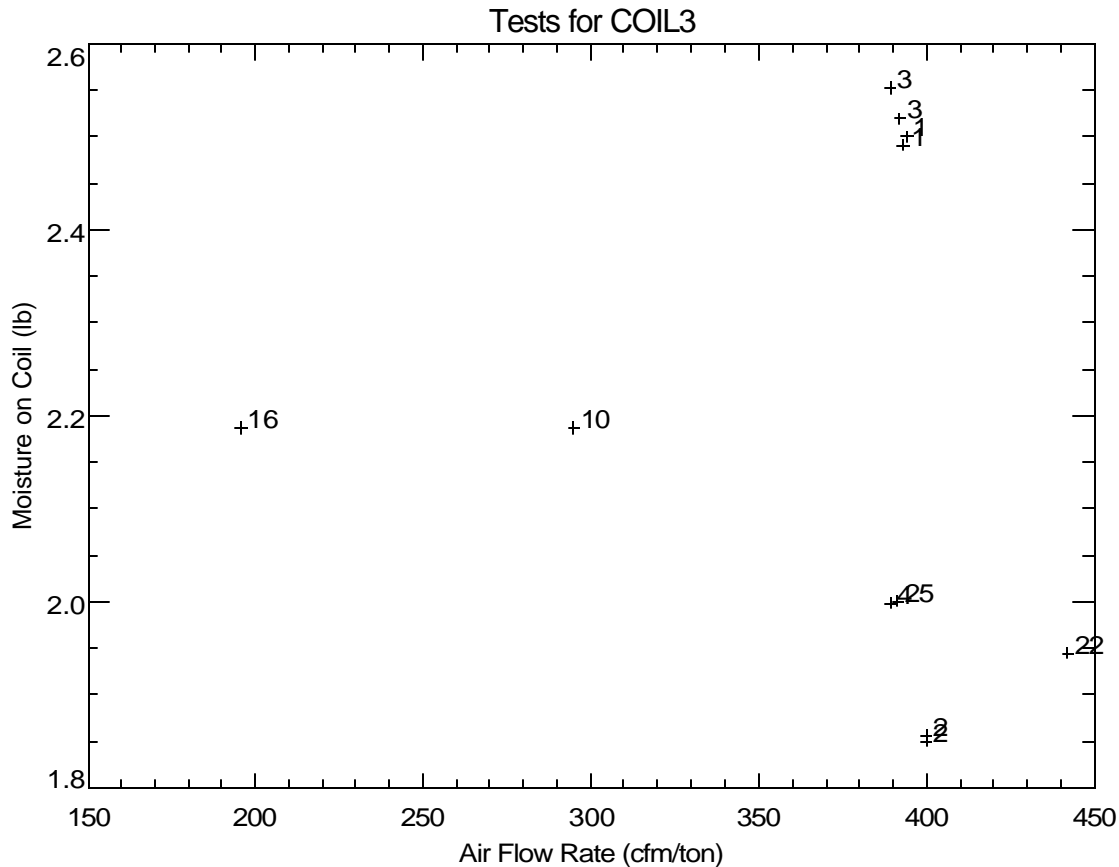
**Figure 10. Comparing Measured and Predicted Initial Moisture Evaporation Rates**

Figure 11 and Figure 12 below evaluate whether the amount of moisture retained on the cooling coil is a function of air flow or entering air conditions. At higher dew points (Figure 11) the moisture holding capacity of the coil approaches the equilibrium value. At lower dew points the moisture holding capacity is less, especially for Tests #6, #9, and #24. For these tests, parts of the coil were not fully wetted because the coil surfaces were warmer than the entering air dew point temperature. For the other test conditions, where the coil surfaces were fully wetted, the amount of retained moisture on the cooling coil ranges from 1.5 to 2.8 lbs.

Figure 12 shows a 10-15% decrease in the amount of retained moisture with higher air flow rates. The variation of retained moisture with air flow rate for Coil 3 was similar to that seen for Coil 1 (except for Tests #1 and #3).



**Figure 11. Variation of Retained Moisture (based on Off-Cycle Sensible ) with Flow and Dew Point**



**Figure 12. Variation of Retained Moisture with Air Flow at Nominal Entering Conditions of 80°F, 60.4°F dew point**

Another way to detect the amount of retained moisture is to measure the static air-side pressure drop across the cooling coil. The difference between the pressure drop across the coil under wet and dry conditions should provide an indication of the amount of retained moisture (the wet coil pressure drop is measured at steady-state conditions while the dry coil pressure drop is taken as the average pressure drop during the last part of the off-cycle). Figure 13 shows the variation of the wet-dry pressure difference with various entering humidity conditions at multiple air flow rates. Comparing the values for each air flow rate generally shows a trend of pressure drops reaching a plateau once the humidity of the entering air is sufficiently high to fully wet the coil. For air flow rates of 200 cfm/ton and 300 cfm/ton, the wet-dry pressure difference remained fairly constant for the range of entering air dew point temperatures that were tested, indicating a fully wetted coil. The wet-dry pressure drops for Tests #6, #9 and #24 are all significantly lower than expected, again confirming that less moisture was retained on the cooling coil at these drier/higher air flow conditions.

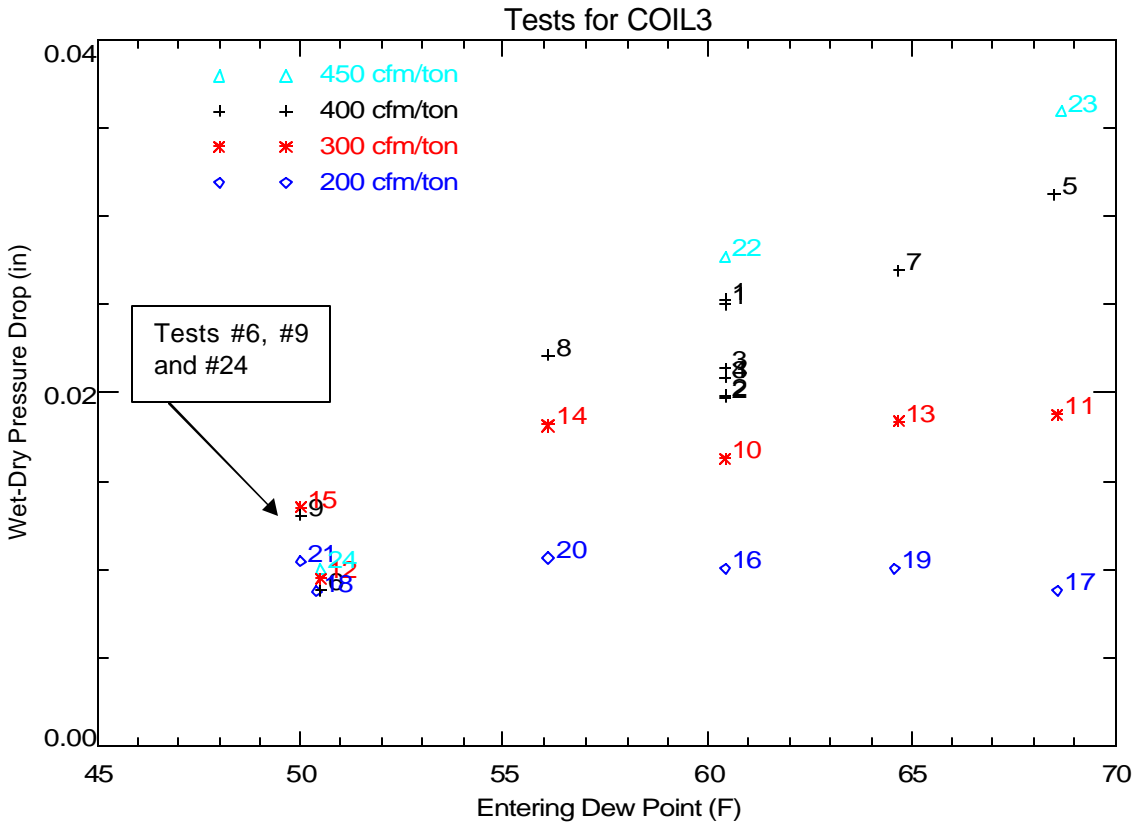


**Figure 13. Variation of Wet-Dry Pressure Drop with Entering Conditions and Air Flow Rate**

Figure 14 confirms that the wet-dry pressure drop is a linear function of air flow rate, which implies laminar flow in the wetted cooling coil.

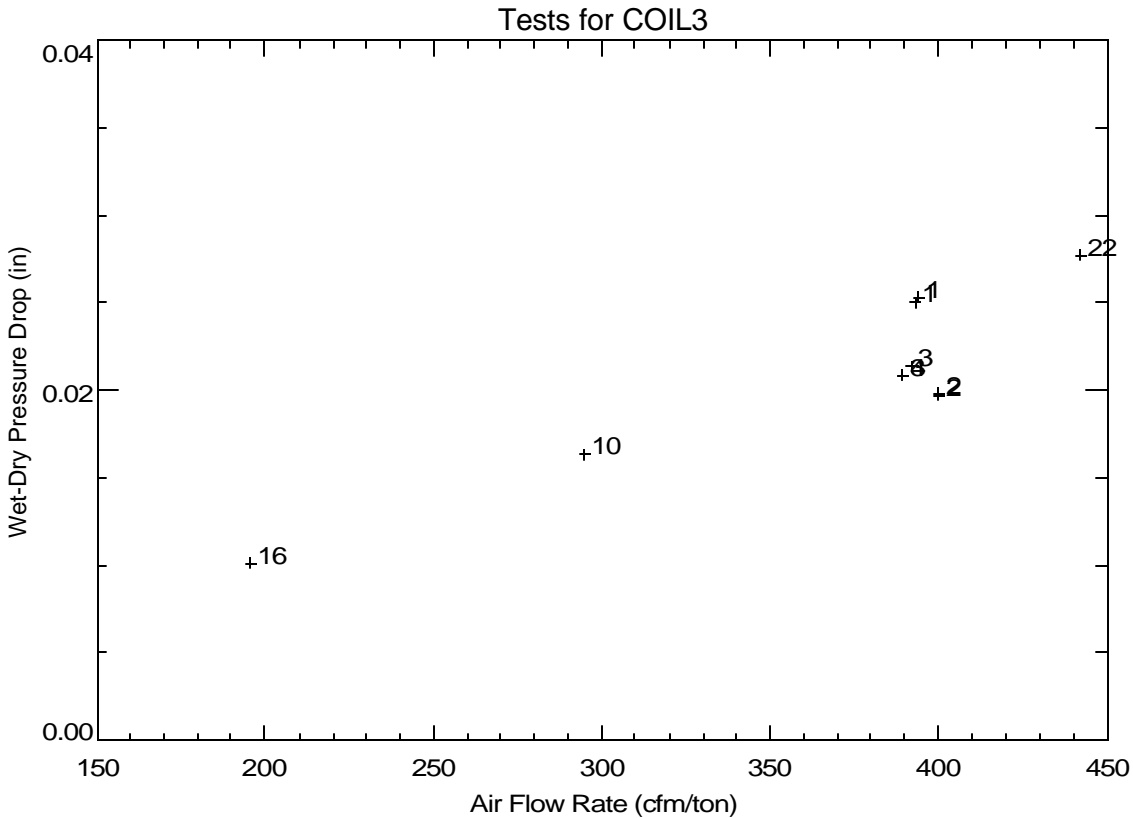


**Figure 14. Trend of Wet-Dry Pressure Drop with Flow at Nominal Entering Conditions of 80°F, 60.4°F dew point**

The series of plots in Figure 15 show the impact of coil suction temperature on performance. The steady-state performance of the system shows the expected trends of lower SHR and greater latent capacity at lower coil temperatures (i.e., lower saturated suction temperatures). In addition, the plots for moisture on coil and wet-dry pressure drop show that more moisture is retained when the coil is colder.

The graph of fan power versus saturated suction temperature in Figure 15 is not relevant in this case since the AHU fan was turned off during all tests. For this cooling coil, an external booster fan was used to obtain the desired air flow rate for each test.

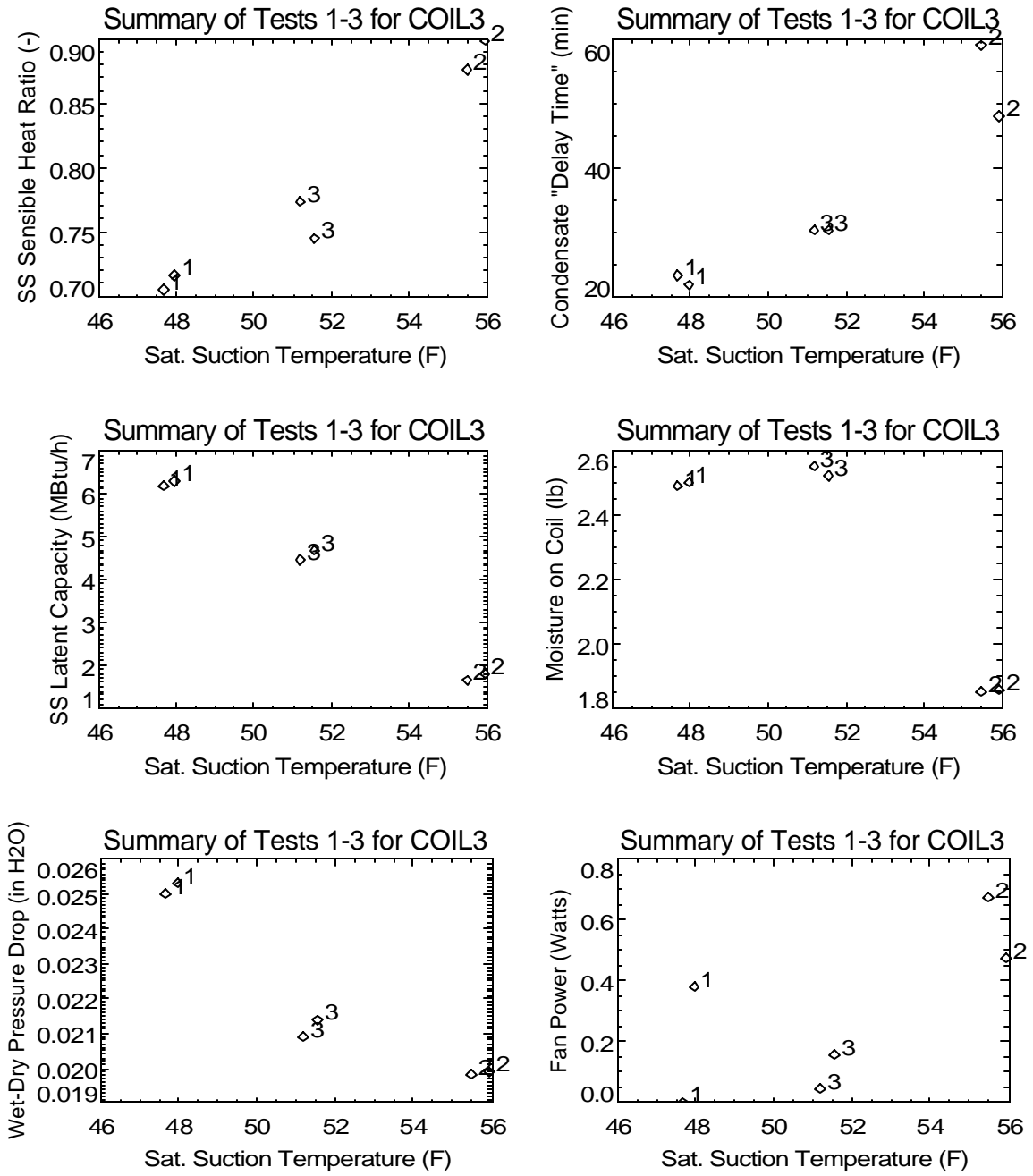


**Figure 15. Trend of Various Parameters with Saturated Suction Temperature**



## Overall Latent Degradation Trends

Several quasi-steady cyclic tests were also completed in the laboratory to quantify the overall part-load degradation of latent capacity. Table 2 lists the cycling test runs. These conditions correspond to a conventional thermostat with a maximum cycle rate of 3 cycles per hour (at 50% runtime).

**Table 2. Cyclic Test Conditions**

CONST FAN <sup>1</sup>	AUTO FAN <sup>2</sup>	Number of Times Test Repeated	ON Time (minutes)	OFF Time (minutes)	Runtime Fraction (-)	Cycle Rate (cycles/h)
Run						
31	41	2	45	45	0.500	0.667
32	42	3	30	6	0.833	1.667
33	43	3	16	7.25	0.688	2.581
34	44	3	10	10	0.500	3.000
35	45	3	7	17.5	0.286	2.449
	46	3	5.5	55	0.091	0.992

Notes: <sup>1</sup>Constant fan tests performed at 80°F db/60.4°F dp inlet air with 400 cfm/ton (runs 31-35) and 300 cfm/ton (runs 71-75) air flow. Tests also conducted at 75°F db/56°F dp (runs 61-65) and 75°F db/64°F dp (runs 51-55) inlet air with 400 cfm/ton air flow.

<sup>2</sup>Auto fan tests performed at 80°F db/60.4°F dp inlet air with 400 cfm/ton air flow.

Figure 16 through Figure 19 show the net impact of part-load unit operation based on cyclic tests completed in the lab. All of these tests are in the constant fan mode (continuous air flow over the cooling coil while the coil cycles on/off), but at various entering air and flow rate conditions:

- Nominal: 80°F & 60.4°F dew pt. with 400 cfm/ton (Figure 16)
- Humid: 75°F & 64°F dew pt. with 400 cfm/ton (Figure 17)
- Dry: 75°F & 56°F dew pt. with 400 cfm/ton (Figure 18)
- Low Flow: 80°F & 60.4°F dew pt. with 300 cfm/ton (Figure 19)

The measured data generally compare well to the model from Henderson and Rengarajan (1996) using the model parameters shown on each plot. These parameters were always taken from the 2<sup>nd</sup> occurrence of the first test in each sequence (i.e., Tests #31, 51, 61 and 71), which were completed as part of the suite of cycling tests listed in Table 2 for the constant fan mode. The latent time constant ( $\tau$ ) of 20 seconds was selected based on qualitative observations of the coil's response time. The solid black line corresponds to the linear off-cycle evaporation model. The black dotted line assumes an off-cycle evaporation trend that corresponds to an exponential decay. The purple line is the new part load LHR model that uses the more realistic evaporation model from Stabat et al. (2001) and also allows for variable amounts of moisture on the coil at the end of the on cycle. The parameters NTU and  $t_p$  were determined from the specific measured data from each test sequence (the purple solid line) as well as the average NTU and  $t_p$  from all the data (the purple dotted line), including Figure 9 above. The parameter  $t_p$  is defined in the improved model development section of this report.

The measured data corresponding to the 2<sup>nd</sup> and 3<sup>rd</sup> repetition (cycle) of each test showed the best agreement with the models, since quasi-steady conditions had been achieved.

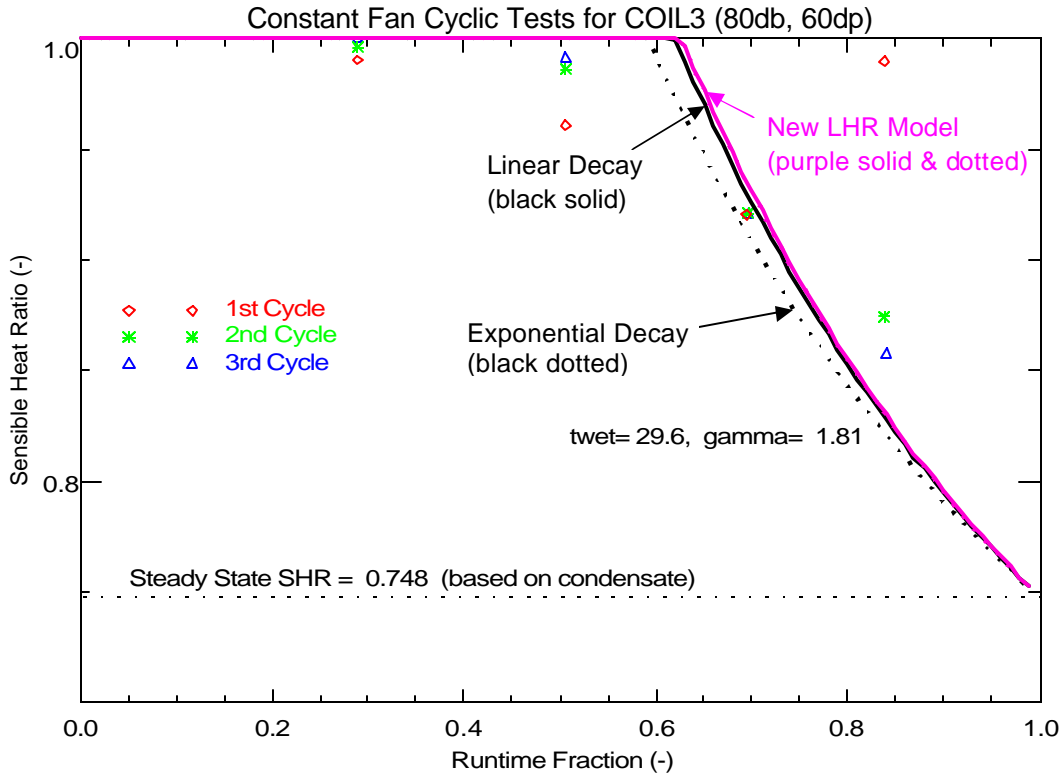


Figure 16. Comparing Measured Latent Degradation to the LHR Models: Nom. Conditions (80°F / 60.4°Fdp)

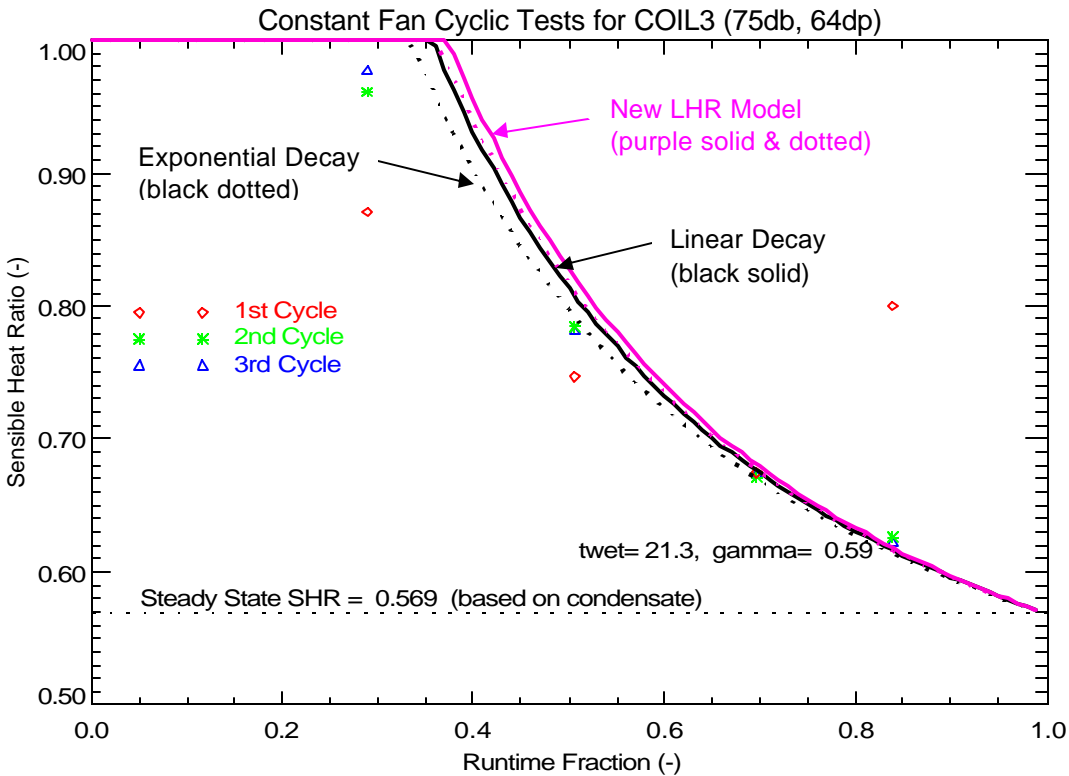


Figure 17. Comparing Measured Latent Degradation to the LHR Models: (75°F / 64°Fdp)

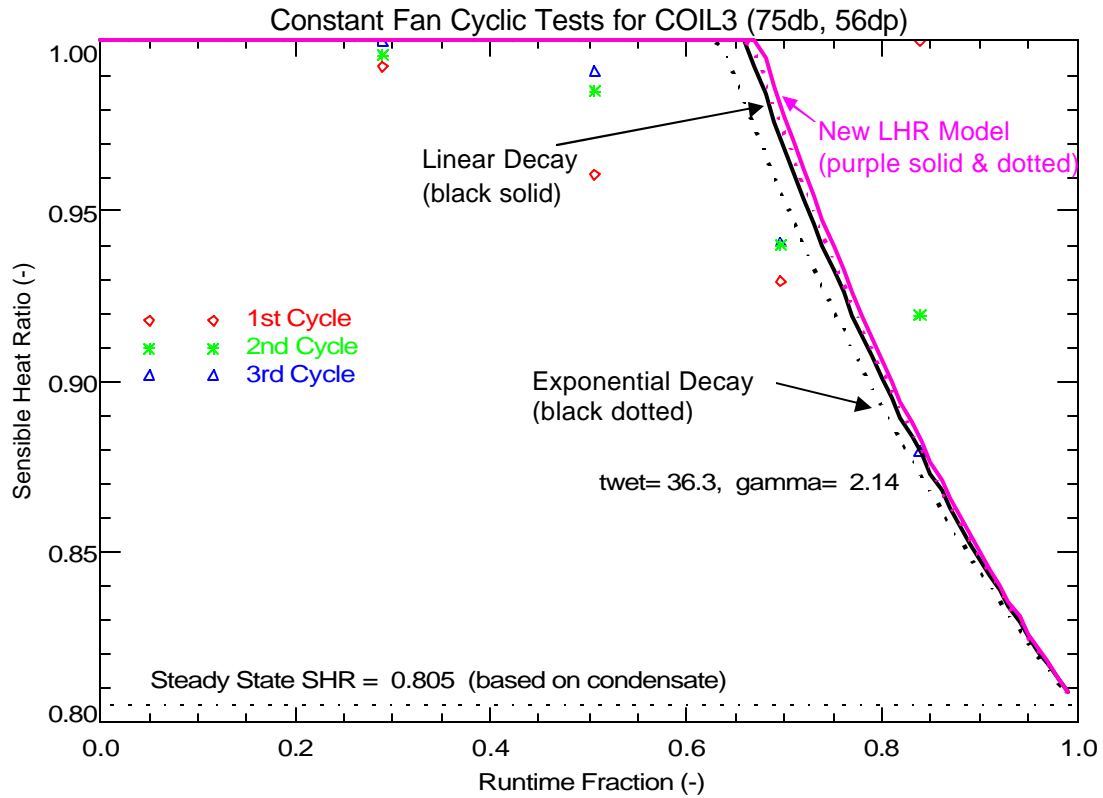


Figure 18. Comparing Measured Latent Degradation to the LHR Models: (75° F / 56° Fdp)

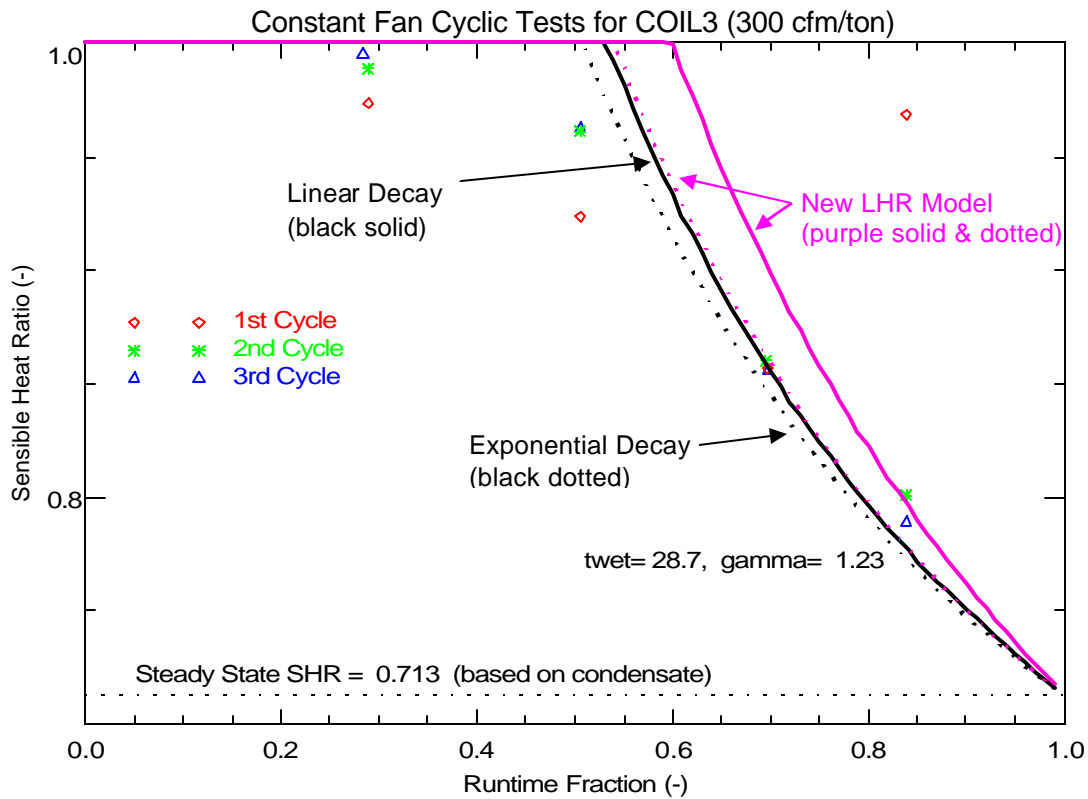
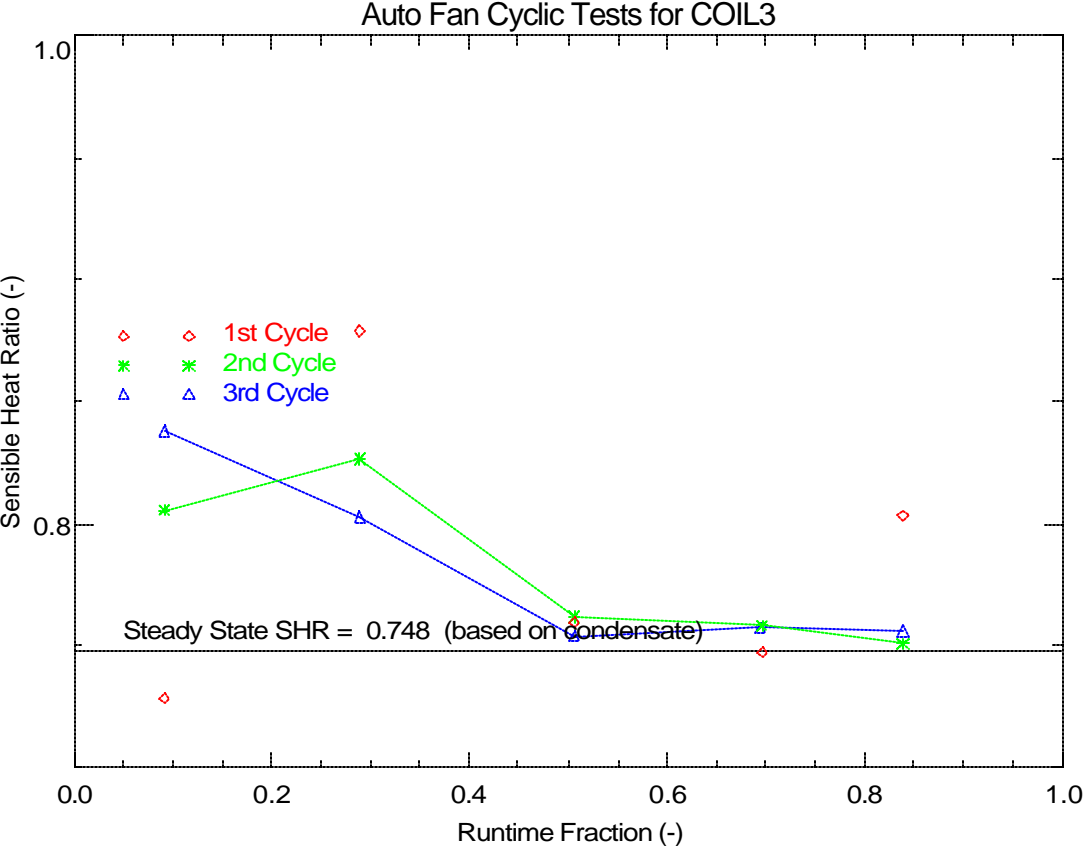


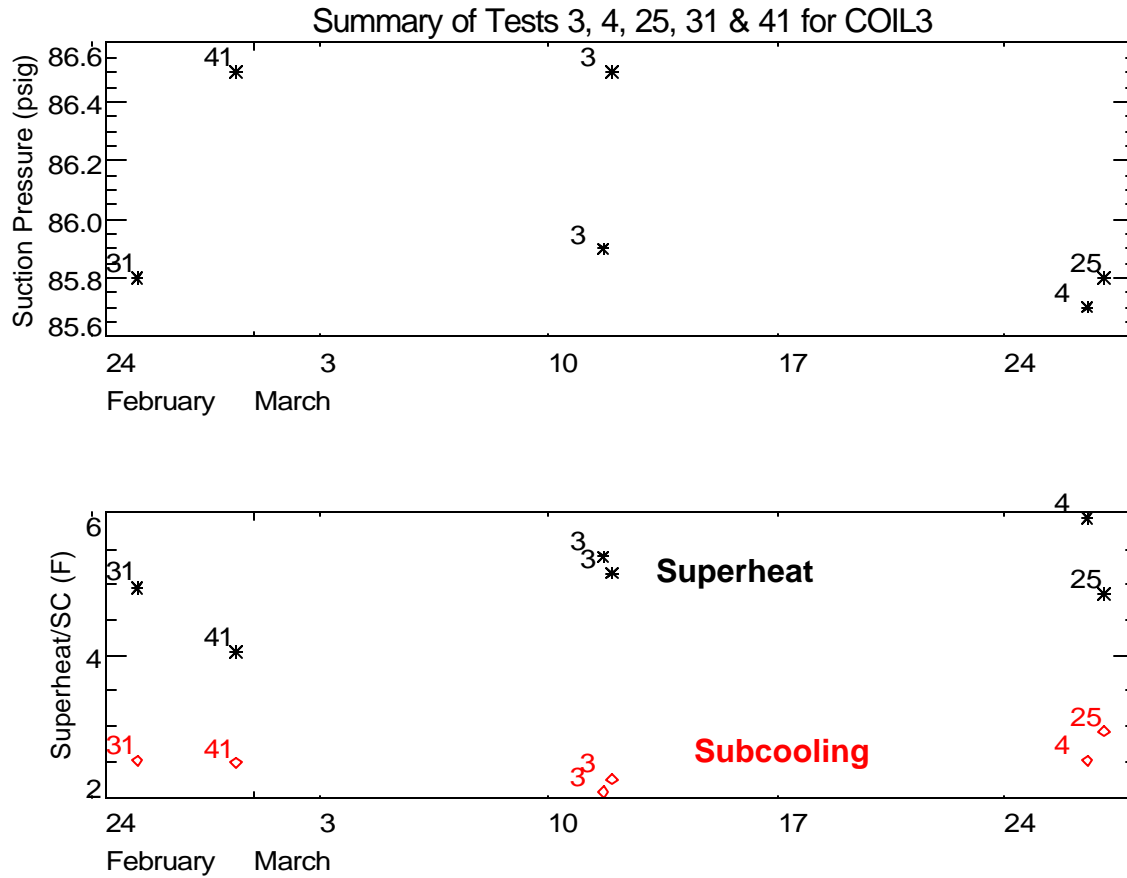
Figure 19. Comparing Measured Latent Degradation to the LHR Models: 300 cfm/ton, 80° F / 60.4° Fdp

Figure 20 shows some latent degradation can be detected in the AUTO fan mode (i.e., the supply air flow across the cooling coil starts and stops with compressor operation) for Coil 3. The degradation is similar to what was seen for Coil 1 but different from Coil 2 (this is somewhat surprising since Coil 2 was the same physical coil as Coil 3). The 2<sup>nd</sup> and 3<sup>rd</sup> repetition (cycle) show fairly good agreement with each other.



**Figure 20. Measured AUTO Fan Latent Degradation**

The tests were completed over a period of 6 weeks. Figure 21 shows little evidence of a change in suction pressure, subcooling or superheat over the test period. This implies that no significant loss of refrigerant charge occurred over the test period.



**Figure 21. Long-Term Variation in Suction Pressure, Superheat and Subcooling**

**References**

Henderson, H., and K. Rengarajan. 1996. A model to predict the latent capacity of air conditioners and heat pumps at part-load conditions with constant fan operation. *ASHRAE Transactions* 102(1): 266-274.

Stabat, P., Marchio, D. and M. Orphelin. 2001. Pre-Design and Design Tools for Evaporative Cooling. *ASHRAE Transactions* 107 (1): 501-510.

**COIL 3 Test Runs**

File Name	Date	Start Time	Sequence No.	Run/Test No.	Inlet DB (F)	Inlet DewPt (F)	Air Flow (cfm)	Test Duration (min)	Comp Runtime (min)
coil3_test_1a.out	4/8/2003	17:02:28	1	1	80	60.4	584.5	359.7	180
coil3_test_1a.out	4/8/2003	23:02:25	2	1	80	60.4	589.7	359.6	179.9
coil3_test_1a.out	4/9/2003	5:02:16	3	1	80	60.4	591.5	359.7	179.9
coil3_test_2b.out	4/1/2003	15:01:15	1	2	80	60.4	597.4	359.7	180
coil3_test_2b.out	4/1/2003	21:01:16	2	2	80	60.4	599.8	359.7	180
coil3_test_2b.out	4/2/2003	3:01:16	3	2	80	60.4	600.2	359.7	180
coil3_test_3.out	3/11/2003	10:20:28	1	3	80	60.4	583.2	359.7	180
coil3_test_3.out	3/11/2003	16:20:28	2	3	80	60.4	583.8	359.8	180
coil3_test_3.out	3/11/2003	22:20:29	3	3	80	60.4	588.2	359.7	180
Coil3 Test 4b 10b 16b 22b 25b.out	3/26/2003	9:12:50	1	4	80	60.4	589.7	179.7	90
Coil3 Test 4b 10b 16b 22b 25b.out	3/26/2003	12:12:49	2	4	80	60.4	583.8	179.7	90
Coil3 Test 4b 10b 16b 22b 25b.out	3/26/2003	15:12:49	3	10	80	60.4	442.3	179.8	90
Coil3 Test 4b 10b 16b 22b 25b.out	3/26/2003	18:12:50	4	16	80.1	60.4	293.6	199.7	100
Coil3 Test 4b 10b 16b 22b 25b.out	3/26/2003	21:32:50	5	22	80	60.4	663.5	179.7	90
Coil3 Test 4b 10b 16b 22b 25b.out	3/27/2003	0:32:49	6	25	80	60.4	587.6	180	90
Coil3 Test 5b 11b 17b 23b.out	4/7/2003	9:28:49	1	5	80.6	67.8	587.5	239.7	120
Coil3 Test 5b 11b 17b 23b.out	4/7/2003	13:28:46	2	5	80.1	68.5	581.4	239.8	120
Coil3 Test 5b 11b 17b 23b.out	4/7/2003	17:28:47	3	11	80.2	68.6	436.7	239.7	120
Coil3 Test 5b 11b 17b 23b.out	4/7/2003	21:28:47	4	17	80.2	68.6	287.8	239.7	120
Coil3 Test 5b 11b 17b 23b.out	4/8/2003	1:28:46	5	23	80.1	68.7	665.2	299.9	149.9
Coil3 Test 6b 12b 18b 24b.out	3/5/2003	13:37:07	1	6	80	50.9	587.1	194.7	134.9
Coil3 Test 6b 12b 18b 24b.out	3/5/2003	16:52:05	2	6	80.1	50.5	587.6	194.7	135
Coil3 Test 6b 12b 18b 24b.out	3/5/2003	20:07:05	3	12	80.2	50.5	442	194.8	135
Coil3 Test 6b 12b 18b 24b.out	3/5/2003	23:22:06	4	18	80.3	50.4	290.4	224.7	135
Coil3 Test 6b 12b 18b 24b.out	3/6/2003	3:07:02	5	24	80	50.5	669	180	135
Coil3 Test 7c 13c 19c.out	4/2/2003	10:52:03	1	7	75.2	64.6	593.5	179.7	90
Coil3 Test 7c 13c 19c.out	4/2/2003	13:52:02	2	7	75.2	64.7	592.1	179.7	89.9
Coil3 Test 7c 13c 19c.out	4/2/2003	16:51:59	3	13	75.3	64.7	442.9	209.7	90
Coil3 Test 7c 13c 19c.out	4/2/2003	20:21:59	4	19	75.5	64.6	291.8	239.7	90
Coil3 Test 8c 14c 20c.out	4/3/2003	9:40:35	1	8	76	56	595.7	179.8	90
Coil3 Test 8c 14c 20c.out	4/3/2003	12:40:36	2	8	75.1	56.1	591.8	179.8	90
Coil3 Test 8c 14c 20c.out	4/3/2003	15:40:37	3	14	75.1	56.1	447.8	179.8	90
Coil3 Test 8c 14c 20c.out	4/3/2003	18:40:38	4	20	75.4	56.1	295.5	200	100
Coil3 Test 9c 15c 21c.out	4/3/2003	22:00:37	1	9	75.1	50.2	594.1	204.7	115
Coil3 Test 9c 15c 21c.out	4/4/2003	1:25:37	2	9	75.1	50	595.7	179.7	90
Coil3 Test 9c 15c 21c.out	4/4/2003	4:25:35	3	15	75.2	50	454.5	179.7	90
Coil3 Test 9c 15c 21c.out	4/4/2003	7:25:35	4	21	75.9	50	297.9	199.7	100
Coil3 Test cycling constant.out	2/25/2003	8:03:36	1	31	81.8	60.4	595.6	89.3	44.5
Coil3 Test cycling constant.out	2/25/2003	9:33:07	2	31	80	60.4	591.1	89.8	45
Coil3 Test cycling constant.out	2/25/2003	11:03:08	3	32	80	60.4	590.8	35.8	30
Coil3 Test cycling constant.out	2/25/2003	11:39:09	4	32	80.1	60.4	587.3	35.8	30
Coil3 Test cycling constant.out	2/25/2003	12:15:10	5	32	80.1	60.4	585.6	35.7	30
Coil3 Test cycling constant.out	2/25/2003	12:51:11	6	33	80.2	60.5	587.8	23	16
Coil3 Test cycling constant.out	2/25/2003	13:14:26	7	33	80.2	60.4	587	23	16
Coil3 Test cycling constant.out	2/25/2003	13:37:42	8	33	80.3	60.4	586.2	23	16
Coil3 Test cycling constant.out	2/25/2003	14:00:58	9	34	80.1	60.5	588.1	19.8	10
Coil3 Test cycling constant.out	2/25/2003	14:20:59	10	34	80.2	60.4	589	19.8	10
Coil3 Test cycling constant.out	2/25/2003	14:41:01	11	34	80.1	60.5	589.2	19.7	10
Coil3 Test cycling constant.out	2/25/2003	15:01:01	12	35	80.2	60.5	589.1	24.3	7
Coil3 Test cycling constant.out	2/25/2003	15:25:32	13	35	80	60.5	589.1	24.3	7
Coil3 Test cycling constant.out	2/25/2003	15:50:03	14	35	80.1	60.5	588.2	24.3	7
Coil3 Test cycling constant 75 56.out	2/26/2003	7:49:58	1	61	76.6	56	593.1	89.8	45
Coil3 Test cycling constant 75 56.out	2/26/2003	9:19:59	2	61	75	56	591.7	149.8	90
Coil3 Test cycling constant 75 56.out	2/26/2003	11:50:00	3	62	75	56	589	35.8	30
Coil3 Test cycling constant 75 56.out	2/26/2003	12:26:01	4	62	75.1	56	586.4	35.8	30
Coil3 Test cycling constant 75 56.out	2/26/2003	13:02:02	5	62	75.2	56.1	584.2	35.8	30
Coil3 Test cycling constant 75 56.out	2/26/2003	13:38:03	6	63	75.3	56	583.4	23	16
Coil3 Test cycling constant 75 56.out	2/26/2003	14:01:19	7	63	75.3	56	583.9	23	16
Coil3 Test cycling constant 75 56.out	2/26/2003	14:24:35	8	63	75.3	56	583.7	23	16
Coil3 Test cycling constant 75 56.out	2/26/2003	14:47:51	9	64	75.3	56.1	584.6	19.8	10
Coil3 Test cycling constant 75 56.out	2/26/2003	15:07:52	10	64	75.2	56.1	584.7	19.8	10
Coil3 Test cycling constant 75 56.out	2/26/2003	15:27:53	11	64	75.2	56.1	585.1	19.8	10
Coil3 Test cycling constant 75 56.out	2/26/2003	15:47:54	12	65	75.3	56.1	585.5	24.3	7
Coil3 Test cycling constant 75 56.out	2/26/2003	16:12:25	13	65	75.3	56.2	587	24.3	7
Coil3 Test cycling constant 75 56.out	2/26/2003	16:36:56	14	65	75.1	56.3	588.8	24.3	7

**COIL 3 Test Runs (cont)**

File Name	Date	Start Time	Sequence No.	Run/Test No.	Inlet DB (F)	Inlet DewPt (F)	Air Flow (cfm)	Test Duration (min)	Comp Runtime (min)
Coil3 Test cycling constant 75 64.out	2/27/2003	8:49:50	1	51	80.2	64	589.8	89.8	45
Coil3 Test cycling constant 75 64.out	2/27/2003	10:19:51	2	51	75.3	64	584.9	149.7	90
Coil3 Test cycling constant 75 64.out	2/27/2003	12:49:52	3	52	75.5	64	583.7	35.7	30
Coil3 Test cycling constant 75 64.out	2/27/2003	13:25:53	4	52	75.5	64	580.7	35.7	30
Coil3 Test cycling constant 75 64.out	2/27/2003	14:01:53	5	52	75.4	64	581.1	35.8	30
Coil3 Test cycling constant 75 64.out	2/27/2003	14:37:54	6	53	75.8	64	581.6	23	16
Coil3 Test cycling constant 75 64.out	2/27/2003	15:01:10	7	53	75.7	64	583.1	23	16
Coil3 Test cycling constant 75 64.out	2/27/2003	15:24:26	8	53	75.8	64	582.2	23	16
Coil3 Test cycling constant 75 64.out	2/27/2003	15:47:42	9	54	75.9	64	581.2	19.8	10
Coil3 Test cycling constant 75 64.out	2/27/2003	16:07:43	10	54	76	64.1	582.9	19.8	10
Coil3 Test cycling constant 75 64.out	2/27/2003	16:27:44	11	54	76	64.1	582.5	19.8	10
Coil3 Test cycling constant 75 64.out	2/27/2003	16:47:45	12	55	76.1	64.2	583.2	24.3	7
Coil3 Test cycling constant 75 64.out	2/27/2003	17:12:16	13	55	76.1	64	583.7	24.3	7
Coil3 Test cycling constant 75 64.out	2/27/2003	17:36:47	14	55	76.1	64.1	585.3	24.3	7
Coil3 Test cycling constant 300d.out	4/10/2003	13:07:22	1	71	80	60.4	455	232.2	112.5
Coil3 Test cycling constant 300d.out	4/10/2003	16:59:52	2	71	80	60.4	454.5	239.7	120
Coil3 Test cycling constant 300d.out	4/10/2003	20:59:49	3	72	80	60.4	458	35.7	30
Coil3 Test cycling constant 300d.out	4/10/2003	21:35:50	4	72	80	60.4	455.9	35.7	30
Coil3 Test cycling constant 300d.out	4/10/2003	22:11:50	5	72	80	60.3	455.9	35.8	30
Coil3 Test cycling constant 300d.out	4/10/2003	22:47:51	6	73	80.1	60.3	456.6	23	16
Coil3 Test cycling constant 300d.out	4/10/2003	23:11:07	7	73	80	60.3	456.7	23	16
Coil3 Test cycling constant 300d.out	4/10/2003	23:34:22	8	73	79.9	60.3	455.5	23	16
Coil3 Test cycling constant 300d.out	4/10/2003	23:57:38	9	74	81	59.9	456.1	19.8	10
Coil3 Test cycling constant 300d.out	4/11/2003	0:17:39	10	74	80	60.4	455.3	19.8	10
Coil3 Test cycling constant 300d.out	4/11/2003	0:37:40	11	74	79.9	60.2	458.2	19.8	10
Coil3 Test cycling constant 300d.out	4/11/2003	0:57:41	12	75	80	60.1	456.8	24.2	7
Coil3 Test cycling constant 300d.out	4/11/2003	1:22:11	13	75	79.8	60.1	458.7	24.3	7
Coil3 Test cycling constant 300d.out	4/11/2003	1:46:42	14	75	80.1	60.1	460	24.7	7
Coil3 Test cycling auto.out	2/28/2003	8:50:38	1	41	80.5	60.4	592.5	89.8	45
Coil3 Test cycling auto.out	2/28/2003	10:20:39	2	41	80	60.4	588.5	149.8	90
Coil3 Test cycling auto.out	2/28/2003	12:50:40	3	42	79.8	60.3	588.6	35.7	30
Coil3 Test cycling auto.out	2/28/2003	13:26:40	4	42	79.8	60.4	587.6	35.8	30
Coil3 Test cycling auto.out	2/28/2003	14:02:41	5	42	79.9	60.3	586.3	35.8	30
Coil3 Test cycling auto.out	2/28/2003	14:38:42	6	43	79.9	60.4	585.1	23	16
Coil3 Test cycling auto.out	2/28/2003	15:01:58	7	43	79.9	60.3	588.1	23	16
Coil3 Test cycling auto.out	2/28/2003	15:25:14	8	43	79.8	60.4	586.9	23	16
Coil3 Test cycling auto.out	2/28/2003	15:48:29	9	44	79.8	60.3	587.3	19.8	10
Coil3 Test cycling auto.out	2/28/2003	16:08:30	10	44	80	60.4	587.3	19.8	10
Coil3 Test cycling auto.out	2/28/2003	16:28:31	11	44	79.9	60.4	588.1	19.7	10
Coil3 Test cycling auto2.out	3/3/2003	12:07:05	3	45	79.6	60.3	589.5	24.3	7
Coil3 Test cycling auto2.out	3/3/2003	12:31:36	4	45	80	60.3	588.5	24.3	7
Coil3 Test cycling auto2.out	3/3/2003	12:56:07	5	45	79.8	60.1	589	24.3	7
Coil3 Test cycling auto2.out	3/3/2003	13:20:38	6	46	80.2	60.4	588.7	60.3	5.5
Coil3 Test cycling auto2.out	3/3/2003	14:21:09	7	46	79.7	60.2	589.6	60.3	5.5
Coil3 Test cycling auto2.out	3/3/2003	15:21:40	8	46	79.7	60.1	587.1	60.5	5.5

## **APPENDIX H4**

### **Summary of Laboratory Data for Coil 4**



**Summary of Laboratory Data for Coil 4  
November 2005**



Vertical coil arrangement



14 fins per inch



Coil refrigerant distribution  
(3 circuits)

Manufacturer	Goodman
Model number	H-24F
Nominal size:	2 tons
Baseline Size and Airflow (Test 4):	1.8 tons / 760 cfm
Coil type:	vertical slab, 2 row, 14 fpi, wavy fins, 3 circuits
Coil dimensions:	3.27 ft <sup>2</sup> face area, 24 in x 19-5/8 in, 16 in x 21 in connecting ductwork flange
Coil thickness:	1.5 in
Tube diameter:	3/8 in OD copper
Tube spacing:	1 in, within row (vert) 3/4 in, row-to-row (horiz)
Expansion device:	fixed orifice
Unit supply fan:	none
Compressor power:	inverter

**Table 1. Summary of Steady State Test Conditions Corresponding to Each Run or Test**

	<i>Entering Coil Conditions</i>					
	<i>80/67°F 60°F dp</i>	<i>80/72°F 68°F dp</i>	<i>80/62°F 50°F dp</i>	<i>75/68°F 64°F dp</i>	<i>75/63°F 56°F dp</i>	<i>75/58°F 45°F dp</i>
400 cfm/ton	#4 (or 3)	#5	#6	#7	#8	#9
300 cfm/ton	#10	#11	#12	#13	#14	#15
200 cfm/ton	#16	#17	#18	#19	#20	#21
450 cfm/ton	#22	#23	#24			
400-200 cfm/ton (ON & OFF)	#25					
Low suction (40°F)	#1					
High suction (50°F)	#2					

Notes: Tests 4-25 all at nominal suction of 44°F (set at nominal conditions of test #3/4). A fixed orifice expansion device was used, with nominal superheat of 3-4°F. The refrigerant charge established during Test 4 was not changed for the remaining tests. The Table 1 test points denote the target testing conditions. Drier test conditions with dew points below 50°F (such as Tests #9, #15, and #21) could not be achieved. In these cases, entering conditions were typically held near 50°F dp. For each test, the compressor is ON for 180 minutes and then the compressor is OFF for at least 90 minutes. The booster fan runs continuously for all tests (when the compressor is both ON and OFF).

**Steady State Performance**

The nominal performance characteristics for this coil (based on steady-state conditions from Run #4 below) are:

Total Capacity:	21.5 MBtu/h (1.8 tons)
Sensible Capacity:	15.4 MBtu/h
Latent Capacity (condensate):	6.1 MBtu/h
Sensible Heat Ratio:	0.72

Latent capacity can be calculated two ways: 1) using dew point readings and air flow, and 2) using the condensate flow rate. Figure 1 compares the latent capacity calculated these two ways. The number of each data point corresponds to the test number listed in Table 1. In general, the condensate readings resulted in a slightly lower capacity, which was probably due to the condensate measurement device (i.e., the tipping bucket mechanism) wearing out.

Figure 2 shows the trend of steady-state sensible heat ratio (SHR) with relative humidity and airflow rate. The cooling capacities used to calculate SHR in Figure 2 are based on airflow measurements and the psychrometric conditions entering and leaving the cooling coil. This performance map is typical for a cooling coil (i.e., SHR is mostly a function of the entering relative humidity, with some dependence on the air flow rate).

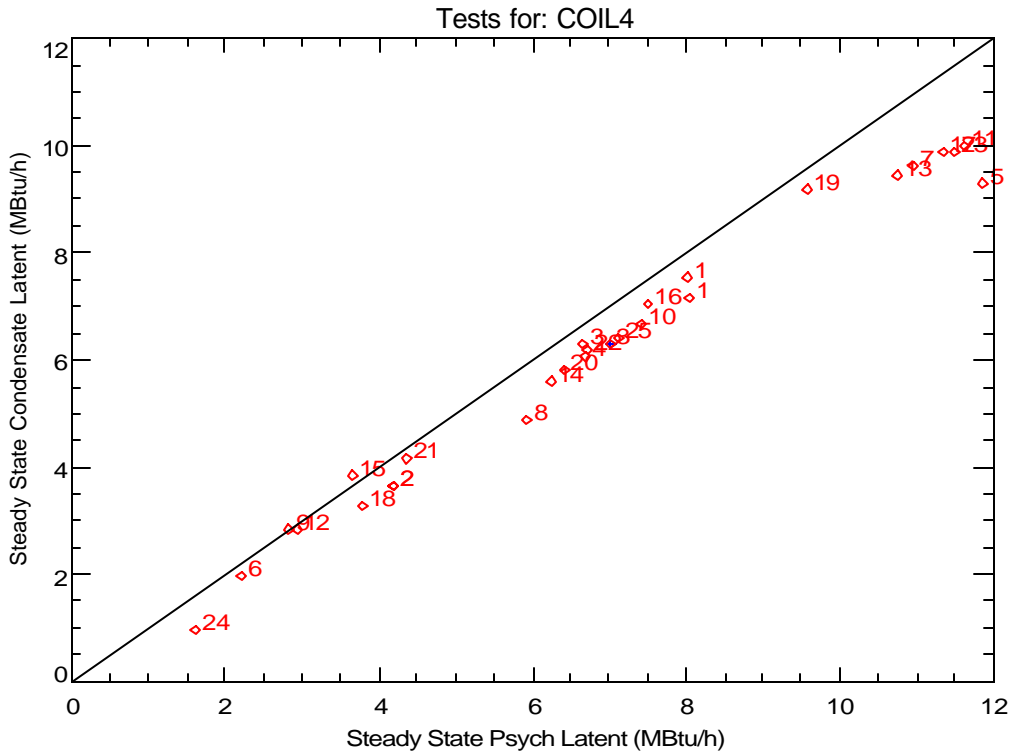


**Figure 1. Comparing Steady-State Latent Capacity Calculated From Psychrometric State Points and Condensate Removal Rates**

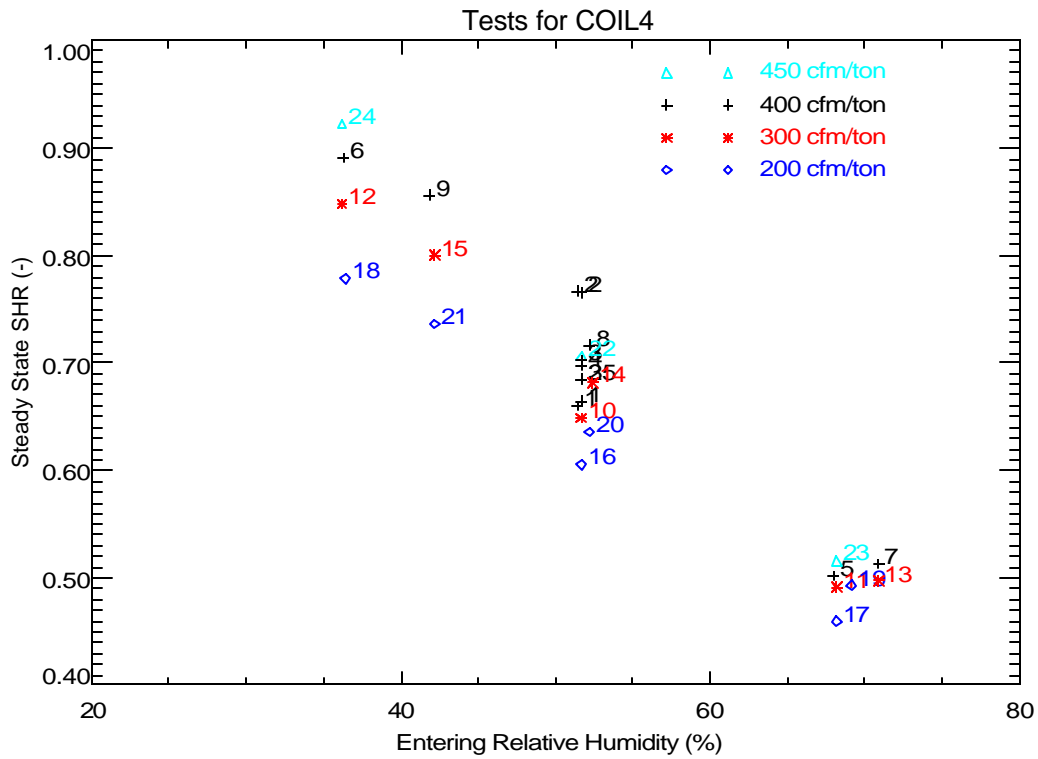


**Figure 2. Variation of Steady State SHR with Entering Humidity and Nominal Air Flow**

## **Typical Transient Performance**

Figure 3 shows the typical transient performance of the cooling coil at nominal conditions (i.e., for Cycle 2 of Run #4). The compressor runs for 180 minutes and is off for 90 minutes<sup>1</sup>. The booster fan remains on during the entire test (separate external fan used to maintain the desired air flow rate across the cooling coil). A portion of the moisture removed by the coil during the compressor on cycle evaporates back into the air stream during the off cycle. During the off cycle the coil acts as an evaporative cooler, so the sensible capacity is nearly equal to the absolute value of the latent capacity (i.e., the sum of latent and sensible is zero).

If we integrate the off cycle sensible capacity (after allowing for a 1-minute off-cycle delay to account for refrigerant movement and other transient effects), we can determine the energy associated with the moisture retained on the coil. To minimize the integration of any measurement errors, the off-cycle integration stops at the time labeled “Integration Pt.” on the plot. This point corresponds to the time when the temperature and dew point differences across the coil have first reached the terminal values (i.e., the averages from the end of the off-cycle). In this case the integration indicates that the sensible cooling is equivalent to 1.91 lbs of moisture being retained on the coil. The integrated latent capacity – which is harder to measure precisely – equals 1.95 lbs.

The value “twet” from Henderson and Rengarajan (1996) can then be calculated by dividing the retained moisture mass (expressed as Btu; mass x 1060 Btu/lb) and the steady state psychrometric latent capacity ( $QL = 6.7 \text{ MBtu/h}$ ). Figure 3 shows that the values of twet based on integrated sensible and latent off-cycle capacity are 18.2 and 18.5 minutes respectively. These values of twet are similar to the measured delay of 23.5 minutes for the first condensate pulse to fall from the drain pan. The value of gamma (0.85), which is the initial off-cycle moisture evaporation rate divided by the steady-state psychrometric latent capacity, uses the off-cycle moisture evaporation rate (5.7 MBtu/h) once the transition point was been detected. For this coil, we detect the transition by determining where the change in off-cycle sensible capacity between each 15-second interval first drops below 3% of the steady-state on cycle sensible capacity (QS). At this transition point where gamma is determined, it is assumed that all coil heat and mass transfer with the air stream is adiabatic (the refrigerant flow could not be used as the indicator to detect this point for this coil). In this case it took 1.75 minutes for the change in off-cycle sensible capacity to drop below 3% of the steady-state on cycle value QS.

---

<sup>1</sup> The runtime was increased from 45 and 90 minutes for the previous coil tests to ensure steady state was achieved during the on cycle and full moisture evaporation occurred during the off cycle.

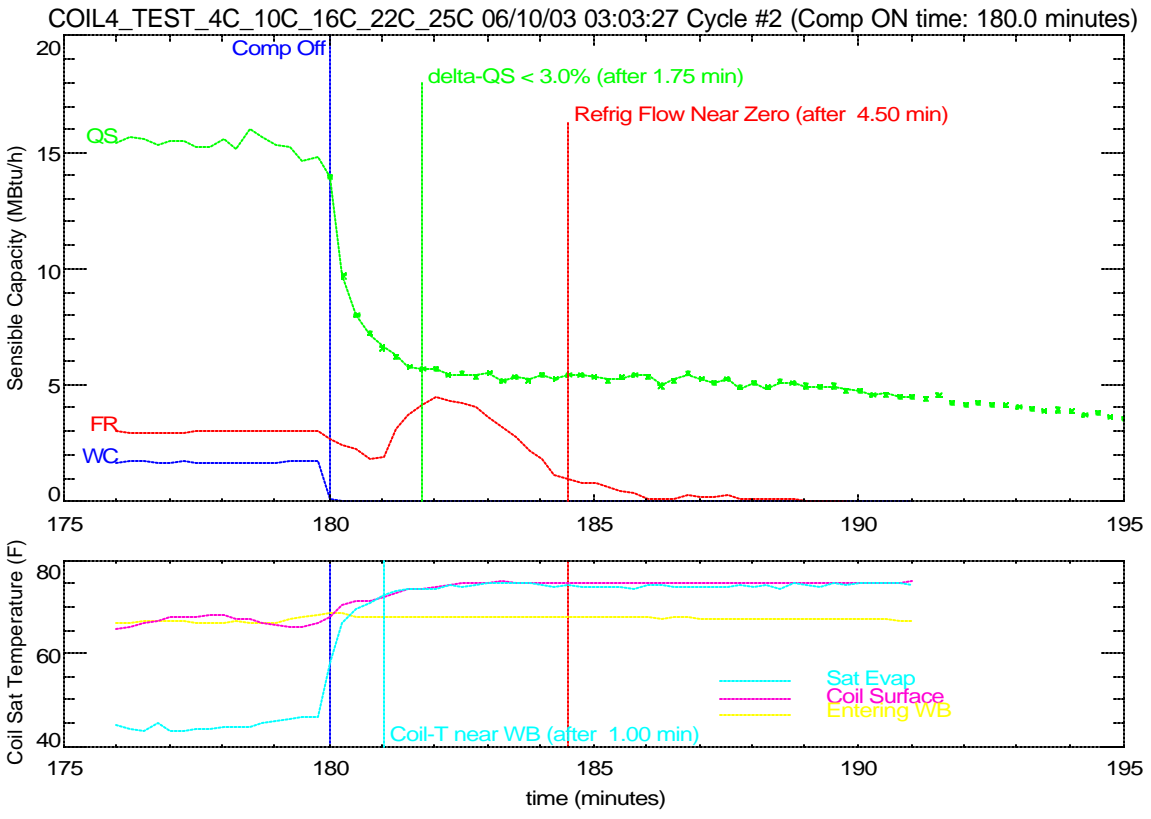
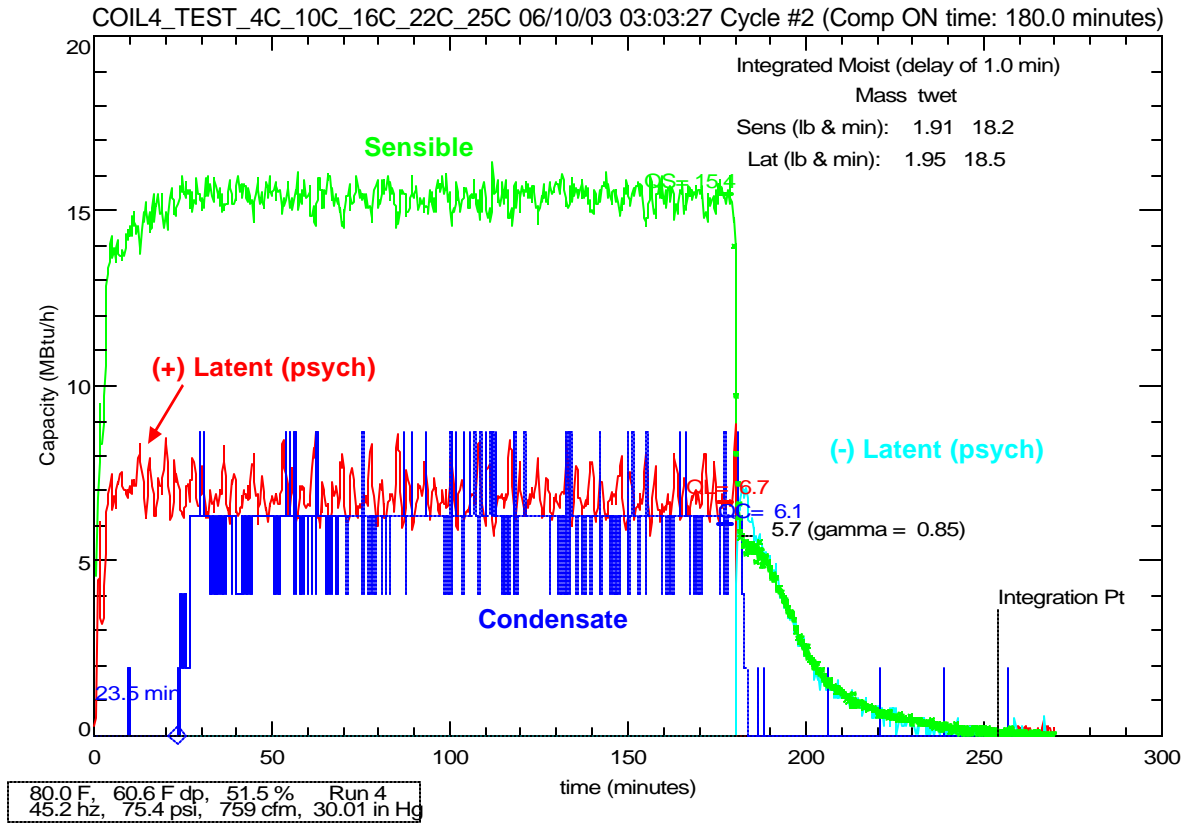
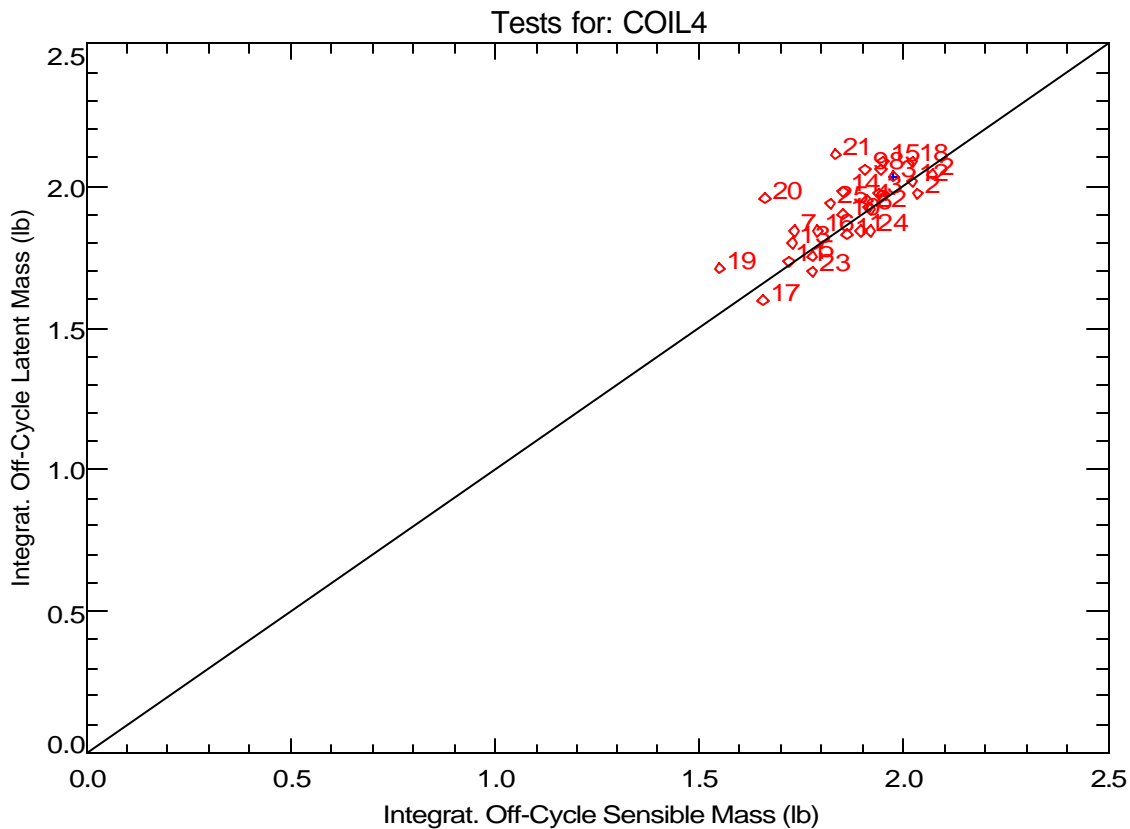


Figure 3. Example Plots of Detailed Data for Coil 4

## Part Load Latent Capacity Parameters

The amount of moisture held on the cooling coil (and drain pan) can be calculated by integrating the off-cycle capacity from the coil (and dividing by the heat of vaporization, 1060 Btu/lb, to get the moisture mass). The integration is delayed for the first minute of the off-cycle so that the overshoot response of the chilled dew point hygrometers does not skew the results of the integration<sup>2</sup>. The integration terminates once steady state conditions are reached for the off cycle. If we assume the coil acts as an evaporative cooler, then sensible and latent capacity should be equal. Figure 4 compares the off-cycle integrated latent and sensible capacity calculated for each run. No systematic bias is evident and Figure 5 shows that the bias is not a function of dew point as was observed from tests of Coil 1.

Since we expect that off-cycle latent and sensible capacity should sum to zero, we have selected the integrated off-cycle sensible capacity as the most consistent and believable indication of the moisture mass held on the cooling coil (and drain pan).



**Figure 4. Comparing Stored Moisture Mass Calculated by Integrating Sensible and Latent Off-Cycle Capacity (Integrated with a 1 minute delay)**

<sup>2</sup>The 1-minute delay causes the estimate of moisture mass to be low by as much as 0.09 lbs (or 5%).

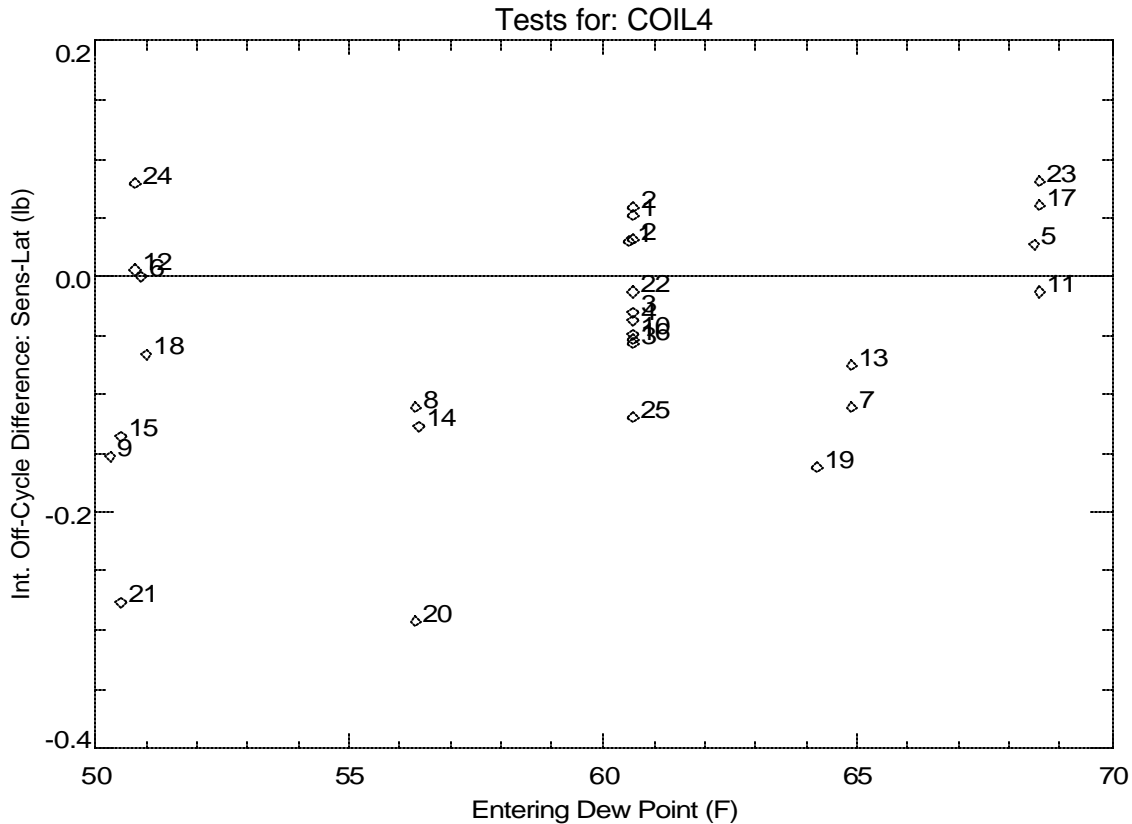


**Figure 5. Variation of Off-Cycle Sensible-Latent Difference with Entering Dew Point**

The parameter “twet” is the moisture mass held on the cooling coil times the enthalpy of vaporization (1060 Btu/lb) divided by the steady-state latent capacity of the cooling coil. The parameter should physically correspond to the time it takes for moisture to first fall from the coil (ignoring startup delays and other effects). Figure 6 compares the calculated “twet” (determined from integrating sensible capacity during the off-cycle and then dividing by the steady-state psychrometric latent capacity during the on-cycle) to the condensate delay time for all test runs. In general, there is fair agreement between these two values. The worst agreement is apparent in tests #6, #9, #12 and #24, which have either drier entering conditions, warmer coil temperatures, or higher air flows. The deviations between twet and the condensate delay time were greater for Coil 4 than for any of the other laboratory-tested coils. The wider deviation may have been due to the tipping bucket “sticking” or resisting the first tipping cycle.

Figure 7a and 7b show that both twet and the condensate delay time are a function of the entering air dew point temperature. Figure 7b uses different symbols to show the 1<sup>st</sup> and 2<sup>nd</sup> cycles in each test sequence with flow rate of 400 cfm/ton for all tests. The delay time was generally the same for the first and second cycles for this coil. The large difference seen for test 6 is due to the low inlet dew point temperature not being properly reached during the 1<sup>st</sup> cycle.

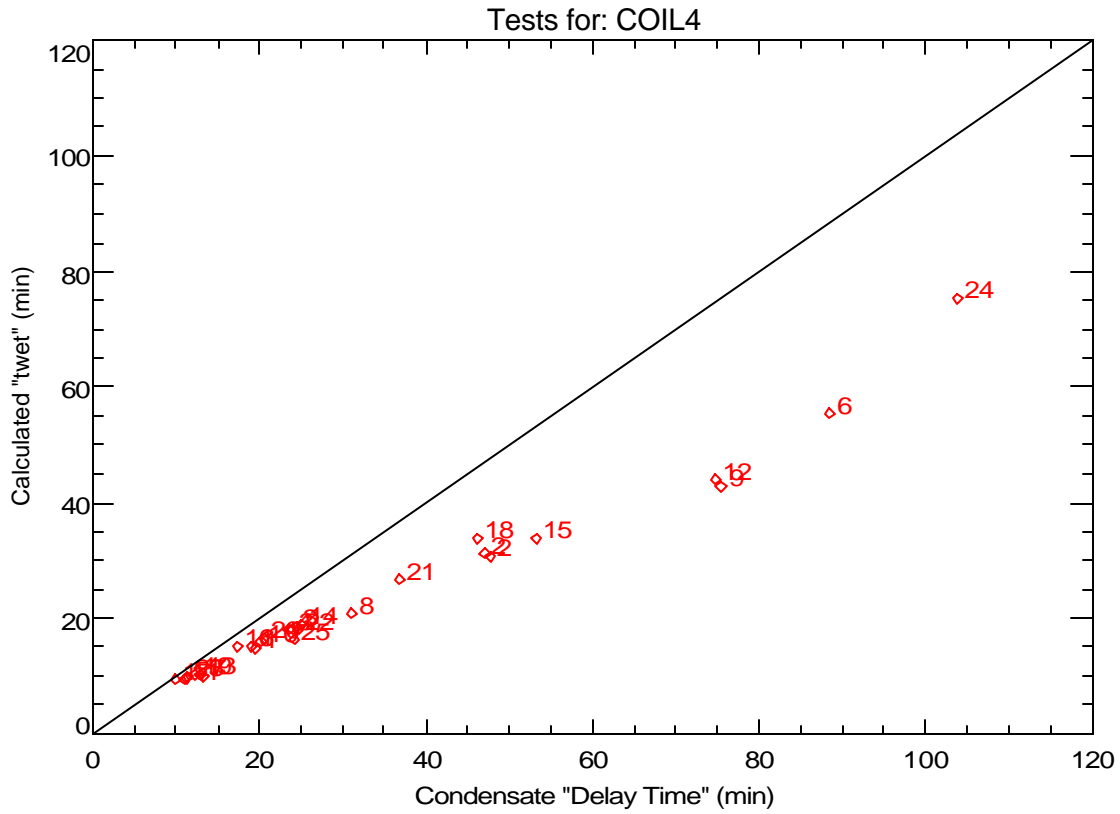


**Figure 6. Comparing “twet” (calculated with off-cycle sensible and steady state latent) to the Condensate Delay Time**



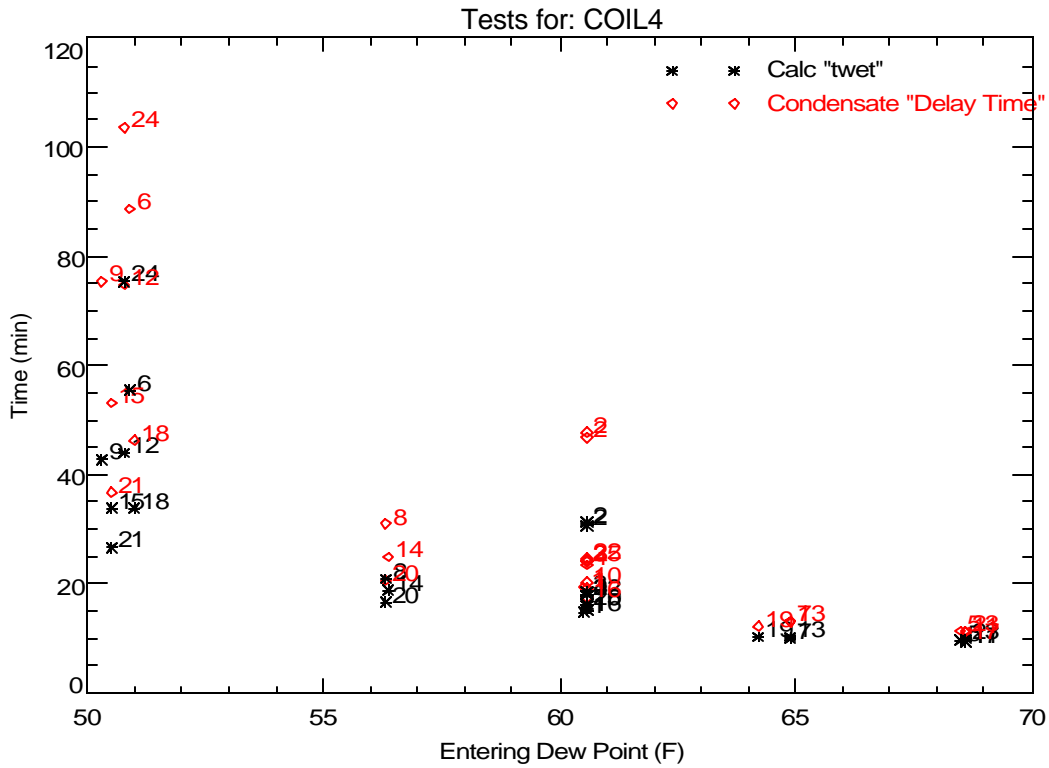


Figure 7a. Impact of Dew Point on “twet” and Condensate Delay Time

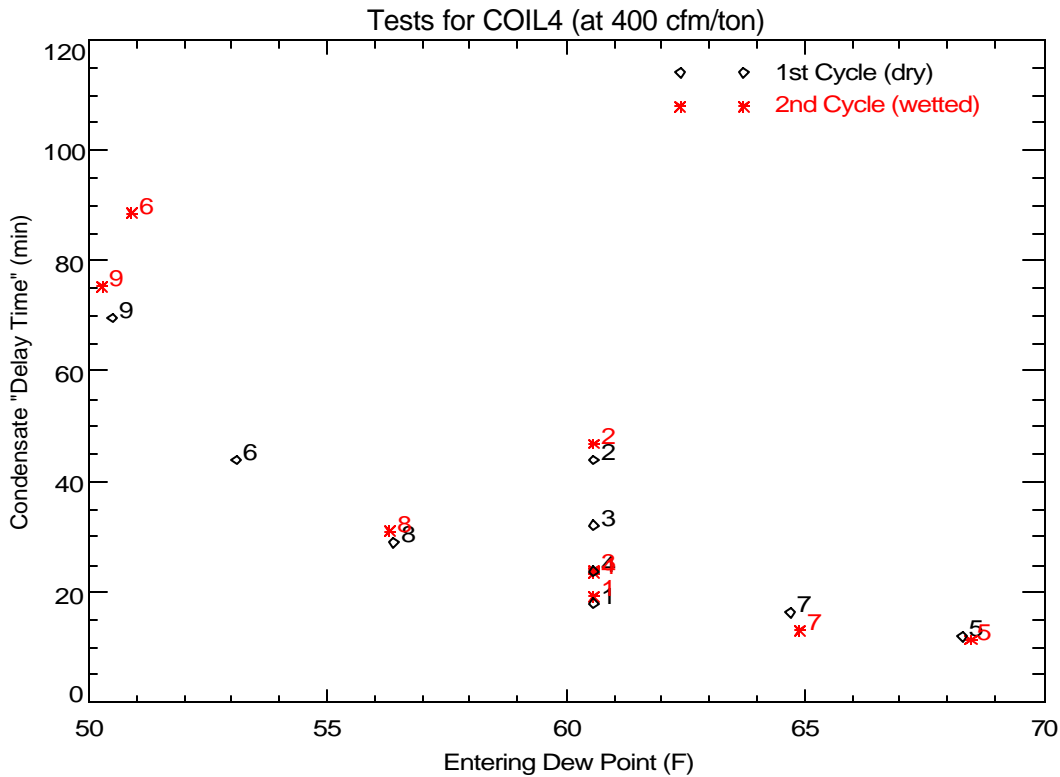


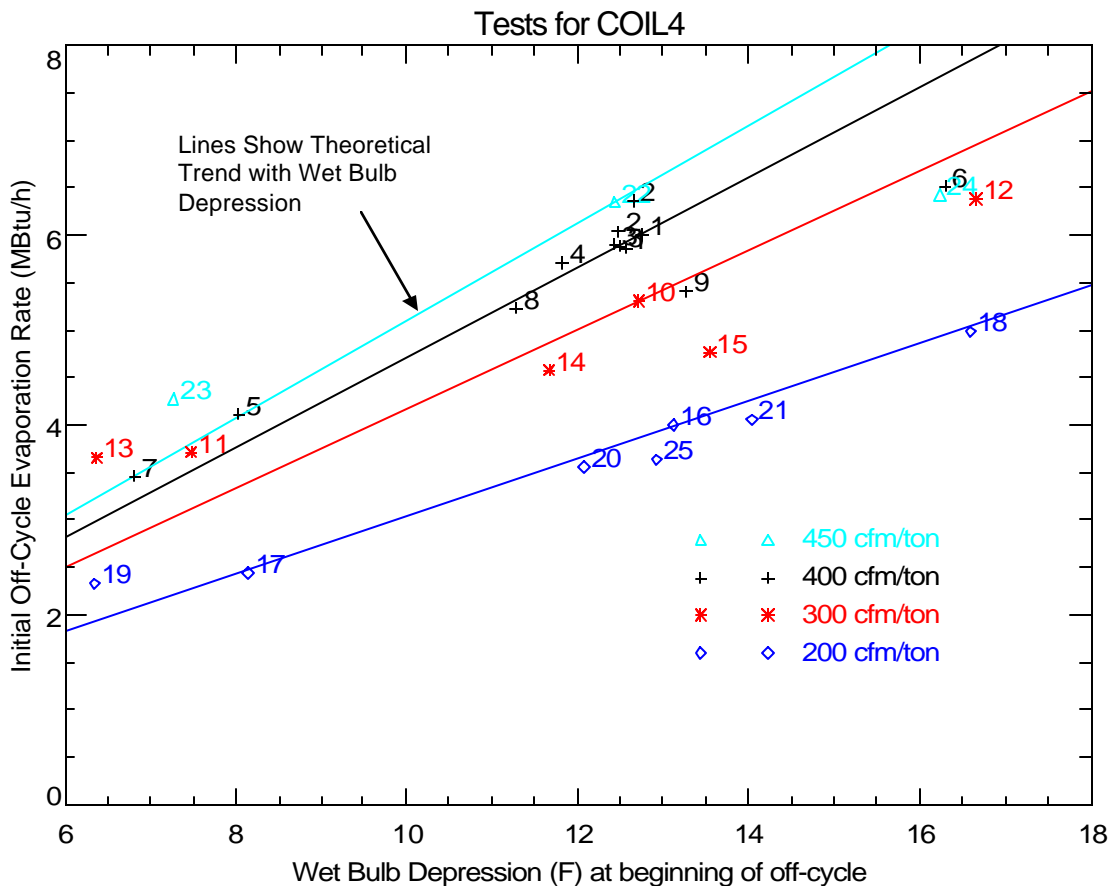
Figure 7b. Impact of Dew Point and Coil Wettedness on Condensate Delay Time

Figure 8 shows the initial off-cycle moisture evaporation rate varies with wet bulb depression. As expected, the evaporation rate is highest when the entering air has a larger wet bulb depression (i.e., has a lower relative humidity) and a higher airflow rate.

The model developed by Henderson and Rengarajan (1996) used the following simple evaporative cooler model to predict the moisture evaporation rate at off-design conditions:

$$Q_{\text{evap}} = Q_{\text{evap}_o} \times \frac{(DB - WB)}{(80 - 67)}$$

where  $Q_{\text{evap}_o}$  is the evaporation rate at the nominal entering air conditions of 80°F dry bulb (DB) and 67°F wet bulb (WB). This simple model is shown as the lines in Figure 8. For each airflow rate, the line is based on the nominal test results at 80°F DB/67°F WB extended to pass through zero. The measured data show essentially the same slope as the theoretical lines. The notable exceptions are the points with higher airflow and drier entering air conditions. Specifically, Tests #6, #9, #24 and #15 deviate significantly from the line. These runs have a much lower initial moisture evaporation rate because the entering air dew point temperature was close to the cooling coil temperature, so the fin surfaces were not fully wetted. The smaller wetted surface area reduces the initial moisture evaporation rate.



**Figure 8. Measured Variation of Initial Evaporation Rate with Wet Bulb Depression**

Stabat et al. (2001) reviewed the theoretical performance of direct evaporative coolers and showed that the saturation effectiveness of an evaporative cooler is:

$$h_{evp} = 1 - e^{-NTU} \quad \text{where} \quad NTU = K/cfm^{0.2} \quad \text{for an air-water mixture.}$$

The line shown on Figure 9 is the best fit of the equation above to the measured data. The resulting constant K was 4.0, which is equivalent to an NTU of 1.06 at 760 cfm. While there is considerable scatter due to the experimental uncertainty of predicting the initial off-cycle moisture evaporation rate, the slope of the line is still fairly representative of the overall trend.

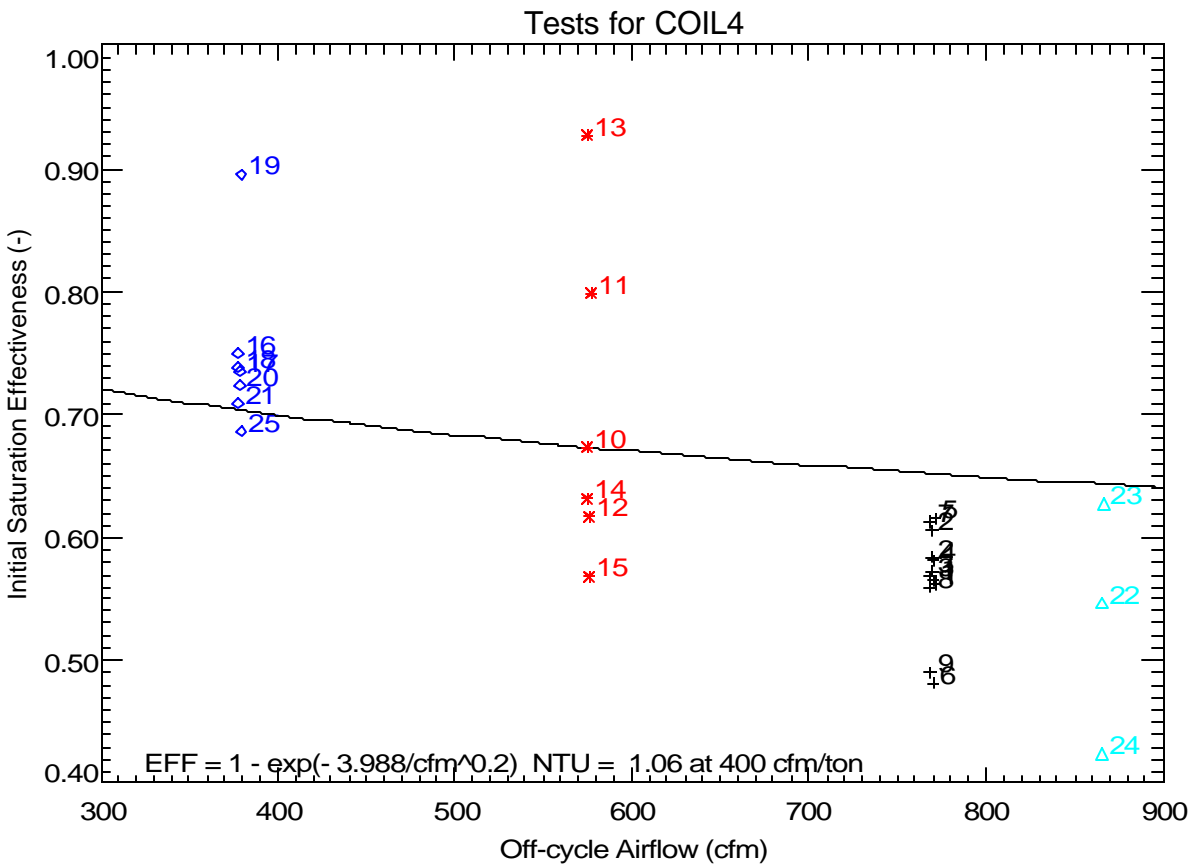


**Figure 9. Evaporative Effectiveness versus Airflow**

Figure 10 compares the measured initial off-cycle moisture evaporation rate for each test to the predicted initial evaporation rate using the effectiveness model above. The model and measured data generally agree when presented in this form (i.e., the overall agreement visually appears better than in Figure 9 above). Again, the variation that occurs for Tests #6, #9 and #24 was due to partial coil dryout, as mentioned above.

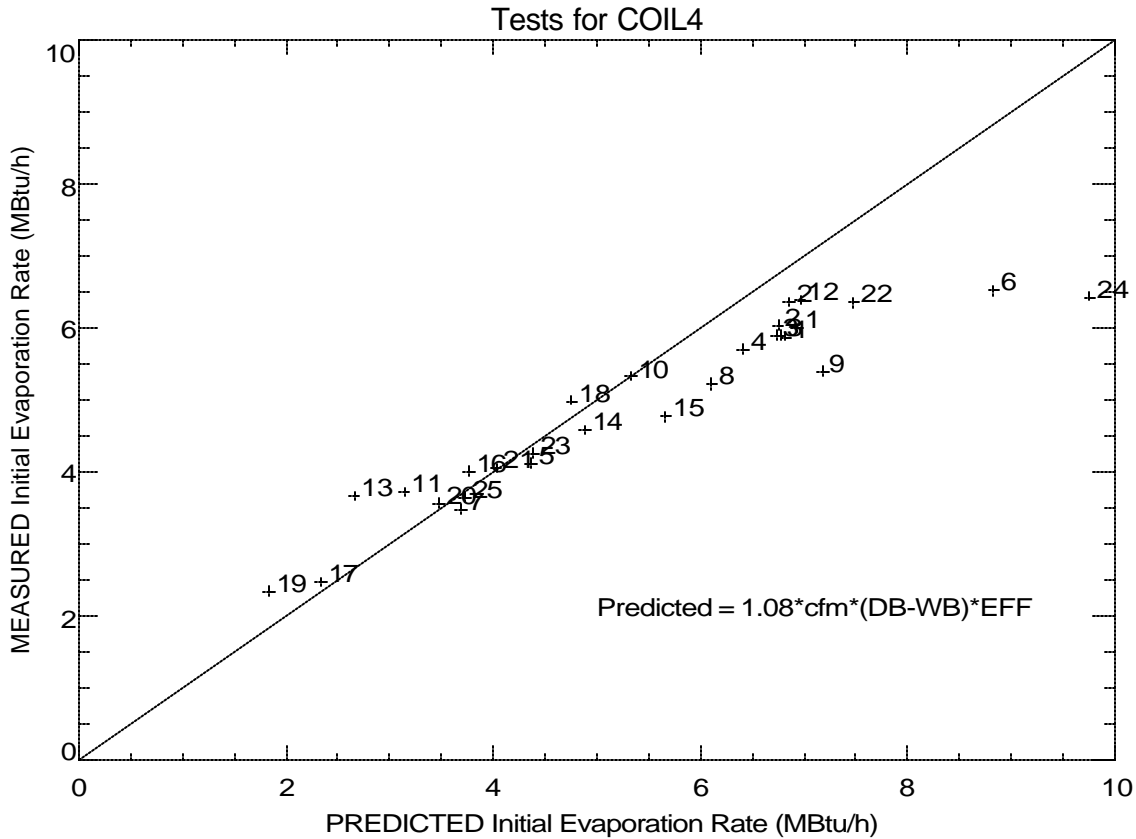


**Figure 10. Comparing Measured and Predicted Initial Moisture Evaporation Rates**

Figure 11 and Figure 12 below evaluate whether the amount of moisture retained on the cooling coil is a function of air flow or entering air conditions. The results for this coil were unusual in that the moisture holding capacity is slightly lower at higher dew points (Figure 11). Most other tested coils showed the opposite trend. Surprisingly, the data also show less evidence of partial coil dryout than we have seen with other coils, despite the known refrigerant distribution problems with this coil (and the degraded evaporation trends for tests #6, #9, and #24 in Figure 8 mentioned above). The amount of retained moisture for Coil 4 ranges from 1.6 to 2.1 lbs.

Figure 12 shows the unexpected trend of a modest decrease in the amount of retained moisture on the cooling coil with lower air flow rates.

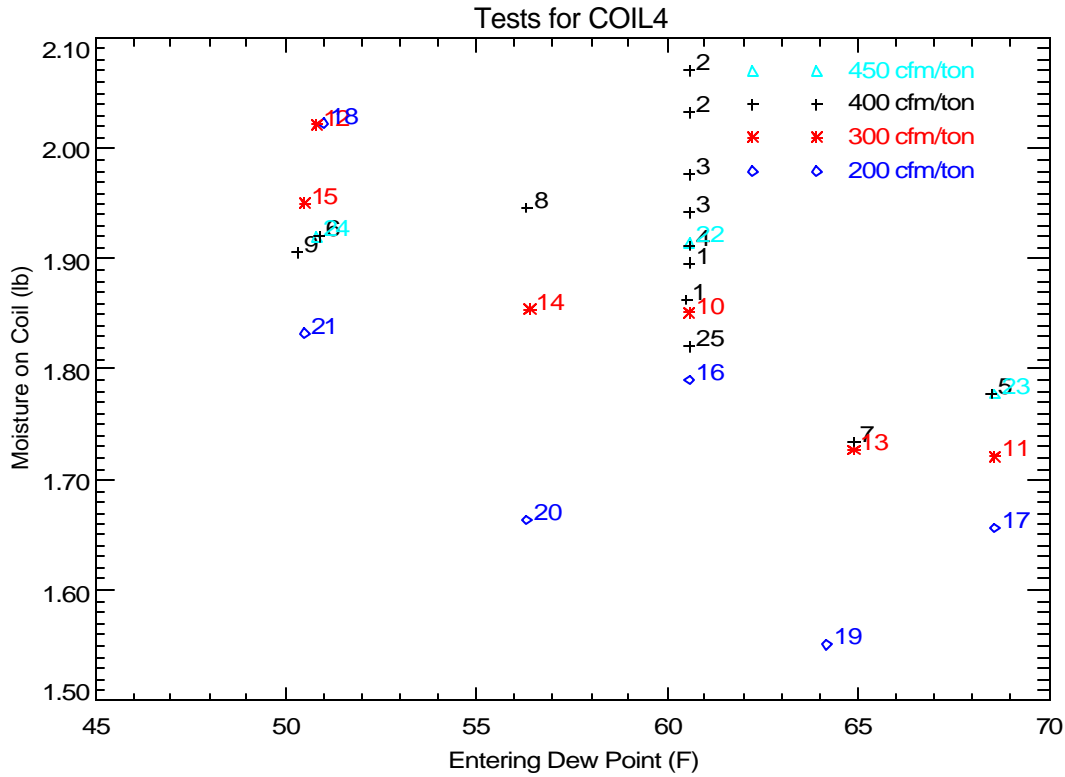


Figure 11. Variation of Retained Moisture (based on Off-Cycle Sensible) with Flow and Dew Point

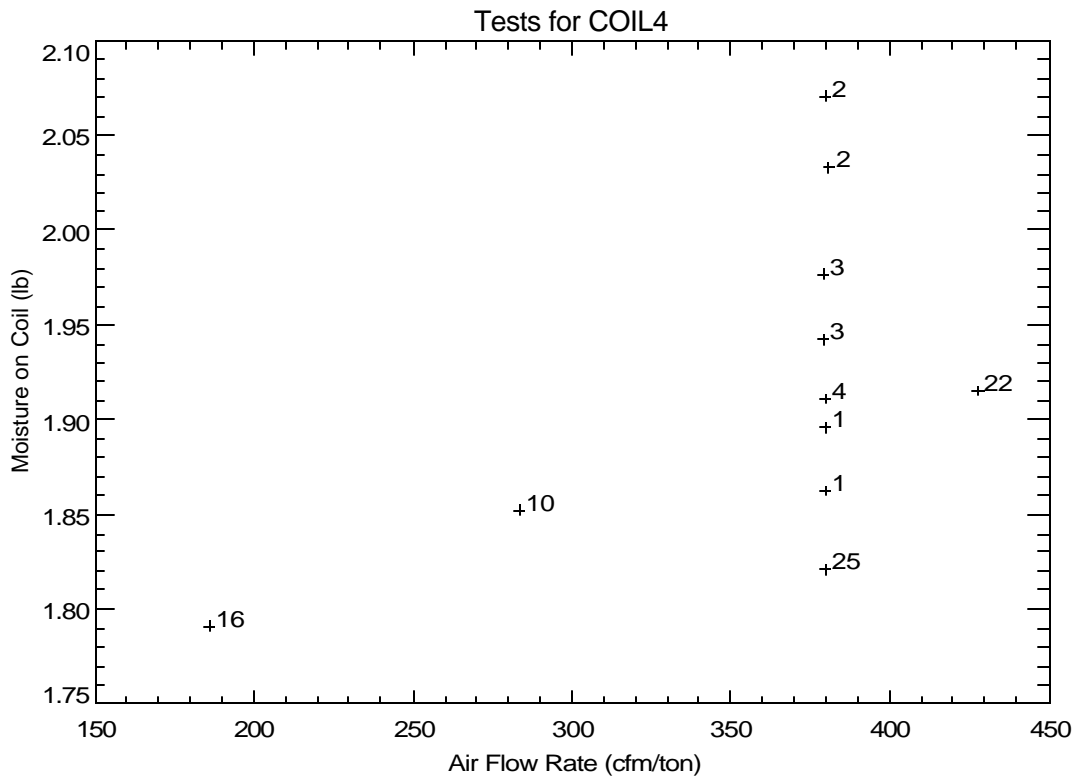
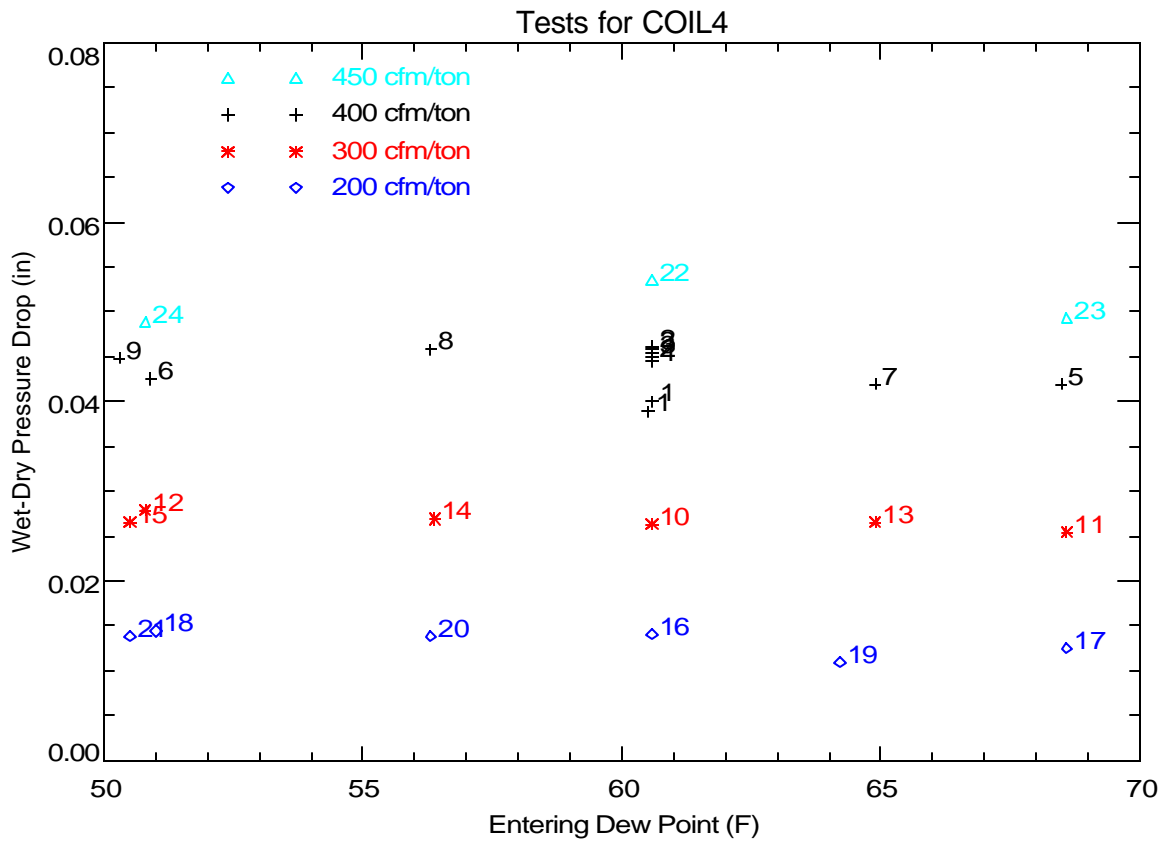


Figure 12. Variation of Retained Moisture with Air Flow at Nominal Entering Conditions of 80°F, 60.4°F dew point

Another way to detect the amount of retained moisture is to measure the static air-side pressure drop across the cooling coil. The difference between the pressure drop across the coil under wet and dry conditions should provide an indication of the amount of retained moisture (the wet coil pressure drop is measured at steady-state conditions while the dry coil pressure drop is taken as the average pressure drop during the last part of the off-cycle). Figure 13 shows the variation of the wet-dry pressure difference with various entering humidity conditions at multiple air flow rates. Comparing the values for each air flow rate generally shows that the pressure drop is not a function of humidity, as had been observed with the other coils. This implies the coil surfaces are consistently at the same temperature and therefore are consistently wetted (and this conflicts with some of the results in Figure 11 above).



**Figure 13. Variation of Wet-Dry Pressure Drop with Entering Conditions and Air Flow Rate**

Figure 14 confirms that the wet-dry pressure drop is a linear function of air flow rate, which implies laminar flow in the wetted cooling coil.

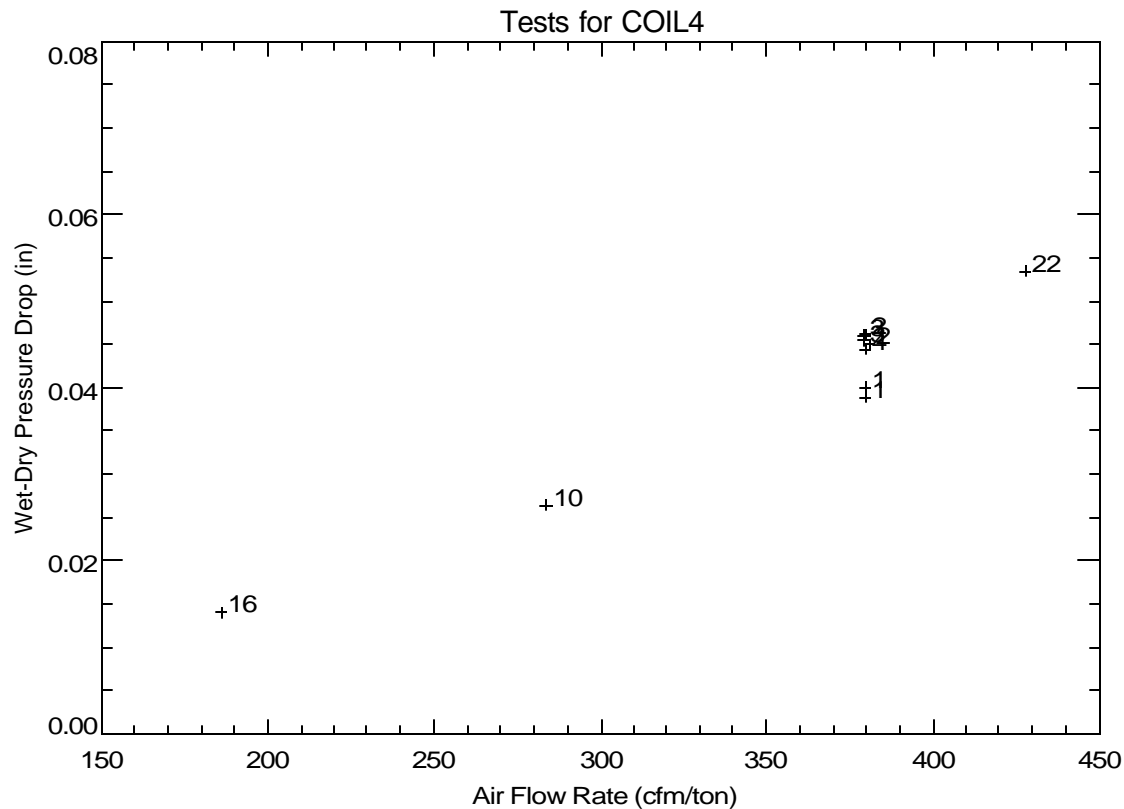


**Figure 14. Trend of Wet-Dry Pressure Drop with Flow at Nominal Entering Conditions of 80°F, 60.4°F dew point**

The series of plots in Figure 15 show the impact of coil suction temperature on performance. The steady-state performance of the system shows the expected trends of lower SHR and greater latent capacity at lower coil temperatures (i.e., lower saturated suction temperatures). On the other hand, the plots for moisture on coil and wet-dry pressure drop show the unexpected trend of less moisture retention at lower coil temperatures. It is not clear what caused this unexpected result.

The graph of fan power versus saturated suction temperature in Figure 15 is not relevant in this case since there was no AHU fan. For this cooling coil, an external booster fan was used to obtain the desired air flow rate for each test.

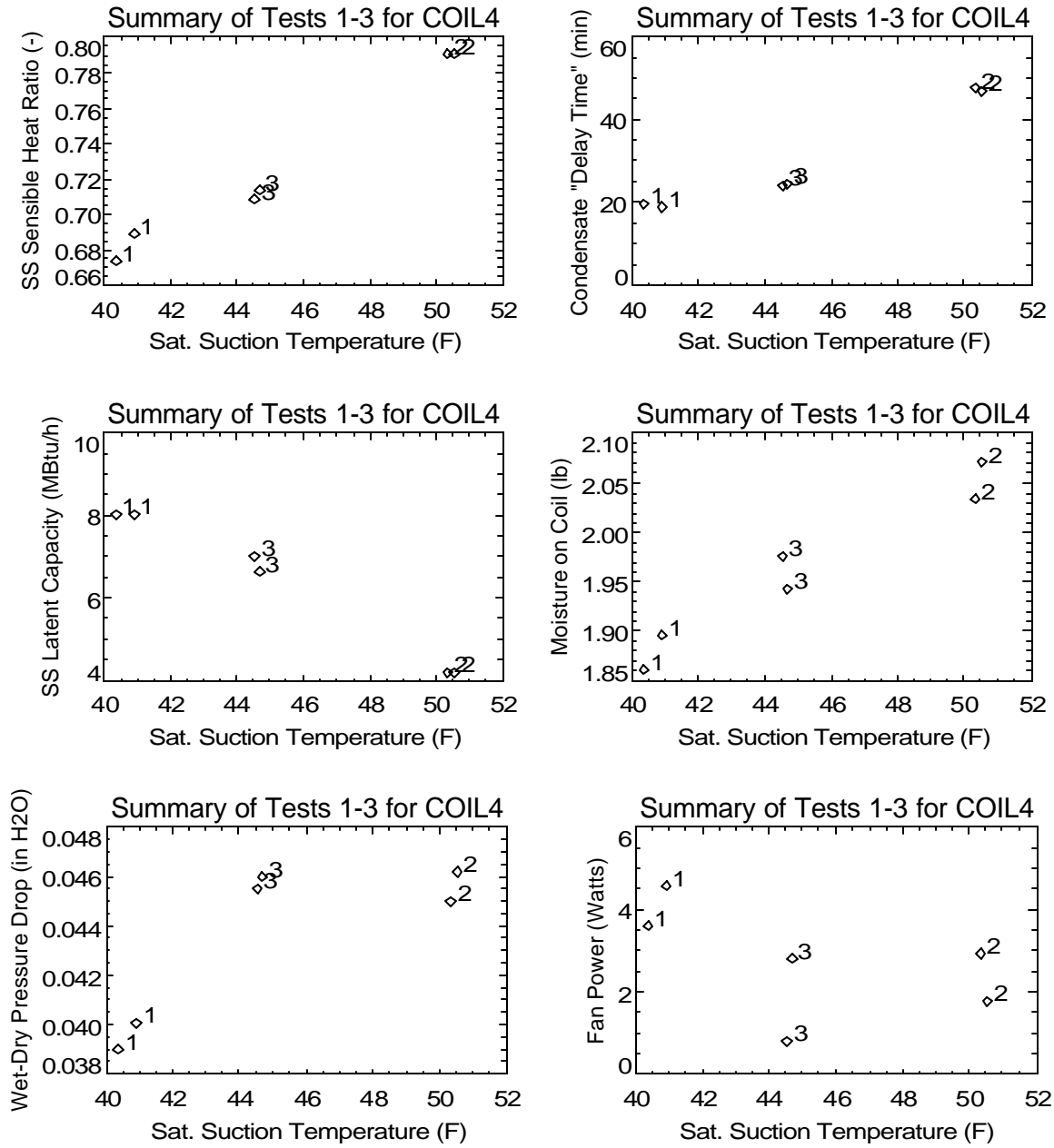


**Figure 15. Trend of Various Parameters with Saturated Suction Temperature**



## Overall Latent Degradation Trends

Several quasi-steady cyclic tests were also completed in the laboratory to quantify the overall part-load degradation of latent capacity. Table 2 lists the cycling test runs. These conditions correspond to a conventional thermostat with a maximum cycle rate of 3 cycles per hour (at 50% runtime).

**Table 2. Cyclic Test Conditions**

CONST FAN <sup>1</sup>	AUTO FAN <sup>2</sup>	Number of Times Test Repeated	ON Time (minutes)	OFF Time (minutes)	Runtime Fraction (-)	Cycle Rate (cycles/h)
Run						
31	41	2	45	45	0.500	0.667
32	42	3	30	6	0.833	1.667
33	43	3	16	7.25	0.688	2.581
34	44	3	10	10	0.500	3.000
35	45	3	7	17.5	0.286	2.449
	46	3	5.5	55	0.091	0.992

Notes: <sup>1</sup>Constant fan tests performed at 80°F db/60.4°F dp inlet air with 400 cfm/ton (runs 31-35) and 300 cfm/ton (runs 71-75) air flow. Tests also conducted at 75°F db/56°F dp (runs 61-65) and 75°F db/64°F dp (runs 51-55) inlet air with 400 cfm/ton air flow.

<sup>2</sup>Auto fan tests performed at 80°F db/60.4°F dp inlet air with 400 cfm/ton air flow.

Figure 16 through Figure 19 show the net impact of part-load unit operation based on cyclic tests completed in the lab. All of these tests are in the constant fan mode (continuous air flow over the cooling coil while the coil cycles on/off), but at various entering air and flow rate conditions:

- Nominal: 80°F & 60.4°F dew pt. with 400 cfm/ton (Figure 16)
- Humid: 75°F & 64°F dew pt. with 400 cfm/ton (Figure 17)
- Dry: 75°F & 56°F dew pt. with 400 cfm/ton (Figure 18)
- Low Flow: 80°F & 60.4°F dew pt. with 300 cfm/ton (Figure 19)

The measured data generally compare well to the model from Henderson and Rengarajan (1996) using the model parameters shown on each plot. These parameters were always taken from the 2<sup>nd</sup> occurrence of the first test in each sequence (i.e., Tests #31, 51, 61 and 71), which were completed as part of the suite of cycling tests listed in Table 2 for the constant fan mode. The latent time constant ( $\tau$ ) of 20 seconds was selected based on qualitative observations of the coil's response time. The solid black line corresponds to the linear off-cycle evaporation model. The black dotted line assumes an off-cycle evaporation trend that corresponds to an exponential decay. The purple line is the new part load LHR model that uses the more realistic evaporation model from Stabat et al. (2001) and also allows for variable amounts of moisture on the coil at the end of the on cycle. The parameters NTU and  $t_p$  were determined from the specific measured data from each test sequence (the purple solid line) as well as the average NTU and  $t_p$  from all the data (the purple dotted line), including Figure 9 above. The parameter  $t_p$  is defined in the improved model development section of this report. This was the first coil where the new model (purple line) was observed to be closer to the measured data than the original LHR model (e.g., Figure 19).

The measured data corresponding to the 2<sup>nd</sup> and 3<sup>rd</sup> repetition (cycle) of each test showed the best agreement with the models, since quasi-steady conditions had been achieved.

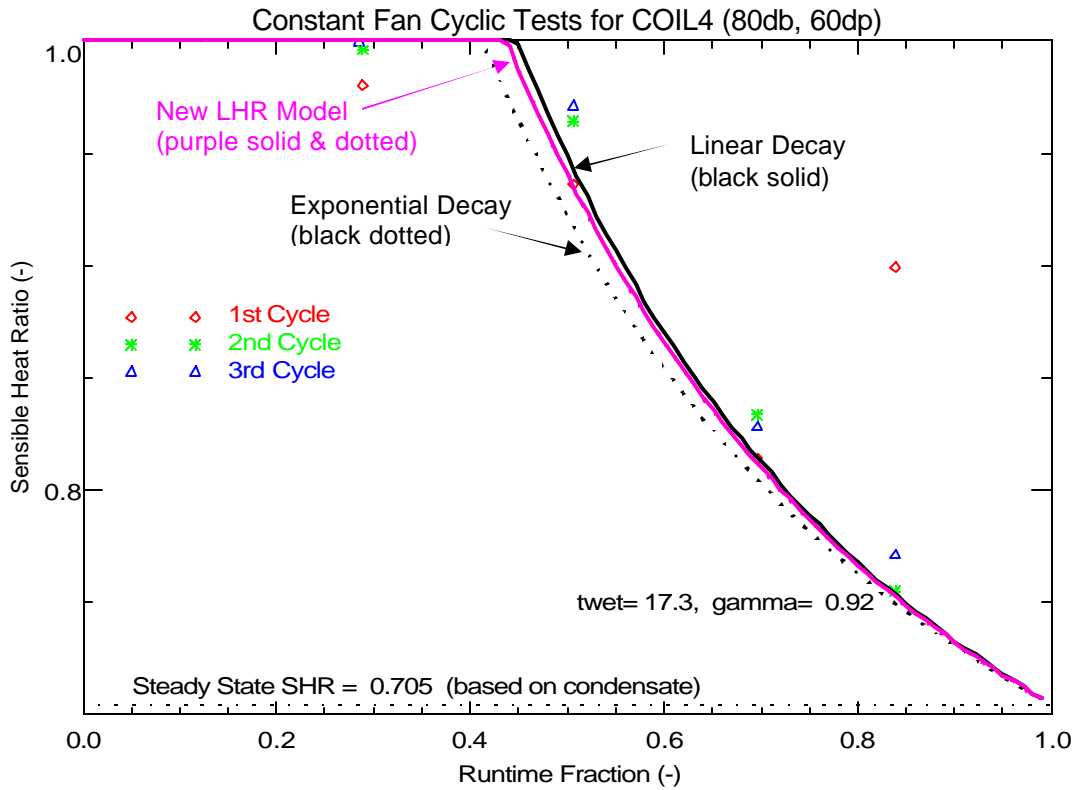


Figure 16. Comparing Measured Latent Degradation to the LHR Models: Nom. Conditions (80°F / 60.4°Fdp)

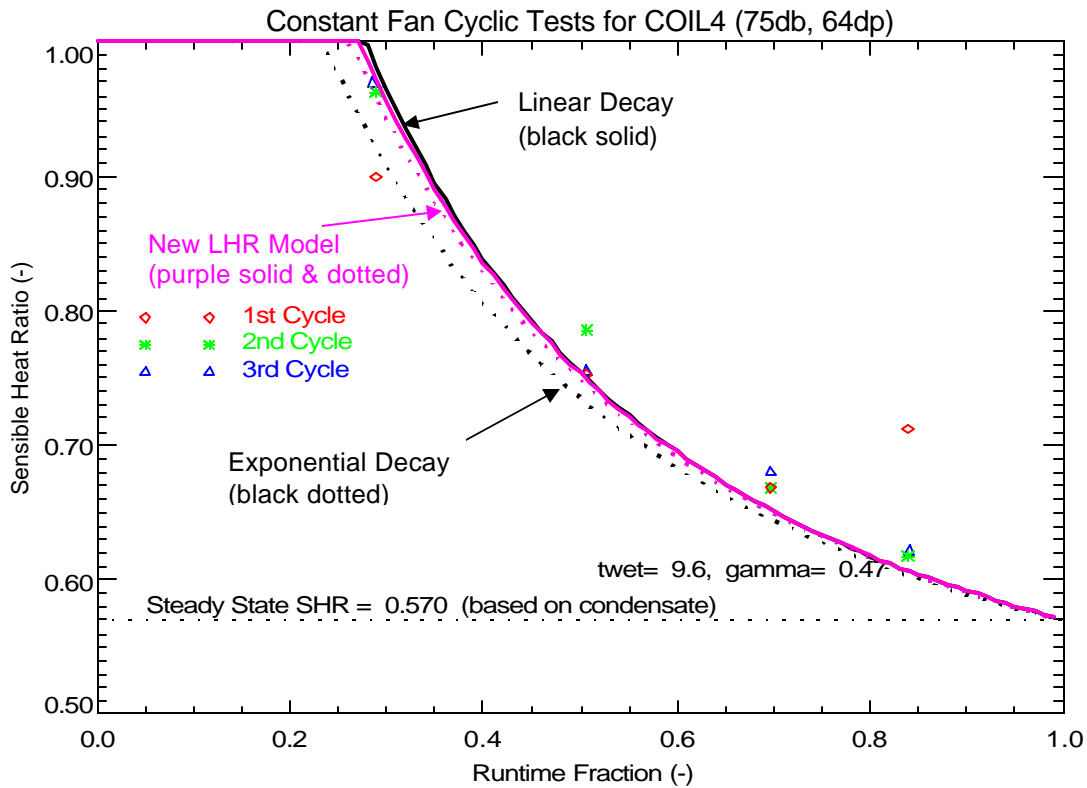


Figure 17. Comparing Measured Latent Degradation to the LHR Models: 75°F / 64°Fdp

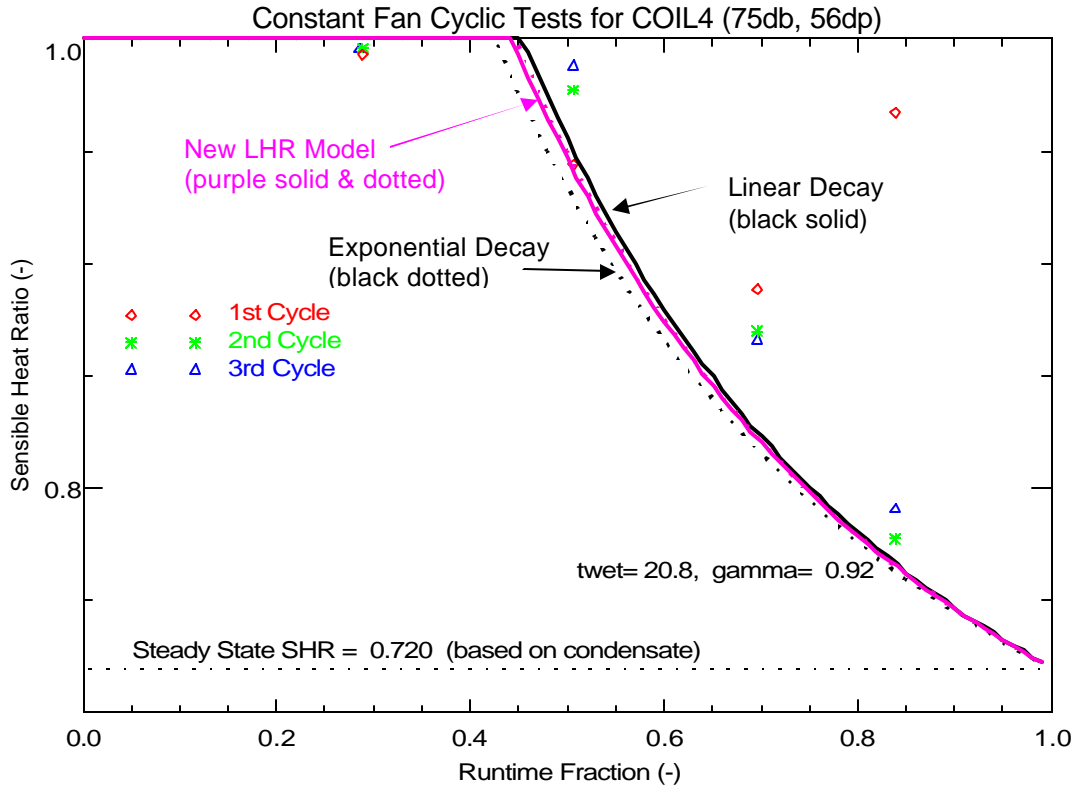


Figure 18. Comparing Measured Latent Degradation to the LHR Models: 75°F / 56°Fdp

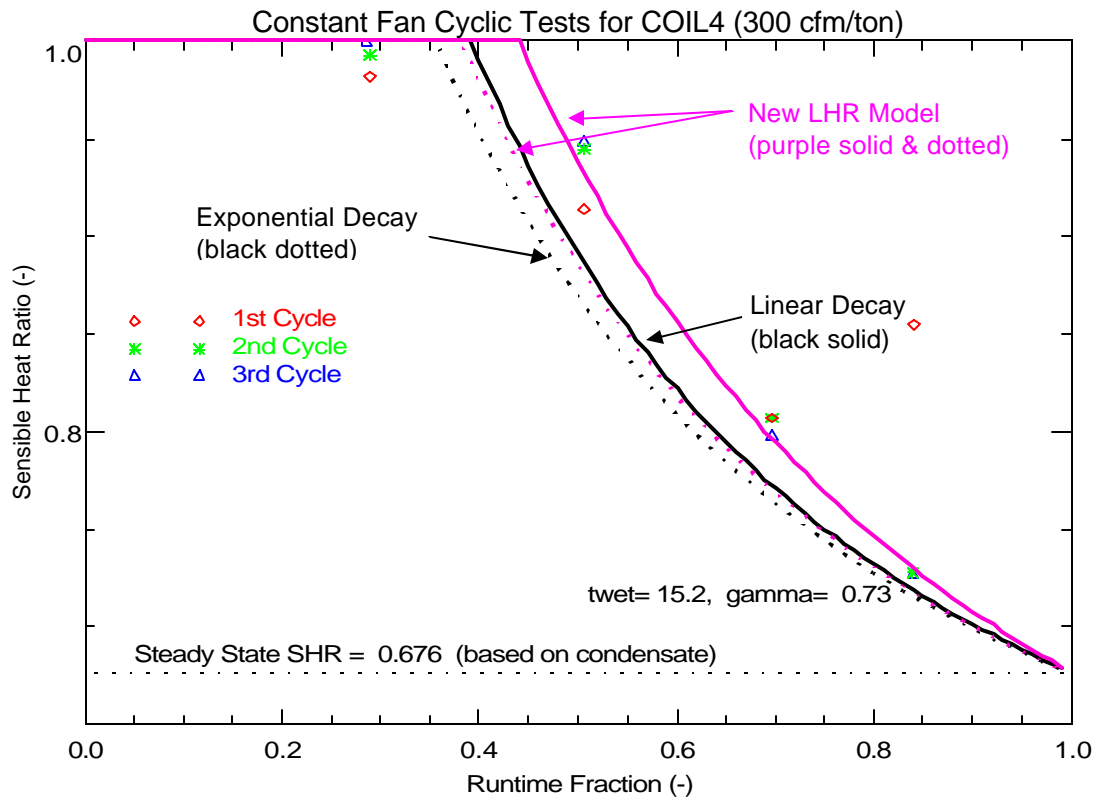
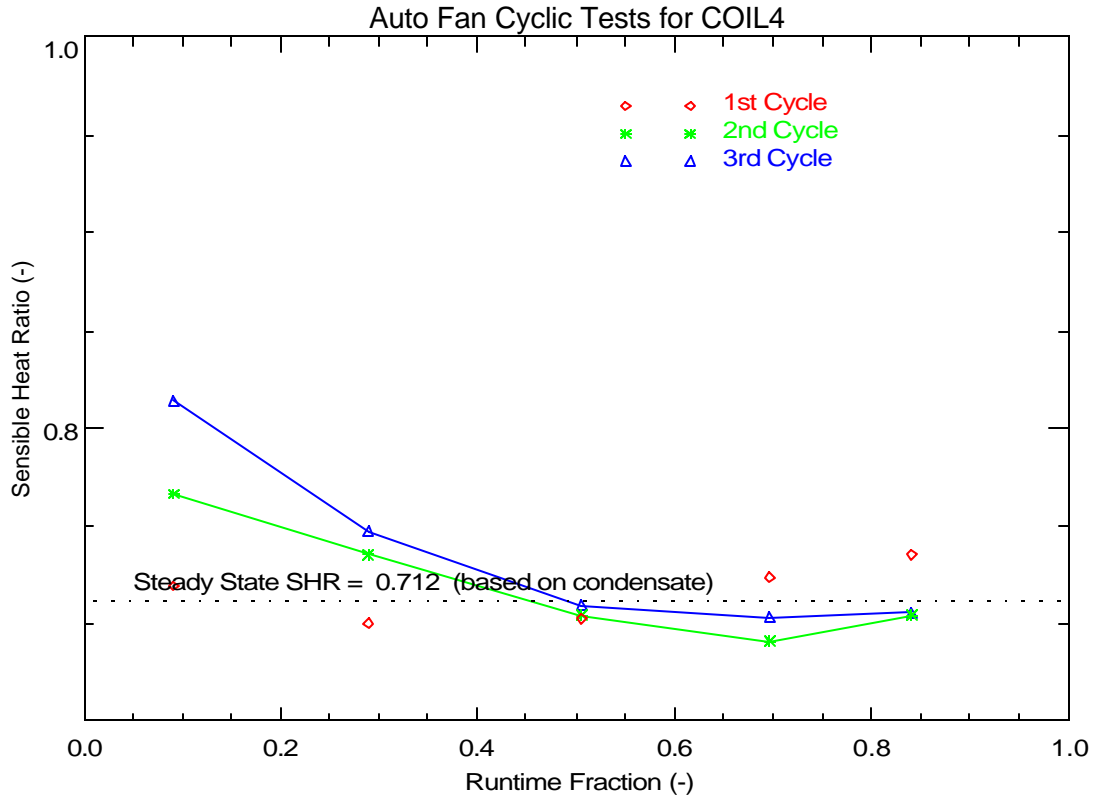


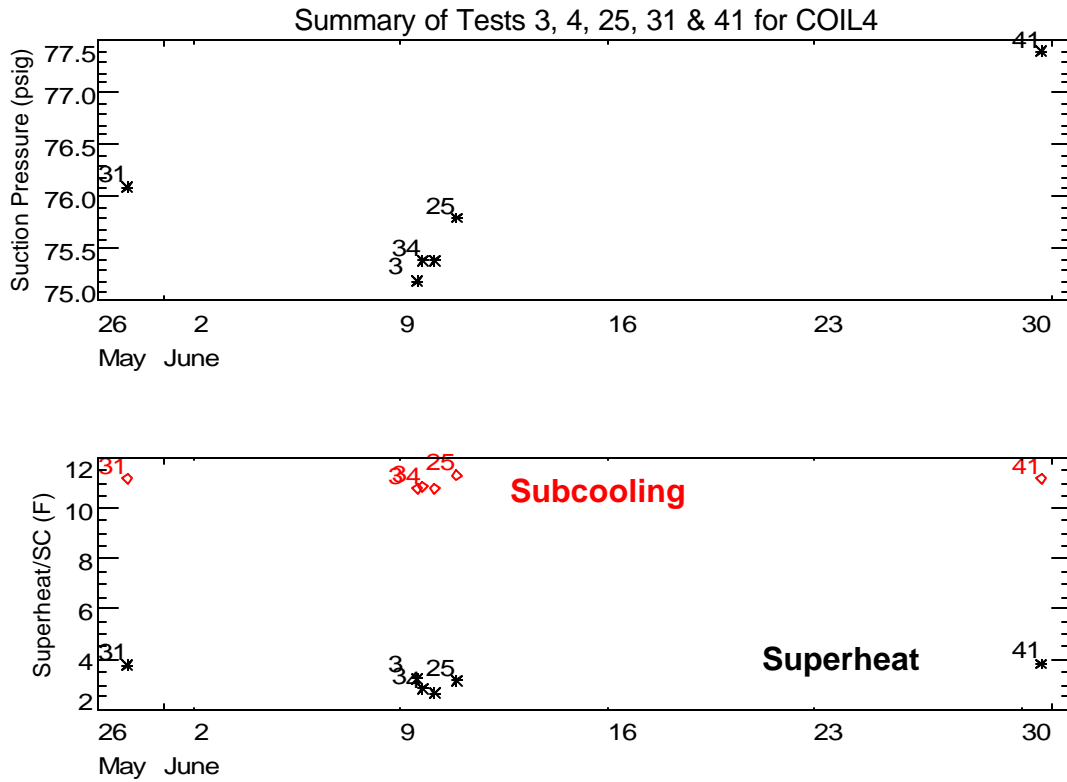
Figure 19. Comparing Measured Latent Degradation to the LHR Models: 300 cfm/ton, 80°F / 60.4°Fdp

Figure 20 shows some latent degradation can be detected in the AUTO fan mode (i.e., the supply air flow across the cooling coil starts and stops with compressor operation) for Coil 4 (similar degradation was seen for Coil 1 and Coil 3). The 2<sup>nd</sup> and 3<sup>rd</sup> repetition (cycle) show relatively good agreement with each other.



**Figure 20. Measured AUTO Fan Latent Degradation**

The tests were completed over a period of 5 weeks. Figure 21 shows little evidence of a change in suction pressure, subcooling or superheat over the test period. This implies that no significant loss of refrigerant charge occurred over the test period.



**Figure 21. Long-Term Variation in Suction Pressure, Superheat and Subcooling**

**References**

Henderson, H., and K. Rengarajan. 1996. A model to predict the latent capacity of air conditioners and heat pumps at part-load conditions with constant fan operation. *ASHRAE Transactions* 102(1): 266-274.

Stabat, P., Marchio, D. and M. Orphelin. 2001. Pre-Design and Design Tools for Evaporative Cooling. *ASHRAE Transactions* 107 (1): 501-510.

**COIL 4 Test Runs**

File Name	Date	Start Time	Sequence No.	Run/Test No.	Inlet DB (F)	Inlet DewPt (F)	Air Flow (cfm)	Test Duration (min)	Comp Runtime (min)
coil4_test_1.out	6/17/2003	12:35:40	1	1	80	60.6	759.9	270.3	180.6
coil4_test_1.out	6/17/2003	17:06:15	2	1	80	60.6	759.5	270.4	180.6
coil4_test_1.out	6/17/2003	21:36:52	3	1	80	60.5	759.4	270.3	180.5
coil4_test_2a.out	6/23/2003	17:40:24	1	2	80	60.6	759.9	269.8	180.1
coil4_test_2a.out	6/23/2003	22:10:29	2	2	80.1	60.6	759.5	269.9	180.1
coil4_test_2a.out	6/24/2003	2:40:38	3	2	80	60.6	761.6	269.9	180.1
coil4_test_3c.out	6/9/2003	9:03:14	1	3	80.1	60.6	757.4	269.5	179.8
coil4_test_3c.out	6/9/2003	13:33:02	2	3	80	60.6	758.7	269.8	180
coil4_test_3c.out	6/9/2003	18:03:06	3	3	80	60.6	758.6	270.2	180.1
coil4_Test_4c_10c_16c_22c_25c.out	6/9/2003	22:33:16	1	4	80.1	60.6	759.7	269.9	180.2
coil4_Test_4c_10c_16c_22c_25c.out	6/10/2003	3:03:27	2	4	80	60.6	759.3	269.8	180
coil4_Test_4c_10c_16c_22c_25c.out	6/10/2003	7:33:31	3	10	80	60.6	567.5	269.8	180
coil4_Test_4c_10c_16c_22c_25c.out	6/10/2003	12:03:33	4	16	80	60.6	372.3	279.8	180.1
coil4_Test_4c_10c_16c_22c_25c.out	6/10/2003	16:43:37	5	22	80	60.6	855.6	269.8	180.1
coil4_Test_4c_10c_16c_22c_25c.out	6/10/2003	21:13:42	6	25	80	60.6	759.4	280.1	180.1
coil4_Test_5c_11c_17c_23c.out	6/11/2003	1:53:50	1	5	80	68.3	761.4	279.9	180.1
coil4_Test_5c_11c_17c_23c.out	6/11/2003	6:33:59	2	5	80	68.5	762	280	180.3
coil4_Test_5c_11c_17c_23c.out	6/11/2003	11:14:18	3	11	80	68.6	568.7	300	180.2
coil4_Test_5c_11c_17c_23c.out	6/11/2003	16:14:33	4	17	80	68.6	374	279.9	180.1
coil4_Test_5c_11c_17c_23c.out	6/11/2003	20:54:42	5	23	80	68.6	857.2	280.3	180.2
coil4_Test_6c_12c_18c_24c.out	6/12/2003	1:34:57	1	6	80	53.1	758.8	270.4	180.6
coil4_Test_6c_12c_18c_24c.out	6/12/2003	6:05:35	2	6	80	50.9	762.2	269.9	180.1
coil4_Test_6c_12c_18c_24c.out	6/12/2003	10:35:43	3	12	80	50.8	569.5	269.8	180.1
coil4_Test_6c_12c_18c_24c.out	6/12/2003	15:05:48	4	18	80	51	374	269.8	180.1
coil4_Test_6c_12c_18c_24c.out	6/12/2003	19:35:53	5	24	80	50.8	858.7	270.1	180.1
coil4_Test_7c_13c_19c.out	6/13/2003	0:05:59	1	7	75.2	64.7	760.3	269.9	180.1
coil4_Test_7c_13c_19c.out	6/13/2003	4:36:08	2	7	75	64.9	759.8	269.8	180.1
coil4_Test_7c_13c_19c.out	6/13/2003	9:06:13	3	13	75	64.9	568.9	299.9	180.1
coil4_Test_7c_13c_19c.out	6/13/2003	14:06:20	4	19	75	64.2	374.6	300.3	180.2
coil4_Test_8c_14c_20c.out	6/13/2003	19:06:35	1	8	75	56.4	758	269.8	180
coil4_Test_8c_14c_20c.out	6/13/2003	23:36:38	2	8	75	56.3	758.7	269.8	180.1
coil4_Test_8c_14c_20c.out	6/14/2003	4:06:42	3	14	75	56.4	567.9	270	180.2
coil4_Test_8c_14c_20c.out	6/14/2003	8:36:57	4	20	75	56.3	374.7	270.1	180.1
coil4_Test_9c_15c_21c.out	6/14/2003	13:07:03	1	9	75	50.5	759.8	269.8	180.1
coil4_Test_9c_15c_21c.out	6/14/2003	17:37:08	2	9	75	50.3	759.2	269.9	180.1
coil4_Test_9c_15c_21c.out	6/14/2003	22:07:15	3	15	75	50.5	569.3	269.9	180.1
coil4_Test_9c_15c_21c.out	6/15/2003	2:37:22	4	21	75	50.5	374.4	269.8	180.1
coil4_Test_cycling_constantb.out	5/30/2003	15:10:15	1	31	80	60.6	721.9	180	120.2
coil4_Test_cycling_constantb.out	5/30/2003	18:10:29	2	31	80	60.6	721.4	240.2	180.4
coil4_Test_cycling_constantb.out	5/30/2003	22:10:58	3	32	80	60.6	733.4	35.8	30.1
coil4_Test_cycling_constantb.out	5/30/2003	22:47:05	4	32	80	60.6	727.8	35.8	30
coil4_Test_cycling_constantb.out	5/30/2003	23:23:09	5	32	80	60.5	728.1	35.9	30.1
coil4_Test_cycling_constantb.out	5/30/2003	23:59:17	6	33	79.2	61.1	725.1	23.1	16.1
coil4_Test_cycling_constantb.out	5/31/2003	0:22:38	7	33	80	60.5	730.9	23.1	16.1
coil4_Test_cycling_constantb.out	5/31/2003	0:45:59	8	33	80	60.6	729.6	23.1	16
coil4_Test_cycling_constantb.out	5/31/2003	1:09:19	9	34	80	60.6	731	19.8	10
coil4_Test_cycling_constantb.out	5/31/2003	1:29:23	10	34	80	60.5	732	19.8	10
coil4_Test_cycling_constantb.out	5/31/2003	1:49:27	11	34	80	60.6	733.4	19.8	10
coil4_Test_cycling_constantb.out	5/31/2003	2:09:31	12	35	80	60.4	733.8	24.3	7
coil4_Test_cycling_constantb.out	5/31/2003	2:34:05	13	35	79.9	60.6	737.6	24.3	7
coil4_Test_cycling_constantb.out	5/31/2003	2:58:38	14	35	80	60.5	737.1	24.6	7
coil4_Test_cycling_constant_75_56b.out	6/1/2003	3:49:41	1	61	75	56.4	727.4	180.2	120.4
coil4_Test_cycling_constant_75_56b.out	6/1/2003	6:50:12	2	61	75	56.2	729.1	240.1	180.4
coil4_Test_cycling_constant_75_56b.out	6/1/2003	10:50:37	3	62	75	56.3	730.8	35.8	30.1
coil4_Test_cycling_constant_75_56b.out	6/1/2003	11:26:43	4	62	75	56.4	721.8	35.8	30.1
coil4_Test_cycling_constant_75_56b.out	6/1/2003	12:02:49	5	62	75	56.4	719.3	35.8	30
coil4_Test_cycling_constant_75_56b.out	6/1/2003	12:38:54	6	63	75	56.3	721.4	23.1	16
coil4_Test_cycling_constant_75_56b.out	6/1/2003	13:02:14	7	63	75	56.4	720.1	23.1	16
coil4_Test_cycling_constant_75_56b.out	6/1/2003	13:25:34	8	63	75	56.4	719.6	23.1	16
coil4_Test_cycling_constant_75_56b.out	6/1/2003	13:48:54	9	64	74.9	56.5	720	19.8	10
coil4_Test_cycling_constant_75_56b.out	6/1/2003	14:08:58	10	64	75	56.3	719.7	19.8	10
coil4_Test_cycling_constant_75_56b.out	6/1/2003	14:29:02	11	64	75	56.3	720.1	19.8	10
coil4_Test_cycling_constant_75_56b.out	6/1/2003	14:49:06	12	65	75	56.1	721.1	24.3	7
coil4_Test_cycling_constant_75_56b.out	6/1/2003	15:13:39	13	65	75.1	56.4	723.7	24.3	7
coil4_Test_cycling_constant_75_56b.out	6/1/2003	15:38:12	14	65	75.1	56.5	724.5	24.6	7

**COIL 4 Test Runs (cont)**

File Name	Date	Start Time	Sequence No.	Run/Test No.	Inlet DB (F)	Inlet DewPt (F)	Air Flow (cfm)	Test Duration (min)	Comp Runtime (min)
coil4_Test_cycling_constant_75_64b.out	5/31/2003	15:36:28	1	51	75.2	64.1	716.3	180	120.2
coil4_Test_cycling_constant_75_64b.out	5/31/2003	18:36:46	2	51	75	64.2	721.7	240.3	180.5
coil4_Test_cycling_constant_75_64b.out	5/31/2003	22:37:18	3	52	75.1	64.2	730.4	35.9	30.1
coil4_Test_cycling_constant_75_64b.out	5/31/2003	23:13:26	4	52	75.1	64.2	726	35.8	30.1
coil4_Test_cycling_constant_75_64b.out	5/31/2003	23:49:33	5	52	75.5	64.3	727	35.9	30.1
coil4_Test_cycling_constant_75_64b.out	6/1/2003	0:25:42	6	53	75.1	64.2	727.8	23.1	16.1
coil4_Test_cycling_constant_75_64b.out	6/1/2003	0:49:03	7	53	75.1	64.3	727.6	23.1	16
coil4_Test_cycling_constant_75_64b.out	6/1/2003	1:12:24	8	53	75.1	64.1	727.3	23.1	16.1
coil4_Test_cycling_constant_75_64b.out	6/1/2003	1:35:45	9	54	75.1	64.2	728.5	19.8	10
coil4_Test_cycling_constant_75_64b.out	6/1/2003	1:55:49	10	54	75.1	64	732.5	19.8	10.1
coil4_Test_cycling_constant_75_64b.out	6/1/2003	2:15:54	11	54	75.2	64.3	731.8	19.8	10.1
coil4_Test_cycling_constant_75_64b.out	6/1/2003	2:35:59	12	55	75.3	64.2	735.9	24.3	7
coil4_Test_cycling_constant_75_64b.out	6/1/2003	3:00:33	13	55	75.3	64.4	735.3	24.3	7
coil4_Test_cycling_constant_75_64b.out	6/1/2003	3:25:07	14	55	75.3	63.9	732.3	24.6	7
coil4_Test_cycling_constant_300b.out	5/31/2003	3:23:12	1	71	80	60.6	555.6	180.2	120.4
coil4_Test_cycling_constant_300b.out	5/31/2003	6:23:41	2	71	80	60.6	556	240.4	180.6
coil4_Test_cycling_constant_300b.out	5/31/2003	10:24:19	3	72	80	60.5	556.3	35.8	30.1
coil4_Test_cycling_constant_300b.out	5/31/2003	11:00:27	4	72	80	60.6	552.5	35.9	30.1
coil4_Test_cycling_constant_300b.out	5/31/2003	11:36:35	5	72	80	60.6	551.1	35.8	30.1
coil4_Test_cycling_constant_300b.out	5/31/2003	12:12:42	6	73	80	60.6	549.4	23	16
coil4_Test_cycling_constant_300b.out	5/31/2003	12:36:02	7	73	80	60.6	551.5	23	16
coil4_Test_cycling_constant_300b.out	5/31/2003	12:59:21	8	73	80	60.6	549.7	23	16
coil4_Test_cycling_constant_300b.out	5/31/2003	13:22:40	9	74	80	60.7	551	19.8	10
coil4_Test_cycling_constant_300b.out	5/31/2003	13:42:44	10	74	80	60.6	550	19.8	10
coil4_Test_cycling_constant_300b.out	5/31/2003	14:02:47	11	74	80	60.5	549.4	19.8	10
coil4_Test_cycling_constant_300b.out	5/31/2003	14:22:49	12	75	80.2	60.5	549.4	24.3	7
coil4_Test_cycling_constant_300b.out	5/31/2003	14:47:22	13	75	80.1	60.6	550.5	24.3	7
coil4_Test_cycling_constant_300b.out	5/31/2003	15:11:55	14	75	80.1	60.5	550.1	24.5	7
coil4_Test_cycling_autoc.out	6/30/2003	13:27:12	1	41	80.8	61.4	758.7	171.9	111.2
coil4_Test_cycling_autoc.out	6/30/2003	16:19:24	2	41	80.7	61.4	756.8	275.2	183.9
coil4_Test_cycling_autoc.out	6/30/2003	20:54:50	3	42	80.7	61.4	761.3	36.5	30.6
coil4_Test_cycling_autoc.out	6/30/2003	21:31:36	4	42	80.7	61.4	758.8	36.5	30.7
coil4_Test_cycling_autoc.out	6/30/2003	22:08:23	5	42	80.7	61.3	759.4	36.5	30.7
coil4_Test_cycling_autoc.out	6/30/2003	22:45:11	6	43	80.7	61.5	759.6	23.5	16.4
coil4_Test_cycling_autoc.out	6/30/2003	23:08:55	7	43	80.6	61.7	758.3	23.5	16.4
coil4_Test_cycling_autoc.out	6/30/2003	23:32:41	8	43	80.6	61.5	758.5	23.5	16.4
coil4_Test_cycling_autoc.out	6/30/2003	23:56:26	9	44	79.9	61.3	757.3	20.1	10.2
coil4_Test_cycling_autoc.out	7/1/2003	0:16:51	10	44	80.3	61.7	759.5	20.1	10.2
coil4_Test_cycling_autoc.out	7/1/2003	0:37:16	11	44	80.6	61.7	762.4	20.1	10.2
coil4_Test_cycling_autoc.out	7/1/2003	0:57:41	12	45	80.5	62.1	761.6	24.7	7.2
coil4_Test_cycling_autoc.out	7/1/2003	1:22:39	13	45	80.6	61.8	761.4	24.7	7.2
coil4_Test_cycling_autoc.out	7/1/2003	1:47:37	14	45	80.6	61.7	757.7	24.7	7.2
coil4_Test_cycling_autoc.out	7/1/2003	2:12:35	15	46	80.5	62.1	760.6	61.3	5.6
coil4_Test_cycling_autoc.out	7/1/2003	3:14:09	16	46	80.6	61.9	762.4	61.3	5.6
coil4_Test_cycling_autoc.out	7/1/2003	4:15:43	17	46	80.5	61.8	759.1	61.8	5.6

## **APPENDIX H5**

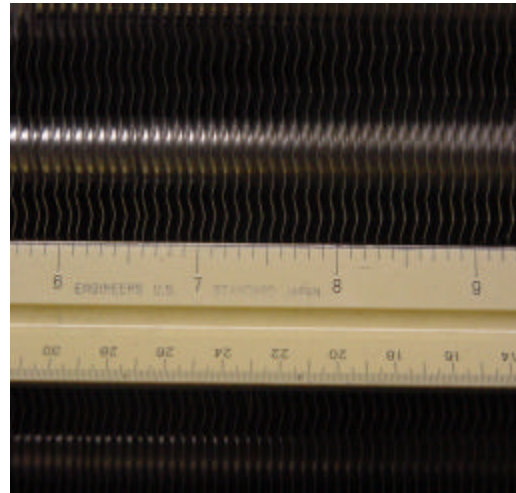
### **Summary of Laboratory Data for Coil 5**



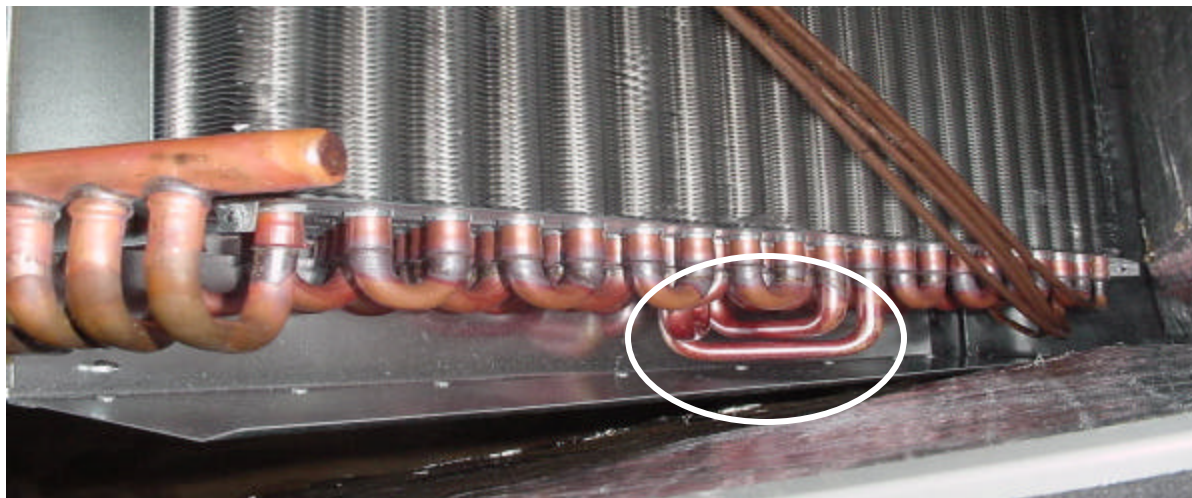
**Summary of Laboratory Data for Coil 5  
November 2005**



Slanted coil arrangement



12 fpi, wavy fin



Cross-flow refrigerant circuit

Manufacturer & Model number:	Trane, TVF025A140A1
Nominal size:	2 tons
Baseline Size and Airflow (Test 4):	2.3 tons / 915 cfm
Coil type:	slanted coil, 4 rows, 12 fpi
Coil dimensions:	2.26 ft <sup>2</sup> face area (manu. data sheet says 2.22 ft <sup>2</sup> ) (1.7 ft <sup>2</sup> open area, excluding filter flange)
	16 1/4 in x 20 in
Coil thickness:	3 in
Tube diameter:	3/8 in OD copper
Tube spacing:	1 in within row (vert), 3/4 in row-to-row (horiz)
Expansion device	fixed orifice, 4 refrig. circuits
Unit supply fan:	off
Compressor power:	direct

**Table 1. Summary of Steady State Test Conditions Corresponding or Each Run or Test**

	<i>Entering Coil Conditions</i>					
	<i>80/67°F 60°F dp</i>	<i>80/72°F 68°F dp</i>	<i>80/62°F 50°F dp</i>	<i>75/68°F 64°F dp</i>	<i>75/63°F 56°F dp</i>	<i>75/58°F 45°F dp</i>
400 cfm/ton	#4 (or 3)	#5	#6	#7	#8	#9
300 cfm/ton	#10	#11	#12	#13	#14	#15
200 cfm/ton	#16	#17	#18	#19	#20	#21
450 cfm/ton	#22	#23	#24			
400-200 cfm/ton (ON & OFF)	#25					
Low suction (40°F)	#1					
High suction (49°F)	#2					

Notes: Tests 4-25 all at nominal suction of 45°F (set at nominal conditions of test #3/4). A fixed orifice expansion device was used, with nominal superheat of 20-22°F. The refrigerant charge established during Test 4 was not changed for the remaining tests. The Table 1 test points denote the target testing conditions. Drier test conditions with dew points below 50°F (such as Tests #9, #15, and #21) could not be achieved. In these cases, entering conditions were typically held near 50°F dp. For each test, the compressor is ON for 60-120 minutes and then the compressor is OFF for at least 60 minutes. The booster fan runs continuously for all tests (when the compressor is both ON and OFF).

**Steady State Performance**

The nominal performance characteristics for this coil (based on steady-state conditions from Run #4 below) are:

Total Capacity:	27.8 MBtu/h (2.3 tons)
Sensible Capacity:	18.6 MBtu/h
Latent Capacity (condensate):	9.2 MBtu/h
Sensible Heat Ratio:	0.67

Latent capacity can be calculated two ways: 1) using dew point readings and air flow, and 2) the condensate flow rate. Figure 1 compares the latent capacity calculated these two ways. The number of each data point corresponds to the test number listed in Table 1. In general, the condensate and psychrometric readings agree for this coil (the tipping bucket was replaced for this test).

Figure 2 shows the trend of steady-state sensible heat ratio (SHR) with relative humidity and airflow rate. The cooling capacities used to calculate SHR in Figure 2 are based on airflow measurements and the psychrometric conditions entering and leaving the cooling coil. This performance map is typical for a cooling coil (i.e., SHR is mostly a function of the entering relative humidity, with some dependence on the air flow rate).

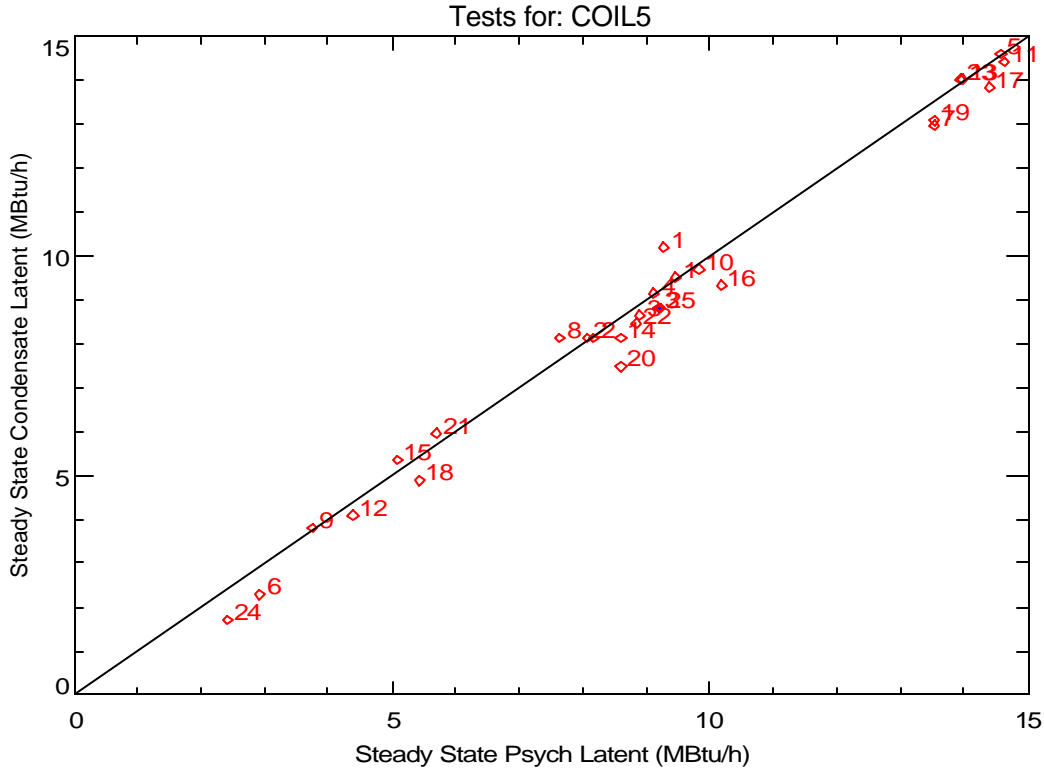


**Figure 1. Comparing Steady-State Latent Capacity Calculated From Psychrometric State Points and Condensate Removal Rates**

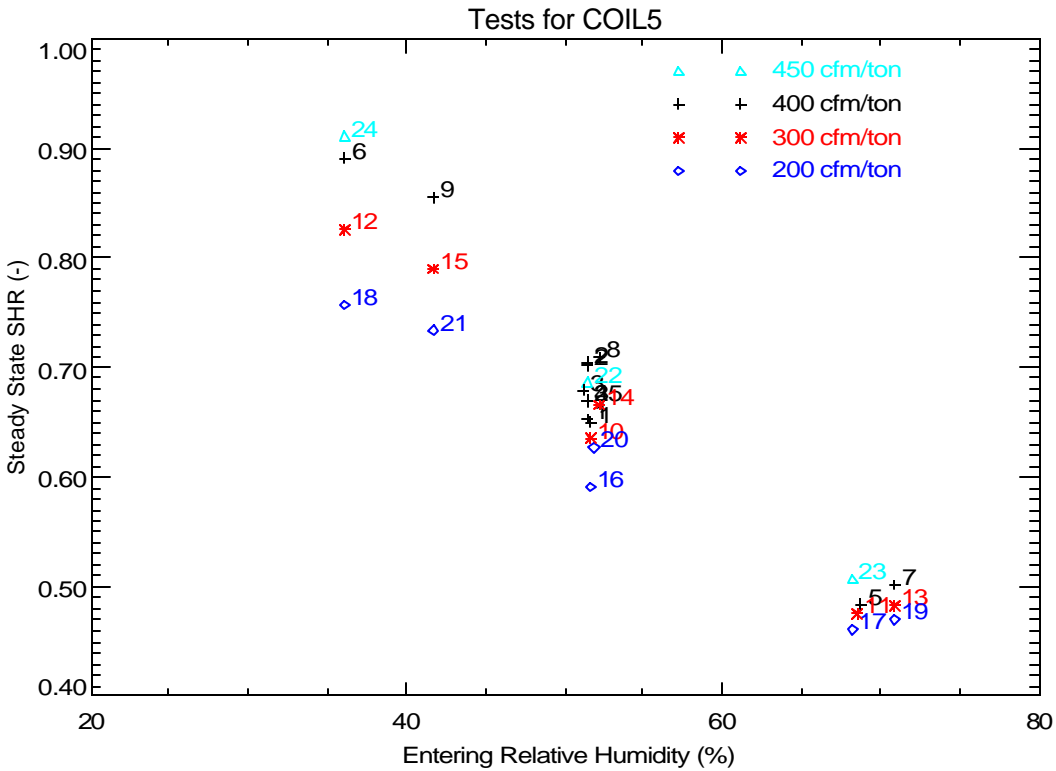


**Figure 2. Variation of Steady State SHR with Entering Humidity and Nominal Air Flow**

## **Typical Transient Performance**

Figure 3 shows the typical transient performance of the cooling coil at nominal conditions (i.e., for Cycle 2 of Run #4). The compressor runs for 120 minutes and is off for 90 minutes. The booster fan remains on during the entire test (separate external fan used to maintain the desired air flow rate across the cooling coil). A portion of the moisture removed by the coil during the compressor on cycle evaporates back into the air stream during the off cycle. During the off cycle the coil acts as an evaporative cooler, so the sensible capacity is nearly equal to the absolute value of the latent capacity (i.e., the sum of latent and sensible is zero).

If we integrate the off cycle sensible capacity (after allowing for a 1-minute off-cycle delay to account for refrigerant movement and other transient effects), we can determine the energy associated with the moisture retained on the coil. To minimize the integration of any measurement errors, the off-cycle integration stops at the time labeled “Integration Pt.” on the plot. This point corresponds to the time when the temperature and dew point differences across the coil have first reached the terminal values (i.e., the averages from the end of the off-cycle). In this case the integration indicates that the sensible cooling is equivalent to 1.37 lbs of moisture being retained on the coil. The integrated latent capacity – which is harder to measure precisely – equals 1.12 lbs.

The value “ $t_{wet}$ ” from Henderson and Rengarajan (1996) can then be calculated by dividing the retained moisture mass (expressed as Btu; mass x 1060 Btu/lb) and the steady state psychrometric latent capacity ( $Q_L = 9.1$  MBtu/h). Figure 3 shows that the values of  $t_{wet}$  based on integrated sensible and latent off-cycle capacity are 9.6 and 7.8 minutes respectively. These values of  $t_{wet}$  are similar to the measured delay of 11.5 minutes for the first condensate pulse to fall from the drain pan. The value of  $\gamma$  (0.93), which is the initial off-cycle moisture evaporation rate divided by the steady-state psychrometric latent capacity, uses the off-cycle moisture evaporation rate (8.5 MBtu/h) once the transition point was been detected. For this coil, we detect the transition by determining where the change in off-cycle sensible capacity between each 15-second interval first drops below 3% of the steady-state on cycle sensible capacity ( $Q_S$ ). At this transition point where  $\gamma$  is determined, it is assumed that all coil heat and mass transfer with the air stream is adiabatic (the refrigerant flow could not be used as the indicator for this point for this coil). In this case it took 1.55 minutes for the change in off-cycle sensible capacity to drop below 3% of the steady-state on cycle value  $Q_S$ .

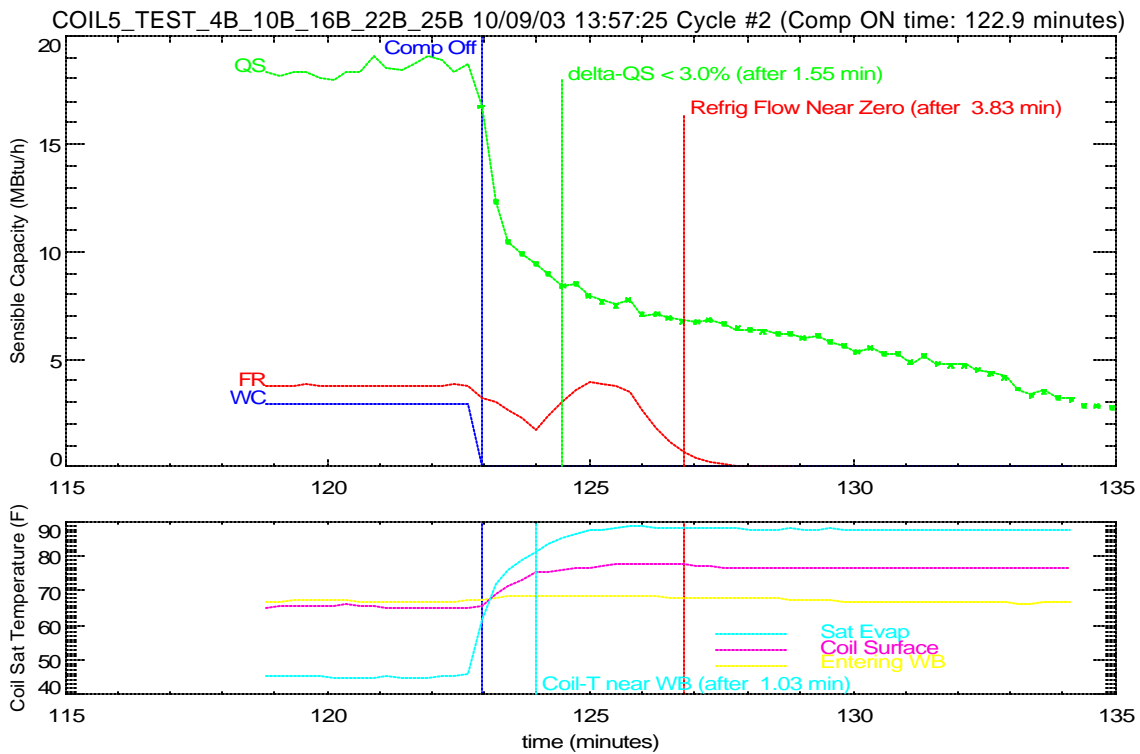
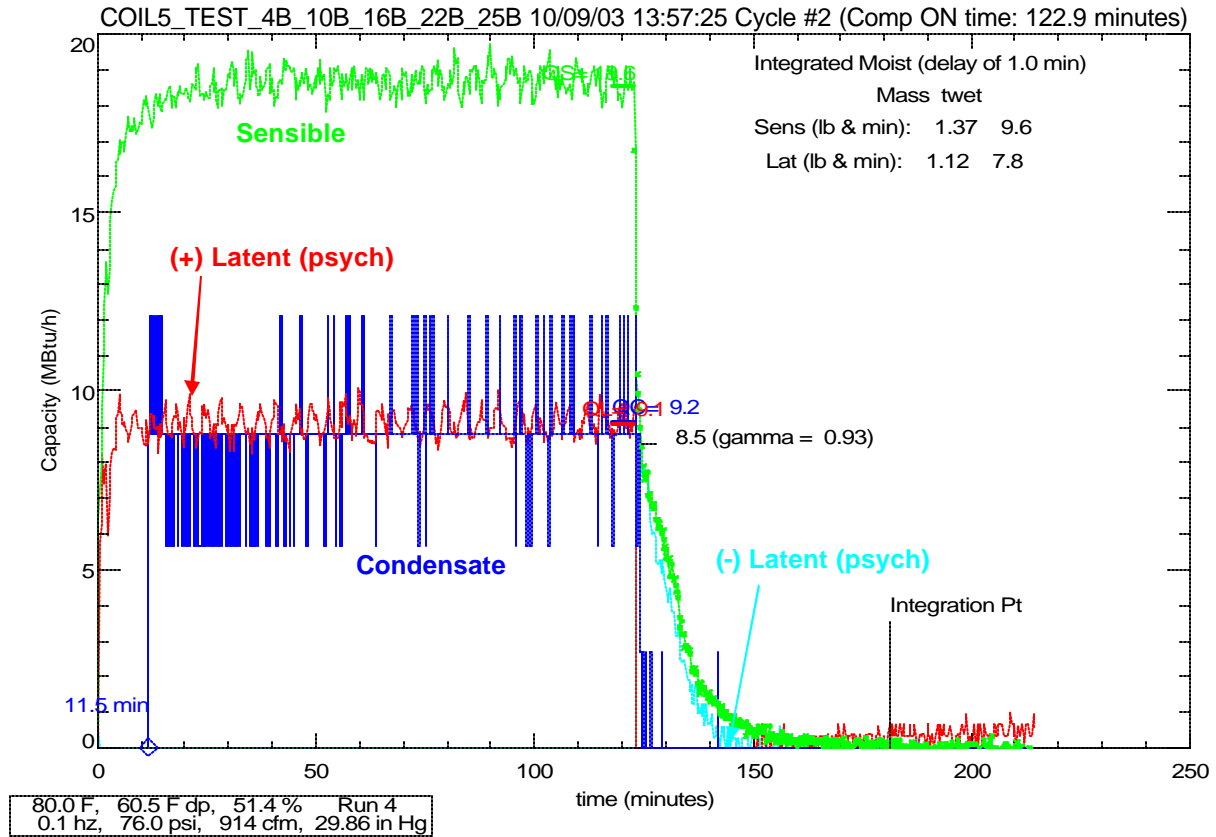
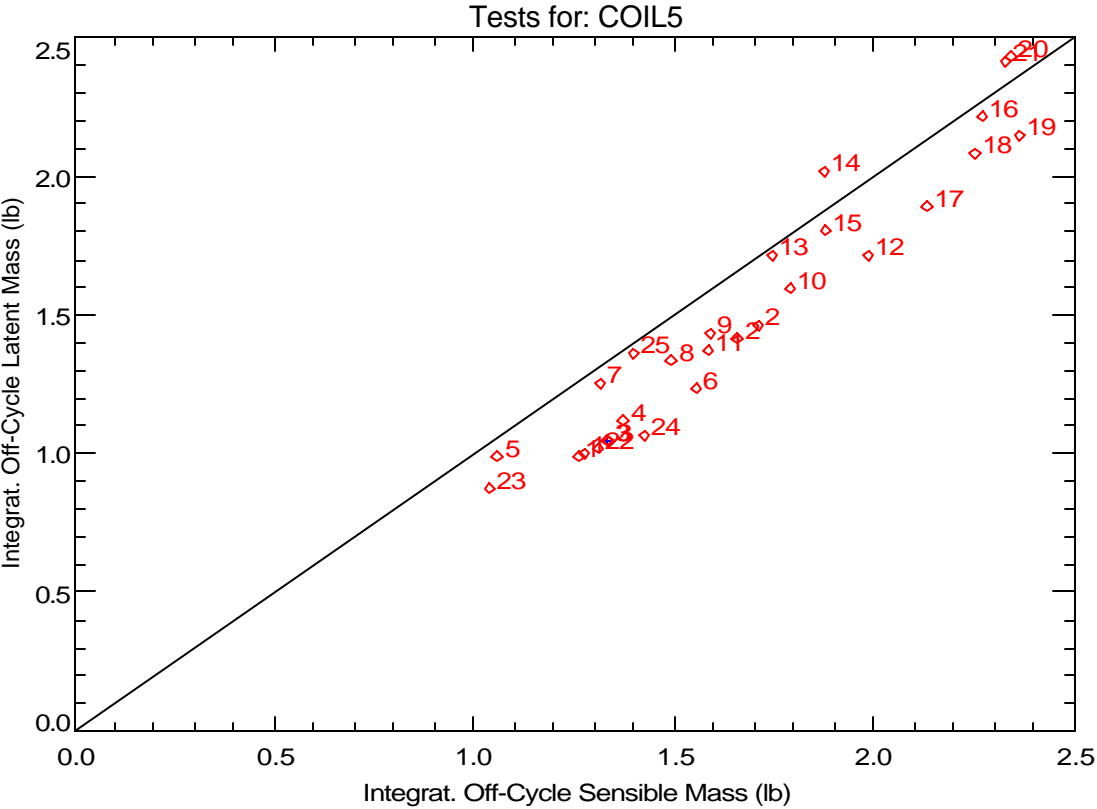


Figure 3. Example Plots of Detailed Data for Coil 5

**Part Load Latent Capacity Parameters**

The amount of moisture held on the cooling coil (and drain pan) can be calculated by integrating the off-cycle capacity from the coil (and dividing by the heat of vaporization, 1060 Btu/lb, to get the moisture mass). The integration is delayed for the first minute of the off-cycle so that the overshoot response of the chilled dew point hygrometers does not skew the results of the integration<sup>1</sup>. The integration terminates once steady state conditions are reached for the off cycle. If we assume the coil acts as an evaporative cooler, then sensible and latent capacity should be equal. Figure 4 compares the off-cycle integrated latent and sensible capacity calculated for each run. No systematic bias is evident and Figure 5 shows that any bias is not a function of dew point as was observed from tests of Coil 1.

Since we expect that off-cycle latent and sensible capacity should sum to zero, we have selected the integrated off-cycle sensible capacity as the most consistent and believable indication of the moisture mass held on the cooling coil (and drain pan).



**Figure 4. Comparing Stored Moisture Mass Calculated by Integrating Sensible and Latent Off-Cycle Capacity (Integrated with a 1 minute delay)**

<sup>1</sup>The 1-minute delay causes the estimate of moisture mass to be low by as much as 0.13 lbs (or 10%).

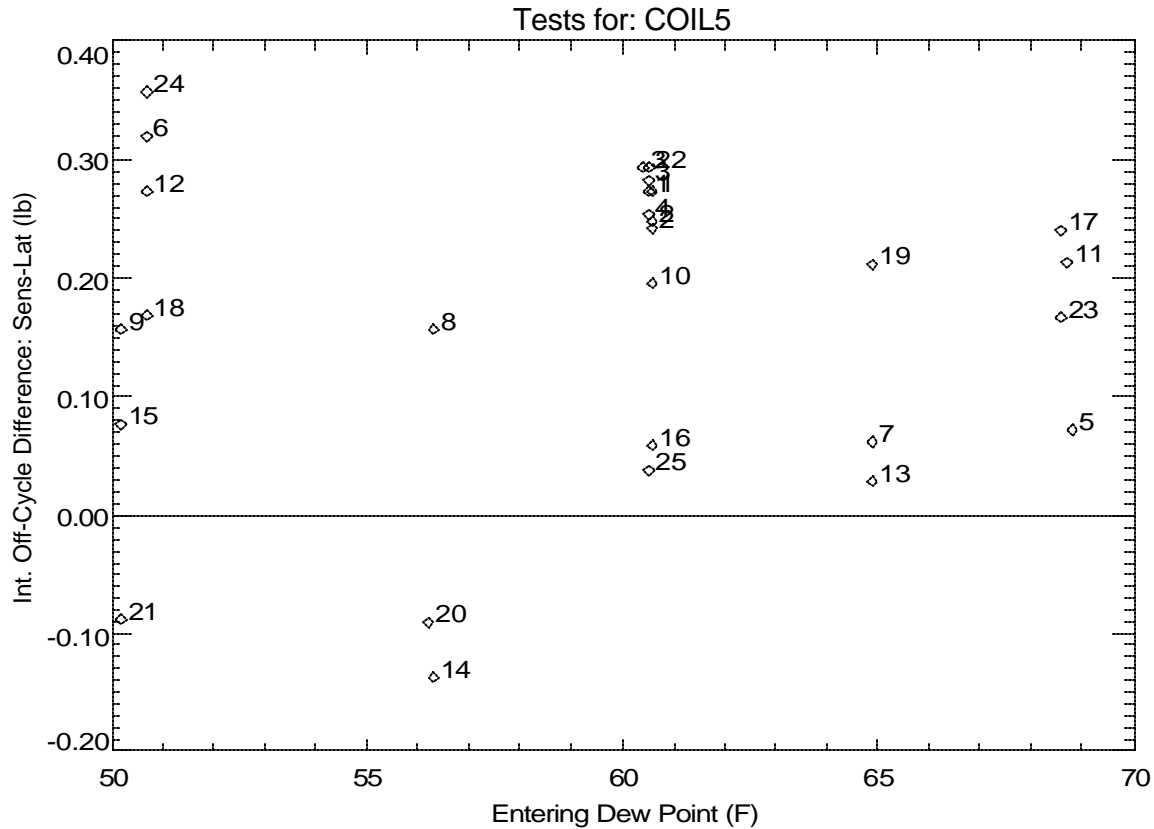


**Figure 5. Variation of Off-Cycle Sensible-Latent Difference with Entering Dew Point**

The parameter “twet” is the moisture mass held on the cooling coil (times the enthalpy of vaporization, 1060 Btu/lb) divided by the steady-state latent capacity of the cooling coil. The parameter should physically correspond to the time it takes for moisture to first fall from the coil (ignoring startup delays and other effects). Figure 6 compares the calculated “twet” (determined from integrating sensible capacity during the off-cycle and then dividing by the steady-state psychrometric latent capacity during the on-cycle) to the condensate delay time for all the test runs. In general, there is fair agreement between these two values. The worst agreement is apparent in tests #6, #9 and #24, which have either drier entering conditions, warmer coil temperatures, or higher air flows.

Figure 7a and 7b show that both twet and the condensate delay time are a function of the entering air dew point temperature. Figure 7b uses different symbols to show the 1<sup>st</sup> and 2<sup>nd</sup> cycles in each test sequence with flow rate of 400 cfm/ton for all tests. The delay time was generally the same for the 1<sup>st</sup> and 2<sup>nd</sup> cycles for this coil. The large difference seen for tests 6 and 9 is due to the low inlet dew point temperature not being properly reached during the 1<sup>st</sup> cycle.

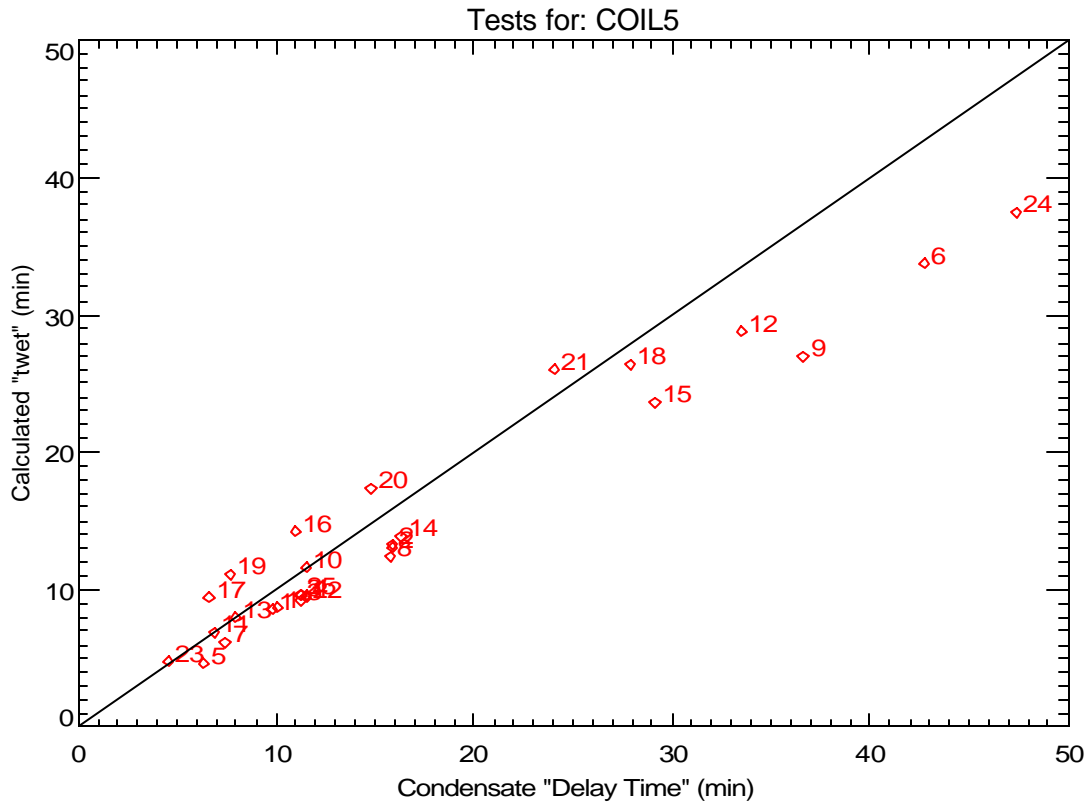


**Figure 6. Comparing “twet” (calculated with off-cycle sensible and steady state latent) to the Condensate Delay Time**



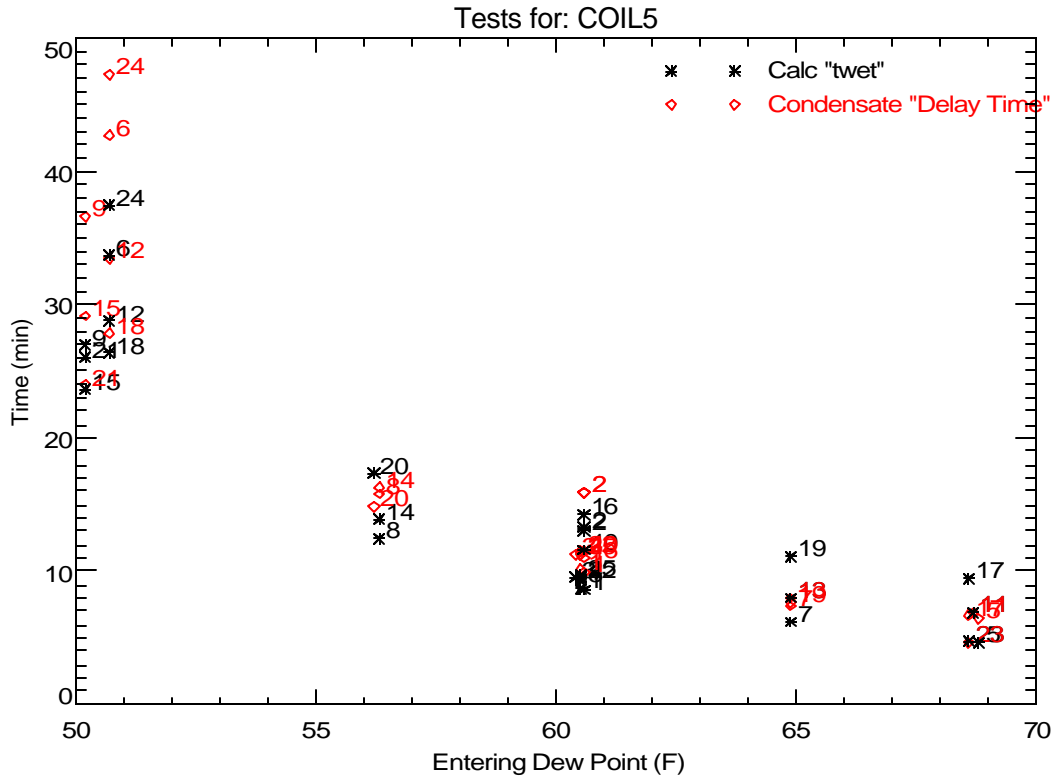


Figure 7a. Impact of Dew Point on “twet” and Condensate Delay Time

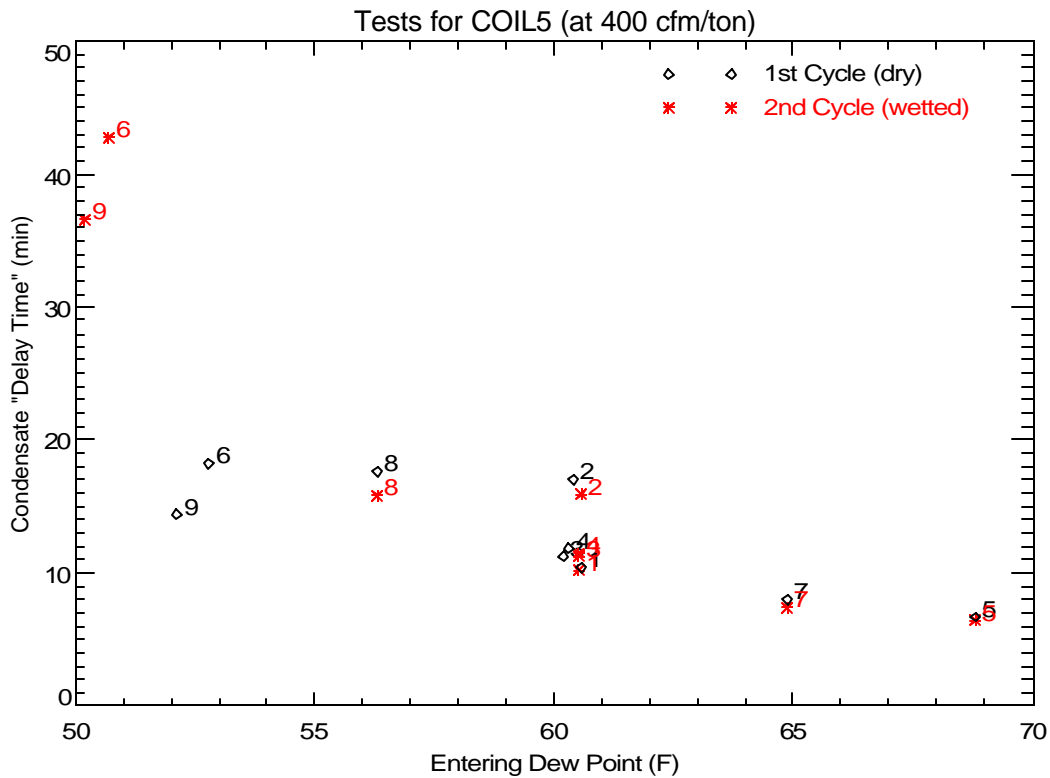


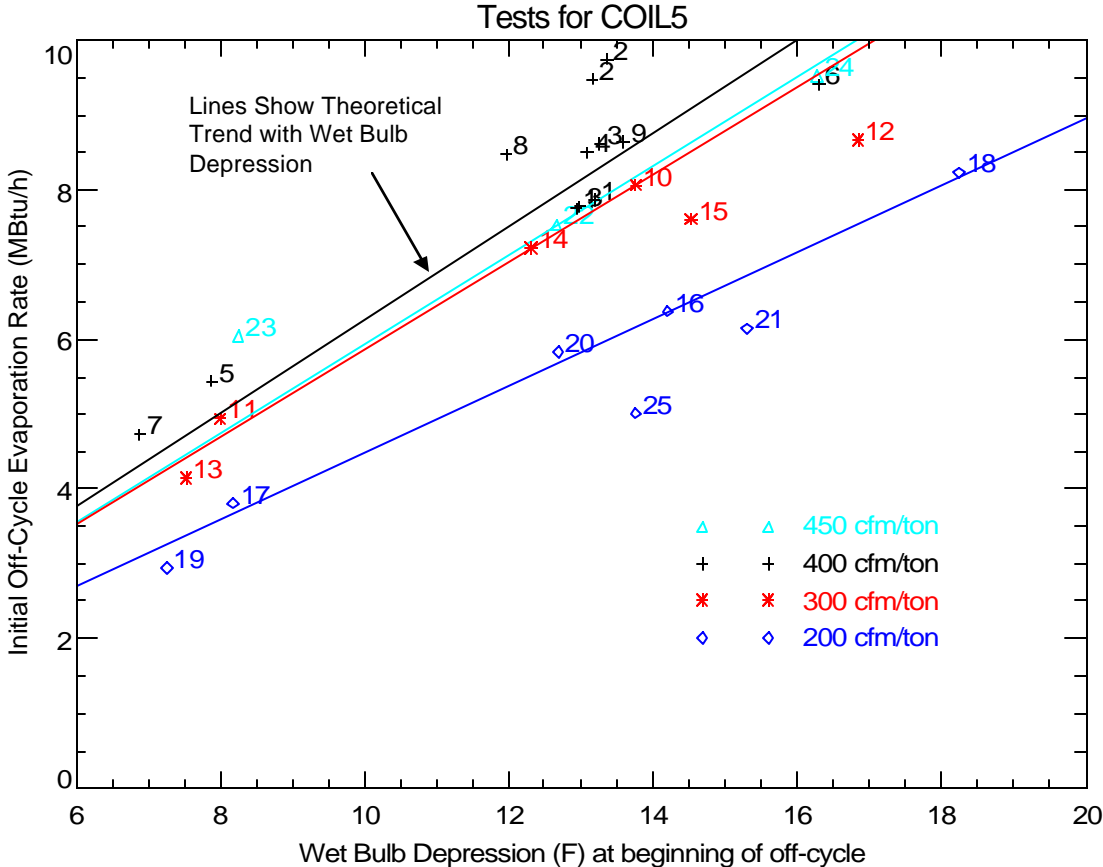
Figure 7b. Impact of Dew Point and Coil Wettedness on Condensate Delay Time

Figure 8 shows the initial off-cycle moisture evaporation rate varies with wet bulb depression. As expected, the evaporation rate is highest when the entering air has a larger wet bulb depression (i.e., has a lower relative humidity) and a higher air flow rate.

The model developed by Henderson and Rengarajan (1996) used the following simple evaporative cooler model to predict the moisture evaporation rate at off-design conditions:

$$Q_{\text{evap}} = Q_{\text{evap}_o} \times \frac{(DB - WB)}{(80 - 67)}$$

where  $Q_{\text{evap}_o}$  is the evaporation rate at the nominal entering air conditions of 80°F dry bulb (DB) and 67°F wet bulb (WB). This simple model is shown as the lines in Figure 8. For each air flow rate, the line is based on the nominal test results at 80°F DB/67°F WB extended to pass through zero. The measured data show essentially the same slope as the theoretical lines. Two of the tests at 450 cfm/ton (#22 and #24) were observed to have a lower than expected evaporation rate (and this caused the turquoise line for 450 cfm/ton to be lower than the black line for 400 cfm/ton). It is not clear what caused this unexpected trend.



**Figure 8. Measured Variation of Initial Evaporation Rate with Wet Bulb Depression**

Stabat et al. (2001) reviewed the theoretical performance of direct evaporative coolers and showed that the saturation effectiveness of an evaporative cooler is:

$$h_{evp} = 1 - e^{-NTU} \quad \text{where} \quad NTU = K/cfm^{0.2} \quad \text{for an air-water mixture.}$$

The line shown on Figure 9 is the best fit of the equation above to the measured data. The resulting constant K was 5.17, which is equivalent to an NTU of 1.32 at 920 cfm. While there is considerable scatter due to the experimental uncertainty of predicting the initial off-cycle moisture evaporation rate, the slope of the line is still fairly representative of the overall trend.

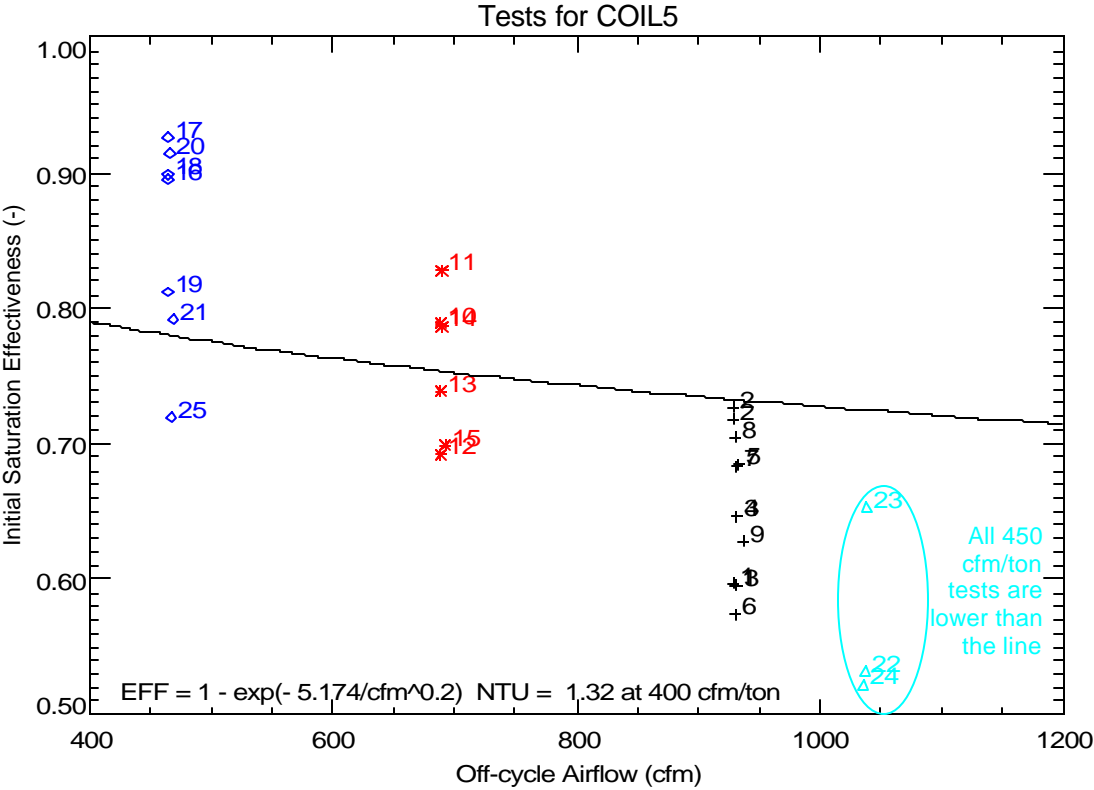


**Figure 9. Evaporative Effectiveness versus Airflow**

Figure 10 compares the measured initial off-cycle moisture evaporation rate for each test to the predicted initial evaporation rate using the effectiveness model above. The model and measured data generally agree when presented in this form (i.e., the overall agreement visually appears better than in Figure 9 above). Again, the variation that occurs with Tests #6 and #24 was due to partial coil dryout.

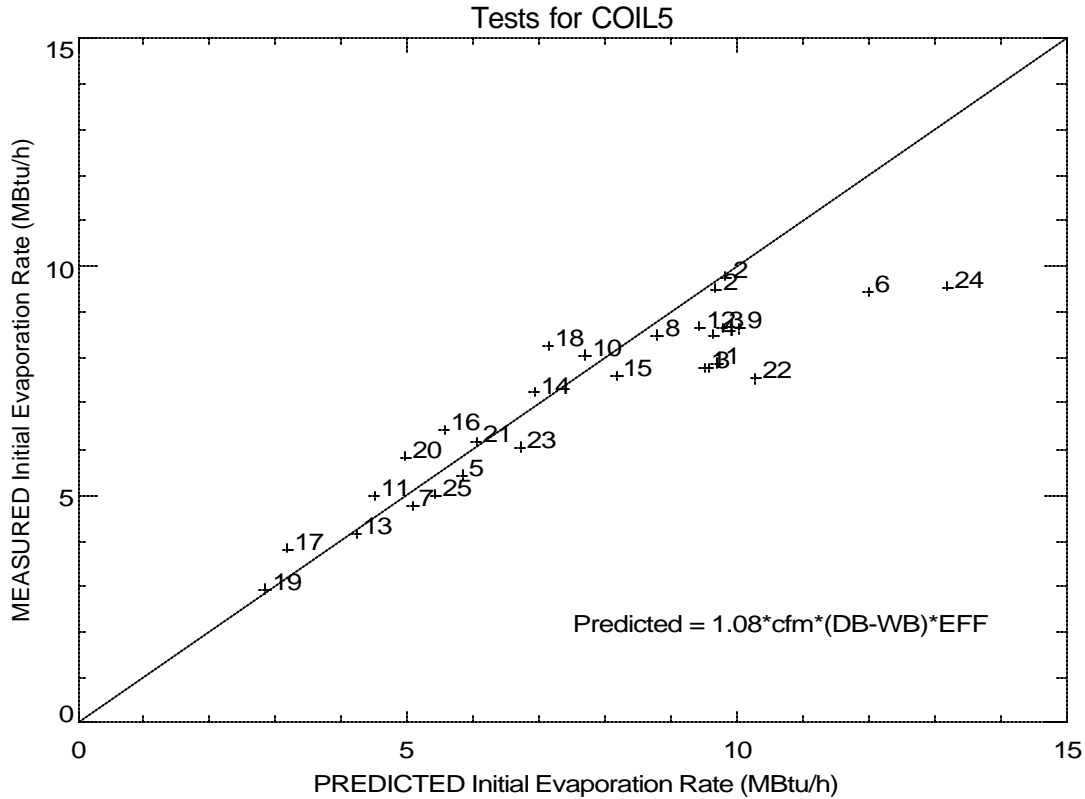


**Figure 10. Comparing Measured and Predicted Initial Moisture Evaporation Rates**

Figure 11 and Figure 12 below evaluate whether the amount of moisture retained on the cooling coil is a function of air flow or entering air conditions. The results for this coil were unusual in that the moisture holding capacity is slightly lower at higher dew points (Figure 11). The data also show little evidence of partial coil dryout, which implies that this slanted coil had good airflow and refrigerant distribution so that all surfaces were at the same temperature. The amount of retained moisture ranges from 1 to 2.3 lbs.

Figure 12 shows the expected trend of more retained moisture on the cooling coil with lower air flow rates.

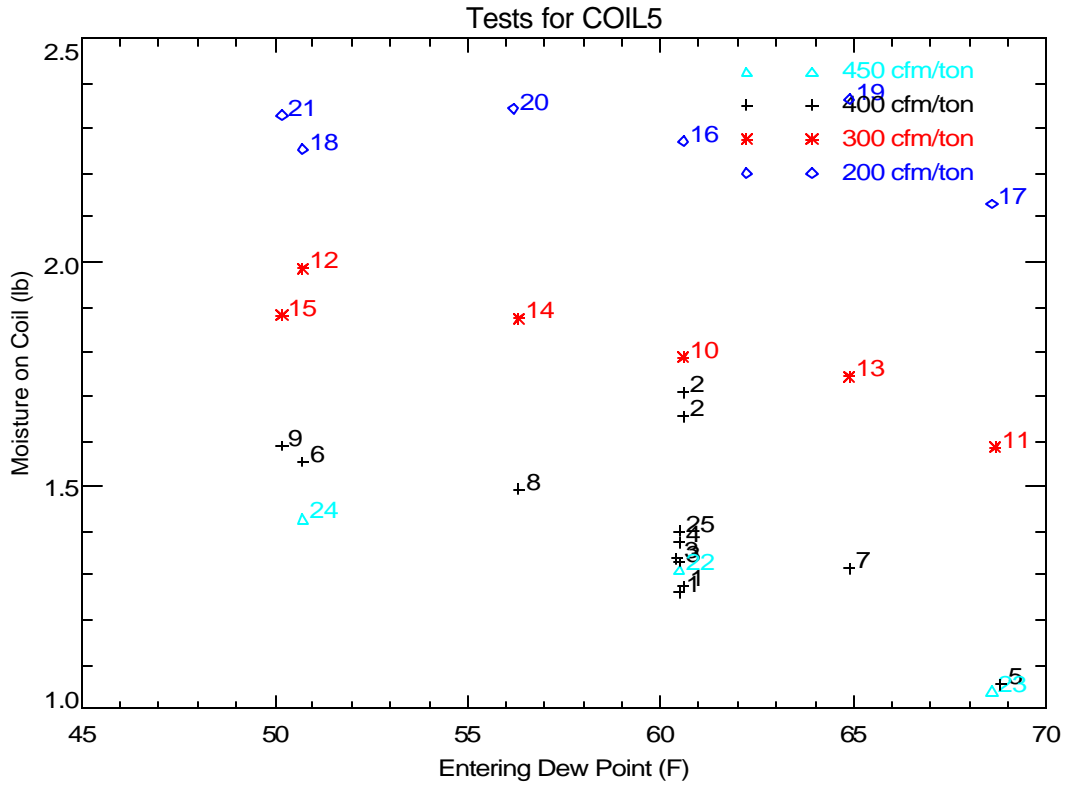


Figure 11. Variation of Retained Moisture (based on Off-Cycle Sensible) with Flow and Dew Point

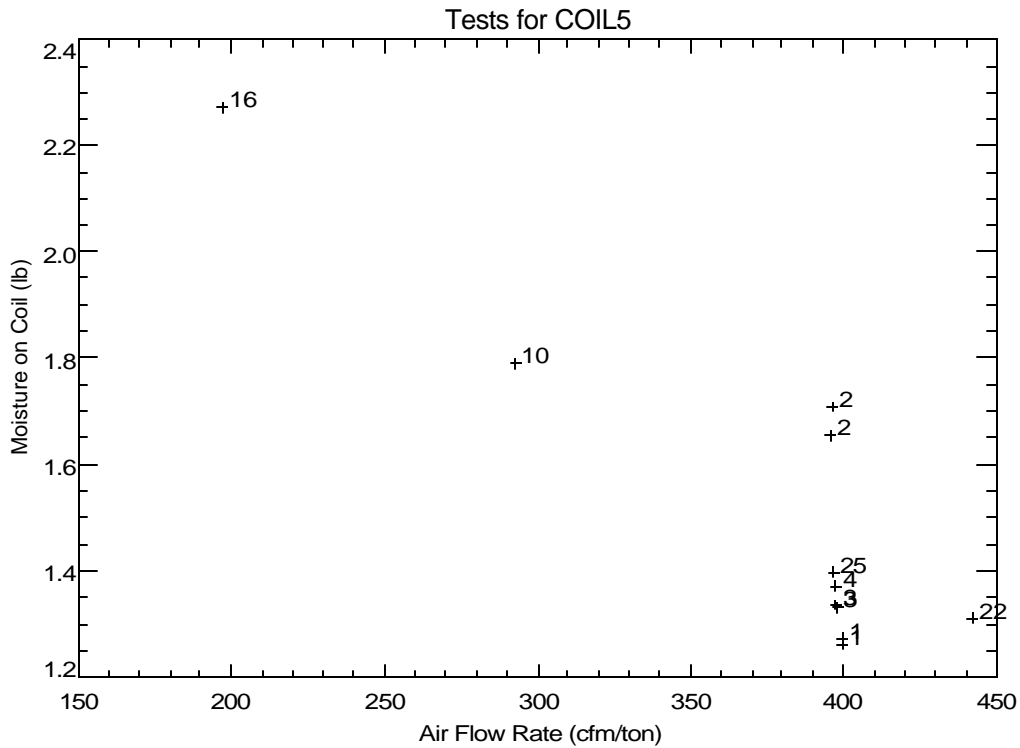
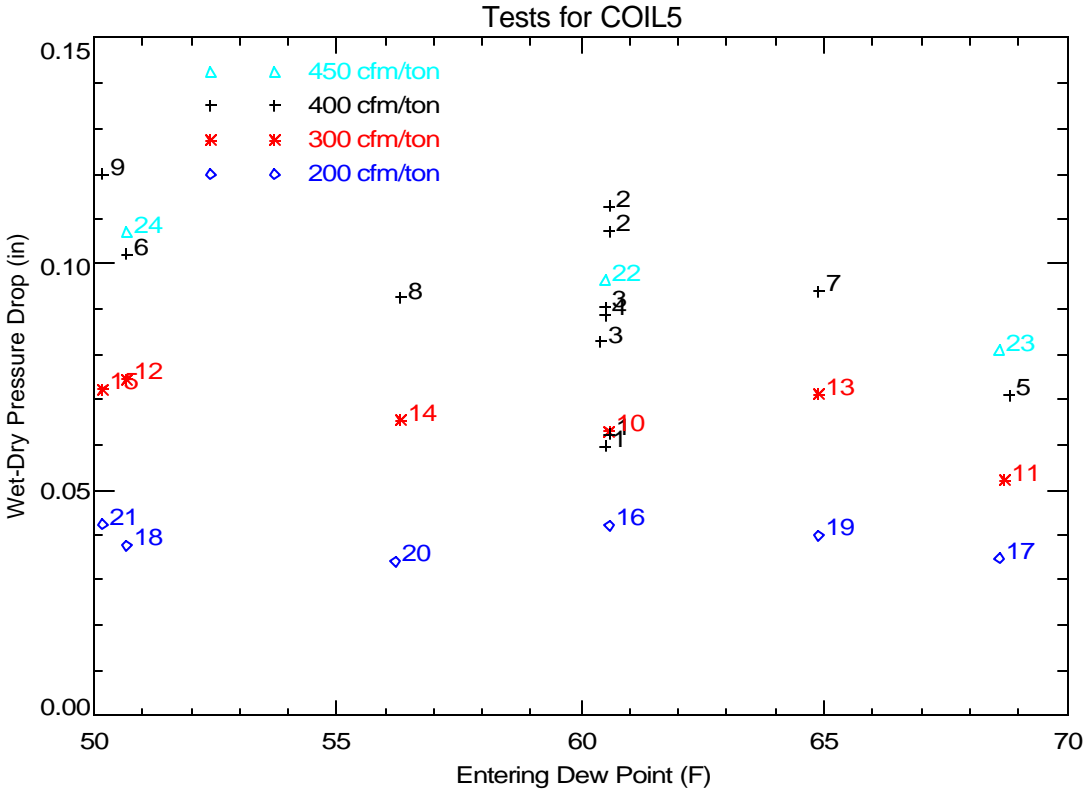


Figure 12. Variation of Retained Moisture with Air Flow at Nominal Entering Conditions of 80°F, 60.4°F dew point

Another way to detect the amount of retained moisture is to measure the static air-side pressure drop across the cooling coil. The difference between the pressure drop across the coil under wet and dry conditions should provide an indication of the amount of retained moisture (the wet coil pressure drop is measured at steady-state conditions while the dry coil pressure drop is taken as the average pressure drop during the last part of the off-cycle). Figure 13 shows the variation of the wet-dry pressure difference with various entering humidity conditions at multiple air flow rates. Comparing the values for each air flow rate generally shows that the pressure drop is not a function of humidity, especially at the lower air flow rates (200 and 300 cfm/ton). This implies that the modest trend of more moisture at lower dew points (Figure 11 above) was caused by a bias in the procedures to determine retained moisture.



**Figure 13. Variation of Wet-Dry Pressure Drop with Entering Conditions and Air Flow Rate**

Figure 14 confirms that the wet-dry pressure drop is a linear function of air flow rate, which implies laminar flow in the wetted cooling coil.

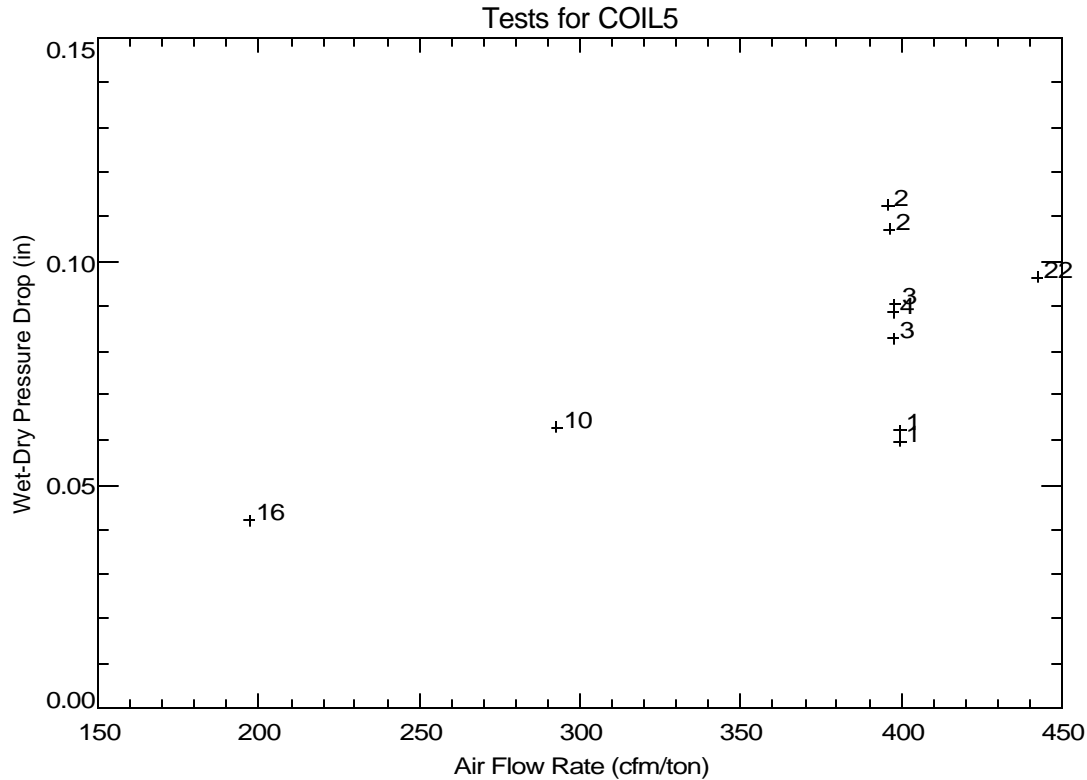


**Figure 14. Trend of Wet-Dry Pressure Drop with Flow at Nominal Entering Conditions of 80°F, 60.4°F dew point**

The series of plots in Figure 15 show the impact of coil suction temperature on performance. The steady-state performance of the system shows the expected trends of lower SHR and greater latent capacity at lower coil temperatures (i.e., lower saturated suction temperatures). Like Coil 4, however, the plots for moisture on coil and wet-dry pressure drop show the unexpected trend of less moisture retention at lower coil temperatures. It is not clear what caused this unexpected result.

The graph of fan power versus saturated suction temperature in Figure 15 is not relevant since the AHU fan was turned off during all tests. For this cooling coil, an external booster fan was used to obtain the desired air flow rate for each test.

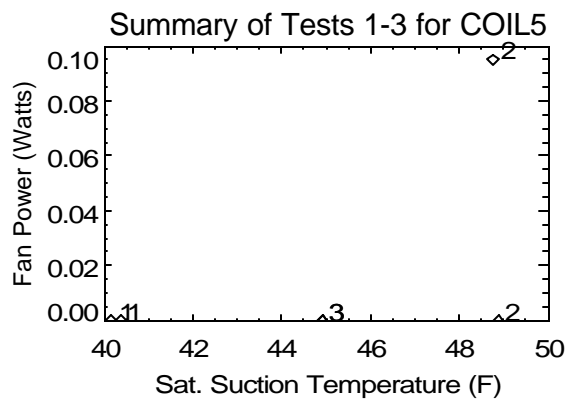
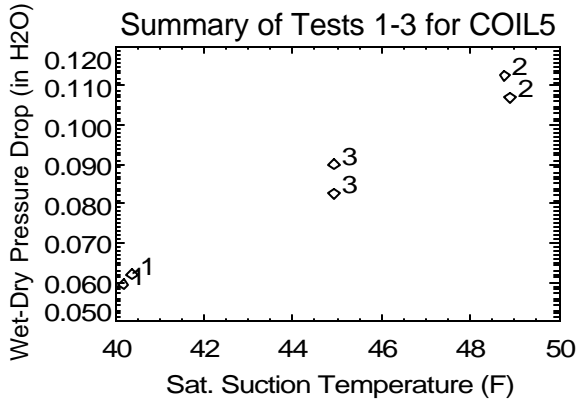
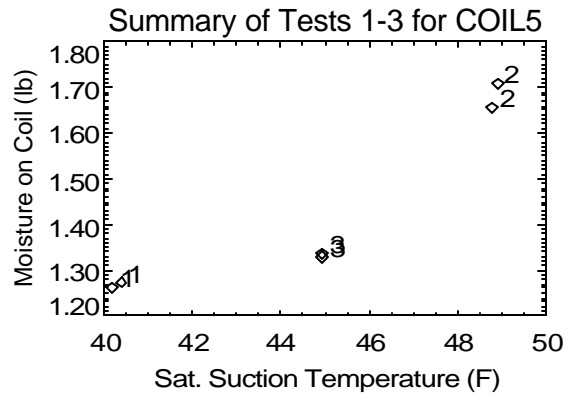
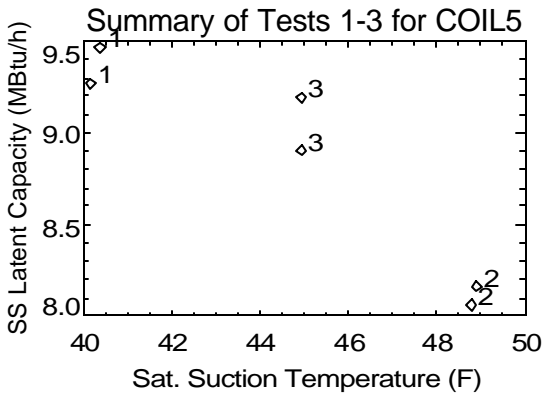
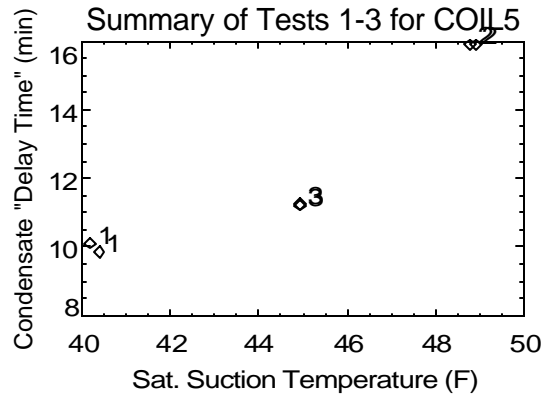
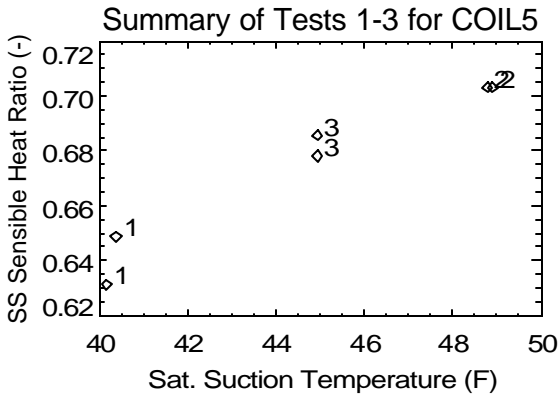


Figure 15. Trend of Various Parameters with Saturated Suction Temperature



## Overall Latent Degradation Trends

Several quasi-steady cyclic tests were also completed in the laboratory to quantify the overall part-load degradation of latent capacity. Table 2 lists the cycling test runs. These conditions correspond to a conventional thermostat with a maximum cycle rate of 3 cycles per hour (at 50% runtime).

**Table 2. Cyclic Test Conditions**

CONST FAN <sup>1</sup>	AUTO FAN <sup>2</sup>	Number of Times Test Repeated <sup>3</sup>	ON Time (minutes)	OFF Time (minutes)	Runtime Fraction (-)	Cycle Rate (cycles/h)
Run						
31	41	2	45	45	0.500	0.667
32	42	3	30	6	0.833	1.667
33	43	3	16	7.25	0.688	2.581
34	44	3	10	10	0.500	3.000
35	45	3, 5	7	17.5	0.286	2.449
	46	5	5.5	55	0.091	0.992

Notes: <sup>1</sup>Constant fan tests performed at 80°F db/60.4°F dp inlet air with 400 cfm/ton (runs 31-35) and 300 cfm/ton (runs 71-75) air flow. Tests also conducted at 75°F db/56°F dp (runs 61-65) and 75°F db/64°F dp (runs 51-55) inlet air with 400 cfm/ton air flow.

<sup>2</sup>Auto fan tests performed at 80°F db/60.4°F dp inlet air with 400 cfm/ton air flow.

<sup>3</sup>Tests were repeated 5 times for runs 45 & 46.

Figure 16 through Figure 19 show the net impact of part-load unit operation based on cyclic tests completed in the lab. All of these tests are in the constant fan mode (continuous air flow over the cooling coil while the coil cycles on/off), but at various entering air and flow rate conditions:

- Nominal: 80°F & 60.4°F dew pt. with 400 cfm/ton (Figure 16)
- Humid: 75°F & 64°F dew pt. with 400 cfm/ton (Figure 17)
- Dry: 75°F & 56°F dew pt. with 400 cfm/ton (Figure 18)
- Low Flow: 80°F & 60.4°F dew pt. with 300 cfm/ton (Figure 19)

The measured data generally compare well to the model from Henderson and Rengarajan (1996) using the model parameters shown on each plot. These parameters were always taken from the 2<sup>nd</sup> occurrence of the first test in each sequence (i.e., Tests #31, 51, 61 and 71), which were completed as part of the suite of cycling tests listed in Table 2 for the constant fan mode. The latent time constant (tau) of 20 seconds was selected based on qualitative observations of the coil's response time. The solid black line corresponds to the linear off-cycle evaporation model. The black dotted line assumes an off-cycle evaporation trend that corresponds to an exponential decay. The purple line is the new part load LHR model that uses the more realistic evaporation model from Stabat et al. (2001) and also allows for variable amounts of moisture on the coil at the end of the on cycle. The parameters NTU and tp were determined from the specific measured data from each test sequence (the purple solid line) as well as the average NTU and tp from all the data (the purple dotted line), including Figure 9 above. The parameter tp is defined in the improved model development section of this report.

The measured data corresponding to the 2<sup>nd</sup> and 3<sup>rd</sup> repetition (cycle) of each test showed the best agreement with the models, since quasi-steady conditions had been achieved.

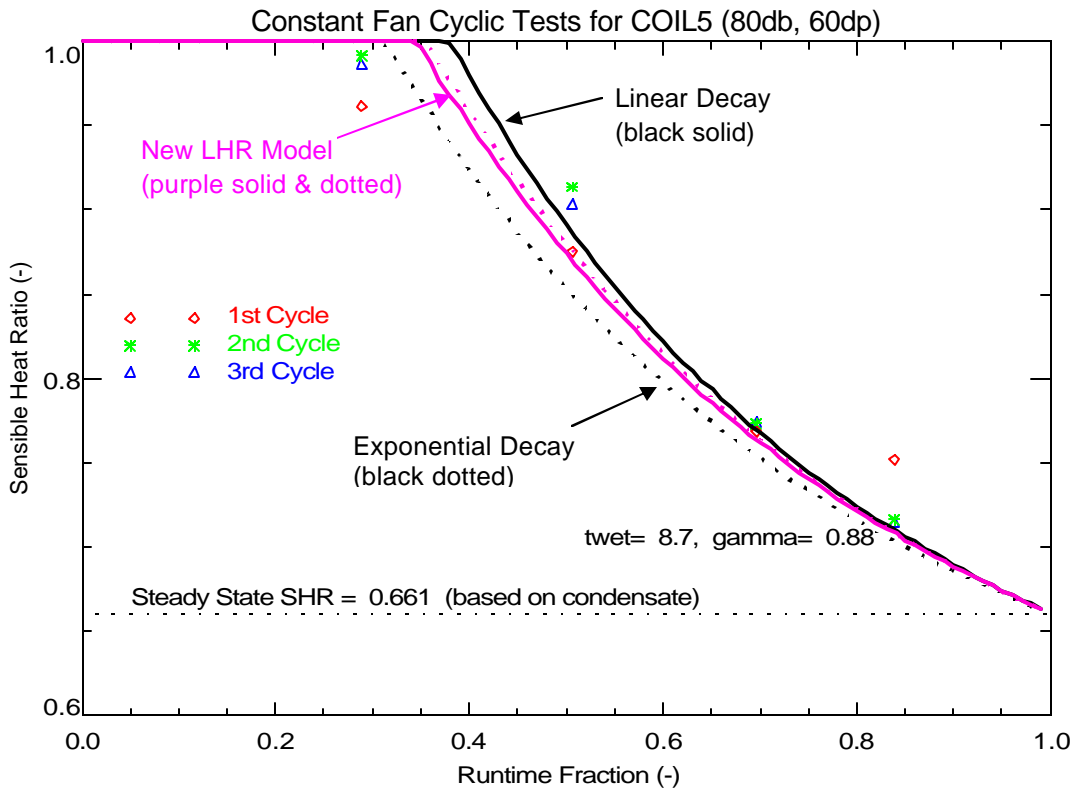


Figure 16. Comparing Measured Latent Degradation to the LHR Models: Nom. Conditions (80°F / 60.4°Fdp)

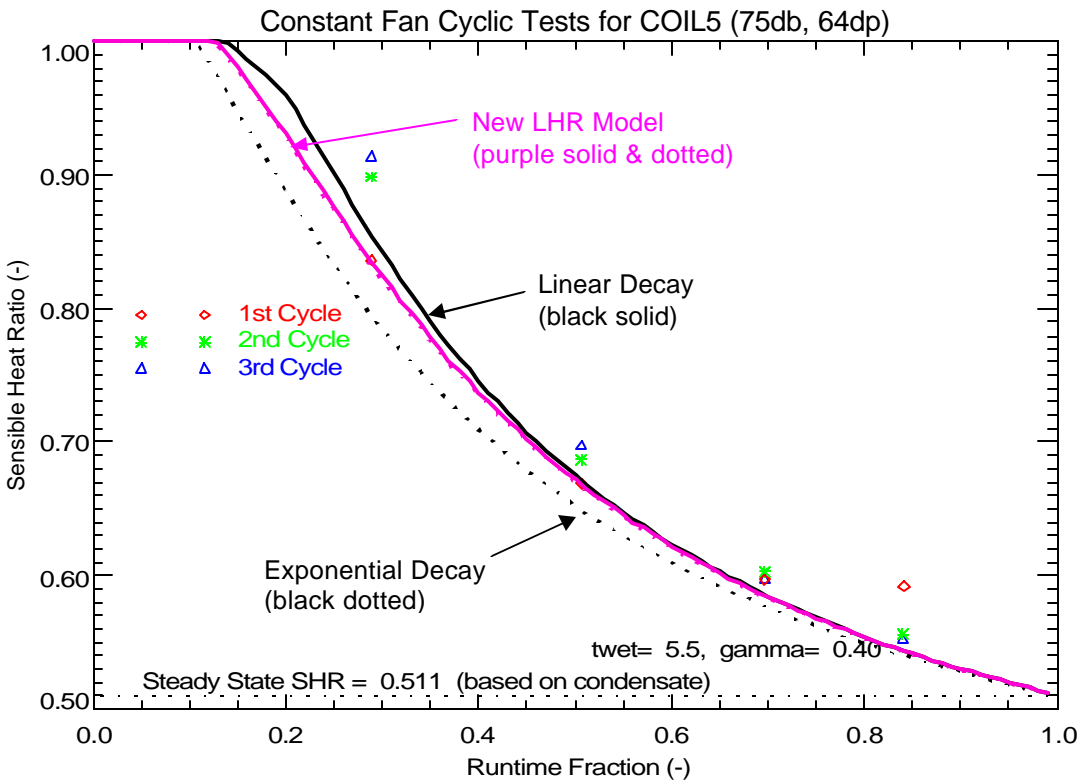


Figure 17. Comparing Measured Latent Degradation to the LHR Models: (75°F / 64°Fdp)

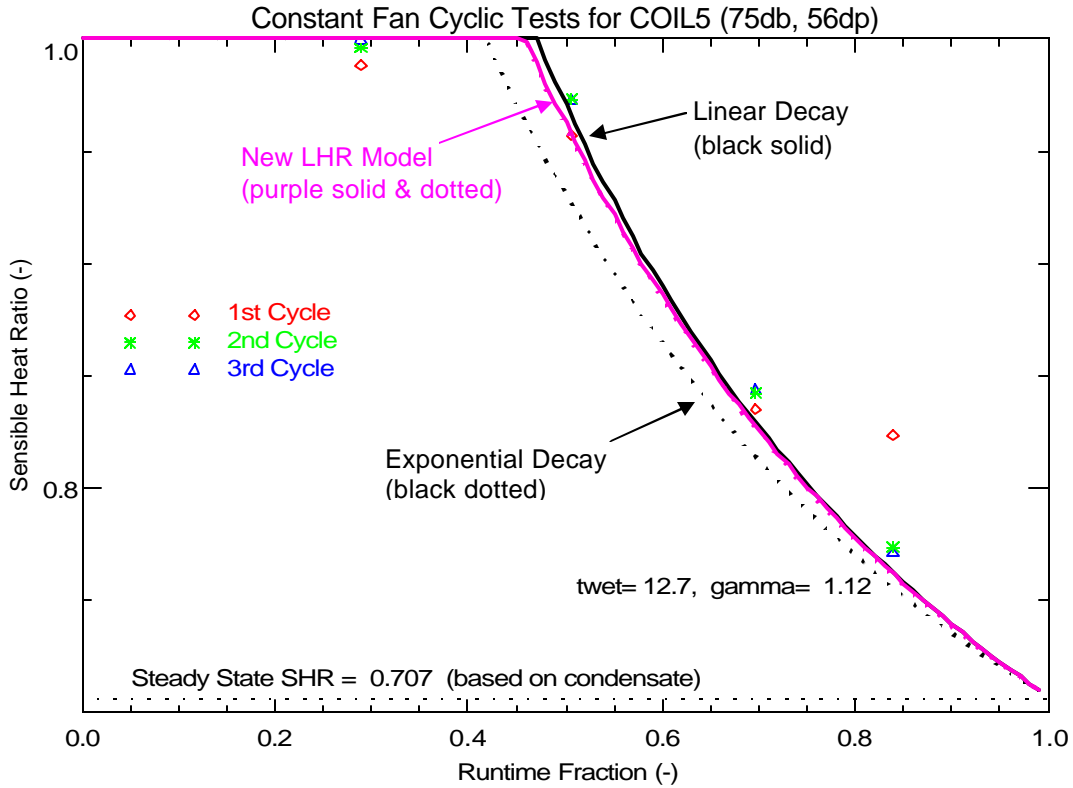


Figure 18. Comparing Measured Latent Degradation to the LHR Models: (75° F / 56° Fdp)

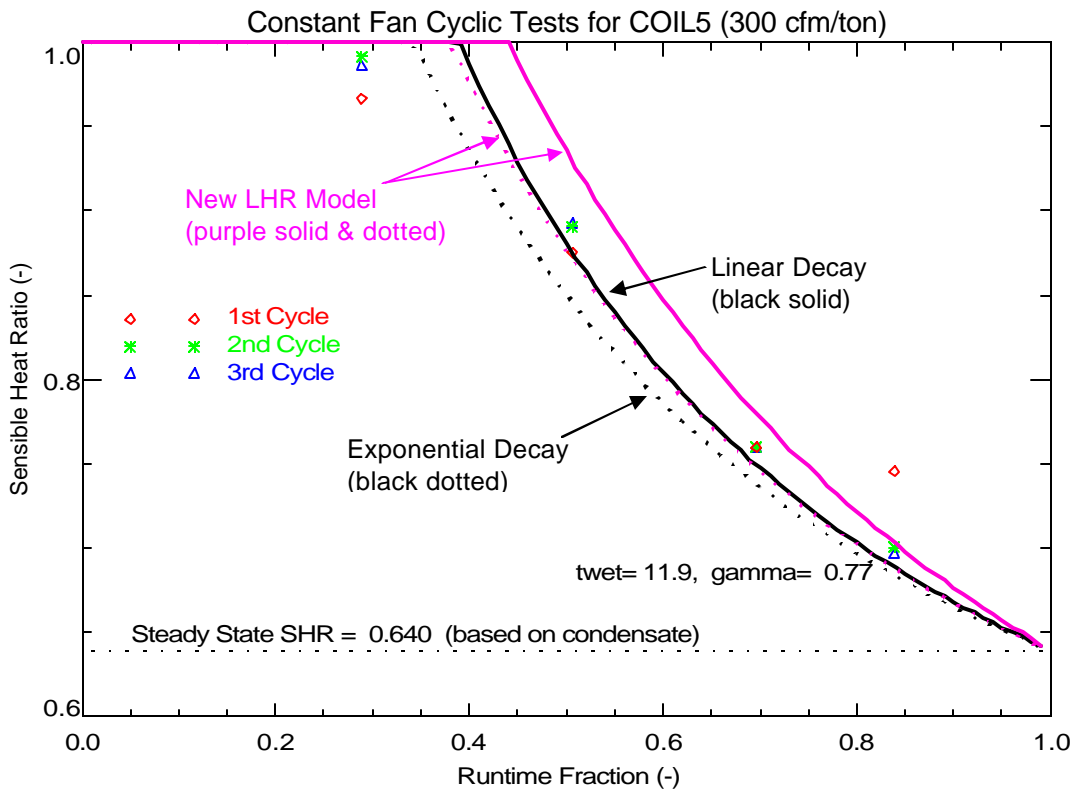
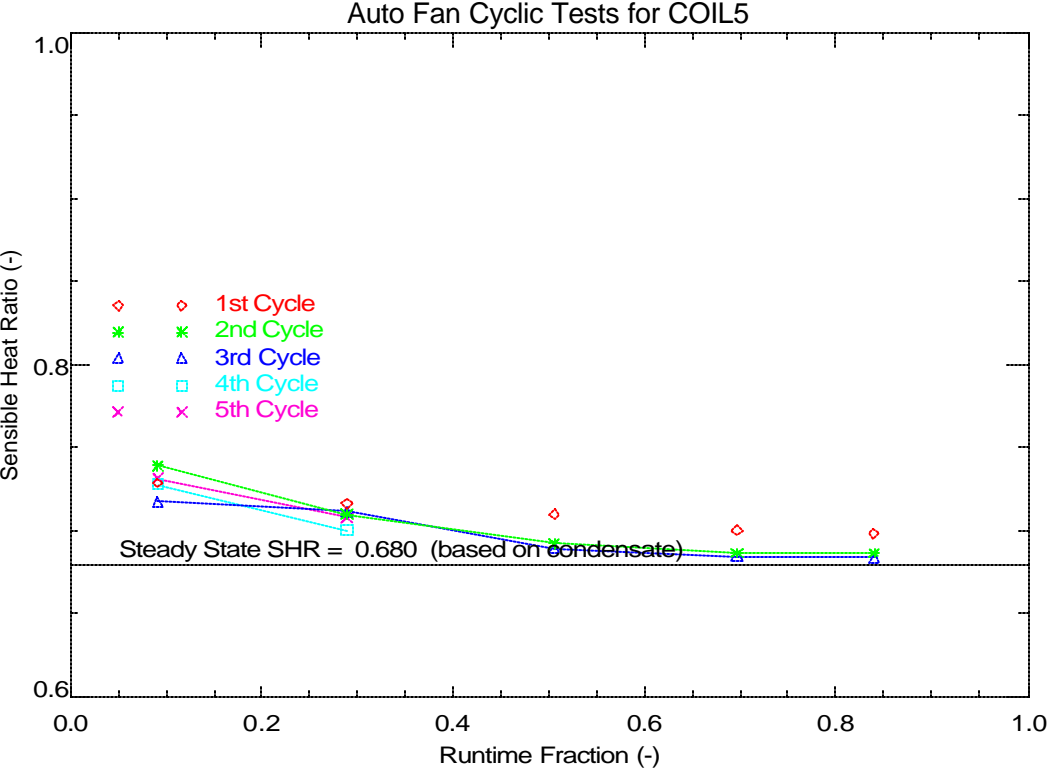


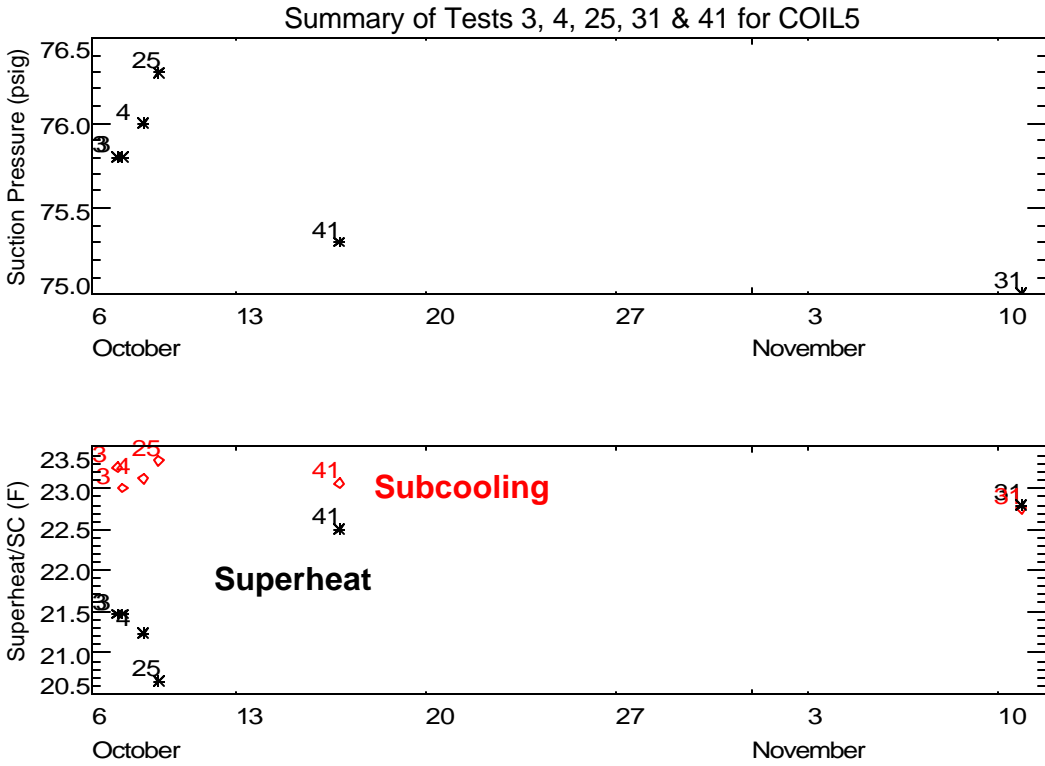
Figure 19. Comparing Measured Latent Degradation to the LHR Models: 300 cfm/ton

Figure 20 shows some latent degradation can be detected in the AUTO fan mode (i.e., the supply air flow across the cooling coil starts and stops with compressor operation) for Coil 5 (similar degradation was seen for Coils 1, 3 and 4). The last repetitions (cycles) show good agreement with each other.



**Figure 20. Measured AUTO Fan Latent Degradation**

The tests were completed over a period of 6 weeks. Figure 21 shows little evidence of a change in suction pressure, subcooling or superheat over the test period. This implies that no significant loss of refrigerant charge occurred over the test period.



**Figure 21. Long-Term Variation in Suction Pressure, Superheat and Subcooling**

**References**

Henderson, H., and K. Rengarajan. 1996. A model to predict the latent capacity of air conditioners and heat pumps at part-load conditions with constant fan operation. *ASHRAE Transactions* 102(1): 266-274.

Stabat, P., Marchio, D. and M. Orphelin. 2001. Pre-Design and Design Tools for Evaporative Cooling. *ASHRAE Transactions* 107 (1): 501-510.

**COIL 5 Test Runs**

File Name	Date	Start Time	Sequence No.	Run/Test No.	Inlet DB (F)	Inlet DewPt (F)	Air Flow (cfm)	Test Duration (min)	Comp Runtime (min)
coil5_test_1.out	10/27/2003	13:01:57	1	1	80	60.6	919.4	120.7	60.7
coil5_test_1.out	10/27/2003	15:02:55	2	1	80	60.5	919.3	120.7	60.7
coil5_test_1.out	10/27/2003	17:03:54	3	1	80	60.6	918.7	120.6	60.7
coil5_test_2d.out	11/18/2003	11:04:59	1	2	80.9	60.4	915.1	90.5	45.7
coil5_test_2d.out	11/18/2003	12:35:46	2	2	80.1	60.6	911.2	120.8	60.7
coil5_test_2d.out	11/18/2003	14:36:53	3	2	80.1	60.6	910.4	113.2	60.7
coil5_test_3b.out	10/8/2003	12:55:27	1	3	80	60.2	916.1	214	122.6
coil5_test_3b.out	10/8/2003	16:29:43	2	3	80	60.5	914.7	214.1	122.7
coil5_test_3b.out	10/8/2003	20:04:08	3	3	80	60.4	914.5	214.2	122.8
coil5_Test_4b_10b_16b_22b_25b.out	10/9/2003	10:22:40	1	4	80	60.3	914.9	214.5	123
coil5_Test_4b_10b_16b_22b_25b.out	10/9/2003	13:57:25	2	4	80	60.5	914.2	214.5	122.9
coil5_Test_4b_10b_16b_22b_25b.out	10/9/2003	17:32:10	3	10	80	60.6	673.3	214.3	122.9
coil5_Test_4b_10b_16b_22b_25b.out	10/9/2003	21:06:45	4	16	80	60.6	453.3	214.3	122.9
coil5_Test_4b_10b_16b_22b_25b.out	10/10/2003	0:41:21	5	22	80	60.5	1017.5	214.3	122.8
coil5_Test_4b_10b_16b_22b_25b.out	10/10/2003	4:15:56	6	25	80	60.5	913.3	214.2	122.8
coil5_Test_5e_11e_17e_23e.out	11/5/2003	16:24:23	1	5	80.1	68.8	922.6	122.2	61.4
coil5_Test_5e_11e_17e_23e.out	11/5/2003	18:26:52	2	5	80	68.8	921.8	122.2	61.3
coil5_Test_5e_11e_17e_23e.out	11/5/2003	20:29:22	3	11	80	68.7	681.8	122.3	61.4
coil5_Test_5e_11e_17e_23e.out	11/5/2003	22:31:55	4	17	80	68.6	461.2	122.3	61.4
coil5_Test_5e_11e_17e_23e.out	11/6/2003	0:34:27	5	23	80	68.6	1026	122.3	61.4
coil5_Test_6b_12b_18b_24b.out	10/11/2003	1:44:39	1	6	79.9	52.8	908.9	214.6	123
coil5_Test_6b_12b_18b_24b.out	10/11/2003	5:19:31	2	6	80	50.7	911.9	214.4	122.8
coil5_Test_6b_12b_18b_24b.out	10/11/2003	8:54:08	3	12	80	50.7	673	214.3	122.8
coil5_Test_6b_12b_18b_24b.out	10/11/2003	12:28:43	4	18	80	50.7	456.1	214.3	122.8
coil5_Test_6b_12b_18b_24b.out	10/11/2003	16:03:18	5	24	80	50.7	1017.6	214.3	122.8
coil5_Test_7c_13c_19c.out	10/18/2003	4:57:31	1	7	75.3	64.9	913.7	214.3	122.9
coil5_Test_7c_13c_19c.out	10/18/2003	8:32:06	2	7	75	64.9	914.4	214.4	122.9
coil5_Test_7c_13c_19c.out	10/18/2003	12:06:43	3	13	75	64.9	674.9	214.4	122.9
coil5_Test_7c_13c_19c.out	10/18/2003	15:41:22	4	19	75	64.9	456.7	214.3	122.8
coil5_Test_8f_14f_20f.out	11/17/2003	14:39:29	1	8	75.2	56.3	913.6	122.2	61.4
coil5_Test_8f_14f_20f.out	11/17/2003	16:41:56	2	8	75	56.3	914.5	122.1	61.3
coil5_Test_8f_14f_20f.out	11/17/2003	18:44:18	3	14	75	56.3	675.5	122.1	61.3
coil5_Test_8f_14f_20f.out	11/17/2003	20:46:40	4	20	75.1	56.2	458.3	122.1	61.3
coil5_Test_9c_15c_21c.out	10/25/2003	7:53:27	1	9	75.1	52.1	914.3	214.3	122.8
coil5_Test_9c_15c_21c.out	10/25/2003	11:28:03	2	9	75	50.2	915.3	214.2	122.7
coil5_Test_9c_15c_21c.out	10/25/2003	15:02:32	3	15	75	50.2	677.4	214.2	122.7
coil5_Test_9c_15c_21c.out	10/25/2003	18:36:58	4	21	75	50.2	459	214.2	122.7
coil5_Test_cycling_constantc.out	11/10/2003	17:54:30	1	31	79.7	60.5	919.6	122.2	61.3
coil5_Test_cycling_constantc.out	11/10/2003	19:56:56	2	31	80	60.6	921	122.2	61.3
coil5_Test_cycling_constantc.out	11/10/2003	21:59:23	3	32	80	60.6	922.2	36.5	30.6
coil5_Test_cycling_constantc.out	11/10/2003	22:36:11	4	32	80	60.6	918.7	36.5	30.6
coil5_Test_cycling_constantc.out	11/10/2003	23:12:59	5	32	80	60.6	920.7	36.5	30.7
coil5_Test_cycling_constantc.out	11/10/2003	23:49:48	6	33	79.7	60.3	922.5	23.5	16.4
coil5_Test_cycling_constantc.out	11/11/2003	0:13:35	7	33	79.8	60.5	923.1	23.5	16.4
coil5_Test_cycling_constantc.out	11/11/2003	0:37:21	8	33	80	60.6	926.5	23.5	16.4
coil5_Test_cycling_constantc.out	11/11/2003	1:01:07	9	34	80	60.7	926.4	20.1	10.2
coil5_Test_cycling_constantc.out	11/11/2003	1:21:33	10	34	80	60.4	925.4	20.2	10.2
coil5_Test_cycling_constantc.out	11/11/2003	1:41:59	11	34	80	60.6	925.6	20.1	10.2
coil5_Test_cycling_constantc.out	11/11/2003	2:02:25	12	35	80	60.6	930.2	24.7	7.1
coil5_Test_cycling_constantc.out	11/11/2003	2:27:24	13	35	80	60.4	932	24.7	7.2
coil5_Test_cycling_constantc.out	11/11/2003	2:52:24	14	35	80	60.8	928.5	24.7	7.2
coil5_Test_cycling_constant_75_56e.out	11/25/2003	15:59:07	1	61	75.1	56.3	911.2	122.1	61.3
coil5_Test_cycling_constant_75_56e.out	11/25/2003	18:01:27	2	61	75	56.2	911.1	122.1	61.3
coil5_Test_cycling_constant_75_56e.out	11/25/2003	20:03:52	3	62	75	56.2	916.7	36.5	30.6
coil5_Test_cycling_constant_75_56e.out	11/25/2003	20:40:38	4	62	74.9	56.3	911	36.5	30.6
coil5_Test_cycling_constant_75_56e.out	11/25/2003	21:17:26	5	62	75	56.3	912.9	36.5	30.6
coil5_Test_cycling_constant_75_56e.out	11/25/2003	21:54:12	6	63	74.9	56.2	913.6	23.5	16.4
coil5_Test_cycling_constant_75_56e.out	11/25/2003	22:17:59	7	63	75	56.2	913	23.5	16.4
coil5_Test_cycling_constant_75_56e.out	11/25/2003	22:41:45	8	63	75	56.2	917.3	23.5	16.4
coil5_Test_cycling_constant_75_56e.out	11/25/2003	23:05:31	9	64	74.9	56.3	919.4	20.2	10.2
coil5_Test_cycling_constant_75_56e.out	11/25/2003	23:25:57	10	64	75	56.2	922.8	20.2	10.2
coil5_Test_cycling_constant_75_56e.out	11/25/2003	23:46:23	11	64	75	56.2	920.7	20.2	10.2
coil5_Test_cycling_constant_75_56e.out	11/26/2003	0:06:49	12	65	75.1	56.2	921.6	24.7	7.2
coil5_Test_cycling_constant_75_56e.out	11/26/2003	0:31:48	13	65	75.1	56.2	926.8	24.7	7.2
coil5_Test_cycling_constant_75_56e.out	11/26/2003	0:56:48	14	65	75.2	56.2	924.6	24.7	7.2

**COIL 5 Test Runs (cont)**

File Name	Date	Start Time	Sequence No.	Run/Test No.	Inlet DB (F)	Inlet DewPt (F)	Air Flow (cfm)	Test Duration (min)	Comp Runtime (min)
coil5_Test_cycling_constant_75_64e.out	12/1/2003	16:16:31	1	51	75.2	64.1	918.5	122.3	61.3
coil5_Test_cycling_constant_75_64e.out	12/1/2003	18:19:03	2	51	75.1	64.1	919.2	122.5	61.5
coil5_Test_cycling_constant_75_64e.out	12/1/2003	20:21:51	3	52	75.2	64.1	924	36.6	30.8
coil5_Test_cycling_constant_75_64e.out	12/1/2003	20:58:45	4	52	75.1	64.1	918.6	36.6	30.7
coil5_Test_cycling_constant_75_64e.out	12/1/2003	21:35:38	5	52	75.1	64.1	918.1	36.6	30.8
coil5_Test_cycling_constant_75_64e.out	12/1/2003	22:12:32	6	53	75.2	64	916.5	23.6	16.4
coil5_Test_cycling_constant_75_64e.out	12/1/2003	22:36:23	7	53	75.2	64	920.4	23.5	16.4
coil5_Test_cycling_constant_75_64e.out	12/1/2003	23:00:12	8	53	75.3	64.1	920.9	23.5	16.4
coil5_Test_cycling_constant_75_64e.out	12/1/2003	23:24:01	9	54	75.3	64	921.4	20.2	10.2
coil5_Test_cycling_constant_75_64e.out	12/1/2003	23:44:29	10	54	75.4	64	920.9	20.2	10.3
coil5_Test_cycling_constant_75_64e.out	12/2/2003	0:04:58	11	54	75.6	64	925.1	20.2	10.2
coil5_Test_cycling_constant_75_64e.out	12/2/2003	0:25:26	12	55	75.5	63.9	926.8	24.8	7.2
coil5_Test_cycling_constant_75_64e.out	12/2/2003	0:50:31	13	55	75.5	63.9	929.6	24.8	7.2
coil5_Test_cycling_constant_75_64e.out	12/2/2003	1:15:34	14	55	75.5	63	929.8	24.8	7.2
coil5_Test_cycling_constant_300b.out	10/15/2003	1:48:04	1	71	80	60.6	672.5	214.6	123
coil5_Test_cycling_constant_300b.out	10/15/2003	5:22:59	2	71	80	60.6	673.3	214.7	123
coil5_Test_cycling_constant_300b.out	10/15/2003	8:57:57	3	72	79.9	60.6	679.5	36.7	30.8
coil5_Test_cycling_constant_300b.out	10/15/2003	9:34:52	4	72	80	60.5	677	36.6	30.8
coil5_Test_cycling_constant_300b.out	10/15/2003	10:11:47	5	72	80	60.6	676.5	36.7	30.8
coil5_Test_cycling_constant_300b.out	10/15/2003	10:48:42	6	73	80	60.6	676.7	23.6	16.4
coil5_Test_cycling_constant_300b.out	10/15/2003	11:12:33	7	73	80	60.6	679.7	23.6	16.4
coil5_Test_cycling_constant_300b.out	10/15/2003	11:36:23	8	73	80	60.6	677.4	23.6	16.4
coil5_Test_cycling_constant_300b.out	10/15/2003	12:00:14	9	74	80	60.6	679.3	20.2	10.3
coil5_Test_cycling_constant_300b.out	10/15/2003	12:20:44	10	74	79.9	60.6	679	20.2	10.2
coil5_Test_cycling_constant_300b.out	10/15/2003	12:41:12	11	74	79.9	60.6	680.3	20.2	10.3
coil5_Test_cycling_constant_300b.out	10/15/2003	13:01:42	12	75	80	60.6	683.8	24.8	7.2
coil5_Test_cycling_constant_300b.out	10/15/2003	13:26:47	13	75	80	60.6	683.4	24.8	7.2
coil5_Test_cycling_constant_300b.out	10/15/2003	13:51:51	14	75	80	60.6	684.2	24.8	7.2
coil5_Test_cycling_autob.out	10/16/2003	15:16:31	1	41	79.9	60.5	916.8	214.9	123.2
coil5_Test_cycling_autob.out	10/16/2003	18:51:42	2	41	80	60.6	912.9	214.8	123.1
coil5_Test_cycling_autob.out	10/16/2003	22:26:44	3	42	80	60.6	908.3	36.7	30.8
coil5_Test_cycling_autob.out	10/16/2003	23:03:40	4	42	80	60.5	907	36.7	30.8
coil5_Test_cycling_autob.out	10/16/2003	23:40:36	5	42	79.8	60.6	909.6	36.7	30.8
coil5_Test_cycling_autob.out	10/17/2003	0:17:33	6	43	80	60.5	903.2	23.6	16.4
coil5_Test_cycling_autob.out	10/17/2003	0:41:24	7	43	80	60.6	903.8	23.6	16.4
coil5_Test_cycling_autob.out	10/17/2003	1:05:14	8	43	80	60.6	904.8	23.6	16.4
coil5_Test_cycling_autob.out	10/17/2003	1:29:04	9	44	80	60.6	895.5	20.2	10.3
coil5_Test_cycling_autob.out	10/17/2003	1:49:33	10	44	80	60.6	894.4	20.2	10.3
coil5_Test_cycling_autob.out	10/17/2003	2:10:03	11	44	80	60.5	892.6	20.2	10.3
coil5_Test_cycling_autob.out	10/17/2003	2:30:33	12	45	80	60.6	884.9	24.8	7.2
coil5_Test_cycling_autob.out	10/17/2003	2:55:37	13	45	80	60.6	888.8	24.8	7.2
coil5_Test_cycling_autob.out	10/17/2003	3:20:40	14	45	80	60.5	886.7	24.8	7.2
coil5_Test_cycling_autob.out	10/17/2003	3:45:44	15	45	80	60.6	891.1	24.8	7.2
coil5_Test_cycling_autob.out	10/17/2003	4:10:48	16	45	80	60.6	887.4	24.8	7.2
coil5_Test_cycling_autob.out	10/17/2003	4:35:52	17	46	80.1	60.7	875.8	61.5	5.7
coil5_Test_cycling_autob.out	10/17/2003	5:37:41	18	46	80.1	60.6	882.7	61.6	5.6
coil5_Test_cycling_autob.out	10/17/2003	6:39:31	19	46	80	60.6	877.4	62	5.7
coil5_Test_cycling_autob.out	10/17/2003	7:41:51	20	46	80	60.5	878.7	62	5.7
coil5_Test_cycling_autob.out	10/17/2003	8:44:11	21	46	80	60.7	879.2	62.1	5.7

## **APPENDIX H6**

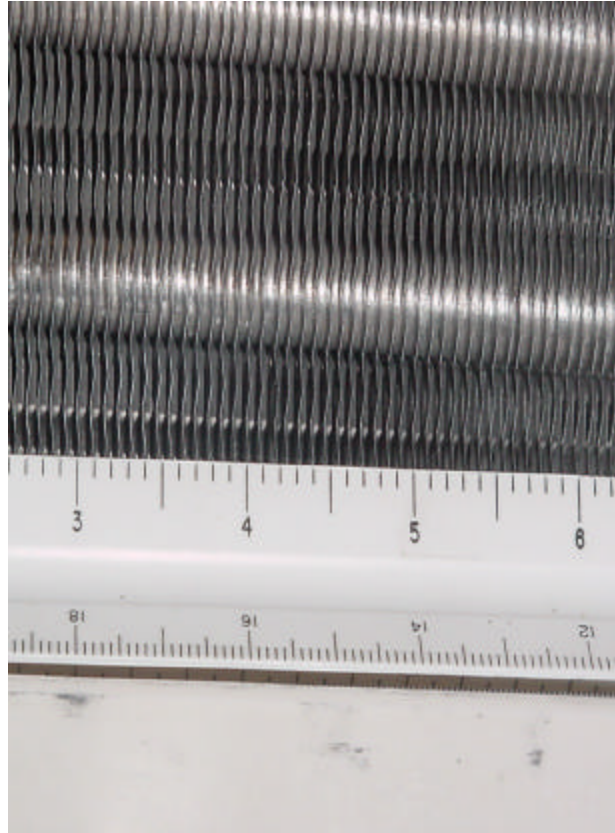
### **Summary of Laboratory Data for Coil 6**



**Summary of Laboratory Data for Coil 6  
November 2005**



A-frame coil arrangement



13 fpi, wavy fin

Manufacturer:	Lennox
Model number:	CB30M-21/26-2P
Nominal size:	1.5 - 2 tons
Baseline Size and Airflow (Test 4):	1.6 tons / 680 cfm
Coil type:	A-frame coil
Coil dimensions:	3 rows, 13 fpi, 3.56 ft <sup>2</sup> total face area 16 in x 16 in total dimension (2 ea.) 3.38 ft <sup>2</sup> open face area (25 in <sup>2</sup> obstruction to air flow)
Coil thickness:	2.5 in
Tube diameter:	3/8 in OD copper
Tube spacing, within row (vert):	1 in
Tube spacing, row-to-row (horiz):	7/8 in
Expansion device:	TXV (12°F superheat)
Unit supply fan:	off
Compressor power:	inverter

**Table 1. Summary of Steady State Test Conditions Corresponding to Each Run or Test**

	<i>Entering Coil Conditions</i>					
	<i>80/67°F 60°F dp</i>	<i>80/72°F 68°F dp</i>	<i>80/62°F 50°F dp</i>	<i>75/68°F 64°F dp</i>	<i>75/63°F 56°F dp</i>	<i>75/58°F 45°F dp</i>
400 cfm/ton	#4 (or 3)	#5	#6	#7	#8	#9
300 cfm/ton	#10	#11	#12	#13	#14	#15
200 cfm/ton	#16	#17	#18	#19	#20	#21
450 cfm/ton	#22	#23	#24			
400-200 cfm/ton (ON & OFF)	#25					
Low suction (50°F)	#1					
High suction (57.5°F)	#2					

Notes: Tests 4-25 all at nominal suction of 53.5°F (set at nominal conditions of test #3/4). A thermal expansion device was used, with nominal superheat of 12°F. The refrigerant charge established during Test 4 was not changed for the remaining tests. The Table 1 test points denote the target testing conditions. Drier test conditions with dew points below 50°F (such as Tests #9, #15, and #21) could not be achieved. In these cases, entering conditions were typically held near 50°F dp. For each test, the compressor is ON for at least 155 minutes and then the compressor is OFF for at least 90 minutes. The booster fan runs continuously for all tests (when the compressor is both ON and OFF).

### **Steady State Performance**

The nominal performance characteristics for this coil (based on steady-state conditions from Run #4 below) are:

Total Capacity:	19.6 MBtu/h (1.6 tons)
Sensible Capacity:	15.3 MBtu/h
Latent Capacity (condensate):	4.3 MBtu/h
Sensible Heat Ratio:	0.78

Latent capacity can be calculated two ways: 1) using dew point readings and air flow, and 2) the condensate flow rate. Figure 1 compares the latent capacity calculated these two ways. The number of each data point corresponds to the test number listed in Table 1. In general, the condensate readings resulted in a slightly lower capacity (probably due to degradation in tipping bucket performance).

Figure 2 shows the trend of steady-state sensible heat ratio (SHR) with relative humidity and airflow rate. The cooling capacities used to calculate SHR in Figure 2 are based on airflow measurements and the psychrometric conditions entering and leaving the cooling coil. This performance map is typical of a cooling coil (i.e., SHR is mostly a function of the entering relative humidity, with some dependence on the air flow rate).

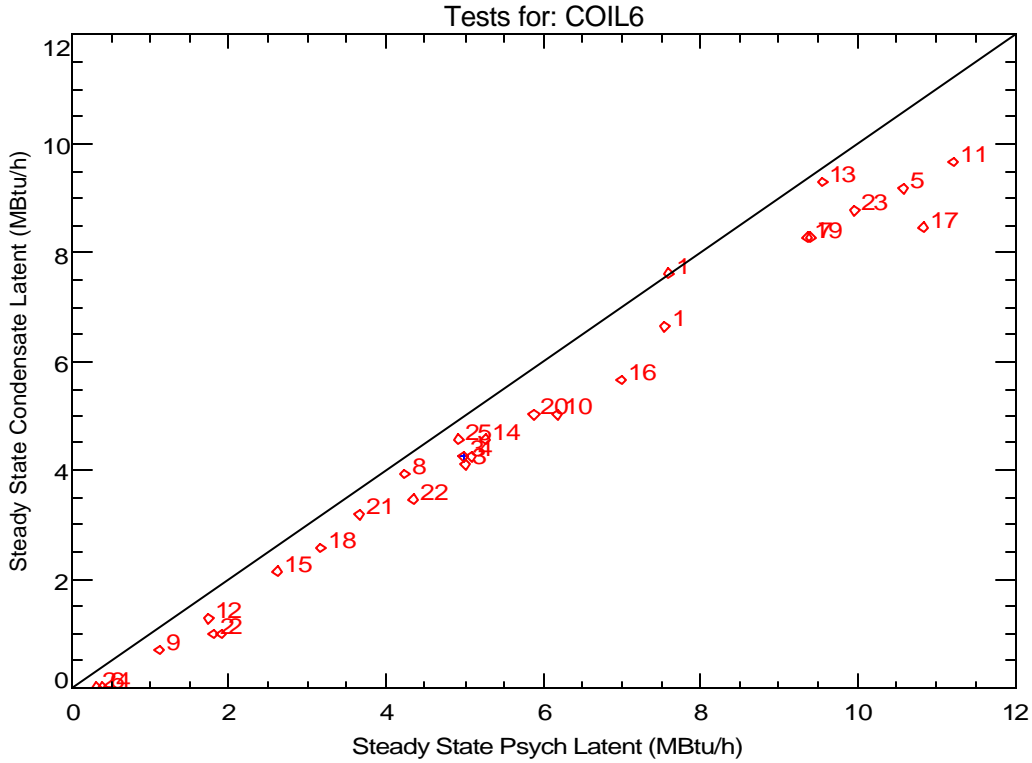


**Figure 1. Comparing Steady-State Latent Capacity Calculated From Psychrometric State Points and Condensate Removal Rates**

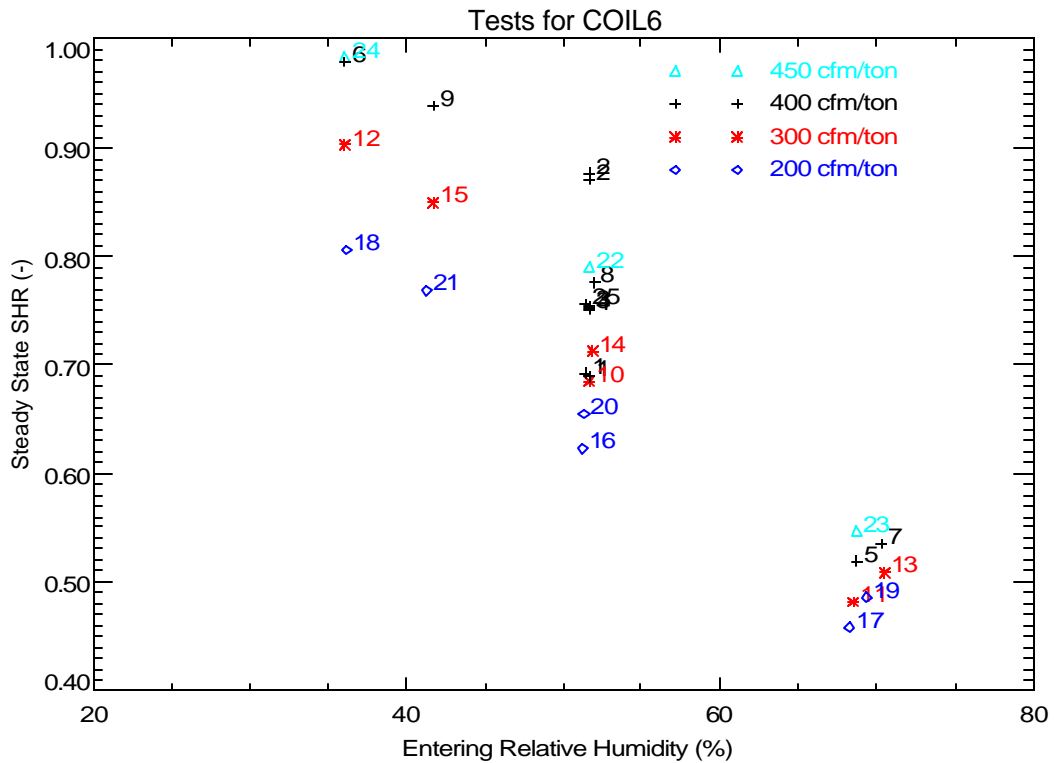


**Figure 2. Variation of Steady State SHR with Entering Humidity and Nominal Air Flow**

## **Typical Transient Performance**

Figure 3 shows the typical transient performance of the cooling coil at nominal conditions (i.e., for Cycle 2 of Run #4). The compressor runs for 155 minutes and is off for 90 minutes. The booster fan remains on during the entire test (separate external fan used to maintain the desired air flow rate across the cooling coil). A portion of the moisture removed by the coil during the compressor on cycle evaporates back into the air stream during the off cycle. During the off cycle the coil acts as an evaporative cooler, so the sensible capacity is nearly equal to the absolute value of the latent capacity (i.e., the sum of latent and sensible is zero).

If we integrate the off cycle sensible capacity (after allowing for a 1-minute off-cycle delay to account for refrigerant movement and other transient effects), we can determine the energy associated with the moisture retained on the coil. To minimize the integration of any measurement errors, the off-cycle integration stops at the time labeled “Integration Pt.” on the plot. This point corresponds to the time when the temperature and dew point differences across the coil have first reached the terminal values (i.e., the averages from the end of the off-cycle). In this case the integration indicates that the sensible cooling is equivalent to 2.66 lbs of moisture being retained on the coil. The integrated latent capacity – which is harder to measure precisely – equals 2.55 lbs.

The value “twet” from Henderson and Rengarajan (1996) can then be calculated by dividing the retained moisture mass (expressed as Btu; mass x 1060 Btu/lb) and the steady state psychrometric latent capacity ( $QL = 5.1 \text{ MBtu/h}$ ). Figure 3 shows that the values of twet based on integrated sensible and latent off-cycle capacity are 33.3 and 31.9 minutes respectively. These values of twet are similar to the measured delay of 33.8 minutes for the first condensate pulse to fall from the drain pan. The value of gamma (1.76), which is the initial off-cycle moisture evaporation rate divided by the steady-state psychrometric latent capacity, uses the off-cycle moisture evaporation rate (9.0 MBtu/h) once the transition point was been detected. For this coil, we detect the transition by determining where the change in off-cycle sensible capacity between each 15-second interval first drops below 3% of the steady-state on cycle sensible capacity (QS). At this transition point where gamma is determined, it is assumed that all coil heat and mass transfer with the air stream is adiabatic (the refrigerant flow could not be used as the indicator to detect this point for this coil). In this case it took 1.28 minutes for the change in off-cycle sensible capacity to drop below 3% of the steady-state on cycle value QS.

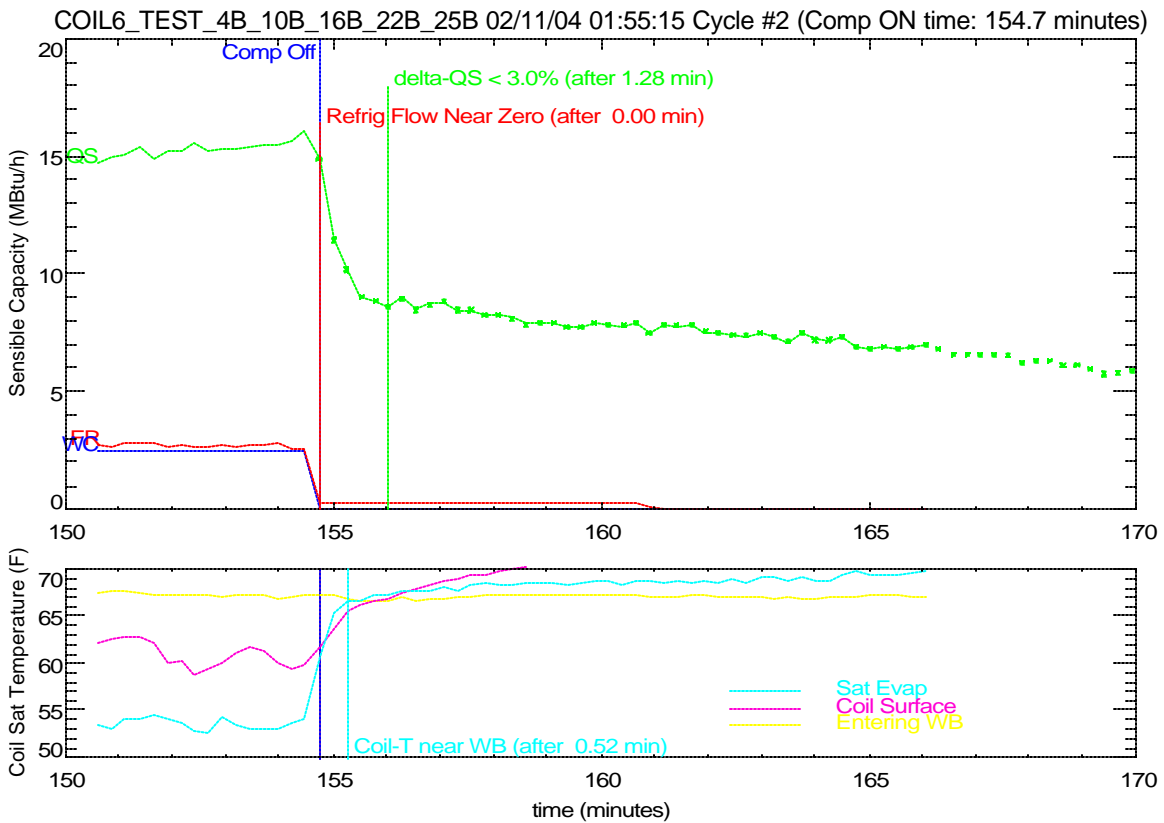
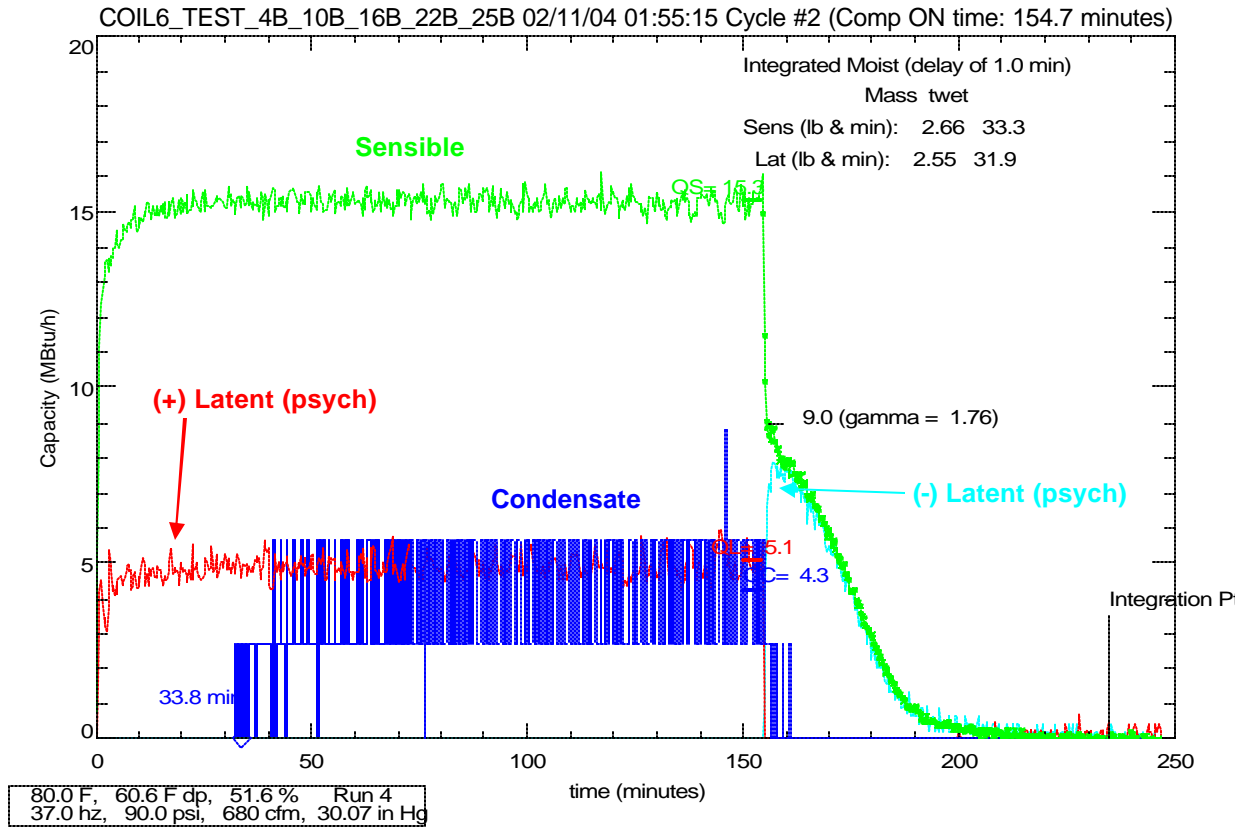
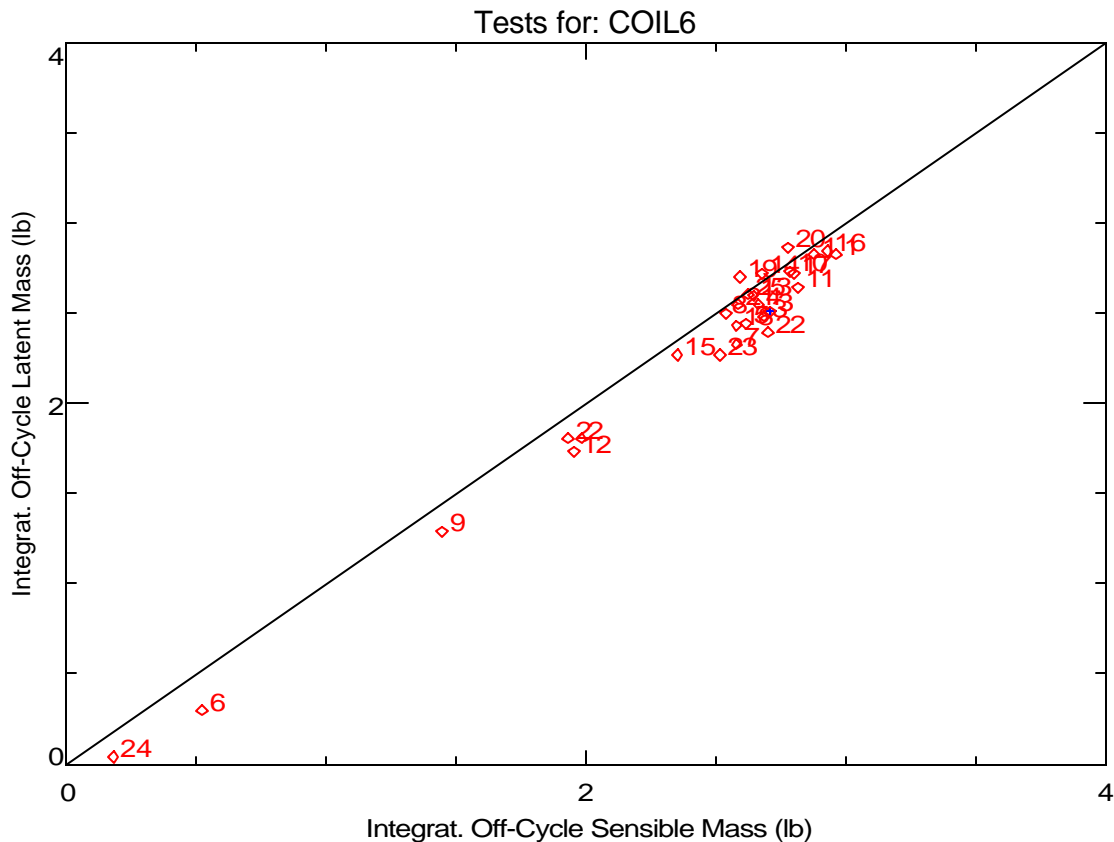


Figure 3. Example Plots of Detailed Data for Coil 6

## Part Load Latent Capacity Parameters

The amount of moisture held on the cooling coil (and drain pan) can be calculated by integrating the off-cycle capacity from the coil (and dividing by the heat of vaporization, 1060 Btu/lb, to get the moisture mass). The integration is delayed for the first minute of the off-cycle so that the overshoot response of the chilled dew point hygrometers does not skew the results of the integration<sup>1</sup>. The integration terminates once steady state conditions are reached for the off cycle. If we assume the coil acts as an evaporative cooler, then sensible and latent capacity should be equal. Figure 4 compares the off-cycle integrated latent and sensible capacity calculated for each run. No systematic bias is evident and Figure 5 shows that any bias is not a function of dew point as was observed for Coil 1.

Since we expect that off-cycle latent and sensible capacity should sum to zero, we have selected the integrated off-cycle sensible capacity as the most consistent and believable indication of the moisture mass held on the cooling coil (and drain pan).



**Figure 4. Comparing Stored Moisture Mass Calculated by Integrating Sensible and Latent Off-Cycle Capacity (Integrated with a 1 minute delay)**

<sup>1</sup>The 1-minute delay causes the estimate of moisture mass to be low by as much as 0.14 lbs (or 5%).

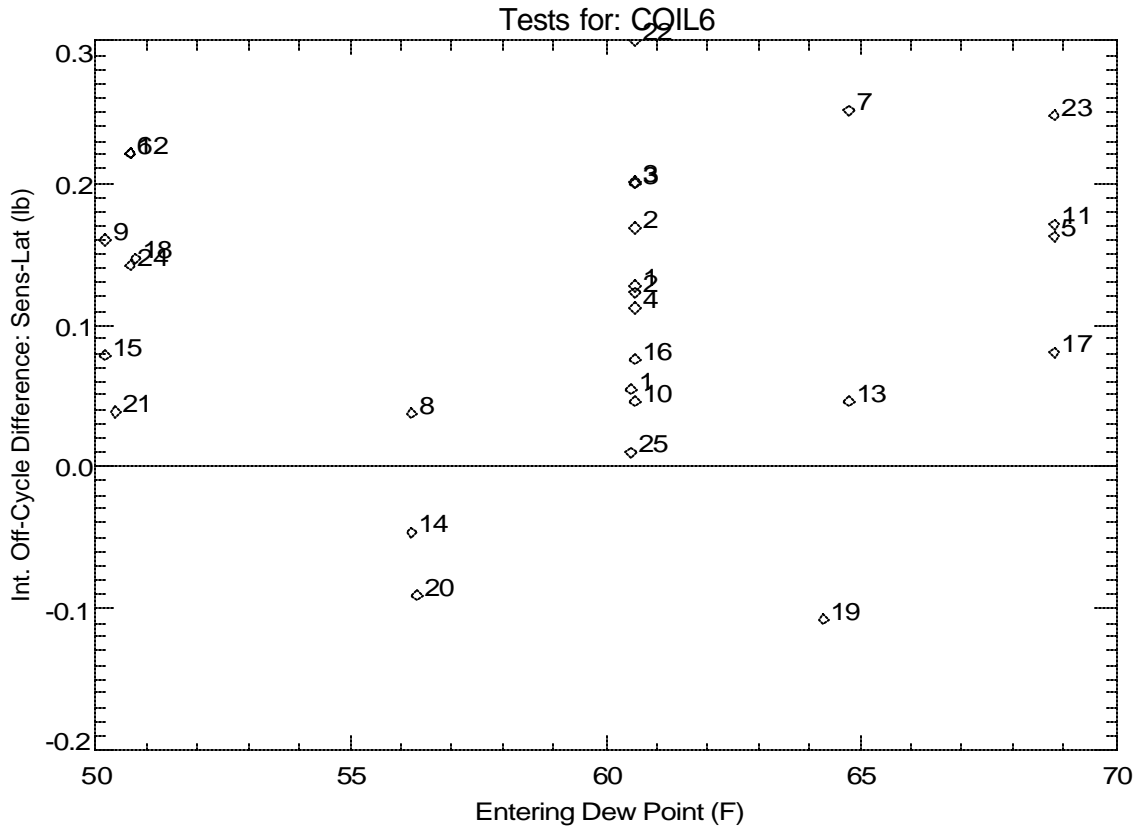


**Figure 5. Variation of Off-Cycle Sensible-Latent Difference with Entering Dew Point**

The parameter “twet” is the moisture mass held on the cooling coil (times the enthalpy of vaporization, 1060 Btu/lb) divided by the steady-state latent capacity of the cooling coil. The parameter should physically correspond to the time it takes for moisture to first fall from the coil (ignoring startup delays and other effects). Figure 6 compares the calculated “twet” (determined from integrating sensible capacity during the off-cycle and then dividing by the steady-state psychrometric latent capacity during the on-cycle) to the condensate delay time for all test runs. In general, there is good agreement between these two values.

Figure 7a and 7b show that both twet and the condensate delay time are a function of the entering dew point temperature. Figure 7b uses different symbols to show the 1<sup>st</sup> and 2<sup>nd</sup> cycles in each test sequence with flow rate of 400 cfm/ton for all tests. The delay time was generally the same for the 1<sup>st</sup> and 2<sup>nd</sup> cycles for this coil, although some difference was seen for tests 8 and 9.

Test 6 registered a single “stray” pulse after 2.3 minutes of coil operation, which explains why this point is an outlier compared to all the other data in Figures 6 and 7.

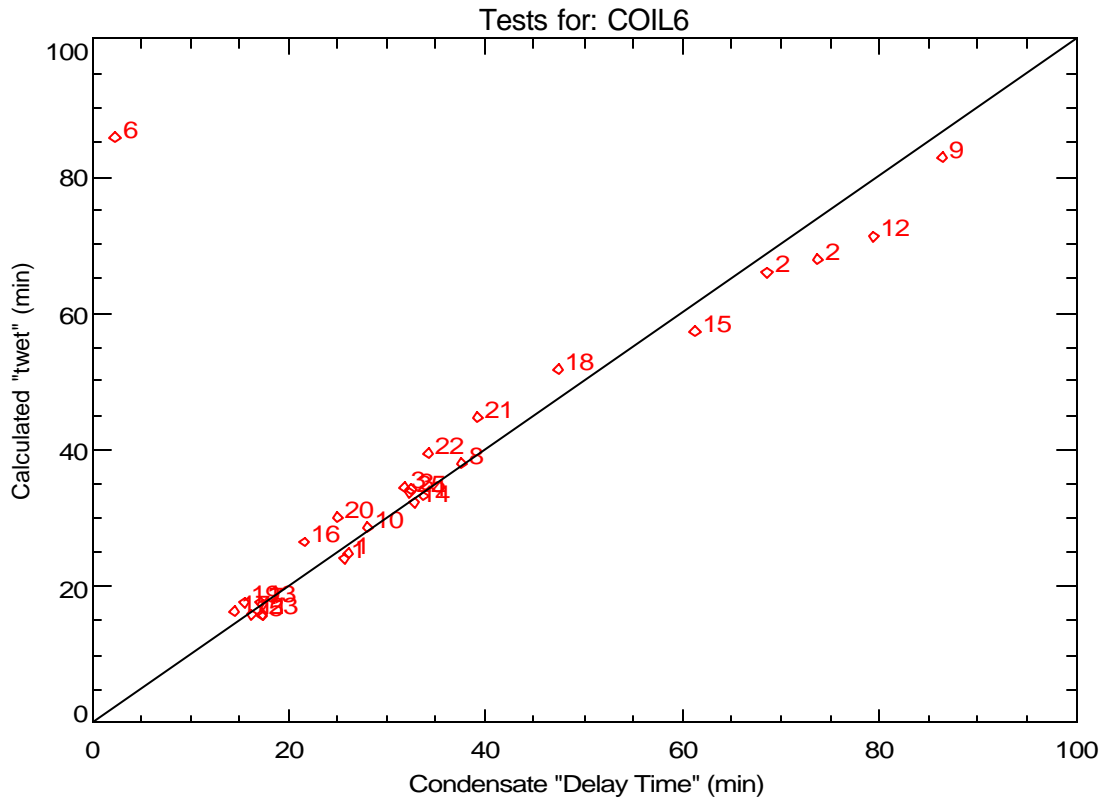


**Figure 6. Comparing “twet” (calculated with off-cycle sensible and steady state latent) to the Condensate Delay Time**



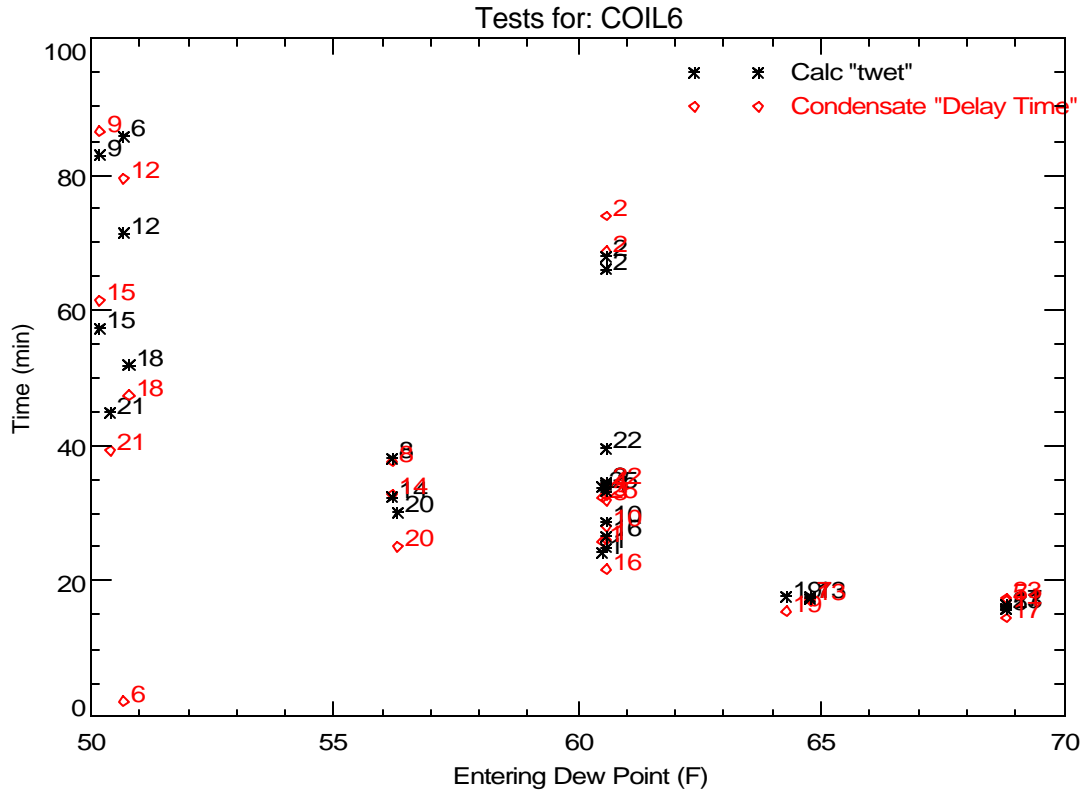


Figure 7a. Impact of Dew Point on “twet” and Condensate Delay Time

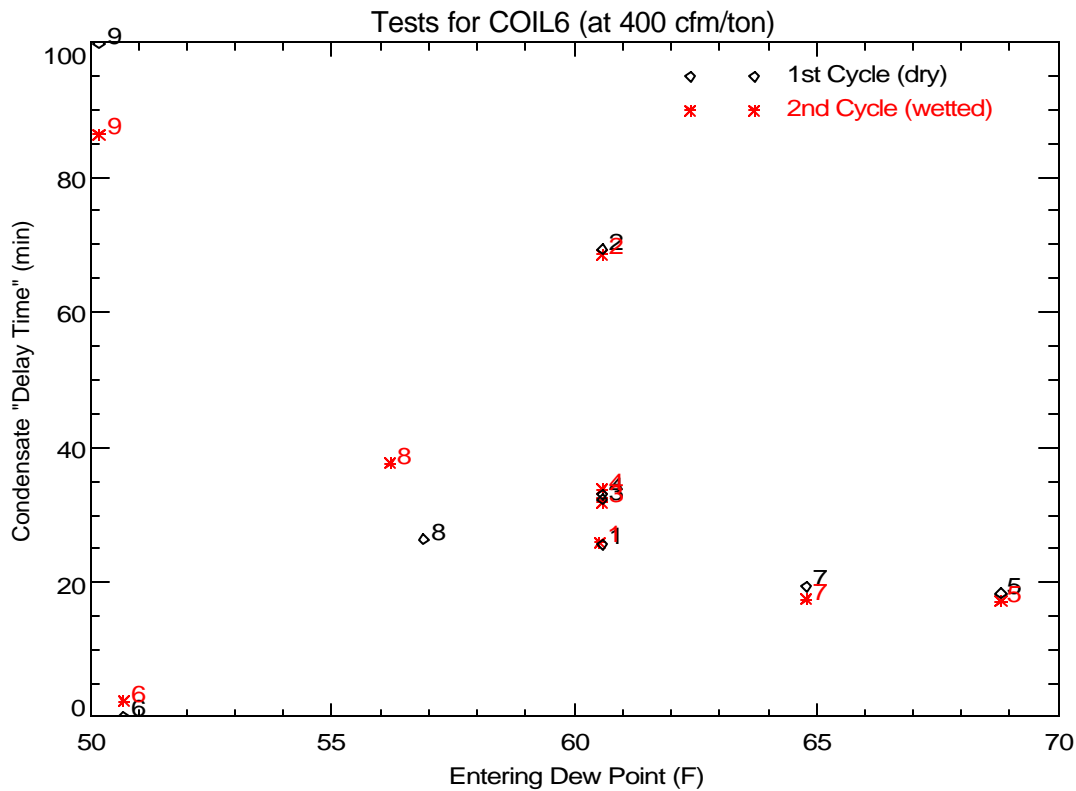


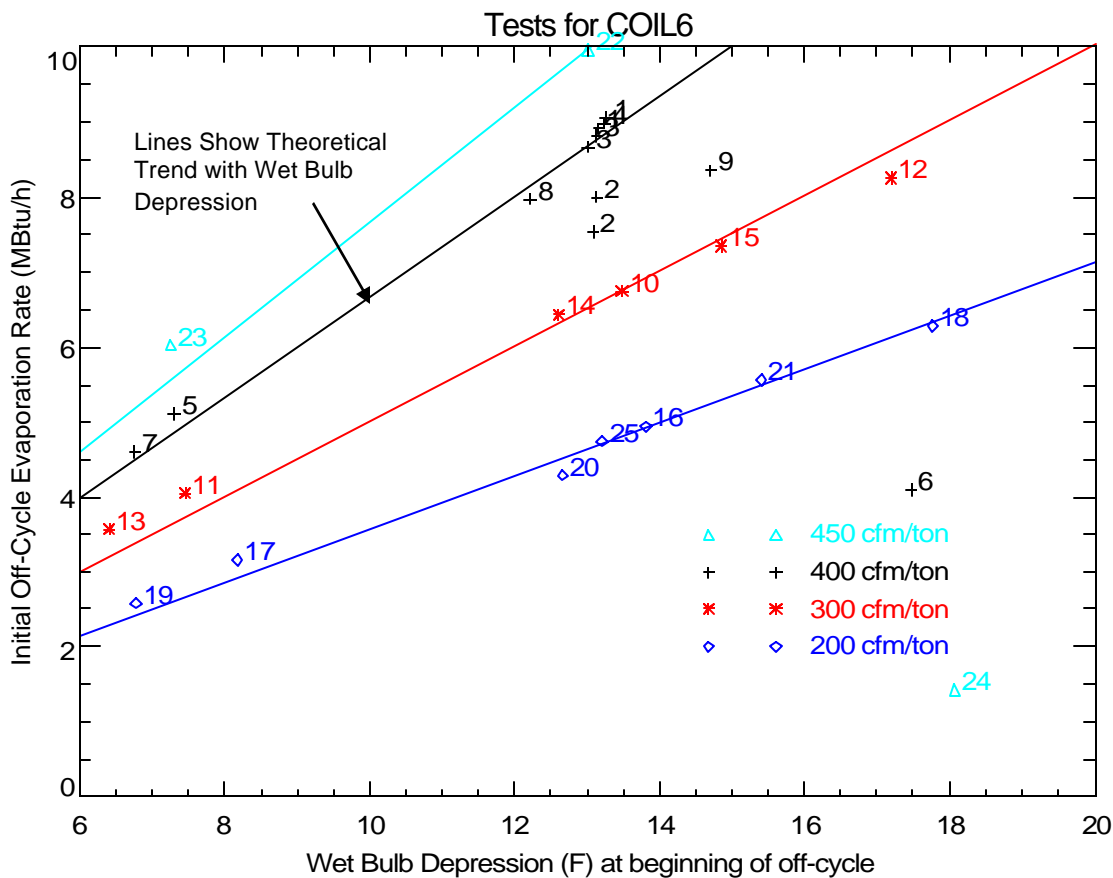
Figure 7b. Impact of Dew Point and Coil Wettedness on Condensate Delay Time

Figure 8 shows the initial off-cycle moisture evaporation rate varies with wet bulb depression. As expected, the evaporation rate is highest when the entering air has a larger wet bulb depression (i.e., has a lower relative humidity) and a higher airflow rate.

The model developed by Henderson and Rengarajan (1996) used the following simple evaporative cooler model to predict the moisture evaporation rate at off-design conditions:

$$Q_{\text{evap}} = Q_{\text{evap}_o} \times \frac{(DB - WB)}{(80 - 67)}$$

where  $Q_{\text{evap}_o}$  is the evaporation rate at the nominal entering air conditions of 80°F dry bulb (DB) and 67°F wet bulb (WB). This simple model is shown as the lines in Figure 8. For each airflow rate, the line is based on the nominal test results at 80°F DB/67°F WB extended to pass through zero. The measured data show essentially the same slope as the theoretical lines. The notable exceptions are the points with higher air flow and drier entering air conditions. Specifically, Tests #6, #9 and #24 deviate significantly from the lines. These runs have a much lower initial moisture evaporation rate because the entering air dew point temperature was close to the cooling coil temperature, so the fin surfaces were not fully wetted (as shown in Figure 4 above). The smaller wetted surface area reduces the initial moisture evaporation rate.



**Figure 8. Measured Variation of Initial Evaporation Rate with Wet Bulb Depression**

Stabat et al. (2001) reviewed the theoretical performance of direct evaporative coolers and showed that the saturation effectiveness of an evaporative cooler is:

$$h_{evp} = 1 - e^{-NTU} \quad \text{where} \quad NTU = K/\text{cfm}^{0.2} \quad \text{for an air-water mixture.}$$

The line shown on Figure 9 is the best fit of the equation above to the measured data. The resulting constant K was 9.99, which is equivalent to an NTU of 2.71 at 680 cfm. While there is some scatter due to the experimental uncertainty of predicting the initial off-cycle moisture evaporation rate, the slope of the line is still representative of the overall trend.

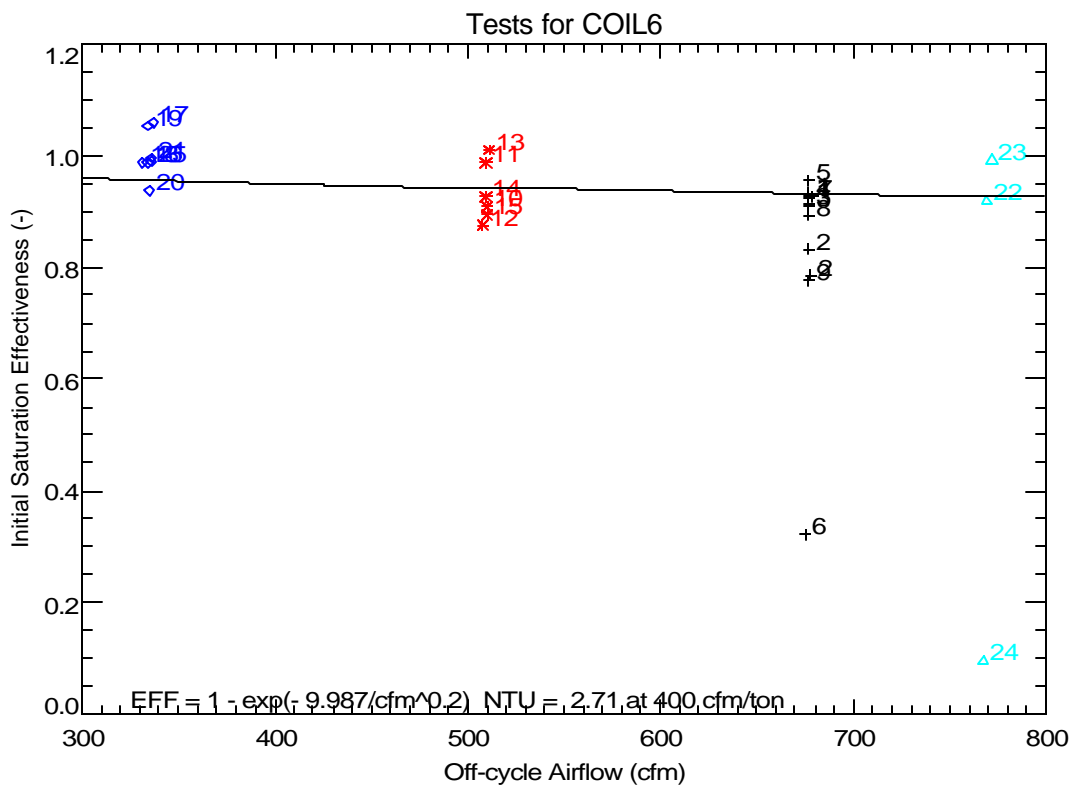


**Figure 9. Evaporative Effectiveness versus Airflow**

Figure 10 compares the measured initial off-cycle moisture evaporation rate for each test to the predicted initial evaporation rate using the effectiveness model above. The model and measured data generally agree when presented in this form (i.e., the overall agreement visually appears better than in Figure 9 above). Again, the variation that occurs for Tests #6, #9 and #24 was due to coil dryout, as mentioned above.

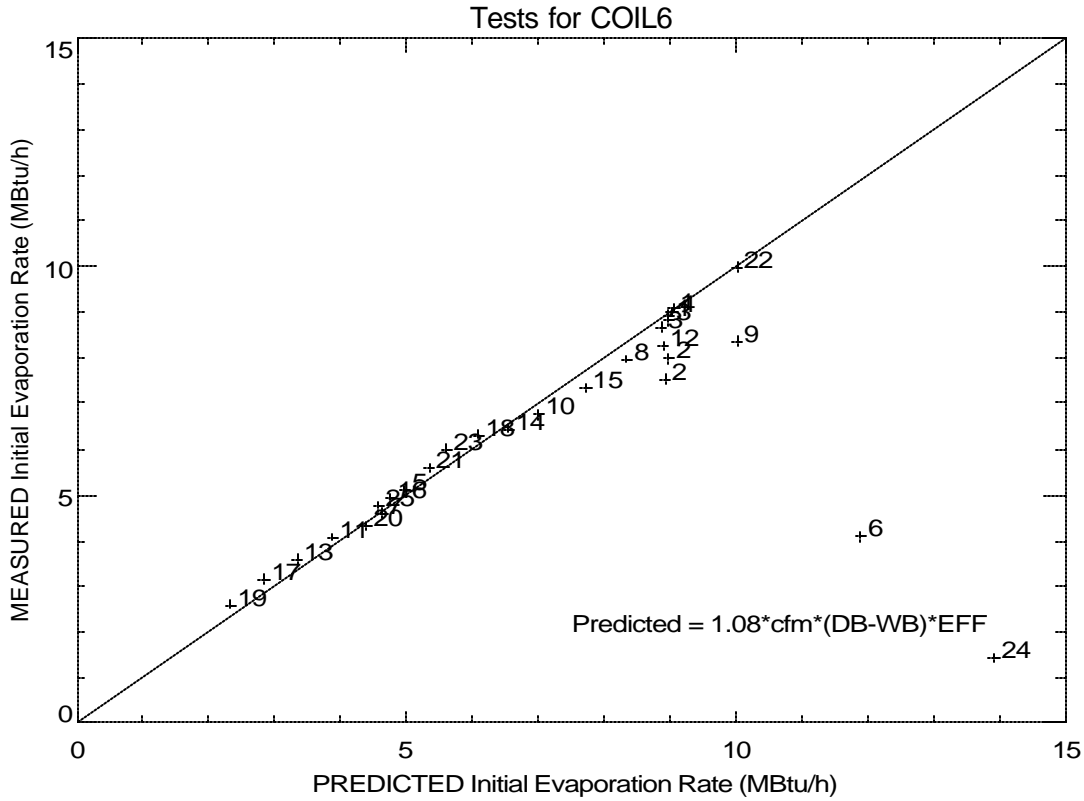


**Figure 10. Comparing Measured and Predicted Initial Moisture Evaporation Rates**

Figure 11 and Figure 12 below evaluate whether the amount of moisture retained on the cooling coil is a function of air flow or entering air conditions. The results for this coil show very little variation at higher dew points (Figure 11). The data also show evidence of coil dryout at low dew points for Tests #6, #9, and #24. For the other test conditions, where the coil surfaces were fully wetted, the amount of retained moisture ranges from 2 to 3 lbs.

Figure 12 shows the expected increase in retained moisture with lower air flow rates. Test 2 with the high refrigerant temperature resulted in a warmer coil with much less moisture retention.

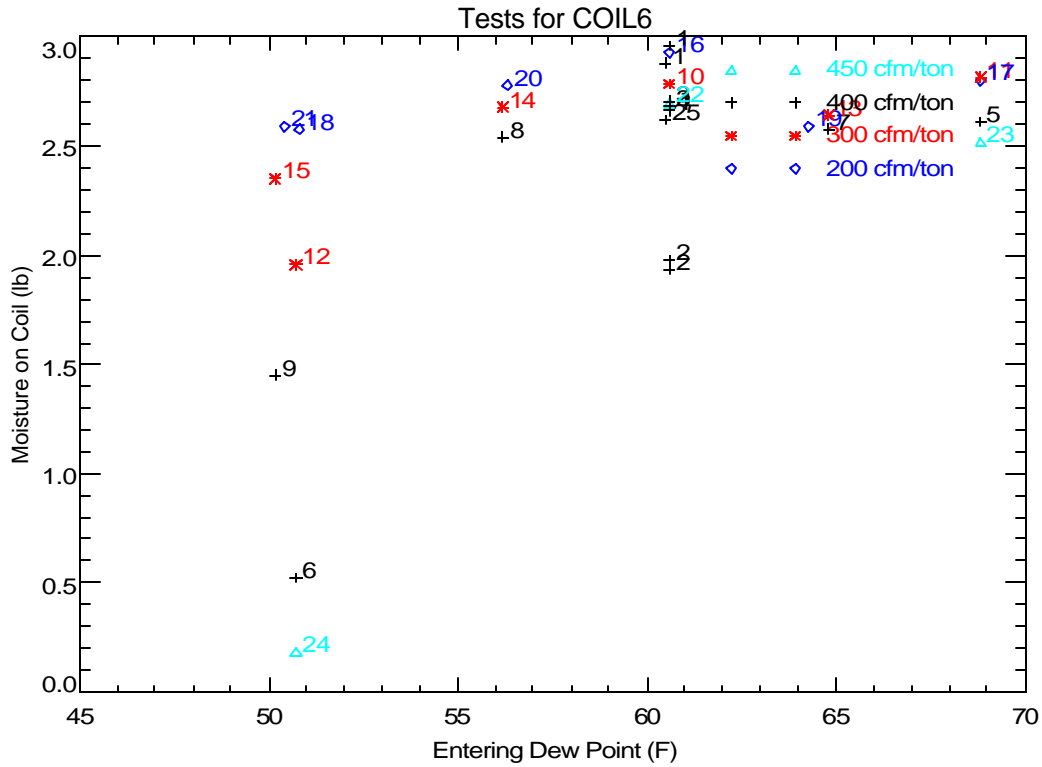


Figure 11. Variation of Retained Moisture (based on Off-Cycle Sensible) with Flow and Dew Point

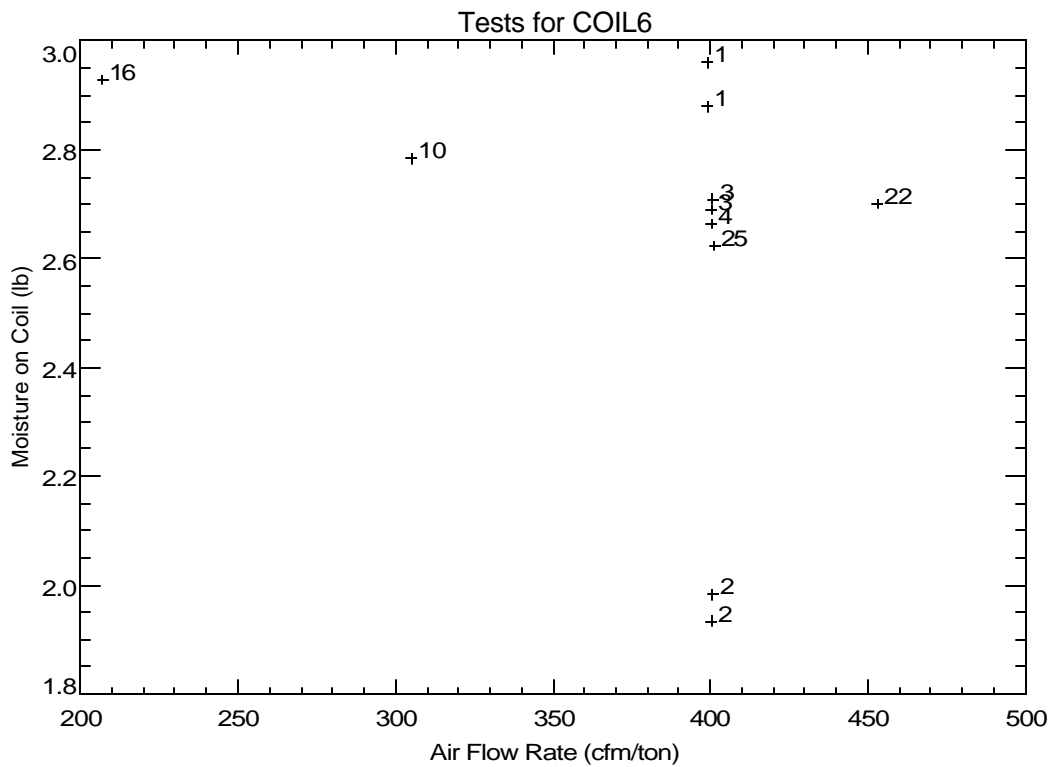
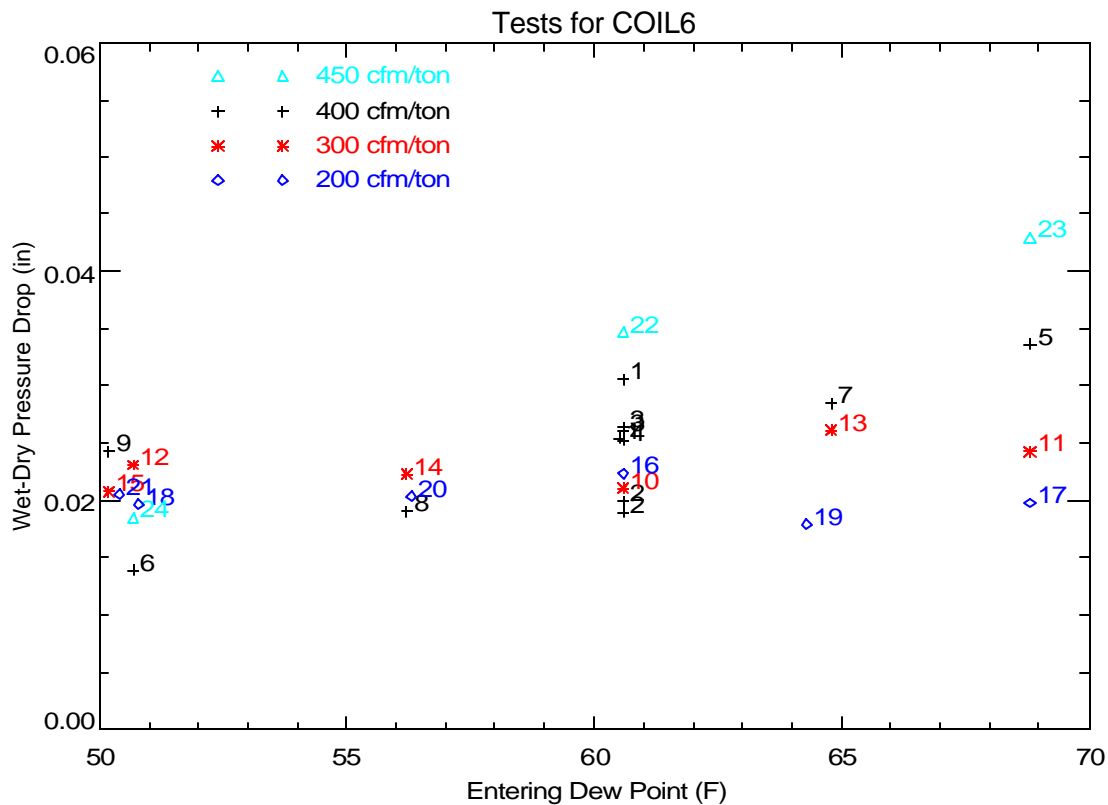


Figure 12. Variation of Retained Moisture with Air Flow at Nominal Entering Conditions of 80°F, 60.4°F dew point

Another way to detect the amount of retained moisture is to measure the static air-side pressure drop across the cooling coil. The difference between the pressure drop across the coil under wet and dry conditions should provide an indication of the amount of retained moisture (the wet coil pressure drop is measured at steady-state conditions while the dry coil pressure drop is taken as the average pressure drop during the last part of the off-cycle). Figure 13 shows the variation of the wet-dry pressure difference with various entering humidity conditions at multiple air flow rates. Comparing the values for each air flow rate generally shows a trend of pressure drops reaching a plateau once the humidity of the entering air is sufficiently high to fully wet the coil. For air flow rates of 200 cfm/ton and 300 cfm/ton, the wet-dry pressure difference remained fairly constant for the range of entering air dew point temperatures that were tested, indicating a fully wetted coil. The wet-dry pressure drops for Tests #6 and #24 are significantly lower than expected, again confirming that less moisture was retained on the cooling coil at these drier/higher air flow conditions.



**Figure 13. Variation of Wet-Dry Pressure Drop with Entering Conditions and Air Flow Rate**

Figure 14 confirms that the wet-dry pressure drop is nearly a linear function of air flow rate, which implies laminar flow in the wetted cooling coil.

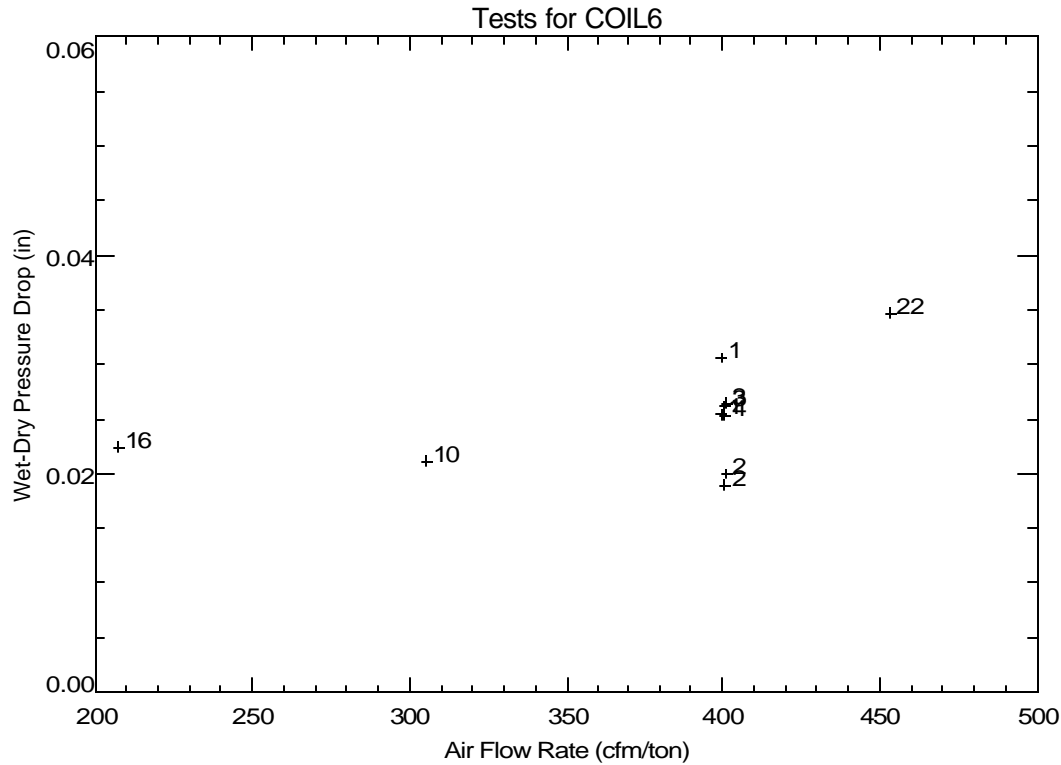


**Figure 14. Trend of Wet-Dry Pressure Drop with Flow at Nominal Entering Conditions of 80° F, 60.4° F dew point**

The series of plots in Figure 15 show the impact of coil suction temperature on performance. The steady-state performance of the system shows the expected trends of lower SHR and greater latent capacity at lower coil temperatures (lower saturated suction temperatures). Like Coil 1 and Coil 3, the plots for moisture on coil and wet-dry pressure drop show that more moisture is retained when the coil is colder.

The graph of fan power versus saturated suction temperature in Figure 15 is not relevant since the AHU fan was turned off during all tests. For this cooling coil, an external booster fan was used to obtain the desired air flow rate for each test.

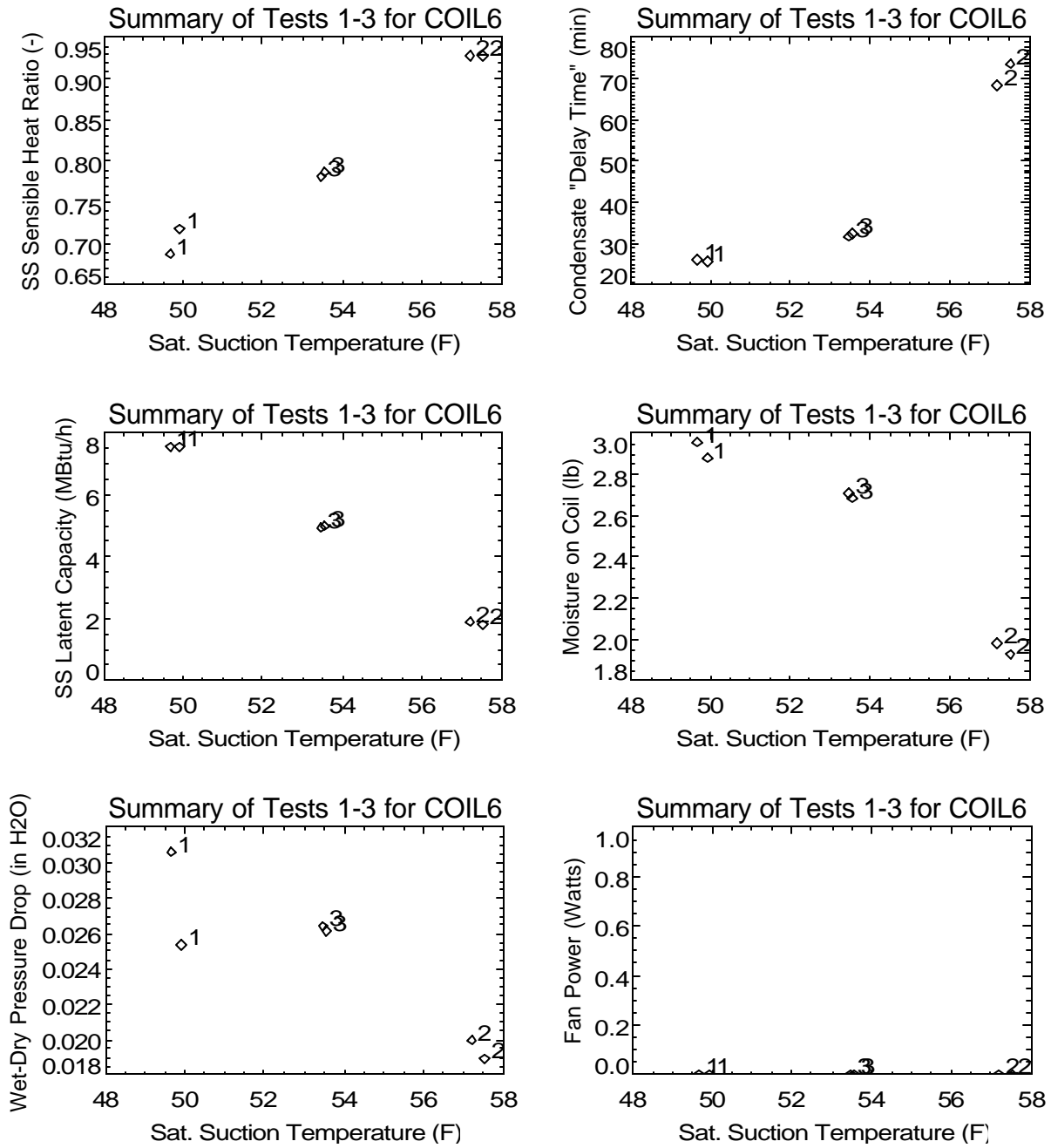


**Figure 15. Trend of Various Parameters with Saturated Suction Temperature**



## Overall Latent Degradation Trends

Several quasi-steady cyclic tests were also completed in the laboratory to quantify the overall part-load degradation of latent capacity. Table 2 lists the cycling test runs. These conditions correspond to a conventional thermostat with a maximum cycle rate of 3 cycles per hour (at 50% runtime).

**Table 2. Cyclic Test Conditions**

CONST FAN <sup>1</sup>	AUTO FAN <sup>2</sup>	Number of Times Test Repeated <sup>3</sup>	ON Time (minutes)	OFF Time (minutes)	Runtime Fraction (-)	Cycle Rate (cycles/h)
Run						
31	41	2	45	45	0.500	0.667
32	42	4, 3	30	6	0.833	1.667
33	43	3	16	7.25	0.688	2.581
34	44	3	10	10	0.500	3.000
35	45	3, 5	7	17.5	0.286	2.449
	46	5	5.5	55	0.091	0.992

Notes: <sup>1</sup>Constant fan tests performed at 80°F db/60.4°F dp inlet air with 400 cfm/ton (runs 31-35) and 300 cfm/ton (runs 71-75) air flow. Tests also conducted at 75°F db/56°F dp (runs 61-65) and 75°F db/64°F dp (runs 51-55) inlet air with 400 cfm/ton air flow.

<sup>2</sup>Auto fan tests performed at 80°F db/60.4°F dp inlet air with 400 cfm/ton air flow.

<sup>3</sup>Tests repeated 5 times for runs 45 & 46. Tests repeated 4 times for runs 32, 62 and 72

Figure 16 through Figure 19 show the net impact of part-load unit operation based on cyclic tests completed in the lab. All of these tests are in the constant fan mode (continuous air flow over the cooling coil while the coil cycles on/off), but at various entering air and flow rate conditions:

- Nominal: 80°F & 60.4°F dew pt. with 400 cfm/ton (Figure 16)
- Humid: 75°F & 64°F dew pt. with 400 cfm/ton (Figure 17)
- Dry: 75°F & 56°F dew pt. with 400 cfm/ton (Figure 18)
- Low Flow: 80°F & 60.4°F dew pt. with 300 cfm/ton (Figure 19)

The measured data generally compare well to the model from Henderson and Rengarajan (1996) using the model parameters shown on each plot. These parameters were always taken from the 2<sup>nd</sup> occurrence of the first test in each sequence (i.e., Tests #31, 51, 61 and 71), which were completed as part of the suite of cycling tests listed in Table 2 for the constant fan mode. The latent time constant ( $\tau$ ) of 20 seconds was selected based on qualitative observations of the coil's response time. The solid black line corresponds to the linear off-cycle evaporation model. The black dotted line assumes an off-cycle evaporation trend that corresponds to an exponential decay. The purple line is the new part load LHR model that uses the more realistic evaporation model from Stabat et al. (2001) and also allows for variable amounts of moisture on the coil at the end of the on cycle. The parameters NTU and  $t_p$  were determined from the specific measured data from each test sequence (the purple solid line) as well as the average NTU and  $t_p$  from all the data (the purple dotted line), including Figure 9 above. The parameter  $t_p$  is defined in the improved model development section of this report.

The measured data corresponding to the last repetitions (cycles) of each test showed the best agreement with the models, since quasi-steady conditions had been achieved.

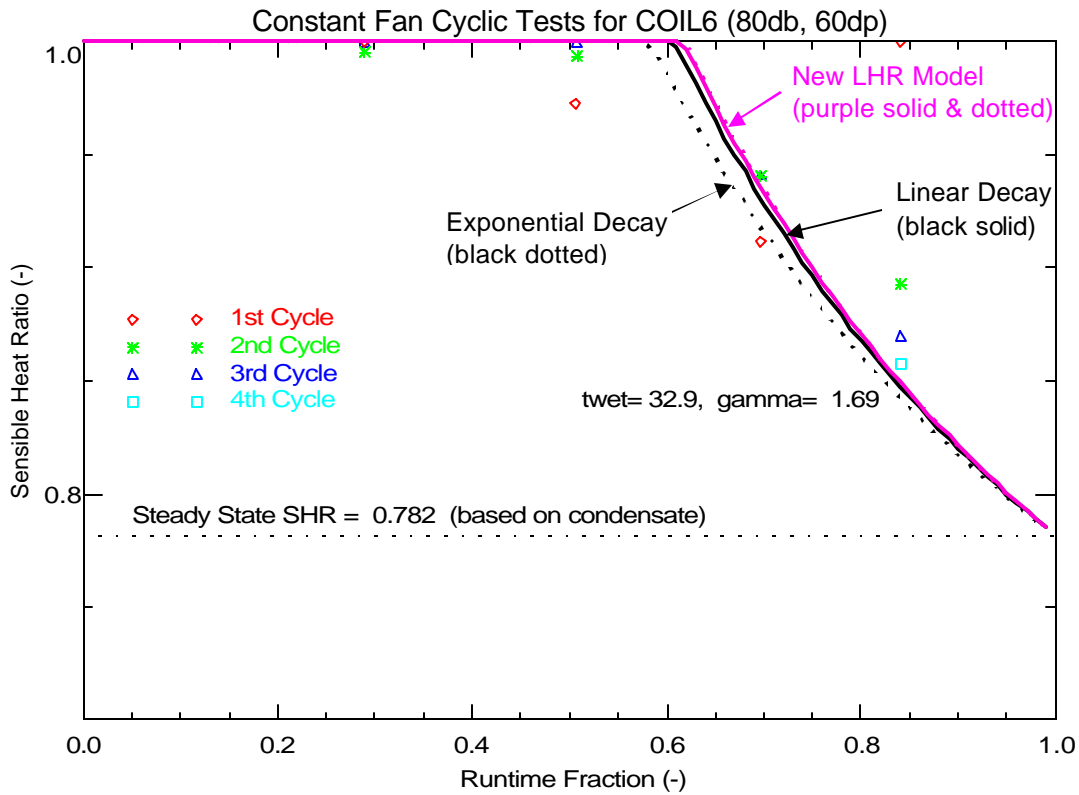


Figure 16. Comparing Measured Latent Degradation to the LHR Models: Nom. Conditions (80°F / 60.4°Fdp)

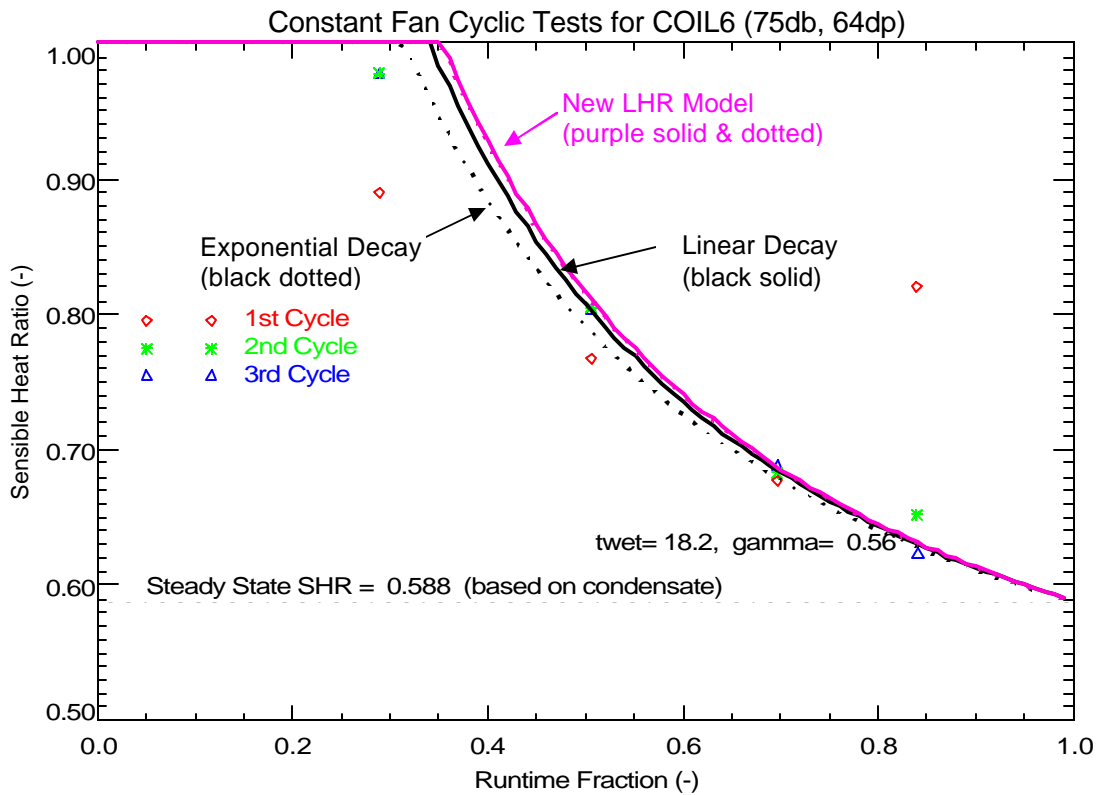


Figure 17. Comparing Measured Latent Degradation to the LHR Models: (75°F / 64°Fdp)

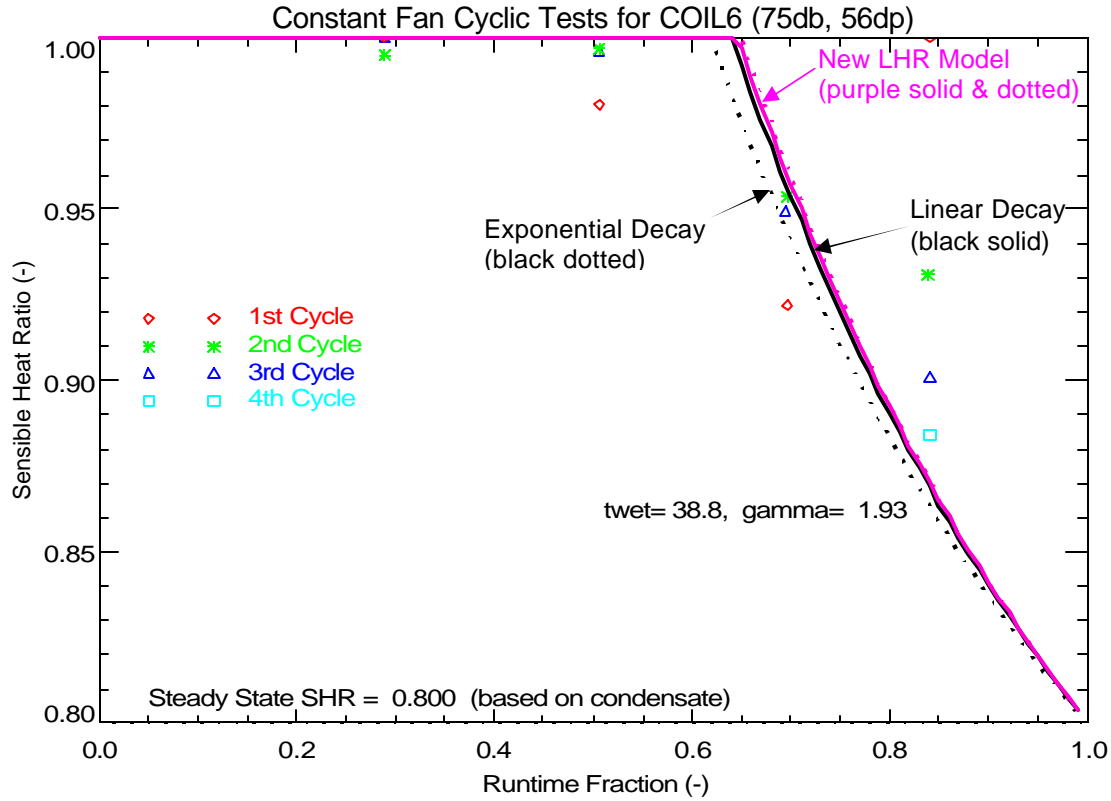


Figure 18. Comparing Measured Latent Degradation to the LHR Models: (75°F / 56°Fdp)

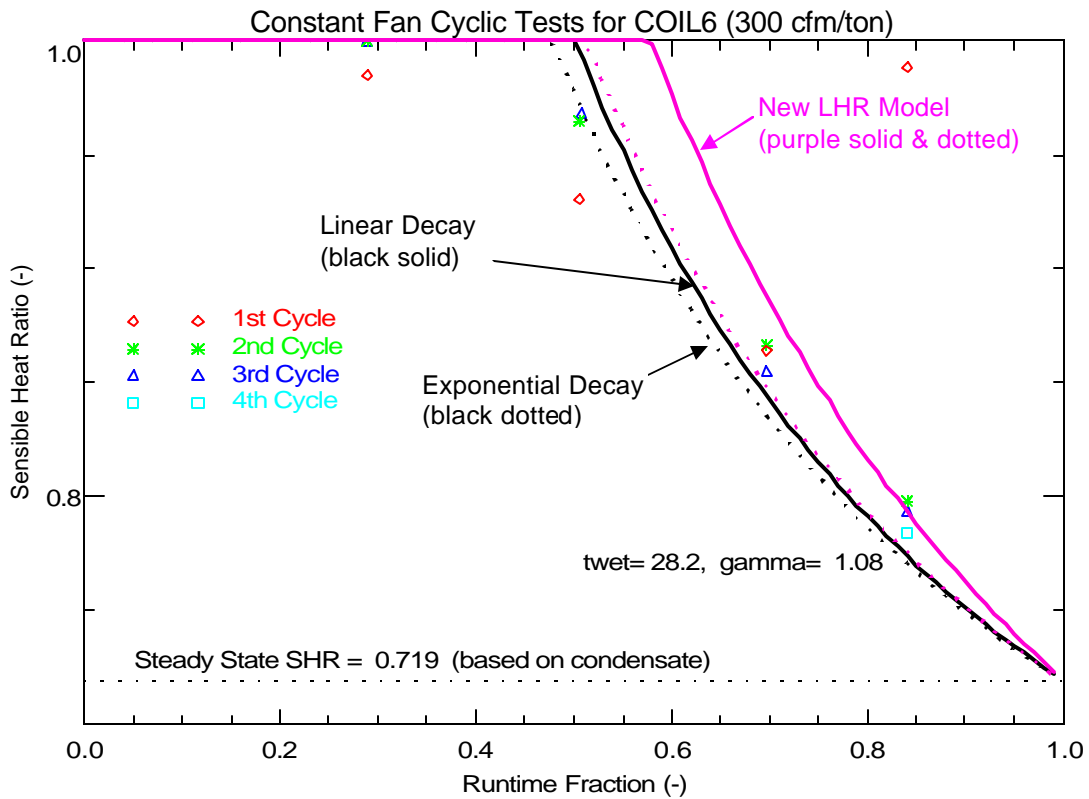
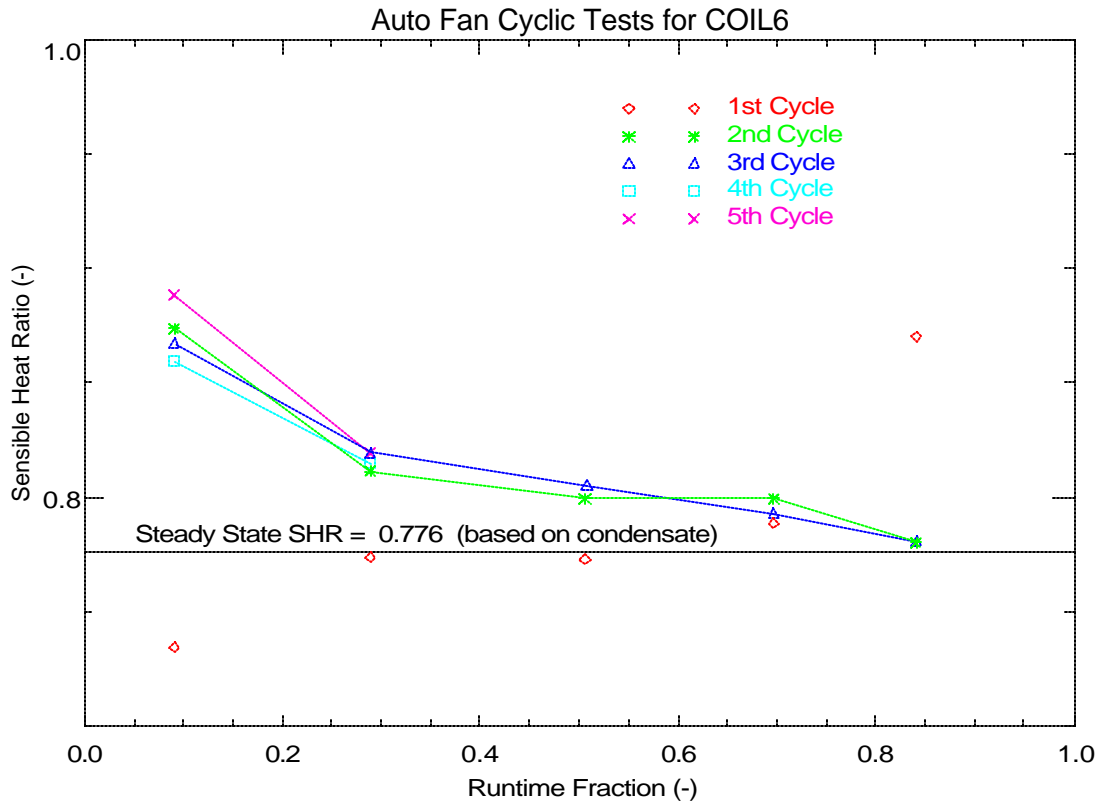


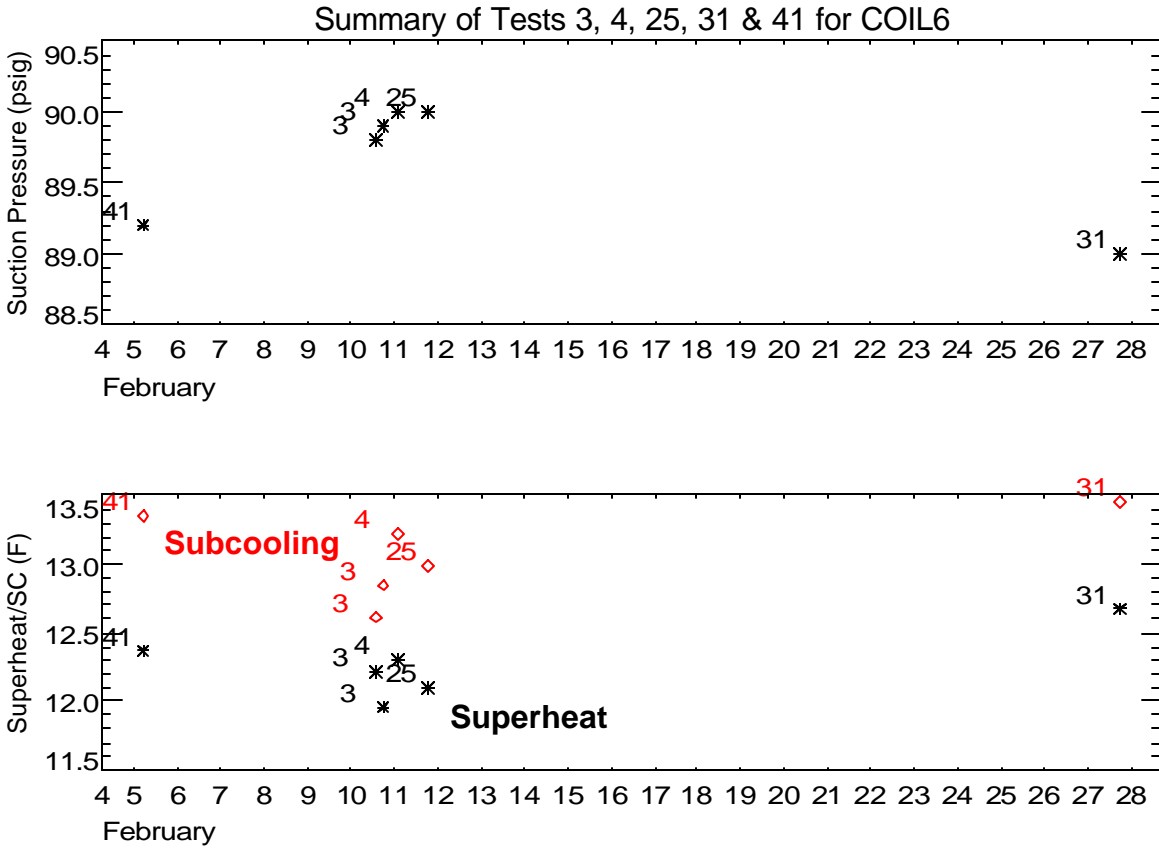
Figure 19. Comparing Measured Latent Degradation to the LHR Models: 300 cfm/ton, 80°F / 60.4°Fdp

Figure 20 shows some latent degradation can be detected in the AUTO fan mode (i.e., the supply air flow across the cooling coil starts and stops with compressor operation) for Coil 6 (similar degradation has been seen for other coils). For this coil the number of repeated cycles at low runtime fractions was increased to 5 to ensure quasi-steady conditions are achieved. The last repetitions (cycles) show good agreement with each other.



**Figure 20. Measured AUTO Fan Latent Degradation**

The tests were completed over a period of 4 weeks. Figure 21 shows little evidence of a change in suction pressure, subcooling or superheat over the test period. This implies that no significant loss of refrigerant charge occurred over the period.



**Figure 21. Long-Term Variation in Suction Pressure, Superheat and Subcooling**

**References**

Henderson, H., and K. Rengarajan. 1996. A model to predict the latent capacity of air conditioners and heat pumps at part-load conditions with constant fan operation. *ASHRAE Transactions* 102(1): 266-274.

Stabat, P., Marchio, D. and M. Orphelin. 2001. Pre-Design and Design Tools for Evaporative Cooling. *ASHRAE Transactions* 107 (1): 501-510.

**COIL 6 Test Runs**

File Name	Date	Start Time	Sequence No.	Run/Test No.	Inlet DB (F)	Inlet DewPt (F)	Air Flow (cfm)	Test Duration (min)	Comp Runtime (min)
coil6_test_1.out	3/1/2004	18:46:50	1	1	80	60.6	679.3	247.1	154.8
coil6_test_1.out	3/1/2004	22:54:15	2	1	80	60.5	679.3	247	154.7
coil6_test_1.out	3/2/2004	3:01:30	3	1	80	60.6	678.9	247	154.7
coil6_test_2.out	3/2/2004	12:18:29	1	2	80	60.6	682.5	324.5	232.3
coil6_test_2.out	3/2/2004	17:43:16	2	2	80	60.6	681.9	324.6	232.4
coil6_test_2.out	3/2/2004	23:08:09	3	2	80	60.6	681.1	324.5	232.4
coil6_test_3c.out	2/10/2004	9:25:40	1	3	80	60.6	682.7	247.1	154.9
coil6_test_3c.out	2/10/2004	13:33:03	2	3	80	60.6	681.9	247.1	154.9
coil6_test_3c.out	2/10/2004	17:40:28	3	3	80	60.6	680.8	247.2	154.9
coil6_Test_4b_10b_16b_22b_25b.out	2/10/2004	21:47:56	1	4	80.1	60.6	681.6	247.1	154.8
coil6_Test_4b_10b_16b_22b_25b.out	2/11/2004	1:55:15	2	4	80	60.6	680.4	247	154.8
coil6_Test_4b_10b_16b_22b_25b.out	2/11/2004	6:02:31	3	10	80	60.6	519.2	247.1	154.8
coil6_Test_4b_10b_16b_22b_25b.out	2/11/2004	10:09:53	4	16	80.2	60.6	352.1	247.1	154.9
coil6_Test_4b_10b_16b_22b_25b.out	2/11/2004	14:17:17	5	22	80	60.6	770.6	247.1	154.8
coil6_Test_4b_10b_16b_22b_25b.out	2/11/2004	18:24:39	6	25	80	60.5	682.3	247.1	154.9
coil6_Test_5d_11d_17d_23d.out	2/26/2004	14:39:10	1	5	80.1	68.8	676.5	247.5	155
coil6_Test_5d_11d_17d_23d.out	2/26/2004	18:46:56	2	5	80	68.8	679.1	247.5	155
coil6_Test_5d_11d_17d_23d.out	2/26/2004	22:54:42	3	11	80.1	68.8	518.9	278.4	155.1
coil6_Test_5d_11d_17d_23d.out	2/27/2004	3:33:24	4	17	80.2	68.8	349.9	299	155
coil6_Test_5d_11d_17d_23d.out	2/27/2004	8:32:39	5	23	80	68.8	768.9	247.5	155.1
coil6_Test_6c_12c_18c_24c.out	2/19/2004	12:47:06	1	6	80.1	50.7	684.3	247.8	155.3
coil6_Test_6c_12c_18c_24c.out	2/19/2004	16:55:08	2	6	80	50.7	682.8	247.9	155.4
coil6_Test_6c_12c_18c_24c.out	2/19/2004	21:03:19	3	12	80	50.7	520.2	248	155.4
coil6_Test_6c_12c_18c_24c.out	2/20/2004	1:11:34	4	18	80	50.8	348.8	247.9	155.4
coil6_Test_6c_12c_18c_24c.out	2/20/2004	5:19:45	5	24	80	50.7	772.8	247.9	155.4
coil6_Test_7c_13c_19c.out	2/23/2004	9:57:59	1	7	75.1	64.8	678.8	248	155.5
coil6_Test_7c_13c_19c.out	2/23/2004	14:06:13	2	7	75.1	64.8	678.3	248.1	155.5
coil6_Test_7c_13c_19c.out	2/23/2004	18:14:32	3	13	75	64.8	513.7	278.9	155.5
coil6_Test_7c_13c_19c.out	2/23/2004	22:53:44	4	19	75	64.3	348.4	299.4	155.4
coil6_Test_8b_14b_20b.out	2/14/2004	8:19:53	1	8	75	56.9	681.2	247.3	155
coil6_Test_8b_14b_20b.out	2/14/2004	12:27:25	2	8	75	56.2	682.1	247.1	154.9
coil6_Test_8b_14b_20b.out	2/14/2004	16:34:49	3	14	75.1	56.2	518.9	247	154.8
coil6_Test_8b_14b_20b.out	2/14/2004	20:42:07	4	20	75.5	56.3	351.5	247.2	154.9
coil6_Test_9b_15b_21b.out	2/16/2004	10:16:50	1	9	75	50.2	684.5	247	154.8
coil6_Test_9b_15b_21b.out	2/16/2004	14:24:06	2	9	75	50.2	683.1	247.1	154.9
coil6_Test_9b_15b_21b.out	2/16/2004	18:31:29	3	15	75	50.2	521.7	247	154.7
coil6_Test_9b_15b_21b.out	2/16/2004	22:38:44	4	21	75.5	50.4	353.6	247	154.8
coil6_test_cycling_constantb.out	2/27/2004	13:21:48	1	31	80	60.7	681.3	247.3	155
coil6_test_cycling_constantb.out	2/27/2004	17:29:19	2	31	80	60.5	681.4	216.1	123.9
coil6_test_cycling_constantb.out	2/27/2004	21:05:45	3	32	80	60.6	682.9	36.9	31
coil6_test_cycling_constantb.out	2/27/2004	21:42:54	4	32	79.9	60.6	682.9	36.9	31
coil6_test_cycling_constantb.out	2/27/2004	22:20:04	5	32	79.9	60.6	680.8	36.9	31
coil6_test_cycling_constantb.out	2/27/2004	22:57:15	6	32	79.9	60.6	680.6	36.9	31
coil6_test_cycling_constantb.out	2/27/2004	23:34:24	7	33	79.8	60.6	681.2	23.7	16.5
coil6_test_cycling_constantb.out	2/27/2004	23:58:24	8	33	79.7	60.4	680.5	23.7	16.5
coil6_test_cycling_constantb.out	2/28/2004	0:22:24	9	33	79.8	60.5	683.3	23.7	16.5
coil6_test_cycling_constantb.out	2/28/2004	0:46:23	10	34	79.7	60.1	684.5	20.4	10.3
coil6_test_cycling_constantb.out	2/28/2004	1:07:01	11	34	79.7	60.6	683.7	20.4	10.3
coil6_test_cycling_constantb.out	2/28/2004	1:27:39	12	34	79.7	60.5	683.6	20.4	10.3
coil6_test_cycling_constantb.out	2/28/2004	1:48:17	13	35	79.6	60.6	686.2	25	7.2
coil6_test_cycling_constantb.out	2/28/2004	2:13:30	14	35	79.8	60.3	685.7	25	7.2
coil6_test_cycling_constantb.out	2/28/2004	2:38:45	15	35	79.9	60.6	684.8	25	7.2
coil6_test_cycling_constant_75_56b.out	2/28/2004	16:15:03	1	61	75.2	56.3	681.3	216.1	123.8
coil6_test_cycling_constant_75_56b.out	2/28/2004	19:51:26	2	61	75	56.2	682.1	216.1	123.9
coil6_test_cycling_constant_75_56b.out	2/28/2004	23:27:52	3	62	75	56.2	683.1	36.9	31
coil6_test_cycling_constant_75_56b.out	2/29/2004	0:05:04	4	62	74.9	56.3	682.6	36.9	31
coil6_test_cycling_constant_75_56b.out	2/29/2004	0:42:13	5	62	74.9	56.3	681.6	36.9	31
coil6_test_cycling_constant_75_56b.out	2/29/2004	1:19:25	6	62	74.9	56.3	682.7	36.9	31
coil6_test_cycling_constant_75_56b.out	2/29/2004	1:56:33	7	63	74.9	56.3	682.7	23.8	16.5
coil6_test_cycling_constant_75_56b.out	2/29/2004	2:20:34	8	63	74.9	56.3	683	23.7	16.5
coil6_test_cycling_constant_75_56b.out	2/29/2004	2:44:34	9	63	74.9	56.3	683.6	23.8	16.5
coil6_test_cycling_constant_75_56b.out	2/29/2004	3:08:35	10	64	74.8	56.4	683.5	20.4	10.3
coil6_test_cycling_constant_75_56b.out	2/29/2004	3:29:14	11	64	74.8	56.2	686.3	20.4	10.3
coil6_test_cycling_constant_75_56b.out	2/29/2004	3:49:53	12	64	74.8	56.2	682.4	20.4	10.3
coil6_test_cycling_constant_75_56b.out	2/29/2004	4:10:30	13	65	74.8	56.4	687.4	25	7.2
coil6_test_cycling_constant_75_56b.out	2/29/2004	4:35:44	14	65	74.9	56.2	684.3	25	7.2
coil6_test_cycling_constant_75_56b.out	2/29/2004	5:00:59	15	65	75	56.2	683.8	25	7.2

**COIL 6 Test Runs (cont)**

File Name	Date	Start Time	Sequence No.	Run/Test No.	Inlet DB (F)	Inlet DewPt (F)	Air Flow (cfm)	Test Duration (min)	Comp Runtime (min)
coil6_test_cycling_constant_75_64b.out	2/25/2004	10:39:34	1	51	76.5	64.1	677.8	248.3	155.6
coil6_test_cycling_constant_75_64b.out	2/25/2004	14:48:08	2	51	75.4	64.2	677.4	217.2	124.5
coil6_test_cycling_constant_75_64b.out	2/25/2004	18:25:36	3	52	75.4	64.1	680	37	31.1
coil6_test_cycling_constant_75_64b.out	2/25/2004	19:02:55	4	52	75.2	64.1	678.7	37.1	31.1
coil6_test_cycling_constant_75_64b.out	2/25/2004	19:40:15	5	52	75.2	64.1	678.4	37	31.1
coil6_test_cycling_constant_75_64b.out	2/25/2004	20:17:34	6	53	75.4	64.1	676.9	23.8	16.6
coil6_test_cycling_constant_75_64b.out	2/25/2004	20:41:40	7	53	75.3	64	680	23.8	16.6
coil6_test_cycling_constant_75_64b.out	2/25/2004	21:05:46	8	53	75.4	64.1	676.9	23.8	16.6
coil6_test_cycling_constant_75_64b.out	2/25/2004	21:29:52	9	54	75.4	64	678.7	20.4	10.4
coil6_test_cycling_constant_75_64b.out	2/25/2004	21:50:34	10	54	75.4	64	677.7	20.4	10.4
coil6_test_cycling_constant_75_64b.out	2/25/2004	22:11:15	11	54	75.4	63.9	678	20.4	10.4
coil6_test_cycling_constant_75_64b.out	2/25/2004	22:31:57	12	55	75.3	64	680.3	25	7.3
coil6_test_cycling_constant_75_64b.out	2/25/2004	22:57:16	13	55	75.5	63.9	682	25.1	7.3
coil6_test_cycling_constant_75_64b.out	2/25/2004	23:22:36	14	55	75.6	64	683.2	25.1	7.3
coil6_test_cycling_constant_300b.out	2/28/2004	3:04:00	1	71	80	60.5	518.1	216.1	123.8
coil6_test_cycling_constant_300b.out	2/28/2004	6:40:22	2	71	80	60.6	515.7	216.1	123.9
coil6_test_cycling_constant_300b.out	2/28/2004	10:16:48	3	72	80	60.5	516.2	36.9	31
coil6_test_cycling_constant_300b.out	2/28/2004	10:53:57	4	72	79.9	60.6	517.8	36.9	31
coil6_test_cycling_constant_300b.out	2/28/2004	11:31:08	5	72	79.9	60.6	514.6	36.9	31
coil6_test_cycling_constant_300b.out	2/28/2004	12:08:19	6	72	80	60.6	517.3	36.9	31
coil6_test_cycling_constant_300b.out	2/28/2004	12:45:28	7	73	79.9	60.6	516.1	23.8	16.5
coil6_test_cycling_constant_300b.out	2/28/2004	13:09:29	8	73	79.9	60.6	517.6	23.7	16.5
coil6_test_cycling_constant_300b.out	2/28/2004	13:33:29	9	73	79.9	60.7	516.2	23.7	16.5
coil6_test_cycling_constant_300b.out	2/28/2004	13:57:28	10	74	79.8	60.6	517.9	20.4	10.3
coil6_test_cycling_constant_300b.out	2/28/2004	14:18:05	11	74	79.8	60.7	518.1	20.4	10.3
coil6_test_cycling_constant_300b.out	2/28/2004	14:38:42	12	74	79.9	60.7	515.9	20.4	10.3
coil6_test_cycling_constant_300b.out	2/28/2004	14:59:19	13	75	79.8	60.7	519	25	7.3
coil6_test_cycling_constant_300b.out	2/28/2004	15:24:34	14	75	79.8	60.7	519.2	25	7.2
coil6_test_cycling_constant_300b.out	2/28/2004	15:49:49	15	75	79.9	60.5	517.1	25	7.2
coil6_test_cycling_auto.out	2/5/2004	1:42:41	1	41	79.9	60.6	683.7	216	123.9
coil6_test_cycling_auto.out	2/5/2004	5:18:56	2	41	80	60.5	682.2	215.9	123.8
coil6_test_cycling_auto.out	2/5/2004	8:55:07	3	42	80	60.6	680.4	36.9	31
coil6_test_cycling_auto.out	2/5/2004	9:32:17	4	42	80	60.5	679.3	36.9	31
coil6_test_cycling_auto.out	2/5/2004	10:09:28	5	42	80	60.5	681.7	36.9	31
coil6_test_cycling_auto.out	2/5/2004	10:46:37	6	43	80	60.5	677.3	23.7	16.5
coil6_test_cycling_auto.out	2/5/2004	11:10:35	7	43	80	60.4	676.4	23.7	16.5
coil6_test_cycling_auto.out	2/5/2004	11:34:35	8	43	80	60.5	674.2	23.7	16.5
coil6_test_cycling_auto.out	2/5/2004	11:58:35	9	44	79.9	60.5	669.4	20.3	10.3
coil6_test_cycling_auto.out	2/5/2004	12:19:11	10	44	80	60.6	669.7	20.3	10.3
coil6_test_cycling_auto.out	2/5/2004	12:39:48	11	44	79.9	60.5	668.3	20.4	10.3
coil6_test_cycling_auto.out	2/5/2004	13:00:25	12	45	80	60.4	661.6	25	7.2
coil6_test_cycling_auto.out	2/5/2004	13:25:39	13	45	80	60.6	664.8	24.9	7.2
coil6_test_cycling_auto.out	2/5/2004	13:50:52	14	45	79.9	60.5	662	24.9	7.2
coil6_test_cycling_auto.out	2/5/2004	14:16:05	15	45	79.9	60.3	663.2	24.9	7.2
coil6_test_cycling_auto.out	2/5/2004	14:41:18	16	45	80.1	60.7	664.8	25	7.2
coil6_test_cycling_auto.out	2/5/2004	15:06:32	17	46	80.1	60.7	656	61.9	5.7
coil6_test_cycling_auto.out	2/5/2004	16:08:40	18	46	80.2	60.8	658.5	61.9	5.7
coil6_test_cycling_auto.out	2/5/2004	17:10:49	19	46	80.1	60.7	660.3	62.4	5.7
coil6_test_cycling_auto.out	2/5/2004	18:13:29	20	46	80.1	60.5	655	62.3	5.7
coil6_test_cycling_auto.out	2/5/2004	19:16:07	21	46	80.1	60.4	659.1	62.4	5.7

## **APPENDIX H7**

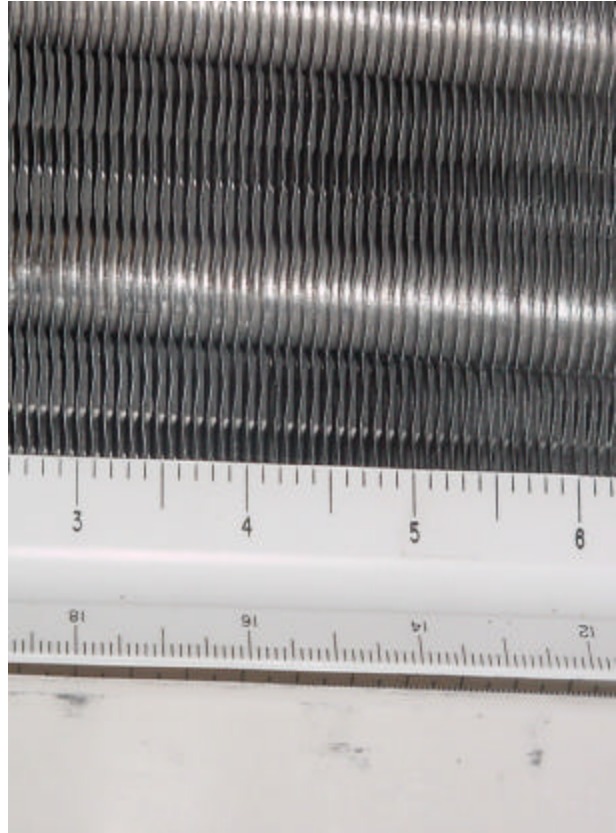
### **Summary of Laboratory Data for Coil 7**



**Summary of Laboratory Data for Coil 7 (same physical coil as Coil 6)  
November 2005**



A-frame coil arrangement



13 fpi, wavy fin

Manufacturer:	Lennox
Model number:	CB30M-21/26-2P
Nominal size:	1.5 - 2 tons
Baseline Size and Airflow (Test 4):	2.0 tons / 800 cfm
Coil type:	A-frame coil
Coil dimensions:	3 rows, 13 fpi, 3.56 ft <sup>2</sup> total face area 16 in x 16 in total dimension (2 ea.) 3.38 ft <sup>2</sup> open face area (25 in <sup>2</sup> obstruction to air flow)
Coil thickness:	2.5 in
Tube diameter:	3/8 in OD copper
Tube spacing, within row (vert):	1 in
Tube spacing, row-to-row (horiz):	7/8 in
Expansion device:	TXV (13°F superheat)
Unit supply fan:	off
Compressor power:	inverter

**Table 1. Summary of Steady State Test Conditions Corresponding to Each Run or Test**

	<i>Entering Coil Conditions</i>					
	<i>80/67°F 60°F dp</i>	<i>80/72°F 68°F dp</i>	<i>80/62°F 50°F dp</i>	<i>75/68°F 64°F dp</i>	<i>75/63°F 56°F dp</i>	<i>75/58°F 45°F dp</i>
400 cfm/ton	#4 (or 3)	#5	#6	#7	#8	#9
300 cfm/ton	#10	#11	#12	#13	#14	#15
200 cfm/ton	#16	#17	#18	#19	#20	#21
450 cfm/ton	#22	#23	#24			
400-200 cfm/ton (ON & OFF)	#25					
Low suction (46.5°F)	#1					
High suction (55.5°F)	#2					

Notes: Tests 4-25 all at nominal suction of 51.5°F (set at nominal conditions of test #3/4). A thermal expansion device was used, with nominal superheat of 13°F. The refrigerant charge established during Test 4 was not changed for the remaining tests. The Table 1 test points denote the target testing conditions. Drier test conditions with dew points below 50°F (such as Tests #9, #15, and #21) could not be achieved. In these cases, entering conditions were typically held near 50°F dp. For each test, the compressor is ON for 120-260 minutes and then the compressor is OFF for at least 90 minutes. The booster fan runs continuously for all tests (when the compressor is both ON and OFF).

### **Steady State Performance**

The nominal performance characteristics for this coil (based on steady-state conditions from Run #4 below) are:

Total Capacity:	24.4 MBtu/h (2.0 tons)
Sensible Capacity:	17.9 MBtu/h
Latent Capacity (condensate):	6.5 MBtu/h
Sensible Heat Ratio:	0.73

Latent capacity can be calculated two ways: 1) using dew point readings and air flow, and 2) using the condensate flow rate. Figure 1 compares the latent capacity calculated these two ways. The number of each data point corresponds to the test number listed in Table 1. The two readings were in very good agreement for this test.

Figure 2 shows the trend of steady-state sensible heat ratio (SHR) with relative humidity and airflow rate. The cooling capacities used to calculate SHR in Figure 2 are based on airflow measurements and the psychrometric conditions entering and leaving the cooling coil. This performance map is typical for a cooling coil (i.e., SHR is mostly a function of the entering relative humidity, with some dependence on the air flow rate).

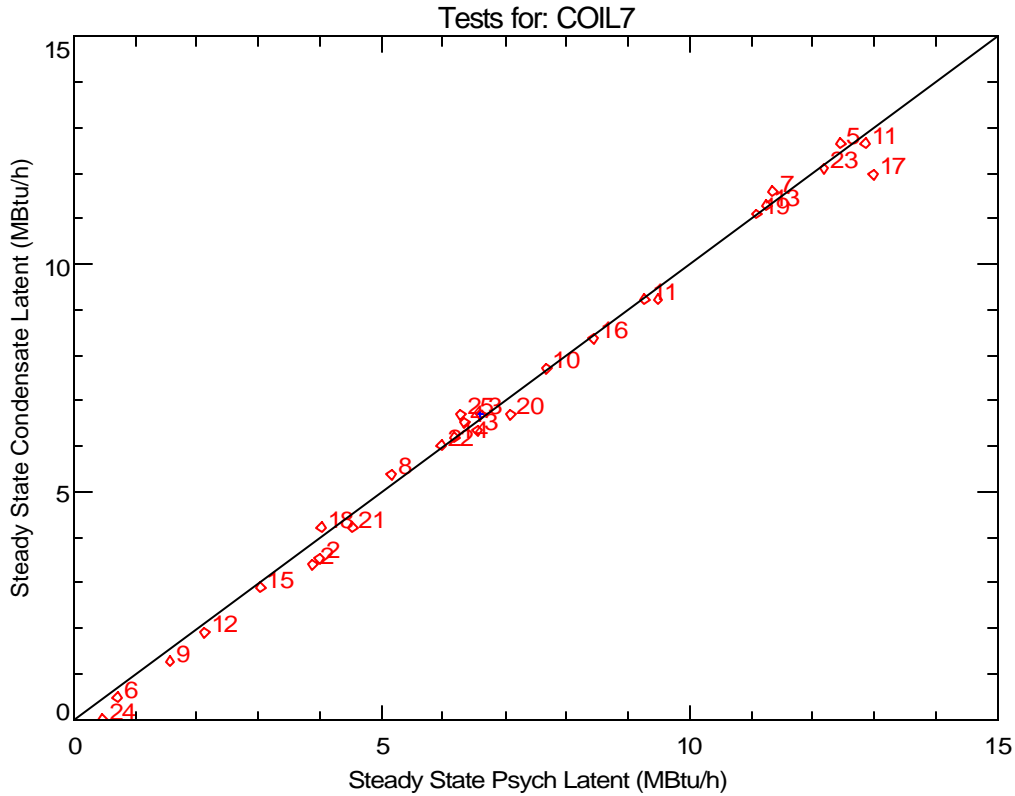


**Figure 1. Comparing Steady-State Latent Capacity Calculated From Psychrometric State Points and Condensate Removal Rates**

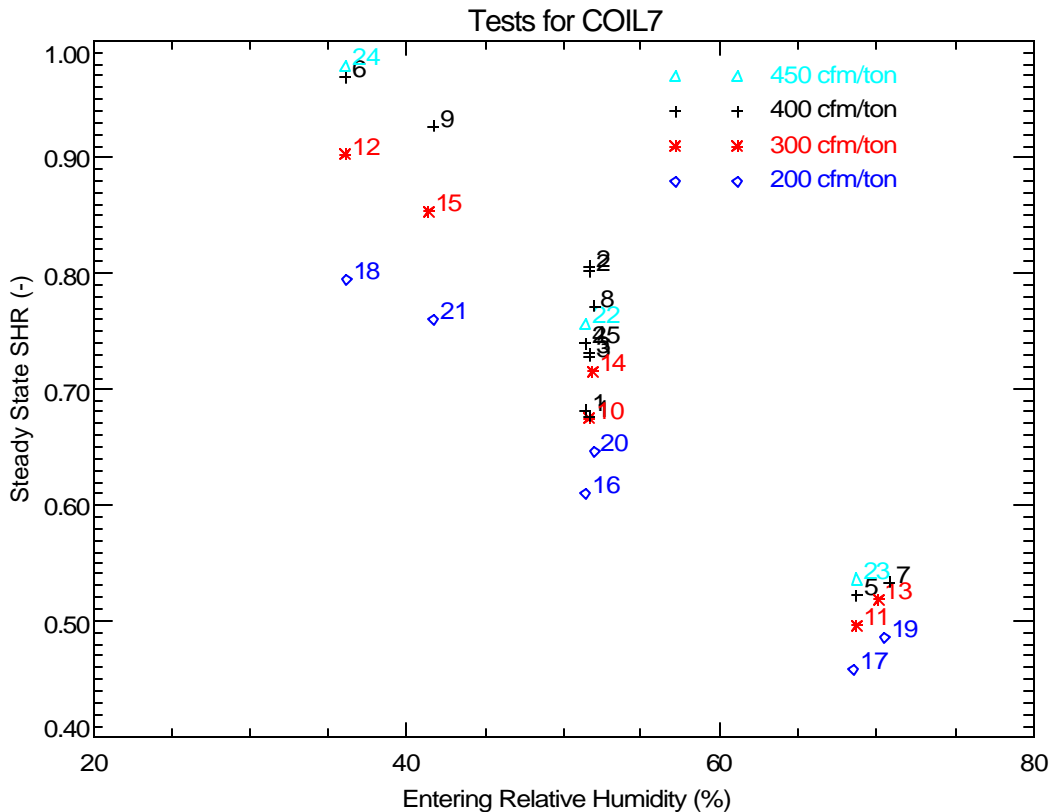


**Figure 2. Variation of Steady State SHR with Entering Humidity and Nominal Air Flow**

## **Typical Transient Performance**

Figure 3 shows the typical transient performance of the cooling coil at nominal conditions (i.e., for Cycle 2 of Run #4). The compressor runs for 155 minutes and is off for 90 minutes. The booster fan remains on during the entire test (separate external fan used to maintain the desired air flow rate across the cooling coil). A portion of the moisture removed by the coil during the compressor on cycle evaporates back into the air stream during the off cycle. During the off cycle the coil acts as an evaporative cooler, so the sensible capacity is nearly equal to the absolute value of the latent capacity (i.e., the sum of latent and sensible is zero).

If we integrate the off cycle sensible capacity (after allowing for a 1-minute off-cycle delay to account for refrigerant movement and other transient effects), we can determine the energy associated with the moisture retained on the coil. To minimize the integration of any measurement errors, the off-cycle integration stops at the time labeled “Integration Pt.” on the plot. This point corresponds to the time when the temperature and dew point differences across the coil have first reached the terminal values (i.e., the averages from the end of the off-cycle). In this case the integration indicates that the sensible cooling is equivalent to 2.65 lbs of moisture being retained on the coil. The integrated latent capacity – which is harder to measure precisely – equals 2.35 lbs.

The value “ $t_{wet}$ ” from Henderson and Rengarajan (1996) can then be calculated by dividing the retained moisture mass (expressed as Btu; mass x 1060 Btu/lb) and the steady state psychrometric latent capacity ( $QL = 6.3$  MBtu/h). Figure 3 shows that the values of  $t_{wet}$  based on integrated sensible and latent off-cycle capacity are 26.6 and 23.6 minutes respectively. These values of  $t_{wet}$  are similar to the measured delay of 26.8 minutes for the first condensate pulse to fall from the drain pan. The value of  $\gamma$  (1.53), which is the initial off-cycle moisture evaporation rate divided by the steady-state psychrometric latent capacity, uses the off-cycle moisture evaporation rate (9.7 MBtu/h) once the transition point was been detected. For this coil, we detect the transition by determining where the change in off-cycle sensible capacity between each 15-second interval first drops below 3% of the steady-state on cycle sensible capacity (QS). At this transition point where  $\gamma$  is determined, it is assumed that all coil heat and mass transfer with the air stream is adiabatic (the refrigerant flow could not be used as the indicator to detect this point for this coil). In this case it took 1.03 minutes for the change in off-cycle sensible capacity to drop below 3% of the steady-state on cycle value QS.

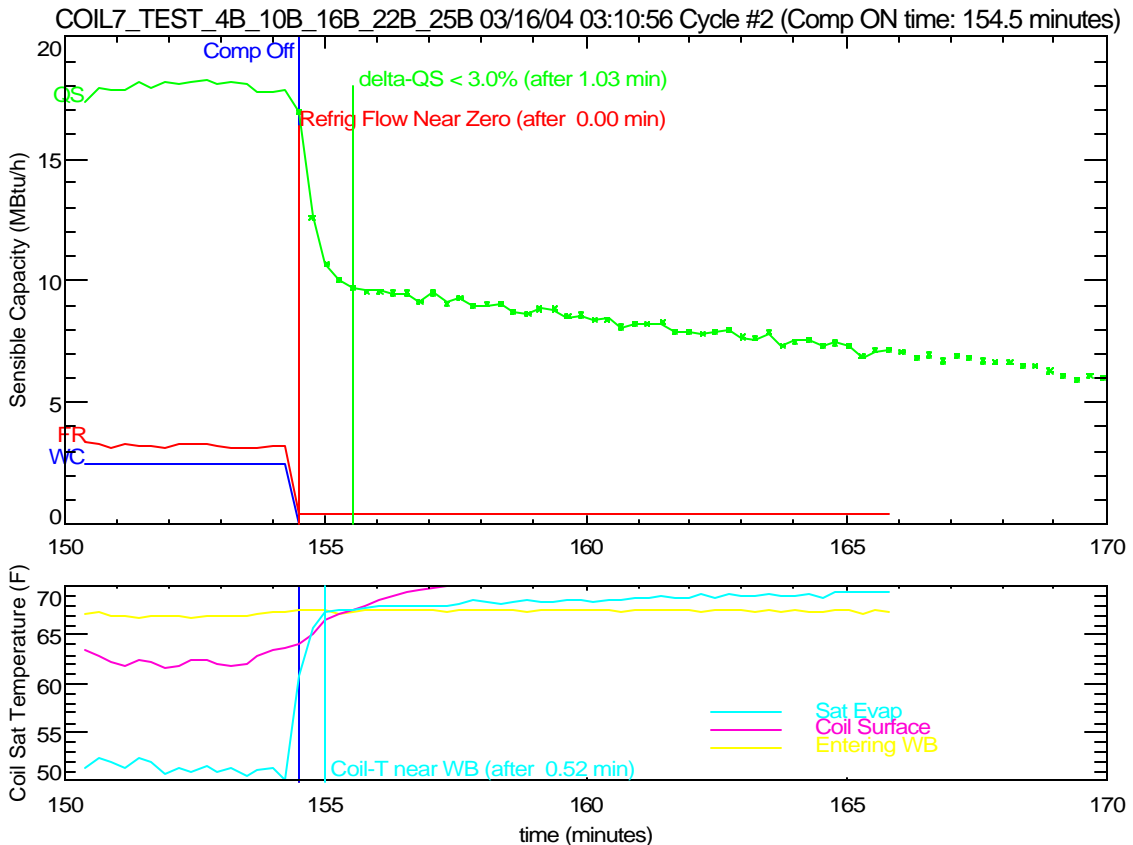
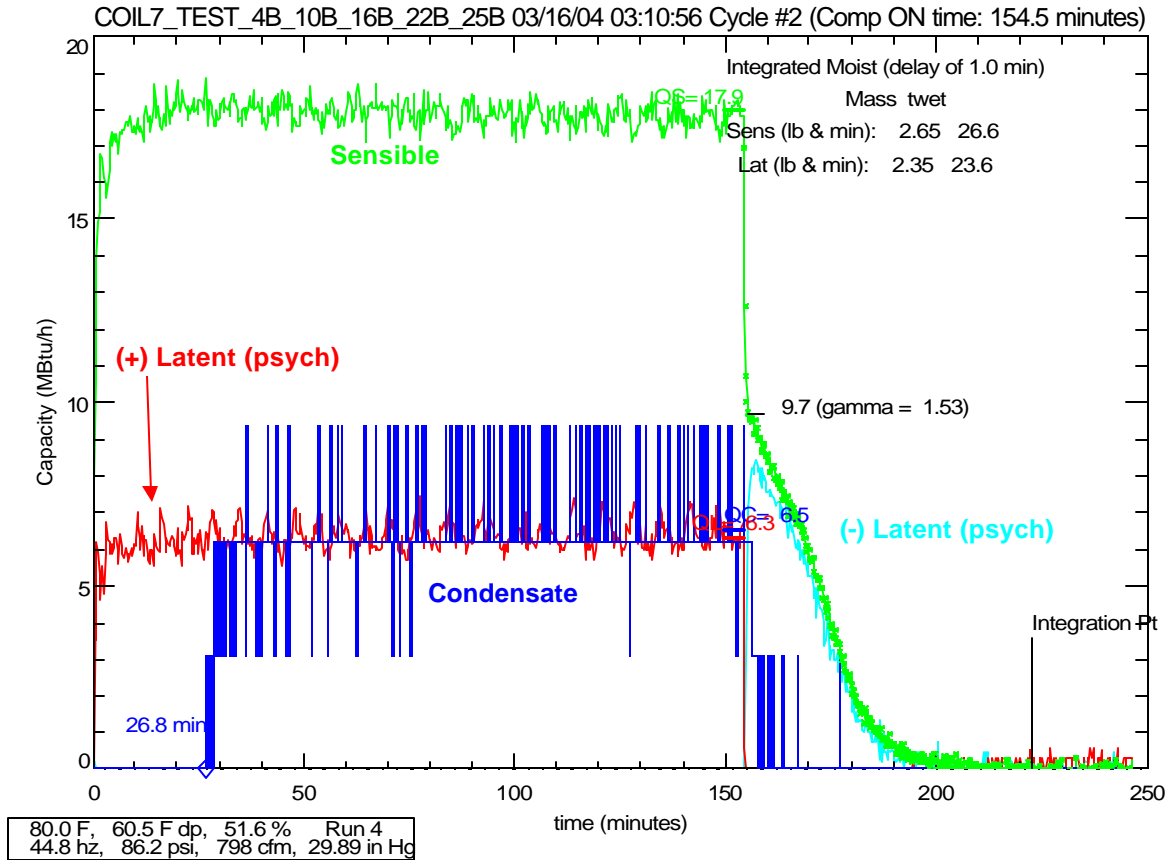
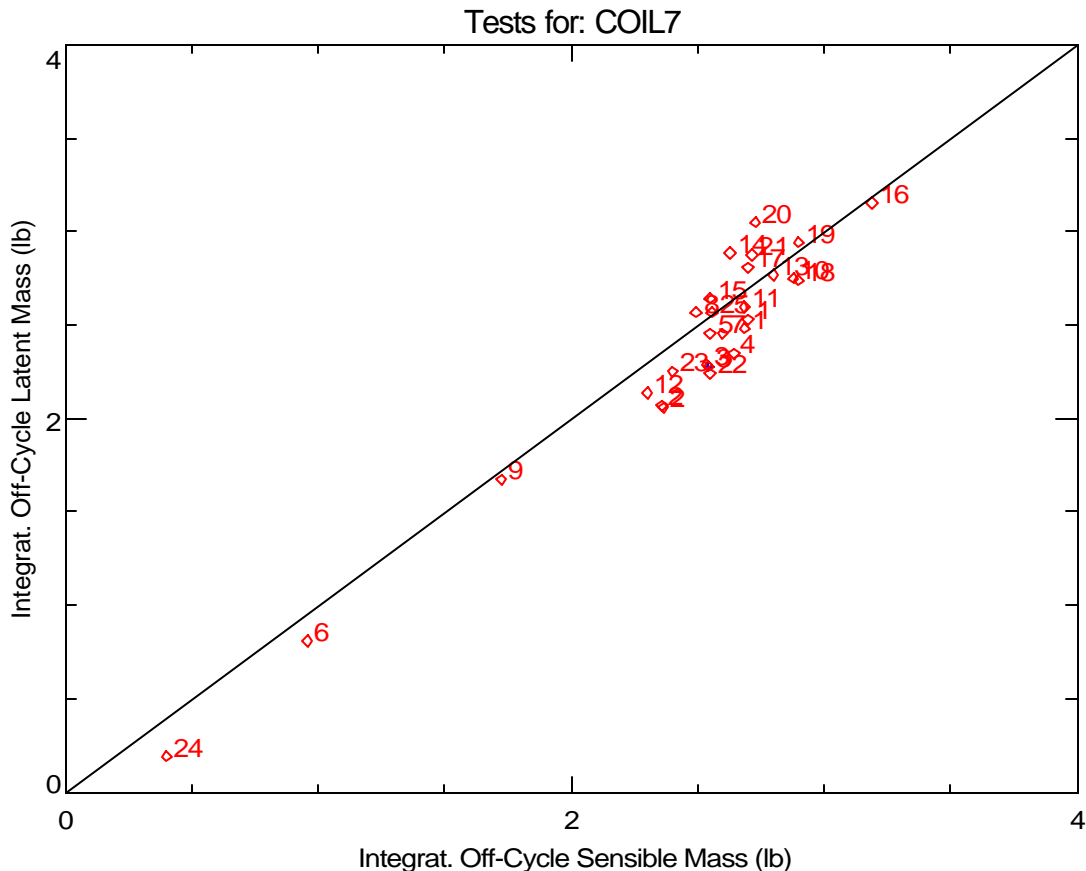


Figure 3. Example Plots of Detailed Data for Coil 7

## Part Load Latent Capacity Parameters

The amount of moisture held on the cooling coil (and drain pan) can be calculated by integrating the off-cycle capacity from the coil (and dividing by the heat of vaporization, 1060 Btu/lb, to get the moisture mass). The integration is delayed for the first minute of the off-cycle so that the overshoot response of the chilled dew point hygrometers does not skew the results of the integration<sup>1</sup>. The integration terminates once steady state conditions are reached for the off cycle. If we assume the coil acts as an evaporative cooler, then sensible and latent capacity should be equal. Figure 4 compares the off-cycle integrated latent and sensible capacity calculated for each run. No systematic bias is evident and Figure 5 shows that any bias is not a function of dew point as was observed from tests of Coil 1.

Since we expect that off-cycle latent and sensible capacity should sum to zero, we have selected the integrated off-cycle sensible capacity as the most consistent and believable indication of the moisture mass held on the cooling coil (and drain pan).



**Figure 4. Comparing Stored Moisture Mass Calculated by Integrating Sensible and Latent Off-Cycle Capacity (Integrated with a 1 minute delay)**

<sup>1</sup>The 1-minute delay causes the estimate of moisture mass to be low by as much as 0.15 lbs (or 6%).

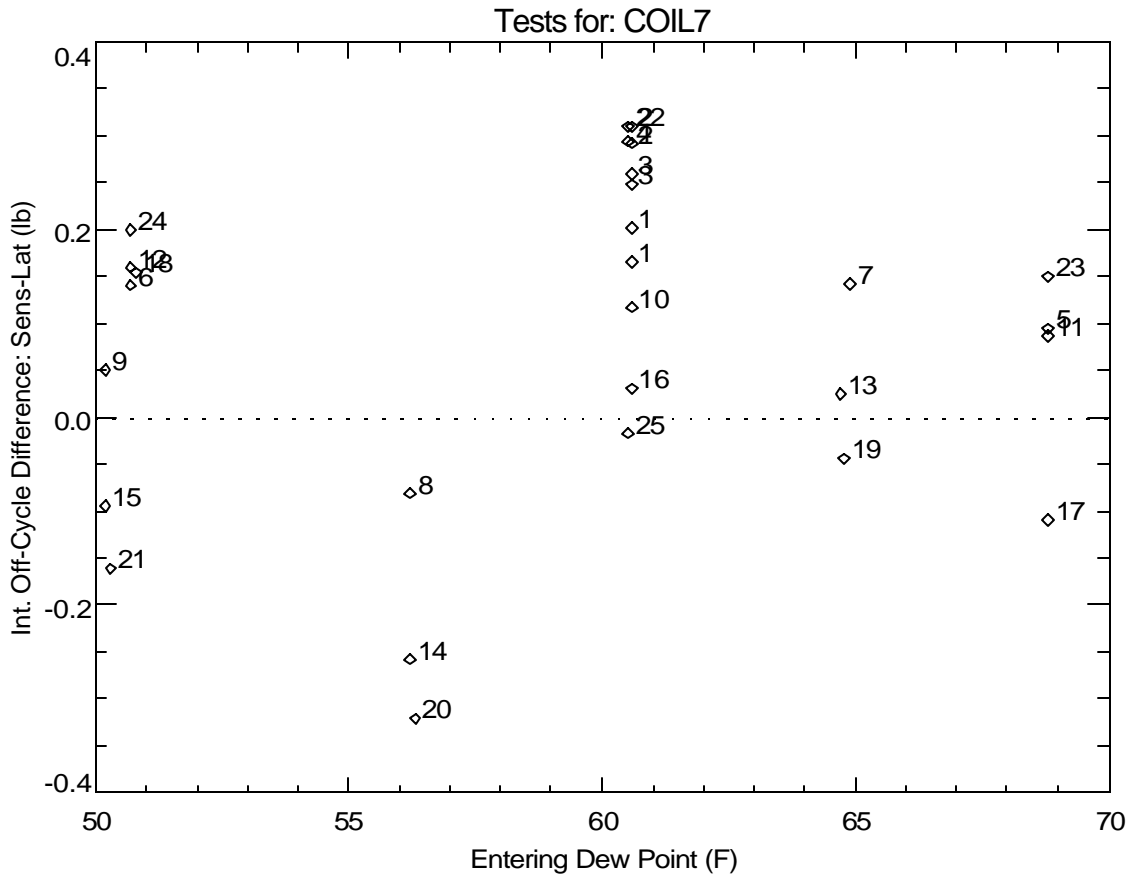


**Figure 5. Variation of Off-Cycle Sensible-Latent Difference with Entering Dew Point**

The parameter “twet” is the moisture mass held on the cooling coil times the enthalpy of vaporization (1060 Btu/lb) divided by the steady-state latent capacity of the cooling coil. The parameter should physically correspond to the time it takes for moisture to first fall from the coil (ignoring startup delays and other effects). Figure 6 compares the calculated “twet” (determined from integrating sensible capacity during the off-cycle and then dividing by the steady-state psychrometric latent capacity during the on-cycle) to the condensate delay time for all test runs. In general, there is good agreement between these two values. The worst agreement is apparent for test #6, which has dry entering air conditions.

Figure 7a and 7b show that both twet and the condensate delay time are a function of the entering air dew point temperature. Figure 7b uses different symbols to show the 1<sup>st</sup> and 2<sup>nd</sup> cycles in each test sequence with flow rate of 400 cfm/ton for all tests. The delay time was generally the same for the first and second cycles for this coil.

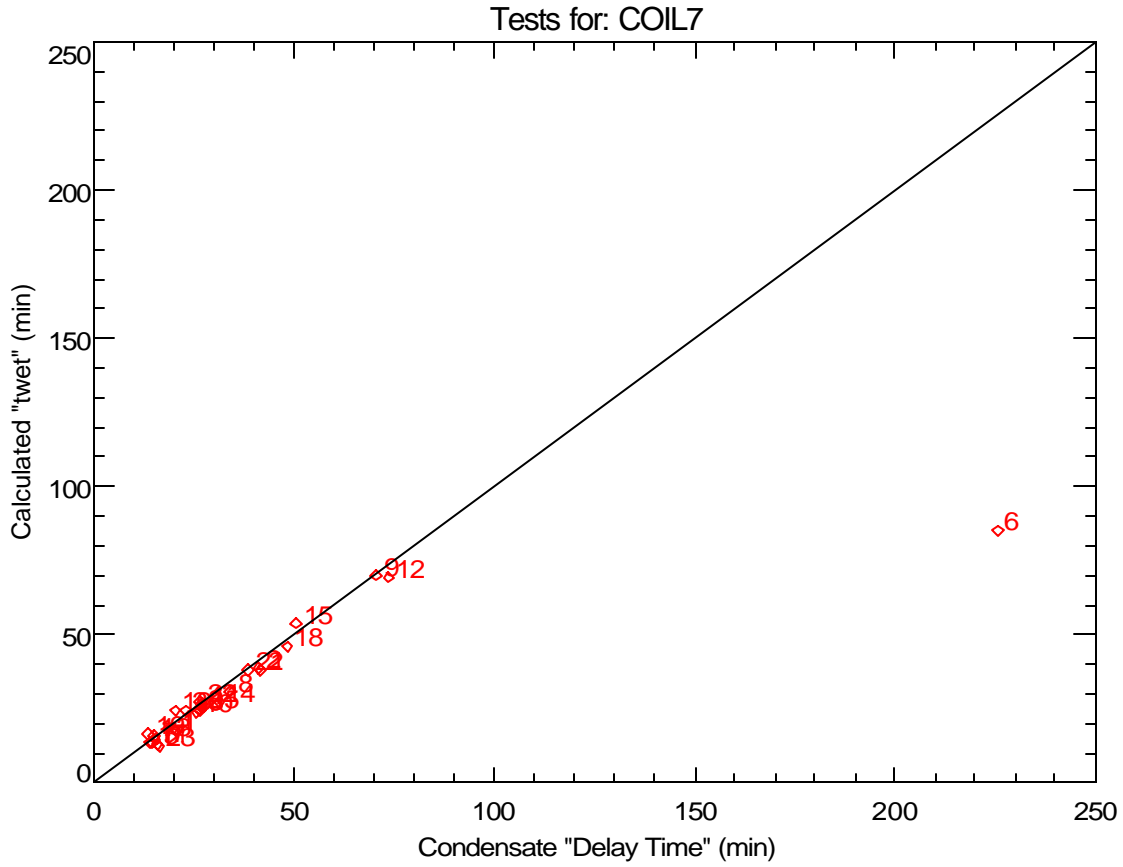


**Figure 6. Comparing “twet” (calculated with off-cycle sensible and steady state latent) to the Condensate Delay Time**



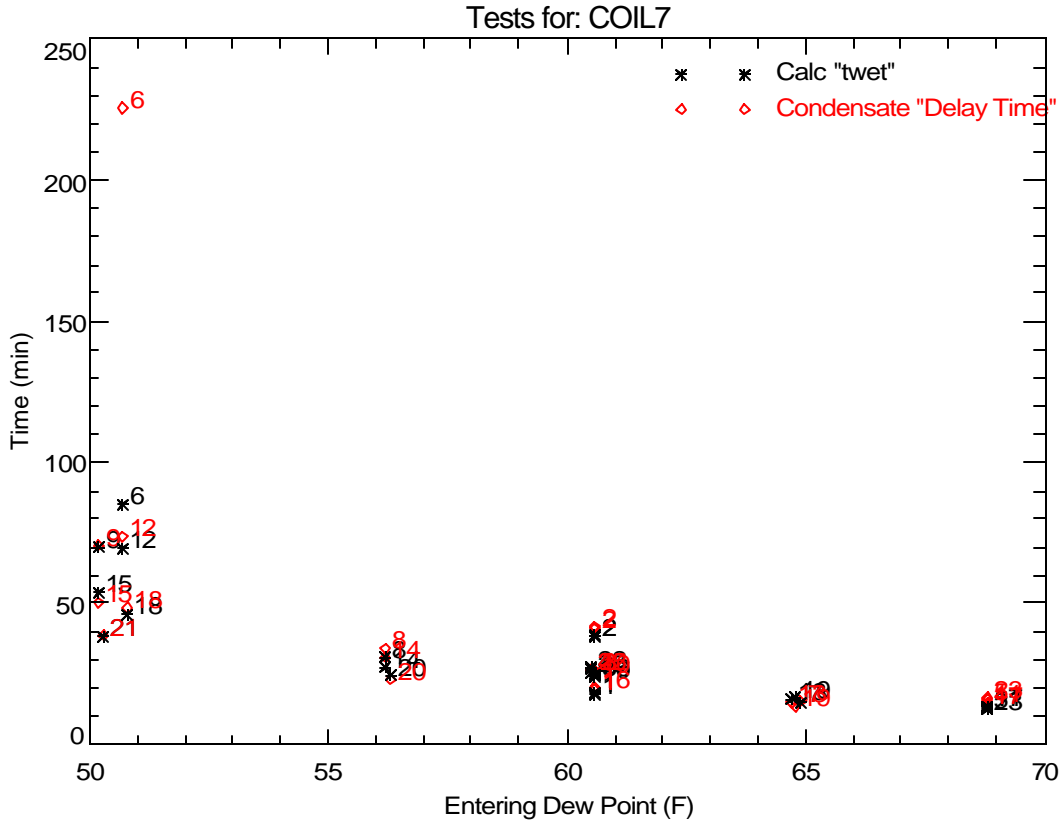


Figure 7a. Impact of Dew Point on “twet” and Condensate Delay Time

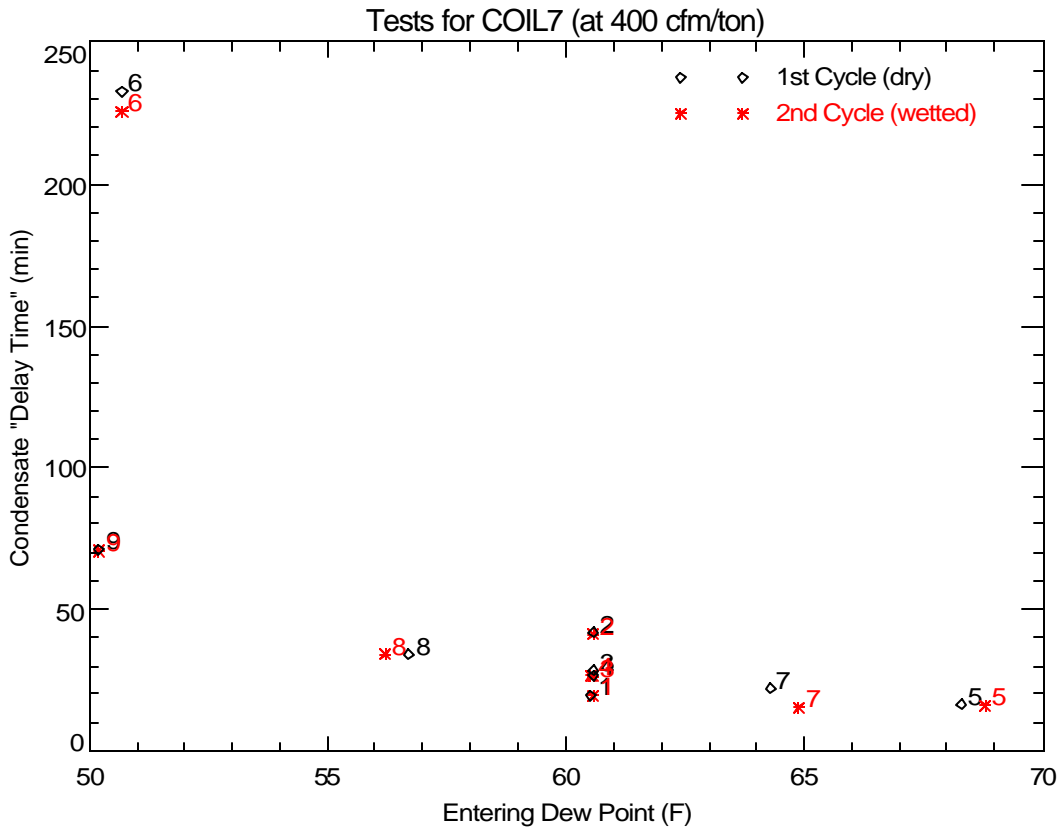


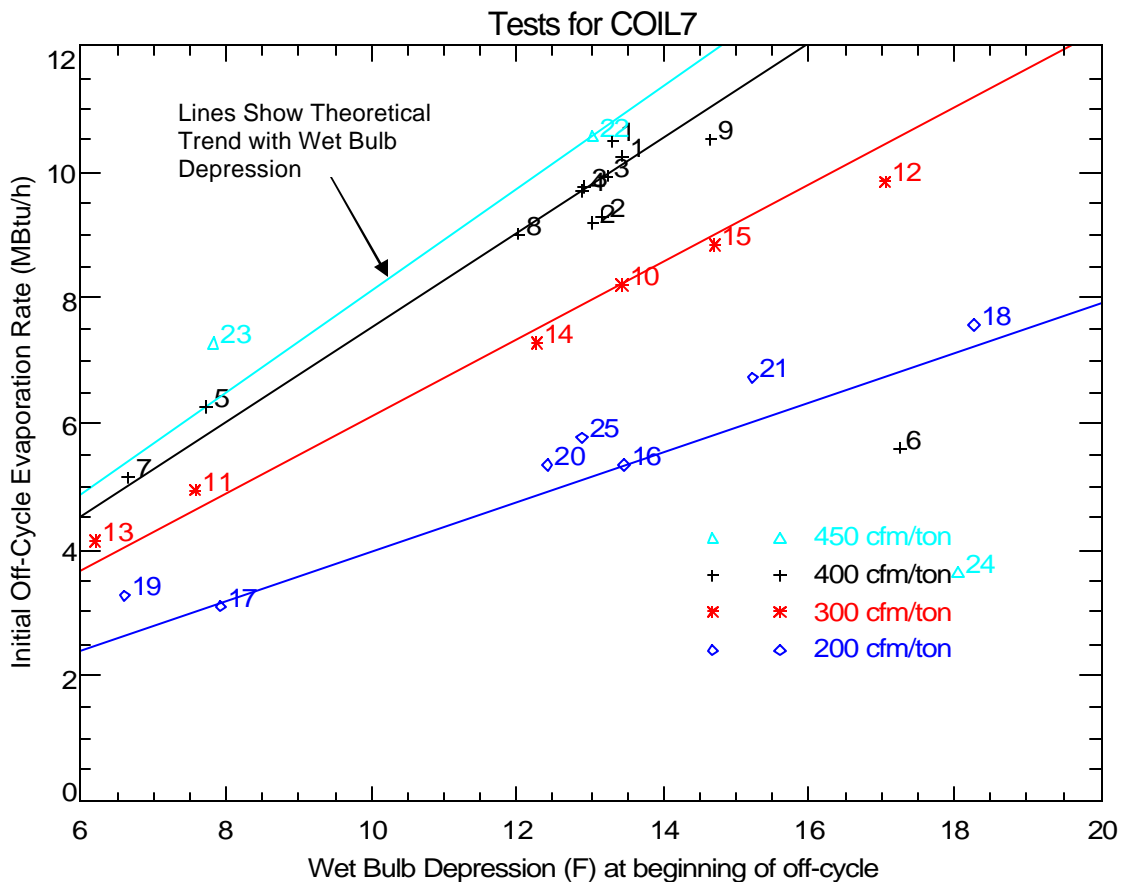
Figure 7b. Impact of Dew Point and Coil Wettedness on Condensate Delay Time

Figure 8 shows the initial off-cycle moisture evaporation rate varies with wet bulb depression. As expected, the evaporation rate is highest when the entering air has a larger wet bulb depression (i.e., has a lower relative humidity) and a higher airflow rate.

The model developed by Henderson and Rengarajan (1996) used the following simple evaporative cooler model to predict the moisture evaporation rate at off-design conditions:

$$Q_{\text{evap}} = Q_{\text{evap}_o} \times \frac{(DB - WB)}{(80 - 67)}$$

where  $Q_{\text{evap}_o}$  is the evaporation rate at the nominal entering air conditions of 80°F dry bulb (DB) and 67°F wet bulb (WB). This simple model is shown as the lines in Figure 8. For each airflow rate, the line is based on the nominal test results at 80°F DB/67°F WB extended to pass through zero. The measured data show essentially the same slope as the theoretical lines. The notable exceptions are the points with higher air flow and drier entering air conditions. Specifically, Tests #6 and #24 deviate significantly from the line. These runs have a much lower initial moisture evaporation rate because the entering air dew point temperature was close to the cooling coil temperature, so the fin surfaces were not fully wetted. The smaller wetted surface area reduces the initial moisture evaporation rate.



**Figure 8. Measured Variation of Initial Evaporation Rate with Wet Bulb Depression**

Stabat et al. (2001) reviewed the theoretical performance of direct evaporative coolers and showed that the saturation effectiveness of an evaporative cooler is:

$$h_{evp} = 1 - e^{-NTU} \quad \text{where} \quad NTU = K/cfm^{0.2} \quad \text{for an air-water mixture.}$$

The line shown on Figure 9 is the best fit of the equation above to the measured data. The resulting constant K was  $9.02^2$ , which is equivalent to an NTU of 2.37 at 800 cfm. While there is considerable scatter due to the experimental uncertainty of predicting the initial off-cycle moisture evaporation rate, the slope of the line is still representative of the overall trend.

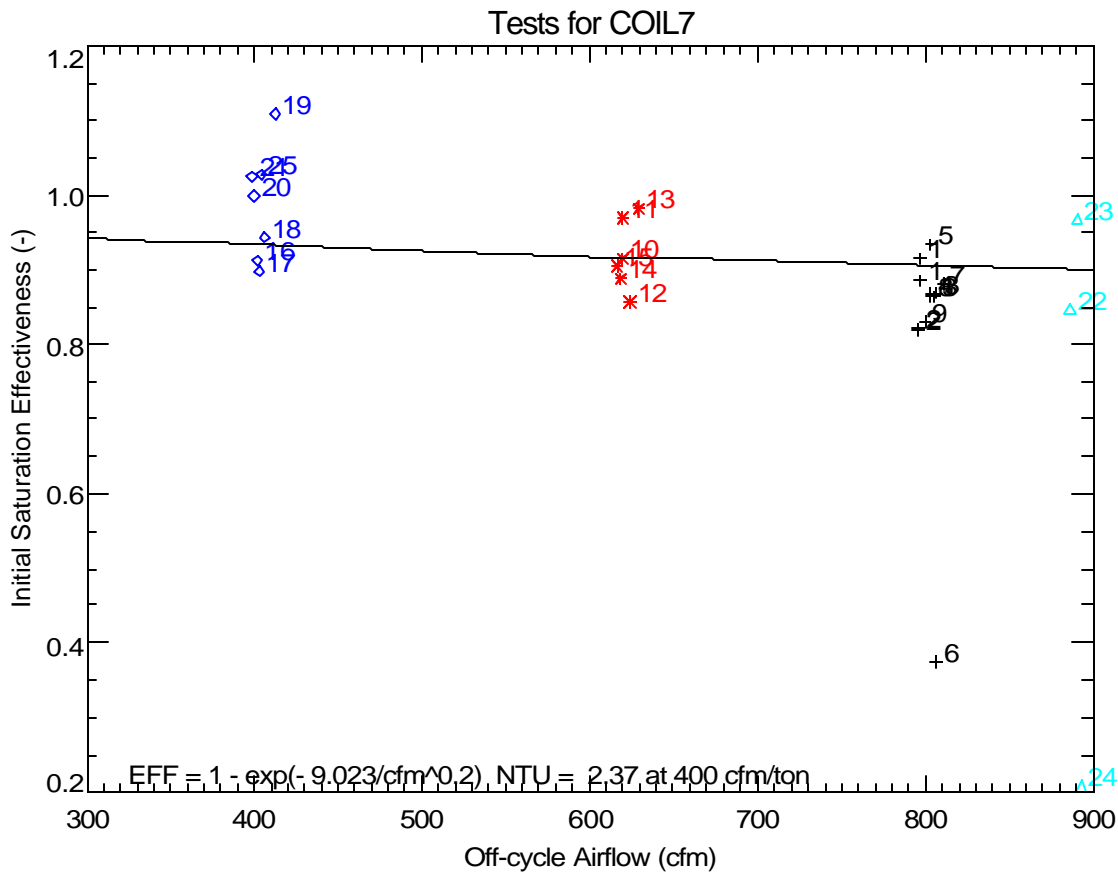


**Figure 9. Evaporative Effectiveness versus Airflow**

Figure 10 compares the measured initial off-cycle moisture evaporation rate for each test to the predicted initial evaporation rate using the effectiveness model above. The model and measured data generally agree when presented in this form (i.e., the overall agreement visually appears better than in Figure 9 above). Again, the variation that occurs for Tests #6 and #24 was due to partial coil dryout, as mentioned above.

<sup>2</sup> For Coil #6, which was the same physical coil,  $K=9.99$  which is in good agreement with the value 9.02 calculated here for Coil #7.

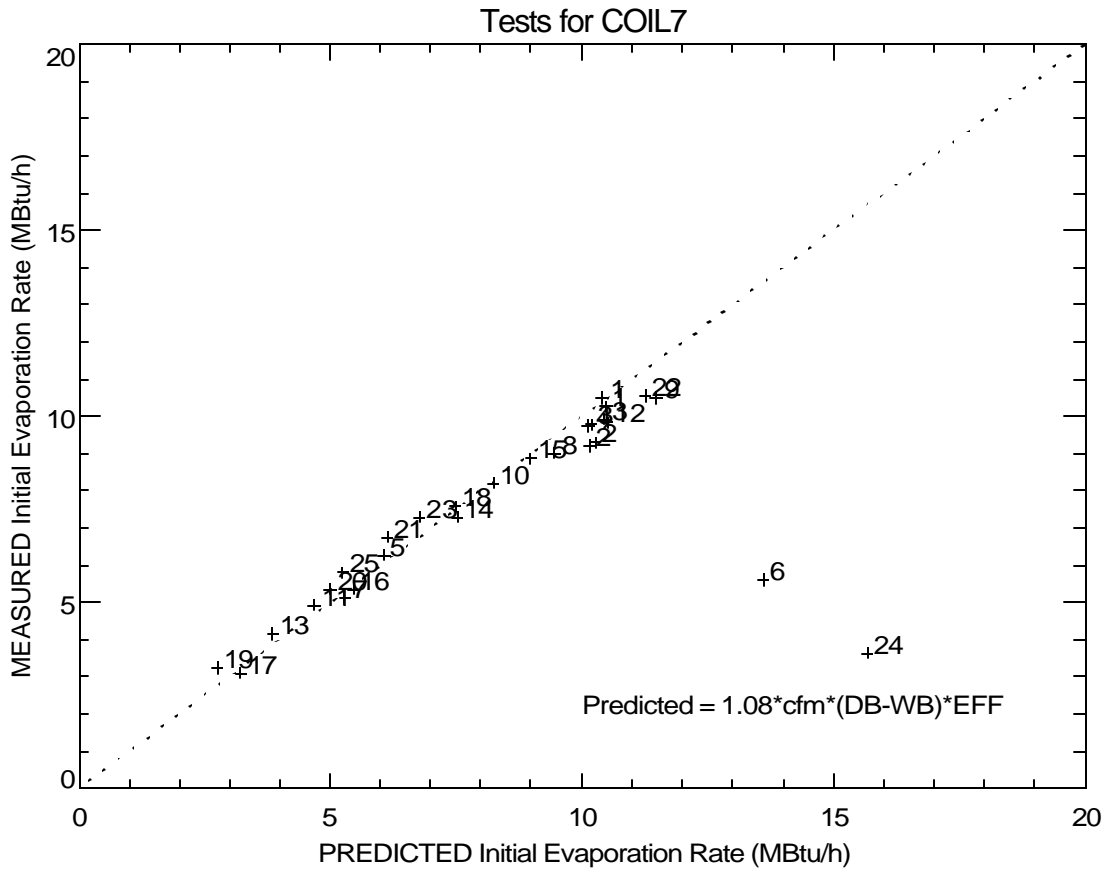


**Figure 10. Comparing Measured and Predicted Initial Moisture Evaporation Rates**

Figure 11 and Figure 12 below evaluate whether the amount of moisture retained on the cooling coil is a function of air flow or entering air conditions. The results for this coil show very little variation at higher dew points (Figure 11). The data also show evidence of dryout at low dew points for Tests #6, #9 and #24. For the other test conditions, where the coil surfaces were fully wetted, the amount of retained moisture ranges from 2.4 to 3.2 lbs.

Figure 12 shows the expected increase in retained moisture with lower air flow rates. Test 2 with high refrigerant temperature resulted in a warmer coil with less moisture retention.

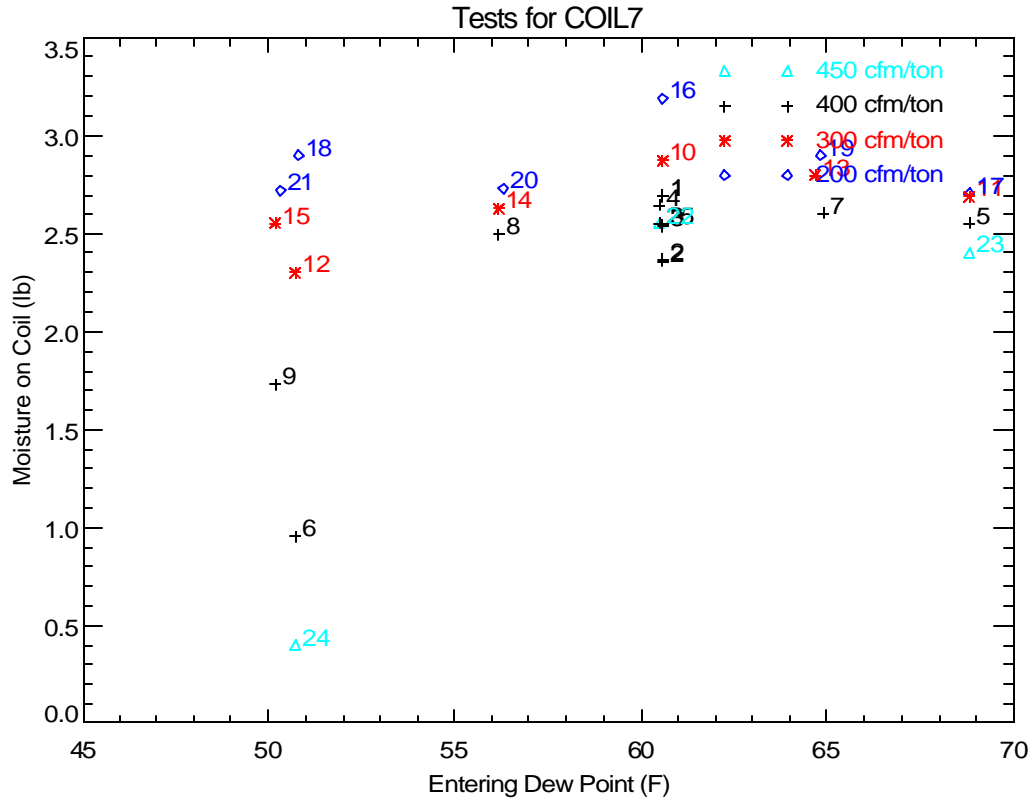


Figure 11. Variation of Retained Moisture (based on Off-Cycle Sensible) with Flow and Dew Point

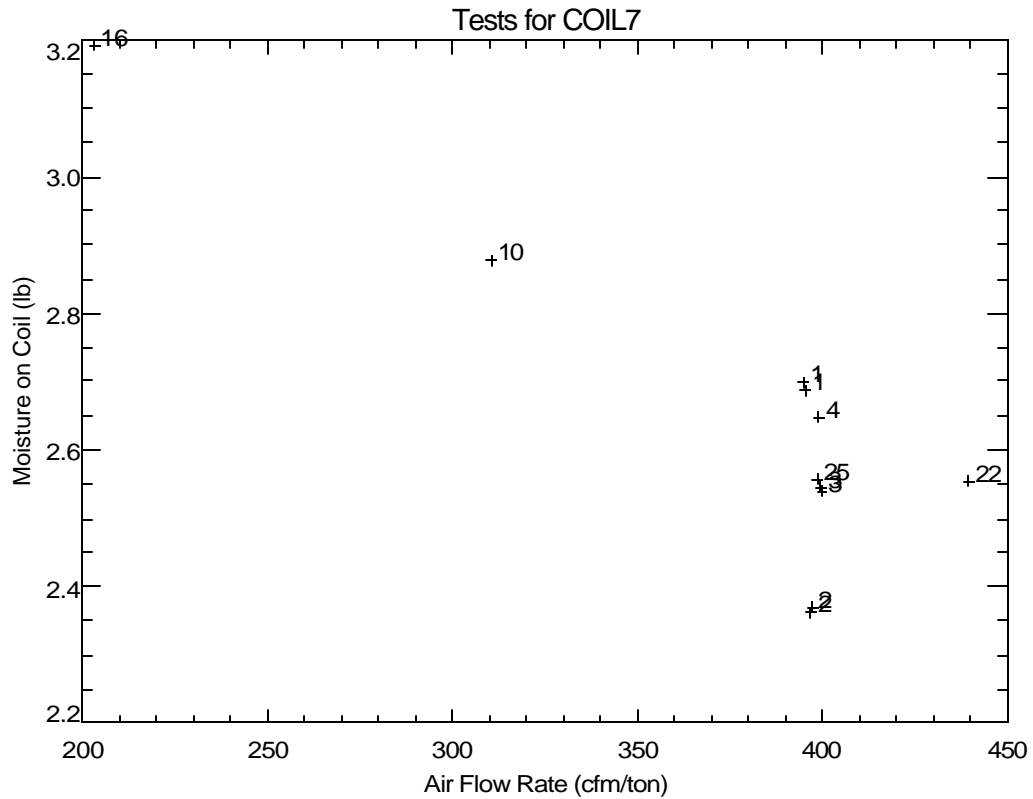
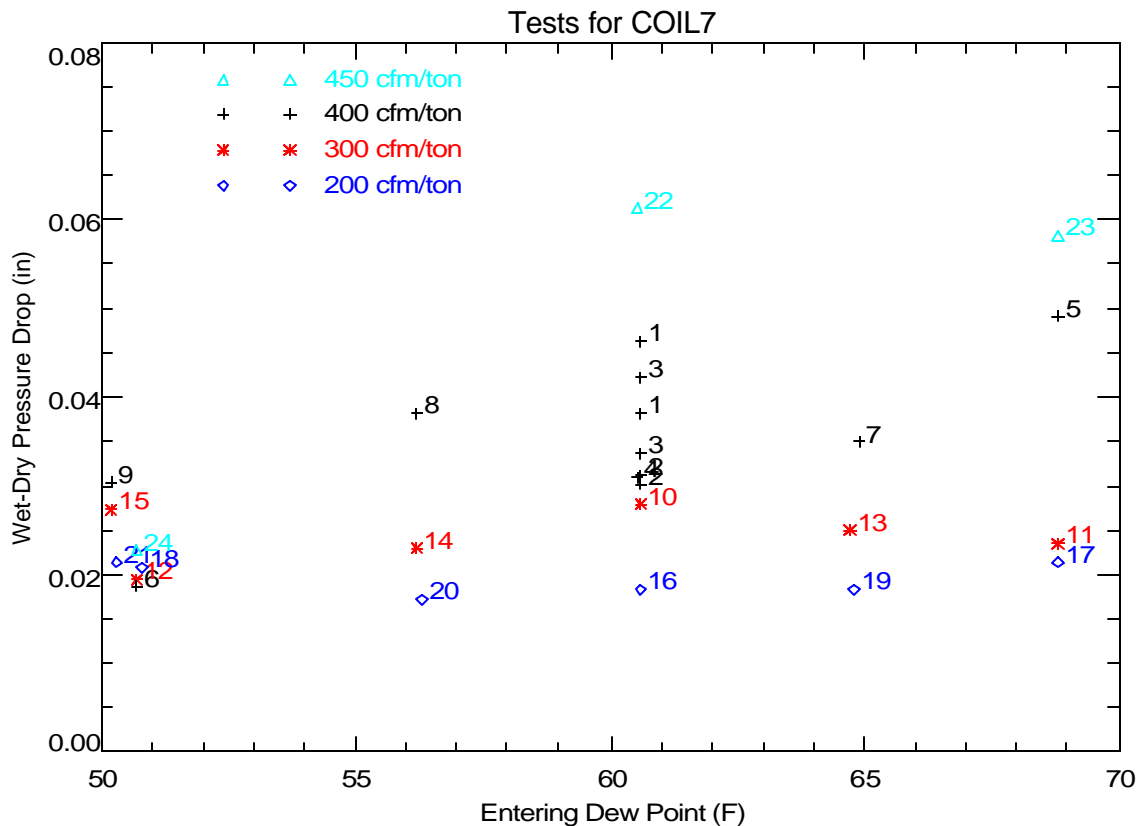


Figure 12. Variation of Retained Moisture with Air Flow at Nominal Entering Conditions of 80°F, 60.4°F dew point

Another way to detect the amount of retained moisture is to measure the static air-side pressure drop across the cooling coil. The difference between the pressure drop across the coil under wet and dry conditions should provide an indication of the amount of retained moisture (the wet coil pressure drop is measured at steady-state conditions while the dry coil pressure drop is taken as the average pressure drop during the last part of the off-cycle). Figure 13 shows the variation of the wet-dry pressure difference with various entering humidity conditions at multiple air flow rates. Comparing the values for each air flow rate generally shows a trend of pressure drops reaching a plateau once the humidity of the entering air is sufficiently high to fully wet the coil. For air flow rates of 200 cfm/ton and 300 cfm/ton, the wet-dry pressure difference remained fairly constant for the range of entering air dew point temperatures that were tested, indicating a fully wetted coil. The wet-dry pressure drops for Tests #6 and #24 are significantly lower than expected, again confirming that less moisture was retained on the cooling coil at these drier/higher air flow conditions.



**Figure 13. Variation of Wet-Dry Pressure Drop with Entering Conditions and Air Flow Rate**

Figure 14 confirms that the wet-dry pressure drop is a linear function of air flow rate, which implies laminar flow in the wetted cooling coil.

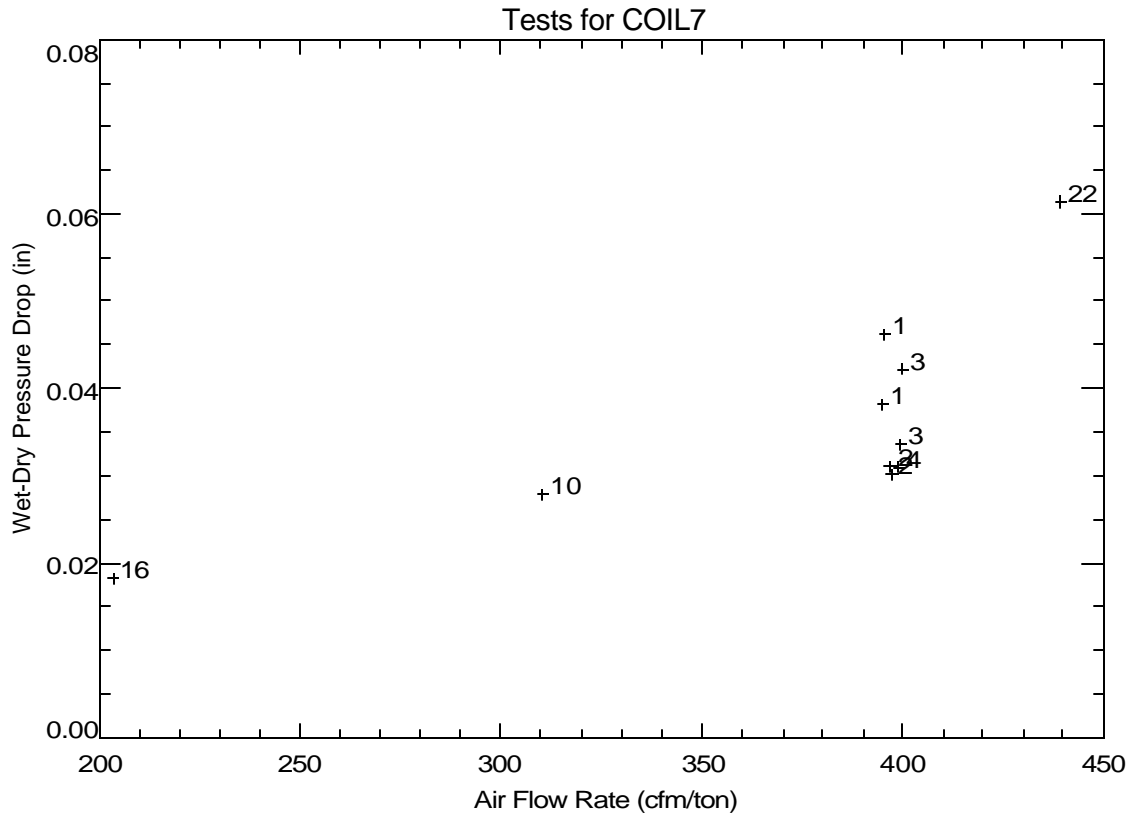


**Figure 14. Trend of Wet-Dry Pressure Drop with Flow at Nominal Entering Conditions of 80° F, 60.4° F dew point**

The series of plots in Figure 15 show the impact of coil suction temperature on performance. The steady-state performance of the system shows the expected trends of lower SHR and greater latent capacity at lower coil temperatures (i.e., lower saturated suction temperatures). Like Coil 1, Coil 3 and Coil 6, the plots for moisture on coil and wet-dry pressure drop show that more moisture is retained when the coil is colder.

The graph of fan power versus saturated suction temperature in Figure 15 is not relevant since the AHU fan was turned off during all tests. For this cooling coil, an external booster fan was used to obtain the desired air flow rate for each test.

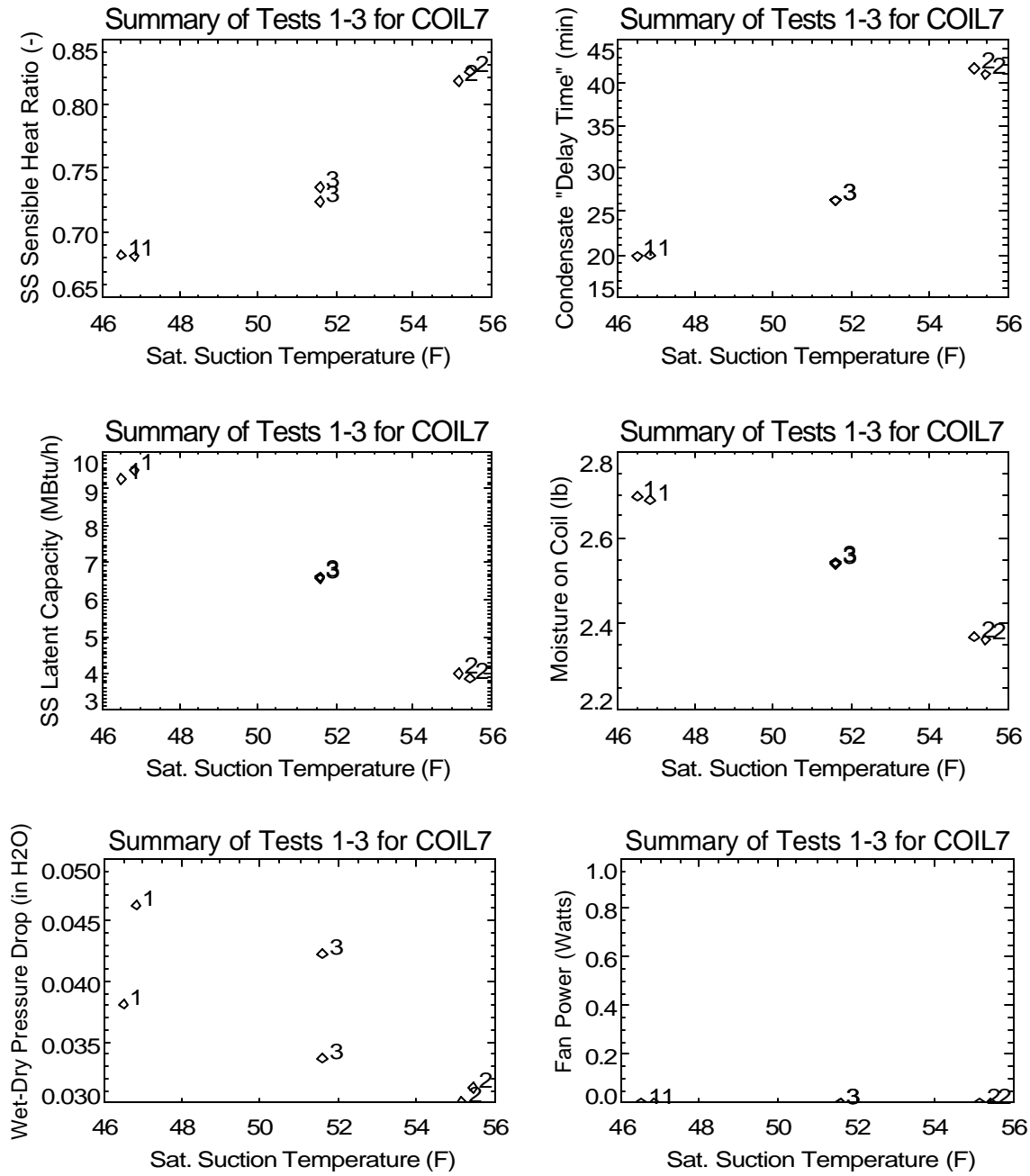


**Figure 15. Trend of Various Parameters with Saturated Suction Temperature**



## Overall Latent Degradation Trends

Several quasi-steady cyclic tests were also completed in the laboratory to quantify the overall part-load degradation of latent capacity. Table 2 lists the cycling test runs. These conditions correspond to a conventional thermostat with a maximum cycle rate of 3 cycles per hour (at 50% runtime).

**Table 2. Cyclic Test Conditions**

CONST FAN <sup>1</sup>	AUTO FAN <sup>2</sup>	Number of Times Test Repeated <sup>3</sup>	ON Time (minutes)	OFF Time (minutes)	Runtime Fraction (-)	Cycle Rate (cycles/h)
Run						
31	41	2	45	45	0.500	0.667
32	42	4	30	6	0.833	1.667
33	43	3	16	7.25	0.688	2.581
34	44	3	10	10	0.500	3.000
35	45	3, 5	7	17.5	0.286	2.449
	46	5	5.5	55	0.091	0.992

Notes: <sup>1</sup>Constant fan tests performed at 80°F db/60.4°F dp inlet air with 400 cfm/ton (runs 31-35) and 300 cfm/ton (runs 71-75) air flow. Tests also conducted at 75°F db/56°F dp (runs 61-65) and 75°F db/64°F dp (runs 51-55) inlet air with 400 cfm/ton air flow.

<sup>2</sup>Auto fan tests performed at 80°F db/60.4°F dp inlet air with 400 cfm/ton air flow.

<sup>3</sup>Tests were repeated 5 times for runs 45 & 46.

Figure 16 through Figure 19 show the net impact of part-load unit operation based on cyclic tests completed in the lab. All of these tests are in the constant fan mode (continuous air flow over the cooling coil while the coil cycles on/off), but at various entering air and flow rate conditions:

- Nominal: 80°F & 60.4°F dew pt. with 400 cfm/ton (Figure 16)
- Humid: 75°F & 64°F dew pt. with 400 cfm/ton (Figure 17)
- Dry: 75°F & 56°F dew pt. with 400 cfm/ton (Figure 18)
- Low Flow: 80°F & 60.4°F dew pt. with 300 cfm/ton (Figure 19)

The measured data generally compare well to the model from Henderson and Rengarajan (1996) using the model parameters shown on each plot. These parameters were always taken from the 2<sup>nd</sup> occurrence of the first test in each sequence (i.e., Tests #31, 51, 61 and 71), which were completed as part of the suite of cycling tests listed in Table 2 for the constant fan mode. The latent time constant ( $\tau$ ) of 20 seconds was selected based on qualitative observations of the coil's response time. The solid black line corresponds to the linear off-cycle evaporation model. The black dotted line assumes an off-cycle evaporation trend that corresponds to an exponential decay. The purple line is the new part load LHR model that uses the more realistic evaporation model from Stabat et al. (2001) and also allows for variable amounts of moisture on the coil at the end of the on cycle. The parameters NTU and  $t_p$  were determined from the specific measured data from each test sequence (the purple solid line) as well as the average NTU and  $t_p$  from all the data (the purple dotted line), including Figure 9 above. The parameter  $t_p$  is defined in the improved model development section of this report. For the conditions shown in Figure 17, the parameters for the new LHR model could not be determined from the data in that test sequence so the solid purple line is not plotted.

The measured data corresponding to the 3<sup>rd</sup> and 4<sup>th</sup> repetition (cycle) of each test showed the best agreement with the models, since quasi-steady conditions had been achieved.

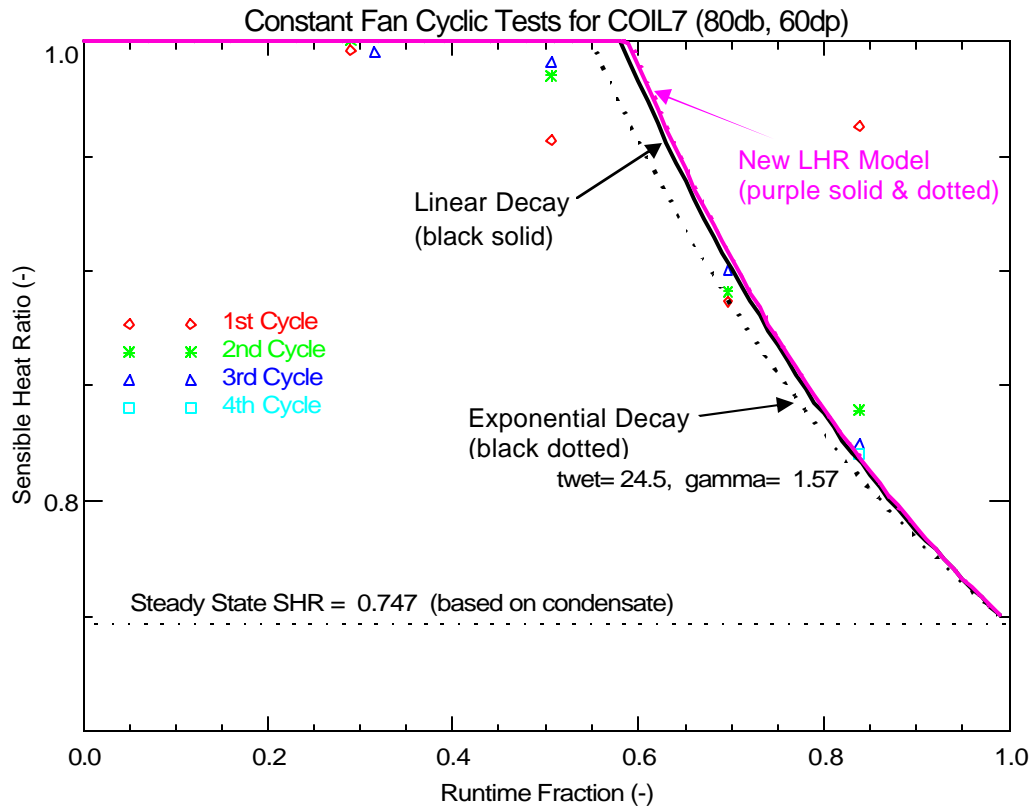


Figure 16. Comparing Measured Latent Degradation to the LHR Models: Nom. Conditions (80°F / 60.4°Fdp)

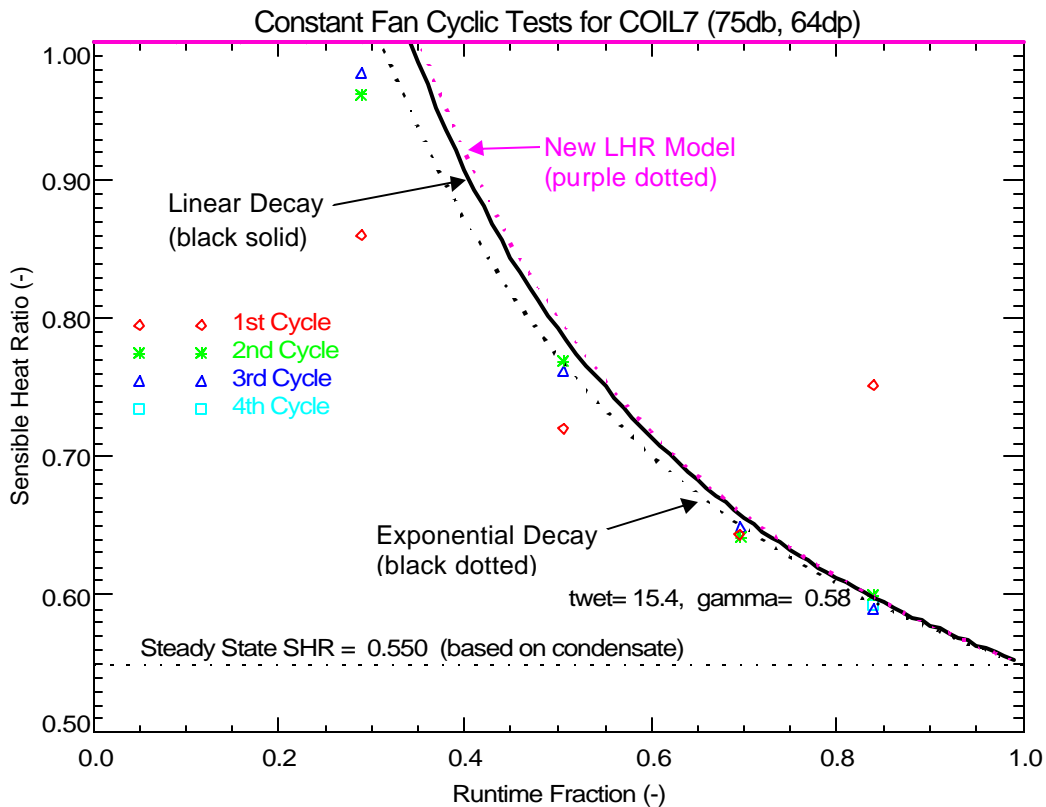


Figure 17. Comparing Measured Latent Degradation to the LHR Models: 75°F / 64°Fdp

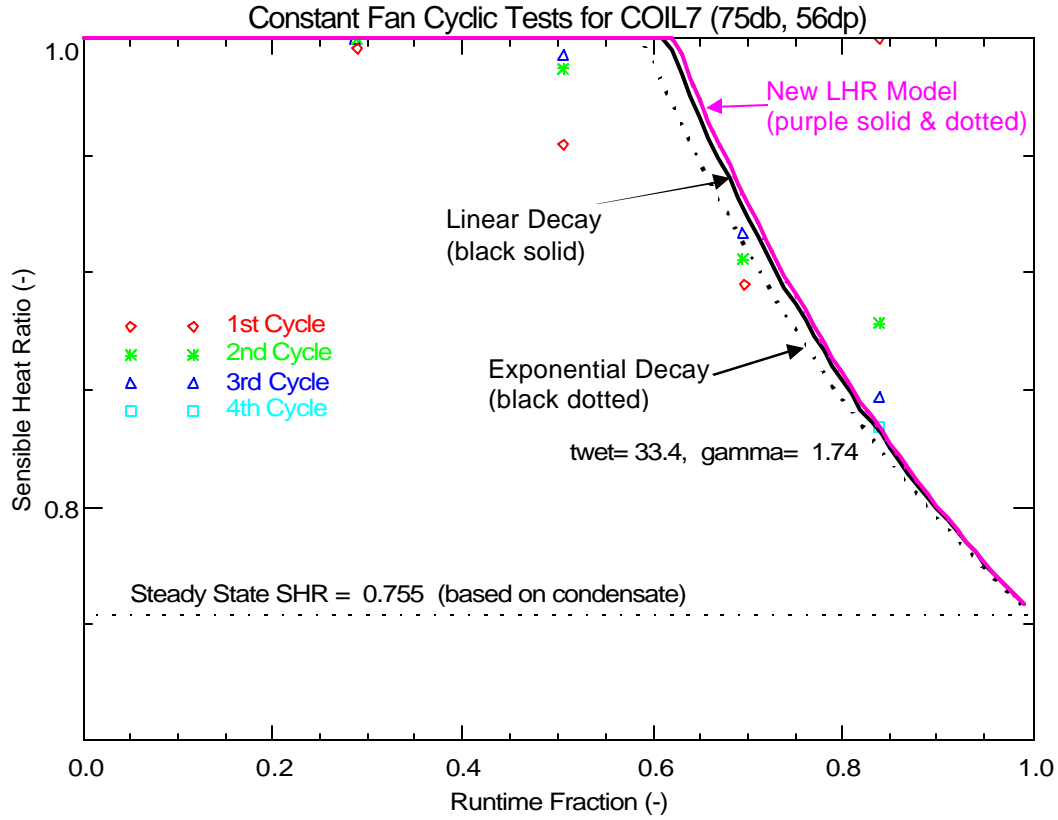


Figure 18. Comparing Measured Latent Degradation to the LHR Models: 75°F / 56°Fdp

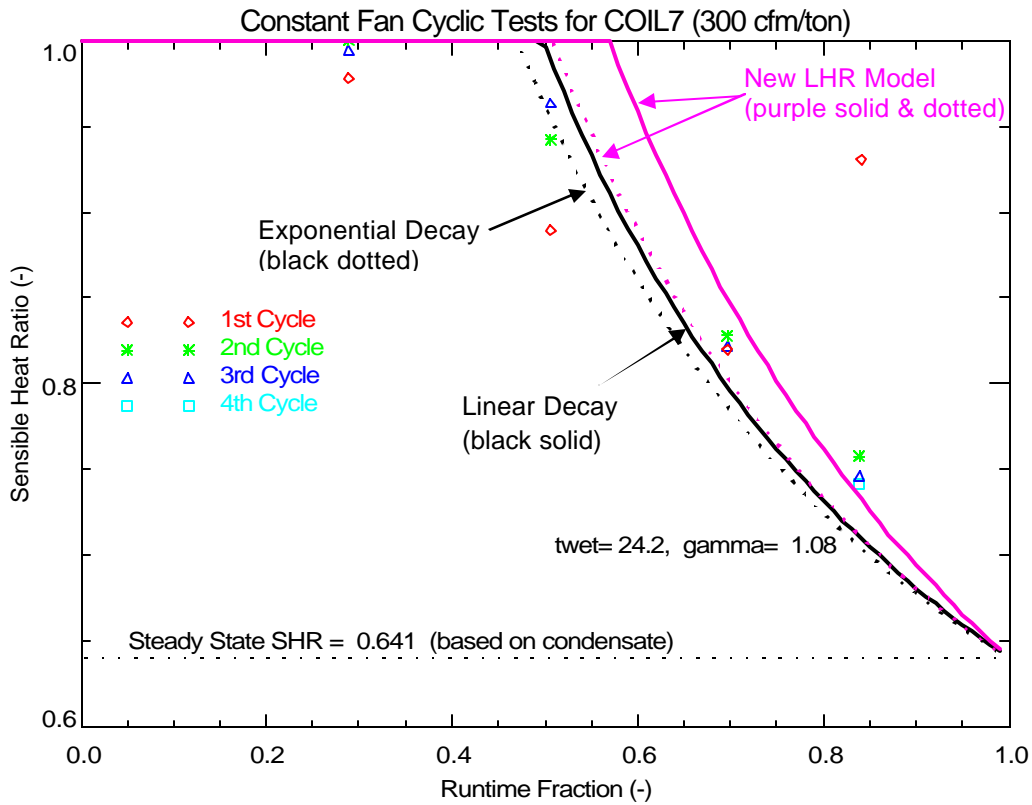
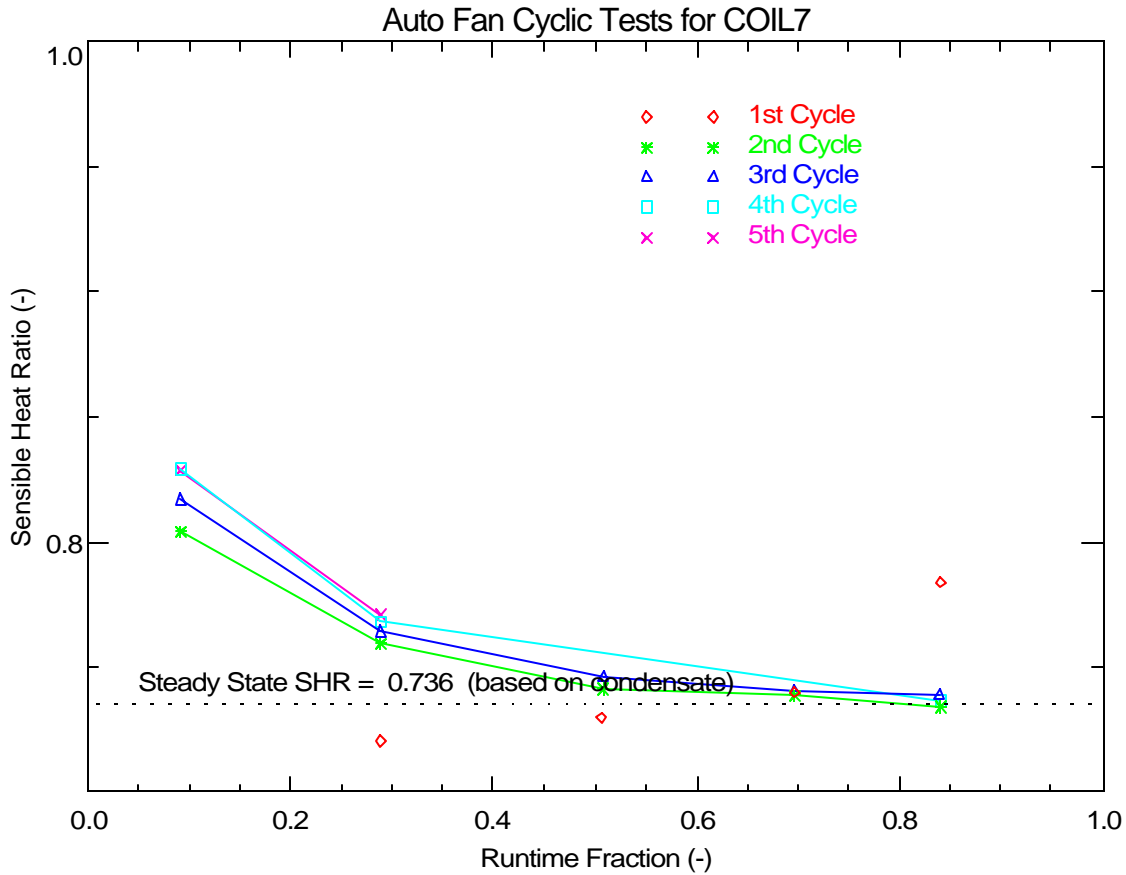


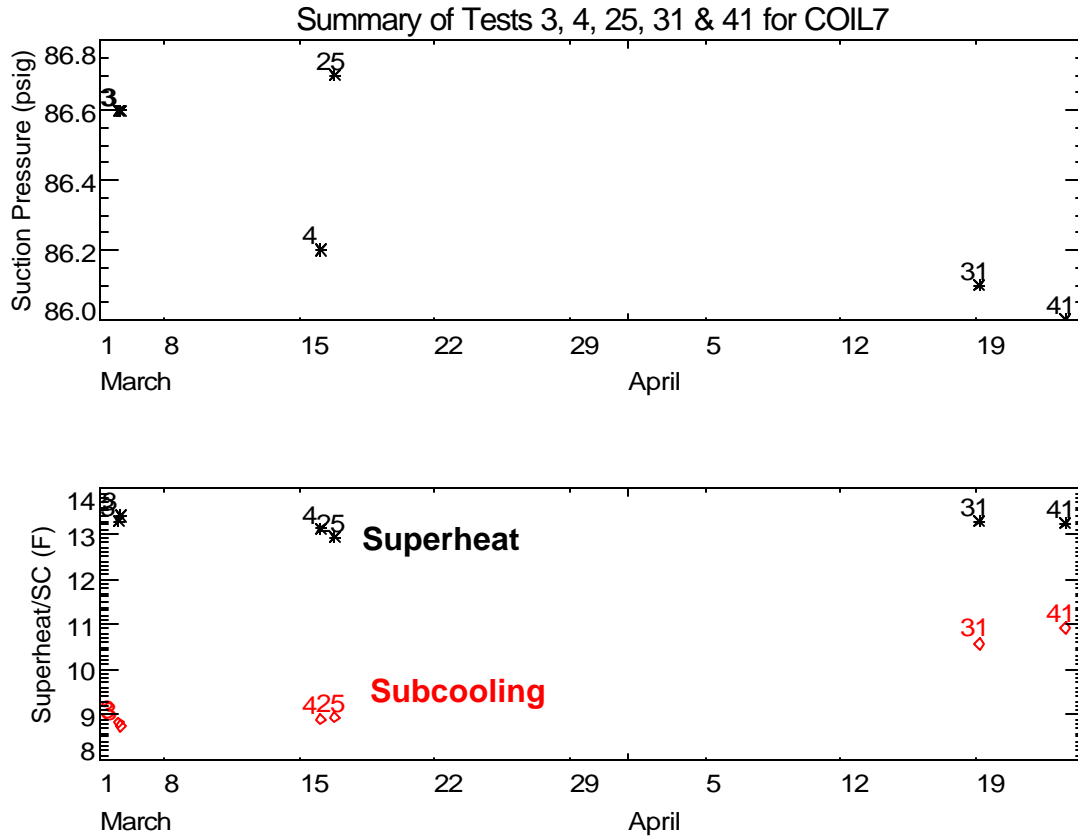
Figure 19. Comparing Measured Latent Degradation to the LHR Models: 300 cfm/ton, 80°F / 60.4°Fdp

Figure 20 shows some latent degradation can be detected in the AUTO fan mode (i.e., the supply air flow across the cooling coil starts and stops with compressor operation) for Coil 7 (similar degradation has been seen for other coils). For this coil the number of repeated cycles at low runtime fractions was increased to 5 to ensure quasi-steady conditions are achieved. The last repetitions (cycles) show good agreement with each other.



**Figure 20. Measured AUTO Fan Latent Degradation**

The tests were completed over a period of 7 weeks. Figure 21 shows some evidence of a modest change in suction pressure, subcooling and superheat over the test period. This implies that a small loss of refrigerant charge may have occurred over the test period.



**Figure 21. Long-Term Variation in Suction Pressure, Superheat and Subcooling**

**References**

Henderson, H., and K. Rengarajan. 1996. A model to predict the latent capacity of air conditioners and heat pumps at part-load conditions with constant fan operation. *ASHRAE Transactions* 102(1): 266-274.

Stabat, P., Marchio, D. and M. Orphelin. 2001. Pre-Design and Design Tools for Evaporative Cooling. *ASHRAE Transactions* 107 (1): 501-510.

**COIL 7 Test Runs**

File Name	Date	Start Time	Sequence No.	Run/Test No.	Inlet DB (F)	Inlet DewPt (F)	Air Flow (cfm)	Test Duration (min)	Comp Runtime (min)
coil7_test_1b.out	4/5/2004	18:57:47	1	1	80	60.5	790.1	215.9	123.3
coil7_test_1b.out	4/5/2004	22:33:54	2	1	80.1	60.6	790.3	215.9	123.4
coil7_test_1b.out	4/6/2004	2:10:03	3	1	80	60.6	790.8	215.9	123.3
coil7_test_2.out	4/6/2004	13:45:29	1	2	80	60.6	794.5	216	123.7
coil7_test_2.out	4/6/2004	17:21:45	2	2	80	60.6	793.5	216.1	123.8
coil7_test_2.out	4/6/2004	20:58:11	3	2	80	60.6	794.2	216.1	123.8
coil7_test_3.out	3/5/2004	11:09:15	1	3	80.1	60.6	798.7	247.5	154.9
coil7_test_3.out	3/5/2004	15:17:01	2	3	80	60.6	799.2	247.7	155.1
coil7_test_3.out	3/5/2004	19:25:01	3	3	80	60.6	799.8	247.7	155.1
coil7_Test_4b_10b_16b_22b_25b.out	3/15/2004	23:03:53	1	4	80.1	60.6	799.1	246.8	154.6
coil7_Test_4b_10b_16b_22b_25b.out	3/16/2004	3:10:56	2	4	80	60.5	798.3	246.7	154.5
coil7_Test_4b_10b_16b_22b_25b.out	3/16/2004	7:17:56	3	10	80	60.6	621.2	246.9	154.7
coil7_Test_4b_10b_16b_22b_25b.out	3/16/2004	11:25:07	4	16	80.1	60.6	407	246.9	154.8
coil7_Test_4b_10b_16b_22b_25b.out	3/16/2004	15:32:20	5	22	80	60.5	879	246.9	154.6
coil7_Test_4b_10b_16b_22b_25b.out	3/16/2004	19:39:30	6	25	80	60.5	797.2	246.8	154.4
coil7_Test_5e_11e_17e_23e.out	4/16/2004	16:53:10	1	5	80	68.3	795.8	247.4	154.9
coil7_Test_5e_11e_17e_23e.out	4/16/2004	21:00:49	2	5	80	68.8	796.8	247.3	154.8
coil7_Test_5e_11e_17e_23e.out	4/17/2004	1:08:21	3	11	80	68.8	621.5	278	154.6
coil7_Test_5e_11e_17e_23e.out	4/17/2004	5:46:34	4	17	80.1	68.8	410.5	324.4	154.6
coil7_Test_5e_11e_17e_23e.out	4/17/2004	11:11:12	5	23	80	68.8	882.4	247.8	155.2
coil7_Test_6c_12c_18c_24c.out	3/23/2004	16:56:21	1	6	80.3	50.7	805.3	324.8	232.3
coil7_Test_6c_12c_18c_24c.out	3/23/2004	22:21:26	2	6	80	50.7	807.7	324.8	232.3
coil7_Test_6c_12c_18c_24c.out	3/24/2004	3:46:29	3	12	80	50.7	628.8	299	206.4
coil7_Test_6c_12c_18c_24c.out	3/24/2004	8:45:45	4	18	80	50.8	414.9	247.6	155
coil7_Test_6c_12c_18c_24c.out	3/24/2004	12:53:39	5	24	80	50.7	893.1	351	258.5
coil7_Test_7b_13b_19b.out	3/19/2004	14:12:45	1	7	75.6	64.3	804	247.5	155.2
coil7_Test_7b_13b_19b.out	3/19/2004	18:20:30	2	7	75	64.9	804	246.9	154.6
coil7_Test_7b_13b_19b.out	3/19/2004	22:27:38	3	13	75.1	64.7	625.7	277.7	154.6
coil7_Test_7b_13b_19b.out	3/20/2004	3:05:37	4	19	75	64.8	410.8	298.2	154.6
coil7_Test_8c_14c_20c.out	4/17/2004	15:19:17	1	8	75.2	56.7	798.7	247.7	155.1
coil7_Test_8c_14c_20c.out	4/17/2004	19:27:17	2	8	75	56.2	799.1	247.6	155
coil7_Test_8c_14c_20c.out	4/17/2004	23:35:12	3	14	75.1	56.2	623.3	247.6	155
coil7_Test_8c_14c_20c.out	4/18/2004	3:43:01	4	20	75.1	56.3	408.5	247.2	154.7
coil7_Test_9f_15f_21f.out	4/19/2004	14:34:23	1	9	75.1	50.2	800.8	247.4	154.9
coil7_Test_9f_15f_21f.out	4/19/2004	18:42:02	2	9	75	50.2	800.6	247.3	154.8
coil7_Test_9f_15f_21f.out	4/19/2004	22:49:35	3	15	75.2	50.2	622	247.2	154.8
coil7_Test_9f_15f_21f.out	4/20/2004	2:57:06	4	21	75.1	50.3	411.5	247	154.4
coil7_test_cycling_constantb.out	4/19/2004	0:21:48	1	31	80	60.5	797	216.6	124
coil7_test_cycling_constantb.out	4/19/2004	3:58:39	2	31	80	60.6	797.2	216.5	123.9
coil7_test_cycling_constantb.out	4/19/2004	7:35:26	3	32	79.9	60.5	801.9	37	31
coil7_test_cycling_constantb.out	4/19/2004	8:12:41	4	32	79.9	60.6	798.6	37	31
coil7_test_cycling_constantb.out	4/19/2004	8:49:55	5	32	79.9	60.6	799.3	37	31
coil7_test_cycling_constantb.out	4/19/2004	9:27:09	6	32	79.9	60.6	798.5	37	31
coil7_test_cycling_constantb.out	4/19/2004	10:04:22	7	33	79.8	60.6	799.2	23.8	16.5
coil7_test_cycling_constantb.out	4/19/2004	10:28:25	8	33	79.8	60.6	797.7	23.8	16.6
coil7_test_cycling_constantb.out	4/19/2004	10:52:29	9	33	79.8	60.6	802.5	23.8	16.5
coil7_test_cycling_constantb.out	4/19/2004	11:16:32	10	34	79.7	60.5	800.6	20.4	10.4
coil7_test_cycling_constantb.out	4/19/2004	11:37:14	11	34	79.7	60.5	802.6	20.4	10.4
coil7_test_cycling_constantb.out	4/19/2004	11:57:56	12	34	79.7	60.4	802.7	20.5	10.4
coil7_test_cycling_constantb.out	4/19/2004	12:18:39	13	35	79.7	60.3	803.2	25	7.3
coil7_test_cycling_constantb.out	4/19/2004	12:43:58	14	35	79.7	60.4	802.5	25	7.3
coil7_test_cycling_constantb.out	4/19/2004	13:09:17	15	35	79.7	60.3	802.8	23	7.3
coil7_test_cycling_constant_75_56.out	3/30/2004	11:15:02	1	61	75	56.4	791.8	216.6	124
coil7_test_cycling_constant_75_56.out	3/30/2004	14:51:54	2	61	75	56.2	791.1	216.7	124.1
coil7_test_cycling_constant_75_56.out	3/30/2004	18:28:53	3	62	75	56.2	795.5	36.9	31
coil7_test_cycling_constant_75_56.out	3/30/2004	19:06:05	4	62	74.9	56.3	792.2	36.9	31
coil7_test_cycling_constant_75_56.out	3/30/2004	19:43:16	5	62	75	56.3	791.9	37	31
coil7_test_cycling_constant_75_56.out	3/30/2004	20:20:29	6	62	74.9	56.3	790.4	36.9	31
coil7_test_cycling_constant_75_56.out	3/30/2004	20:57:41	7	63	74.9	56.2	792.5	23.8	16.5
coil7_test_cycling_constant_75_56.out	3/30/2004	21:21:43	8	63	74.9	56.3	793.8	23.8	16.5
coil7_test_cycling_constant_75_56.out	3/30/2004	21:45:45	9	63	74.9	56.4	794.1	23.8	16.5
coil7_test_cycling_constant_75_56.out	3/30/2004	22:09:47	10	64	74.8	56.5	793.5	20.4	10.3
coil7_test_cycling_constant_75_56.out	3/30/2004	22:30:27	11	64	74.8	56.5	794.4	20.4	10.3
coil7_test_cycling_constant_75_56.out	3/30/2004	22:51:09	12	64	74.8	56.4	795.8	20.4	10.3
coil7_test_cycling_constant_75_56.out	3/30/2004	23:11:49	13	65	74.7	56.3	796.3	25	7.2
coil7_test_cycling_constant_75_56.out	3/30/2004	23:37:08	14	65	74.9	56.3	799.3	25	7.2
coil7_test_cycling_constant_75_56.out	3/31/2004	0:02:26	15	65	74.9	56.3	799.3	25	7.2

**COIL 7 Test Runs (cont)**

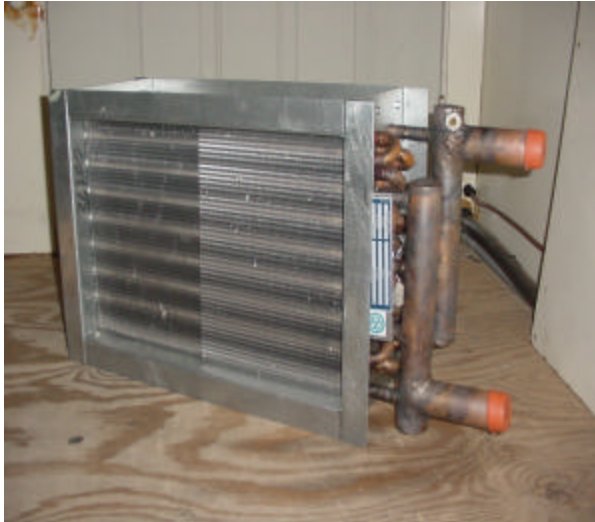
File Name	Date	Start Time	Sequence No.	Run/Test No.	Inlet DB (F)	Inlet DewPt (F)	Air Flow (cfm)	Test Duration (min)	Comp Runtime (min)
coil7_test_cycling_constant_75_64.out	3/29/2004	22:03:32	1	51	75.5	64.1	791.1	216.4	123.8
coil7_test_cycling_constant_75_64.out	3/30/2004	1:40:10	2	51	75.1	64.2	791.3	216.2	123.7
coil7_test_cycling_constant_75_64.out	3/30/2004	5:16:37	3	52	75.2	64.1	791.9	36.8	30.9
coil7_test_cycling_constant_75_64.out	3/30/2004	5:53:42	4	52	75.1	64.1	790.4	36.8	30.9
coil7_test_cycling_constant_75_64.out	3/30/2004	6:30:49	5	52	75.1	64.1	791.4	36.8	30.9
coil7_test_cycling_constant_75_64.out	3/30/2004	7:07:57	6	52	75.1	64.1	791	36.9	31
coil7_test_cycling_constant_75_64.out	3/30/2004	7:45:07	7	53	75.2	64	789.2	23.8	16.5
coil7_test_cycling_constant_75_64.out	3/30/2004	8:09:08	8	53	75.2	64.1	791.9	23.7	16.5
coil7_test_cycling_constant_75_64.out	3/30/2004	8:33:09	9	53	75.3	64	791.7	23.7	16.5
coil7_test_cycling_constant_75_64.out	3/30/2004	8:57:10	10	54	75.4	64.1	792	20.4	10.3
coil7_test_cycling_constant_75_64.out	3/30/2004	9:17:49	11	54	75.4	64	792.5	20.4	10.3
coil7_test_cycling_constant_75_64.out	3/30/2004	9:38:28	12	54	75.3	63.9	791.6	20.4	10.3
coil7_test_cycling_constant_75_64.out	3/30/2004	9:59:07	13	55	75.4	63.9	794.6	25	7.2
coil7_test_cycling_constant_75_64.out	3/30/2004	10:24:25	14	55	75.6	63.9	796	25	7.2
coil7_test_cycling_constant_75_64.out	3/30/2004	10:49:43	15	55	75.7	64	796.1	25	7.3
coil7_test_cycling_constant_300.out	3/29/2004	8:51:01	1	71	80.4	60.5	613.1	216.7	124.2
coil7_test_cycling_constant_300.out	3/29/2004	12:27:59	2	71	80	60.6	614	216.5	123.9
coil7_test_cycling_constant_300.out	3/29/2004	16:04:44	3	72	80	60.5	615.6	37	31.1
coil7_test_cycling_constant_300.out	3/29/2004	16:42:01	4	72	79.9	60.6	611.8	36.9	31
coil7_test_cycling_constant_300.out	3/29/2004	17:19:13	5	72	79.9	60.5	612.3	37	31
coil7_test_cycling_constant_300.out	3/29/2004	17:56:26	6	72	79.9	60.5	614.2	36.9	31
coil7_test_cycling_constant_300.out	3/29/2004	18:33:38	7	73	79.8	60.5	614.8	23.8	16.5
coil7_test_cycling_constant_300.out	3/29/2004	18:57:40	8	73	79.8	60.5	615.7	23.7	16.5
coil7_test_cycling_constant_300.out	3/29/2004	19:21:41	9	73	79.8	60.5	614.5	23.7	16.5
coil7_test_cycling_constant_300.out	3/29/2004	19:45:41	10	74	79.7	60.5	614.8	20.4	10.3
coil7_test_cycling_constant_300.out	3/29/2004	20:06:21	11	74	79.7	60.4	615.2	20.4	10.3
coil7_test_cycling_constant_300.out	3/29/2004	20:27:01	12	74	79.8	60.4	616.5	20.4	10.3
coil7_test_cycling_constant_300.out	3/29/2004	20:47:40	13	75	79.6	60.4	617.3	25	7.2
coil7_test_cycling_constant_300.out	3/29/2004	21:12:57	14	75	79.6	60.5	616.1	25	7.2
coil7_test_cycling_constant_300.out	3/29/2004	21:38:15	15	75	79.7	60.5	618.2	25	7.2
coil7_test_cycling_autof.out	4/23/2004	13:23:17	1	41	80	60.5	790.1	138.7	77.4
coil7_test_cycling_autof.out	4/23/2004	15:42:16	2	41	80	60.6	789.4	138.8	77.4
coil7_test_cycling_autof.out	4/23/2004	18:01:18	3	42	80	60.5	789	36.9	31
coil7_test_cycling_autof.out	4/23/2004	18:38:29	4	42	80	60.5	789.5	36.8	30.9
coil7_test_cycling_autof.out	4/23/2004	19:15:35	5	42	80	60.5	792.1	36.8	30.9
coil7_test_cycling_autof.out	4/23/2004	19:52:41	6	42	80	60.5	790.2	36.8	30.9
coil7_test_cycling_autof.out	4/23/2004	20:29:45	7	43	80	60.4	792.1	23.7	16.5
coil7_test_cycling_autof.out	4/23/2004	20:53:42	8	43	80	60.5	791.4	23.7	16.5
coil7_test_cycling_autof.out	4/23/2004	21:17:39	9	43	80	60.5	790.3	23.7	16.5
coil7_test_cycling_autof.out	4/23/2004	21:41:35	10	44	79.9	60.5	789	20.3	10.3
coil7_test_cycling_autof.out	4/23/2004	22:02:11	11	44	80	60.5	789.7	20.3	10.3
coil7_test_cycling_autof.out	4/23/2004	22:22:46	12	44	80	60.4	791.8	20.3	10.3
coil7_test_cycling_autof.out	4/23/2004	22:43:22	13	45	80.1	60.3	788.6	24.9	7.2
coil7_test_cycling_autof.out	4/23/2004	23:08:34	14	45	80	60.6	792	24.9	7.2
coil7_test_cycling_autof.out	4/23/2004	23:33:45	15	45	80.1	60.5	791.5	24.9	7.2
coil7_test_cycling_autof.out	4/23/2004	23:58:56	16	45	79.5	60.2	789.9	24.9	7.2
coil7_test_cycling_autof.out	4/24/2004	0:24:08	17	45	79.9	60.4	789.7	24.9	7.2
coil7_test_cycling_autof.out	4/24/2004	0:49:18	18	46	79.9	60.6	792.5	61.8	5.7
coil7_test_cycling_autof.out	4/24/2004	1:51:23	19	46	80	60.6	794.1	61.8	5.7
coil7_test_cycling_autof.out	4/24/2004	2:53:28	20	46	80	60.6	789.5	62.3	5.7
coil7_test_cycling_autof.out	4/24/2004	3:56:05	21	46	80.1	60.8	792.6	62.3	5.7
coil7_test_cycling_autof.out	4/24/2004	4:58:41	22	46	79.9	60.7	791.5	62.3	5.7

## **APPENDIX H8**

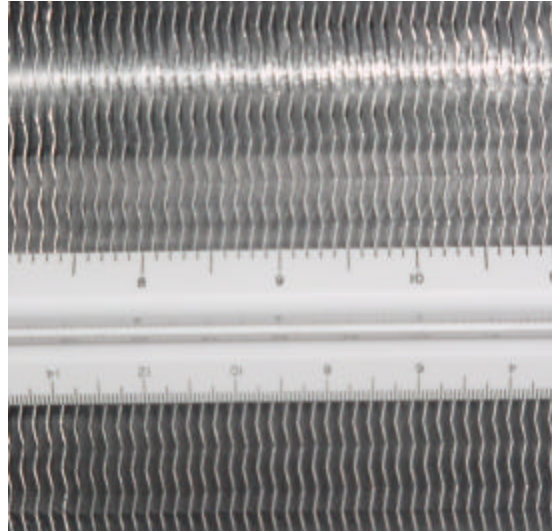
### **Summary of Laboratory Data for Coil 8**



**Summary of Laboratory Data for Coil 8  
November 2005**



Vertical coil arrangement



10 fpi, wavy fin

Manufacturer:	Colmac
Model number:	BWL-12x18-4R-10F-WR-1
Nominal size:	2 tons
Baseline Size and Airflow (Test 4):	1.5 tons / 740 cfm
Coil type:	vertical slab coil, chilled water
Coil dimensions:	4 rows, 10 fpi, 1.5 ft <sup>2</sup> total face area 12 in x 18 in total dimension
Coil thickness:	5 ¼ in
Tube diameter:	5/8 in OD copper
Tube spacing, within row (vert):	1 ½ in
Tubes per row	8
Tube spacing, row-to-row (horiz):	1 3/8 in
Expansion device	not applicable (na)
Unit supply fan:	none
Compressor power	na

**Table 1. Summary of Steady State Test Conditions Corresponding or Each Run or Test**

	<i>Entering Coil Conditions</i>					
	<i>80/67°F 60°F dp</i>	<i>80/72°F 68°F dp</i>	<i>80/62°F 50°F dp</i>	<i>75/68°F 64°F dp</i>	<i>75/63°F 56°F dp</i>	<i>75/58°F 45°F dp</i>
400 cfm/ton	#4 (or 3)	#5	#6	#7	#8	#9
300 cfm/ton	#10	#11	#12	#13	#14	#15
200 cfm/ton	#16	#17	#18	#19	#20	#21
450 cfm/ton	#22	#23	#24			
400-200 cfm/ton (ON & OFF)	#25					
Low water temp (41.5°F)	#1					
High water temp (51.5°F)	#2					

Notes: Tests 4-25 all at nominal entering chilled water temperature of 46°F. The nominal chilled water flow was 8.8 gpm. The Table 1 test points denote the target testing conditions. Drier test conditions with dew points below 50°F (such as Tests #9, #15, and #21) could not be achieved. In these cases, entering conditions were typically held near 50°F dp. For each test, the coil solenoid valve is ON for 60 to 255 minutes and then the coil is OFF for at least 55 minutes. The booster fan runs continuously for all tests (when the coil is both ON and OFF).

### Steady State Performance

The nominal performance characteristics for this chilled coil (based on steady-state conditions from Run #4 below) are:

Total Capacity:	18.1 MBtu/h (1.5 tons)
Sensible Capacity:	15.2 MBtu/h
Latent Capacity (condensate):	2.9 MBtu/h
Sensible Heat Ratio:	0.84

Latent capacity can be calculated two ways: 1) using dew point readings and air flow, and 2) using the condensate flow rate. Figure 1 compares the latent capacity calculated these two ways. The number of each data point corresponds to the test number listed in Table 1. In general, the condensate readings resulted in a slightly lower capacity.

Figure 2 shows the trend of steady-state sensible heat ratio (SHR) with relative humidity and airflow rate. The cooling capacities used to calculate SHR in Figure 2 are based on airflow measurements and the psychrometric conditions entering and leaving the cooling coil. This performance map is typical for a chilled water cooling coil (i.e., SHR is mostly a function of the entering relative humidity, with some dependence on the air flow rate). As might be expected, the SHR is much more dependent on entering humidity conditions for this chilled water coil than had been observed for the DX coils (Coils 1 - 7).

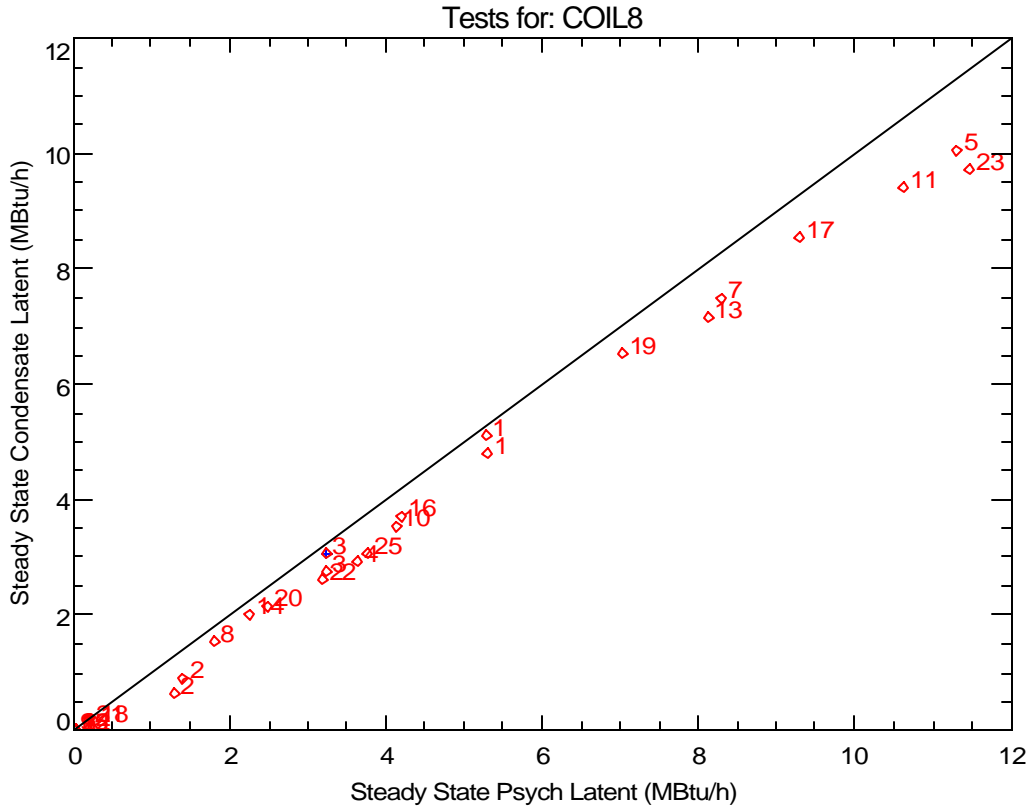


**Figure 1. Comparing Steady-State Latent Capacity Calculated From Psychrometric State Points and Condensate Removal Rates**

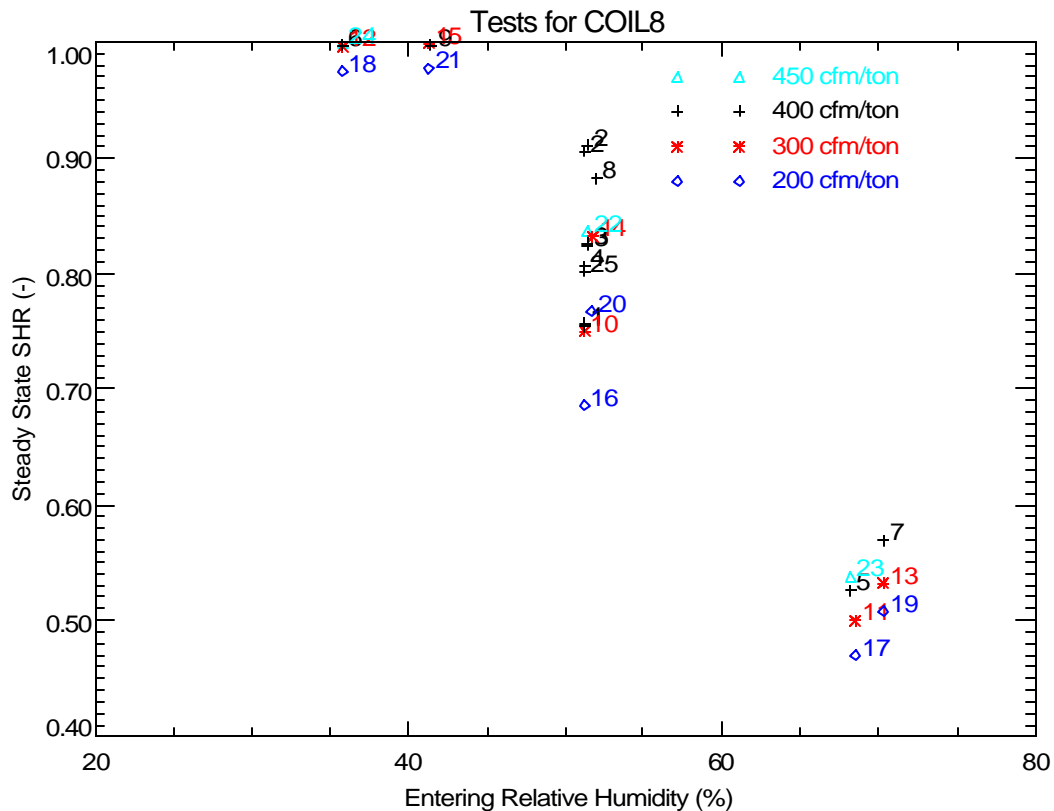


**Figure 2. Variation of Steady State SHR with Entering Humidity and Nominal Air Flow**

## **Typical Transient Performance**

Figure 3 shows the typical transient performance of the cooling coil at nominal conditions (i.e., for Cycle 2 of Run #4). The coil is on for 90 minutes and is off for 75 minutes. The booster fan remains on during the entire test (separate external fan used to maintain the desired air flow rate across the cooling coil). A portion of the moisture removed by the coil during the coil on cycle evaporates back into the air stream during the off cycle. During the off cycle the coil acts as an evaporative cooler, so the sensible capacity is nearly equal to the absolute value of the latent capacity (i.e., the sum of latent and sensible is zero).

If we integrate the off cycle sensible capacity (after allowing for a 1-minute off-cycle delay for transient effects), we can determine the energy associated with the moisture retained on the coil. To minimize the integration of any measurement errors, the off-cycle integration stops at the time labeled “Integration Pt.” on the plot. This point corresponds to the time when the temperature and dew point differences across the coil have first reached the terminal values (i.e., the averages from the end of the off-cycle). In this case the integration indicates that the sensible cooling is equivalent to 1.43 lbs of moisture being retained on the coil. The integrated latent capacity – which is harder to measure precisely – equals 1.24 lbs. The difference in integrated capacities is primarily due to the significant thermal mass of the cooling coil and the water contained within the coil.

The value “ $t_{wet}$ ” from Henderson and Rengarajan (1996) can then be calculated by dividing the retained moisture mass (expressed as Btu; mass x 1060 Btu/lb) and the steady state psychrometric latent capacity ( $QL = 3.7$  MBtu/h). Figure 3 shows that the values of  $t_{wet}$  based on integrated sensible and latent off-cycle capacity are 24.9 and 21.6 minutes, respectively. These values of  $t_{wet}$  are similar to the measured delay of 26.5 minutes for the first condensate pulse to fall from the drain pan. The value of  $\gamma$  (2.23), which is the initial off-cycle moisture evaporation rate divided by the steady-state psychrometric latent capacity, uses the off-cycle moisture evaporation rate (8.1 MBtu/h) once the transition point was been detected. For this coil, we detect the transition by determining where the change in off-cycle sensible capacity between each 15-second interval first drops below 3% of the steady-state on cycle sensible capacity (QS). At this transition point where  $\gamma$  is determined, it is assumed that all coil heat and mass transfer with the air stream is adiabatic. In this case it took 2.25 minutes for the change in off-cycle sensible capacity to drop below 3% of the steady-state on cycle value QS. In contrast, the chilled water flow had stopped after 0.25 minutes.

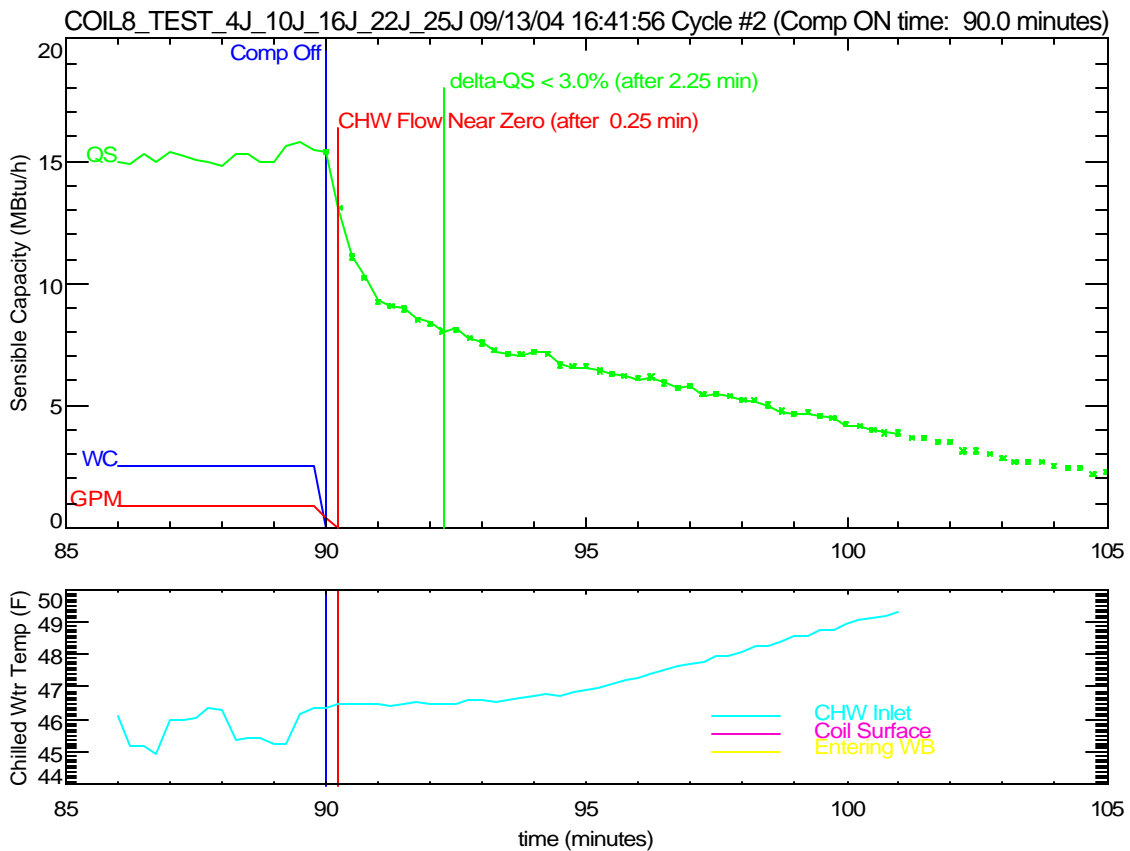
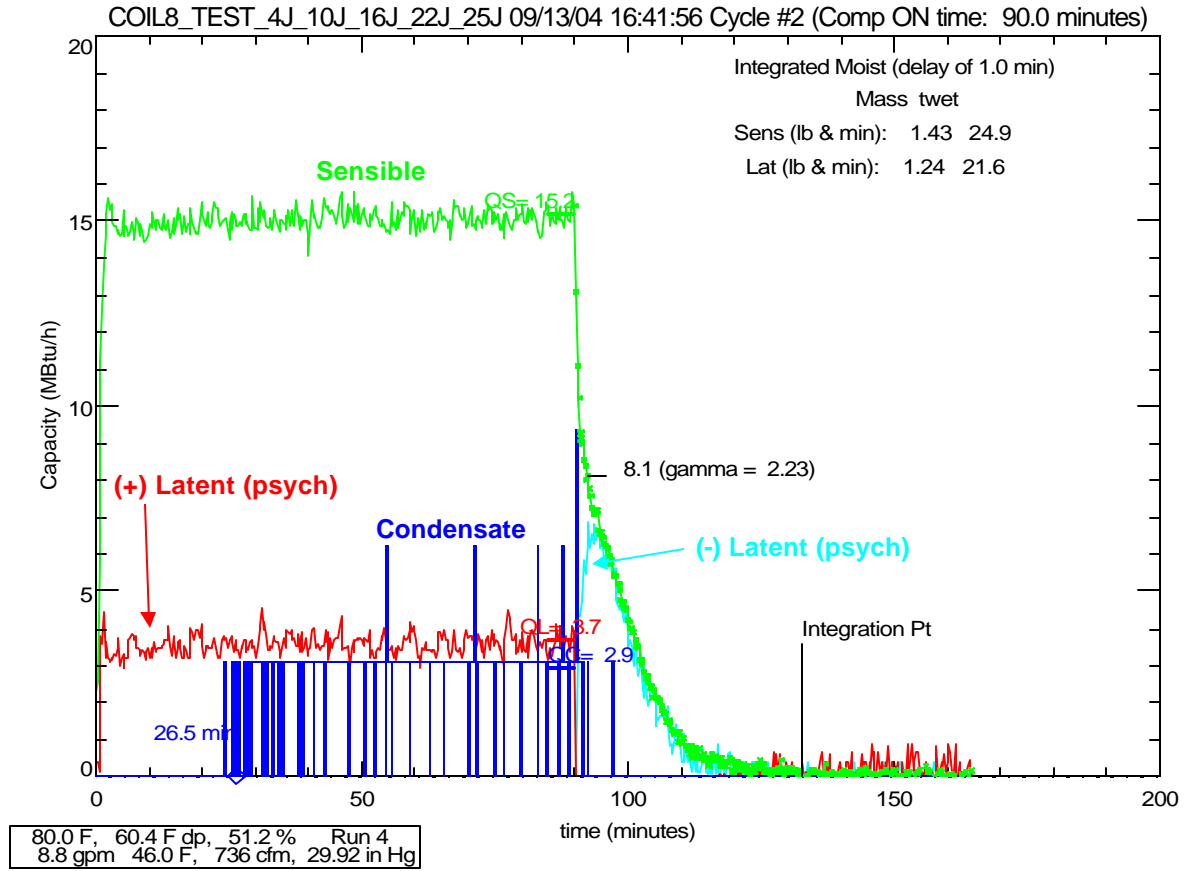
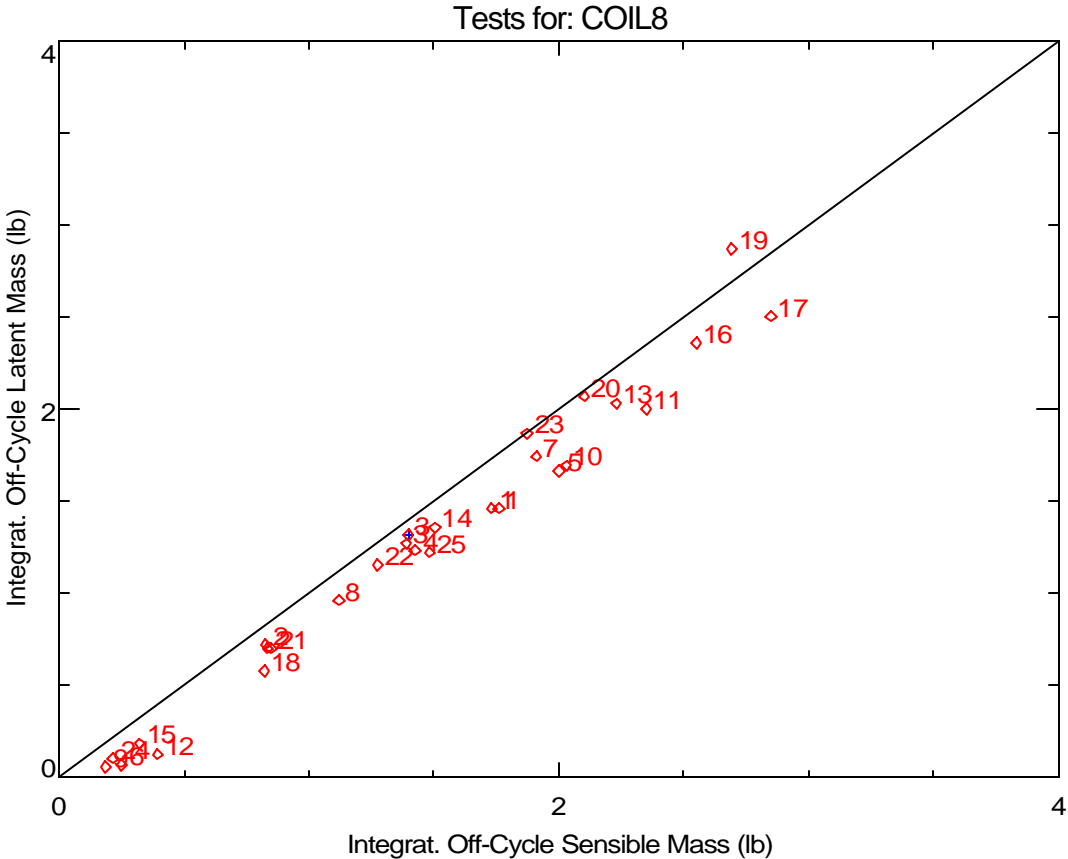


Figure 3. Example Plots of Detailed Data for Coil 8

**Part Load Latent Capacity Parameters**

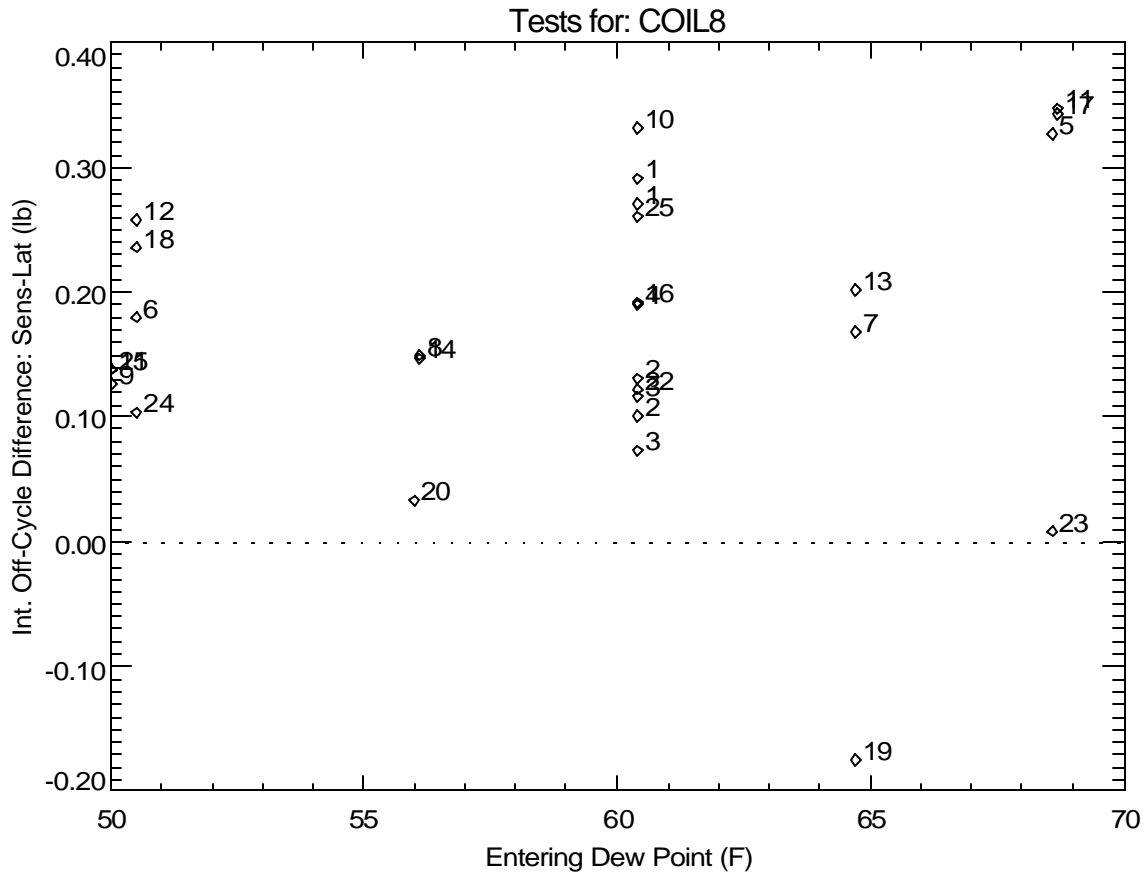
The amount of moisture held on the cooling coil (and drain pan) can be calculated by integrating the off-cycle capacity from the coil (and dividing by the heat of vaporization, 1060 Btu/lb, to get the moisture mass). The integration is delayed for the first minute of the off-cycle so that the overshoot response of the chilled dew point hygrometers does not skew the results of the integration<sup>1</sup>. The integration terminates once steady state conditions are reached for the off cycle. If we assume the coil acts as an evaporative cooler, then sensible and latent capacity should be equal. Figure 4 compares the off-cycle integrated latent and sensible capacity calculated for each run. No systematic bias is evident and Figure 5 shows that any bias is not a function of dew point as was observed from tests of Coil 1.

Since we expect that off-cycle latent and sensible capacity should sum to zero, we have selected the integrated off-cycle sensible capacity as the most consistent and believable indication of the moisture mass held on the cooling coil (and drain pan).



**Figure 4. Comparing Stored Moisture Mass Calculated by Integrating Sensible and Latent Off-Cycle Capacity (Integrated with a 1 minute delay)**

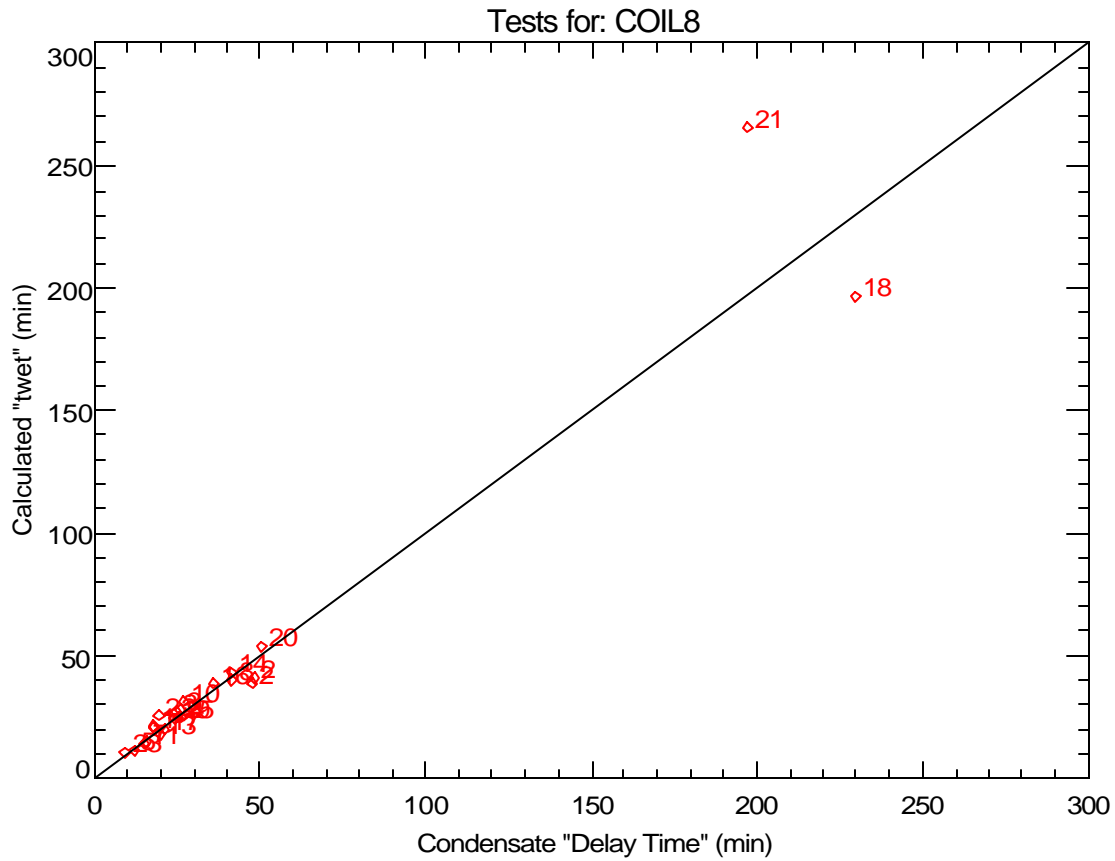
<sup>1</sup>The 1-minute delay causes the estimate of moisture mass to be low by as much as 0.13 lbs (or 9%).



**Figure 5. Variation of Off-Cycle Sensible-Latent Difference with Entering Dew Point**

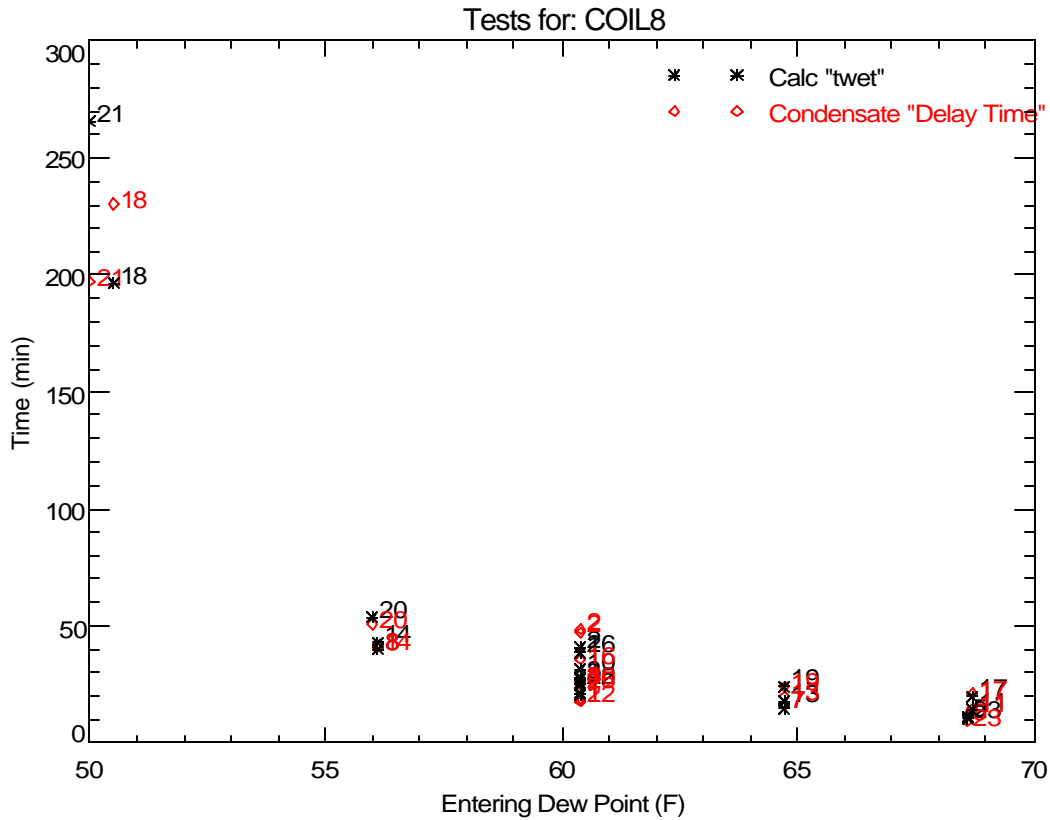
The parameter “twet” is the moisture mass held on the cooling coil times the enthalpy of vaporization (1060 Btu/lb) divided by the steady-state latent capacity of the cooling coil. The parameter should physically correspond to the time it takes for moisture to first fall from the coil (ignoring startup delays and other effects). Figure 6 compares the calculated “twet” (determined from integrating sensible capacity during the off-cycle and then dividing by the steady-state psychrometric latent capacity during the on-cycle) to the condensate delay time for all test runs. In general, there is fair agreement between these two values. The worst agreement is apparent for tests #21 and #18, which correspond to the dry entering air conditions at 200 cfm/ton. The nearly dry coil tests for the DX coils (#6, #9, #15 and #24) are already fully dry for this chilled water coil, and are therefore not being plotted.

Figure 7a and 7b show that both twet and the condensate delay time are a function of the entering air dew point temperature. Figure 7b uses different symbols to show the 1<sup>st</sup> and 2<sup>nd</sup> cycles in each test sequence with flow rate of 400 cfm/ton for all tests. The delay time was generally the same for the first and second cycles for this coil.

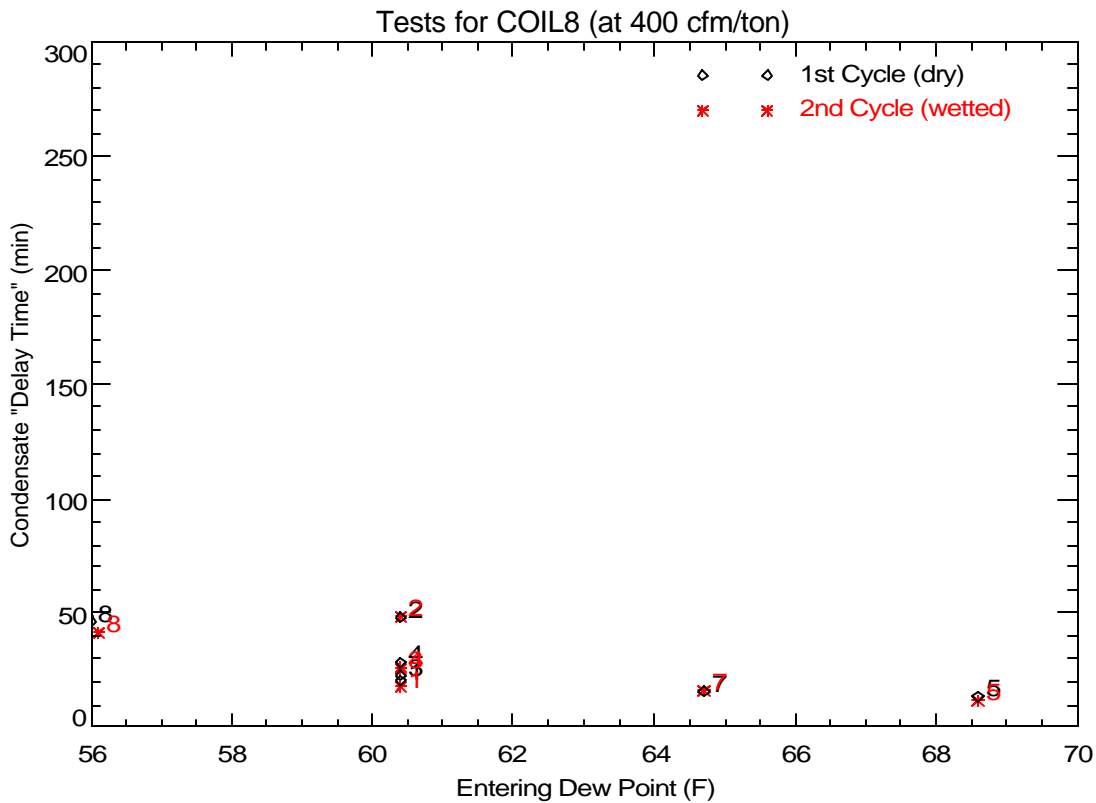


**Figure 6. Comparing “twet” (calculated with off-cycle sensible and steady state latent) to the Condensate Delay Time**





**Figure 7a. Impact of Dew Point on “twet” and Condensate Delay Time**



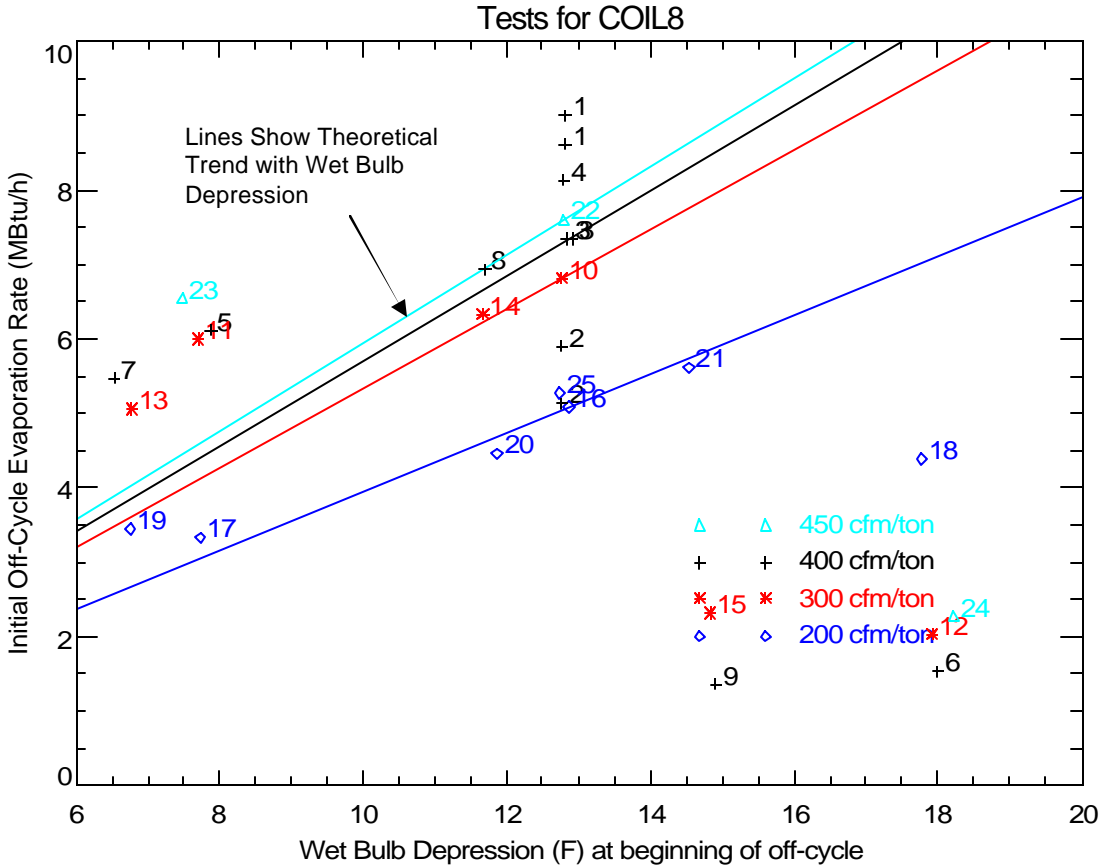
**Figure 7b. Impact of Dew Point and Coil Wettedness on Condensate Delay Time**

Figure 8 shows the initial off-cycle moisture evaporation rate varies with wet bulb depression. As expected, the evaporation rate is highest when the entering air has a larger wet bulb depression (i.e., has a lower relative humidity) and a higher airflow rate.

The model developed by Henderson and Rengarajan (1996) used the following simple evaporative cooler model to predict the moisture evaporation rate at off-design conditions:

$$Q_{\text{evap}} = Q_{\text{evap}_o} \times \frac{(DB - WB)}{(80 - 67)}$$

where  $Q_{\text{evap}_o}$  is the evaporation rate at the nominal entering air conditions of 80°F dry bulb (DB) and 67°F wet bulb (WB). This simple model is shown as the lines in Figure 8. For each airflow rate, the line is based on the nominal test results at 80°F DB/67°F WB extended to pass through zero. The measured data show essentially the same slope as the theoretical lines, though this chilled water coil shows a high degree of scatter. The widest deviations are observed for the points with higher airflow and drier entering air conditions. Specifically, Tests #6, #9, #12, #15, #18 and #24 deviate significantly from the line. These runs have a much lower initial moisture evaporation rate because the entering air dew point temperature was close to the cooling coil temperature, so the fin surfaces were not fully wetted. The smaller wetted surface area reduces the initial moisture evaporation rate.



**Figure 8. Measured Variation of Initial Evaporation Rate with Wet Bulb Depression**

Stabat et al. (2001) reviewed the theoretical performance of direct evaporative coolers and showed that the saturation effectiveness of an evaporative cooler is:

$$h_{evp} = 1 - e^{-NTU} \quad \text{where} \quad NTU = K/cfm^{0.2} \quad \text{for an air-water mixture.}$$

The line shown on Figure 9 is the best fit of the equation above to the measured data. The resulting constant K was 5.64, which is equivalent to an NTU of 1.50 at 740 cfm. While there is considerable scatter due to the experimental uncertainty of predicting the initial off-cycle moisture evaporation rate, the slope of the line is still fairly representative of the overall trend.

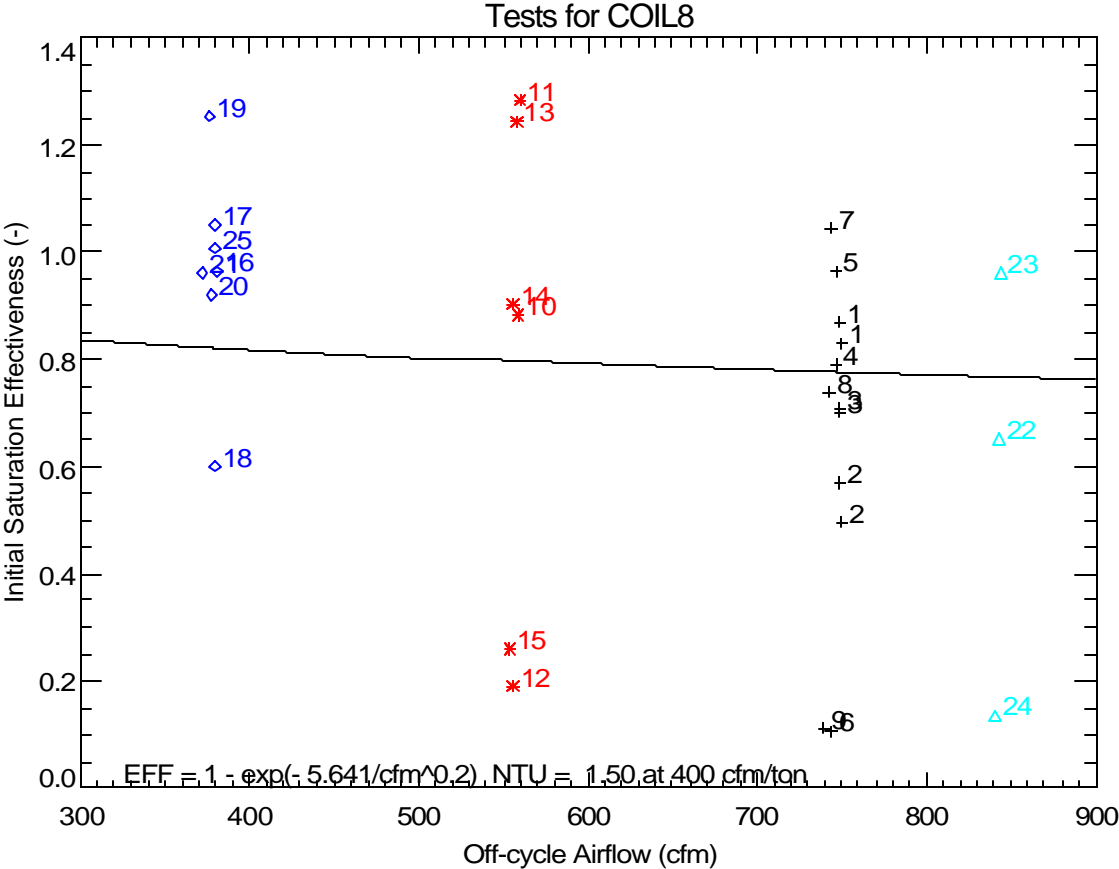


**Figure 9. Evaporative Effectiveness versus Airflow**

Figure 10 compares the measured initial off-cycle moisture evaporation rate for each test to the predicted initial evaporation rate using the effectiveness model above. The model and measured data generally agree when presented in this form (i.e., the overall agreement visually appears better than in Figure 9 above). Again, the variation that occurs for Tests #6, #9, #12, #15, #18 and #24 was due to partial coil dryout, as mentioned above.

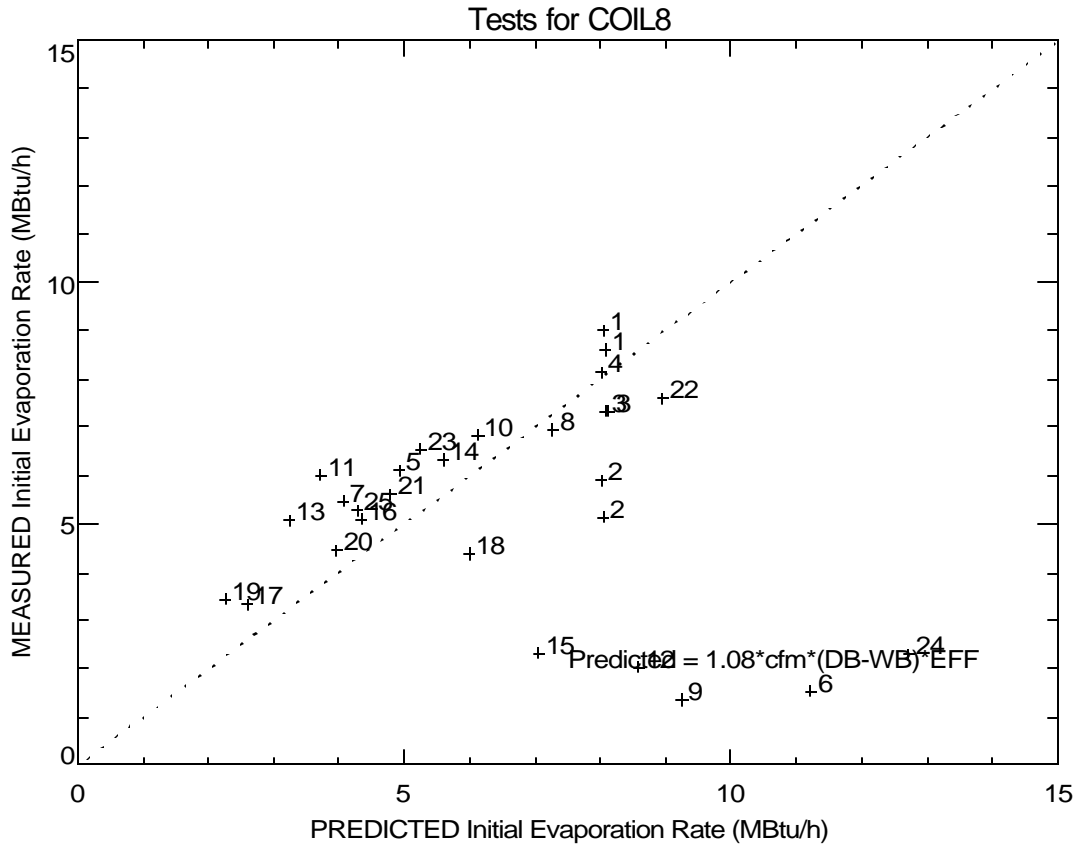


**Figure 10. Comparing Measured and Predicted Initial Moisture Evaporation Rates**

Figure 11 and Figure 12 below evaluate whether the amount of moisture retained on the cooling coil is a function of air flow or entering air conditions. This chilled water coil demonstrated a strong dependence of retained moisture on the entering air dew point temperature (Figure 11). More water was also retained at lower air flow rates (Figure 12). The amount of retained moisture ranges from 0.3 to 3 lbs.

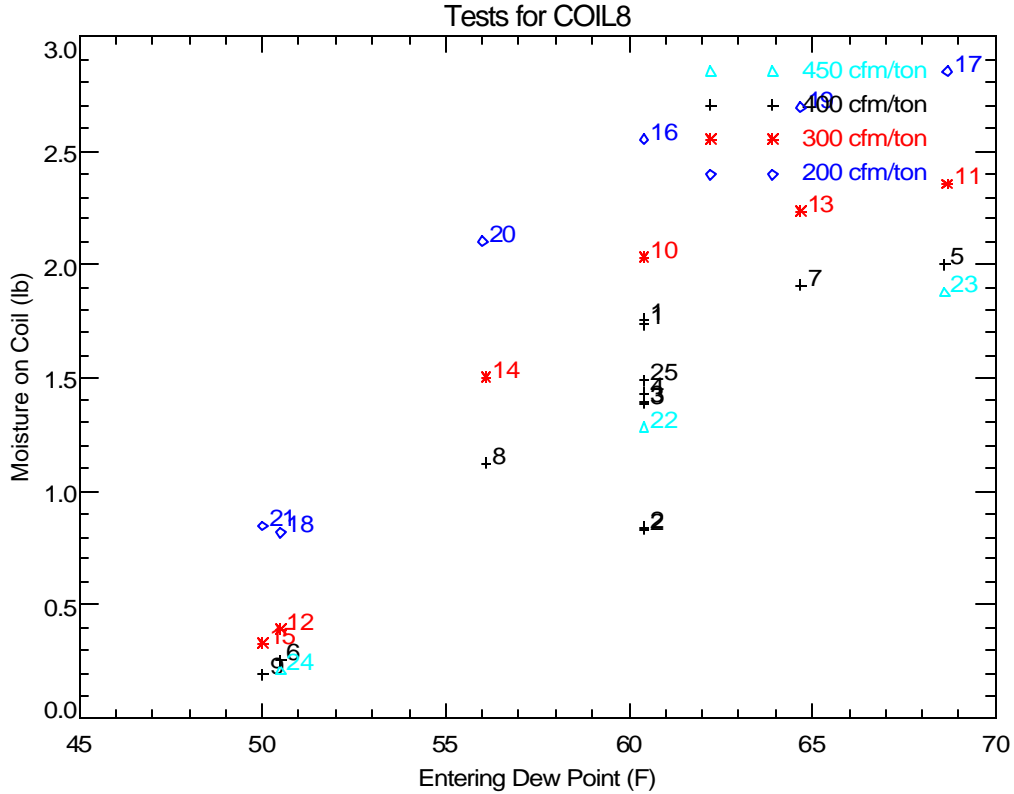


Figure 11. Variation of Retained Moisture (based on Off-Cycle Sensible) with Flow and Dew Point

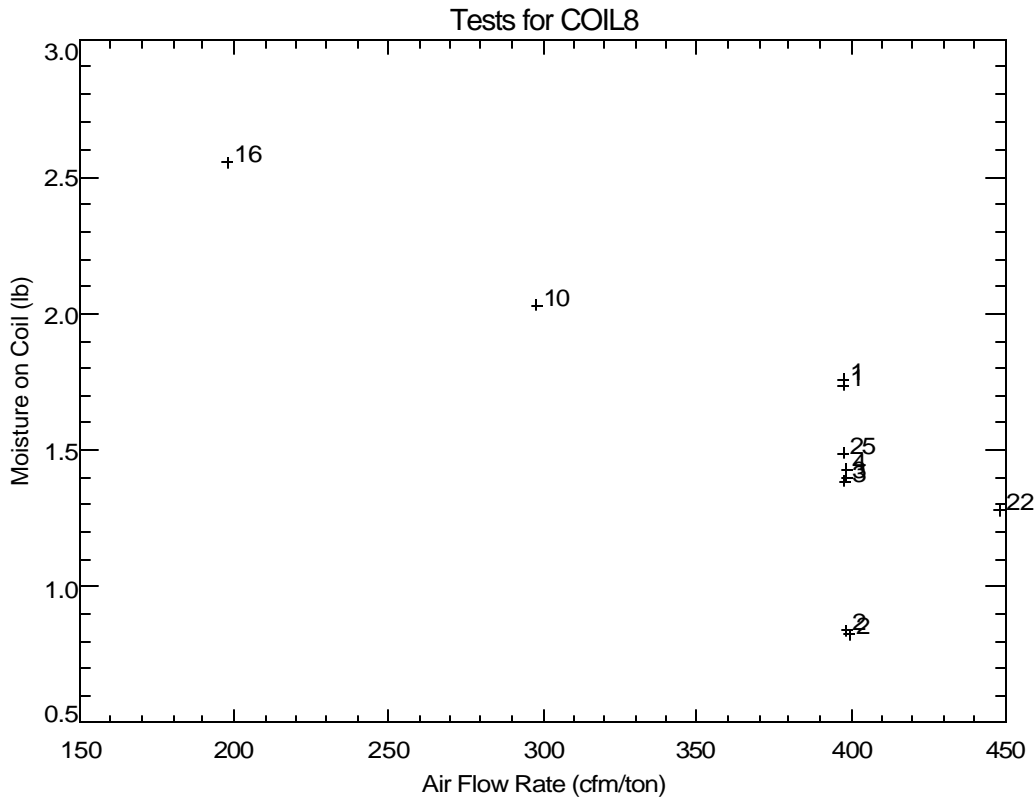
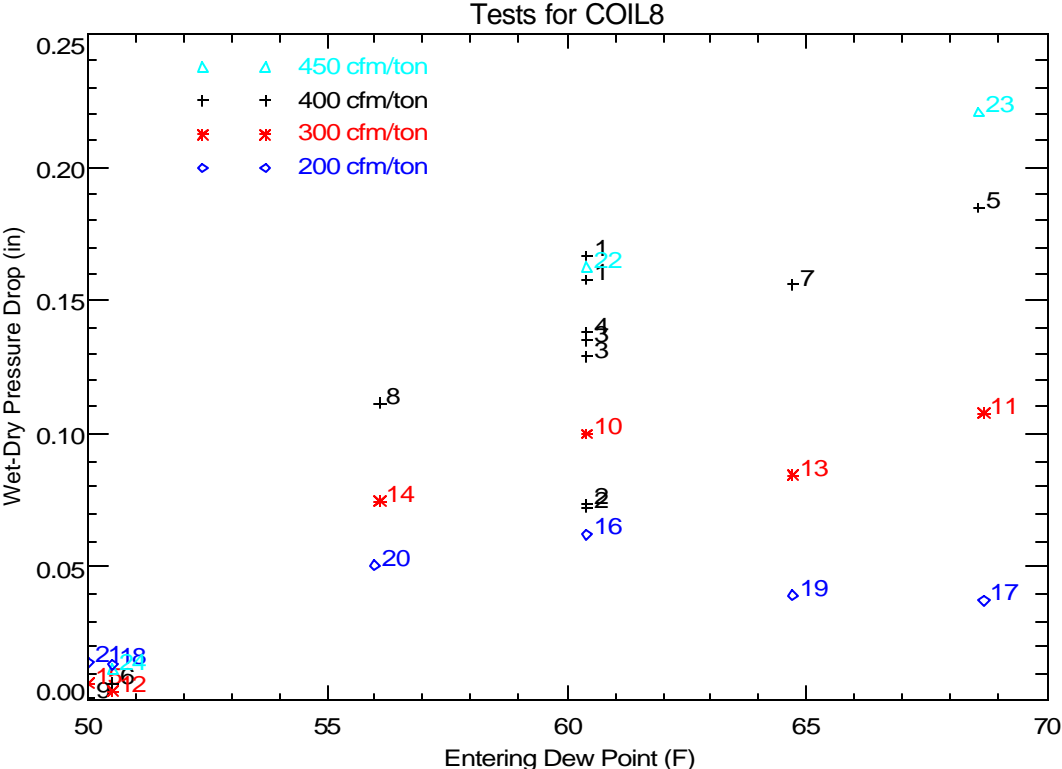


Figure 12. Variation of Retained Moisture with Air Flow at Nominal Entering Conditions of 80°F, 60.4°F dew point

Another way to detect the amount of retained moisture is to measure the static air-side pressure drop across the cooling coil. The difference between the pressure drop across the coil under wet and dry conditions should provide an indication of the amount of retained moisture (the wet coil pressure drop is measured at steady-state conditions while the dry coil pressure drop is taken as the average pressure drop during the last part of the off-cycle). Figure 13 shows the variation of the wet-dry pressure difference with various entering humidity conditions at multiple air flow rates. The pressure drop data confirm that moisture retention is a strong function of the entering air dew point temperature, particularly at the higher air flow rates of 400 cfm/ton and 450 cfm/ton.



**Figure 13. Variation of Wet-Dry Pressure Drop with Entering Conditions and Air Flow Rate**

Figure 14 shows that the wet-dry pressure drop is a linear function of air flow rate, as had been observed for the other tested cooling coils. Test #2 had a warmer chilled water inlet temperature so less moisture was retained.

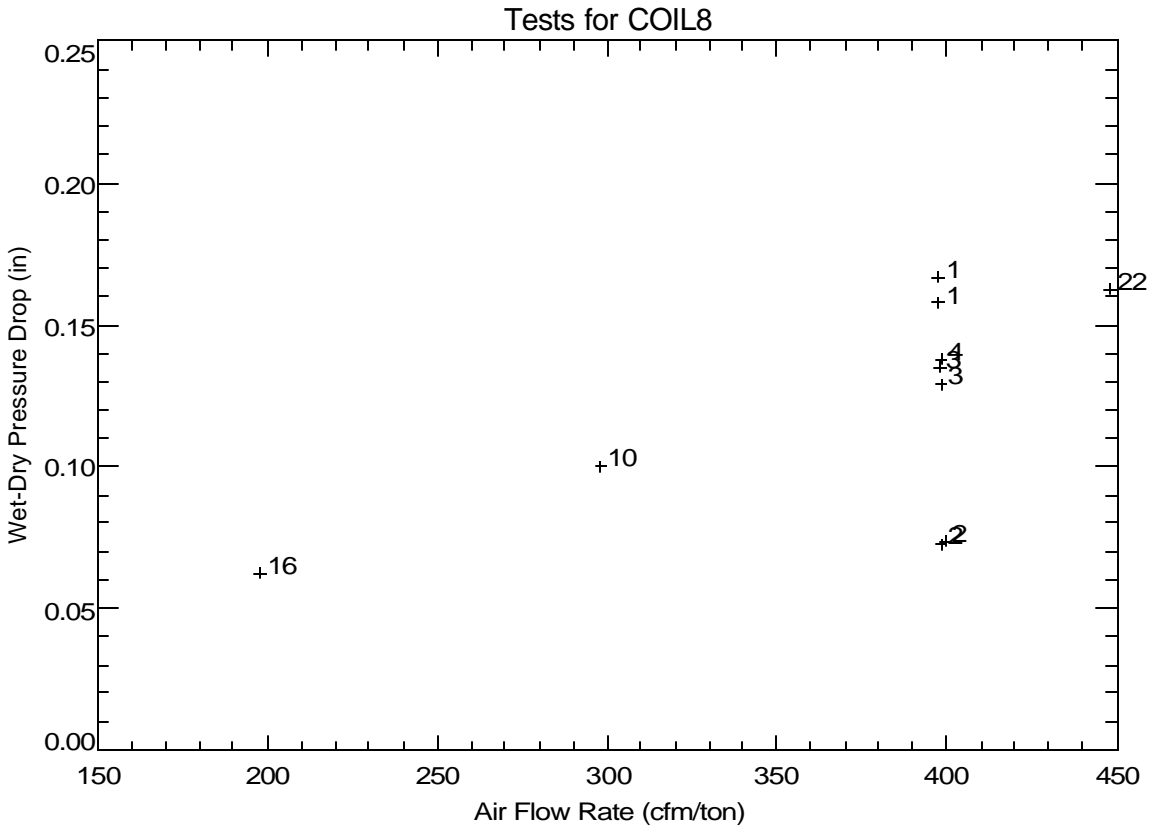


**Figure 14. Trend of Wet-Dry Pressure Drop with Flow at Nominal Entering Conditions of 80°F, 60.4°F dew point**

The series of plots in Figure 15 show the impact of chilled water inlet temperature on performance. The steady-state performance of the system shows the expected trends of lower SHR and greater latent capacity at lower chilled water temperatures. Like Coils 1, 3, 6 and 7, the plots for moisture on coil and wet-dry pressure drop show that more moisture is retained when the coil is colder.

The graph of fan power versus chilled water temperature plot in Figure 15 is not relevant in this case since there was no AHU fan. An external booster fan was used to obtain the desired air flow rate for each test.

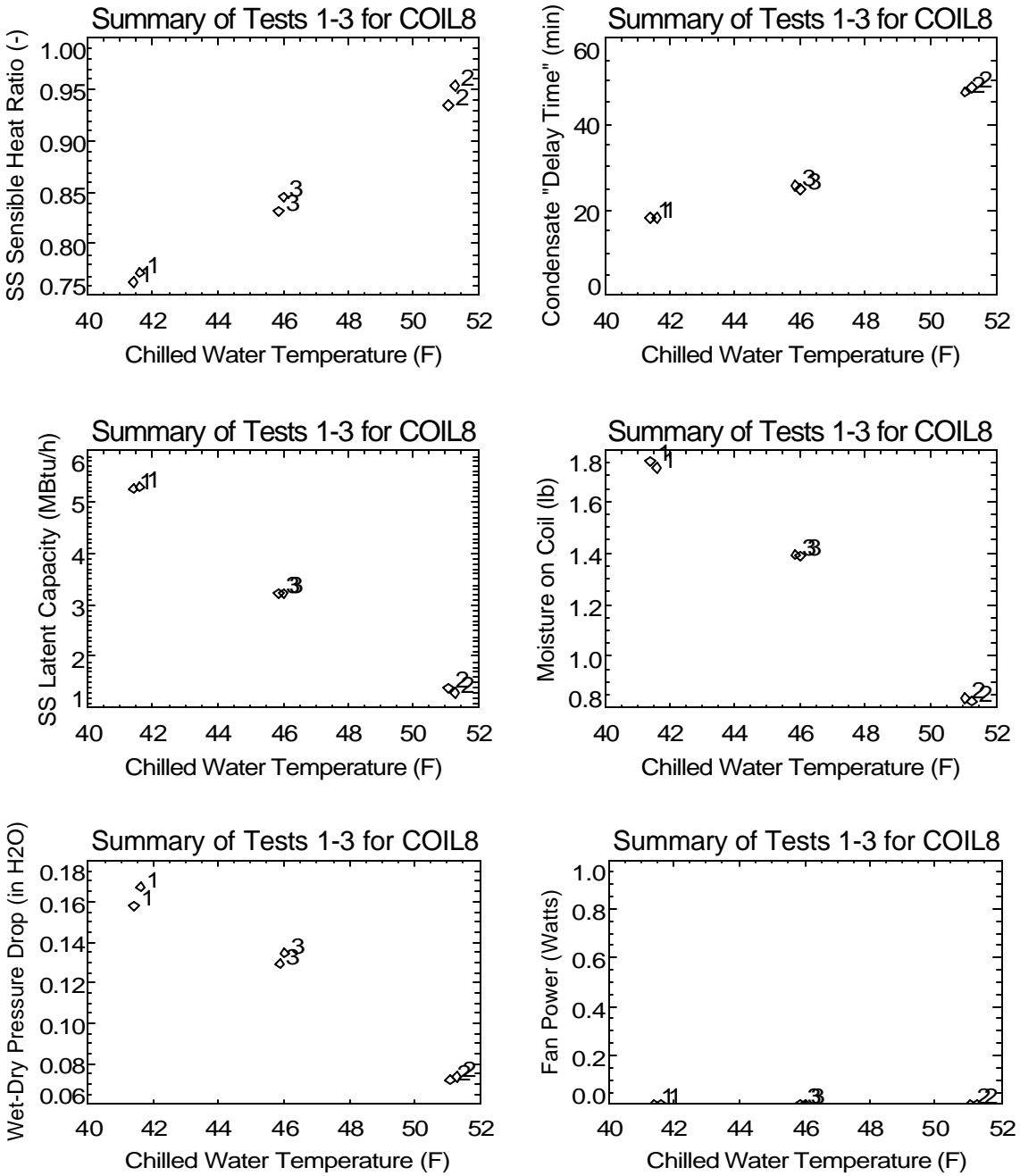


**Figure 15. Trend of Various Parameters with Chilled Water Temperature**



## Overall Latent Degradation Trends

Several quasi-steady cyclic tests were also completed in the laboratory to quantify the overall part-load degradation of latent capacity. Table 2 lists the cycling test runs. These conditions correspond to a conventional thermostat with a maximum cycle rate of 3 cycles per hour (at 50% runtime).

**Table 2. Cyclic Test Conditions**

CONST FAN <sup>1</sup>	AUTO FAN <sup>2</sup>	Number of Times Test Repeated <sup>3</sup>	ON Time (minutes)	OFF Time (minutes)	Runtime Fraction (-)	Cycle Rate (cycles/h)
Run						
31	41	2	45	45	0.500	0.667
32	42	4	30	6	0.833	1.667
33	43	3	16	7.25	0.688	2.581
34	44	3	10	10	0.500	3.000
35	45	3, 5	7	17.5	0.286	2.449
	46	5	5.5	55	0.091	0.992

Notes: <sup>1</sup>Constant fan tests performed at 80°F db/60.4°F dp inlet air with 400 cfm/ton (runs 31-35) and 300 cfm/ton (runs 71-75) air flow. Tests also conducted at 75°F db/56°F dp (runs 61-65) and 75°F db/64°F dp (runs 51-55) inlet air with 400 cfm/ton air flow.

<sup>2</sup>Auto fan tests performed at 80°F db/60.4°F dp inlet air with 400 cfm/ton air flow.

<sup>3</sup>Tests were repeated 5 times for runs 45 & 46.

Figure 16 through Figure 19 show the net impact of part-load unit operation based on cyclic tests completed in the lab. All of these tests are in the constant fan mode (continuous air flow over the cooling coil while the coil cycles on/off), but at various entering air and flow rate conditions:

- Nominal: 80°F & 60.4°F dew pt. with 400 cfm/ton (Figure 16)
- Humid: 75°F & 64°F dew pt. with 400 cfm/ton (Figure 17)
- Dry: 75°F & 56°F dew pt. with 400 cfm/ton (Figure 18)
- Low Flow: 80°F & 60.4°F dew pt. with 300 cfm/ton (Figure 19)

The measured data generally compare well to the model from Henderson and Rengarajan (1996) using the model parameters shown on each plot. These parameters were always taken from the 2<sup>nd</sup> occurrence of the first test in each sequence (i.e., Tests #31, 51, 61 and 71), which were completed as part of the suite of cycling tests listed in Table 2 for the constant fan mode. The latent time constant (tau) of 60 seconds was selected based on qualitative observations of the coil's response time. This chilled water coil had a slower response than the other DX coils (a tau of 20 seconds had been used for the DX coils). The solid black line corresponds to the linear off-cycle evaporation model. The black dotted line assumes an off-cycle evaporation trend that corresponds to an exponential decay. The purple line is the new part load LHR model that uses the more realistic evaporation model from Stabat et al. (2001) and also allows for variable amounts of moisture on the coil at the end of the on cycle. The parameters NTU and tp were determined from the specific measured data from each test sequence (the purple solid line) as well as the average NTU and tp from all the data (the purple dotted line), including Figure 9 above. The parameter tp is defined in the improved model development section of this report.

The measured data corresponding to the 3<sup>rd</sup> and 4<sup>th</sup> repetition (cycle) of each test showed the best agreement with the models, since quasi-steady conditions had been achieved.

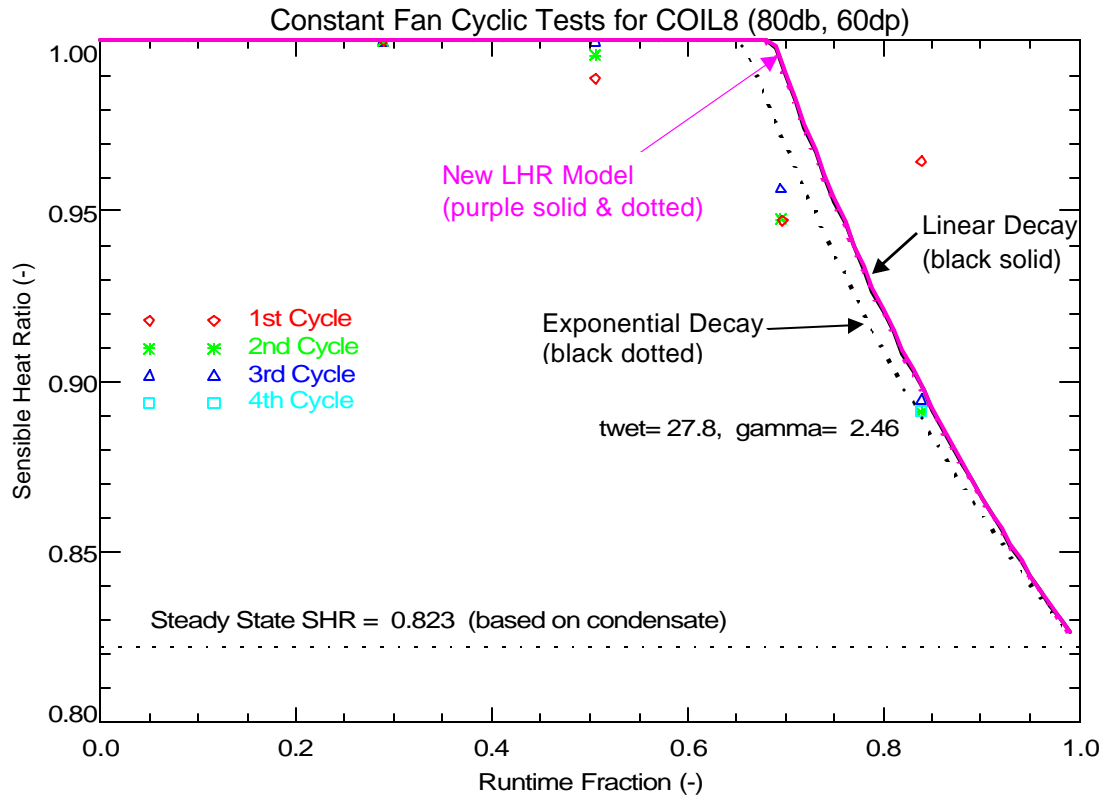


Figure 16. Comparing Measured Latent Degradation to the LHR Models: Nom. Conditions (80°F / 60.4°Fdp)

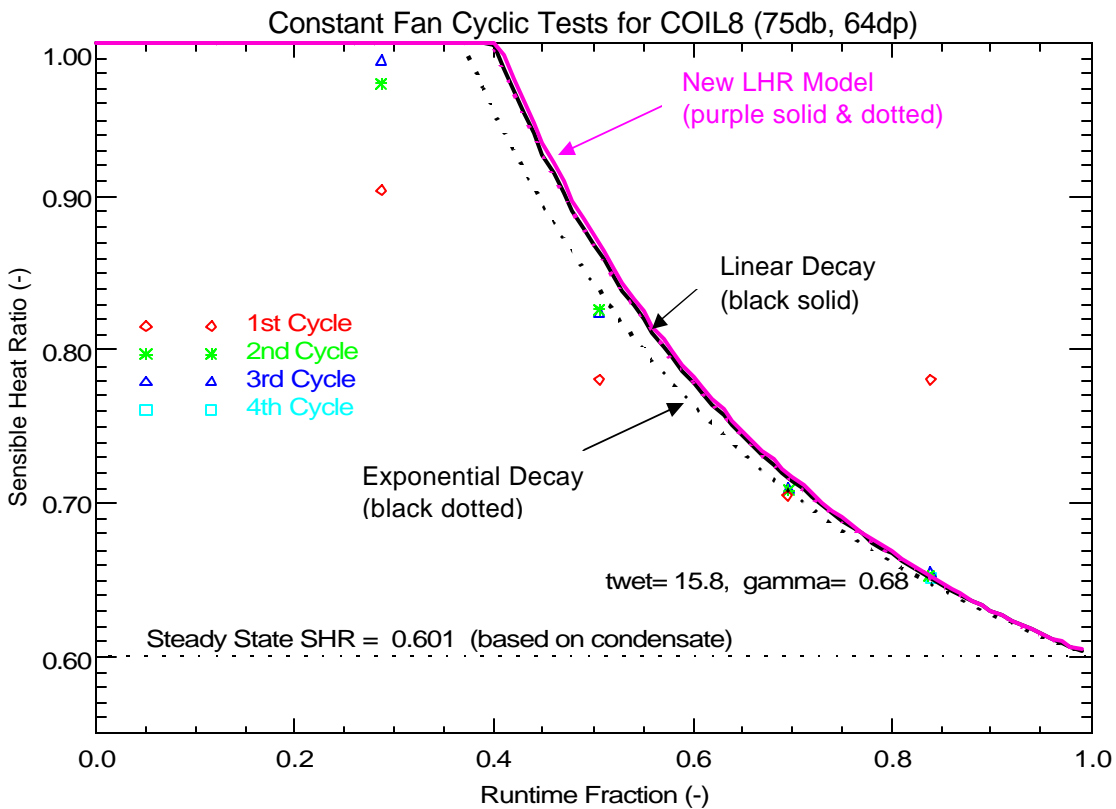


Figure 17. Comparing Measured Latent Degradation to the LHR Models: 75°F / 64°Fdp

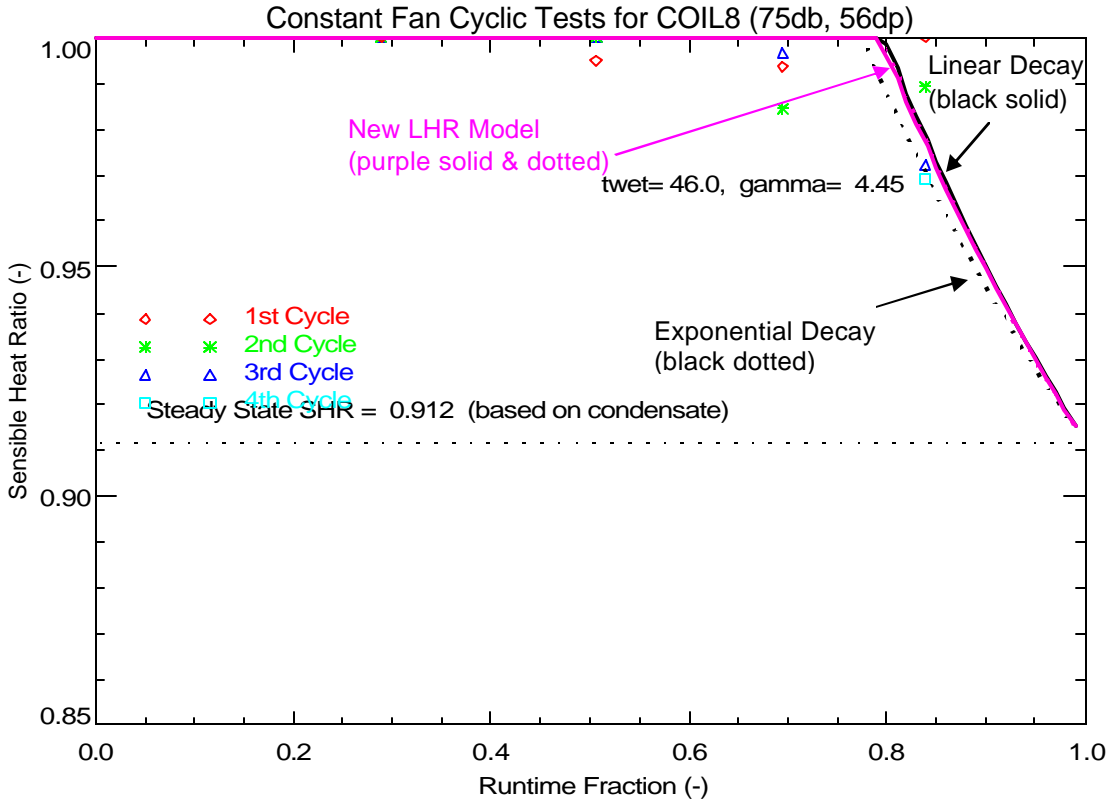


Figure 18. Comparing Measured Latent Degradation to the LHR Models: 75°F / 56°Fdp

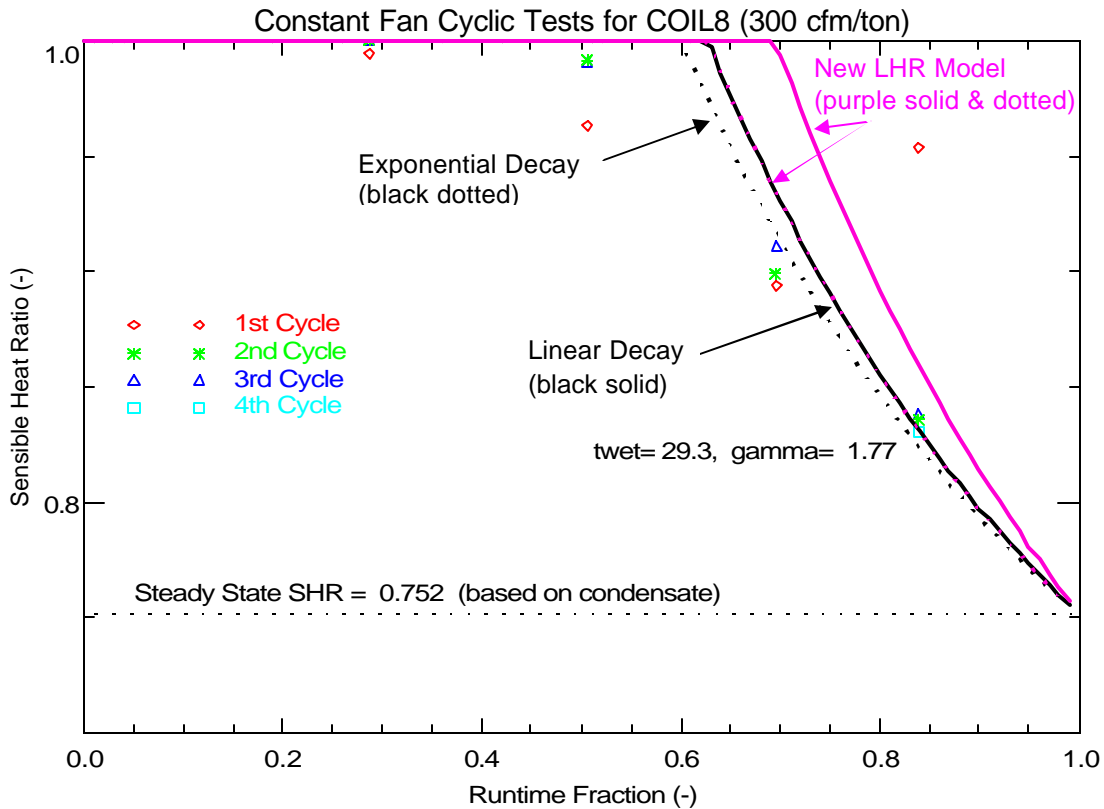
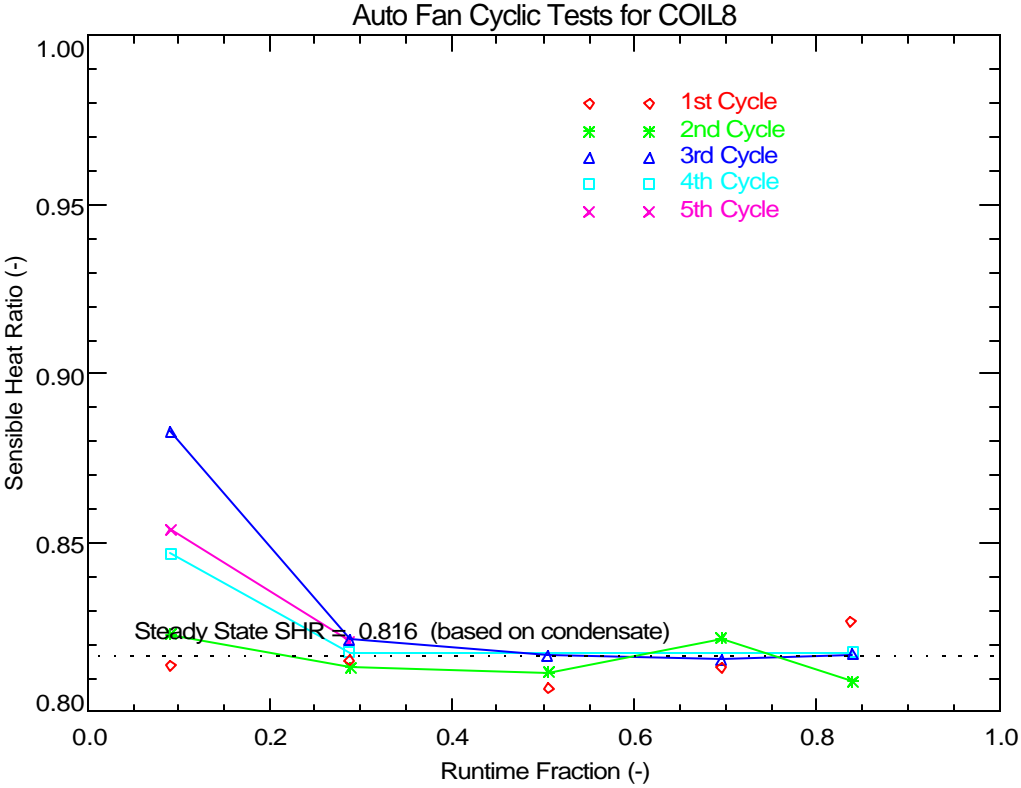


Figure 19. Comparing Measured Latent Degradation to the LHR Models: 300 cfm/ton, 80°F / 60.4°Fdp

Figure 20 shows some latent degradation can be detected in the AUTO fan mode (i.e., the supply air flow across the cooling coil starts and stops with coil operation) for Coil 8 (similar degradation was seen for other coils). For this coil the number of repeated cycles at low runtime fractions was increased to 5 to ensure quasi-steady conditions are achieved. The last repetitions (cycles) show good agreement with each other.



**Figure 20. Measured AUTO Fan Latent Degradation**

Chilled water coils rarely cycle on and off as was simulated with the tests above. Instead, cooling capacity is modulated by varying the chilled water flow rate through the coil. Figure 21 and Figure 22 show the measured steady-state SHR of the coil at various chilled water flow rates. Each plot shows the results for four different entering air conditions. The chilled water flow rate drops from 9 to 1 gpm in each case. The degree of latent degradation varies with the entering air temperature and humidity conditions. The amount of SHR degradation is greater at more humid inlet air conditions.

Figure 23 and 24 show the same data but with total capacity on the x axis. On this scale the latent degradation looks more pronounced since the cooling capacity at very low water flow rates corresponds to about half of the cooling coil capacity at the full water flow rate.

**References**

Henderson, H., and K. Rengarajan. 1996. A model to predict the latent capacity of air conditioners and heat pumps at part-load conditions with constant fan operation. *ASHRAE Transactions* 102(1): 266-274.

Stabat, P., Marchio, D. and M. Orphelin. 2001. Pre-Design and Design Tools for Evaporative Cooling. *ASHRAE Transactions* 107 (1): 501-510.

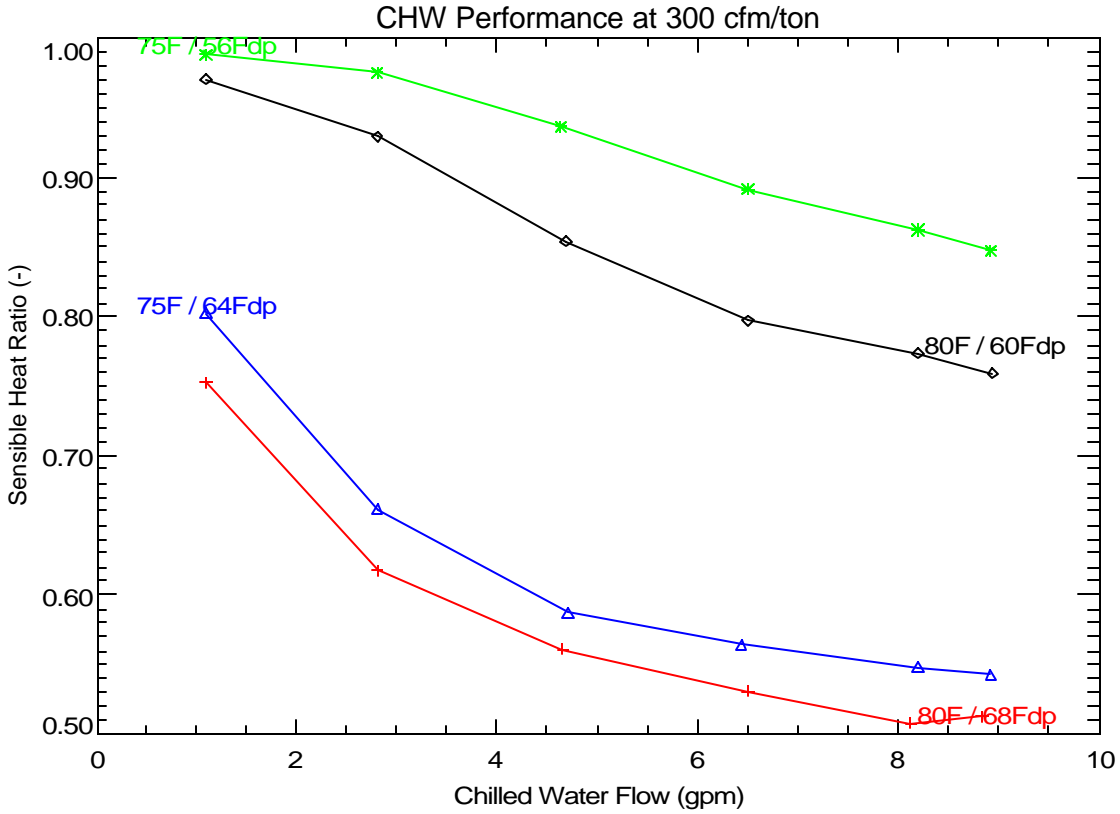


Figure 21. Variation of Coil SHR with Chilled Water Flow Rate at 300 cfm/ton

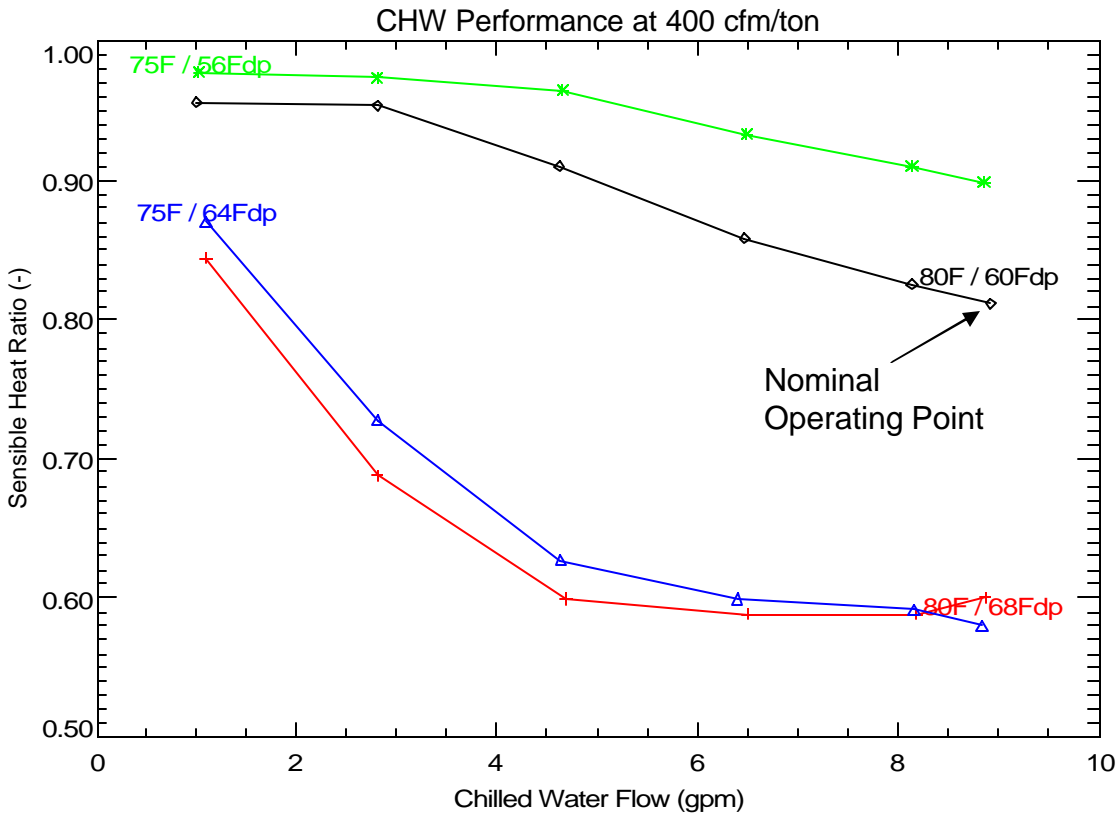
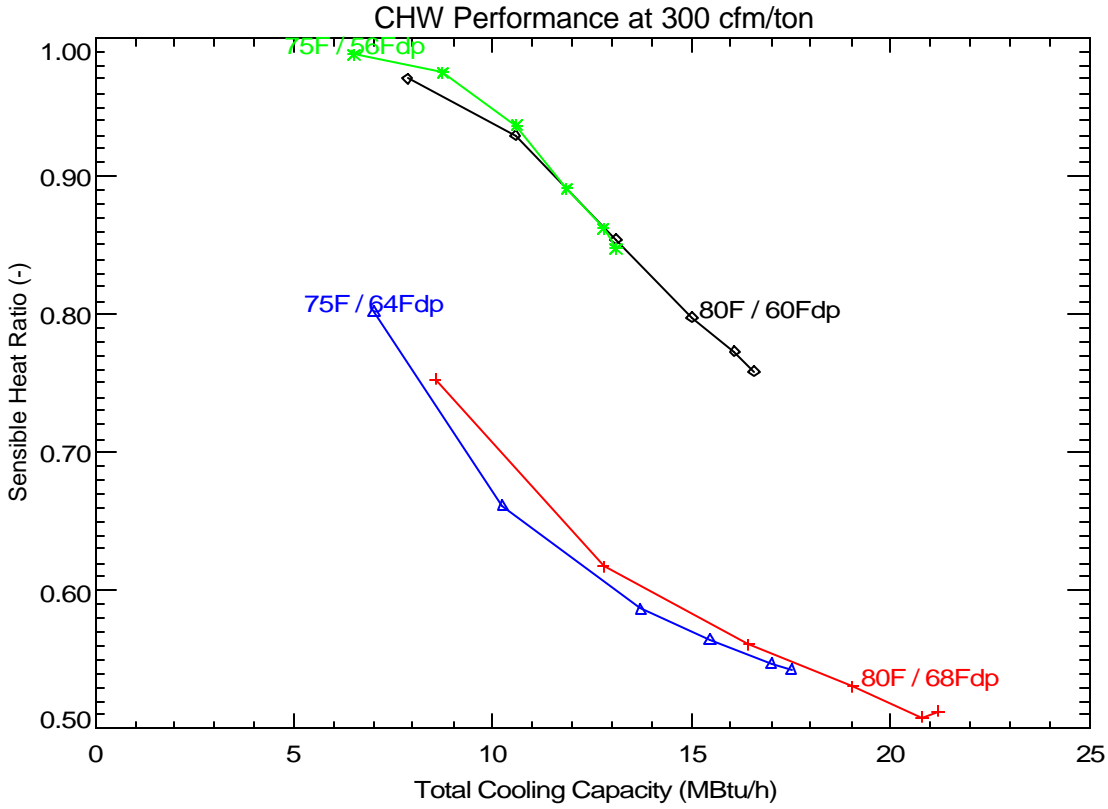
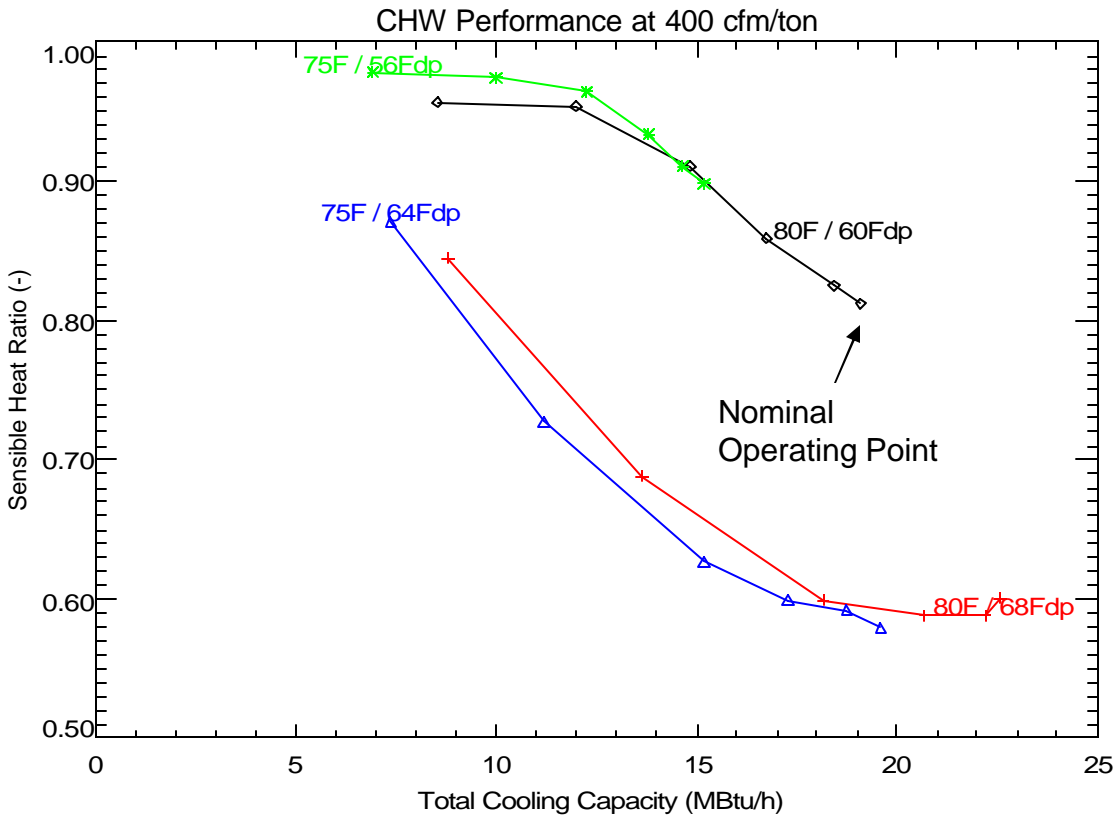


Figure 22. Variation of Coil SHR with Chilled Water Flow Rate at 400 cfm/ton



**Figure 23. Variation of Coil SHR with Cooling Capacity at 300 cfm/ton**



**Figure 24. Variation of Coil SHR with Cooling Capacity at 400 cfm/ton**

**COIL 8 Test Runs**

File Name	Date	Start Time	Sequence No.	Run/Test No.	Inlet DB (F)	Inlet DewPt (F)	Air Flow (cfm)	Test Duration (min)	Comp Runtime (min)
coil8_test_1.out	8/24/2004	9:03:27	1	1	79.9	60.4	734.5	134.8	75
coil8_test_1.out	8/24/2004	11:18:27	2	1	80	60.4	734.9	134.8	75
coil8_test_1.out	8/24/2004	13:33:27	3	1	80	60.4	735.7	138.2	78.4
coil8_test_2.out	8/23/2004	9:15:30	1	2	79.8	60.4	738.1	149.8	75
coil8_test_2.out	8/23/2004	11:45:31	2	2	79.9	60.4	739.5	149.9	75.2
coil8_test_2.out	8/23/2004	14:15:40	3	2	80	60.4	737.6	149.8	75
coil8_test_3e.out	8/17/2004	9:54:08	1	3	80	60.4	736.5	164.7	90
coil8_test_3e.out	8/17/2004	12:39:07	2	3	79.9	60.4	736.9	164.8	90
coil8_test_3e.out	8/17/2004	15:24:07	3	3	79.9	60.4	736.6	164.8	90
coil8_Test_4j_10j_16j_22j_25j.out	9/13/2004	13:56:56	1	4	80	60.4	736.6	164.8	90
coil8_Test_4j_10j_16j_22j_25j.out	9/13/2004	16:41:56	2	4	80	60.4	736.9	164.8	90
coil8_Test_4j_10j_16j_22j_25j.out	9/13/2004	19:26:56	3	10	80	60.4	551.7	179.8	90
coil8_Test_4j_10j_16j_22j_25j.out	9/13/2004	22:26:56	4	16	80	60.4	365.9	199.8	100
coil8_Test_4j_10j_16j_22j_25j.out	9/14/2004	1:46:58	5	22	79.9	60.4	829	164.8	90
coil8_Test_4j_10j_16j_22j_25j.out	9/14/2004	4:31:58	6	25	80	60.4	735.7	189.8	90
coil8_Test_5i_11i_17i_23i.out	8/24/2004	17:07:03	1	5	80.1	68.6	738.2	114.8	60
coil8_Test_5i_11i_17i_23i.out	8/24/2004	19:02:03	2	5	80	68.6	738.9	114.8	60
coil8_Test_5i_11i_17i_23i.out	8/24/2004	20:57:04	3	11	80	68.7	553.5	149.8	70
coil8_Test_5i_11i_17i_23i.out	8/24/2004	23:27:04	4	17	80	68.7	366.6	239.8	90
coil8_Test_5i_11i_17i_23i.out	8/25/2004	3:27:05	5	23	80	68.6	831.8	119.8	60
coil8_Test_6f_12f_18f_24f.out	10/1/2004	14:03:18	1	6	80	50.4	734.6	320.3	229
coil8_Test_6f_12f_18f_24f.out	10/1/2004	19:23:53	2	6	80	50.5	734.7	289.9	229.1
coil8_Test_6f_12f_18f_24f.out	10/2/2004	0:14:01	3	12	80	50.5	549.2	290	229.2
coil8_Test_6f_12f_18f_24f.out	10/2/2004	5:04:16	4	18	80	50.5	364.9	346	254.5
coil8_Test_6f_12f_18f_24f.out	10/2/2004	10:50:28	5	24	80	50.5	827.3	290.1	229.2
coil8_Test_7f_13f_19f.out	8/25/2004	5:27:05	1	7	75.2	64.7	737.7	164.8	90
coil8_Test_7f_13f_19f.out	8/25/2004	8:12:05	2	7	75	64.7	736.4	164.8	90
coil8_Test_7f_13f_19f.out	8/25/2004	10:57:05	3	13	75	64.7	550.9	189.8	100
coil8_Test_7g_13g_19g.out	9/14/2004	17:44:42	4	19	75	64.7	366.2	284.8	125
coil8_Test_8g_14g_20g.out	8/20/2004	22:43:29	1	8	74.9	56	734.6	239.8	150
coil8_Test_8g_14g_20g.out	8/21/2004	2:43:31	2	8	74.9	56.1	734.4	239.8	150
coil8_Test_8g_14g_20g.out	8/21/2004	6:43:32	3	14	75	56.1	549.3	239.8	150
coil8_Test_8g_14g_20g.out	8/21/2004	10:43:32	4	20	75	56	365.1	289.8	200
coil8_Test_9g_15g_21g.out	10/2/2004	15:40:50	1	9	75.2	50	732.5	290	229.2
coil8_Test_9g_15g_21g.out	10/2/2004	20:31:04	2	9	75	50	733.3	289.9	229.1
coil8_Test_9g_15g_21g.out	10/3/2004	1:21:16	3	15	75.1	50	548.6	289.9	229.1
coil8_Test_9g_15g_21g.out	10/3/2004	6:11:26	4	21	75.1	50	364	345.8	254.5
coil8_test_cycling_constantb.out	9/17/2004	15:18:43	1	31	80	60.5	736.4	167.6	91.6
coil8_test_cycling_constantb.out	9/17/2004	18:06:36	2	31	80	60.4	736.4	213.5	122.1
coil8_test_cycling_constantb.out	9/17/2004	21:40:19	3	32	80	60.4	737.3	36.4	30.6
coil8_test_cycling_constantb.out	9/17/2004	22:16:59	4	32	80	60.4	736.8	36.4	30.5
coil8_test_cycling_constantb.out	9/17/2004	22:53:39	5	32	80	60.4	735.9	36.4	30.5
coil8_test_cycling_constantb.out	9/17/2004	23:30:18	6	32	80	60.4	736.7	36.4	30.5
coil8_test_cycling_constantb.out	9/18/2004	0:06:56	7	33	79.9	60.4	736.6	23.4	16.3
coil8_test_cycling_constantb.out	9/18/2004	0:30:37	8	33	80.1	60.3	738.5	23.4	16.3
coil8_test_cycling_constantb.out	9/18/2004	0:54:17	9	33	80.1	60.4	734.7	23.4	16.3
coil8_test_cycling_constantb.out	9/18/2004	1:17:57	10	34	80	60.3	735.3	20.1	10.2
coil8_test_cycling_constantb.out	9/18/2004	1:38:19	11	34	79.9	60.3	735.3	20.1	10.2
coil8_test_cycling_constantb.out	9/18/2004	1:58:41	12	34	80	60.3	736	20.1	10.2
coil8_test_cycling_constantb.out	9/18/2004	2:19:03	13	35	80.1	60.3	737.3	24.7	7.1
coil8_test_cycling_constantb.out	9/18/2004	2:43:59	14	35	80	60.4	740.9	24.7	7.1
coil8_test_cycling_constantb.out	9/18/2004	3:08:56	15	35	79.8	60.4	738.5	24.7	7.1
coil8_test_cycling_constant_300b.out	9/18/2004	3:33:54	1	71	80	60.4	552.3	213.5	122.2
coil8_test_cycling_constant_300b.out	9/18/2004	7:07:38	2	71	80	60.4	552.9	213.4	122.1
coil8_test_cycling_constant_300b.out	9/18/2004	10:41:17	3	72	80.1	60.4	555.3	36.4	30.5
coil8_test_cycling_constant_300b.out	9/18/2004	11:17:56	4	72	79.9	60.4	554.4	36.4	30.5
coil8_test_cycling_constant_300b.out	9/18/2004	11:54:35	5	72	80.1	60.4	554.4	36.4	30.5
coil8_test_cycling_constant_300b.out	9/18/2004	12:31:13	6	72	80	60.4	554.7	36.4	30.5
coil8_test_cycling_constant_300b.out	9/18/2004	13:07:52	7	73	80	60.3	557.3	23.4	16.3
coil8_test_cycling_constant_300b.out	9/18/2004	13:31:33	8	73	80	60.3	558.8	23.4	16.3
coil8_test_cycling_constant_300b.out	9/18/2004	13:55:13	9	73	80	60.3	557.1	23.4	16.3
coil8_test_cycling_constant_300b.out	9/18/2004	14:18:54	10	74	80	60.3	562.2	20.1	10.2
coil8_test_cycling_constant_300b.out	9/18/2004	14:39:16	11	74	80	60.3	562.9	20.1	10.2
coil8_test_cycling_constant_300b.out	9/18/2004	14:59:38	12	74	80.1	60.3	563	20.1	10.2
coil8_test_cycling_constant_300b.out	9/18/2004	15:20:00	13	75	80	60.2	567.7	24.7	7.1
coil8_test_cycling_constant_300b.out	9/18/2004	15:44:56	14	75	80.1	60.3	566.7	24.7	7.1
coil8_test_cycling_constant_300b.out	9/18/2004	16:09:53	15	75	79.9	60.2	568.8	24.7	7.1

**COIL 8 Test Runs (cont)**

File Name	Date	Start Time	Sequence No.	Run/Test No.	Inlet DB (F)	Inlet DewPt (F)	Air Flow (cfm)	Test Duration (min)	Comp Runtime (min)
coil8_test_cycling_constant_75_56b.out	9/20/2004	9:17:00	1	61	75	56	734.5	212.5	121.6
coil8_test_cycling_constant_75_56b.out	9/20/2004	12:49:48	2	61	75	56	734.5	212.6	121.6
coil8_test_cycling_constant_75_56b.out	9/20/2004	16:22:37	3	62	75	56	734.8	36.3	30.4
coil8_test_cycling_constant_75_56b.out	9/20/2004	16:59:07	4	62	75	56	733.9	36.3	30.4
coil8_test_cycling_constant_75_56b.out	9/20/2004	17:35:38	5	62	75	56	733	36.2	30.4
coil8_test_cycling_constant_75_56b.out	9/20/2004	18:12:07	6	62	75	56	733.5	36.3	30.4
coil8_test_cycling_constant_75_56b.out	9/20/2004	18:48:38	7	63	75	56	734.1	23.3	16.2
coil8_test_cycling_constant_75_56b.out	9/20/2004	19:12:12	8	63	75	56	734.3	23.3	16.2
coil8_test_cycling_constant_75_56b.out	9/20/2004	19:35:46	9	63	75	56	734.1	23.3	16.2
coil8_test_cycling_constant_75_56b.out	9/20/2004	19:59:21	10	64	75	56	734.1	20	10.1
coil8_test_cycling_constant_75_56b.out	9/20/2004	20:19:38	11	64	75	55.9	730.2	20	10.1
coil8_test_cycling_constant_75_56b.out	9/20/2004	20:39:55	12	64	75	56	736.6	20	10.1
coil8_test_cycling_constant_75_56b.out	9/20/2004	21:00:11	13	65	75.1	56	734.2	24.6	7.1
coil8_test_cycling_constant_75_56b.out	9/20/2004	21:25:01	14	65	75.1	55.9	737	24.6	7.1
coil8_test_cycling_constant_75_56b.out	9/20/2004	21:49:51	15	65	74.9	55.9	736.8	24.6	7.1
coil8_test_cycling_constant_75_64b.out	9/18/2004	16:34:49	1	51	75.2	63.6	736.8	213.6	122.3
coil8_test_cycling_constant_75_64b.out	9/18/2004	20:08:41	2	51	75	63.9	736.3	213.5	122.2
coil8_test_cycling_constant_75_64b.out	9/18/2004	23:42:26	3	52	75	64	735.8	36.4	30.5
coil8_test_cycling_constant_75_64b.out	9/19/2004	0:19:05	4	52	75	64	736	36.4	30.5
coil8_test_cycling_constant_75_64b.out	9/19/2004	0:55:45	5	52	75	63.9	736.2	36.4	30.5
coil8_test_cycling_constant_75_64b.out	9/19/2004	1:32:24	6	52	75	63.9	735.4	36.4	30.5
coil8_test_cycling_constant_75_64b.out	9/19/2004	2:09:04	7	53	75	63.8	735.1	23.4	16.3
coil8_test_cycling_constant_75_64b.out	9/19/2004	2:32:44	8	53	75	63.9	733.3	23.4	16.3
coil8_test_cycling_constant_75_64b.out	9/19/2004	2:56:25	9	53	75.1	63.8	733.6	23.5	16.3
coil8_test_cycling_constant_75_64b.out	9/19/2004	3:20:07	10	54	75	63.8	733.3	20.1	10.2
coil8_test_cycling_constant_75_64b.out	9/19/2004	3:40:30	11	54	75.1	63.7	731.7	20.1	10.2
coil8_test_cycling_constant_75_64b.out	9/19/2004	4:00:52	12	54	75	63.8	735.7	20.1	10.2
coil8_test_cycling_constant_75_64b.out	9/19/2004	4:21:15	13	55	75.1	63.8	736.5	24.7	7.1
coil8_test_cycling_constant_75_64b.out	9/19/2004	4:46:11	14	55	75	63.7	736.3	24.7	7.1
coil8_test_cycling_constant_75_64b.out	9/19/2004	5:11:08	15	55	75	63.8	739	24.7	7.1
coil8_test_cycling_autoc.out	9/22/2004	14:19:41	1	41	80	60.4	737.1	146.6	76.4
coil8_test_cycling_autoc.out	9/22/2004	16:46:30	2	41	80	60.4	733.9	91.5	61.1
coil8_test_cycling_autoc.out	9/22/2004	18:18:15	3	42	80	60.4	730	36.4	30.5
coil8_test_cycling_autoc.out	9/22/2004	18:54:55	4	42	80	60.4	731.6	36.4	30.5
coil8_test_cycling_autoc.out	9/22/2004	19:31:36	5	42	79.9	60.3	730.3	36.4	30.5
coil8_test_cycling_autoc.out	9/22/2004	20:08:16	6	42	80	60.4	730.3	36.4	30.5
coil8_test_cycling_autoc.out	9/22/2004	20:44:57	7	43	79.9	60.4	724.1	23.4	16.3
coil8_test_cycling_autoc.out	9/22/2004	21:08:38	8	43	80	60.3	724.6	23.5	16.3
coil8_test_cycling_autoc.out	9/22/2004	21:32:21	9	43	79.9	60.4	724.7	23.5	16.3
coil8_test_cycling_autoc.out	9/22/2004	21:56:03	10	44	79.9	60.5	719.3	20.2	10.2
coil8_test_cycling_autoc.out	9/22/2004	22:16:28	11	44	79.9	60.5	715.9	20.1	10.2
coil8_test_cycling_autoc.out	9/22/2004	22:36:52	12	44	80	60.5	718.2	20.1	10.2
coil8_test_cycling_autoc.out	9/22/2004	22:57:17	13	45	79.9	60.3	713.7	24.8	7.1
coil8_test_cycling_autoc.out	9/22/2004	23:22:17	14	45	79.8	60.2	715.7	24.8	7.2
coil8_test_cycling_autoc.out	9/22/2004	23:47:18	15	45	79.9	60.4	709.2	24.8	7.1
coil8_test_cycling_autoc.out	9/23/2004	0:12:19	16	45	79.9	60.3	712.3	24.8	7.1
coil8_test_cycling_autoc.out	9/23/2004	0:37:19	17	45	79.8	60.2	709.9	24.8	7.1
coil8_test_cycling_autoc.out	9/23/2004	1:02:19	18	46	79.7	60.2	702.1	61.5	5.6
coil8_test_cycling_autoc.out	9/23/2004	2:04:07	19	46	80.1	60.3	702.9	61.5	5.6
coil8_test_cycling_autoc.out	9/23/2004	3:05:55	20	46	80	60.2	700.4	61.5	5.6
coil8_test_cycling_autoc.out	9/23/2004	4:07:43	21	46	80	60.4	704.4	61.5	5.6
coil8_test_cycling_autoc.out	9/23/2004	5:09:31	22	46	80	60.4	706.7	61.5	5.6



# **APPENDIX I**

## **Field Test Site Summaries**

## **APPENDIX I1**

### **Summary of Data for Field Test Site 1**

## Site #1 – Herndon, VA



**Figure 1. South Exposure**

### **System Description**

This site has two conventional AC units: a 3-ton downstairs unit and a 2.5-ton upstairs unit. The upstairs unit meets the majority of the cooling load.

#### Unit #1 – Upstairs Unit

- Heat pump
- York E1FD030806A Condensing Unit
- AHU nameplate unknown (York Unit)
- 2.5-ton

#### Unit #2 – First Floor and Basement Unit

- Heat pump
- York E1FD036S06B Condensing Unit
- G/HC036SB AHU
- 3.0-ton

## Sensors and Data Logger Connections

**Table 1. Data Logger Channel Assignments and Sensor Identification**

Channel	Data Point	Description	Units	Sensor
SE1	PSUC1	Compressor Suction Pressure - Unit #1	psig	Setra C207
SE2	RHM1	Return/Mixed RH - Unit #1 - Unit #1	%	Vaisala HMD60U
SE3	RHS1	Supply RH - Unit #1	%	Vaisala HMD60U
SE4	DPC1	Pressure Drop Across Coil - Unit #1	in WC	Setra 267MR (0.25, 0.5, 1.0 inches)
SE5	IB1	AHU Fan Current - Unit #1	amps	Veris H721LC
SE6	PSUC2	Compressor Suction Pressure - Unit #2	psig	Setra C207
SE7	RHM2	Return/Mixed RH - Unit #2	%	Vaisala HMD60U
SE8	RHS2	Supply RH - Unit #2	%	Vaisala HMD60U
SE9	DPC2	Pressure Drop Across Coil - Unit #2	in WC	Setra 267MR (0.25, 0.5, 1.0 inches)
SE10	IB2	AHU Fan Current - Unit #2	amps	Veris H721LC
SE11	TC MUX			
SE12	TC MUX			
P1	WC1	Compressor Power - Unit #1	kWh	Ohio Semitronic SWH-2100 100 AMP
P2	WC2	Compressor Power - Unit #2	kWh	Ohio Semitronic SWH-2100 100 AMP
C1	DMUX-cntrl			
C2	DMUX-cntrl			
C3	DMUX-cntrl			
C4	TC MUX-cntrl			
C5	TC MUX-cntrl			
C6				
C7				
C8	WF1	AHU Fan Power - Unit #1	kWh	Ohio Semitronic SWH-2100 100 AMP
DMUX-1				
DMUX-2				
DMUX-3	FC2	Condensate Removal - Unit #2	pulse	Texas Tipping Bucket
DMUX-4	SC1	Compressor Status - Unit #1	min	Veris H800
DMUX-5	SC2	Compressor Status - Unit #2	min	Veris H800
DMUX-6				
DMUX-7	WF2	AHU Fan Power - Unit #2	kWh	Ohio Semitronic SWH-2100 100 AMP
DMUX-8	FC1	Condensate Removal - Unit #1	pulse	Texas Tipping Bucket
TCMX-1	TEVP1	Coil Return Bend Temperature - Unit #1	F	Watlow TC AFEC0TA040U8250
TCMX-2	TSUC1	Suction Temperature - Unit #1	F	Watlow TC AFEC0TA040U8400
TCMX-3	TLIQ1	Liquid Line Temperature - Unit #1	F	Watlow TC AFEC0TA040U8250
TCMX-4	TAM1	Mixed Air Temperature - Unit #1	F	Watlow TC AFGCNTA120U8250
TCMX-5	TAS1	Supply Air Temperature - Unit #1	F	Watlow TC AFGCNTA120U8250
TCMX-6	TEVP2	Coil Return Bend Temperature - Unit #2	F	Watlow TC AFEC0TA040U8250
TCMX-7	TSUC2	Suction Temperature - Unit #2	F	Watlow TC AFEC0TA040U8400
TCMX-8	TLIQ2	Liquid Line Temperature - Unit #2	F	Watlow TC AFEC0TA040U8250
TCMX-9	TAM2	Mixed Air Temperature - Unit #2	F	Watlow TC AFGCNTA120U8250
TCMX-10	TAS2	Supply Air Temperature - Unit #2	F	Watlow TC AFGCNTA120U8250
TCMX-11	TAO	Outdoor Temperature	F	Watlow TC AFEC0TA040U8400

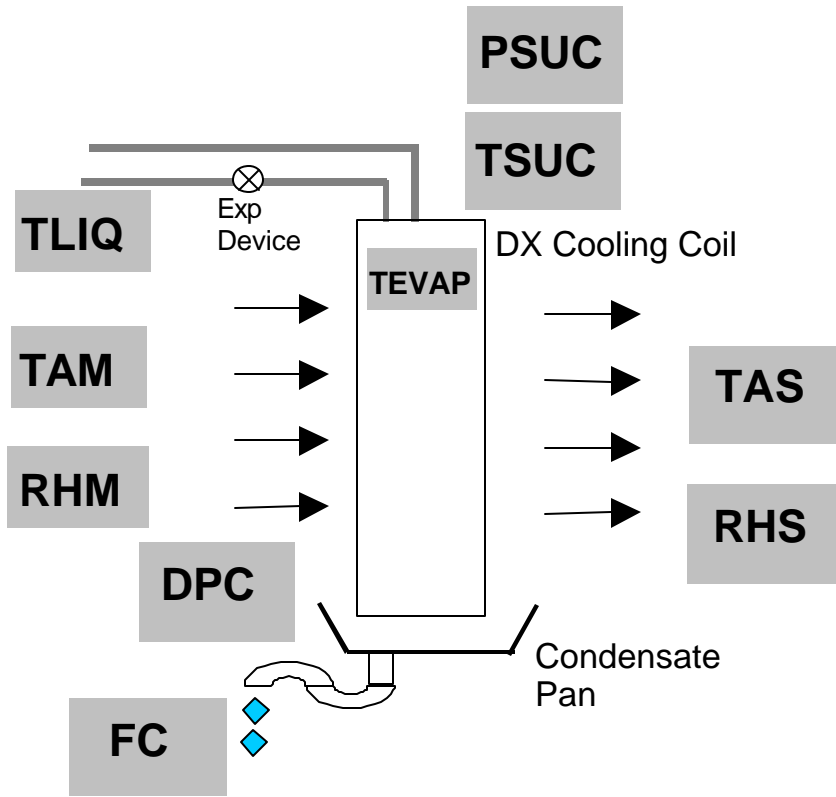
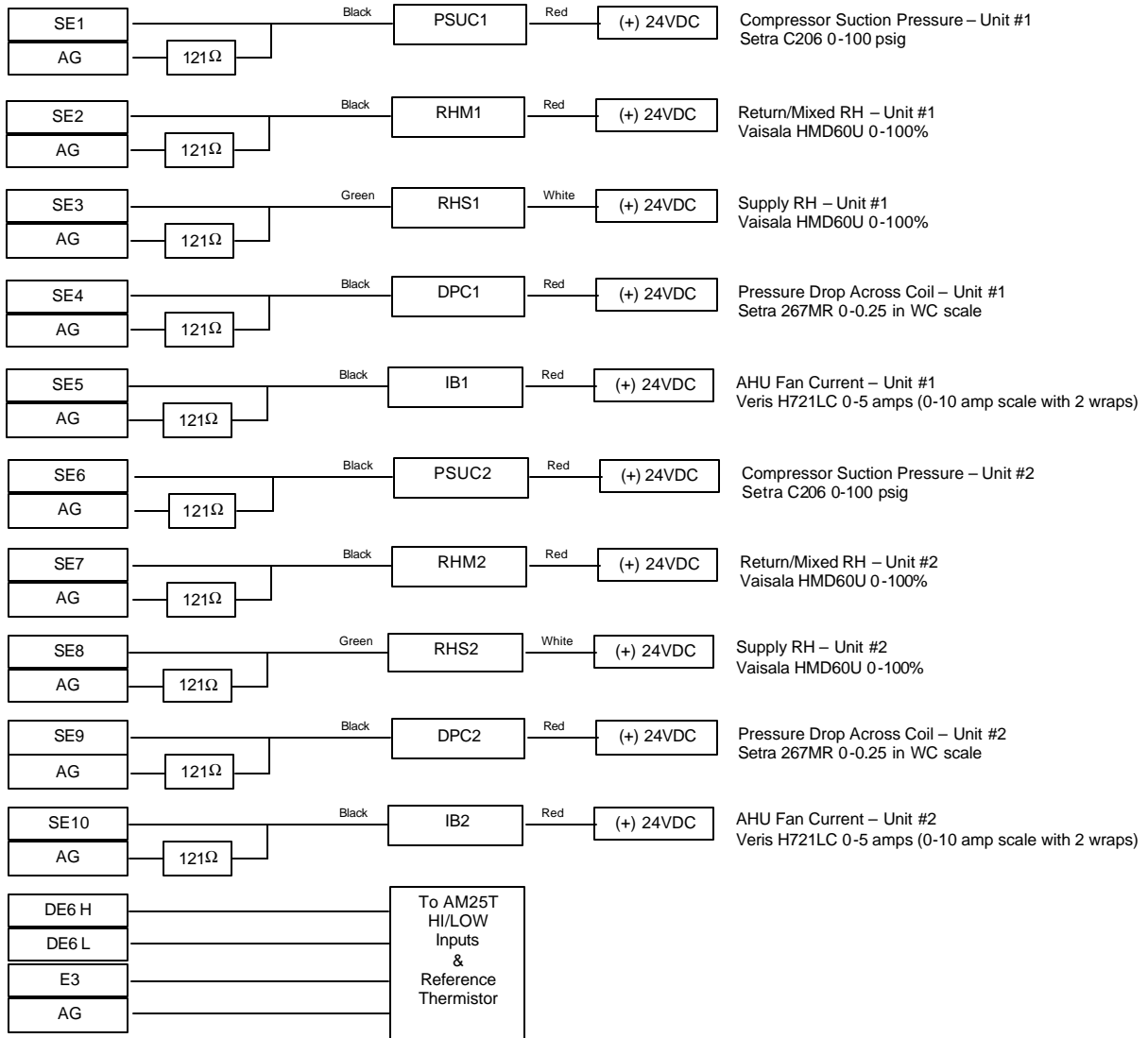


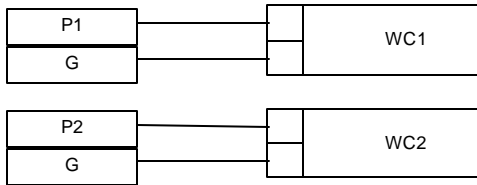
Figure 2. System Schematic

**CR10X Data Logger  
Analog Terminals**



**Figure 3. CR10X Analog Terminals Wiring Schematic**

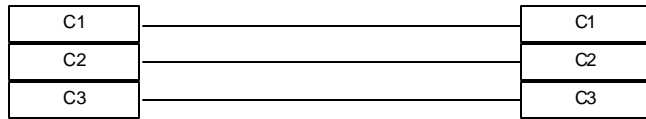
**CR10X Data Logger  
Pulse Terminals**



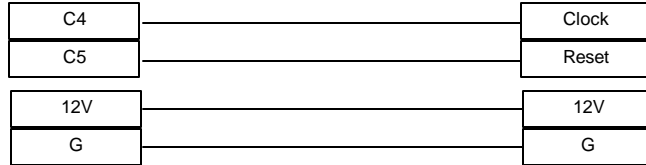
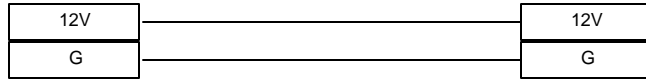
Compressor Power – Unit #1 (includes condenser fan)  
Ohio Semtronic SWH-2100 (0.01 Wh/pulse)

Compressor Power – Unit #2 (includes condenser fan)  
Ohio Semtronic SWH-2100 (0.01 Wh/pulse)

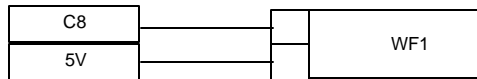
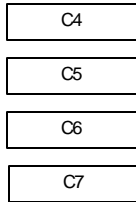
**CR10X Data Logger  
Digital Terminals**



Communications with SDM-SW8A  
Digital Multiplexer



Communications with AM25T  
Thermocouple Multiplexer



AHU Fan Power – Unit #1  
Ohio Semtronic SWH-2100 (0.01 Wh/pulse)

**Figure 4. CR10X Digital Terminals Wiring Schematic**

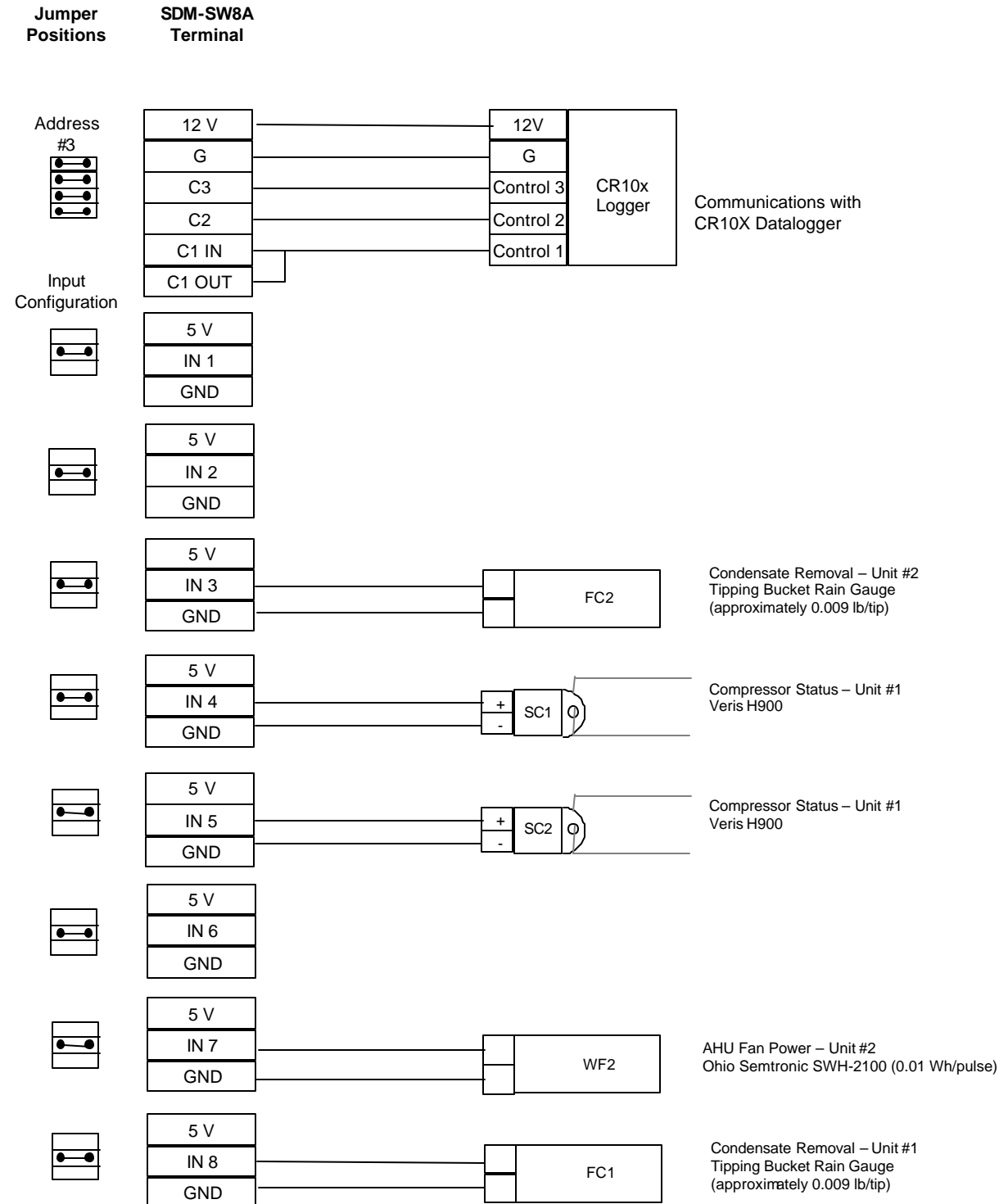


**Figure 5. Data Logger Connections to SDM-SW8A #0**



**AM25T  
Input Terminals**

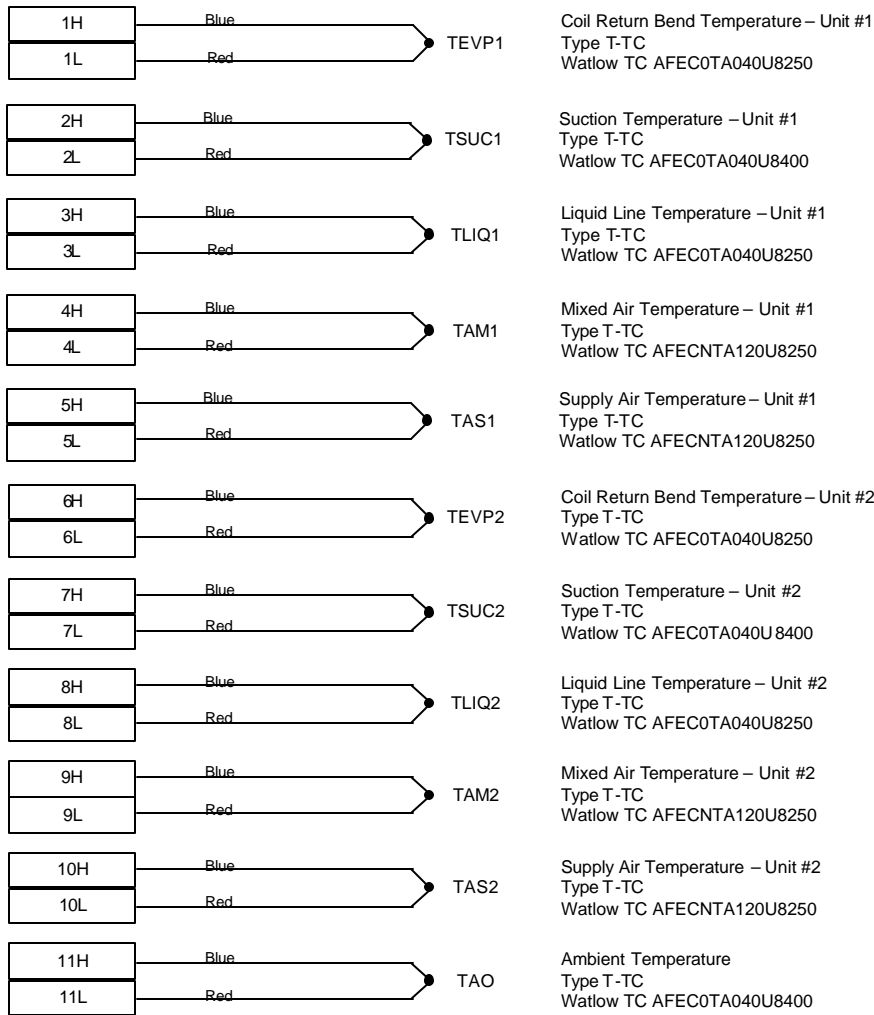


**Figure 6. AM25T Thermocouple Multiplexer Input Connections**

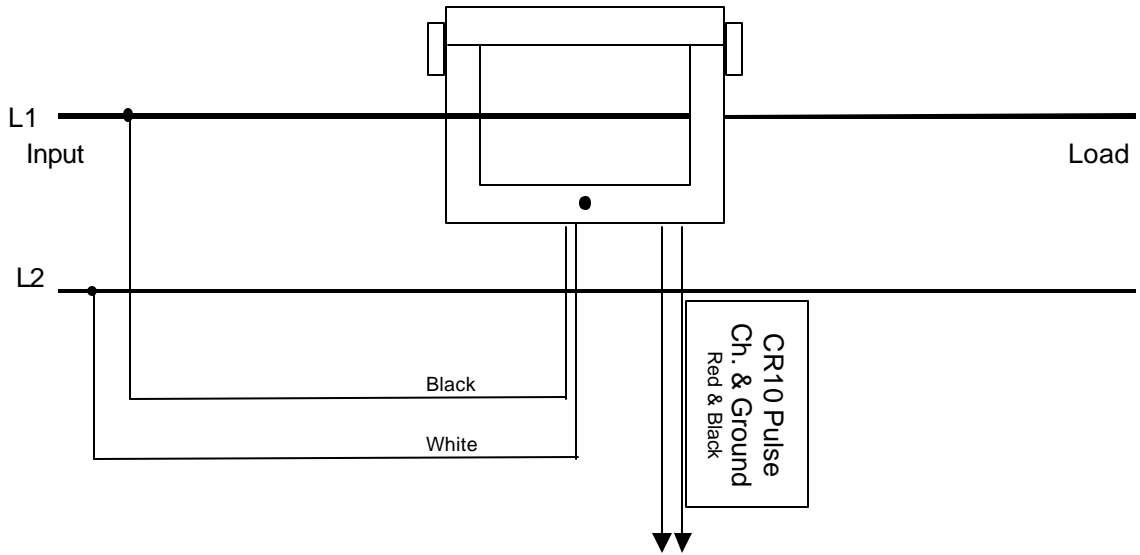


**Figure 7. Connection Diagram for SWH-2100 for Single Phase 2-wire Circuit (240V)**

**Coil Measurements**

Coil Type	“V” coil	
Coil Face Area	542.9 sq. in. 574.9 sq. in. w/o blockage	
Number of rows x Tubes/row	3 x 18	
Fin spacing	11 fpi	
Tubing diameter	¼”	
Coil depth	2.75 in	
Exp device	orifice	
Notes:	Small sheet metal “L” bracket at bottom of coil partial blocks air flow around a portion of the lower right side coil. This appears to be the same coil as Unit #2, with smaller angle between the coil sides.	

**Figure 8. AHU#1 Coil Dimensions**

Gross fin area: $(2.75 \text{ in}) \times (11 \text{ fins/in}) \times (2 \text{ sides/fin}) \times (574.9 \text{ sq in.}) / 144 \text{ sq in/ft}^2 = \underline{241.5 \text{ ft}^2}$
--

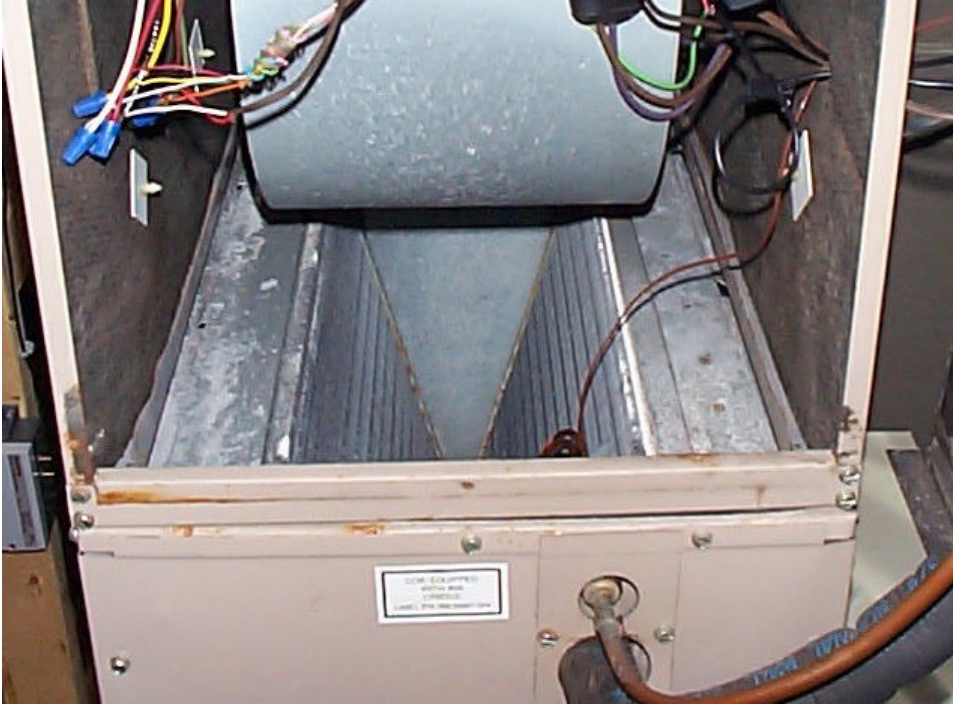


**Figure 9. Coil AHU #1**

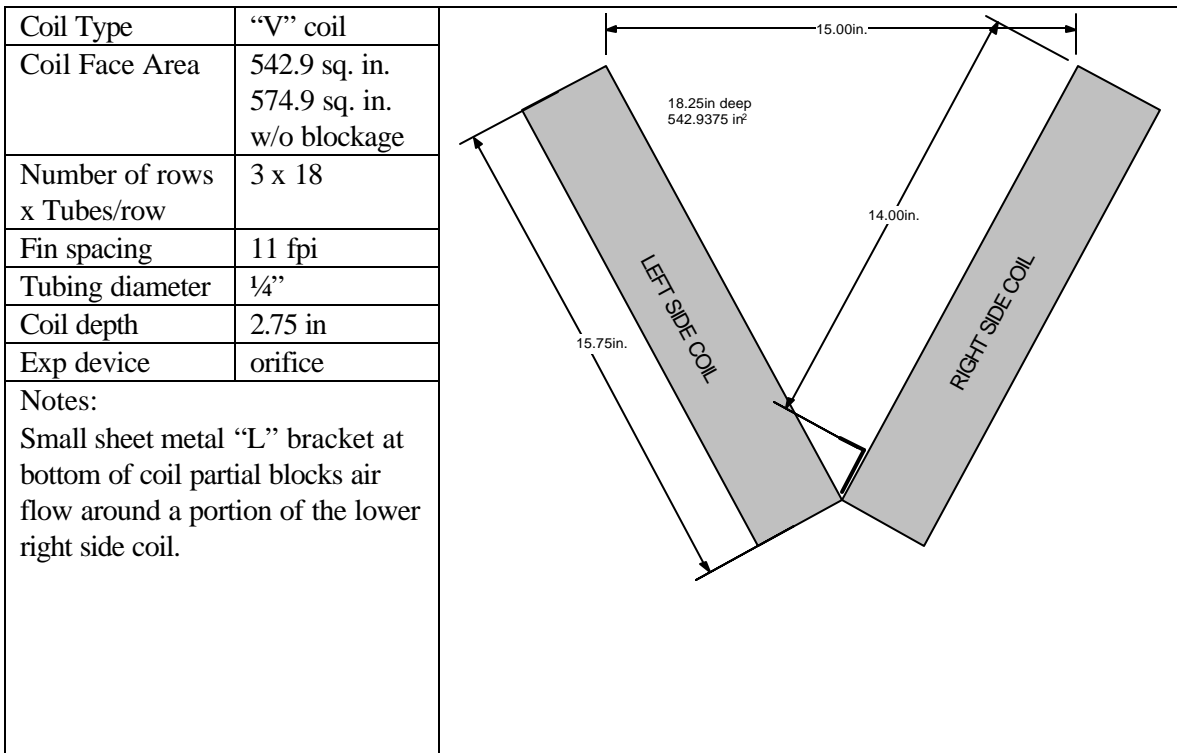


**Figure 10. AHU#2 Coil Dimensions**

Gross fin area: $(2.75 \text{ in}) \times (11 \text{ fins/in}) \times (2 \text{ sides/fin}) \times (574.9 \text{ sq in.}) / 144 \text{ sq in/ft}^2 = \underline{241.5 \text{ ft}^2}$
--



**Figure 11. Coil in AHU #2**

## **One Time Measurements**

**Table 2. Comparing Data Logger Measurements to TSI hand held probe**

<b>Sensor</b>	<b>Campbell</b>	<b>TSI</b>
Unit #1 – Supply (T/RH)	53.3°F / 82.2%	53.8°F / 78.1%
Unit #1 – Supply (T/RH)	53.2°F / 82.3%	53.6°F / 78.6%
Unit #1 – Return (T/RH)	72.2°F / 49.3%	71.9°F / 49.6%
Unit #2 – Supply (T/RH)	53.1°F / 84.4%	53.2°F / 80.5%
Unit #2 – Supply (T/RH)	53.0°F / 84.2%	53.1°F / 81.6%
Unit #2 – Return (T/RH)	71.5°F / 46.2%	70.9°F / 48.0%
Unit #2 – Return (T/RH)	71.5°F / 47.0%	71.1°F / 48.6%

**Table 3. One-Time Measurements**

Measurement				
Unit #1 Heat Balance:				
Electric Heat and Fan Power		10.75 kW (44.5 amps @ 240 VAC)		
Temperature Readings:				
TAM	75.2°F	75.8°F	76.0°F	76.3°F
TAS	108.4°F	110.0°F	110.5°F	111.7°F
TAS (TSI hand probe)	103.4°F	104.8°F	106.0°F	106.9°F
Average Temperature Rise (TAS-TAM)				
		34.3°F → 990 SCFM		
Average Temperature Rise (TSI – TAM)				
		29.5°F → 1,154 SCFM		
Average Difference between TAS and TSI				
		4.9°F		
Unit #2 Heat Balance:				
Electric Heat and Fan Power		13.15 kW (53.0 amps @ 240 VAC)		
Temperature Readings:				
TAM	76.5°F	77.0°F	77.3°F	77.5°F
TAS	110.0°F	110.9°F	111.8°F	112.7°F
TAS (TSI hand probe)	103.5°F	104.3°F	105.0°F	105.6°F
Average Temperature Rise (TAS-TAM)				
		34.3°F → 1,212 SCFM		
Average Temperature Rise (TSI – TAM)				
		27.5°F → 1,510 SCFM		
Average Difference between TAS and TSI				
		6.75°F		
AHU #1 Blower Power				
		500 watts 2.1 A @ 240 VAC		
AHU #2 Blower Power				
		Not measured by hand		
Compressor/Condenser #1 Power				
		2.46 kW 11.9 A @ 240 VAC		
Compressor/Condenser #2 Power				
		3.10 kW 13.2 A @ 240 VAC		

Note: The location of the supply air thermocouples exposes them to radiation from the electric heat elements. The TSI hand held probe was used to take a reading in a supply trunk near the thermocouple but out of line-of-sight with the elements.

## **Data Collection Summary**

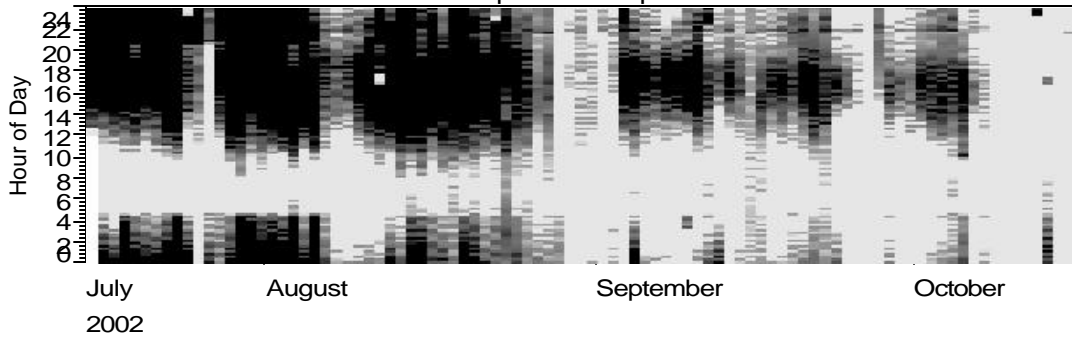
Table 4 summarizes the monitoring and site events that occurred during the monitoring period. The downstairs unit operated in the Constant Fan Mode for about three weeks starting on August 18, but was in the Auto Fan Mode for all other times. The upstairs unit was always in the Auto Fan Mode.

**Table 4. Data Collection Events**

July 1, 2002	Datalogger installed
July 15, 2002	Verified Data Collection Begins
Aug 18 to Sep 4, 2002	Downstairs Unit Set to “Constant” Fan Mode
October 12-13, 2002	Last Day of Significant Cooling
October 15, 2002	Beginning of Significant Heating Activity

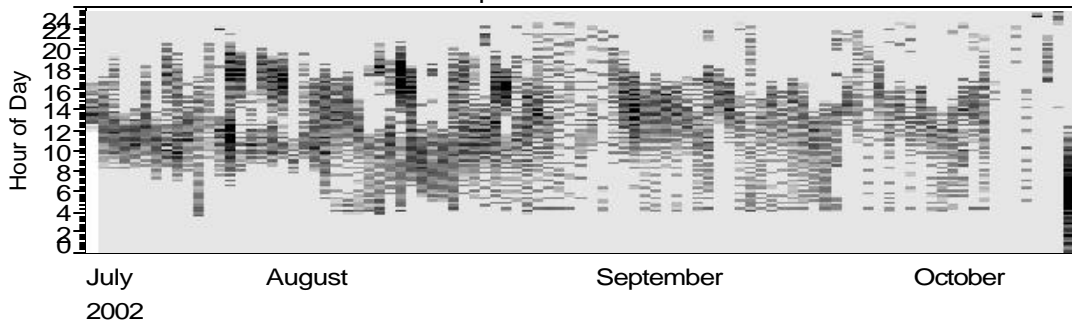
The shade plots in Figure 12 qualitatively show the operating patterns for the compressor, supply fan, and condensate flow on both the upstairs and downstairs AC units. Each day is qualitatively shown as a vertical stripe on the plot, with darker shades of gray indicating more operation or use. The period when the downstairs supply fan ran constantly from August 18 to September 4 is evident on the shade plot. The first significant day of heating on the downstairs unit is apparent on the early morning of the October 15.

07/15/02 00:15:00 to 10/15/02 23:45:00  
Compressor - Upstairs



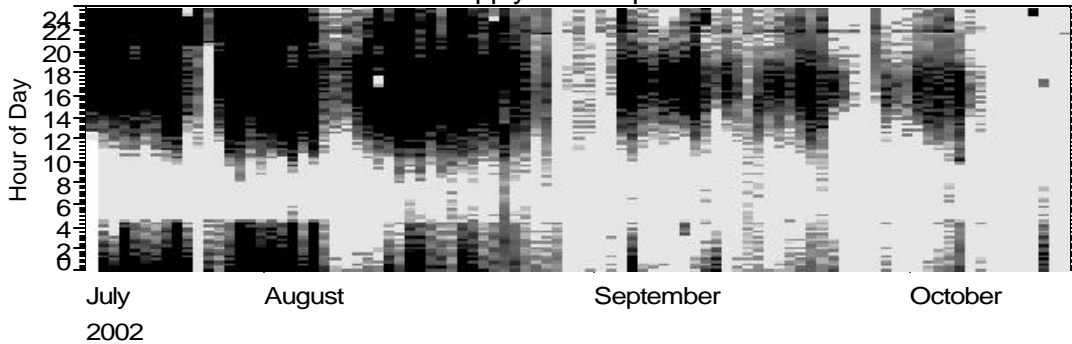
Day (MAX/MIN = 15.00/ 0.00 minutes)

Compressor - Downstairs



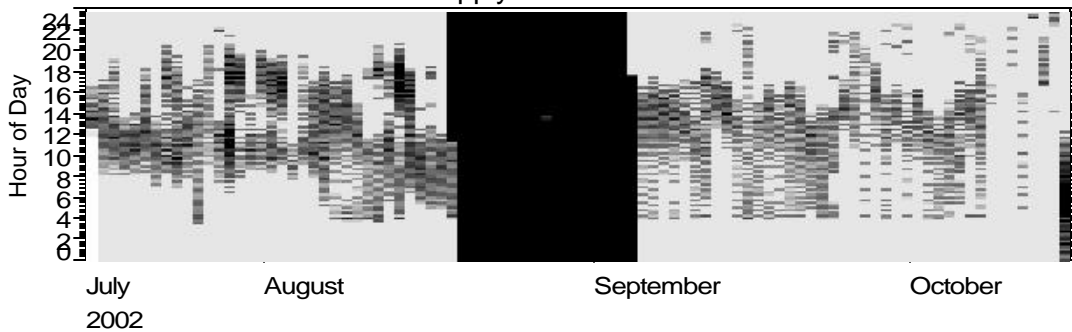
Day (MAX/MIN = 15.00/ 0.00 minutes)

Supply Fan - Upstairs



Day (MAX/MIN = 15.00/ 0.00 minutes)

Supply Fan - Downstairs



Day (MAX/MIN = 15.00/ 0.00 minutes)

Figure 12. Shade Plots of Compressors and Supply Fans

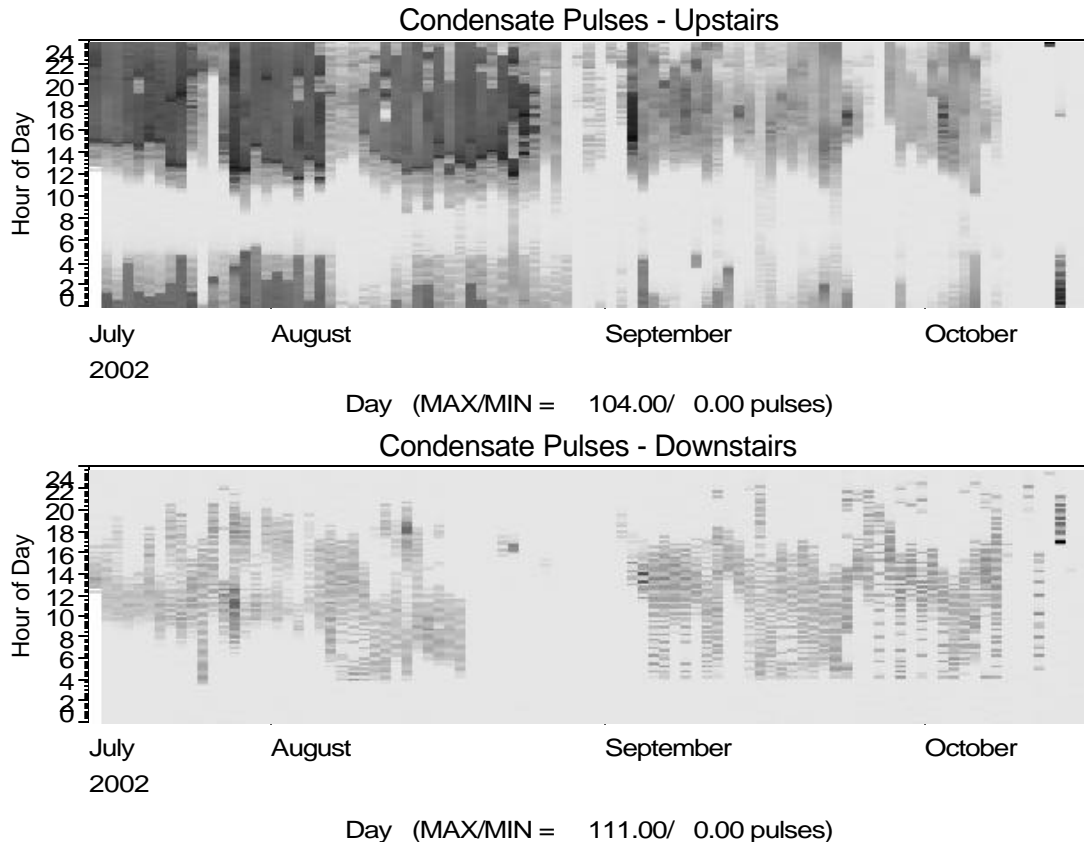


**Figure 13. Shade Plots of Condensate Flow Rate**

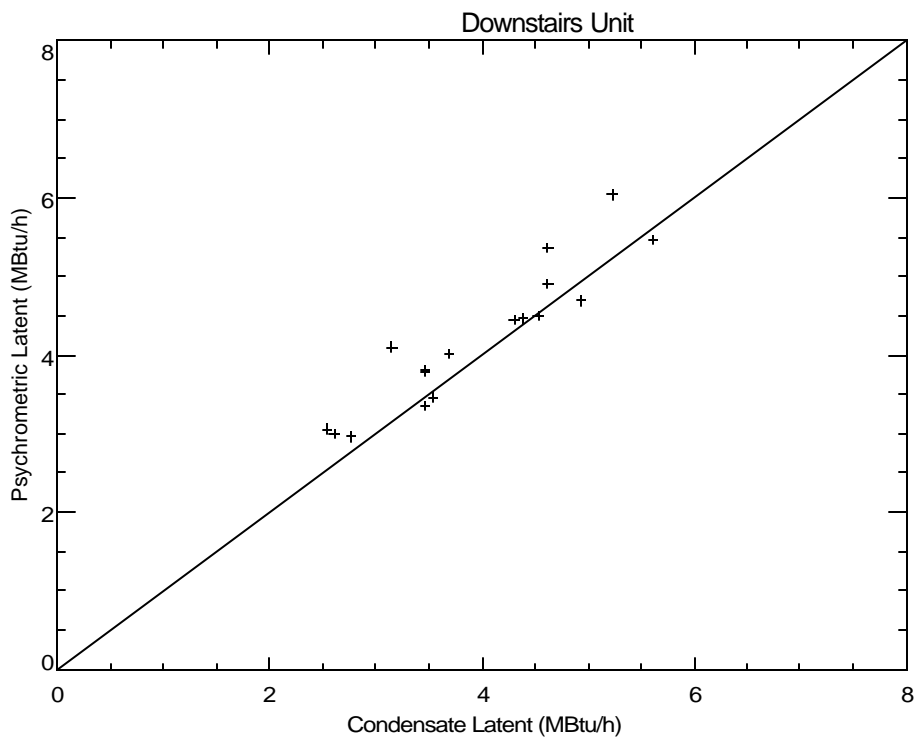
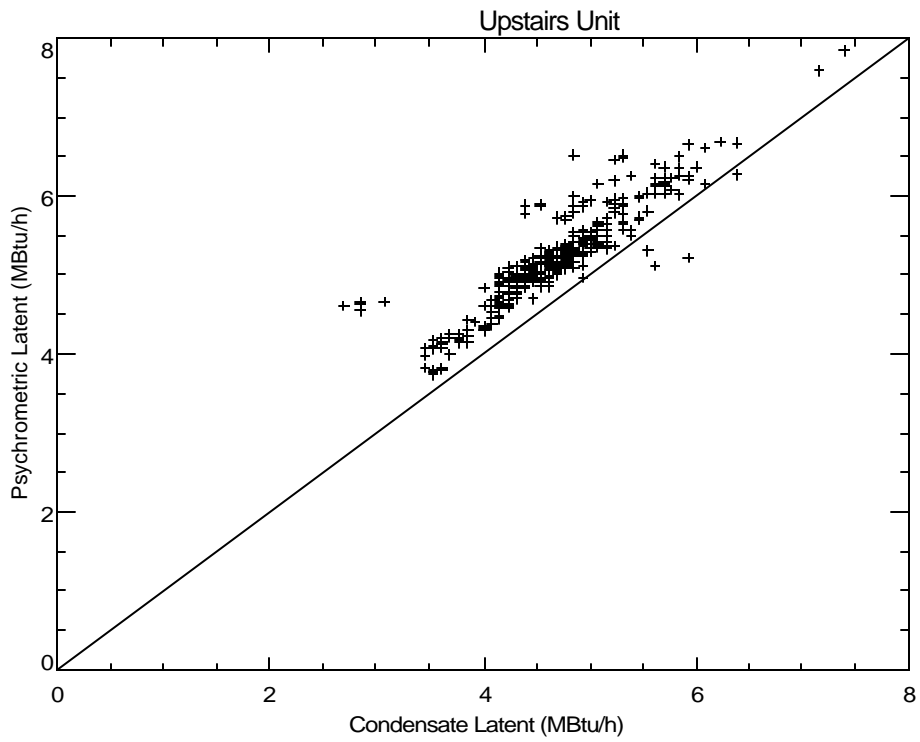
### Latent Capacity

Figure 14 compares the latent capacity of each unit calculated from the condensate flow as well as from psychrometric state-points and the airflow. The plots only include data records when the compressor had been on continuously to ensure steady state was achieved (for the upstairs unit, the unit had to be on for 30 minutes prior; for the downstairs unit, the compressor had to be on for 15 minutes prior). For the upstairs AC unit, the steady state data was limited to only periods where the entering temperature was greater than 73°F and the relative humidity was between 48 and 52%. The latent capacity based on condensate removal is slightly lower than the psychrometric-based capacity for the both the upstairs and downstairs units.

Figure 15 shows the process line for cooling on the psychrometric chart for both units. The smaller data points correspond to the 15-minute data records. The line and the larger three points correspond to the average of conditions: 1) at the coil inlet, 2) at the coil outlet, but before the fan and 3) after the supply fan.

The average SHR for the coils – or the slope of the process line - are also shown on the plots. The sensible heat ratio is 0.80 for the upstairs unit, which met most of the load and had slightly more humid inlet conditions. The SHR is 0.85 for the downstairs unit, which has slightly drier entering conditions. The saturated suction temperatures were 42.4° F for both AC units.





**Figure 14. Comparing Condensate and Psychrometric-Based Latent Capacity**

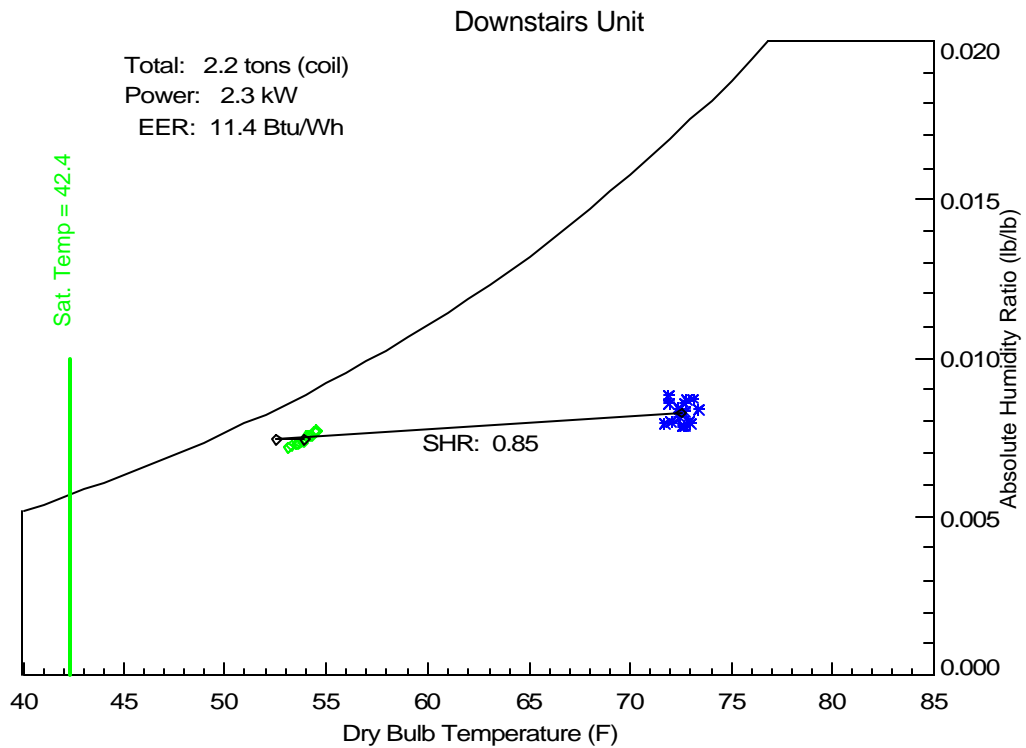
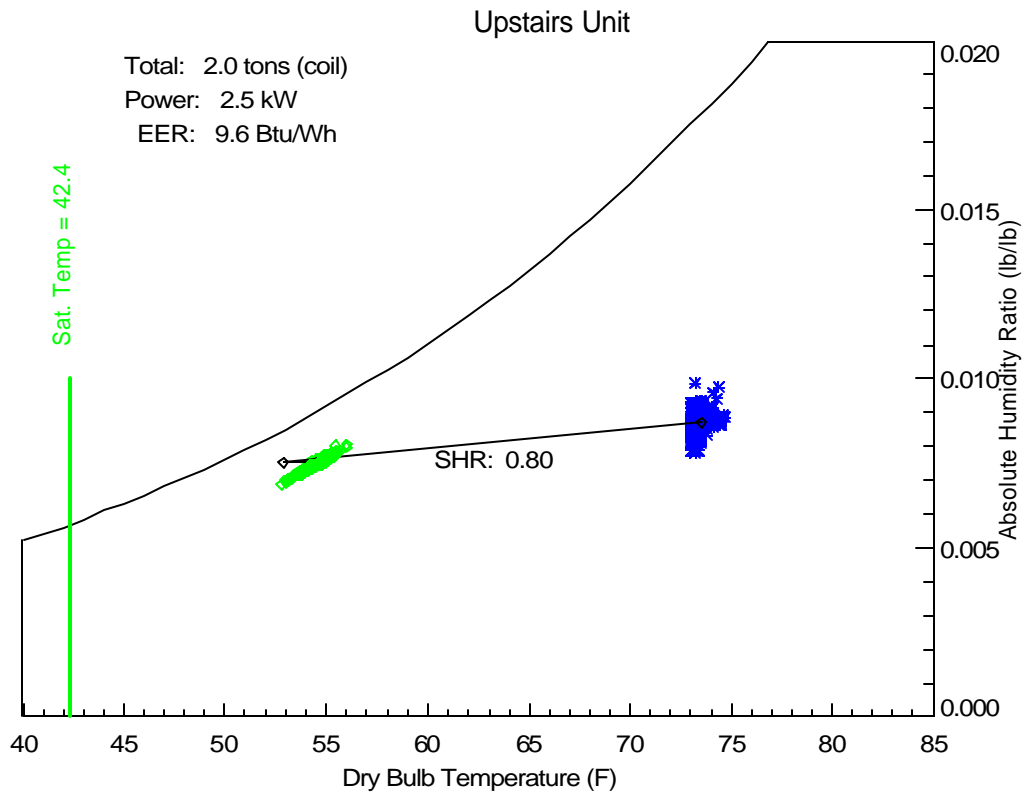


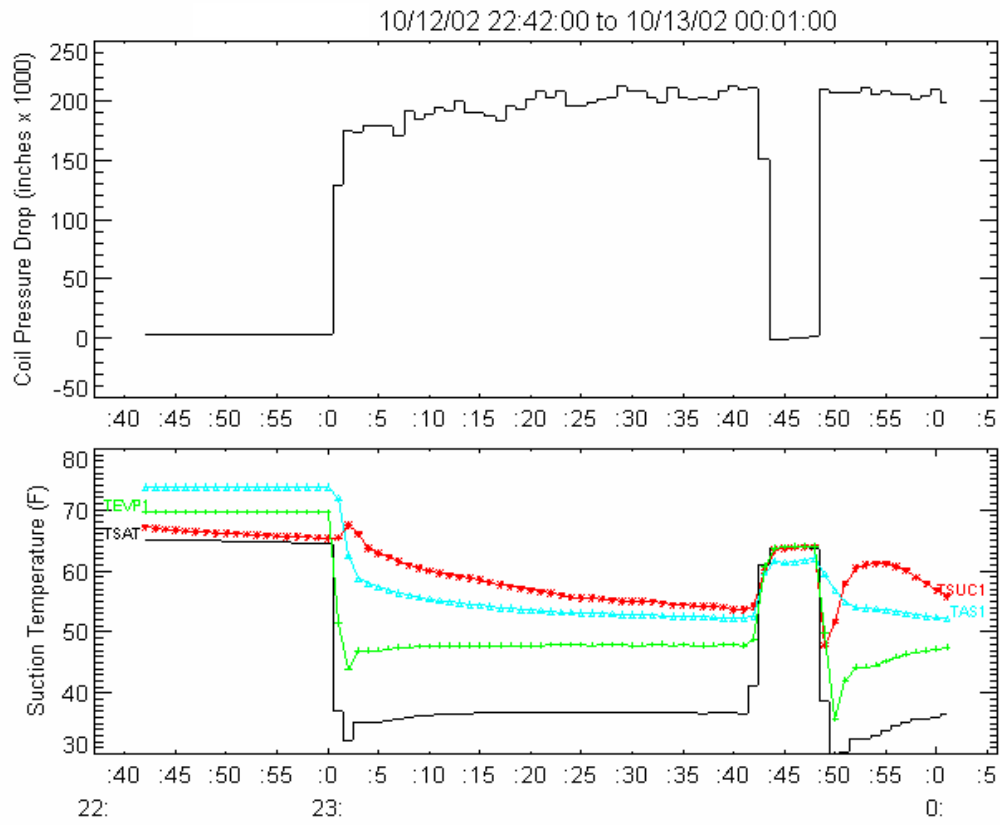
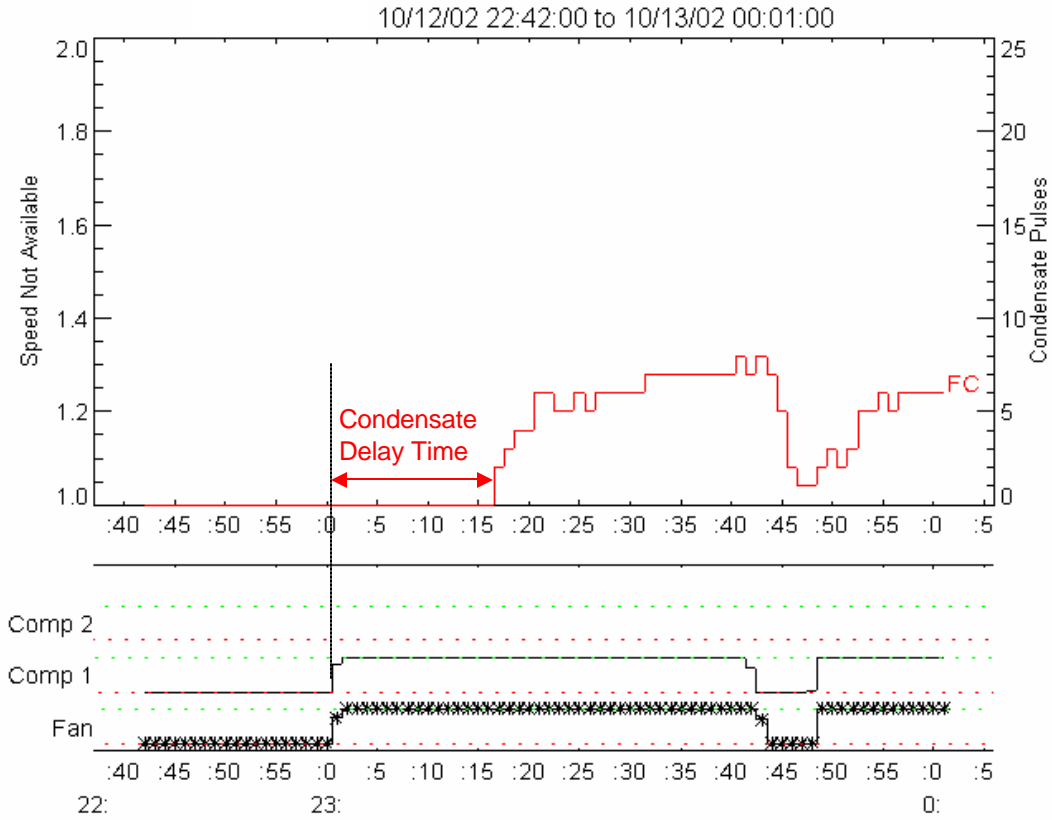
**Figure 15. Cooling Process Lines for AC Coils at Steady State Conditions**

## **Control Details in Various Modes**

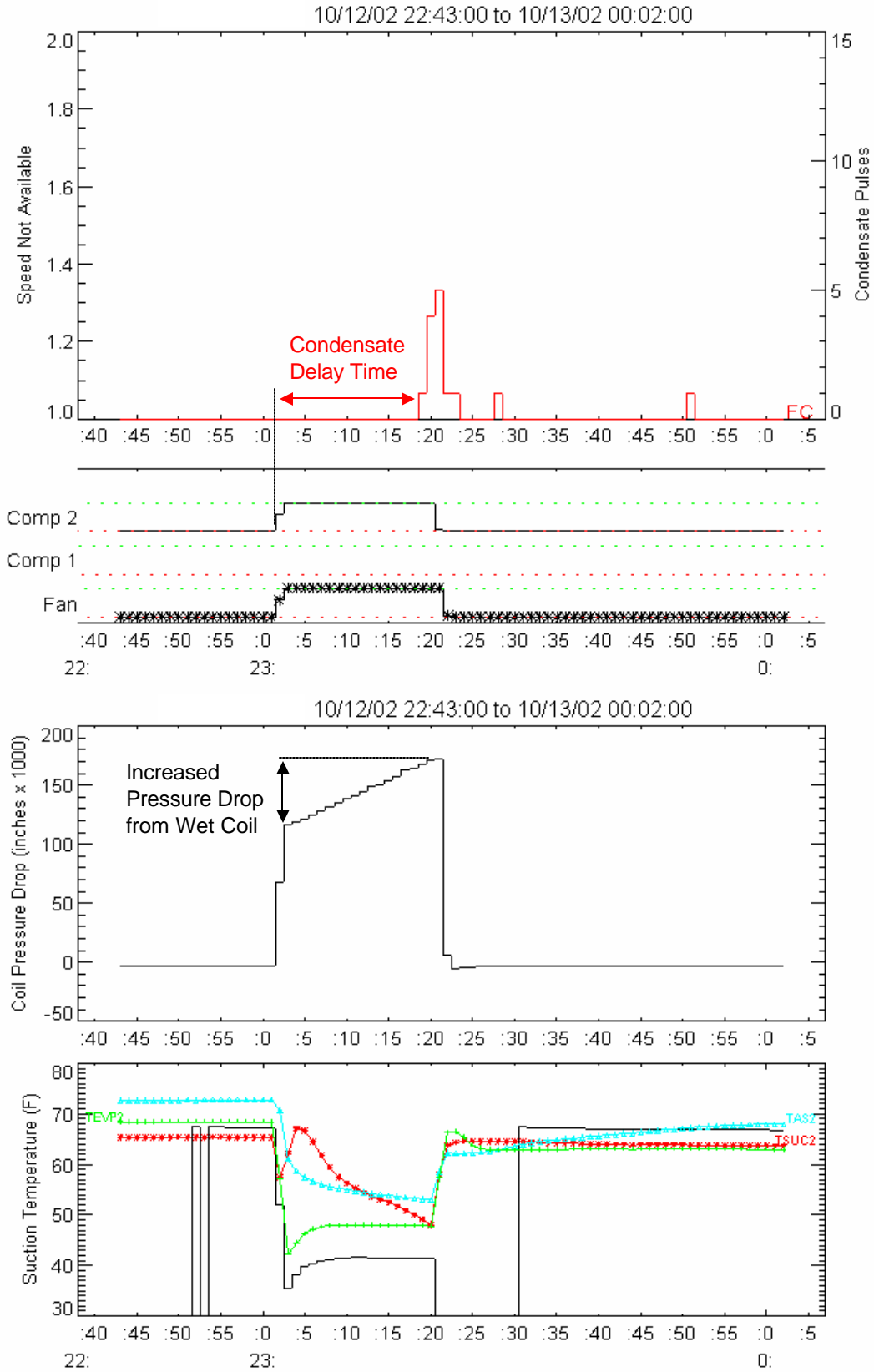
Figure 16 shows some typical operating cycles for the upstairs AC unit. The upstairs unit operated in auto fan mode for the entire period as shown in Figure 12. The operating data shown on the plot are for October 12, a day of significant cooling operation that occurred after homeowners returned from vacation. This warm humid day was selected since it resulted in a long cycle of consistent compressor operation with the space humidity near the nominal dew point of 60°F. The time delay for the first condensate pulse to occur after compressor startup is shown on the plot.

Figure 17 and Figure 18 show typical operating cycles for the downstairs AC unit in both the Auto and Constant Fan Modes. Figure 17 shows a long operating cycle in the Auto Fan mode after the downstairs unit had been off for several days (i.e., October 12). The Auto Fan Mode produced more condensate removal, especially this day when the entering dew point was high. The Constant Fan Mode operation in Figure 18 shows that short compressor cycles result in no condensate removal. The shade plot Figure 13 also confirms that throughout the 3-week period of Constant Fan operation, almost no condensate pulses were ever recorded for the downstairs unit.

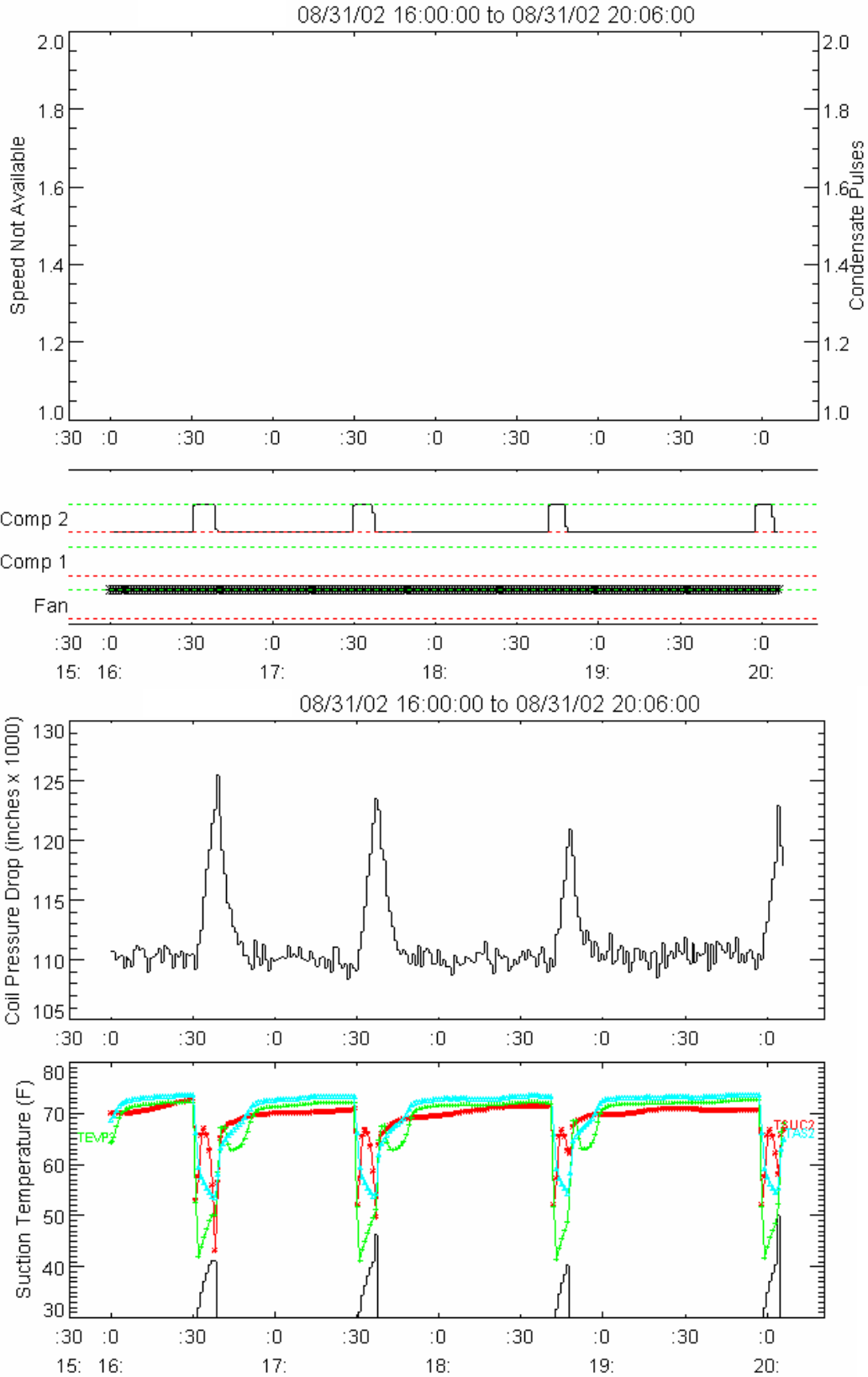
Both the Constant Fan and Auto Fan plots (Figure 17 and Figure 18) for the downstairs unit show the increase in static pressure drop for the coil as moisture forms on the fins. The wet-dry pressure drop difference builds to more than 0.050 inches by the time condensate falls from the coil. The static pressure buildup of 0.010-0.015 inches during the constant fan cycles in Figure 18 confirm that sufficient moisture had not yet built up for condensate to fall from the coil.



**Figure 16. A Typical Operating Cycle: Upstairs Unit, Oct 12**



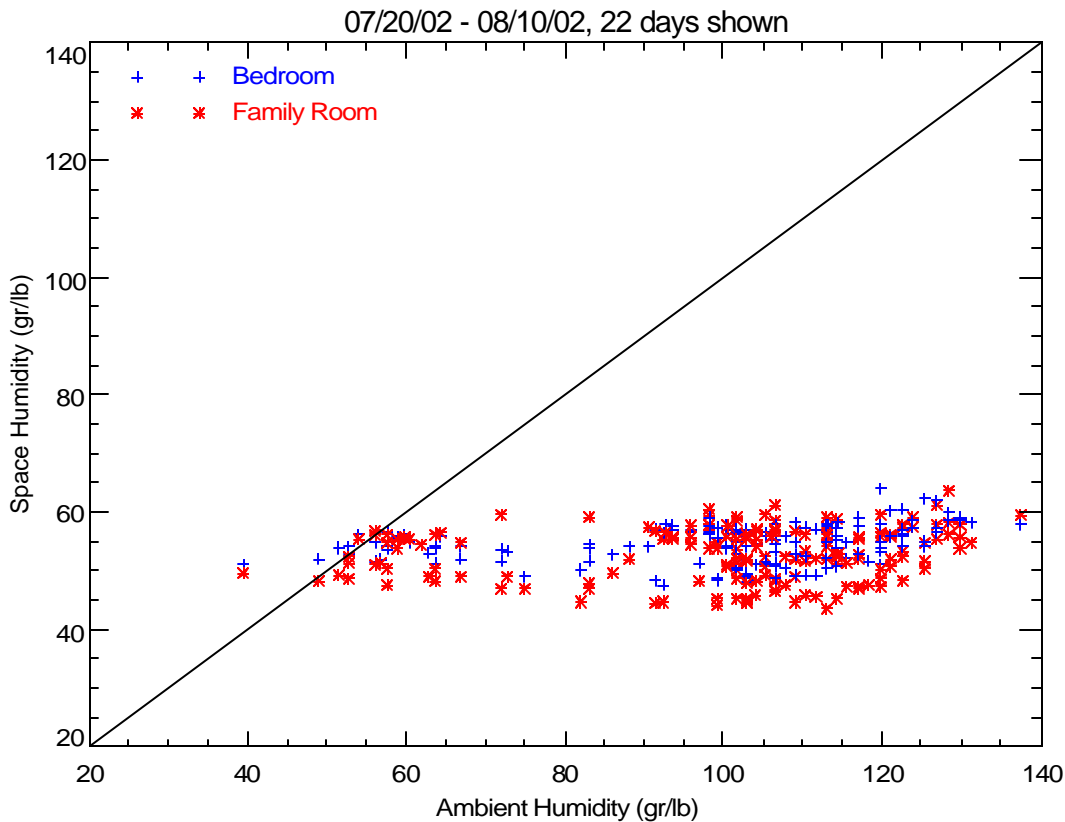
**Figure 17. A Typical Operating Cycle: Downstairs Unit, Oct 12 (Auto Fan Mode)**



**Figure 18. A Typical Operating Cycle: Downstairs Unit, Aug 31 (Constant Fan Mode)**

## Space Conditions

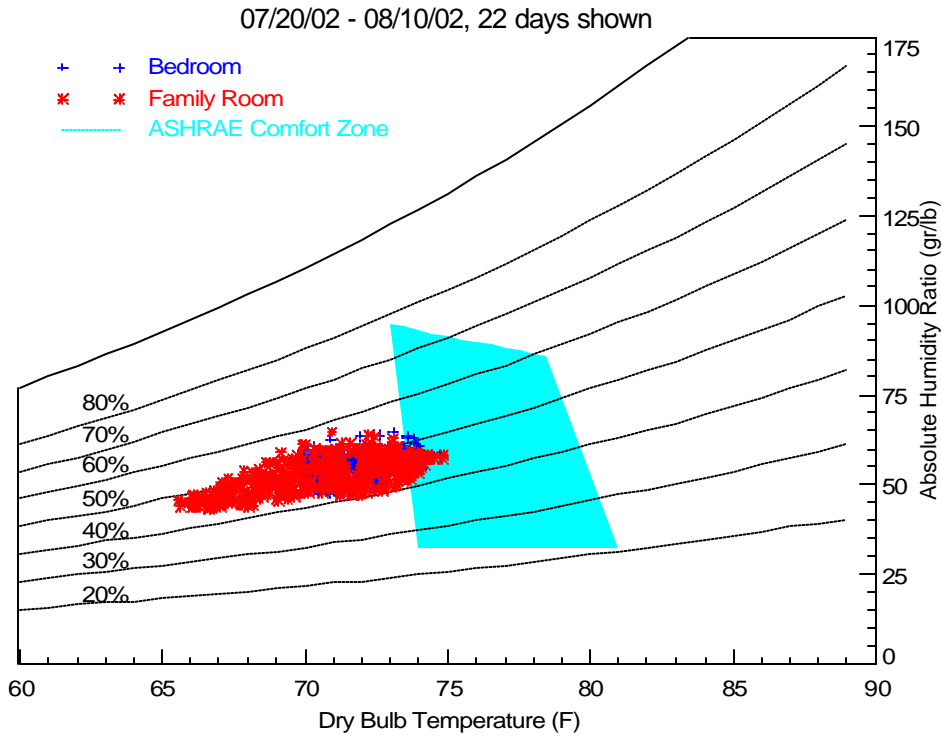
In addition to the return air sensors, two HOBO T/RH dataloggers were installed in the house in the upstairs bedroom and the downstairs family room. The resulting hourly space humidity trends are shown in Figure 19 and Figure 20. In Figure 19 the space humidity is compared to ambient hourly humidity data from nearby Dulles Airport (NCDC data). Both Figures show that the upstairs bedroom is slightly warmer and more humid than the downstairs family room. This concurs with the cooling coil process lines in Figure 15, which also indicate that the upstairs AC unit had slightly more humid inlet conditions.



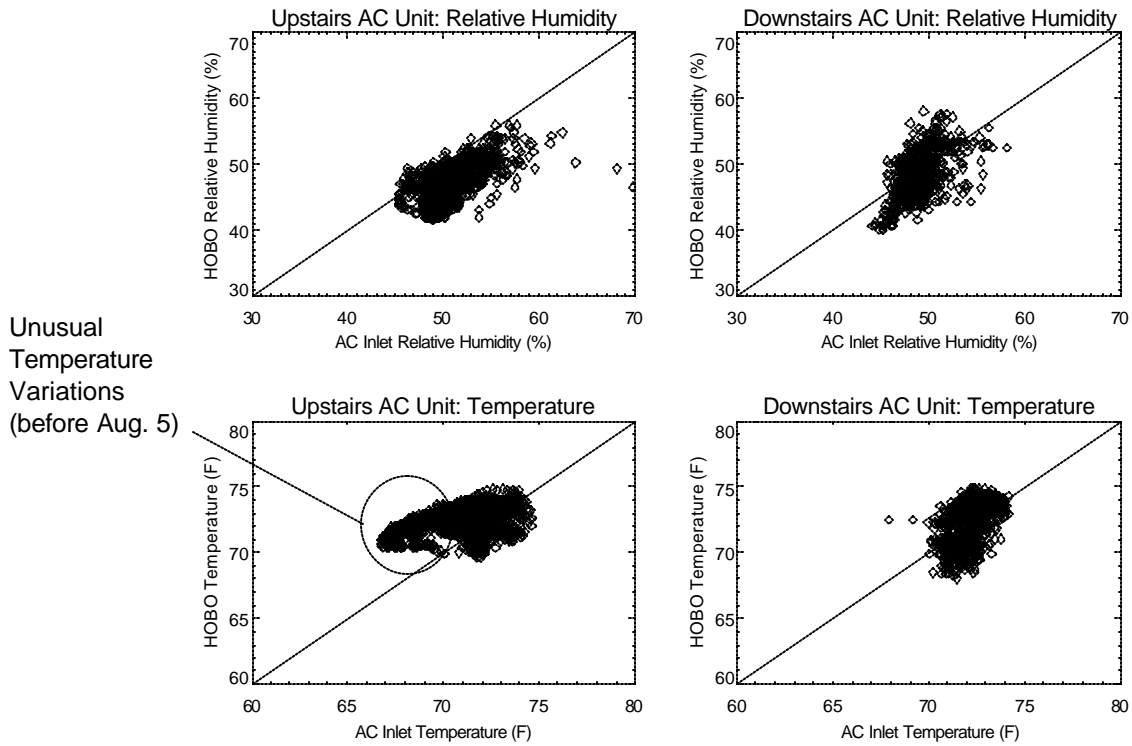
**Figure 19. Space Humidity Trend with Ambient HOBO loggers compared to NCDC Ambient Data**

Figure 21 shows that the HOBO space readings are in fair agreement with the return air conditions at the AC coil inlet (the Bedroom is matched to the upstairs AC unit while the Family Room is the downstairs unit). The only significant variation is the differences between the upstairs return temperature and the bedroom temperature. Prior to August 5, the inlet temperature varies 4-5° F from the HOBO sensor during the overnight period. This variation may be due to doors being closed at night.

Figure 22 shows the typical daily space temperature and humidity profiles for a hot day in August. The daily trend shows the expected variation with time of day and compressor operation.



**Figure 20. Space Conditions Shown on the Psychrometric Chart**



**Figure 21. Comparison of Hobo and AC Inlet Conditions**



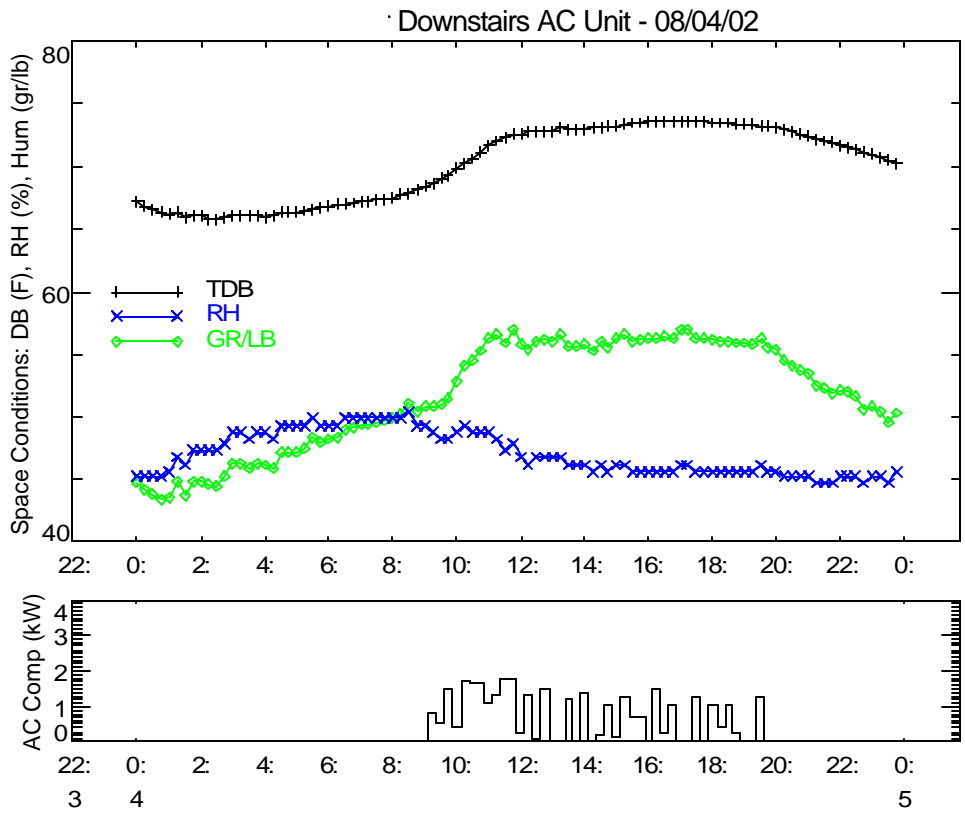
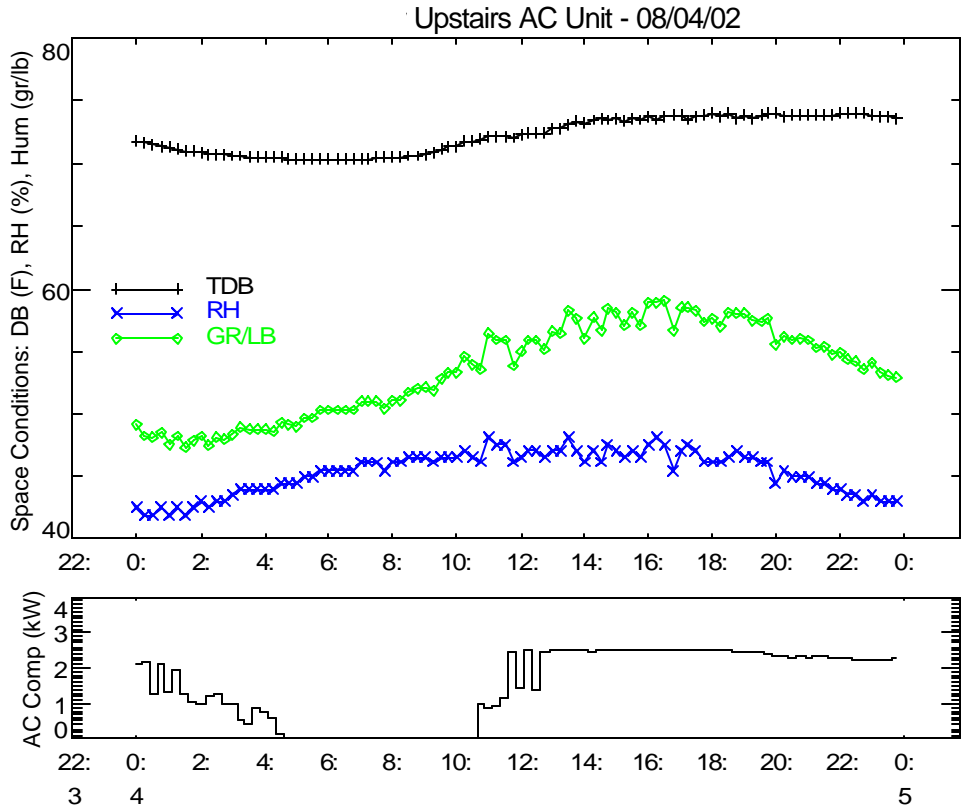


Figure 22. Daily Profile of Space Conditions for a Hot Summer Day (August 4, 2002)

## Condensate Delay Time

One key indication of the coil's moisture-holding capacity is the time it takes for condensate to first fall from the coil. This time delay is similar to the parameter  $t_{wet}$  from the LHR Model. Figure 16 and Figure 17 show operating cycles for both AC units from October 12, a day when both units had been off for an extended time and then started up under fairly humid conditions. For both units, this event was the one time over the entire season when the coil was fully dry and then ran continuously for several minutes.

Figure 23 shows the condensate delay times for a few compressor startup cycles for the upstairs and downstairs units. The criteria for including cycles on the plots were:

- There were no condensate pulses in the previous 2 hours before compressor startup,
- The compressor was continuously on at least until the first condensate pulse occurred,
- The condensate event was followed by at least one other condensate pulse.

For the upstairs unit, only one recorded condensate pulse/on cycle met the criteria above (it is also shown in Figure 16). Several cycles met the criteria for the downstairs unit, though many of these had much lower delay times, which implies that the coil was not fully dry before these cycles occurred. Data from the lab and other field test sites typically showed a decreasing condensate delay time with increasing dew point temperature. However, not enough data were available to detect that trend here.

Table 2 summarizes the nominal condensate delay time and the increased pressure drop due to the wet coil. The entering dew point of 58°F approximately corresponds to nominal entering conditions of 60°F dew point (and the laboratory data shows that dew point is the primary factor affecting the condensate delay time). The condensate delay time for both units was about 15-16 minutes.

**Table 5. Summary of Nominal Condensate Delay and Wet-Dry Pressure Drop Calculations**

	Upstairs AC Unit	Downstairs AC Unit
Entering Dew Point (F) (avg conditions before first pulse)	58	58
Time Delay for First Condensate Pulse (minutes)	15.2	16.4
Wet-Dry Coil Pressure Drop (in H <sub>2</sub> O x 1000)	36.5	54

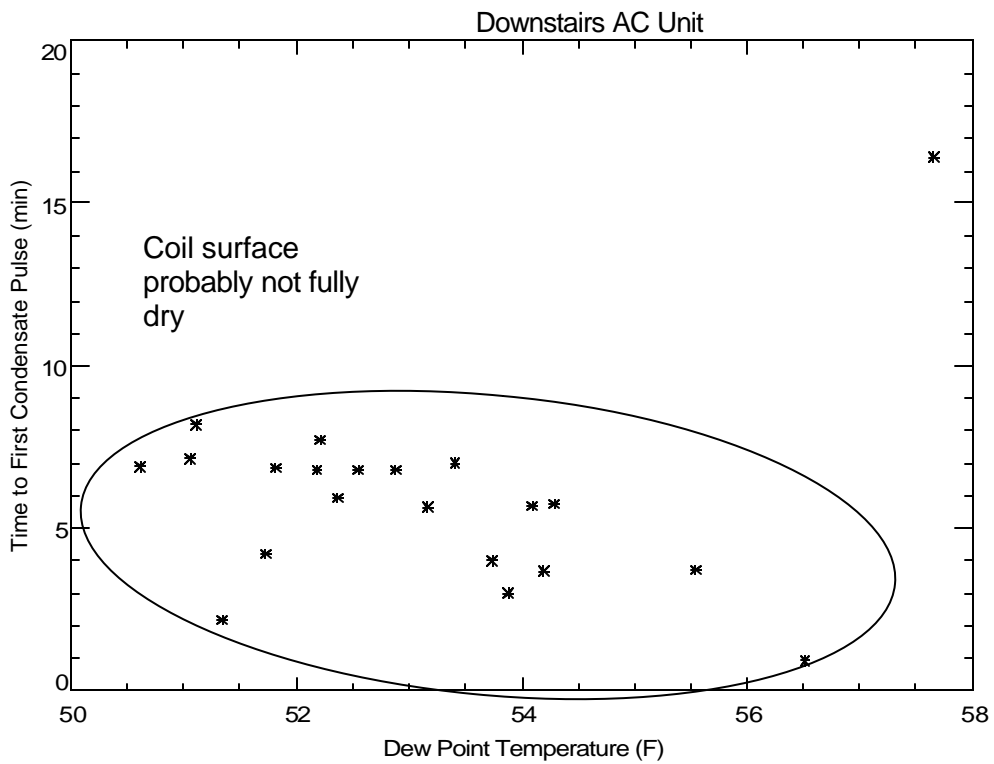
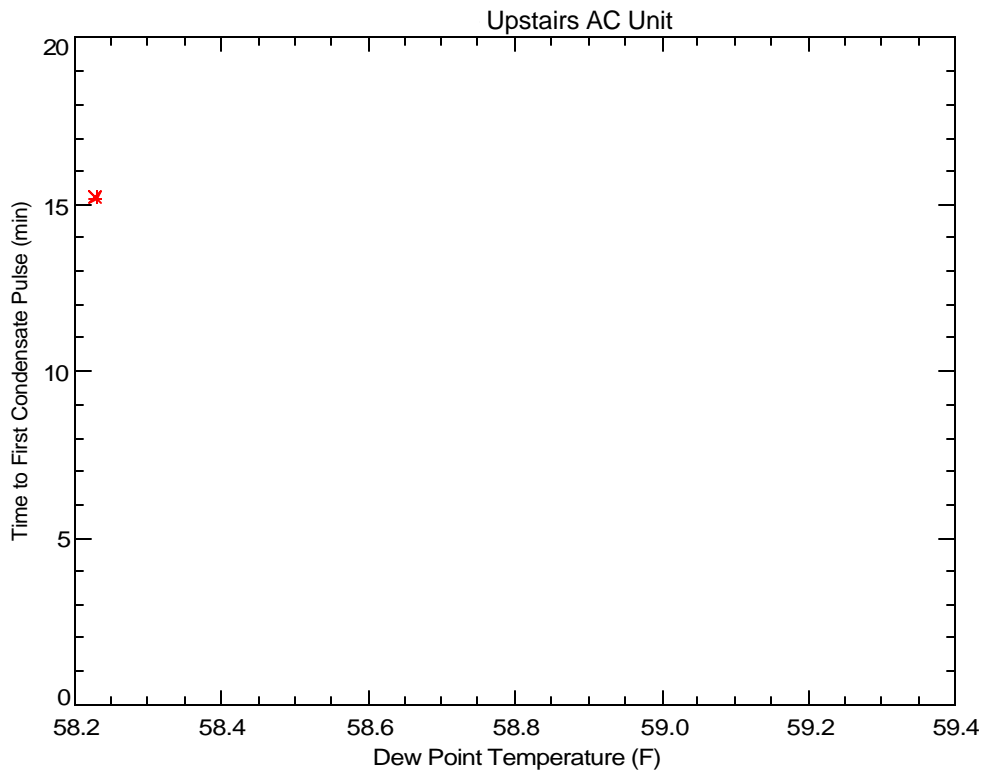


**Figure 23. Condensate Delay Time as a Function of Entering Dew Point for Upstairs and Downstairs Units**

## **Thermostat Cycling Rate**

Thermostat behavior for single stage AC system is expected to follow a parabolic trend with runtime fraction as shown in Figure 24 below. The single-parameter parabolic curve is defined as

$$N = 4 \cdot N_{\max} \cdot X \cdot (1-X)$$

Where  $N_{\max}$  is the peak cycling rate and occurs at a runtime fraction ( $X$ ) of 0.5. Most residential and small commercial systems have a value of  $N_{\max}$  around 3. For upstairs and downstairs AC units, the values of  $N_{\max}$  calculated from the average  $N$  for  $X$  in the range of 0.48-0.52 are 3.5 and 2.9, respectively. In each case the measured data were determined from 1-minute records by calculating the exact length of each total on/off cycle ( $t_{\text{cyc}}$ ) as well as the compressor runtime ( $t_{\text{on}}$ ). Then for each cycle the runtime fraction ( $X = t_{\text{on}}/t_{\text{cyc}}$ ) and the cycle rate ( $N = 1/t_{\text{cyc}}$ ) can be determined. The degree of scatter on Figure 24 is most likely due to user thermostat adjustment, thermostat setup and setback, and any built-in control delays in the AC unit.

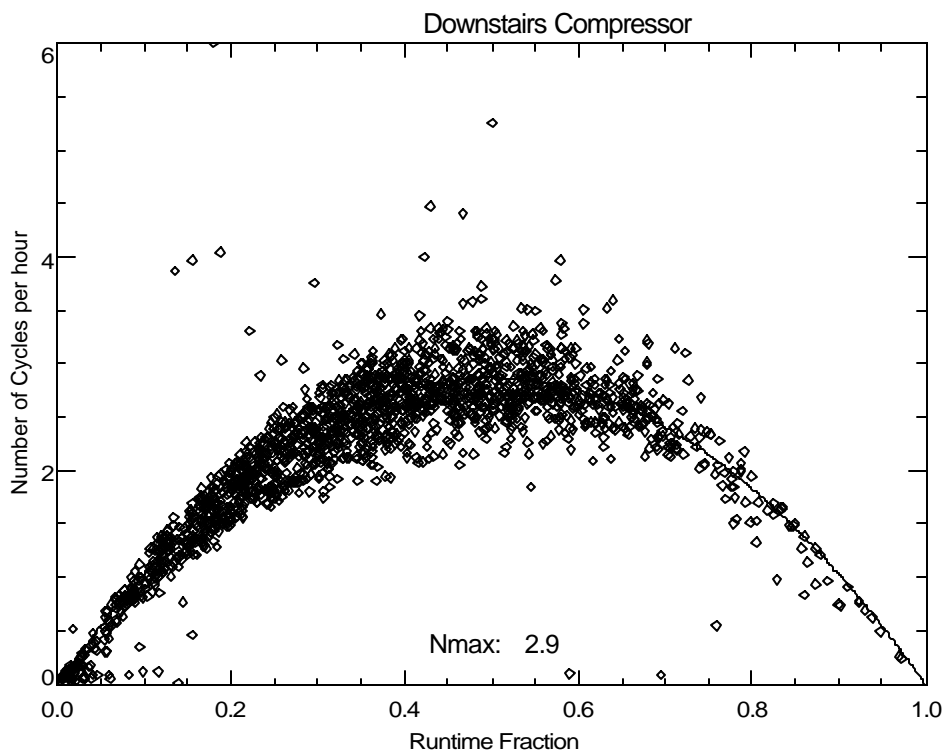
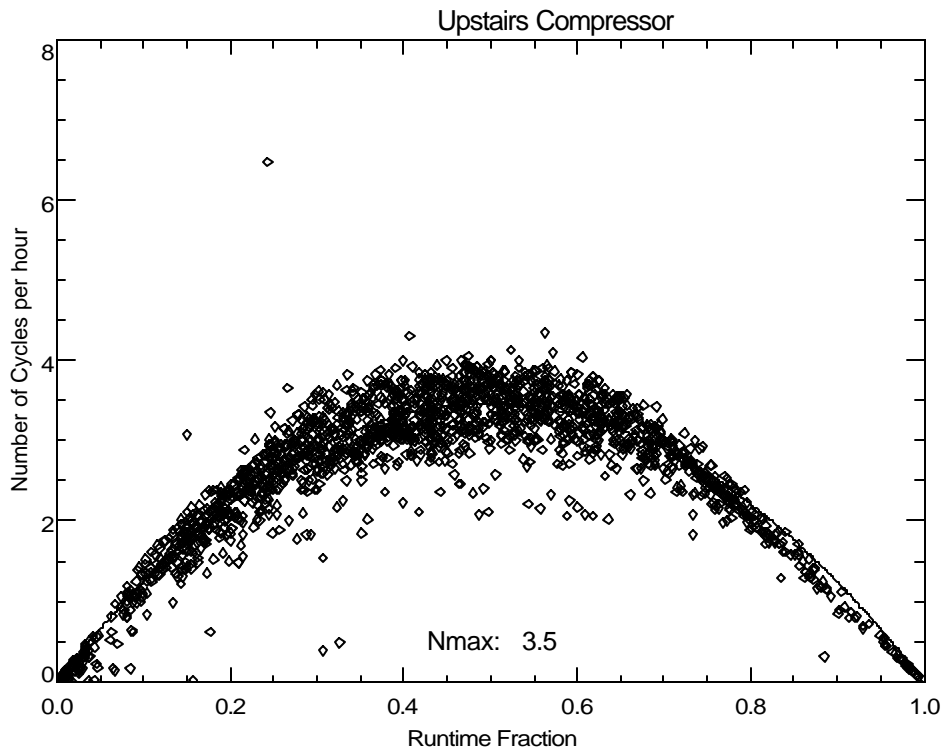


**Figure 24. Thermostat Cycling Curves for Both Units**

## Cooling Energy Trends

Total cooling energy use for both units shows a linear trend with the daily average ambient temperature. The upstairs unit ran the most and uses about 60% of the total annual energy use.

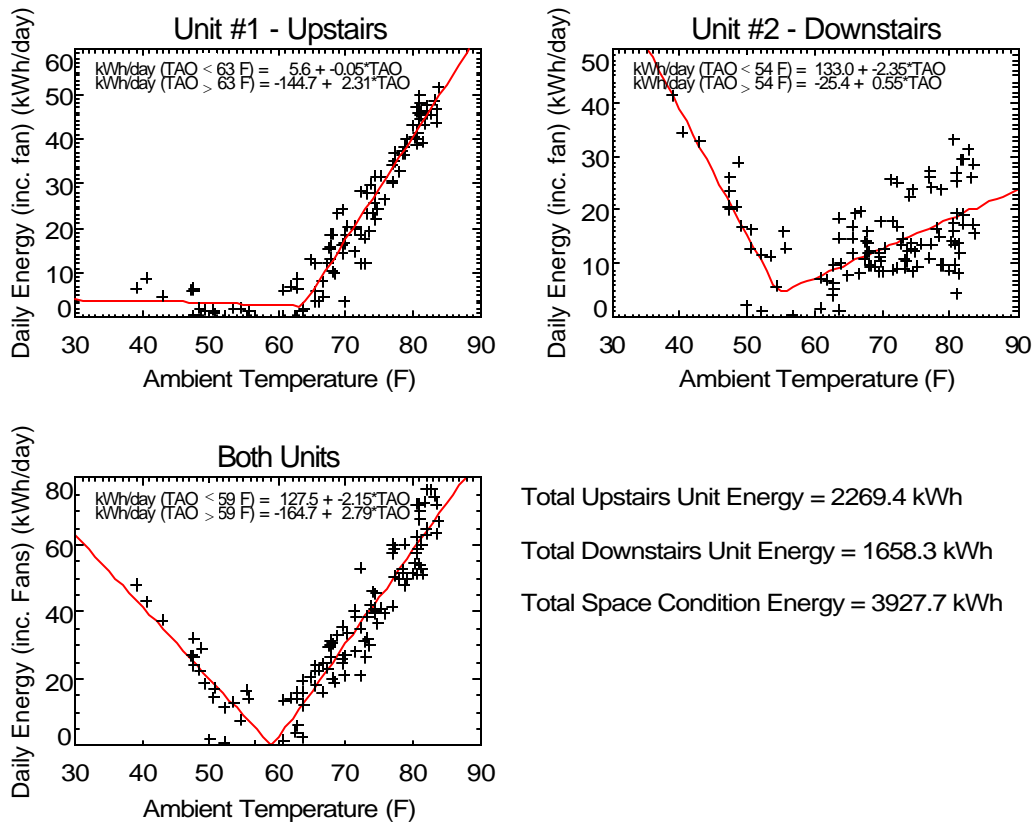


**Figure 25. Cooling Load Lines for Both Units**

## Off-Cycle Evaporation Rates

The downstairs unit operated for an extended period in the constant fan mode, which allowed the off-cycle performance of that cooling coil to be evaluated. Figure 26 shows the off-cycle sensible capacity for several cycles when the compressor had just stopped operating, and one or more condensate pulses had occurred in the last 10 minutes of compressor operation. The plot includes ‘\*’s after the 2<sup>nd</sup> minute, which is about the time when we estimate that refrigerant dynamics have died down and sensible capacity is driven by the evaporation process. We make the assumption, based on laboratory data, that the coil operates an evaporative cooler with latent and sensible capacity summing to zero.

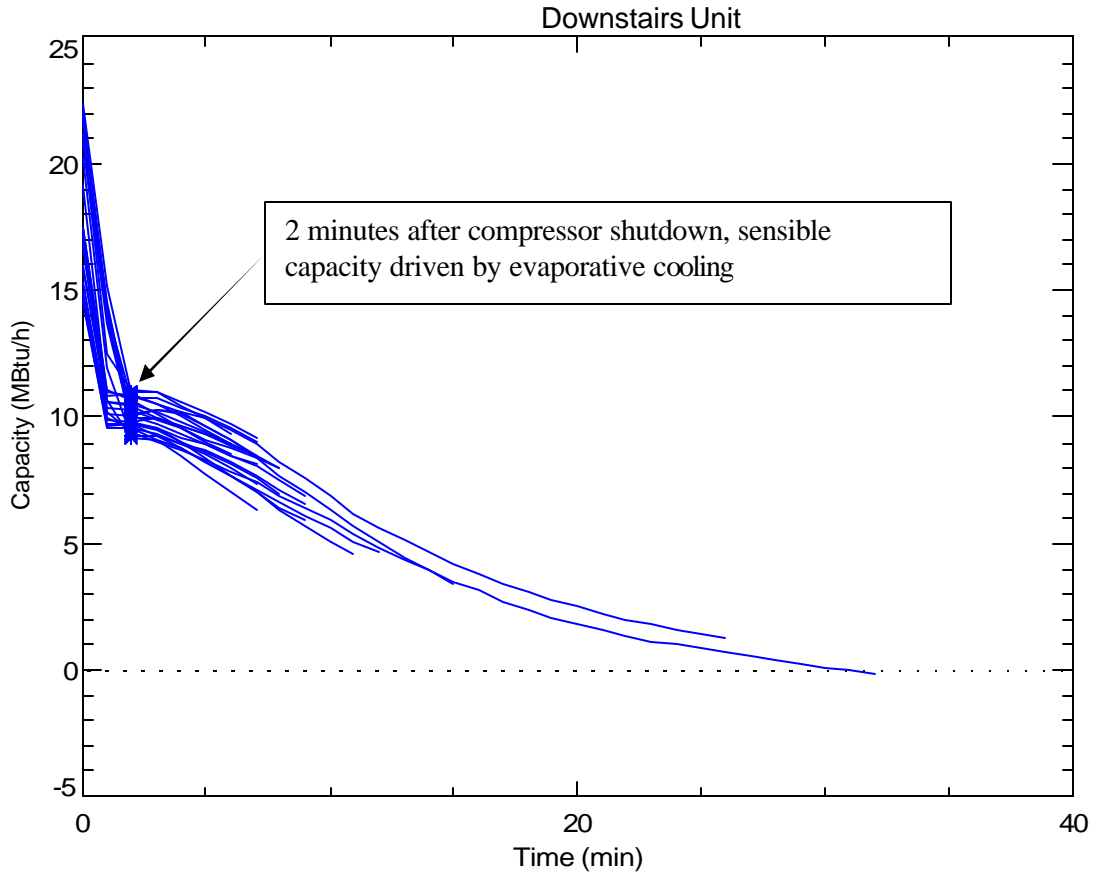


**Figure 26. The Trend of Sensible Capacity for Several “Wetted” Off-Cycles**

Figure 27 and Figure 28 compare the initial evaporation rate (i.e., the points noted as \*s on Figure 26 above) for each off-cycle meeting the criteria for being fully wetted. The initial evaporation rate is about 10 MBtu/h. Figure 27 shows that the evaporation rate is clearly a function of the wet bulb depression (i.e., the DB minus the WB), as would be expected. The line on the plot shows the theoretical trend projected to zero evaporation at no wet bulb depression. The saturation effectiveness, which is defined below, is shown on Figure 28.

$$\eta_{\text{sat}} = Q_{\text{evp}} / (1.08 \times \text{cfm} \times (\text{DB} - \text{WB}))$$

The average effectiveness is 0.782, which corresponds to an NTU of 1.52. The NTU of the coil as an evaporative cooler is defined as:

$$\text{NTU} = (k \times A) / \text{cfm}^{0.2}$$

Where A is fin surface area of the coil (241.5 ft<sup>2</sup>) and the cfm is 1100 cfm. Using these parameter values, the constant k = 0.026, which is similar to the values determined from the laboratory measurements for other coils.

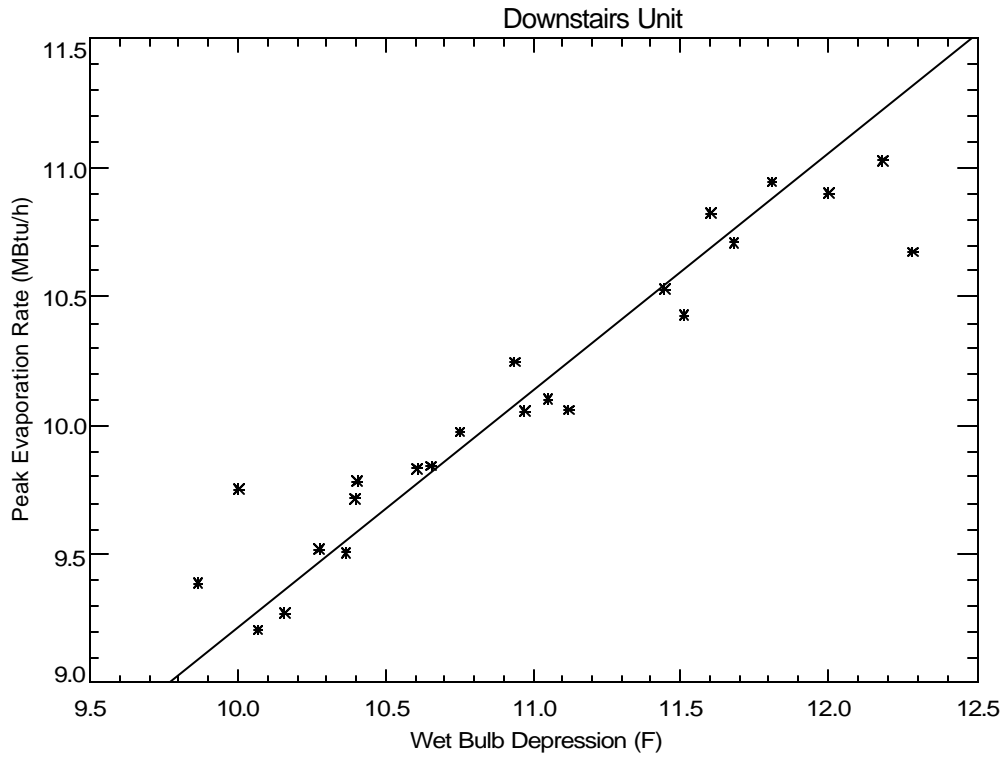


**Figure 27. The Trend of Peak Off-Cycle Evaporation Rate With Wet Bulb Depression**

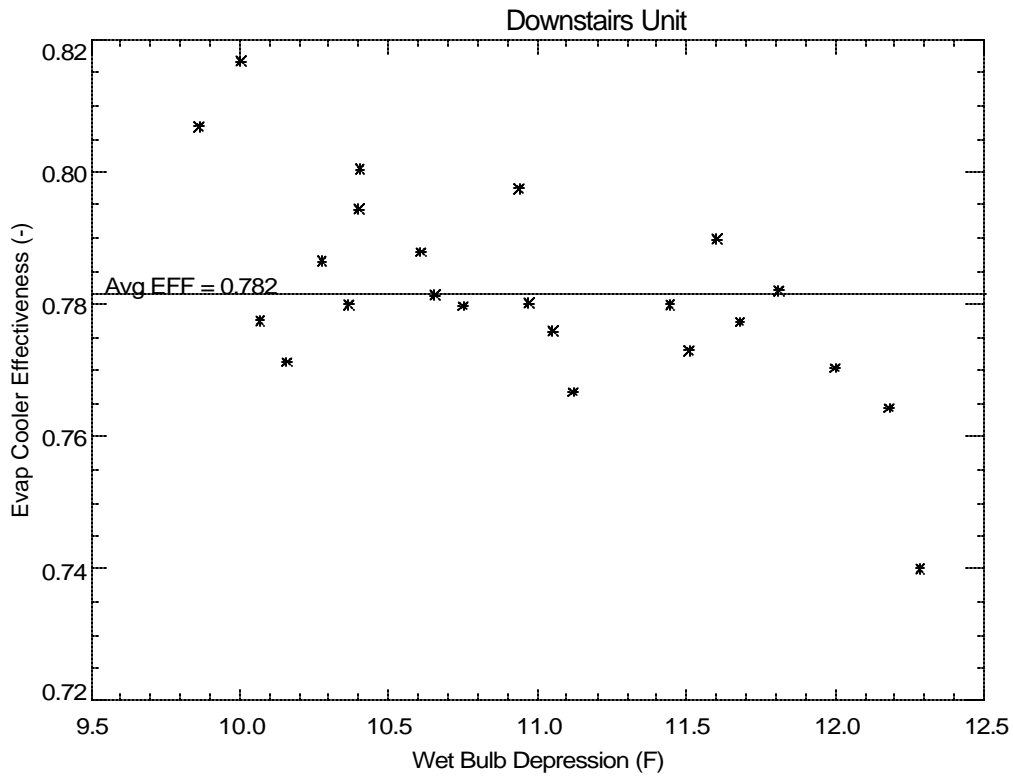


**Figure 28. Evaporative Cooler Saturation Effectiveness of Cooling Coil**



## **Part Load SHR**

The moisture removal capacity of a cooling coil is reduced at part load conditions. This part load degradation is especially prevalent when the fan operates continuously. However, Figure 29 shows that it is also true when the fan cycles on and off with the compressor (the auto fan mode). The SHR is calculated using the coil temperature difference, air flow, and condensate readings on an hourly basis. Data are only included on the plot when the hourly average entering conditions are between 71 to 74 °F and 48 to 52 % relative humidity. The steady state SHR listed on each plot with a dotted line approximately corresponds to the SHR of the process lines shown on Figure 15.

The graph at the bottom of the Figure shows that the downstairs unit operated in both the constant and the auto fan modes. In constant fan mode, the SHR for the downstairs unit is essentially zero until the hourly runtime fraction reaches 0.6. In the auto fan mode, both units show a similar degradation rate where the latent capacity linearly approaches zero (or SHR approaches 1) as the runtime fraction approaches zero.

The red line of the plot is the LHR model with the parameters:

$t_{\text{wet}}$	$\cong$	15 minutes		
gamma	$\cong$	$Q_{\text{evp}} / Q_L$	=	11 MBtuh / 5 MBtuh = 2.2
$N_{\text{max}}$	=	3 cycles/h		
Model type	-	linear		
AC time const	-	60 seconds		

The parameters correspond the entering conditions used to select the data (approximately 54-56°F dew point). They were determined from the plots above.

The nominal values of  $t_{\text{wet}}$  and gamma at 80°F/67°F would be closer to:

Nominal gamma:	1.7 ( $Q_{\text{evp}} = 12.5 \text{ MBtuh}$ ; $Q_L = 7.5 \text{ MBtuh}$ )
Nominal $t_{\text{wet}}$ :	16.4 minutes

The mass of water stored on the coil is equivalent to  $Q_L \times t_{\text{wet}}$ , or

$$\text{Mass} = 7.5 \text{ MBtu/h} \times 16.4 \text{ minutes} \times 1 \text{ hr}/60 \text{ minutes} / 1.06 \text{ MBtu/lb} = 1.9 \text{ lbs}$$

This mass is per unit fin area becomes: 8 lb per 1000 ft<sup>2</sup>, which is similar to what has been observed in the lab.

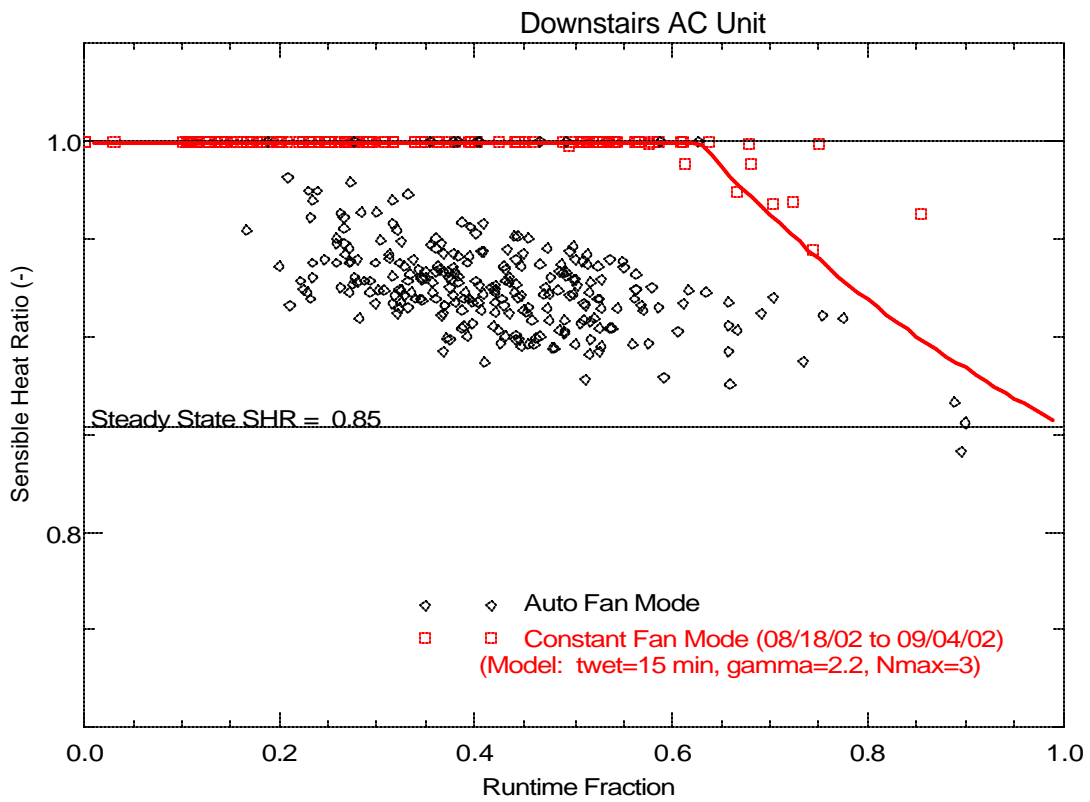
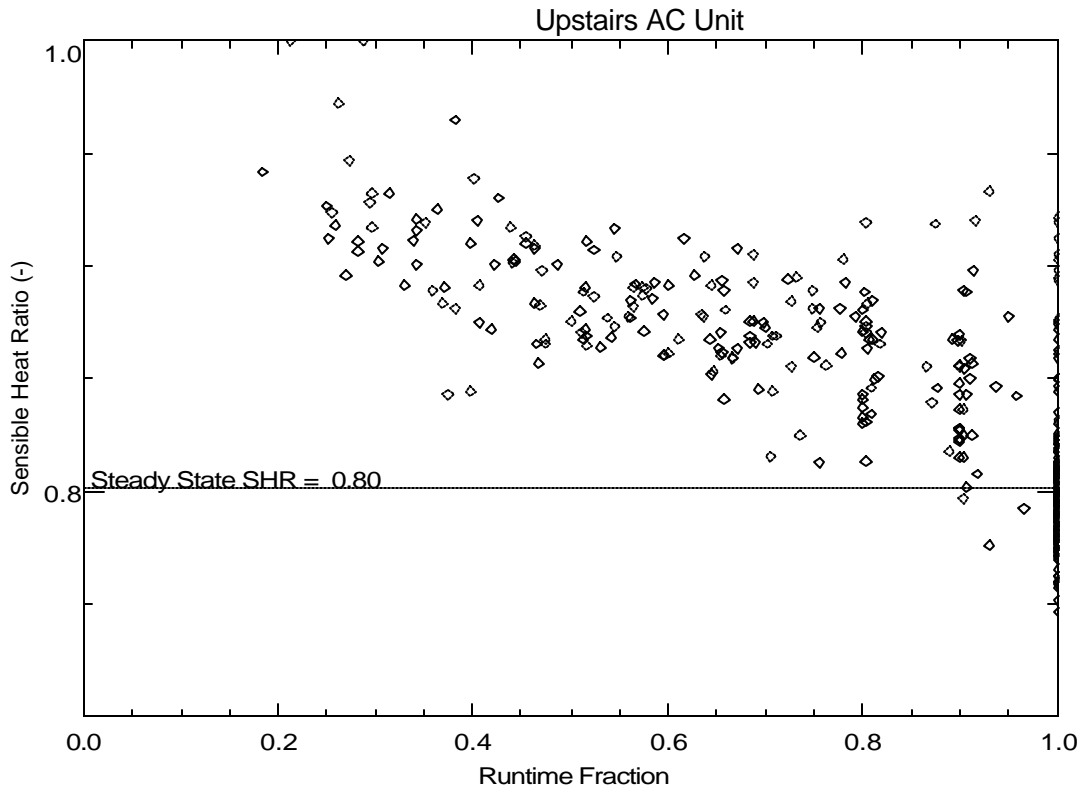


**Figure 29. Part-Load Sensible Heat Ratio**

## Indoor-Outdoor Humidity Ratio for Different Fan Control Modes

The indoor and outdoor humidity were averaged for days with cooling activity. Figure 30 shows the plot of the humidity ratios for the downstairs AC Unit. With significant cooling activity, constant fan mode is expected to cause greater indoor humidity than auto fan mode, however there may not be enough compressor run-time during the day to notice the trend for the downstairs AC Unit.

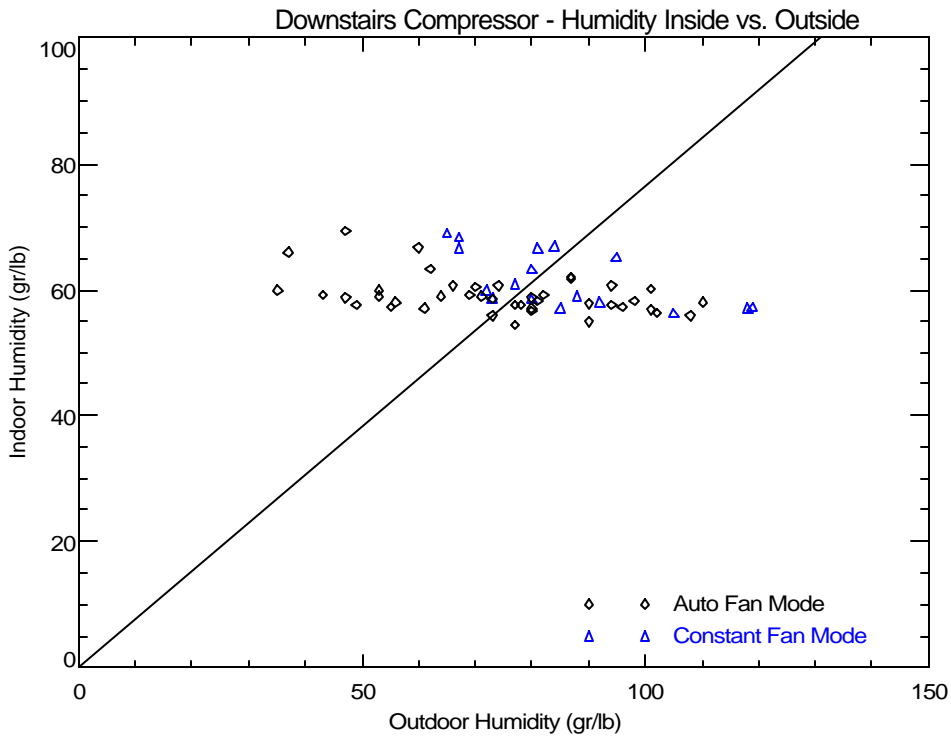


**Figure 30. Daily Humidity Ratios for Constant vs. Auto Fan Mode for Downstairs AC Unit**

## **APPENDIX I2**

### **Summary of Data for Field Test Site 2**

## Site #2 – Merritt Island, FL



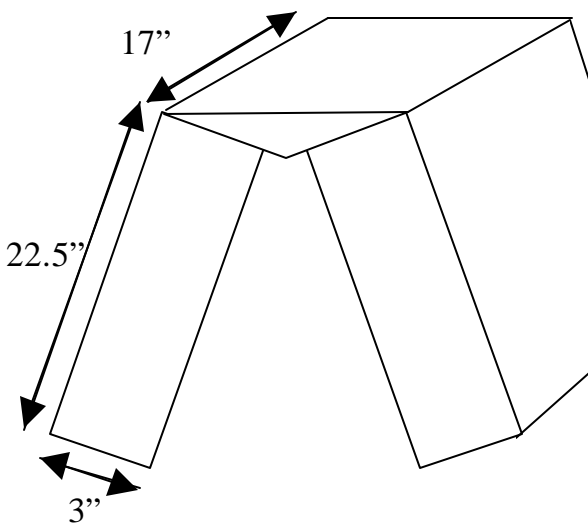
Figure 1. East Exposure

### System Description

This site has a 2-stage, 3-ton heat pump system. The site is located on the intercoastal waterway in Merritt Island, Florida. The unit has a multi-speed ECM fan motor that operates at various speeds depending on the control settings. The nominal operating speed for 1<sup>st</sup> and 2<sup>nd</sup> stage are 550 and 1,100 rpm. The unit has an enhanced humidity control mode that operates the fan at a fraction of nominal speed for several minutes during startup.

#### Heat Pump

Trane XL1800 2-speed condensing unit  
Model No: TWZ036A100A2  
Serial No: Z371UHD1F

Coil Type	"A" coil	
Coil Face Area	765 sq. in.	
Rows / depth	4 tubes / 3 in.	
Tubes per row	21 (each side)	
Fin Space / Type	14 fpi / Wavy	
Initial AHU Settings:		
Switch	Setting	
1	On	
2	-	
3	-	
4	-	
*5	On	
*6	On	
7	-	
8	-	
*Switches 5 and 6 are for Enhanced Mode		
Exp device: TXV		

**Figure 2. AHU Coil Dimensions and Settings**

Gross fin area: $(3 \text{ in}) \times (14 \text{ fins/in}) \times (2 \text{ sides/fin}) \times (765 \text{ sq in.}) / 144 \text{ sq in/ft}^2 = \underline{446.3 \text{ ft}^2}$
---

**Table 1. Sensor Verification Readings**

Data Point	Data Logger	TSI
TAO (F)	75.9	77.4
TAS (F)	63.1	63.0
TAR (F)	75.8	76.6
RHO (%)	91.1	87.9
RHS (%)	86.7	83.2
RHR (%)	58.6	59.5

## Sensors and Data Logger Connections

Channel	Data Point	Description	Units	Sensor Description
SE1	TREF	Reference Temperature	C	
SE2	TAO	Outdoor Temperature	F	Type-T TC
SE3	AMUX CH 1			
SE4				
SE5				
SE6	AMUX CH 2			
SE7	TEVP1	Coil Return Bend Temperature	F	Watlow TC AFEC0TA040U8250
SE8	TEVP2	Temperature Leaving Evaporator	F	Watlow TC AFEC0TA040U8400
SE9	TSUC1	Suction Temperature	F	Watlow TC AFEC0TA040U8400
SE10	TLIQ1	Liquid Line Temperature	F	Watlow TC AFEC0TA040U8250
SE11	TAM1	Mixed Air Temperature	F	Watlow TC AFGCNTA120U8250
SE12	TAS1	Supply Air Temperature	F	Watlow TC AFGCNTA120U8250
P1	VF1	Fan Speed	RPM	Monarch ROS-5P photo tach
P2	WC1	Compressor Power	kWh	Ohio Semitronic SWH-2100 100 AMP
C1	AMUX RES			
C2	AMUX CLK			
C3	SC1	Compressor Stage 1 Status	min	Veris H800
C4	SC2	Compressor Stage 2 Status	min	Veris H800
C5				
C6				
C7	FC1	Condensate Removal	pulse	Texas Tipping Bucket
C8	WF1	AHU Fan Power	kWh	Ohio Semitronic SWH-2100 100 AMP
		****Analog MUX****		
AM-1-1H	PSUC1	Compressor Suction Pressure	psig	Setra C207
AM-1-2H	RHM1	Return/Mixed RH	%	Vaisala HMD60U
AM-2-1H	RHS1	Supply RH	%	Vaisala HMD60U
AM-2-2H	DPC1	Pressure Drop Across Coil	in wc *100	Setra 267MR (0.25, 0.5, 1.0 inches)
AM-3-1H	IB1	AHU Fan Current	amps	Veris H721LC
AM-3-2H	FA1	Supply Air Velocity	in wc *100	Pitot Tube/Setra C264
AM-4-1H	RHO	Outdoor RH	%	Vaisala HMD60U

**Table 2. CR10X Data Logger Channel Assignments and Sensors Identification**

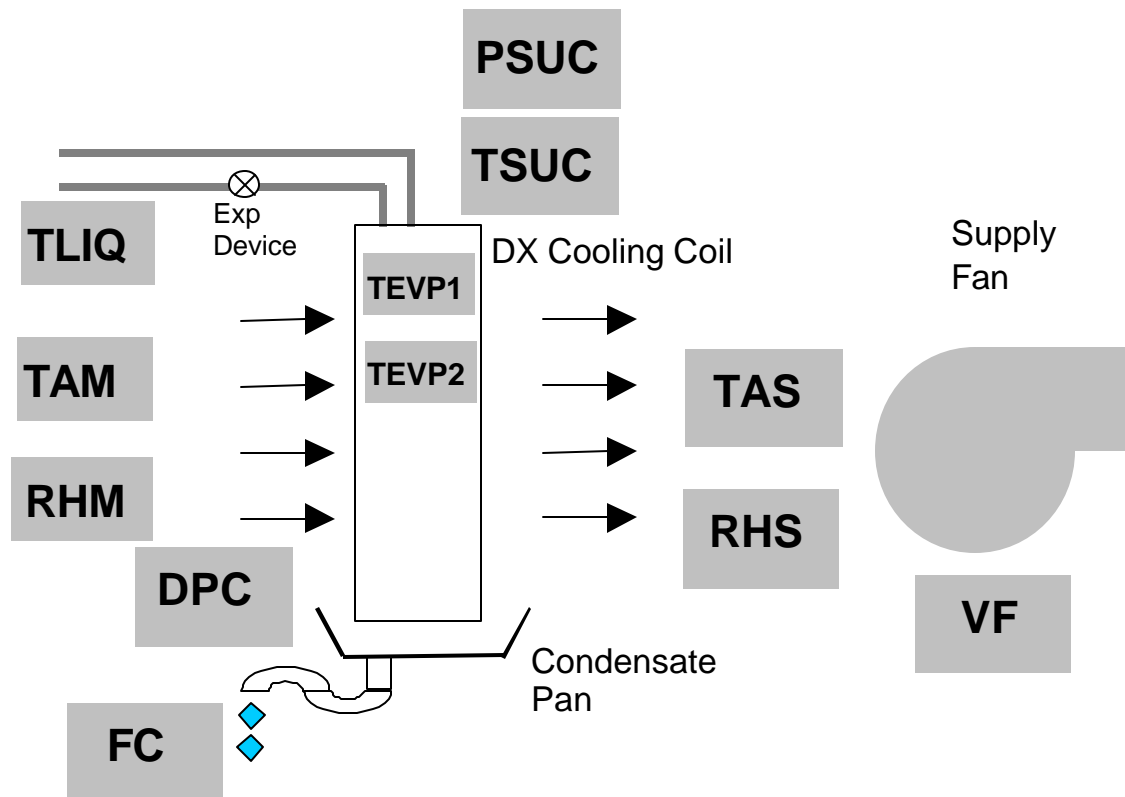


Figure 3. System Schematic

**Site Photos**

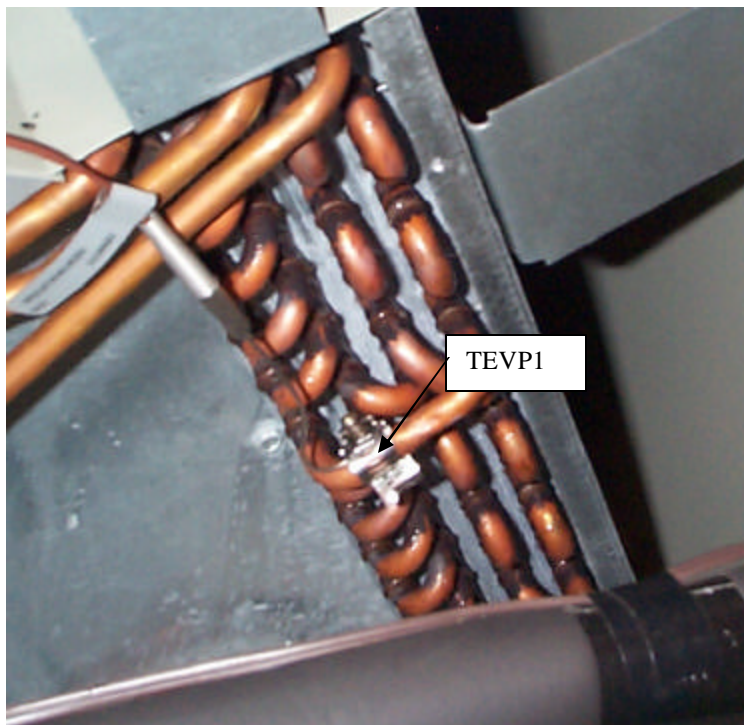


Figure 4. Coil Return Bend Temperature Sensor



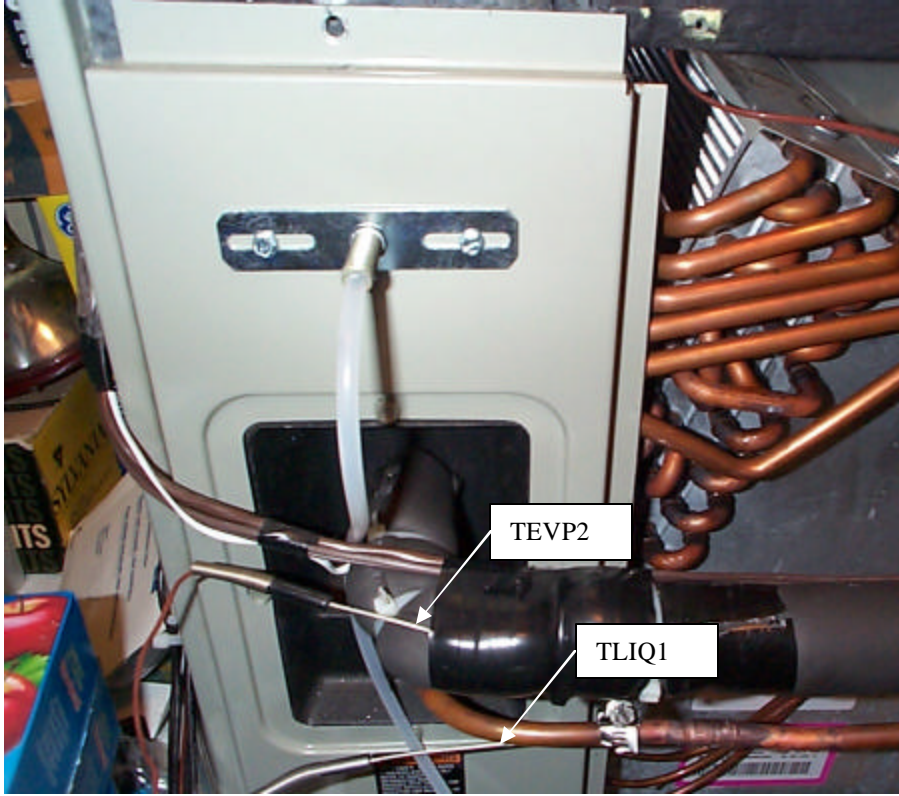


Figure 5. Evaporator Leaving Temperature Sensor

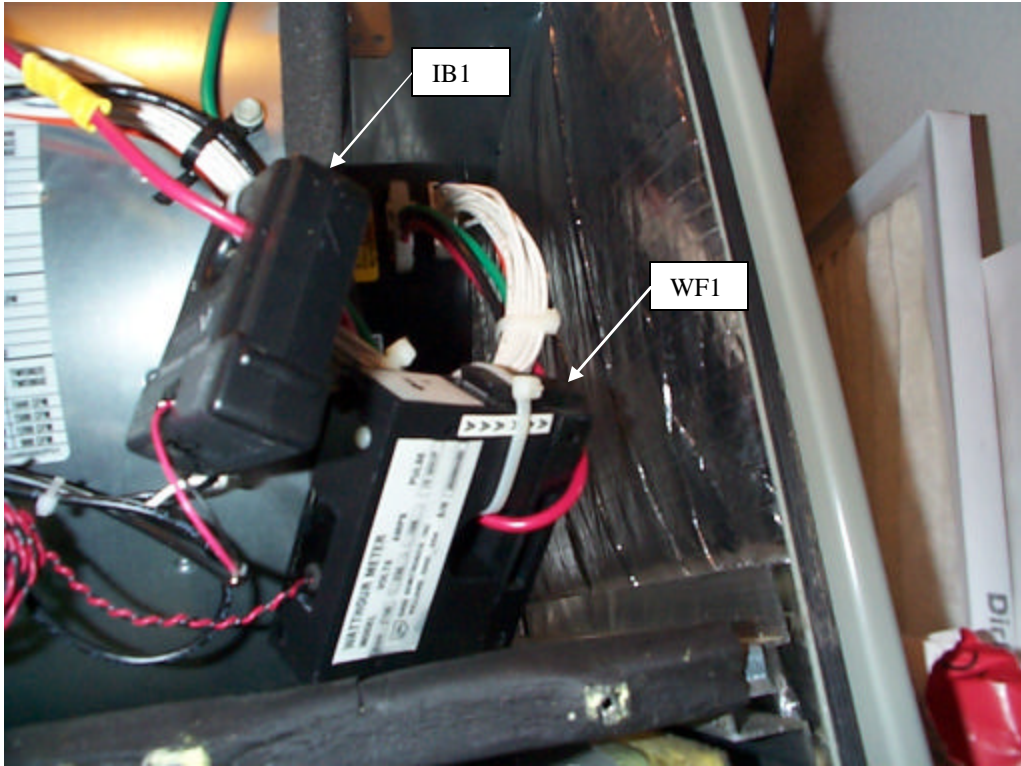


Figure 6. AHU Fan Power and Current Sensors

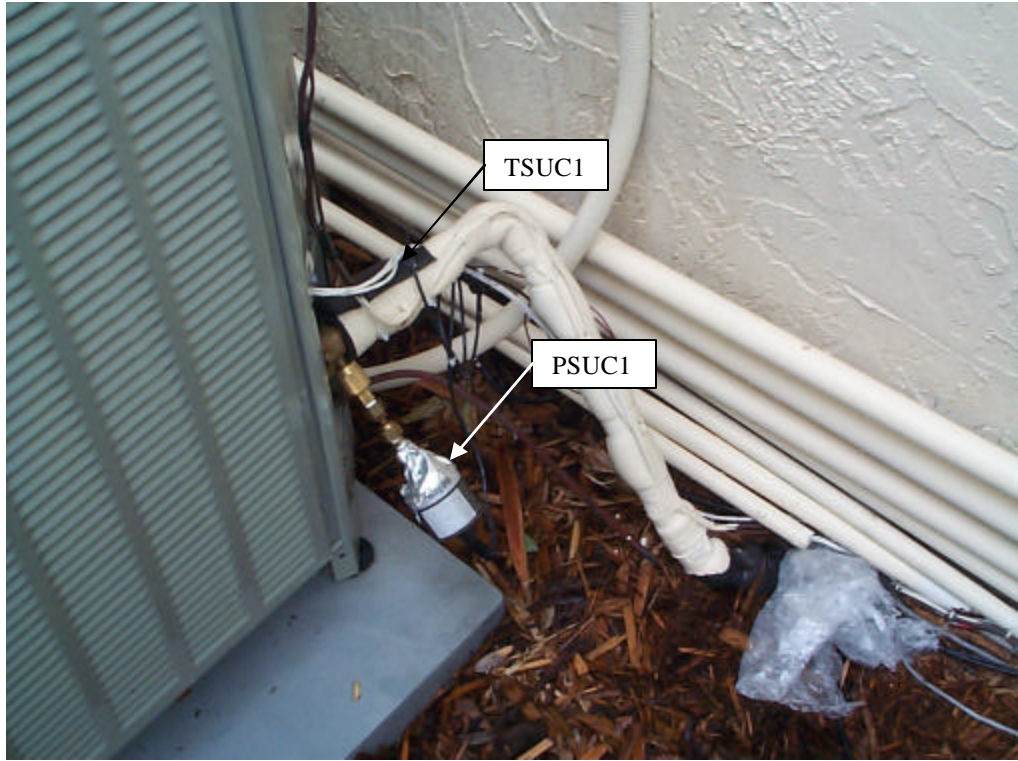


Figure 7. Condenser Unit Sensors

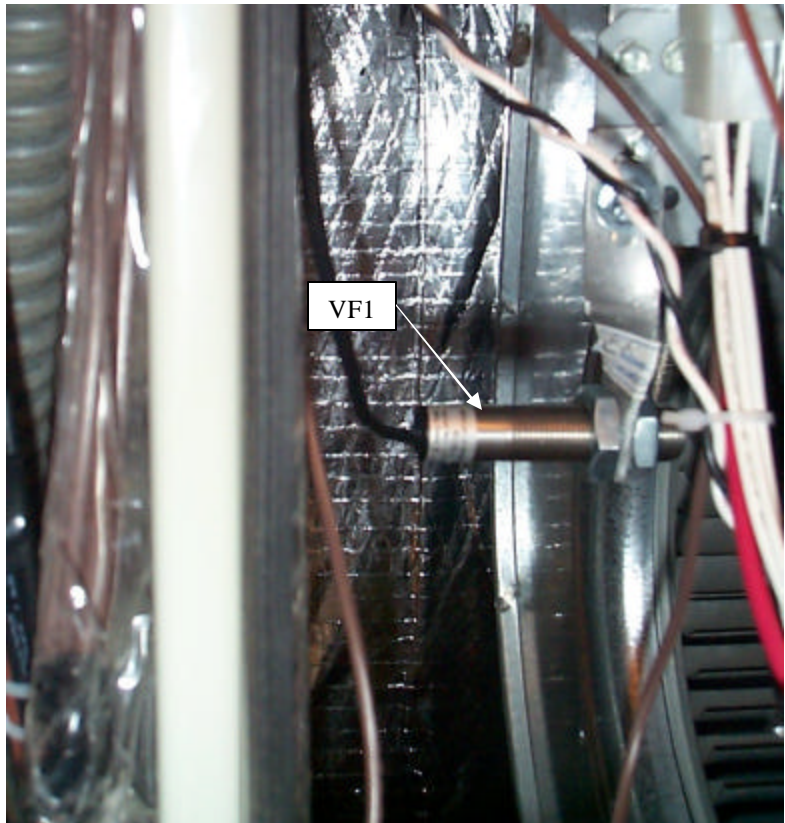


Figure 8. AHU Fan Speed Sensor

# CR10X Data Logger Wiring Schematics

## CR10X Data Logger Analog Terminals

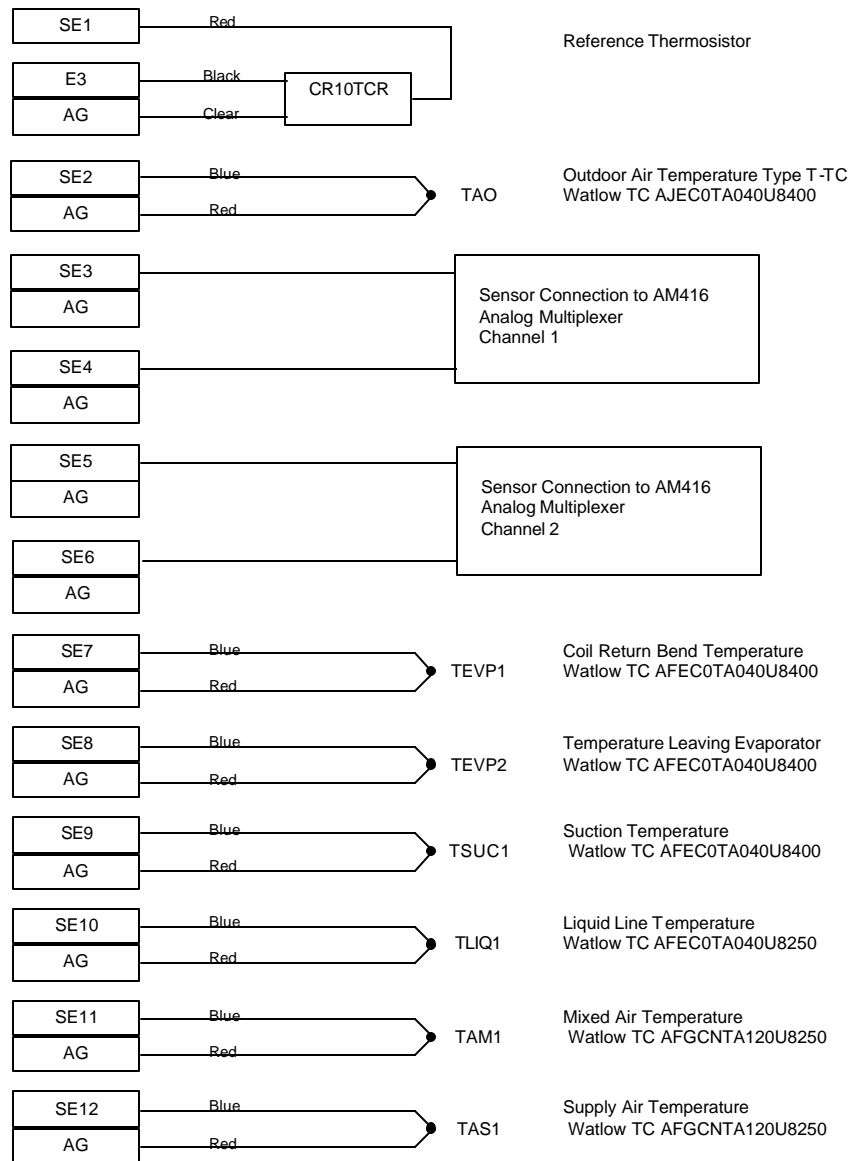
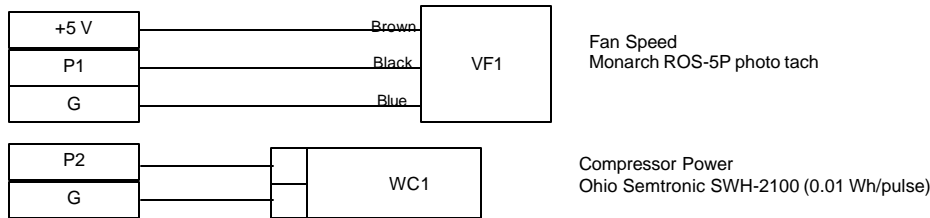
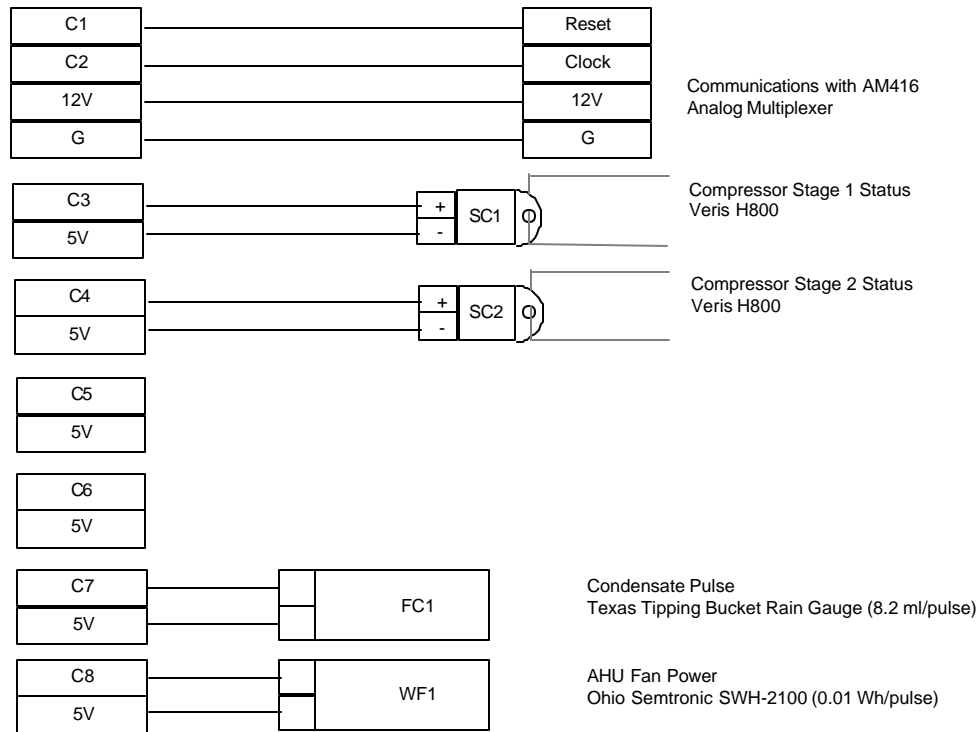


Figure 9. CR10X Analog Terminals Wiring Schematic

**CR10X Data Logger  
Pulse Terminals**



**CR10X Data Logger  
Digital Terminals**



**Figure 10. CR10X Digital Terminals Wiring Schematic**

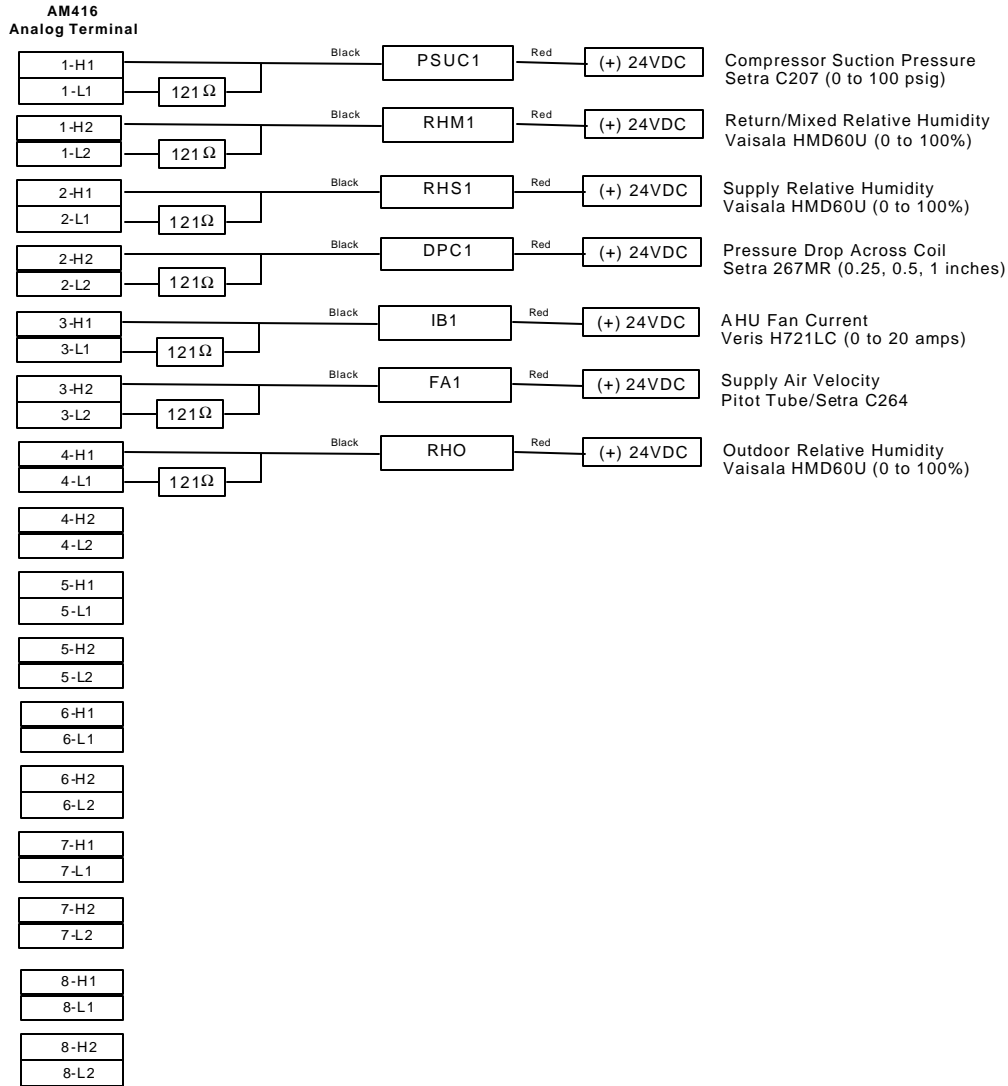


Figure 11. Data Logger Connections to AM416

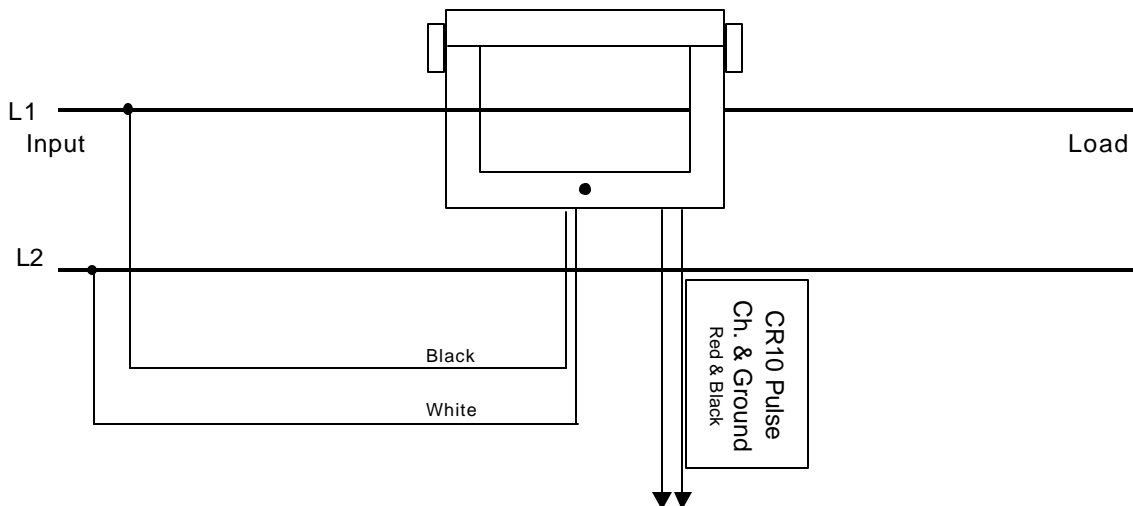


Figure 12. Connection Diagram for SWH-2100 for Single Phase 2-wire Circuit (240V)

## Data Collection Summary

Table 3 summarizes the monitoring and site events that occurred during the monitoring period in 2002 and 2003. Data collection began on July 9, 2002 with the enhanced mode enabled.

However, due to a control wiring problem, the supply fan ran at 1,100 rpm with the 1<sup>st</sup> stage of cooling. This wiring problem was fixed on August 13, 2002 by the local contractor, so that the supply fan ran at 550 rpm in 1<sup>st</sup> stage. The unit then ran in the enhanced mode from August 13 to 31, 2002. The unit was switched to the “regular mode” with no fan delays from September 1 to 26, 2002. From September 27 to October 15, 2002 the supply fan was set to run continuously (i.e., in the constant fan mode). On October 16, 2002 the fan was again set to run in the enhanced mode. However there was very little operation for the remainder of the fall. In the summer of 2003 the unit continued to operate in the enhanced mode. On August 19, 2003, the controls were jumpered to make the unit operate as a single stage unit with enhanced fan operation. On September 5, 2003 the regular fan mode was enabled in the single stage mode.

**Table 3. Summary of Site and Data Collection Events**

July 9, 2002	Data Collection Begins
August 13, 2002	Control problem fixed
August 13-31, 2002	Supply Fan set to Enhanced Mode (auto fan)
September 1-26, 2002	Supply Fan set to Regular Mode (auto fan)
September 27- October 15, 2002	Supply Fan set to Constant Fan Mode
October 16-17, 2002	Supply Fan set to Enhanced Mode (auto fan)
October 17-20, 2002	Unit turned off
November 2-4, 2002	Unit turned off
November 7, 2002	Last Day of Cooling Activity
June 1- August 19, 2003	Monitoring Resumes (in Enhanced Mode)
August 19- September 5, 2003	Set to SINGLE STAGE Enhanced Mode (auto fan)
September 5-29, 2003	Set to SINGLE STAGE Regular Mode (auto fan)
October 1-17, 2003	Set Point Increased by Homeowners
After October 17, 2003	Unit put back to Enhanced Mode (auto fan) End of test period
January 2004	Datalogger removed

Figure 13 through Figure 16 are shade plots that show the operation of the two compressor stages, the supply fan, the supply fan speed, and the condensate removal rate for the 2002 and 2003 seasons. The shade plots qualitatively show the 15-minute data records with shades of gray. Each day is shown as vertical stripe on the plot. Darker shades indicate more operation or activity.

The unit rarely operated in 2<sup>nd</sup> stage cooling, as would be expected (except when it was setup as a single-stage unit). The fan speed plot for 2002 (Figure 14) confirms the initial problems with high fan speed before August 13, 2002. The periods in the constant fan mode are also apparent.



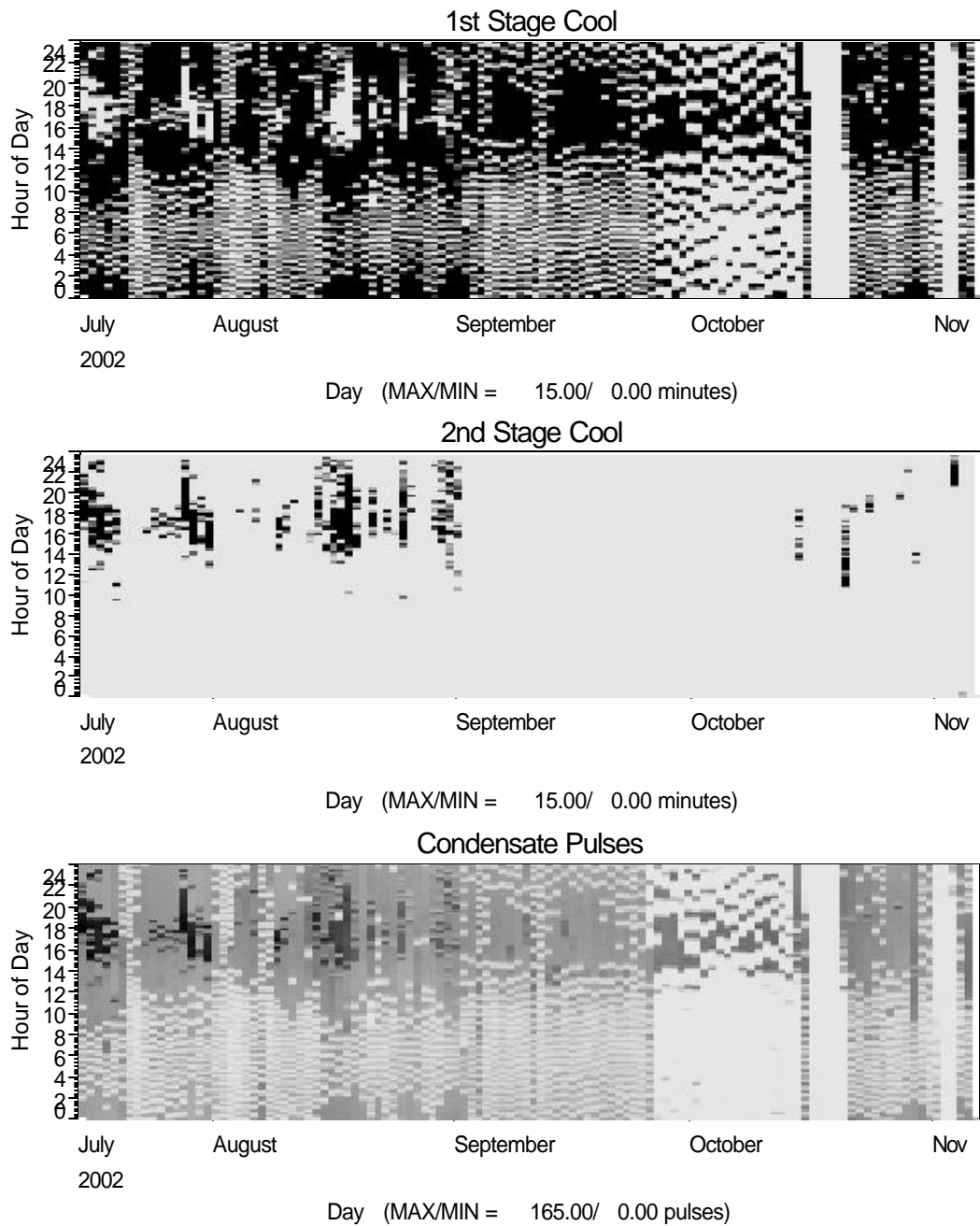


**Figure 13. Shade Plots of Cooling Operation and Condensate Removal for 2002 Season**

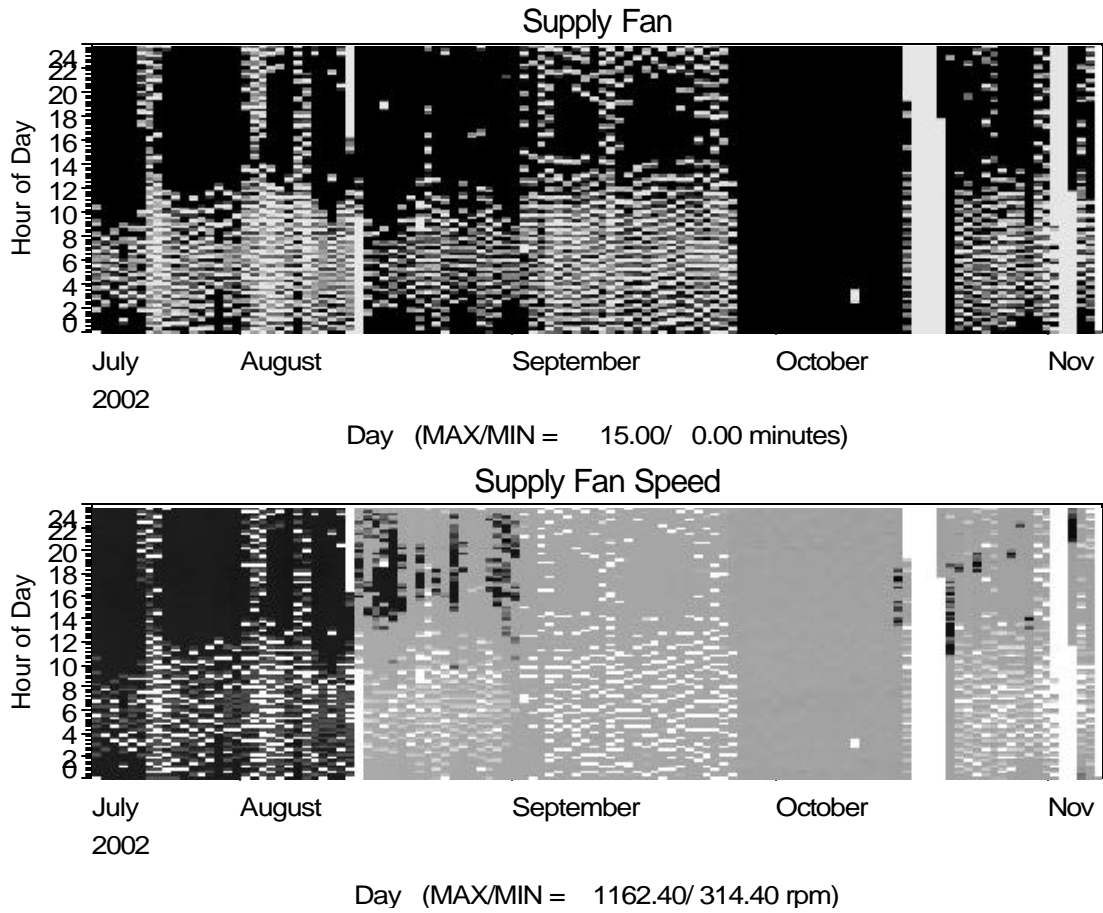


**Figure 14. Shade Plots of Supply Fan Operation for 2002 Season**



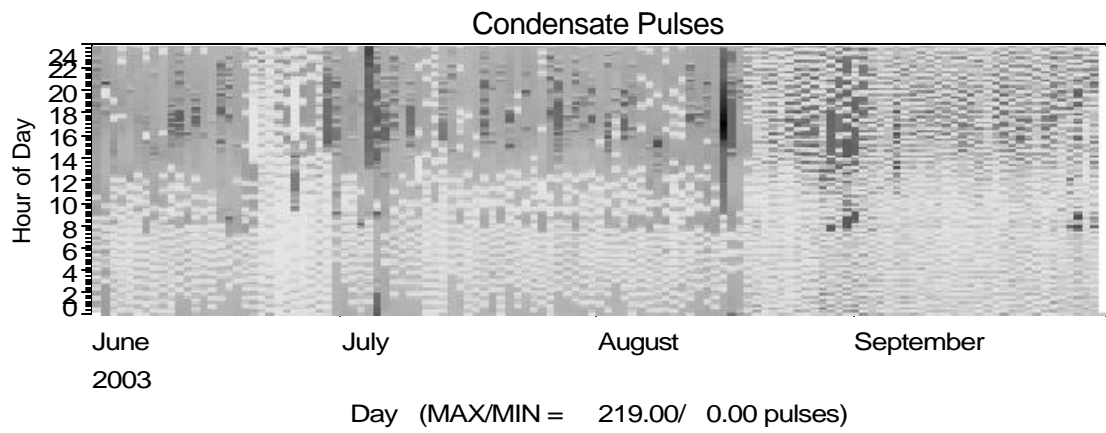
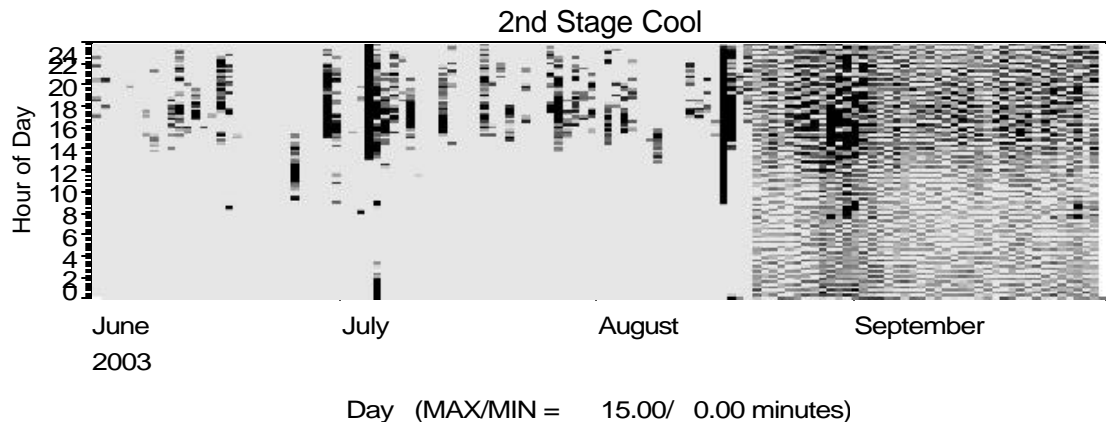
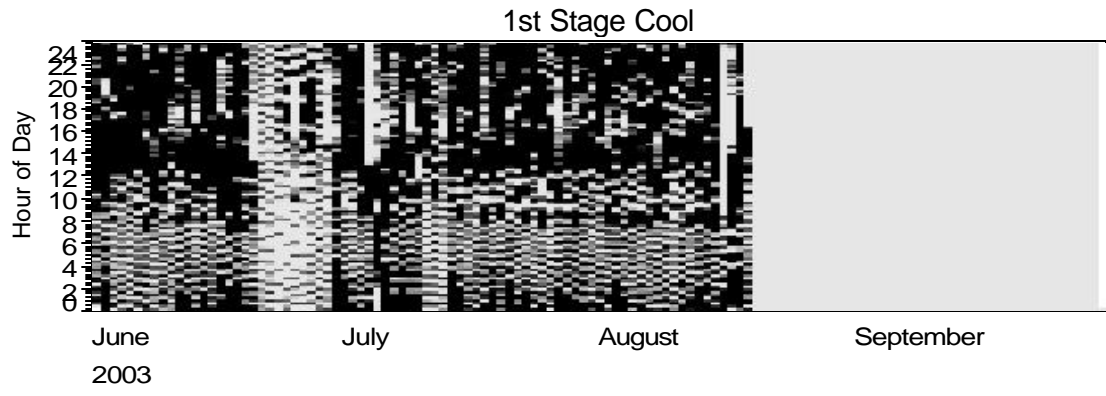


**Figure 15. Shade Plots of Cooling Operation and Condensate Removal for 2003 Season**

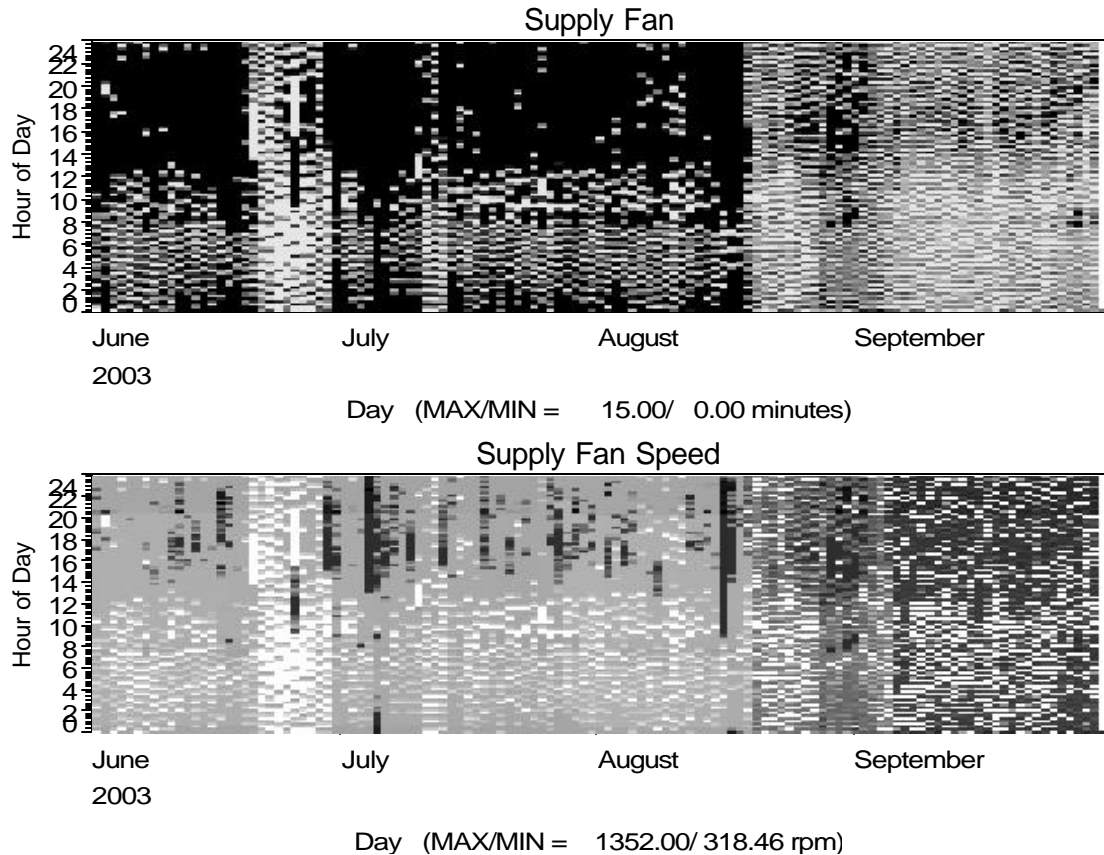


Figure 16. Shade Plots of Supply Fan Operation for 2003 Season

### Steady State Latent Capacity

Figure 17 compares the latent capacity calculated by two methods: 1) the condensate flow and 2) the psychrometric state-point/air flow calculations. Separate plots are shown for each cooling stage. The plots only include data from the hottest summer period (August 15 to September 26, 2002) when the cooling stage (either 1<sup>st</sup> or 2<sup>nd</sup>) had been running for 30 minutes prior to the interval to ensure steady state conditions. The latent capacity based on condensate removal is slightly lower than the psychrometric-based capacity for both the 1<sup>st</sup> and 2<sup>nd</sup> stage cooling.

Figure 18 shows the process line for cooling on the psychrometric chart. The smaller data points correspond to the data for each interval. The steady-state data were selected using the same criteria described above. The line and the larger three points correspond to the average of conditions 1) at the coil inlet, 2) at the coil outlet, but before the fan and 3) after the supply fan.

The average SHR for the coil – as indicated by the slope of the process line – is also shown on the plot. The sensible heat ratio is 0.80 for the 1<sup>st</sup> stage cooling and 0.77 for 2<sup>nd</sup> stage. The saturated suction temperature, which is also shown on plots, was 51°F for low stage and 50°F for 2<sup>nd</sup> stage. The coil or gross capacity is also shown on each plot along with power and EER.

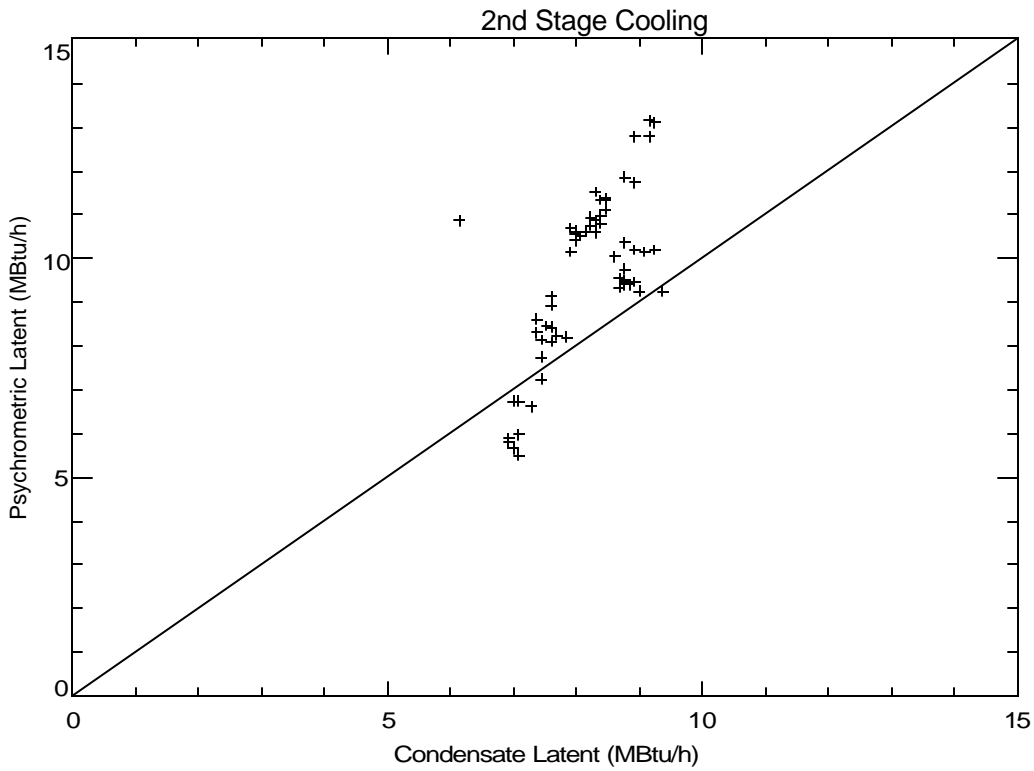
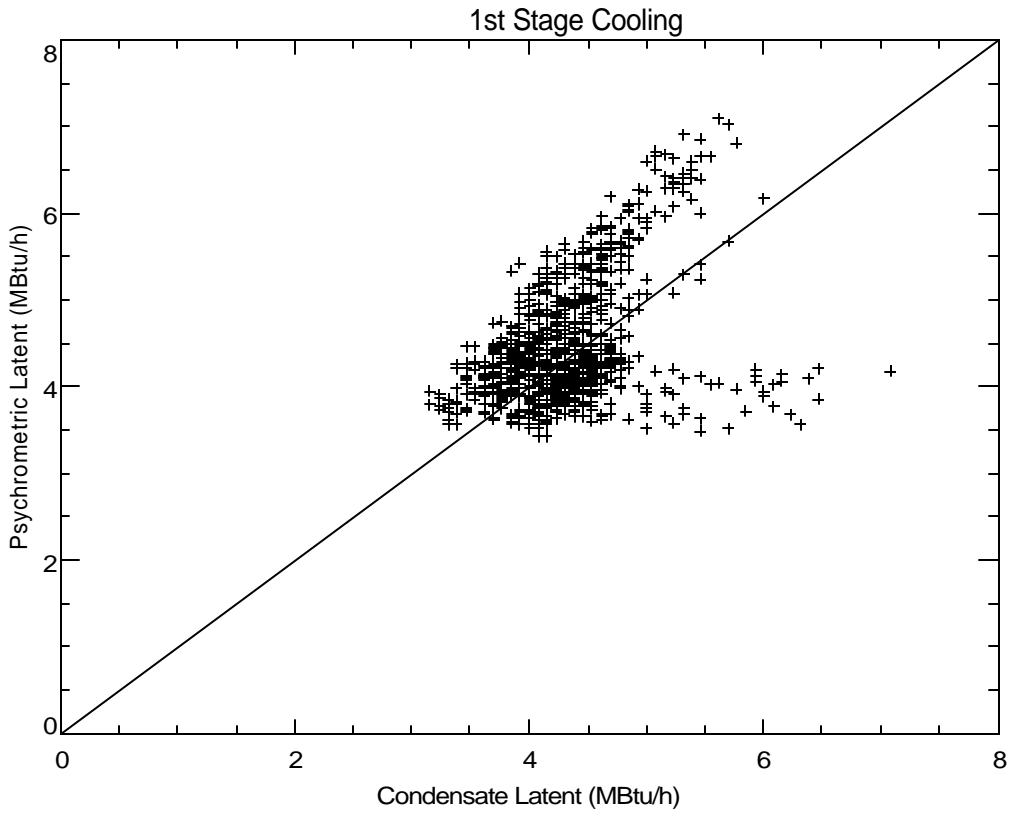
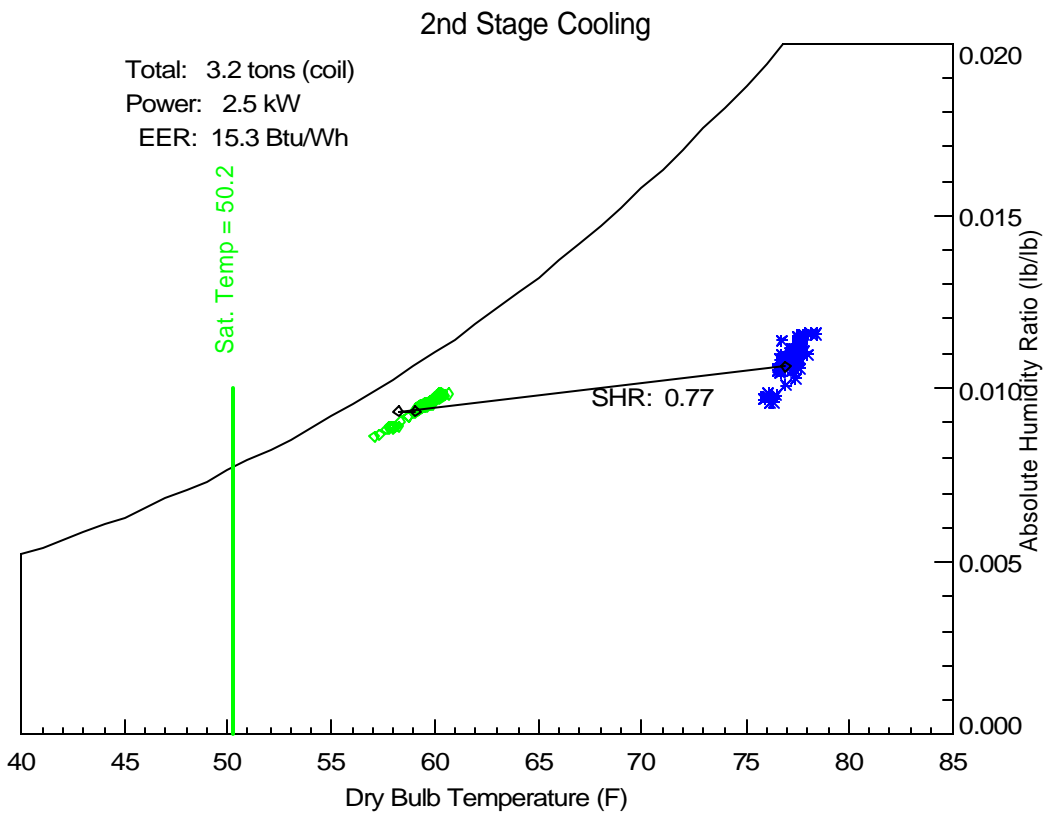
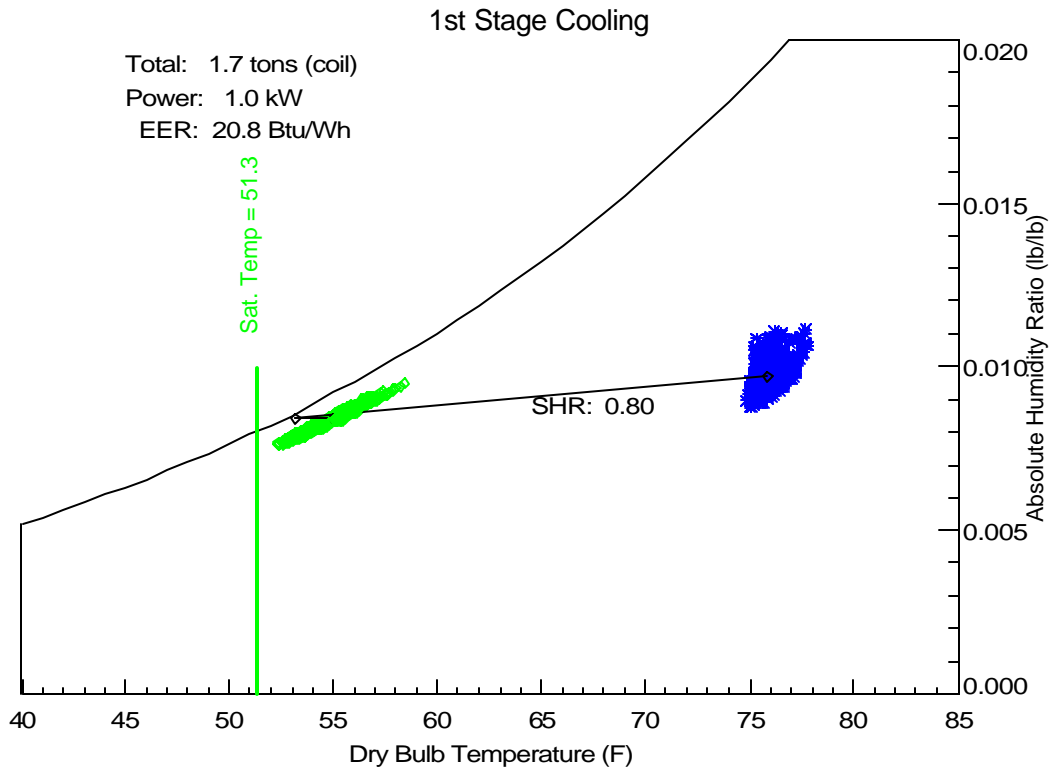


Figure 17. Comparing Condensate and Psychrometric-based Latent Capacity



**Figure 18. Cooling Process Lines for AC Coils at Steady State Conditions**

## Typical Operation in Various Control Modes

Figure 19 through Figure 25 show typical operating cycles for the different operational modes listed in Table 3.

**Control Wiring Problem.** In Figure 19, several operating cycles are shown for the system before the control wiring problem was corrected (July 9 to August 13, 2002). The system showed the stepped fan speed response expected for the enhanced mode, except the nominal fan speed was 1,100 rpm instead of 550 rpm. The fan delays are all typical of the enhanced mode (though the speeds are wrong).

**Enhanced Mode.** Figure 20 shows typical operating cycles for the system in the enhanced mode with the proper fan speed control. Figure 21 zooms in on the first cycle shown in Figure 20. The fan speed initially spends about 1 minute at 50% of the nominal fan speed (i.e., nominal is 550 rpm at 1<sup>st</sup> stage) then goes to 80% on nominal speed for 7.5 minutes. The number of condensate pulses per minute (FC) typically shows an increase when the fan speed reaches the nominal value. The coil return bend temperature (TEVP 1 & 2) and saturated suction temperature (TSAT) both show only a small change when the fan speed reaches the nominal value. When the 1<sup>st</sup> stage compressor cycles off, the fan remains at 550 rpm for 3 minutes before ramping off. This is in contrast to the shut down cycle shown in Figure 19, where the fan speed drops to 50% of full speed (or 550 rpm) during the last three minutes of operation. It is possible that this discrepancy was not intended by the system designers.

Figure 22 shows how the unit switches up to (and back from) 2<sup>nd</sup> stage. Both compressors are off for 1 minute before the 2<sup>nd</sup> stage compressor is enabled. During the 1-minute break, the fan ramps up (or down) to the required speed without any enhanced mode delays. The saturated suction of the coil is 2-3°F lower with the larger compressor operating.

**Regular Mode.** Figure 23 shows typical operating cycles for the system in the regular mode (AUTO fan). Figure 24 zooms in on the first cycle shown in Figure 23. In this case, the fan goes to full speed upon compressor startup without any delay. However, there is still an off-cycle delay of about 1 minute for fan shutdown at the end of the cycle.

**Constant Fan Mode.** Figure 25 shows typical operating cycles for the system with the fan operating continuously. In this mode, the coil starts off totally dry for most cycles, so the time delay between compressor startup and the first condensate pulse is related to the amount of moisture held on the coil surfaces. Similarly, the buildup of moisture on the coil fins is indicated by the change in pressure drop across the coil over each on cycle. These concepts are discussed further in the following section. The 10-15 rpm speed change shown in Figure 25 is due the self-compensating control features built into the ECM motor controller.

**Single-Stage Operation.** As mentioned Table 3 above, the unit controls were changed in 2003 to operate the unit as a single-stage system (by jumpering Y to Ylow at the air handler terminal block). This mode was conceived to test the enhanced features for a constant speed unit. Figure 26 shows single-stage operation with the enhanced fan mode. Figure 27 show single-stage operation with regular fan control.

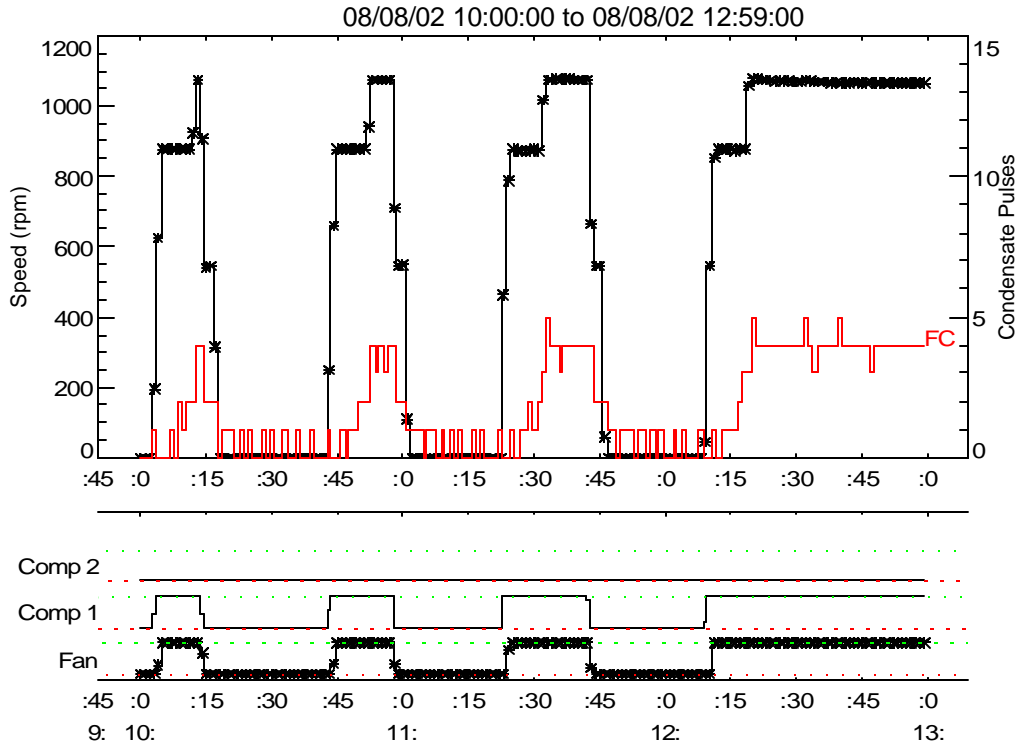


Figure 19. Initial Control Wiring Problem: Typical Operating Cycles on August 8

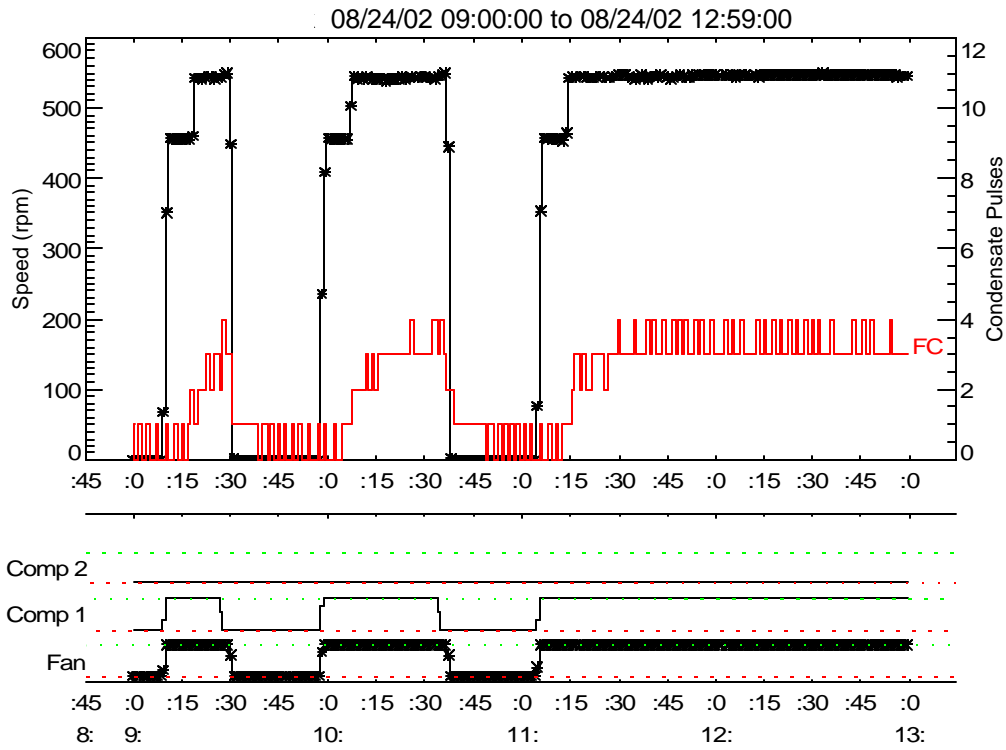


Figure 20. Enhanced Mode: Typical Operating Cycles on August 24

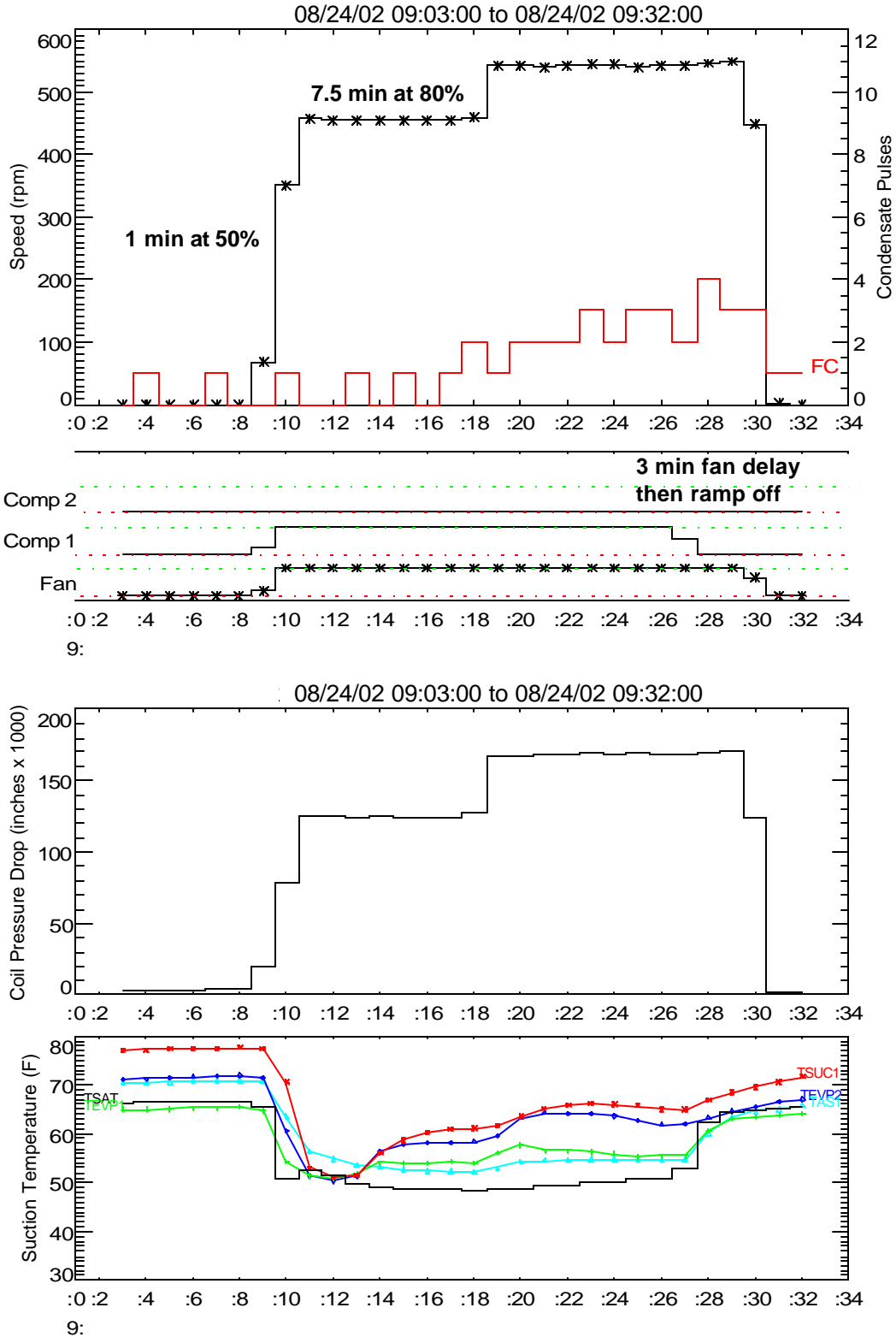


Figure 21. Enhanced Mode: Details of a 1<sup>st</sup> Stage Cycle on August 24

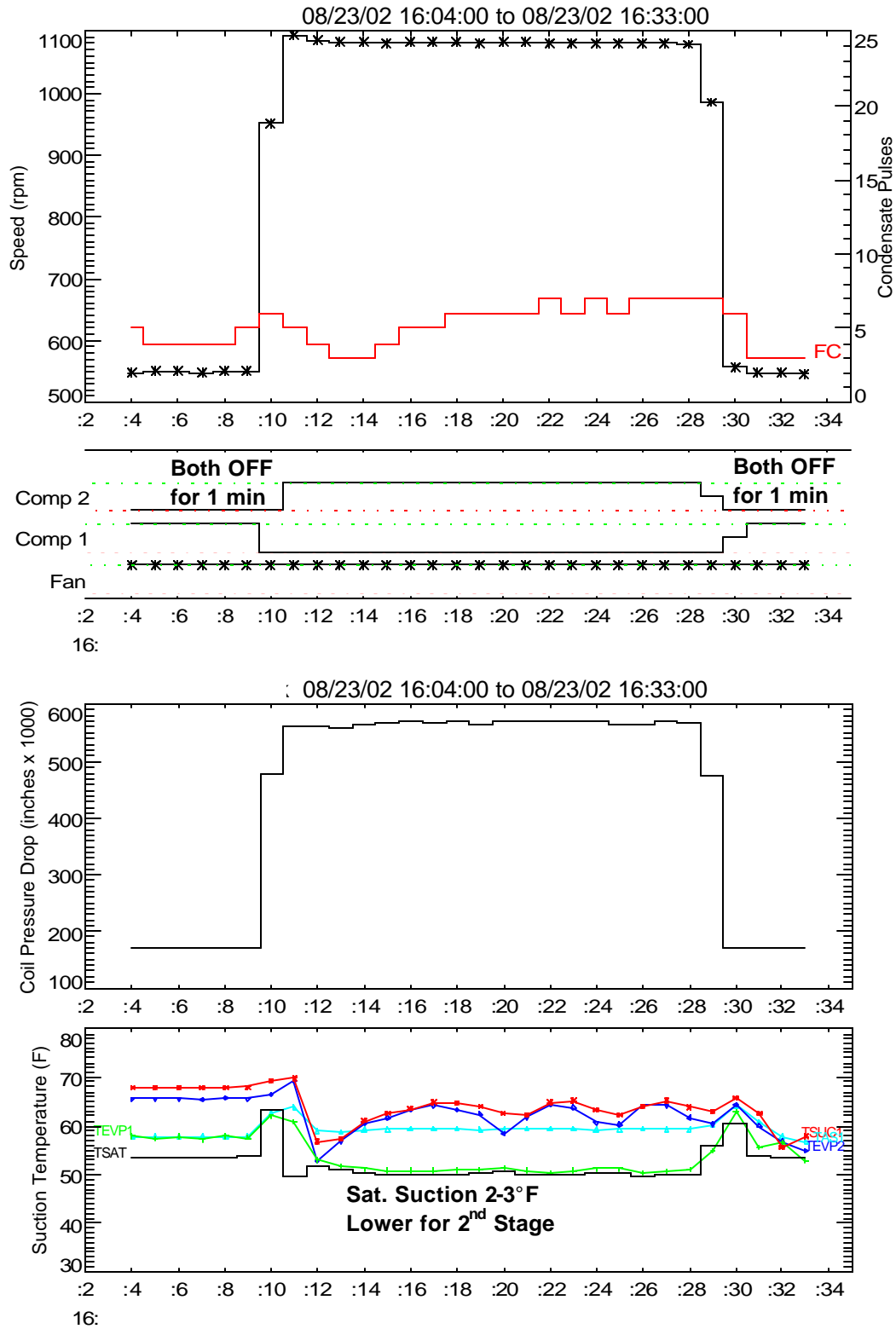


Figure 22. Enhanced Mode: Details of a 2<sup>nd</sup> Stage Cycle on August 23



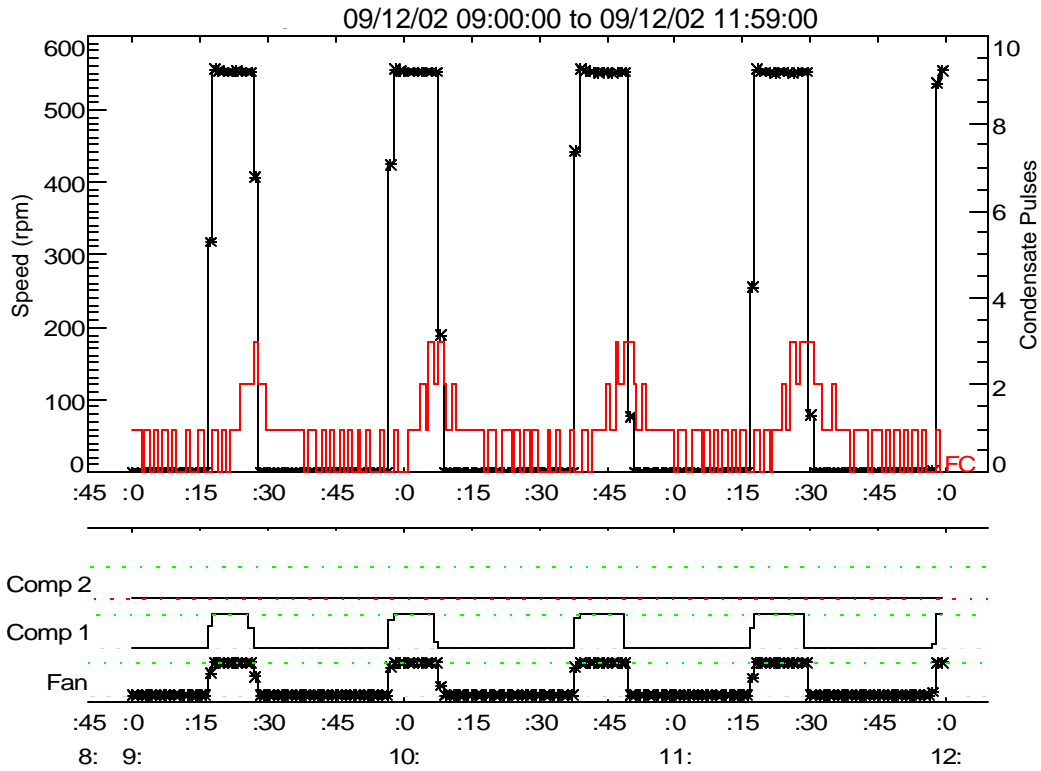


Figure 23. Regular Mode: Typical Operating Cycles on September 12

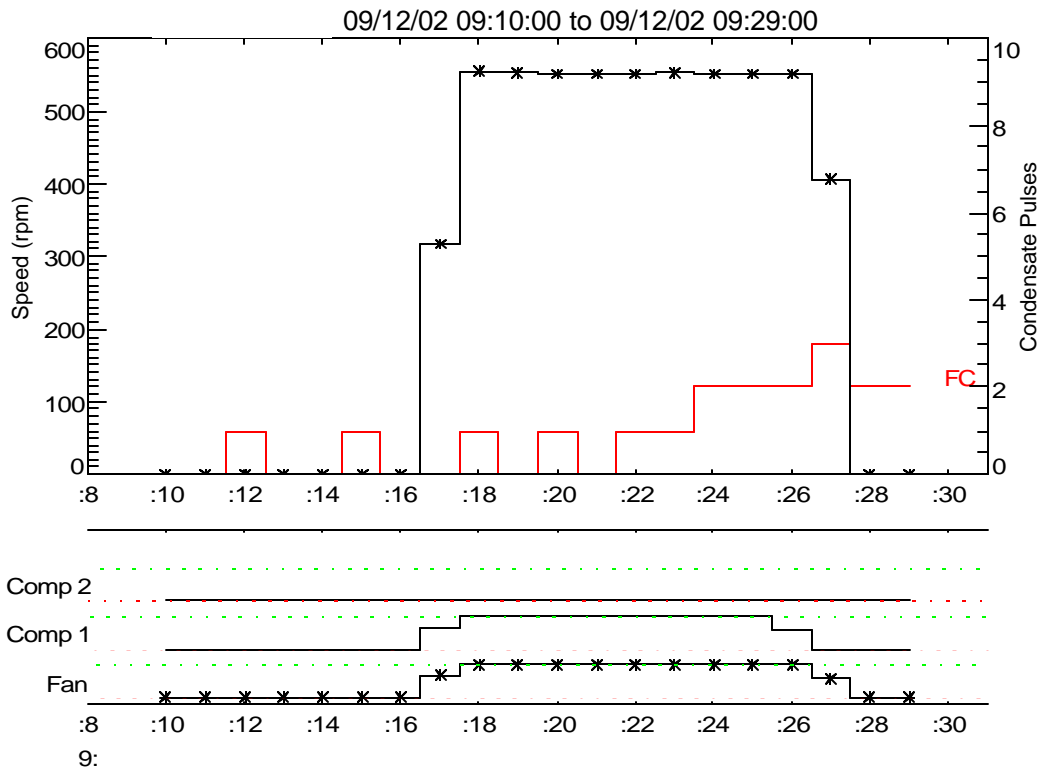


Figure 24. Regular Mode: Details of a 1<sup>st</sup> Stage Cycle on September 12

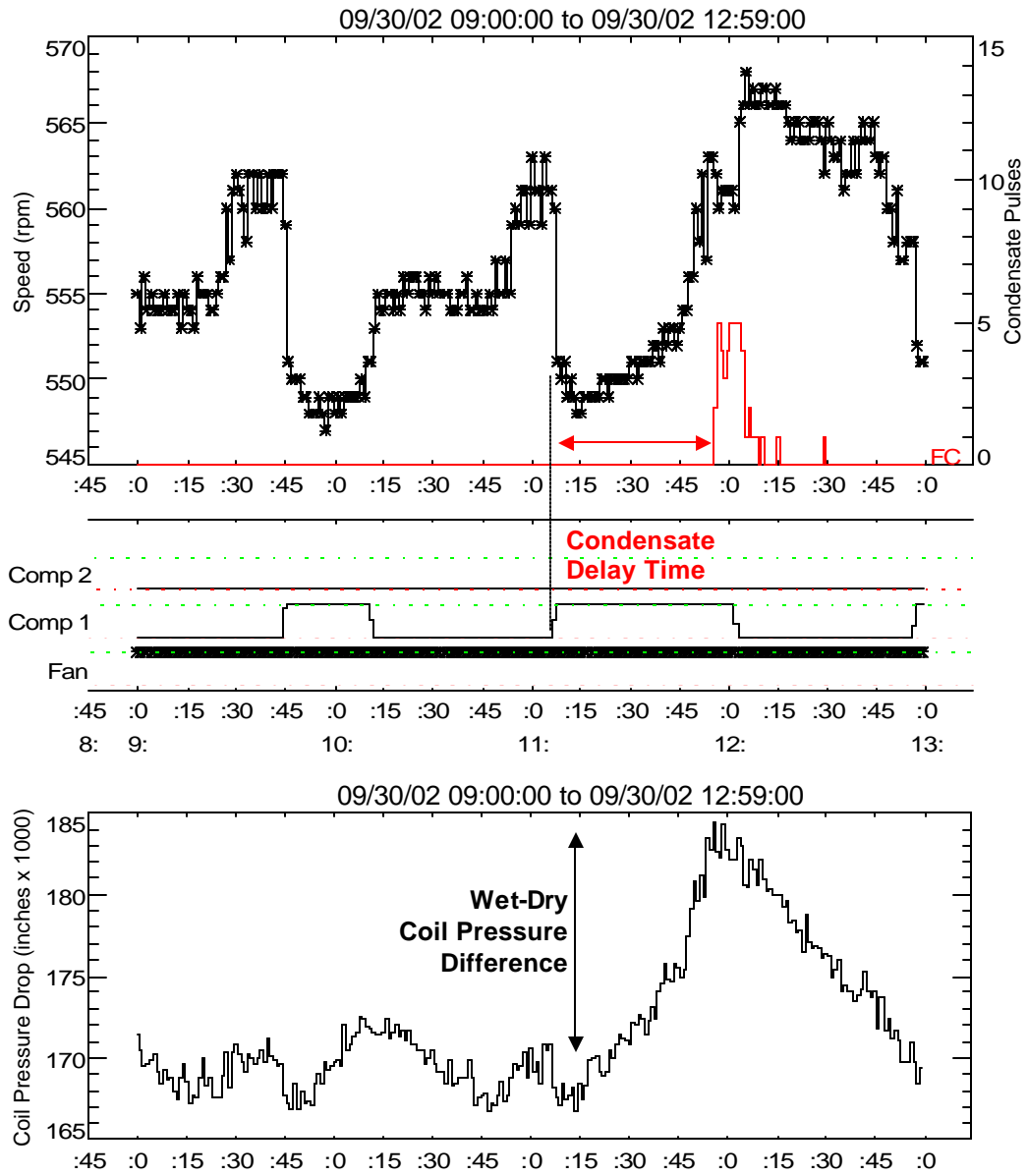


Figure 25. Constant Fan Mode: Typical Operating Cycles on September 30

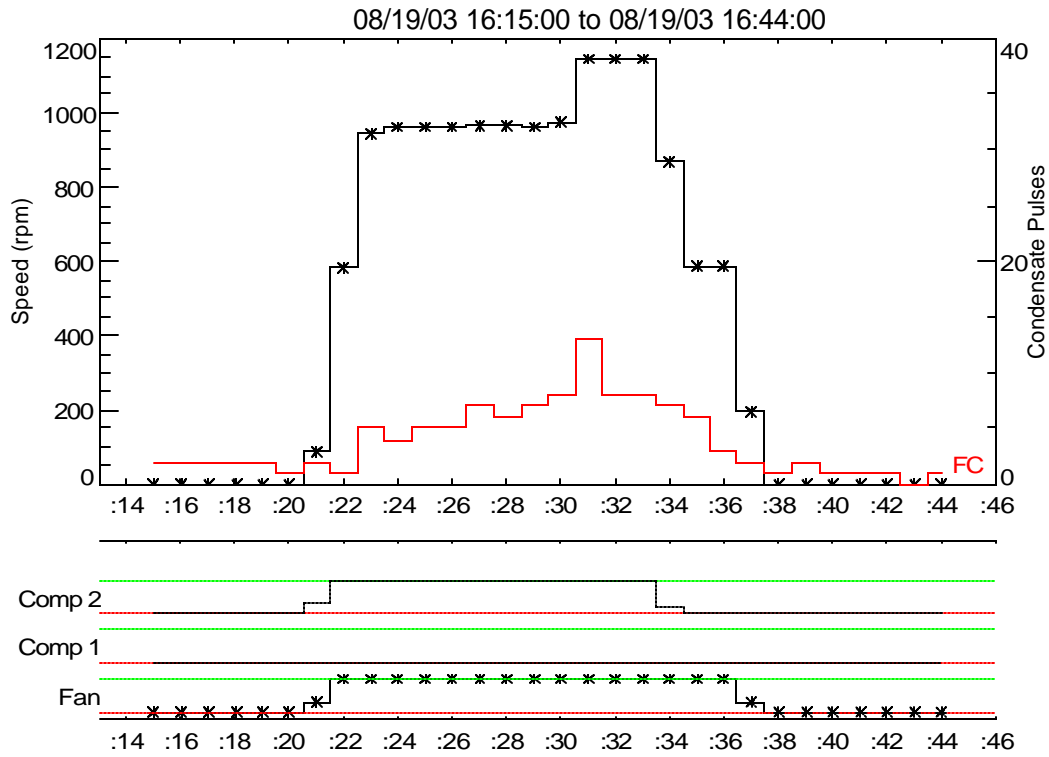


Figure 26. Single Stage Enhanced: Typical Operating Cycles on August 19

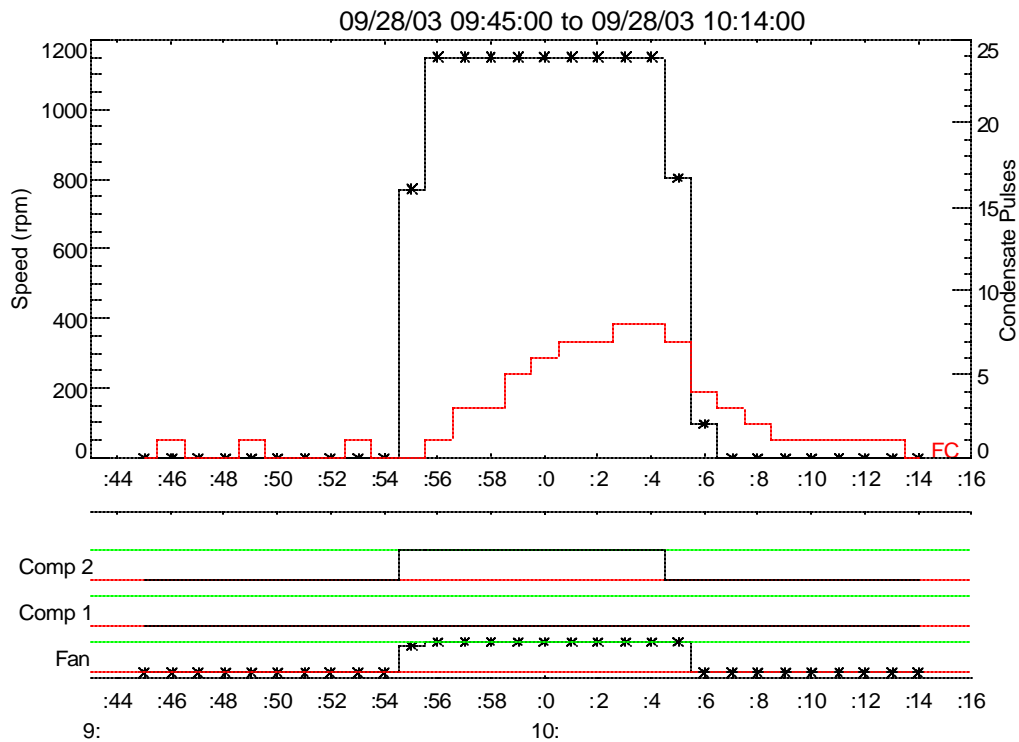


Figure 27. Single Stage Regular: Typical Operating Cycles on September 28

## Condensate Delay Time

One key indication of the coil's moisture-holding capacity is the time it takes for condensate to first fall from the coil. This time delay is similar to the parameter  $t_{\text{wet}}$  from the LHR Degradation Model developed by Henderson and Rengarajan (1996). Figure 25 shows operating cycles for the AC unit from September 30<sup>th</sup>, a day when both stages had been off prior to starting up and under fairly humid conditions in the morning.

Figure 28 shows the condensate delay times for several compressor startup cycles for 1<sup>st</sup> stage cooling. The criteria for including cycles on the plots were:

- There were no condensate pulses in the previous 2 hours before compressor startup,
- The 1<sup>st</sup> stage cooling was continuously on at least until the first condensate pulse occurred,
- The condensate event was followed by at least one other condensate pulse.

Several cycles met the criteria for the AC unit, though none of these had 2<sup>nd</sup> stage cooling active before the first condensate pulse fell. Data from the lab testing and other field test sites typically showed a decreasing condensate delay time with increasing dew point temperature.

The plot on the bottom of Figure 28 shows wet-dry pressure drop as function of dew point. Very little variation with dew point is apparent, which implies the amount of moisture on the coil is not changing significantly with entering dew point conditions.

Table 4 summarizes the nominal condensate delay time and the increased pressure drop due to the wet coil. The entering dew point of 61°F approximately corresponds to nominal entering conditions of 80°F DB / 67°F WB.

**Table 4. Summary of Nominal Condensate Delay and Wet-Dry Pressure Drop Calculations**

	<b>Unit</b>
Entering Dew Point (F) (avg conditions before first pulse)	61
Time Delay for First Condensate Pulse (minutes)	40-50
Wet-Dry Coil Pressure Drop (in H <sub>2</sub> O x 1000)	15-19

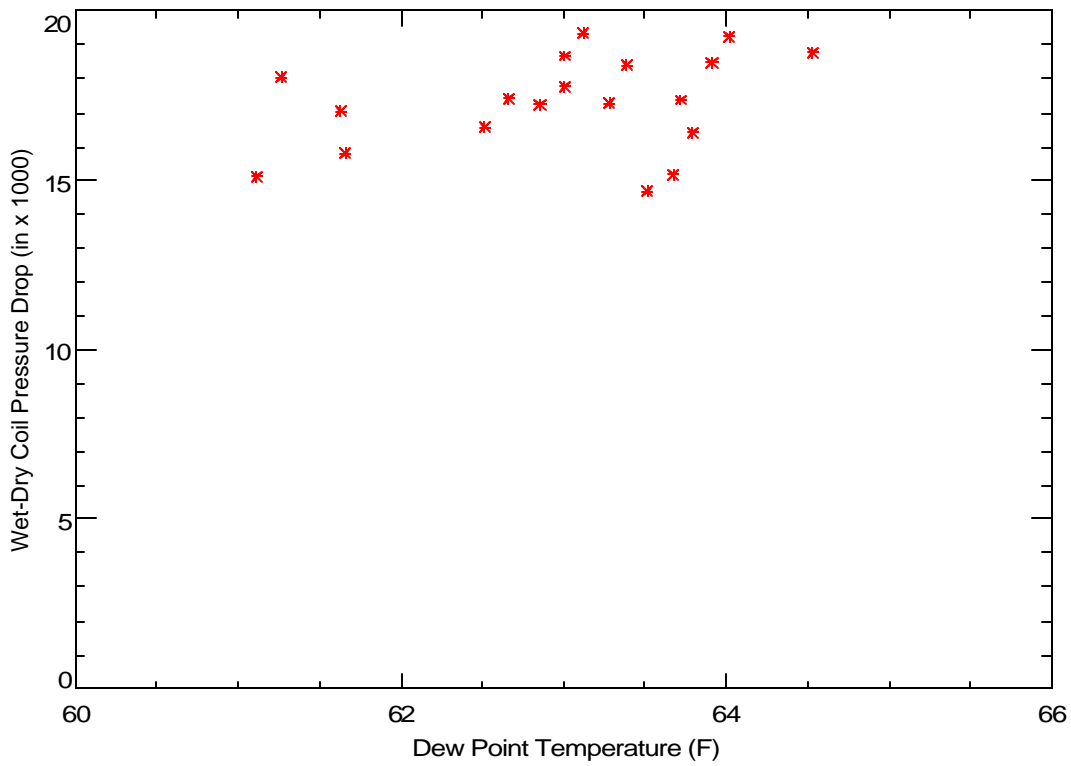
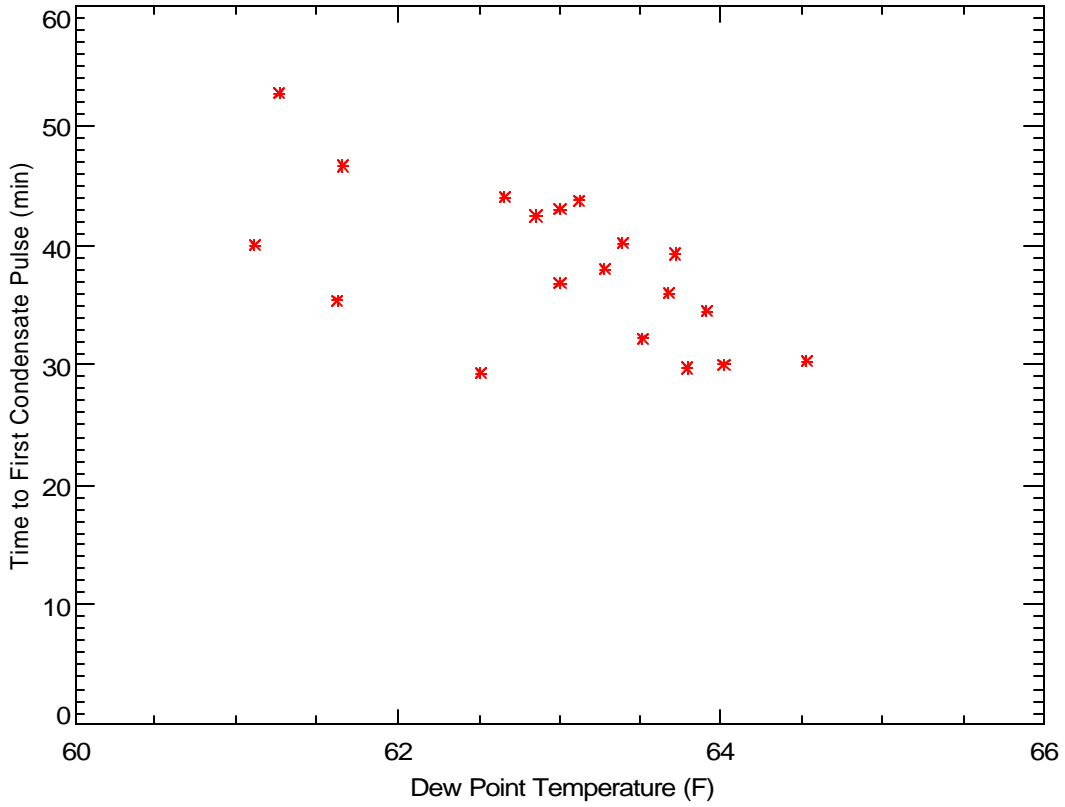


Figure 28. Condensate Delay Time and Wet Coil Pressure Drop vs. Entering Dew Point for 1<sup>st</sup> Stage Cooling

## Cooling Energy Trends

Total cooling energy use for the AC unit is approximately linear with the daily average ambient temperature above 68°F, as shown in Figure 29. The energy use is constant for temperatures between 58°F and 68°F since the unit was in the constant fan mode for these days. Energy use in the heating mode was also linear with ambient temperature below 58°F.

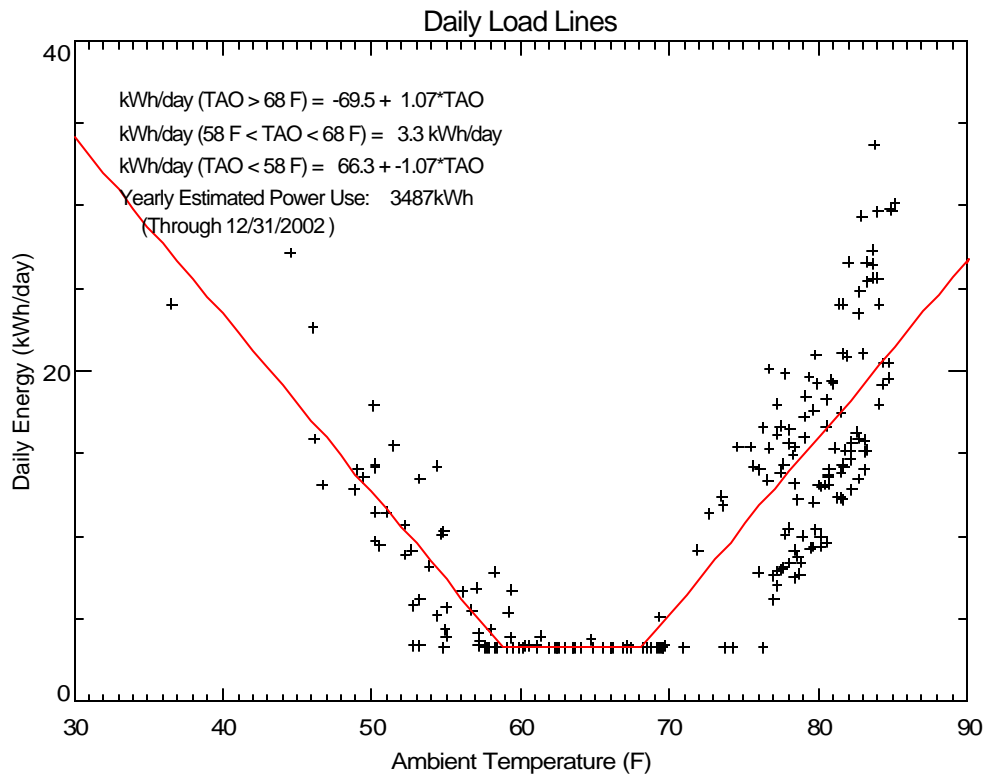
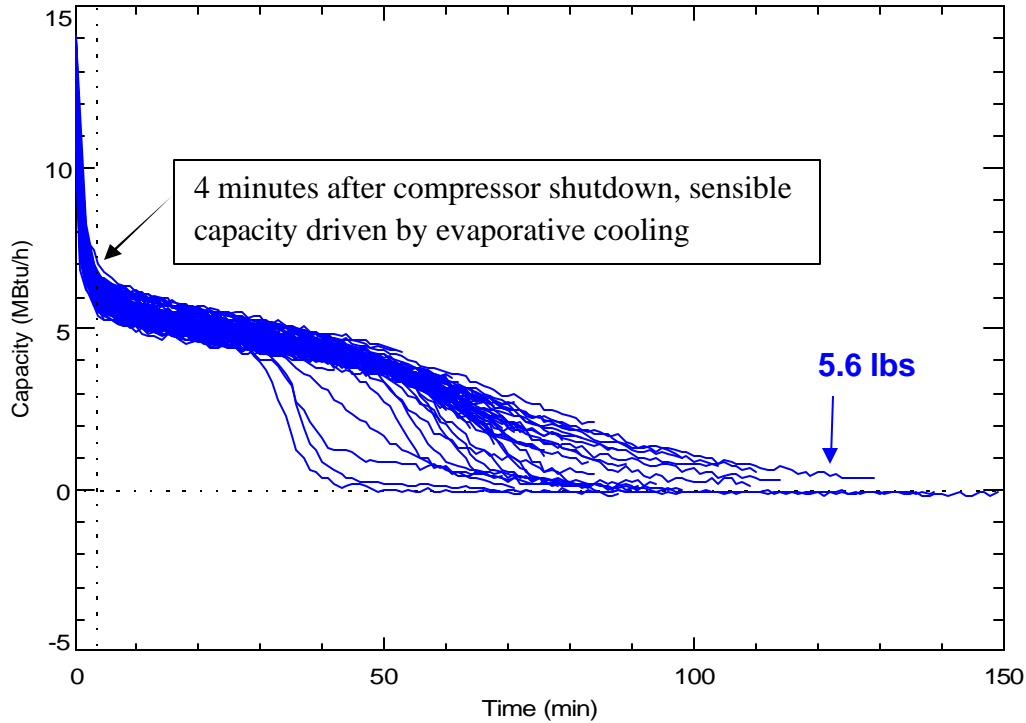


Figure 29. Daily Energy Trends for Heating and Cooling

## Off-Cycle Evaporation Rates

The unit operated for an extended period in the constant fan mode, which allowed the off-cycle cooling performance of the coil to be evaluated (some of these off cycles are shown in Figure 25). Figure 30 shows the off-cycle sensible capacity for several cycles when the compressor had just shut off but the fan continued to run (at 550 rpm). The plot only includes off cycles where one or more condensate pulses had occurred during the last 10 minutes of compressor operation. The plot has vertical line at the 4<sup>th</sup> minute, which was about the time when refrigerant dynamics have died down and sensible capacity is driven by the evaporation process. We make the assumption – based on laboratory measurements of other coils – that the coil operates as an evaporative cooler starting in the 4<sup>th</sup> minute with latent and sensible capacity summing to zero.



**Figure 30. The Trend of Sensible Capacity for Several “Wetted” Off-Cycles**

Integrating the longest off cycle sensible capacity trend in Figure 30 above indicates that this coil holds about 5.6 lbs of moisture. Based on the total fin area of 446.3 ft<sup>2</sup>, the coil holds about 12.5 lb per 1000 ft<sup>2</sup>. This is towards the high end of the range for the coils tested in the laboratory. The higher moisture mass is probably due to the lower airflow across the coil (the face velocity is 126 fpm). The lab tested coils typically demonstrated a 30-50% higher moisture mass as the air flow dropped from 400 to 200 cfm per ton.

Figure 31 and Figure 32 compare the initial evaporation rate (i.e., the vertical line noted on Figure 30 above) for each off-cycle meeting the criteria for being fully wetted. The initial evaporation rate is about 7 MBtu/h. Figure 31 shows that the evaporation rate is clearly a function of the wet bulb depression (i.e., the DB minus the WB), as would be expected. The line on the plot shows the theoretical trend projected to zero evaporation at no wet bulb depression. The saturation effectiveness, which is defined below, is shown on Figure 32.

$$\eta_{\text{sat}} = Q_{\text{evp}} / (1.08 \times \text{cfm} \times (\text{DB} - \text{WB}))$$

The average effectiveness is 0.852, which corresponds to an NTU of 1.91. Based on the total coil area of 446.3 ft<sup>2</sup> and an airflow of 671 cfm, the estimated value of k for this coil is 0.016, which is on the low end of values determined in the lab tests.

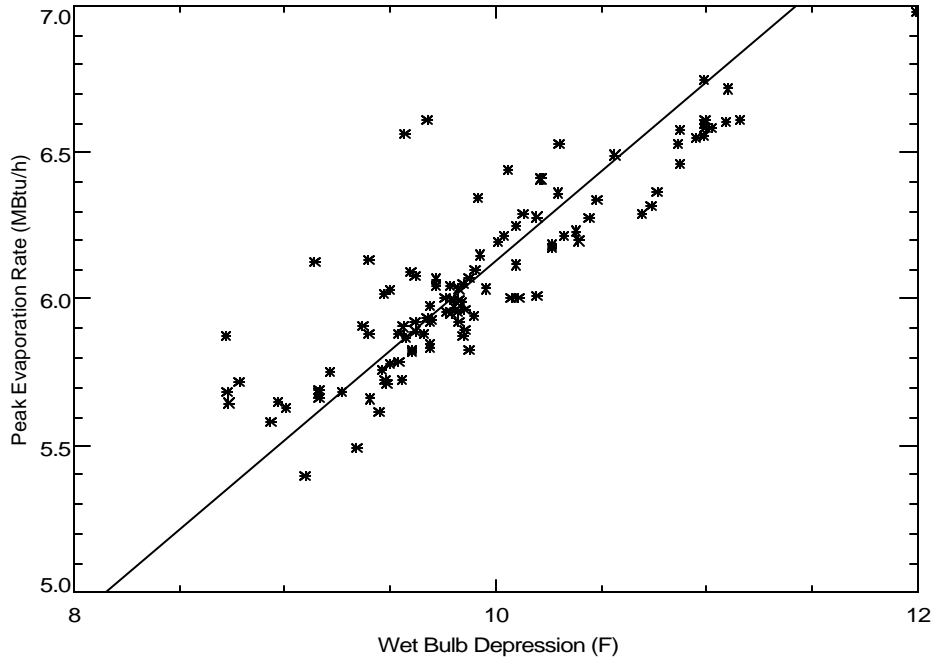


**Figure 31. The Trend of Peak Off-Cycle Evaporation Rate With Wet Bulb Depression**

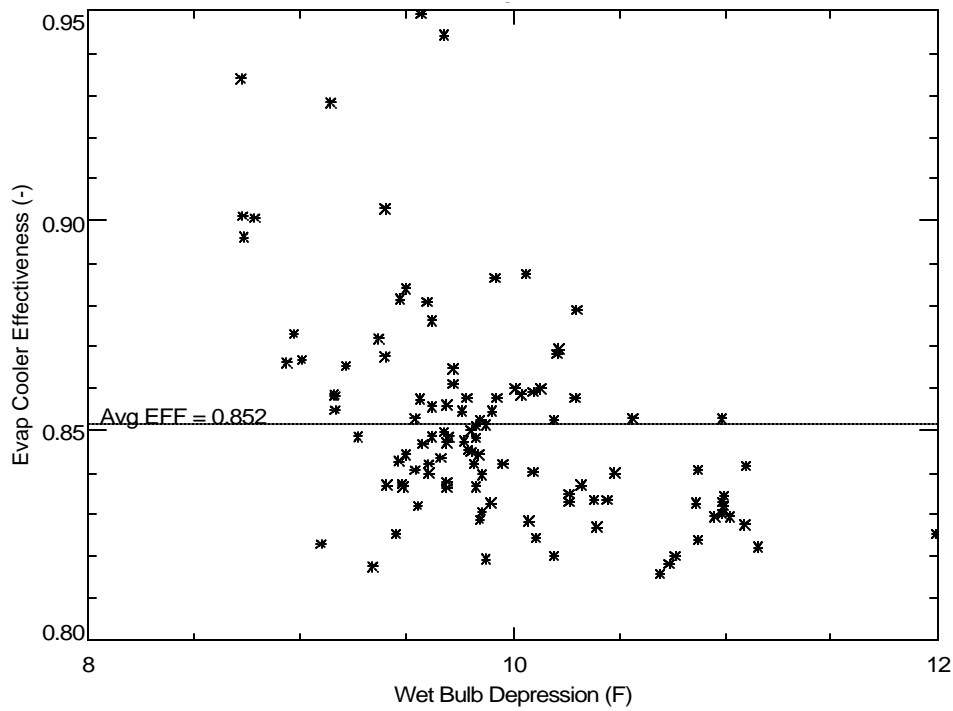


**Figure 32. Evaporative Cooler Saturation Effectiveness Calculated for the Cooling Coil**



## Part Load SHR

The moisture removal capacity of a cooling coil is reduced at part load conditions. This part load degradation is especially prevalent when the fan operates continuously. The SHR is calculated using the coil temperature difference, air flow, and condensate readings aggregated into 2-hour averages. Data are only included on the plot when the average entering conditions are between 75-80 °F and 50-65% RH for the interval.

Figure 33 shows the SHR trend with Runtime fraction (RTF). In this case, times when the 2<sup>nd</sup> stage ran for the entire interval correspond to RTF = 1. Times when the 1<sup>st</sup> stage ran for the entire interval correspond to RTF = 0.5. The steady state SHR with the 2<sup>nd</sup> stage fully on is shown on the plot with a horizontal line. The value of 0.78 based on condensate, approximately corresponds to the SHR of 0.77 from the process line for 2<sup>nd</sup> stage shown in Figure 18. Most of the degradation for this system happened with the 1<sup>st</sup> stage compressor cycling on and off (i.e., RTF between 0 and 0.5). The data from the constant fan mode was from a slightly cooler period, so no 2<sup>nd</sup> stage operation occurred (i.e., the RTF was never over 0.5). The data for the constant fan mode (“\*”)s showed slightly more SHR degradation at low RTFs than the auto fan operating modes. However, from the laboratory testing of coils, we know that the amount of degradation would have been even greater – i.e., the “\*”s would shift to the right on the plot – had the humidity been the same as for the other operating modes (Figure 38 in the next section shows that the space humidity was much higher in the constant fan mode).

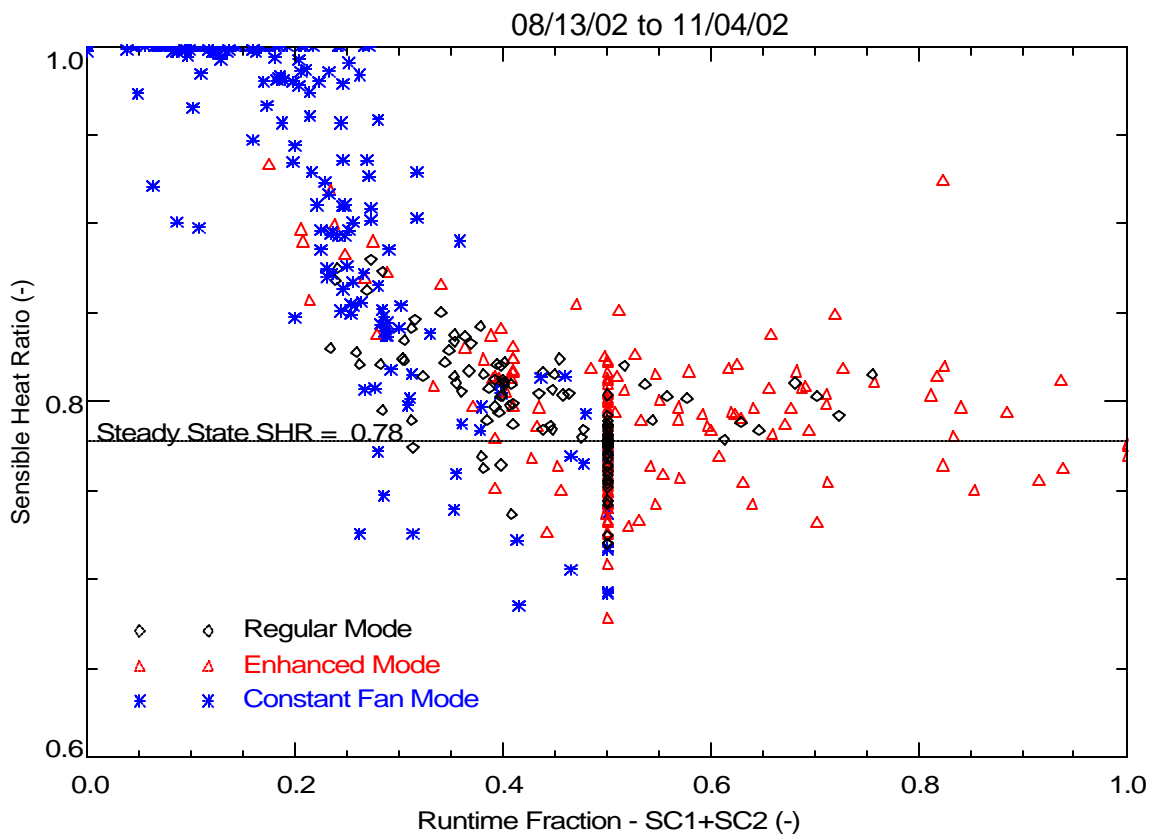


Figure 33. Part-Load Sensible Heat Ratio vs. Runtime Fraction

The data in Figure 33 show about the same amount of SHR degradation for the enhanced and regular modes (triangles and diamonds, respectively). Figure 34 shows the SHR trend when the return humidity is limited to between 50 to 55% RH (this range eliminates most of the constant fan data). This plot also confirms that the degradation trends for the enhanced and regular modes are very similar.

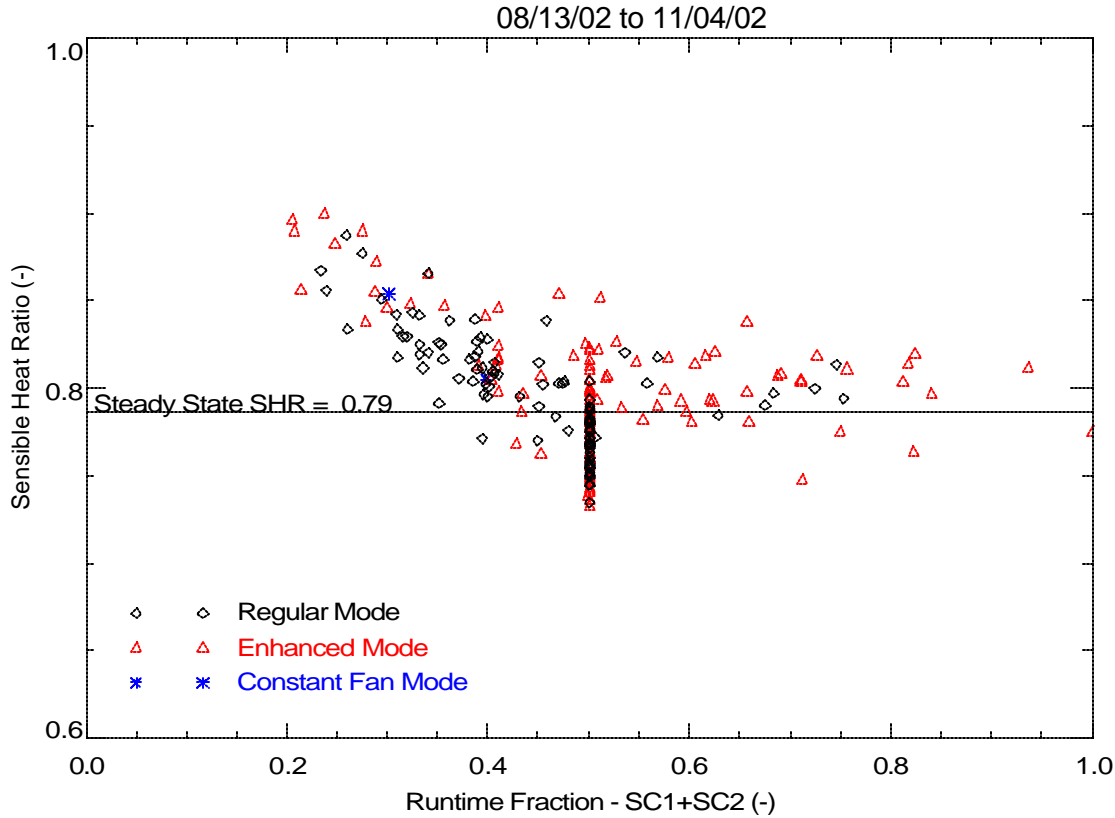
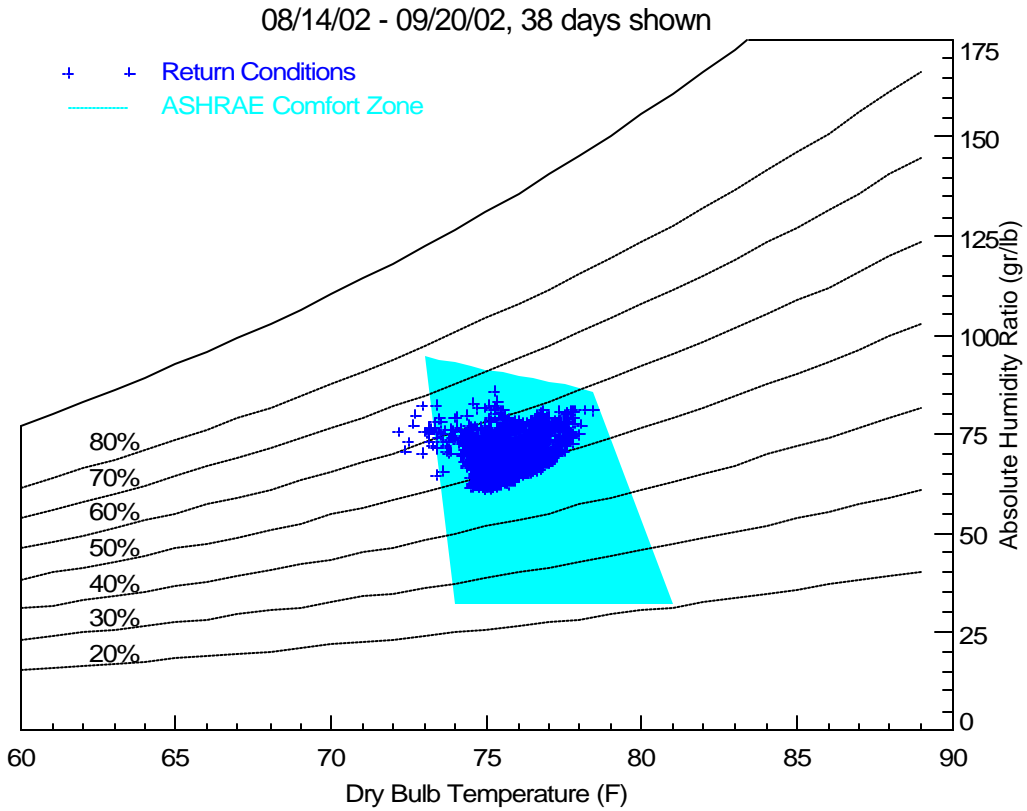


Figure 34. Part-Load Sensible Heat Ratio vs. Runtime Fraction: humidity between 50-55% RH

## Space Conditions

Figure 35 shows the return conditions for the unit in cooling during the hottest period of the summer when the unit operated in the auto fan mode. The return conditions are expected to be very close to the space conditions in this house since the air handler is located in the conditioned space. The conditions indicate the unit maintains the space within the ASHRAE comfort zone for most of the time.



**Figure 35. Return/Space Conditions Compared to the ASHRAE Comfort Region (all AUTO Fan Data)**

Figure 36 shows a daily profile of space conditions with compressor power for a warm summer day when the unit was in the Enhanced Mode. The humidity and temperature show some modest variation with compressor operation, as would be expected. The space is held at 50% RH.

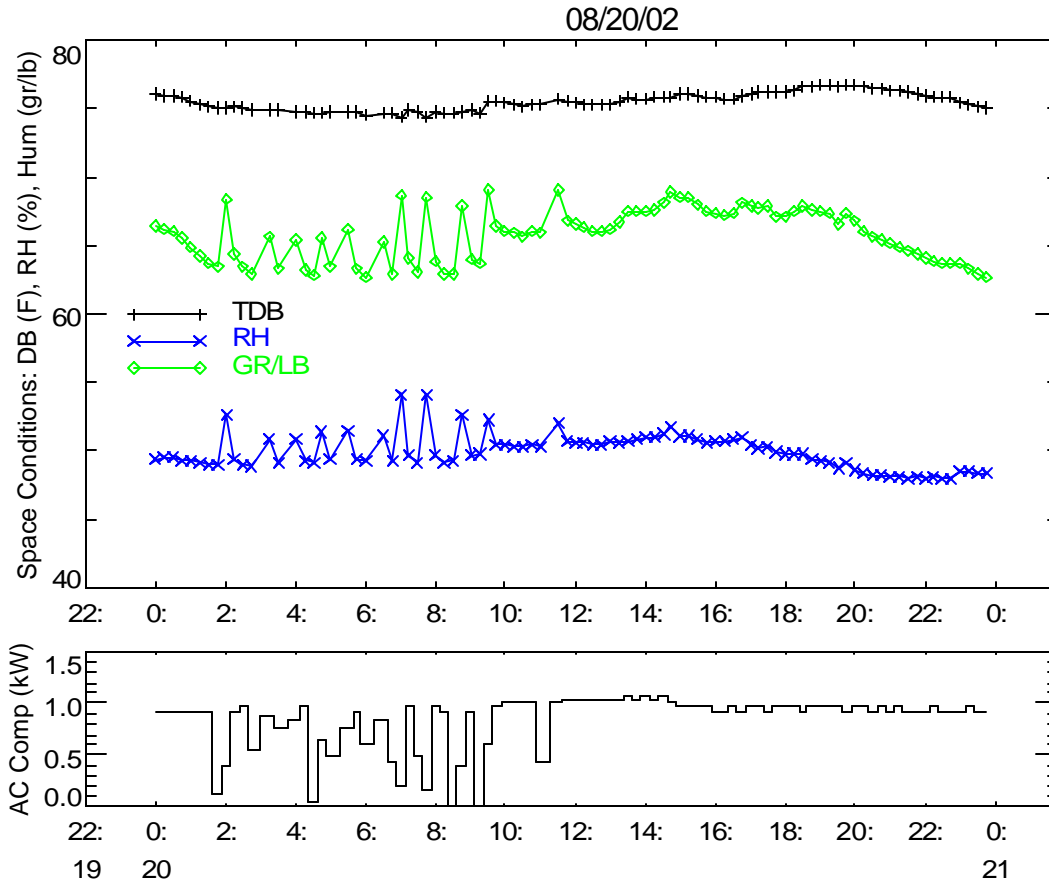


Figure 36. Profile of Space/Return Air Conditions for a Hot Day (August 20, 2002)

### The Impact of Different Control Modes on Indoor Humidity

The characteristic trend of indoor and outdoor humidity generally follow a repeatable pattern for most building/HVAC combinations. We compared this characteristic trend under the various control modes to discern any impact on space humidity levels. The indoor and outdoor humidity were averaged over each day for periods when the supply fan ran. The plots only include days with at least 5 hours of cooling activity. The data point corresponding to October 21 is noted on each plot because this was the first day of operation after the AC was shut down for 4 days.

Figure 37 compares the humidity levels before and after the fan control wiring problem was fixed. Operating the fan at 1100 rpm with 1<sup>st</sup> stage compressor clearly affected indoor humidity levels. Lowering the nominal fan speed lowered the space humidity levels by 10-15 gr/lb.

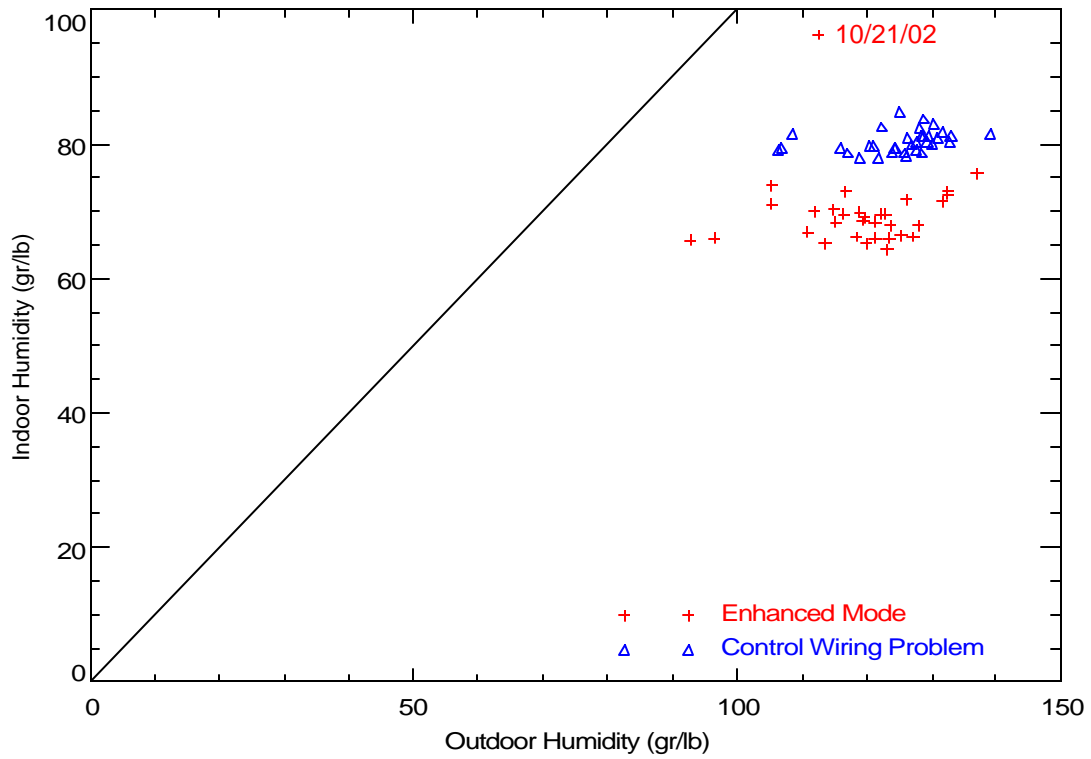
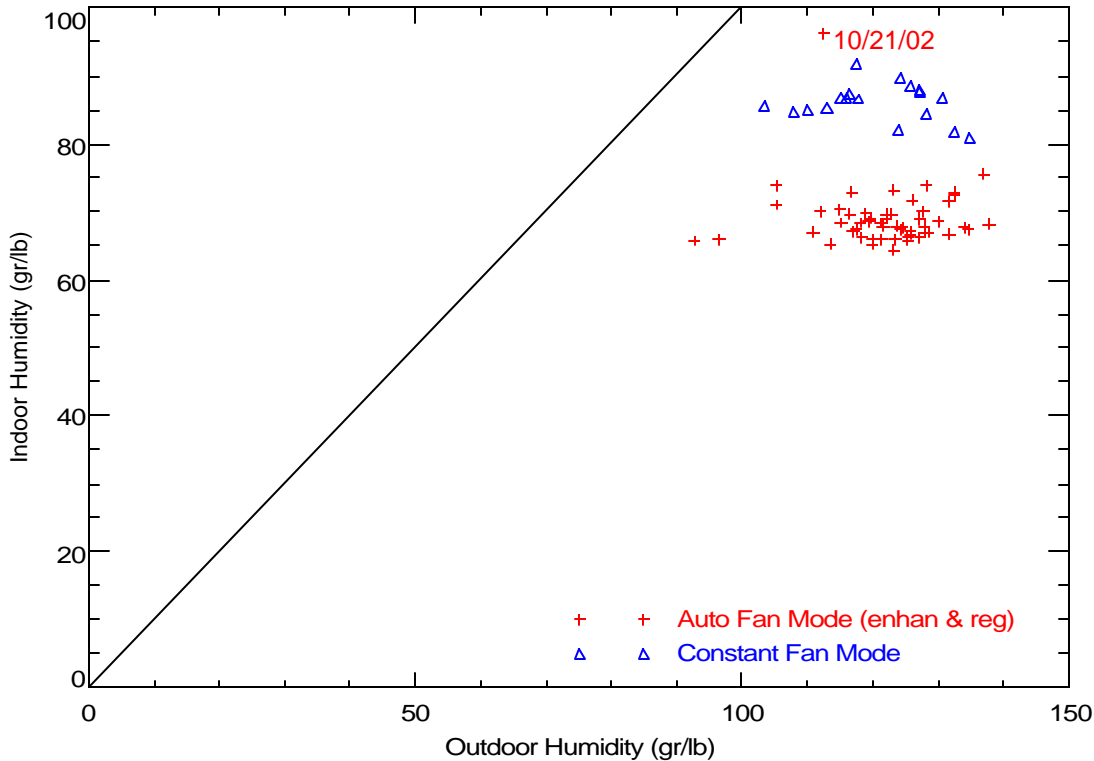


Figure 37. Impact of Control Modes on Indoor Humidity: Control Wiring Problem vs. Enhanced

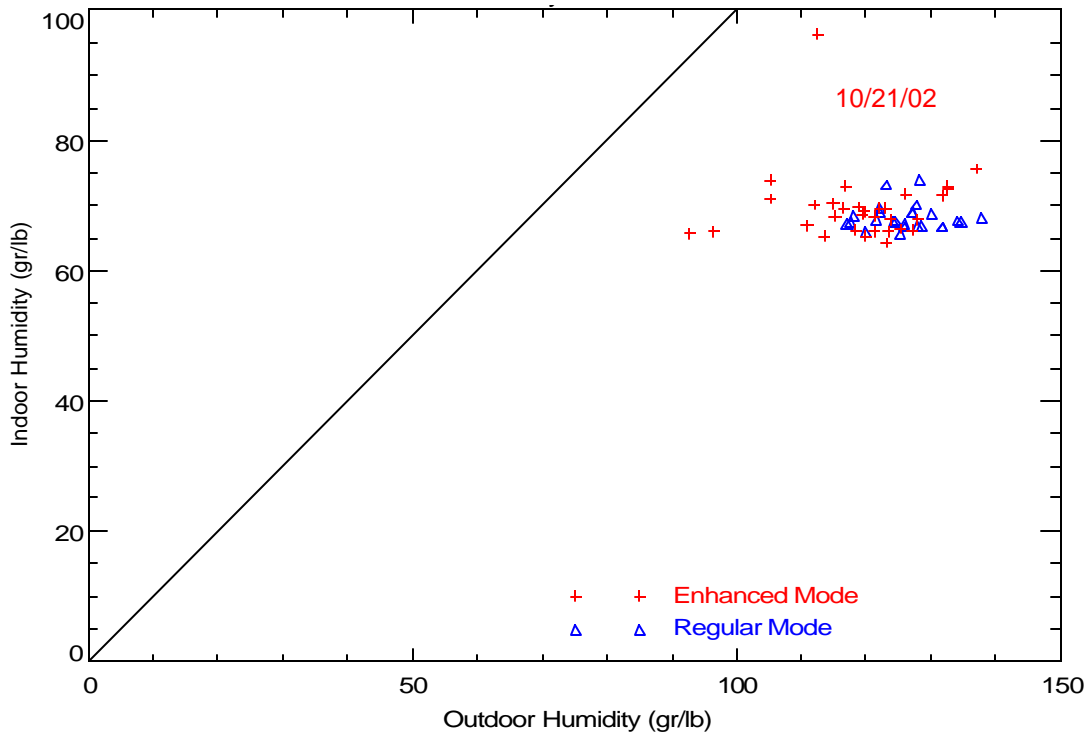
Figure 38 compares indoor humidity levels for the constant and auto fan modes (the auto fan mode includes both regular and enhanced mode operation). Constant fan operation clearly shows a detrimental impact on indoor humidity, in spite of the fact that this is a two-stage unit operating with low speed fan during the off cycle.



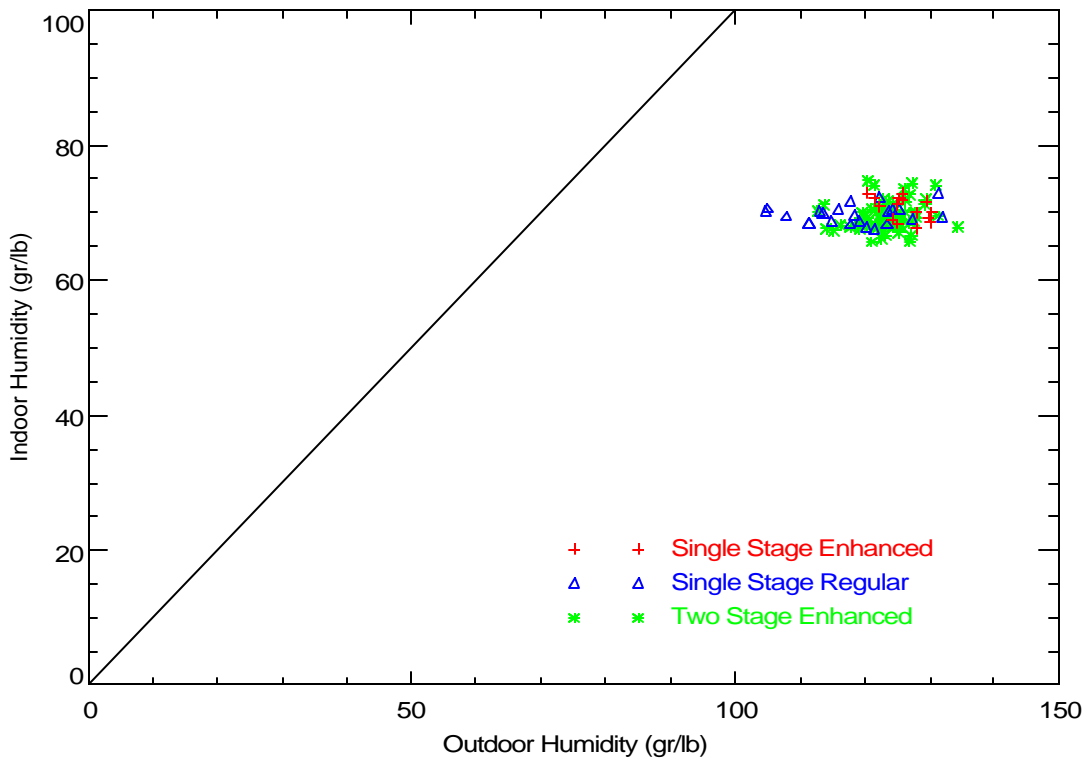
**Figure 38. Impact of Control Modes on Indoor Humidity: Auto Fan vs. Constant Fan**

Figure 39 compares indoor humidity levels with the Enhanced and Regular modes. Very little difference could be discerned between these modes. One theory was that two-stage compressor operation already provides sufficient humidity control so that enhanced fan control provides little additional benefit.

To test this hypothesis, the unit controls were jumpered to act as a single stage unit (in high stage) for 2003. From August 20 to September 5, the unit operated as a single-stage unit with the enhanced fan controls. From September 5 to the end of the month the unit acted as at a single stage unit with regular fan controls. In the beginning of the summer (June 1 to August 20), the unit operated as a two-stage unit in the enhanced mode. Figure 41 shows that the same indoor humidity was maintained for all three of these control modes. As shown above in Figure 18, the unit actually has a slightly lower suction and lower steady state SHR at high stage. So the penalty of short cycles for the single stage unit apparently was compensated for by the lower high stage SHR. For the single-stage unit, not difference could be detected for the enhanced mode.



**Figure 39. Impact of Control Modes on Indoor Humidity: Enhanced vs. Regular**



**Figure 40. Impact of Control Modes on Indoor Humidity: SINGLE-STAGE vs. Two Stage**

## Problems with Fan Speed Readings

During the monitoring period, the fan speed readings from the photo tachometer periodically pegged to erroneous values (i.e., 4000 rpm). This problem was intermittent in nature though it seemed to always occur at the same time each day. The shade plot in Figure 41 shows the erroneous fan speeds typically occur during two times of day: 6 am to 9 am and 6 pm to 1 am. The problem got progressively worse later in the year. The problem was thought to be an electrical noise issue possibly related to all the sprinkler and lighting control timers located in the closet with the air handler. No other sensors appear to be affected.

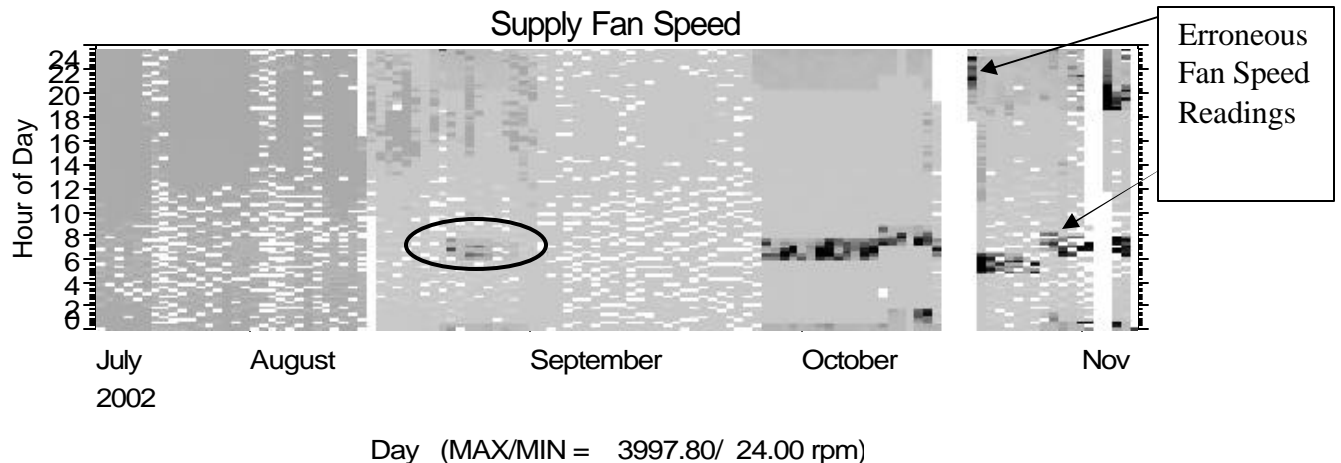


**Figure 41. Shade Plot of Erroneous Fan Speed Readings**

Other fan data were available to quantify fan performance and correct for the erroneous speed readings. Figure 42 shows the relationship between fan speed and fan current using data where the fan had been on for the entire 15-minute interval. Two linear regression models were fit to the data as shown on the plot. These linear models were used to replace the erroneous fan speed readings (i.e., values detected to be far from the current-speed trend). The corrected fan speeds are used in this report.



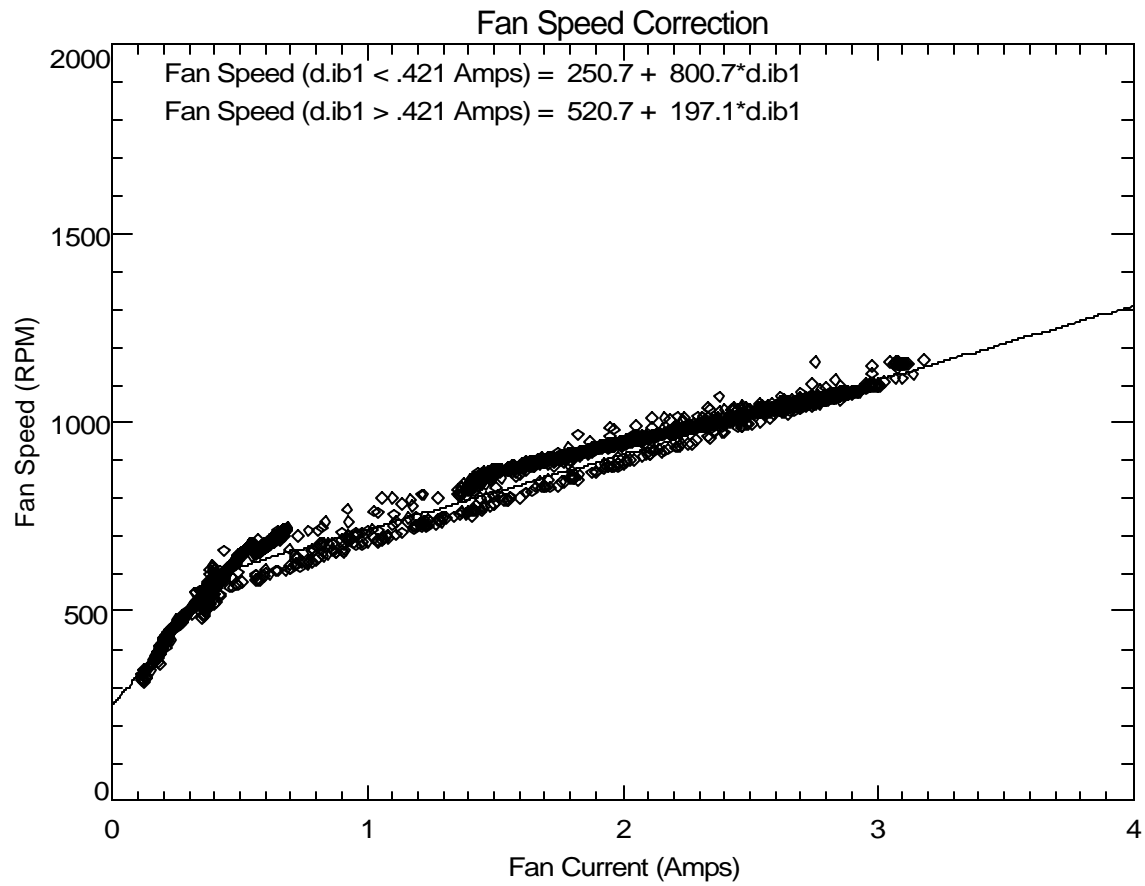


**Figure 42. Trend of Fan Speed with Fan Current**

## **APPENDIX I3**

### **Summary of Data for Field Test Site 3**

## Site #3 – Danbury, CT



**Figure 1. Photo of Home from the East**

### System Description

Size: Estimated 3,500 sq. ft.  
Age: Existing construction on the order of 25 years old  
Construction: Stick frame construction faced with brick, estimated R20 wall, R30 roof

#### Heat pump

4-ton ECR Earthlink DX  
Forced air heating and cooling

#### Ancillary Equipment

(1) HP circulation pumps in heat exchanger, controlled off compressor contactor. Grundfos UP2626BF 240 V  
Measured Power: 200 watts 0.6 A @ 235 VAC (each)

#### (1) Air Handling Unit

Sun Therm B15-55-15-C1BACP1X/CA048A695  
SN FF266079

Measured Power – Blower only: 700 watts 33 A @ 236 VAC (0.90 PF)  
Emergency heat: 15.52 kW 67 A @ 236 VAC (1.00 PF)

#### Backup/Additional heat

(3) Electric resistance elements  
Measured Power: 14.82 kW

#### Hot water

Dedicated heat pump hot water heat exchanger.

DHW production takes precedence over space heating.

(1) DHW Tank – Tank replaced after DAS was installed, model unknown. Element size assumed to be 4.5 kW.

Lower element disconnected and aquastat used to control HP.

Ground heat exchanger

Four 3-inch diameter, 100 foot deep bores under driveway.

In each bore is a copper U-tube consisting of a 3/4" liquid refrigerant supply line and a 1" refrigerant suction line. The U-tubes are connected together at the top of the bores with a single liquid line and suction line header which is connected back to the heat pump.

**Table 1. Data Logger Channel Assignments and Sensor Identification**

Channel	Data Point	Description	Units	Sensor
SE1	TREF	Datalogger Reference Temperature	C	Campbel TCR-10X
SE2	SC	Compressor Status	min	Veris H800
SE3	AMUX	Connection to AM416 Analog Multiplexer		
SE4	AMUX	Connection to AM416 Analog Multiplexer		
SE5	SDHW	DHW Tank Element Status	min	Veris H800
SE6	TRB	Coil Return Bend Temperature	F	Watlow TC AJEC0TA040U8400
SE7	TAS	Supply Air Temperature	F	Watlow TC AJGCNTA120U8400
SE8	TAR	Return/Mixed Air Temperature	F	Watlow TC AJGCNTA120U8400
SE9	TCW	Cold Water Temperature	F	Watlow TC AJEC0TA040U8400
SE10	TDHW	DHW Temperature	F	Watlow TC AJEC0TA040U8400
SE11	THXE2	Ref to Water HX2 Entering Water Temperature	F	Watlow TC AJEC0TA040U8400
SE12	THXL2	Ref to Water HX2 Leaving Water Temperature	F	Watlow TC AJEC0TA040U8400
P1	FDHW	DHW Water Use	gallons	Omega FTB4607
P2				
C1	AMUX	Connection to AM416 Analog Multiplexer		
C2	AMUX	Connection to AM416 Analog Multiplexer		
C3	SB	Blower Status	min	Veris H800
C4	SPHX2	Ref to Water HX2 Circulator Pump Status	min	Veris H800
C5	SRV	Reversing Valve Status	min	Veris H800
C6	WAHU	Total Air Handler Energy	kWh	Ohio Semitronic SWH-2100 50 AMP
C7	FC	Condensate Flow	lbm	Hydrolynx 5050P Tipping Bucket
C8	WU	Total HP Energy	kWh	Ohio Semitronic SWH-2100 50 AMP
AMUX 1H-1L	PD	Comp Discharge Pressure	psi	Setra C206 0-500 psig
AMUX 2H-2L	PS	Comp Suction Pressure	psi	Setra C206 0-100 psig
AMUX 3H-3L	TAO	Ambient Temperature	F	Mamac TE211Z-OAWP-3
AMUX 4H-4L	RHR	Return/Mixed Air Humidity	%	Vaisala HMD60U
AMUX 5H-5L	IB	Supply Fan Current	Amps	Veris H720
AMUX 6H-6L	PCD	Pressure Drop Across Coil	in. WC	Setra C264 0-2.5 in WC

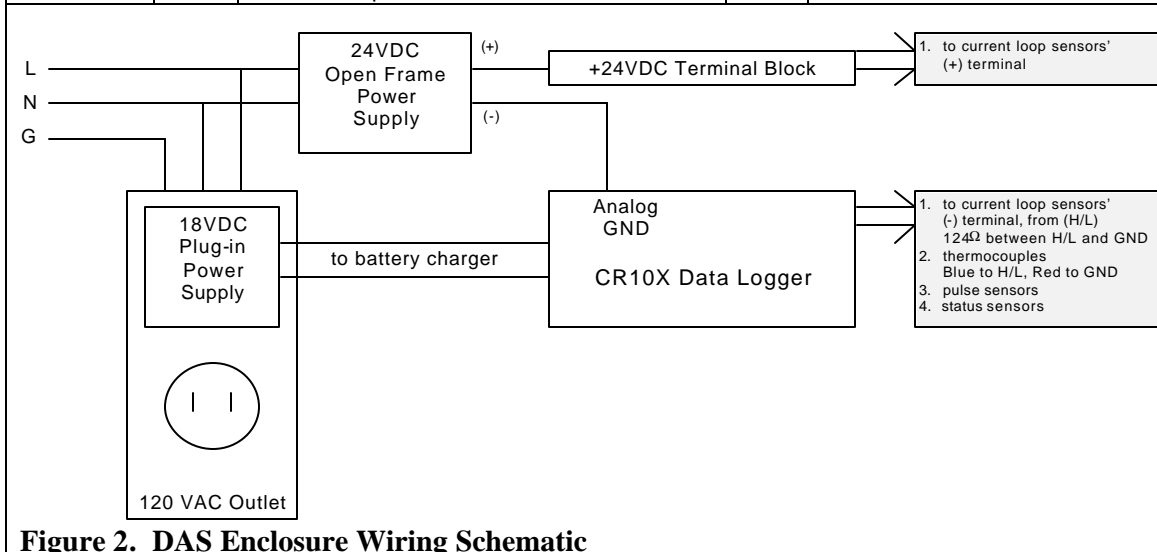


**Figure 2. DAS Enclosure Wiring Schematic**

**CR10X Data Logger  
Analog Terminals**

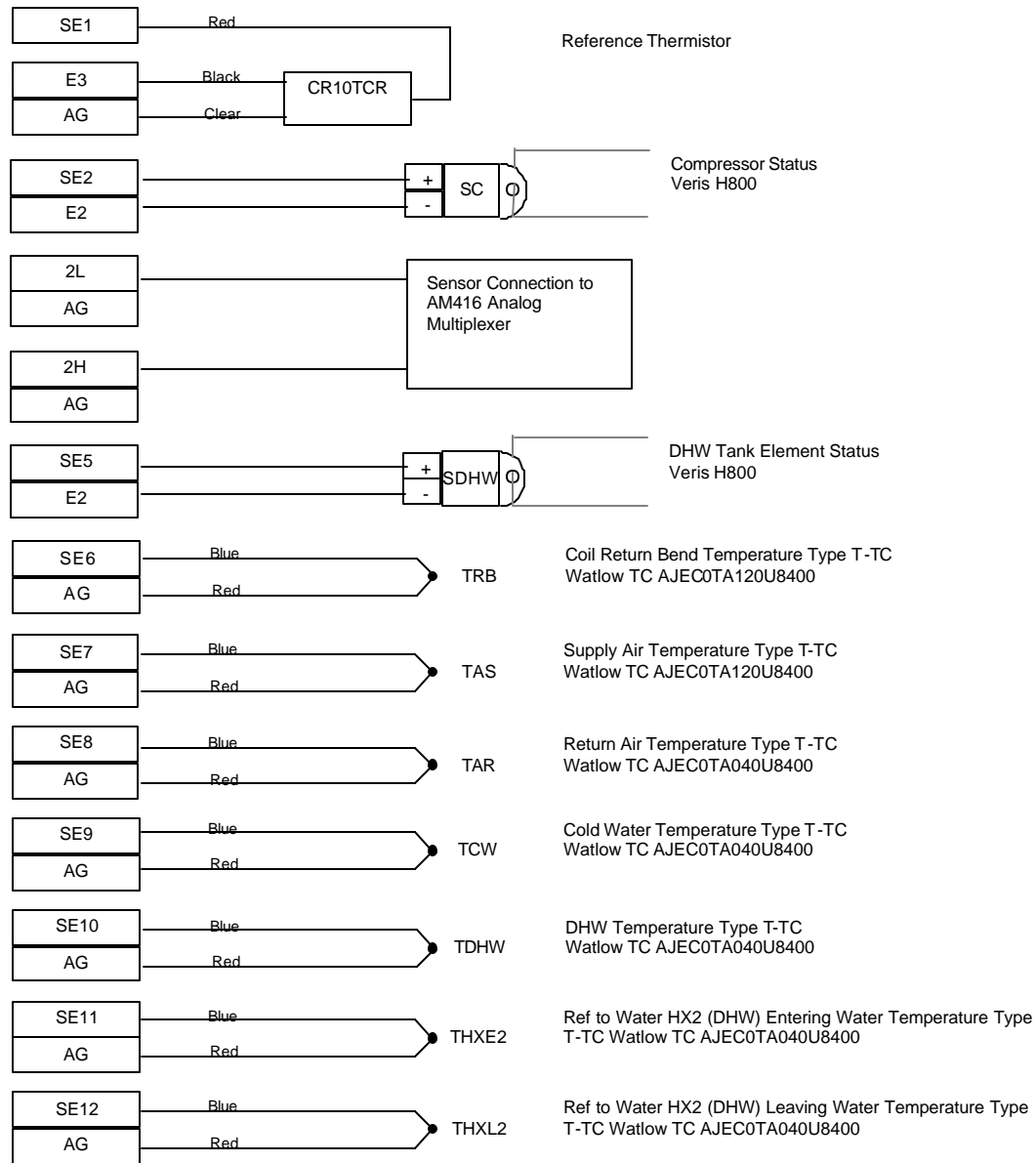
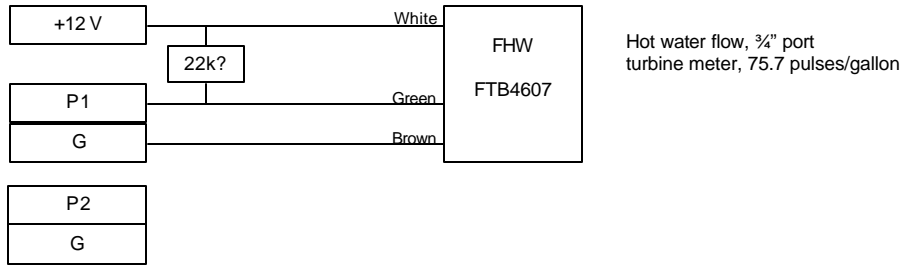


**Figure 3. CR10X Analog Terminals Wiring Schematic**

**CR10X Data Logger  
Pulse Terminals**



**CR10X Data Logger  
Digital Terminals**

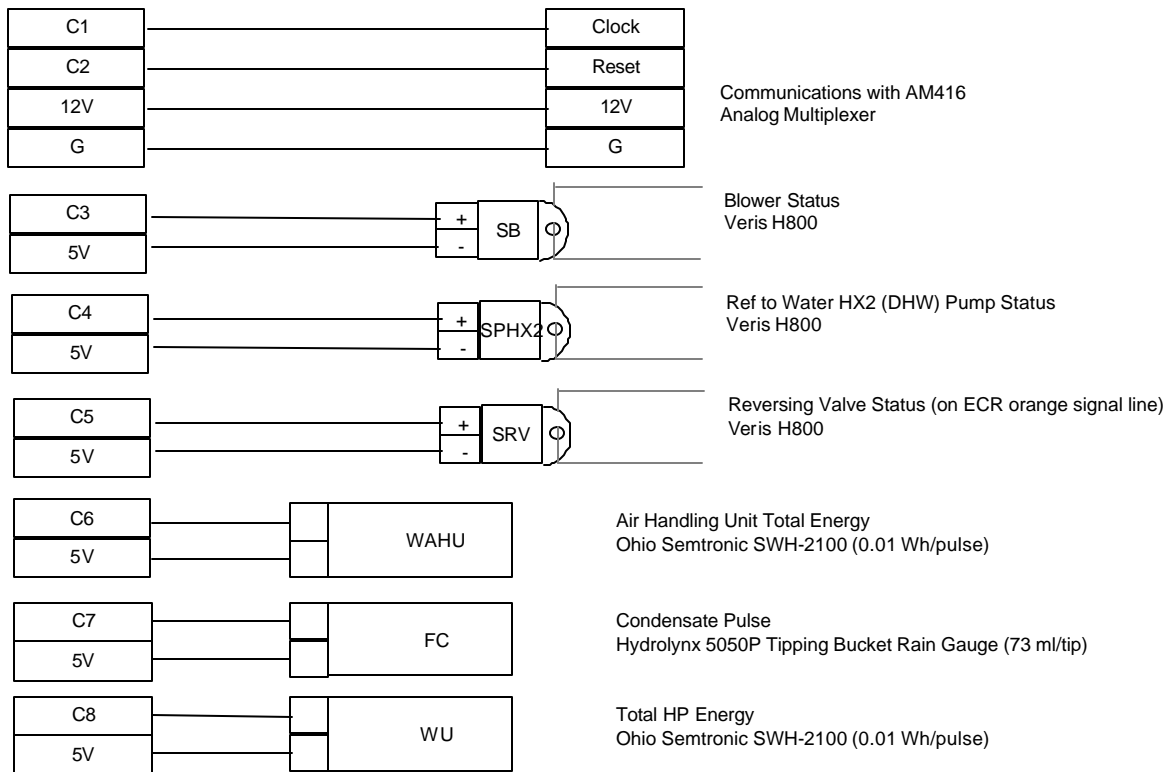


**Figure 4. CR10X Digital Terminals Wiring Schematic**

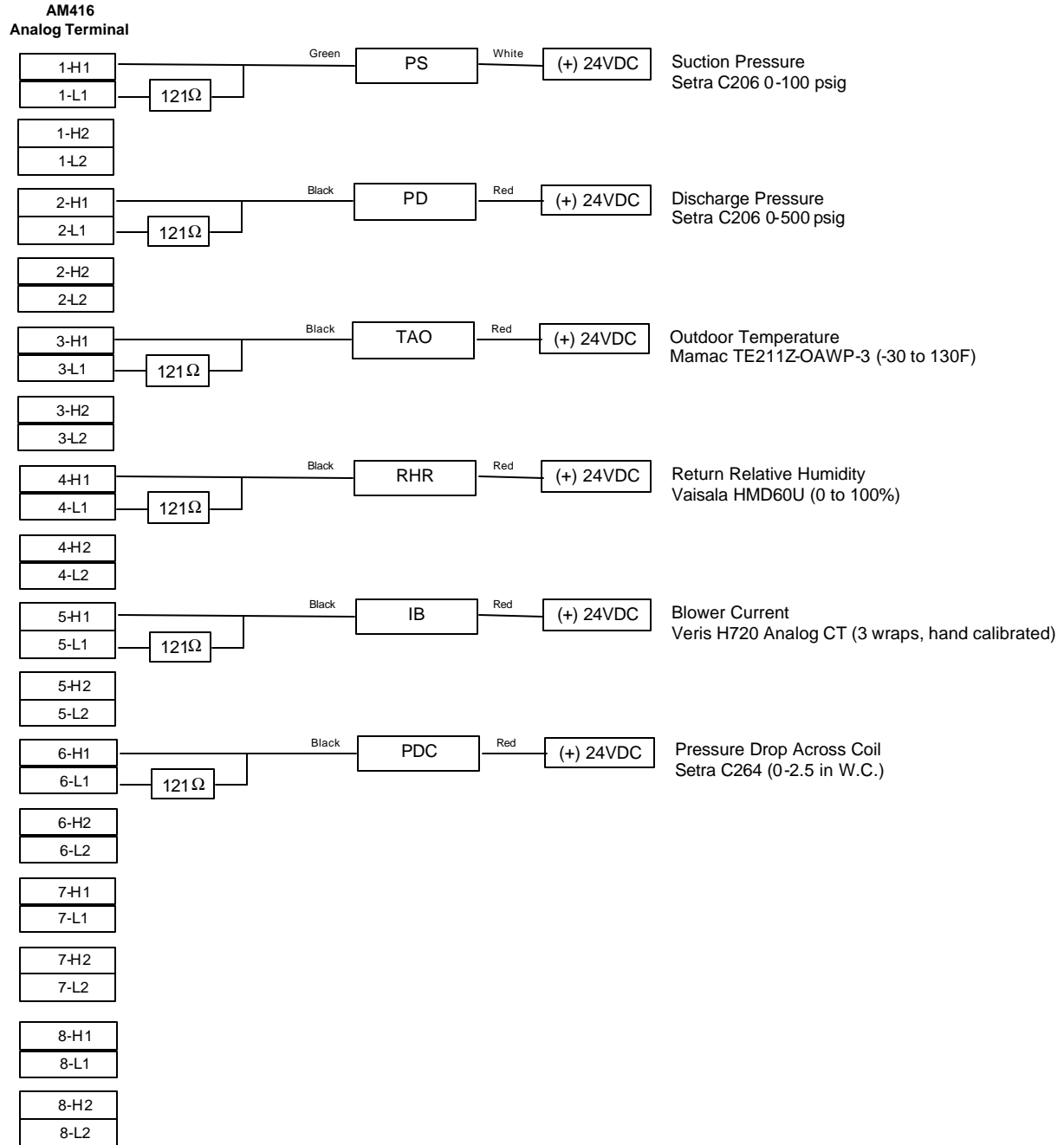


**Figure 5. Data Logger Connections to AM416**

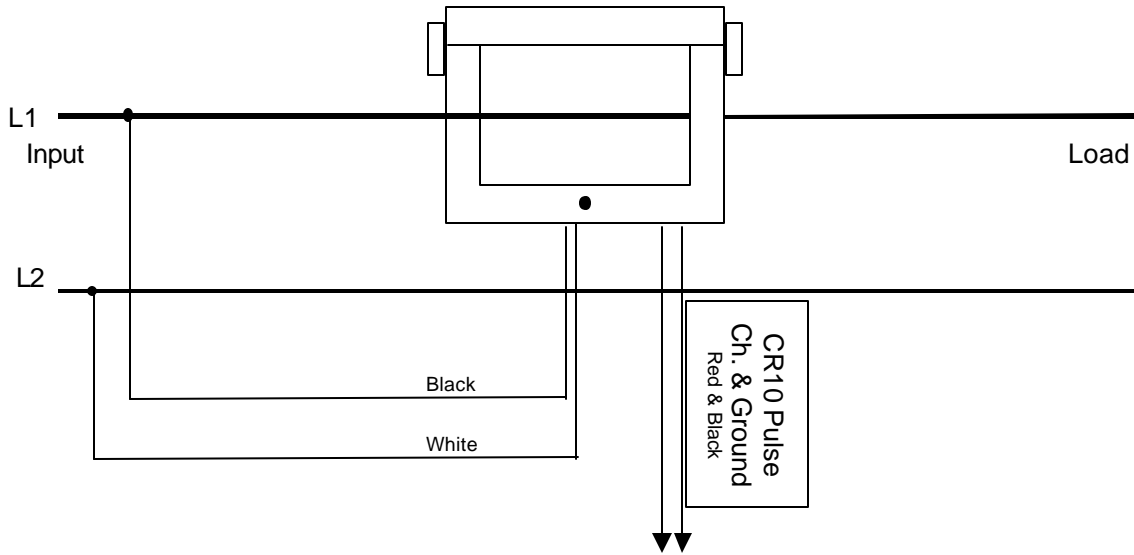


**Figure 6. Connection Diagram for SWH-2100 for Single Phase 2-wire Circuit (240V)**

**Table 2. One-Time Measurements**

Measurement	Data
System flow rate measured using equal area traverse on return duct (12 points, 60 measurements) Duct size 24 inch x 16 inch with ½ inch interior insulation. Total interior area = 345 sq. in. / 2.396 sq. ft.	660 FPM avg 1,581 SCFM
System flow rate measured using energy balance with emergency heat and temperature difference across unit. Compressor OFF.  Total AHU power (4.96 kW + 10.56 kW) = 15.52 kW Supply air temperature = Return air temperature = Temperature rise = 31.5°F	Calculated SCFM:  $Q = 1.08 \times SCFM \times \Delta T$ $Q = 15.52 \text{ kW} \times 3413 \frac{\text{BTU}_h}{\text{kW}} = 52,969 \text{ BTU}_h$ $SCFM = \frac{52,969 \text{ BTU}_h}{1.08 \times 31.5^\circ \text{F}}$ $SCFM = 1,557$
Total HP Power	3.06 kW 13.5 A @ 236 VAC
HX Circulator Pump Power	210 watts 0.6 A @ 236 VAC
Blower Power	700 watts 3.2 A @ 236 VAC
Hydronic Tank Resistance Element	4.4 kW 18.3 A @ 236 VAC
DHW Tank Resistance Element (old tank)	4.15 kW 17.7 A @ 236 VAC
Pressure drop across coil (dry)	0.18 in WC

**Notes:**

Space conditions monitored by HOBO data loggers

**Coil Info:**

A-coil, 4 row, 14 FPI, wavy fins, fixed orifice expansion device

Coil dimensions: 20 3/8 inch X 19 3/4 inch on each side X 3 inch depth

Coil face area: 804.8 sq. in / 5.589 sq. ft. total area

20 1/4 inch tubes per row

Gross fin area: (3 in) x (14 fins/in) x (2 sides/fin) x (804.8 sq in.) / 144 sq in/ft<sup>2</sup> = 469.5 ft<sup>2</sup>



## Site Photos

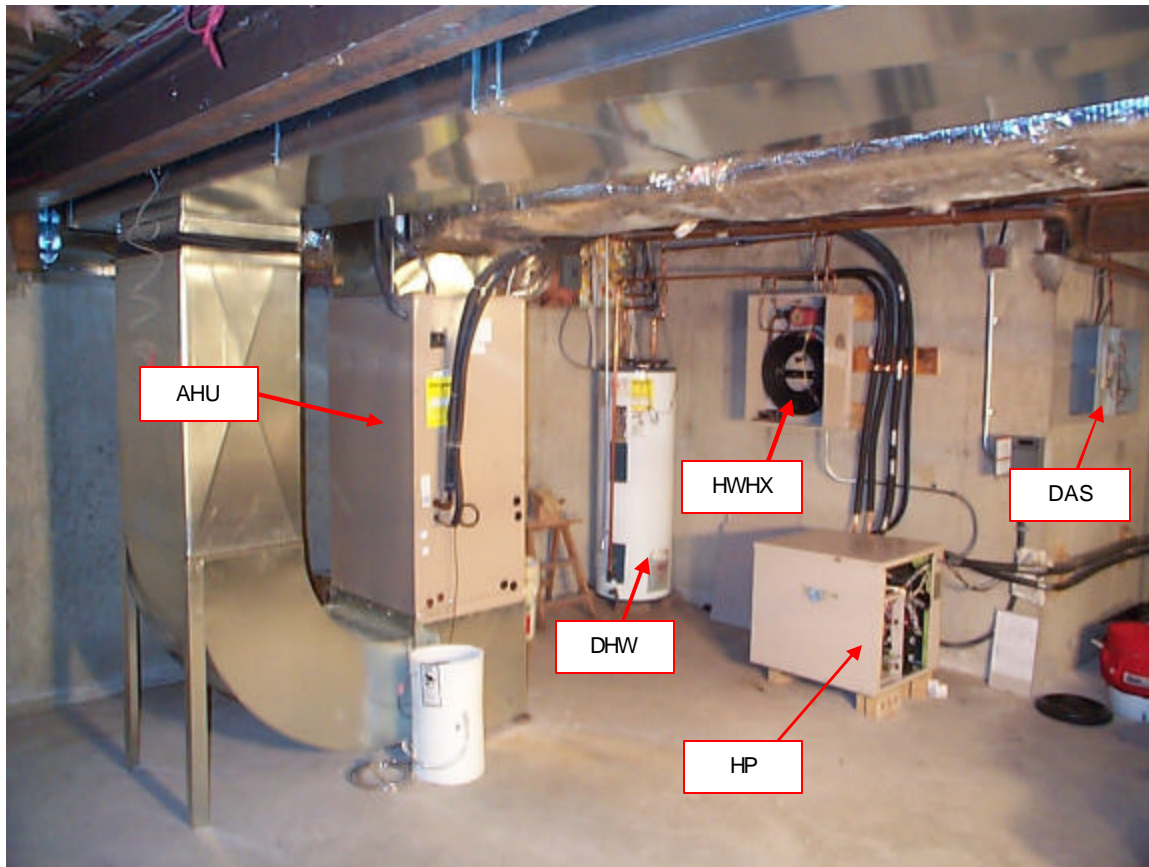


**Figure 7. Entire System**

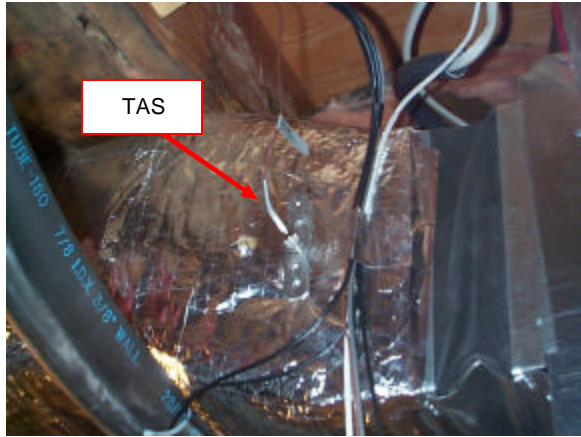


**Figure 8. Supply and Return Air Sensors**

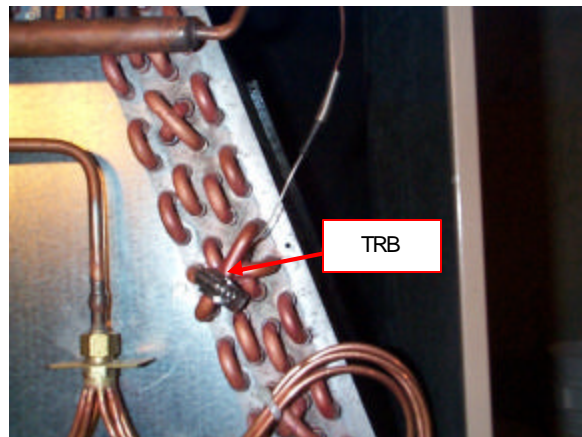
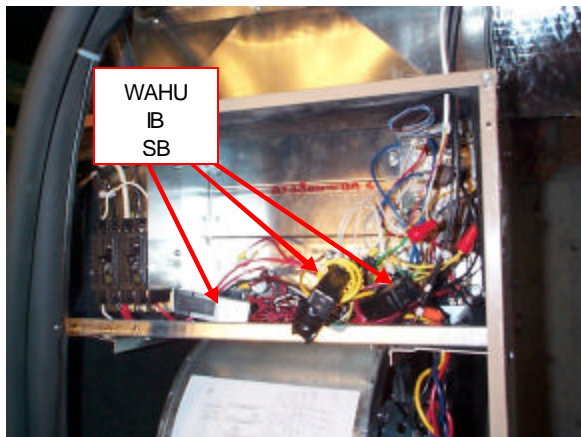


**Figure 9. AHU Power and Status Sensors, Coil Return Bend Sensor**

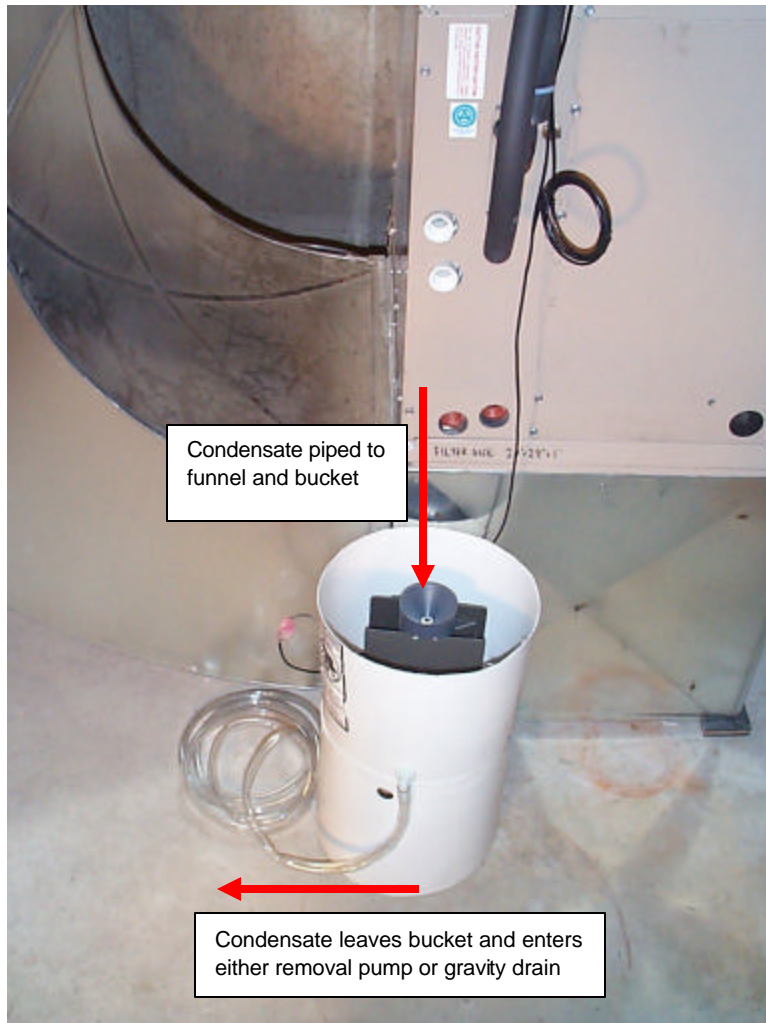


**Figure 10. Tipping Bucket Condensate Sensors**

### **Data Collection Summary**

Thirteen analog and ten digital data points are monitored on the heat pump and DHW systems to quantify each system's performance. All readings are measured once every five seconds, and recorded as the average reading over a 15-minute period (for the analog channels) or the total over a 15-minute period (for the digital channels). Short time step data (1-minute records) are also recorded when the blower operates. Event based data is collected when a component of the system changes state (i.e. a pump turns on or off).

Table 3 summarizes the monitoring and site events that occurred during the monitoring period. Data collection began on April 5<sup>th</sup> with the first significant cooling observed on April 17<sup>th</sup>. The supply fan was set to "constant" fan mode from June 11<sup>th</sup> to July 3<sup>rd</sup> and remained in "auto" mode for the rest of the cooling season. Space conditioning was turned off from July 9<sup>th</sup> to July 11<sup>th</sup>.

**Table 3. Summary of Site and Data Collection Events**

April 5, 2002	Data logger installed and data collection begins
April 17-19, 2002	First significant cooling operation observed during April heat wave
May 28, 2002	Full time cooling operation begins.
June 11 – July 3, 2002	Thermostat fan control set to “constant”. Blower does cycle off during DHW operation.
July 3, 2002	Thermostat fan control changed back to “auto” mode.
July 5-9, 2002	House unoccupied. Homeowners turn off water main from street while away. No change in thermostat set point was observed while owners were away.
July 9, 2002 5:00 AM – July 11, 2002 9:00 PM	DHW HX pump cycles 3-minutes on, 3-minutes off for 2 days straight. Compressor cycles on for 6-minutes every 90-minutes. No blower operation or space conditioning occurs during this period.
July 18, 2002 2:00 PM	Space conditioning operation resumes.
August 16, 2002	Data collection stopped due to data logger malfunction.
August 21, 2002	Data logger repaired and data collection resumes. Additional sensors added to the data logger include supply RH and compressor suction header temperature. Discharge pressure sensor replaced.
October 2, 2002	Last day with significant cooling operation

Figure 11 below shows shade plots of system activity for the compressor, supply fan, condensate tip bucket.

### **Latent Capacity**

Figure 12 compares the latent capacity calculated from the condensate flow as well as from psychrometric calculations. The plot only includes data records where the compressor ran for 15 minutes in cooling (i.e., at steady state conditions). The relative humidity sensor for the supply air flow was not installed until the end of August, causing a small sample of data in the primary cooling season.

Figure 13 shows the process line for cooling on the psychrometric chart. The smaller data points correspond to the performance data. The line and the larger three points correspond to the average of conditions 1) at the coil inlet, 2) at the coil outlet, but before the fan and 3) after the supply fan.

The average SHR for the coil – or the slope of the process line – is also shown on the plot. The sensible heat ratio is 0.773 for the unit during the few hours of steady state operation after August 21 (when the supply RH sensor was installed). The saturated suction temperature for the coil for these periods was fairly cold at 35°F.

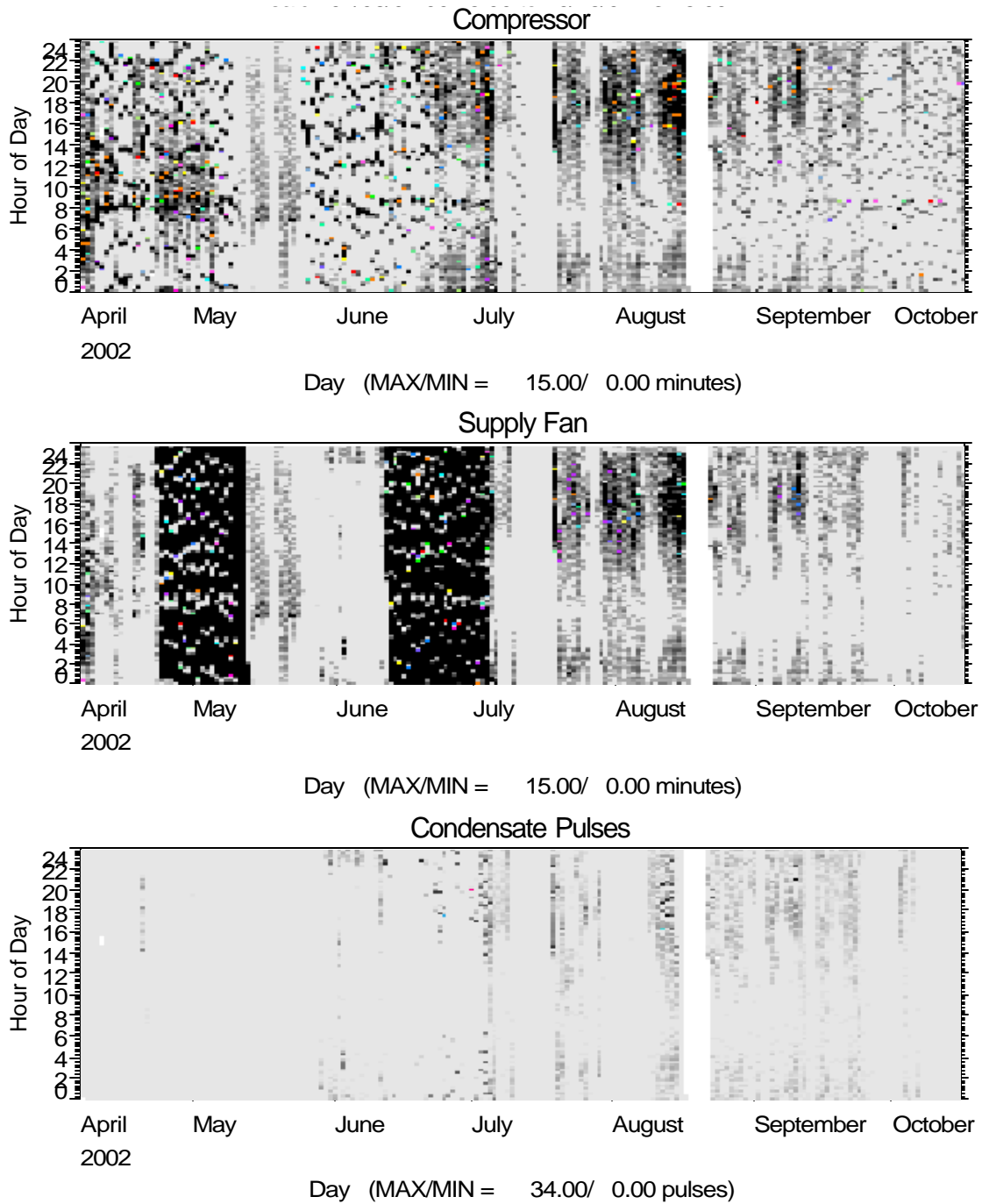


**Figure 11. Shade Plots of Compressor, Supply Fan and Condensate Tip Bucket**



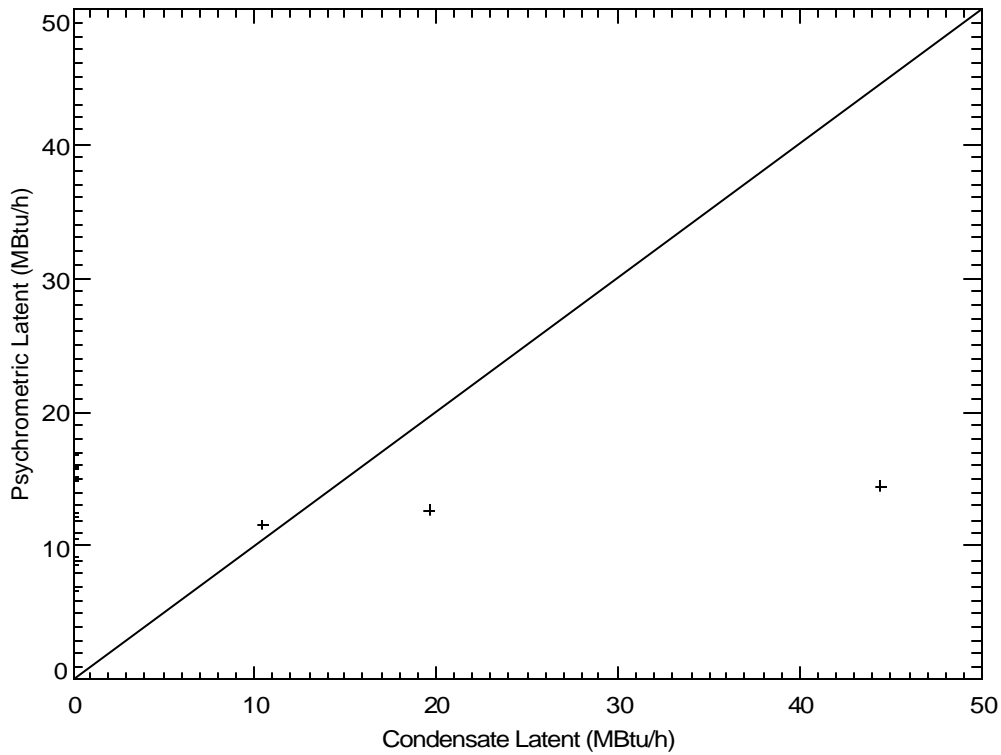


**Figure 12. Comparing Condensate and Psychrometric-based Latent Capacity**

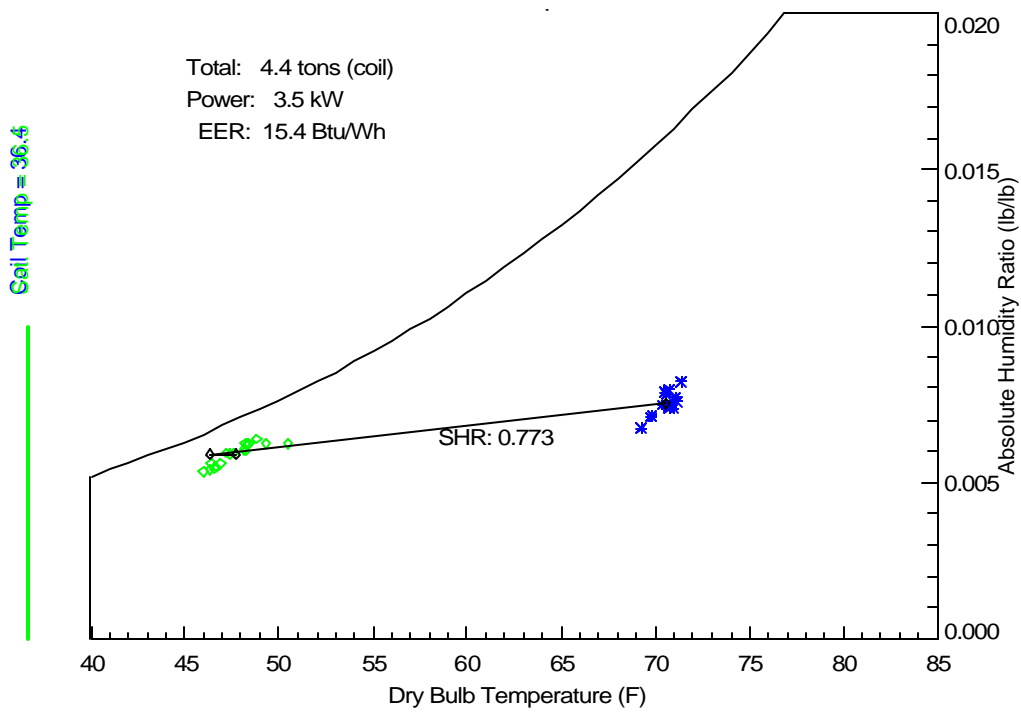


**Figure 13. Cooling Process Lines for AC Coils at Steady State Conditions**

## Space Conditions

Figure 14 shows the return air conditions as compared to the ASHRAE comfort zone. The return conditions for the AC unit are expected to approximate the space conditions. For the 38 days shown, there are no periods where the return conditions fall within the comfort zone. The dry bulb temperature is generally five degrees lower than the lower limits of the summer comfort zone.

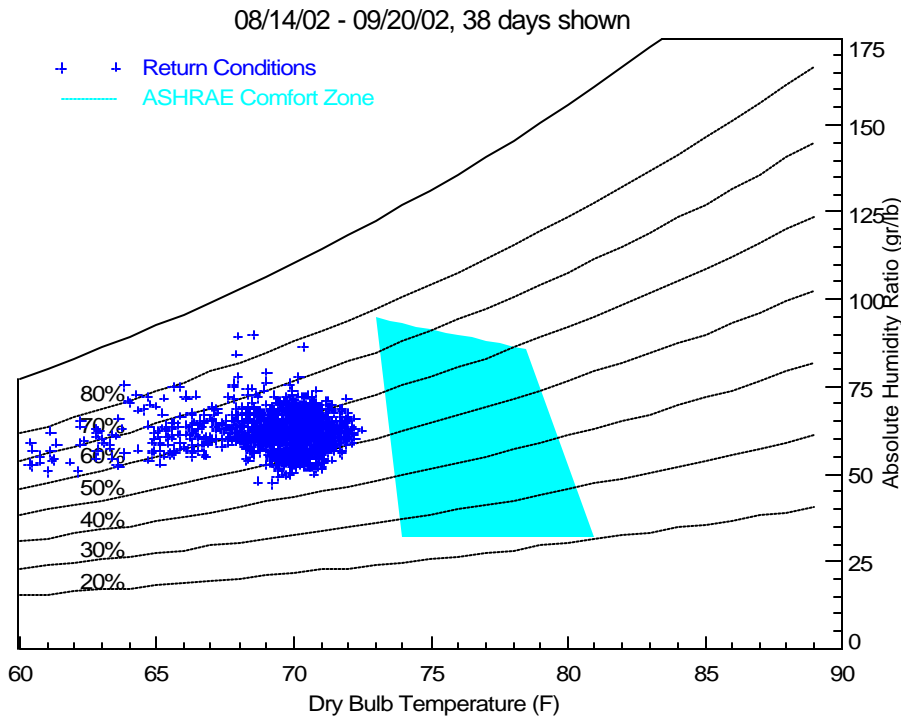


**Figure 14. Space Conditions Show on the Psychrometric Chart**

## Part Load SHR

The moisture removal capacity of a cooling coil is reduced at part load conditions. This part load degradation is especially prevalent when the fan operates continuously. The SHR is calculated using the coil temperature difference, air flow, and condensate readings on an hourly basis. Data for the plot are averaged hourly. The steady state SHR listed on the plot with a dotted line is higher than the SHR of the process lines shown on Figure 13 (the process line only corresponds to a brief period when supply RH data was available). The steady state SHR for this period averaged 0.864.

Figure 15 shows the SHR trending with Runtime fraction (RTF), the percentage of time the cooling stages were running for the given period. The shows a fair amount of scatter. The scatter may be due to the fact that compressor runtime fraction (RTF) is also driven by compressor operation for water heating.

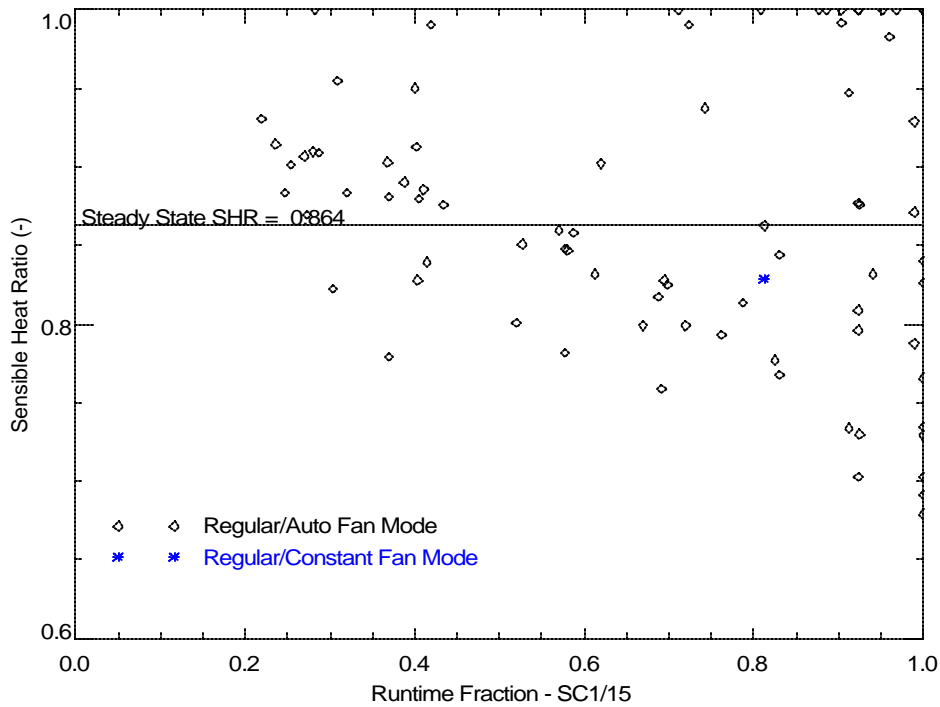


**Figure 15. Part-Load Sensible Heat Ratio**

### **Indoor-Outdoor Humidity Ratio for Different Control Modes**

The indoor and outdoor humidity were averaged daily during the cooling period. Figure 16 shows the plot of indoor and outdoor humidity for auto and constant fan operating modes. The plot shows that constant fan mode causes higher indoor humidity when compared to auto fan mode at similar outdoor humidity levels.



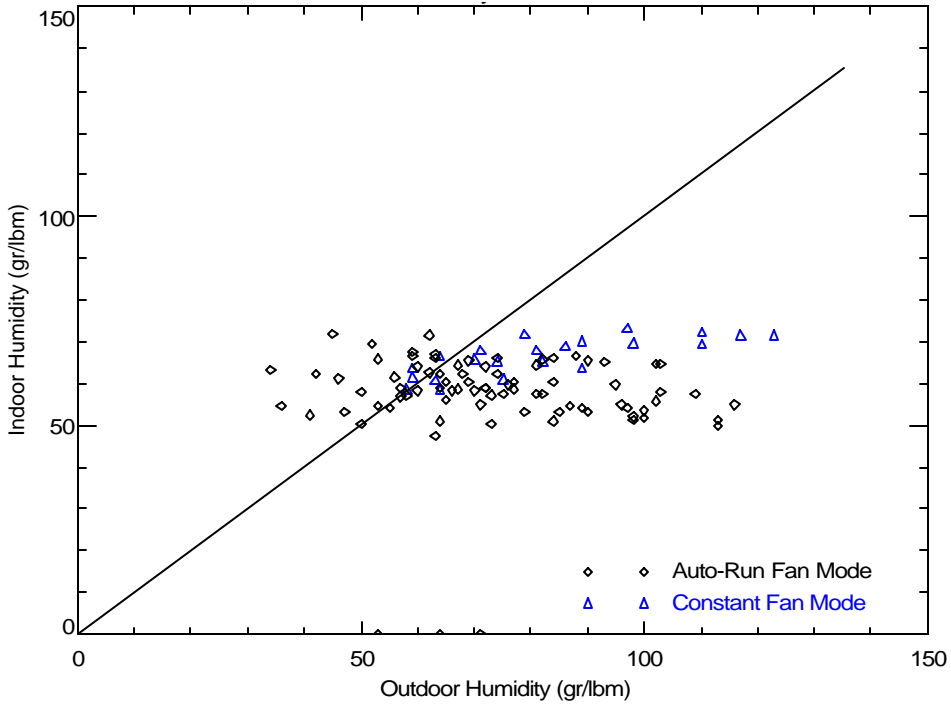


**Figure 16. Daily Humidity Ratios for Auto vs. Constant Fan Mode Settings**

## **APPENDIX I4**

### **Summary of Data for Field Test Site 4**

## Site #4 – Commercial RTU – Brookline MA



**Figure 1. RTU With DAS System Installed**

### **System Description**

This 10-ton rooftop unit (RTU) is conventional two-stage system that serves a portion of a 20,000 sq. ft. retail area in Boston. The RTU has two separate compressors and refrigeration circuits with face-split evaporator coils. The unit is time-clock controlled by the building energy management system (EMS). The RTU supply fan operated continuously each day to provide ventilation during the occupied period (8 am to 9 pm Monday to Saturday; 10 am to 5 pm Sundays).

York 2-stage RTU w/ Natural gas heater  
Model D1EG120N16546JSE  
10-ton nominal cooling capacity (Stage 1 5-tons, Stage 2 5-tons)

## Sensors and Data Logger Connections

**Table 1. Data Logger Channel Assignments and Sensor Identification**

Channel	Data Point	Description	Units	Sensor
SE1	TREF			
SE2	TEVP1	Coil Return Bend Temperature - Unit 1	F	Type-T TC
SE3	TSUC1	Suction Temperature - Unit 1	F	Type-T TC
SE4	TLIQ1	Liquid Line Temperature - Unit 1	F	Type-T TC
SE5	TAM1	Mixed Air Temperature - Unit 1	F	Mamac TE211Z Avg probe (40-140)
SE6	TAS1	Supply Air Temperature - Unit 1	F	Mamac TE211Z Avg probe (40-140)
SE7	PSUC1	Compressor Suction Pressure - Unit 1	psig	Setra C207
SE8	RHM1	Return/Mixed RH - Unit 1	%	Vaisala HMD60U
SE9	RHS1	Supply RH - Unit 1	%	Vaisala HMD60U
SE10	DPC1	Pressure Drop Across Coil - Unit 1	in wc	Setra 267MR (0.25, 0.5, 1.0 inches)
SE11	IB1	AHU Fan Current - Unit 1	amps	Veris H721LC
SE12	TAO	Ambient Temperature - Unit 1	F	Mamac RTD
P1	WU	Total Power - Unit 1	kWh	Veris 8500 100 amp
P2				
C3	SC1		min	Veris H800
C4	SC2		min	Veris H800
C5				
C6				
C7	FC1	Condensate Removal - Unit 1	pulse	Tipping Bucket HydroLynx
C8				

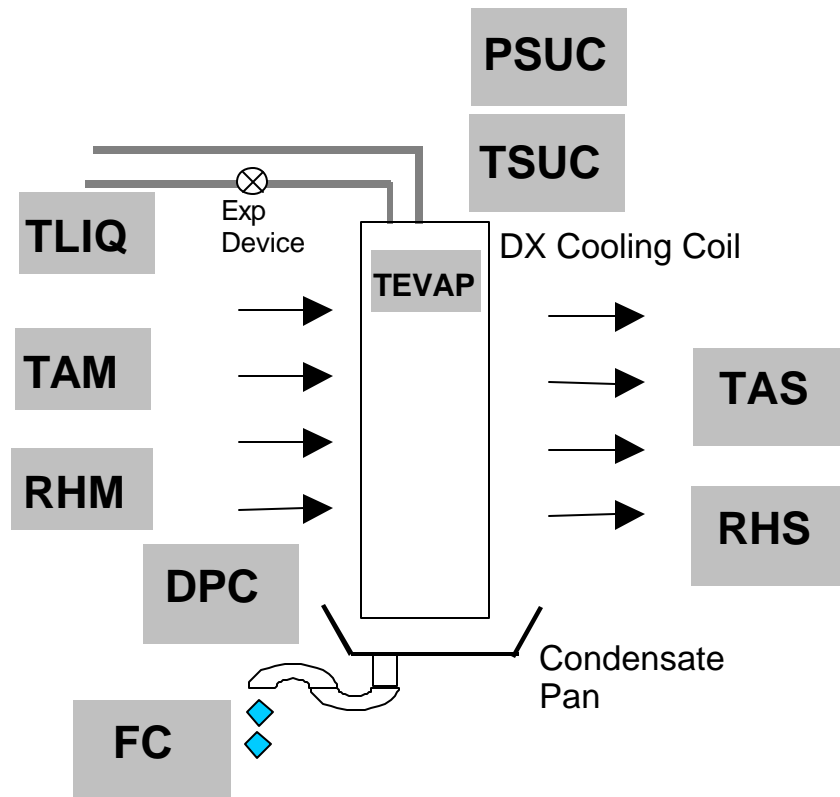
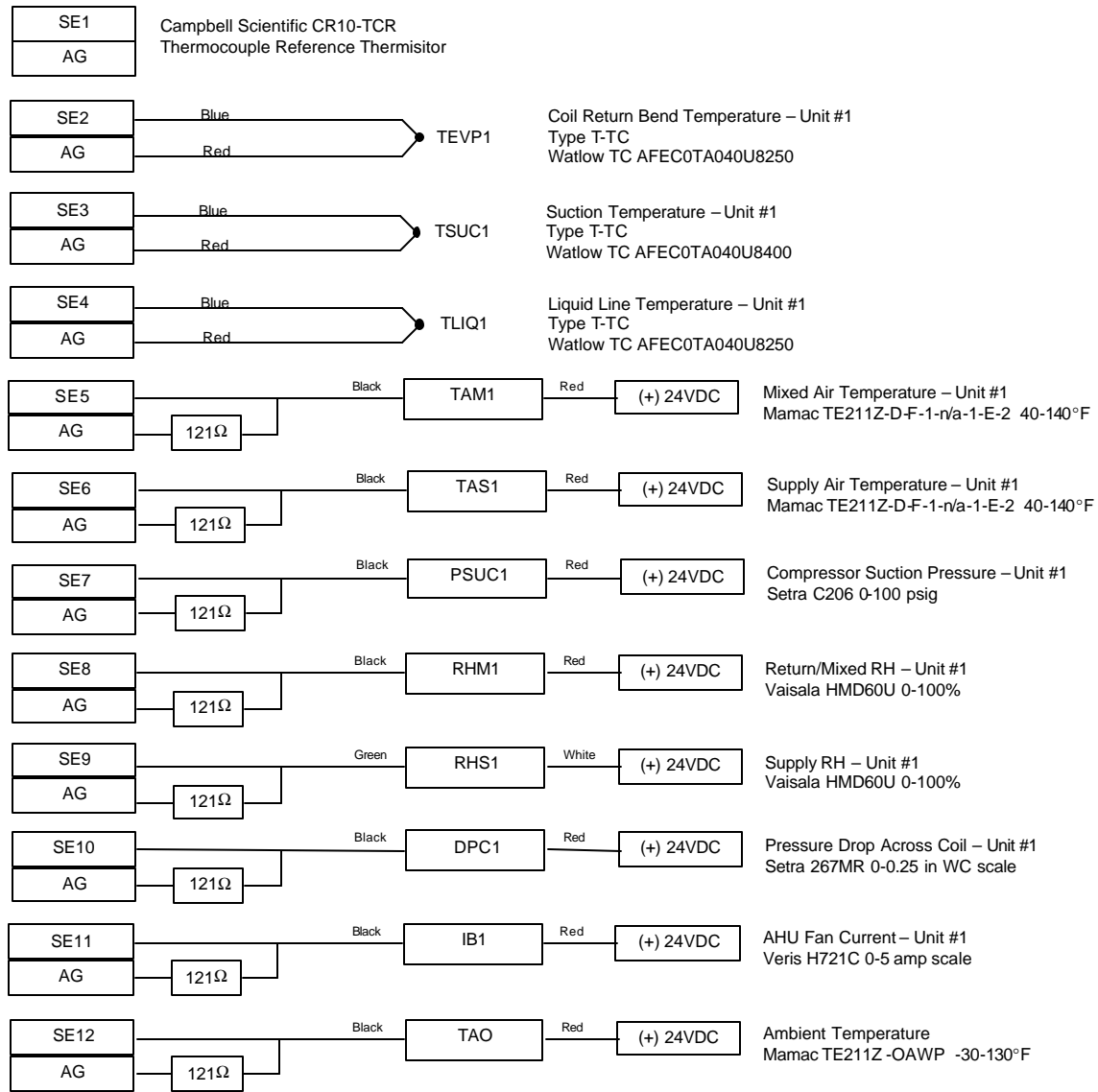


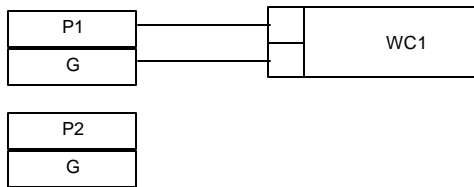
Figure 2. System Schematic

**CR10X Data Logger  
Analog Terminals**



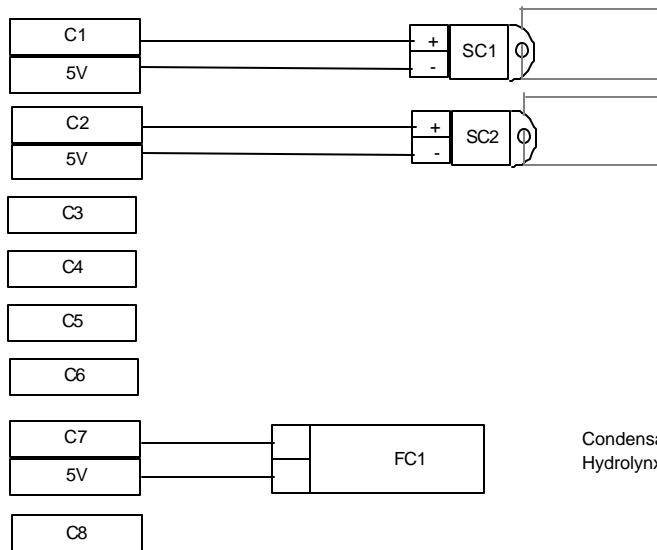
**Figure 3. CR10X Analog Terminals Wiring Schematic**

**CR10X Data Logger  
Pulse Terminals**



Total Power – Unit #1 (includes condenser fan)  
Veris H8053-100 Power Transducer 0.1 kWh/pulse

**CR10X Data Logger  
Digital Terminals**



Compressor Stage 1 Status – Unit #1  
Veris H900

Compressor Stage 2 Status – Unit #1  
Veris H900

Condensate Removal – Unit #1  
Hydrolynx Tipping Bucket Rain Gauge

**Figure 4. CR10X Digital Terminals Wiring Schematic**

## Coil Measurements

Coil Type	“Flat” coil	
Coil Face Area	1,535.25 sq. in.	
Number of rows	3 / 2.75 in deep	
Tubes per row	34	
Tubing diameter	Unknown	
Notes: 13 FPI Straight Fins		
Exp device: TXV, each coil section.		
Coil split: approx 50% each circuit		

**Figure 5. RTU Coil Dimensions**

Gross fin area: $(2.75 \text{ in}) \times (13 \text{ fins/in}) \times (2 \text{ sides/fin}) \times (1535.3 \text{ sq in.}) / 144 \text{ sq in/ft}^2 = \underline{762.3 \text{ ft}^2}$
---

## One Time Measurements

**Table 2. Comparing Data Logger Measurements to TSI hand held probe**

Sensor	Campbell	TSI / Handheld
Unit #1 – Supply (T/RH)	61.6°F / 60.6%	62.6°F / 53.2%
Unit #1 – Mixed (T/RH)	74.7°F / 38.6%	74.0°F / 38.2%
Ambient (T)	75.9°F	74.2°F
Unit #1 – Suction (T)	60.1°F	N/A
Unit #1 – Liquid Line (T)	79.0°F	N/A
Unit #1 – Return Bend (T)	61.0°F	N/A
Unit #1 – Suction Pressure (psig/T)	60.1 psig/33.9°F SST 29.3°F TC	N/A
Unit #1 – Pressure Drop Across Coil	0.139 in WC	0.12 in WC
Unit #1 – AHU Fan Current	3.82 amps	3.7 Amps
Unit #1 – Total Power	6.8 kW	7.0 kW (10.6 amps @ 460 VAC)



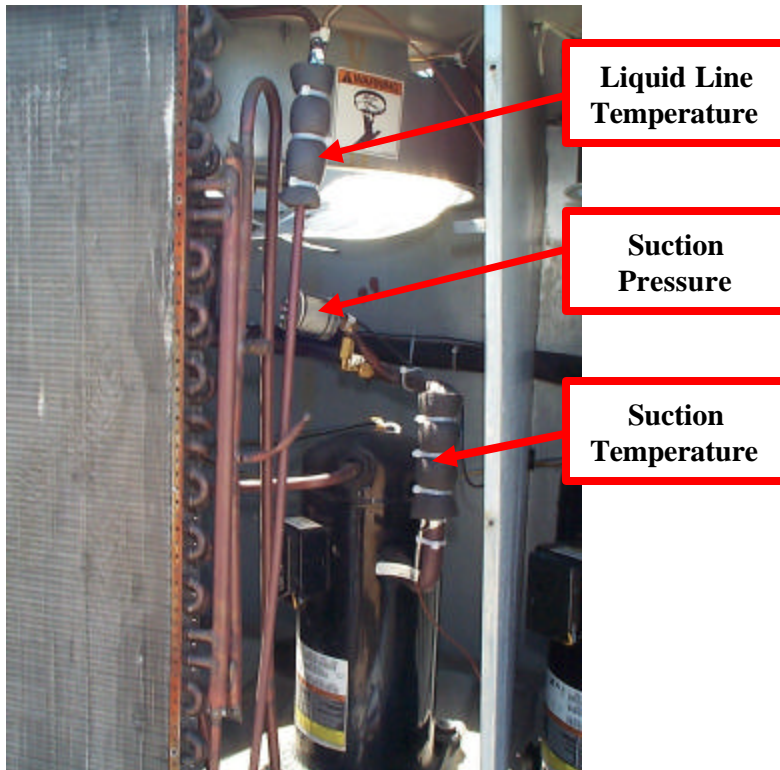
## Site Photos



**Figure 6. Supply Temperature and RH**



**Figure 7. Mixed Temperature and RH**



**Liquid Line  
Temperature**

**Suction  
Pressure**

**Suction  
Temperature**

**Figure 8. Sensors in Condensing Unit Section**

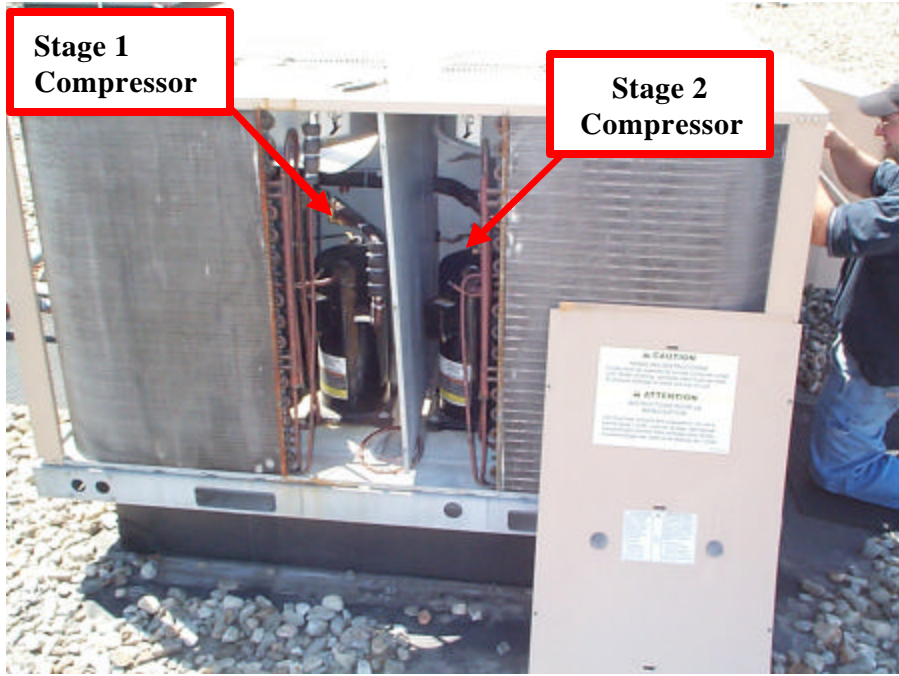


Figure 9. Condensing Section

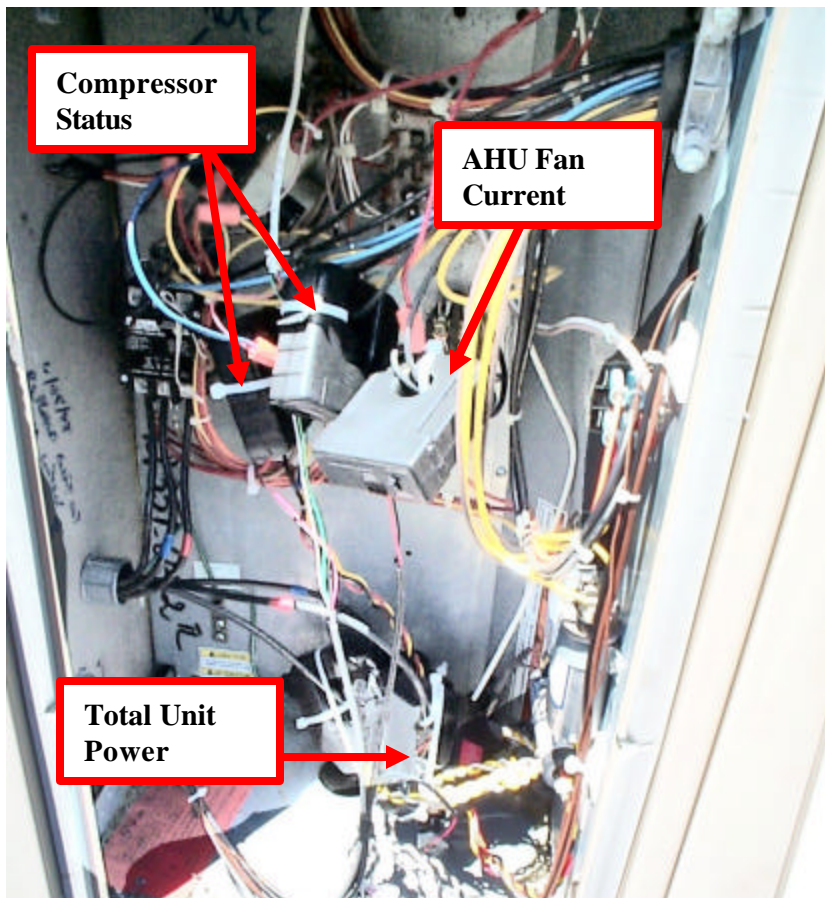
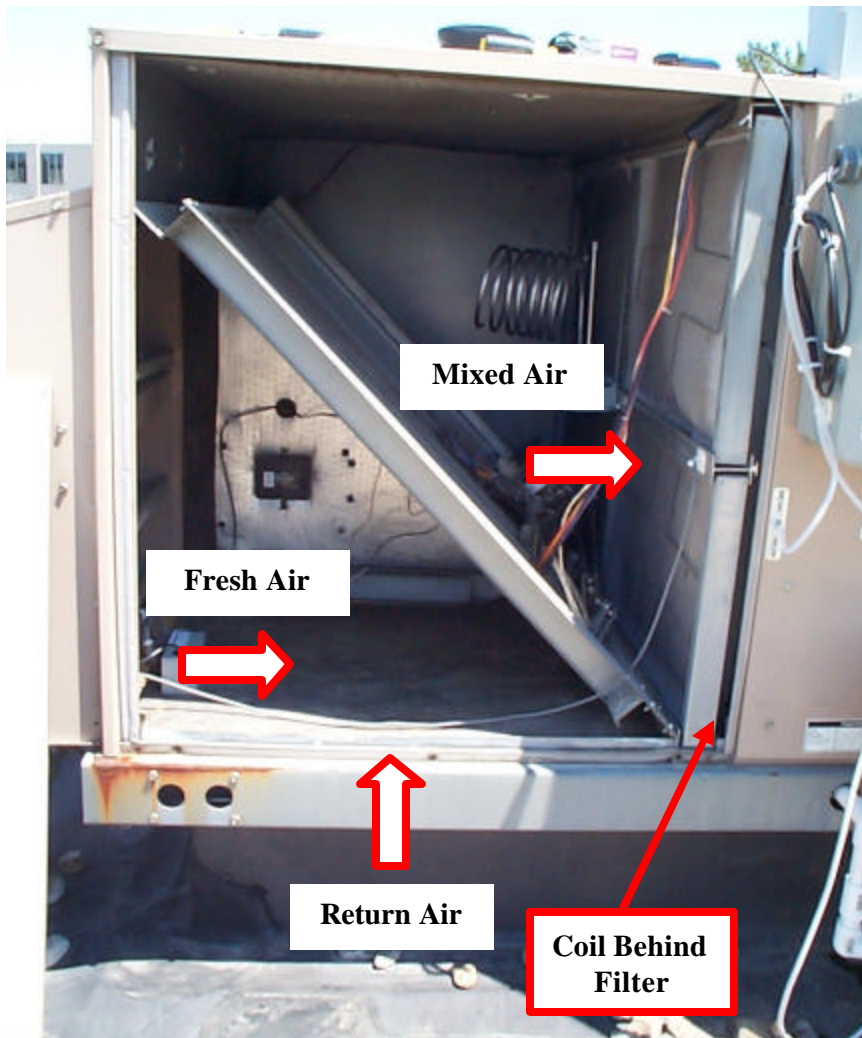


Figure 10. Sensors in Electrical Service Panel



**Figure 11. Ambient Temperature Sensor Under Fresh Air Intake**



**Figure 12. Return/Mixed Air Section**



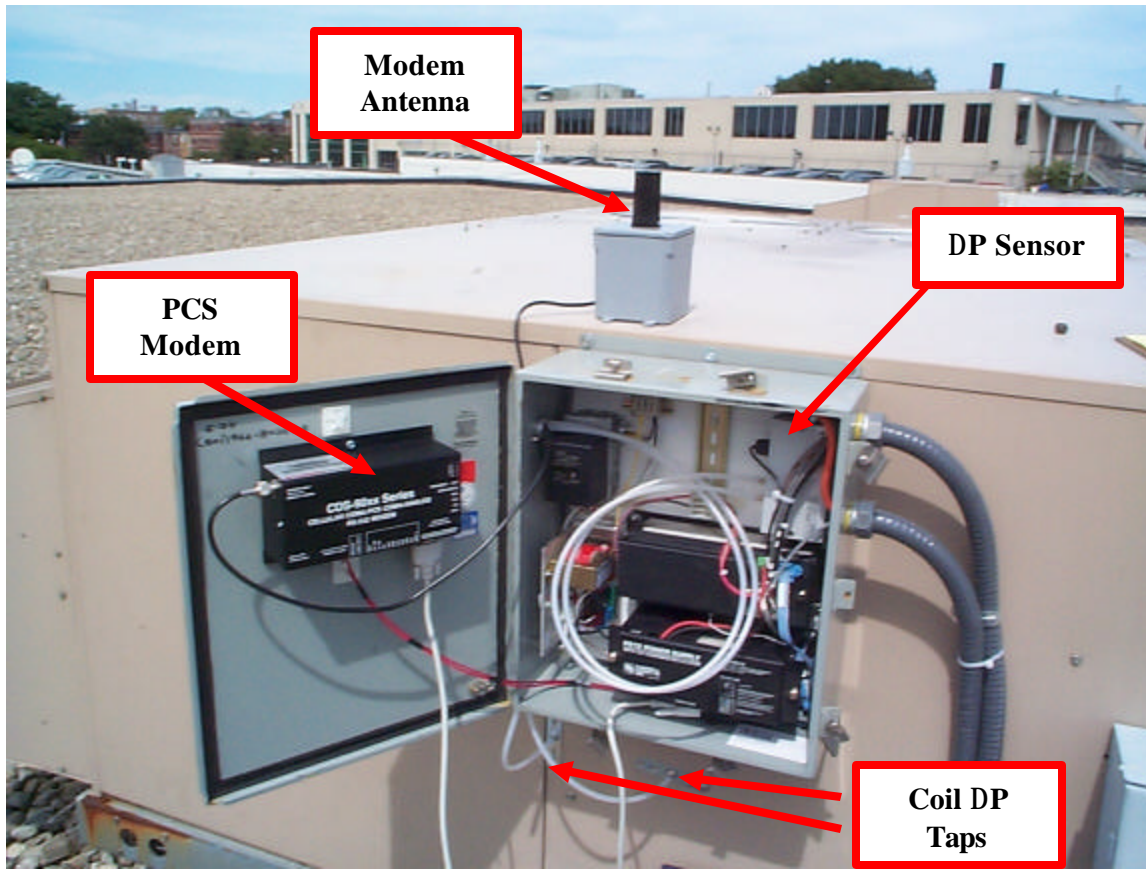


Figure 13. Data Logger Panel

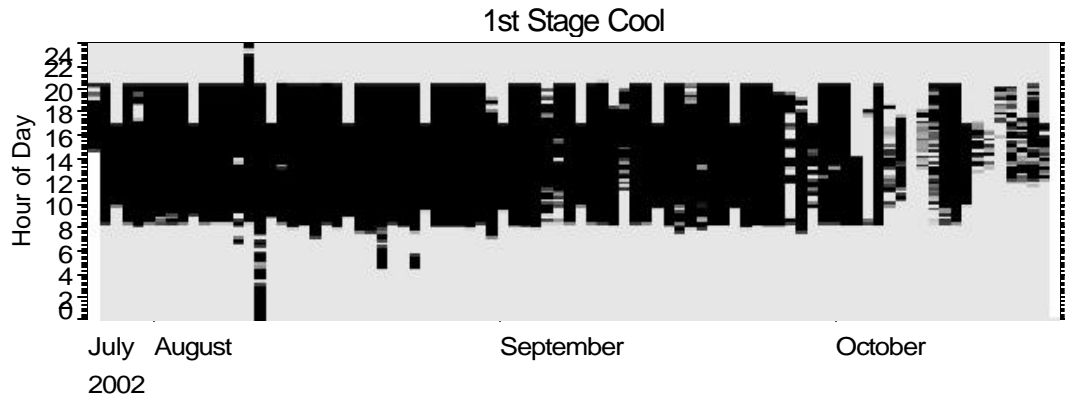
## Data Collection Summary

Data collection for the RTU began on July 26. The unit is controlled/scheduled by the building control system. A brief period of 24-hour fan operation was observed on October 6-10. After October 10 the RTU fan was switched to the auto fan mode by the EMS (as appears to be the building owner's policy). Table 3 below summarizes the major events that occurred over the monitoring period.

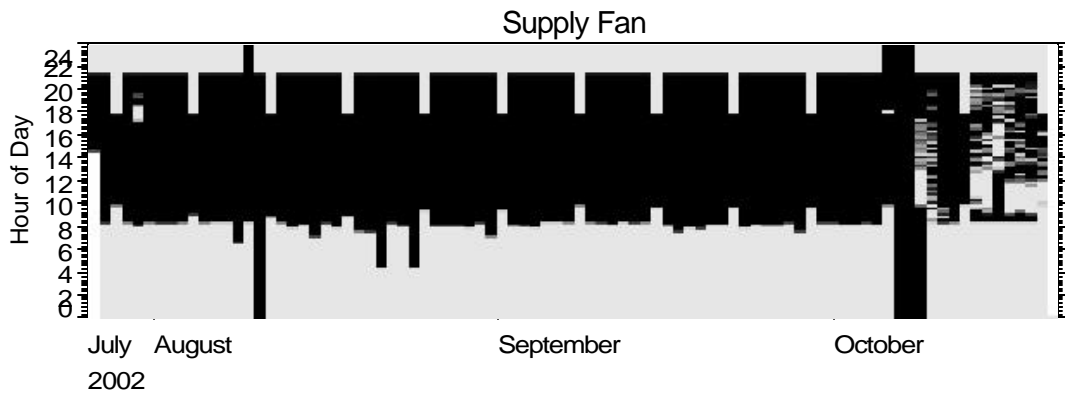
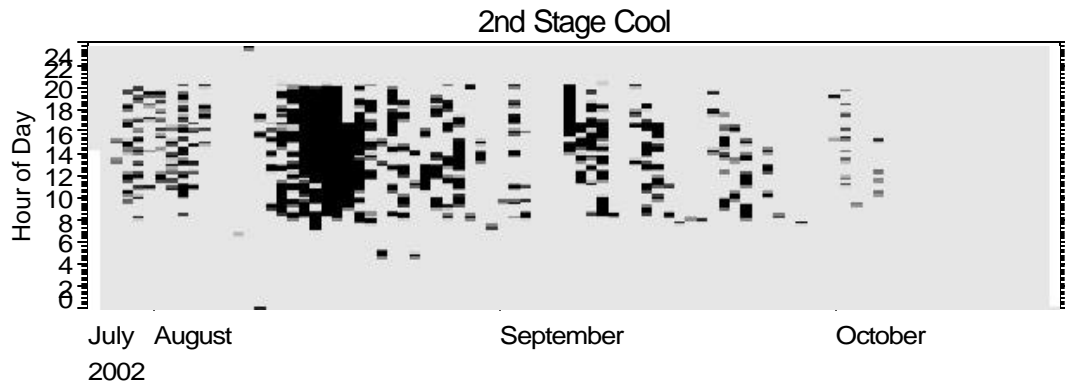
**Table 3. Summary of Site and Data Collection Events**

July 26, 2002	Data collection begins
October 6-10, 2002	RTU supply fan runs constantly
October 10, 2002	RTU supply fan switched to auto mode (cycles with heating & cooling)
October 21, 2002	Last day of cooling activity

Figure 14 below includes shade plots of system activity for the two compressors, supply fan, and condensate tipping bucket. Each day of operation is qualitatively shown as a vertical stripe on the shade plot, with darker shades indicating more operation or use. During the cooling season, the supply fan ran continuously during the day. The RTU runs nearly all the time in 1<sup>st</sup> stage cooling during the summer months. In the fall, 1<sup>st</sup> stage compressor operation becomes more sporadic. The 2<sup>nd</sup> stage compressor operated sporadically, except during the hottest days of August.



Day (MAX/MIN = 15.00/ 0.00 minutes)



Day (MAX/MIN = 15.00/ 0.00 minutes)

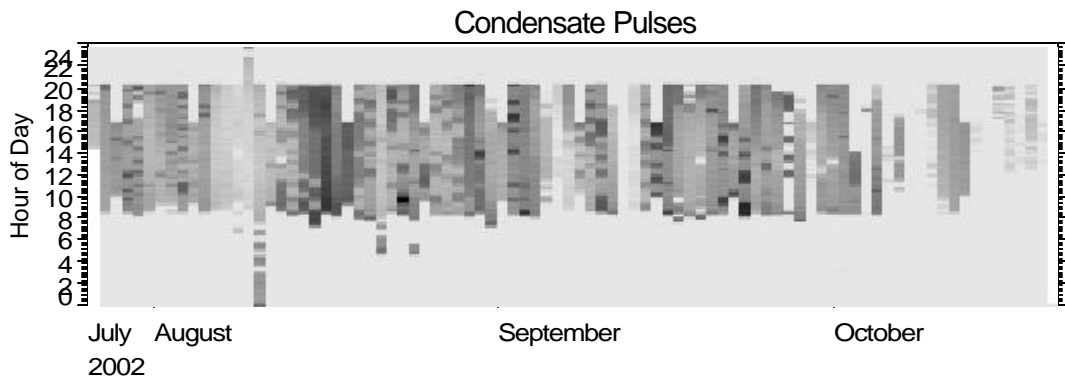


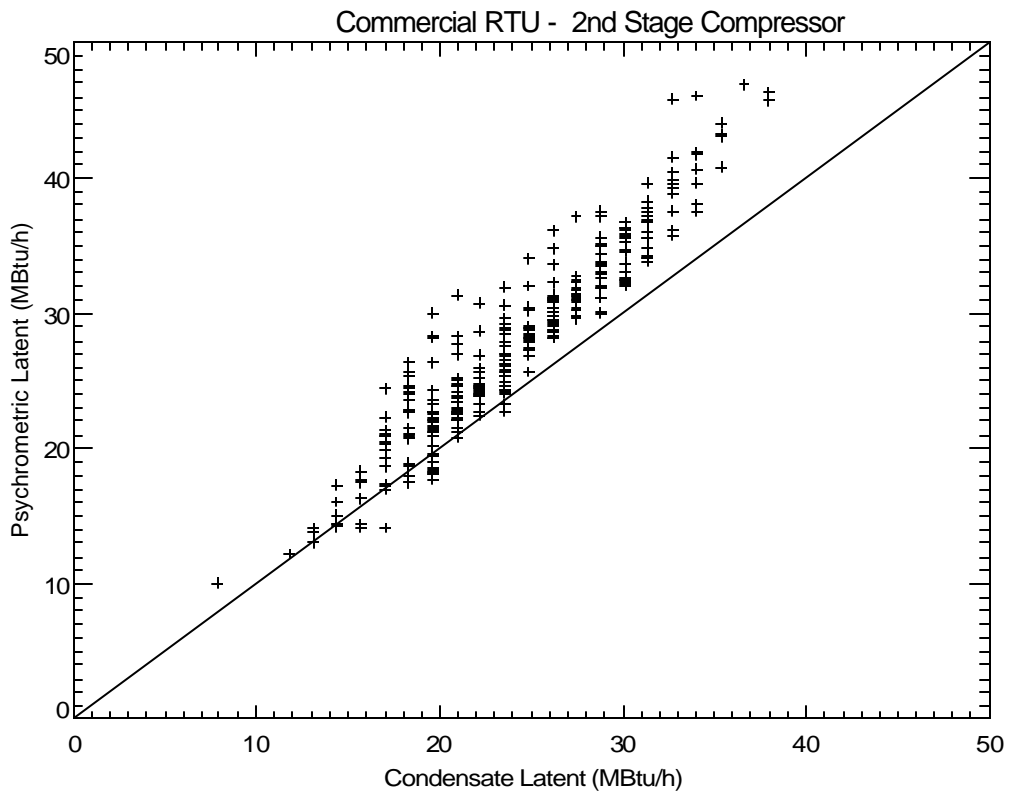
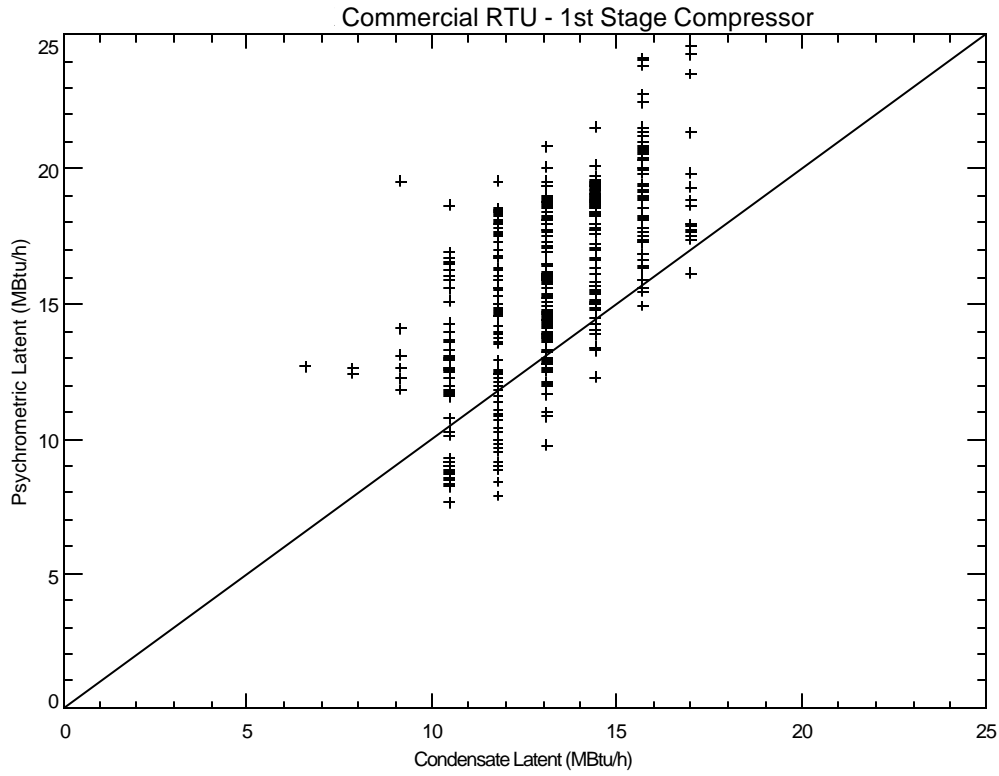
Figure 14. Shade Plots of Compressor, Supply Fan, and Condensate Flow

## **Latent Capacity**

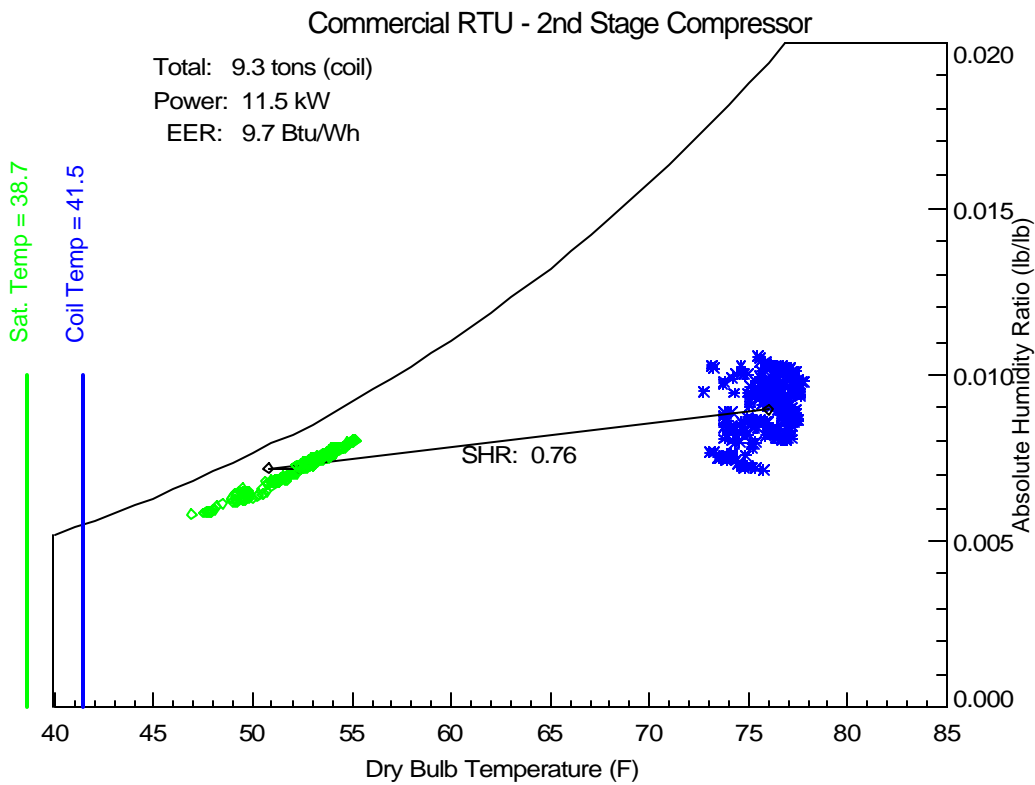
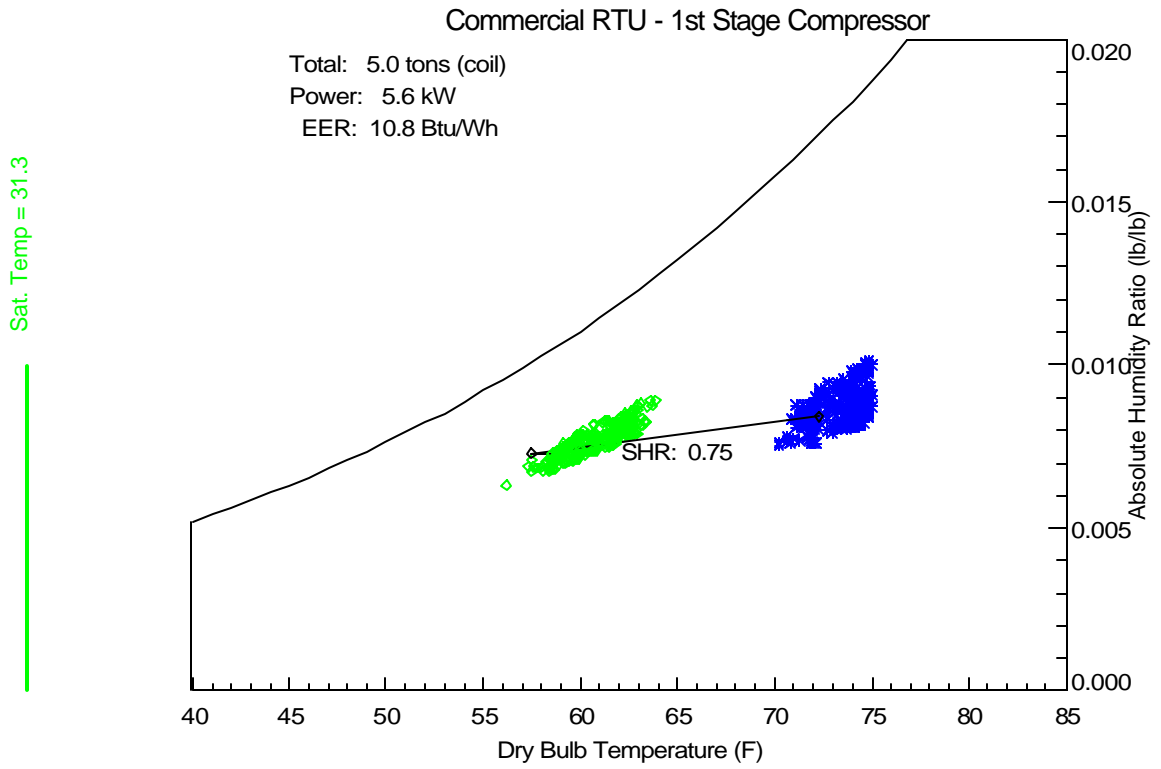
Figure15 compares the latent capacity of each stage calculated from the condensate flow as well as from the psychrometric state points and airflow. The plots only include data when the compressor had been on continuously for 30 minutes prior to ensure steady state was achieved. Additionally for first stage cooling, points are only plotted for periods when the second stage had not run during the previous 30 minutes and when the entering temperature was between 70° and 75° F and relative humidity between 45 and 55 %. The latent capacity based on condensate removal is slightly lower than the psychrometric -based capacity for both cooling stages.

Figure16 shows the process line for cooling on the psychrometric chart. The smaller data points correspond to the 15-minute data records described above. The line and the larger three points correspond to the average conditions: 1) at the coil inlet, 2) at the coil outlet, but before the fan and 3) after the supply fan.

The average SHR for the coil – or the slope of the process line – is also shown on the plot. The sensible heat ratio is 0.75 for first stage and 0.76 for the second stage. The similar SHRs for both stages are expected since the evaporator coil is face split. The saturated suction temperature (SST) with the 1<sup>st</sup> stage compressor on is only 31° F. When the 2<sup>nd</sup> stage comes on, the SST for compressor increases to 38°F. The suction temperature as recorded by the thermocouple on the return bend of the 2<sup>nd</sup> stage evaporator section is about 41° F. The SST of the 1<sup>st</sup> stage compressor increases in part because the entering conditions are 3-4°F higher when stage 2 is on.



**Figure 15. Comparing Condensate and Psychrometric-based Latent Capacity**



**Figure 16. Cooling Process Lines for AC Coils at Steady State Conditions**



## Space Conditions

Two HOBO T/RH dataloggers were installed in the store. The resulting daily space humidity trends are shown in Figure 17 and compared to daily ambient humidity for Logan Airport (from NCDC). The HOBO space sensors were also found to be in reasonable agreement with the inferred return air condition at the RTU. Figure 17 and Figure 18 show that the east sensor is maintained at slightly cooler and drier conditions than the west sensor. The west sensor was closer to the RTU entering conditions.

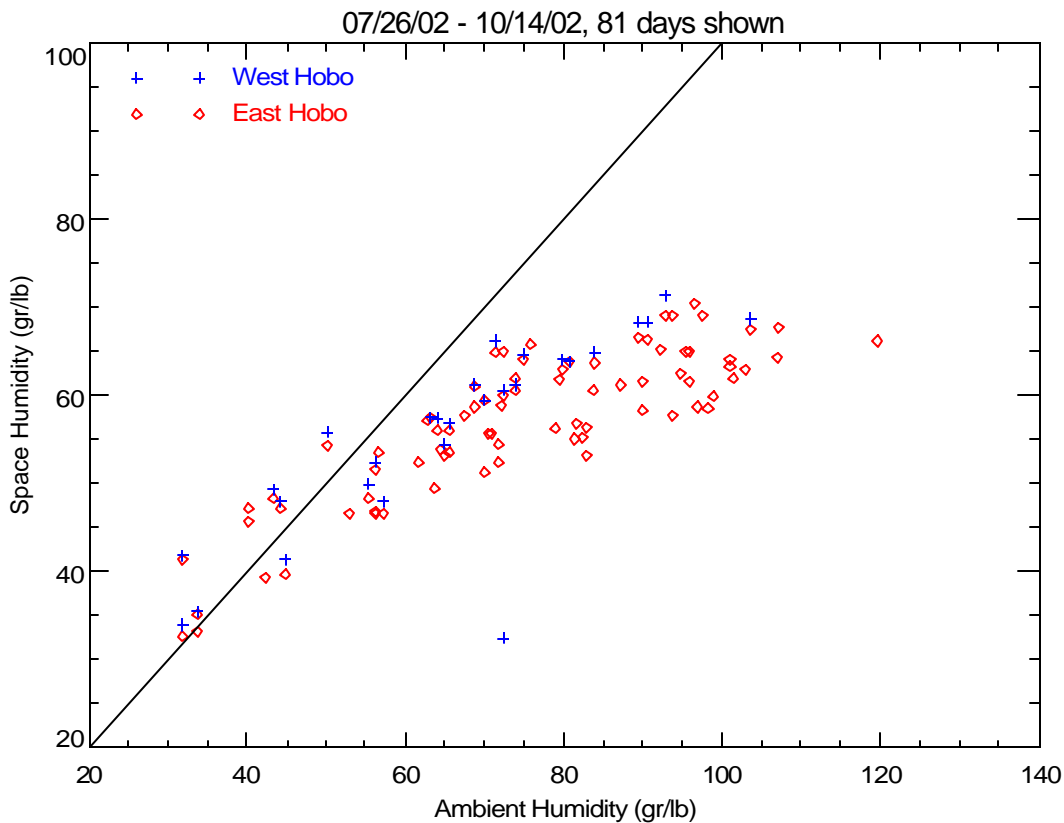


**Figure 17. Space Humidity Trend with Ambient, Based on HOBO Loggers on the East and West of the Store**

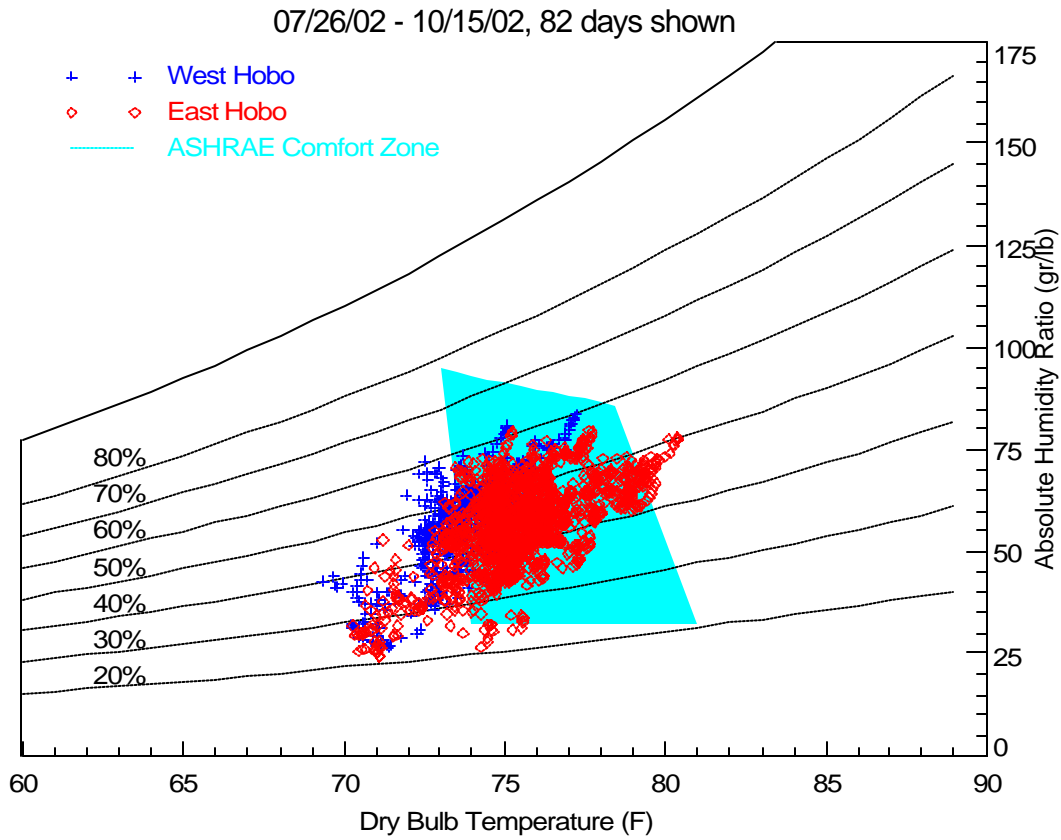


**Figure 18. Space Conditions Shown on the Psychrometric Chart**

Figure 19 shows the typical daily space temperature and humidity profile (based on the east-side HOB0 data) for a hot day in July. The daily trend shows the expected variation with time of day and compressor operation. Both humidity and temperature increase at night with the unit off.

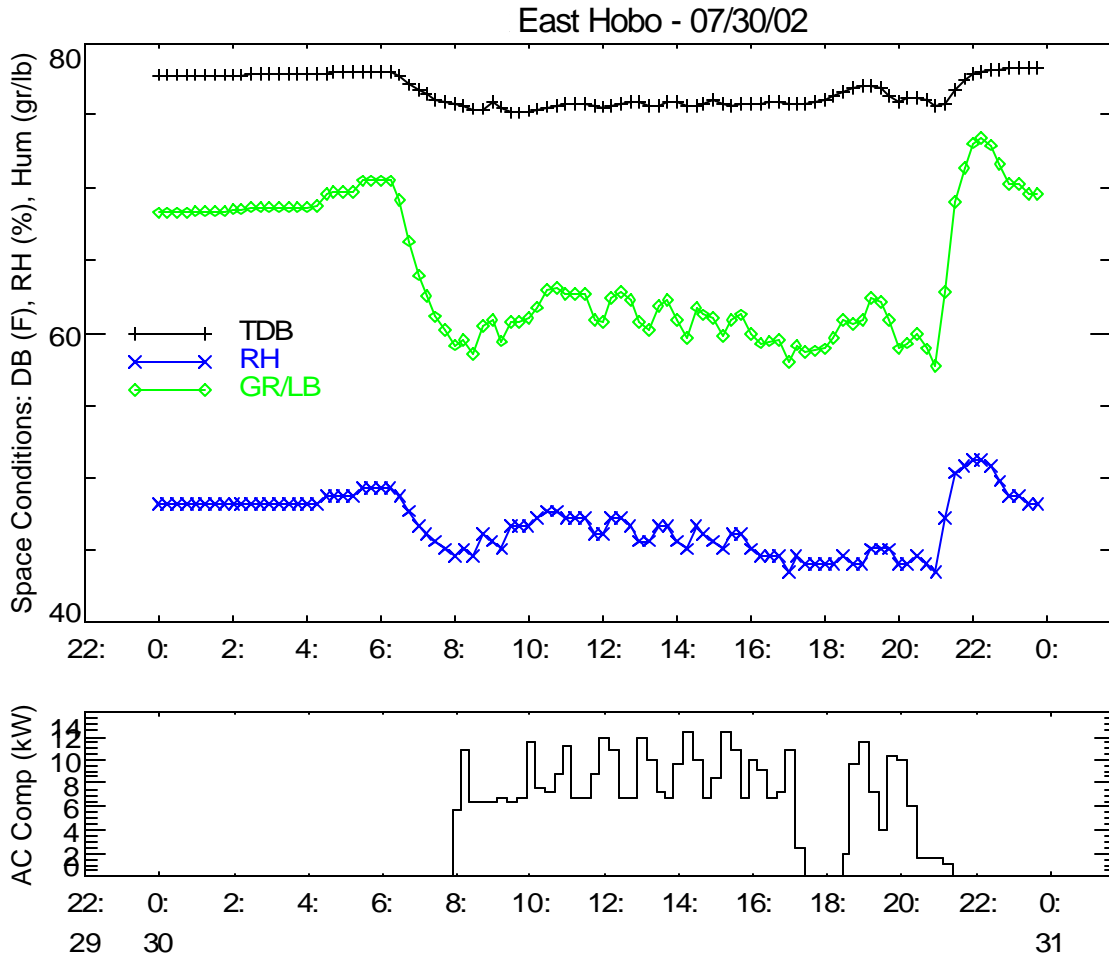


**Figure 19. Daily Profile of Space Conditions for a Hot Summer Day (July 30, 2002)**

## **Control Details**

Figure 20 shows a typical early morning operating pattern for the RTU. The system is controlled by the EMS to start slightly after 8 am. Then if the space temperature is high enough, the second stage compressor is allowed to come on after a 10-minute delay. The condensate delay time (i.e., the time between initial compressor startup and the first recorded condensate pulse), is shown on the plot to be about 15 minutes in this case. The first stage cooling typically runs throughout the day during the cooling season while second stage cycles on and off as required (see Figure 14).

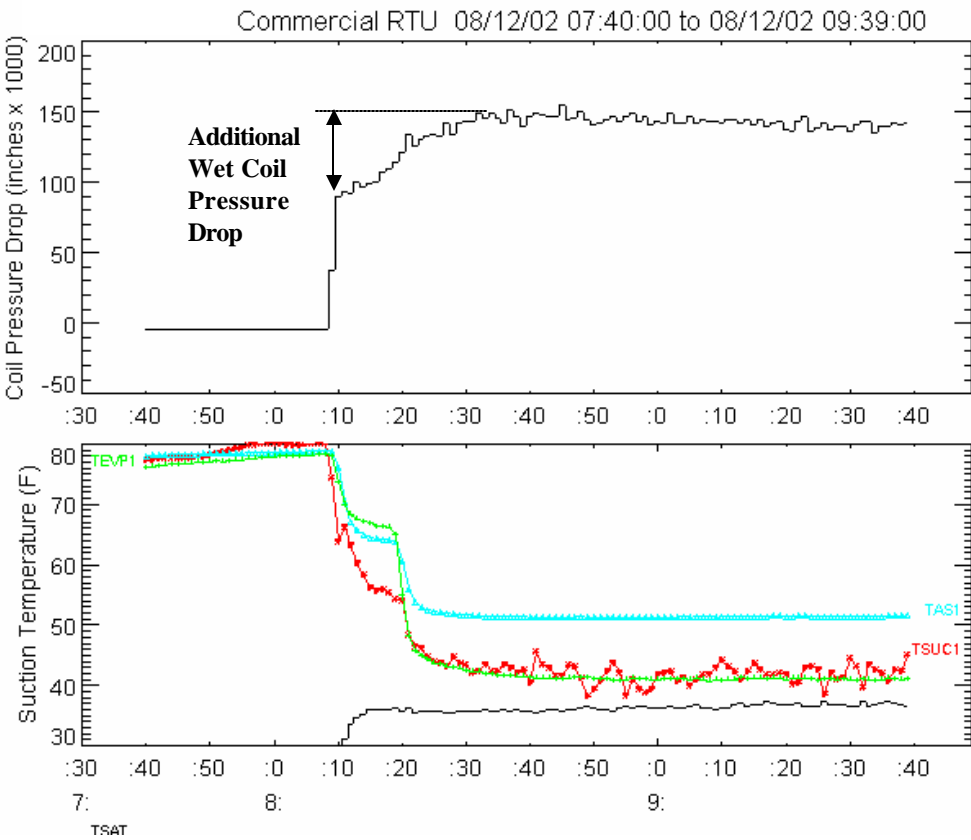
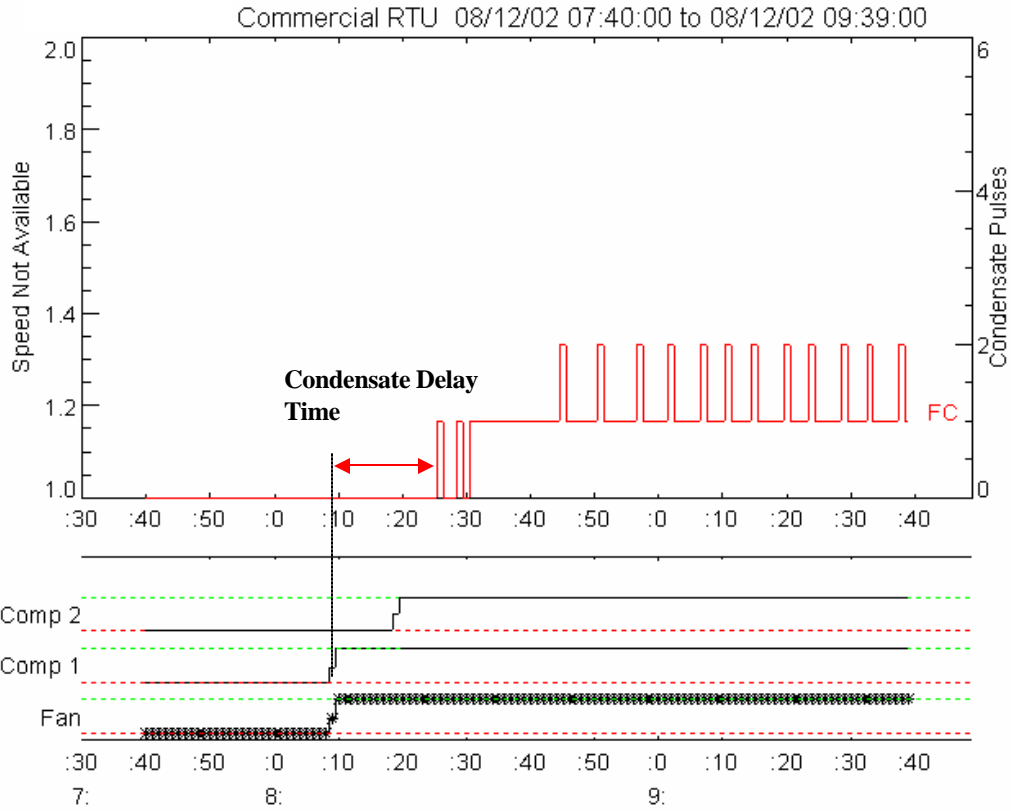


**Figure 20. A Typical Morning Startup Cycle When Both Stages Operated: August 12**

## Condensate Delay Time

One key indication of the coil's moisture-holding capacity is the time it takes for condensate to first fall from the coil. This time delay is similar to the parameter  $t_{\text{wet}}$  from LHR Model. Figure 19 shows operating cycles for the AC unit from August 12, a day when both units had been off overnight and then started up under fairly humid conditions in the morning.

Figure 21 shows the condensate delay times for several compressor startup cycles for 1<sup>st</sup> stage cooling alone and with both cooling stages on. The criteria for including cycles on the plots were:

- There were no condensate pulses in the previous 2 hours before compressor startup,
- The 1<sup>st</sup> stage cooling was continuously on at least until the first condensate pulse occurred,
- The condensate event was followed by at least one other condensate pulse.

Several cycles met the criteria for the AC unit with both stages and single-stage cooling active. Data from the lab and other field test sites typically showed a decreasing condensate delay time with increasing dew point temperature. The same trend is also apparent here. Because of how this RTU was controlled each morning, the delayed operation of the 2<sup>nd</sup> compressor at startup seems to have very little impact on the condensate delay time.

Table 4 summarizes the nominal condensate delay time and the increased pressure drop due to the wet coil. The wet coil pressure drop demonstrates two distinct operating levels corresponding to first and second stage operation (where the coil is 50% of 100% wetted).

**Table 4. Summary of Nominal Condensate Delay and Wet-Dry Pressure Drop Calculations**

	<b>RTU Unit</b>
Entering Dew Point (F) (avg conditions before first pulse)	60
Time Delay for First Condensate Pulse (minutes)	8-12
Wet-Dry Coil Pressure Drop (in H <sub>2</sub> O x 1000)	20-50 (1 <sup>st</sup> stage only), 50-60 (both stages)

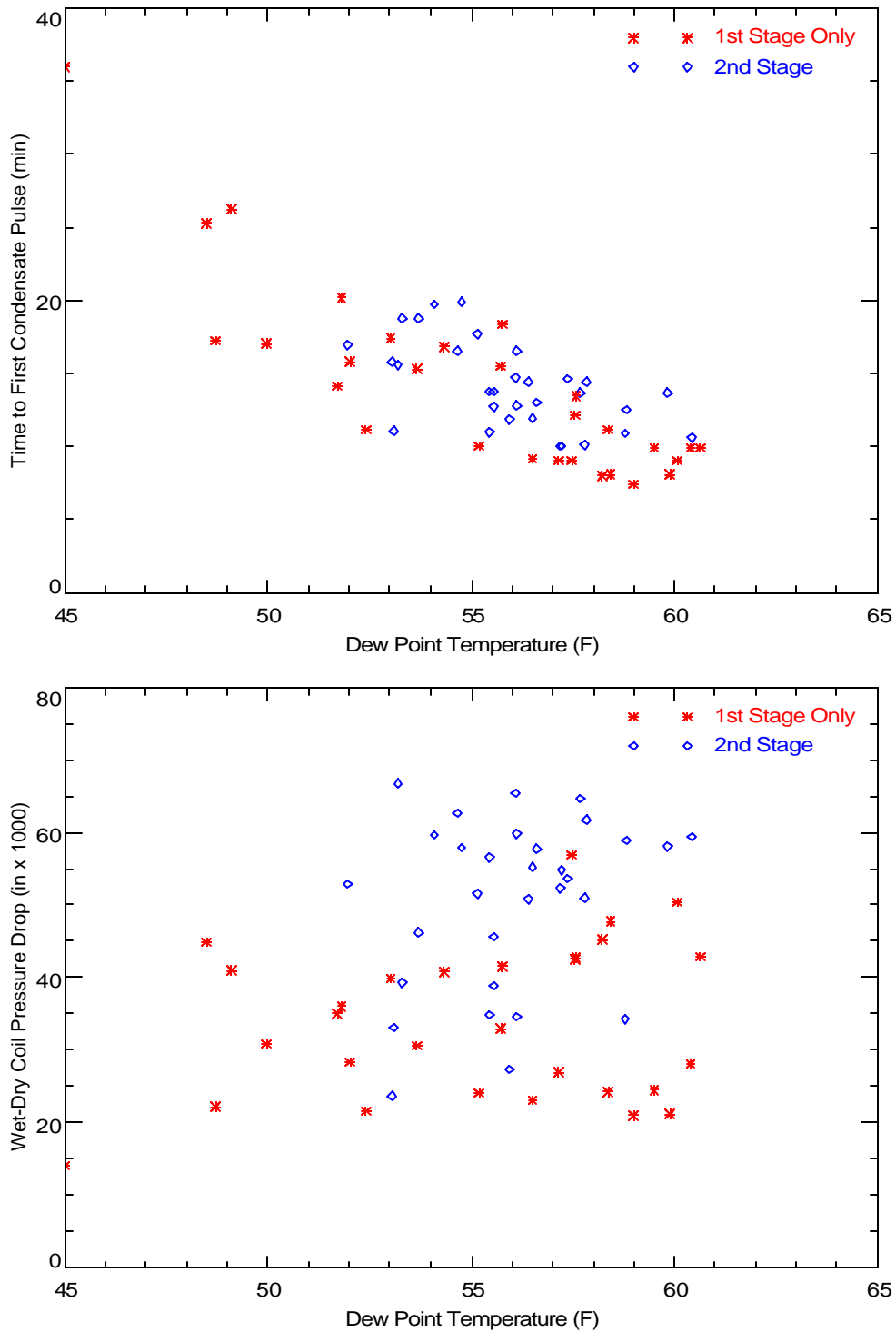


**Figure 21. Condensate Delay Time and Wet-Dry Pressure Drop as a Function of Entering Dew Point**

## Thermostat Cycling Rate

On a single stage AC system, the compressor cycling rate can typically be described by the parabolic curve shown in Figure 22 below. The single-parameter parabolic curve is defined as

$$N = 4 \cdot N_{\max} \cdot X \cdot (1-X)$$

Where  $N$  is the number of on-off cycles per hour and  $X$  is the runtime fraction. The behavior of the 2<sup>nd</sup> stage RTU compressor approximately follows this trend. Deviations from the line are due to forced on/off cycles by the EMS time clock controls.

The maximum cycling rate  $N_{\max}$  occurs at a runtime fraction ( $X$ ) of 0.5. While most single stage AC systems have a value of  $N_{\max}$  around 3, the data here imply a value closer to 0.9 cycles/hour. The measured data shown on the plot were determined from 1-minute records by calculating the exact length of each total on/off cycle ( $t_{\text{cyc}}$ ) as well as the compressor runtime ( $t_{\text{on}}$ ). Then for each cycle the runtime fraction ( $X = t_{\text{on}}/t_{\text{cyc}}$ ) and the cycle rate ( $N = 1/t_{\text{cyc}}$ ) can be determined.

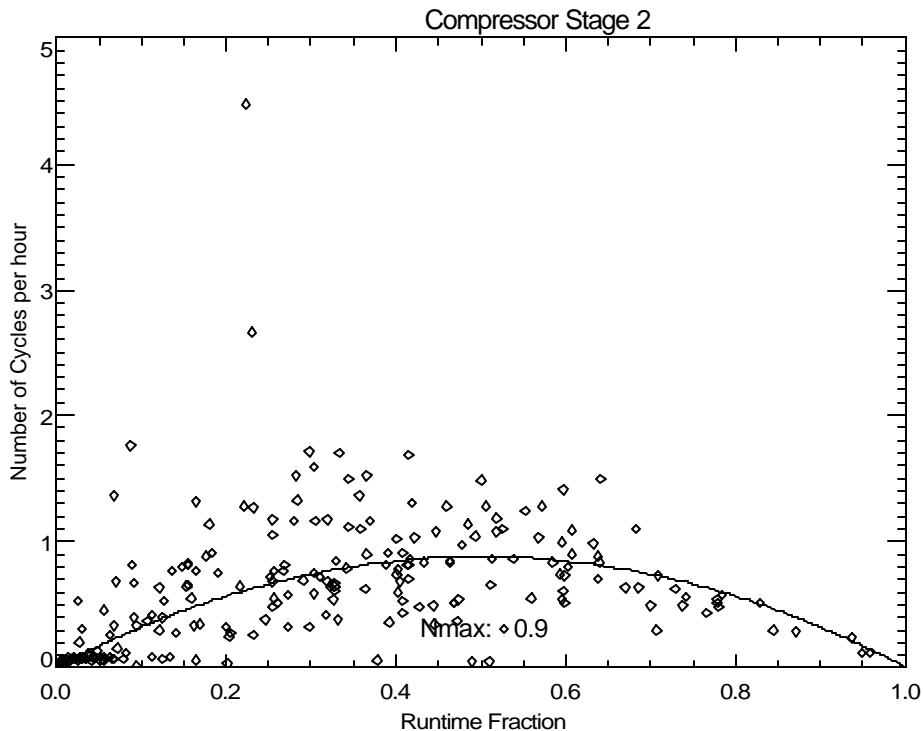


**Figure 22. Thermostat Cycling for 2<sup>nd</sup> Stage Compressor Operation**

## Cooling Energy Trends

Figure 23 shows that the total cooling energy use for the RTU demonstrates a clear linear trend with the daily average ambient temperature. The ambient temperature is from the NCDC data for Logan Airport in Boston. Energy use is flat below 44°F since only the supply fan operates when heating is required.

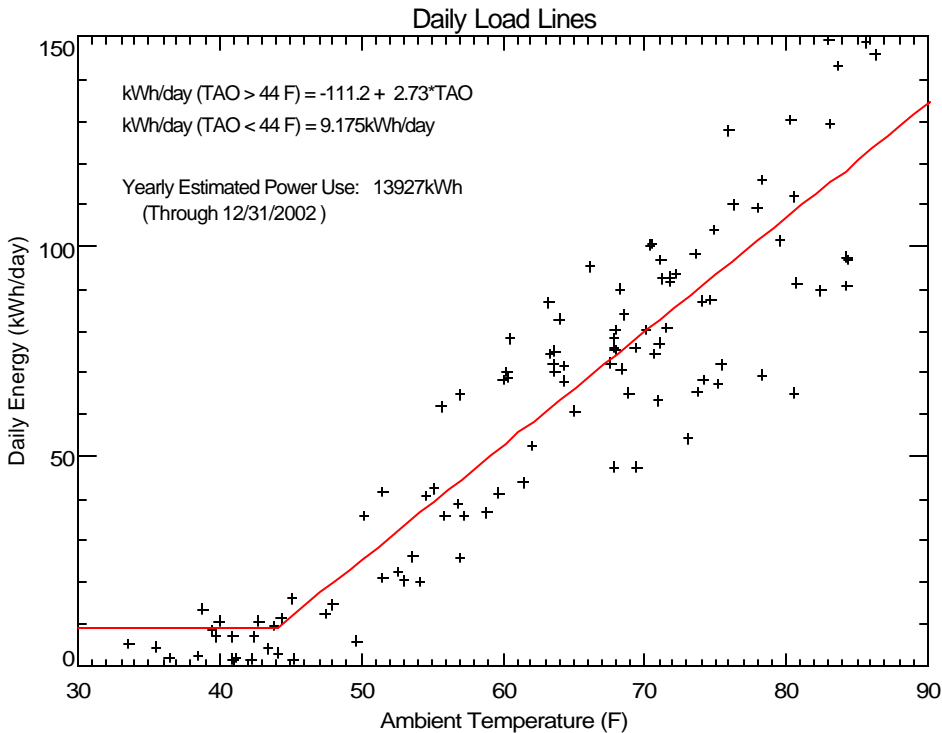


**Figure 23. Cooling Load Line for Both Units Combined**

## Off-Cycle Evaporation Rates

Each day the AC unit operates as if it were in the constant fan mode during occupied hours, allowing off-cycle performance of the cooling coil to be evaluated. Figure 24 shows the off-cycle sensible capacity for several cycles when the compressor had just stopped operating, and one or more condensate pulses had occurred in the last 10 minutes of compressor operation. The plot includes ‘\*’s after the third minute, which is about the time when refrigerant dynamics appear to have died down and the sensible capacity is driven by the evaporation process. We make the assumption, based on laboratory data, that the coil operates as an evaporative cooler with latent and sensible capacity summing to zero after this time.



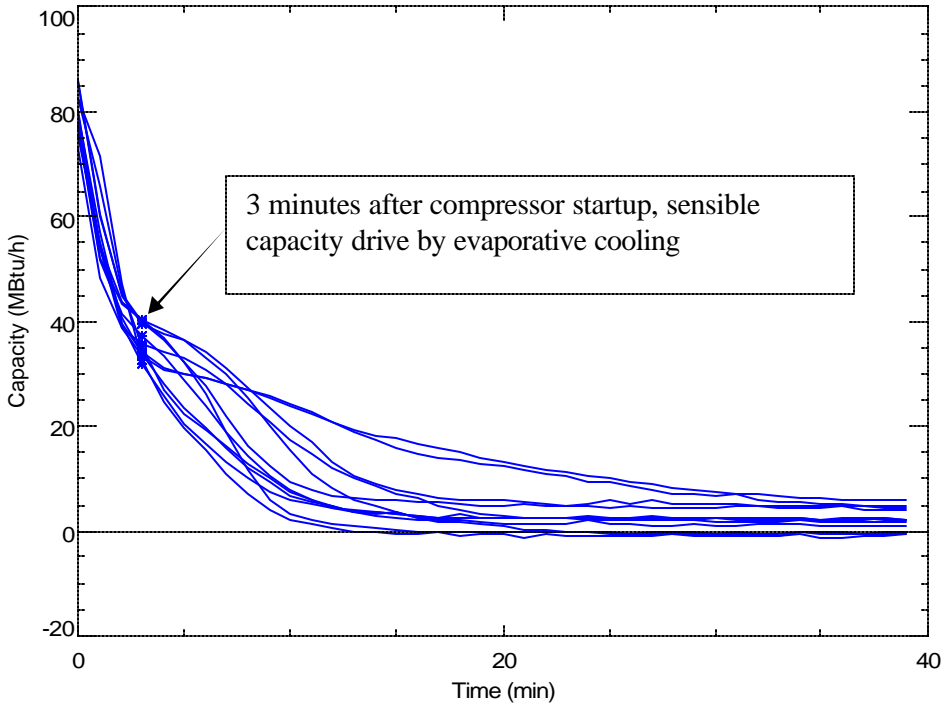


**Figure 24. The Trend of Sensible Capacity for Several “Wetted” Off-Cycles**

Figure 25 and Figure 26 compare the initial evaporation rate (i.e., the points noted as \*s on Figure 21 above) for each off-cycle meeting the criteria for being fully wetted. The initial evaporation rate is about 40 MBtu/h. Figure 25 shows that the evaporation rate is a function of the wet bulb depression (i.e., the DB minus the WB), as would be expected. The line on the plot shows the theoretical trend projected to zero evaporation at no wet bulb depression. The saturation effectiveness, which is defined below, is shown on Figure 26.

$$\eta_{\text{sat}} = Q_{\text{evp}} / (1.08 \times \text{cfm} \times (\text{DB} - \text{WB}))$$

The average effectiveness is 0.863, which corresponds to an NTU of 1.99. The NTU of the coil as an evaporative cooler is defined as:

$$\text{NTU} = (k \times A) / \text{cfm}^{0.2}$$

Where A is fin surface area of the coil (762.3 ft<sup>2</sup>) and the cfm is 3200 cfm. Using these parameter values, the constant k = 0.013, which is lower by a factor of two compared to the values determined from the laboratory measurements for other coils. The value k may have been lower because the second stage section of the cooling coil was not fully wetted or because of the uncertainty in precisely identifying the initial evaporation rate (Q<sub>evp</sub>) in Figure 24 above.

The data in both Figure 25 and Figure 26 demonstrate much more scatter than we have observed at the other sites, in part due to the narrow range of wet bulb depressions shown on the plot.

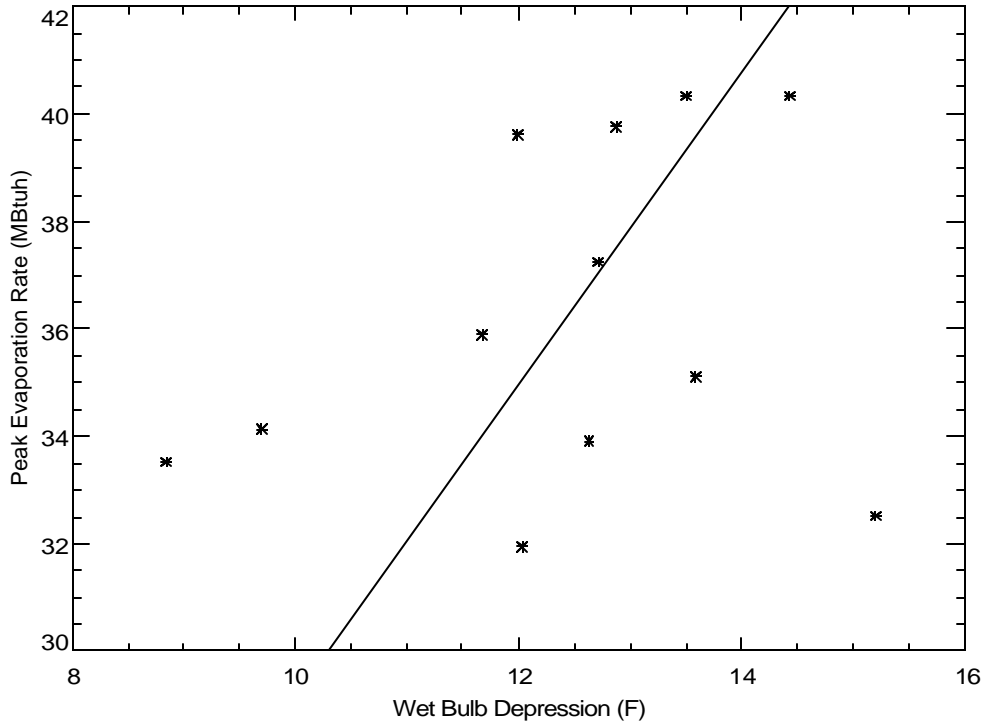


**Figure 25. The Trend of Peak Off-Cycle Evaporation Rate With Wet Bulb Depression**

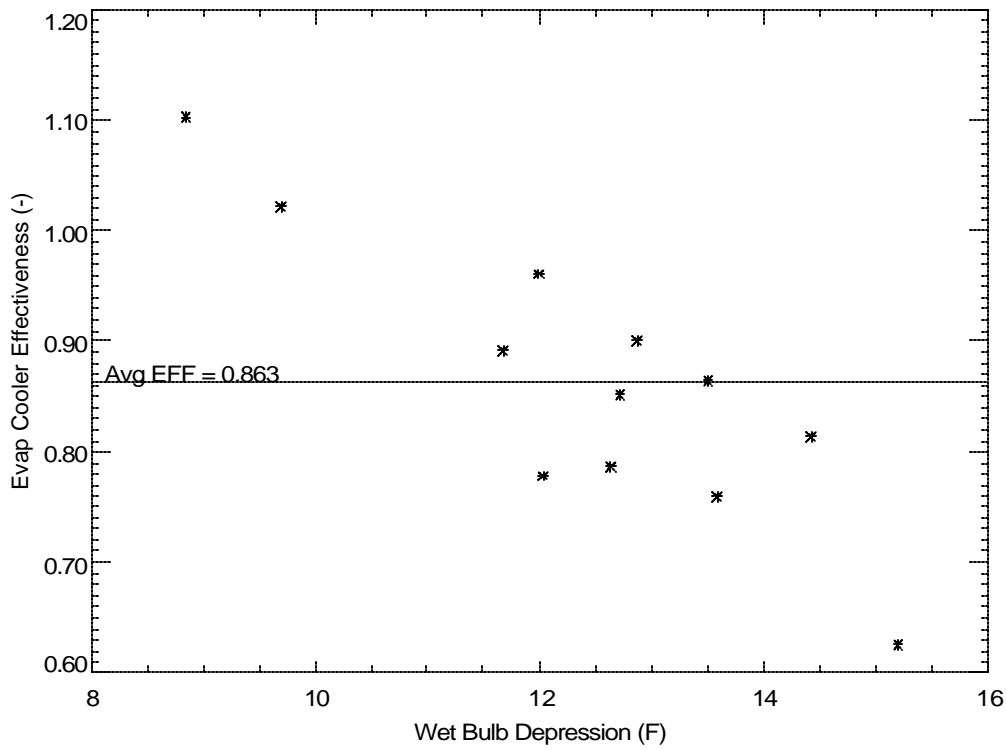
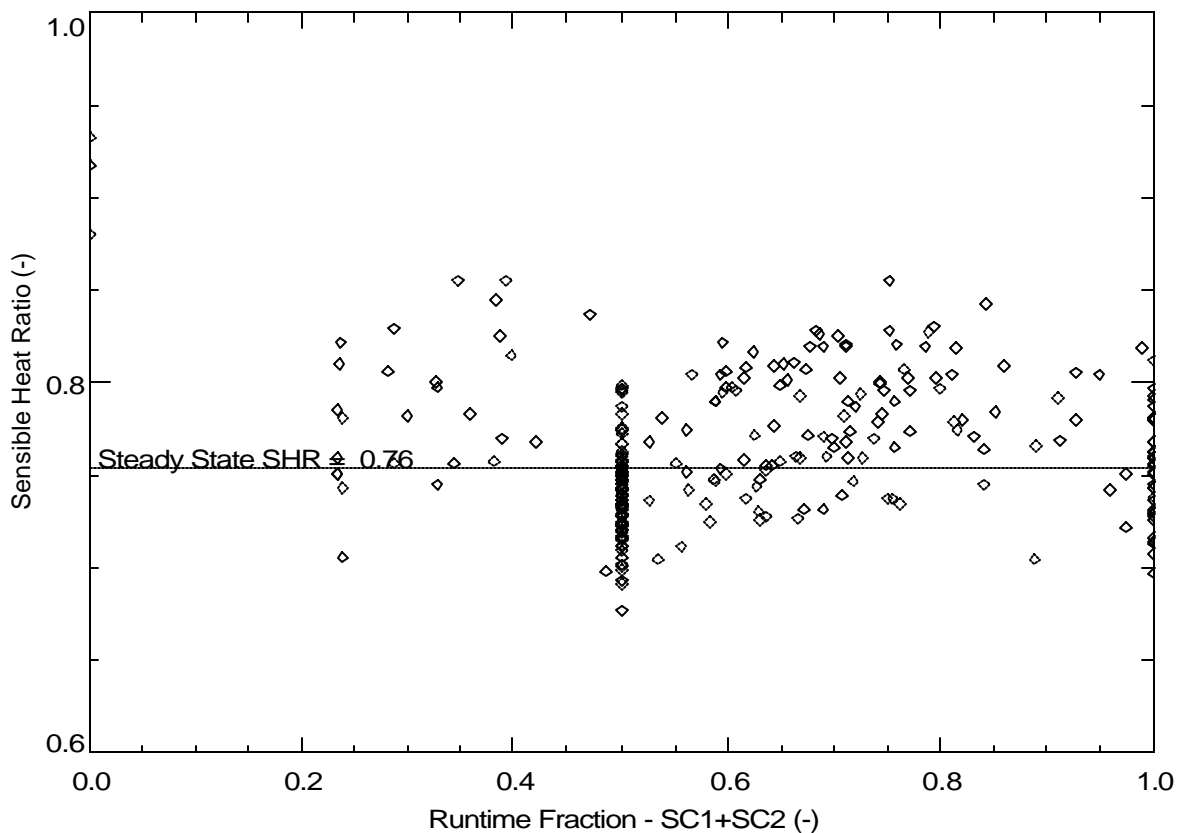


**Figure 26. Evaporative Cooler Saturation Effectiveness of Cooling Coil**

## **Part Load SHR**

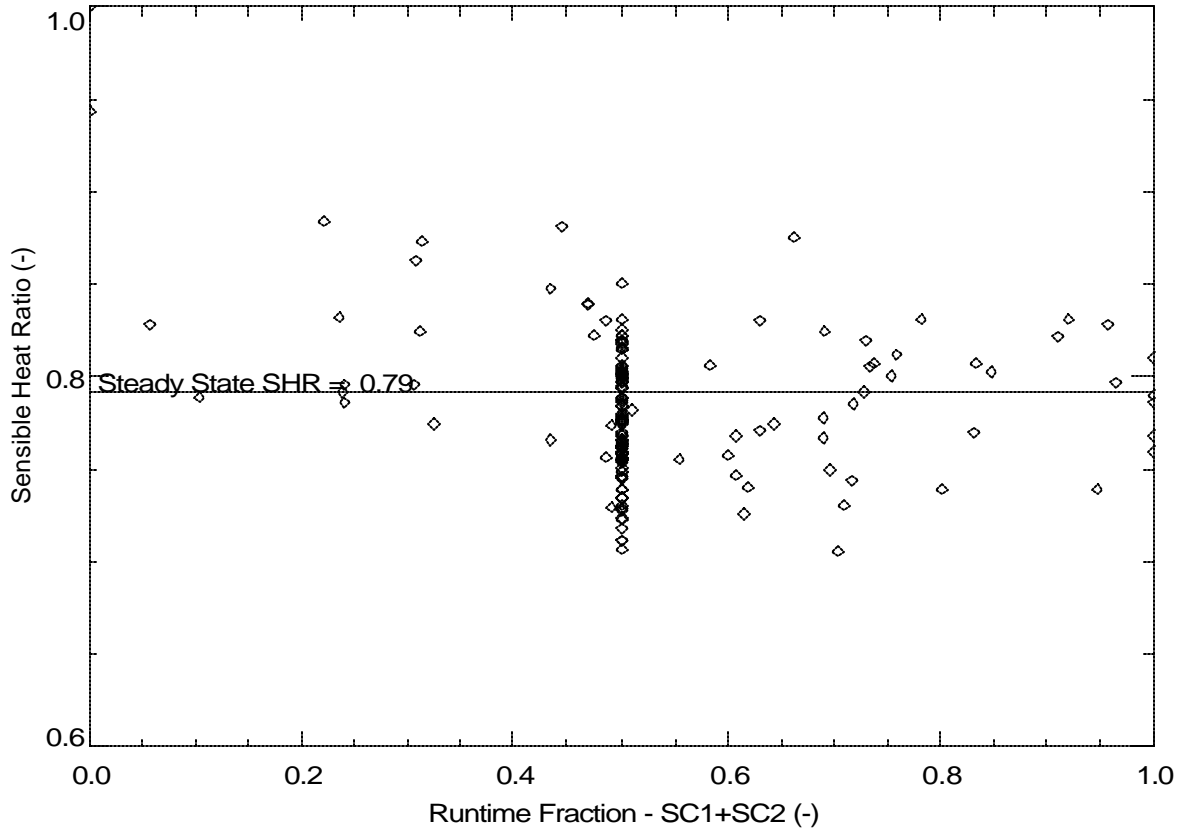
The moisture removal capacity of a cooling coil is reduced at part load conditions. The SHR is calculated using the coil temperature difference, air flow, and condensate readings on an hourly basis. Data are only included on the plot when the hourly average entering conditions are between 75° to 80° F and 45 to 55 % relative humidity. Both the runtime fraction (RTF) and SHR are averaged hourly. The runtime fraction in this case is SC1+ SC2 divided by 2. The steady state SHR listed on the plot with a dotted line approximately corresponds to the SHR of the process lines shown on Figure 16.

Figure 27 shows the SHR trend with the runtime fraction. There is little to no degradation at runtime fractions above 0.5, since compressor 1 is running continuously at these conditions. Only a mild amount of degradation is apparent as compressor 1 cycles on and off (for the RTF below 0.5), even in the constant fan mode.



**Figure 27. Part-Load Sensible Heat Ratio vs. Runtime Fraction (DB: 75-80° F, RH: 45-55%)**

Figure 28 shows the same trend but with data limited to the cooler range 70° to 75° F (and still with 45 to 55% relative humidity). This puts a little more bias towards the conditions when 1<sup>st</sup> stage operation is more likely to operate alone. This plot shows slightly more degradation since conditions are cooler (and drier in absolute terms). As a result, the steady-state SHR is higher as well.



**Figure 28. Part-Load Sensible Heat Ratio vs. Runtime Fraction (DB: 70-75°F, RH: 45-55%)**

The moisture holding capacity of the coil was difficult to determine by off-cycle integration in this case since the system rarely had two compressors running followed by a long off-cycle. Therefore we estimated the moisture holding capacity using the measured delay time (a good surrogate for  $t_{wet}$ ) and the steady-state latent capacity of the unit. The steady state latent capacity of the unit was 30 MBtu/h (25% of 10 tons). The nominal delay time from Table 4 above was 8-12 minutes.

The mass of water stored on the coil is equivalent to  $Q_L \times t_{wet}$ , assuming a delay of 10 or 12 minutes:

$$\text{Mass} = 30 \text{ MBtu/h} \times 10 \text{ or } 12 \text{ minutes} \times 1 \text{ hr}/60 \text{ minutes} / 1.06 \text{ MBtu/lb} = 4.7 - 5.7 \text{ lbs}$$

This mass in per unit fin area becomes: 6.2 - 7.4 lb per 1000 ft<sup>2</sup>, which is similar to what has been observed in the lab.

## **APPENDIX I5**

### **Summary of Data for Field Test Site 5**

## Site #5 – Cocoa, FL



**Figure 1. East Exposure**

### **System Description**

This site utilizes a single 3 ½-ton split heat pump system. The condensing unit is located on the south side of the house adjacent to the garage. The variable-speed air handler is located in the garage. The return air is ducted separately from the living room, family room, and back bedrooms to a common return plenum. Supply air is similarly distributed via attic ductwork throughout the home. The unit was installed in April 2002. Prior to the start of this project an air conditioning contractor was hired to install a new thermostat. The new thermostat (Carrier “thermidistat”) was purchased for this project to enable super dehumidify mode operation; however, only enhanced and 0/0 mode operation were tested since indoor humidity levels were typically maintained between 40% and 45% RH.

Unit #1 – Split System Heat Pump, 3.5 ton  
Bryant Condensing Unit #663CJX042000ABAA  
Carrier AHU #FK4CNB006000AGAA

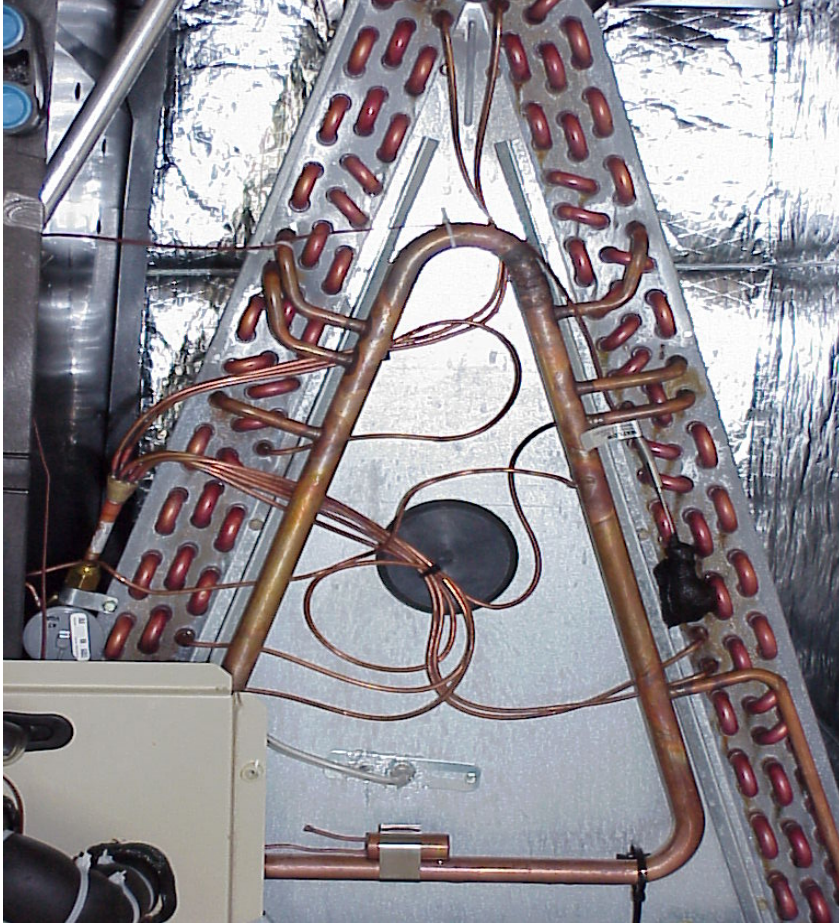


**Figure 2. AHU A-Coil**

**Carrier AHU Easy Select Board Settings**

Aux Heat kW/cfm = 4  
 AC/HP Size = 3  
 Type = HP-eff  
 CFM adjust = NOM  
 ON/OFF delay = enh, 0/0 (alternated setting during data collection)  
 Cont Fan = medium

**Thermidistat Setpoints**

8:00 am	78 Cool	60 Heat	Day
4:45 pm	78 Cool	68 Heat	Evening
10:00 pm	79 Cool	60 Heat	Sleep
6:00 am	78 Cool	68 Heat	Wake

High humidity setpoint = 60% RH

## Sensors and Data Logger Connections

**Table 1. Data Logger Channel Assignments and Sensor Identification**

Channel	Data Point	Description	Units	Sensor
DI1	TC MUX			
DI2	VOLT MUX			
SE5	TREF	Thermocouple Reference Temperature	C	Campbell Scientific TC107
SE6	FSA	Supply Air Flow Rate	CFM	Setra 264 (0 - 0.25 inches)
DI4	Not Used			
DI5	DPC	Pressure Drop Across Coil	in WC	Setra 267 MR (0 - 1 inch)
DI6	Not Used			
P1	WU	Compressor Power	kWh	Ohio Semitronic (W062B)
P2	WF	Fan Power	kWh	Ohio Semitronic (W005B)
C1	Not Used			
C2	Not Used			
C3	Not Used			
C4	MUX-cntrl			
C5	MUX-cntrl			
C6	SF	Fan Status	On/Off	Veris (Hawkeye 900)
C7	FC	Condensate (Interrupt Subroutine 97)	lbs	Texas Electronics tipping bucket
C8	SC	Compressor Status (Interrupt Sub 98)	On/Off	Veris (Hawkeye 900)
MUX-1	TAM	Return Air Thermocouple	F	Type-T Thermocouple
MUX-2	RHM	Return Air Relative Humidity	%	Vaisala HMD60U
MUX-3	TAS	Supply Air Thermocouple	F	Type-T Thermocouple
MUX-4	RHS	Supply Air Relative Humidity	%	Vaisala HMD60U
MUX-5	TSUC	Suction Thermocouple	F	Type-T Thermocouple
MUX-6	TFR	Family Room Space Temperature	F	General Eastern Space Mount
MUX-7	TEVAP	Evaporator Thermocouple (1st U-bend)	F	Type-T Thermocouple
MUX-8	RHFR	Family Room Space Relative Humidity	%	General Eastern Space Mount
MUX-9	TLIQ	Liquid Line Thermocouple (before EXP)	F	Type-T Thermocouple
MUX-10	PSUC	Suction Pressure at Condenser	psi	Setra C207
MUX-11	TAO	Outdoor Temperature	F	Type-T Thermocouple
MUX-12	RHO	Outdoor Relative Humidity	%	Vaisala HMD60U
MUX-13	TCSUC	Suction Thermocouple at Condenser	F	Type-T Thermocouple
MUX-14	IB	Fan current	amps	Veris (Hawkeye 922)



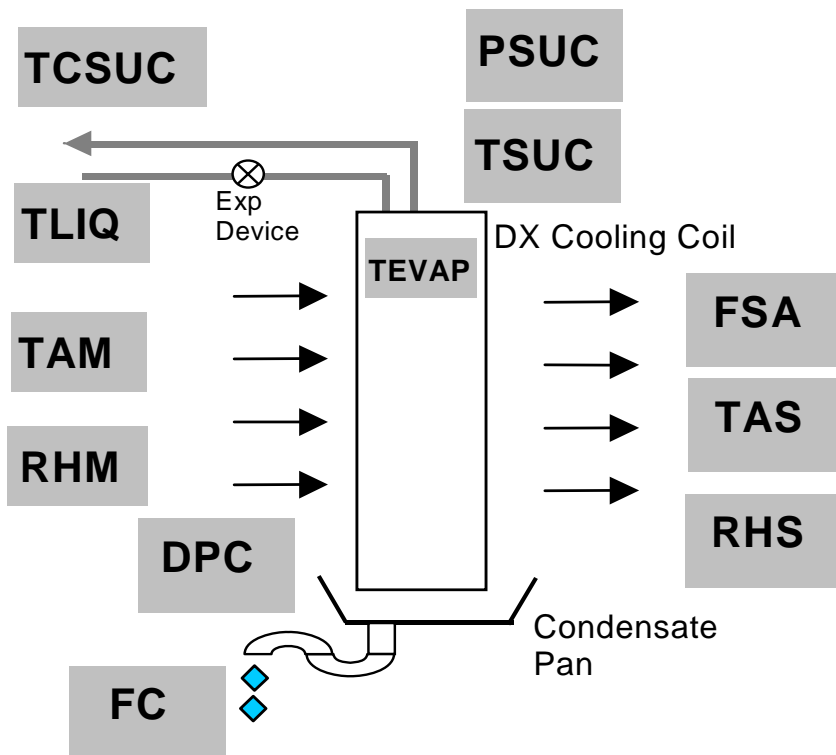


Figure 3. System Schematic

### Coil Measurements

Coil Type	"A" coil	
Coil Face Area	1049 sq. in.	
Number of rows	3 (per side)	
Tubes per row	30	
Tubing diameter	3/8" OD	
Notes:	<p>Total surface area, including area behind some small flanges = <math>2 \times (17 \frac{5}{8}'' \text{ wide} \times 29 \frac{3}{4}'' \text{ tall}) = 1049 \text{ in}^2 = 7.28 \text{ ft}^2</math>. Manufacturer's data says <math>7.42 \text{ ft}^2</math> (about 2% larger). Total exposed surface area (excluding area blocked by flanges) = <math>2 \times (17 \frac{5}{16}'' \text{ wide} \times 29 \frac{1}{16}'' \text{ tall}) = 1006 \text{ in}^2 = 6.99 \text{ ft}^2</math>. One inch tube spacing within a coil row, approx. <math>\frac{3}{4}''</math> tube spacing row-to-row, approx. coil thickness = <math>2 \frac{1}{4}''</math>. Fin spacing is 15.5 fpi, lanced sine-wave fins. Copper tubing, aluminum fins. Coil has 8 circuits.</p>	

$$\text{Gross fin area: } (2.25 \text{ in}) \times (15.5 \text{ fins/in}) \times (2 \text{ sides/fin}) \times (1049 \text{ sq in.}) / 144 \text{ sq in/ft}^2 = \underline{508.1 \text{ ft}^2}$$

## One-Time Measurements

The air-conditioning system supply air flow rate was correlated to supply air duct static pressure using an Energy Conservatory Flow Grid. Measurements were made at 75% and 100% fan speed. The differential pressure measured by the flow grid was used to calculate supply air flow rate which was then correlated to supply air duct static pressure for continuous monitoring of system air flow rate.

Fan Speed	Grid dP	SA Duct Static	Conversion	CFM
70 %	29.2 Pa	10 Pa	$158.3 (29.2)^{0.5} =$	855.4
100 %	63.5 Pa	25 Pa	$158.3 (63.5)^{0.5} =$	1261.4

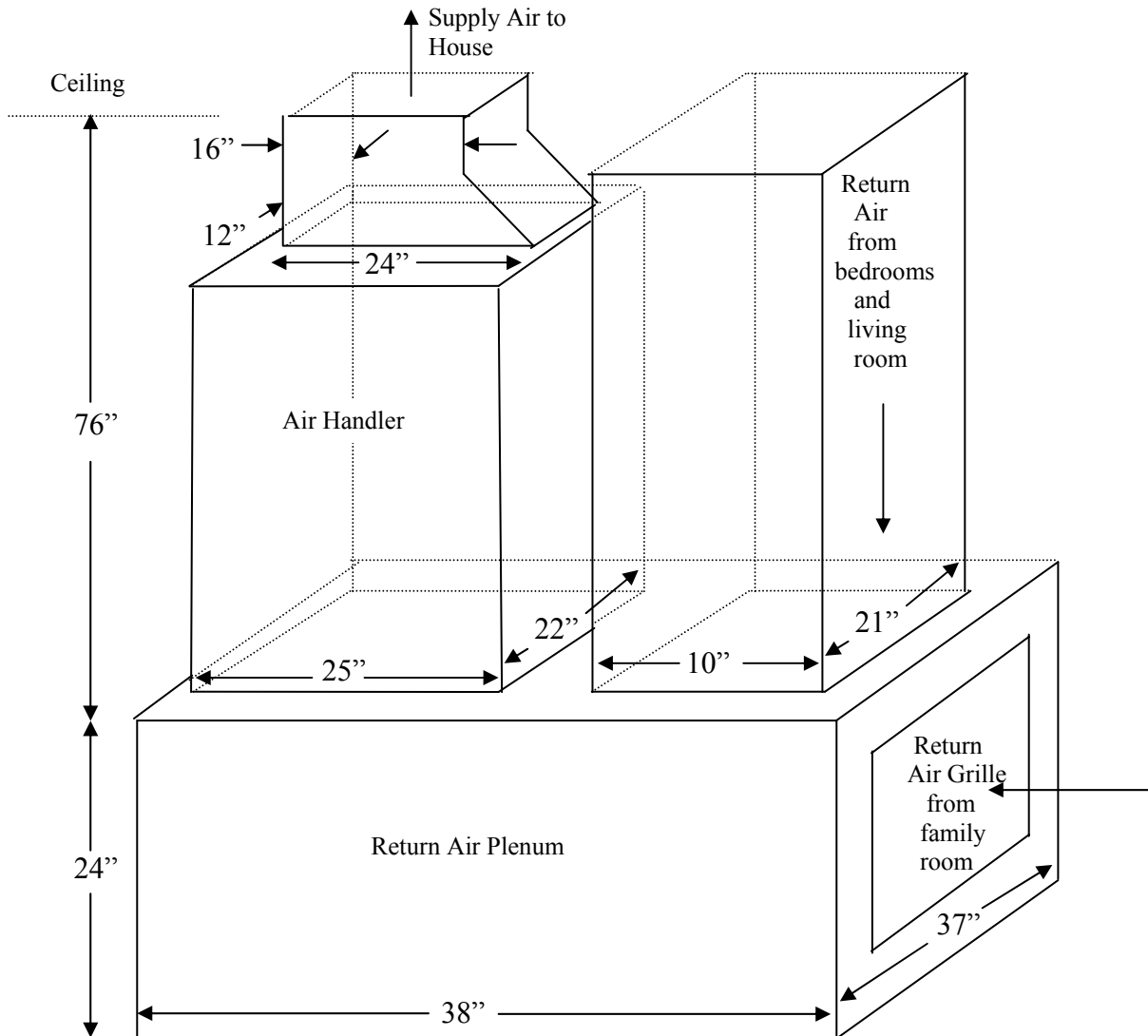
## Instrumentation

Parameter	Manufacturer	Model Number	Location, Accuracy
Temperature	Omega	TT-T-24-TWSH-SLE	Air temperature, $\pm 1^\circ\text{F}$
Relative Humidity	Viasala	HMD-60	Air relative humidity, $\pm 5\% \text{ RH}$
Power/Energy	Ohio Semitronics	W-062B / W-005B	Compressor/Fan energy, $\pm 0.5\% \text{ FS}$
Pressure	Setra	Model 264	Coil pressure drop, $\pm 1\% \text{ FS}$
		Model 267 MR	SA flow rate, $\pm 1\% \text{ FS}$
		Model 207	Refrigerant pressure, $\pm 0.013\% \text{ FS}$
Condensate	Texas Electronics	TB-525I	Tipping bucket mechanism calibrated at 0.0128 lb/tip

## Sensor Calibration

Relative humidity sensors were verified and calibrated using a General Eastern Hygo-M1 chilled mirror hygrometer ( $\pm 0.36^\circ\text{F}$  accuracy) and Type-T thermocouples with special limits of error ( $\pm 1^\circ\text{F}$  accuracy). The relative humidity sensors were placed in an environmental chamber to collect a wide range of humidity data for several days. The output of each sensor was correlated back to the reference relative humidity and a calibration equation was used to verify operation and further increase the accuracy of the sensors output to better than  $\pm 2\%$ .

The condensate tipping bucket was calibrated by weighing a known volume of water into the tipping bucket at 3 separate flow rates. The number of “tips” were recorded for each test as follows: 87 tips/1.0396 lbs at 4.31 lb/hr, 81 tips/1.0396 at 5.71 lb/hr, and 76 tips/1.0396 lbs at 18.53 lb/hr. A nominal “lb/tip” of 0.0128 lb/tip was used corresponding to a typical condensate flow rate of approximately 6 lb/hr as measured from the AC units condensate drain.



**Schematic Diagram of Air Handler Duct Layout**

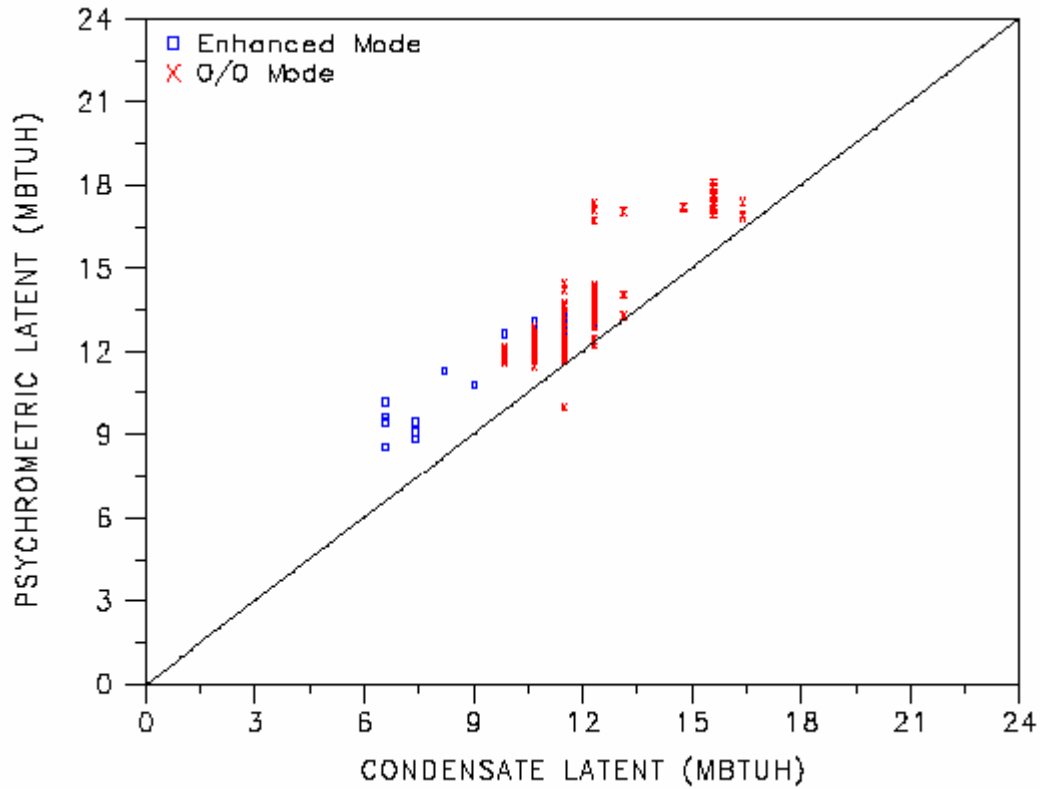
**Table 2. Data Collection Summary**

August 1, 2002	Data collection officially begins. Air handler configured in “Enhanced” mode (as configured by the installer).
Aug. 1, 2002 – Aug. 12, 2002	Space temperature sensor malfunction
Aug. 27, 2002 – Sept. 3, 2002	Supply air relative humidity sensor malfunction
Sept. 2, 2002 – Sept. 3, 2002	Condensate tipping bucket malfunction
<b>August 30, 2002</b>	<b>Switched air handler control from Enhanced to 0/0 mode</b>
Sept. 17, 2002 – Sept. 25, 2002	Supply air relative humidity sensor malfunction
Sept. 21, 2002 – Sept. 30, 2002	Coil air-side pressure drop sensor malfunction
<b>November 13, 2002</b>	<b>Switched air handler control from 0/0 to Enhanced mode</b>
Feb. 4, 2003	Performed cycling tests prior to terminating data collection

**Note:** In enhanced mode, supply air fan operation is delayed (no flow) for 30 seconds after the compressor turns on. The fan runs at 70% flow for the next 150 seconds of compressor operation, and then operates at 100% flow for the duration of the on cycle. The supply air fan quickly ramps down to no flow when the compressor on cycle is complete. In 0/0 mode, the supply air fan operates at 100% flow while the compressor runs and quickly ramps down to no flow when compressor operation stops.

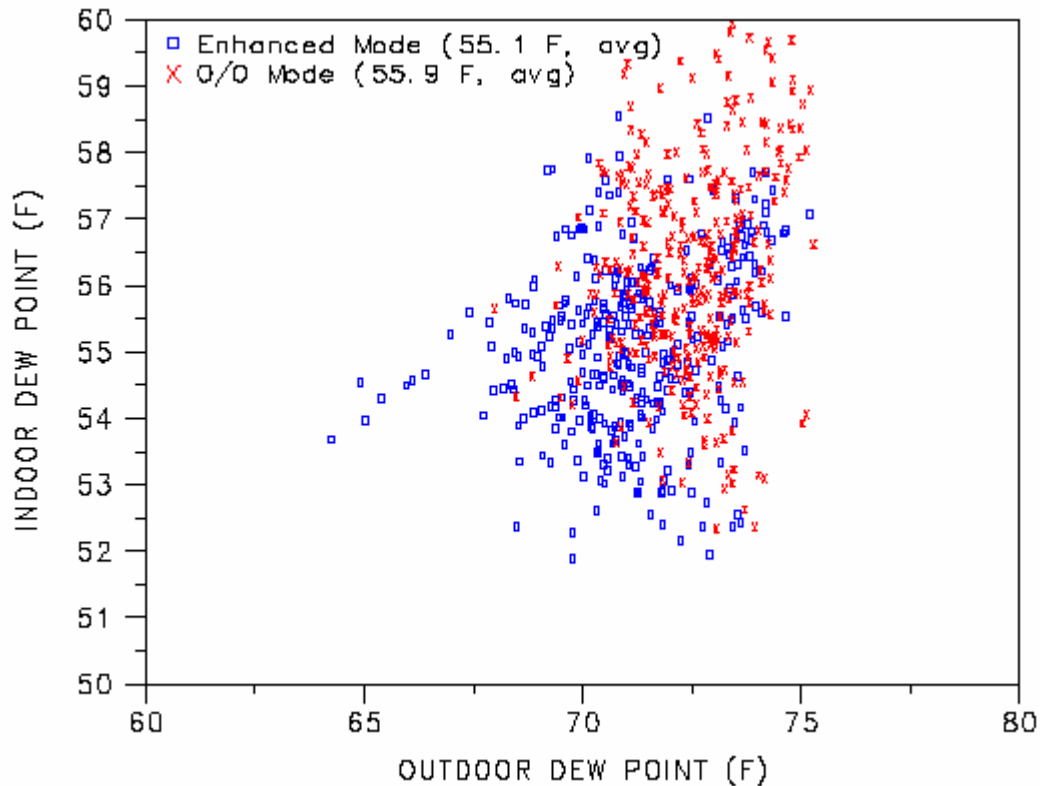
### **Data Analysis**

Figure 4 shows the comparison of psychrometric latent capacity versus measured condensate. The data was collected at times when there was at least 15 minutes of continuous compressor run time. Each data point is a 1-minute average (data scanned at 10-second intervals) of return and supply air conditions and a summation of condensate over the same interval. Typical compressor on-time was 10-minutes or less at this site; however, a small amount of data was available where the compressor ran for more than 15 minutes allowing this figure to be generated. The figure shows a fairly good correlation between the air-side humidity measurements and the measured condensate leaving the AC unit. The trend of higher psychrometric-based latent capacity compared to condensate removal is consistent with what has been observed at other field test sites being monitored for this project. Invalid data points have been removed.



**Figure 4. Comparing Condensate and Psychrometric-based Latent Capacity**

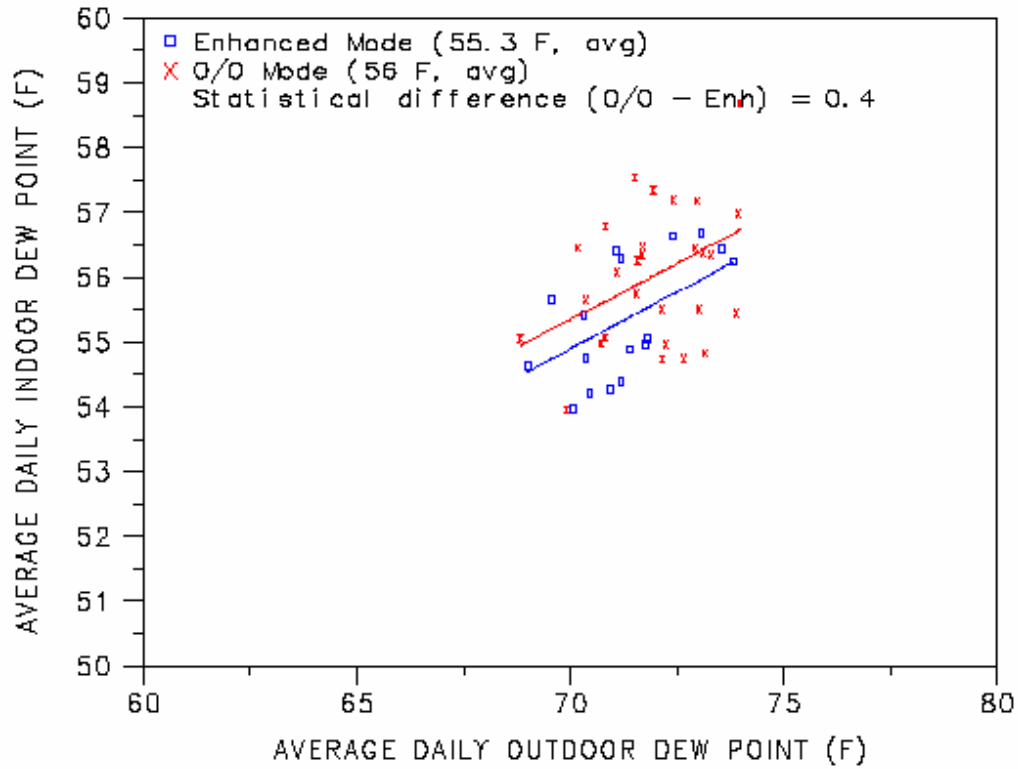
Figure 5 shows average hourly data from August 16 through August 29 for enhanced mode fan operation and August 31 through September 13 for 0/0 mode fan operation. The data show similar scattered patterns of indoor dew point temperatures over a rather limited range of outdoor dew point temperatures for each fan mode tested. Although the enhanced fan mode data show a lower average dewpoint temperature (55.1°F) over the 0/0 fan mode data (55.9°F), the difference in indoor conditions is rather small. Comparing the resulting relative humidity for these two dewpoint temperatures at this site’s typical indoor dry-bulb temperature of 80°F yields a difference of only 1.2% RH (42.4 % RH versus 43.6 % RH).



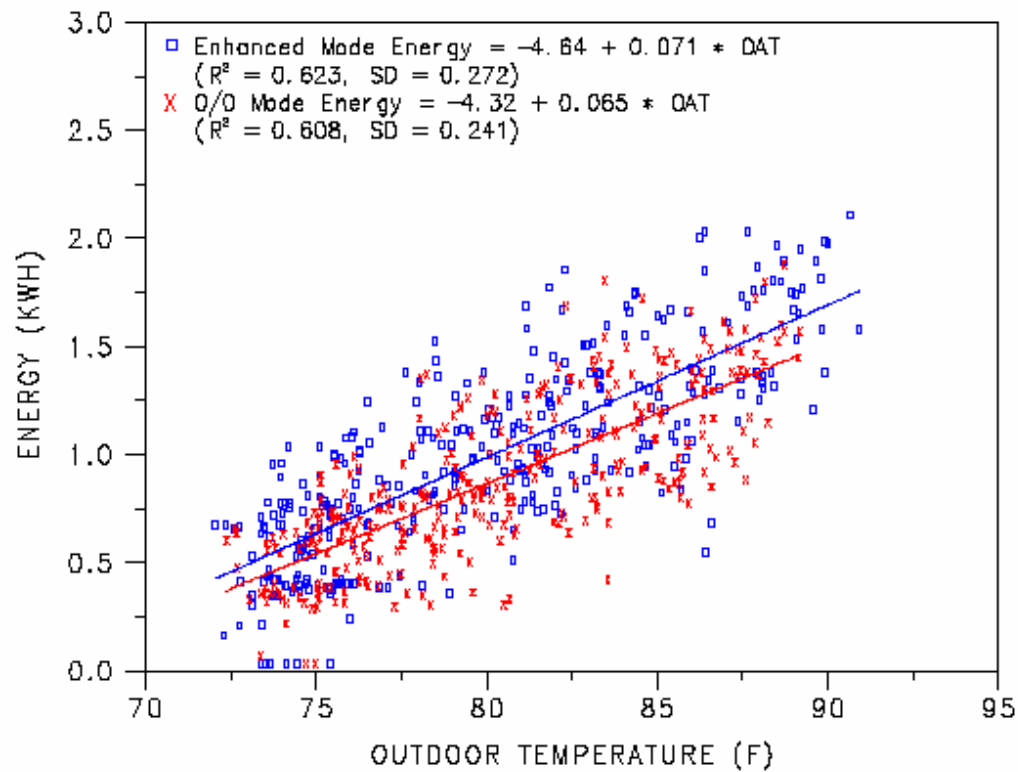
**Figure 5. Measured Indoor Dewpoint Temperature versus Outdoor Dew Point Temperature**

Figure 6 shows average daily data from August 13 through August 29 for enhanced mode fan operation and August 31 through September 27 for 0/0 mode fan operation. Figure 6 is similar to Figure 5 except that data is plotted as average daily values versus average hourly values shown in Figure 5. The data was fitted using a simple linear equation to describe average daily indoor dew point as a function of average daily outdoor dew point ( $\text{Indoor DP} = A_0 + A_1 * \text{Outdoor DP} + A_2 * \text{INF}$ ). An indicator variable (INF) was used to describe the fan mode operation as  $\text{INF} = 1$  during enhanced mode and  $\text{INF} = 0$  during 0/0 mode fan operation. Parameter  $A_2$  was found to be  $-0.4$  with a statistical T-value of  $-1.5$ . A T-value of less than 2.0 shows that this parameter describes the variation in indoor dew point based on the fan mode selected at less than a 95% confidence level. However, the trend is for a slightly lower indoor dew point temperature when using the enhanced fan control mode.

Figure 7 compares hourly energy consumption for two weeks in the enhanced mode and two weeks in the 0/0 mode (same time periods used for Figure 2). Condensing unit and supply air fan energy were added to yield total energy use. A least-squares curve fit of the measured data was developed using a linear relationship of energy use to outdoor temperature. The curve fit t-values are high: 19,23 and 18,22 for offset and slope in enhanced and 0/0 fan mode operation, respectively. Standard deviations for the curve-fit equations are 0.27 and 0.24 for enhanced and 0/0 mode, respectively. The resulting curve-fit equations indicate a difference in hourly energy usage of less than 0.2 kWh (0.17 kWh @ 85°F) for the different fan operating modes, however, the statistical t-values are high denoting that the difference is statistically significant.

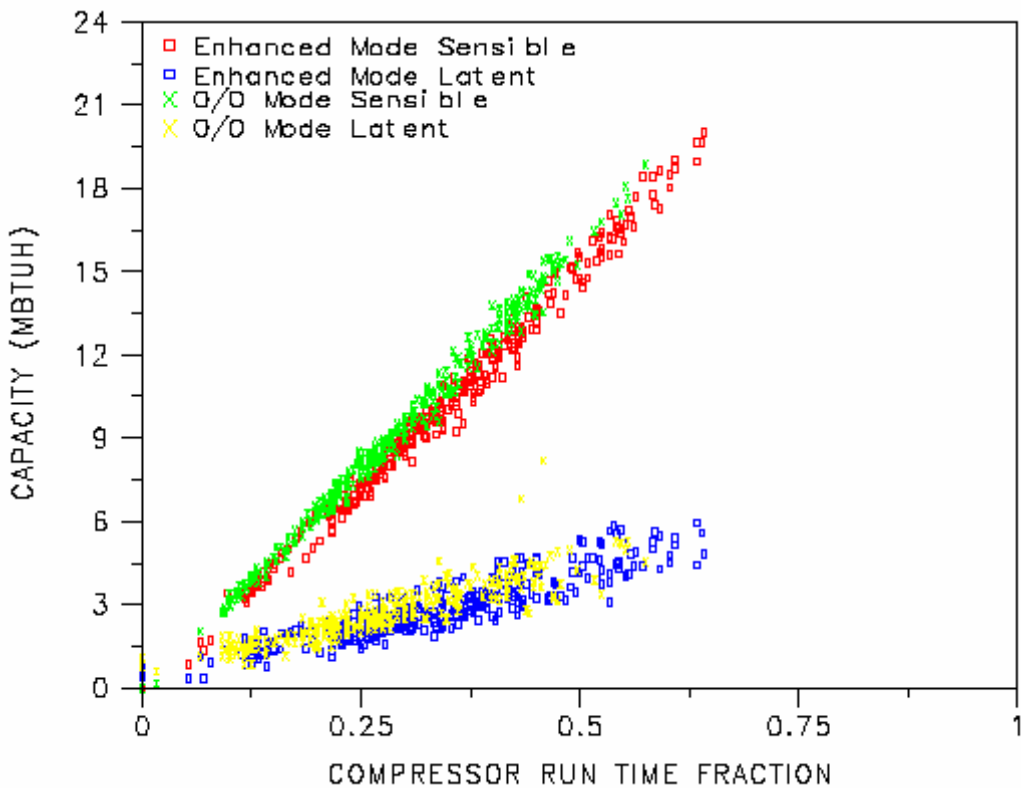


**Figure 6. Comparing Average Daily Indoor Dew Point versus Outdoor Dew Point Temperature**



**Figure 7. Hourly Energy Consumption versus Outdoor Dry-Bulb Temperature**

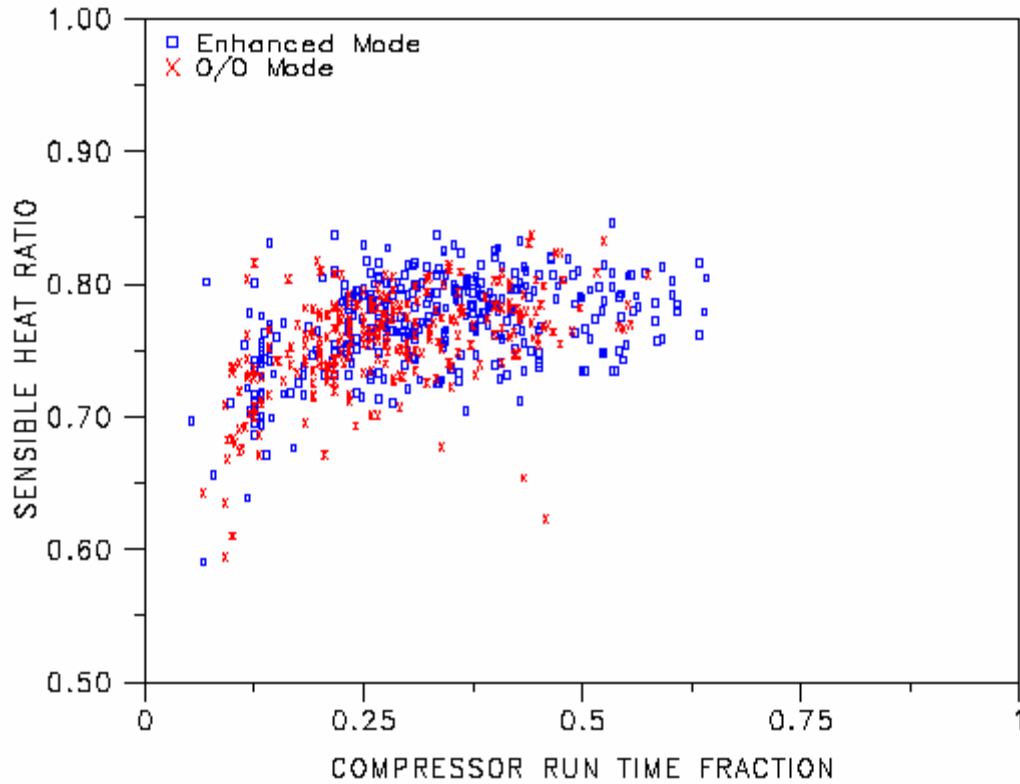
Figure 8 contains average hourly data for the same 2-week period before and after August 30, 2002. Data were removed when the condensate tipping bucket failed on September 2, 2002 and September 3, 2002. The sensible capacity shown in the figure is based on a return air temperature sensor in the return plenum, a supply air temperature sensor located just after the fan, and the supply air flow rate as indicated by a pitot tube located in the supply ductwork (calibrated with an Energy Conservatory air flow grid). Latent capacity is based solely on condensate tipping bucket measurements during the entire hour (including the condensate that continues to exit the air handler when the compressor and supply air fan are not operating). The measured data indicate that this system is oversized compared to the load, since the compressor runtime fraction rarely exceeds 60%. This is due in part to the homeowner's preferred thermostat setpoint of 78 – 79°F. The unit's delivered sensible capacity is lower in the enhanced mode compared to the 0/0 mode due to the reduced supply airflow rate at the start of each period of compressor operation. The measured latent capacity also appears to be lower when the unit operates in the enhanced mode.



**Figure 8. Hourly Sensible and Latent Capacity**

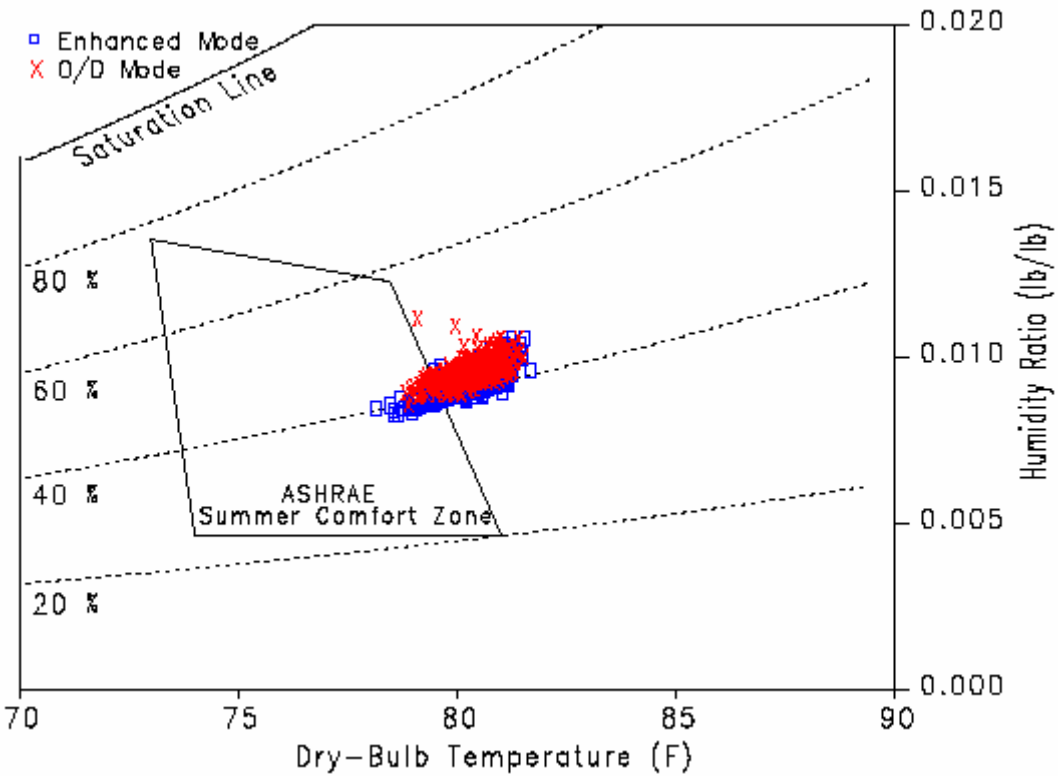
Figure 9 contains the same hourly data used for Figure 8. The sensible heat ratio (SHR) is calculated based on the ratio of sensible capacity to total (sensible + latent) capacity. The delivered sensible heat ratio for this 4-week period is roughly 0.75 to 0.8 for both fan operating modes (enhanced and 0/0). There is a trend toward lower SHR values at lower compressor runtime fractions, which is strongly influenced by condensate continuing to exit the air handler during the portions of the hour when the compressor and supply air fan are not operating. The impact of continued moisture removal has a greater impact on the calculated SHR at lower compressor runtime fractions.





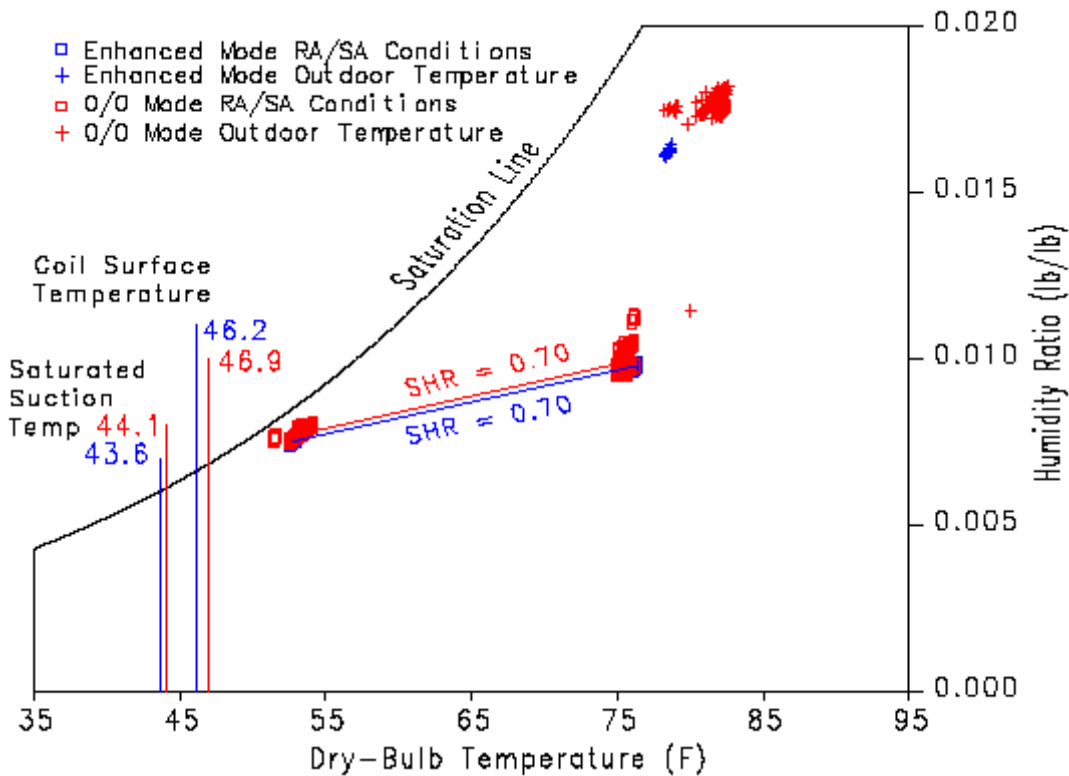
**Figure 9. Measured Sensible Heat Ratio (Hourly)**

Figure 10 compares hourly indoor air (temperature & humidity) conditions for the same 2 week period before and after August 30, 2002. This data shows a relatively high thermostat set point. Indoor air conditions are shown to be very similar regardless of the selected fan mode.



**Figure 10. Comparing Indoor Conditions to ASHRAE Comfort Zone**

Figure 11 compares steady-state performance data under both fan control modes. Coil surface temperature is measured on a single U-bend of the evaporator coil. Saturated suction temperature is determined by measuring refrigerant (R-22) pressure at the compressor inlet (suction). Data are only plotted for outdoor air temperatures between 78°F and 83°F to minimize the impact of outdoor temperature on performance. Extrapolation of the SHR line to the saturation curve matches the coil surface measurements fairly well. The SHR shown in Figure 11 is lower than that shown in Figure 9 due to the longer compressor runtime constraint used to generate the steady-state performance shown in Figure 11. Steady-state performance of this unit is shown to be identical regardless of the type of fan control selected. This result is expected, as this data is the resulting performance after the compressor and fan have operated for an extended period of time. Typical compressor runtime was 10 minutes or less at this site; however, a small amount of data was available where the compressor ran for more than 15 minutes allowing this figure to be generated.



**Figure 11. Steady-State Performance During Cooling Operation**

Figure 12 shows the trend of unit cycling rate versus compressor runtime fraction. The same 2-week period before and after August 30, 2002 was used to generate this plot. The compressor on and off period was calculated based on an individual compressor on cycle followed by a compressor off cycle (data is measured in seconds with a resolution of 10 seconds). Cycles per hour and run time fraction are calculated as follows:

$$\text{Cycling rate (cycles/hour)} = 60 / (\text{on time}/60 + \text{off time}/60)$$

$$\text{Compressor runtime fraction (RTF)} = \text{on time} / (\text{on time} + \text{off time})$$

The resulting data points were curve-fitted according to the equation for both modes of fan operation:

$$\text{cycling rate (cph)} = 4 \times N_{\max} \times \text{RTF} \times (1 - \text{RTF})$$

where  $N_{\max}$  = maximum cycling rate at 50% compressor runtime fraction  
 RTF = compressor runtime fraction (on time / on+off time)  
 cph = cycles per hour

Figure 13 is similar to Figure 12 except only the unoccupied hours between 9 a.m. and 5 p.m. were plotted. Weekends and holidays were classified as occupied hours and removed from the data set. Note that the scatter of data is much less in Figure 13 than in Figure 12 due to the removal of hours where occupant generated cooling loads impact the thermostat's response.

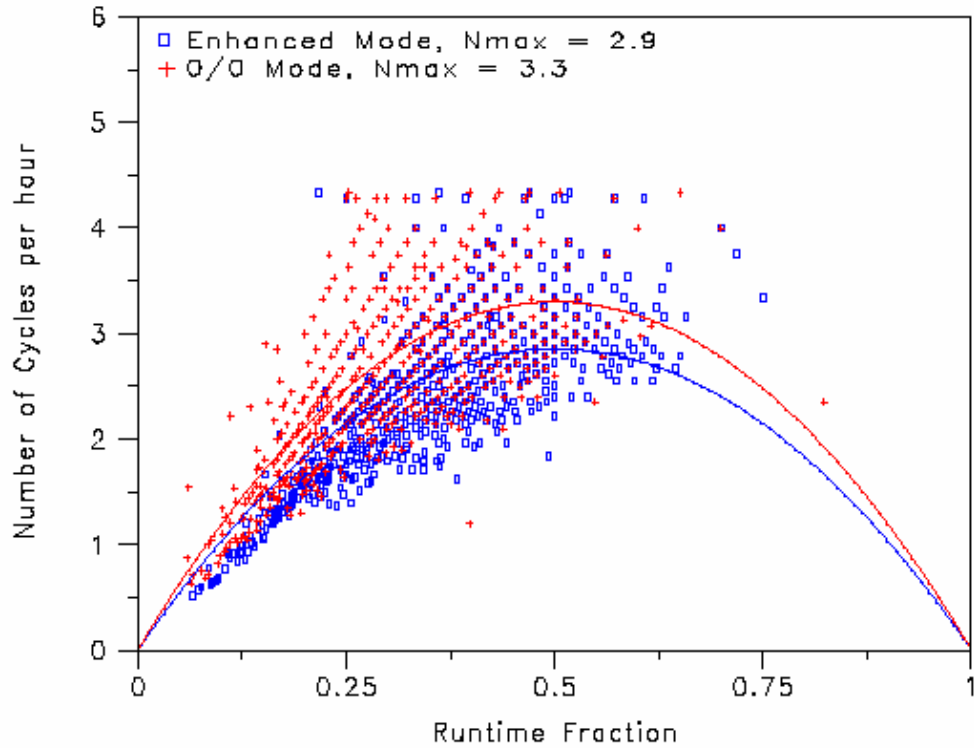


**Figure 12. Thermostat Cycling Curves for Enhanced and 0/0 Mode Operation**

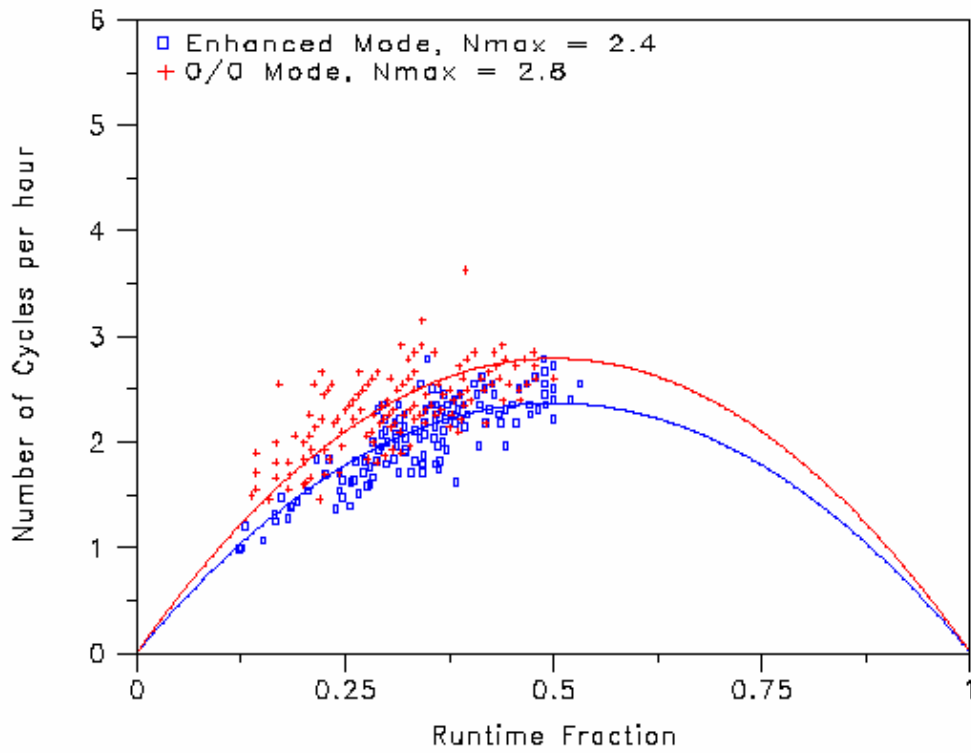


**Figure 13. Thermostat Cycling Curves for Enhanced and 0/0 Mode Operation (Unoccupied Hours)**

Figure 14 compares the measured return air and supply air temperature, relative humidity and supply airflow rate when enhanced fan mode and 0/0 fan mode operation are used (fan mode changed from enhanced to 0/0 at hour 12.3). Delaying the fan for 30 seconds after the compressor has started results in a colder coil temperature at the onset of fan operation (blue line in Figure 12). This is evident by the sharp decline in supply air temperature after the fan speed is increased to 70% of the maximum flow rate (blue line in Figure 14). In 0/0 fan mode operation, the supply air temperature is shown to exponentially decline to a steady state value. In both modes of fan operation, the steady state supply air temperature reached is nearly the same.

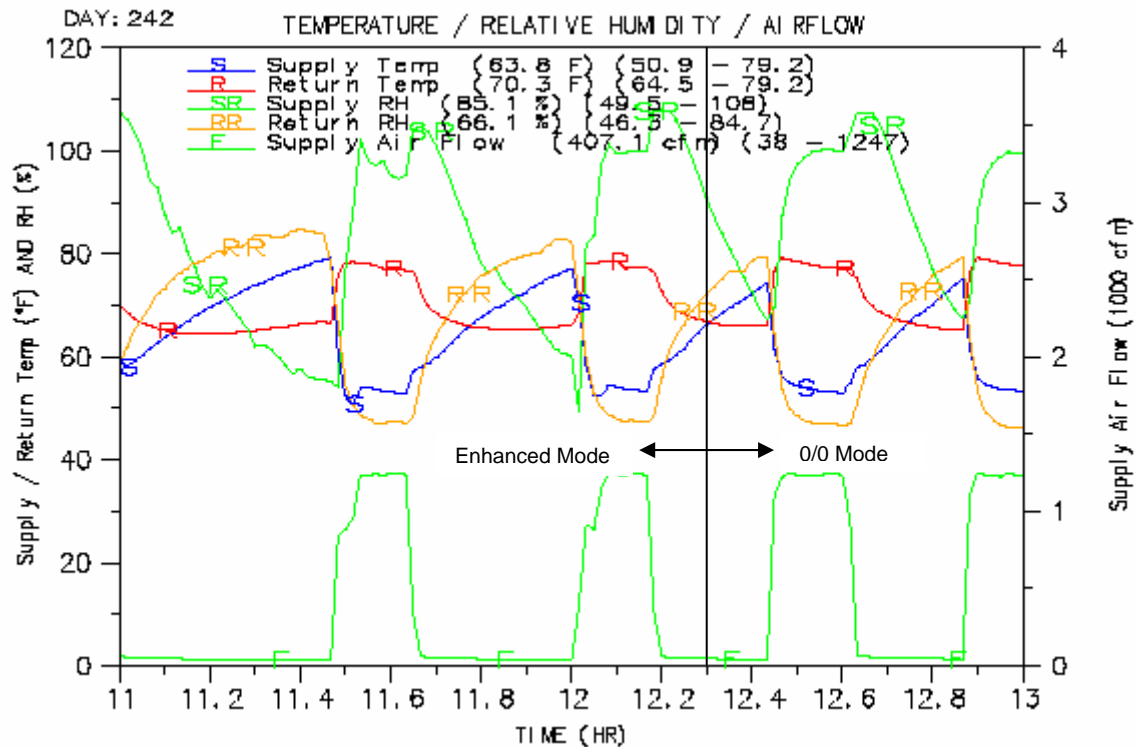


**Figure 14. Comparing SA and RA Conditions for Enhanced and 0/0 Fan Mode Operation**

Figure 15 shows refrigerant temperatures and pressure at various locations throughout the system. A pressure transducer was installed on the condenser suction line near the compressor inlet. Notice in Figure 15 that the compressor suction pressure, using a delayed fan operation approach in enhanced mode, goes much lower when the compressor first starts operating than in the 0/0 fan mode operation where the fan starts at the same time as the compressor. This results in a colder coil temperature and therefore a colder supply air temperature as shown in Figure 14 above. Condensate is also shown to leave the unit at a faster initial rate due to the colder surface temperature of the cooling coil.

Figure 16 compares the fan and compressor energy and status along with the airside pressure drop of the cooling coil. The impact of delaying the operation of the fan is shown to reduce both fan energy and air side pressure drop, however, compressor power remains fixed regardless of the mode chosen.

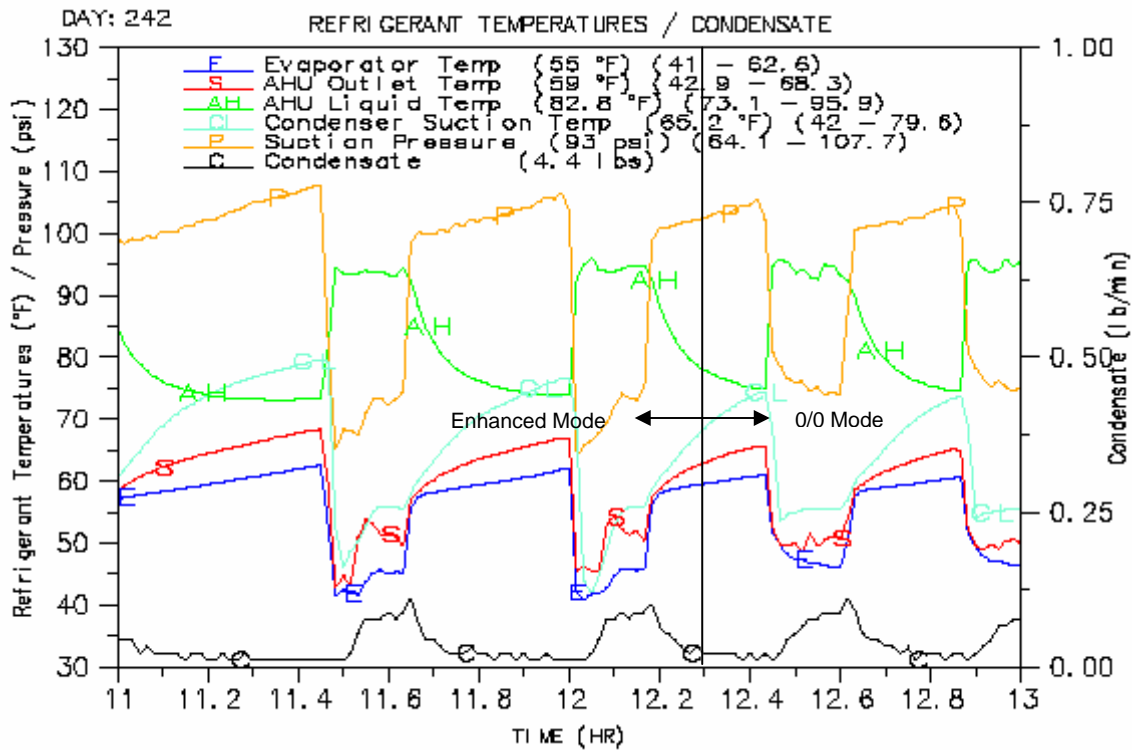


Figure 15. Refrigerant Temperatures and Pressure for Enhanced and 0/0 Fan Mode Operation

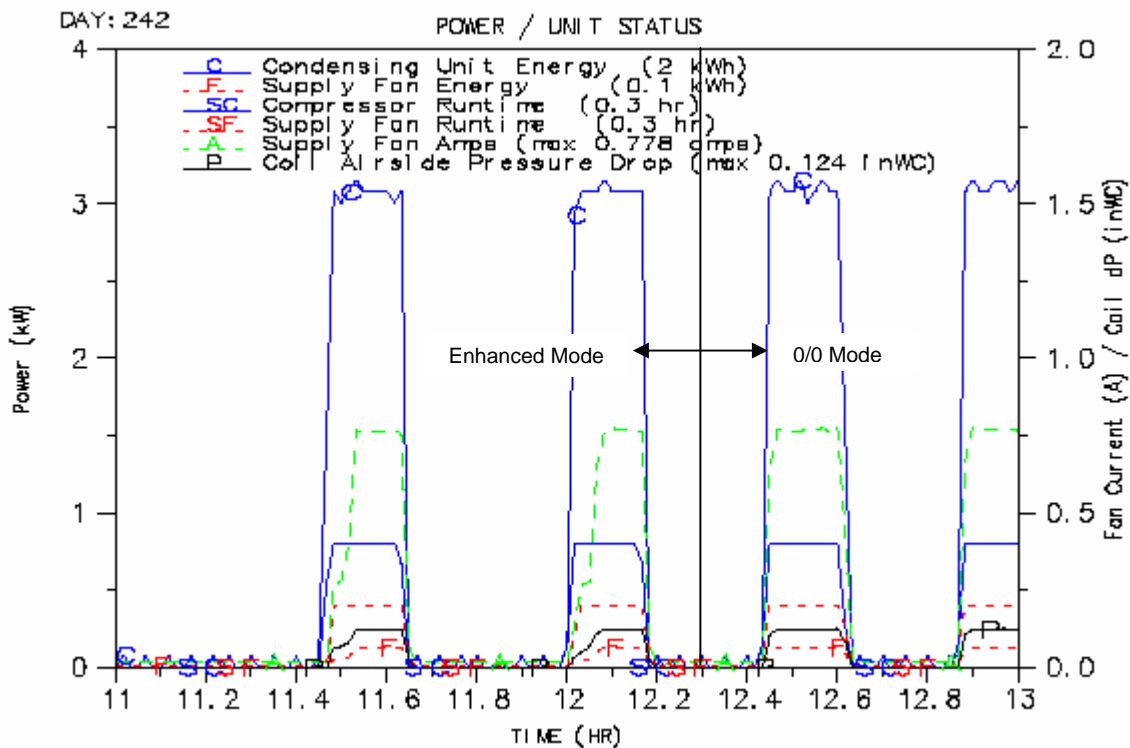
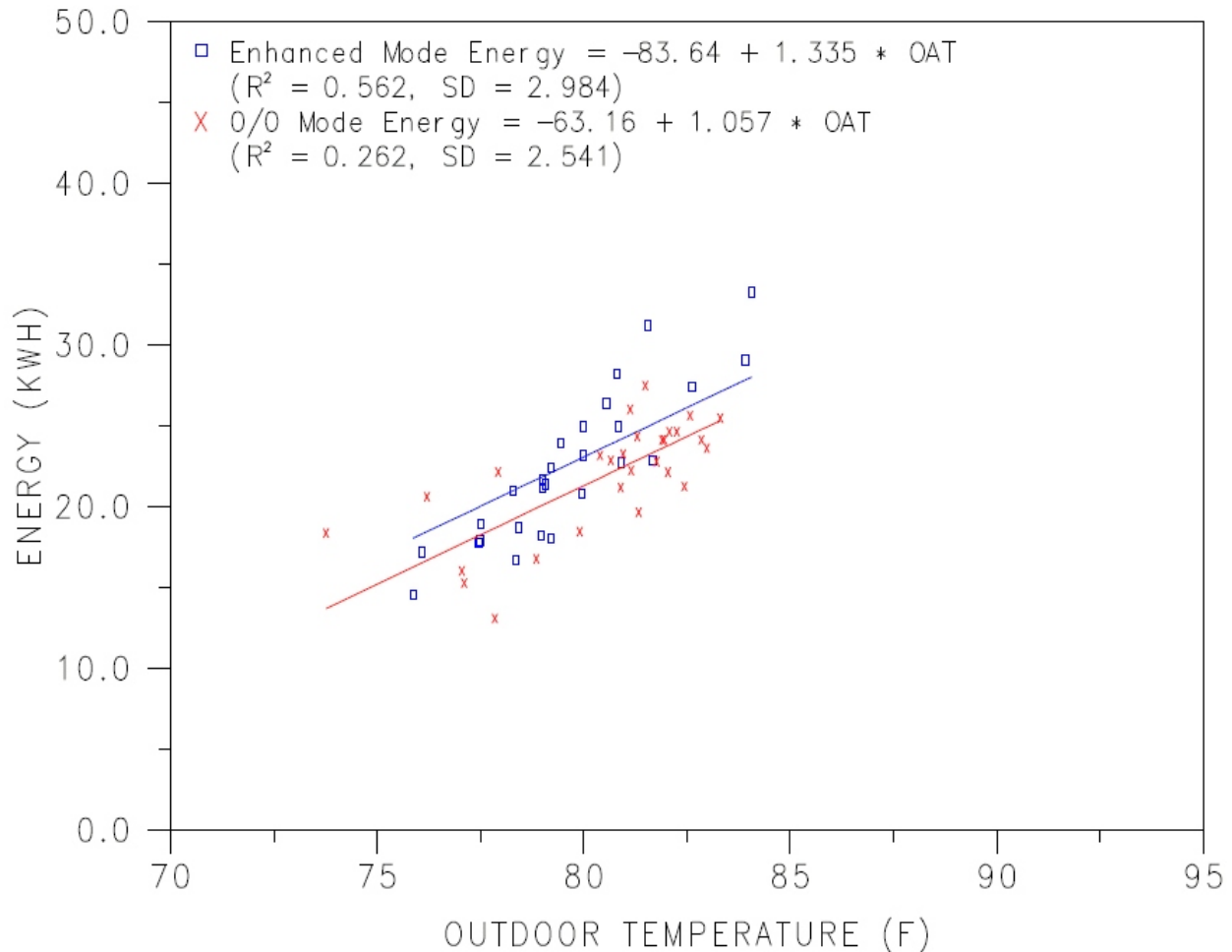


Figure 16. Compressor and Fan Energy and Runtime for Enhanced and 0/0 Fan Mode Operation

Figure 17 shows daily energy use versus average daily outdoor dry-bulb temperature. Measured data from four weeks prior and four weeks after the change from enhanced to 0/0 mode fan operation on August 30, 2002 were used to generate this figure. The measured daily energy use was curve-fitted using least squared regression with daily outdoor dry-bulb temperature as the independent variable.



**Figure 17. Daily Energy Consumption versus Outdoor Dry-Bulb Temperature**

Figure 18 through Figure 21 compares the sensible, condensate, latent, and sensible heat ratio performance of the unit for the two modes of fan operation tested at this site. One-minute data collected during both fan operation modes was analyzed to determine differences in unit performance. Compressor operation was used to provide cyclic performance of the unit for enhanced mode fan operation two days prior to the fan mode operation change on August 28 and 29, 2002. A similar two day period for 0/0 mode fan operation was analyzed on August 31 and September 1, 2002. Outdoor conditions were similar over this 5 day period. The figures show complete cycles starting when the compressor turned on through the entire on and off cycle of the compressor. The data were further grouped to determine if previous cycles had an influence on performance. Data collected where previous total cycle times were between 10 and 20 minutes are shown in blue. Similar traces are shown for other previous total cycle times as well. Figure 18 and Figure 19 compare the cyclic performance of the unit for air side sensible capacity and condensate for each fan mode operation tested. There appears to be a trade off in sensible

and latent capacity based on the fan mode selected. In the case of enhanced mode operation, sensible capacity of the unit is shown at a reduced level at the start of the compressor on cycle in Figure 15 where the latent capacity is shown to be slightly higher and starts more quickly in Figure 16. Figure 20 and Figure 21 show the cyclic performance for net latent capacity based on condensate (similar to Figure 19) and the resulting sensible heat ratio, respectively.

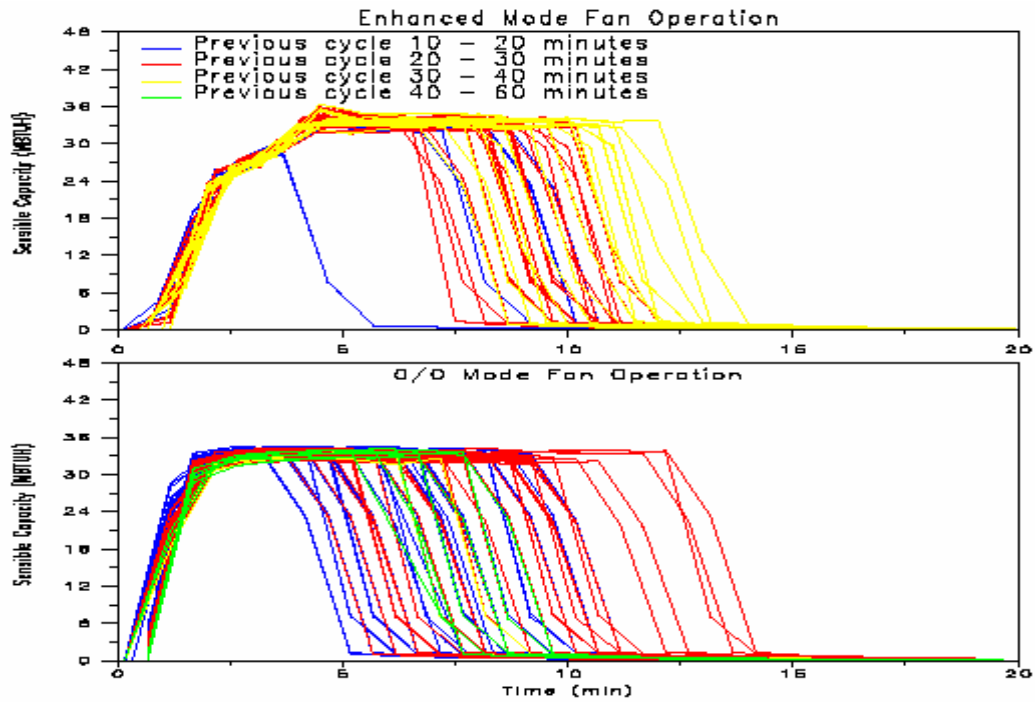


Figure 18. Characteristic Sensible Capacity Profiles



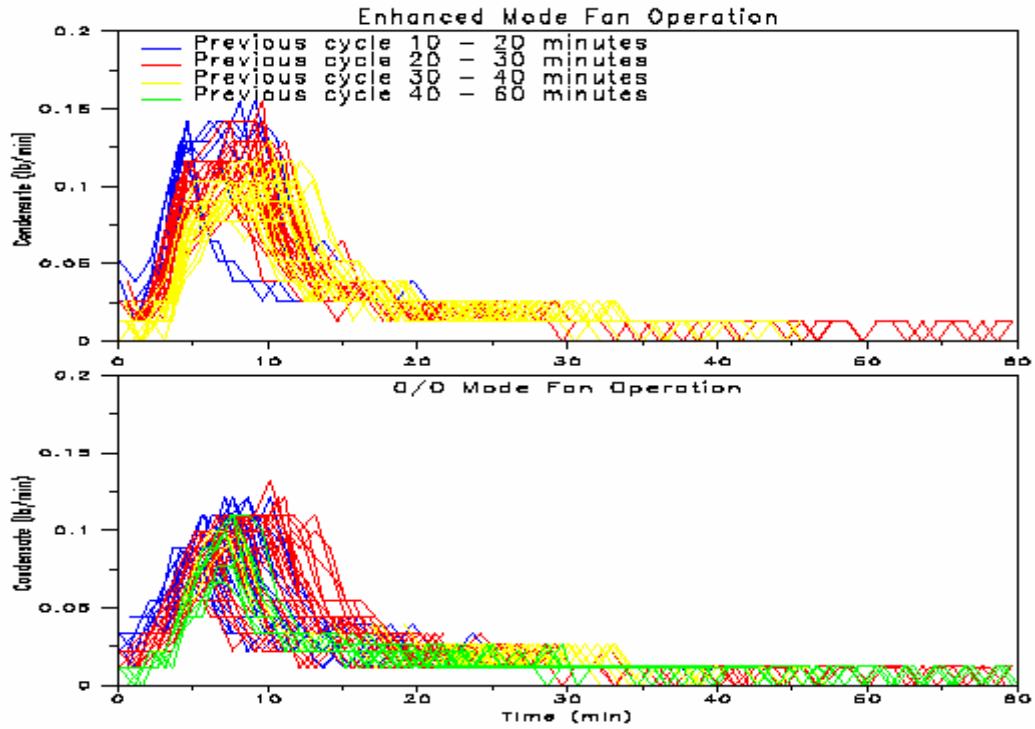


Figure 19. Characteristic Condensate Discharge Profiles

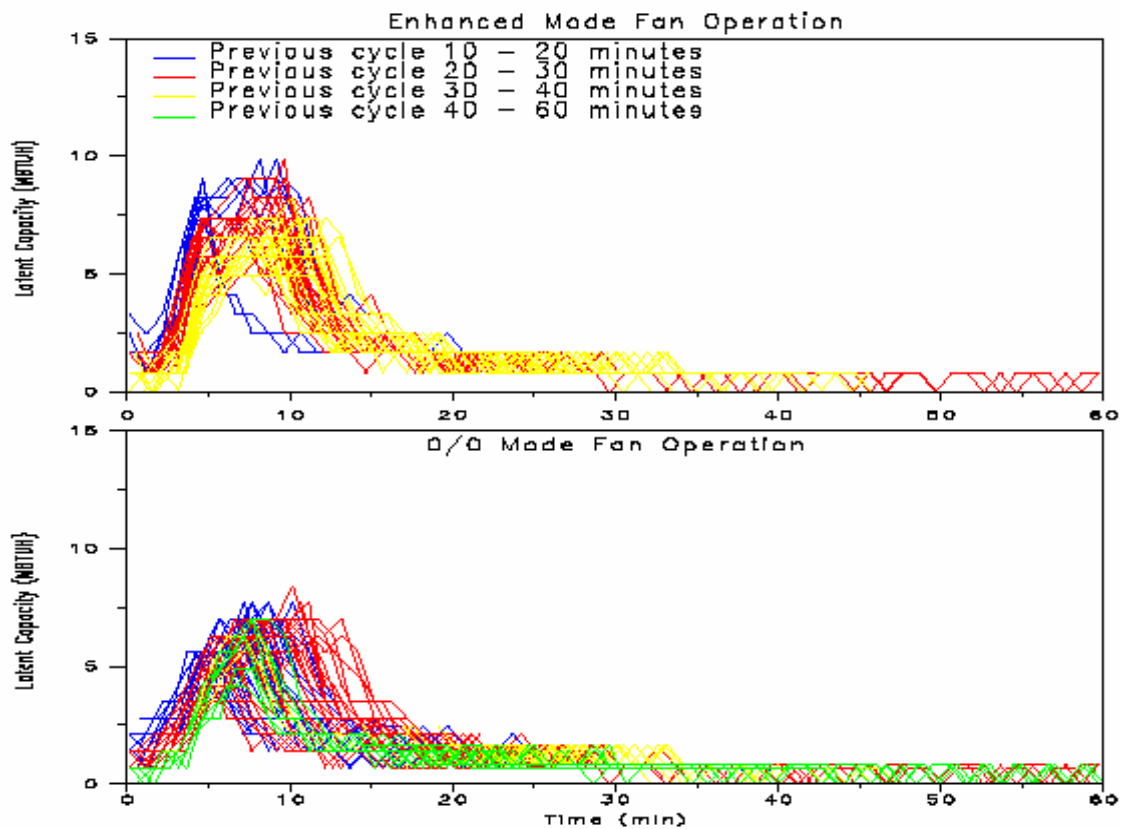
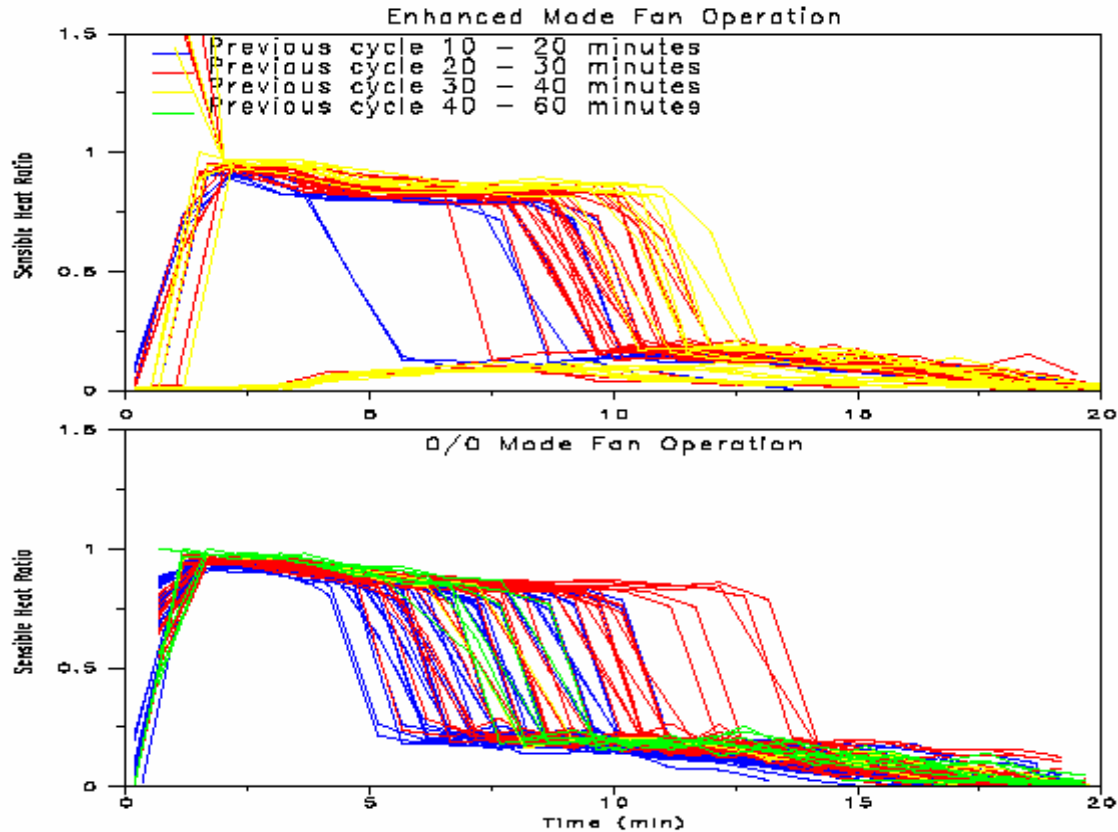


Figure 20. Characteristic Latent Capacity Profiles (based on condensate discharge)



**Figure 21. Characteristic Sensible Heat Ratio Profiles**

Collected data had shown that the coil required a long length of time to completely shed moisture from the coil's surface. Figure 22 shows a day where system loads were small and compressor operation occurred during the morning hours. This plot shows the long drip-down time required to completely shed the accumulated moisture from the surface of this coil. This particular air handler is rated for use with condensing systems ranging from 3.5 to 5 tons. This air handler, installed with a 3.5 ton condensing unit, results in a large coil surface area with respect to the available compressor capacity (2 sqft/ton). This coil is shown to discharge condensate (~1.6 oz/pulse) for a period of 7-10 hours with decreasing frequency. Even after this sustained off cycle, the coil continues to show the presence of moisture for the remainder of the day with a discharge of condensate around 2 p.m., 6 p.m., and again at 7 a.m. the following morning (not shown in this figure).

Figure 23 is an attempt to show the delay to first condensate pulse for this cooling coil. As described previously, this coil retained moisture for long periods of time after the compressor turned off. Due to the frequent discharge of condensate, calculating the delay to first condensate pulse posed a problem. An alternative method was required to estimate this parameter for this particular coil. The compressor operating time was summed until the first burst of condensate pulses was detected. Notice here again that a condensate discharge occurred shortly after the first compressor on cycle and was not considered to be due to a fully moisture laden coil. Disregarding this phantom condensate pulse allowed the first time to condensate pulse to be estimated based on the accumulated compressor runtime for the first two compressor cycles and a portion of the third in Figure 23 as 24.5 minutes. Outdoor temperature at this time was noted as

83°F. Indoor temperature and humidity were recorded at approximately 79°F and 49 % RH, respectively.

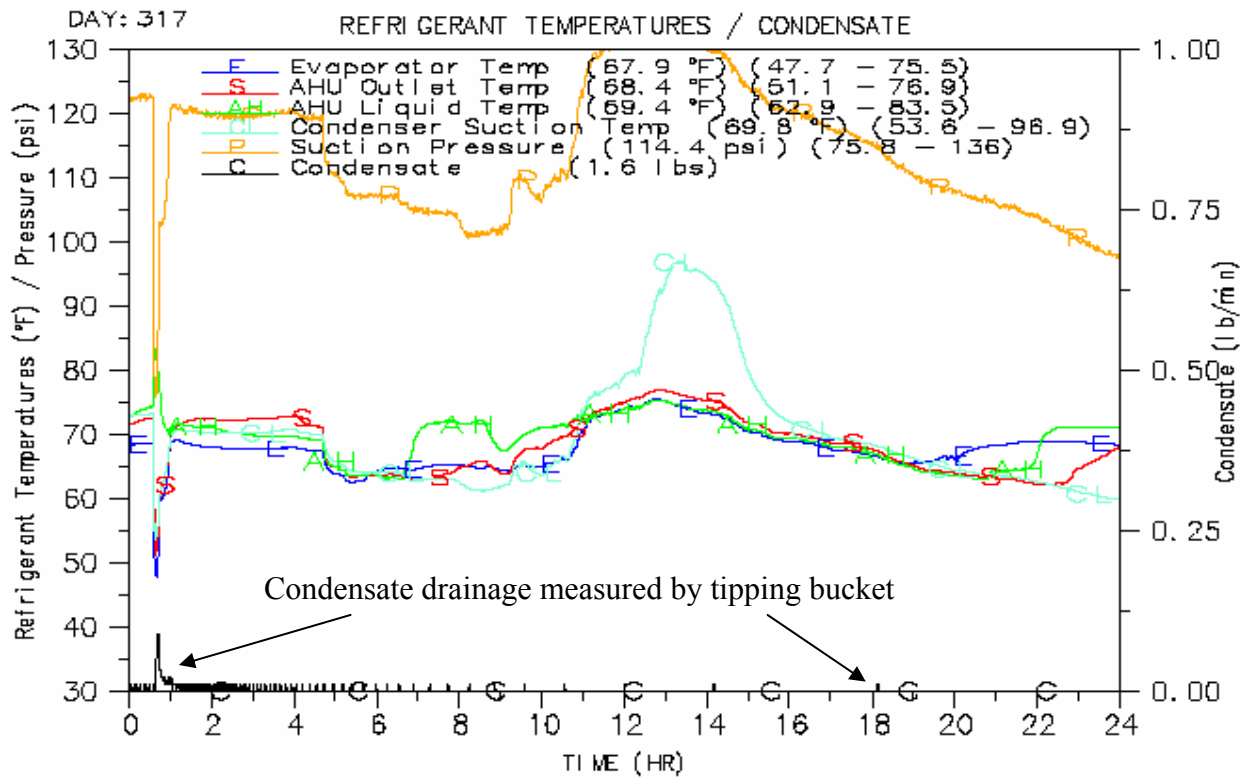
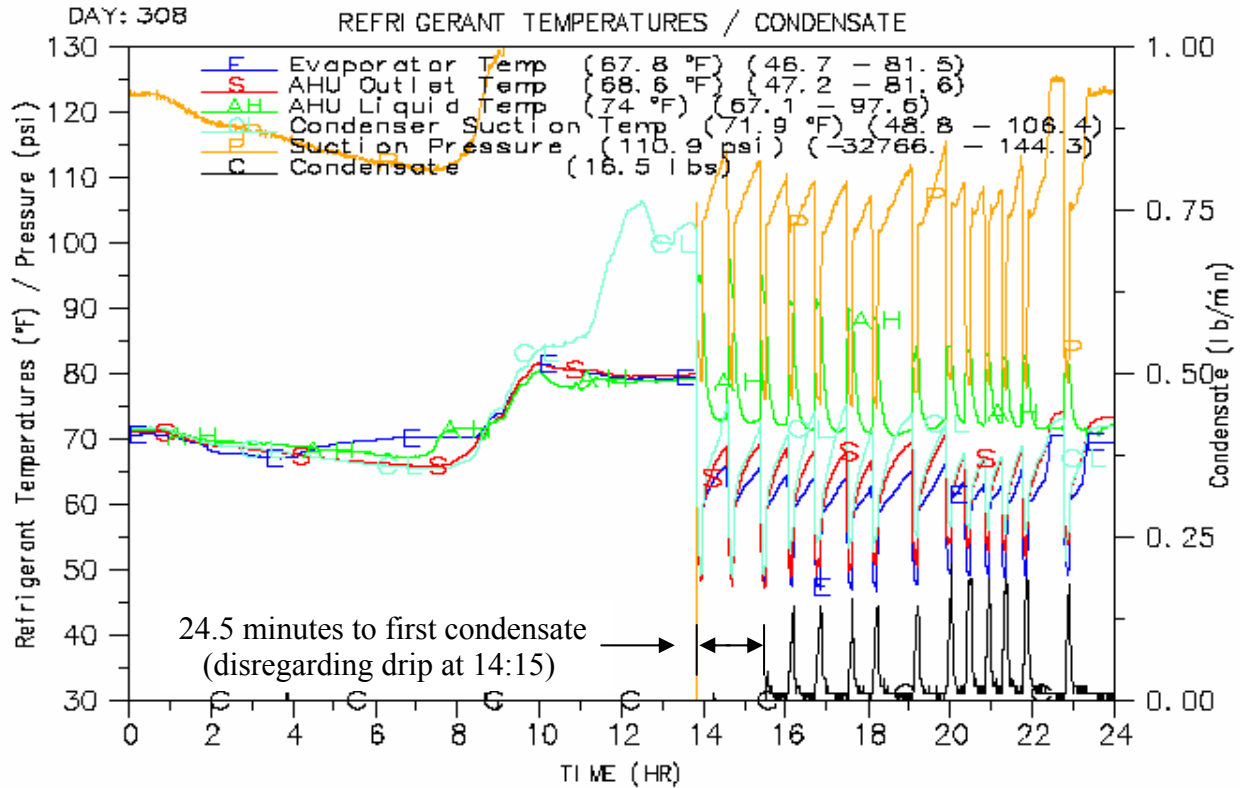
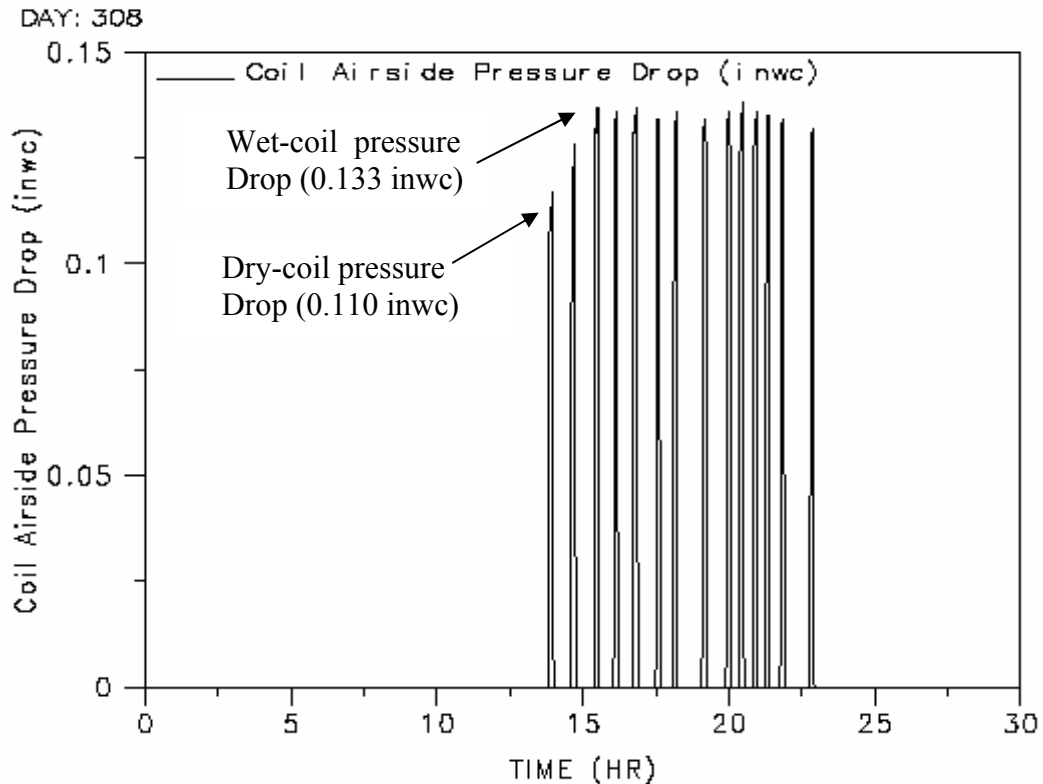


Figure 22. Representative Drip-down delay time



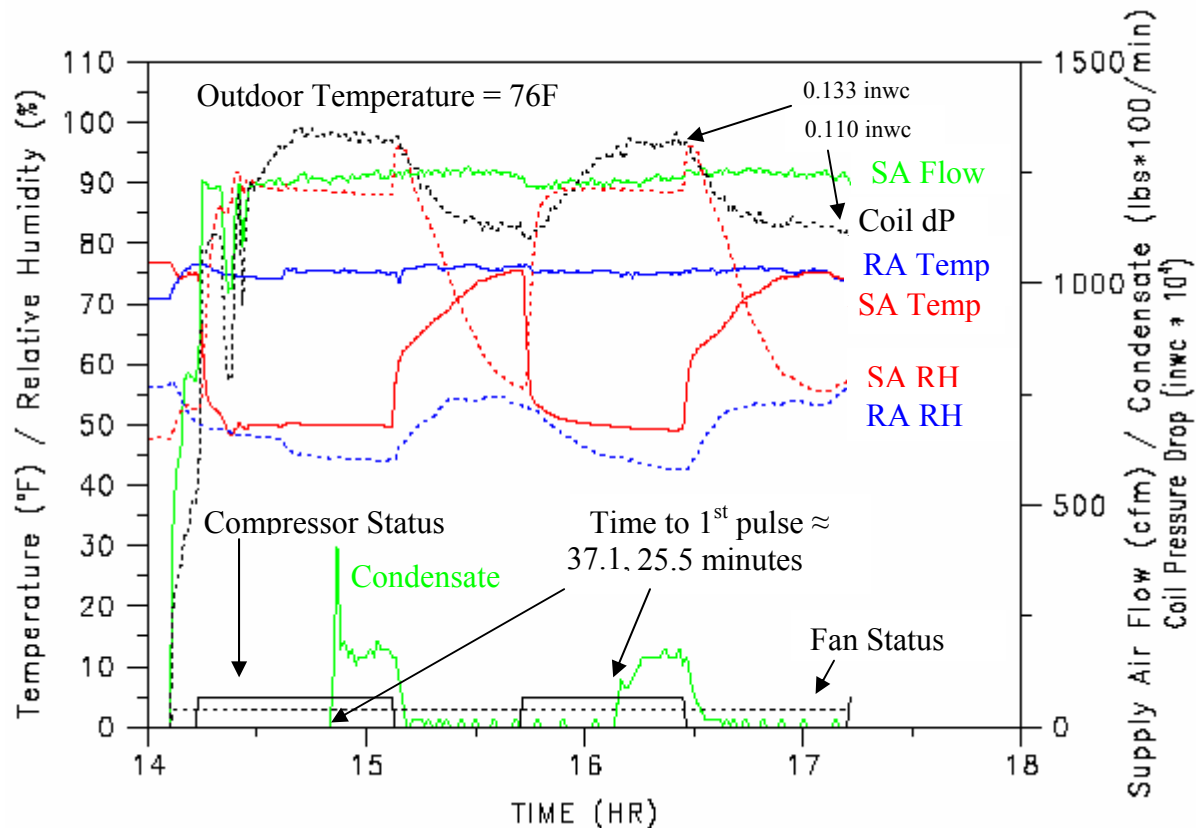
**Figure 23. Alternate Method for Calculation of Twet Parameter**

Figure 24 shows how the airside pressure drop increases with increasing moisture accumulation on the surface of the cooling coil. A day was selected where the system had been off for a sufficient time to allow the accumulated moisture to drain from the coil surface. The first on cycle is shown to have an airside pressure drop of 0.11 in wc. As the compressor continued to cycle and moisture continued to accumulate, the airside pressure drop increased to a steady state value near 0.133 in wc.



**Figure 24. Coil Air-side Pressure Drop Comparison for Dry and Wet Coil**

Additional tests were performed on this unit just before the data collection period ended. The fan had been configured to operate in auto fan mode during the entire data collection period. It was, however, desirable to operate the AC system using constant fan mode operation to quantify parameters associated with this coil in order to compare to similar data collected in the laboratory. At the end of the data collection period, fan mode operation was changed to constant speed and the AC unit was cycled on and off for two complete cycles. Space heaters were used to maintain the indoor temperature at  $75^{\circ}\text{F} \pm 1^{\circ}\text{F}$ ; however, moisture levels were not controlled during the test. Figure 25 shows supply and return air conditions, airflow, condensate, and status of the compressor and fan. At the beginning of the test, the fan was enabled and the supply air flow rate was found to be approximately 790 cfm. The air handling unit was configured to operate the fan at around 60% of nominal flow in constant fan mode when the compressor is not operating. Since it was desirable to collect data at full fan speed when the compressor was off, the condenser unit breaker was used to operate the compressor when desired. The thermostat was programmed to operate in constant fan mode and the temperature set point was lowered to  $60^{\circ}\text{F}$  to provide continuous cooling when desired throughout this test period.



**Figure 25. Performance Data for Constant Fan Mode Operation**

The fan was enabled at approximately 2:10 p.m. and allowed to operate alone for a short period of time as shown in the figure. The compressor was then enabled using the condensing unit's breaker. Supply air flow is shown at approximately 1250 cfm at the start of compressor operation. The reduction in supply air flow near the beginning of compressor operation was due to the Carrier's thermostad humidity control function. During times when space humidity exceeds the setpoint (60% RH) and the thermostat called for cooling, supply air fan speed is reduced to 80% of the nominal value. This control was quickly disabled for the remainder of testing (RH setpoint was increased to 90%).

The AC system was allowed to operate until steady state performance was observed for more than 10 minutes. The compressor was then turned off, while the supply air fan continued to operate, to allow moisture collected on the coil to fully evaporate. This cycle was repeated a second time in part due to the reconfiguration of the thermostat at the beginning of the first cycle. Additionally, laboratory data has shown that the second cycle yields more repeatable data than the first cycle after the coil has completely dried.

As shown in the figure, the time to first condensate pulse was recorded as 37.1 and 25.5 minutes for the first and second compressor cycles, respectively. This value is an indication of the moisture retention capacity of the coil. For the first compressor cycle, the coil was completely dry prior to the start of the compressor on cycle; however, airflow over the coil was not constant during the entire period. For the second cycle, the coil had not fully drained the moisture from

the coil's surface (as seen by the condensate discharge prior to the start of the second compressor on cycle) and the time to first condensate pulse appears to be underestimated. For these reasons, the time to first condensate pulse is estimated at 35 minutes.

Collected data also allowed the comparison of the coil's wet-dry pressure drop. The difference between the pressure drop for the coil under wet and dry conditions should provide an indication of the amount of retained moisture. Figure 25 shows the variation of the wet-dry difference while the retained moisture on the coil increased during the compressor on cycle and decreased during the off cycle evaporation period. At the end of the second compressor on cycle, the moisture retained on the coil had caused the airside pressure drop to increase to a steady state value of 0.133 in wc. When the compressor turns off, the amount of moisture on the coil decreased during the evaporation process to 0.11 in wc at which time the coil was relatively dry. These values are shown to be identical to those shown in Figure 24 using an alternative method to derive the coil's wet-dry pressure drop characteristics.

Figure 26 shows the off-cycle sensible (solid) and latent (dotted) capacity for the two cycles shown in Figure 25 above. The plot shows measured capacities starting the first minute after the compressor stopped operating. The capacity curves were then integrated to provide a reference for the amount of accumulated moisture on the evaporator coil. The integration began the second minute after the compressor turned off to allow refrigerant pressures and flow to stabilize. Measured fan energy was used to calculate the actual temperature difference across the cooling coil. The integration of the first and second off-cycle shows sensible capacities due to the evaporation process of 5.51 and 5.54 Mbtu, respectively. The assumption is then made that the coil operates as an evaporative cooler with the latent and sensible capacity summing to zero. With this in mind, the energy associated with the sensible cooling is equivalent to 5.23 pounds of moisture retained on the coil. Integration of the airside psychrometric latent capacity yields a slightly lower evaporation rate and totals 4.04 Mbtu (3.81 lbs) and 4.64 Mbtu (4.38 lbs) for the first and second off-cycles, respectively. Further calculations using latent capacity will rely on net latent capacity as measured at the unit's condensate discharge.

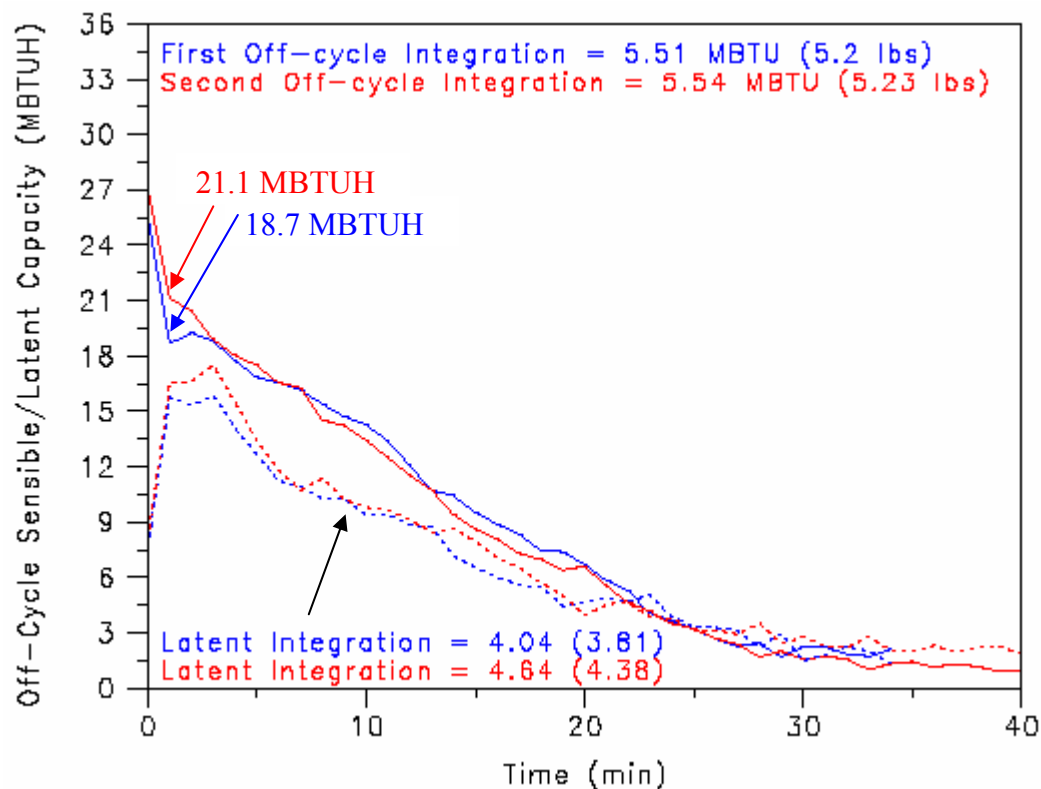


**Figure 26. The Trend of Sensible Capacity for "Wetted" Off-Cycles**

For this coil, the value “twet” from Henderson and Rengarajan (1996) can then be calculated by multiplying the retained moisture mass by the heat of condensation of water and then dividing by the steady-state latent capacity (8.39 MBtu/h based on the last 10 minutes of condensate discharge during the second cycle shown in Figure 25). The value of twet based on the integrated sensible and latent capacity is 39.4 (5.23 lb x 1060 Btu/lb / 8390 Btu/h) and 33.2 (4.38 lb x 1060 Btu/lb / 8390 Btu/h) minutes, respectively. This value of twet is slightly higher than the estimated delay of 35 minutes for the first condensate pulse to fall from the drain pan. This discrepancy may be the result of the dry inlet conditions entering the evaporator coil during this test (75 F DB, 47% RH) and although steady state performance was perceived in the field, the coil may not have been fully wetted. In addition, condensate is shown to continue to leave the unit and the moisture retained on the coil had not fully evaporated.

The value of gamma (2.67), which is the initial off-cycle moisture evaporation rate divided by the steady-state psychrometric latent capacity (7.9 Mbtu/h, based on the psychrometric latent capacity during the last 10 minutes of compressor operation during the second cycle), uses the off-cycle moisture evaporation rate (21.1 MBtu/h) once the refrigerant flow rate has reached zero (and all coil heat and mass transfer with the air stream is assumed to be adiabatic). The off-cycle sensible capacity also shows a clear change in the decay trend at this point. For this unit, it took about 2.0 minutes for refrigerant flow to settle to zero.



## **APPENDIX I6**

### **Summary of Data for Field Test Site 6**

## Site #6 – Commercial Building in Cocoa, Florida

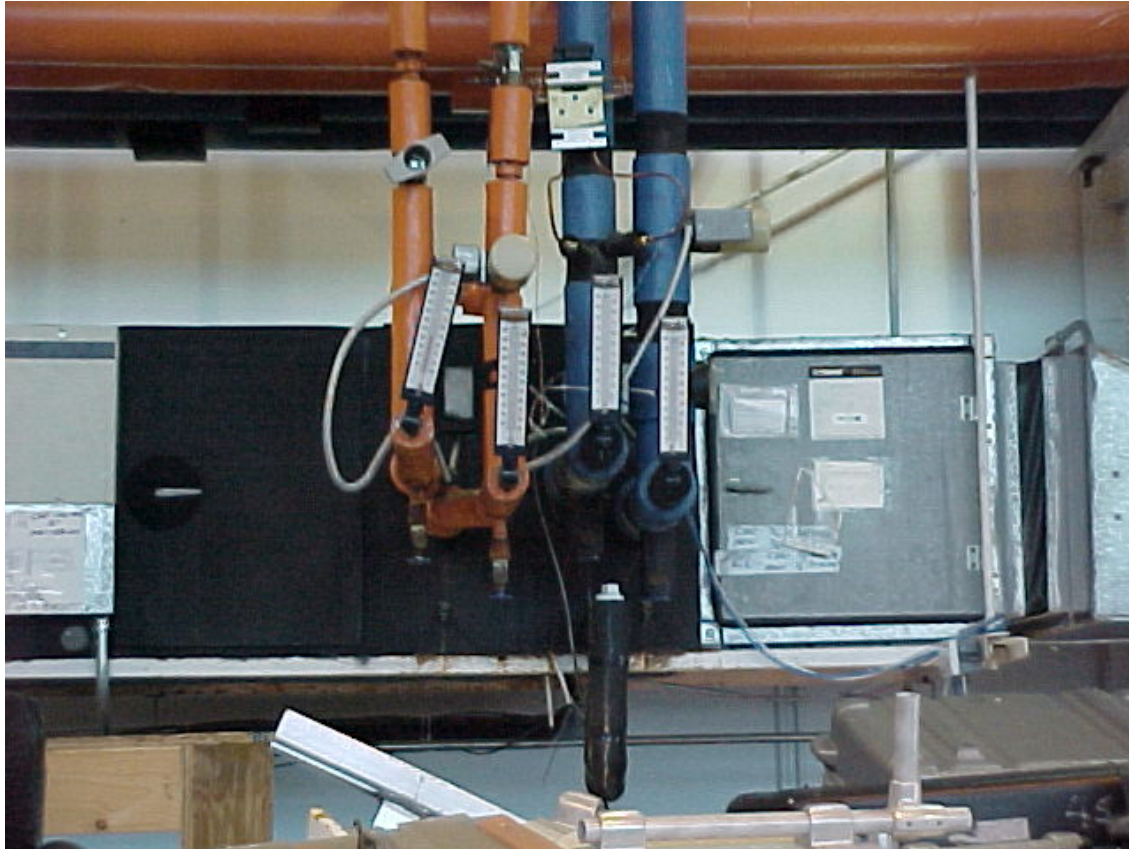
This site is a single-story laboratory facility located in Cocoa on Florida's East coast, approximately 45 miles east of Orlando. The facility is conditioned by multiple chilled water, constant volume air handlers. One of these air handlers was monitored for this project.



Figure 1. Southern Exposure for Site #6 in Cocoa, Florida

### Chilled Water Air Handler Description

The system, a Trane modular air handler CLCH-3, was installed in 1995. This air handler is located in a high-bay area and is used to condition a portion of adjacent low-bay laboratories. The area where the air handler is mounted is unconditioned during the summer months and hot water coils are used to minimally heat the area during the winter months. Figure 2 shows the unit installed at 10' above the finished floor. The unit is comprised of a filter rack section (right of figure), chilled water coil section, hot water coil section, and finally, a fan (draw-through) section. The air volume flow rate is constant, and two-way modulating valves are used to control the cooling and heating coil capacities based on thermostat temperature.



**Figure 2. Constant-Air-Volume Air Handler at Test Site #6**

The design specifications for the air handler are provided below:

Model:	Trane CLCH-3
Total Supply Air Flow:	1,248 cfm
Outside Air Flow:	15 cfm
Total Cooling Capacity:	34,500 Btu/hr
Sensible Cooling Capacity:	29,900 Btu/hr
Rows/Fin Spacing:	6 rows / 12 fpi
Entering Water Temp:	45°F
Leaving Water Temp:	60°F
Design Water Flow Rate:	4.8 gpm
Entering Air Conditions:	74.9°F DB / 62.5°F WB ( $\approx$ 50 % RH)
Leaving Air Conditions:	53.1°F DB / 52.9°F WB
Fan Motor Size:	1½ hp
Coil Type:	Vertical slab
Capacity Modulation:	Two-way modulating chilled water valve

## Sensors and Data Logger Connections

Table 1 summarizes the points being monitored by the data logger and the sensors installed for each measurement. Figure 3 shows a basic schematic of the cooling coil along with sensor locations.

**Table 1. Data Logger Channel Assignments and Sensor Identification for Site #6**

Channel	Data Point	Description	Units	Sensor
DI1	TCWE	Chilled Water Entering Temperature	F	Type-T Thermocouple
DI2	TCWL	Chilled Water Leaving Temperature	F	Type-T Thermocouple
DI3	TAM	Return Air Mixed Temperature	F	Type-T Thermocouple
DI4	TAS	Supply Air Temperature	F	Type-T Thermocouple
DI5	Not Used			
SE11	SF	Fan Status	On/Off	Setra (Hawkeye 900)
SE12	TREF	Thermocouple Reference Temperature	C	Campbell Scientific TC107
P1	WF	Fan Power	kWh	Ohio Semitronics (W005B)
P2	FC	Condensate	Lb	Texas Electronics tipping bucket
C1	MUX-cntrl			
C2	MUX-cntrl			
C3-8	Not Used			
MUX-1	RHM	Return Air Relative Humidity	%	Vaisala HMD60U
MUX-2	RHS	Supply Air Relative Humidity	%	Vaisala HMD60U
MUX-3	PDB	Pressure Drop at Balancing Valve	Psi	Setra 230 (0 – 2 psi)
MUX-4	DPC	Pressure Drop across CW Coil	In WC	Setra 267MR (0.25, 0.5, 1.0 inches)
MUX-5	CWVP	CW Valve Position (6-9 Vdc)	Vdc	Voltage divider

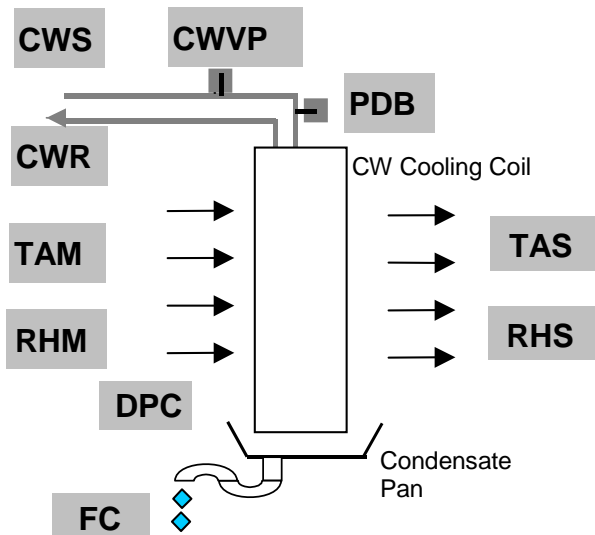


**Figure 3. System Schematic With Sensor Locations for Site #6**

## Cooling Coil Characteristics

Figure 4 shows dimensional data for the cooling coil monitored at this site. The coil is a vertical slab configuration with air flowing horizontally. Figure 5 shows the u-bend circuiting of the 6-row coil which has a wavy fin design as shown in Figure 6.

Coil Type	Vertical Slab	
Coil Face Area	470.25 sq. in.	
Number of rows	6	
Fins per inch	12	
Tubes per row	16	
Tube-to-tube in row	1 1/4"	
Row spacing	1 1/16"	
Tubing diameter	1/2"	
Coil depth	6 3/8"	
Fan Configuration	Draw Thru	
Notes:		

**Figure 4. AHU Cooling Coil Dimensions for Site #6**

Gross fin area: $(6.375 \text{ in}) \times (12 \text{ fins/in}) \times (2 \text{ sides/fin}) \times (470.25 \text{ sq in.}) / 144 \text{ sq in/ft}^2 = 499.6 \text{ ft}^2$
--



**Figure 5. Coil U-bends**

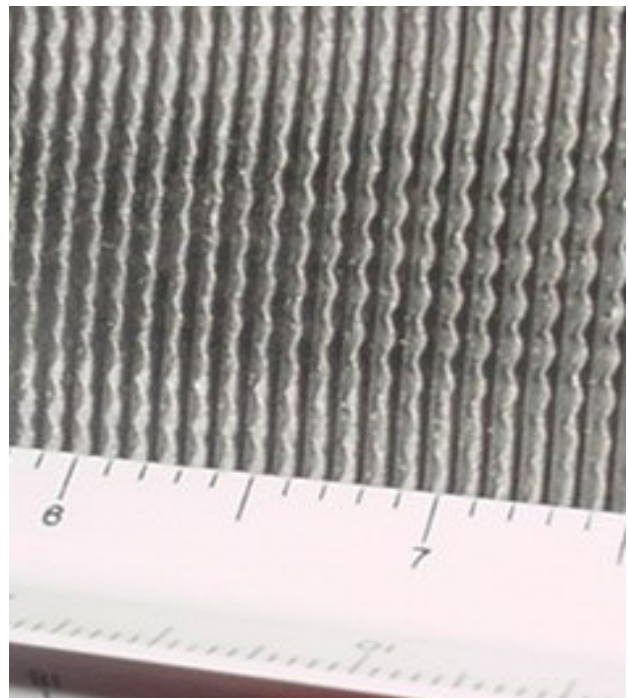


**Figure 6. Coil Fin Spacing**

## **Temperature set point schedule**

The temperature set point schedule for this air handler, as controlled by the building's energy management system, is provided below:

4:30 am	78°F Cool 68°F Heat	Occupied Mode
3:00 am	85°F Cool 55°F Heat	Unoccupied Mode

## **One-Time Measurements**

Air flow measurements were made using a 30-point pitot tube duct traverse. Measurements were made approximately 10 feet downstream of the unit in the supply air duct. Duct static pressure and coil air-side pressure drop were also measured to document these characteristics for the selected coil assembly.

Supply duct static pressure =	40 Pascals (0.16 in WC)
Duct dimension =	12 in x 18 in
Duct area =	1.5 sq ft
Average velocity =	941.4 ft/min
Air flow (1248 cfm design) =	1412 cfm
Coil air-side pressure drop =	0.46 in WC
Test time =	10/2/02 @ 4:00 pm

Velocity Pressure (Pa)					
23.9	34.5	31.2	24.5	14.5	7.9
24	28.1	22.9	22.5	16.6	10.4
18.6	22.8	17.8	12	10.8	9.9
10.6	16.5	9.5	7.8	7.1	8.1
6.4	9.8	5.6	4.6	4.9	5.1
Velocity (ft/min)					
1238.3	1487.8	1414.8	1253.8	964.5	711.9
1240.9	1342.7	1212.1	1201.5	1032.0	816.9
1092.4	1209.5	1068.7	877.5	832.4	797.0
824.7	1028.9	780.7	707.4	674.9	720.9
640.8	792.9	599.4	543.3	560.7	572.0

## **Chilled Water Flow Rate Measurements**

The method selected to determine chilled water (CW) flow rate was to monitor the pressure drop across a chilled water loop circuit setter. The circuit setter was adjusted by the testing and balancing firm upon installation in 1995 and was not changed prior to or during this project. A mathematical correlation was developed for chilled water flow versus pressure drop across the ¾" Gerand Engineering venturi based on manufacturer's tabular data. Figure 7 below shows tabular data and the resulting correlation.



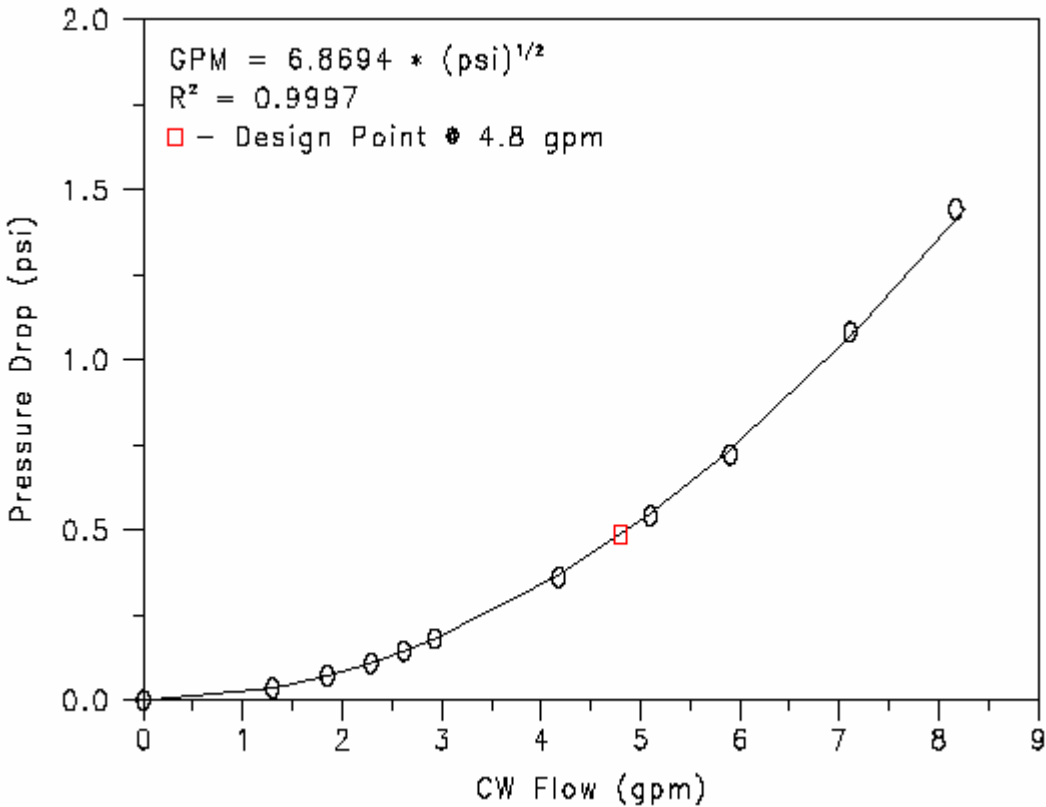


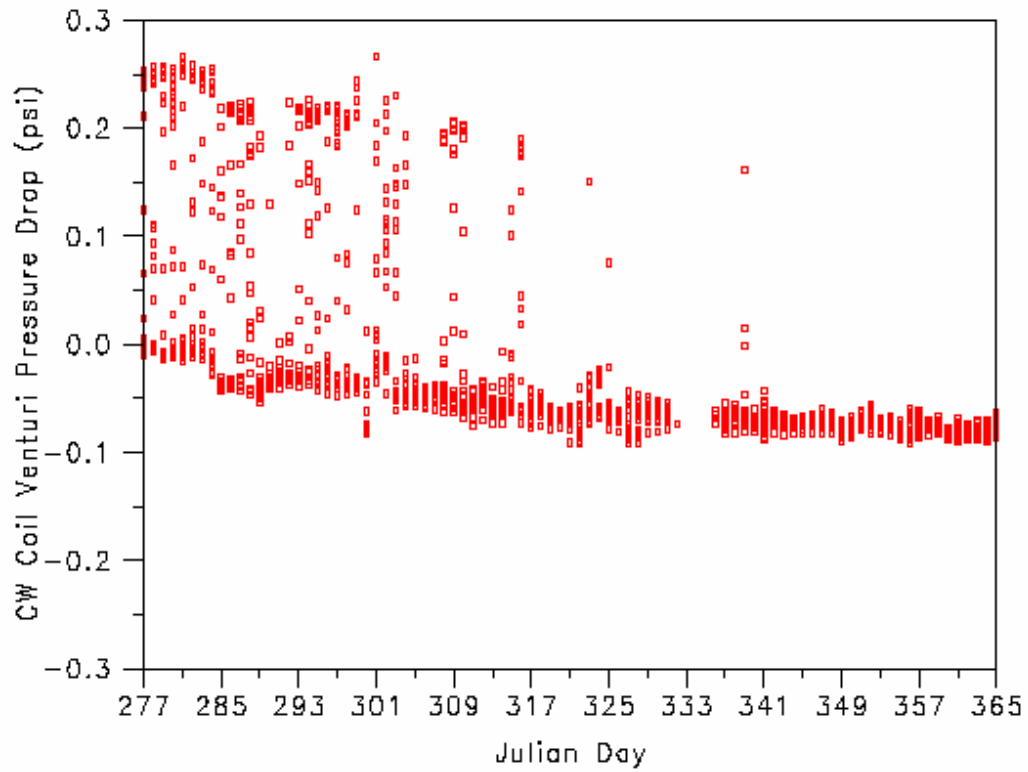
**Figure 7. Capacity Curve for Gerand Venturi Model 3/4" - 550**

A precision differential pressure sensor was installed to measure the pressure drop across the circuit setter. The sensor manufacturer's zero and span shift specification is 1.8%FS/50°C each, with long-term stability at 0.5%FS/year. The pressure range selected for this application was 0-2 pounds per square inch (psi) differential.

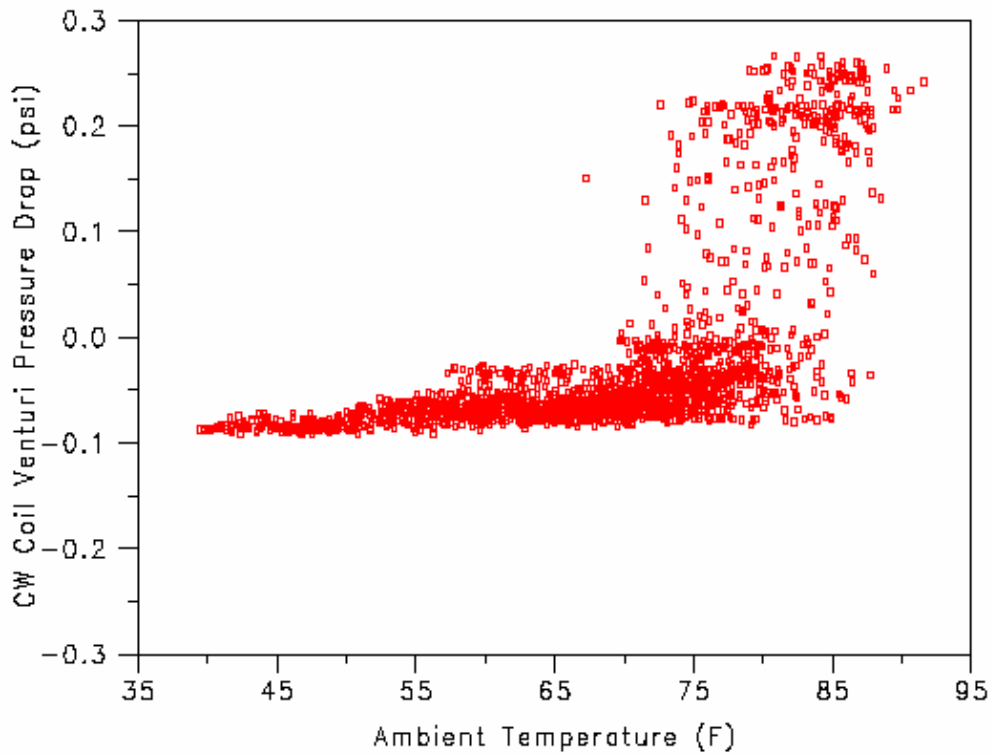
Figure 8 below shows the average hourly differential pressure for the first 89 days of monitoring. The sensor is shown to have a minimum pressure differential near zero on October 4, 2002 (Julian Day 277). Over the course of time, however, the sensor's zero output shows signs of drift continuing through December 31, 2002 (Julian Day 365).

Figure 9 shows the same differential pressure sensor output with respect to the outdoor temperature measured at a nearby weather station. The sensor's minimum pressure output is shown to be relatively insensitive to outdoor temperature for the range of temperatures experienced at this site.

To account for the zero drift of this sensor over time, the minimum pressure differential detected for each day was used to offset the measured pressures for that day. The result of modifying the data in this manner is shown in Figure 10. This method of "zeroing" the pressure measurements for each day was applied prior to determining the chilled water flow rate using the mathematical correlation shown in Figure 7.



**Figure 8. Long-term Differential Pressure Sensor Output**



**Figure 9. Differential Pressure Sensor Output versus Outdoor Temperature**



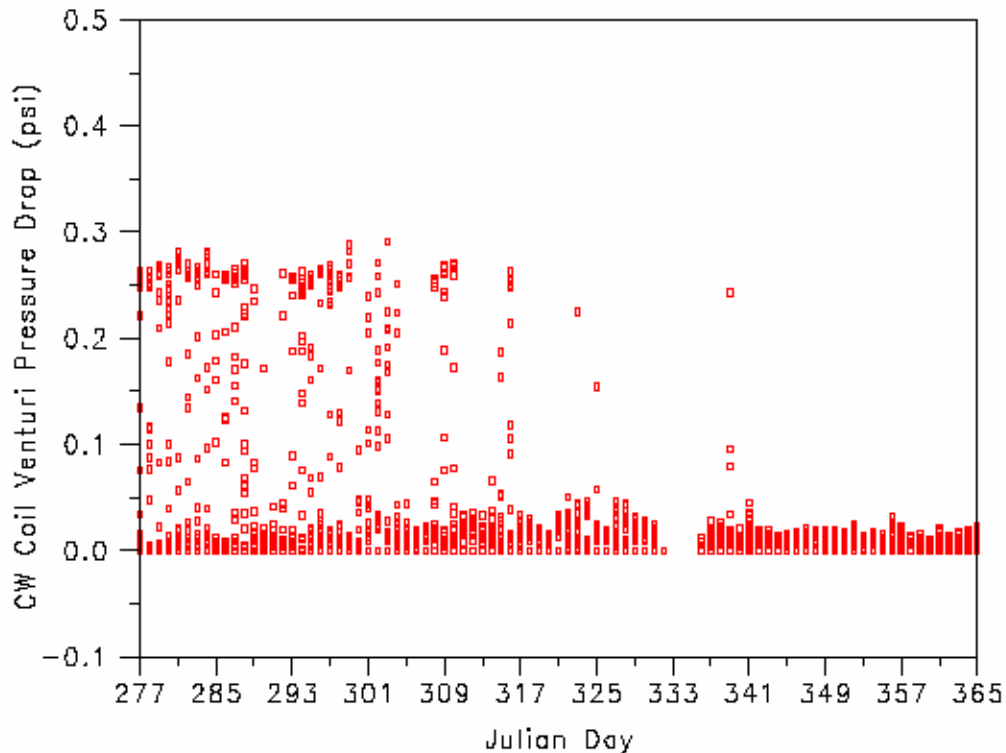


**Figure 10. Differential Pressure Sensor Output using Daily Zero Adjustment**

### **Chilled Water Valve Position Versus Flow Rate**

One objective of these field tests was to determine if lower cost methods can be used to measure the performance of air-conditioning systems instead of the more difficult and costly methods typically used. One of the performance parameters typically required is the measurement of chilled water flow rate. A potential surrogate measurement for chilled water flow through the cooling coil is the control voltage for the chilled water valve actuator, which was measured using a simple voltage divider. The chilled water valve is fully open at 6 Vdc and closes as the voltage increases to approximately 8 Vdc. The chilled water valve control signal was compared to the measured chilled water flow rate (pressure measurement across the circuit setter converted to flow rate) to determine its feasibility as a surrogate measurement for water flow rate.

Figure 11 shows measured data collected at 1-minute intervals from October 4 – October 10, 2002. Measured data for chilled water valve position was plotted versus CW flow rate for the 7-day period. The data shows that a good correlation can be made with this type of measurement within a certain range. As the valve continues to open, a point is reached where the chilled water flow rate reaches its maximum value, in this case 6.4 Vdc. The same trend is shown as the valve fully closes, however, the differential pressure measurement at the circuit setter is so small that accurate measurements of actual chilled water flow rate were not possible.

Other issues must also be considered when using such a method for monitoring the flow rate of chilled water systems (control voltage to CW valve as a surrogate for chilled water flow rate). If a low-cost technique such as this is chosen as the primary measurement of chilled water flow rate, a method must be used to correlate chilled water valve position with actual chilled water flow rate. In this case a circuit setter, with known pressure drop versus flow characteristics, was

available for comparison. A clamp-on flow meter may also be used to correlate valve position to actual flow rate. However, these meters are expensive to purchase and can also be quite expensive to rent for extended periods of time. Insertion type flow meters are also costly to purchase, although to a lesser degree, and must be installed directly into the flow stream. Insertion type flow meters either require the chilled water pump to be turned off during installation or experienced technicians can install a hot-tap port while the system remains pressurized.

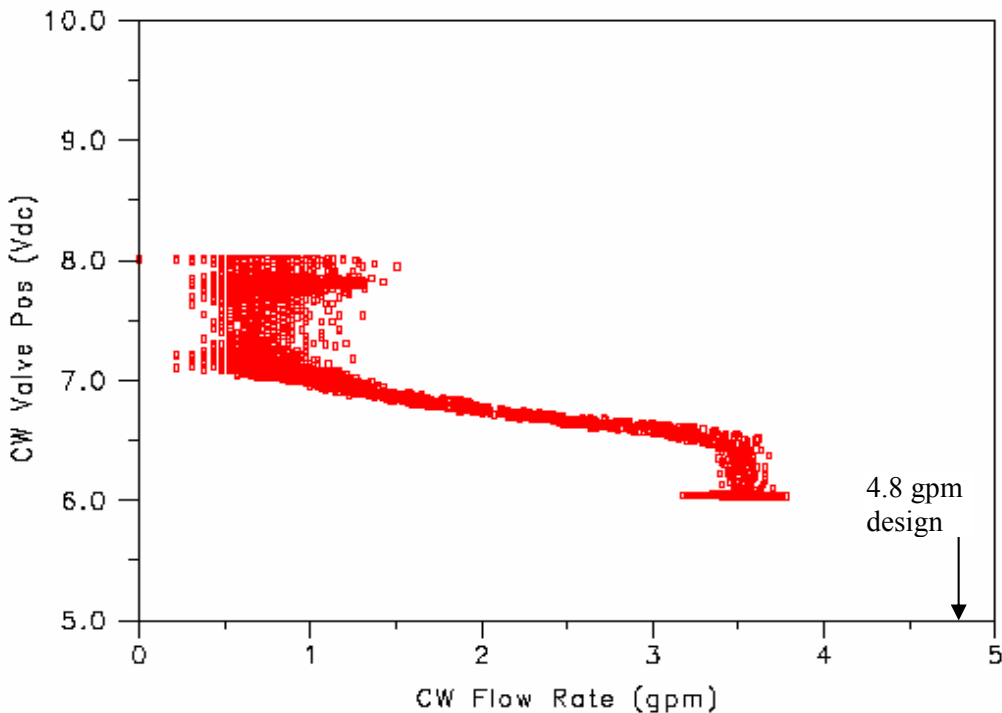
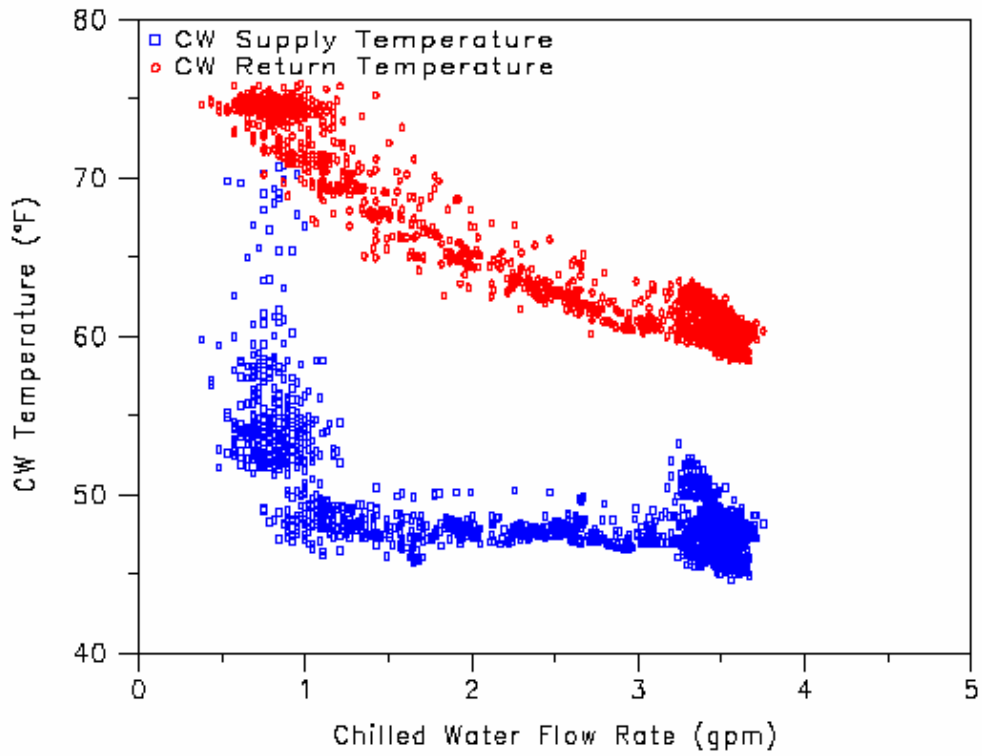


**Figure 11. Chilled Water Valve Position versus Chilled Water Flow Rate**

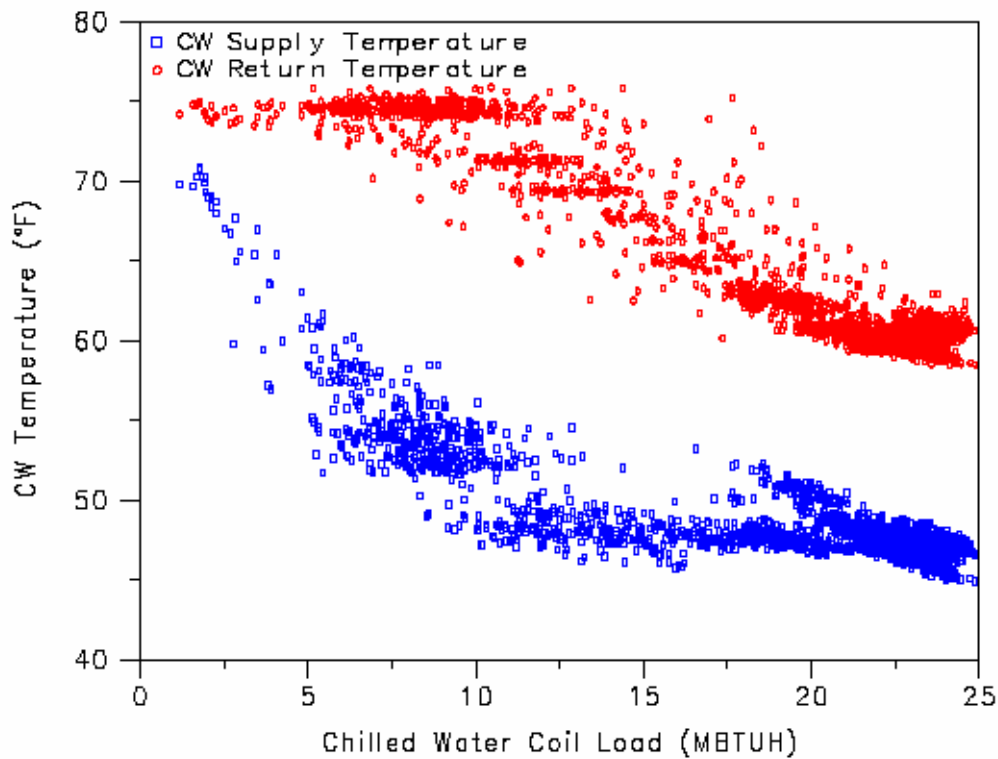
### **Measured Cooling and Dehumidification Performance**

Figure 12 and Figure 13 show the measured chilled water temperature entering and leaving the cooling coil. The data were collected from October 4 – October 10, 2002 at 1-minute intervals and are plotted only for periods with air entering the cooling coil at  $74 \pm 2^\circ\text{F}$  and  $67 \pm 3\%$  RH. Figure 12 shows that as the chilled water valve opens and water begins to flow, the supply water temperature quickly approaches the design temperature of  $45^\circ\text{F}$ . However at low flow rates, the return water temperature remains well above  $70^\circ\text{F}$ . As the chilled water flow rate increases (4.8 gpm design), the return water temperature begins to approach the design leaving water temperature of  $60^\circ\text{F}$ .

Figure 13 shows the same chilled water return and supply temperature data versus total chilled water coil load (water side). As the load on the coil increases, the chilled water valve opens to provide additional capacity for meeting the increased load. As the chilled water flow rate increases, the air-side surface of the coil becomes colder. At low chilled water flow rates (or low coil load conditions), only a small portion of the coil is cold enough to condense moisture. As the chilled water flow rate increases, more and more of the coil's surface becomes colder and is able to condense moisture.



**Figure 12. Chilled Water Temperatures versus Chilled Water Flow Rate**



**Figure 13. Entering and Leaving Chilled Water Temperatures vs Total Water-side Coil Load**

Figure 14 shows the measured supply air dry-bulb temperature versus chilled water coil load for the same time period. The supply air temperature profile is typical for a constant volume air handler under varying load conditions. Since the airflow rate is fixed at a constant value, the supply air temperature must be lowered as the load increases to provide the necessary sensible cooling capacity. This type of control has a negative impact on the air handler's latent capacity by reducing the amount of moisture removed from the air stream as the cooling load decreases. At low-load conditions, the supply air temperature is shown to be approximately 73°F. At this point, the chilled water coil has little chance to remove moisture from the air stream. As the load increases, the supply air temperature gradually reduces to near 60°F where the chilled water coil is more fully loaded and can readily dehumidify the entering air stream. This figure shows quite well why this type of control provides poor dehumidification at part-load conditions. The measured minimum supply air temperature of 59°F is 6°F higher than design (53°F), which supports the difference seen between measurements of maximum chilled water flow rate and air volume flow rate versus the corresponding design values (measured maximum chilled water flow of 3.6 gpm vs. 4.8 gpm design, 1412 cfm measured air flow rate vs. 1248 cfm design).

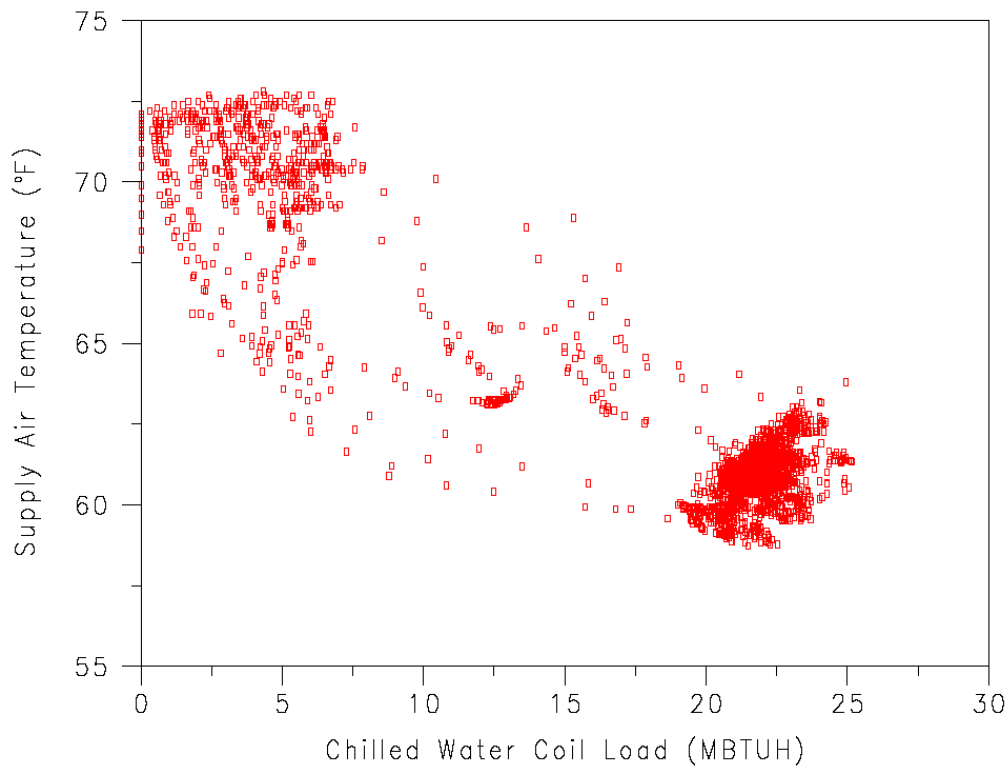


**Figure 14. Supply Air Temperature versus Total Chilled Water Coil Load**

The impact that chilled water flow rate has on this cooling coil's exiting air conditions is shown in Figure 15. The figure shows 1-minute data collected from April 30, 2003 through May 6, 2003. The return and supply air conditions entering and exiting the cooling coil are shown on a psychrometric chart. The return air conditions were limited to  $74 \pm 2^\circ\text{F}$  and  $67 \pm 3\%$  RH. The supply air conditions vary over a far broader range of temperatures depending on the current coil load. The air handler is able to remove moisture only at times when the leaving air humidity ratio is lower than the entering air humidity ratio (the average entering air humidity ratio is shown as a dotted horizontal line). At this point, the coil load and chilled water flow rate are large enough to provide a low supply air temperature and the air leaving the cooling coil is drier (has a lower

humidity ratio) than the entering air. At all other times, the supply air humidity ratio is greater than or equal to the entering air humidity ratio. When the leaving air humidity ratio is higher than the entering air humidity ratio, moisture on the cooling coil is evaporated back into the supply air stream and relative humidity in the conditioned space tends to rise.

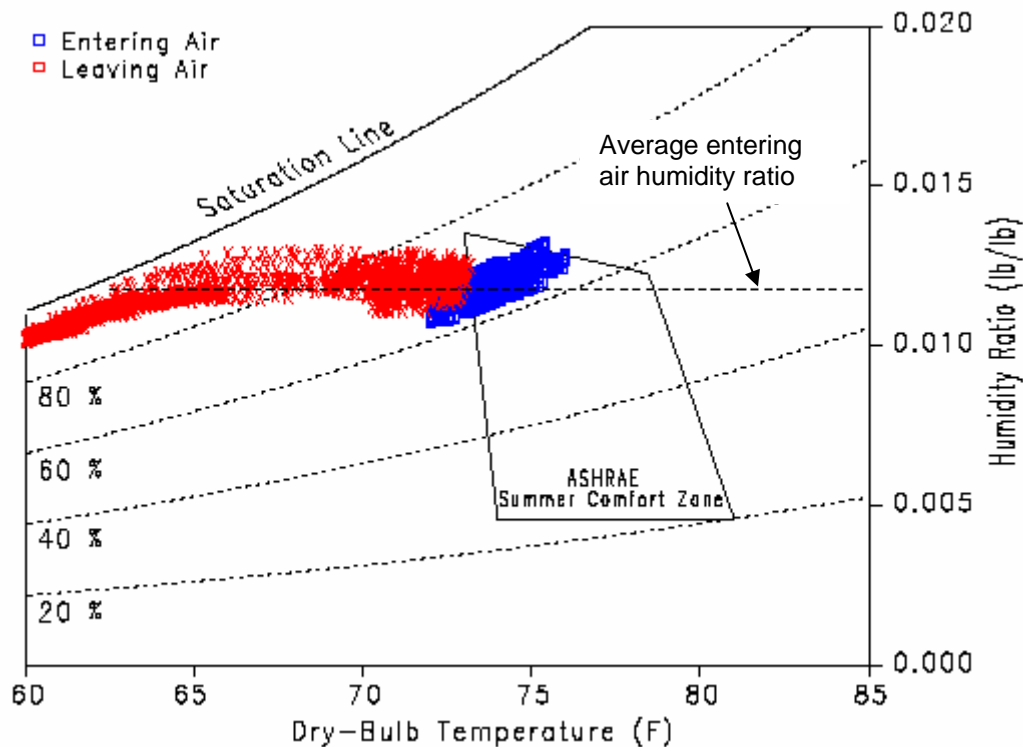
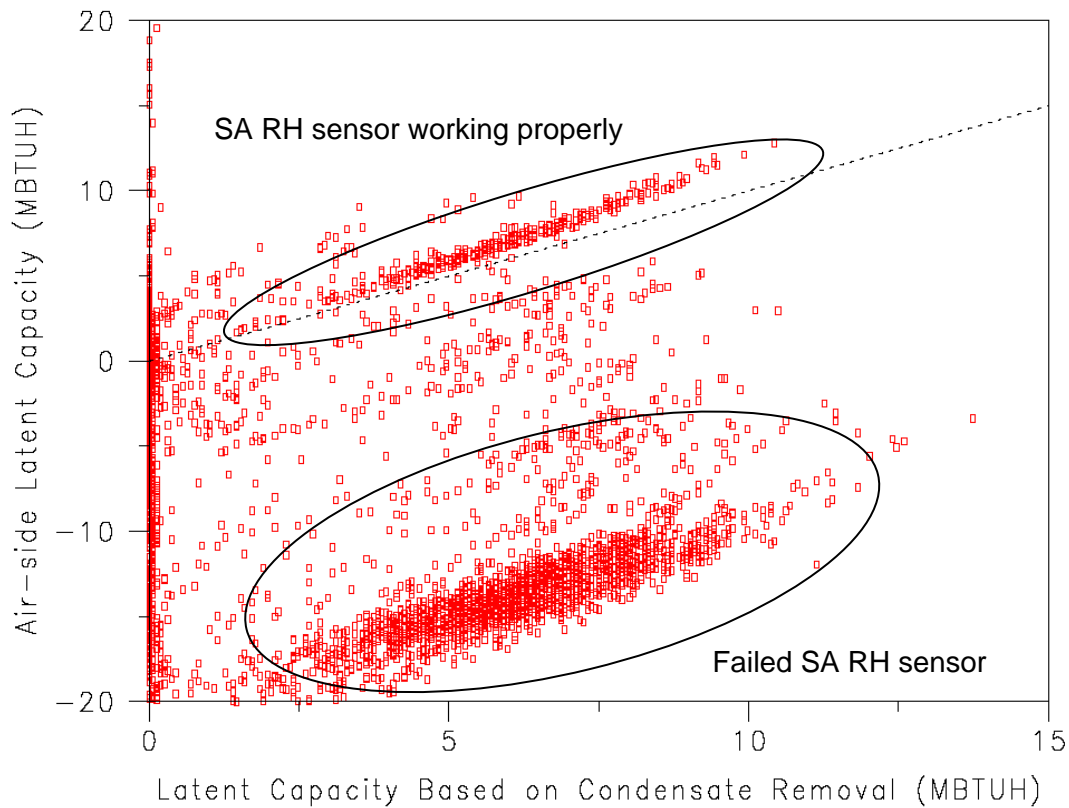


Figure 15. Chilled Water Coil Air-side Performance Data

### Comparison of Air-Side and Water-Side Measurements

Figure 16 compares the air-side latent cooling capacity based on entering and leaving air humidity conditions with latent capacity based on condensate removed. Average hourly data collected from October 4, 2002 through January 23, 2004 were plotted to determine if the air-side humidity measurements could be reliably used for other portions of the analysis. Air-side latent capacity was calculated using the temperature and relative humidity of the return and supply air, along with the one-time measurement of airflow at 1,412 cfm. At times when the surface of the coil is relatively dry and the capacity of the unit is increased (increase in CW flow rate and a colder coil surface temperature), there is a time delay while moisture builds up on the coil's surface before it drains from the unit. This is shown as a positive air-side latent capacity at zero or low condensate removal rates. As capacity fluctuates throughout the day this delay is seen as scatter in the data set. Air-side humidity measurements show relatively good agreement to condensate measurements when sensor accuracy is not compromised. However, over time the supply air relative humidity sensor's output drifted upward and exceeded 100% RH. The failure of the supply air relative humidity sensor required the use of condensate measurements to determine air-side latent capacity later in the project. The supply air relative humidity sensor measurements were unreliable after May 15, 2003.



**Figure 16. Comparison of Air-side and Condensate-based Latent Cooling Capacity**

Figure 17 compares air-side versus water-side total cooling capacity for the same time period. The air-side sensible capacity was calculated using the average (hourly) return and supply air temperatures and the one-time measurement of airflow at 1,412 cfm. The impacts of fan heat and temperature sensor offset were accounted for based on measurements of return and supply air temperatures when chilled water flow was completely stopped. Air-side latent capacity was calculated based on measured condensate removal since supply air humidity measurements became unreliable midway through the testing period. Chilled water coil return and supply water temperatures and the chilled water flow rate (based on pressure difference across the circuit setter and the correlation for water flow versus pressure drop) were used to calculate water-side total cooling capacity.

There is general agreement between the measured air-side and water-side total cooling capacity. However, there is a significant amount of scatter in the plotted data due to many factors, such as uncertainty regarding chilled water flow rate, time lag between actual moisture removal and measurement by the condensate tipping bucket, time lag in the measurement of coil water temperatures due to sensor location on pipe exterior, and thermal capacitance of the cooling coil.

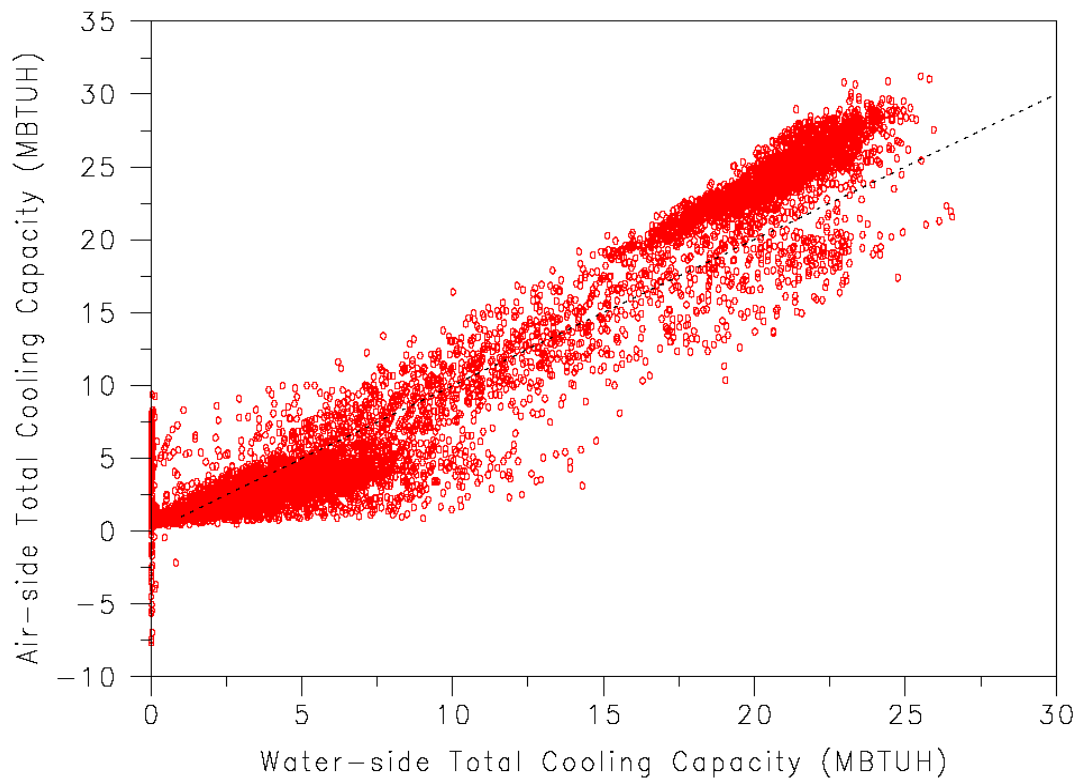


**Figure 17. Air-side versus Water-side Total Cooling Capacity**

### **Moisture-Holding Capacity of the Cooling Coil**

Tests were performed to quantify the moisture-holding capacity of this chilled water cooling coil. The chilled water valve was fully opened for a period of 1 to 2 hours in an attempt to produce a fully-wetted cooling coil. Then, water flow through the coil was stopped for several hours while the supply air fan continued to operate. Once the moisture on the cooling coil had been fully evaporated into the supply air stream, the chilled water valve was reopened and measurements were collected until condensate removal was detected by the tipping bucket mechanism. This test sequence was performed twice during the monitoring period and the results are described below.

Figure 18 shows air-side performance data collected on May 6, 2003 when this test sequence was being performed. The chilled water control valve was fully opened from 10 am until just after 12 noon. Chilled water flow was stopped from 12:08 pm to 3:15 pm using a manual isolation valve. When chilled water flow was stopped, the moisture on the coil's surface was evaporated back in to the supply air stream. The air-side sensible and latent capacities were integrated starting at 12:08 pm and ending at 2:00 pm (hour 14 in Figure 18). Based on these integrated values and assuming an enthalpy of vaporization equal to 1060 Btu/lb<sub>moisture</sub>, the moisture holding capacity of the cooling coil was estimated to be between 3.44 and 2.71 pounds. During this same integration period, 0.7 pounds of moisture exited the unit through the condensate drain line. The value of  $T_{wet}$  is calculated based on a retained moisture mass of 3.44 (based on sensible integration) and an average latent capacity just prior to the off-cycle of 8.84 MBtu/hr (based on condensate). The average inlet air temperature, humidity, and dew point conditions just prior to the off-cycle (11:57 am – 12:07 pm) were 75.33 °F, 70.31 %, and 64.97 °F, respectively. Multiplying the retained moisture mass by the heat of vaporization for water (1060 Btu/lb) and dividing by the steady-state latent capacity yields 24.7 minutes.

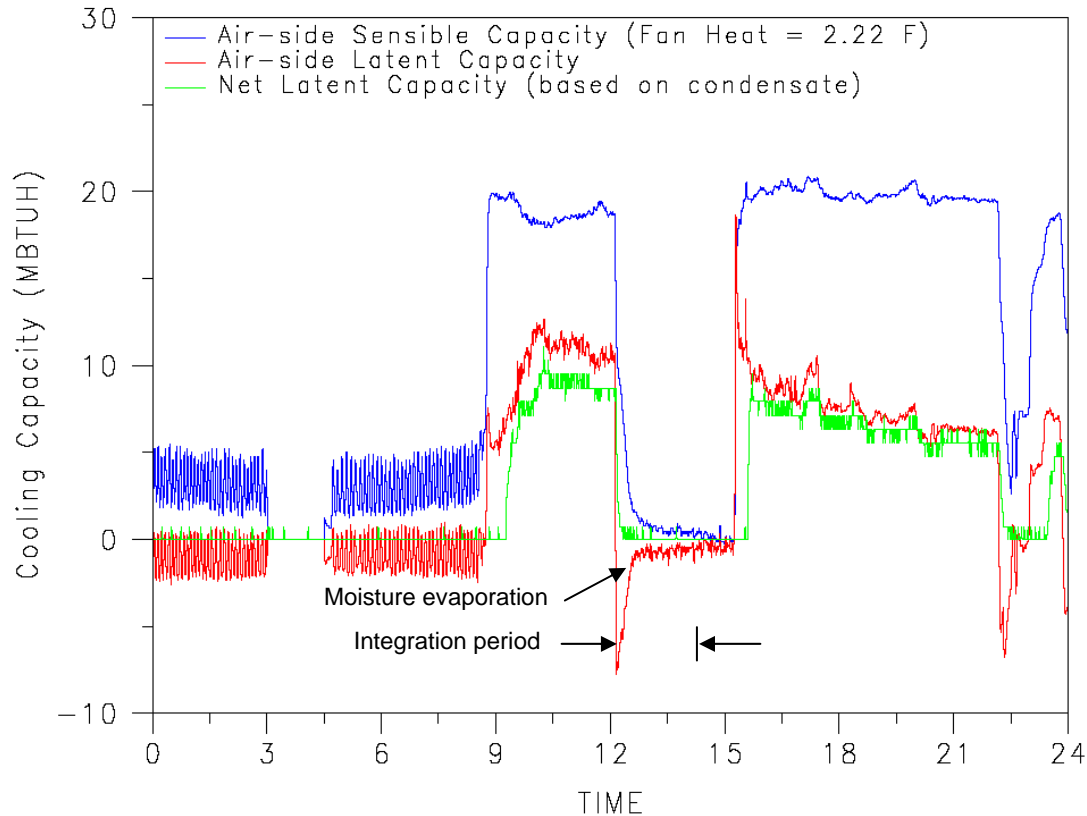
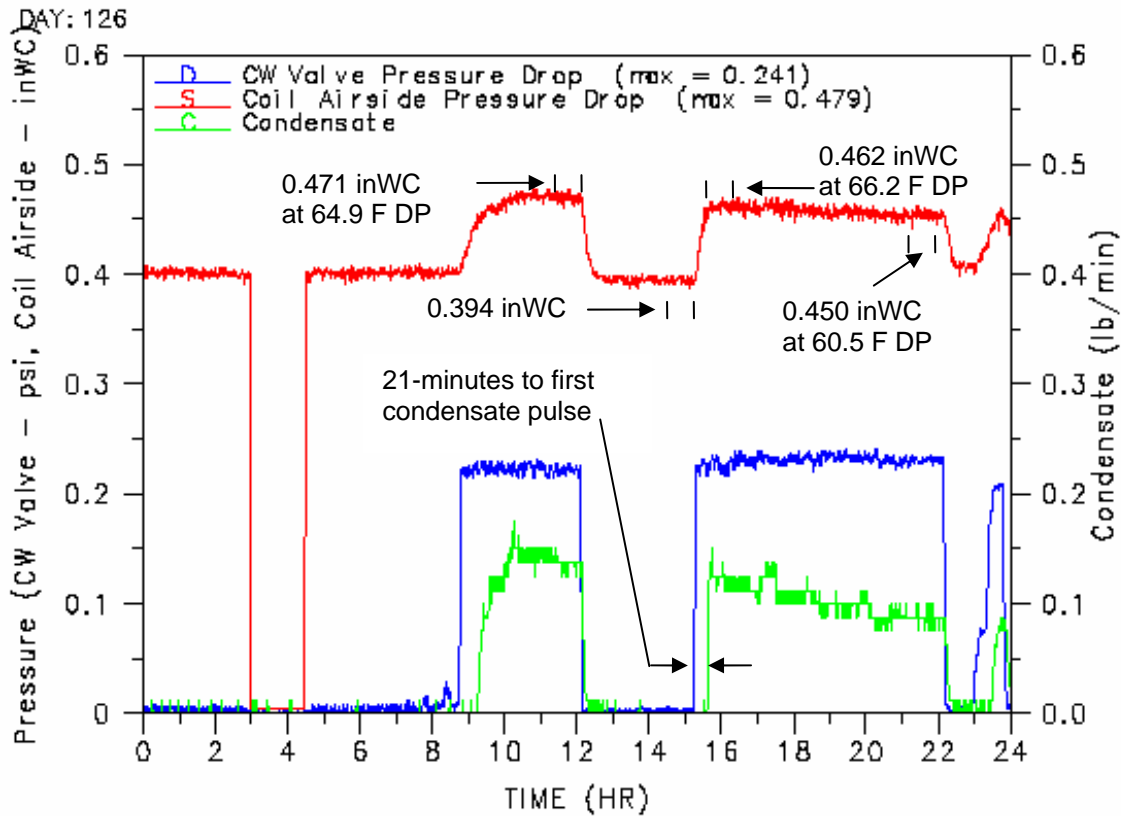


**Figure 18. Measured Sensible and Latent Capacity for May 6, 2003**

Figure 19 shows additional data measurements collected during this test sequence, including the impacts of coil moisture retention on air-side pressure drop. The coil was relatively dry prior to 8:45 am and the coil loaded up with moisture until 9:15 am where condensate began rapidly leaving the unit through the drain line (average airside pressure drop from 11:45 – 12:00 pm = 0.471 in. WC). The coil isolation valve was closed at 12:08 pm. Since the supply air fan continued to run, the moisture retained on the coil was rapidly evaporated back into the supply air stream (see Figure 18). After a sufficient period of time the coil was assumed to be completely dry and the air-side pressure drop was measured at 0.394 in. WC. The isolation valve was then opened to allow full chilled water flow through the coil. The air-side pressure drop plateaued at 0.462 in. WC at approximately 3:30 pm and gradually reduced to 0.45 in. WC at 10:10 pm as the inlet air dew point decreased due to the rapid moisture removal by the cooling coil. The air-side pressure drop for the wet coil was 0.077 in. WC (20%) higher than when the coil was dry. The air-side pressure drop due to moisture on the coil also varies based on the inlet air dew point temperature as shown from 3:30 pm to 10:10 pm.

After the isolation valve was reopened, 21 minutes elapsed before any condensate removal was measured. With latent capacity of approximately 8,000 Btu/hr (based on condensate) and a condensate delay time of 21 minutes, this coil holds approximately 2.64 pounds of moisture. This method of estimating the moisture-holding capacity of the cooling coil agrees fairly well with the previously-described method of integrating air-side latent and sensible capacities during the moisture evaporation period when chilled water flow is fully stopped.





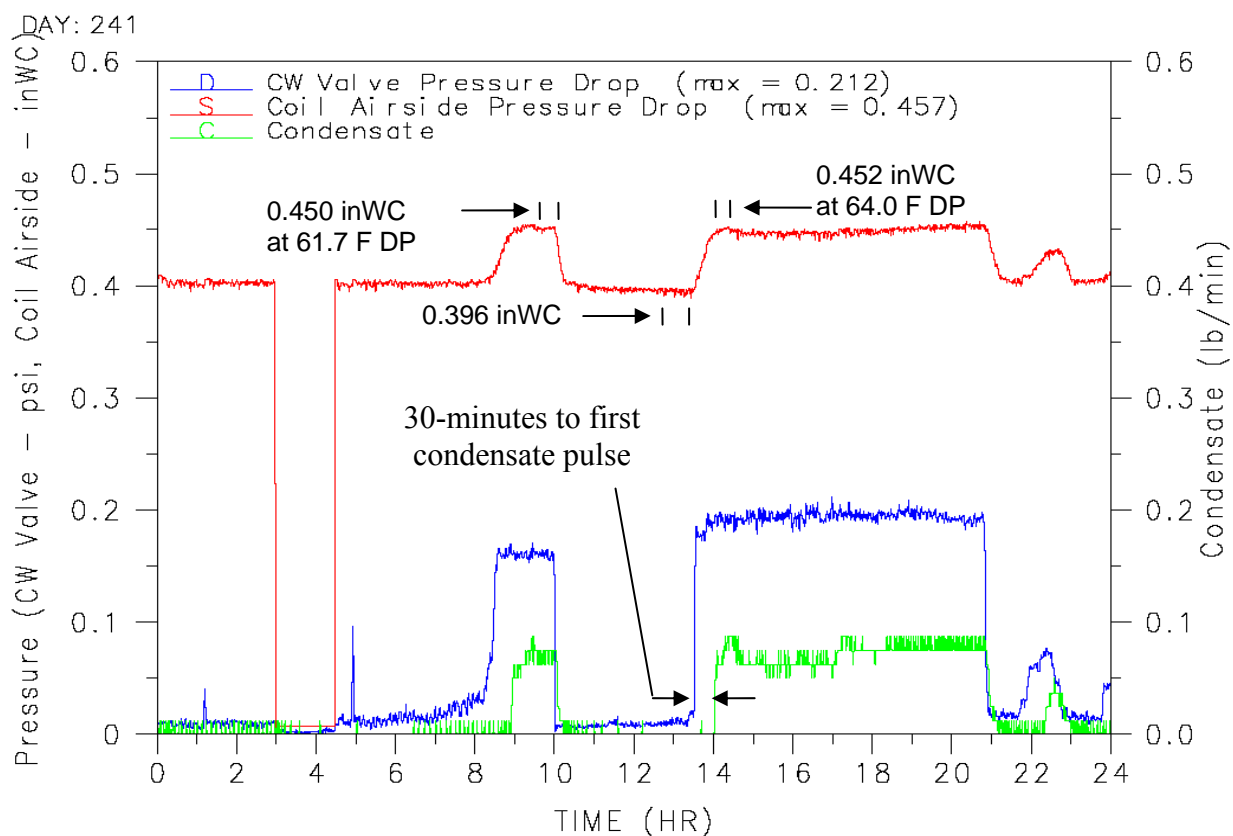
**Figure 19. Wet-dry Coil Pressure Drop and Condensate Removal for May 6, 2003**

Figure 20 shows similar measurements for data collected on August 29, 2003. For this day, the coil was relatively dry prior to 8:15 a.m. and the coil loaded up with moisture until 9:00 am when condensate began rapidly leaving the unit (average air-side pressure drop from 9:45 – 10:00 am = 0.450 in. WC). Just after 10 am the isolation valve was closed to prevent chilled water from circulating through the coil. Since the supply air fan continued to run, the moisture retained on the coil was rapidly evaporated back into the supply air stream. After a sufficient period of time the coil was assumed to be completely dry and the air-side pressure drop was measured at 0.396 in. WC. The isolation valve was then opened to allow full chilled water flow through the coil. The air-side pressure drop plateaued at 0.452 in WC around 2:20 pm.

For these operating conditions, moisture retention on the cooling coil increased the air-side pressure drop by 0.056 in. WC (14%). This result is somewhat lower than for the similar data collected on May 6, 2003 (Figure 19), indicating less moisture retention on the cooling coil during this latter test. The pressure drop across the circuit setter was lower during the August 2003 test (Figure 20) than during the May 2003 test (Figure 19). This indicates a lower chilled water flow rate during the August test which would have reduced the amount of moisture held on the coil. Drier inlet air conditions were also present during the August test which would have also reduced coil moisture retention the time measured to the first condensate pulse.

Integrating the sensible capacity during the off-cycle evaporation period (10:03 a.m. to 12:00 p.m.) yields 2.92 lb of moisture retained on the coil surface. After the isolation valve was

opened, 30 minutes elapsed before condensate removal was measured. With latent capacity of approximately 4,700 Btu/hr (based on condensate) and a condensate delay time of 30 minutes, the moisture on the cooling coil is estimated at 2.22 lb.



**Figure 20. Wet-dry Coil Pressure Drop and Condensate Removal for August 29, 2003**

### **Part-Load Dehumidification Performance**

Figure 21 and Figure 22 show hourly performance data for the constant-air-volume chilled water air handler. Data collected from October 4, 2002 through January 23, 2004 were averaged over one-hour intervals to provide performance data over a wide range of load conditions. Air-side sensible capacity was calculated using the temperature difference between the return and supply air streams and the one-time measurement of supply air flow rate. The impacts of fan heat and temperature sensor offset were accounted for based on measurements of return and supply air temperatures when chilled water flow was completely stopped. Latent capacity was calculated using the measured condensate removal. The sensible heat ratio was calculated as the ratio of the delivered sensible capacity to total (sensible plus condensate) capacity. Chilled water coil return and supply water temperatures and the chilled water flow rate (based on pressure difference across the circuit setter and the correlation for water flow versus pressure drop) were used to calculate water-side total cooling capacity (Figure 22). Performance data in each figure is shown for return air temperatures of  $75 \pm 1^\circ\text{F}$  and return air relative humidities of  $66.5 \pm 1.5\% \text{RH}$ .

Although the performance data plotted versus water-side cooling load (Figure 21) shows a slight degree of scatter, both figures show that the latent capacity of this unit is virtually zero below 15,000 Btu/hr of gross cooling capacity. From this point, the latent capacity of this coil gradually

increases with increasing cooling load. These data indicate that the cooling coil must be loaded more than 50% of its maximum capacity at these operating conditions to provide any dehumidification. These data confirm the expected drop in part-load latent capacity for this type of cooling system.

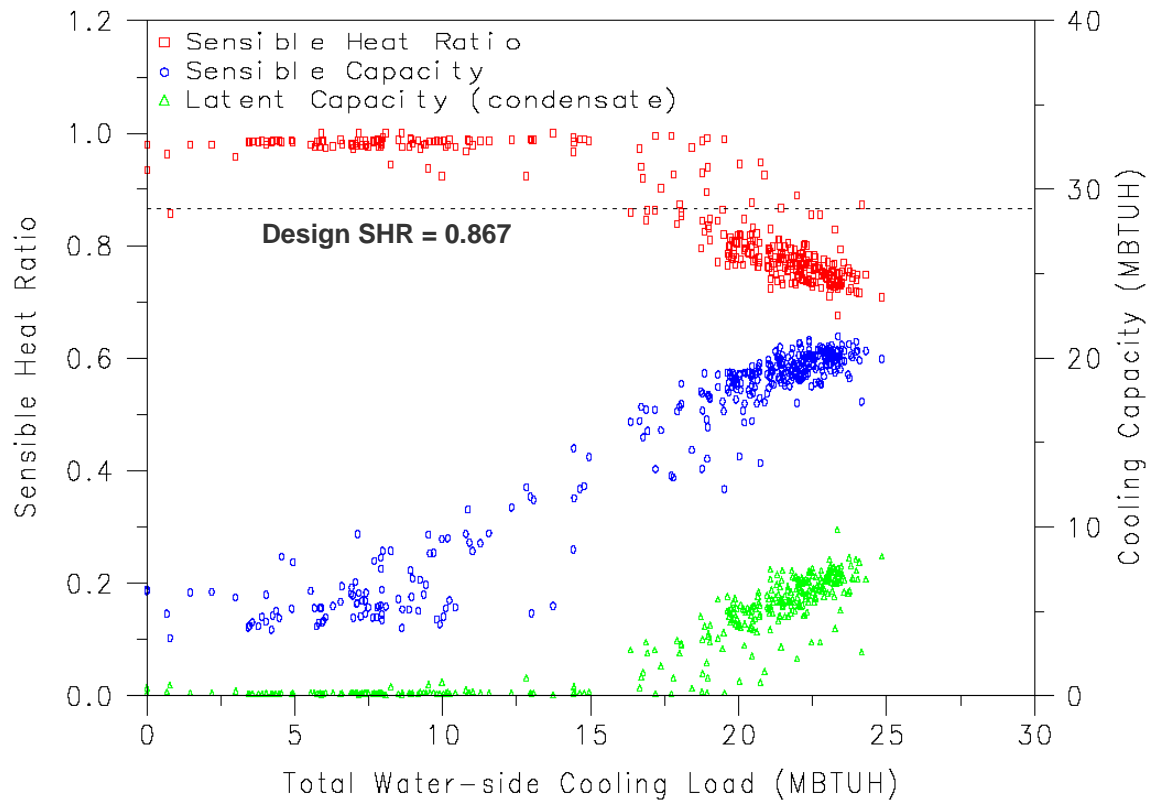


**Figure 21. Hourly Air-side Capacity and SHR versus Total Water-side Cooling Load**

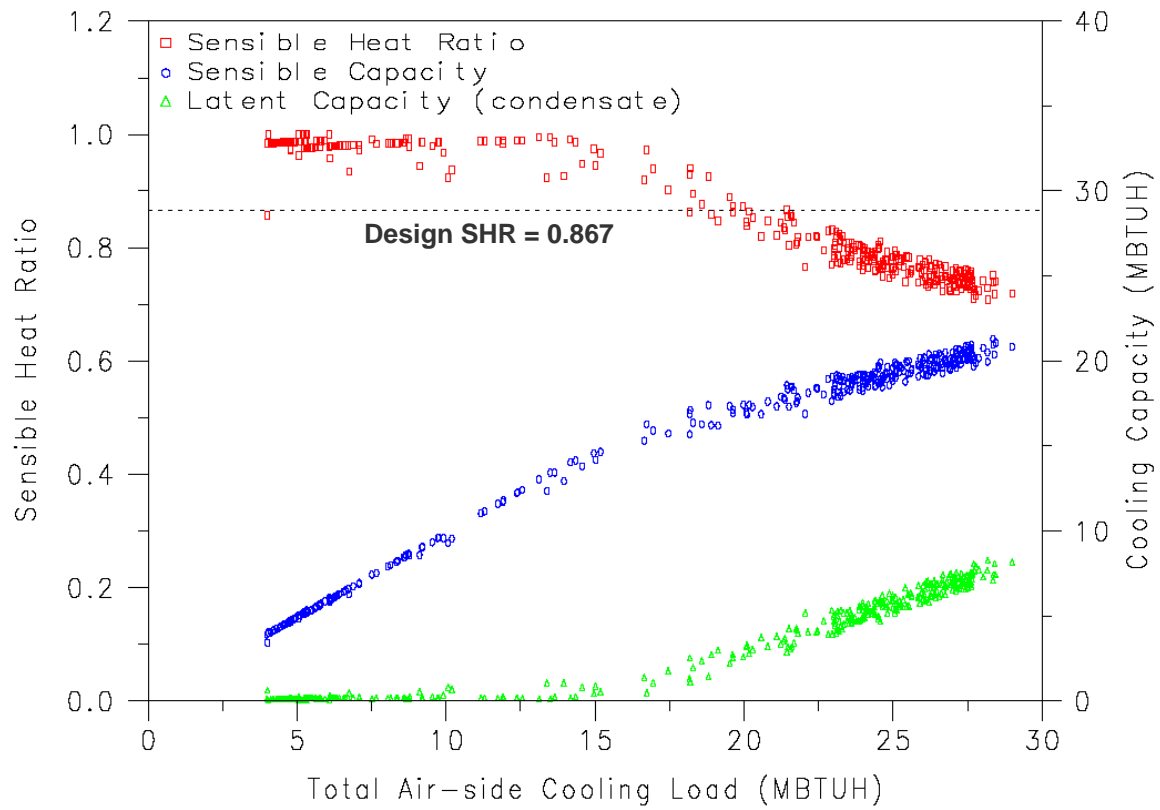


**Figure 22. Hourly Air-side Capacity and SHR versus Total Air-side Cooling Load**

## **APPENDIX I7**

### **Summary of Data for Field Test Site 7**

## Site #7 – Commercial Building in Cocoa, Florida

### Building Description

This site is a two-story office facility located in Cocoa on Florida's East coast, approximately 45 miles east of Orlando. The facility is conditioned by multiple chilled water, variable volume air handlers. One of these air handlers was monitored for this project.



Figure 1. Eastern exposure for Site #7 in Cocoa, Florida

### Chilled Water Air Handler Description

The system was installed in 1995. Trane modular air handler, CLCH-6. This system has a design cooling capacity of approximately 7 tons. The air handler is located in a mechanical room and is used to condition a portion of the offices in the main building. The area where the air handler is mounted is conditioned year round.

Figure 2 shows the unit installed in the first floor mechanical room of the 2-story office building. The unit is comprised of a filter rack section (bottom left of figure), chilled water coil section (bottom middle of figure), and a fan (draw-through at upper right of figure) section. The air volume flow rate is variable, and a two-way modulating valve is used to control the cooling capacity based on thermostat temperature. Figure 3 shows the coil's copper header assembly and Figure 4 shows the fin spacing of the cooling coil to be 11 fins per inch (fpi).





**Figure 2. VAV Air Handler**



**Figure 3. Coil Header Connection**

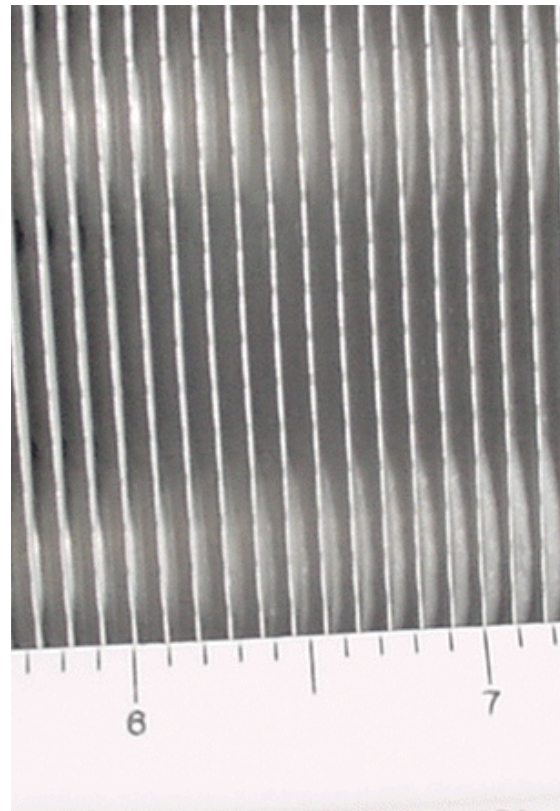


**Figure 4. 11 Fins Per Inch Fin Spacing**

**Design Data:**

Variable Air Volume AHU Trane CLCH-6  
 Design CFM – 2888 CFM  
 Design Outside Air – 545 CFM  
 Minimum Outside Air – 200 CFM  
 Total Capacity – 83600 BTUH  
 Sensible Capacity – 69520 BTUH  
 Rows/fpi – 6 / 12 (11 actual)  
 Entering Water Temp/LWT – 45 F / 60 F  
 Entering Air Temp – 73.3 DB / 61.9 WB  
 Leaving Air Temp – 51.8 DB / 51.7 WB  
 Chilled Water Flow Rate – 11.9 GPM  
 Coil Type – Vertical Slab  
 Fan HP/Configuration – 5 / Draw-Thru

**Thermostat Setpoints**

8:00 am	75 Cool	Occupied
	68 Heat	
5:00 pm	85 Cool	Unoccupied
	65 Heat	

**Sensors and Data Logger Connections**

**Table 1. Data Logger Channel Assignments and Sensor Identification for Site #7**

Channel Data Point Description			Units	Sensor
DI1	TCWE	Chilled Water Entering Temperature	F	Type-T Thermocouple
DI2	TCWL	Chilled Water Leaving Temperature	F	Type-T Thermocouple
DI3	TAM	Return Air Mixed Temperature	F	Type-T Thermocouple
DI4	TAS	Supply Air Temperature	F	Type-T Thermocouple
DI5	Not Used			
SE11	SF	Fan Status	On/Off	Veris H904
SE12	TREF	Thermocouple Reference Temperature	C	Campbell Scientific TC107
P1	WF	Fan Power	kWh	Ohio Semitronic WL40R-052
P2	FC	Condensate	lb	Texas Electronics tipping bucket
C1	MUX-cntrl			
C2	MUX-cntrl			
C3-8	Not Used			
MUX-1	RHIN	Return Air Relative Humidity	%	Vaisala HMD60U
MUX-2	RHOUT	Supply Air Relative Humidity	%	Vaisala HMD60U
MUX-3	PDB	Pressure Drop at Balancing Valve	Psi	Setra Model 230 – 2 psi
MUX-4	PDC	Pressure Drop across CW Coil	In WC	Setra 267MR (0.25, 0.5, 1.0 inches)
MUX-5	VP	CW Valve Position (6-9 Vdc)	Vdc	Voltage divider



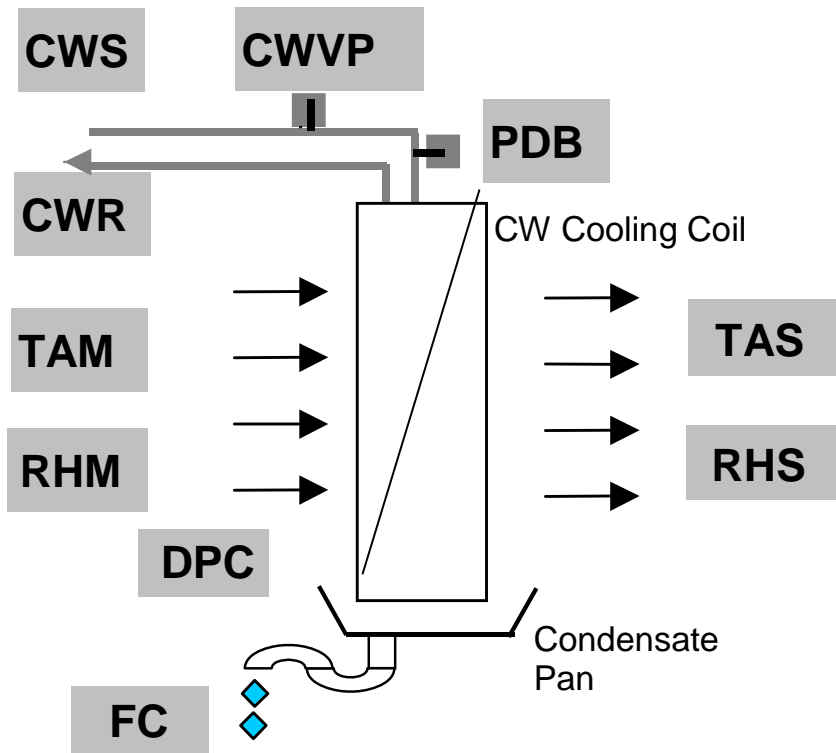


Figure 5. System Schematic

**Coil Measurements**

Coil Type	Vertical Slab	
Coil Face Area	825.3 sq. in.	
Number of rows	6	
Tubes per row	18	
Tubing diameter	1/2" OD	
Tube Spacing	1 1/4" row-row	
Coil Thickness	8"	
Fin Spacing	11 fpi	
Fan Configuration	Draw Thru	
Notes:		

Gross fin area:  $(8 \text{ in}) \times (11 \text{ fins/in}) \times (2 \text{ sides/fin}) \times (825.3 \text{ sq. in.}) / 144 \text{ sq in/ft}^2 = 1008.7 \text{ ft}^2$

## One-Time Measurements

### Air Flow using Pitot Tube Measurements

The air flow rate through the cooling coil is monitored using a surrogate measurement of coil air-side pressure drop. Since this air handler is a variable-air volume unit, the air flow rate through the cooling coil should be proportional to the square root of air-side pressure drop across the cooling coil. The chilled water valve is controlled to maintain a constant 50 °F supply air temperature while air flow through the unit is varied to provide the desired capacity. This control will provide a wetted coil surface throughout the day and pressure affects due to varying amounts of moisture on the cooling coil surface are neglected for this portion of the analysis. The following one-time measurements describe the 30-point pitot tube traverse of the return air duct when the supply air fan was set at 60 Hz. The coil air-side pressure drop was measured at 1.01 inwc and the calculated air flow rate was 3654.5 cfm. Similar measurements were made at 53, 45, and 37.7 Hz to provide a range of air flow through the unit used to calibrate the surrogate measurement of coil air-side pressure drop.

#### AHU 2 - Variable Air Volume CW Air Handler @ 60 Hz

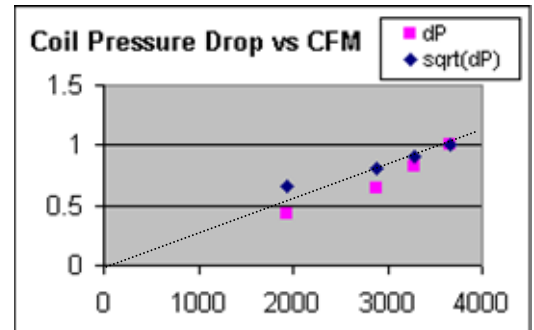
Duct Static Pressure = 563 Pa  
 Duct Dimension = 32x15 in  
 Duct Area = 3.3333 sqft  
 Average velocity = 1096.4 ft/min  
 Airflow (2888 cfm design) = 3654.5 cfm  
 Coil pressure drop = 1.01 inwc  
 Test time = 10/3/02 @ 8:35 am

Pressure (Pa):  
 Before filter -171  
 Filter/Coil -243  
 Coil/Fan -460  
 After fan 563  
 Time = 10/3/02 @ 9:10 am

Pressure (Pa)					
9.3	8.4	14.5	21.4	34.6	36.4
7.8	7.2	16.4	25.1	25.3	35.1
7.4	7.1	13.4	20.6	25.7	33.4
7.1	8.5	12.9	16.7	25.4	42.7
6.2	9.3	18.1	26.9	43.1	52.6

Velocity (ft/min)					
772.5	734.1	964.5	1171.8	1489.9	1528.2
707.4	679.7	1025.8	1269.0	1274.1	1500.7
689.0	674.9	927.2	1149.7	1284.1	1463.9
674.9	738.5	909.8	1035.1	1276.6	1655.2
630.7	772.5	1077.6	1313.7	1662.9	1837.1

CFM	dP	sqrt(dP)
3654.5	1.01	1.004988
3285.1	0.826	0.908845
2877.199	0.649	0.805605
1938.209	0.43	0.655744



### Chilled Water Flow Rate using Gerand Venturi Circuit Setter

The method selected to determine chilled water flow rate was to monitor the pressure drop across a chilled water loop circuit setter. The circuit setter was adjusted by the testing and balancing firm upon installation in 1995 and was not changed prior to or during this project. The manufacturer's water flow rate versus pressure drop curve for the 1 ¼" Gerand Engineering venturi was used to calibrate the measured venturi pressure drop to CW coil flow rate in units of gallons per minute (gpm). Figure 6 shows the results of the least squares fit used for calibration.

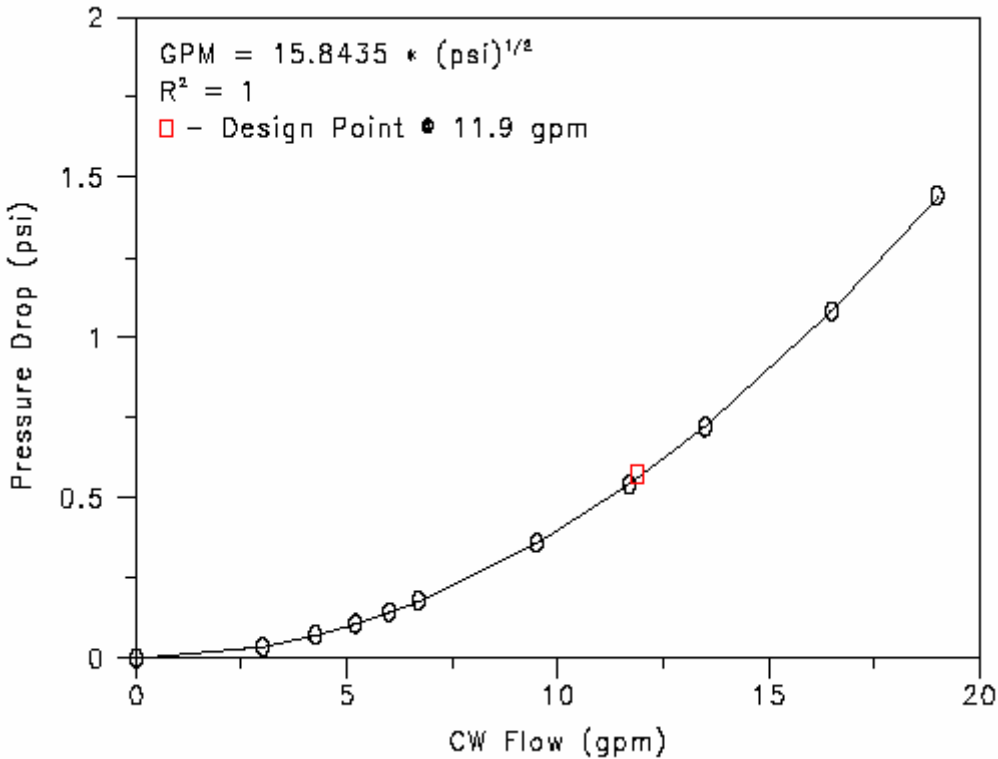
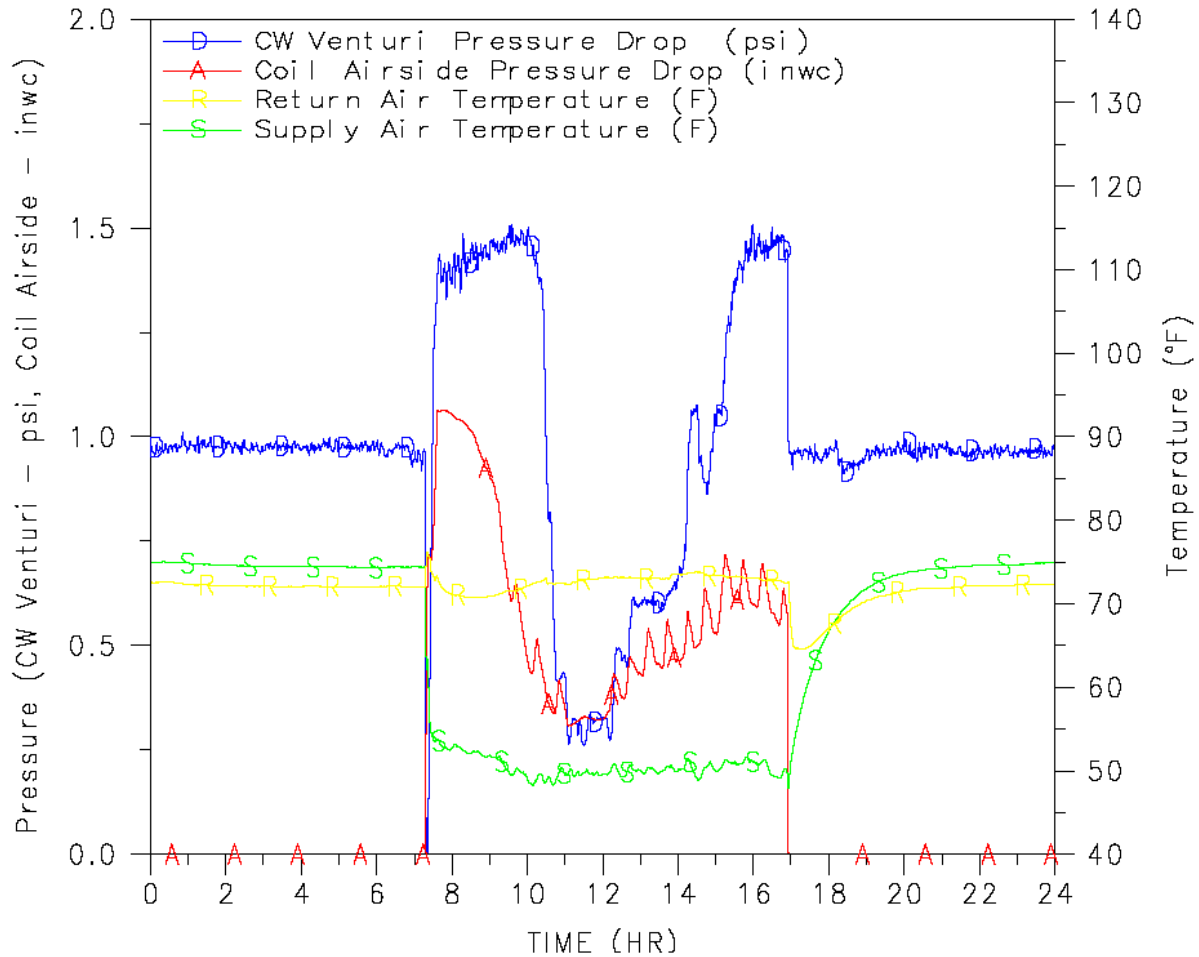


Figure 6. Capacity Curve for Gerand Venturi Model 3/4" - 550

### Measuring Chilled Water Flow Rate using a Balancing Valve Venturi

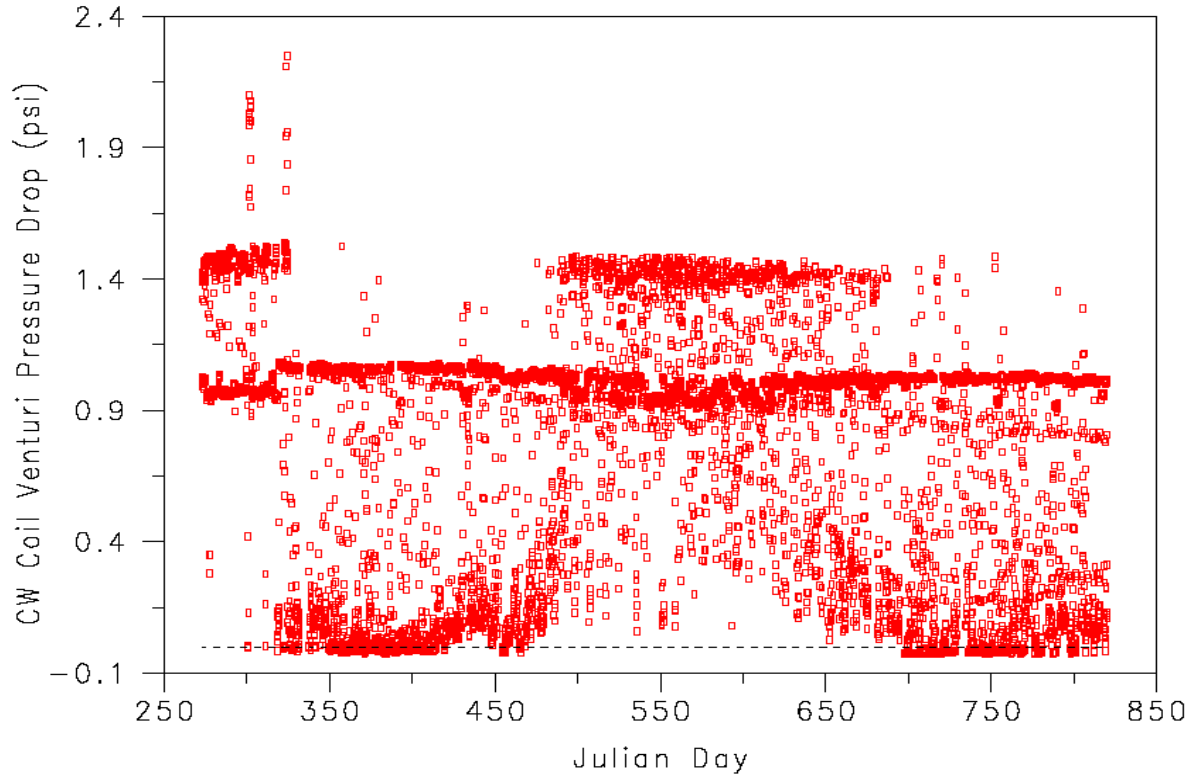
Chilled water flow rate was monitored using a balancing port circuit setter. A precision differential pressure sensor was installed to measure the pressure drop associated with chilled water flow through the venturi. The examination of air-side and water-side pressure drops and supply air temperature for a typical summer day will provide insight into the operation of this air handler.

Figure 7 below shows the pressure drop across the balancing port circuit setter along with the air-side pressure drop across the chilled water coil and supply air temperature for May 16, 2003. The air handler operated from 7:15 a.m. to 5:00 p.m. as seen from the increased air-side pressure drop across the cooling coil. During unoccupied hours the chilled water flow rate is continuous with a CW venturi pressure drop of approximately 1.0 psi. At 7 a.m., the coil air-side pressure drop increases to a maximum pressure of 1.2 inwc at 7:15 a.m. as the air handler ramps up in the morning during pull-down. The air-side pressure decreases gradually until approximately 11:00 a.m. as the variable-air-volume air handler reduces fan speed based on space temperature. During this time, the supply air temperature is shown to be above the 50 °F set point temperature. As the supply air temperature approaches 50 °F, the chilled water valve closes to maintain the 50 °F supply air temperature set point. As the afternoon loads increase, the coil air-side pressure drop increases as the fan speed is raised in response to the space thermostat. Return air temperature entering the cooling coil is shown to be approximately 72 °F.



**Figure 7. CW Venturi and Air-Side Pressure Drop**

Figure 8 below shows the output of the differential pressure sensor for the duration of the project. The sensor manufacturer's zero and span shift specification is 1.8%FS/50°C each, with long-term stability at 0.5%FS/year. The pressure range selected for this application was 0-2 pounds per square inch (psi) differential. Using average hourly data, the sensor's output is shown to have a minimum average pressure reading near 0.0 from September 30, 2002 (Julian Day 273) through March 30, 2004 (Julian Day 365 [end of 2002] + 365 [year 2003] + Julian Day 90 [March 30, 2004] = 820). Over the course of time, the sensor's zero output is shown to be relatively stable near 0.0 psi and adjustments to the sensors output regarding zero shift were not necessary. The grouped set of data near 1 psi reflects the large amount of time chilled water is flowing through the coil during unoccupied hours. Data above this value to the far left and center of the figure is during summer months when loads are high. Data below this value is during winter and shoulder months when loads are lower and require less chiller water flow. The raw data shown in Figure 8 will be used throughout this analysis to provide a measurement of chilled water flow rate through the cooling coil.



**Figure 8. Long-term Differential Pressure Sensor Output**

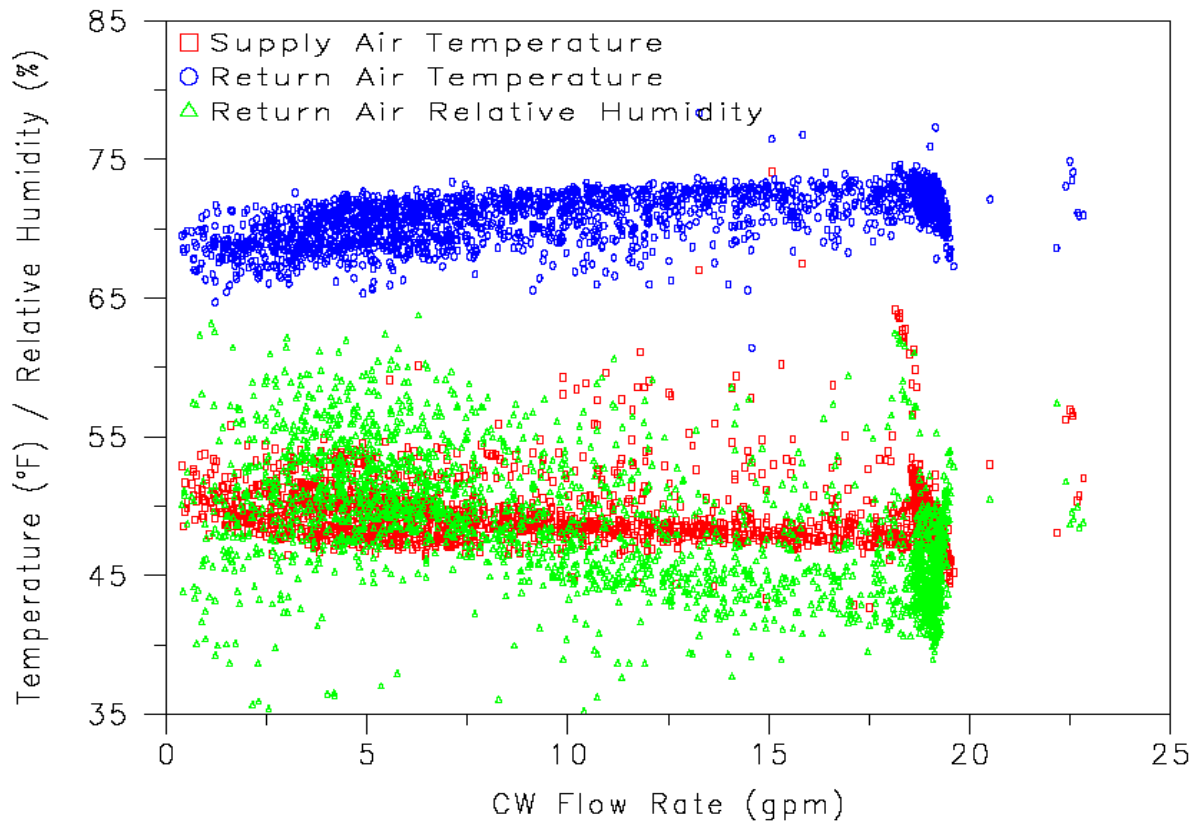


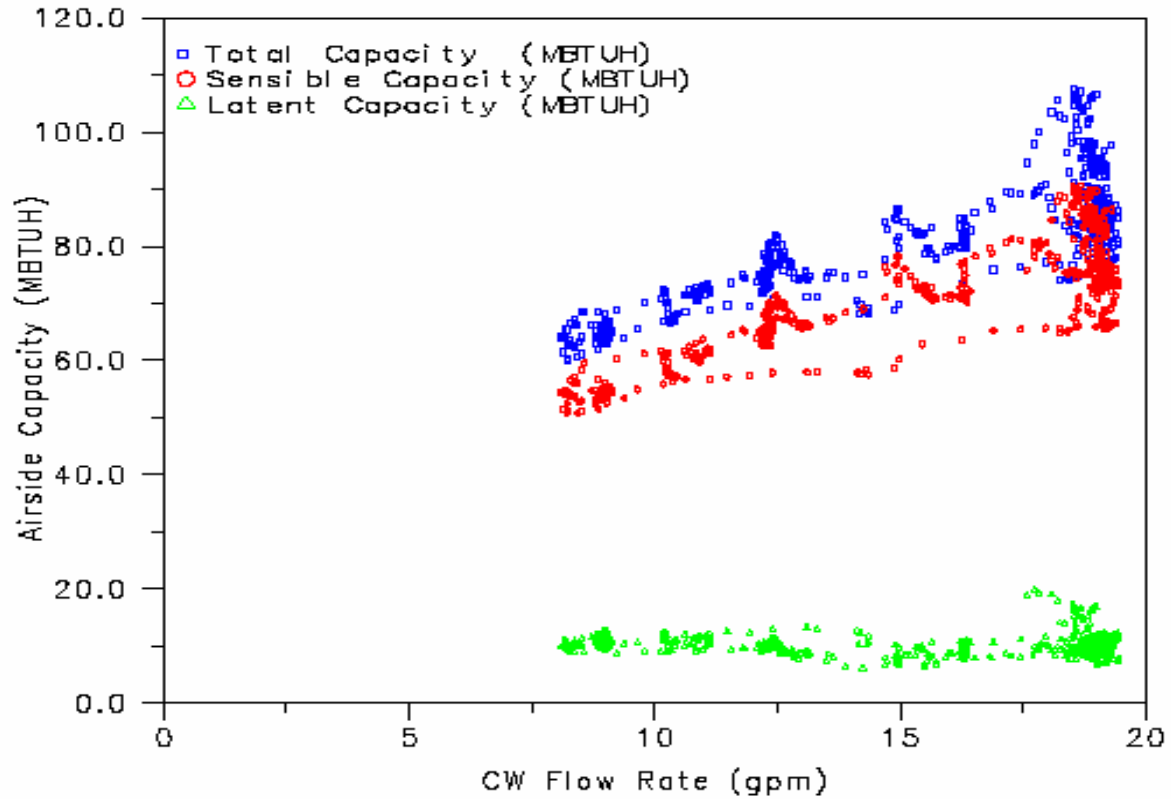
**Figure 9. Return and Supply Air Temperature versus CW Flow Rate**

## **Measured Cooling and Dehumidification Performance**

Figure 9 shows the return air temperature entering the air handler and supply air temperature leaving the air handler as a function of chilled water flow rate. The same hourly data set presented in Figure 8 was converted to gallons per minute (gpm) using the correlation shown in Figure 6. Collected data was screened to provide only occupied hours between the hours of 9 a.m. and 5 p.m. to eliminate weekends and morning pull-down hours where the average hourly supply air temperatures were considered invalid. Supply air temperature for this variable air volume air handler is controlled at 50 °F. The supply air temperature shown in the figure is adjusted for supply air fan heat to reflect the air temperature leaving the cooling coil. The return air temperature shown is a mixture of pre-treated outdoor air and varying amounts of recirculation air. The control system is shown to maintain a coil exiting supply air temperature of approximately 50 °F. A supply air temperature reset strategy is not used.

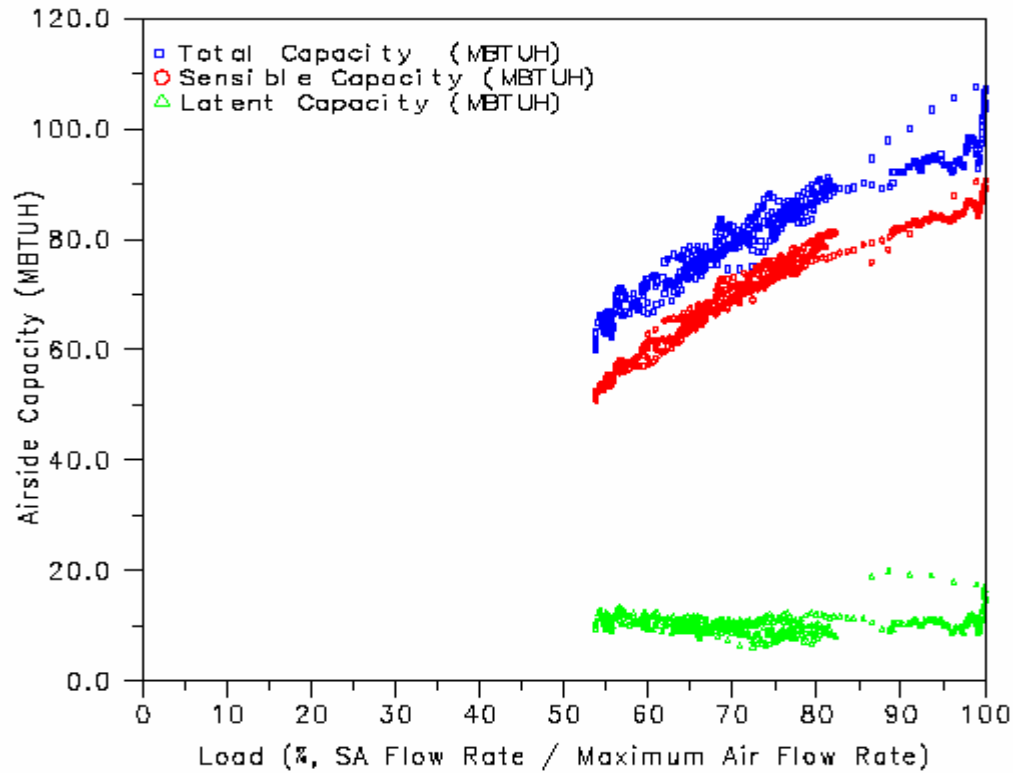
The energy management system also monitors other parameters to control and pre-treat the outdoor air entering the building. Carbon dioxide (CO<sub>2</sub>) sensors are located in the return air stream and monitored to control the CO<sub>2</sub> levels at or below 1000 ppm recommended by ASHRAE Standard 62-1989. This air is pre-treated by heat-pipe assisted chilled water coils to maintain a 60 °F supply air temperature off the outdoor air coils. The heat pipes are used to avoid over cooling the space during low load conditions. The amount of outdoor air supplied to the building is also controlled. Based on the amount of outdoor air entering the building, the minimum outdoor air volume set point, and the worst (or minimum) variable-air-volume box position, an outdoor air damper is set to provide the minimum amount of outdoor air. Due to this control scheme, relative humidity in the space is shown to rarely exceed 60 %.

Figure 10 shows the measured air-side total, sensible and latent capacities plotted as a function of chilled water flow rate. The same data set was used as in Figure 7, however, only data collected between the hours of 7:30 a.m. and 4:56 p.m. were plotted. Sensible capacity was adjusted for fan heat to provide an accurate assessment of this chilled water coil. The maximum air-side sensible capacity is shown to be quite similar to the design value of 69,520 MBTUH with slightly higher capacities occurring during pull-down hours. Air-side latent capacity is shown to be relatively constant at approximately 10 MBTUH which tends to support the fact that variable-air volume air handlers are much more capable of removing moisture from the air stream over a wide range of load conditions.



**Figure 10. Air-side Capacity versus CW Flow Rate**

Figure 11 shows the same air-side performance data as in Figure 10, however, this time the performance data is plotted versus air handler load with respect to supply air flow rate. Since a variable-air volume air handler modulates air flow rate to maintain space temperature, the performance data for sensible capacity is shown to be more linearly correlated to air flow as opposed to chilled water flow rate as shown in Figure 10.



**Figure 11. Airside Capacity versus Air Handler Load**

Figure 12 shows a comparison of measured air-side latent capacity to the condensate collected from the condensate drain pan using the same hourly data set previously described in Figure 8. Although the air-side latent capacity is shown to be slightly higher (~10% at higher capacities) than the condensate measurements, the fair correlation shown indicates that the more difficult measurements of air flow rate and inlet and outlet humidity ratio's are measured within a reasonable tolerance for this analysis.



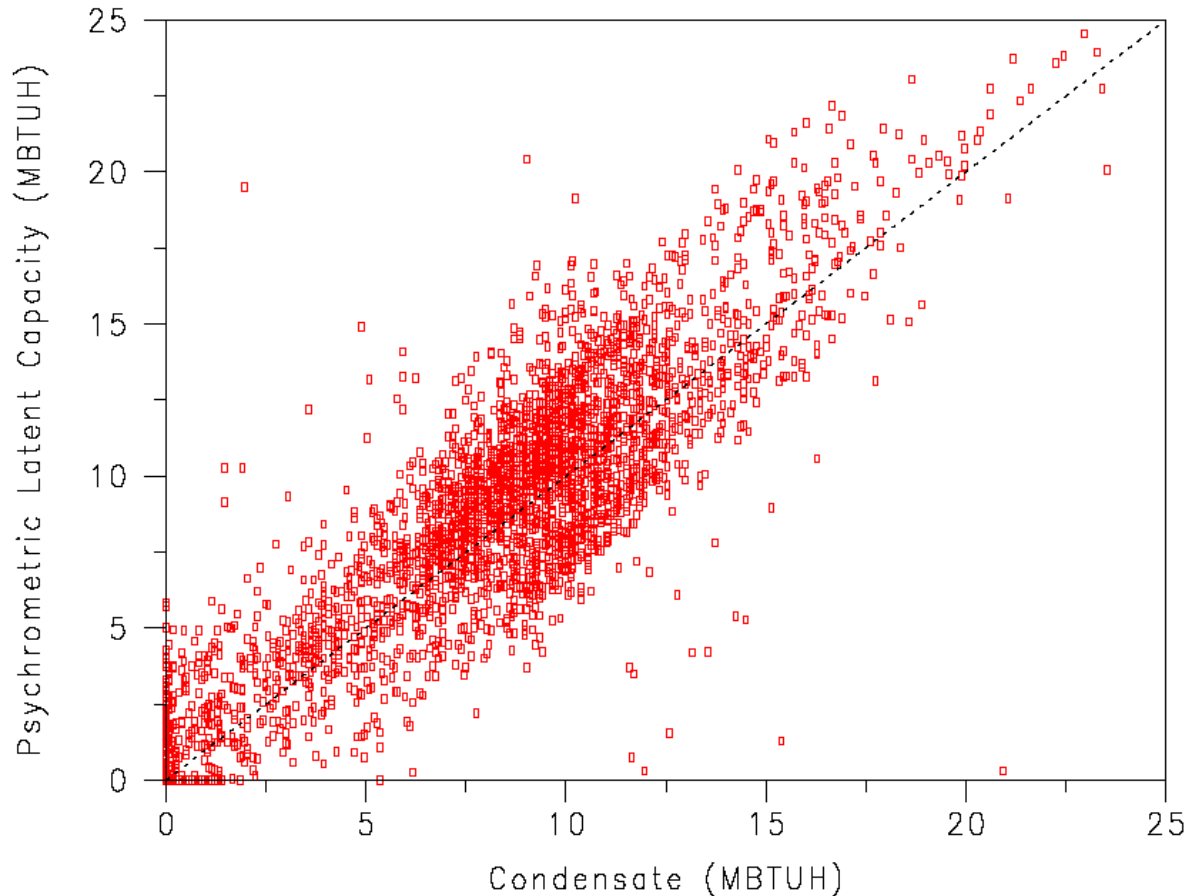


**Figure 12. Psychrometric Latent Capacity versus Condensate**

Figure 13 combines information discussed in previous figures to compare the measured air-side total capacity to that measured on the water-side. Return and supply air temperature and humidity measurements combined with the air flow rate through the cooling coil provides a measure of air-side total capacity. Fan heat was added to the air side sensible capacity to provide an indication of gross coil capacity. Measurement of chilled water supply and return temperatures along with the calculated chilled water flow rate provided an independent measurement of the coil's total capacity yielding an energy balance. Winter data from December 2002 through February 2003 and December 2003 through February 2004 were removed to analyze only cooling data.

There is general agreement between the measured air-side and water-side total cooling capacity. However, there is a significant amount of scatter in the plotted data due to many factors, such as uncertainty regarding chilled water flow rate, time lag between a change in chilled water flow rate and the air-side total capacity, time lag in the measurement of coil water temperatures due to sensor location on pipe exterior, and thermal capacitance of the cooling coil. Field measurements typically depict these types of uncertainties and every effort must be made to assure accurate measurements depending on the required project outcome.

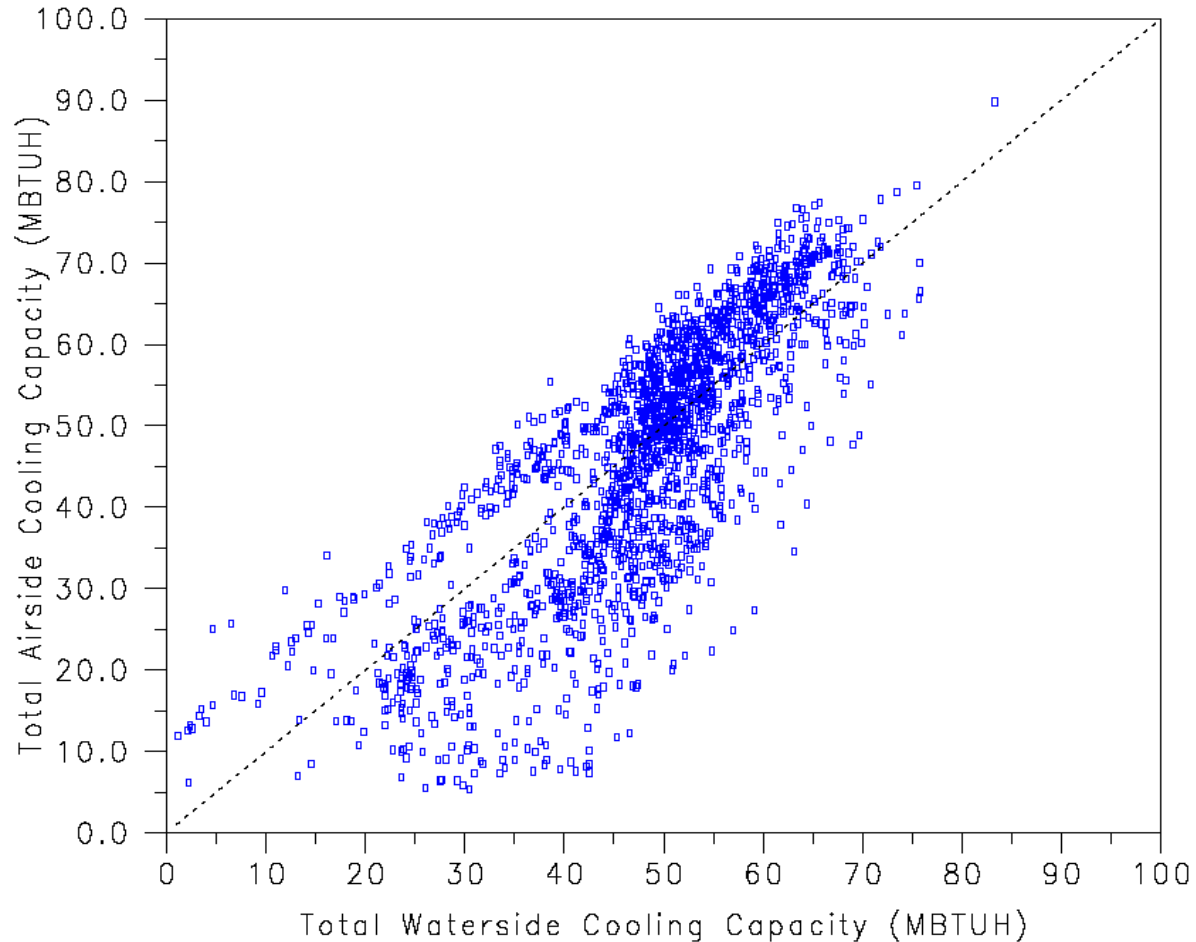


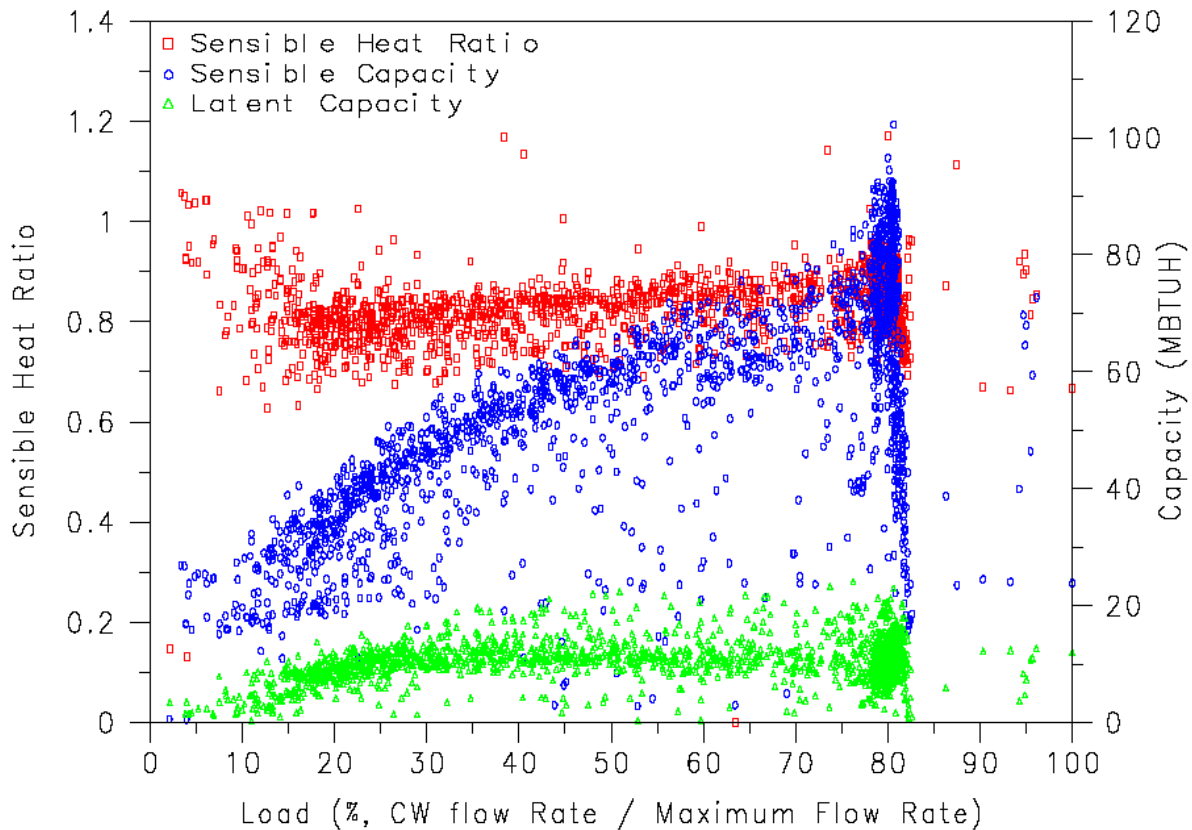
**Figure 13. Air-side Capacity versus Water-side Capacity**

The required outcome for this project is to define the part-load latent degradation characteristics for this particular cooling coil. The part-load degradation characteristic of interest is latent capacity with respect to the steady state latent capacity of the cooling coil. Latent capacity of an air conditioner is a measure of the coil’s ability to remove moisture from the air as it passes over the cooling coil’s surface. Performance of an air conditioner is also measured using the sensible heat ratio (SHR) of the system and is defined as the sensible cooling capacity divided by total cooling capacity (sensible plus latent). The latent heat ratio ( $1 - \text{SHR}$ ) is a measure of the latent (moisture removal) cooling capacity divided by the total cooling capacity. The latent capacity of an air conditioner can be measured in different ways. In this project, temperature and relative humidity sensors were installed in the return and supply air streams. The measure of humidity ratio, when combined with air flow rate yields the psychrometric latent capacity of the air conditioner. In addition to these sensors, a condensate measuring device was installed at the end of the condensate drain line. This device measures the actual moisture leaving the AC unit and is considered to be a measure of the air handler’s net latent capacity.

The term “part-load” above refers the actual total capacity delivered compared to the maximum total capacity available. This analysis requires that the actual coil load be defined with respect to some measured parameter. For a variable-air-volume air handler, capacity is controlled by modulating air flow across a cooling coil. This is accomplished by controlling the supply air fan

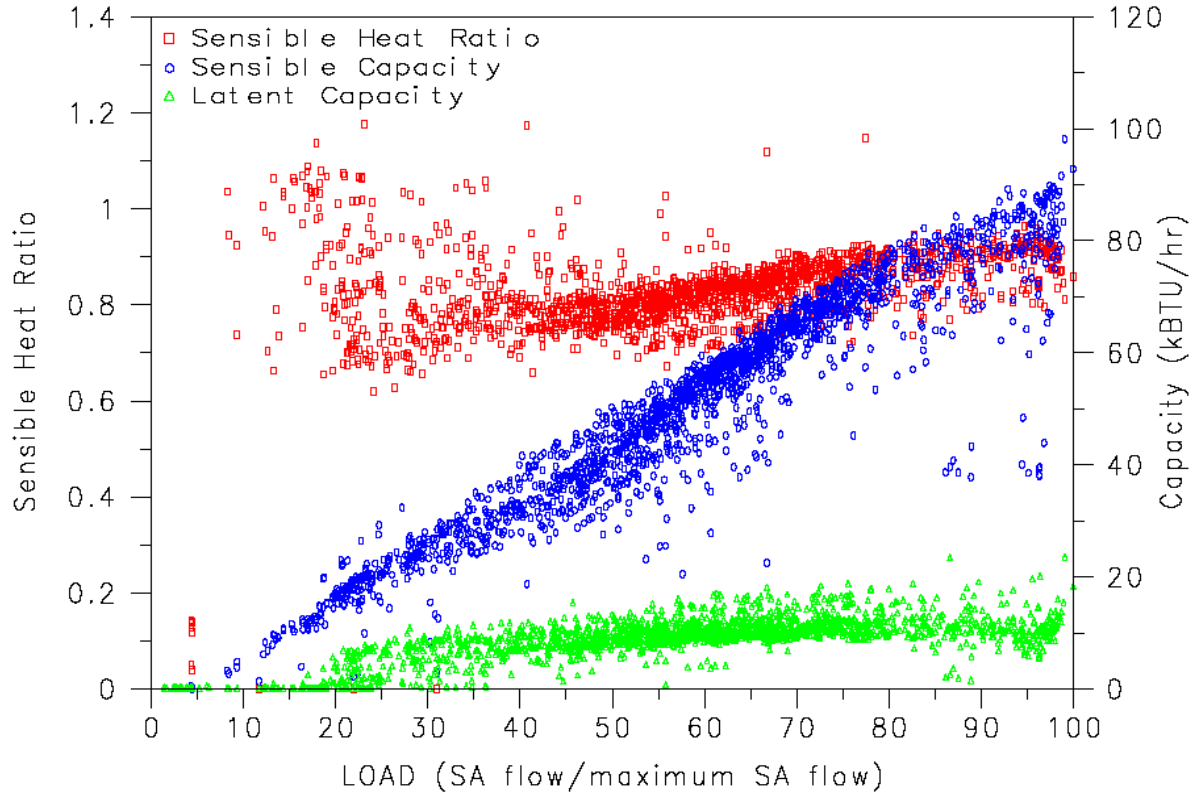
to maintain a constant supply air static pressure. As the space temperature is reduced, individual variable-air-volume boxes close a damper to provide less cooling to the individual spaces. This in turn raises the supply air static pressure and fan speed is reduced to maintain the supply air static pressure set point. At this same time, chilled water is modulated through the cooling coil to maintain a desired supply air temperature set point. With the uncertainties between air-side and water-side measurements previously mentioned, a single plot of sensible heat ratio may yield unexplainable results and further investigations are warranted. To complete the analysis, the data set will be analyzed using both chilled water flow rate through the cooling coil and supply air flow rate across the cooling coil as a measure of “load” on the system. In addition, the measurements of air-side latent capacity and condensate will also be presented in the following figures.

Figure 14 through Figure 18 shows the same hourly data set described in Figure 13. Figure 14 shows the air-side sensible and psychrometric latent capacity as a function of chilled water flow rate through the cooling coil.



**Figure 14. Summer Sensible Heat Ratio and Capacity versus Load (gpm, latent)**

Figure 15 shows the air-side sensible and psychrometric latent capacity as a function of supply air flow rate through the cooling coil. Figure 16 and Figure 17 show the same air-side sensible capacity plotted versus chilled water flow rate and supply air flow rate, respectively. However, latent capacity and SHR are now with respect to the condensate discharged through the drain line.



**Figure 15. Summer Sensible Heat Ratio and Capacity versus Load (SA Flow, latent)**

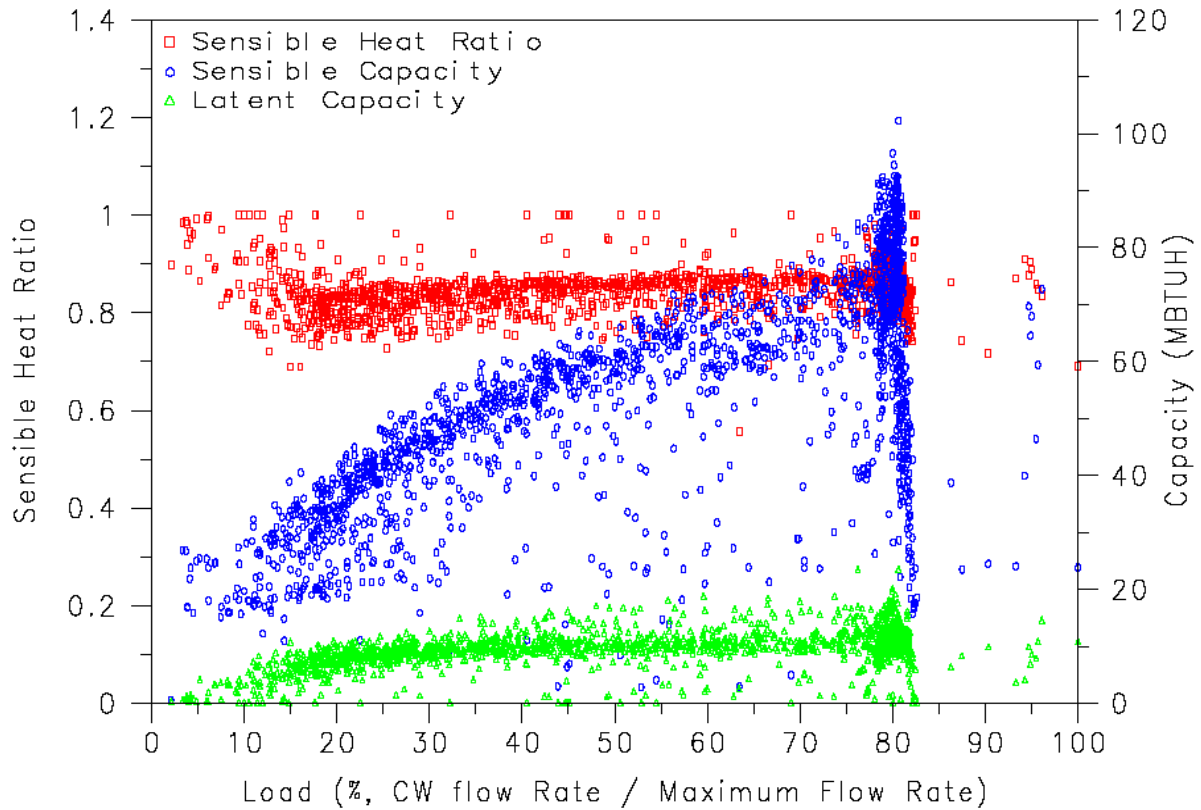


**Figure 16. Summer Sensible Heat Ratio and Capacity versus Load (gpm, condensate)**

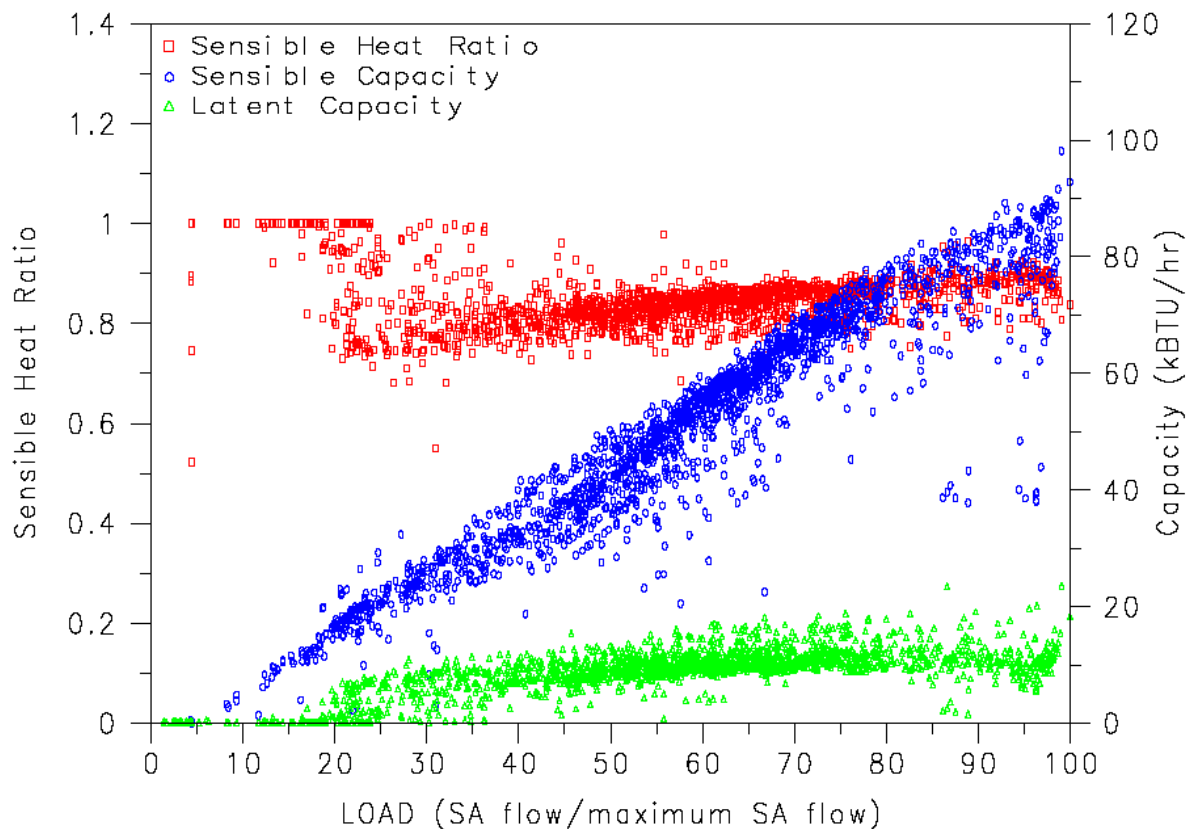


**Figure 17. Summer Sensible Heat Ratio and Capacity versus Load (SA Flow, condensate)**

These figures, when combined as in Figure 18, show the sensible heat ratio of this cooling coil when capacity is a function of different load criteria (i.e. load with respect to supply air flow rate or chilled water flow rate) and when latent capacity is a function of different measurements in the system (i.e., latent capacity measured with temperature and relative humidity sensors or condensate measurements).

Each of these methods provides an indication of the part-load performance of this particular cooling coil. In all cases, the sensible heat ratio is shown to be approximately 0.8 at a part-load ratio of 40 % and 0.89 at a part load ratio of 100%. This would seem to be a reasonable assessment of performance for this cooling coil when configured as a variable-air-volume system. The part-load performance shows a somewhat different pattern as the “load” on the system falls below 40 % depending on the measured data selected for analysis. In the case of load as a function of chilled water flow rate, the sensible heat ratio rises sharply as the load drops below 15 % and tends to approach a value of 1.0. If supply air flow rate is selected as the measure of coil load, SHR is shown to begin to rise and appear more scattered as the load on the system is reduced below a 40 % part-load condition.

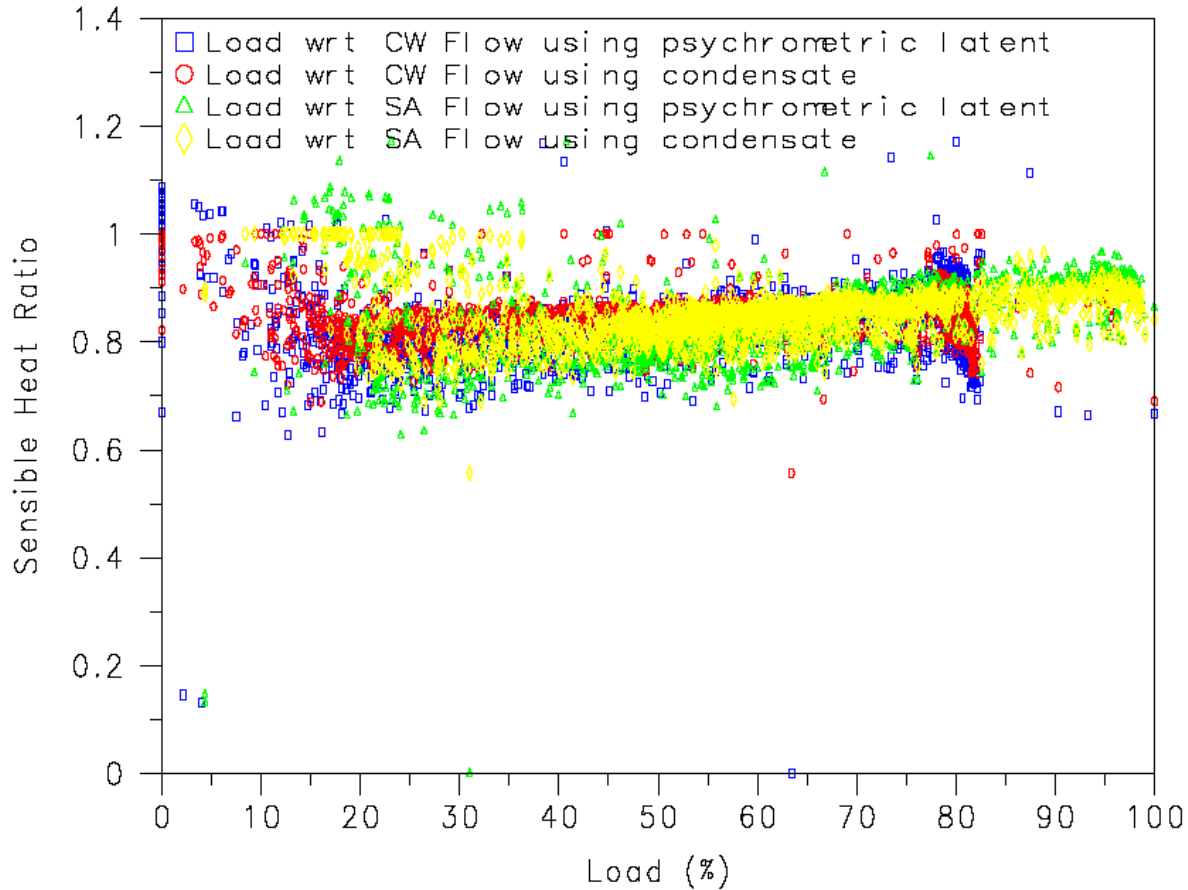


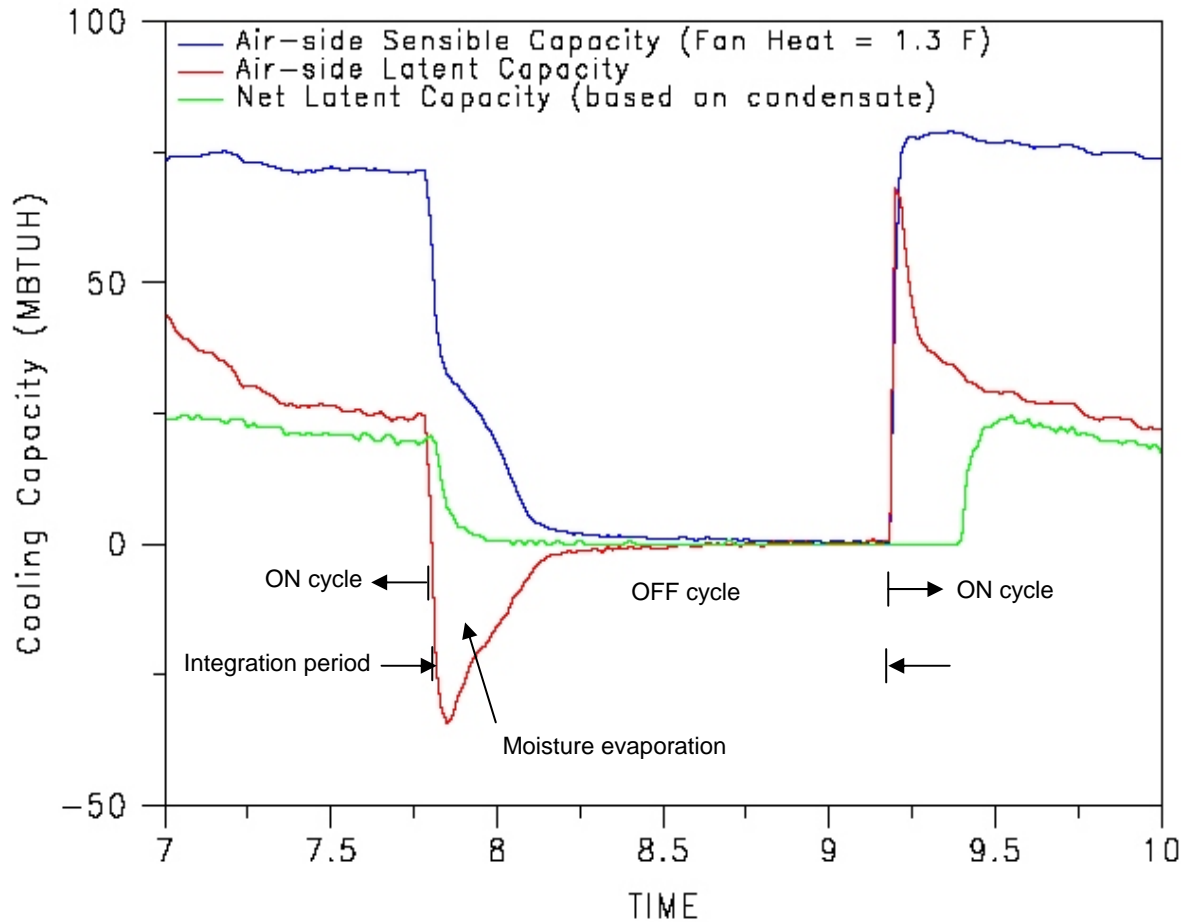
**Figure 18. Sensible Heat Ratio Comparison**

### **Moisture-Holding Capacity of the Cooling Coil**

Tests were performed to quantify the moisture-holding capacity of this chilled water cooling coil. For this variable-air-volume air handler, the fan was fixed at 45 Hz to provide approximately the design air flow rate of 2888 CFM. The chilled water valve was fully opened for a short period of time in an attempt to produce a fully-wetted cooling coil. Then, water flow through the coil was stopped for one or two hours while the supply air fan continued to operate. Once the moisture on the cooling coil had been fully evaporated into the supply air stream, the chilled water valve was reopened and measurements were collected until condensate removal was detected by the tipping bucket mechanism. This test sequence was performed twice during the monitoring period and the results are described below.

Figure 19 shows air-side performance data collected on October 7, 2004 when this test sequence was being performed. The chilled water control valve was fully opened from 6:47 a.m. when the unit turned on until just after 7:47 a.m.. Chilled water flow was stopped from 7:47 a.m. to 9:19 a.m. using a manual isolation valve. When chilled water flow was stopped, the moisture on the coil's surface was evaporated back in to the supply air stream. The air-side sensible and latent capacities were integrated starting at 7:48 a.m. and ending at 9:19 a.m. Based on these integrated values and assuming an enthalpy of vaporization equal to 1060 Btu/lb<sub>moisture</sub>, the moisture holding capacity of the cooling coil was estimated to be between 7.51 and 6.11 pounds,

respectively. During this same integration period, 1.02 pounds of moisture exited the unit through the condensate drain line. The value of  $T_{wet}$  is calculated based on a retained moisture mass of 7.51 (based on sensible integration) and an average latent capacity just prior to the off-cycle of 19.85 MBtu/hr (based on condensate). The average inlet air temperature, humidity, and dew point conditions just prior to the off-cycle (7:38 – 7:48 am) were 71.67 °F, 50.28 %, and 52.2 °F, respectively. Multiplying the retained moisture mass by the heat of vaporization for water (1060 Btu/lb) and dividing by the steady-state latent capacity yields 24.1 minutes.



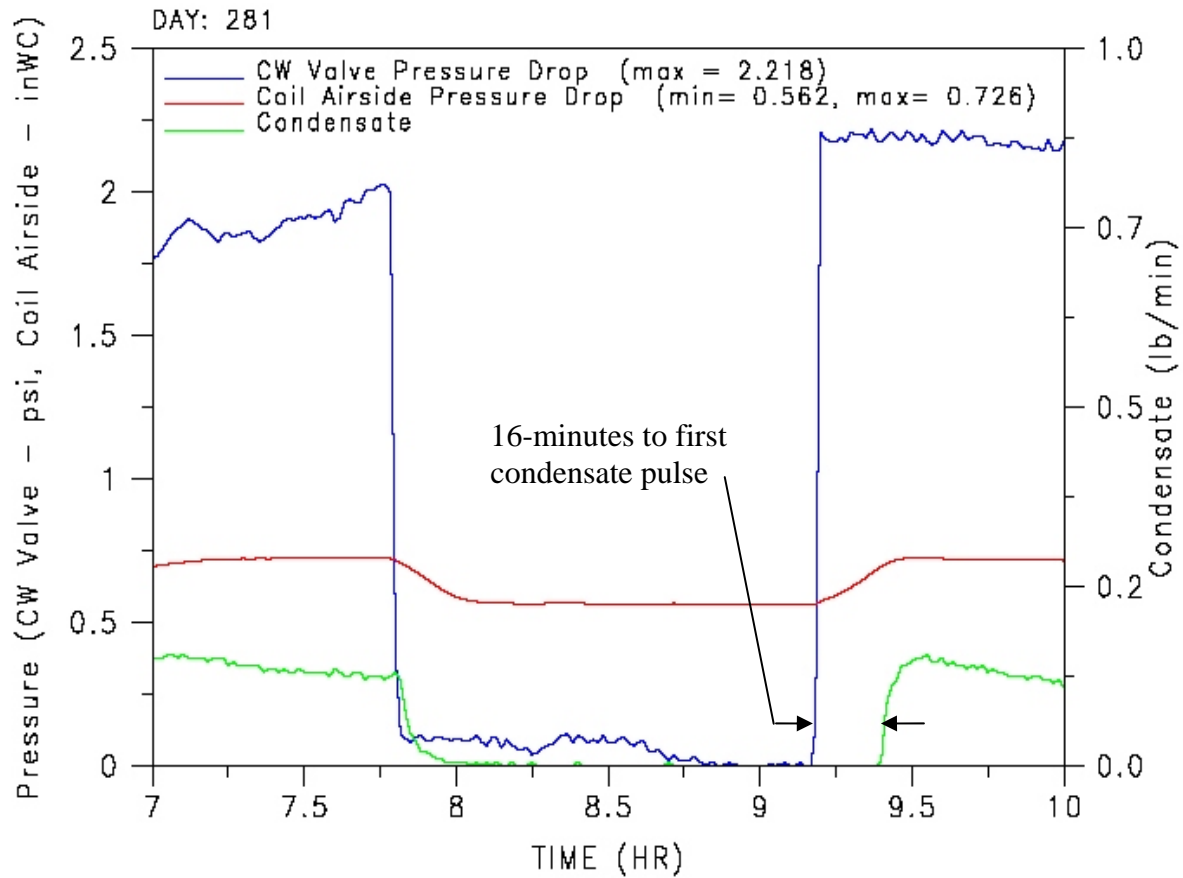
**Figure 19. Measured Sensible and Latent Capacity for October 7, 2004**

Figure 20 shows additional measurements collected during this test sequence, including the impacts of coil moisture retention on air-side pressure drop. Since this is a variable-air-volume air handler, the coil was loaded up with moisture at 7:00 am and condensate is seen to be leaving the unit at a relatively constant rate. The air side pressure drop is shown to be 0.726 in. WC while the coil is fully laden with moisture and 0.562 in. WC during the time when the coil is dry. The air-side pressure drop for the wet coil was 0.164 in. WC (29%) higher than when the coil was dry.

After the isolation valve was reopened, 16 minutes elapsed before any condensate removal was measured. With latent capacity of approximately 22,390 Btu/hr (based on condensate) and a condensate delay time of 16 minutes, this coil holds approximately 5.63 pounds of moisture at these conditions. This method of estimating the moisture-holding capacity of the cooling coil



agrees fairly well with the previously-described method of integrating air-side latent and sensible capacities during the moisture evaporation period when chilled water flow is fully stopped.



**Figure 20. Wet-dry Coil Pressure Drop and Condensate Removal for October 7, 2004**

Figure 21 shows a similar test to that described in Figure 19. The moisture reevaporation test was performed the following day to measure the moisture retention characteristics of this coil under similar conditions. On this day the air handler turned on at 7:08 a.m. and operated at full chilled water flow rate with the fan speed set at 45 Hz. At 7:53 a.m. the CW valve was manually closed and the amount of moisture retained on the coil was again measured. Based on the psychrometric sensible and latent capacities measured during the off cycle integration period, this coil holds 7.27 and 6.61 lbs of moisture, respectively. Condensate leaving the drain line was measured at 1.02 lbs moisture during the off cycle. Upon opening the CW valve, the first condensate pulse was measured 15-minutes into the on cycle. With an average latent capacity of 19.85 Mbtu/hr based on condensate measured at approximately 10 a.m., this alternate measurement of moisture retention using steady-state latent capacity and condensate delay time yields 4.7 lbs of moisture.



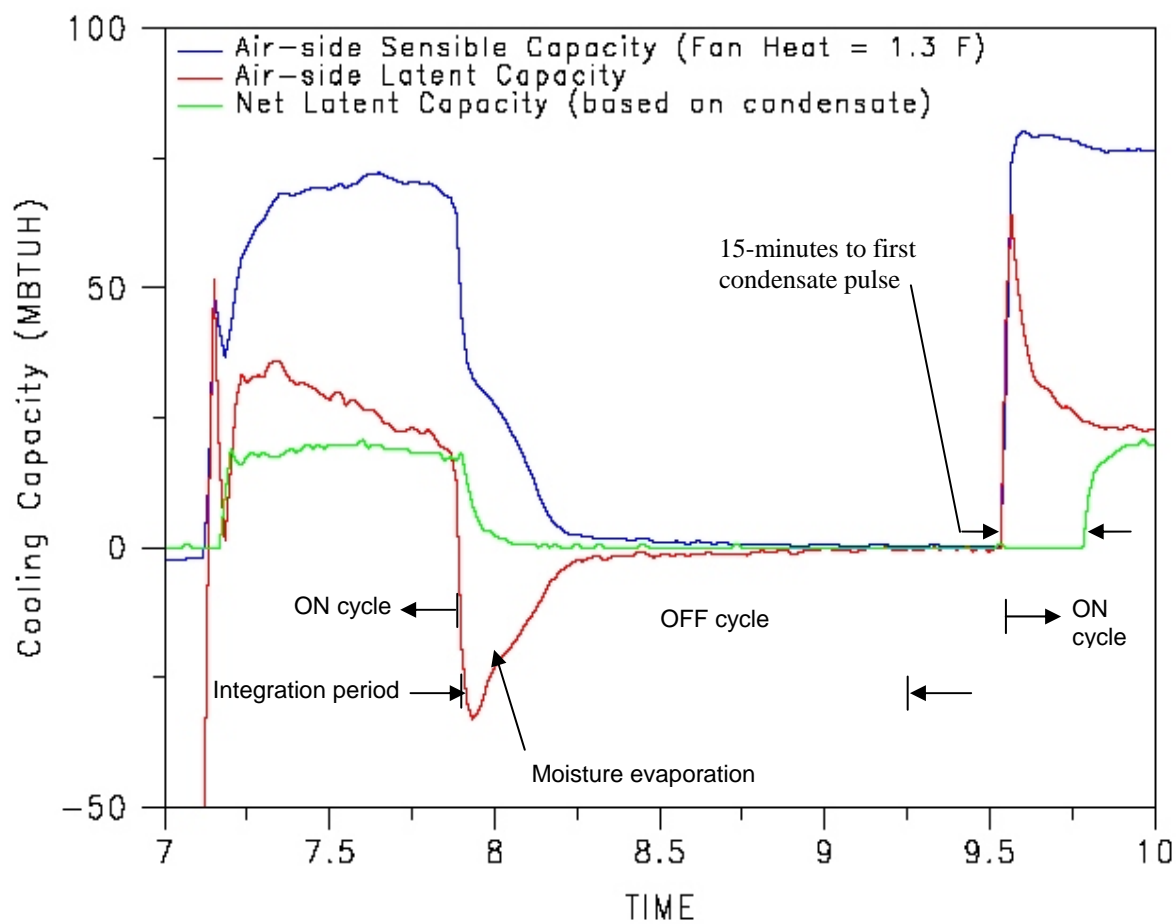


Figure 21. Measured Sensible and Latent Capacity for October 8, 2004